SPECIALIST PERIODICAL REPORTS

RS•C
ROYAL SOCIETY OF CHEMISTRY

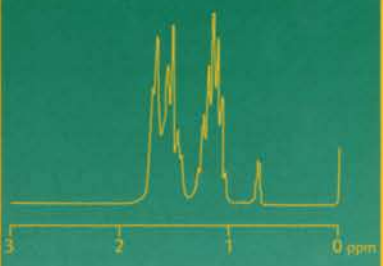

Nuclear magnetic *resonance*

Volume 31

senior reporter G.A. WEBB

Nuclear Magnetic Resonance

Volume 31

SPECIALIST PERIODICAL REPORTS

RS•C
ROYAL SOCIETY OF CHEMISTRY

Systematic and detailed review coverage in major areas of chemical research.

A unique service for the active research chemist with annual or biennial, in-depth accounts of progress in particular fields of chemistry, in print and online.

NOW AVAILABLE ELECTRONICALLY - chapters from volumes published 1998 onwards are now available online, fully searchable by key word, on a pay-to-view basis.

Contents pages can be viewed free of charge.

Now available online:

- Amino Acids, Peptides & Proteins *Vol.29 - 32*
- Carbohydrate Chemistry *Vol.30 - 32*
- Catalysis *Vol.14 - 15*
- Chemical Modelling *Vol.1*
- Electron Paramagnetic Resonance *Vol.16 - 17*
- Nuclear Magnetic Resonance *Vol.27 - 30*
- Organometallic Chemistry *Vol.26 - 29*
- Organophosphorus Chemistry *Vol.29 - 31*
- Photochemistry *Vol.29 - 32*
- Spectroscopic Properties of Inorganic and Organometallic Compounds *Vol.31 - 34*

Titles for 2002:

- Amino Acids, Peptides & Proteins *Vol.33*
- Carbohydrate Chemistry *Vol.33*
- Catalysis *Vol.16*
- Chemical Modelling *Vol.2*
- Electron Paramagnetic Resonance *Vol.18*
- Nuclear Magnetic Resonance *Vol.31*
- Organometallic Chemistry *Vol.30*
- Organophosphorus Chemistry *Vol.32*
- Photochemistry *Vol.33*
- Spectroscopic Properties of Inorganic and Organometallic Compounds *Vol.35*

RSCA2K/10101/60-NONO

ROYAL SOCIETY OF CHEMISTRY *Investing in Chemical Science*

Or visit our web pages today:

www.rsc.org/spr

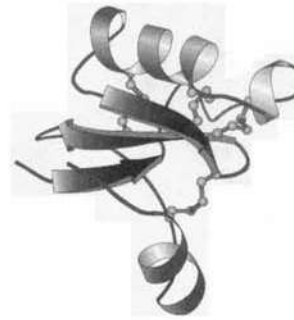

Orders & further details **Sales & Customer Care Dept** · Royal Society of Chemistry
Thomas Graham House · Science Park · Milton Road · Cambridge · CB4 0WF · UK
T +44(0)1223 432360 · F +44(0)1223 426017 · E sales@rsc.org
Or visit our websites: **www.rsc.org** and **www.chemsoc.org**
Registered Charity No. 207890

A Specialist Periodical Report

Nuclear Magnetic Resonance
Volume 31

A Review of the Literature Published between June 2000 and May 2001

Senior Reporter
G.A. Webb, *formerly Department of Chemistry of Surrey, Guildford, UK*

Reporters
A.E. Aliev, *University College, London, UK*
S. Ando, *Tokyo Institute of Technology, Tokyo, Japan*
T. Baba, *Kitami Institute of Technology, Kitami, Japan*
I. Barsukov, *University of Leicester, UK*
A.C. de Dios, *Georgetown University, Washington, DC, USA*
H. Fukui, *Kitami Institute of Technology, Kitami, Japan*
E.F. Hounsell, *Birkbeck College, London, UK*
C.J. Jameson, *University of Illinois at Chicago, USA*
K. Kamieńska-Trela, *Polish Academy of Sciences, Warszawa, Poland*
C.L. Khetrapal, *Sanjay Gandhi Post Graduate Institute of Medical Sciences, Lucknow, India*
S. Kuroki, *Tokyo Institute of Technology, Tokyo, Japan*
H. Kurosu, *Nara Women's University, Nara City, Japan*
R.V. Law, *Imperial College of Science, Technology and Medicine, London, UK*
R. Ludwig, *Universität Dortmund, Germany*
S.J. Matthews, *Imperial College of Science, Technology and Medicine, London, UK*
G.A. Nagana Gowda, *Sanjay Gandhi Post Graduate Institute of Medical Sciences, Lucknow, India and Indian Institute of Science, Bangalore, India*
M.J.W. Prior, *University of Nottingham, UK*
K.V. Ramanathan, *Indian Institute of Science, Bangalore, India*
W. Schilf, *Polish Academy of Sciences, Warszawa, Poland*
T. Watanabe, *Tokyo University of Fisheries, Tokyo, Japan*
J. Wójcik, *Polish Academy of Sciences, Warszawa, Poland*
T. Yamanobe, *University of Gunma, Japan*

RS•C
ROYAL SOCIETY OF CHEMISTRY

ISBN 0-85404-337-3
ISSN 0305-9804

Copyright © The Royal Society of Chemistry 2002

All rights reserved

Apart from any fair dealing for the purposes of research or private study, or criticism or review as permitted under the terms of the UK Copyright, Designs and Patents Act, 1988, this publication may not be reproduced, stored or transmitted, in any form or by any means, without the prior permission in writing of The Royal Society of Chemistry, or in the case of reprographic reproduction only in accordance with the terms of the licences issued by the Copyright Licensing Agency in the UK, or in accordance with the terms of the licences issued by the appropriate Reproduction Rights Organization outside the UK. Enquiries concerning reproduction outside the terms stated here should be sent to The Royal Society of Chemistry at the address printed on this page.

Published by The Royal Society of Chemistry,
Thomas Graham House, Science Park, Milton Road, Cambridge CB4 0WF, UK

Registered Charity Number 207890

For further information see our web site at www.rsc.org

Typeset by Computape (Pickering) Ltd, Pickering, North Yorkshire, UK
Printed by Athenaeum Press Ltd, Gateshead, Tyne and Wear, UK

Preface

It is my great pleasure to introduce Volume 31 of the Specialist Periodical Reports on NMR. The chapter coverage aims to provide a comprehensive account of the NMR literature appearing between June 2000 and May 2001. Between them the reporters have produced, with a high degree of celerity, very valuable accounts of the fourteen areas of science covered in this volume.

I am very happy to have the opportunity to thank the authors, all of whom have reported in previous volumes, for their very commendable efforts. Dr S. Ando is retiring from the reporting team with this volume; my thanks and best wishes go with him. Finally, I am very grateful for the dedicated work of the production team at the Royal Society of Chemistry.

G.A. Webb

Contents

Chapter 1 **NMR Books and Reviews** **1**
By W. Schilf
1 Books 1
2 Regular Reviews Series 1
3 Edited Books and Symposia 8
4 Reviews in Periodicals 18
5 Reviews and Books in Foreign Languages 41

Chapter 2 **Theoretical and Physical Aspects of Nuclear Shielding** **48**
By C.J. Jameson and A.C. de Dios
1 Theoretical Aspects of Nuclear Shielding 48
1.1 General Theory 48
1.2 *Ab initio* Calculations 57
1.3 Semi-empirical Calculations 58
2 Physical Aspects of Nuclear Shielding 58
2.1 Anisotropy of the Shielding Tensor 58
2.2 Shielding Surfaces and Rovibrational Averaging 63
2.3 Isotope Shifts 66
2.4 Intermolecular Effects on Nuclear Shielding 67
2.5 Absolute Shielding Scales 73
3 References 74

Chapter 3 **Applications of Nuclear Shielding** **79**
By S. Ando and S. Kuroki
1 Introduction 79
2 Various Chemical and Physical Influences on Nuclear Shielding 79
2.1 Substituent Effects 79
2.2 Conformation Effects 81
2.3 Intermolecular and Hydrogen Bonding Effects 83
2.4 Solvent Effects 85
2.5 Isotope Effects 86
3 Shielding of Particular Nuclear Species 88
3.1 Group 1 (^{1}H, ^{2}H, ^{3}H, ^{6,7}Li, ^{23}Na, ^{87}Rb, ^{133}Cs) 88
3.1.1 Hydrogen (^{1}H) (I = 1/2) 88
3.1.2 Deuterium (^{2}H) (I = 1) 88
3.1.3 Lithium (^{6,7}Li) (I = 1, 3/2) 88
3.1.4 Sodium (^{23}Na) (I = 3/2) 90
3.1.5 Rubidium (^{87}Rb) (I = 3/2) 90
3.1.6 Caesium (^{133}Cs) (I = 7/2) 91

Nuclear Magnetic Resonance, Volume 31
© The Royal Society of Chemistry, 2002

3.2 Group 2 (^{9}Be, ^{25}Mg, ^{137}Ba) 91
3.2.1 Beryllium (^{9}Be) (I = 3/2) 91
3.2.2 Magnesium (^{25}Mg) (I = 5/2) 91
3.2.3 Barium (^{137}Ba) (I = 3/2) 91
3.3 Group 3 and Lanthanoids (^{45}Sc, ^{89}Y, ^{139}La, ^{153}Eu) 91
3.3.1 Scandium (^{45}Sc) (I = 7/2) 91
3.3.2 Yttrium (^{89}Y) (I = 1/2) 91
3.3.3 Lanthanum (^{139}La) (I = 7/2) 92
3.3.4 Europium (^{153}Eu) (I = 5/2) 92
3.4 Group 4 (^{47,49}Ti) 92
3.4.1 Titanium (^{47,49}Ti) (I = 5/2, 7/2) 92
3.5 Group 5 (^{51}V and ^{93}Nb) 92
3.5.1 Vanadium (^{51}V, ^{93}Nb) (I = 7/2) 92
3.5.2 Niobium (^{93}Nb) (I = 9/2) 93
3.6 Group 6 (^{95}Mo, ^{183}W) 93
3.6.1 Molybdenum (^{95}Mo) (I = 5/2) 93
3.6.2 Tungsten (^{183}W) (I = 1/2) 94
3.7 Group 7 (^{55}Mn, ^{99}Tc) 94
3.7.1 Manganese (^{55}Mn) (I = 5/2) 94
3.7.2 Technetium (^{99}Tc) (I = 3/2) 94
3.8 Group 8 (^{57}Fe, ^{99}Ru) 94
3.8.1 Iron (^{57}Fe) (I = 1/2) 94
3.8.2 Ruthenium (^{99}Ru) (I = 3/2) 95
3.9 Group 9 (^{59}Co, ^{103}Rh) 95
3.9.1 Cobalt (^{59}Co) (I = 7/2) 95
3.9.2 Rhodium (^{103}Rh) (I = 1/2) 95
3.10 Group 10 (^{195}Pt) 95
3.10.1 Platinum (^{195}Pt) (I = 1/2) 95
3.11 Group 11 (^{63}Cu, ^{107,109}Ag) 97
3.11.1 Copper (^{63}Cu) (I = 3/2) 97
3.11.2 Silver (^{107,109}Ag) (I = 1/2, 1/2) 97
3.12 Group 12 (^{67}Zn, ^{111,113}Cd, ^{199}Hg) 97
3.12.1 Zinc (^{67}Zn) (I = 5/2) 97
3.12.2 Cadmium (^{111,113}Cd) (I = 1/2, 1/2) 97
3.12.3 Mercury (^{199}Hg) (I = 1/2) 98
3.13 Group 13 (^{11}B, ^{27}Al, ^{71}Ga, ^{203,205}Tl) 98
3.13.1 Boron (^{11}B) (I = 3/2) 98
3.13.2 Aluminium (^{27}Al) (I = 5/2) 99
3.13.3 Gallium (^{71}Ga) (I = 3/2) 101
3.13.4 Thallium (^{203,205}Tl) (I = 1/2, 1/2) 102
3.14 Group 14 (^{13}C, ^{29}Si, ^{73}Ge, ^{117,119}Sn, ^{207}Pb) 102
3.14.1 Carbon (^{13}C) (I = 1/2) 102
3.14.2 Silicon (^{29}Si) (I = 1/2) 102
3.14.3 Germanium (^{73}Ge) (I = 9/2) 103
3.14.4 Tin (^{117,119}Sn) (I = 1/2, 1/2) 103
3.14.5 Lead (^{207}Pb) (I = 1/2) 104
3.15 Group 15 (^{14,15}N, ^{31}P) 104
3.15.1 Nitrogen (^{14,15}N) (I = 1, 1/2) 104
3.15.2 Phosphorus (^{31}P) (I = 1/2) 105
3.16 Group 16 (^{17}O, ^{33}S, ^{77}Se, ^{125}Te) 105

3.16.1 Oxygen (^{17}O) ($I = 5/2$) 105
3.16.2 Sulfur (^{33}S) ($I = 3/2$) 105
3.16.3 Selenium (^{77}Se) ($I = 1/2$) 106
3.16.4 Tellurium (^{125}Te) ($I = 1/2$) 106
3.17 Group 17 (^{19}F, $^{35,37}Cl$) 107
3.17.1 Fluorine (^{19}F) ($I = 1/2$) 107
3.17.2 Chlorine ($^{35,37}Cl$) ($I = 3/2, 3/2$) 107
3.18 Group 18 (^{3}He, ^{129}Xe) 107
3.18.1 Helium (^{3}He) ($I = 1/2$) 107
3.18.2 Xenon (^{129}Xe) ($I = 1/2$) 107
4 References 108

Chapter 4 Theoretical Aspects of Spin–Spin Couplings 122
By H. Fukui and T. Baba
1 Introduction 122
2 Relativistic Calculation of Spin–Spin Couplings 122
3 Density Functional Theory 129
4 *Ab Initio* Calculations 134
4.1 Correlation Effects 134
4.2 Scalar Couplings as a Function of Interatomic Distance 134
4.3 Anisotropy of the Spin–Spin Coupling Tensor 135
4.4 Effects of Internal Rotation and Bond Stretching 136
5 Through-space and Hydrogen Bond Scalar Couplings 137
5.1 Through-space Scalar Coupling 137
5.2 Hydrogen Bond Scalar Couplings 138
6 References 140

Chapter 5 Applications of Spin–Spin Couplings 144
By K. Kamieńska-Trela and J. Wójcik
1 Introduction 144
2 New Methods 145
3 One-bond Couplings to Hydrogen 147
4 One-bond Couplings not Involving Hydrogen 149
5 Two-bond Couplings to Hydrogen 156
6 Two-bond Couplings not Involving Hydrogen 158
7 Three-bond Hydrogen–Hydrogen Couplings 159
8 Three-bond Couplings Between Hydrogen and Heteronuclei 166
9 Three-bond Couplings not Involving Hydrogen 171
10 Couplings over More than Three Bonds and Through Space 172
11 Couplings Through Hydrogen Bonds 175
12 References 178

Chapter 6 Nuclear Spin Relaxation in Liquids and Gases 192
By R. Ludwig
1 Introduction 192
2 General, Physical and Experimental Aspects of Nuclear Spin Relaxation 195
2.1 General Aspects 195
2.2 Experimental Aspects 196
2.3 Relaxation in Coupled Spin Systems 197

2.4 Dipolar Couplings and Distance Information 200
2.5 Exchange Spectroscopy 201
2.6 Radiation Damping 203
2.7 Quadrupolar Interactions 204
2.8 Intermolecular Dipolar Interaction in Diamagnetic and Paramagnetic Solution 206
2.9 Slow Motions in Glasses 207
2.10 Models for Molecular Dynamics 209
3 Selected Applications of Nuclear Spin Relaxation 210
3.1 Pure Liquids 210
3.2 Non-electrolyte Solutions 211
3.3 Electrolyte Solutions 211
3.4 Transition Metal Complexes 212
3.5 Molten Salts 213
4 Nuclear Spin Relaxation in Gases 213
5 Self-diffusion in Liquids 215
5.1 Experimental and Theoretical Aspects 215
5.2 Selected Examples 215
6 References 216

Chapter 7 Solid-state NMR Spectroscopy 225
A.E. Aliev and R.V. Law
1 Introduction 225
2 Reviews 225
3 Theory 226
4 Experiment 230
4.1 New Technique Developments 230
4.1.1 ^{1}H NMR 230
4.1.2 Fast MAS 231
4.1.3 2D Correlation Spectroscopy 232
4.1.4 2D MQ MAS 234
4.1.5 Other Experiments 236
4.2 Distance and Angle Measurements by REDOR and Other Solid-state NMR Techniques 239
4.3 NMR Parameters: Experimental and Theoretical Studies 242
4.4 Exotic and Troublesome Nuclei 246
5 Applications 247
5.1 Organic Solids 247
5.2 Organometallic and Coordination Compounds 250
5.3 Natural Products 251
5.4 Biochemical, Medical and Pharmaceutical Applications 253
5.4.1 Proteins 253
5.4.2 Peptides 254
5.4.3 Lipids and Membranes 254
5.4.4 Biomedical Applications 256
5.5 Coal, Soil Organic Matter and Other Related Materials 257
5.5.1 Coals and Carbonaceous Materials 257
5.5.2 Soils 257
5.6 Polymers 258
5.7 Glasses and Amorphous Solids 263

5.8 Cements 266
5.9 Micro- and Mesoporous Solids 266
5.10 Surface Science and Catalysis 269
5.11 Inorganic and Other Related Materials 271
6 References 276

Chapter 8 Multiple Pulse NMR 289
By I. Barsukov
1 Introduction 289
2 Shaped Radiofrequency Pulses and Solvent Suppression 289
2.1 Adiabatic Pulses and Isotropic Mixing 289
2.2 Shaped Pulses and Other Homonuclear Experiments 290
3 NOE, Chemical Exchange and Relaxation 291
3.1 NOE and Chemical Exchange 291
3.2 Relaxation Rate Measurements 292
3.3 Cross-correlated Relaxation Experiments 293
4 Coupling Constants Measurements 295
4.1 Scalar Couplings 295
4.2 Couplings across Hydrogen Bonds 296
4.3 Residual Dipolar Couplings 297
5 Inverse Proton Detected Correlation Spectroscopy 300
5.1 Isotope Filtered Experiments 300
5.2 Isotope Edited Experiments 301
5.3 Heteronuclear Double Resonance Experiments 301
5.3.1 HSQC/HMQC 301
5.3.2 TROSY 303
5.4 Heteronuclear Triple Resonance Experiments 304
6 References 309

Chapter 9 NMR of Proteins and Nucleic Acids 312
By S.J. Matthews
1 Introduction 312
2 Emerging NMR Methodology 312
2.1 Dipolar Couplings 312
2.2 Transverse Relaxation Optimized Spectroscopy (TROSY) 316
2.3 General Methodology 318
3 Solution Structures 319
3.1 Free Proteins 319
3.2 Protein–Small Molecule Complexes 320
3.3 Protein–Metal Complexes 322
3.4 Protein–Protein Complexes 322
3.5 Protein–Nucleic Acid Complexes 324
4 Protein Relaxation and Dynamics 325
5 Protein Folding 330
6 References 332

Chapter 10 NMR of Carbohydrates, Lipids and Membranes 338
By E.F. Hounsell
1 Introduction 338
2 Bacterial Natural Products 339

2.1 Bacteria Causing Mammalian Pathogenesis 339
2.2 Bacteria Causing Disease in Plants 341
2.3 Marine Bacteria 341
3 Fungal Natural Products 342
4 Plant Natural Products Characterised by ^{1}H and ^{13}C NMR 342
5 Other Organisms 344
6 Lipid Conjugates 344
7 Glycosylphosphatidylinositol Anchors 345
8 Membrane Studies 346
9 Mammalian Glycoproteins and Carbohydrate–Protein Recognition Studies 346
9.1 Structural Studies 346
9.2 Conformational Studies 347
9.3 *In vivo* Studies 348
10 References 348

Chapter 11 Synthetic Macromolecules 353
By H. Kurosu and T. Yamanobe
1 Introduction 353
2 Primary Structure 353
3 Liquid Crystalline Polymers 353
4 Characterization of the Synthetic Macromolecules 364
5 Dynamics of the Synthetic Macromolecules 370
6 Gels and Crosslinking Macromolecules 372
7 Polymer Blend and Diffusion of the Synthetic Macromolecules 373
8 References 374

Chapter 12 NMR in Living Systems 388
By M.J.W. Prior
1 General Applications and New Methodology 388
1.1 Applications, Methodologies and Instrumentation 388
1.2 Spectral Editing 388
1.3 Localisation 389
1.4 Spectral Analysis 389
1.5 Data Analysis 390
1.6 Intracellular Ions 391
1.7 Cellular Metabolites 391
1.8 pH 392
2 Cells 392
2.1 Microorganisms 392
2.2 Blood 394
2.3 Cultured and Tumour Cells 394
2.4 Reproductive 396
3 Plants and Algae 397
3.1 Cells 397
3.2 Seeds and Fruits 397
3.3 Tissues 398
4 Animal Tissues 398
4.1 Brain 398
4.2 Eye 401

4.3 Heart 402
4.4 Liver 406
4.5 Muscle 408
4.6 Smooth Muscle 409
4.7 Tumour 409
4.8 Whole Animal 410
5 Clinical Studies 411
5.1 Brain 411
5.2 Heart 415
5.3 Liver 415
5.4 Muscle 416
5.5 Tumour 418
6 References 418

Chapter 13 Nuclear Magnetic Resonance Imaging 428
By T. Watanabe
1 Introduction 428
2 General Aspects and Reviews 429
3 Instruments 432
3.1 NMR Apparatus for Education 432
3.2 Receiver Coil and Flux Guide 432
3.3 Probe 433
4 Pulse Sequences and Data Processing 433
5 Solid State NMR Imaging 434
6 Other Nuclei 435
6.1 Hyperpolarized Noble Gases 435
6.1.1 Applications to Dynamics 435
6.1.2 Chemical Shift 436
6.1.3 Application to *In Vivo* Systems 436
6.2 Other Nuclei 436
6.2.1 Application to Materials and Plants 436
6.2.2 Application to *In Vivo* Systems 436
7 Diffusion, Flow and Velocity Imaging 439
7.1 Diffusion 439
7.2 Flow: Velocity, Rheometry 440
7.3 Mass Transport: Absorption, Dissolution, Swelling, Drying 441
7.3.1 Water Absorption, Transport Processes of Water 441
7.3.2 Drug Delivery 441
8 Porosity, Fluid Assisted Imaging 442
8.1 Porosity, Porosimetry, Structure 442
8.1.1 Porosimetry 442
8.1.2 Cork and Coal 443
8.2 Migration of Liquids in Porous Media 443
8.3 Packed Beds, Granual Media: Flow, Voidage 443
8.3.1 Velocity and Voidage 443
8.3.2 Resin Column 444
9 Polymers 444
9.1 Crosslinked Structures 444
9.2 Swelling, Diffusion, Hydrophilicity 446
9.3 Dosimetry 447

10 Plants: *In Vivo* 447
11 Food 449
12 *In Vivo* and *Ex Vivo* 449
12.1 *In Vivo* Applications 449
12.1.1 Sponges and Insects 449
12.1.2 Apparent Diffusion Coefficient (ADC) 450
12.1.3 Flow, CBV, Ischemic Tissue 451
12.1.4 Magnetic Resonance Spectroscopic Imaging (MRSI) 451
12.1.5 Therapy Effect 451
12.1.6 Pharmacological MRI and Neuropharmocolgical MRI 452
12.1.7 BOLD Effect, High Field 452
12.1.8 Gene Expression 453
12.1.9 Paramagnetic Effects: Endogenous 453
12.1.10 Paramagnetic Effect and Pharmacokinetics: Exogenous 454
12.1.11 Toxicity 455
12.2 *Ex Vivo* Experiments 455
12.2.1 Cartilage 455
12.3 Miscellaneous 456
13 Miscellaneous 457
14 References 457

Chapter 14 Oriented Molecules 464
By C.L. Khetrapal, G.A. Nagana Gowda and K.V. Ramanathan
1 Introduction 464
2 Reviews, Theory and General Studies 465
3 New Techniques and Emerging Areas 466
3.1 General 466
3.2 Quantum Computing 467
4 Dynamic NMR Studies 469
5 Smectic, Lyotropic, Polymeric and Chiral Systems 471
6 Weak Ordering and Biomolecular Structural Studies 473
6.1 New Methodologies and Protein Studies 474
6.2 Nucleic Acids, Oligosaccharides and their Complexes 481
7 Membranes and Molecules Oriented Therein 483
8 Relaxation Studies 484
9 Structure and Conformation of Small Molecules and Orientational Order 485
10 References 489

Symbols and Abbreviations

These lists contain the symbols and abbreviations most frequently used in this volume, but they are not expected to be exhaustive. Some specialized notation is only defined in the relevant chapter. An attempt has been made to standardize usage throughout the volume as far as is feasible, but it must be borne in mind that the original research literature certainly is not standardized in this way, and some difficulties may arise from this fact. Trivial use of subscripts *etc.* is not always mentioned in the symbols listed below. Some of the other symbols used in the text, *e.g.* for physical constants such as h or π, or for the thermodynamic quantities such as H or S, are not included in the list since they are considered to follow completely accepted usage.

Symbols

a_N	hyperfine (electron–nucleus) interaction constant
A	(i) hyperfine (electron–nucleus) interaction constant (ii) parameter relating to electric field effects on nuclear shielding
B	(i) magnetic induction field (magnetic flux density) (ii) parameter relating to electric field effects on nuclear shielding
B_0	static magnetic field of NMR or ESR spectrometer
B_1, B_2	r.f. magnetic fields associated with ν_1, ν_2
C_x	spin-rotation coupling constant of nucleus X (used sometimes in tensor form): $C^2 = {}^1/_3(C_\parallel^2 + 2C_\perp^2)$.
$C_\parallel, C_\perp$	components of C parallel and perpendicular to a molecular symmetry axis
D	(i) self-diffusion coefficient (ii) zero-field splitting constant
D	rotational diffusion tensor
$D_\parallel, D_\perp$	components of D parallel and perpendicular to a molecular symmetry axis
D_{int}	internal diffusion coefficient
D_0	overall isotropic diffusion coefficient
E	electric field
E_n	eigenvalue of $\hat{\mathscr{H}}$ (or a contribution to $\hat{\mathscr{H}}$)
g	nuclear or electronic g-factor
G	magnetic field gradient
H_{ij}	element of matrix representation of $\mathscr{H}$
$\mathscr{H}$	Hamiltonian operator–subscripts indicate its nature
I_i	nuclear spin operator for nucleus i
I_{ix}, I_{iy}, I_{iz}	components of I_i
I	(i) ionization potential (ii) moment of inertia
${}^nJ$	nuclear spin–spin coupling constant through n bonds (in Hz). Further information may be given by subscripts or in brackets. Brackets are used for indicating the species of nuclei coupled, *e.g.* $J({}^{13}C, {}^1H)$ or additionally, the coupling path, *e.g.* J(POCF)
J_r	reduced splitting observed in a double resonance experiment
J	rotational quantum number
${}^nK$	reduced nuclear spin–spin coupling constant (see the notes concerning ${}^nJ$)
m_i	eigenvalue of I_{iz} (magnetic component quantum number)
M_0	equilibrium macroscopic magnetization of a spin system in the presence of B_0
M_x, M_y, M_z	components of macroscopic magnetization

M_n	the number of average mol. wt.
P_A	valence p orbital of atom A
P_j	fractional population (or rotamers *etc.*)
P_{uv}	element of bond-order, charge-density matrix
q	electric field gradient
Q	(i) nuclear quadrupole moment (ii) quality factor for an r.f. coil
s_A	valence s-orbital of atom A
$S_A^2(0)$	electron density in S_A at nuclear A
S	(i) singlet state (ii) electron (or, occasionally, nuclear spin) *cf.* I (iii) ordering parameter for oriented systems (iv) overlap integral between molecular orbitals
t	elapsed time
T	(i) temperature (ii) triplet state
T_c	coalescence temperature for an NMR spectrum
T_g	the glass transition temperature (of a polymer)
T_1^X	spin–lattice relaxation time of the X nuclei (further subscripts refer to the relaxation mechanism)
T_2^X	spin–spin relaxation time of the X nucleus (further subscripts refer to the relaxation mechanism)
T'_2	inhomogeneity contribution to dephasing time for M_x or M_y
T^*_2	total dephasing time for M_x or M_y; $(T^*_2)^{-1} = T_2^{-1} + (T'_2)^{-1}$
T_3	decay time following 90_0–τ–90_{90} pulse sequences
$T_{1\rho}^X$, $T_{2\rho}^X$	spin–lattice and spin–spin relaxation time of the X nuclei in the frame of reference rotating with B_1
T_{1D}	dipolar spin–lattice relaxation time
X_i	mole fraction of compound
Z_A	atomic number of atom A
α	(i) nuclear spin wavefunction (eigenfunction of I_z) for a spin $-^1/_2$ nucleus (ii) polarizability
β	nuclear spin wavefunction (eigenfunction of I_z) for a spin $-^1/_2$ nucleus
γ_X	magnetogyric ratio of nucleus X
δ_X	chemical shift of a nucleus of element X (positive when the sample resonates to high frequency of the reference). Usually in p.p.m.
δ_{ij}	Kronecker delta ($=1$ if $i=j$, and $=0$ otherwise)
$\delta(r_{KA})$	Dirac delta operator
Δ	(i) time between field gradient pulses (ii) spectral width
ΔJ	anisotropy in J ($\Delta J = J_\parallel - J_\perp$, for axial symmetry)
Δn	population difference between nuclear states
$\Delta\delta$	change of difference in δ
$\Delta_{\nu^{1/2}}$	full width (in Hz) of a resonance line at half-height
$\Delta\sigma$	(i) anisotropy in σ($\Delta\sigma = \sigma_\parallel - \sigma_\perp$, for axial symmetry) (ii) differences in σ for two different situations
$\Delta\chi$	(i) susceptibility anisotropy ($\Delta_\chi = \chi_\parallel - \chi_\perp$, for axial symmetry (ii) differences in electronegativities
ε_r	relative permittivity
ε_0	permittivity of a vacuum
η	(i) nuclear Overhauser effect (ii) asymmetry factor (*e.g.* in e^2qQ/h) (iii) refractive index (iv) viscosity
μ	magnetic dipole moment
μ_0	permeability of a vacuum
μ_B	Bohr magneton
μ_N	nuclear magneton
ν_i	Larmor precession frequency of nucleus i (in Hz)
ν_0	(i) spectrometer operating frequency

ν_1	frequency of 'observing' r.f. magnetic field
ν_2	frequency of 'irradiating' r.f. magnetic field
σ_i	shielding parameter of nucleus i (used sometimes in tensor form). Usually in p.p.m. Subscripts may alternatively indicate contributions to σ.
$\sigma_{\parallel}, \sigma_{\perp}$	components of σ parallel and perpendicular to a molecular symmetry axis
σ^{d}	diagrammatic contribution to σ
σ^{p}	paramagnetic contribution to σ
τ	(i) pre-exchange lifetime of molecular species (ii) time between r.f. pulses (general symbol)
τ_c	correlation time
τ_{coll}	mean time between molecular collisions in the liquid state
τ_j	angular momentum correlation time
τ_p	pulse duration
τ_t	translational magnetic relaxation correlation time
χ	(i) magnetic susceptibility (ii) electronegativity (iii) nuclear quadrupole coupling constant ($= e^2qQ/h$)
ω	carrier frequency in rad s^{-1}
$\omega_i, \omega_0, \omega_1, \omega_2$	as for $\nu_i, \nu_0, \nu_1, \nu_2$ but in rad s^{-1}
ω_m	modulation angular frequency (in rad s^{-1})
ω_r	sample rotation (rad s^{-1})

Abbreviations

(a) *Physical properties*

a.f.	audiofrequency
a.u.	atomic unit
a.m.	amplitude modulation
b.c.c.	body-centred cubic
c.m.c.	critical micelle concentration
e.d.	electron diffraction
e.f.g.	electric field gradient
f.c.c.	face-centred cubic
f.m.	frequency modulation
h.c.p.	hexagonal close-packed
h.f.	hyperfine
i.d.	inside diameter
i.f.	intermediate frequency
l.c.	liquid crystalline
mol. wt.	molecular weight
o.d.	outside diameter
p.p.m.	parts per million
r.f.	radiofrequency
r.m.s.	root mean square
s.h.f.	super-high frequency
u.h.f.	ultra-high frequency
ADC	analogue-to-digital converter
AEE	average excitation energy approximation
AQ	acquire
ARP	adiabatic rapid passage
BIRD	bilinear rotation decoupling
CCPPA	coupled cluster polarization propagator approximation
CH-COSY	carbon-hydrogen correlation spectroscopy
CHESS	chemical shift selection
CHF	coupled Hartree–Fock molecular orbital calculations
CIDEP	chemically induced dynamic electron polarization

CIDNP	chemically induced dynamic nuclear polarization
COSY	correlation spectroscopy
CP	cross polarization
CPMG	Carr–Purcell pulse sequence. Meiboom–Gill modification
CSA	chemical shielding anisotropy
CSI	chemical shift imaging
CW	continuous wave
DAC	digital-to-analogue converter
DD	dipole-dipole (interaction or relaxation mechanism)
DEPT	distortionless enhancement by polarization transfer
DLB	differential line broadening
DNP	dynamic nuclear polarization
DQ	double quantum
DQF	double quantum filter
ECOSY	exclusive correlation spectroscopy
EHT	extended Hückel molecular orbital theory
ENDOR	electron–nucleus double resonance
EOM	equations of motion
ESR	electron spin resonance
EXSY	exchange spectroscopy
FC	Fermi contact
FID	free induction decay
FLASH	fast low angle shot
FPT	finite perturbation theory
FT	Fourier transform
GIAO	gauge included atomic orbitals
HMQ	heteronuclear multiquantum
HOHAHA	homonuclear Hartman–Hahn
HRPA	higher random phased approximation
IDESS	improved depth selective single surface coil spectroscopy
IGLO	individual gauge for different localized orbitals
INADEQUATE	incredible natural abundance double quantum transfer experiment
INDO	intermediate neglect of differential overlap
INDO/S	intermediate neglect of differential overlap calculations for spectroscopy
INDOR	internuclear double resonance
INEPT	insensitive nuclei enhanced by polarization transfer
IR	infrared
ISIS	image selected *in vivo* spectroscopy
LIS	lanthanide induced shift
LORG	local origin
LSR	lanthanide shift reagent
MASS	magic angle sample spinning
MBPT	many body perturbation theory
MEM	maximum entropy method
MINDO	modified INDO
MQ	multiple quantum
MQC	multiple quantum coherence
MQF	multiple quantum filter
NMR	nuclear magnetic resonance
NOE	nuclear Overhauser enhancement
NOESY	nuclear Overhauser enhancement spectroscopy
NQCC	nuclear quadrupole coupling constant
NQR	nuclear quadrupole resonance
PFG	pulsed field gradient
PRE	proton relaxation enhancement
QF	quadrupole moment/field gradient
QPD	quadrature phase detection
REX	relativistically extended Hückel molecular orbital theory
ROESY	rotating frame Overhauser enhancement spectroscopy
RPA	random phase approximation

SCPT	self consistent perturbation theory
SD	spin dipolar
SECSY	spin echo correlation spectroscopy
SEFT	spin echo Fourier transform
SLITDRESS	slice interleaved depth resolved surface coil spectroscopy
SOPPA	second order polarization propagator approach
SPI	selective population inversion
SPT	selective population transfer
SR	spin rotation (interaction or relaxation mechanism)
TART	tip angle reduced T_1 imaging
TOCSY	total correlation spectroscopy
UV	ultraviolet
WAHUHA	Waugh, Huber and Häberlen (cycle of pulses)
ZQ	zero quantum
ZQC	zero quantum coherence

(b) *Chemical species**

acac	acetylacetonato
ACTH	adrenocorticotropic hormone (corticotropin)
ADP	adenosine diphosphate
AMP	adenosine monophosphate
ATP	adenosine triphosphate
BSA	bovine serum albumin
CMP	cytidine monophosphate
cp	cyclopentadienyl
DAP	dodecylammonium propionate
DME	1,2-dimethoxyethane
DMF	dimethylformamide
DML	dimyristoyl-lecithin
DMS	dimethylsiloxane
DMSO	dimethyl sulfoxide
DNA	deoxyribonucleic acid
DPG	2,3-diphosphoglycerate
DPI	dipalmitoyl-lecithin
dpm	dipivaloylmethanato
DPPH	diphenylpicrylhydrazyl
DSS	2,2-dimethyl-2-silapentane-5-sulfonate (usually as the sodium salt)
DTBN	di-t-butyl nitroxide
EBBA	*N*-(*p*-ethoxybenzylidene)-*p*-butylaniline
EDTA	ethylenediaminetetra-acetic acid
EVA	ethylene-vinyl acetate
fod	1,1,1,2,2,3,3-heptafluoro-7,7-dimethyloctane-4,6-dionato
HAB	4,4′-bis(heptyl)azoxybenzene
HMPA	hexamethylphosphoramide
HOAB	*p*-n-heptyloxyazoxybenzene
IHP	inositolhexaphosphate
KDP	potassium dihydrogen phosphate
MBBA	*N*-(*p*-methoxybenzylidene)-*p*-butylaniline
NADH(P)	nicotinamide adenine dinucleotide (phosphate)
NMF	*N*-methylformamide
PAA	*p*-azoxyanisole
PBA	pyrene butyric acid
PBLG	poly(L-benzyl μ-glutamate)
PC	phosphatidyl choline (lecithin)
PCB	polychlorinated biphenyl
PDMS	polydimethylsiloxane
PMA	poly(methacrylic acid)
PMMA	poly(methyl methacrylate)
POM	poly(oxymethylene)
PS	phosphatidylserine

* Lower case initials are used when the species is a ligand.

PTFE	polytetrafluoroethylene
PVC	poly(vinyl chloride)
PVF	poly(vinyl fluoride)
PVP	poly(vinyl pyrrolidone)
RNA	ribonucleic acid (tRNA, transfer RNA)
SDS	sodium dodecyl sulfate
TAB	trimethylammonium bromide
TCNQ	tetracyanoquinodimethane
TFA	trifluoroacetic acid
THF	tetrahydrofuran
TMS	tetramethylsilane
UTP	uridine triphosphate

Amino-acid residues

Ala	alanine	Leu	leucine
Arg	arginine	Lys	lysine
Asn	asparagine	Met	methionine
Asp	aspartic acid	Phe	phenylalanine
Cys	cysteine	Pro	proline
Gln	glutamine	Ser	serine
Glu	glutamic acid	Thr	threonin
Gly	glycine	Trp	tryptophan
His	histidine	Tyr	tyrosine
Hyp	hydroxyproline	Val	valine
Ile	isoleucine		

1
NMR Books and Reviews

BY W. SCHILF

1 Books

R1 E. D. Backer, *High Resolution NMR: Theory and Chemical Applications, Third Edition*, Academic, San Diego, CA., 1999

R2 J. P. Hornak, *The Basics of NMR*, ed. J. P. Hornak, Rochester, N.Y., 1997, Available URL:http://www.cis.rit.edu/htbooks/nmr/

2 Regular Reviews Series

Accounts of Chemical Research vol. 33, 2000

R3 A. Badia, R. B. Lennox and L. Reven, 'A Dynamic View of Self-Assembled Monolayers', p. 475

R4 F. A. Cotton and D. G. Nocera, 'The Whole Story of the Two-Electron Bond, with the δ Bond as a Paradigm', p. 483

R5 A. Bagno and G. Scorrano, 'Selectivity in Proton Transfer, Hydrogen Bonding, and Solvation', p. 609

vol. 34, 2001

R6 H. W. Roesky, M. G. Walawalkar and R. Murugavel, 'Is Water a Friend or Foe in Organometallic Chemistry? The Case of Group 13 Organometallic Compounds', p. 201

R7 V. J. Hruby, 'Design in Topographical Space of Peptide and Peptidomimetic Ligands that Affect Behavior. A Chemist's Glimpse at the Mind-Body Problem', p. 389

Annual Reports on NMR Spectroscopy, ed. G. A. Webb, Academic Press Ltd., London vol. 41, 2000

R8 J. C. C. Chan and S. C. F. Au-Yeung, 'Cobalt-59 NMR Spectroscopy', p. 1

R9 R. H. Contreras, J. E. Peralta, C. G. Giribet, M. C. Ruiz De Azua and J. C. Facelli, 'Advances in Theoretical and Physical Aspects of Spin-Spin Coupling Constants', p. 55

R10 S. Dusold and A. Sebald, 'Dipolar Recoupling under Magic-Angle-Spinning Conditions', p. 185

Nuclear Magnetic Resonance, Volume 31
© The Royal Society of Chemistry, 2002

R11 P. J. Barrie, 'Characterization of Porous Media Using NMR Methods', p. 265
vol. 42, 2000
R12 A. Lycka, 'Multinuclear NMR of Azo Dyes and their Metal Complexes', p. 1
R13 C. Ye, S. Ding and C. A. Mcdowell, 'Recent Progress in Solid-State NMR', p. 59
R14 D. J. Craik and M. J. Scanlon, 'Pharmaceutical Applications of NMR', p. 115
vol. 43, 2001
R15 M. J. Duer, 'Solid-State NMR Studies of Molecular Motion', p. 1
R16 J. Higinbotham and I. Marshall, 'NMR Lineshapes and Lineshape Fitting Procedures', p. 59
R17 M. E. Smith, 'Recent Progress in Solid-State NMR of Low-γ Nuclei', p. 121

Annual Reports on the Progress of Chemistry, Section B: Organic Chemistry, Royal Society of Chemistry, vol. 96, 2000
R18 C. Halkides and C. K. McClure, 'NMR Spectroscopic Methods' p. 497

Annual Reports on the Progress of Chemistry, Section C: Physical Chemistry, Royal Society of Chemistry, vol. 96, 2000
R19 W. S. Price, 'NMR Gradient Methods in the Study of Proteins', p. 3

Annual Review of Biochemistry vol. 69, 2000
R20 P. E. Dawson and S. B. H. Kent, 'Synthesis of Native Proteins by Chemical Ligation', p. 923

Annual Review of Biophysics and Biomolecular Structure, vol. 29, 2000
R21 W. A. Eaton, V. Munoz, S. J. Hagen, G. S. Jas, L. J. Lapidus, E. R. Henry and J. Hofrichter, 'Fast Kinetics and Mechanisms in Protein Folding', p. 327

Annual Review on Physical Chemistry, vol. 51, 2000
R22 S. Mukamel, 'Multidimensional Femtosecond Correlation Spectroscopies of Electronic and Vibrational Excitations', p. 691

Biological Magnetic Resonance, vol. 15
In Vivo Carbon-13 NMR, ed. L. J. Berliner and P.-M. Robitaille, Kluwer Academic/Plenum Publ., New York, N.Y., 1998
R23 M. R. Laughlin and J. K. Kelleher, 'Tracer Theory and ^{13}C NMR', p. 1
R24 E. D. Lewandowski, 'Metabolic Flux and Subcellular Transport of Metabolites', p. 117
R25 R. G. Weiss and G. Gerstenblith, 'Assessing Cardiac Metabolic Rates During Pathologic Conditions with Dynamic ^{13}C NMR Spectra', p. 161

R26 G. F. Mason, 'Applications of ^{13}C Labeling to Studies of Human Brain Metabolism in Vivo', p. 181

R27 P.-M. L. Robitaille, 'In Vivo ^{13}C NMR Spectroscopy: A Unique Approach in the Dynamic Analysis of Tricarboxylic Acid Cycle Flux and Substrate Selection', p. 215

vol. 16

Modern Techniques in Protein NMR, ed. N. R. Krishna and L. J. Berliner, Kluwer Academic/Plenum Publ., New York, N.Y., 1998

R28 G. M. Clore and A. M. Gronenborn, 'Determining Structures of Large Proteins and Protein Complexes by NMR', p. 3

R29 K. H. Gardner and L. E. Kay, 'Multidimensional ^{2}H-Based NMR Methods for Resonance Assignment, Structure Determination, and the Study of Protein Dynamics', p. 27

R30 B. T. Farmer II and R. A. Venters, 'NMR of Perdeuterated Large Proteins', p. 75

R31 F. M. Marassi, J. J. Gesell and S. J. Opella, 'Recent Developments in Multidimensional NMR Methods for Structural Studies of Membrane Proteins', p. 121

R32 E. Kupce, H. Matsuo and G. Wagner, 'Homonuclear Decoupling in Proteins', p. 149

R33 G. W. Vuister, M. Tessari, Y. Karimi-Nejad and B. Whitehead, 'Pulse Sequences for Measuring Coupling Constants', p. 195

R34 C. Griesinger, M. Hennig, J. P. Marino, B. Reif, C. Richter and H. Schwalbe, 'Methods for the Determination of Torsion Angle Restraints in Biomacromolecules', p. 259

vol. 17

Structure Computation and Dynamics in Protein NMR, ed. N. R. Krishna and L. J. Berliner, Kluwer Academic/Plenum Publishers, 1999

R35 Y. Xu, C. H. Schein and W. Braun, 'Combined Automated Assignment of NMR Spectra and Calculation of Three-Dimensional Protein Structures', p. 37

R36 G. T. Montelione, C. B. Rios, G. V. T. Swapna and D. E. Zimmerman, 'NMR Pulse Sequences and Computational Approaches for Automated Analysis of Sequence-Specific Backbone Resonance Assignments of Proteins', p. 81

R37 S. I. O'Donoghue and M. Nilges, 'Calculation of Symmetric Oligomer Structures from NMR Data', p. 131

R38 A. Mujeeb, N. B. Ulyanov, T. M. Billeci, S. Farr-Jones and T. L. James, 'Conformational Ensemble Calculations: Analysis of Protein and Nucleic Acid NMR Data', p. 201

R39 J. Engelke and H. Ruterjans, 'Recent Developments in Studying the Dynamics of Protein Structures from ^{15}N and ^{13}C Relaxation Time Measurements', p. 357

R40 B. Halle, V. P. Denisov and K. Venu, 'Multinuclear Relaxation Dispersion Studies of Protein Hydration', p. 419

Carbohydrate Chemistry, Royal Society of Chemistry, vol. 31, 2000
R41 Anonymous (U.K.), 'NMR Spectroscopy and Conformational Features', p. 312
R42 Anonymous (U.K.), 'Other Physical Methods', p. 322
vol. 32, 2001
R43 Anonymous (U.K.), 'NMR Spectroscopy and Conformational Features', p. 312
R44 Anonymous (U.K.), 'Separatory and Analytical Methods', p. 342

Chemical Reviews, vol. 100, 2000
R45 J. O. Duus, C. H. Gotfredsen and K. Bock, 'Carbohydrate Structural Determination by NMR Spectroscopy: Modern Methods and Limitations', p. 4589
vol. 101, 2001
R46 R. H. Mitchell, 'Measuring Aromaticity by NMR', p. 1301

Coordination Chemistry Reviews, vol. 206–207, 2000
R47 D. S. Frohnapfel and J. L. Templeton, 'Transition Metal η^2-Vinyl Complexes', p. 199
R48 A. Bianchi, L. Calabi, F. Corana, S. Fontana, P. Losi, A. Maiocchi, L. Paleari and B. Valtancoli, 'Thermodynamic and Structural Properties of Gd(III) Complexes with Polyamino-Polycarboxylic Ligands: Basic Compounds for the Development of MRI Contrast Agents', p. 309
vol. 208, 2000
R49 H. Yersin and J. Strasser, 'Triplets in Metal-Organic Compounds. Chemical Tunability of Relaxation Dynamics', p. 331
vol. 209, 2000
R50 A. K. Singh and S. Sharma, 'Recent Developments in the Ligand Chemistry of Tellurium', p. 49
vol. 210, 2000
R51 A. Sekiguchi, V. Y. Lee and M. Nanjo, 'Lithiosilanes and their Application to the Synthesis of Polysilane Dendrimers', p. 11
R52 K. K. Lalli, 'Nitro and Nitroso Transformations in Superacids', p. 47
vol. 212, 2001
R53 T. W. Hambley and A. R. Jones, 'Molecular Mechanics Modeling of Pt/Nucleotide and Pt/DNA Interactions', p. 35

Current Drug Metabolism, vol. 1, 2000
R54 R. Martino, M. Malet-Martino and V. Gilard, 'Fluorine Nuclear Magnetic Resonance, a Privileged Tool for Metabolic Studies of Fluoropyrimidine Drugs', p. 271

Current Issues in Molecular Biology, vol. 2, 2000
R55 M. Auger, 'Biological Membrane Structure by Solid-State NMR', p. 119

Current Medical Chemistry, vol. 8, 2001

R56 X. Han and X. Gao, 'Sequence Specific Recognition of Ligand-DNA Complexes Studied by NMR', p. 551

Current Opinion on Biotechnology, vol. 11, 2000

R57 H. Weber and L. Brecker, 'Online NMR for Monitoring Biocatalysed Reactions', p. 572

Current Opinion on Chemistry and Biology, vol. 4, 2000

R58 R. Tycko, 'Solid-State NMR as a Probe of Amyloid Fibril Structure', p. 500

Current Opinion in Clinical Nutrition & Metabolic Care, vol. 2, 1999

R59 J.-L. Sebedio, S. Gnaedig and J.-M. Chardigny, 'Recent Advances in Conjugated Linoleic Acid Research', p. 499

Current Opinion in Colloid & Interface Science, vol. 5, 2000

R60 M. M. Robins, 'Emulsions. Creaming Phenomena', p. 265

Current Opinion in Drug Discovery & Development, vol. 3, 2000

R61 B. J. Stockman, 'Flow NMR Spectroscopy in Drug Discovery', p. 269

R62 A. Williams, 'Recent Advances in NMR Prediction and Automated Structure Elucidation Software', p. 298

R63 O. Brummer, B. Clapham and K. D. Janda, 'Recent Developments and Applications of Polymer-Supported Reagents in Synthetic Organic Chemistry', p. 462

Current Opinion on Plant Biology, vol. 3, 2000

R64 C. Giersch, 'Mathematical Modeling of Metabolism', p. 249

Current Opinion on Structural Biology, vol. 10, 2000

R65 D. A. Case, 'Interpretation of Chemical Shifts and Coupling Constants in Macromolecules', p. 197

R66 E. T. Mollova and A. Pardi, 'NMR Solution Structure Determination of RNAs', p. 298

R67 N. K. Goto and L. E. Kay, 'New Developments in Isotope Labeling Strategies for Protein Solution NMR Spectroscopy', p. 585

R68 H. J. M. De Groot, 'Solid-State NMR Spectroscopy Applied to Membrane Proteins', p. 593

vol. 11, 2001

R69 C. E. Bell and M. Lewis, 'The Lac Repressor: A Second Generation of Structural and Functional Studies', p. 19

R70 J.-M. Perez-Canadillas and G. Varani, 'Recent Advances in RNA-Protein Recognition', p. 53

Current Organic Chemistry, vol. 4, 2000

R71 H. U. Shetty and W. Huang, 'Measurement of Myo-Inositol in

Biological Systems by Mass Spectrometric and in Vivo ^{1}H Magnetic Resonance Spectroscopic Techniques', p. 1

R72 W.-C. Haase and P. H. Seeberger, 'Recent Progress in Polymer-Supported Synthesis of Oligosaccharides and Carbohydrate Libraries', p. 481

R73 S. Grivas, '2,1,3–Benzoselenadiazoles as Valuable Synthetic Intermediates', p. 707

vol. 5, 2001

R74 R. Araya-Maturana, T. Delgado-Castro, W. Cardona and B. E. Weiss-Lopez, 'Use of Long-Range C-H (^{n}J n>3) Heteronuclear Multiple Bond Connectivity in the Assignment of ^{13}C NMR Spectra of Complex Organic Molecules', p. 253

R75 T. Dziembowska and Z. Rozwadowski, 'Application of the Deuterium Isotope Effect on NMR Chemical Shift to Study Proton Transfer Equilibrium', p. 289

R76 N. P. Sahu and B. Achari, 'Advances in Structural Determination of Saponins and Terpenoid Glycosides', p. 315

R77 M. Liu and J. C. Lindon, 'Recent Advances in Editing and Selective Detection Methods for ^{1}H NMR Spectroscopy', p. 351

Current Protein and Peptide Science, vol. 1, 2000

R78 T. Fukumizo, 'Chitinolytic Enzymes: Catalysis, Substrate Binding, and their Application', p. 105

R79 B. Asboth and G. Naray-Szabo, 'Mechanism of Action of D-Xylose Isomerase', p. 237

NATO Advanced Study Institute Series, Series A, vol. 301, 1998

R80 A. M. Gronenborn and G. M. Clore, 'Determining Structures of Protein/DNA Complexes by NMR', p. 1

R81 O. Jardetzky, 'What Can NMR Tell US About Protein Motions?', p. 103

R82 R. A. Atkinson and J.-F. Lefevre, 'The Investigation of Protein Dynamics via the Spectral Density Function', p. 129

R83 L. Spyracopoulos, S. M. Gagne, W. Gronwald, L. E. Kay and B. D. Sykes, 'NMR Studies of Protein Sidechain Dynamics: Examples from Antifreeze and Calcium-Regulatory Proteins', p. 147

R84 S. Yoshizawa and J. D. Puglisi, 'NMR Structure Determination of an Antibiotic-RNA Complex', p. 173

vol. 305, 1999

R85 B. Halle, 'Magnetic Relaxation Dispersion: Principles and Applications', p. 221

R86 B. Halle, 'Water in Biological Systems: The NMR Picture', p. 233

R87 D. J. Tobias, 'Water and Membranes: Molecular Details from MD Simulations', p. 293

R88 J. Parello, 'Workshop on NMR and Hydration of Biomacromolecules in Aqueous Solutions', p. 379

vol. 313, 2000

R89 J. Timbrell, 'Biomarkers of Organ Toxicity', p. 189
Series C, vol. 538, 1999

R90 P. Sozzani, A. Comotti and R. Simonutti, 'NMR and Crystallinity of Nanostructured Materials', p. 443
vol. 546, 2000

R91 I. Bertini, J. Faraone-Mennella, C. Luchinat and A. Rosato, 'The Use of the Electron-Nucleus Hyperfine Interaction for Solution Structure Determination', p. 1
vol. 560, 2000

R92 E. G. Derouane, S. B. Derouane-Abd Hamid, I. I. Ivanova, H. He and J. C. Vedrine, 'In Situ Investigations of Catalysts and Catalytic Reaction Mechanisms, Part 1. General Introduction and Applications of in Situ MAS NMR Spectroscopy', p. 99
Series II, vol. 2, 2000

R93 J. A. Weil, 'A Demi-Century of Magnetic Defects in α-Quartz', p. 197
Series 2, vol. 55, 1999

R94 I. Ahlers, 'Metabolic and Hormonal Changes in Irradiated Animals', p. 389
Series 3, vol. 70, 1999

R95 E. C. Thiel, Y. Ke, Z. Gdaniec and H. Sierzputowska-Gracz, 'The IRE Model for Families of RNA Structures: Selective Recognition by Binding Proteins (IRPs), NMR Spectroscopy and Probing with Metal Coordination Complexes', p. 241
vol. 74, 2000

R96 P. W. Kuchel and P. J. Mulquiney, 'Combined NMR Experimental and Computer Simulation Study of 2,3–Bisphosphoglycerate Metabolism in Human Erythrocytes', p. 139

R97 K. M. Brindle and P. M. Haggie, 'Probing the Cell Interior with NMR Spectroscopy', p. 191

Progress in Nuclear Magnetic Resonance Spectroscopy, ed. J. W. Emsley, J. Feeney and L. H. Sutcliffe, vol. 36, 2000

R98 D. Grucker, 'Oxymetry by Magnetic Resonance: Applications to Animal Biology and Medicine', p. 241

R99 A. L. Breeze, 'Isotope-Filtered NMR Methods for the Study of Biomolecular Structure and Interactions', p. 323
vol. 37, 2000

R100 F. C. Oliveira, M. J. P. Ferreira, C. V. Nunez, G. V. Rodriguez and V. P. Emerenciano, '^{13}C NMR Spectroscopy of Eudesmane Sesquiterpenes', p. 1

R101 L. Ernst, 'NMR Studies of Cyclophanes', p. 47

R102 J. J. van der Klink and H. B. Brom, 'NMR in Metals, Metal Particles and Metal Cluster Compounds', p. 89

R103 A. Kumar, R. G. R. Christy and P. K. Madhu, 'Cross-Correlation in NMR', p. 191

R104 P. Hodgkinson and L. Emsley, 'Numerical Simulation of Solid-State NMR Experiments', p. 201
R105 J. C. Martins, M. Biesemans and R. Willem, 'Tin NMR Based Methodologies and their Use in Structural Tin Chemistry', p. 271
R106 R. H. Contreras and J. E. Peralta, 'Angular Dependence of Spin-Spin Coupling Constants', p. 321
vol. 38, 2001
R107 N. Nestle, A. Schaff and W. S. Veeman, 'Mechanically Detected NMR, an Evaluation of the Applicability for Chemical Investigations', p. 1
R108 E. C. Reynhardt and G. L. High, 'Nuclear Magnetic Resonance Studies of Diamond', p. 37
R109 N. Jamin and F. Toma, 'NMR Studis of Protein-DNA Interactions', p. 83
R110 R. Sharp, L. Lohr and J. Miller, 'Paramagnetic NMR Relaxation Enhancement. Recent Advances in Theory', p. 115
R111 V. A. Mandelshtam, 'FDM. The Filter Diagonalization Method for Data Processing in NMR Experiments', p. 159
R112 D. M. Korzhnev, M. Billeter, A. S. Arseniev and V. Y. Orekhov, 'NMR Studies of Brownian Tumbling and Internal Motions in Proteins', p. 197
R113 M. Pons and O. Millet, 'Dynamic NMR Studies of Supramolecular Complexes', p. 267
R114 J. A. Jones, 'NMR Quantum Computation', p. 325

Spectroscopic Properties of Inorganic and Organometallic Compounds, ed. G. Davidson, Royal Society of Chemistry, vol. 33, 2000
R115 B. E. Mann, 'Nuclear Magnetic Resonance Spectroscopy', p. 1
R116 K. B. Dillon, 'Nuclear Quadrupole Resonance Spectroscopy', p. 192

3 Edited Books and Symposia

ACS Symposia Series vol. 729, 2000
R117 A. C. Dagger and J. A. Semlyen, 'Hydrogenated and Deuterated Cyclic Poly(dimethylsiloxanes)', p. 38
vol. 758, 2000
R118 G. D. Manners, S. Hasegawa, R. D. Bennett and R. Y. Wong, 'LC-MS and NMR Techniques for the Analysis and Characterization if Citrus Limonoids', p. 40
vol. 760, 2000
R119 W. P. Weber, J. K. Paulasaari, D. Huang, S. Gupta, T. M. Londergan, J. R. Sargent and J. M. Mabry, 'New Applications of "Carbonylbis(-triphenylphosphine)ruthenium" Catalysis in Polymer Synthesis', p. 24
R120 C.-H. Jun, H. Lee, J.-B. Hong and D.-Y. Lee, 'Modification of Polybutadiene by Transition Metal Catalysts: Hydroacylation of Polybutadiene', p. 94
vol. 764, 2000

R121 X. Chen, Y. Shen and R. A. Gross, 'High-Molecular-Weight [L]-Polylactides Containing Pendant Functional Groups', p. 129
vol. 765, 2000

R122 T. E. Hogen-Esch, H. Zhang and D. Xie, 'Synthesis and Characterization of Well Defined End-Functionalized Hydrocarbon and Perfluorocarbon Derivatives of Polyethyleneoxide and Poly(N,N-Dimethylacrylamide)', p. 179
vol. 774, 2001

R123 B. C. Hamper, T. J. Owen, K. D. Jerome, A. S. Scates, S. A. Kolodziej, R. C. Chott and A. S. Kesselring, 'Preparation of Small Molecule Libraries for Agrochemical Discovery. Development of Parallel Solution and Solid Phase Synthesis Methods', p. 180
vol. 775, 2001

R124 R. E. Wrolstad, M. M. Giusti, L. E. Rodriguez-Saona and R. W. Durst, 'Anthocyanins from Radishes and Red-Flashed Potatoes', p. 66
vol. 777, 2001

R125 M. J. Schocken, 'In Vitro Methods in Metabolism and Environmental Fate Studies', p. 30

Adsorption Science and Technology, Proceedings of the Second Pacific Basin Conference, ed. D. D. Do, World Scientific Publishing Co. Pte. Ltd, Singapore, 2000

R126 B. M. Odintsov, R. L. Belford, R. B. Clarkson, V. D. Skirda, A. N. Temnikov and R. S. Vartapetian, 'Characterization of Porous Materials by Means of Advanced Magnetic Resonance Techniques', p. 466

Advances in Superconductivity XII, Proceedings of 12th International Symposium on Superconductivity (ISS'99), ed. T. Yamashita and T. Keiishi, Springer-Verlag Tokyo, Japan, 2000

R127 J. L. Tallon, 'Antiferromagnetic Correlations and the Pseudogap in HTS Cuprates', p. 185

Aminophosphonic and Aminophosphinic Acids, ed. V. P. Kukhar and H. R. Hudson, John Wiley & Sons Ltd, Chichester, U.K., 2000

R128 G. Hagele, 'Physical Properties and NMR-Spectroscopic Characterization of Aminophosphonates and Aminophosphinates', p. 217

Bioorganic Chemistry, ed. U. Diederichsen, Wiley-VCH Verlag GmbH, Weinheim, Germany, 1999

R129 P. Jeschke, W. Etzel, A. Harder, M. Schindler, A. Gohrt, U. Pleiss, H. Kleikauf, R. Zocher, G. Thielking, W. Gau and G. Bonse, 'Cyclodepsipeptides: From Natural Product to Anthelmintically Active Synthetic Enniatins', p. 207

R130 M. Kock and J. Junker, 'Marine Natural Products: New Ways in the Constitutional Assignment', p. 365

R131 T. Weimar, 'NMR Techniques for the Investigation of Carbohydrate-Protein Interactions', p. 396
R132 H.-C. Siebert, 'Carbohydrate-Protein Interaction Studies by Various NMR Methods and Computational Calculations', p. 418

Carbohydrates in Chemistry and Biology, vol. 2, ed. B. Ernst, G. W. Hart and P. Sinay, Wiley-VCH Verlag GmbH, Weinheim, Germany, 2000
R133 S. W. Homans, 'Conformational Analysis in Solution by NMR', p. 947
R134 J. F. G. Vliegenthart and H.-C. Siebert, 'Carbohydrate-Protein Interactions: Use of the Laser Photo Chemically Induced Dynamic Nuclear Polarization (CIDNP) - NMR Technique', p. 1025

Characterization of Nanophase Materials, ed. Z.-L. Wang, Wiley-VCH Verlag GmbH, Weinheim, Germany, 2000
R135 L.-Q. Wang, G. J. Exarhos and J. Liu, 'Nuclear Magnetic Resonance. Characterization of Self-Assembled Nanostructural Materials', p. 243

Comprehensive Natural Products Chemistry, Volume 6: Prebiotic Chemistry, Molecular Fossils, Nucleosides and RNA, ed. D. Soell, S. Nashimura and P. B. Moore, Elsevier Science B. V., Amsterdam, Netherlands, 1999
R136 P. B. Moore, 'A Spectroscopist's View of RNA Conformation: RNA Structural Motifs', p. 3

Comprehensive Natural Products Chemistry, Volume 7: DNA and Aspects of Molecular Biology, ed. E. T. Kool, Elsevier Science B. V., Amsterdam, Netherlands, 1999
R137 C. De Los Santos, 'Probing DNA Structure by NMR Spectroscopy', p. 55

Current Advances in Mycorrhizae Research, ed. G. K. Podila and D. D. Douds Jr., American Phytopathological Society, St.Paul, Minn, 2000
R138 B. Bago, Y. Shachar-Hill and P. E. Pfeffer, 'Dissecting Carbon Pathways in Arbuscular Mycorrhizas with NMR Spectroscopy', p. 111

Cyclic Polymers, Second Edition, ed. J. A. Semlyen, Kluwer Academic Publishers, Dordrecht, Netherlands, 2000
R139 P. C. Griffiths, 'Neutron Scattering and Nuclear Magnetic Resonance Investigations of Cyclic Polymers', p. 385

Enzyme Chemistry, (3rd Ed.), ed. C. J. Suckling, C. L. Gibson and A. R. Pitt, Blackie Academic & Professional, London, U.K., 1998
R140 T. J. Wess, 'Enzyme Structure', p. 51

Fission and Properties of Neutron-Rich Nuclei, Proceedings of the Second International Conference, St.Andrews, Scotland, 1999, ed. J. H. Hamilton, W. R. Phillips and H. K. Carter, World Scientific Publishing Co. Pte. Ltd., Singapore, 2000

R141 N. J. Stone, 'Recent on-Line NMR/on Nuclar Magnetic Dipole Moments Near ^{132}Sn: Meson Exchange Current Effects at the Shell Closure and Shell Model Treatment of Variation with Proton and Neutron Number', p. 166

Flavor Chemistry, 30 Years of Progress, Proceedings of American Chemical Society Symposium, 1998, ed. R. Teranishi, E. L. Wick and I. Hornstein, Kluwer Academic/Plenum Publishers, New York, N.Y., 1999

R142 H.-L. Schmidt, D. Weber, A. Rossmann and R. A. Werner, 'The Potential of Intermolecular and Intramolecular Isotopic Correlations for Authenticity Control', p. 55

Fluoropolymers, vol. 2, ed. G. Hougham, Kluwer Academic/Plenum Publishers, New York, N.Y., 1999

R143 T. Davidson, R. N. Gounder, D. K. Weber and S. M. Wecker, 'A Perspective on Solid State Microstructure in Polytetrafluoroethylene', p. 3

R144 S. Ando, T. Matsuura and S. Sasaki, 'Synthesis and Properties of Perfluorinated Polyimides', p. 277

Hydrocolloids, vol. 1, 1998, ed. K. Nishinari, Elsevier Science B. V., Amsterdam, Netherlands, 2000

R145 W. Cui and P. J. Wood, 'Relationships Between Structural Features, Molecular Weight and Rheological Properties of Cereal β-D-Glucans', p. 159

International Contributions to: Wood Adhesion Research, [Proceedings of Forest Products Society Annual Meeting, 1998], ed. A. W. Christiansen and L. A. Pilato, Forest Products Society, Madison, Wis., 1999

R146 A. Pizzi, 'Phenolic and Tannin Adhesives for Panel Products', p. 13

Lipid Bilayers. Structure and Interactions, ed. J. Katsaras and T. Gutberlet, Springer-Verlag, Berlin, Germany, 2001

R147 R. S. Prosser and C. R. Sanders II, 'Solid State NMR Approaches to the Study of Membrane Proteins in Magnetically Aligned Model Membranes', p. 207

Liquid Crystals, ed. S. Kumar, Cambridge University Press, Cambridge, U.K., 2001

R148 P. Ukleja and D. Finotello, 'NMR Studies of Orientational Order', p. 155

Macromolecular Systems: Microscopic Interaction and Macroscopic Properties, ed. H. Hoffmann, M. Schwoerer and T. Vogtmann, Wiley-VCH Verlag GmbH, Weinheim, Germany, 2000

R149 S. Limmer, G. Ott and M. Sprinzl, 'Site-Directed Spectroscopy and Site-Directed Chemistry of Biopolymers', p. 369

Metal Clusters in Chemistry, ed. P. Braunstein, L. A. Oro and P. R. Raithby, Wiley-VCH Verlag GmbH, Weinheim, Germany, 1999

R150 B. T. Heaton, J. A. Iggo, I. S. Podkorytov, D. J. Smawfield and S. P. Tunik, 'Multinuclear NMR Studies on Homo- and Heterometallic Rhodium Clusters Containing 6 or More Metal Atoms', p. 960

Metallothionein IV, [The Proceedings of the Fourth International Meeting (MT-97)], ed. C. D. Klaassen, Birkhaeuser Verlag, Basel, Switzerland, 1999

R151 G. Oz, D. L. Pountney and I. M. Armitage, 'Metallothionein Structure Update', p. 37

Methods in Plant Electron Microscopy and Cytochemistry, ed. W. V. Dashek, Humana Press Inc., Totowa, N. J., 2000

R152 W. V. Dashek, 'Methods for he Detergent Release of Particle-Bound Plant Proteins', p. 169

Microbial Sediments, ed. R. E. Riding and S. M. Awramik, Springer-Verlag, Berlin, Germany, 2000

R153 A. W. Decho, 'Exopolymer Microdomains as a Structuring Agent for Heterogeneity within Microbial Biofilms', p. 9

Molecular Appproaches to Heart Failure Therapy, ed. G. Hasenfuss and E. Marban, Dr.Dietrich Steikopff Verlag GmbH & Co. KG, Darmstadt, Germany, 2000

R154 M. J. Lohse and S. Engelhardt, 'Cardiac Overexpression of β-Adrenergic Receptors', p. 26

New Advances in Analytical Chemistry, ed. Atta-ur-Rahman, Harwood Academic Publishers, Amsterdam, Netherlands, 2000

R155 L. Cugunov, 'Parametrization of ESR Spectra in Disordered Solids: Measurement Aspects', p. P1/1

R156 W. S. Price, 'Probing Molecular Dynamics in Biochemical and Chemical Systems Using Pulsed Field Gradient NMR Diffusion Measurements', p. P1/31

R157 G. Kogan and D. Uhrin, 'Current NMR Methods in the Structural Elucidation of Polysaccharides', p. P1/73

R158 P. Novak, Drazenvikic-Topic, V. Smrecki and Z. Meic, 'Isotope Effects in NMR Spectra as a Structural Tool for Organic Molecules', p. P1/135

R159 M. Piotto, 'Applications of B_0 Field Gradients to the Study of Natural Products by NMR', p. P1/211

R160 S. H. Alarcon and A. C. Olivieri, 'Residual Dipolar Coupling Effects in Solid State MAS NMR. Investigation of Proton Transfer Processes in Solids' p. P1/263

R161 J. Zakrzewska, Z. Zujovic and D. Vucelic, 'Application of NMR Spectroscopy for Structural Studies of Lignins, Humic Materials and Oil Shales', p. P1/291

R162 M. J. Potrzebowski, 'Solid State NMR Studies of Carbohydrates and their Analogues', p. P1/359

R163 R. C. R. Grace and N. Syryaprakash, 'Application of Z-Cosy Technique for the Analyses of NMR Spectra of Oriented Molecules', p. P1/441

R164 N. Chandrakumar, 'High Resolution NMR as a Probe of Molecular Structure, Dynamics and Diffusion', p. P1/485

R165 W. Schilf and L. Stefaniak, 'Application of ^{14}N and ^{15}N NMR for Determination of Protonation Site and Hydrogen Bond Strength in Nitrogen Organic Compounds', p. P1/659

R166 M. Mackowiak, 'Nuclear Quadrupole Resonance Studies of Electron Density Distribution and Molecular Dynamics', p. P2/433

NMR in Microbiology. Theory and Applications, ed. J.-N. Barbotin and J.-C. Portais, Horizon Scientific Press, Wymondham, U.K., 2000

R167 J.-M. Franconi, D. Cailleu, J.-C. Portais and P. Canioni, 'NMR Basic Principles', p. 1

R168 J.-P. Grivet, 'NMR and Microorganisms', p. 27

R169 J. V. Shanks, 'In Situ NMR Systems', p. 47

R170 A. A. de Graaf, 'Use of ^{13}C Labelling and NMR Spectroscopy in Metabolic Flux Analysis', p. 73

R171 T.-D. Son, 'Data Analysis and Modelization', p. 105

R172 J. Skalicky and T. Szyperski, 'Two-Dimensional NMR Spectroscopy', p. 155

R173 D. Uhrin and J.-R. Brisson, 'Structure Determination of Microbial Polysaccharides by High Resolution NMR Spectroscopy', p. 165

R174 G. Gemmecker and E. Bernhard, 'NMR Studies of the Bacterial Sugar Transport System', p. 191

R175 Z.-Y Wang and T. Nozawa, 'In Situ Measurements of Enzyme Activities by NMR', p. 221

R176 M. Auger, 'Biological Membrane Structure by Solid-State NMR', p. 243

R177 S. Guillouet, P. A. Lessard and A. J. Sinskey, 'Investigating Microbial Metabolic Pathways with NMR: Metabolism of Amino Acids in Corynebacteria', p. 259

R178 P. Boyaval and C. Deborde, 'Metabolic Behavior of Lactic and Propionic Acid Bacteria', p. 283

R179 H. J. Fogel and E. M. Lohmeier-Vogel, 'NMR Investigations of Yeast Metabolism: Biochemistry and Biotechnology Applications', p. 309

R180 I. Gosselin, J.-N. Barbotin and J.-C. Portais, 'NMR Investigations of Polymer Biosynthesis. The Case of a Multiproductive Bacterium, Sinorhizobium Meliloti', p. 331

R181 O. M. M. Bouvet and M.-N. Rager, 'Sugar Transport and Metabolism in Fermentative Bacteria', p. 349

R182 A.-M. Delort and B. Combourieu, 'Microbial Degradation of Xenobiotics', p. 411

R183 D. W. Hopkins, J. A. Chudek, S. F. I. Haslam and E. A. Webster, 'Application of Solid-State NMR to Investigate Organic Biogeochemistry in Soils', p. 431

R184 U. Sauer, T. Szyperski and J. E. Bailey, 'Future Trends in Complex Microbial Reaction Studies', p. 479

Organosilicon Chemistry IV, ed. N. Auner and J. Weis, Wiley-VCH Verlag GmbH, Weinheim, Germany, 2000

R185 N. Auner, T. Muller, M. Ostermeier, J. Schuppan and H.-U. Steiberger, 'Intramolecularly π-Stabilized Silyl Cations', p. 127

R186 H.-U. Siehl and M. Fuss, 'Silyl Effects in Hypercoordinated Carbocations', p. 140

R187 N. W. Mitzel and H. Oberhammer, 'N,O-Dimethyl-N-Silylhydroxylamine, a Compound with Steeply Pyramidal Nitrogen Coordination', p. 158

R188 W. Krumlacher, H. Siegl and K. Hassler, 'Hypersilyl Compounds of Elements of Group 15', p. 367

R189 E. Brendler, K. Trommer and G. Roewer, '^{29}Si-MAS-NMR Investigations of Aminosubstituted Chloromethylpolysilanes', p. 372

Oxford Handbook of Nucleic Acid Structure, ed. S. Neidle, Oxford University Press, Oxford, U.K., 1999

R190 U. Schmitz, F. J. H. Blocker and T. L. James, 'Standard DNA Duplexes and RNA:DNA Hybrids in Solution', p. 253

R191 H. M. Berman and B. Schneider, 'Nucleic Acid Hydration', p. 295

R192 D. J. Patel, S. Bouaziz, A. Kettani and Y. Wang, 'Structures of Guanine-Rich and Cytosine-Rich Quadruplexes Formed in Vitro by Telomeric, Centromeric, and Triplet Repeat Disease DNA Sequences', p. 389

R193 J. Nowakowski and I. Tinoco Jr., 'RNA Structure in Solution', p. 567

Peptides for the New Millennium, [Proceedings of the 16th American Peptide Symposium, 1999], ed. G. B. Fields, J. P. Tam and G. Barany, Kluwer Academic Publishers, Dordrecht, Netherlands, 2000

R194 P. A. Keifer, 'NMR Analysis Tools for the Peptide Sciences', p. 396

Peroxide Chemistry, ed. W. Adam, Wiley-VCH Verlag GmbH, Weinheim, Germany, 2000

R195 W. R. Thiel, M. Barz, H. Glas and A.-K. Pleier, 'Olefin Epoxidation

Catalyzed by Molybdenum Peroxo Complexes: A Mechanistic Study', p. 433

Pesticide/Soil Interaction, ed. J. Cornejo and P. Jamet, Institut National de la Recherche Agronomique, Paris, France, 2000

R196 A. Piccolo, G. Celano and P. Conte, 'Methods of Isolation and Characterization of Humic Substances to Study their Interaction with Pesticides', p. 103

Phytochemicals as Bioactive Agents, ed. W. R. Bidlack, Technomic Publishing Co., Inc., Lancaster, Pa, 2000

R197 S. O. Duke, A. M. Rimando, F. E. Dayan, C. Canel, D. E. Wedge, M. R. Tellez, K. K. Schrader, L. A. Weston, T. J. Smillie, R. N. Paul and M. V. Duke, 'Strategies for the Discovery of Bioactive Phytochemicals', p. 1

Plant Cell and Tissue Culture for the Production of Food Ingredients, ed. T.-J. Fu, G. Singh and W. R. Curtis, Kluwer/Plenum Publishers, New York, N.Y., 1999

R198 J. V. Shanks, S. K. Rijhwani, J. Morgan, S. Vani, R. Bhadra and C.-H. Ho, 'Quantification of Metabolic Fluxes for Metabolic Engineering of Plant Products', p. 45

Prix Nobel 1999, Almqvist & Wiksell International, 2000

R199 A. H. Zewail, 'Femtochemistry. Atomic-Scale Dynamics of the Chemical Bond Using Ultrafast Lasers. Nobel Lecture, December 8, 1999', p. 110

Proceedings of ECSOC-1, The First International Electronic Conference on Synthetic Organic Chemistry, Proceedings of ECSOC-2, The Second International Electronic Conference on Synthetic Organic Chemistry, CD-ROM edition Editors: S.-K. Lin and E. Pombo-Villar, Molecular Diversity Preservation International, Basel, Switzerland, 1999

R200 W. Ganci, U. Ringeisen and P. Ruedi, 'Synthesis of Rigid Acetylcholine Mimics as Inhibitors of Serine Hydrolases', p. 439

R201 S. Furegati, A. Linden, G. Przibille, D. Rentsch and P. Ruedi, 'Synthesis, ee-Determination and Absolute Configuration of Chiral Organophosphorus Inhibitors of Serine Hydrolases', p. 726

Proceedings of the Eleventh Conversation, Part 1, Journal of Biomolecular Structure & Dynamics, Conversation 11, Issue Number 1, ed. R. H. Sarma and M. H. Sarma, Adenine Press, Schenectady, N.Y., 2000

R202 H. G. Khorana, 'Molecular Biology of Light Transduction by the Mammalian Photoreceptor, Rhodopsin', p. 1

Proceedings of the Eleventh Conversation, Part 2, Journal of Biomolecular Structure and Dynamics, Conversation 11, Issue Number 2, 1999, ed. R. H. Sarma and M. H. Sarma, Adenine Press, Schenectady, N. Y, 2000

R203 S. H. Chou, 'NMR Studies of DNA Structures Containing Sheared Purine-Purine and Purine-Pyrimidine Base Pairs', p. 303

Proceedings of the 1998 ERDEC Scientific Conference on Chemical and Biological Defense Research, 1998, ed. D. A. Berg, National Technical Information Service, Springfield, Va., 1999

R204 M. D. Brickhouse, R. Matteson, H. D. Durst and R. J. O'Connor, 'Traditional and Novel Relaxation Agents to Improve Quantitative NMR Analysis of Organic and Aqueous Solutions', p. 591

Proceedings of the 25th European Peptide Symposium, 1998, ed. S. Bajusz and F. Hudecz, Akademiai Kiado, Budapest, Hungary, 1999

R205 F. Jordan, D. Bao, W. P. Huskey, K. Haghjoo, C. Kettner and L. Polgar, 'Hydrogen Bonding at Serine Protease Active Centers in the Absence and Presence of Potent Peptide-Based Inhibitors Studied by NMR Methods', p. 784

Proceedings of ICCR '98, ed. G. Chen, International Academic Publishers, Beijing, People's Republic of China, 1998

R206 S. W. Van Sciver, Y. S. Hascicek, W. D. Markiewicz, J. Schwartz and H. J. Schneider-Montau, 'High Field HTS Magnet Technology and Applications', p. 499

Proceedings of International Symposium on Fuels and Lubricants, Symposium Papers, 2nd, vol. 1, ed. S. P. Srivastava, Allied Publishers Ltd, New Delhi, India, 2000

R207 R. N. Rao, 'Role of Modern Analytical Techniques in Quality Assurance of Fuels and Lubricants', p. 185

Real-Time Analysis of Biomolecular Interactions, ed. K. Nagata and H. Handa, Springer-Verlag Tokyo, Tokyo, Japan, 2000

R208 I. Shimada, 'NMR Analysis for Interactions between Biomacromolecules', p. 223

Ribozyme, ed. G. Krupp and R. K. Gaur, Eaton Publishing Co., Natick, Mass., 2000

R209 A. Pichler, C. Berens and R. Schroeder, 'Localization of Metal Ion Binding Sites in Group I Intron RNA', p. 7

R210 M. Zheng and I. Tinoco Jr., 'High Resolution NMR Spectroscopy of Ribozymes', p. 297

R211 M. Egli and G. Minasov, 'Recent Advances in RNA Crystallography', p. 315

Second Topical Meeting on Decontamination, Decommissioning and Reutilization of Commercial and Government Facilities, Knoxville, Tennessee, 1999, [computer optical disk], American Nuclear Society, La Grange Park, Ill., 1999

R212 L. Bishop, R. Meehan and K. Yuracko, 'Leveraging Legacy Material to Accelerate Cleanup', 14

Solid State Ionics, Materials and Devices, [Proceedings of 7th Asian Conference], ed. B. V. R. Chowdari and W. Wang, World Scientific Publishing Co. Pte. Ltd., Singapore, 2000

R213 D. Brinkmann, S. Bergar and J. Ross, 'Exploring Glasses on the Microscopic Level by NMR. xLiF. (1–x)$LiPO_3$', p. 167

Structure and Dynamics of Biomolecules, ed. E. Fanchon, Oxford University Press, Oxford, U.K., 2000

R214 H. B. Stuhrmann, 'Nuclear Spin Contrast Variation Studies on Macromolecular Complexes', p. 390

Structure and Imperfections in Amorphous and Crystalline Silicon Dioxide, ed. R. A. B. Devine, J.-P. Duraud and E. Dooryhee, John Wiley & Sons Ltd., Chichester, U.K., 2000

R215 R. Dupree, 'Nuclear Magnetic Resonance as a Structural Probe of SiO_2', p. 107

Supramolecular and Colloidal Structures in Biomaterials and Biosubstrates, Proceedings of the Fifth Royal Society-Unilever Indo-UK Forum in Material Science and Engineering, 1999, ed. M. Lal, Imperial College Press, London, U.K., 2000

R216 N. Chandrakumar, 'C-13 NMR Imaging: Techniques and Applications to Materials and Biological Systems', p. 33

Synthesis and Application of Isotopically Labelled Compounds, 1997, Proceedings of Sixth International Symposium, Philadelphia, USA, 14–18 September 1997, ed. J. R. Heys and D. G. Melillo, Wiley & Sons, Chichester, U.K., 1998

R217 V. Anderson, 'Mechanism of Bond Distortions in Enoyl-CoA Hydratase', p. 273

The Chemistry of Dienes and Polyenes, Volume 2, ed. Z. Rappoport, John Wiley & Sons Ltd, Chichester, U.K., 2000

R218 Y. Takeuchi and T. Takayama, 'NMR Spectroscopy of Dienes and Polyenes', p. 59

The Male Gameta: From Basic Science to Clinical Applications, ed. C. Gagnon, Cache River Press, Vienna, Ill, 1999

R219 R. Balhorn, M. Cosman, K. Thornton, V. V. Krishnan, M. Corzett,

G. Bench, C. Kramer, J. Lee IV, N. V. Hud, M. Allen, M. Prieto, W. Meyer-Ilse, J. T. Brown, J. Kirz, X. Zhang, E. M. Bradbury, G. Maki, R. E. Braun and W. Breed, 'Protamine Mediated Condensation of DNA in Mammalian Sperm', p. 55

Water Management in the Design and Distribution of Quality Foods, [International Symposium on the Properties of Water in Foods, ISOPOW 7, 1998], ed. Y. H. Roos, R. B. Leslie and P. J. Lillford, Technomic Publishing Co., Inc., Lancaster, Pa., 1999

R220 B. P. Hills, 'NMR Studies of Water Mobility in Foods', p. 107

R221 P. Auffinger and E. Westhof, 'Roles of Hydration on the Structure and Dynamics of Nucleic Acids', p. 165

Wood and Cellulosic Chemistry, Second Edition, Revised, and Expanded, ed. D. N.-S. Hon and N. Shiraishi, Marcel Dekker, Inc., New York, N.Y., 2001

R222 F. Hori, 'Structure of Cellulose: Recent Developments in its Characterization', p. 83

4 Reviews in Periodicals

R223 D. Acquotti and S. Sonnino, 'Use of Nuclear Magnetic Resonance Spectroscopy in Evaluation of Ganglioside Structure, Conformation, and Dynamics', *Methods Enzymol.*, 2000, **312**, 247

R224 T. M. Alam and M. K. Alam, 'Chemometric Analysis of Nuclear Magnetic Resonance Spectroscopy Data', *Spectroscopy (Eugene, Oreg.)*, 2001, **16**, 18

R225 A. D. Albert and P. L. Yeagle, 'Domain Approach to Three-Dimensional Structure of Rhodopsin Using High-Resolution Nuclear Magnetic Resonance', *Methods Enzymol.*, 2000, **315**, 107

R226 H. M. A. Al-Hazimi, 'Naturally Occurring Flavans and Isoflavans', *J. Saudi. Chem. Soc.*, 2000, **4**, 67

R227 S. Al-Karadaghi, O. Kristensen and A. Liljas, 'A Decade of Progress in Understanding the Structural Basis of Protein Synthesis', *Prog. Biophys. Mol. Biol.*, 2000, **73**, 167

R228 D. Allen, C. Flaum, T. S. Ramakrishnan, D. Fairhurst, T. Pritchard, J. Bedford, G. Gubelin, N. Heaton, C. C. Minh, R. Ramamoorthy, K. Castelijns, M. A. Norville and M. R. Seim, 'Trends in NMR Logging', *Oilfield Rev.*, 2000, **12**, 2

R229 B. Andersen and E. Sletten, 'NMR Studies on Metal Complexes of DNA Oligomers', *J. Inorg. Biochem.*, 2000, **79**, 353

R230 Z. Argov, M. Lofberg and D. L. Arnold, 'Insights into Muscle Diseases Gained by Phosphorus Magnetic Resonance Spectroscopy', *Muscle Nerve*, 2000, **23**, 1316

R231 K. Asayama, Y. Kitaoka, G.-Q. Zheng, K. Ishida and Y. Tokunaga,

'NMR Study of Strongly Correlated Superconductors (Heavy Fermion, High T_c and Related Materials)', *Stud. High Temp. Supercond.*, 1999, **29**, 59

R232 D. Astruc, J.-C. Blais, E. Cloutet, L. Djakovitch, S. Rigaut, J. Ruiz, V. Sartor and C. Valerio, 'The First Organometallic Dendrimers: Design and Redox Functions', *Top. Curr. Chem.*, 2000, **210**, 229

R233 R. H. Atalla, 'The Individual Structures of Native Celluloses', *Lenzinger Ber.*, 2000, **79**, 5

R234 Y. Ba, C. I. Ratcliffe and J. A. Ripmeester, 'Double Resonance NMR Echo Spectroscopy of Aluminosilicates', *Adv. Mater. (Weinheim, Ger.)*, 2000, **12**, 603

R235 F. Babonneau and J. Maquet, 'Nuclear Magnetic Resonance Techniques for the Structural Characterization of Siloxane-Oxide Hybrid Materials', *Polyhedron*, 2000, **19**, 315

R236 M. Badertscher, A. Korytko, K.-P. Schulz, M. Madison, M. E. Munk, P. Portmann, M. Junghans, P. Fontana and E. Pretsch, 'Assemble 2.0: A Structure Generator', *Chemom. Intell. Lab. Syst.*, 2000, **51**, 73

R237 A. Bagno, 'Acyl Group vs Nitrogen Protonation of Carboxylic and Non-Carboxylic Amides in the Gas Phase and Water', *J. Phys. Org. Chem.*, 2000, **13**, 574

R238 R. Bakhtiar and F. L. S. Tse, 'Biological Mass Spectrometry: A Primer', *Mutagenesis*, 2000, **15**, 415

R239 J. D. Baleja, 'Structure Determination of Membrane-Associated Proteins from Nuclear Magnetic Resonance Data', *Anal. Biochem.*, 2001, **288**, 1

R240 G. Balogh, 'NMR Spectroscopy', *Prog. Pharm. Biomed. Anal.*, 2000, **4**, 441

R241 L. Banci and C. Presenti, 'Perspectives in Inorganic Structural Biology: Solution Structures of Metalloproteins', *JBIC, J. Biol. Inorg. Chem.*, 2000, **5**, 422

R242 F. E. Barton II and D. S. Himmelsbach, 'The Need for 2–D Correlation in NIR Spectroscopy', *AIP Conf. Proc.*, 2000, **503**, 163

R243 A. K. Basu, J. M. McNulty and W. G. McGregor, 'Solution Conformation and Mutagenic Specificity of 1,N^6-Ethenoadenine', *IARC Sci. Publ.*, 1999, **150**, 325

R244 D. Bauman, 'Application of Spectroscopic Methods to Study of Liquid Crystalline Phases', *Proc.SPIE-Int. Soc. Opt. Eng.*, 2000, **4147**, 126

R245 R. C. Baxter, 'Insulin-Like Growth Factor (IGF) - Binding Proteins: Interactions with IGFs and Intrinsic Bioactivities', *Am. J. Physiol.*, 2000, **278**, E967

R246 P. Bayer, L. Varani and G. Varani, 'Nuclear Magnetic Resonance Methods to Study RNA-Protein Complexes', *Methods Enzymol.*, 2000, **317**, 198

R247 B. Bechinger, 'Solid-State NMR Investigations on the Structure and Topological Equilibria of Polypeptides Associated with Biological Membranes', *Phys. Chem. Chem. Phys.*, 2000, **2**, 4569

R248 B. Bechinger, 'Biophysical Investigations of Membrane Perturbations by Polypeptides Using Solid-State NMR Spectroscopy', *Mol. Membr. Biol.*, 2000, **17**, 135

R249 M.-C. Bellissent-Funel, 'Structure of Supercritical Water', *J. Mol. Liq.*, 2001, **90**, 313

R250 J. Belloque and M. Ramos, 'Application of NMR Spectroscopy to Milk and Dairy Products', *Trends Food Sci. Technol*, 1999, **10**, 313

R251 P. S. Belton, 'Nuclear Magnetic Resonance Studies of the Hydration of Proteins and DNA', *Cell. Mol. Life Sci.*, 2000, **57**, 993

R252 M. Benedikt, F. Caspers and M. Lindroos, 'Application of Magnetic Markers for Precise Measurement of Magnetic Fields in Ramped Accelerators', *Part. Accel.*, 1999, **63**, 57

R253 L. J. Berliner, V. Khramtsov, H. Fujii and T. L. Clanton, 'Unique in Vivo Applications of Spin Traps', *Free Radical Biol. Med.*, 2001, **30**, 489

R254 O. O. Bernal, 'NMR/μSR and Non-Fermi-Liquid Behavior in Heavy Fermion Systems', *Phys. Status Solidi B*, 2000, **220**, 335

R255 I. Bertini, A. Rosato and P. Turano, 'Solution Structure of Paramagnetic Metalloproteins', *Pure Appl. Chem.*, 1999, **71**, 1717

R256 T. Bizouarn, O. Fjellstrom, J. Meuller, M. Axelsson, A. Bergkvist, C. Johansson, B. G. Karlsson and J. Rydstrom, 'Proton Translocating Nicotinamide Nucleotide Transhydrogenase from *E. coli*. Mechanism of Action Deduced from its Structural and Catalytic Properties', *Biochim. Biophys. Acta*, 2000, **1457**, 211

R257 C. Boesch, 'Molecular Aspects of Magnetic Resonance Imaging and Spectroscopy', *Mol. Aspects Med.*, 1999, **20**, 185

R258 E. N. Bogacheva and A. B. Shishkov, 'Tritium Planigraphy: A Tool for Studying the Spatial Structure of Proteins and their Complexes', *Mol. Biol.*, 2000, **34**, 712

R259 Y. Boulanger, M. Labelle and A. Khiat, 'Role of Phospholipase A_2 on the Variations of the Choline Signal Intensity Observed by ^{1}H Magnetic Resonance Spectroscopy in Brain Diseases', *Brain Res. Rev.*, 2000, **33**, 380

R260 C. Branca, A. Faraone, S. Magazu, G. Maisano, P. Migliardo and V. Villari, 'Polyethylene Oxide: A Review of Experimental Findings by Spectroscopic Techniques', *J. Mol. Liq.*, 2000, **87**, 21

R261 E. V. Brandt, R. Bekker and D. Ferreira, 'Structure and Absolute Configuration of Biflavonoids with Benzofuranoid Constituent Units', *Basic Life Sci.*, 1999, **66**, 245

R262 K. P. J. Braun, W. P. Vandertop, R. H. J. M. Gooskens, K. A. F. Tulleken and K. Nicolay, 'NMR Spectroscopic Evaluation of Cerebral Metabolism in Hydrocephalus: A Review', *Neurol. Res.*, 2000, **22**, 51

R263 P. J. Bray, 'C. Nuclear Quadrupole Resonance (NQR) Studies of Glass Structure', *Ser. Dir. Condens. Matter Phys.*, 2000, **17**, 249

R264 L. Brecker and D. W. Ribbons, 'Biotransformations Monitored in Situ by Proton Nuclear Magnetic Resonance Spectroscopy', *Trends Biotechnol.*, 2000, **18**, 197

R265 S. R. Breeze, S. J. Lang, A. V. Nosov, A. Sanchez, I. L. Moudrakovski, C. I. Ratcliffe and J. A. Ripmeester, 'Probing the Pore Space in Mesoporous Solids with NMR Spectroscopy and Magnetic Resonance Microimaging', *Stud. Surf. Sci. Catal.*, 2000, **129**, 491

R266 S. E. Brenner, 'Target Selection for Structural Genomics', *Nat. Struct. Biol.*, 2000, **7**, 967

R267 C. Brunel and P. Romby, 'Probing RNA Structure and RNA-Ligand Complexes with Chemical Probes', *Methods Enzymol.*, 2000, **318**, 3

R268 B. Brutscher, 'Principles and Applications of Cross-Correlated Relaxation in Biomolecules', *Concepts Magn. Reson.*, 2000, **12**, 207

R269 A. L. Buchachenko, 'Compressed Atoms', *J. Phys. Chem.B*, 2001, **105**, 5839

R270 A. S. V. Burgen, 'Targets of Drug Action', *Annu. Rev. Pharmacol. Toxicol.*, 2000, **40**, 1

R271 K. Burgess, 'Organometallic Chemistry', *Chem. Int. (London, U.K.)*, 2001, **6**, 189

R272 E. E. Burnell, D. Capitani, C. Casieri and A. L. Segre, 'A Proton Nuclear Magnetic Resonance Relaxation Study of $C_{12}E_6/D_2O$', *J. Phys. Chem. B*, 2000, **104**, 8782

R273 V. Busico and A. L. Segre, 'Recent Advances in the NMR Description of Polypropylene', *Polym. Prepr. (Am. Chem. Soc., Div.Polym.Chem.)*, [computer optical disk], 2001, **42**, 6

R274 A. Bussmann-Holder and N. Dalal, 'Polarizability Induced Cooperative Proton Ordering, Coexistence of Order/Disorder and Displacive Dynamics and Isotope Effect in Hydrogen-Bonded Ferroelectrics', *Ferroelectrics*, 2000, **237**, 305

R275 R. Cappai, M. F. Jobling, C. J. Barrow and S. Collins, 'Structural Biology of Prions', *Contrib. Microbiol.*, 2001, **7**, 32

R276 M. Carrion-Vazquez, A. F. Oberhauser, T. E. Fisher, P. E. Marszalek, H. Li and J. M. Fernandez, 'Mechanical Design of Proteins Studied by Single-Molecule Force Spectroscopy and Protein Engineering', *Prog. Biophys. Mol. Biol.*, 2000, **74**, 63

R277 F.-T. Chau and A. K.-M. Leung, 'Applications of Wavelet Transform in Spectroscopic Studies', *Data Handl. Sci. Technol.*, 2000, **22**, 241

R278 Y. W. Chen, E. J. Dodson and G. J. Kleywegt, 'Does NMR Mean "Not for Molecular Replacement"? Using NMR-Based Search Models to Solve Protein Crystal Structures', *Structure (London)*, 2000, **8**, R213

R279 H. N. Cheng, 'Computer-Aided NMR Methods for Polymers', *Polym. News*, 2000, **25**, 114

R280 M. Cisero, G. Fronza, C. Fuganti, C. Guillou and F. Reniero, 'Biogeneration of Aromas: Mechanistic Aspects of the Microbial Generation of Several Aroma Components and Authentication of their Origin Using the ^{2}H NMR Spectroscopy', *Proc. Phytochem. Soc. Eur.*, 2000, **46**, 121

R281 J. F. Clark, 'Creatine in Cardiovascular Metabolism During Physiolo-

gical and Pathological Conditions: NMR Studies', *Med. Sci. Symp. Ser.*, 2000, **14**, 25

R282 W. W. Cleland, 'Low-Barrier Hydrogen Bonds and Enzymic Catalysis', *Arch. Biochem. Biophys.*, 2000, **382**, 1

R283 M. Colic and J. Miller, 'The Significance of Interfacial Water Structure in Colloidal Systems – Dynamic Aspects', *Surfactant Sci. Ser.*, 2000, **88**, 35

R284 V. Conte, O. Bortolini, M. Carraro and S. Moro, 'Models for the Active Site of Vanadium - Dependent Haloperoxidases: Insight into the Solution Structure of Peroxo Vanadium Compounds', *J. Inorg. Biochem.*, 2000, **80**, 41

R285 D. G. Cory, R. Laflamme, E. Knill, L. Viola, T. F. Havel, N. Boulant, G. Boutis, E. Fortunato, S. Lloyd, R. Martinez, C. Negrevergne, M. Pravia, Y. Sharf, G. Teklemariam, Y. S. Weinstein and W. H. Zurek, 'NMR Based Quantum Information Processing: Achievements and Prospects', *Los Alamos Natl. Lab., Prepr. Arch., Quantum Phys.* [preprint] 2000, 1–33, arXiv:Quant-ph/0004104, available URL: http://xxx.lanl.gov/pdf/quant-ph/0004104

R286 D. G. Cory, R. Laflamme, E. Knill, L. Viola, T. F. Havel, N. Boulant, G. Boutis, E. Fortunato, S. Lloyd, R. Martinez, C. Negrevergne, M. Pravia, Y. Sharf, G. Teklemariam, Y. S. Weinstein and W. H. Zurek, 'NMR Based Quantum Information Processing: Achievements and Prospects', *Forschr. Phys.*, 2000, **48**, 875

R287 G. P. Crawford, 'Measurement of Surface Elastic Constants', *EMIS Datarev. Ser.*, 2000, **25**, 230

R288 L. Cristofolini and M. P. Fontana, 'Vibrational Properties and Phase Transitions in Lithium Doped Fullerides', *Asian J. Phys.*, 2000, **9**, 609

R289 T. A. Cross and J. R. Quine, 'Protein Structure in Anisotropic Environments: Development of Orientational Constraints', *Concepts Magn. Reson.*, 2000, **12**, 55

R290 T. A. Cross, F. Tian, M. Cotten, J. Wang, F. Kovacs and R. Fu, 'Correlations of Structure, Dynamics and Function in the Gramicidin Channel by Solid-State NMR Spectroscopy', *Novartis Found. Symp.*, 1999, **225**, 4

R291 H. K. Cummings and J. A. Jones, 'Nuclear Magnetic Resonance: A Quantum Technology for Computation and Spectroscopy', *Contemp. Phys.*, 2000, **41**, 383

R292 J. J. Dalluge and B. C. Nelson, 'Determination of Tea Catechins', *J. Chromatogr., A*, 2000, **881**, 411

R293 J. W. Daly and H. M. Garraffo, 'An Arthropod Origin for Bioactive Alkaloids of Amphiabian Skin', *An. Acad. Nac. Cienc. Exactas, Fis. Nat. (Buenos Aires)*, 1999, **51**, 9

R294 T. De Bruyne, L. Pieters, R. Dommisse, H. Kolodziej, V. Wray, D. Vanden Berghe and A. Vlietinck, 'NMR Characterization and Biological Evaluation of Proanthocyanidins: A Systematic Approach', *Basic Life Sci.*, 1999, **66**, 193

R295 J. Dec and J.-M. Bollag, 'Phenoloxidase-Mediated Interactions of Phenols and Anilines with Humic Materials', *J. Environ. Qual.*, 2000, **29**, 665

R296 R. A. De Graaf and D. L. Rothman, 'In Vivo Detection and Quantification of Scalar Coupled ^{1}H NMR Resonances', *Concepts Magn. Reson.*, 2001, **13**, 32

R297 W. J. DeGrip, F. DeLange, C. H. W. Klaassen, P. J. M. Verdegem, S. Wallace-Williams, A. F. L. Creemers, V. Bergo, P. H. M. Bovee, J. Raap, K. J. Rothschild, H. J. M. DeGroot and J. Lugtenburg, 'Photoactivation of Rhodopsin: Interplay between Protein and Chromophore', *Novartis Found. Symp.*, 1999, **224**, 102

R298 D. E. Demko and B. Blumich, 'Solid-State NMR Imaging Methods. Part I: Strong Field Gradients', *Concepts Magn. Reson.*, 2000, **12**, 188

R299 D. E. Demco and B. Blumich, 'Solid-State NMR Imaging Methods. Part II: Line Narrowing', *Concepts Magn. Reson.*, 2000, **12**, 269

R300 M. Destarac and B. Boutevin, 'Use of Polychloro Alkane Initiators for Comparison between Copper-Based Redox Telomerization and Atom Transfer Radical Polymerization', *Curr. Trends Polym. Sci.*, 1999, **4**, 201

R301 B. Devreese and J. Van Beeumen, 'Mass Spectrometric Methods for the Study of Non-Covalent Interactions of Proteins and Other Biomolecules', *Int. J. Bio-Chromatogr.*, 2000, **5**, 313

R302 S. Dey, S. Narayan, A. Singhal and V. K. Jain, 'Palladium and Platinum Organochalcogenolates and their Transformation into Metal Chalcogenides', *Proc.-Indian Acad. Sci., Chem. Sci.*, 2000, **112**, 187

R303 A. J. Dingley, F. Cordier and S. Grzesiek, 'An Introduction to Hydrogen Bond Scalar Couplings', *Concepts Magn. Reson.*, 2001, **13**, 103

R304 K.-P. Dinse, 'FT-EPR and Pulsed ENDOR Studies of Encapsulated Atoms and Ions', *Electron Paramagn. Reson.*, 2000, **17**, 78

R305 V. V. Dmitriev, 'New NMR Modes in Superfluid ^{3}He-B', *Phys. Usp.*, 2000, **43(6)**

R306 J.-G. Dong, A. Kawamura, J. Guo, I. A. Zanze, K. Nakanishi and N. Berova, 'Structure Determination of Saponins with Cardiotonic Activity by Circular Dichroism', *Proc. Phytochem. Soc. Eur.*, 2000, **45**, 79

R307 K. Dorai, T. S. Mahesh, Arvind and Anil Kumar, 'Quantum Computation Using NMR', *Curr.Sci.*, 2000, **79**, 1447

R308 M. J. Duer, 'Solid State NMR', *Phys. Organomet. Chem.*, 1999, **2**, 227

R309 H. Durr, 'Fsec Magnetism', *Schr. Forschungszent. Juelich, Mater. Mater.*, 2000, **3**, E5.1

R310 H. Eckert, 'D. Solid State NMR as a Structural Tool in Glass Science', *Ser. Dir. Condens. Matter Phys.*, 2000, **17**, 283

R311 A. M. Edwards, C. H. Arrowsmith, D. Christendat, A. Dharamsi, J. D. Friesen, J. F. Greenblatt and M. Vedadi, 'Protein Production: Feeding the Crystallographers and NMR Spectroscopists', *Nat. Struct. Biol.*, 2000, **7**, 970

R312 M. R. Egmond and J. De Vlieg, 'Fusarium Solani Pisi Cutinase', *Biochimie*, 2000, **82**, 1015

R313 B. Eichler and R. West, 'Chemistry of Group 14 Heteroallenes', *Adv. Organomet. Chem.*, 2000, **46**, 1

R314 A. Ejchart, 'Non-Classic Constraints in Protein Structure Determination', *Bull. Pol. Acad. Sci., Chem.*, 2000, **48**, 1

R315 J. R. Engen and D. L. Smith, 'Investigating Protein Structure and Dynamics by Hydrogen Exchange MS', *Anal. Chem.*, 2001, **73**, 256A

R316 C. Enjalbal, J. Martinez and J.-L. Aubagnac, 'Mass Spectrometry in Combinatorial Chemistry', *Mass. Spectrom. Rev.*, 2000, **19**, 139

R317 S. E. Evsyukov, 'Chemical, Photo-, and Electrochemical Transformation of Polymers. Chemical Dehydrohalogenation of Polymers', *Phys. Chem. Mater.Low-Dimens. Struct.*, 1999, **21**, 55

R318 S. Failla, P. Finocchiaro and G. A. Consiglio, 'Syntheses, Characterization, Stereochemistry and Complexing Properties of Acyclic and Macrocyclic Compounds Possessing α-Amino or α-Hydroxyphosphonate Units: A Review Article', *Heteroat. Chem.*, 2000, **11**, 493

R319 A. L. Feig, 'The Use of Manganese as a Probe for Elucidating the Role of Magnesium Ions in Ribozymes', *Met. Ions Biol. Syst.*, 2000, **37**, 157

R320 S. A. Feller, 'A Summary of the Second International Conferance on Borate Glases, Crystals and Melts', *Phys. Chem. Glasses*, 2000, **41**, 211

R321 W. S. Fenton, J. Hibbeln and M. Knable, 'Essential Fatty Acids, Lipid Membrane Abnormalities, and the Diagnosis and Treatment of Schizophrenia', *Biol. Psychiatry*, 2000, **47**, 8

R322 A. N. Ferentz and G. Wagner, 'NMR Spectroscopy: A Multifaceted Approach to Macromolecular Structure', *Q. Rev. Biophys.*, 2000, **33**, 29

R323 J. A. Ferretti, 'The Homeobox and Genetic Disease: Structure and Dynamics of Wild Type and Mutant Homeodomain Proteins', *J. Biochem. Mol. Biol.*, 2001, **34**, 1

R324 D. Fick, 'Study of Single Crystal Surfaces with Polarized ^{8}Li', *Hyperfine Interact.*, 2000, **127**, 463

R325 L. Fielding, 'Determination of Association Constants (K_a) from Solution NMR Data', *Tetrahedron*, 2000, **56**, 6151

R326 F. Fillaux, 'Hydrogen Bonding and Quantum Dynamics in the Solid State', *Int. Rev. Phys. Chem.*, 2000, **19**, 553

R327 R. H. Fillingame, W. Jiang, O. Y. Dmitriev and P. C. Jones, 'Structural Interpretations of F_o Rotary Function in the *Escherichia coli* F_1F_0 ATP Synthase', *Biochim. Biophys. Acta*, 2000, **1458**, 387

R328 R. H. Fillingame, W. Jiang and O. Y. Dmitriev, 'The Oligomeric Subunit c Rotor in the F_0 Sector of ATP Synthase: Unresolved Question in our Understanding of Function', *J. Bioenerg. Biomembr.*, 2000, **32**, 433

R329 A. Foldesi, A. Trifonova, M. K. Kundu and J. Chattopadhyaya, 'The Synthesis of Deuteronucleosides', *Nucleosides, Nucleotides Nucleic Acids*, 2000, **19**, 1615

R330 S. Fritzsche, R. Haberlandt, S. Jost and A. Schuring, 'Modeling

Diffusion in Zeolites by Molecular Dynamics Simulations', *Mol. Simul.*, 2000, **25**, 27

R331 D. C. Fry and S. D. Emerson, 'Applications of Biomolecular NMR to Drug Discovery', *Drug Des. Discovery*, 2000, **17**, 13

R332 T. Fukai and T. Nomura, 'New NMR Structure Determination Methods for Prenylated Phenols', *Basic Life Sci.*, 1999, **66**, 259

R333 Y. G. Gakh, A. A. Gakh and A. M. Gronenborn, 'Fluorine as an NMR Probe for Structural Studies of Chemical and Biological Systems', *Magn. Res. Chem.*, 2000, **38**, 551

R334 P. N. Gambhir and S. Nagarajan, 'Application of Nuclear Magnetic Resonance in Agriculture', *PINSA-A: Proc. Indian Natl. Sci. Acad., Part A*, 1999, **65**, 731

R335 K. Ganicz, 'Solid State NMR Spectroscopy as a Tool for Investigation of Structure and Dynamics of Amino Acids and Model Peptides', *Bull. Pol. Acad. Sci., Chem.*, 2000, **48**, 57

R336 E. Geiler, N. Eisenreich, A. Geiler and C. Hubner, 'Analysis and Test Methods for Service Life Prediction of Energetic Materials', *Int. Annu. Conf. ICT*, 2000, **31**, 149/1

R337 W. Geithner, U. Georg, S. Kappertz, M. Keim, A. Klein, P. Lievens, R. Neugart, M. Neuroth, L. Vermeeren and S. Wilbert, 'Measurement of Nuclear Moments and Radii by Collinear Laser Spectroscopy and by β-NMR Spectroscopy', *Hyperfine Interact.*, 2000, **129**, 271

R338 G. Gemmecker, 'Direct Detection of Hydrogen Bonds in Biopolymers by NMR Spectroscopy', *Angew. Chem., Int. Ed.*, 2000, **39**, 1224

R339 J. Gergely, 'Molecular Switches in Troponin', *Adv. Exp. Med. Biol.*, 1998, **453**, 169

R340 G. J. Gerwig and J. F. G. Vliegenthart, 'Analysis of Glycoprotein-Derived Glycopeptides', *EXS*, 2000, **88**, 159

R341 V. L. Ginzburg, V. V. Dmitriev and A. I. Smirnov, 'New NMR Modes in Superfluid ^{3}He-B', *Phys.-Usp.* , 2000, **43**, 639

R342 M. Glasbeek, 'Excited State Spectroscopy and Excited State Dynamics of Rh(III) and Pd(II) Chelates as Studied by Optically Detected Magnetic Resonance Techniques', *Top. Curr. Chem.*, 2001, **213**, 95

R343 S. J. Glaser, 'NMR Quantum Computing', *Angew. Chem., Int. Ed.*, 2001, **40**, 147

R344 A. Gold and R. Weiss, 'High-Valent Iron Porphyrins', *J. Porphyrins Phthalocyanines*, 2000, **4**, 344

R345 F. M. Goni and A. Alonso, 'Spectroscopic Techniques in the Study of Membrane Solubilization, Reconstitution and Permeabilization by Detergents', *Biochim. Biophys. Acta*, 2000, **1508**, 51

R346 G. N. Greaves, Y. Vaills, S. Sen and R. Winter, 'Density Fluctuations, Phase Separation and Microsegregation in Silicate Glasses', *J. Optoelectron. Adv. Mater.*, 2000, **2**, 299

R347 N. S. Green, M. M. Miller and K. N. Houk, 'Evaluation of Isoprenoid Conformation in Solution and in the Active Site of Protein-Farnesyl

Transferase Using Carbon-13 Labelling in Conjunction with Solution- and Solid-State NMR', *Chemtracts*, 2000, **13**, 749

R348 J. A. Grijalvo, M. T. Blanco-Varela, F. P. Maroto, A. P. Sanchez and T. V. Moreno, 'Thaumasite Formation in Hydraulic Mortars and Concretes', *Am. Concr. Inst.,SP,* 2000, **SP-192 (vol. 2)**, 1173

R349 D. Grinstein, S. Braverman and H. E. Gottlieb, 'NMR Identification of Trichloromethyl Sulfoxides, Sulfones and their Precursors', *Phosphorus, Sulfur Silicon Relat. Elem.*, 1998, **136, 137&138**, 259

R350 M. L. Gross, 'Charge-Remote Fragmentation: An Account of Research on Mechanisms and Applications', *Int.J. Mass Spectrom.*, 2000, **200**, 611

R351 F. P. Guengerich, S. Langouet, A. N. Mican, S. Akasaka, M. Muller and M. Persmark, 'Formation of Etheno Adducts and their Effects on DNA Polymerases', *IARC Sci. Publ.*, 1999, **150**, 137

R352 S. Guyot, C. Le Guerneve, N. Marnet and J.-F. Drilleau, 'Methods for Determining the Degree of Polymerization of Condensed Tannins: A New ^{1}H-NMR Procedure Applied to Cider Apple Procyanidins', *Basic Life Sci.*, 1999, **66**, 211

R353 A. Haase, F. Odoj, M. Von Kienlin, J. Warnking, F. Fidler, A. Weisser, M. Nittka, E. Rommel, T. Lanz, B. Kalusche and M. Griswold, 'NMR Probeheads for in Vivo Applications', *Concepts Magn. Reson.*, 2000, **12**, 361

R354 K. M. Haider, M. Spiteller, J. Dec and A. Schaffer, 'Silylation of Soil Organic Matter: Extraction of Humic Compounds and Soil-Bound Residues', *Soil Biochem.*, 2000, **10**, 139

R355 P. J. Hajduk, R. P. Meadows and S. W. Fesik, 'NMR-Based Screening in Drug Discovery', *Q. Rev. Biophys.*, 1999, **32**, 211

R356 J. M. Hakumaki and R. A. Kauppinen, '^{1}H NMR Visible Lipids in the Life and Death of Cells', *Trends Biochem. Sci.*, 2000, **25**, 357

R357 R. B. Hallock, 'The Two-Dimensional World of ^{3}He in ^{3}He-^{4}He Mixture Films', *J. Low Temp. Phys.*, 2000, **121**, 441

R358 M. R. Hansen, P. Hanson and A. Pardi, 'Filamentous Bacteriphage for Aligning RNA, DNA, and Proteins for Measurement of Nuclear Magnetic Resonance Dipolar Coupling Interactions', *Methods Enzymol.*, 2000, **317**, 220

R359 I. Haq and J. Landbury, 'Drug-DNA Recognition: Energetics and Implications for Design', *J. Mol. Recognit.*, 2000, **13**, 188

R360 T. Hard, 'NMR Studies of Protein-Nucleic Acid Complexes: Structures, Solvation, Dynamics and Coupled Protein Folding', *Q. Rev. Biophys.*, 1999, **32**, 57

R361 T. K. Harris, Q. Zhao and A. S. Mildvan, 'NMR Studies of Strong Hydrogen Bonds in Enzymes and in a Model Compound', *J. Mol. Struct.*, 2000, **552**, 97

R362 J. Heberle, J. Fitter, H. J. Sass and G. Buldt, 'Bacteriorhodopsin: The Functional Details of a Molecular Machine Are Being Resolved', *Biophys. Chem.*, 2000, **85**, 229

R363 A. Heerschap, C. Houtman, H. J. A. In't Zandt, A. J. Van den Bergh

and B. Wieringa, 'Introduction to in Vivo ^{31}P Magnetic Resonance Spectroscopy of (Human) Skeletal Muscle', *Proc. Nutr. Soc.*, 1999, **58**, 861

R364 W. Heink, J. Karger and S. Vasenkov, 'Application of Pulsed Field Gradient NMR to Characterize the Transport Properties of Microporous Membranes', *Membr. Sci. Technol. Ser.*, 2000, **6**, 97

R365 P. J. F. Henderson, C. K. Hoyle and A. Ward, 'Expression, Purification and Properties of Multidrug Efflux Proteins', *Biochem. Soc. Trans.*, 2000, **28**, 513

R366 M. Herberhold, A. M. Dietel, J. Peuker, A. Pfeifer and W. Milius, 'Sandwich and Half-Sandwich Complexes Derived from Pentamethylcyclopentadienyl Tetracarbonyl Vanadium, $Cp^*V(CO)_4$', *Appl. Organomet. Chem.*, 2000, **14**, 519

R367 P. J. Hernes and J. I. Hedges, 'Geochemistry of Tannin. Methods and Applications', *Basic Life Sci.*, 1999, **66**, 853

R368 J. Herzfeld and B. Tounge, 'NMR Probes of Vectoriality in the Proton-Motive Photocycle of Bacteriorhodopsin: Evidence for an "Electrostatic Steering" Mechanism', *Biochim. Biophys. Acta*, 2000, **1460**, 95

R369 M. P. Heyn, B. Borucki and H. Otto, 'Chromophore Reorientation During the Photocycle of Bacteriorhodopsin: Experimental Methods and Functional Significance', *Biochim. Biophys. Acta*, 2000, **1460**, 60

R370 A. Hilgeroth, 'Recent Advances in the Solid-State Photochemistry of 1,4–Dihydropyridines', *Recent Res. Dev. Pure Appl. Chem.*, 1999, **3**, 153

R371 J. Hobley, V. Malatesta, R. Millini and W. O. Parker Jr., 'Merocyanine and Photomerocyanine Dyes', *Mol. Cryst. Liq. Cryst. Sci. Technol., Sect. A*, 2000, **345**, 329

R372 J. C. A. Hopkins, K. Clarke and G. K. Radda, 'Control of Cardiac Energetics: From Models to Human Disease', *Magn. Reson. Mater.-Phys., Biol. Med.*, 2000, **11**, 1

R373 K. Hostettmann and C. Terreaux, 'Search for New Lead Compounds from Higher Plants', *Chimia*, 2000, **54**, 652

R374 R. V. Hosur, P. K. Radha, S. Singh and P. K. Patel, 'NMR of Bio-Macromolecules', *PINSA-A: Proc. Indian Natl. Sci. Acad., Part A*, 1999, **65**, 633

R375 P. J. Houghton, 'Chemistry and Biological Activity of Natural and Semi-Synthetic Chromone Alkaloids', *Stud. Nat. Prod. Chem.*, 2000, **21**, 123

R376 L. G. Hubert-Pfalzgraf, 'Tailoring Molecular Precursors for Multicomponent Oxides', *Korean J. Ceram.*, 2000, **6**, 370

R377 S. M. Hubig and J. K. Kochi, 'Structure and Dynamics of Reactive Intermediates in Reaction Mechanism. σ- and π-Complexes in Electrophilic Aromatic Substitutions', *J. Org. Chem.*, 2000, **65**, 6807

R378 F. Humbert, 'Potentials of Radio-Frequency Field Gradient NMR Microscopy in Environmental Science', *J. Ind. Microbiol. Biotechnol.*, 2001, **26**, 53

R379 P. T. Inglefield and A. A. Jones, 'Polycarbonate Dynamics by Nuclear Magnetic Resonance', *Plast. Eng. (N. Y.)*, 2000, **56**, 43

R380 M. Inouye, 'Synthetic Hydrogen-Bonding Receptors for Biologically Essential Monosaccharides', *Yuki Gosei Kagaku Kyokaishi*, 2000, **58**, 1077

R381 Y. P. Irkhin and V. Y. Irkhin, 'Determination of Magnetic Anisotropy of Complex Rare-Earth Compounds from Mössbauer and NMR Spectra', *Phys. Solid State*, 2001, **43**, 284

R382 V. I. Irzhak, 'Solution-Free Methods for the Determination of the Molecular Mass Distribution of Polymers', *Russ. Chem. Rev.*, 2000, **69**, 717

R383 N. Ishida, M. Koizumi and H. Kano, 'The NMR Microscopy: A Unique and Promising Tool for Plant Science', *Ann. Bot. (London)*, 2000, **96**, 259

R384 R. Ishima and D. A. Torchia, 'Protein Dynamics from NMR', *Nat. Struct. Biol.*, 2000, **7**, 740

R385 K. Ito and Y. Ohba, 'Synthesis and Properties of Chiral Homoazacalixarenes Possessing Amino Acid Residues', *Recent Res. Dev. Pure Appl. Chem.*, 1999, **3**, 255

R386 C. Jager, M. Schulz, P. Hartmann, S. Barth, R. Witter and J. Vogel, '2D NMR Investigations of Various Phosphate Materials', *Phosphorus Res. Bull.*, 1999, **10**, 6

R387 W. Jahnke, S. Ruedisser and M. Zurini, 'Spin Label Enhanced NMR Screening', *J. Am. Chem. Soc.*, 2001, **123**, 3149

R388 V. K. Jain, A. Singhal and S. Narayan, 'Chemistry of Palladium and Platinum with Selenium and Tellurium Ligands', *Phosphorus, Sulfur Silicon Relat. Elem.*, 1998, **136, 137 & 138**, 483

R389 J. Jaklic and P. Prelovsek, 'Finite-Temperature Properties of Doped Antiferromagnets', *Adv. Phys.*, 2000, **49**, 1

R390 M. C. Jarvis and M. C. McCann, 'Macromolecular Biophysics of the Plant Cell Wall: Concepts and Methodology', *Plant Physiol. Biochem. (Paris)*, 2000, **38**, 1

R391 J. Jazwinski, 'Nitrogen NMR Investigation of Compounds Containing 1,3–Diphenyl- and 2,3–Diphenyl-1,2,3,4–Tetrazolium Ring', *Bull. Pol. Acad. Sci. Chem.*, 2000, **48**, 35

R392 L. W. Jelinski and M. T. Melchior, 'High-Resolution NMR of Solids', *Appl. Spectrosc. Rev.*, 2000, **35**, 25

R393 J. Jimenez-Barbero, J. F. Espinoza, J. L. Asensio, F. J. Canada and A. Poveda, 'The Conformation of C-Glycosyl Compounds', *Adv. Carbohydr. Chem. Biochem.*, 2001, **56**, 235

R394 J. A. Jones, 'NMR Quantum Computation', *Los Alamos Natl. Lab., Prepr. Arch., Quantum Phys., [preprint]* 1 Sep. 2000, 1, arXiv:quant-ph/0009002, URL; http://xxx.lanl.gov/pdf/quant-ph/0009002

R395 S. Kaizaki, 'Roles of Solvation in Variability of Ligand Field and Stereochemistry for Transition Metal Complexes as Revealed by UV-Vis, CD and/or Paramagnetic NMR Spectroscopy', *Trends Inorg. Chem.*, 1999, **6**, 105

R396 S. G. Kalko, M. Chagoyen, N. Jimenez-Lozano, N. Verdaguer, I. Fita

and J. M. Carazo, 'The Need for a Shared Database Infrastructure: Combining X-Ray Crystallography and Electron Microscopy', *Eur. Biophys. J.*, 2000, **29**, 457

R397 K. Kato, W. H. Fridman, Y. Arata and C. Sautes-Fridman, 'A Conformational Change in the Fc Precludes the Binding of Two Fcγ Receptor Molecules to One IgG', *Immunol. Today*, 2000, **21**, 310

R398 M. A. S. H. Kersten, C. Van der Drift, H. J. M. Op den Camp, J. J. P. Baars, L. J. L. D. Van Griensven, P. J. Schaap, Y. Muller, J. Visser and J. A. M. Leunissen, 'The Glutamine Synthetase from the Edible Mushroom Agaricus Bisporus', *Mushroom Sci.*, 2000, **15**, 71

R399 M. S. Keshavan, J. A. Stanley and J. W. Pettegrew, 'Magnetic Resonance Spectroscopy in Schizophrenia: Methodological Issues and Findings - Part II', *Biol. Psychiatry*, 2000, **48**, 369

R400 J. Keske, D. A. McWhorter and B. H. Pate, 'Molecular Rotation in the Presence of Intramolecular Vibrational Energy Redistribution', *Int. Rev. Phys. Chem.*, 2000, **19**, 363

R401 A. D. Khanolkar, S. L. Palmer and A. Makriyannis, 'Molecular Probes for the Cannabinoid Receptors', *Chem. Phys. Lipids*, 2000, **108**, 37

R402 C. D. Kilts, 'In Vivo Imaging of the Pharmacodynamics and Pharmacokinetics of Lithium', *J. Clin. Psychiatry*, 2000, **61, (Suppl. 9)**, 41

R403 H. Kim, J. Ralph, N. Yahiaoui, M. Pean and A.-M. Boudet, 'Cross-Coupling of Hydroxycinnamyl Aldehydes into Lignins', *Org. Lett.*, 2000, **2**, 2197

R404 C. M. Kinart and W. J. Kinart, 'Physicochemical Methods Used to Study Internal Structures of Liquid Binary Mixtures', *Phys. Chem. Liq.*, 2000, **38**, 155

R405 M. Kira and T. Iwamoto, 'Stable Cyclic and Acyclic Persilyldisilenes', *J. Organomet. Chem.*, 2000, **611**, 236

R406 M. Kitagawa, K. Yamashina, S. Tojyo and D. Ulam-Orgikh, 'In Search for Molecules which Calculate Quantum Mechanically', *Mem. Inst. Sci. Ind. Res., Osaka Univ.*, 2000, **57**, 96

R407 A. Klein, G. Strecker, G. Lamblin and P. Roussel, 'Structural Analysis of Mucin – Type O – Linked Oligosaccharides', *Methods Mol. Biol. (Totowa, N. J.)*, 2000, **125**, 191

R408 J. Klein, 'Membrane Breakdown in Acute and Chronic Neurodegeneration: Focus on Choline-Containing Phospholipids', *J. Neural Transm.*, 2000, **107**, 1027

R409 E. Kleinpeter, 'Recent Advances in Studying Tautomerism in Solution and in the Solid State', *Adv. Mol. Struct. Res.*, 2000, **6**, 97

R410 J. L. Koenig, 'Spectroscopic Characterization of the Molecular Structure of Elastomeric Networks', *Rubber Chem. Technol.*, 2000, **73**, 385

R411 I. Kogel-Knabner, 'Analytical Approaches for Characterizing Soil Organic Matter', *Org. Geochem.*, 2000, **31**, 609

R412 M. Kojima, M. Tanokura and K. Takahashi, 'Structure – Function Relationship of Ribonuclease T_1 Based on Molecular Structure', *Bioimages*, 2000, **8**, 45

R413 P. Komarek, 'Advances in Large Scale Applications of Superconductors', *Supercond. Sci. Technol.*, 2000, **13**, 456

R414 P. Komarek, 'Advances in Large Scale Applications of Superconductors', *Inst. Phys. Conf. Ser.*, 2000, **167**, 17

R415 E. Komor, 'Source Physiology and Assimilate Transport: The Interaction of Sucrose Metabolism, Starch Storage and Phloem Export in Source Leaves and the Effects on Sugar Status in Phloem', *Aust. J. Plant Physiol.*, 2000, **27**, 497

R416 G. J. J. Kortstee, K. J. Appeldoorn, C. F. C. Bonting, E. W. J. Van Niel and H. W. Van Veen, 'Recent Developments in the Biochemistry and Ecology of Enhanced Biological Phosphorus Removal', *Biochemistry (Moscow)*, 2000, **65**, 332

R417 Y. Koyama and R. Fujii, 'Cis-Trans Carotenoids in Photosynthesis: Configurations, Excited-State Properties and Physiological Functions', *Adv. Photosynth.*, 1999, **8**, 161

R418 M. Kralik, B. Corain and M. Zecca, 'Catalysis by Metal Nanoparticles Supported on Functionalized Polymers', *Chem. Pap.*, 2000, **54**, 254

R419 Zh.A. Krasnaya, 'Dienone⇆2H-Pyran Valence Isomerization', *Chem.-Heterocycl. Compd. (N. Y.)*, 1999, **35**, 1255

R420 H.-M. Krenzlin, 'Dynamics of Complex Molecules and Multidimensional Nuclear Magnetic Resonance', *Ber. Forschungszent. Juelich*, 1999,(**Juel-3726**), i–iii, 1–125

R421 N. R. Krishna and P. K. Agrawal, 'Molecular Structure of the Carbohydrate-Protein Linkage Region Fragments from Connective-Tissue Proteoglycans', *Adv. Carbohydr. Chem. Biochem.*, 2001, **56**, 201

R422 E. Kupce and S. Smallcombe, '900 MHz Nuclear Magnetic Resonance Shows Great Promise', *Spectrosc. Eur.*, 2001, **13**, 12

R423 K. Kurotobi, T. Murafuji and Y. Sugihara, 'Borepinothiophene, Synthesis and Characterization', *Trends Organomet. Chem.*, 1999, **3**, 211

R424 J. B. Lambert, C. E. Shawl and J. A. Stearns, 'Nuclear Magnetic Resonance in Archeology', *Chem. Soc. Rev.*, 2000, **29**, 175

R425 B. R. Landau, 'Quantifying the Contribution of Gluconeogenesis to Glucose Production in Fasted Human Subjects Using Stable Isotopes', *Proc. Nutr. Soc.*, 1999, **58**, 963

R426 J. Lapham and D. M. Crothers, 'Site-Specific Cleavage of Transcript RNA', *Methods Enzymol.*, 2000, **317**, 132

R427 W. Laurent, J. M. Bonny and J. P. Renou, 'Muscle Characterization by NMR Imaging and Spectroscopic Techniques', *Food Chem.*, 2000, **69**, 419

R428 P. Lens and M. A. Hemminga, 'Introduction to Journal of Industrial Microbiology and Biotechnology', *J. Int. Microbiol. Biotechnol.*, 2001, **26**, 1

R429 D. F. V. Lewis and P. Hlavica, 'Interaction between Redox Partners in Various Cytochrome P450 Systems: Functional and Structural Aspects', *Biochim. Biophys. Acta*, 2000, **1460**, 353

R430 J. Lhomme, J.-F. Constant and M. Demeunynck, 'Abasic DNA Structure, Reactivity, and Recognition', *Biopolymers*, 1999, **52**, 65

R431 J. C. Lindon and J. K. Nicholson, 'Advancing Hyphenated Chromatographic Systems', *Anal. Chem.*, 2000, **72**, 534A

R432 J. C. Lindon, J. K. Nicholson, E. Holmes and J. R. Everett, 'Metabonomics: Metabolic Processes Studied by NMR Spectroscopy of Biofluids', *Concepts Magn. Reson.*, 2000, **12**, 289

R433 J. C. Lindon, J. K. Nicholson and I. D. Wilson., 'Directly Coupled HPLC-NMR and HPLC-NMR-MS in Pharmaceutical Research and Development', *J. Chromatogr., B: Biomed. Sci. Appl.*, 2000, **748**, 233

R434 S. Liu and S. Sun., 'Recent Progress in the Studies of Endohedral Metallofullerenes', *J. Organomet. Chem.*, 2000, **599**, 74

R435 T. S. Lobana, 'Stereochemical Trends of Metal Derivatives of Some Heterocyclic-2–Thiones and Thiosemicarbazones', *Proc.-Indian Acad. Sci., Chem. Sci.*, 2000, **112**, 323

R436 R. N. Loeppky, W. Cui, P. Goelzer, M. Park and Q. Ye, 'Glyoxal-Guanine DNA Adducts: Detection, Stability and Formation in Vivo from Nitrosamines', *IARC Sci. Publ.*, 1999, **150**, 155

R437 S. R. Lynch, M. I. Recht and J. D. Puglisi, 'Biochemical and Nuclear Magnetic Resonance Studies of Aminoglycoside-RNA Complexes', *Methods Enzymol.*, 2000, **317**, 240

R438 D. G. Lynn and S. C. Meredith, 'Review: Model Peptides and the Physicochemical Approach to β-Amyloids', *J. Struct. Biol.*, 2000, **130**, 153

R439 P. M. Macdonald, K. J. Crowell, C. M. Franzin, P. Mitrakos and D. Semchyschyn, '^{2}H NMR and Polyelectrolyte-Induced Domains in Lipid Bilayers', *Solid State Nucl. Magn. Reson.*, 2000, **16**, 21

R440 K. J. D. MacKenzie, 'Applications of Solid State NMR Spectroscopy to Ceramic Research', *Br. Ceram. Trans.*, 2000, **99**, 231

R441 A. Madl and S. Spange, 'On the Importance of the Amide-Bonded Hydrogen Atom in the Cationically Induced Oligomerization of N-Vinylamides', *Macromolecules*, 2000, **33**, 5325

R442 A. Madl and S. Spange, 'Synthesis and Application of Oligo(vinylamine)', *Macromol. Symp.*, 2000, **161**, 149

R443 H. Maeda and R. Kakehashi, 'Effects of Protonation on the Thermodynamic Properties of Alkyl Dimethylamine Oxides', *Adv. Colloid Interface Sci.*, 2000, **88**, 275

R444 S. Magazu, 'NMR, Static and Dynamic Light and Neutron Scattering Investigations on Polymeric Aqueous Solutions', *J. Mol. Struct.*, 2000, **523**, 47

R445 G. Malandrinos, K. Dodi, M. Louloudi and N. Hadjiliadis, 'On the Mechanism of Action of Thiamin Enzymes in the Presence of Bivalent Metal Ions', *J. Inorg. Biochem.*, 2000, **79**, 21

R446 A. K. Malik and W. Faubel, 'A Review of Capillary Electrophoretic Separations and their Studies by Nuclear Magnetic Resonance', *J. Capillary Electrophor. Microchip Technol.*, 1999, **6**, 97

R447 P. T. Manoharan and G. V. R. Chandramouli, 'Evolution of Magnetic Resonance Spectroscopy', *PINSA-A: Proc. Indian. Natl. Sci. Acad., Part A*, 1999, **65**, 613

R448 L. A. Marky and D. W. Kupke, 'Enthalpy - Entropy Compensations in Nucleic Acids: Contribution of Electrostriction and Structural Hydration', *Methods Enzymol.*, 2000, **323**, 419

R449 A. F. Martins, 'Measurement of Viscoelastic Coefficients for Nematic Mesophases Using Magnetic Resonance', *EMIS Datarev. Ser.*, 2000, **25**, 405

R450 N. J. Mathers, X. A. Mao, Z. H. Xu, P. G. Saffigna, S. J. Berners-Price and M. C. S. Perera, 'Recent Advances in the Application of ^{13}C and ^{15}N NMR Spectroscopy to Soil Organic Matter Studies', *Aust. J. Soil Res.*, 2000, **38**, 769

R451 K. H. Mayo, 'Recent Advances in the Design and Construction of Synthetic Peptides: For the Love of Basics or Just for the Technology of it', *Trends Biotechnol.*, 2000, **18**, 212

R452 I. K. McDonald, S. C. Holmes, K. J. Young, J. S. Vyle, T. J. Pickering and J. A. Grasby, 'Functional Group Mutagenesis of the Hairpin Ribozyme', *Collect. Symp. Ser.*, 1999, **2**, 306

R453 K. D. McReynolds and J. Gervay-Hague, 'Examining the Secondary Structures of Unnatural Peptides and Carbohydrate-Based Compounds Utilizing Circular Dichroism', *Tetrahedron: Asymmetry*, 2000, **11**, 337

R454 M. S. Meier, H. P. Spielmann, R. C. Haddon, R. G. Bergosh, M. E. Gallagher, M. A. Hamon and B. R. Weedon, 'Reactivity, Spectroscopy, and Structure of Reduced Fullerenes', *Carbon*, 2000, **38**, 1535

R455 S. C. J. Meskers and H. P. J. M. Dekkers, 'Enantioselective Quenching of Luminescence: Molecular Recognition of Chiral Lanthanide Complexes by Biomolecules in Solution', *J. Phys. Chem. A*, 2001, **105**, 4589

R456 M. Michalik, M. Hein and M. Frank, 'NMR Spectra of Fluorinated Carbohydrates', *Carbohydr. Res.*, 2000, **327**, 185

R457 L.-J. Ming, 'NMR Studies of Paramagnetic Multinuclear Metalloproteins', *Trends Inorg. Chem.*, 1998, **5**, 205

R458 S. Miyajima, 'Measurement of Translational Diffusion in Nematics', *EMIS Datarev. Ser.*, 2000, **25**, 457

R459 H. E. Moller, K. Ullrich and J. Weglage, 'In Vivo Proton Magnetic Resonance Spectroscopy in Phenylketonuria', *Eur. J. Pediatr.*, 2000, **159**, S121

R460 G. T. Montelione, D. Zheng, Y. J. Huang, K. C. Gunsalus and T. Szyperski, 'Protein NMR Spectroscopy in Structural Genomics', *Nat.Struct. Biol.*, 2000, **7**, 982

R461 K. Morikawa and M. Shirikawa, 'Three-Dimensional Structural View of Damaged-DMA Recognition: T4 Endonuclease V, E. coli Vsr. Protein, and Human Nucleotide Excision Repair Factor XPA', *Mutat. Res.*, 2000, **460**, 257

R462 Y. Morishima, 'Self-Assembling Amphiphilic Polyelectrolytes and their Nanostructures', *Chin. J. Polym. Sci.*, 2000, **18**, 323

R463 T. Moriya and K. Ueda, 'Spin Fluctuations and High Temperature Superconductivity', *Adv. Phys.*, 2000, **49**, 555

R464 B. A. Morrow and I. D. Gay, 'Infrared and NMR Characterization of the Silica Surface', *Surfactant Sci. Ser.*, 2000, **90**, 9

R465 B. Mulloy and M. J. Forster, 'Conformation and Dynamics of Heparin and Heparin Sulfate', *Glycobiology*, 2000, **10**, 1147

R466 H. Murai, S. Tero-Kubota and S. Yamauchi, 'Pulsed and Time-Resolved EPR Studies of Transient Radicals, Radical Pairs and Excited States in Photochemical Systems', *Electron Paramagn. Reson.*, 2000, **17**, 130

R467 P. Mustarelli, 'The NMR Information on Phosphate Glasses: A Review', *Phosphorus Res. Bull.*, 1999, **10**, 25

R468 K. Nagashima and F. D. Blum, 'Adsorption and Dynamics of Sodium Alkylbenzenesulfonates on Alumina', *Colloids Surf., A*, 2001, **176**, 17

R469 M. Nakahara, N. Matubayasi, C. Wakai and Y. Tsujino, 'Structure and Dynamics of Water: From Ambient to Supercritical', *J. Mol. Liq.*, 2001, **90**, 75

R470 H. Nakazawa, 'The Chemistry of Transition Metal Complexes Containing a Phosphenium Ligand', *J. Organomet. Chem.*, 2000, **611**, 349

R471 R. Neugart, 'Properties of Halo Nuclei Measured by Laser and β-NMR Spectroscopy', *Hyperfine Interact.*, 2000, **127**, 101

R472 P. J. Nieuwenhuizen, J. G. Haasnoot and J. Reedijk, 'Raw Materials and Applications: Model Compound Vulcanization – an Established Technique for the Next Century', *Kautsch. Gummi Kunstst.*, 2000, **53**, 144

R473 K. Nishinari, 'Konjac Glucomannan', *Dev. Food Sci.*, 2000, **41**, 309

R474 A. Nordon, C. A. McGill and D. Littlejohn, 'Process NMR Spectroscopy', *Analyst (Cambridge, U.K.)*, 2001, **126**, 260

R475 O. Nureki, S.-i. Sekine, S. Fukai, M. Inoue, I. Kim, N. Handa, T. Ito, D. G. Vassylyev, Y. Muto and S. Yokoyama, 'Interactions of Multidomain Protein and RNA', *Front. Sci. Ser.*, 2000, **31**, 147

R476 C. O'Driscoll, 'Stretching [of Polymers] – the Truth', *Chem. Br.*, 2000, **36**, 20

R477 F. Ooms, S. Jegham, P. George, F. Durant and J. Wouters, 'Molecular Interaction between Reversible MAO-A Inhibitors and the Enzyme: Application to Aryloxazolidinone, a Prototype Series', *Neurobiology (Budapest)*, 2000, **8**, 81

R478 F. Ozawa, 'The Chemistry of Organo(silyl)platinum(II) Complexes Relevant to Catalysis', *J. Organomet. Chem.*, 2000, **611**, 332

R479 M. Ozawa, Y. Sano and Y. Tanaka, 'CMPO-TRUEX Process and its Application in the Separation of Actinides from High-Level Liquid Wastes', *Miner. Process. Extr. Metall. Rev.*, 2000, **21**, 249

R480 N. Pant, D. C. Jain, R. S. Bhakuni and R. P. Sharma, 'Polyhydroxy Alkaloids from Plants: NMR Shielding Behavior', *Indian J. Chem., Sect.B: Org. Chem. Incl. Med. Chem.*, 2000, **39B**, 483

R481 G. F. Pauli, 'qNMR - a Versatile Concept for the Validation of Natural Product Reference Compounds', *Phytochem. Anal.*, 2001, **12**, 28

R482 P. L. Pedersen, Y. H. Ko and S. Hong, 'ATP Synthases in the Year 2000: Evolving Views about the Structures of these Remarkable Enzyme Complexes', *J. Bioenerg. Biomembr.*, 2000, **32**, 325

R483 M. Pelecanou, K. Chryssou and C. I. Stassinopoulou, 'Trends in NMR Chemical Shifts and Ligand Mobility of TcO(V) and ReO(V) Complexes with Aminothiols', *J. Inorg. Biochem.*, 2000, **79**, 347

R484 P. Pelupessy and E. Chiarparin, 'Hartmann-Hahn Polarization Transfer in Liquids: An Ideal Tool for Selective Experiments', *Concepts Magn. Reson.*, 2000, **12**, 103

R485 S. X. Peng, 'Hyphenated HPLC-NMR and its Applications in Drug Discovery', *Biomed. Chromatogr.*, 2000, **14**, 430

R486 A. S. Peregudov and D. N. Kravtsov, 'Electronegativity and Chemical Hardness of Organoelement Groups', *Appl. Organomet. Chem.*, 2001, **15**, 27

R487 K. Pervushin, 'Imapct of Transverse Ralaxation Optimized Spectroscopy (TROSY) on NMR as a Technique in Structural Biology', *Q. Rev. Biophys.*, 2000, **33**, 161

R488 K. F. Petersen and G. I. Shulman, 'Hepatic Glycogen Metabolism in Type 1 Diabetic and Glycokinase-Deficient Subjects', *Front. Diabetes*, 2000, **15**, 153

R489 K. E. Peuschel, 'Pitfalls in Prion Research', *Med. Hypotheses*, 2000, **54**, 698

R490 B. L. Philips, 'NMR Spectroscopy of Phase Transitions in Minerals', *Rev. Mineral. Geochem.*, 2000, **39**, 203

R491 J. C. Philips, 'Dual Nature of Molecular Glass Transitions', *Ser. Dir. Condens. Matter Phys.*, 2000, **17**, 53

R492 T. Pietrass, 'Optically Polarized ^{129}Xe in Magnetic Resonance Techniques', *Magn. Reson. Rev.*, 2000, **17**, 263

R493 C. Piguet, C. Edder, S. Rigault, G. Bernardinelli, J.-C. G. Bunzli and G. Hopfgartner, 'Isolated d-f Pairs in Supramolecular Complexes with Tunable Structural and Electronic Properties', *Dalton*, 2000, **22**, 3999

R494 E. P. Pioro, 'Proton Magnetic Resonance Spectroscopy (^{1}H-MRS) in ALS', *Amyotrophic Lateral Scler. Other Mot. Neuron Disord.*, 2000, **1**, S7

R495 M. B. Pratt, S. A. Forman, S. S. Husain, B. Dubois, M. A. Kloczewiak, G. H. Addona, J. Yu, D. C. Chiara, J. B. Cohen and K. W. Miller, 'Sites of Anesthetic Action on the Nicotinic Acetylcholine Receptor', *Prog. Anesth. Mech.*, 2000, **6**, 285

R496 J. H. Prestegard, 'Orientational Constraints of Polypeptide Folds: The Role of NMR in Structural Genomics', *Polym. Prepr. (Am. Chem. Soc., Div. Polym. Chem.)* [computer optical disk], 2001, **42**, 60

R497 T. B. Price, D. L. Rothman and R. G. Shulman, 'NMR of Glycogen in Exercise', *Proc. Nutr. Soc.*, 1999, **58**, 851

R498 R. S. Prosser and I. V. Shiyanovskaya, 'Lanthanide Ion Assisted Magnetic Alignment of Model Mambranes and Macromolecules', *Concepts Magn. Reson.*, 2001, **13**, 19

R499 J. Qin, Y. Yang, A. Velyvis and A. Gronenborn, 'Molecular Views of Redox Regulation: Three-Dimensional Structures of Redox Regulatory Proteins and Protein Complexes', *Antioxid. Redox Signaling*, 2000, **2**, 827

R500 D. L. Rabenstein, 'NMR Spectroscopy: Past and Present', *Anal. Chem.*, 2001, **73**, 214A

R501 P. Raghunathan, 'Magnetic Resonance Imaging and Spectroscopy in Biomedicine', *PINSA-A: Proc. Indian. Natl. Sci. Acad., Part A*, 1999, **65**, 699

R502 J. W. Rathke, K. W. Kramarz, R. J. Klingler, M. J. Chen, D. E. Fremgen and R. E. Gerald II, 'Carbonylation with Cobalt Catalysts', *Trends Organomet. Chem.*, 1999, **3**, 201

R503 H. Rauvala, H. J. Huttunen, C. Fages, M. Kaksonen, T. Kinnunen, S. Imai, E. Raulo and I. Kilpelainen, 'Heparin-Binding Proteins HB-GAM (Pleiotrophin) and Amphoterin in the Regulation of Cell Motility', *Matrix Biol.*, 2000, **19**, 377

R504 W. Richter and W. S. Warren, 'Intermolecular Multiple Quantum Coherence in Liquids', *Concepts Magn. Reson.*, 2000, **12**, 396

R505 P. C. Riedi, Cz. Kapusta, Y. Kohori and G. J. Tomka, 'Volume Dependence of NMR of Ordered Correlated Electron Systems', *Hyperfine Interact.*, 2000, **128**, 167

R506 R. Riek, K. Pervushin and K. Wuthrich, 'TROSY and CRINEPT: NMR with Large Molecular and Supramolecular Structures in Solution', *Trends Biochem. Sci.*, 2000, **25**, 462

R507 R. Righini, 'Rotational Diffusion of Liquid Crystals in the Nematic Phases', *EMIS Datarev. Ser.*, 2000, **25**, 464

R508 J. Rikovska and N. J. Stone, 'Beta-NMR/ON On-Line at the NICOLE Facility, ISOLDE. Recent Magnetic Moment Studies Near Double Magic ^{68}Ni', *Hyperfine Interact.*, 2000, **129**, 131

R509 J. A. Ripmeester, 'Hydrate Research - From Correlations to a Knowledge – Based Discipline the Importance of Structure', *Ann. N.Y. Acad. Sci.*, 2000, **912**, 1

R510 G. C. K. Roberts, 'Applications of NMR in Drug Discovery', *Drug Discovery Today*, 2000, **5**, 230

R511 M. Roden, K. F. Petersen and G. I. Shulman, 'Nuclear Magnetic Resonance Studies of Hepatic Glucose Metabolism in Humans', *Recent Prog. Horm. Res.*, 2001, **56**, 219

R512 D. Rojo, K. Suetomi and J. Navarro, 'Structural Biology of Chemokine Receptors', *Biol. Res.*, 1999, **32**, 263

R513 R. M. Romano and C. O. Della Vedova, 'N-Sulfinylimine Compounds, R-N:S:O: a Chemistry Family with Strong Temperament', *J. Mol.-Struct.*, 2000, **522**, 1

R514 J. P. Rosenbusch, 'Folding Patterns of Membrane Proteins: Diversity and the Limitations of their Prediction', *Novartis Found. Symp.*, 1999, **225**, 207

R515 J. P. Rosenbusch, A. Lustig, M. Grabo, M. Zulauf and M. Regenass,

'Approaches to Determining Membrane Protein Structures to High Resolution: Do Selections of Subpopulations Occur?', *Micron 2001*, 2000, **32**, 75

R516 L. Rosendahl, A. Rudbeck, A. M. Scharff and P. Mouritzen, 'Assimilation of Fixed Nitrogen Studied by Membrane Vesicle Transport and in Vivo ^{15}N-NMR Spectroscopy in Pea', *Curr. Plant Sci. Biotechnol. Agric.*, 2000, **38**, 351

R517 B. D. Ross, 'Real or Imaginary? Human Metabolism through Nuclear Magnetism', *IUBMB Life*, 2000, **50**, 177

R518 R. Rothchild, 'NMR Methods for Determination of Enantiomeric Excess', *Enantiomer*, 2000, **5**, 457

R519 R. R. Ruan and P. L. Chen, 'Nuclear Magnetic Resonance Techniques in Cereal Chemistry Research', *Curr. Top. Cereal Chem.*, 1999, **2**, 1

R520 W. Runde, 'Spectroscopies for Environmental Studies of Actinide Species', *Los Alamos Sci.*, 2000, **26**, 412

R521 H. Sahm, L. Eggeling and A. A. De Graaf, 'Pathway Analysis and Metabolic Engineering in Corynebacterium Glutamicum', *Biol. Chem.*, 2000, **381**, 899

R522 H. R. Saibil, 'Conformational Changes Studied by Cryoelectron Microscopy', *Nat. Struct. Biol.*, 2000, **7**, 711

R523 H. R. Saibil, 'Macromolecular Structure Determination by Cryoelectron Microscopy', *Acta Crystallogr., Sect.D: Biol. Crystallogr.*, 2000, **D56**, 1215

R524 C. R. Sanders and K. Oxenoid, 'Customizing Model Membranes and Samples for NMR Spectroscopic Studies of Complex Membrane Proteins', *Biochim. Biophys. Acta*, 2000, **1508**, 129

R525 L. K. Sanders, W. D. Arnold and E. Oldfield, 'NMR, IR, Mössbauer and Quantum Chemical Investigations of Metalloporphyrins and Metalloproteins', *J. Porphyrins Phthalocyanines*, 2001, **5**, 323

R526 A. V. S. Sarma and A. C. Kunwar, 'Pharmaceutical Application of NMR Spectroscopy', *PINSA-A: Proc. Indian Natl. Sci. Acad., Part A*, 1999, **65**, 655

R527 D. J. Schibli and H. J. Vogel, 'Structural Studies of Lactoferricin B and its Antimicrobial Active Peptide Fragments', *Int. Congr. Ser.*, 2000, **1195**, 27

R528 M. Schnitzer, 'A Lifetime Perspective on the Chemistry of Soil Organic Matter', *Adv. Agron.*, 2000, **68**, 1

R529 M. D. Schonemann, A. K. Ryan, L. Erkman, R. J. McEvilly, J. Bermingham and M. G. Rosenfeld, 'POU Domain Factors in Neural Development', *Adv. Exp. Med. Biol.*, 1998, **449**, 39

R530 T. Schopke, 'Non-NMR Methods for Structure Elucidation of Saponins', *Proc. Phytochem. Soc. Eur.*, 2000, **45**, 95

R531 K. B. Schowen, H.-H. Limbach, G. S. Denisov and R. L. Schowen, 'Hydrogen Bonds and Proton Transfer in General Catalytic Transition-State Stabilization in Enzyme Catalysis', *Biochim. Biophys. Acta*, 2000, **1458**, 43

R532 J. Schraml, 'Derivatives of Hydroxamic Acids', *Appl. Organomet. Chem.*, 2000, **14**, 604

R533 H.-R. Schulten and P. Leinweber, 'New Insights into Organic-Mineral Particles: Composition, Properties and Models of Molecular Structure', *Biol. Fertil. Soils*, 2000, **30**, 399

R534 J. E. Scott, 'Secondary and Tertiary Structures in Solutions of Hyaluronan and Related "Shape Module" Anionic Glykosaminoglycans', *Int. Congr. Ser.*, 2000, **1196**, 11

R535 B. N. Shelimov, J.-F. Lambert, M. Che and B. Didillon, 'Molecular-Level Studies of Transition Metal – Support Interactions During the First Steps of Catalysts Preparation: Platinum Speciation in the Hexachloroplatinate/Alumina System', *J. Mol. Catal. A: Chem.*, 2000, **158**, 91

R536 K. Shimizu, 'An Overview on Metabolic Systems Engineering Approach and its Future Perspectives for Efficient Microbial Fermentation', *J. Chin. Inst. Chem. Eng.*, 2000, **31**, 429

R537 H. Shinohara, 'Endohedral Matallofullerenes', *Rep. Prog. Phys.*, 2000, **63**, 843

R538 R. G. Shulman and D. L. Rothman, 'The Glycogen Shunt in Exercising Muscle: A Role for Glycogen in Muscle Energetics and Fatigue', *Proc. Natl. Acad. Sci. U.S.A.*, 2001, **98**, 457

R539 G. I. Shulman, 'Cellular Mechanisms of Insulin Resistance', *J. Clin.-Invest.*, 2000, **106**, 171

R540 L. A. "Pete" Silks, R. Wu, R. B. Dunlap and J. D. Odom., 'Synthesis and Applications of Chiral Selones', *Phosphorus, Sulfur Silicon Relat. Elem.*, 1998, **136, 137 & 138**, 209

R541 G. J. Simpson, 'New Tools for Surface Second-Harmonic Generation', *Appl. Spectrosc.*, 2001, **55**, 16A

R542 N. J. Skelton and W. J. Chazin, 'Solution Structure Determination of Proteins by Nuclear Magnetic Resonance Spectroscopy', *Drugs Pharm. Sci.*, 2000, **101**, 683

R543 J. S. Soares and R. B. Innis, 'Brain Imaging Findings in Bipolar Disorder', *Med. Psychiatry*, 2000, **15**, 227

R544 L. Sobczyk, 'NMR Studies on Hydrogen Bonding and Proton Transfer in Mannich Bases', *Appl. Magn. Reson.*, 2000, **18**, 47

R545 K. Sohlberg, S. J. Pennycook and S. T. Pantelides, 'The Bulk and Surface Structure of γ-Alumina', *Chem. Eng. Commun.*, 2000, **181**, 107

R546 L. Sokoloff, 'Historical Review of Developments in the Field of Cerebral Blood Flow and Metabolism', *Keio Univ. Symp. Life Sci. Med.*, 2000, **6**, 3

R547 D. Solis, J. Jimenez-Barbero, H. Kaltner, A. Romero, H.-C. Siebert, C.-W. von der Lieth and H.-J. Gabius, 'Towards Defining the Role of Glycans as Hardware in Information Storage and Transfer: Basic Principles, Experimental Approaches and Recent Progress', *Cells Tissues Organs*, 2001, **168**, 5

R548 S. Spange, 'Silica Surface Modification by Cationic Polymerization and Carbenium Intermediates', *Prog. Polym. Sci.*, 2000, **25**, 781

R549 H. W. Spiess, 'Multidimensional Solid State NMR Studies of Complex Dynamics in Polymers', *AIP Conf. Proc.*, 2000, **519**, 33

R550 O. Spring, 'Chemotaxonomy Based on Metabolites from Glandular Trichomes', *Adv. Bot. Res.*, 2000, **31**, 153

R551 M. Springborg, 'Density-Functional Theory', *Chem. Modell.*, 2000, **1**, 306

R552 A. J. Stanley, J. W. Pettegrew and M. S. Keshavan, 'Magnetic Resonance Spectroscopy in Schizophrenia: Methodological Issues and Findings – Part I', *Biol. Psychiatry*, 2000, **48**, 357

R553 D. A. Stead, 'Current Methodologies for the Analysis of Aminoglycosides', *J. Chromatogr., B: Biomed. Sci. Appl.*, 2000, **747**, 69

R554 J. F. Stebbins, J. V. Oglesby and S. K. Lee, 'Oxygen Sites in Silicate Glasses: A New View from Oxygen-17 NMR', *Chem. Geol.*, 2001, **174**, 63

R555 M. J. Steward and V. Steenkamp, 'The Biochemistry and Toxicity of Atractyloside. A Review', *Ther.Drug Monit.*, 2000, **22**, 641

R556 R. Sun, P. Rowlands and J. M. Lawther, 'Rapid Isolation and Physicochemical Characterization of Wheat Straw Lignins', *Recent Res. Dev. Agric. Food Chem.*, 2000, **4**, 1

R557 C. Szantay Jr. and A. Demeter, 'NMR Spectroscopy', *Prog. Pharm. Biomed. Anal.*, 2000, **4**, 109

R558 G. Tarkanyi, 'NMR Spectroscopy', *Prog. Pharm. Biomed. Anal.*, 2000, **4**, 562

R559 G. Tastevin, 'Optically Polarized Helium-3 for NMR Imaging in Medicine', *Phys. Ser., T*, 2000, **T86**, 46

R560 G. Te Velde, F. M. Bickelhaupt, E. J. Baerends, G. C. Fonseca, S. J. A. Van Gisbergen, J. G. Snijders and T. Ziegler, 'Chemistry with ADF', *J. Comput. Chem.*, 2001, **22**, 931

R561 B. Thony, G. Auerbach and N. Blau, 'Tetrahydrobiopterin Biosynthesis, Regeneration and Functions', *Biochem. J.*, 2000, **347**, 1

R562 A. Thorpe, 'Interpreting NMR Spectra', *Chem. Rev. (Deddington, U.K.)*, 2000, **10**, 10

R563 R. Tian and J. S. Ingwall, 'The Molecular Energetics of the Failing Heart from Animal Models – Small Animal Models', *Heart Failure Rev.*, 1999, **4**, 245

R564 A. M. Torres and P. W. Kuchel, 'The Platypus and its Venom', *Biochemist*, 2000, **22**, 33

R565 Y. Tsuji and Y. Obora, 'Structure and Fluxional Behavior of Platinum and Palladium Complexes Having M-Si or M-Sn (M=Pt or Pd) Inter-Element Linkages', *J. Organomet. Chem.*, 2000, **611**, 343

R566 V. V. Turov and R. Leboda, '^{1}H-NMR Spectroscopy of Adsorbed Molecules and Free Surface Energy of Carbon Adsorbents', *Chem. Phys. Carbon*, 2001, **27**, 67

R567 G. Tzimas, 'Recent Advances in the Application of Instrumental Methods of Analysis in Toxicology', *Pharmakeutike*, 2000, **13**, 32

R568 L. M. K. Vandersypen, C. S. Yannoni and I. L. Chuang, 'Liquid State

NMR Quantum Computing', *Los Alamos Natl.Lab., Prepr. Arch., Quantum Phys.* [preprint] 20 Dec 2000,1, arXiv:quant-ph/0012108, Avail. URL:http://xxx.lanl.gov/pdf/quant-ph/0012108

R569 C. P. M. van Mierlo and E. Steensma, 'Protein Folding and Stability Investigated by Fluorescence, Circular Dichroism (CD), and Nuclear Magnetic Resonance (NMR) Spectroscopy: The Flavodoxin Story', *J. Biotechnol.*, 2000, **79**, 281

R570 M. Vasak, D. W. Hasler and P. Faller, 'Metal-Thiolate Clusters in Neuronal Growth Inhibitory Factor (GIF)', *J. Inorg. Biochem.*, 2000, **79**, 7

R571 C. Vigano, L. Manciu, F. Buyse, E. Goormaghtigh and J.-M. Ruysschaert, 'Attenuated Total Reflection IR Spectroscopy as a Tool to Investigate the Structure, Orientation and Tertiary Structure Changes in Peptides and Membrane Proteins', *Biopolymers*, 2001, **55**, 373

R572 M. Von Kienlin, 'Methodological Advances in Cardiac ^{31}P-MR Spectroscopy', *Magn. Reson. Mater. Phys., Biol. Med.*, 2000, **11**, 36

R573 A. G. J. Voragen, P. J. H. Daas and H. A. Schols, 'Enzymes as Tools for Structural Studies of Pectins', *Proc. Phytochem. Soc. Eur.*, 2000, **44**, 129

R574 V. K. Voronov, 'The Use of NMR for Solving the Problems of Quantum Computers', *Los Alamos Natl. Lab., Prepr. Arch., Quantum Phys.* [preprint] 2 Feb 2001, 1, Avail. URL: http://xxx.lanl.gov/ps/quant-ph/0102021

R575 B. A. Wallace, 'X-Ray Crystallographic Structures of Gramicidin and their Relation to the Streptomyces Lividans Potassium Channel Structure', *Novartis Found Symp.*, 1999, **225**, 23

R576 A. J. Wand, J. L. Urbauer, M. R. Ehrhardt and A. L. Lee, 'NMR Studies of Protein-Peptide Complexes: Examples from the Calmodulin System', *Drugs Pharm. Sci.*, 2000, **101**, 727

R577 G. Wider, 'Structure Determination of Biological Macromolecules in Solution Using Nuclear Magnetic Resonance Spectroscopy', *BioTechniques,* 2000, **29**, 1278

R578 C. R. Wilson, J.-M. Sauer and S. B. Hooser, 'Taxines: A Review of the Mechanism and Toxicity of Yew (Taxus Spp.) Alkaloids', *Toxicon*, 2001, **39**, 175

R579 I. D. Wilson, 'Multiple Hyphenation of Liquid Chromatography with Nuclear Magnetic Resonance Spectroscopy, Mass Spectrometry and Beyond', *J. Chromatogr., A*, 2000, **892(1+2)**, 315

R580 I. D. Wilson, L. Griffiths, J. C. Lindon and J. K. Nicholson, 'HPLC/NMR and Related Hyphanated NMR Methods', *Prog. Pharm. Biomed. Anal.*, 2000, **4**, 299

R581 D. E. Woessner, 'The Early Days of NMR in the Southwest', *Concepts Magn. Reson.*, 2001, **13**, 77

R582 J.-L. Wolfender, K. Ndjoko and K. Hostettmann, 'The Potential of LC-NMR in Phytochemical Analysis', *Phytochem. Anal.*, 2001, **12**, 2

R583 S. Woodward, 'Decoding the "Black Box" Reactivity that is Organocuprate Conjugate Addition Chemistry', *Chem. Soc. Rev.*, 2000, **29**, 393

R584 J. Workman Jr., K. E. Creasy, S. Doherty, L. Bond, M. Koch, A. Ullman and D. J. Veltkamp, 'Process Analytical Chemistry', *Anal. Chem.*, 2001, **73**, 2705

R585 R. Wu, C. C. Orji, R. Michalczyk, J. G. Schmidt, Z. Li, E. M. Stocking, D. A. Ashburn, J. A. Kelly, O. Khalsa, R. A. Martinez, S. V. S. Mariappan, C. J. Unkefer and L. A. "Pete" Silks, 'Synthesis and Application of Labeled Nucleic Acids, Amino Acids and Carbohydrates', *Recent Res. Dev. Org. Bioorg. Chem.*, 1999, **3**, 1

R586 P. Wzietek, S. Lefebvre, H. Mayaffre, S. Brown, C. Bourbonnais, D. Jerome, C. Meziere and P. Batail, 'Two-Dimensional Organic Superconductors Studied by NMR under Pressure', *Hyperfine Interact.*, 2000, **128**, 183

R587 Z. Xia, G. Ying, A. L. Hansson, H. Karlsson, Y. Xie, A. Bergstrand, J. W. DePierre and L. Nassberger, 'Antidepressant-Induced Lipidosis with Special Reference to Tricyclic Compounds', *Prog. Neurobiol. (Oxford)*, 2000, **60**, 501

R588 Y. Yamamoto and K.-Y. Akiba, 'The Chemistry of Group 15 Element Porphyrins Bearing Element-Carbon Bonds: Synthesis and Properties', *J. Organomet. Chem.*, 2000, **611**, 200

R589 L. Yang, 'Surface Composition and Structural Stability of Bimetallic Catalysts', *Curr. Top. Catal.*, 1999, **2**, 59

R590 E. Yashima, 'Polysaccharide-Based Chiral Stationary Phases for High-Performance Liquid Chromatographic Enantioseparation', *J. Chromatogr., A*, 2001, **906**, 105

R591 T. Yoshida, T. Hatano, H. Ito and T. Okuda, 'Chemical and Biological Perspectives of Ellagitannin Oligomers from Medicinal Plants', *Stud. Nat. Prod. Chem.*, 2000, **23**, 395

R592 Z. Yu and R. A. Dahlgren, 'Evaluation of Methods for Measuring Polyphenols in Conifer Foliage', *J. Chem. Ecol.*, 2000, **26**, 2119

R593 M. Zenetti, S. Lomakin and G. Camino, 'Polymer Layered Silicate Nanocomposites', *Macromol. Mater. Eng.*, 2000, **279**, 1

R594 A. H. Zewail, 'Femtochemistry: Atomic-Scale Dynamics of the Chemical Bond Using Ultrafast Lasers (Nobel Lecture)', *Angew. Chem., Int. Ed.*, 2000, **39**, 2586

R595 H. Zhou, A. Vermeulen, F. M. Jucker and A. Pardi, 'Incorporating Residual Dipolar Couplings into the NMR Solution Structure Determination of Nucleic Acids', *Biopolymers*, 1999–2000, **52**, 168

R596 J. Zhou and N. Tan, 'Application of a New TLC Chemical Method for Detection of Cyclopeptides in Plants', *Chin. Sci. Bull.*, 2000, **45**, 1825

5 Reviews and Books in Foreign Languages

Chinese

R597 X. Chen and K.-L. Yong, 'Application of Analysis Techniques to Fermentation Bioprocess Monitoring', *Shanghai Daxue Xuebao, Ziran Kexueban*, 2000, **6**, 124

R598 Y.-g. Chen, '^{1}H NMR Spectroscopic Characteristics of Lignans from Plants of Schisandraceae', *Bopuxue Zazhi*, 2000, **17**, 427

R599 Z.-W. Chen and Z. Chen., 'Hyphenation of Supercritical Fluid Separation with Nuclear Magnetic Resonance and their Applications', *Guangpu Shiyanshi*, 2001, **18**, 139

R600 R.-J. Cheng and P.-Y. Chen., 'Electronic Structures of Metalloporphyrins - Applications of Paramagnetic Nuclear Magnetic Resonance Spectroscopy', *Huaxue*, 2000, **58**, 459

R601 J. Cui and C. Lin, 'Application of NMR in the Analysis of Enantiomeric Purity and its Absolute Configuration', *Guangxi Daxue Xuebao, Ziran Kexueban*, 1999, **24**, 296

R602 J. Gao, Y. Zhan and J. Zhu, 'Analytical Methods for Sulfides in Liquefied Petroleum Gas', *Fenxi Yiqi*, 2001, **1**, 32

R603 X.-w. Han, W.-p. Zhang and X.-h. Bao, 'Methods for the Investigation of Solid Catalysts. 7. In Situ MAS NMR Method (Part 1)', *Shiyou Huagong*, 2000, **29**, 884

R604 C.-H. Hsu, 'Determination of Tertiary Structure of Carbohydrate Molecules', *Huaxue*, 2000, **58**, 323

R605 H. Li, S.-C. Zhang and B. R. Kowalski, 'Advance in Second Order Calibration', *Jisuanji Yu Yingyong Huaxue*, 200, **17**, 8

R606 W.-c. Lin and L.-s. Kan, 'DNA Triplex', *Huaxue*, 2000, **58**, 661

R607 L.-S. Ling, Z.-K. He, F.-W. Wu, Q.-Y. Luo and Y.-E. Zeng, 'Progress of the Nucleic Acid Molecular "Light Switch"', *Gaodeng Xuexiao Huaxue Xuebao*, 2000, **21**, 527

R608 X. Shao, C. Pang and L. Sun, 'Wavelet Transform and Signal Processing in Analytical Chemistry', *Huaxue Jinzhan*, 2000, **12**, 233

R609 B. Su and Z. Jia, 'Structure Elucidation of Iridoil Glycosides by Spectroscopic Technique', *Lanzhou Daxue Xuebao, Ziran Kexueban*, 2000, **36**, 58

R610 X. Wang, Z. Zong, Z. Qin, X. Wei and L. He, 'Progress of Organic Spectroscopy Applied to Coal Molecular Chemistry', *Meitan Zhuanhua*, 2001, **24**, 5

R611 Z. Wang, Y. Zhao, Y. Chen and B. Ma, 'Triterpenoid Compounds of Prunella Genus and their Features of ^{13}C NMR Spectroscopy, *Zhongguo Zhongyao Zazhi*, 2000, **25**, 583

R612 C. Yang and Y. Si, 'Nuclear Magnetic Resonance Spectroscopy in Drug Metabolism Study', *Yaowu Fenxi Zazhi*, 1999, **19**, 422

R613 S. Yu, F. Chen and M. Wang, 'Calibration of Elemantal Analysis Data for Structure Determination of New Organic Compounds', *Huaxue Tongbao*, 2001, **2**, 124

R614 D.-w. Zhang, L.-w. Guo, X. Gao and S.-h. Wu, 'Powerful Tool for the Structural Characterisation of [60]Fullerene and its Derivatives - ^{3}He NMR', *Youji Huaxue*, 2000, **20**, 719

R615 L.-J. Zhang, 'Progress in Nuclear Magnetic Resonance', *Hebei Shifan Daxue Xuebao, Ziran Kexueban*, 2000, **24**, 224

R616 M. Zhang and P. Yang, 'Determination of the Secondary Structure of Proteins by Nuclear Magnetic Resonance', *Huaxue Tongbao*, 2000, **12**, 26

R617 R. Zhao, Q. Gu and H. Guan, 'Study on Progress of Extraction and Analysis Methods for Peptides', *Zhongguo Haiyang Yaowu*, 2000, **19**, 48

R618 J.-Y. Zhou, W.-M. Chen and Q.-C. Fang, 'The ^{13}C-NMR Features of Natural Taxane Diterpenoid Compounds', *Zhiwu Xuebao*, 2000, **42**, 1

French

R619 B. Garrigues, 'Conformation of Thiophene Derivatives', *Roum. Chem. Q. Rev.*, 2000, **8**, 55

R620 M. Martin and G. Martin, 'Frauds in Food Products: A Challenge for Analytical Chemistry', *Actual. Chim.*, 2000, **11**, 18

German

R621 A. Golloch and C. Luhr, 'Amber Analysis', *Anal.-Taschenb.*, 2000, **21**, 179

R622 A. De Graaf, 'In Vivo NMR Spectroscopy. Determination of Metabolic Activity in Living Microorganisms', *BIOspektrum*, 2000, **6**, 370

R623 F. H. Frimmel and C. Zwiener, 'Trends in Environmental Analysis', *GIT Labor-Fachz.*, 2000, **44**, 1142

R624 U. Hahn, 'GBM Promotion Prize of the Knoll AG 2000: Multi-Dimensional NMR Studies on the Human Proteins MDM2 and MIA', *BIOspectrum*, 2001, **7**, 55

R625 T. Maurer, 'TROSY and Other NMR Methods for Screening Biological Active Materials', *Nachr. Chem.*, 2000, **48**, 1336

R626 A. Preiss and K. Levsen, 'Use of High-Peformance Liquid Chromatography Complex with Nuclear Resonance Spectroscopy (HPLC/NMR) and with Mass Spectrometry (HPLC/MS) for Analysis of Complex Water Samples', *Biol. Abwasserreinig.*, 1999, **11**, 169

R627 G. Schilling, 'Determination of Enantiomers of Free Amino Acids Using Pd Complexes via NMR', *GIT Labor-Fachz.*, 2000, **44**, 1469

R628 H. F. Schroder, 'Possibilities for Determining Individual Haloorganic Substances', *ATV-DVWK-Schriftenr.*, 2000, **18**, 159

R629 L. F. Trueb, 'From Micro- to Nanotechnology. Machines and Systems in the Micro- and Nanometer Range', *Naturwiss. Rundsch.*, 2000, **53**, 329

Greek

R630 T. Mauromoustakos, I. Daliani, A. Kolokouris and E. Theodoro-

poulou, 'Use of Solid State NMR Spectroscopy in Archaeometry', *Chem. Chron., Genike Ekdose*, 2000, **62**, 41

R631 T. Mavromoustakos, I. Daliani, P. Zoumboulakis and A. Kolocouris, 'Solid State Nuclear Magnetic Resonance. A Valuable Tool in Pharmaceutical Chemistry', *Pharmakeutike*, 2000, **13**, 37

R632 M. Sotiris and A.-V. Ekaterini, 'The Contribution of Simple NMR Spectroscopy Techniques in the Study of Supramolecular Interactions of Cyclodextrins with Various Drugs', *Pharmakeutike*, 1999, **12**, 79

Hungarian

R633 S. Gorog, 'Forty Years in Pharmaceutical Analysis', *Magy. Kem. Foly.*, 2000, **106**, 51

R634 E. B. Hethelyi, I. Koczka and J. Bernath, 'Chemotaxonomical Varieties of Tanacetum Vulgare L. in Hungary and Canada', *Olaj, Szappan, Kozmet.*, 2000, **49**, 143

R635 K. Kanai, M. Feher, A. Lopata, B. Podanyi, I. Novik, E. Susan, I. Hermecz and P. Aranyi, 'Molecular Modeling and CoMFA Studies on Prolyl Endopeptidase Inhibitors', *Acta Pharm. Hung.*, 1999, **69**, 240

R636 L. Toke, 'Supramolecular Chemistry, Crown Ethers', *Magy. Kem. Foly.*, 2000, **106**, 277

Italian

R 637 S. Aime, M. Botta, L. Frullano and E. Terreno, 'Contrast Media for MRI: State of the Art and Prospects', *Chim. Int. (Milan)*, 2000, **82**, 55

R638 L. Conte, R. Bortolomeazzi, S. Moret, L. Pizzale and S. Vichi, 'Current Developments in the Field of Evaluation of Identity, Quality and Stability of Food Lipids', *Riv. Ital. Sostanze Grasse*, 2000, **77**, 431

R639 L. Pellicioli and F. Negroni, 'Vulcanization and Solid-State ^{13}C NMR Spectroscopy', *Ind. Gomma*, 2000, **44**, 37

Japanese

R640 K. Akasaka and H. Li, 'A Novel Picture of Protein from High Pressure NMR', *Tanpakushitsu Kakusan Koso*, 2001, **46**, 208

R641 M. Annaka, 'Determination of Diffusion Coefficients by NMR', *Maku*, 2000, **25**, 312

R642 K. Asai, 'Studies of Ferromagnetic Oxides with Ordered Double Perovskite Structure by Nuclear Probes', *KURRI-KR*, 2000, (KURRI-KR-49, Proceedings of the Specialist Research Meeting on New Developments in Solid State Physics with Probes of Radiations and Nuclei, 1999), 229

R643 S. Asai, 'High-Dimensional Structural Analysis of Plastic Moldings: Mesostructural Analysis', *Seikei Kako*, 2000, **12**, 710

R644 M. Demura, 'Binding Feature of Mastoparan Inducing Phase Change of Lipid Bilayers', *Seibutsu Butsuri*, 2001, **41**, 20

R645 H. Fujii, '^{1}H NMR of Kagome-Lattice Antiferromagnetic m-N-Alkylpyridinium α-Nitronyl Nitroxide (m-AlkylPYNN) Organic Radical Salts', *Bunssei Kenkyu*, 2000, **75**, 107

R646 N. Fujii, 'Maintenance and Performance Factors of Spectroscopic Instruments. V. Nuclear Magnetic Resonance', *Bunko Kenkyu*, 2000, **49**, 259

R647 T. Hasegawa, 'NMR Spin-Spin Network Analysis', *CACS Forum*, 1999, **19**, 29

R648 K. Hirayama, 'Structural Characterization of Immune Components; Immunoglobulin G and its Receptor', *J. Mass Spectrom. Soc. Jpn.*, 2000, **48**, 101

R649 K. Hirayama, 'Study of the Mechanism of Biological Systems Using Mass Spectrometry - from Proteome Analysis to Structural Biology', *J. Mass Spectrom. Soc. Jpn.*, 2000, **48**, 289

R650 H. Hiroaki, 'Bridging of Structure Biology and Drug Discovery by NMR', *Seibutsu Kogaku Kaishi*, 2000, **78**, 428

R651 T. Hirose, K. Naito and K. Taniguchi, 'Development of Sensing Agents Using Kemp's Triacid Derivatives for Metal Ions and Chiral Amines', *CACS Forum*, 2000, **20**, 58

R652 K. Ishimaru and E. Matsuura, 'Flavonoids and a Polyacetylene in Pratia Nummularia-Chemistry, Bio Activity Analysis and Biotechnology', *Foods Food Ingredients J. Jpn*, 2000, **186**, 33

R653 M. Isobe, M. Kuse, T. Fujii, H. Takahashi, K. Ohshima, H. Mori, J.-Y. Ahn and M. Tsukasa, 'Molecular Mechanisms of Bioluminescence of Symplectin, a Photoprotein from Okinawan Squid, Symplectoteuthis Oualaniensis L', *Tennen Yuki Kagobutsu Toronkai Koen Yoshishu*, 2000, **42**, 97

R654 M. Isobe, S. Suwan and T. Franz, 'Recent Progress in Ultramicroanalysis by LC-Q-TOF', *Jasco Rep.*, 2000, **42**, 1

R655 Y. Ito, T. Machi, N. Watanabe and N. Koshizuka, 'Nuclear Spin Lattice Relaxation by Ni Impurity in $YBa_2Cu_4O_8$', *Bussei Kenkyu*, 2000, **74**, 461

R656 M. Itoh, 'Orbital Order Using NMR and Observation of Charge Order', *Bussei Kenkyu*, 2000, **74**, 407

R657 F. Iwasaki, 'Future of Organic Crystal Chemistry', *Nippon Kessho Gakkaishi*, 2000, **42**, 304

R658 M. Katahira, 'Structure of Telomere-Sequence DNA/RNA-Binding Protein, hnRNP DO, and Transformation of DNA/RNA Quadruplex to a Single Strand by hnRNP DO', *Seibutsu Butsuri*, 2000, **40**, 326

R659 K. Kato, 'Structural Basis of the Interaction between Immunoglobulins and Fc Receptors Provided by NMR Spectroscopy', *Yakagaku Zasshi*, 2001, **121**, 345

R660 T. Kato, 'NMR Pulsed-Gradient Spin Echo of Surfactant Systems', *Nihon Yukagakkaishi*, 2000, **49**, 1173

R661 H. Kikuchi, 'Possibility of a Gapless Chiral State of Frustrated S=1 One-Dimensional Antiferromagnetic CaV_2O_4', *Bussei Kenkyu*, 2000, **75**, 143

R662 J. Kikuchi and S. Motoya, 'NMR of Spin Singlet System', *Bussei Kenkyu*, 2000, **74**, 331

R663 I. Kitagawa, T. Ishizu, K. Ohashi and H. Shibuya, 'Chirality of Natural Products: Hyoscyamine and Scopolamine', *Yakugaku Zasshi*, 2000, **120**, 1017

R664 M. Kitagawa, 'Quantum Computer Made of Molecules', *Kagaku to Kogyo (Tokyo)*, 2001, **54**, 459

R665 M. Kodama, H. Hioki and S. Yoshio, 'Asymmetric Total Synthesis of Terpenoids Possessing Novel Structure or Biological Activity', *Yuki Gosei Kagaku Kyokaishi*, 2000, **58**, 1167

R666 D. Kohda, 'Molecular Basis of Presequence Recognition by the Mitochondrial Import Receptors', *Seibutsu Butsuri*, 2000, **40**, 44

R667 C. Kojima and M. Kainosho, 'Direct Observation of Hydrogen Bonding in Biomolecules by NMR', *Seibutsu Butsuri*, 2000, **40**, 379

R668 K. Komata and K. Kabuto, 'NMR Absolute Configuration Using Single Diastereomer Chiral Derivatizing Agent', *Kagaku (Kyoto)*, 2000, **55**, 62

R669 H. Koshino and H. Satoh, 'Can Structure Determination for Natural Organic Compounds Be Automated? Development of Accurate Prediction System for ^{13}C-NMR Chemical Shifts with Stereochemical Consideration', *Kagaku to Seibutsu*, 2000, **38**, 708

R670 S. Kuramitsu, K. Miki, M. Miyamo, N. Kamiya and S. Yokoyama, 'Structural Genomics', *Nippon Kessho Gakkaishi*, 2001, **43**, 45

R671 S. Kurano, 'Attempts to Determine the Number and the Binding Sites of the Sulfate Groups on Glycoconjugates Using Mass Spectrometry', *J. Mass Spectrom. Soc. Jpn.*, 1999, **47**, 409

R672 T. Miyagawa and Y. Yoshida, 'Paper Physics Evaluation Test and Analysis Instruments', *Kami Parupu Gijutsu Taimusu*, 2000, **43**, 5

R673 K. Nagayama, 'The Nobel Prize and Spectroscopy. I. High Resolution NMR. One Leap to Higher Dimensions by Ernst', *Bunko Kenkyu*, 2001, **50**, 28

R674 T. Nakagawa, 'Gas Permeability of Biodegradable Polyester Films', *Nippon Hoso Gakkaishi*, 2000, **9**, 157

R675 M. Nakahara, 'In Situ NMR Observation of Supercritical Water as a Novel Reaction Field', *Chorinkai Saishin Gijutsu*, 2000, **4**, 57

R676 N. Nakamura, 'Solid-State NMR Spectroscopy of Microporous Materials', *Seisan to Gijutsu*, 1999, **51**, 10

R677 H. Nakazawa and K. Miyoshi, 'Synthesis and Property of Phosphenium Complexes Containing Double Bond Character between a Transition Metal and a Phosphorus Atom', *Yuki Gosei Kagaku Kyokaishi*, 2001, **59**, 52

R678 K. Nokihara, 'Recent Progress in Combinatorial Chemistry. Combinatorial Analysis for Assaying Library. Hyphenated Techniques', *Kagaku to Seibutsu*, 2001, **39**, 56

R679 T. Ohama, 'Charge Order of α-NaV_2O_5', *Bussei Kenkyu*, 2000, **74**, 391

R680 N. Ohata, H. Masuda and O. Yamauchi, 'Unique Self-Organized Structures of Metal (II)-Arginine Complexes through Directed Hydrogen Bonds', *Kobunshi Ronbunshu*, 2000, **57**, 167

R681 T. Okamura and K. Ueyama, 'Synthesis and Properties of New Peptide Complex Having Ferrocene Structure as Main Chain', *Kobunshi Kako*, 2000, **49**, 261

R682 M. Osanai and M. Okudaira, 'Biosynthesis of Nonessential Amino Acids and the Urea-Cycle in Silkworms', *Tanpakushitsu Kakusan Koso*, 2001, **46**, 733

R683 M. Sakakura, '^{13}C-NMR for Proteins Using Cryoprobe', *Farumashia*, 2000, **36**, 1071

R684 A. Satake, 'Synthesis of neutral π-Allylpalladium Complexes Having Bisnitrogen Ligands and Palladium-Catalysed Cyclopropanation of Ketene Silyl Acetals with Allylic Acetates', *Yuki Gosei Kagaku Kyokaishi*, 2000, **58**, 736

R685 K. Shibata, Y. Ono and K. Kikukawa, 'Molecular Design of Functionalized Host Compounds and their Application for Organic Chemistry. Part 2. Molecular Recognition with Functionalized Calixresorcin[4]-Arene Derivatives', *Kurume Kogyo Daigaku Kenkyu Hokoku*, 2000, **24**, 67

R686 K. Shimizu, 'Metabolic Network Systems Analysis and its Application to Microbial Cultivation Processes', *Bio. Ind.*, 2000, **17**, 21

R687 S. Shuto, 'A New Method for Conformational Restriction Based on Repulsion between Adjacent Substituents on a Cyclopropane Ring and its Application to the Development of Potent N-Methyl-D-Aspartic Acid (NMDA) Receptor Antagonists', *Yukugaku Kenkyu no Shinpo*, 1999, **16**, 43

R688 Y. Sugiura, 'Molecular Mechanisms of DNA Recognition and Function by Bioactive Compounds', *Yakugaku Zasshi*, 2000, **120**, 1409

R689 H. Takeya, 'The Structure and Function of Disintegrins', *Nippon Kessen Shiketsu Gakkaishi*, 2000, **11**, 211

R690 A. Tanatani, I. Azumaya and H. Kagechika, 'Aromatic Architecture Based on Cis Conformational Preference of N-Methylated Amides', *Yuki Gosei Kagaku Kyokaishi*, 2000, **58**, 556

R691 Y. Tezuka, 'Structural Study on Cellulose Derivatives with Carbonyl Groups as Sensitive NMR Probe', *Cellul. Commun.*, 1999, **6**, 73

R692 H. Tomoda and S. Omura, 'Lactacystin, a Proteasome Inhibitor: Discovery and its Application in Cell Biology', *Yakugaku Zasshi*, 2000, **120**, 935

R693 Y. Tozuka, 'Is Crystal Structure Predictable even when a Single Crystal is Not Available?', *Farumashia*, 2000, **36**, 995

R694 K. Tsuji, 'Studies in Organic-Functionalized Molecular Sieves (OFMSs)', *Zeoraito*, 2000, **17**, 162

R695 M. Ueno and H. Kashiwagi, 'Interaction of Liposomes with Detergents', *Nihon Yukagakkaishi*, 2000, **49**, 1131

R696 T. Wakahara, T. Akasaka, K. Kobayashi and S. Nagase, 'Frontier of Endohedral Metallofullerene Chemistry', *Kagaku (Kyoto, Jpn.)*, 2001, **56**, 60

R697 H. Yasuoka, 'NMR of High Temperature Superconductors', *JAERI-Rev.*, 2000, **(2000-003)**, 65

R698 N. Yoshii, S. Miura and S. Okazaki, 'Computer Simulation of Supercritical Water and Aqueous Solutions', *Koatsuryoku no Kagaku to Gijutsu*, 2000, **10**, 275

Korean

R699 S.-H. Hong, 'Advanced Cement Based Materials Center in USA', *Seramisutu*, 1999, **2**, 62

Polish

R700 J. Abildgaard and P. E. Hansen, 'Model Quantum-Mechanical Calculations in Chemistry. Structure, Vibrational Spectra, Chemical Shifts, and Isotope Effects on Chemical Shifts', *Wiad. Chem.*, 2000, **54**, 845

R701 J. Goralski, J. Grams, I. Ludomirska, T. Paryjczak and I. Rzeznicka, 'Carbonaceous Deposits on Catalysts and Methods for their Study', *Wiad. Chem.*, 2000, **54**, 591

R702 P. Minkiewicz, J. Dziuba and D. Nalecz, 'Current Methods of Separation and Structure Determination of Peptides and Food Proteins', *Przem. Spozyw.*, 2000, **54**, 34

R703 J. Pietras, 'Methods for Detection and Determination of Toxins. General Characteristics and Possibilities of the Use of Toxins', *Biul.-Wojsk. Inst. Chem. Radiom.*, 2000, **1**, 57

R704 P. Polaczek, 'DNA Mismatch Repair (MMR): Evolution of the System from Bacteria to Humans', *Kosmos (Krakow)*, 1999, **48**, 353

Portugal

R705 C. M. Fernandes and F. J. B. Veiga, 'The Cyclodextrins in Pharmaceutical Technology. III. Preparation and Characterization of Inclusion Complexes in the Solid State', *Rev. Cienc. Farm. (Sao Paulo)*, 1999, **20**, 375

R706 C. R. Kaiser, '2D NMR: Inverse Detection and Field Gradient in Structure Determination of Organic Compounds', *Quim. Nova*, 2000, **23**, 231

R707 A. Ramos, A. R. Neves, J. Almeida and H. Santos, 'Nuclear Magnetic Resonance: A Noninvasive Technique for Real-Time Observation of Metabolites in Living Cells', *Quimica (Lisboa)*, 2000, **77**, 8

Russian

R708 L. P. Smirnov, 'NMR Study of Network Polymer Structures', *Vysokomol.Soedin.,Ser. A. Ser. B*, 2000, **42**, 1775

Spanish

R709 J. Colmenero, 'Molecular Motion in Polymeric Materials', *Rev. Plast. Mod.*, 2000, **80**, 427

Turkish

R710 R. Ertan and O. Bozdag, 'Oral Antidiabetic 2,4–Thiazolidinedione Derivative Agents II', *FABAD Farm. Bilimler Derg.*, 2000, **25**, 57

2
Theoretical and Physical Aspects of Nuclear Shielding

BY CYNTHIA J. JAMESON AND ANGEL C. DE DIOS

1 Theoretical Aspects of Nuclear Shielding

1.1 General Theory. – *Ab initio* fully relativistic four-component calculations of nuclear shielding have only recently appeared and reviewed in the previous volume of this series,[1–3] although the theory had been laid out as early as 1983 by Pyykko and Pyper.[4,5] Nakatsuji and co-workers have used a Dirac–Fock finite perturbation theory using the no-pair Dirac–Coulomb Hamiltonian to obtain fully relativistic wavefunctions.[2] In this reporting period they have applied this Dirac–Fock method to both H and heavy nuclei in the series of molecules H_2O, H_2S, H_2Se, and H_2Te.[6] Hada *et al.* seem to have overlooked the earlier work of Visscher *et al.* when they state that this work is the first in the world to apply the *ab initio* four component calculations to heavy nuclei. They also used the Gordon decomposition first proposed for shielding calculations by Pyper in 1983 to convert the single term into a sum of four terms which is formally equivalent but in practice is deficient in a finite basis set. They compare these two sets of results to those obtained using their version of the quasi-relativistic approach employing the Douglas–Kroll method, and also to non-relativistic values. The Gordon decomposition permits comparison term-by-term with the quasi-relativistic methods and also permits the analysis of contributions coming from the small components *versus* the large components of the four-component wavefunction. They find small component contributions to be negligible for protons but significant for the Te shielding, −1748 ppm (small components) and +6486 ppm (large components) respectively. In particular the small component terms are significant for the paramagnetic and the spin-dipolar terms. Only the isotropic shieldings are reported, unfortunately.

Except for the efforts mentioned above, relativistic calculations of shielding evaluate the main relativistic effects using one or two component limits of the four-component formalism, quasi-relativistic approaches. These avoid the variational collapse in the calculation of the scalar relativistic terms by employing frozen cores,[7,8] or effective core potentials.[9,10] Some include the one-electron spin–orbit terms,[11,12] and sometimes the higher order spin–orbit terms too.[13,14] Others include both scalar and spin–orbit terms.[15–17] Ziegler

Nuclear Magnetic Resonance, Volume 31
© The Royal Society of Chemistry, 2002

and co-workers have introduced to shielding calculations the zero-order regular approximation (ZORA),[18] which is characterized by variational stability and also is a more complete theory in that one- and two-electron spin orbit contributions and magnetic field dependence of the spin–orbit are included, as well as orbital contraction effects on the spin–orbit contribution. The ZORA method appeared to yield results superior to the quasi-relativistic methods that employ a Pauli Hamiltonian, in every case.[18–20] More recently, a comparison between the Pauli approach and the ZORA approach to the worst cases, uranium compounds, seems to indicate that there are systems where the Pauli approach actually provides more accurate results.[21] Ordinarily, theoretical-computational papers ignore completely the various aspects of the experimental data they are using in comparisons. Schreckenbach *et al.* consider not only the usual computational aspects, how to handle relativistic effects, electron correlation, basis sets, molecular geometries; they also consider chemical shifts referencing as well as intermolecular effects in condensed phase data. In the ZORA approach, the ZORA orbital energies are scaled to improve agreement with the one-electron Dirac energies.[18] Schreckenbach *et al.*[21] have found that the scaling procedure has practically no effect on the ligand (^{19}F) shieldings but the difference between scaled and unscaled calculations are as large as 3140 ppm for the absolute shielding of the ^{235}U nucleus. The core orbitals on the heavy nucleus are the most influenced by scaling, so the relative shieldings or chemical shifts are not affected very much by scaling. For a nucleus as heavy as ^{235}U, the scaling is still useful even when only chemical shifts are desired, but perhaps not absolutely necessary when one takes into account the other sources of ambiguities such as solvent effects, and molecular geometries in solution, *etc.* The use of effective core potentials on the heavy nuclei for calculations of shieldings of the ligand nuclei was found to be unsuccessful. DFT-ECP methods are not recommended as a general approach. Of course, they are of no use at all in the calculations of shielding for the nuclei at which the ECP are used. The Pauli approach was found to be superior to ZORA for the proton shieldings in the $UF_{6-n}(OCH_3)_n$ compounds.[21]

The ligand nuclei in transition metal oxides and carbonyl complexes were among the earliest targets for relativistic shielding calculations. Recently, the ZORA method has been applied to the more difficult problem of the shielding of the transition metal nucleus.[22] The origin of the relativistic effects on the metal shieldings is considered. There are relativistic effects, changes in the molecular orbitals and their energies during the SCF calculations, in addition to the use of a relativistic Hamiltonian for the shielding. The relativistic effects on the bond lengths were not investigated; the experimental geometries were used. The core contribution to the diamagnetic shielding is large (on the order of 10 000 ppm for the 5d metals) and the additional relativistic corrections to the core diamagnetic part are also large. These large diamagnetic core contributions are important only for the absolute shielding calculations; they are essentially unchanged from one compound to the next and are therefore irrelevant for the chemical shifts. They, of course, remain exactly unchanged in

the frozen core approximation used in the Pauli approach. Comparisons of the results for SCF calculations and shielding calculations using either Pauli or ZORA method were presented. Basis sets used were not identical, since tight basis functions can be used in ZORA but not in the Pauli approach. Also the former is an all-electron calculation while the latter uses frozen cores. The Pauli-based method neglected some relativistic terms that were here shown to contribute significantly to the isotropic shieldings. Another factor not taken into account in comparing with experiments is that the experiments have intermolecular effects that are not uniform across the compounds studied. A large part of the discrepancies (of the order of 200 ppm) could easily be accounted for by the differential intermolecular effects between the compounds studied and the chemical shift reference.

A method of calculating the shielding of light nuclei in compounds containing heavy elements, such as to include both the scalar relativistic and spin–orbit effects, is implemented by incorporating scalar relativistic effects *via* quasi-relativistic effective core potentials and combined with a third order perturbation theory treatment of the spin–orbit effect (including the second order SO terms due to the magnetic field dependence of the one-electron part of the SO Hamiltonian interacting with the Fermi contact mechanism) using spin–orbit effective core potentials, so-called SO-ECPs.[23] The method employs DFT and uses IGLO for local gauge origins. The method is applied to the standard test set of molecules HX and CH_3X (X = F, Cl, Br, I). The spin–orbit pseudopotentials have been previously used by Nakatsuji *et al.* at the UHF level. This recent work is a systematic study, at an electron-correlated level, of the succession of non-relativistic, scalar relativistic, and spin–orbit-corrected scalar relativistic shieldings using ECPs. As a test of the halogen ECPs, two sets of comparisons with all-electron calculations are made. The results using halogen ECPs compare favorably with all-electron calculations,[13] when the present work on shieldings including scalar relativistic terms are compared with non-relativistic all-electron calculations, and also when the total shieldings including both scalar relativistic and one-electron spin–orbit terms are compared with all electron calculations using atomic mean-field spin–orbit operators.[13] The SO-ECP method that incorporates the coupling between scalar relativistic and spin–orbit effects gives somewhat larger SO contributions to ^{13}C and also to ^{1}H shieldings as compared to the all electron SO calculations. Since the changes in the second order and third order SO shielding terms, as the basis set is changed, are found to be canceling to some extent, this offers hope that the overall basis set dependence of the SO contributions is not so critical and application to larger systems is possible.[23] The method is further applied to other standard test sets, namely the ^{13}C chemical shifts in transition metal carbonyls and methyl mercury compounds. For these sets of molecules both scalar relativistic and spin–orbit terms had previously been included by Ziegler *et al.*[17] and Kaupp *et al.*[16] In third row transition metal hexacarbonyls the scalar relativistic and the spin–orbit effects act in the same direction, whereas in the Au and Hg dicarbonyls the SO effect is deshielding, leading to partial cancellation of the two relativistic effects. An

interesting point is that in most cases the use of IGLO leads to larger SO corrections than a common gauge origin at the metal.[23] In methyl mercury compounds CH_3HgX (X = CN, Cl, CH_3, H, SiH_3), consideration of both the scalar relativistic and the spin orbit effects is necessary; both are deshielding and important. The results for ^{13}C here are not as encouraging as in the hexacarbonyls. The absolute deviations from experimental chemical shifts are not much worse, the largest being about 10 ppm, but the chemical shift range is much smaller, 40 ppm compared to about 120 ppm for the hexacarbonyls. The treatment of the spin orbit effects may be inadequate for the compounds containing elements on the right side of the sixth period in the Periodic Table.[23]

Nakatsuji and co-workers have recently adopted a quasi-relativistic Hamiltonian that includes a relativistic correction to the magnetic interaction terms, the one-electron SO term in Douglas–Kroll form and the two-electron SO term of Breit–Pauli form.[24] The important coupling between the scalar relativistic terms (mass–velocity and Darwin terms) and the SO terms is therefore included. Quasi-relativistic calculations of ^{199}Hg shieldings in dimethyl mercury and its silyl and germyl analogs leads to total quasi-relativistic shieldings that are quite different from those obtained by Ziegler *et al.* using the ZORA method; for example, there is a huge difference between the 8019.0 ppm obtained by DFT-ZORA[18] and the 15128 ppm[24] obtained by Nakatsuji *et al.* The difference is more than 7000 ppm between methods. There are several reasons why these results should be different: One is that there is no electron correlation included in the latter, whereas the former has the built-in electron correlation in the DFT method. Another is the GIAO method of taking care of the gauge problem in the former, whereas the common origin method is used in the latter. And the relativistic methods used are different. The SO part in the ZORA calculation is 2461 ppm, whereas in a level 2 calculation that includes only SO but not the scalar relativistic terms the SO contribution is found in the latter to be −264 ppm, while the scalar relativistic terms calculated separately was found to be −1083 ppm. Thus, Nakatsuji *et al.* find the coupling between the SO and scalar relativistic effects to be a very large positive shielding contribution.[24] When the differences between three molecules (the chemical shifts) are only of the order of 400 ppm, as in this case, then it is difficult to believe that the proposed agreement with experimental shifts mean anything at all, if different computational methods can give absolute shieldings that differ by over 7000 ppm for one of the compounds.

Other developments in general theory include improvements in density functional theory,[25] the development of a pseudopotential-based theory of NMR chemical shifts for finite and for infinitely periodic systems,[26] and a combined quantum mechanics–molecular mechanics approach to chemical shifts in large molecules.[27] We consider these in turn below.

The general conclusion from studies of calculated HOMO–LUMO gaps in a wide variety of compounds including organic pi systems and small molecules of first row atoms, and now also transition metal compounds, is that using the local density approximation and different GGAs calculated band gaps that are

too small. Hartree–Fock on the other hand, overestimates the HOMO–LUMO gap and therefore the band gap, because HF theory describes virtual MOs by an electron that is moving in the field of n electrons rather than $(n-1)$.[28] Admixture of Hartree–Fock exchange into the hybrid functionals leads to HOMO–LUMO gaps that are larger than those for the GGAs or LDA, bringing them into much better agreement with experimental excitation energies. Construction of the exact XC potential from high-level *ab initio* densities shows that the LDA and GGA potentials show the wrong asymptotic behavior in the limit of $r \rightarrow \infty$, decaying exponentially rather than proportional to $-1/r$.[29–31] Tozer and Handy stress that in order to improve calculated properties, attention has to be paid to the exchange correlation potential, in addition to the exchange correlation energy. Thus, they have been constructing XC functionals that have the correct asymptotic behavior of the XC potential for training sets of small molecules containing first and second row atoms. Although this is clearly the right approach, these new functionals with asymptotic correction have so far produced disappointing results.[32] For the meantime, Handy and co-workers are testing out a second approach, which is to empirically find the best fraction of Hartree–Fock exchange to obtain specifically best agreement with NMR chemical shifts.[33] Wilson, Amos and Handy use a small admixture of the exact exchange (optimized at 5% to obtain best agreement with experimental data), the MOs and orbital energies are then used as an input to an uncoupled pure DFT shielding tensor calculation.[33] The latter method, a hybrid DFT followed by a non-hybrid DFT non-iterative uncoupled sum-over-states calculation of the paramagnetic contribution, has recently been implemented into the DALTON code, with gauge-including atomic orbitals (GIAO), rather than the LORG method of distributed gauge origins used earlier.[34] One of the disadvantages of this approach is that the "best" fraction is dependent on the form of the approximate exchange-correlation functional used. When used with B3LYP they call the method $B3LYP^{0.05}{}_{GGA}$. Application to the specially challenging cases of NNO and 1-cyclopropylcyclopropylidenemethyl-cation show that $B3LYP^{0.05}{}_{GGA}$ results are much closer to the best *ab initio* results, respectively GIAO-CCSD and GIAO-CCSD(T),[35,36] than any of the other DFT methods.

A non-empirical improvement of DFT method of calculating magnetic properties has been proposed and implemented by Ziegler *et al.*[25] The presence of the self-interaction has been identified as the cause of some of the qualitative failures of approximate DFT: incorrect dissociative limits for some symmetric bonds, positive energies of the HOMO in many anions, *etc.* Among the XC functionals popular in applications, only the Lee–Yang–Parr correlation functional is self-interaction-free. A self-interaction corrected (SIC) density functional theory for calculation of magnetic properties has been implemented by Ziegler and co-workers[25] using the Vosko–Wilk–Nusair (VWN) functional. The SIC-VWN implementation leads to improvements over BP86 and VWN for the light nuclei (^{1}H, ^{13}C, ^{15}N, ^{17}O, ^{19}F) in a large number of test molecules, including the pathological cases (N_2, CO, CH_2N_2 and O_3), especially for individual tensor components. The improvements are thought to arise from a

better description of the Kohn–Sham orbital energies, leading to a general decrease in the paramagnetic contribution to the shielding. Removal of self-interaction is said to correct the tendency toward excessively covalent chemical bonds, characteristic of popular approximate density functionals. The increased importance of self-interaction for nitrogen and oxygen, compared to carbon and hydrogen, arises from the lone pairs becoming increasingly important for N, O, and F; N and O atoms also exhibit a propensity for forming short multiple bonds. Both factors lead to compact electron density distributions that typically exhibit large self-interaction corrections. In many systems the major effect of the SIC potential is the increase in the HOMO–LUMO gap accompanied by a general increase in the separation between Kohn–Sham orbital eigenvalues. The insufficient separation between the occupied and virtual MOs, leading to excessively large paramagnetic contributions, has previously been identified as the major reason for the deficiencies in the calculated NMR chemical shifts for N and O.[37–39] SIC methods account for both changes in orbital energies and orbital shapes which become less delocalized when self-interaction is removed. Since the excessive covalency in popular DFT functionals is known to present a bigger problem for heavier elements and particularly for transition metals, SIC methods may significantly improve our ability to calculate shielding in transition metal complexes.

The ^{57}Fe shielding offers a typical example of the difficulties associated with DFT calculations in transition metal complexes, particularly of the shielding of transition metal nuclei.[40] It appeared that the question of whether GGA (generalized gradient approximations) or hybrid functionals (B3LYP, for example) are superior can change back and forth, depending on the transition metal complexes and the nuclei under study. It had been claimed that a dramatic effect of including Hartree–Fock exchange is observed, in particular for Fe chemical shifts.[41] To better understand the influence of the exchange-correlation functional on the calculated electronic structure and on the calculated shielding, Schreckenbach has carried out a detailed study of ^{57}Fe in ferrocene and in $Fe(CO)_5$.[40] Using DFT-GIAO, he investigated a number of XC functionals BLYP, B3LYP, BP86, BPW91, B3PW91, using the Amsterdam density functional package or the Gaussian program package. Differences between the two program packages have to do with frozen-core *vs.* all-electron, Slater type orbitals *vs.* Gaussian basis sets, small *vs.* large basis sets. Nevertheless, agreement between the two packages is good. Geometry is very important; the shielding derivative with respect to metal–ligand distance is known theoretically to be very large; and this is known from experiments as well.[42] The present calculations are all in the experimental geometry of the molecules. In the detailed analysis of $Fe(CO)_5$ and $Fe(C_5H_5)_2$, Schreckenbach finds that the ^{57}Fe diamagnetic shielding is not contributing to the relative chemical shifts since it is relatively constant for both compounds, the paramagnetic shielding is dominated by the occupied-virtual contributions, which in turn are determined by d→d couplings, the strength of the coupling is inversely proportional to the energy difference between the orbitals involved; this is the major factor responsible for the difference in shielding between the

two compounds. This verifies that which was known as far back as the late 1950s and early 1960s.[43,44] Nowadays, one explains the numerically larger paramagnetic shielding in $Fe(C_5H_5)_2$ compared to $Fe(CO)_5$ in terms of the larger HOMO–LUMO gap in $Fe(CO)_5$. The thrust of the study is in the comparison of the Fe shieldings using various XC functionals, different GGAs (BLYP, BP86, BPW91) and hybrid functionals (B3LYP, B3PW91) within the same platform (GAUSSIAN) followed by analysis using ADF. All three GGAs give very similar results with differences of about 100 ppm at most. The hybrids also give similar results to each other. The marked difference of as much as 1916 ppm in ferrocene is between the GGA and its hybrid. Part of the difference between including or not including Hartree–Fock exchange is lost when the relative chemical shifts are taken. The error in band gaps is largely due to deficiencies of these model XC functionals. Incorporating Hartree–Fock exchange increases the occupied-virtual gaps, which tend to reduce the paramagnetic shielding. This effect is, however, offset by two other dominating effects on the matrix elements of the shielding: Another consequence of mixing in Hartree–Fock exchange is the more diffuse virtual MOs, leading to increased magnitudes of the paramagnetic shielding and, also, the larger couplings leads to an increase in magnitude of the paramagnetic shielding. The combined result is a net improvement which is an increase in the magnitude of the (negative) paramagnetic shielding. Wilson *et al.* also came to the same conclusion in their calculations on complexes of V, Cr, Mn, Fe Co, Ni, that the poor performance of non-hybrid functionals is that they underestimate the numerator rather than any deficiencies in the description of the eigenvalue differences that appear in the denominator.[45] Wilson found this also to be the case in a comparison of various functionals including their $B3LYP^{0.05}{}_{GGA}$ for a variety of Se shieldings,[46] where the results could be measured against the CCSD benchmark calculations that Gauss *et al.* have carried out.[47] Thus, merely correcting the HOMO–LUMO gap by a factor something like the 'Malkin correction',[48] does not take care of the other two effects, which turn out to be very pronounced in transition metal compounds, although less so for molecules of only first row atoms. Incidentally, apparently also for ^{99}Ru in its complexes, the hybrid B3LYP does give results that correlate better with experimental chemical shifts than BPW91,[49] and for ^{59}Co in the hexa-coordinated Co(III) porphyrin system, the B3LYP result is recommended by the authors over the BLYP result,[50] although the comparison with experiment leaves too much wiggle room in this case; for example, is there or is there no hydrogen bonding? and what is actually the axial ligand orientation? The discrepancy between electric field gradients and anisotropy inferred from relaxation in the solution data and the solid state anisotropy that has been reported leave the cobalt porphyrins an unsettled problem.

Mauri *et al.* have provided the only *ab initio* shielding calculation method for extended periodic networks, which they have applied to crystals and also to small molecules containing atoms in the first row of the Periodic Table.[51] In an effort to extend the *ab initio* calculations of shielding in extended networks using periodic boundary conditions to involve other than light atoms, Mauri *et*

al. consider the viability of all-electron calculations using a pseudopotential approximation.[26] We have seen wide applications of pseudopotentials to represent the core in relativistic calculations of shielding. The pseudopotential approximation explicitly neglects the form of the electronic wavefunctions near the nucleus; the correct nodal structure of the wavefunction is lost. For those properties for which the matrix elements are dominated by regions outside the core, the use of pseudopotentials provides a good approximation. The basis for the approach of Mauri *et al.*[26] is their recent finding that if a careful separation of core and valence contributions that ensures that they are individually gauge invariant is carried out, the core contributions to the shielding can be separately described and is found to be rigid (unchanging with molecule formation).[52] These authors derive a gauge-including projector augmented-wave method (GIPAW) that, by construction, imposes the translational invariance in a uniform magnetic field. The current is computed using the GIPAW operators and the wavefunctions; the current is also translationally invariant. The theory is formulated and implemented in a plane wave pseudopotential electronic structure code. The method is tested with an all-electron plane-wave calculation for diamond as an example of the application to large extended systems. GIPAW calculations performed using pseudopotentials generated by an all-electron atomic code for small molecules involving first and second row atoms are compared with calculations using the IGAIM method. Using various available pseudopotentials leads to total shifts that differ by only about 1 ppm. The comparison with IGAIM is flawed by use of two different density functionals; the GIPAW-LDA calculations used parameters of Ceperley-Alder, while the IGAIM calculations used VWN. Even so, differences are small for light atoms, larger for ^{31}P (worst case was 15 ppm difference between IGAIM and the new method for P_2 molecule).[26]

Mauri's method is explicitly the only *ab initio* approach to infinite extended networks that actually does the same level calculations for the entire network. (In order to do calculations in a system that has a distribution of geometries, polymorphs with different internal coordinates have to be created and the larger unit cells of these are then used to make the periodic network.[53]) When the system is not periodic, but very large, as a molecule in a hydrogen-bonded fluid, or for smaller molecules associated with very large intermolecular partners such as polymers, proteins, or zeolites, properly accounting for shielding can require an impossibly large *ab initio* calculation. Various methods are employed to circumvent the problems of size. For example, *ab initio* shielding calculations may be carried out on a cluster carved out of the crystalline structure;[54–59] *ab initio* shielding of one or several small clusters are sometimes used to represent the liquid structure or crystalline structure.[60,61] *Ab initio* shielding in a molecule in the presence of other molecules, or in the presence of fragments of the zeolite used as intermolecular partners of the molecule,[62,63] or *ab initio* shielding tensor calculations as a function of geometry in a fragment of the protein[64,65] are some of the approaches that have been introduced. Averaging over many configurations of the large system takes on many forms, too. For example, a smaller representation of the full

system is taken to generate *ab initio* shielding surfaces *via* local geometry modifications in the midst of the rest of the crystal or protein which is incorporated in the form of a charge field; CFP-GIAO (charge-field perturbation GIAO) is an approach introduced by de Dios and Oldfield.[64] Partition functions may be calculated from a finite number of cluster types that may be present (as in a hydrogen-bonded liquid),[60,61] or else using grand ensemble Monte Carlo methods,[66–71] or using classical molecular dynamics[72] to circumvent calculations of partition functions entirely. These methods incorporated what could be described as the onion approach. More recently, the onion approach has become more popular and taken other forms, such as that introduced by Morokuma *et al.*, which they explicitly label ONIOM.[73] A recent addition to onion approaches is the combined QM/MM approach to molecular properties by Cui and Karplus.[27] We discuss it here because it is not explicitly an intermolecular method (although that is the rationale for its introduction) but could be used for local properties such as nuclear shielding in macromolecular systems such as polymers and crystals. The idea is the same as in previous onion approaches, the local electronic environment is described at a high level while the outlying environment is described by possibly less accurate methods. This time the outlying environment is described by molecular mechanics, using the CHARMM force field. The MM atoms are permitted to contribute indirectly to the shielding by contributing explicitly electric charge effects (as parametrized in CHARMM) to the derivatives of the one-electron matrix elements in the GIAO basis. Magnetic anisotropy effects from the MM atoms are not included nor are the electrons of the MM atoms permitted to contribute any repulsion effects. This approach is therefore the same as the charge-field perturbation approach introduced by de Dios, Pearson and Oldfield,[64] except that AMBER partial charges were used in the earlier CFP-GIAO work (1993) rather than the CHARMM partial charges used here.[27] Re-inventing previously established methods is a normal part of doing science. In this way we re-validate each other's techniques and results. Example systems to which the QM/MM method has been applied are the water dimer (an old favorite), *N*-methylacetamide–water complex, cytosine monophosphate, paired and stacked nucleic acid bases, imidazole–metal complexes and metal ion complexes of deoxyribose. In the nucleic acid bases, the MM atoms contribute substantially to the shielding of the base atoms, typically 5–10 ppm and as large as 27 ppm for oxygen. Unfortunately, the authors did not compare their calculated tensors with the experimental ones for the bases.

Gauss has done the definitive shielding calculations, ranging from full CI, CCSD(T) and CCSD to various levels of MBPT on small molecules that now are used as benchmarks for testing other methods. In this reporting period, he investigates the application of schemes that exploit the "local" character of electron correlation toward an efficient implementation of MP2 level calculations for slightly larger molecules.[74] The scheme for calculating shielding using local second order Møller–Plessset using GIAO (GIAO-LMP2) is compared to conventional GIAO-MP2 for ^{13}C, ^{15}N and ^{17}O shieldings in

molecules of the size of CH_3COCH_3. Some of the cases are specially challenging, all require some level of correlation calculation to come close to the experimental absolute shielding. The results are very promising. Differences are small, typically less than 1 ppm for ^{13}C. It is anticipated that with efficiently implemented code, GIAO-LMP2 might easily compete with Hartree–Fock and DFT as a routine tool for treatment of such cases.

Shielding polarizabilities, the derivatives of the shielding with respect to external electric fields and field gradients, have traditionally been more demanding of basis set size and level of electron correlation than the shieldings themselves. They have been calculated by a number of methods, including SCF, MP2, MP3, L-CCD, MCSCF, previously reviewed in this series. Recently, Lazzeretti *et al.*[75] make use of an extension of CTOCD-DZ continuous transformation of the origin by annihilation of diamagnetic contributions to the electron current density, an approach originally suggested by Keith and Bader[76] with another name. The calculation is at the coupled-Hartree–Fock level. Shielding polarizabilities evaluated by this method are gauge-origin independent and the constraints for charge and current conservation are exactly fulfilled, no matter the size of the basis set used in the calculations. The price to pay for this theoretical purity is that the basis sets that need to be used should be larger than those used in GIAO calculations. The set of molecules include H_2O_2, F_2, $HC{\equiv}CH$, H_2CO, NH_3, HCN and HNC, and comparisons are made with previous calculations by other methods.[75]

1.2 ***Ab initio* Calculations.** – A comparative study of the performance of various well-established functionals, hybrid and non-hybrid in the calculations of ^{31}P shielding complexes are presented by van Wullen.[77] who appears not to be convinced of the superiority of Wilson, Amos and Handy's $B3LYP^{0.05}{}_{GGA}$, even though the latter offers substantial improvements in the pathological cases of PN and PCl_3 compared to others. Most of the density functional calculations reported in this review period are for one or two specific molecules. For example ^{13}C in the C_{84} fullerene,[78] ^{31}P in R_2N-P=N-Mes,[79] ^{31}P in vanadium phosphorus oxides,[80] ^{11}B chemical shifts in hexagonal boron nitrides,[81] formamide and carbazole,[82,83] ^{13}C in 1- and 2-methyl adamantanes and bicyclic alcohols,[84,85] silanes,[86] and some cations.[87,88] With complete prediction of the ^{1}H spectra for aromatic and aliphatic organic molecules *via* B3LYP calculations as the stated goal, Bagno finds that the spectrum does lie in the right general region and systematic errors in the chemical shifts (generally less than 0.5 ppm) lead to spectra offset from theoretical ones but still fairly recognizable in the groupings of peaks.[89] Authors of the DFT calculations of ^{19}F chemical shifts for fluoroaromatic compounds complexed with benzene in various geometries come to the unenlightened conclusion that counterpoise corrections are not appropriate for this system because the results with counterpoise corrections do not agree with experiment![90] Unfortunately, these types of papers arising from the GAUSSIAN program package in the wrong hands, seemingly an unavoidable consequence of its popularity appear

more and more often in the literature; they are also a testament to the lack of fundamental knowledge among the referees.

1.3 Semi-empirical Calculations. – An interesting analysis of the shielding tensor in terms of local bond structure starts out assuming that the field-induced electron current density is entirely perpendicular to the applied magnetic field.[91] This has two interesting consequences: (1) The resulting shielding tensor is perfectly symmetric. Thus asymmetry in a shielding tensor is an indication of current density that is not orthogonal to the applied field. (2) The orientation dependence of the shielding at a point of interest is related explicitly to the isotropic average of the shielding at every point in the surrounding region. A good correlation with experimental tensors is obtained with just 1–2 adjustable parameters in several series of compounds, including silicates, phosphates, carboxyls and amides, when the assumption is made that the important contribution to the shielding anisotropy comes primarily from the regions of the directly bonded neighbors.

2 Physical Aspects of Nuclear Shielding

2.1 Anisotropy of the Shielding Tensor. – The fact that the shielding tensor, the magnitude of its principal components and their orientation offers much more information than the isotropic value alone continues to serve as a driving force behind a significant number of papers published this year on nuclear magnetic resonance. In most of these papers, *ab initio* methods are utilized to either complement or further elucidate the experimental observations. Furthermore, considerable attention is now placed on how each of the principal components is influenced by local geometry as well as intermolecular interactions. There is a recent series of studies on ^{17}O tensors from Wu's group.[92–96] One example involves the ^{17}O shielding tensor in *p*-toluenesulfonic acid monohydrate (TAM).[92] This tensor is axially symmetric, with an isotropic value of 278 ppm and an anisotropy of 87 ppm. *Ab initio* computations are employed with a model consisting of an H_3O^+ ion bound to three hydrogen sulfite (HSO_3^-) ions. Calculations using HF/cc-pVTZ produces an isotropic value of 285.3 ppm with an anisotropy of 48 ppm. On the other hand, DFT calculations using B3LYP/cc-pVTZ yields 266.8 ppm, with a similar anisotropy. RHF shows deshielding of 25 ppm when bound while B3LYP indicates 39 ppm. The experimentally observed difference between the ^{17}O shielding in TAM and that of aqueous H_3O^+ is 21 ppm. In addition, the hydrogen bonding environment in TAM reduces the ^{17}O quadrupole coupling constant, while all shielding tensor components are also decreased, leading to an overall deshielding and very small changes in the anisotropy.[92] Additional studies have been performed on carbonyl oxygen sites in the following amides, benzamide,[93,94] benzanilide, *N*-methylbenzamide and acetanilide.[95] These measurements demonstrate ^{17}O shielding tensors characterized by spans of about 560–630 ppm. In these compounds, the most shielded component lies normal to the

amide plane while the least shielded component usually lies in the amide plane and is about 20° off the direction of the C=O vector. As in TAM, comparison between theory and experiment reveals the importance of incorporating a hydrogen bonding partner in the model used in the computation. Without an additional formamide molecule as a hydrogen bond partner, calculations produce values for the least shielded component that are in error by as much as 160 ppm. The introduction of a formamide molecule reduces this error in half. The dramatic improvement is also seen in the electric field gradient (efg) tensor. Experiment and theory indicate that σ_{11} and σ_{22} become more shielded while the opposite happens to σ_{33}, which becomes less shielded with hydrogen bonding. These changes correlate very well, according to *ab initio* computations, with the hydrogen bond distance.[95] One important conclusion from these shielding tensor measurements is the success of current computational methods in predicting the orientation of the ^{17}O shielding tensor in these hydrogen-bonded systems.

A series of papers from the Wasylishen laboratory describe a combination of experiment and theory.[97–101] Although hybrid density functional methods, in most cases, produce spans and skews that are in better agreement with experiment, Hartree–Fock calculations appear to reproduce the ^{15}N shielding tensor orientation closer to experiment than a hybrid density functional method in pyridine and aniline-containing cobaloximes.[97] It seems that when two components are relatively close to each other (for example, when σ_{11} and σ_{22} differ by only 73 ppm while the span of the tensor is 484 ppm, as illustrated by the ^{15}N shielding in a pyridine ligand complexed to a cobaloxime), the B3LYP methodology fails in predicting the correct orientation of these two components. This difficulty is perhaps a characteristic of ^{15}N shielding, and not necessarily of Group 15 nuclei. The problem does not appear in the case of ^{31}P nuclei in which the two components close to each other in value are only 16 ppm apart with a tensor span of about 150 ppm; both B3LYP and RHF methods yield orientations for the shielding tensor that are in good agreement with experiment. This is demonstrated by the case of ^{31}P shielding tensors in tetramethyldiphosphine disulfide.[98] With a 6–311++G(3df,3pd) basis, RHF calculated spans and skews lie very close to experiment although the isotropic value is a bit shielded (by about 24 ppm). In comparison, B3LYP/6–311G(d,p) reproduces a less shielded (by about 16 ppm) value and overestimates the span by as much as 33%. B3LYP underestimates the least shielded component while overestimating the most shielded component. Thus, these studies show that B3LYP does not necessarily perform better than RHF in computing shieldings of nuclei other than ^{13}C.

Measurements of ^{13}C shielding tensor components in an ethylene ligand bound to Pt(0) and Pt(II) reveal that the least shielded and intermediate principal values are especially sensitive, increasing (greater shielding) significantly upon coordination to platinum.[99] Thus, compared to free ethylene, the span of bound ethylene is greatly reduced. These two components also show a marked difference between Pt(0) and Pt(II), with the sites bound to Pt(II) having a shielding tensor lying somewhere between that of free ethylene and an

ethylene bound to Pt(0). This behavior is explained by the stronger coordination to Pt(0) which is reflected effectively in the values of σ_{11} and σ_{22}, the components that lie farthest from the Pt–C vector.

The first ^{11}B chemical shielding tensors have been measured.[100] Trimesitylborane gives an axially symmetric tensor with a span of 121 ppm and a positive skew, while triphenyl borate is characterized by a tensor that is less than 10 ppm wide. Interestingly, the span observed for trimesitylborane corresponds to the known chemical shift range of tricoordinated boron. Both RHF and B3LYP reproduce nicely these experimental findings. The ^{13}C, ^{15}N, and ^{77}Se shielding tensors in selenocyanate salts are all found to be axially symmetric, as may be expected from the linear geometry of the $[SeCN]^-$ ion in these salts.[101] The spans of the ^{13}C and ^{77}C tensors in $[SeCN]^-$ are much smaller than the corresponding values in the SeCSe molecule. *Ab initio* calculations show that the tensor components perpendicular to the molecular ion axis involve less efficient mixing of sigma and pi orbitals in the ion compared to carbon diselenide molecule, leading to smaller paramagnetic shielding.

Grant's laboratory continues to add new techniques that they use to advantage in experimental determination of ^{13}C shielding tensors.[102–107] A new method has been introduced by Hu *et al.*[102] that combines Gan's magic angle turning (MAT) experiment[108] with the two-dimensional chemical shift anisotropy–chemical shift anisotropy (2D CSA-CSA) correlation experiment of Hughes *et al.*[109] This recently introduced experiment has been illustrated to be capable of resolving the overlapping CSA-CSA patterns (which provide information regarding the relative orientation of shielding tensors) of the methoxy carbons in 1,2,3–trimethoxybenzene. Using MAT and separated-local-field (SLF) experiments, Hu *et al.*[103] determine the ^{13}C shielding tensors in polyethylene. Their results indicate that the tensors are practically identical for all-*trans* crystalline structures with long and short longitudinal relaxation times. Polymorphs are distinct crystalline forms of the same chemical compound. Their physical properties are different. They are of considerable interest to pharmaceutical companies since each crystalline form can be separately patented and different crystalline forms may have different efficacy due to differing solubility and other physical properties. Upon comparison of *ab initio* results with experimentally measured tensors, it is suggested that the polymorphous verbenol is composed of two sites that differ in the orientation of a hydroxy hydrogen.[104] The relevant dihedral angle consisting of the C3–C4–O–H atoms is found to be between 45° and 80°, in agreement with X-ray values, while it is predicted that the other form has a dihedral angle near either 60° or 180°. White and yellow forms of dimethyl-3,6-dichloro-2,5-dihydroxyterephthlate have also been studied by FIREMAT experiments.[105] Isotropic shieldings of the aromatic carbon sites appear to be sensitive to the polymorphic form while those of the carboxyl and methyl sites are only slightly different between the two forms. The principal components, however, are much more sensitive to dihedral angles and hydrogen-bonding patterns. These are some of the structural parameters in which the two polymorphs exhibit significant differences. Using known structures, theoretical calculations are

shown to approach experimental numbers when the models used take into account strong intermolecular interactions. *Ab initio* calculations have likewise been utilized in the assignment of ^{13}C chemical shielding tensors in polycyclic aromatic compounds obtained *via* FIREMAT and PHORMAT experiments.[106,107]

It is frequently stated that the full shielding tensor information, the components as well as the orientation of the principal axes, can provide vital local structural and conformational information in substrate–enzyme complexes, for example. Accurate determination of shielding tensor orientations in model compounds with known structure is a very important first step towards application of shielding tensor orientations to determination of conformations in target compounds of unknown structure/conformation. In a combination of ^{31}P single crystal NMR studies in one case and ^{13}C MAS NMR experiments with ^{31}P rotary resonance recoupling on polycrystalline powder samples in two cases, it was possible to determine without ambiguity the ^{31}P shielding tensors in two phosphoenolpyruvate compounds.[110] The ^{31}P tensor assignments from the powder agree with the single crystal experiments, and are unambiguous for both compounds. Only some of the orientational parameters of the three ^{13}C shielding tensors could be derived. Homonuclear ^{13}C dipolar recoupling methods are needed to complete the tensor information. Although success in theoretical calculations reproducing experimental shielding tensors for first and second row atoms has now become very common, the shielding tensors of heavier elements still remain a challenge, as exemplified by the work of Grossmann *et al.*[111] on bis(dineopentoxyphosphorthioyl) diselenide. Using SOS-DFT-IGLO, the calculated ^{31}P shielding tensor, its principal components and their orientations, agrees favorably with experimental values obtained through single crystal NMR measurements. In contrast, the two components, σ_{11} and σ_{22}, of the ^{77}Se shielding tensor are underestimated by about 100–200 ppm. The magnified deshielding contributions are attributed to the diffuse nature of the lone pairs on Se rendering it extremely susceptible to the level of theory and the large basis set requirements of a fourth period element. The authors, however, noted that the principal axis system derived from computations for both nuclei perfectly agree with those obtained in the single crystal experiments.

Considerable interest continues in utilizing shielding tensors in characterizing samples of biological relevance. Studying two β-lactam antibiotics, Rich *et al.*[112] have shown that it is feasible to reproduce the ^{13}C shielding tensors by employing isolated molecules. The two antibiotics penicillin-V and ampicillin contain carbonyl, carboxyl, aromatic, nonaromatic cyclic and methyl sites. As observed by other workers in the field, agreement between theory and experiment is excellent even with gas phase isolated models except for the carbonyl and carboxyl carbons, which participate in hydrogen bonding in the condensed phase. Lee *et al.*[113] have reported a two-dimensional solid-state NMR experiment that correlates chemical shift anisotropy and dipolar coupling. Since the dipolar interaction between the amide N and its proton is linked to the N–H vector, this offers an additional tool in deciphering the orientation for the ^{15}N

shielding tensor. The potential application of *ab initio* calculations of shielding tensors in the study of biologically relevant molecules is highlighted in a paper of Brender *et al.*,[114] which shows that the tensor orientation of ^{15}N shielding is insensitive to the size of basis set, suggesting that routine applications of these computations on large molecules may be not as expensive as first thought. Basis sets ranging from 4–31G to 6–311++G(2d,p) have been used in this recent evaluation. A recent work by Cornilescu and Bax[115] shows that in terms of CSA values and tensor orientation, a significant range is observed for the residues in the protein ubiquitin for amide N and H as well as carbonyl C sites. The observed range is wide enough that it may not be advisable to assume a uniform tensor for these sites.

As novel solution and solid state experiments enabling the determination of shielding tensor quantities in peptides and proteins become widespread, it is strongly recommended that practitioners stick to precise definitions of terms that have accepted meanings within the solid state NMR community. As a reminder, we list again the modern terms: The difference between the most shielded (σ_{33}) and the least shielded (σ_{11}) tensor component is the span.

$$\text{Span} = \Omega \equiv (\sigma_{33} - \sigma_{11}) \text{ where } \sigma_{33} \geqslant \sigma_{22} \geqslant \sigma_{11}$$

Since, the chemical shifts $\delta \equiv (\nu - \nu_{ref})/\nu_{ref} = (\sigma_{ref} - \sigma)(1 - s_{ref})$ then this leads to $\delta_{11} \geqslant \delta_{22} \geqslant \delta_{33}$ and

$$\Omega = (\delta_{11} - \delta_{33}) \times (1 - \sigma_{ref}) \approx (\delta_{11} - \delta_{33}).$$

Span is always a positive quantity.

$$\text{Skew} = \kappa \equiv 3(\sigma_{iso} - \sigma_{22})/(\sigma_{33} - \sigma_{11})$$

The skew κ characterizes the shielding tensor without being affected by the choice of reference substance. Converting shielding into chemical shift,

$$\kappa = 3(\delta_{22} - \delta_{iso})/(\delta_{11} - \delta_{33})$$

The old conventions, are still in use, for example, in the compendium of chemical shift tensors by T. M. Duncan.[116] Depending on which component δ_{11} or δ_{33} is farther from δ_{iso}, for $|\delta_{11} - \delta_{iso}| \geqslant |\delta_{33} - \delta_{iso}|$

$$\text{anisotropy} = (3/2)(\delta_{11} - \delta_{iso}) = \delta_{11} - \tfrac{1}{2}(\delta_{22} + \delta_{33})$$
$$\text{and asymmetry} = \eta = (\delta_{22} - \delta_{33})/(\delta_{11} - \delta_{iso})$$

For $|\delta_{11} - \delta_{iso}| \leqslant |\delta_{33} - \delta_{iso}|$

$$\text{anisotropy} = (3/2)(\delta_{33} - \delta_{iso}) = \delta_{33} - \tfrac{1}{2}(\delta_{11} + \delta_{22})$$
$$\text{and asymmetry} = \eta = (\delta_{22} - \delta_{11})/(\delta_{33} - \delta_{iso})$$

Thus, at $\delta_{22} = \delta_{iso}$, the anisotropy $= \pm(3/2)(\delta_{33} - \delta_{iso})$, and the asymmetry $\eta = 1.0$. Although most authors usually define the terms and symbols that they have used in their paper, it can still happen that readers may not pay due attention to these very important details, especially for terms related to the shielding tensor. For example, the term anisotropy is now very carelessly used in some of these recently developed experiments to describe the difference

between the shielding magnitude along a vector, normally a bond direction, and at all directions normal to such a vector. This can result in a misunderstanding when other workers do not carefully read the text and simply assume that the anisotropy being described is the same as the conventional one, as listed above. This confusion is recently exemplified in a paper by Hong,[117] where anisotropies obtained *via* a solid state NMR technique have been incorrectly compared directly to values obtained by Tjandra and Bax,[118] who have employed cross-correlated relaxation experiments in solution. The chemical shift anisotropy cited by Tjandra and Bax is not identical to the one defined by the above equation. Instead, the anisotropy described in the solution work is with reference to the value of the shielding along the C–H bond. Therefore, the large difference observed between helical and sheet sites is not primarily due to the tensors having different spans or different anisotropy, but rather, to a dramatic change in the orientation of the shielding tensors, as already predicted by quantum mechanical calculations of Walling *et al.*[65]

2.2 Shielding Surfaces and Rovibrational Averaging. – Shielding surfaces, which mathematically describe how the shielding property changes with the internal coordinates of a molecule, illustrate very clearly how experimental and theoretical means can be used in complementary ways to establish the relationship between shielding and geometry. As computational results approach experimental values, the remaining gap is basically the one arising from a frozen molecule inside a computer and a real molecule that is rotating and vibrating at 300 K. Hence, a thorough evaluation of present theoretical methods requires incorporation of motional averaging. On the other hand, the persistence of a distribution of local structural features (such as O–Si–O angles) will produce ranges of chemical shifts. However, the range of local geometry variables in the systems accessible *via* experiments is usually limited. In this area, *ab initio* methods offer a huge advantage as the geometry of any molecule inside a computer can be set at any desired configuration, permitting a more extensive exploration of shielding surfaces. Although shielding surfaces and rovibrational averaging have become popular, there are still questions that need to be answered. Similar to the task of reproducing isotropic shielding values at a specific geometry, the same questions with regard to basis set and level of theory need to be addressed.

Since the proton shielding range is relatively small, contributions from electron correlation, finite basis sets, and vibrational effects can play quite a dramatic role. Ruud *et al.*[119] have studied a series of organic compounds and have evaluated the zero-point vibrational corrections to proton shieldings in a wide variety of organic molecules. In this compilation, it is suggested that the vibrational effects are transferable from one molecule to another. These results are summarized in Table 2.1. In contrast, the corrections to the shielding of non-hydrogen atoms do not display transferability. For corrections to proton shieldings, interesting to note is the opposite sign of the correction when the proton belongs to an alcohol. On the other hand, a carboxyl proton bears the usual deshielding correction. It has been known since the 1970s that the

Table 2.1 *Zero-point vibrational contributions to proton shieldings in various functional groups*[119]

Functional group	*Corrections* (ppm)
Methane	−0.59
$-CR_2H$	−0.70 ± 0.11
=CRH	−0.46 ± 0.13
≡CH	−0.76 ± 0.01
H–CRO	−0.55 ± 0.06
RO–H	0.48 ± 0.13
$RN-H_2$	−0.18 ± 0.03
RCOO–H	−0.49 ± 0.06
Ar–H	−0.39 ± 0.06

derivative of the shielding with respect to bond extension is usually negative (that is, deshielding occurs as the bond stretches) and vibrational corrections are usually dominated by stretching motions.[120–123] For these reasons, vibrational corrections are usually negative based on shielding derivatives with respect to bond length. Indeed, a large number of calculations since the 1970s bear this out; as do the recent examples shown in Table 2.1. Based on a more detailed and careful investigation,[124] it turns out that the hydroxyl proton is a special case, because of the two possible conformations (*trans* and *gauche*) an ethanol molecule, for example, can assume. Depending on the level of the theory, either conformation can be of lowest energy. In fact, with density functional theory, Borowski *et al.*[124] arrive at a 0 ppm value for the vibrational correction to the shielding of a hydroxyl proton. In an attempt to reproduce the liquid spectrum of ethanol, Borowski *et al.* have found that the starting geometry should be obtained at a correlated level and with a large basis set, B3LYP/6–311G(d,p). Similarly, the NMR shieldings should be calculated at the same level with a 6–311++G(d,p) basis. The results obtained using an isolated molecule compare favorably with gas phase chemical shifts. To match the spectrum in the liquid, it appears that clusters of ethanol between a trimer and a tetramer are necessary. This novel work also points out the importance of basis sets in deriving populations of various clusters within the quantum cluster equilibrium (QCE) theory of liquids.[125]

Averaging over an internal rotation is discussed by Baaden *et al.*[126] using vinyl derivatives $H_2C{=}CH{-}X$, where the rotation occurs about the C–X bond. This averaging leads to a correction to the ^{13}C shieldings of about 2 ppm in the isotropic value, and as much as 17 ppm when individual tensor components are considered. Large amplitude internal motions in the solid state can also lead to an averaging of the shielding tensor orientation, which in turn leads to temperature-sensitive powder NMR spectra. Hallock *et al.*[127] discuss in detail the effects of librations on the ^{13}C shielding tensor in β-calcium formate. The motion of interest in this system is a wagging type centered around an axis that lies approximately on the carboxylate plane and is perpendicular to the C–H vector. This axis is parallel to the direction of the intermediate shielding

component, thus, both σ_{11} and σ_{22} are motion-averaged and are dependent on temperature. The same motion can account for the observed temperature dependence of the ^{2}H electric field gradient tensor on deuterium-labeled β-calcium formate.

^{87}Rb NMR shieldings have been shown experimentally to depend linearly on the distance of the Rb^{+} ion to its nearest neighbor shell of halide ions in the family of Rb-doped alkali halides, and theoretical calculations bear out the experimental linear trends.[128] The shielding derivatives with respect to the ionic distance are positive and are very similar, largely independent of the identity of the halide ion for the distances that naturally occur in the alkali halide lattices. At much shorter distances, we would not expect this to be the case.

One area that continues to illustrate the significance of shielding surfaces is the prediction of isotope shifts, to be discussed in detail in the next section. Gee and Raynes[129] have recently added the molecule methyl fluoride to the short list of polyatomic molecules whose shielding surfaces have been totally determined. The shielding derivative of the ^{13}C shielding with respect to the C–H bond length is about -15 ppm/Å, while for ^{19}F it is -29 ppm/Å. The dependence on the C–F bond is greater, with the first derivative for ^{13}C being -102 ppm/ Å and for ^{19}F -169 ppm/ Å. The second derivatives are fairly substantial that these can no longer be safely discounted in predicting the vibrational corrections for the shielding of both ^{13}C and ^{19}F nuclei. Moreover, the contributions arising from the C–H stretching motion are twice as much as the contributions coming from the C–F bond, in terms of the vibrational corrections to the ^{19}F shielding. Lastly, second order contributions from bending motions are also deemed necessary in calculating the isotope shifts and the temperature dependence of the ^{13}C and ^{19}F NMR chemical shifts in methyl fluoride.

An interesting study of the shielding of Si and its variation with Si–O–Si angle presents probably the most complete shielding calculation relating to this dependence.[53] Previous treatments, by the Tossell[130] and Sauer[58] groups, and others, had used small fragments rather than an extended network to calculate the shielding. Mauri *et al.* calculated the correlation between the ^{29}Si shieldings and the Si–O–Si bond angles for the full range of angles (including 180°) found in vitreous silica.[53] Using their theory of NMR shielding in infinite extended periodic networks,[51] and DFT, they constructed a set of polymorphs with different Si–O–Si angles, and the large unit cells of the polymorphs are used to generate the periodic network. The ^{29}Si NMR spectrum of vitreous silica is compared with their theoretical spectra for a parametrized Si–O–Si angle distribution function. A very good description of the experimental NMR spectrum is achieved. Calculated and measured chemical shifts in crystals (quartz, cristobalite, tridymite) are in excellent agreement and confirm the method's accuracy. The only outliers are the shifts from coesite. Distributions derived from diffraction data which are characterized by different first and second moments exhibit large deviations from the experimental NMR spectrum. Thus, the method can distinguish among various proposed angle

distributions, and using a parametrized distribution function with this method offers a general approach that may be very useful in interpreting the multidimensional spectra obtained in solids that are correlations of anisotropic and quadrupolar lineshapes with isotropic chemical shifts.

The shielding tensors for CO, NO, and O_2 bound to iron porphyrin model complexes have been the subject of several experimental and theoretical studies. Of particular interest are the bend and tilt angles that define the geometry of the Fe–O–O, for example, with respect to the porphyrin ring, whether the NMR parameters can provide unequivocal information about this geometry and also, what is the extent and nature of the dynamic averaging that is taking place at the temperatures of the NMR experiment. The theoretical ^{17}O shielding and electric field gradient tensors have been studied recently for the O_2 complex of the picket fence porphyrin, $Fe(T_{piv}PP)(2\text{-}MeIm)(O_2)$, using the results of the large scale *ab initio* molecular dynamics simulations of the Car–Parinello type as the basis for structural and dynamical information. The SOS-DFPT(IGLO) approach was used with the Loc1 approximation of the Malkin correction.[131] The variation of the ^{17}O isotropic shielding and the nuclear quadrupole coupling constant as a function of Fe–O–O angle for both the terminal and the bridging oxygen have been investigated. The comparison of the computed and experimental shift tensor components suggests that, in contrast to the interpretations that accompanied the experimental solid state NMR studies,[132] even at 77 K, the rotation of the O_2 ligand above the porphyrin plane is not frozen in. The nuclear quadrupole coupling constants that were calculated do not agree with the values that were found by fitting the solid state spectra. The calculations do not resolve the difference between the solution and solid state chemical shifts, nor the temperature dependence observed. The authors concede that the electronic structure of the Fe–O–O in these oxyheme complexes remains to some extent an unsolved puzzle.

The variation of the ^{13}C and ^{15}N chemical shifts as a function of the glycosidic torsion angle in nucleic acids has been investigated using B3LYP-GIAO.[133] Torsion angle and base-pairing information is apparently encoded in the chemical shifts.

2.3 Isotope Shifts. – Isotope shifts are intimately related to shielding surfaces. Gee and Raynes[129] have utilized their calculated shielding surfaces for ^{13}C and ^{19}F in methyl fluoride to arrive at the following deuterium-induced isotope shifts at 300 K. On going from CH_3F to CH_2DF, to CHD_2F, to CD_3F the increments for each deuterium-induced isotope shift on ^{19}F are, 0.626 ppm, 0.618 and 0.616 ppm, respectively. The corresponding numbers for ^{13}C are 0.297 ppm, 0.294 ppm and 0.291 ppm. All are in the same direction, that is, heavy atom substitution leads to increased shielding. The apparent lack of strict additivity is attributed to angular contributions.

Isotope effects acting over a network of more than three bonds have been illustrated in the case of methyl groups contributing in a steric fashion to the shielding of another carbon nucleus (at least five bonds away, but close in

space).[134] The shifts are in the order of +0.055 ppm to −0.035 ppm, with both sign and magnitude depending on the initial steric effect of the methyl group. The sign of the deuterium-induced shift is, of course, opposite to that of the initial effect attributed to the methyl group. In fact, if one plots the isotope shift (Δ) against the initial methyl substituent effect (δ), one finds a linear equation (determined from 12 different compounds): Δ (in ppb) = -7.3δ (in ppm) -5.5. Although isotope effects due to deuterium substitution are most common, isotope effects due to other isotopes are also observed. In this reporting period, $^{37}Cl/^{35}Cl$ and $^{13}C/^{12}C$ isotope effects have been measured for the ^{19}F shielding in a series of two-carbon chlorofluoro-substituted ethanes and ethenes.[135] The measured $^{13/12}C$-induced ^{19}F shifts are 0.094–0.160 ppm for one-bond isotope shifts and 0.013–0.049 ppm two-bond isotope shifts, while the two- or three-bond $^{37}Cl/^{35}Cl$-induced ^{19}F shifts are within the range of 0.045 to 0.076 ppm for these molecules. All signs are usual, that is, heavy atom substitution leads to increase in shielding. Large ^{15}N-, ^{13}C-, ^{18}O-isotope-induced one-bond and two-bond shifts in ^{31}P spectra have been reported in phosphalkynes.[136]

2.4 Intermolecular Effects on Nuclear Shielding. – Since hydrogen bonding is crucial in biologically relevant molecules, it is with no surprise that a significant amount of attention has always been given to changes in shielding caused by hydrogen bonding. Arnold and Oldfield have applied Bader's theory of Atoms in Molecules in describing the electronic structure of various types of hydrogen bonds.[137] A short strong hydrogen bond (SSHB), characterized by a dramatic deshielding of the proton (about 20 ppm), apparently consists of an interaction that has attained significant covalent character. A related work by Barich *et al.*[138] shows that electron correlation contributes significantly to the proton shieldings (by about 1–2 ppm) in short strong hydrogen bonded systems. A combined theoretical and experimental study of crystalline urea provides interesting insight. It is found that the ^{17}O shielding tensor in the crystalline state cannot be reproduced without the use of a model that includes a cluster containing seven urea molecules.[96] With B3LYP/6–311++G**, the value obtained in an isolated monomer is 80 ppm away from the experimental value, in which the discrepancy is mostly present in the two components σ_{11} and σ_{22}. In contrast to C=O in other amides, the least shielded component of the observed ^{17}O shielding tensor in urea does not lie parallel to the C=O bond direction. It still lies in the plane of the molecule, but it is perpendicular to the carbonyl bond. It is the intermediate component that lies parallel to the C=O vector. The three-dimensional hydrogen bonding network employed in this work consists of a urea molecule lying at the origin of a Cartesian frame with additional urea molecules at each axis. Four of the six neighboring urea molecules are interacting with the center urea molecule acting as a hydrogen bond acceptor. Two of these four lie on the same plane as the center urea molecule, while the other two approach the urea molecule from directions normal to this plane. It is interesting to note that two additional molecules (to complete the six neighbors) are also necessary to make the results approach the

experimental values. These two additional urea molecules, unlike the other four, are hydrogen bond acceptors to the center urea molecule. Thus, although this hydrogen bonding takes place with the amide protons and not the carbonyl group carrying the ^{17}O nucleus of interest, its effects are very much present in the ^{17}O shielding tensor.

Witanowski *et al.*[139] have found that the ^{15}N shieldings in *N,N*-dimethylacetamidine are extremely sensitive to solvents. A range of about 120 ppm is observed for a set of solvents that includes cyclohexane, diethyl ether, benzene, ethanol and water. Among solvents that cannot serve as hydrogen bond donors, the range reduces to about 8 ppm. The large increase in nitrogen shielding of about 120 ppm in going from cyclohexane to water is attributed to a complete proton transfer to the =NH moiety in the latter solvent. The great sensitivity of the ^{15}N shielding to hydrogen bonding arises from the low-lying $n \rightarrow \pi^*$ magnetic dipole transition that is largely responsible for the paramagnetic shielding of a nitrogen with a lone pair and involved in a pi bond. When a proton is accepted, the lone pair character disappears, leading to a more positive shielding. This is indeed what is observed in the proton-donating solvents. For nonspecific interactions, Manalo *et al.*[140] have found that a polarizable continuum model (PCM) is able to reproduce solvent effects on ^{15}N NMR shieldings in 1,2,4,5–tetrazine and isomeric tetrazoles. It has been shown that the observed solvent-induced shielding variation is more strongly related to the intensity of the solvent reaction field rather than on the change of molecular geometry induced by the solvent. The approach used, however, does not take into account the consequences of specific solute–solvent interactions such as hydrogen bonding, thus, as an example, PCM is not expected to reproduce the 120 ppm shift seen *N,N*-dimethylacetamidine.

The knowledge of shielding tensors, their anisotropy and orientation, can facilitate the design of experimental work as illustrated by Czerneky.[141] Using Watson–Crick base pairs, the shieldings of the ^{15}N nuclei have been studied as a function of hydrogen bond distance in this recent work. It is claimed that the SOS-DFT-IGLO method produces values similar to those of B3LYP-GIAO, yet the former requires shorter computational times. With a triple-zeta basis set, basis set superposition errors are found to be negligible. Geometry optimization at each hydrogen separation does not affect appreciably the calculated shielding tensors. Finally, based on the calculated CSA autocorrelation and cross-correlation parameters, improvements in the resolution of heteronuclear correlated spectra are expected *via* the application of transverse relaxation-optimized spectroscopy (TROSY). Barfield *et al.*[142] have likewise shown that the ^{15}N shielding correlates with coupling constants in the hydrogen bonding regions of a DNA triplex. Other work on the shielding of the nucleic acid bases, some paired and stacked, are mentioned elsewhere in this review chapter.[27,133]

Comparative calculations[143] of the shielding constants in water dimer reveal the following. SCF calculations with a medium-size basis set (as in 6–31++G**) are reliable for proton shieldings. On the other hand, for ^{17}O, the requirements are much more stringent. First, larger basis sets, at least triple-

zeta quality, are imperative. Second, basis set superposition errors are present and need to be corrected. Third, electron correlation is very important. None of these are surprising or new. To illustrate the importance of these requirements, it is cited that, in the case of the shielding of the proton donor, SCF calculations even give the opposite sign for the shift upon dimer formation. Lastly, the MP2 method tends to overestimate the correlation, thus, either CCSD- or MP4-level calculations are recommended. In any case, the water dimer is too small a model for water in the condensed phase. For this, as we shall see below, the rest of the liquid has to be taken into account. Theoretical investigations of hydrogen-bonding-induced shielding changes have been performed on CH···O systems.[144] In this paper, fluorinated methane derivatives have been used as donors with water, methanol and formaldehyde as acceptors. The effects, as expected, are smaller compared to systems where the proton is attached to an N, O, or F atom. Since these changes in shielding are much smaller, they are much more sensitive to basis set size, superposition errors and level of theory. Aminova *et al.*[145] have calculated the effects of hydrogen bonding on the shielding of ^{1}H, ^{13}C and ^{17}O nuclei in formic acid, acrylic acid and their complexes with water and dimethyl sulfoxide. Their work suggests that chemical shifts of methyl protons can be used as an indicator for C–H···O hydrogen bonding. Effects of hydrogen bonding have likewise been investigated for the following hetero- and homo-dimers; CH_2O–H_2O, C_2H_2–H_2O, CH_3OH–H_2O and $(HCOOH)_2$.[146] Felemez *et al.*[147] suggest that the unusual deshielding of the ^{31}P nucleus of the P-1 site in *myo*-inositol 1,4,5-tris(phosphate) is due to C–H···O hydrogen bonding. The ^{31}P shielding tensor in dipalmitoylphosphatidic acid has been demonstrated to be particularly sensitive to complexation with amines.[148] With regard to geometrical parameters describing a hydrogen bond interaction, Facelli,[149] using a pyridine–methanol complex as a model system, has discovered that hydrogen bond effects are significantly more sensitive to the distance between molecules than to the orientation between them. Therefore, the principal components of the ^{15}N shielding tensor, especially the most deshielded principal value, can be employed as a good indicator for the separation between the pyridine nitrogen nucleus and an interacting proton. In a range of N–O distances of 2.59 to 3.49 Å, a variation of as much as 35 ppm is predicted for the σ_{11} component.

Although shielding is a local property, the question of where one should truncate a condensed system into a manageable model still remains to be answered in some cases. Using clusters that include up to fourth nearest neighbor atoms, Casanovas *et al.*[150] have been able to reproduce ^{29}Si chemical shifts observed for defect sites (≡Si-H, ≡Si-OH, =Si(H)$_2$, and =Si(OH)$_2$) in silica. The QM/MM method of Cui and Karplus,[27] which can provide a means of incorporating intermolecular effects on shielding, including averaging in condensed phases, has already been discussed in Section 1.1. In this method, the outer shells of the onion in the model are treated with molecular mechanics (MM) whereas the local electronic structure is described with quantum mechanics. CHARMM charges are incorporated in the MM region. Examples of systems to which the method has been applied include paired and stacked

nucleic acid bases and metal ion complexes of deoxyribose.[27] Stueber *et al.*[151] propose, in what they call an embedded ion method, the utilization of Ewald lattice sums (implemented in *Gaussian98*) as a way of accounting for polarization contributions to the chemical shielding in ionic lattices. The method generates point charge arrays that simulate the Ewald potential over a defined region at the center of the array. Applied to the computation of ^{13}C shieldings in potassium methyl-trithiocarbamate (KS_2CSCH_3), it is observed that incorporation of an Ewald potential results in a substantial improvement of the calculated shieldings, based on their closer agreement to experimental values. Furthermore, the orientation of the principal axis system for the shielding tensor of the central C appears to be sensitive to the addition of an Ewald sum lattice. This is a self-consistent way of including the ionic lattice effects.

Calculating shieldings in a hetero- or homo-dimer as a means of eliciting the solvent shifts or gas-to-liquid shifts may be sufficient if one is primarily interested in qualitative trends, but such calculations are clearly inadequate to reproduce gas-to-liquid shifts or gas-to-solutions shifts in strongly associated systems like water. Two methods of treating the shielding in liquid water (and in ice, too) that go well beyond the usual (inadequate) dimer or even the 17–mer of Pulay *et al.*,[54] have been reported. The QM/MM approach of Cui and Karplus uses molecular dynamics simulations in a 16 Å water sphere with a deformable stochastic boundary potential.[27] The calculated gas to-liquid-shift in water, found by doing QM(within 3 Å radius of the nucleus)/MM for 100 MD snapshots averaging 7–8 water molecules in the QM region, could only provide a part of the observed values, −22.3 ppm for the ^{17}O and −2.9 ppm for the ^{1}H. These are the difference between the shielding of the water in clusters and the water monomer, both configurations taken from the liquid MD trajectory. The MM contributions are −5 ppm and −0.5 ppm for the ^{17}O and ^{1}H respectively. Using a larger basis set showed that the basis set deficiencies cause errors of roughly 7 ppm and 0.5 ppm for the ^{17}O and ^{1}H respectively. Within these errors, the authors consider their results in agreement with the results of the supermolecule, up to $(H_2O)_{13}$, calculations of Malkin *et al.*, −36.8 ppm for the ^{17}O and −3.4 ppm for the ^{1}H.[152] Experimental values are −36.0 ppm at 300 K[153] and −4.368 ppm at 298.2 K.[154] It appears that the TIP3P potential model they used for liquid water is adequate to produce the needed small but not negligible long-range effects in the molecular dynamics simulations. Pfrommer *et al.*[155] use the method they developed for extended periodic networks[51] to calculate the ^{1}H and ^{17}O chemical shifts in hexagonal ice and in liquid water. A super-cell technique extends the method they previously used for crystals (diamond, for example)[51] to amorphous materials (such as silica glass)[53] and liquids. Liquid water is modeled by nine snapshots from an *ab initio* (BLYP) Car–Parinello molecular dynamics simulation at 300 K. A cubical supercell with 32 water molecules inside and an edge length of 9.865 Å is periodically replicated. The results are $\sigma(^{1}H, H_2O$, liquid model, 300 K) $-\sigma(^{1}H$, static H_2O monomer) = -5.83 ± 0.10 ppm. For ^{17}O the corresponding value found is -36.6 ± 0.5 ppm.[155] Hexagonal ice is a crystal with static and/or dynamic

Table 2.2 *The ^1H shielding in ice, ppm; the basis for the absolute shielding values is a series of translations from TMS or liquid water back to the absolute shielding scale; the experimental monomer shielding using the same absolute scale is $\sigma_0(^1H, H_2O$, gas, 403–463 K) = 30.05 ± 0.015*[157]

Author	*Phase*	σ_{11}, σ_{22}	σ_{33}	$\Delta\sigma$	σ_{iso}	σ_{iso} − 30.05 ± 0.015	*Ref*
Pines *et al.*	Ice, 183 K	12.4	46.4	34 ± 2	23.7	−6.4	158
Ryan *et al.*	Ice, 173 K	19.2	53.4	34.2 ± 1	30.6	+0.6	159
Rhim *et al.*	Single	13.2	41.7	28.5 ± 1	22.7	−7.4	160
Burum *et al.*	Ice, 77 K crystal, 77 K	10.8	39.5	28.7	20.4	−9.7	161
Pulay *et al.*	$(H_2O)_5$	12.30, 13.32	47.72	33.92	24.45	−5.6	54
Pulay *et al.*	$(H_2O)_{17}$	11.97,	46.91	34.83	23.69	−6.36	54
Pfrommer *et al.*	Periodic hexagonal, 0 K			33.4 ± 0.2		−8.0 ± 0.1	155

disorder. Thus, the simulations are restricted to a static periodic model of ice which is designed to resemble the disordered phase. Supercells have the oxygen atoms exactly at their symmetric averaged lattice sites, with the hydrogen atoms placed at arbitrary sites following the "ice rules".[155] The results indicate molecules beyond the first solvation shell influence the proton shielding *via* electrostatic polarization. It is worthwhile to repeat here (in Table 2.2) the absolute ^1H shieldings that the experimental chemical shifts in ice translate into, especially since accidental misrepresentations of the data keep recurring in the literature when the experimental data are compared with calculations. The absolute shielding for ^1H derives from $\sigma(^1H, H_2O$, spherical liquid, 307.9 K) = 25.790 ± 0.014 ppm based on H atom beam and g value of the electron in the H atom.[156] We see that the present calculations[155] provide as good agreement with experiments of Pines *et al.*[158] as does the earlier work by Pulay and co-workers using $(H_2O)_{17}$ in the ice geometry.[54]

It is known that a molecule that crystallizes in two (or more) crystalline forms is found to have different geometries in the different crystalline forms and have different solid state NMR spectra. Thus, when doing a shielding calculation for comparison with a solid state experiment, it is important to incorporate the changes in geometry that are imposed by the local electric potential in the solid. This could be done using the Ewald potential described by Stueber *et al.*[151] In the method introduced by Mauri *et al.*[51] for extended networks of periodic systems, geometry optimization of the molecule is carried out in the presence of counterions, using periodic boundary conditions, which correctly account for the interactions between atoms belonging to different periodic cells in crystals. They find that geometry optimization affects the calculated ^{13}C shieldings in retinylidene iminium salts.[162] The changes upon

relaxation of the geometry translate to a closer agreement between calculated and measured ^{13}C chemical shifts.

An oversimplified polarization model would place two partial charges +q and −q at some orientation and distance from the isolated molecule to see how much the ^{13}C shieldings would change in aromatic groups in 1-X,2-methoxynaphthalenes.[163] Lau and Gerig[164] have attempted to reproduce ^{19}F chemical shifts in fluorine-labeled proteins. However, due to the presence of motion and various factors contributing to the measured ^{19}F NMR chemical shifts, agreement between experiment and theory is not satisfactory. Perczel and Csaszar[165] have performed theoretical work on chemical shifts of the nuclei in valine at various conformations, a repetition of the earlier work done by de Dios and Oldfield.[166] Unfortunately, Perczel and Csaszar, in their recent work, have claimed excellent correlation by plotting the theoretical and experimental chemical shifts for all nuclei, ^{1}H, ^{13}C and ^{15}N, in one graph!

In this reporting period, ^{129}Xe continues to serve as an excellent probe for porous surfaces and nonspecific surface interactions. Sozzani *et al.*[167] have used continuous flow hyperpolarized Xe NMR in studying tris(*o*-phenylenedioxy)cyclophosphazene (TPP) channels. Their work illustrates the dependence of the Xe NMR lineshape on the concentration of Xe in the gas used for the continuous flow experiment. The ^{129}Xe NMR chemical shifts measured in solutions containing myoglobin at various concentrations has a non-monotonic dependence on the concentration of the protein.[168] After the initial addition of protein, the ^{129}Xe resonance becomes more deshielded compared to its resonance in water. However, at higher protein concentrations, a shielding effect begins to occur. It is suggested that the initial deshielding is caused by nonspecific interactions between Xe and the surface atoms of myoglobin while the increased shielding observed is due to Xe binding to a specific site within the protein. Such suggestion is supported by the observation of a monotonic deshielding with increasing protein concentration when denatured myoglobin is used.

Gas phase NMR measurements at various densities have long been applied to provide the shielding for an isolated molecule that permits closer comparisons with theoretical values. Jackowski *et al.*[169–171] have done gas phase measurements in order to obtain chemical shifts at the zero-density limit; they then insert these values into some previously determined absolute shielding scale. They measured the ^{13}C and ^{1}H chemical shifts of acetylene (relative to liquid TMS) in binary mixtures with Xe or CO_2 gas and extrapolated to zero density.[169] They also list their measurements of the values for $\sigma_0(^{13}C, HCCH) - \sigma_0(^{13}C, CO) = 115.98$ ppm and $\sigma_0(^{1}H, HCCH) - \sigma_0(^{1}H, CH_4) = -1.334 \pm 0.002$ ppm, but do not state how these were obtained. (Did they use a mixture of acetylene and CO or did they measure the rather broad peak of ^{13}CO in the gas against liquid TMS?) When placed on the existing absolute ^{13}C and ^{1}H shielding scales, the observed values at 300 K for the isolated molecule is $\sigma_0(^{13}C, HCCH) = 116.58 \pm 0.9$ ppm, in agreement with a previously reported value, 116.8 ppm[172] and $\sigma_0(^{1}H, HCCH) = 29.278 \pm 0.024$ ppm for ^{1}H. The absolute scale they used is based on $\sigma_0(^{13}C, CO) = 0.6 \pm 0.9$ ppm and $\sigma_0(^{1}H,$

CH_4) = 30.611 ± 0.024 ppm. They measured the ^{17}O chemical shifts for CO, CO_2, OCS and NNO in the gas phase relative to liquid H_2O at various densities.[170] After extrapolation to zero-density they used the value $\sigma_0(^{17}O, H_2O)$ = 307.9 ppm from the ^{17}O absolute shielding scale of Wasylishen *et al.*[173] that is based on the absolute $\sigma_0(^{17}O, CO) = -42.3 \pm 17$ ppm to convert the measured chemical shifts at zero density into absolute shieldings: $\sigma_0(^{17}O, CO_2)$ = 225.8 ppm, $\sigma_0(^{17}O, NNO)$ = 184.4 ppm, $\sigma_0(^{17}O, OCS)$ = 90.7 ppm, and $\sigma_0(^{17}O, CO) = -59.5$ ppm. These numbers are all in excellent agreement with the earlier gas phase data of Wasylishen *et al.*[173] Having been extrapolated to zero density the Jackowski data should be more precise. Jackowski[171] also reports ^{33}S in OCS and SF_6 gas. Using Wasylishen's ^{33}S absolute shielding scale based on $\sigma_0(^{33}S, OCS) = 843 \pm 12$ ppm,[174] he thus places SF_6 as $\sigma_0(^{33}S, SF_6)$ = 398.9 ppm, which is somewhat different from Wasylishen's earlier value of 417.2 ppm.[174]

2.5 Absolute Shielding Scales. – Gee and Wasylishen[175] have recommended that the microwave study of AlH be repeated, as the previous one[176] failed to account for the ^{27}Al nuclear spin–rotation interaction. Their *ab initio* calculations give a range of values depending on the method used but are all of the order of 300 kHz.[175] The value of the spin–rotation constant for ^{27}Al in AlF, on the other hand, has been measured, $C_\perp = 8.2 \pm 1.3$ kHz,[177] which leads to $(\sigma_\parallel - \sigma_\perp) = 320 \pm 50$ ppm for ^{27}Al in AlF and

$$\sigma_{iso}(^{27}Al, AlF, v = 0) = 580 \pm 50 \text{ ppm}.$$

To have a usable ^{27}Al absolute shielding scale, what is still needed is the ^{27}Al chemical shift between a commonly used reference substance such as $[Al(H_2O)_6]^{3+}$ in infinite dilution and the isolated AlF molecule.

A microwave study of the spin–rotation tensor of GaF in the gas phase has been reported by Wasylishen *et al.*[178] This provides spin–rotation constants for both the ^{19}F and the ^{69}Ga nucleus. A value of $(\sigma_\parallel - \sigma_\perp) = 945 \pm 35$ ppm for ^{69}Ga is derived from the experimental spin–rotation constant. The absolute ^{69}Ga isotropic shielding obtained from the experimental spin–rotation constant at the ground vibrational state of GaF is

$$\sigma_{iso}(^{69}Ga, GaF, v = 0) = 2005 \pm 35 \text{ ppm},$$

using a non-relativistic calculation for the diamagnetic part. This provides an independent point on the Ga absolute shielding scale, in addition to the

$$\sigma_{iso}(^{71}Ga, [Ga(OD_2)_6]^{3+}, \text{infinitely dilute in } D_2O) = 1840 \pm 45 \text{ ppm},$$

obtained by an atomic beam of Ga atoms measured at the same time in the same field as the solution at infinite dilution.[179] The non-relativistic value of 2638.6 ppm[180] is used for the free atom to arrive at this absolute shielding. On the other hand, *ab initio* calculations (MP2/6–311G(2df,2pd)) of the Ga shielding in GaF gives 2038 ppm.[178] The value of $(\sigma_\parallel - \sigma_\perp) = 945 \pm 35$ ppm for ^{69}Ga is compared with other Group 13 fluorides, using values derived in the same way from the spin–rotation constants of the diatomic molecules: ($\sigma_\parallel$

$-\sigma_{\perp}$) = 320 ppm for Al in AlF, 945 ppm for Ga in GaF, ~1660 ppm for In in InF and ~5300 ppm for Tl in TlF.

3 References

1 L. Visscher, T. Enevoldsen, T. Saue, H. J. A. Jensen and J. Oddershede, *J. Comput. Chem.*, 1999, **20**, 1262.
2 Y. Ishikawa, T. Nakajima, M. Hada and H. Nakatsuji, *Chem. Phys. Lett.*, 1998, **283**, 119.
3 M. Hada, Y. Ishikawa, J. Nakatani and H. Nakatsuji, *Chem. Phys. Lett.*, 1999, **310**, 342.
4 P. Pyykkö, A. Gorling and N. Rösch, *Mol. Phys.*, 1987, **61**, 195.
5 N. C. Pyper, *Chem. Phys. Lett.*, 1983, **96**, 211.
6 M. Hada, R. Fukuda and H. Nakatsuji, *Chem. Phys. Lett.*, 2000, **321**, 452.
7 G. Schreckenbach and T. Ziegler, *J. Phys. Chem.*, 1995, **99**, 606.
8 G. Schreckenbach, R. M. Dickson, Y. Ruiz-Morales and T. Ziegler, in *Density Functional Theory in Chemistry*, ed. B. Laird, R. Ross and T. Ziegler, ACS Symposium Series 629, American Chemical Society, Washington D.C., 1996, p. 328.
9 M. Kaupp, V. G. Malkin, O. L. Malkina and D. R. Salahub, *Chem. Phys. Lett.*, 1995, **235**, 382.
10 M. Kaupp, V. G. Malkin, O. L. Malkina and D. R. Salahub, *J. Am. Chem. Soc.*, 1995, **117**, 1851.
11 H. Nakatsuji, H. Takashima and M. Hada, *Chem. Phys. Lett.*, 1995, **233**, 95.
12 V. G. Malkin, O. L. Malkina and D. R. Salahub, *Chem. Phys. Lett.*, 1996, **261**, 335.
13 O. L. Malkina, B. Schimmelpfennig, M. Kaupp, B. A. Hess, P. Chandra, U. Wahlgren and V. G. Malkin, *Chem. Phys. Lett.*, 1998, **296**, 93.
14 M. Kaupp, C. Aubauer, G. Engelhardt, T. M. Klapotke and O. L. Malkina, *J. Chem. Phys.*, 1999, **110**, 3897.
15 C. C. Ballard, M. Hada, H. Kaneko and H. Nakatsuji, *Chem. Phys. Lett.*, 1996, **254**, 170.
16 M. Kaupp and O. L. Malkina, *J. Chem. Phys.*, 1998, **108**, 3648.
17 S. K. Wolff and T. Ziegler, *J. Chem. Phys.*, 1998, **109**, 895.
18 S. K. Wolff, T. Ziegler, E. van Lenthe and E. J. Baerends, *J. Chem. Phys.*, 1999, **110**, 7689.
19 T. M. Gilbert and T. Ziegler, *J. Phys. Chem.*, 1999, **103**, 7535.
20 A. Rodriguez-Fortea, P. Alemany and T. Ziegler, *J. Phys. Chem.*, 1999, **103**, 8288.
21 G. Schreckenbach, S. K. Wolff, T. Ziegler, *J. Phys. Chem.*, 2000, **104**, 8244.
22 R. Bouten, E. J. Baerends, E. van Lenthe, L. Visscher, G. Schreckenbach and T. Ziegler, *J. Phys. Chem.*, 2000, **104**, 5600.
23 J. Vaara, O. L. Malkina, H. Stoll, V. G. Malkin, M. Kaupp, *J. Chem. Phys.*, 2001, **114**, 61.
24 J. Wan, R. Fukuda, M. Hada and H. Nakatsuji, *J. Phys. Chem.*, 2001, **105**, 128.
25 S. Patchkovskii, J. Autschbach and T. Ziegler, *J. Chem. Phys.*, 2001, **115**, 26.
26 C. J. Pickard and F. Mauri, *Phys. Rev. B*, 2001, **63**, 5101.
27 Q. Cui and M. Karplus, *J. Phys. Chem. B*, 2000, **104**, 3721.
28 R. McWeeney, *Methods of Molecular Quantum Mechanics*, 2nd. Ed., Academic, New York, 1998.

29 R. van Leeuwen and E. J. Baerends, *Phys. Rev. A*, 1994, **49**, 2421.
30 D. J. Tozer and N. C. Handy, *J. Chem. Phys.*, 1998, **108**, 2545.
31 D. J. Tozer and N. C. Handy, *J. Phys. Chem. A*, 1998, **101**, 5383.
32 P. J. Wilson, R. D. Amos and N. C. Handy, *Mol. Phys.*, 1999, **97**, 757.
33 P. J. Wilson, R. D. Amos and N. C. Handy, *Chem. Phys. Lett.*, 1999, **312**, 475.
34 T. Helgaker, P. J. Wilson, R. D. Amos and N. C. Handy, *J. Chem. Phys.*, 2000, **113**, 2983.
35 J. Gauss and J. F. Stanton, *J. Chem. Phys.*, 1995, **102**, 251.
36 J. F. Stanton, J. Gauss and H. U. Siehl, *Chem. Phys. Lett.*, 1996, **262**, 183.
37 V. G. Malkin, O. L. Malkina, L. A. Eriksson and D. R. Salahub, in *Modern Density Functional Theory: A Tool for Chemistry*, Vol. 2 of Theoretical and Computational Chemistry, ed. P. Politzer and J. M. Seminario, Elsevier, Amsterdam, 1995, p. 273.
38 L. Olson and D. Cremer, *J. Chem. Phys.*, 1996, **105**, 8995.
39 L. Olson and D. Cremer, *J. Phys. Chem.*, 1996, **100**, 16881.
40 G. Schreckenbach, *J. Chem. Phys.*, 2000, **110**, 11936.
41 M. Bühl, *Chem. Phys. Lett.*, 1997, **267**, 251.
42 C. J. Jameson, D. Rehder and M. Hoch, *J. Am. Chem. Soc.*, 1987, **109**, 2589.
43 J. S. Griffith and L. E. Orgel, *Trans. Faraday Soc.*, 1957, **53**, 601.
44 W. G. Schneider and A. D. Buckingham, *Disc. Faraday Soc.* 1962, **34**, 147.
45 P. J. Wilson, R. D. Amos and N. C. Handy, *Phys. Chem. Chem. Phys.*, 2000, **2**, 187.
46 P. J. Wilson, *Mol. Phys.*, 2001, **99**, 363.
47 M. Bühl, J. Gauss and J. F. Stanton, *Chem. Phys. Lett.*, 1995, **241**, 248.
48 V. G. Malkin, O. L. Malkina, M. E. Casida and D. R. Salahub, *J. Am. Chem. Soc.*, 1994, **116**, 5898.
49 M. Bühl, S. Gaemers, C. J. Elsevier, *Chem. Eur. J.*, 2000, **6**, 3272.
50 X. P. Xu and S. C. F. Au-Yeung, *J. Am. Chem. Soc.*, 2000, **122**, 6468.
51 F. Mauri, B. G. Pfrommer, S. G. Louie, *Phys. Rev. Lett.*, 1996, **77**, 5300.
52 T. Gregor, F. Mauri and R. Car, *J. Chem. Phys.*, 1999, **111**, 1815.
53 F. Mauri, A. Pasquarello, B. G. Pfrommer, Y. G. Yoon and S. G. Louie, *Phys. Rev. B*, 2000, **62**, R4786.
54 J. F. Hinton, P. Guthrie, P. Pulay and K. Wolinski, *J. Am. Chem. Soc.*, 1992, **114**, 1604.
55 J. A. Tossell, *Phys. Chem. Miner., 1992*, **19**, 338.
56 J. A. Tossell, *Phys. Chem. Miner.*, 1999, **27**, 70.
57 F. Haase and J. Sauer, *J. Phys. Chem.*, 1994, **98**, 3083.
58 G. Ricchiardi and J. Sauer, *Z. Phys. Chem. (Part 1)*, 1999, **209**, 21.
59 G. Valerio, A. Goursot, R. Vetrivel, O. L. Malkina, V. G. Malkin and D. R. Salahub, *J. Am. Chem. Soc.*, 1998, **120**, 11426.
60 R. Ludwig, F. Weinhold and T. C. Farrar, *Ber. Bunsenges. Phys. Chem.*, 1998, **102**, 205.
61 R. Ludwig, F. Weinhold and T. C. Farrar, *J. Phys. Chem.*, 1997, **101**, 8861.
62 C. J. Jameson and H. M. Lim, *J. Chem. Phys.*, 1995, **103**, 3885.
63 A. C. de Dios and C. J. Jameson, *J. Chem. Phys.*, 1997, **107**, 4253.
64 A. C. de Dios, J. G. Pearson and E. Oldfield, *Science*, 1993, **260**, 1491.
65 A. E. Walling, R. E. Pargas, A. C. de Dios, *J. Phys. Chem.*, 1997, **101**, 7299.
66 C. J. Jameson, A. K. Jameson, B. I. Baello and H. M. Lim, *J. Chem. Phys.*, 1994, **100**, 5965.
67 C. J. Jameson, A. K. Jameson, H. M. Lim and B. I. Baello, *J. Chem. Phys.*, 1994, **100**, 5977.

68 C. J. Jameson, A. K. Jameson, R. E. Gerald and H. M. Lim, *J. Chem. Phys.*, 1995, **103**, 8811.
69 C. J. Jameson, A. K. Jameson and H. M. Lim, *J. Chem. Phys.*, 1996, **104**, 1709.
70 C. J. Jameson, A. K. Jameson and H. M. Lim, *J. Chem. Phys.*, 1997, **107**, 4364.
71 C. J. Jameson, A. K. Jameson, P. Kostikin and B. I. Baello, *J. Chem. Phys.*, 2000, **112**, 323.
72 J. H. Kantola, J. Vaara, T. T. Rantala and J. Jokisaari, *J. Chem. Phys.*, 1997, **107**, 6470.
73 P. B. Karadakov and K. Morokuma, *Chem. Phys. Lett.*, 2000, **317**, 589.
74 J. Gauss and H. J. Werner, *Phys. Chem. Chem. Phys.*, 2000, **2**, 2083.
75 M. C. Caputo, M. B. Ferraro and P. Lazzeretti, *J. Chem. Phys.*, 2000, **112**, 6141.
76 T. A. Keith and R. F. W. Bader, *Chem. Phys. Lett.*, 1993, **210**, 223.
77 C. van Wullen, *Phys. Chem. Chem. Phys.*, 2000, **2**, 2137.
78 G. Y. Sun and M. Kertesz, *New J. Chem.*, 2000, **24**, 741.
79 D. Gudat, W. Hoffbauer, A. B. Rozhenko, W. W. Schoeller and M. I. Povolotskii, *Magn. Reson. Chem.*, 2000, **38**, 861.
80 V. Robert, S. Petit, S. A. Borshch and B. Bigot, *J. Phys. Chem.*, 2000, **104**, 4586.
81 C. M. Marian and M. Gastreich, *Solid State Nucl. Magn. Reson.*, 2001, **19**, 29.
82 T. Kupka, I. P. Gerothanassis and I. N. Demetropoulos, *J. Mol. Struct. (Theochem)*, 2000, **531**, 143.
83 T. Kupka, G. Pasterna, M. Jaworska, A. Karali and P. Dais, *Magn. Reson. Chem.*, 2000, **38**, 149.
84 P. R. Seidl and K. Z. Leal, *J. Mol. Struct. (Theochem)*, 2001, **539**, 159.
85 P. R. Seidl, J. G. R. Tostes, J. W. D. Carneiro, C. A. Taft and J. F. Dias, *J. Mol. Struct. (Theochem)*, 2001, **539**, 163.
86 T. Heine, A. Goursot, G. Seifert and J. Webert, *J. Phys. Chem.*, 2001, **105**, 620.
87 G. A. Olah, G. K. S. Prakash and G. Rasul, *J. Am. Chem. Soc.*, 2001, **123**, 3308.
88 G. Rasul, G. K. S. Prakash and G. A. Olah, *J. Org. Chem.*, 2000, **65**, 8786.
89 A. Bagno, *Chem. Eur. J.*, 2001, **7**, 1652.
90 A. DerHovanessian, P.R. Rablen and A. Jain, *J. Phys. Chem.*, 2000, **104**, 6056.
91 J. Herzfeld, D. J. Olbris, E. Furman and V. Benderskiy, *J. Chem. Phys.*, 2000, **113**, 5162.
92 G. Wu, A. Hook, S. Dong and K. Yamada, *J. Phys. Chem.*, 2000, **104**, 4102.
93 G. Wu and S. Dong, *Chem. Phys. Lett.*, 2001, **334**, 265.
94 G. Wu, K. Yamada, S. Dong and H. Grondey, *J. Am. Chem. Soc.*, 2000, **122**, 4215.
95 K. Yamada, S. Dong and G. Wu, *J. Am. Chem. Soc.*, 2000, **122**, 11602.
96 S. Dong, R. Ida and G. Wu, *J. Phys. Chem.*, 2000, **104**, 11194.
97 R. W. Schurko and R. E. Wasylishen, *J. Phys. Chem.*, 2000, **104**, 3410.
98 M. Gee, R. E. Wasylishen, K. Eichele and J. F. Britten, *J. Phys. Chem.*, 2000, **104**, 4598.
99 G. M. Bernard, R. E. Wasylishen and A. D. Phillips, *J. Phys. Chem.*, 2000, **104**, 8131.
100 D. L. Bryce, R. E. Wasylishen and M. Gee, *J. Phys. Chem.*, 2001, **105**, 3633.
101 G. M. Bernard, K. Eichele, G. Wu, C. W. Kirby and R. E. Wasylishen, *Can. J. Chem.*, 2000, **78**, 614.
102 J. Z. Hu, C. H. Ye, R. J. Pugmire and D. M. Grant, *J. Magn. Reson.*, 2000, **145**, 230.
103 J. Z. Hu, W. Wang, S. Bai, R. J. Pugmire, C. M. V. Taylor and D. M. Grant, *Macromolecules*, 2000, **33**, 3359.
104 J. K. Harper and D. M. Grant, *J. Am. Chem. Soc.*, 2000, **122**, 3708.

105 M. Strohmeier, A. M. Orendt, D. W. Alderman and D. M. Grant, *J. Am. Chem. Soc.*, 2001, **123**, 1713.
106 D. H. Barich, J. C. Facelli, J. Z. Hu, D. W. Alderman, W. Wang, R. J. Pugmire and D. M. Grant, *Magn. Reson. Chem.*, 2001, **39**, 115.
107 D. H. Barich, A. M. Orendt, R. J. Pugmire and D. M. Grant, *J. Phys. Chem.*, 2000, **104**, 8290.
108 Z. Gan, *J. Am. Chem. Soc.*, 1992, **114**, 8307.
109 C. D. Hughes, M. H. Sherwood, D. W. Alderman and D. M. Grant, *J. Magn. Reson. A*, 1993, **102**, 58.
110 M. Bechmann, S. Dusold, H. Forster, U. Haeberlen, T. Lis, A. Sebald and M. Stumber, *Mol. Phys.*, 2000, **98**, 605.
111 G. Grossmann, D. Scheller, O. L. Malkina, V. G. Malkin, G. Zahn, H. Schmitt and U. Haeberlen, *Solid State Nucl. Magn. Reson.*, 2000, **17**, 22.
112 J. E. Rich, M. N. Manalo and A. C. de Dios, *J. Phys. Chem.*, 2000, **104**, 5837.
113 D. K. Lee, Y. F. Wei and A. Ramamoorthy, *J. Phys. Chem. B*, 2001, **105**, 4752.
114 J. R. Brender, D. M. Taylor and A. Ramamoorthy, *J. Am. Chem. Soc.*, 2001, **123**, 914.
115 G. Cornilescu and A. Bax, *J. Am. Chem. Soc.*, 2000, **122**, 10143.
116 T. M. Duncan, *A Compilation of Chemical Shift Anisotropies*, Farragut Press, Madison, 1990.
117 M. Hong, *J. Am. Chem. Soc.*, 2000, **122**, 3762.
118 N. Tjandra and A. Bax, *J. Am. Chem. Soc.*, 1997, **119**, 9576.
119 K. Ruud, P. O. Astrand and P. R. Taylor, *J. Am. Chem. Soc.*, 2001, **123**, 4826.
120 C. J. Jameson, *J. Chem. Phys.*, 1977, **66**, 4977.
121 C. J. Jameson, *J. Chem. Phys.*, 1977, **67**, 2814.
122 C. J. Jameson and H. J. Osten, *Annu. Rep. NMR Spectrosc.*, 1986, **17**, 1.
123 D. B. Chesnut and D. W. Wright, *J. Comput. Chem.*, 1991, **12**, 546.
124 P. Borowski, T. Janowski and K. Wolinski, *Mol. Phys.*, 2000, **98**, 1331.
125 F. Weinhold, *J. Chem. Phys.*, 1998, **109**, 367.
126 M. Baaden, P. Granger and A. Strich, *Mol. Phys.*, 2000, **98**, 329.
127 K. J. Hallock, D. K. Lee, A. Ramamoorthy, *J. Chem. Phys.*, 2000, **113**, 11187.
128 A. C. de Dios, A. Walling, I. Cameron, C. I. Ratcliffe and J. A. Ripmeester, *J. Phys. Chem.*, 2000, **104**, 908.
129 C. H. Gee and W. T. Raynes, *Chem. Phys. Lett.*, 2000, **330**, 595.
130 C. G. Lindsay and J. A. Tossell, *Phys. Chem. Miner.*, 1991, **18**, 191.
131 M. Kaupp, C. Rovira, M. Parinello, *J. Phys. Chem. B*, 2000, **104**, 5200.
132 E. Oldfield, H. C. Lee, C. Coretsopoulos, F. Adeboun, K. D. Park, S. Yang, J. Chung and B. Phillips *J. Am. Chem. Soc.*, 1991, **113**, 8680.
133 X. P. Xu and S. C. F. Au-Yeung, *J. Phys. Chem. B*, 2000, **104**, 5641.
134 K. Ibrom, G. Kohn, K. U. Boeckmann, R. Kraft, P. Holba-Schultz and L. Ernst, *Org. Lett.*, 2000, **2**, 4111.
135 M. Tordeux, C. Wakselman, O. Jarjayes and C. G. Beguin, *Magn. Reson. Chem.*, 2001, **39**, 301.
136 G. Heckmann, G. Becker, S. Horner, H. Richard, H. Kraft and P. Dvortsak, *Z. Naturforsch. B*, 2001, **56**, 146.
137 W. D. Arnold and E. Oldfield, *J. Am. Chem. Soc.*, 2000, **122**, 12835.
138 D. H. Barich, J. B. Nicholas and J. F. Haw, *J. Phys. Chem.*, 2001, **105**, 4708.
139 M. Witanowski, W. Sicinska, Z. Biedrzycka and G. A. Webb, *Magn. Reson. Chem.*, 2000, **38**, 177.
140 M. N. Manalo, A. C. de Dios and R. Cammi, *J. Phys. Chem.*, 2000, **104**, 9600.
141 J. Czerneky, *J. Phys. Chem.*, 2001, **105**, 1357.

142 M. Barfield, A. J. Dingley, J. Feigon and S. Grzesiek, *J. Am. Chem. Soc.*, 2001, **123**, 4014.
143 M. Pecul, J. Lewandowski and J. Sadlej, *Chem. Phys. Lett.*, 2001, **333**, 139.
144 S. Scheiner, Y. Gu and T. Kar, *J. Mol. Struct. (Theochem)*, 2000, **500**, 441.
145 R. M. Aminova, G. A. Schamov and A. V. Aganov, *J. Mol. Struct. (Theochem)*, 2000, **498**, 233.
146 M. Pecul, J. Leszczynski and J. Sadlej, *J. Chem. Phys.*, 2000, **112**, 7930.
147 M. Felemez, P. Bernard, G. Schlewer and B. Spiess, *J. Am. Chem. Soc.*, 2000, **122**, 3156.
148 N. Asakawa, D. Sato, M. Sakurai and Y. Inoue, *J. Phys. Chem.*, 2000, **104**, 2716.
149 J. C. Facelli, *Chem. Phys. Lett.*, 2000, **322**, 91.
150 J. Casanovas, F. Illas and G. Pacchioni, *Chem. Phys. Lett.*, 2000, **326**, 523.
151 D. Stueber, F. N. Guenneau and D. M. Grant, *J. Chem. Phys.*, 2001, **114**, 9236.
152 V. G. Malkin, O. L. Malkina, G. Steinebrunner and H. Huber, *Chem. Eur. J.*, 1996, **2**, 452.
153 A. E. Florin and M. Alei, *J. Chem. Phys.*, 1967, **47**, 4268.
154 J. C. Hindman, *J. Chem. Phys.*, 1966, **44**, 4582.
155 B. G. Pfrommer, F. Mauri and S. G. Louie, *J. Am. Chem. Soc.*, 2000, **122**, 123.
156 W. D. Phillips, W. E. Cooke and D. Kleppner, *Phys. Rev. Lett.*, 1975, **15**, 1619.
157 W. T. Raynes, in *Nuclear Magnetic Resonance*, ed. R. J. Abraham, Specialist Periodical Reports, The Chemical Society, London, UK, 1979, Vol. 7, p. 25.
158 A. Pines, D. J. Ruben, S. Vega and M. Mehring, *Phys. Rev. Lett.*, 1976, **36**, 110.
159 L. M. Ryan, R. C. Wilson and B. C. Gerstein, *Chem. Phys. Lett.*, 1977, **52**, 341.
160 W. K. Rhim, D. P. Burum and D. D. Elleman, *J. Chem. Phys.*, 1979, **71**, 3139.
161 D. P. Burum and W. K. Rhim, *J. Chem. Phys.*, 1979, **70**, 3553.
162 F. Buda, P. Giannozzi and F. Mauri, *J. Phys. Chem. B*, 2000, **104**, 9048.
163 R. H. Contreras, O. E. Taurian, F. S. Ortiz and J. E. Peralta, *J. Mol. Struct.*, 2000, **556**, 263.
164 E. Y. Lau and J. T. Gerig, *J. Am. Chem. Soc.*, 2000, **122**, 4408.
165 A. Perczel and A. G. Csaszar, *Chem. Eur. J.*, 2001, **7**, 1069.
166 A. C. de Dios and E. Oldfield, *J. Am. Chem. Soc.*, 1994, **116**, 5307.
167 P. Sozzani, A. Comotti, R. Simonutti, T. Meersmann, J. W. Logan and A. Pines, *Angew. Chem. Intl. Ed.*, 2000, **39**, 2695.
168 S. M. Rubin, M. M. Spence, B. M. Goodson, D. E. Wemmer and A. Pines, *Proc. Natl. Acad. Sci., U.S.A.*, 2000, **97**, 9472.
169 K. Jackowski, M. Wilczek, M. Pecul, J. Sadlej, *J. Phys. Chem.*, 2000, **104**, 9806.
170 W. Makulski and K. Jackowski, *Chem. Phys. Lett.*, 2001, **341**, 369.
171 K. Jackowski, *J. Mol. Struct.*, 2001, **563**, 159.
172 A. K. Jameson and C. J. Jameson, *Chem. Phys. Lett.*, 1987, **134**, 461.
173 R. E. Wasylishen, S. Mooibroek and J. B. Macdonald, *J. Chem. Phys.*, 1984, **81**, 1057.
174 R. E. Wasylishen, C. Connor and J. O. Friedrich, *Can. J. Chem.*, 1984, **62**, 981.
175 M. Gee and R. E. Wasylishen, *J. Mol. Spectrosc.*, 2001, **207**, 153.
176 M. Goto and S. Saito, *Astrophys. J.*, 1995, **452**, L147.
177 R. Honerjäger and R. Tischer, *Z. Naturforsch. A*, 1974, **29**, 342.
178 R. E. Wasylishen, D. L. Bryce, C. J. Evans and M. C. L. Gerry, *J. Mol. Spectrosc.*, 2000, **204**, 184.
179 J. Kodweiss, O. Lutz, W. Messner, K. R. Mohn, A. Nolle, B. Stutz and and D. Zepf, *J. Magn. Reson.*, 1981, **43**, 495.
180 G. Malli and C. Froese, *Int. J. Quantum Chem.*, 1967, **1S**, 95.

3
Applications of Nuclear Shielding

BY SHINJI ANDO AND SHIGEKI KUROKI

1 Introduction

The format of this report remains similar to previous years. Chemical and physical influences on nuclear shieldings are considered in the first section. The shieldings of particular nuclear species are described in the following section according to their position in the Periodic Table. Since a huge number of articles on NMR spectroscopy were published during the period of this review, due to space limitation the coverage of this report is restricted to widely available and common journals, which are published in English.

2 Various Chemical and Physical Influences on Nuclear Shielding

2.1 Substituent Effects. – The ^{13}C NMR substituent-induced chemical shifts (SCS) of aromatic carbons in 1,4-disubstituted benzenes were correlated with inductive and mesomeric effects, expressed in σ_I and σ_R (NMR) scales, and with charge alterations (Δq) provoked by introducing a new substituent (X) at position C1. 105 different compounds with groups attached to C1 (X) and C4 (Y) in a sequence: NMe_2, NH_2, OMe, F, Cl, Br, Me, H, CF_3, CN, C(O)OEt, C(O)Me, NO_2 and CHO were studied.[1]

In a strong magnetic field, hydrogen nuclei located over an aromatic ring experience a reduced magnetic field as a result of the induced magnetic field associated with circulating π electrons. The GIAO-SCF, an *ab initio* subroutine in Gaussian 94, was used to calculate isotropic shielding values and to determine the proton NMR shielding increment for a simple model system: methane held at various positions over a substituted benzene ring.[2]

Both the ^{13}C and ^{15}N chemical shifts of a number of quinoxalines substituted at position 2 with the π-electron excess 2′-benzo[*b*]furanyl substituent, which has at position 3′ a hydroxy or amino group, could be satisfactorily calculated by the GIAO method on the basis of HF and DFT *ab initio* structures.[3] Quantum mechanical calculations using the 3-21G(d) basis-set were performed on some *p*-substituted diaryl tellurides and aryl Me tellurides, and the corresponding cationic radicals of these compounds. Calculated relative radical stabilization energies were shown to correlate with experimental data, and the peak oxidation potentials and ^{125}Te chemical shifts were

Nuclear Magnetic Resonance, Volume 31
© The Royal Society of Chemistry, 2002

determined.[4] A number of phosphine selenide ligands and their gold(I) complexes $R_3P{:}Se{-}Au{-}X$ (X = Cl-, Br- and CN- and R = Ph, cyclohexyl and tolyl) were prepared and ^{31}P NMR showed that the electronegativity of the substituents is the most important factor that distinguishes the ^{31}P chemical shift.[5] The ^{1}H NMR spectra of a number of nitriles of fixed geometry were recorded in diluted $CDCl_3$ solution and assigned.[6] The previous literature data allowed the determination of the cyano substituent chemical shifts (SCS) in a variety of molecules. These SCS were analyzed in terms of the CN electric field, magnetic anisotropy and steric effects for protons more than three bonds removed together with a model for the calculation of the 2- and 3-bond SCS. Fourteen linear and cyclic α- and β-aminophosphonates in which the P-atom is substituted by alkoxy groups have been synthesized and evaluated as ^{31}P NMR pH markers in Krebs–Henseleit buffer.[7]

Substituents placed on the phenyl rings of 3-benzyl-2-phenyl-1,3-thiazolidin-4-one affect the electron density surrounding both the methine proton, H_m, at C2, H_a and H_b at C5, and H_c and H_d at the benzyl C. The electron density changes are also exhibited at the C2, C4, C5 and the benzyl carbons. Correlations for the effects of various substituents in both the 2-Ph and 3-benzyl rings with the ^{1}H and ^{13}C chemical shifts, for the aforementioned sites, are discussed using Hammett σ constants.[8]

Substituents in the aromatic ring of (*E*)-$RCH{:}CHCH_2OC_6H_4NO_{2\text{-}4}$ (R = Ph, 4-tolyl, 4-$MeOC_6H_4$, 2- and 4-ClC_6H_4 and -BrC_6H_4, 2,5-$Cl_2C_6H_3$, 2-, 3- and 4-$O_2NC_6H_4$, 1-naphthyl) affect the chemical shifts and coupling constants of all protons in the molecules.[9] For substituted phenyl-*N*-Bu carbamates (1) and 4-nitrophenyl-*N*-substituted carbamates (2), linear relationships between values of NH proton chemical shift (δ_{NH}), pK_a, and $\log k[OH]$ and Hammett σ constant or Taft substituent constant (σ*) are observed.[10] Eight thia- or aza-substituted $Ph(CH_2)_3CO_2H$ derivatives were prepared and the influence of these substitutions on the chemical shifts of the benzene-ring carbon atoms was studied.[11] ^{1}H NMR study and conformational analysis of a broad series of biological important C5-substituted 2′-deoxyuridines, including alkyl, halogen, vinyl, hydroxymethyl, and hydroxy derivatives as well as nitro, formyl, trifluoromethyl, and dimethylamino substituents, was presented.[12] The ^{13}C NMR spectra of 24 1-X-bicyclo[1.1.1]pentanes were measured.[13] Substituent chemical shifts (SCSs) on C1 correlated linearly with those on C3, although the former correspond to deshielding effects and the latter to shielding effects. Even though the C1 SCSs follow the same trend as α-SCSs in other types of substrates, they are significantly smaller.

The alkyl substituent effect on the intermolecular H-bonding properties of tertiary amides was studied.[14] *N,N*-dimethylformamide, *N,N*-diethylformamide, *N,N*-diisopropylformamide, *N,N*-dimethylacetamide, *N,N*-diethylacetamide and *N,N*-diisopropylacetamide were chosen as proton acceptors for thioacetamide in CCl_4 solution.

Substituent chemical shift values for the acetylation and mesylation of hydroxy-*p*-benzoquinones and for the introduction of acetyloxy and mesyloxy groups into *p*-benzoquinones were derived after complete ^{13}C NMR assign-

ment of all ring carbons for nine perezone derivatives and six thymoquinone derivatives, which follow from one-bond and long-range multiplicities.[15] The ^{1}H and ^{13}C NMR chemical shifts and $^{1}H,^{1}H$ coupling constants of 27 brominated di-Ph ethers are reported.[16] The increment models for the bromine substituent effects on the ^{1}H and ^{13}C NMR chemical shifts were constructed based on a multiple linear regression analysis. The full analysis of ^{1}H NMR spin systems and the charting of substituent chemical shifts offer great potential in the structure elucidation of glycosides.[17] The potential of the method is demonstrated for three kaempferol bisdesmosides by establishing the shift characteristics for 3-O-, 7-O-, and 6″-O-glycosidation.

Prediction of the ^{13}C NMR signals for derivatives of naphthalene was studied using statistical SCS values.[18] ^{19}F, ^{1}H, and ^{13}C NMR spectral data are reported for a variety of oxetane compounds containing fluorine on or near the ring. Effects of substituents on the spectra are analyzed and correlations of chemical shifts and coupling constants in terms of molecular structure are presented.[19] A series of 2-aryl-2-hydroxy-1,1,3,3-tetramethyl-5,8-dioxaspiro[3.4]octanes (1), 3-aryl-3-hydroxyl-2,2,4,4-tetramethylcyclobutanones (2), and 1-aryl-2,2,4-trimethyl-1,3-pentadiones (3) were studied by ^{13}C NMR.[20] The *o*-C chemical shifts of the cyclobutane ring are dependent on the substituent groups on the Ph ring for compounds.

^{13}C and ^{1}H spectral assignments were made for three 2-substituted- and six 2,6-disubstituted naphthalenes with isoPr, 2-hydroxy-2-methylethyl and 2-hydroperoxy-2-methylethyl substituents using proton–proton decoupling, 2-dimensional H,H-COSY and 2-dimensional-C,H-COSY techniques.[21] An excellent additivity of substituent effects was found for both the ^{13}C and ^{1}H spectra of 2,6-disubstituted naphthalenes. Long range substituent effects on the ^{29}Si NMR chemical shifts in alkylene- and arylene-bridged triethoxysilanes were observed over as many as 11 bonds.[22]

Mono- and diesters of fatty acids of peracetylated α-D-glucopyranose were prepared by chemical interesterification. Substituent-induced chemical shift effects on the carbonyl carbons rather than the ring carbons and proton atoms unambiguously show the fatty acyl substituents to be at C1 in the monosubstituted, and at C1 and C6 in the disubstituted products.[23] A series of *m*-, and *p*-substituted Ph 2-thiophenecarboxylates and benzoates was prepared by the reaction of the corresponding acylchlorides and phenols. Their ^{1}H and ^{13}C NMR chemical shifts were analyzed using single substituent parameter (SSP) and dual substituent parameter (DSP) methods.[24] The ^{13}C chemical shifts were measured of the carboxyl carbon atoms for all the 2-, 3- and 4-substituted benzoic acids with H, CH_3, CH_3O, F, Cl, Br, I, and NO_2 substituents, as well as for all 3,4-, 3,5-, and 2,6-disubstituted benzoic acids with combinations of CH_3, CH_3O, Cl (or Br), NO_2 substituents and for symmetrical 2,6-disubstituted derivatives with Et, EtO, PrO, i-PrO, and BuO substituents.[25]

2.2 Conformation Effects. – ^{1}H and ^{13}C chemical shifts and $^{1}H,^{1}H$, $^{13}C,^{1}H$ and $^{13}C,^{13}C$ coupling constants were determined for *O*-vinyl ketoximes.[26] The analysis suggests that *O*-vinyl ketoximes are conformationally homogeneous.

Dynamic two-dimensional ^{1}H and ^{13}C NMR studies of the conformationally restricted amide *N*-(1-naphthoyl)-*cis*-2,6-dimethylpiperidine reveal correlated rotation about the aryl–CO and amide bonds.[27] 9-(1-Adamantylaminomethyl)-9,10-dihydroanthracene was prepared *via* condensation of 1-adamantylnitrile with 9-anthryllithium and its hydride reduction. An NMR study confirmed a boat conformation for the central ring, with the substituent of C9 in a pseudo-axial position.[28] The structure of bis[(1,3)2-oxaadamantano]-18-crown-6 (I) and its potassium picrato complex were studied using NMR, X-ray structure analysis and molecular mechanics calculations.[29] In the gas phase and in $CDCl_3$ solution, in both I and the corresponding complex cation the most stable conformation of C_{2h} symmetry is found.

The ^{1}H and ^{13}C NMR spectra of 2,4,6,8-tetraaryl-3,7-diazabicyclo[3.3.1]-nonan-9-ones [I; Ar = Ph, R = H (II); Ar = p-$CH_3C_6H_4$, R = H (III); Ar = *p*-$CH_3OC_6H_4$, R = H(IV); Ar = Ph, R = CH_3 (V)] were measured.[30] The chemical shifts for II–V were assigned unambiguously and these results clearly indicate a chair–boat conformation for these compounds with (i) all aryl groups orientated equatorially and (ii) the aryl groups of the boat lying in the shielding zone of the aryl groups of the chair.

^{1}H NMR and UV–vis spectroscopic studies as well as molecular mechanics calculations have been performed for the *trans* and *cis* isomers of a series of chlorine substituted stilbenes.[31] In a continuing study on the use of hydroxy protons in conformational analysis of saccharides in aqueous solution by NMR, a number of disaccharides with 1,3-, 1,4- and 1,6-linkages were investigated.[32]

The seven-residue peptide *N*-acetyl-Lys-Leu-Val-Phe-Phe-Ala-Glu-NH_2 is shown by electron microscopy to form highly ordered fibrils upon incubation of aqueous solutions. X-ray powder diffraction and optical birefringence measurements have confirmed that these are amyloid fibrils. The peptide conformation and supramolecular organization in fibrils were investigated by solid state ^{13}C NMR.[33]

Axial equatorial populations were determined for (*E*)-2-X-cyclohexanone oximes and O-Me oxime ethers in $CHCl_3$ by the Eliel method [X = F, Cl, Br, OMe, NMe_2, SMe].[34] A novel approach is presented, which uses ^{1}H NMR data from the protons bonded to C6. The conformational proportions were also obtained from the C4 chemical shifts, the *Z*-isomer spectral parameters being taken as reference for calculation.

Cisproline(i-1)–aromatic(i) interactions have been detected in several short peptides in aqueous solution by analysis of anomalous chemical shifts measured by ^{1}H-NMR.[35] Conformational preferences of esters of 2,2,5,7,8-pentamethylchroman-6-ol were studied by dynamic ^{13}C NMR in solution and the cross-polarization (CP)-magic angle spinning (MAS) technique in the solid phase.[36] Experimental (*anti*/*syn* ratios, ^{15}N NMR chemical shift, and UV) and theoretical [DFT, MP2 and QCISD(T) calculations of optimized structures and *anti*/*syn* ratios and free energy differences, and GIAO calculation of NMR chemical shifts] results establish the conformations of *S*-nitrosothiols.[37] The formation of the cytosine-uracil (C–U) base pair in a duplex was observed in

solution by means of the temperature profile of ^{15}N chemical shifts, and the precise geometry of the C–U base pair was also determined by NOE-based structure calculation.[38]

The relationships between ^{13}C NMR chemical shifts of aromatic carbons and the inter-ring torsion angles (θ) of two Ph rings in biphenyl and its substituted derivatives were systematically examined.[39] The chemical shifts of C1, C2 and C6 carbons of the biphenyl group in the solid state show systematic correlations with θ when the substituent shielding effects are removed from the solid chemical shifts. The isotropic nuclear shielding calculated using *ab initio* molecular orbital theory with the GIAO-CHF method for biphenyl agree well with the experimental results.

A computer program, SHIFT, for evaluating NMR shielding variations on the basis of classical equations describing anisotropy, linear and square electric effects and also sterically induced charge separations is presented.[40] Application of the program is illustrated with the conformational analysis of three cyclophanes.

2.3 Intermolecular and Hydrogen Bonding Effects. – A new method was presented to calculate solid-state effects on NMR chemical shifts. Using full crystal potentials, this new method (CPPCh) eliminates the need to arbitrarily select the point charges that are included in the calculations of the NMR chemical shieldings to take into account intermolecular effects.[41] The complexation of benzonitrile as acceptor with the aromatic donors *o*-, *m*- and *p*-xylene in CCl_4 solution was investigated using ^1H NMR chemical shifts.[42] Structural studies[43] of protein–ligand complexes are often limited by low solubility, poor affinity, and interfacial motion and, in NMR structures, by the lack of intermolecular NOEs. In the absence of other structural restraints, they use a procedure that compares simulated chemical shift perturbations to observed perturbations to better define the binding orientation of ligands with respect to protein surfaces.

IR and ^1H NMR studies on nitrilotriacetic acid suggest that the acid exists in the zwitterion form, which allows the existence of intermolecular hydrogen bonding.[44] The enantiomers of aminoglutethimide [2-(*p*-aminophenyl)-2-ethylglutarimide, AGT] can be resolved using all of three most commonly used native cyclodextrins (CD): α-, β-, and γ-CDs.[45] In order to examine some underlying mechanisms of the chiral recognition the interaction of AGT with the chiral selectors was studied with 1D and 2D NMR and electrospray ionization mass spectrometry (ESI-MS). The Job's and Scott's plots constructed based on the complexation-induced chemical shifts (CICS) observed in NMR spectra provided some preliminary information on the stoichiometry of the intermolecule.

Two different charge models were applied to take into account intermolecular interactions to model the solid-state effects on the ^{19}F NMR chemical shift tensors.[46] The interpretation of ^1H NMR chemical shifts, coupling constants, and coefficients of temperature dependence (δ(OH), *J*(H,OH), and $\Delta\delta(OH)/\Delta T$ values) evidences that, in DMSO solution, the signal of an OH

group involved as donor in an intramolecular hydrogen bond to a hydroxy or alkoxy group is shifted upfield, whereas the signal of an OH group acting as acceptor of an intramolecular hydrogen bond and as donor in an intermolecular hydrogen bond to DMSO is shifted downfield.[47] ^{1}H, ^{13}C and ^{14}N NMR chemical shifts were used to monitor the dilution process of DMF in monosubstituted benzenes.[48] The assignment of solid-state NMR spectra is studied by the use of model systems computed with *ab initio* methods.[49] The investigated system is a hexabenzocoronene derivative, for which a T-like arrangement of dimer units is found in the solid-state structure. Here, a tetramer model is required to explain the intermolecular interactions influencing the spectrum, whereas a dimer model is found to be inadequate.

By using the high-pressure cell, ^{1}H chemical shifts of nonpolar (n-hexane and benzene) and polar (dichloromethane, chloroform, acetonitrile, water, methanol, and ethanol) solute molecules in gaseous and supercritical carbon dioxide were measured in the wide pressure range between 2 and 30 MPa at 313.3 K.[50] The chemical shifts of hydroxy protons of water, methanol, and ethanol in carbon dioxide at 20.0 MPa were shifted to higher frequency due to intermolecular hydrogen bonding with increasing concentration.

The molecular structures and intramolecular hydrogen bonding for salicylic (I), 2-hydroxythiobenzoic (II), 2-hydroxythionobenzoic (III) and 2-hydroxydithiobenzoic acids (IV) were studied precisely by *ab initio* method and density functional theory.[51] The carbonyl ^{17}O electrical field-gradient (EFG) tensor and chemical shift (CS) tensor of a urea-type functional group, $R^{1}NH$-C(O)-NHR^{2} were determined.[52] Quantum chemical calculations revealed very large intermolecular hydrogen bonding effects on the ^{17}O NMR tensors.

A number of disaccharides with 1,3-, 1,4- and 1,6-linkages have been investigated in a continuing study on the use of hydroxy protons in conformational analysis of saccharides in aqueous solution by NMR.[53] The intramolecular N H···O hydrogen bonds formed by a number of heteroconjugated systems (β-enaminones, ketohydrazones, and nitrosoenamines) were studied by X-ray, IR and NMR spectroscopic, and quantum-mechanical calculation.[54]

A review with 49 references was given.[55] Hydrogen bond lengths on enzymes have been derived with high precision ($\leqslant \pm 0.05$ Å) from both the proton chemical shifts (δ) and the fractionation factors (φ) of the proton involved and were compared with those obtained from protein X-ray crystallography.

^{15}N NMR spectra of a series of *N*-(R-salicylidene)-alkylamines in $CDCl_3$ solution were measured.[56] Proton transfer equilibrium was established on the basis of the temperature dependence of the ^{15}N chemical shift and $^{1}J_{NH}$ coupling constants.

A series of amide oligomers have been prepared from isophthalic acid and bisaniline derivatives.[57] These compounds assemble into double-stranded zipper complexes in solution *via* hydrogen-bonding and edge-to-face aromatic interactions. The stability and structures of the complexes were determined by ^{1}H NMR in chloroform solution.

^{1}H NMR spectra of Gly-containing peptides and polypeptides in the solid state were measured at 800 MHz and at high-speed MAS of 30 kHz to

elucidate the relationship between the hydrogen-bond length and ^{1}H NMR chemical shift.[58] Preliminary NMR studies on hydrogen bonding of carboxylic acid–carboxylate systems in an anhydride, aprotic solvent are presented.[59] The question as to whether the CH···O interaction constitutes a true H-bond is examined from the perspective of calculated NMR chemical shieldings.[60] To demonstrate the H-bond-like character of the CH/π interaction, electronic substituent effects on the equilibrium between the stretched and the folded conformers of series of compounds capable of forming CH/π interactions were examined by measurements of NOE enhancements of ^{1}H NMR signals.[61]

Density functional theory calculations of the ^{15}N chemical shifts of pyridine in the presence of a methanol molecule were reported.[62] These calculations were done to study the effects of hydrogen bonding (HB) on the principal components of the nitrogen chemical shift tensors. *Ab initio* calculations demonstrate that relationships exist among the X–Y distance in an X–H–Y H bond, the anharmonic proton-stretching frequency, the ^{1}H NMR chemical shift, and the X–Y spin-spin coupling constant.[63] Structural information related to the type of H bond present may be inferred from these data. The ^{17}O electrical-field-gradient (EFG) and chemical shielding (CS) tensors for an amide functional group were determined.[64] The importance of including intermolecular hydrogen-bonding (HB) interactions in quantum chemical calculations of ^{17}O EFG and CS tensors was demonstrated.

Two 3-diethylaminomethyl-4-R-salicylic aldehydes were obtained and studied in chloroform solutions by FT-IR and NMR spectroscopy.[65] The existence of an equilibrium between the structures with OH···O=C and N···HO intramolecular hydrogen bonds was suggested. Electronic and spatial structure and nuclear magnetic shielding constants of some hydrogen-bonded complexes ({formic acid}$_n$, n = 1-4, {acrylic acid}$_n$, n = 1–2 and their complexes with H_2O and DMSO) were studied by *ab initio* methods using MP2/RHF//6-31G*, RHF/6-31G* basis sets and by using density functional theory within the B3LYP approximation.[66]

2.4 Solvent Effects. – The synthesis of 2,6-diarylpiperidines and the corresponding epimeric alcohols as well as the synthesis of tetrahydrothiopyran-4-one oxime derivatives were reported, and the effect of temperature and solvent chemical shifts in NMR spectra were presented.[67] The ^{33}S NMR gas-to-solution shifts for SF_6 in 13 different solvents were measured.[68] All the ^{33}S shifts were negative (deshielding effect) and ca. 4 times weaker than the ^{19}F NMR gas-to-soln. shifts for a given solvent. The substituent-induced chemical shifts (SCS) of C(α,β) on the ^{13}C NMR spectra of arylalkynes (*i.e.* containing H, Me, Cl and Br) were studied.[69] The solvent effect on the ^{13}C chemical shifts of phenylalkynyl bromide demonstrates a strong dependence on the relative permittivity as well as the shielding character of the solvents.

Theoretical and experimental ^{1}H, ^{13}C, ^{15}N and ^{17}O NMR chemical shifts for uracil and 5-halogenouracils were determined and analyzed.[70] The solvent effect was checked at the HF/3-21G** level by surrounding the uracil molecule by seven water molecules.

Solvent-induced effects on ^{15}N NMR shielding of 1,2,4,5-tetrazine and two isomeric tetrazoles are calculated using density functional theory combined with the polarizable continuum model and using the continuous set gauge transformation.[71] Direct and indirect solvent effects on shielding are also calculated.

Solvent effects on the N shieldings of 3-methylsydnone (1), a zwitterionic isomer of the hypothetical 5-methoxy-1,2,3-oxadiazole, are significantly different from those observed for oxazoles and oxadiazoles.[72] *Ab initio* DFT-GIAO magnetic shielding calculations employing B3PW91 functionals, a 6-311++G** basis set and geometries optimized using the same set are reported for (1) and some related molecules which include all of the existing oxazoles and oxadiazoles.

Concentration-dependent experimental measurements of the EtOH hydroxy-proton chemical shift δ_H for binary solutions were carried out.[73] The solvents used were CCl_4, C_6H_6, $CHCl_3$, MeCN, Me_2CO and DMSO.

It was shown that the polarizable continuum model is able to reproduce the stability of zwitterionic forms of alanine and glycine in aqueous solution at the B3LYP/6-31G (d) level of theory. The model is extended to the calculation of vibrational frequencies, vibrational CD spectra, and NMR chemical shifts.[74] ^{1}H, ^{13}C and ^{14}N NMR chemical shifts were used to monitor the dilution process of DMF in monosubstituted benzenes.[75] Comparison of the ^{15}N chemical shifts of 2,6-di-tert-butylpyridine (DTBP) and pyridine (Py) in a series of solvents demonstrates the inability of the nitrogen atom in DTBP to participate in hydrogen bonds.[76] *Ab initio* calculated values of the nuclear magnetic shielding constants and nuclear quadrupole coupling constants of N atoms in azoles are compared with experimental data.[77] The solvent dependence of the molecular properties is accounted for, and it is described using solvent response theory.

2.5 Isotope Effects. – Important details of the structures of a wide set of homoconjugated ions can be obtained *via* H/D isotope effects on hydrogen bond NMR chemical shifts at low temperatures.[78] A strong increase in solvent polarity does not lead to asymmetrization of the hydrogen bonds of [FHF]- and of the maleate ion. The ^{17}O NMR spectra of ^{17}O isotope-enriched 1,3,5-trinitrobenzene and its Meisenheimer adducts with hydride ion (1), acetone anion (2) and methoxide ion (3) were measured.[79] The adducts 1–3 show ^{17}O signals shifted upfield compared with those of 1,3,5-trinitrobenzene. D-induced isotope shifts in ML_n (L = statistical mixture of 3-oxido-2-phenylpropenal-d0, -1-d and -1,3-d_2) were measured.[80] The ^{13}C NMR isotope shifts, $\delta C(D)$-$\delta C(H)$, for the aldehydic CH of AlL_3, $Al(OiPr)_2L$, Me_2AlL, $SiBr_3L$, $SiL_3{}^{+}HBr_2{}^{-}$, $(CF_3)_3GeL$, $(EtO)_4NbL$, $Rh(CO)_2L$, PdL_2, $SbCl_4L$ and $(EtO)_4TaL$ are small and positive. The ^{19}F, ^{13}C and ^{1}H shielding in Me fluoride and its deuterated isotopomers was calculated from *ab initio* shielding surfaces for selected temperatures.[81] A CD_3 group close in space to (but several bonds distant from) a carbon atom A causes a substituent effect on the chemical shift of CA that is algebraically smaller than the effect of a CH_3

group, in agreement with the notion of shorter C–D relative to C–H bonds.[82] A study of the tautomerism of dehydroacetic acid using ^{1}H, ^{13}C (solution and CP/MAS), gated ^{1}H-decoupling techniques, deuterium-induced isotope effects on ^{13}C chemical shifts, and molecular modeling has shown that this compound exists as the 3-acetyl-4-hydroxy-6-methyl-2*H*-pyran-2-one in solution and in the solid state.[83] Cl isotope effects on ^{19}F and ^{13}C NMR chemical shifts were used for the indirect determination of the number of geminal and vicinal Cl atoms in fluorinated molecules.[84] A chemical shift *vs.* temperature analysis of β-thioxoketones has been performed for the four β-thioxoketones, thioacetylacetone (I), benzoylthioacetone (II), thiobenzoylacetone (III) and monothiodibenzoylmethane (IV).[85] Analysis of chemical shifts and isotope effects on these reveals that a three-component system is involved in the tautomeric equilibrium. The primary D and tritium isotope effects, $\delta(XH)-\delta(XD/T)$, were measured for 55 compounds having $\geqslant 1$ intramolecular H bonds.[86] The primary isotope effects were measured at various temperatures. 2,5-Dihydro-1,2,5-azasilaboroles I (1; R = Me, Et, Ph) (cyclic heterodienes) readily form tricarbonyliron complexes, I·$Fe(CO)_3$ (3) and both are compared with a silole (2) and its tricarbonyliron complex (4). The compounds 1–4 were studied with respect to isotope-induced chemical shifts $1\Delta 12/13C(^{29}Si)$.[87] The authors have synthesized all three monodeuterated anthracenes and shown that their ^{13}C spectra provide the same information that can be obtained from perdeuterated anthracene.[88] The isotope shifts change when the PAH is reduced by an alkali metal. For a planar molecule such as anthracene, the isotope shifts change in proportion to the change in charge density. D isotope effects on ^{15}N NMR chemical shifts and spin–spin coupling constants were studied for the ^{15}N-enriched ammonium chloride in liquid solutions.[89] A review with 164 references was given on isotope effects on chemical shifts of intramolecularly hydrogen bonded systems.[90] The effects are conveniently divided into localized (intrinsic) and equilibrium isotope effects. The review covers both primary and secondary isotope effects on chemical shifts. Bis(diphenylphosphinyl)amine $(Ph_2P)_2NH$ (1), the disulfide $[Ph_2P(S)]_2NH$ 1S and diselenide $[Ph_2P(Se)]_2NH$ (1)Se were selected to show the efficient application of the INEPT-HEED pulse sequence for measuring coupling constants $^{1}J(^{31}P^{15}N)$ and isotope induced chemical shifts $1\Delta 14/15N(^{31}P)$, both at natural abundance of ^{15}N, from ^{31}P NMR spectra.[91] The solution structures of two allenyl-propargyllithium reagents which give ^{13}C NMR chemical shifts intermediate between those expected for the allenyl and propargyl isomers were studied by the Saunders isotope perturbation technique.[92] Variable equilibrium isotope shifts were detected, showing that these reagents adopt structures ranging from equilibrating localized allenyl- and propargyllithium reagents to equilibrating unsymmetrical bridged structures and symmetrical bridged structures, depending mostly on the details of solvation.

A review with 116 references was given.[93] Isotope effects on chemical shifts, $n\Delta^{13}C(D)$, $n\Delta^{1}H(D)$, $1\Delta^{15}N(D)$ and $1\Delta^{13}C(^{18}O)$, and solvent isotope effects in proteins are reviewed and references are provided to related cases.

3 Shielding of Particular Nuclear Species

During the period of this review, the NMR spectra of most elements have received at least some chemical biological or physical investigation. Due to the space limitation, structure determination and related studies of natural products or macromolecules will be excluded, and the review articles are given for the most popular nuclei (^{1}H, ^{2}H, ^{13}C, ^{29}Si, $^{14,15}N$, ^{31}P, and ^{19}F).

3.1 Group 1 (^{1}H, ^{2}H, ^{3}H, $^{6,7}Li$, ^{23}Na, ^{87}Rb, ^{133}Cs). – *3.1.1 Hydrogen (^{1}H) ($I = 1/2$).* Recent advances in structural and conformational analysis of fluorinated carbohydrates by NMR spectroscopy are reviewed.[94] Characteristic ^{1}H, ^{13}C and ^{19}F NMR chemical shifts and coupling constants for selected examples are given and the spectral data of a series of fluorinated carbohydrates were collected. A comprehensive review with 120 references was given on organotin(IV) complexes of the amino acids and peptides.[95] The structures of these complexes are discussed on the basis of IR, electronic, ^{1}H, ^{13}C and ^{119}Sn NMR, X-ray and ^{119}Sn Mössbauer spectral studies. A review with 31 references was given on recent progress on characterizing the site environment relating to the catalytic activity and selectivity of a Brønsted-acid site in a zeolite.[96] Characterization of the site environment using ^{13}C NMR of adsorbed $CH_3{}^{13}COCH_3$ and ^{1}H NMR of CH_3CN was discussed. A review of the applications utilizing ^{1}H–^{15}N heteronuclear shift correlation experiments at natural abundance was given with emphasis placed on the observed long-range coupling pathways.[97]

3.1.2 Deuterium (^{2}H) ($I = 1$). Magic-angle spinning (MAS) ^{2}H and ^{17}O NMR spectra were obtained for water, following addition to an activated carbon.[98] Shortly after addition two peaks are seen: a free liquid resonance and a 2nd broad resonance shifted to low frequency. The latter is attributed to water in the pores of the activated carbon.

3.1.3 Lithium ($^{6,7}Li$) ($I = 1, 3/2$). A review with 117 references was given on the applications of ^{7}Li NMR spectroscopy and imaging in biology and experimental medicine.[99] The interest derives primarily from the clinical use of Li salts to treat mania and manic-depressive illness. One area of investigation is ionic transport across the cellular membrane and compartmentation, so as to elucidate the mechanisms of therapeutic action and toxicity in clinical practice. The second is the development of a noninvasive, *in vivo* analytical tool to measure brain Li concentrations in humans, both as an adjunct to treatment and as a mechanistic probe.

The two chiral lithium amides were found to form symmetrically solvated dimers in diethyl ether (DEE). The addition of tetrahydrofuran (THF) and of 1,3-dimethyl-3,4,5,6-tetrahydro-2-(1*H*)-pyrimidinone (DMPU) did not affect the ^{6}Li NMR chemical shift due to a very strong internal coordination.[100] The ^{6}Li and ^{7}Li MAS-NMR signals of fast ionic conducting $Li_{2-2x}Mg_{1+x}Cl_4$ have

been assigned to the two lithium ion positions of their inverse spinel-type structure.[101] ^{6}Li and ^{27}Al MAS NMR and EPR of low-spin Ni^{3+} were used to study the local environment of aluminium and the electronic structure of $LiNi_{1-y}Al_yO_2$ solid solutions.[102] The accessibility of lithium cations in the high-silica zeolites ZSM-5 and beta was investigated using ^{7}Li MAS NMR.[103] NMR spectra of ^{7}Li nucleus have been measured in $LiCoO_2$ and $LiNiO_2$. Line widths of the spectra decreased with increasing temperature above 400 K.[104] A ^{7}Li NMR study has been carried out on poly(propylene glycol) (PPG) with an average molecular weight of 4000 and poly(ethylene glycol) mono-methyl-ether with an average molecular weight of 350 (PEG) containing lithium salts.[105] The effect of uniaxial stress on the polymer electrolyte long and short range structures was investigated by ^{7}Li NMR. Stretching results in partial alignment of the PEO helices and also induces small but observable changes in the Li^+ solvation sheath.[106] Solid-state ^{7}Li NMR revealed different Ni/Co distributions in an inverse spinel structure of $LiNi_xCo_{1-x}VO_4$ cathode materials prepared by either high- or low-temperature solid-state reaction methods.[107] ^{7}Li MAS NMR provides an effective and unique method for probing different local environments of lithium cations in the microseparated phases of polyether polyurethane urea (PEUU) electrolytes, since it is the source that supplies the high ionic conductivity.[108] ^{7}Li NMR was used to investigate the stoichiometry and stability of a Li^+ complex with 18-crown-6 in pure acetonitrile and its 50:50 (w/w) mixtures with nitrobenzene and nitromethane.[109] HT-Li_xCoO_2 phases were synthesised *via* a solid state reaction with nominal Li/Co ratios $x = 0.90$, 1.0, 1.05 and 1.10 and were studied by ^{7}Li MAS NMR.[110] The ionic conduction mechanism in glasses was studied by comparing ^{7}Li NMR and the temperature dependence of the linewidth and electrical conductivity.[111] Negative electrodes for lithium-ion batteries containing a hard carbon with different binders were characterized by ^{7}Li NMR experiments.[112] Solid-state ^{7}Li NMR was used to probe the effects of the temperature and composition on the dynamic behavior of the ionic species for hybrid organic–inorganic ionic conductors obtained by dissolution of $LiClO_4$ into silica/poly(ethylene glycol) matrices.[113] ^{7}Li and ^{19}F NMR have been performed in the single crystal of the lithium fluoride $BaLiF_3$ with a cubic structure in order to examine the basic requirements for crystal NMR quantum computing devices.[114] A $LiKSO_4$ single crystal grown by the slow evaporation method was investigated by ^{7}Li and ^{39}K NMR.[115] Two solvent-free cross-linked polymer electrolytes doped with $LiN(SO_2CF_3)_2$ were studied by ^{1}H, ^{19}F and ^{7}Li NMR.[116] The effects of carbon black and ceramic (α-Al_2O_3 and γ-Al_2O_3) particles on the cationic and polymer chain mobility were investigated in poly(ethylene oxide)–lithium salt ($LiClO_4$ and $LiBF_4$) solid composite polymer electrolytes by using ^{7}Li NMR.[117] ^{7}Li NMR and ionic conductivity are reported for the polymer electrolytes formed by hydroxyethylcelluloses, poly(ethylene oxide) diisocyanate and $LiClO_4$.[118] Pristine and partially oxidized graphite were lithiated electrochemically and investigated by solid state ^{7}Li NMR.[119] The process of the complexation of lithium with Lasalocid metal salts was studied by ^{7}Li NMR.[120]

3.1.4 Sodium (^{23}Na) ($I = 3/2$) – Sodium ion dynamics in the nonstoichiometric layer-type oxide $Na_{0.67}Ni_{0.33}Ti_{0.67}O_2$ powder was studied by ^{23}Na NMR.[121] ^{23}Na NMR line shapes have been measured over the temperature range from 125 K to 909 K to investigate Na^+ ion dynamics in the polycrystalline ruthenium oxide $Na_{3-x}Ru_4O_9$ with one-dimensional structure.[122] $^{11}B\{^{23}Na\}$ REDOR NMR has been used to probe the spatial relationship between the network former (boron) and the network modifier (sodium) species in sodium borate glasses.[123] The sodium environment in oxide glasses was investigated by ^{23}Na MQ-MAS NMR and compared with molecular dynamics simulations.[124] The isotropic chemical shift distributions were extracted from the MQ-MAS spectra to infer Na–O distance distributions. Structural investigations of nitrate cancrinite (Na_2O-$xSiO_2$-Al_2O_3-$NaNO_3$-H_2O, $1 \leqslant x \leqslant 6$) were performed by ^{29}Si, ^{27}Al and ^{23}Na MAS NMR.[125] The results confirmed the alternating Si, Al ordering of the alumosilicate framework for a Si/Al ratio of 1.0 for all samples. The biologically important compound hydrated disodium adenosine 5′-triphosphate (ATP) was studied by solid-state ^{23}Na MAS, CP-MAS and MQ-MAS NMR.[126] Five binary borosilicate glasses and 54 ternary sodium borosilicate glasses covering the glass-forming regions have been examined by ^{11}B, ^{23}Na and ^{29}Si MAS NMR.[127] One-dimensional heteronuclear correlation solid-state NMR experiments are utilized to determine local structural changes in sodium phosphate glass compositions with ratios of Na/P of 0.25, 0.78, 1 and 1.3. ^{23}Na–^{31}P CPMAS NMR detect direct interactions between distinct phosphorus sites and sodium nuclei in the second coordination sphere.[128] A variety of ^{29}Si, ^{27}Al, ^{23}Na, ^{17}O and ^{1}H NMR data are consistent with the formation of Q^3 AlOH and SiOH groups upon dissolution of H_2O into aluminosilicate glasses.[129] ^{29}Si single-pulse and ^{1}H–^{29}Si CP/MAS data presented more direct evidence for the formation of Q^3 Si species. The cationic coordinations of phosphate based gallium sodium glasses in the system Na_2O-Ga_2O_3-P_{205} have been studied by ^{71}Ga and ^{23}Na MAS NMR in order to study the relationship between the structure and the chemical composition.[130] The process of complexation of Lasalocid, which forms 1:1 or 2:2 complexes with sodium ions, was studied in different solvents at various temperatures by ^{23}Na NMR.[131] ^{23}Na and ^{1}H NMR have been used to study the thermal stability of the double helix structure of an 11-basepair oligonucleotide.[132] The ^{23}Na and ^{27}Al satellite transition spectroscopy NMR MAS spectra of polycrystalline of natural blue sodalite ($Na_8Cl_2(AlSiO_4)_6$) yielded the electric field gradient and chemical shift tensors at both the ^{23}Na and ^{27}Al lattice sites.[133] Static and ^{23}Na MAS and ^{1}H MAS NMR experiments at temperatures down to 100 K as well as high temperature static and ^{23}Na MAS NMR experiments up to 873 K were carried out to study the dynamics of the sodium cation in nitrate cancrinite.[134]

3.1.5 Rubidium (^{87}Rb) ($I = 3/2$). No reference was found during the period of this review.

3.1.6 Caesium (^{133}Cs) ($I = 7/2$). Several new ternary phases including a novel microporous Cs-silicotitanate molecular sieve, SNL-B with the approximate formula of $Cs_3TiSi_3O_{9.5}\cdot 3H_2O$, were investigated by ^{29}Si and ^{133}Cs MAS NMR.[135] A ^{133}Cs NMR experiment was performed on $CsFeCl_3$, which focuses on the field-induced ordered phase around the level-cross field.[136] A new microporous lithosilicate, $Cs_{10}(Li,H)_{14}[Li_8Si_{40}O_{96}]\cdot 12H_2O$, was synthesised and characterized by ^{29}Si, ^{7}Li and ^{133}Cs solid-state NMR.[137] The concentration dependences of ^{133}Cs and ^{19}F chemical shifts for aqueous solutions of caesium perfluorooctanoate are analyzed by using a two-state model.[138]

3.2 Group 2 (^{9}Be, ^{25}Mg, ^{137}Ba). – *3.2.1 Beryllium (^{9}Be) ($I = 3/2$).* The complexes $[Be(OPPh_3)_4](ClO_4)_2$, $[(N(CH_2PPh_2O)_3)Be(OH_2)](ClO_4)_2$ and $[(N(CH_2CH_2PPh_2O)_3)Be(OH_2)](ClO_4)_2$, were characterized by ^{9}Be NMR.[139] ^{31}P and ^{9}Be NMR spectra of mixtures of beryllium(II) and phosphoric acid were interpreted to support the speciation previously proposed on the basis of potentiometric measurements.[140]

3.2.2 Magnesium (^{25}Mg) ($I = 5/2$). The separate effects of 10 wt% MgO, Y_2O_3 and Fe_2O_3 on the silicothermal formation and sintering of X-sialon were investigated by ^{25}Mg NMR.[141] A comparison of ^{25}Mg MAS NMR spectra of crystalline and glassy diopside ($CaMgSi_2O_6$) reveals that the chemical shift in the disordered phase corresponds to that of the mineral, suggesting that sixfold coordination is essentially retained upon vitrification.[142]

3.2.3 Barium (^{137}Ba) ($I = 3/2$). NMR spectra of ^{29}Si and ^{137}Ba were measured in silicon clathrate compounds, $Ba_8Ag_xSi_{46-x}$ ($x = 0$–6), to investigate their electronic properties and superconducting mechanism.[143] Mixed oxide compounds of potential usefulness for fibre coatings (hexagonal celsian, $BaAl_2Si_2O_8$ and lanthanum hexaluminate, $LaAl_{11}O_{18}$) were prepared by hybrid sol-gel synthesis and their thermal crystallization was monitored by solid state ^{137}Ba MAS NMR.[144] ^{137}Ba MAS NMR spectra are presented for 10 ceramic materials and related inorganic compounds. The spectra of compounds in which Ba occurs in highly symmetric sites ($BaZrO_3$, $BaTiO_3$, BaO) show sharp resonances with a well-resolved quadrupolar line shape in the case of $BaTiO_3$.[145]

3.3 Group 3 and Lanthanoids (^{45}Sc, ^{89}Y, ^{139}La, ^{153}Eu). – *3.3.1 Scandium (^{45}Sc) ($I = 7/2$).* ^{45}Sc NMR measurements were performed on the $Sc_{1-x}U_xPd_3$ system, which exhibits an unconventional Kondo effect with a non-Fermi liquid character at low temperatures for the samples with $x < 0.3$.[146]

3.3.2 Yttrium (^{89}Y) ($I = 1/2$). The reaction of periodic acid or alkali-metal periodates with aqueous solutions of scandium, yttrium or lanthanum salts

formed white $M(H_2O)_3\{IO_4(OH)_2\}$ (M = Sc, Y or La). The solution chemistry of $[M(H_2O)_n]^{3+}$ in the presence of H_5IO_6 has been partially explored by ^{45}Sc, ^{89}Y and ^{139}La NMR.[147]

3.3.3 Lanthanum (^{139}La) (I = 7/2). ^{139}La NMR measurements below room temperature have been made on powder samples of $La_3Ni_2O_7$- with ~0.0 and 0.08, and $La_4Ni_3O_{10}$. ^{139}La NMR spectra of these systems are successfully assigned.[148]

3.3.4 Europium (^{153}Eu) (I = 5/2). No reference was found during the period of this review.

3.4 Group 4 ($^{47,49}Ti$). – *3.4.1 Titanium ($^{47,49}Ti$) (I = 5/2, 7/2).* Solid state $^{47,49}Ti$ NMR spectra have been obtained for a number of perovskite and ilmenite $ATiO_3$ compounds.[149]

3.5 Group 5 ($^{51}V^{93}Nb$). – *3.5.1 Vanadium (^{51}V) (I = 7/2).* Multinuclear (^1H, ^{13}C, ^{17}O, ^{51}V) 1D and 2D NMR has been used to characterize the peroxovanadium(V) complexes of glycolic acid in aqueous solution.[150] The vanadotungstogermanic heteropoly acid $H_5GeW_{11}VO_{40}\cdot 22H_2O$ has been prepared for the first time and characterized by ^{51}V NMR.[151] In the case of polydimethylsiloxane-vanadate (PDMSV) materials, single pulses on ^{17}O and ^{51}V nuclei allow an observation of the effect on the quadrupolar splitting of motional changes above the calorimetric glass transition.[152] A charge ordering in NaV_6O_{15} single crystals was investigated by ^{51}V NMR.[153] Monometallic $[Pd_3(PW_9O_{34})_2]^{12-}$, $[Pd_3(PW_9O_{34})_2Pd_nO_xH_y]^{q-}$ (where on the average $n = 3$), bimetallic $[Pd_2Cu(PW_9O_{34})_2]^{12-}$, $[Pd_2Fe(PW_9O_{34})_2]^{11-}$, $[PdFe_2(PW_9O_{34})_2]^{10-}$ and a mixture of $[Pd_3(PW_9O_{34})_2Pd_nO_xH_y]^{q-}$ ($n_{av} = 10$)+$[(VO)_3(PW_9O_{34})_2]^{9-}$ complexes were prepared and characterized by ^{31}P, ^{183}W, ^{51}V NMR.[154] As-synthesised V-containing and V,Mg-containing aluminophosphates of the $AlPO_4$-5 type (AFI structure) with different compositions were characterized by ^{51}V NMR.[155] The magnetic behaviour of VO_2 was studied from high-field ^{51}V NMR data.[156] It was clarified that the transition from the metal to an insulator state in VO_2 is accompanied by the change of the electronic state $2V^{4+} \leftrightarrow V^{3+}+V^{5+}$. The local magnetic properties of β-AV_6O_{15} (A = Ca, Na and Ag) were studied by ^{51}V NMR.[157] Na-deficient $Na_{1-x}V_2O_5$ ($x = 0, 0.02, 0.04$) with single-crystal samples were studied by ^{51}V NMR.[158] Using a combination of potentiometry (glass electrode) and quantitative ^{51}V NMR, the full speciation in the vanadate–peroxide and vanadate–peroxide–imidazole systems was determined.[159] The speciation in the quaternary aqueous $H^+H_2VO_4$-H_2O_2-L-α-alanyl-L-histidine (Ah) system was determined from quantitative ^{51}V NMR measurements.[160] Synthesis and ^{31}P and ^{51}V NMR characterization of $Na_5[PMo_{10}V_2O_{40}]\cdot 14H_2O$ as a mixture of five-Keggin and two-Keggin divanadium(V)-substituted polyoxomolybdates were reported.[161] Vanadium aluminophosphate molecular sieves VAPO-5, -11, -17 and -31 were synthesized hydrothermally and characterized by ^{27}Al , ^{31}P , ^{51}V NMR.[162] The fresh

catalyst $V_2O_5WO_3/TiO_2$ and catalyst used in SCR for 9000 h have been studied by the solid state ^{51}V NMR in static and MAS conditions.[163] A series of catalysts with vanadia contents varying between 4 and 18 wt% were prepared using sol-gel derived alumina-zirconia mixed oxide as a support. The catalysts were characterized by ^{51}V and ^{1}H MAS NMR.[164] Alumina–silica mixed oxide, synthesized by the sol-gel technique, was used as a support for dispersing and stabilizing the active vanadia phase.[165] The catalysts were characterized by ^{51}V and ^{1}H solid-state MAS NMR. The molybdovanadogermanic heteropoly acid $H_5GeMo_{11}VO_40{\cdot}0.24H_2O$ was prepared and characterized by ^{51}V NMR.[166] The reaction of (Bu*t*N=)VNp$_3$ towards dehydroxylated silica was studied by *in situ* ^{13}C CP-MAS and ^{51}V MAS NMR.[167] A novel decavanadium cluster $[(V{=}O)_{10}(\mu^2\text{-}O)_9(\mu^3\text{-}O)_3(C_5H_7O_2)_6]$ bearing ten oxovanadium(V) centers linked with bridging oxygen atoms was prepared and characterized by ^{51}V NMR.[168] The nature of the vanadium species present on V_2O_5/Al_2O_3 catalysts was investigated by solid state ^{51}V NMR.[169] Various Pd-only three-way catalysts containing vanadium and zirconium oxides were prepared by the sol-gel method and investigated with XRD, XPS, ^{51}V NMR, ^{27}Al MAS NMR.[170] Sol-gel derived titania based mixed oxides TiO_2–SiO_2 and TiO_2–ZrO_2 used as supports for preparing a series of catalysts with vanadia contents were characterized by employing ^{51}V and ^{1}H solid-state MAS NMR.[171]

3.5.2 Niobium (^{93}Nb) ($I = 9/2$). – Solid-state ^{93}Nb static and MAS NMR and ^{93}Nb nutation studies of polycrystalline $Pb(Mg_{1/3}Nb_{2/3})O_3$, (PMN) and $(1-x)Pb(Mg_{1/3}Nb_{2/3})O_3/xPbTiO_3$ (x = 0.05 to 0.50) solid-solutions are reported.[172]

3.6 Group 6 (^{95}Mo, ^{183}W). – *3.6.1 Molybdenum (^{95}Mo) ($I = 5/2$).* Reaction of $MoO_2Br_2S_2$ complexes [S = THF, CH_3CN] with bidentate nitrogen donor ligands (L_2) leads to complexes of the type $MoO_2Br_2L_2$ in good yields, L_2 = substituted bipyridylphenanthroline, 1,4-R_2-diazabutadiene and bipyrimidine. The ^{95}Mo NMR data of selected complexes reflect the donor capability of the organic ligands.[173] By using multinuclear (^{1}H, ^{13}C, ^{17}O, ^{95}Mo, ^{183}W) 1D and 2D-NMR, D-gulonic acid is found to form ten and seven complexes, respectively, with tungsten(VI) and molybdenum(VI), in aqueous solution, depending on pH and metal–ligand molar ratios.[174] The complexes *fac*-$[M(CO)_3L_3]$ (M = Mo or W, L_3 = $MeC(CH_2SMe)_3$, $MeC(CH_2SeMe)_3$ or $MeC(CH_2TeMe)_3$) have been prepared from $[M(CO)_3(MeCN)_3]$ and characterized by ^{1}H, $^{13}C\{^{1}H\}$, ^{77}Se, ^{125}Te and ^{95}Mo NMR.[175] Complexes of the type $MoO_2X_2L_2$ were characterized by ^{95}Mo and ^{17}O NMR.[176] The Chevrel-phase pseudo-binary solid solution $Mo_6Se_8Mo_6Te_8$ was studied by solid-state ^{95}Mo NMR.[177] Chiral dioxomolybdenum(VI) complexes of the type $MoO_2Cl_2(L^*)$ (L^* = oxime), $MoO_2(THF)2L^*$ (L^* = *cis-p*-menthane-3,8-diol) and $MoO_2Cl(THF)L^*$ (L^* = 8-phenylthioneomenthol and 8-phenylthioisoneomenthol) were prepared and characterized by solution ^{1}H, ^{13}C, ^{95}Mo NMR.[178] A group of chiral molybdenum(VI) complexes comprising $MoO_2Cl_2L^{**}$, $MoO_2Cl(THF)L^*$

and $MoO_2L_2^*$ [L^{**} = chiral bis(oxazoline) and L^* = chiral 2′-pyridyl alcoholate] were prepared and characterized by ^1H, ^{13}C, ^{17}O, ^{95}Mo NMR.[179]

3.6.2 Tungsten (^{183}W) (I = 1/2). Single crystal of $K_{12}H_2[Ce_4(OH_2)_9(OH)_2(P_2W_{16}O_{59})_2]\cdot 48H_2O$ was prepared, and the ^{183}W NMR spectra (8 lines of equal intensity) of the sample are consistent with the solid state structure.[180] Organophosphoryl derivatives of tungstophosphate of formula $[\alpha_2\text{-}R_2P_2W_{17}O_{61}]^{6-}$ (R = $C_6H_{11}P(O)$; $C_6H_5P(O)$; $C_6H_{11}P(S)$; $C_6H_5P(S)$) were characterized by ^{31}P and ^{183}W.[181] The preparation and crystallization of a tetrameric form of the tri-Ti(IV)-substituted Wells–Dawson-substructure (*i.e.* $[P_2W_{18}O_{62}]^{6-}$-type) heteropolyoxoanion, $[(P_2W_{15}Ti_3O_{60.5})_4]^{36-}$, as its water-soluble potassium salt, are described; the compounds were characterized by solution ^{31}P and ^{183}W NMR.[182] Syntheses and ^{31}P and ^{183}W NMR structural characterization of a novel Dawson-type tungstophosphate $[H_4PW_{18}O_{62}]^{7-}$ and of its lacunary and zinc-substituted derivatives $[H_4PW_{17}O_{61}]^{11-}$ and $[Zn(H_2O)(H_4PW_{17}O_{61})]^{9-}$.[183] Hybrid organophosphoryl polyoxotungstates $[(C_6H_{11}P(O)]_2XW_{11}O_{39}{}^{(8-n)-}]$ were characterized by ^{31}P and ^{183}W NMR.[184] Diorganometallo-substituted γ-Keggin heteropolytungstates γ-$[(RSn)_2SiW_{10}O_{38}]^{6-}$ [R = $MeOCOCH_2CH_2$, $MeOCOCH(Me)CH_2$,$NCCH_2CH_2$], γ-$[(CpTi)_2SiW_{10}O_{38}]^{6-}$ and γ-$[(CpZr)_2SiW_{10}O_{38}]^{6-}$ were prepared and characterized by ^{183}W NMR.[185] The heteropolytungstates, α,β-$K_aH_bXW_9M_3O_{37}(H_2O)_3\cdot nH_2O$ (X = Si,Ge; M = Al, Ga, In, $a + b = 7$) were characterized by ^{183}W NMR.[186] A complex of a novel voltammetrically active isopolyoxotungstate anion, $[H_6W_{18}O_{60}]^{6-}$ was characterized by ^{183}W NMR.[187]

3.7 Group 7 (^{55}Mn, ^{99}Tc). – *3.7.1 Manganese (^{55}Mn) (I = 5/2).* The $La_{0.6}Sr_{0.2}Mn_{1.2-x}Cr_xO_3$ ($0 \leqslant x \leqslant 0.2$) ceramic samples with perovskite-like structure have been studied using X-ray diffraction and ^{55}Mn NMR. The NMR spectra depend strongly on the Cr/Mn ratio.[188] ^{55}Mn NMR in the quasi-1D triangular antiferromagnet $CsMnI_3$ was investigated, and six NMR modes corresponding to six spin orientations of Mn ions in an elementary magnetic cell were observed.[189] The preparation, structure and reactions of glycosylmanganese pentacarbonyl complexes are discussed, and the compounds were characterized by ^{55}Mn NMR chemical shifts and ^{55}Mn, ^{13}C one-bond coupling constants.[190]

3.7.2 Technetium (^{99}Tc) (I = 3/2). No reference was found during the period of this review.

3.8 Group 8 (^{57}Fe, ^{99}Ru). – *3.8.1 Iron (^{57}Fe) (I = 1/2).* ^{13}C, ^{17}O and ^{57}Fe NMR spectra of several carbonmonoxy hemoprotein models with varying polar and steric effects of the distal organic superstructure, constraints of the proximal side, and porphyrin ruffling are reported. Both heme models and heme proteins obey a similar excellent linear δ(13C) *versus* ν(C–O) relationship which is primarily due to modulation of back-bonding from the Fe dπ to CO π* orbital by the distal pocket polar interactions.[191] Mono- and 1,1′-disub-

stituted ferrocene derivatives (substituents are tBu, alkynyl, silyl, germyl, stannyl and boryl groups, and the bridges in the ferrocenophanes are $SiMe_2$ and $Me_2SiSiMe_2$ units) were analyzed by ^{57}Fe NMR.[192]

3.8.2 Ruthenium (^{99}Ru) (I = 3/2). Gradient-coordinate and hybrid variants of density functional theory are used to compute the geometries and ^{99}Ru chemical shifts of RuO_4, $[RuCp_2]$, $[K_4Ru(CN)_6]$, $[Ru_3(CO)_{12}]$, $[Ru(CO)_3X_3]^-$ (X = Cl, I), $[Ru(CO)_2Cl_4]^{2-}$, $[Ru(bipy)_3]^{2+}$ and $[Ru(CO)_2(iPr\text{-}DAB)(X)(Y)]$ [XY = Cl_2, I_2, MeCl, MeI, or $(SnMe_3)_2$].[193]

3.9 Group 9 (^{59}Co, ^{103}Rh). - *3.9.1 Cobalt (^{59}Co) (I = 7/2).* ^{59}Co NMR experiments were performed in melt-spun $Cu_{100-x}Co_x$ samples (x = 10, 15 and 20).[194] An ^{59}Co NMR in intermetallic compounds of the series $Y_{1-x}Gd_xCo_3$was studied,[195] and spectra exhibiting four lines, corresponding to four magnetic sites of these compounds, were observed. The electronic and magnetic properties of superconducting $CuCo_2S_4$ have been investigated with ^{63}Cu and ^{59}Co NMR and ^{59}Co PQR measurements.[196] Selective ^{59}Co-NMR inversion-recovery experiments combined with non-selective experiments on a solution of the cluster $Co_4(CO)_{12}$ at various temperatures yield information about ^{59}Co relaxation data and carbonyl ligand exchange.[197] ^{59}Co NMR experiments were made to study local magnetic properties of an itinerant two-dimensional cobalt oxide $NaCo_2O_4$ with the large thermoelectric power.[198] Two series of cobalt(III)-monodentate phosphine complexes, *trans*-$[Co(acac)_2(PMe_3\text{-}nPh_n)(H_2O)]PF_6$ and *trans*-$[Co(acac)_2(PMe_3\text{-}nPh_n)_2]PF_6$ have been compared in variation of methyl/phenyl substituents of phosphines and evaluated in relation to the ^{59}Co NMR chemical shifts.[199]

3.9.2 Rhodium (^{103}Rh) (I = 1/2). The calculated ^{103}Rh NMR chemical shifts (GIAO-B3LYP/II level) for a range of bis(η^2-alkene)(2,4-pentanedionato)rhodium(I) complexes agree well with solution NMR data.[200] The empirical correlation between transition-metal shifts and stability constants could be confirmed for simple alkenes, since the computed relative Rh-alkene binding energies were found to correlate with $\delta(^{103}Rh)$.

3.10 Group 10 (^{195}Pt). - *3.10.1 Platinum (^{195}Pt) (I = 1/2).* The ^1H, ^{13}C, ^{31}P, and ^{195}Pt NMR spectra of $[Pt^0(PPh_3)_2(\eta^2\text{-}ABC(1)=C(2)XY)]$ compounds (ABC(1)=C(2)XY; A = B = X = Y = H; A = B = X = H, Y = CN; A = H, B = p-NO_2-Ph, X = $COOCH_3$, Y = CN; A = H, B = Ph, X = $COOCH_3$, Y = CN; A = H, B = Ph, X = Y = CN; A = H, B = OEt, X = Y = CN), where X and Y are electron-acceptor substituents, are reported.[201] The Cu(II), Pt(II) and Pd(II) chelates of 3-deoxy-D-*erythro*-hexos-2-ulose bis(thiosemicarbazone) were synthesized and characterized by ^{195}Pt NMR.[202] Two methods for the synthesis of compounds of the type *cis*-PtA_2X_2 (A_2 = bidentate amine or two monodentate amines and X_2 = bidentate or two monodentate carboxylato ligands) were evaluated. The compounds were characterized by ^{195}Pt NMR and IR.[203] A ^{195}Pt NMR measurement has been carried out in heavy fermion

pseudo-binaries $U(Pt_{1-x}Pd_x)_3$ ($0 < x < 0.10$) in order to investigate the evolution of magnetic order.[204] The platinum(IV) carbohydrate complexes of the type $[PtMe_3L]_2SO_4$ (L = 1-amino-1-deoxy-D-glucitol; 1-(*N*-methylamino)-1-deoxy-D-glucitol; 2-amino-2-deoxy-α-D-glucose) were characterized by ^1H, ^{13}C and ^{195}Pt NMR.[205] A novel series of mixed-ligand platinum(II) complexes of the type [PtCl(DMSO)(L)], where L = *N,N*-diethyl-*N'*-(3-R-benzoyl)thiourea, *N,N*-di(2-hydroxyethyl)-*N'*-(3-R-benzoyl)thiourea or *N*-morpholino-*N'*-(3-R-benzoyl)thiourea (R = H, Cl, NO_2, CH_3O, CH_3), have been synthesized and characterized by ^1H and ^{195}Pt NMR.[206] $[Pt_3(\mu\text{-}CO)_3(PPh_3)_3]$ was prepared in high yield by the reaction of $[Pt_3(\mu\text{-}CO)_3(PPh_3)_4]$ with H_2O_2. and characterized by ^{195}Pt NMR.[207] Several novel binuclear Pd^{II}, Pt^{II}, and Pt^{IV} complexes of *trans*-1,2-bis(diphenylphosphino)ethene or *cis,trans,cis*-1,2,3,4-tetrakis(diphenylphosphino)cyclobutane have been prepared and characterized by $^{195}Pt\{^1H\}$ and $^{31}P\{^1H\}$ NMR.[208] An efficient chiral derivatizing agent for the determination of the enantiomeric composition of unsaturated ethers and alcohols, *cis*-dichloro[(*S*)-methylbenzylamine](ethylene)platinum(II) was characterized by ^{195}Pt NMR.[209] The propensity of highly pyramidalized unsaturated dodecahedranes for metal complexation has been tested; structures, complexing strengths and reversibility have been analyzed by ^1H, ^{13}C, ^{31}P, ^{195}Pt NMR.[210] A series of new platinum(IV) complexes of the type $[Pt(IV)(DACH)trans(L)_2Cl_2]$ (where DACH = *trans*-1R,2R-diaminocyclohexane, and L = acetate, propionate, butyrate, valerate, hexanoate, or heptanoate) bearing the carboxylate groups in the axial positions have been synthesized and characterized by ^{195}Pt NMR.[211] Dissociation of coordinated water from *trans*-diaquabisoxalatoplatinum(IV) has been proposed as the first step in the formation of one-dimensional mixed valence polymers of oxalatoplatinum complexes. ^{195}Pt and ^{13}C NMR was used to study hydroxo-aqua protonation states and aqua ligand exchange rates for *trans*-diaquabisoxalatoplatinum(IV).[212] A new class of water-soluble cyclotriphosphazene-(diamine)-platinum(ll) conjugate drugs $[NP(Am{\cdot}Li_2)(Am{\cdot}PtA_2)]_3$ (Am: dicarboxylic amino acid; A_2: diamine) has been synthesized and characterized by means of elemental analysis, multinuclear (^1H, ^{31}P, ^{13}C, ^{195}Pt) NMR.[213] New types of mixed-ligands Pt(II) complexes, *cis*- and *trans*-$Pt(R_2SO)$(pyrimidine)Cl_2 (R_2SO = dimethyl sulfoxide, tetramethylene sulfoxide, di-n-propyl sulfoxide, di-n-butyl sulfoxide, dibenzyl sulfoxide and diphenyl sulfoxide) were synthesized and characterized by ^{195}Pt NMR.[214] The photochemical transformation of the *fac*-$Pt(NO_2)_3Cl_{32}$-complex in water solutions and frozen matrices was studied by ^{195}Pt NMR.[215] The structures of $[MCl_2(maleonitrile\text{-}S_2O_n)]$ (n = 2–5) (M = Pd, Pt) were investigated by 1D and 2D ^1H, ^{13}C and ^{195}Pt NMR.[216] The ionic complexes [M(triphos)Cl]X [M = Pd, X = Cl (1), $SnCl_3$, $SnPh_2Cl_3$; M = Pt, X = Cl, $SnCl_3$, $SnPh_2Cl_3$], $[M(triphos)Cl]_2X$ [X = $SnPh_2Cl_4$, M = Pd, Pt; X = $PtCl_4$, M = Pt] and $[M(triphos)_2]X_2$ [X = $SnPh_2Cl_3$, M = Pd, Pt] where triphos = bis(2-diphenylphosphinoethyl)phenylphosphine, were synthesized and characterized by ^{31}P, ^{195}Pt and ^{119}Sn NMR.[217] Reactions of sodium benzylselenolate with several palladium(II) and platinum(II) complexes were carried out and a variety of products isolated and characterized by ^1H, ^{31}P, ^{77}Se, ^{195}Pt

NMR.[218] The complex $[(CH_3)_4N]_3[Pt(SnCl_3)_5]$ as a molecular precursor to prepare PtSn/c-Al_2O_3 reforming catalysts was characterized by ^{195}Pt and ^{119}Sn NMR.[219] The synthesis and mesomorphic properties of the first thiocyanato-bridged, sheet-shaped di- and tetra-platinum complexes are described, and the compounds were characterized by ^{1}H, ^{13}C, ^{195}Pt NMR.[220]

3.11 Group 11 (^{63}Cu, ^{107,109}Ag). – *3.11.1 Copper (^{63}Cu) ($I = 3/2$).* The ^{63,65}Cu NMR/NQR spectra,[199] ^{199}Hg and ^{19}F NMR spectra and spin–lattice relaxation rate on a series of powder $HgBa_2CuO^{4+}{}_xF_y$ samples with different oxygen and fluorine content have been measured.[221] ^{63}Cu NMR and X-ray diffraction methods have been used to investigate the temperature dependence of the nuclear chemical shifts and the diffraction patterns, respectively, for mixed crystal $Ag_xCu_{1-x}I$ ($0 < x < 0.5$).[222] Bridgman-grown polycrystalline $CuInS_2$ and $CuInSe_2$ containing 2 atom% excess S and Se, respectively, were investigated by ^{63}Cu and ^{115}In NMR.[223] Polycrystalline n- and p-type $CuInSe_2$ was examined by ^{63}Cu NMR.[224]

3.11.2 Silver (^{107,109}Ag) ($I = 1/2, 1/2$). A ^{109}Ag–^{107}Ag double-resonance NMR signal between the very mobile nuclei of a superionic conductor was detected in a silver conductor, namely Ag_9GaSe_6.[225] Two novel coinage metal(I)-triphenylphosphine complexes with a heterocyclic ligand, $[Ag(tetrazole)(PPh_3)_2]_n$, were synthesized and characterized by the solid-state, solution ^{31}P, ^{1}H and ^{13}C, ^{109}Ag NMR.[226]

3.12 Group 12 (^{67}Zn, ^{111,113}Cd, ^{199}Hg). – *3.12.1 Zinc (^{67}Zn) ($I = 5/2$).* Taking advantage of an order of magnitude in sensitivity enhancement obtained by sampling of quadrupolar-echo (QE) solid-state NMR spectra during a quadrupolar Carr–Purcell–Meiboom–Gill (QCPMG) pulse sequence, the coordination environment of low-γ quadrupolar metal nuclei can be studied routinely for powders with these nuclei in natural abundance. The general applicability of the method is demonstrated by ^{39}K, ^{25}Mg, ^{67}Zn and ^{87}Sr QCPMG solid-state NMR experiments for K_2MoO_4, KVO_3, $Mg(VO_3)_2$, $Zn(CH_3COO)_2{\cdot}2H_2O$, $Zn(Ala)_2{\cdot}H_2O$, $Sr(NO_3)_2$ and $SrMoO_4$.[227]

3.12.2 Cadmium (^{111,113}Cd) ($I = 1/2, 1/2$). ^{113}Cd MAS NMR spectra of crystalline CdF_2, $KCdF_3$ and $CdCl_2$ and vitreous $50CdF_2{\cdot}30NaF{\cdot}20BaF_2$, $50CdF_2{\cdot}30NaCl{\cdot}(20-x)BaF_2{\cdot}xBaCl_2$ (x = 0, 5, 10, 15 and 20) and $50CdCl_2{\cdot}15NaCl{\cdot}35BaCl_2$ in mol% were measured so as to reveal the anion coordination environments around Cd^{2+} in the glasses.[228] ^{113}Cd MAS NMR is used to probe the Ca^{2+}-binding site in the water-oxidizing complex of $^{113}Cd^{2+}$-substituted photosystem II of plants. The line width of the proton signal in a WISE (wide-line separation) two-dimensional ^{1}H–^{113}Cd NMR experiment demonstrates that the signal arises from Cd^{2+} in a solid and magnetically undisturbed environment.[229] The use of both slurry and solid-state ^{113}Cd NMR has been applied to the investigation of the chemical moieties involved in cadmium ion binding to a biosorbent.[230] ^{113}Cd NMR in $YbInCu_4$ and

$YbCdCu_4$ have been measured on powdered samples prepared from single crystals.[231] ^1H-^{113}Cd variable-amplitude cross-polarization (VACP) and ^{27}Al-^{113}Cd spin-echo double-resonance (SEDOR) experiments were performed on dried, Cd^{2+}-exchanged beidellite, montmorillonite and vermiculite samples, demonstrating a direct interaction between the adsorbed cations and the clay.[232] ^{113}Cd MAS NMR spectra of crystalline CdF_2,$KCdF_3$ and $CdCl_2$ with known crystal structures and vitreous $50CdF_2{\cdot}30NaCl{\cdot}(20-x)BaF_2{\cdot}xBaCl_2$ in mol% (x : 0, 5, 10, 15 and 20) were measured to reveal the anion-coordination environments around Cd^{2+} in the glasses.[233]

3.12.3 Mercury (^{199}Hg) ($I = 1/2$). The $^{63,65}Cu$ NMR/NQR spectra, ^{199}Hg and ^{19}F NMR spectra and spin–lattice relaxation rate on a series of powder $HgBa_2CuO^{4+}{}_xF_y$ samples with different oxygen and fluorine content have been measured.[221] [HgR(5-(4′-dimethylaminobenzylidene)rhodanine)] and [HgR(5-(2′-thiophenomethylene)rhodanine)] (R = Me, Ph) were synthesized and characterized by ^1H, $^{13}C\{^1H\}$ and ^{199}Hg NMR.[234] Several novel binuclear Hg(II) complexes of *cis,trans,cis*-1,2,3,4-tetrakis(diphenylphosphino)cyclobutane were prepared and characterized by $^{199}Hg\{^1H\}$, $^{31}P\{^1H\}$, ^1H NMR.[235] Mercury(II) complexes of aromatic aminothiolate ligands of formula [Hg(n-$SC_6H_4NH_2)_2$] and [RHg(n-$SC_6H_4NH_2$)], (R = Me, Ph, n = 3 or 4) were obtained and characterized by ^1H, ^{13}C and ^{199}Hg NMR.[236]

3.13 Group 13 (^{11}B, ^{27}Al, ^{71}Ga, $^{203,205}Tl$). – *3.13.1 Boron (^{11}B) ($I = 3/2$).* Experimental and computed ^{11}B NMR signals are assigned for the first time in the yet X-ray unresolved 1,2-$(SH)_2$-1,2-$C_2B_{10}H_{10}$ *ortho*-carborane.[237] Synthetic methodologies as well as ^{11}B-, ^{19}F-NMR, and negative ion elecrospray mass spectrometric (NIEMS) characterization of the 8,8′-difluoro derivative of this anion [commo-3,3′-Co(8-F-3,1,2-$CoC_2B_9H_{10})_2{}^{1-}$] are reported.[238] The compounds of 1-CCPh-2-Ph-3-(-L)-3,1,2-$RhC_2B_9H_9$ (L = C_5H_5 and C_5Me_5) were prepared and characterized by ^{11}B NMR.[239] A series of alkali metal dihydrido borates was prepared by three different routes and characterized by ^{11}B-NMR.[240] The series of compounds m,m'-$M(B_5H_8)_2$, where M = Cd (I), Zn (II), or Hg (III), were prepared, and the NMR spectral assignments were confirmed using $^{11}B\{^1H\}$ selective decoupling experiments and heteronuclear ^{11}B–^1H chemical shift correlation spectroscopy.[241] $^{11}B\{^{23}Na\}$ REDOR NMR was used to probe the spatial relationship between the network former (boron) and the network modifier (sodium) species in sodium borate glasses.[123] The structure of PbO–B_2O_3 glasses was investigated in the composition range of 25–80 mol% PbO by ^{11}B NMR.[242] The effect of Al_2O_3 on the structure change and the phase separation in Na_2O–B_2O_3–SiO_2 glass was investigated using ^{11}B, ^{29}Si-MAS, and ^{27}Al-MAS NMR.[243] Alternating acceptor–donor-conjugated copolymers of cyclodiborazane with dithiafulvene were prepared and characterized by ^1H and ^{11}B NMR.[244] The kinetics of the phase separation in $15Na_2O$–$85B_2O_3$ binary glasses was investigated -P_2O_5, MO–SiO_2–P_2O_5 and MO(M'_2O)–SiO_2–Al_2O_3–B_2O_3 (M = Mg, Ca, Sr and Ba, M′ = Na) glasses were examined.[246] The ^{11}B MAS NMR in the binary glass system $xV_2O_5B_2O_3$

($x = 0.053, 0.43$) and the ternary glass system $xV_2O_5B_2O_3PbO$ ($0.1 \leqslant x \leqslant 1.5$) was investigated.[247] The ^{11}B NMR spectra of $xRb_2S+(1-x)B_2S_3$ glasses in the range $0 \leqslant x \leqslant 0.75$ and of $xCs_2S+(1-x)B_2S_3$ glasses in the range $0 \leqslant x \leqslant 0.60$ are reported.[248] A series of β-irradiated aluminoborosilicate glasses was investigated by ^{11}B NMR.[249] Five binary borosilicate glasses and 54 ternary sodium borosilicate glasses covering the glass-forming regions have been examined by ^{11}B, ^{23}Na and ^{29}Si solid state MAS NMR.[250] Titanium-containing MEL zeolites (Ti-ZSM-11) are prepared by gas–solid reactions between $TiCl_4$ vapor and B-ZSM-11 precursors and characterized by ^{11}B and ^{29}Si MAS NMR.[251] Possible methods of formation of chelated fluoroboron cations $(DD)BF^{2+}$ and $(DD)BFX^+$, where DD is 2,2′-bipyridine, 1,10-phenanthroline, 2,2′,6′,2″-terpyridine and 1,8-bis(dimethylamino)naphthalene were investigated by ^{19}F and ^{11}B NMR.[252] The complex formation between three tris(oxaalkyl) borates and $SbCl_5$ as well as the structure of these complexes were studied by ^{11}B NMR.[253] Thin films of boron-substituted carbons have been synthesized by chemical vapor deposition and characterized by ^{11}B-NMR.[254] Boron adsorption behavior on cross-linked polysaccharide anion exchangers, QAE-Sephadex and QA cellulose, was examined by ^{11}B NMR.[255] The effective incorporation of B in a borosilicate framework was confirmed by ^{11}B MAS NMR.[256] The ^{11}B NMR chemical shift of diphenylboronium perchlorate dissolved in $CD_3NO_2$was determined.[257] A modified *in situ* preparation and the ^1H, ^{13}C and ^{11}B NMR spectra of the chelating monoanionic tricarbene ligands hydrotris(3-R-imidazoline-2-yliden-1-yl)borate (R = Me, Et) were reported.[258]

3.13.2 Aluminium (^{27}Al) ($I = 5/2$). Solid-state ^1H, ^{13}C, ^{27}Al NMR during the continuous-flow of propene monomer was applied to analyze *in situ* propene polymerization on Ziegler–Natta catalysts.[259] ^{27}Al MAS NMR spectra of 12 fluoroaluminate crystals with known crystal structures and $40AlF_3 \cdot (20-x)BaF_2 \cdot xBaCl_2 \cdot 20CaF_2 \cdot 17YF_3 \cdot 3EuF_3$·glasses ($x$ = 0, 3, 6, 9 and 12) in mol% were measured to examine the anion coordination environments around Al^{3+} in the glasses.[260] The lithium fast-ion conductor, $Li_{1+x}Al_xTi_2\text{-}x(PO_4)_3$ (LATP) has been modified *via* changes in stoichiometry during the processing steps. The resultant changes have been followed using ^{27}Al MAS NMR.[261] ^{27}Al MQ MAS NMR combined with global elemental analysis have been used to identify and quantify extra-framework aluminium (EFAL) in Y zeolites stabilized by steaming.[262] The effect of Al_2O_3 on the structure change and the phase separation in Na_2O–B_2O_3–SiO_2 glass was investigated using ^{11}B, ^{29}Si MAS, and ^{27}Al MAS NMR.[243] ^{27}Al and ^{29}Si NMR spectra and spin–lattice relaxation in heavily sodium-doped sodalite $Na_8(AlSiO_4)_6$ were presented.[263] ^{27}Al MAS NMR has been used to study the surface aluminium compounds formed upon interaction of the supported $TiCl_4$/donor/$MgCl_2$ catalyst with $AlEt_3$ in the presence or absence of the external donor.[264] A pillared interlayered clay (PILC) was characterized by ^{27}Al MAS NMR, and Al_{13}-PILC samples contain the expected resonances due to Al(VI) and Al(IV) sites.[265] ZSM-5 zeolites prepared by confined space synthesis are characterized by ^{27}Al

and ^{29}Si-MAS NMR.[266] ^{27}Al{^{1}H} MAS and CP/MAS NMR have been used to follow both the hydration processes of the cement blends and the interactions of chloride ion with the hydrated aluminium species.[267] ^{1}H, ^{27}Al and ^{31}P MAS, and ^{13}C and ^{29}Si CP/MAS NMR was used to characterize catalysts of Pd supported on various solids including SiO_2, $AlPO_4$ and $Mg_3(PO_4)_2$ that were activated with the chiral hydrogen-donor limonene.[268] The effect of pH during sol-gel synthesis on the structural and physicochemical properties of a Pd–Al_2O_3 three-way catalyst prepared by the sol-gel method was investigated by ^{27}Al MAS NMR.[269] Ag^+/Na^+ ion-exchanged R_2O–Al_2O_3–SiO_2 glasses with a uniform concentration profile of Ag^+ and Na^+ were prepared and investigated by ^{29}Si-MAS and ^{27}Al-MAS NMR.[270] ^{27}Al-3QMAS and ^{27}Al{^{19}F}-WISE MAS NMR were used to detect three different Al–F sites on the surface of fluorinated-alumina.[271] Solid state ^{29}Si and ^{27}Al NMR were applied to a series of reduced-charge montmorillonites (RCMs) to discern changes in electronic and structural properties that are induced by Li fixation.[272] The spectrum inversion for the ^{27}Al MQ-MAS was developed, and the Al–O–Si bond angles in sodium aluminosilicate glasses with variable calcium content were investigated.[273] The ^{27}Al NMR spectrum of an emerald ($Be_3Al_2Si_6O_{18}$:Cr^{3+}) single crystal grown by the flux method was investigated in the temperature range of 120-420 K.[274] Zeolite Beta samples that had undergone calcination and/or steam deactivation were examined by ^{27}Al MAS and ^{29}Si MAS NMR.[275] Vanadium aluminophosphate molecular sieves VAPO-5, -11, -17 and -31 were synthesized hydrothermally and characterized by ^{27}Al, ^{31}P, ^{51}V NMR.[276] Aluminium nitride (AlN) powder prepared by the solid–gas reaction of aluminium sulfide (Al_2S_3) with ammonia was investigated by ^{27}Al MAS NMR.[277] A variety of ^{29}Si, ^{27}Al, ^{23}Na, ^{17}O and ^{1}H NMR data are consistent with the formation of Q3 AlOH and SiOH groups upon dissolution of H_2O into aluminosilicate glasses.[129] The local structures of Sm and Al in Sm-doped aluminosilicate glasses prepared by the sol-gel method were investigated by ^{27}Al MAS NMR.[278] The compositional dependence of water incorporation mechanisms in melts and glasses belonging to the quartz-albite join was studied with ^{1}H, ^{23}Na, ^{27}Al and ^{29}Si MAS NMR and ^{1}H–^{29}Si CP-MAS NMR.[279] Al-containing micelle-templated silica with Si/Al atomic ratios in the range 8–45 was synthesized and characterized by ^{27}Al NMR-MAS.[280] Two-dimensional ^{27}Al–^{31}P CPMAS NMR experiments have been performed on sodium aluminophosphate glasses in the $x NaAlO_2 \cdot (1-x) NaPO_3$ compositional range, providing direct detection of particular aluminium species connected to specific phosphorus species.[281] ^{27}Al MAS and 3Q-MAS NMR spectra were recorded for the synthetic amphibole $Ca_{1.8}(Mg_{4.8}Al_{0.4})(Si_{7.6}A_{l0.4})O_{22}(OH)_2$.[282] ^{27}Al MAS NMR showed that aluminium hydroxyphosphate adjuvants contain both tetrahedrally and octahedrally coordinated aluminium.[283] Pigments of titanium dioxide rutile, coated with SiO_2–Al_2O_3, were characterized by ^{27}Al single pulse MAS and 3Q-MAS NMR. Rotational echo double resonance, ^{27}Al{^{1}H} CP and ^{29}Si{^{1}H} CP experiments provide longer range distance information through dipolar coupling to proton.[284] Double resonance NMR echo techniques were developed for the study of

solids, particularly in the ^{29}Si–^{27}Al REAPDOR (rotational echo adiabatic passage double resonance) NMR experiment.[285] The experiment holds the promise of broad applications to the study of aluminosilicates, intra-zeolite chemistry and glassy materials, including complex spectral assignments, structural details, and reaction mechanisms. The combined application of ^{27}Al MAS, 3Q-MAS, as well as CP-MAS and REDOR techniques were applied to study the local environments of several aluminium fluoride-based glasses and the model crystalline compound AlF_3.[286] Glass-forming characteristics, properties and structural features of glasses in the $La_2O_3Al_2O_3P_2O_5$ system have been investigated by ^{27}Al MAS NMR.[287] 2D ^{27}Al MQ-MAS NMR has been used to extract the isotropic chemical shifts and quadrupolar parameters of five amorphous aluminosilicates.[288] Various solid-state NMR techniques, such as CP-MAS, HETCOR, dipolar dephasing, spin counting, double-quantum correlation and REDOR, were applied to hydrous silicate and aluminosilicate glasses.[289] The interaction of aluminium(III) with glucose-6-phosphate in aqueous solutions as studied by ^{31}P, ^{27}Al, ^{13}C NMR.[290] The dealumination of Zeolite MCM-22 by calcination or hydrothermal treatment was investigated by multinuclear solid-state NMR and checked by an ultrahigh-field NMR experiments (19.6 T) with a very fast spin rate (19.1 kHz).[291] Platinum supported on La_2O_3–Al_2O_3 and CeO_2–Al_2O_3 were prepared by the sol-gel method and characterized by ^{27}Al-MAS NMR.[292] ZSM-5 zeolites were prepared using sodium silicate, aluminium sulfate and tetrapropylammonium bromide and characterized by ^{29}Si, ^{27}Al MAS NMR and ^{29}Si, ^{27}Al CP-MAS NMR.[293] Mesoporous MCM-41 molecular sieves substituted with various amounts of Cu(II) and Al(III) were synthesized and characterized by ^{27}Al MAS NMR.[294] Nanocrystalline metal aluminates MAl_2O_4, M = Mn, Cu and Zn, have been prepared and characterized by ^{27}Al MAS NMR.[295] Various Pd-only three-way catalysts containing vanadium and zirconium oxides were prepared and investigated by ^{51}V NMR and ^{27}Al MAS NMR.[296] Steamed zeolite Y samples were examined by ^{27}Al MAS, ^{1}H spin-echo editing MAS, and $^{1}H,^{27}Al\}$ double-resonance MAS NMR in order to evaluate the dealumination process during steaming.[297] A variety of silicon and cobalt substituted mesoporous aluminophosphate materials with different incorporated contents were prepared and characterized by ^{27}Al, ^{31}P MAS NMR.[298] The ^{23}Na and ^{27}Al MAS spectra of polycrystalline of natural blue sodalite ($Na_8Cl_2(AlSiO_4)_6$) yielded the electric field gradient and chemical shift tensors at both the ^{23}Na and ^{27}Al lattice sites.[133] Carbonate hydrotalcites prepared by coprecipitation of metal nitrate salts and Na_2CO_3 were characterized by ^{27}Al MAS NMR.[299] ^{27}Al and ^{29}Si NMR were employed to characterize layered silicates in a suite of eight Argonne Premium coals.[300]

3.13.3 Gallium (^{71}Ga) ($I = 3/2$). With the recent progress in ^{71}Ga solid state NMR, it has become possible to take advantage of the complementary information that can be obtained using NMR and X-ray absorption spectroscopies. Examples of an Al-, Ga-based catalyst are investigated.[301] The solution chemistry and structure of the complex of the triazamacrocyclic

ligand NOTP (1,4,7-triazacyclononane-1,4,7-tris(methylenephosphonate)) with Ga^{3+} in D_2O have been investigated by ^1H, ^{71}Ga and ^{31}P NMR.[302] The cationic coordinations of phosphate based gallium sodium glasses in the system Na_2O–Ga_2O_3–P_{205} have been studied by ^{71}Ga and ^{23}Na MAS-NMR.[303] Ga-containing MCM-41 zeolites were prepared by addition of Ga to the synthesis gel (Ga-MCM-41) or by impregnation of Ga onto MCM-41, and their structure were studied by ^{71}Ga NMR.[304] MFI-type gallosilicalite and galloaluminosilicate were synthesized and characterized by ^{71}Ga MAS NMR.[305] Ga-substituted merlinoite (MER)-type zeolites are hydrothermally synthesized and characterized by ^{29}Si and ^{71}Ga MAS NMR.[306]

3.13.4 Thallium ($^{203,205}Tl$) (I = 1/2,1/2). The semiconductor Tl_2Te_3, in which Tl atoms are placed in galleries formed by puckered Te layers, was examined by ^{203}Tl and ^{205}Tl NMR.[307]

3.14 Group 14 (^{13}C, ^{29}Si, ^{73}Ge, $^{117,119}Sn$, ^{207}Pb). – *3.14.1 Carbon (^{13}C) (I = 1/2) (Review).* Recent advances in structural and conformational analysis of fluorinated carbohydrates by NMR spectroscopy are reviewed. Characteristic ^1H, ^{13}C, and ^{19}F NMR chemical shifts and coupling constants for selected examples are given.[308] The salient aspects concerning the syntheses, characterization, and complexing properties of variously substituted mono- and bis-(α-amino)- and (α-hydroxy)-phosphonates are reviewed. Characterization of these compounds was mainly achieved by ^1H, ^{13}C, and ^{31}P NMR, by FABMS techniques, and by X-ray diffraction analyses.[309] A comprehensive review with 175 references was given on the microstructural analysis of polypropylene using solution-state ^{13}C NMR.[310] The stereoselectivity, regioselectivity, polymerization mechanisms, and polymerization catalysts are discussed. Complete parametrization of peptide backbone ^{13}CO chemical shift anisotropy tensors were obtained for a protein (Binase) in solution.[311] The site-resolved identification of the secondary structure of solid peptides and proteins is presented by the correlation between the backbone conformation and the C_α chemical shift anisotropies of proteins.[312]

3.14.2 Silicon (^{29}Si) (I = 1/2). It is shown that ^{29}Si and ^{15}N NMR chemical shifts are useful for differentiation between hydroxamic and hydroxamic structures of silylated aliphatic dihydroxamic acids, but for determination of *E* and *Z* configurations spin–spin coupling must be used until more data relating ^{29}Si, ^{13}C and ^{15}N chemical shifts to the configuration are available for this class of compounds.[313] The dependence of chemical shifts on Hammett substituent constants in ring-substituted benzhydroxamic acids is discussed. The results of first principles density functional theory (DFT) calculations on the ^1H and ^{29}Si NMR chemical shifts of silane and hydroxyl groups in SiO_2 was reported.[314] Solid state MAS NMR is used to measure the ^{29}Si chemical shift and full width at half maximum in $Na_2O{\cdot}2SiO_2{\cdot}xMnO$ glasses (for $0.0 \leqslant x \leqslant 0.8$).[315] Solid state ^{29}Si and ^{27}Al NMR were applied to a series of reduced-charge montmorillonites (RCM) to discern changes in electronic and structural

properties that are induced by Li fixation.[316] Structure, size and dynamics of domains of hybrid siloxane networks prepared by copolymerization of tetraethoxysilane (TEOS) and dimethyl(diethoxy)silane (DMDEOS) were studied by solid-state ^{1}H and ^{29}Si NMR and *ab initio* MO calculations.[317] The different polymorphs of $Y_2Si_2O_7$ have been synthesized by a sol-gel process and by mixed-powder routes. ^{29}Si NMR spectra are reported for the α, β, γ and δ, polymorphs which are consistent with accepted structural data from the point of view of the number of sites, the populations and the relative chemical shifts.[318] The ^{29}Si NMR chemical shifts for organically modified silane compounds, $Me_xSi(OR)_y(OH)_{4-x-y}$ (OR = OMe, OEt), were evaluated using a partial charge model (PCM) approach to describe the chemical bonding.[319]

3.14.3 Germanium (^{73}Ge) (I = 9/2). ^{73}Ge MAS NMR spectra of organogermanium compounds were observed for the first time. The chemical shifts and half-widths of tetra-Ph germane and tetrabenzyl germane were recorded with and without high-power decoupling.[320]

3.14.4 Tin ($^{117,119}Sn$) (I = 1/2,1/2). A comprehensive review with 120 references was given on organotin(IV) complexes of the amino acids and peptides with special reference to their methods of synthesis, structural and thermal properties as well as their solution studies and biological activity.[321] The structures of these complexes are discussed on the basis of IR, electronic, ^{1}H, ^{13}C and ^{119}Sn NMR, X-ray and ^{119}Sn Mössbauer spectral studies. The solid acid catalyst 30% WO_3/SnO_2 was synthesized and studied by solid state ^{117}Sn NMR.[322] Three dibutyltin perfluoroalkanecarboxylates were synthesized and characterized by ^{1}H-, ^{13}C-, ^{19}F- and ^{117}Sn NMR.[323] Monometallic Ru and heterobimetallic complexes containing Ru–Sn bonds, $[(\eta^5\text{-}C_5H_5)\ P_2RuX]$ and $[(\eta^5\text{-}C_5H_5)P_2Ru(SnX_3)]$, where P = PPh_3, PPh_2Me, P_2 = 1,2-bis(diphenylphosphine)ethane (dppe), and X = F, Cl, Br, were synthesized and characterized by ^{31}P and ^{119}Sn NMR.[324] A family of novel alkaline earth metal stannides, $[Ba(18\text{-crown-}6)(HMPA)_2][SnPh_3]_2$, $[Ca(18\text{-crown-}6)(HMPA)_2][Sn(SnPh_3)_3]_2$, and $[Sr(18\text{-crown-}6)(HMPA)_2][Sn(SnPh_3)_3]_2$ were synthesized and characterized by ^{119}Sn NMR.[325] An improved synthesis of tetrakis(trimethylstannyl)cyclopentadiene is reported with ^{1}H-, ^{13}C- and ^{119}Sn-NMR data.[326] Organotin(IV) compounds of the potentially ambidentate *O*-cholesteryl-*O*-phenyl phosphorothioate ligand formulated as $Me_3SnOSPR'R''$, $Ph_3SnOSPR'R''$, $O(CH_2CH_2S)_2Sn(n\text{-Bu})OSPR'R''$, $S(CH_2CH_2S)_2Sn(n\text{-Bu})OSPR'R''$, (R′ = *O*-Ph; R″ = *O*-cholesteryl) were obtained and characterized by ^{119}Sn NMR.[327] Intra-ribbon dynamics in $[(Me_2Sn)_3\{Co(CN)_6\}_2\cdot 6H_2O]$ were suggested by solid-state ^{13}C, ^{15}N, ^{59}Co and ^{119}Sn CP-MAS NMR.[328] Bis(alkoxyethynyl)dimethyltin derivatives $Me_2Sn(CCOR)_2$ were characterized by ^{1}H, ^{13}C and ^{119}Sn NMR.[329] ^{119}Sn NMR spectra and ^{1}H NMR spin–lattice relaxation times were measured for $(CH_3)_nNH_{4-n}SnCl_3$ (n = 1–4).[330] $E(Si_2Me_4)_2E$, $E(Si_2Me_4)_2E'$, and six-membered-ring compounds $(Me_2ME)_3$ (M = Si, Ge, Sn, E,E′ = Se, Te) were synthesized and characterized by ^{1}H, ^{11}B, ^{13}C, ^{29}Si, ^{77}Se, ^{119}Sn, ^{125}Te NMR.[331] The ionic complexes [M(triphos)Cl]X [M

= Pd, X = Cl, $SnCl_3$, $SnPh_2Cl_3$; M = Pt, X = Cl, $SnCl_3$, $SnPh_2Cl_3$], $[M(triphos)Cl]_2X$ [X = $SnPh_2Cl_4$, M = Pd, Pt; X = $PtCl_4$, M = Pt] and $[M(triphos)_2]X_2$ [X = $SnPh_2Cl_3$, M = Pd, Pt] where triphos = bis(2-diphenylphosphinoethyl)phenylphosphine, were synthesized and characterized by ^{31}P, ^{195}Pt and ^{119}Sn NMR.[332] The functionalized vinylstannanes of the type (*E*)/(*Z*)-$Ph_3SnCR'=CHYR_n$ and (*E*)/(*Z*)-$Ph_3SnC(YR_n)=CHR'$(YR_n = NMe_2, OEt, SMe, SEt; R′ = Ph, Bu (*n*-butyl), Pe (*n*-pentyl), H) were prepared and characterized by ^1H, ^{13}C and ^{119}Sn NMR.[333] The stereospecific $B(C_6F_5)_3$-catalyzed 1,3-isomerization of (*E*,*S*)-1-methoxymethoxy-2-butenyl tributylstannane was investigated by ^1H and ^{119}Sn NMR.[334] The complex $[(CH_3)_4N]_3[Pt(SnCl_3)_5]$ selected as a molecular precursor to prepare PtSn/c-Al_2O_3 reforming catalysts was characterized by ^{195}Pt and ^{119}Sn NMR.[335] The halogen redistribution reaction in the binary $[nBu_2SnCl]_2O/[nBu_2SnBr]_2O$ system is examined by ^{119}Sn and ^{13}C NMR.[336] The triorganotin halides (CabC,P)$SnMe_2X$ (X = Cl, Br) and a tetraorganotin compound (CabC,P)$SnMe_3$ containing the *o*-carboranylphosphino ligand (CabC,P) were prepared and characterized by ^1H, ^{13}C, ^{31}P and ^{119}Sn NMR.[337] Thirteen tris(2-methyl-2-phenylpropyl)tin germylpropionates were synthesized and characterized by ^1H, ^{13}C, ^{119}Sn NMR.[338] The novel compounds 1,3-bis(trimethylstannyl)ferrocene, 1,2,4-tris(trimethylstannyl)ferrocene, 1,1′,3,3′-tetrakis (trimethylstannyl)ferrocene and 1,1′,2,2′,4,4′-hexakis(trimethylstannyl)-ferrocene were prepared and characterized by ^1H, ^{13}C and ^{119}Sn NMR.[339] Methyl 4,6-*o*-benzylidene-2,3-bis-*o*-(Ph_nMe_3-*n*$SnCH_2$)-α-D-glucopyranosides, (3: *n* = 3; 4: *n* = 2; 5: *n* = 1) were investigated by ^{119}Sn and ^{13}C NMR.[340] Equilibrium and spectroscopic (^1H, ^{13}C NMR and ^{119}Sn Mössbauer) studies in aqueous solution are reported for dimethyltin(IV) complexes of 2-hydroxyhippuric acid.[341]

3.14.5 Lead (^{207}Pb) (I = 1/2). Tetrakis(pentafluorophenyl)lead(IV) was characterized by ^{19}F, ^{13}C and ^{207}Pb NMR, and theoretical simulation of ^{207}Pb NMR spectra was presented.[342] A variable temperature ^{207}Pb solid-state NMR study of lead titanate was conducted between −150 and 60 °C, and it was clarified that the isotropic lead chemical shift is only weakly dependent on temperature.[343] Bis(pentacarbonylmanganese)diphenyltin(IV) and bis(pentacarbonylmanganese)diphenyllead(IV) were characterized by solid-state ^{119}Sn and ^{207}Pb CP-MAS NMR.[344]

3.15 Group 15 ($^{14,15}N$, ^{31}P). – *3.15.1 Nitrogen ($^{14,15}N$) (I = 1,1/2) (Review).* A review was given for the applications utilizing ^1H–^{15}N heteronuclear shift correlation experiments at natural abundance with emphasis placed on the observed long-range coupling pathways.[345] Inverse-detected NMR methods coupled with major advances in NMR probe designs have made it possible to acquire long-range ^1H–^{15}N heteronuclear shift correlation data on samples as small as a micromole overnight. The currently available pulse sequences, pulse calibration, parametrization and processing of long-range ^1H–^{15}N data, and the implications of probe selection are discussed. Strategies are discussed for

resolving and assigning peptide backbone and side chain resonances in uniformly ^{13}C,^{15}N-labeled solid peptides.[346] For characterizing the structure of protein/drug complexes the protein differential ^{1}H, ^{13}C, and ^{15}N NMR chemical shifts for the FK506 binding protein (FKBP)–ascomycin complex was compared to free FKBP, FKBP/31-keto-32-desoxy-ascomycin, FKBP/24-desoxy-ascomycin, and FKBP/FK506.[347]

3.15.2 Phosphorus (^{31}P) ($I = 1/2$). A review with 17 references was given.[348] The site of protonation of carboxylic and non-carboxylic amides (whether the amido nitrogen or an atom in the acyl group, generally oxygen) was investigated through quantum chemical calculations and heteronuclear NMR measurements. The relative energies of the various ions deriving from protonation at each site were calculated both in the gas phase and in water, and NMR properties of the involved heteronuclei (nuclear shielding and electric field gradient) were also calculated and compared with chemical shifts and relaxation rates experimentally measured in ^{14}N, ^{17}O and ^{31}P spectra.

^{31}P chemical shifts were measured for the phosphorothioates and a regression analysis with the experimental chemical shift data and a number of data from the DFT and AIM calculations were analyzed using linear least-squares method.[349]

3.16 Group 16 (^{17}O, ^{33}S, ^{77}Se, ^{125}Te). – *3.16.1 Oxygen (^{17}O) ($I = 5/2$).* A sodium ilerite, molar ratios $1Na_2O{:}8.2SiO_2{:}10.2H_2O$, was characterized by solid state ^{2}H MAS, ^{29}Si MAS and ^{17}O NMR.[350] Both the carbonyl (C=O) and the hydroxyl (OH) ^{17}O resonances of the carboxylic group were detected for the first time for Boc-[^{17}O]Tyr(2,6-diClBzl)-OH in DMSO-d_6 by ^{17}O NMR.[351] The ^{17}O NMR spectra of poly(vinyl alcohol) gel as prepared by repeating freezing/thawing cycle were measured to elucidate the structure and dynamics of water molecules.[352] Rate coefficients for steady exchange of oxygens between sites in the $AlO_4Al_{12}(OH)_{24}(H_2O)^{127+}$(aq) ($Al_{13}$) complex and bulk solution were determined using ^{17}O-NMR.[353] Rates of steady exchange of oxygens between bulk solution and sites in the $GaO_4Al_{12}(OH)_{24}(H_2O)^{127+}$(aq) ($GaAl_{12}$) aqueous complex were determined by ^{17}O NMR.[354] Direct experimental evidence of Al–O–Al and Si–O–Si linkages in charge-balanced aluminosilicate glasses with Si/Al = 1, such as $NaAlSiO_4$ (nepheline) and $LiAlSiO_4$ (eucryptite) compositions was detected using ^{17}O 3Q-MAS NMR and quantify the extent of disorder in framework cations (Si/Al).[355] The ^{17}O NMR studies of silicate glasses gives structural information from an "anionic" viewpoint, which is an important complement to more traditional discussions of cation coordination and connectivities. A variety of techniques, such as two-dimensional, high resolution techniques of Dynamic Angle Spinning (DAS) and Triple Quantum Magic Angle Spinning (3QMAS), which have resolved and distinguished peaks for bridging oxygens linking Si, Al and B cations, as well as non-bridging oxygens, are described.[356] The orientations of the ^{17}O electric-field-gradient and chemical shift tensors of [α-^{13}C,^{17}O]benzamide were determined from analysis of ^{17}O MAS and

stationary spectra.[357] The irradiated-oxidation of pentacontane ($C_{50}H_{102}$) and polyisoprene was investigated as a function of oxidation level using ^{17}O NMR.[358] Static, MAS, ^{1}H-decoupled, ^{1}H-^{17}O CP, and 3Q-MAS ^{17}O NMR were performed on crystalline $KHSi_2O_5$ and hydrous and anhydrous $K_2Si_4O_9$ and $KAlSi_3O_8$.[359] The results of *ab initio* density functional theory calculations of the NMR chemical shift of liquid H_2O and hexagonal ice were reported.[360] The carbonyl ^{17}O electric-field-gradient (EFG) tensor and chemical shift (CS) tensor of a urea-type functional group, R_1NH-C(O)-NHR_2, were determined.[361]

3.16.2 Sulfur (^{33}S) ($I = 3/2$). The ^{33}S magnetic shielding constants of several gaseous compounds were reported. The ^{33}S magnetic shielding of an octahedral SF_6 molecule is modestly dependent on intermolecular interactions.[362]

3.16.3 Selenium (^{77}Se) ($I = 1/2$). The Chevrel-phase solid solution Mo_6Se_8–Mo_6Te_8 was studied by ^{77}Se and ^{125}Te. The NMR spectra of the binaries Mo_6Se_8 and Mo_6Te_8 reveal two significant features, attributed to two different chalcogen positions in the R^3 symmetry.[363] A set of new chalcogen-bridged mixed metal clusters $[Fe_2Os_3(\mu_4\text{-E})(\mu_3\text{-E}')(CO)_{17}]$ (EE′ = SeTe; STe; Se_2; SSe) and $[Fe_2Ru_3(\mu_4\text{-E})(\mu_3\text{-E}')(CO)_{17}]$ (EE′ = SeTe; STe; Se_2; SSe) were synthesized and characterized by ^{77}Se and ^{125}Te NMR.[364] Two new sets of products $[(CO)_6Fe_2EE'\{\mu\text{-indanone}\}]$ (E, E′ = Se; E = S, E′ = Se) and $[(CO)_6Fe_2EE'\{\mu\text{-(2-ethoxy, }\alpha\text{-naphthol)}\}]$ (E, E′ = Se; E = S, E′ = Se; E = S, E′ = Te) were isolated from the thermolysis of the cluster-bound Fischer carbene complex and were characterized by ^{1}H, ^{13}C, ^{77}Se and ^{125}Te NMR.[365] The complexes *fac*-$[M(CO)_3L_3]$ (M = Mo or W, L_3 = $MeC(CH_2SMe)_3$, $MeC(CH_2SeMe)_3$ or $MeC(CH_2TeMe)_3$) were prepared and characterized by ^{1}H, $^{13}C\{^{1}H\}$, ^{77}Se, ^{125}Te and ^{95}Mo NMR.[366] The new Mo/Se clusters $[Mo3(\mu^3\text{-Se})(\mu^2\text{-Se}_2)_3\{N(SePPh_2)_2\}_3]Br$ and $[Mo_3(\mu^3\text{-Se})(\mu^2\text{-Se}_2)_3\{Se_2P\text{-}(OCH_2CH_3)_2\}_3]Br$ were synthesized and characterized in solution by ^{31}P and ^{77}Se NMR.[367] The solution behavior of the monomeric two-coordinated complex $[Ag(diphenylselenophosphoryl)]ClO_4$ was probed by variable-concentration and/or -temperature ^{1}H, ^{13}C, ^{31}P and ^{77}Se NMR.[368] Insights into the structure and dynamics of the binary As–Se glass system were obtained from high-temperature ^{77}Se NMR studies of molten samples.[369] A series of 22 ferrocenyl alkyl selenides and tellurides were prepared and characterized by ^{77}Se and ^{125}Te NMR.[370] The electronic properties of the organic molecular complexes $(BETS)_2(X_2TCNQ)$ (X = Cl, Br) were investigated using ^{1}H, ^{13}C, and ^{77}Se NMR.[371]

3.16.4 Tellurium (^{125}Te) ($I = 1/2$). The synthesis and coordination chemistry of telluroether (including hybrid ones), anionic organotellurium and inorganic tellurium (halotellurium, telluride and polytellurides) ligands developed during the last decade are reviewed. The characterization of the metal–tellurium bond containing species by multinuclei NMR (particularly ^{125}Te NMR) and X-ray diffraction on their single crystals is discussed.[372] Alkyl hexynyl tellurides,

n-C_4H_9CCTeR, where R = CH_3, $CH(CH_3)_2$, cyclo-C_6H_{11}, $CH_2CH(CH_3)_2$, $CH_2(CH_2)_6CH_3$, $CH_2(CH_2)_{10}CH_3$, $CH_2CH_2CH(Br)CH_3$, $CH_2C_6H_5$, 4-$CH_2C_6H_4NO_2$, $CH_2CH_2C_6H_5$ and $CH_2CH_2OC_6H_5$, were prepared and characterized by ^1H, $^{13}C\{^1H\}$, ^{125}Te NMR.[373] The organotellurium(IV) compounds $[C_4H_8TeI(S_2PMe_2)]$, $[C_4H_8TeI(S_2PEt_2)]$, $[C_4H_8TeI(S_2CNC_4H_6)]$ and $[C_4H_8TeI(SOCNC_5H_{10})]$ were synthesized and characterized by ^1H, ^{13}C, ^{31}P and ^{125}Te NMR.[374] A series of 22 ferrocenyl alkyl selenides and tellurides were prepared and characterized by ^{77}Se and ^{125}Te NMR.[370]

3.17 Group 17 (^{19}F, $^{35,37}Cl$). – *3.17.1 Fluorine (^{19}F) (I = 1/2).* A review with 206 references was given on recent advances in structural and conformational analysis of fluorinated carbohydrates by NMR. Characteristic ^1H, ^{13}C, and ^{19}F NMR chemical shifts and coupling constants for selected examples are given and the spectral data of a series of fluorinated carbohydrates were collected.[375]

3.17.2 Chlorine ($^{35,37}Cl$) (I = 3/2,3/2). Colloidal palladium particles were prepared by reduction with hydrogen of H_2PdCl_4 in a mixture of H_2O, trioctylamine and cyclohexane, and the process of reduction was monitored by ^{14}N and ^{35}Cl NMR.[376]

3.18 Group 18 (^3He, ^{129}Xe). – *3.18.1 Helium (^3He) (I = 1/2).* Results are reported for high frequency pulsed NMR studies of ^3He adsorbed on hexagonal boron nitride. The commensurate coverage, corresponding to a 0.75 fraction of a monolayer was studied.[377]

3.18.2 Xenon (^{129}Xe) (I = 1/2). The existence and the average size of free volume in bisphenol-A polycarbonate, low-density polyethylene, poly(2,6-dimethyl-phenyleneoxide), and polytetrafluoroethylene were studied by positron annihilation and ^{129}Xe NMR. The ^{129}Xe NMR chemical shifts for xenon adsorbed in the polymers indicated that the average pore size of the free volume increased in the following order: PC, LDPE, PPO, and PTFE.[378] Optically enhanced NMR with ^{129}Xe and ^3He is described as a novel and promising technique for medical imaging of lungs and other tissues. Hyperpolarized ^{129}Xe NMR provides a powerful means of measuring blood oxygenation quantitatively and noninvasively. The interaction of xenon with hemoglobin is responsible for an oxygen-dependent NMR shift of ^{129}Xe in red blood cells, in sharp contrast to the current model of xenon–hemoglobin binding.[379] Purely siliceous and Al-containing MCM-41 and SBA-15 materials have been prepared. The effect of compression on the mesopore structure has been studied by ^{129}Xe NMR.[380] The utility of NMR is extended as a technique to probe porous media structure over length scales of 100–2000 μm by using ^{129}Xe imbibed into the system's pore space. Such length scales are much greater than can be probed with NMR diffusion studies of water-saturated porous media.[381]

4 References

1 E. L. Do Canto, L. Tasic, and R. Rittner, Can. *J. Anal. Sci. Spectrosc.*, 2000, **45**, 30–35.
2 N. H. Martin, N. W. Allen, and J. C. Moore, *J. Mol. Graphics Modell.*, 2000, **18**, 242–246.
3 E. Kleinpeter, L. Hilfert, and A. Koch, *J. Phys. Org. Chem.*, 2000, **13**, 473–479.
4 H. Frisell and L. Engman, *J. Mol. Struct.*, 2000, **526**, 103–114.
5 S. Ahmad, M. N. Akhtar, A. A. Isab, A. R. Al-Arfaj, and M. S. Hussain, *J. Coord. Chem.*, 2000, **51**, 225–234.
6 R. J. Abraham, and M. Reid, *Magn. Reson. Chem.*, 2000, **38**, 570–579.
7 S. Pietri, M. Miollan, S. Martel, F. Le Moigne, B. Blaive, and M. Culcasi, *J. Biol. Chem.*, 2000, **275**, 19505–19512.
8 J. Tierney, D. Sheridan, K. Kovalesky, L. M. Mascavage, K. Schneider, and C. Sheely, *Heterocycl. Commun.*, 2000, **6**, 105–111.
9 V. V. Karpyak, N. D. Obushak, V. L. Mizyuk, and N. I. Ganushchak, *Russ. J. Org. Chem.*, 2000, **36**, 83–87.
10 G. Lin, C. Y. Lai, W. C. Liao, B. H. Kuo, and C. P. Lu, *J. Chin. Chem. Soc. (Taipei)*, 2000, **47**, 489–500.
11 J. Frohlich, F. Sauter, and V. Milata, *Molecules*, 2000, **5**, 616–619.
12 J. Poznanski, K. Felczak, T. Kulikowski, and M. Remin, *Biochem. Biophys. Res. Commun.*, 2000, **272**, 64–74.
13 E. W. Della, I. J. Lochert, J. E. Peralta, and R. H. Contreras, *Magn. Reson. Chem.*, 2000, **38**, 395–402.
14 N. K. Kim, H. J. Lee, K. H. Choi, J. A. Yu, C. J. Yoon, J. Park, and Y. S. Choi, *J. Phys. Chem. A*, 2000, **104**, 5572–5578.
15 E. Burgueno-Tapia, and P. Joseph-Nathan, *Magn. Reson. Chem.*, 2000, **38**, 390–393.
16 J. Hu, E. Kolehmainen, and J. Knuutinen, *Magn. Reson. Chem.*, 2000, **38**, 375–378.
17 G. F. Pauli, *J. Nat. Prod.*, 2000, **63**, 834–838.
18 J. R. Nanney, and C. A. L. Mahaffy, *Spectrosc. Lett.*, 2000, **33**, 255–267.
19 W. S. Brey, and M. L. Brey, *J. Fluorine Chem.*, 2000, **102**, 219–233.
20 S. T. Lin, and W. C. Lin, J. *Chin. Chem. Soc. (Taipei)*, 2000, **47**, 275–278.
21 R. Mazurkiewicz, Z. Stec, J. Zawadiak, *Magn. Reson. Chem.*, 2000, **38**, 213–215.
22 S. A. Myers, R. A. Assink, D. A. Loy, and K. J. Shea, *J. Chem Soc., Perkin 2*, 2000, 545–549.
23 D. Kuang, O. J. Obaje, A. Kassim, G. C. L. Ee, and H. Suhaimi, *J. Am. Oil Chem. Soc.*, 2000, **77**, 43–47.
24 C. K. Lee, J. S. Yu, and J. S. Park, *Bull. Korean Chem. Soc.*, 2000, **21**, 49–55.
25 J. Kulhanek, O. Pytela, and A. Lycka, *Collect. Czech. Chem. Commun.*, 2000, **65**, 106–116.
26 A. V. Afonin, I. A. Ushakov, S. V. Zinchenko, O. A. Tarasova, and B. A. Trofimov, *Magn. Reson. Chem.*, 2000, **38**, 994–1000.
27 E. R. Johnston, R. Fortt, and J. C. Barborak, *Magn. Reson. Chem.*, 2000, **38**, 932–936.
28 M. Sanchez, T. Parella, E. Cervello, C. Jaime, and A. Virgili, *Magn. Reson. Chem.*, 2000, **38**, 925–931.
29 K. Mlinaric-Majerski, A. Visnjevac, G. Kragol, and B. Kojic-Prodic, *J. Mol. Struct.*, 2000, **554**, 279–287.

30 V. Vijayakumar, M. Sundaravadivelu, S. Perumal, and M. J. E. Hewlins, *Magn. Reson. Chem.*, 2000, **38**, 883–885.
31 A. Kvaran, A. E. Konradsson, C. Evans, and J. K. F. Geirsson, *J. Mol. Struct.*, 2000, **553**, 79–90.
32 I. Ivarsson, C. Sandstrom, A. Sandstrom, and L. Kenne, *J. Chem. Soc., Perkin 2*, 2000, 2147–2152.
33 J. J. Balbach, Y. Ishii, O. N. Antzutkin, R. D. Leapman, N. W. Rizzo, F. Dyda, J. Reed, and R. Tycko, *Biochemistry*, 2000, **39**, 13748–13759.
34 D. S. Ribeiro, P. R. Olivato, R. Rittner, Roberto. *Magn. Reson. Chem.*, 2000, **38**, 627–638.
35 F. Nardi, J. Kemmink, M. Sattler, and R. C. Wade, *J. Biomol. NMR*, 2000, **17(1)**, 63–77.
36 S. Witkowski, D. Maciejewska, and I. Wawer, *J. Chem. Soc., Perkin 2*, 2000, 1471–1476.
37 M. D. Bartberger, K. N. Houk, S. C. Powell, J. D. Mannion, K. Y. Lo, J. S. Stamler, and E. J. Toone, *J. Am. Chem. Soc.*, 2000, **122**, 5889–5890.
38 Y. Tanaka, C. Kojima, T. Yamazaki, T. S. Kodama, K. Yasuno, S. Miyashita, A. Ono, M. Kainosho, and Y. Kyogoku, *Biochemistry*, 2000, **39**, 7074–7080.
39 S. Ando, T. Hironaka, H. Kurosu, and I. Ando, *Magn. Reson. Chem.*, 2000, **38**, 241–250.
40 V. Rudiger, and H-J. Schneider, *Magn. Reson. Chem.*, 2000, **38**, 85–89.
41 D. M. Schneider, M. C. Caputo, M. B. Ferraro, and J. C. Facelli, *Int. J. Mol. Sci.*, 2000, **1**, 75–83.
42 M. Asadi,and M. Niad, *Int. J. Chem.*, 2000, **10**, 157–163.
43 M. A. McCoy, and D. F. Wyss, *J. Biomol. NMR*, 2000, **18**, 189–198.
44 E. R. Souaya, W. G. Hanna, E. H. Ismail, and N. E. Milad, *Molecules*, 2000, **5**, 1121–1129.
45 B. Chankvetadze, M. Fillet, N. Burjanadze, D. Bergenthal, C. Bergander, H. Luftmann, J. Crommen, and G. Blaschke, *Enantiomer*, 2000, **5**, 313–322.
46 D. Solis, and M. B. Ferraro, *Theor. Chem. Acta*, 2000, **104**, 323–326.
47 B. Bernet, and A. Vasella, *Helv. Chim. Acta*, 2000, **83**, 995–1021.
48 K. Jackowski, W. Makulski, and Z. Trenkner-Olejniczak, *Bull. Pol. Acad. Sci., Chem.*, 2000, **48**, 81–89.
49 C. Ochsenfeld, *Phys. Chem. Chem. Phys.*, 2000, **2**, 2153–2159.
50 M. Kanakubo, T. Aizawa, T. Kawakami, O. Sato, Y. Ikushima, K. Hatakeda, and N. Saito, *J. Phys. Chem. B*, 2000, **104**, 2749–2758.
51 Y. Kwon, *THEOCHEM*, 2000, **532**, 227–237.
52 S. Dong, R. Ida, and G. Wu, *J. Phys. Chem. A*, 2000, **104**, 11194–11202.
53 I. Ivarsson, C. Sandstrom, A. Sandstrom, and L. Kenne, *J. Chem. Soc., Perkin 2*, 2000, 2147–2152.
54 P. Gilli, V. Bertolasi, V. Ferretti, and G. Gilli, *J. Am. Chem. Soc.*, 2000, **122**, 10405–10417.
55 T. K. Harris, Q. Zhao, and A. S. Mildvan, *J. Mol. Struct.*, 2000, **552** 97–109.
56 W. Schilf, B. Kamienski, T. Dziembowska, Z. Rozwadowski, and A. Szady-Chelmieniecka, *J. Mol. Struct.*, 2000, **552** 33–37.
57 A. P. Bisson, F. J. Carver, D. S. Eggleston, R. C. Haltiwanger, C. A. Hunter, D. L. Livingstone, J. F. McCabe, C. Rotger, and A. E. Rowan, *J. Am. Chem. Soc.*, 2000, **122**, 8856–8868.
58 K. Yamauchi, S. Kuroki, K. Fujii, and I. Ando, *Chem. Phys. Lett.*, 2000, **324**, 435–439.

59 A. Brueck, L. L. McCoy, and K. V. Kilway, *Org. Lett.*, 2000, 2007–2009.
60 S. Scheiner, Y. Gu, and T. Kar, *THEOCHEM*, 2000, **500**, 441–452.
61 H. Suezawa, T. Hashimoto, K. Tsuchinaga, T. Yoshida, T. Yuzuri, K. Sakakibara, M. Hirota, and M. Nishio, *J. Chem. Soc., Perkin 2*, 2000, 1243–1249.
62 J. C. Facelli, *Chem. Phys. Lett.*, 2000, **322**, 91–96.
63 J. E. Del Bene, and M. J. T. Jordan, *J. Am. Chem. Soc.*, 2000, **122**, 4794–4797.
64 G. Wu, K. Yamada, S. Dong, and H. Grondey, *J. Am. Chem. Soc.*, 2000, **122**, 4215–4216.
65 A. Szady-Chelmieniecka, Z. Rozwadowski, T. Dziembowska, E. Grech, G. Wojciechowski, and B. Brzezinski, *J. Mol. Struct.*, 2000, **520**, 39–43.
66 R. M. Aminova, G. A. Schamov, and A. V. Aganov, *THEOCHEM*, 2000, **498**, 233–246.
67 C. Palanivel, K. Suganya, C. Ramalingan, and S. Kabilan, *Orient. J. Chem.*, 2000, **16**, 441–446.
68 M. Wilczek, W. Makulski, and K. Jackowski, *Mol. Phys. Rep.*, 2000, **29**, 180–182.
69 S-T. Lin, C-C. Lee, and D. W. Liang, *Tetrahedron*, 2000, **56**, 9619–9623.
70 E. Bednarek, J. C. Dobrowolski, K. Dobrosz-Teperek, L. Kozerski, W. Lewandowski, and A. P. Mazurek, *J. Mol. Struct.*, 2000, **554**, 233–243.
71 M. N. Manalo, A. C. de Dios, and R. Cammi, *J. Phys. Chem. A*, 2000, **104**, 9600–9604.
72 M. Witanowski, Z. Biedrzycka, and Z. Grabowski, *Magn. Reson. Chem.*, 2000, **38**, 580–586.
73 T. D. Ferris, M. D. Zeidler, and T. C. Farrar, *Mol. Phys.*, 2000, **98**, 737–744.
74 L. Gontrani, B. Mennucci, and J. Tomasi, *THEOCHEM*, 2000, **500**, 113–127.
75 K. Jackowski, W. Makulski, and Z. Trenkner-Olejniczak, *Bull. Pol. Acad. Sci., Chem.*, 2000, **48**, 81–89.
76 D. Farcasiu, M. Lezcano, and A. Vinslava, *New J. Chem.*, 2000, **24**, 199–201.
77 M. Jaszunski, K. V. Mikkelsen, A. Rizzo, and M. Witanowski, *J. Phys. Chem. A*, 2000, **104**, 1466–1473.
78 P. Schah-Mohammedi, I. G. Shenderovich, C. Detering, H-H. Limbach, P. M. Tolstoy, S. N. Smirnov, G. S. Denisov, and N. S. Golubev, *J. Am. Chem. Soc.*, 2000, **122**, 12878–12879.
79 V. Machacek, A. Lycka, and J. Kavalek, *Magn. Reson. Chem.*, 2000, **38**, 1001–1004.
80 C. L. Perrin, and Y-J. Kim, *J. Phys. Org. Chem.*, 2000, **13**, 752–756.
81 C. H. Gee, and W. T. Raynes, *Chem. Phys. Lett.*, 2000, **330**, 595–602.
82 K. Ibrom, G. Kohn, K-U. Boeckmann, R. Kraft, S. P. Holba-Schulz, and L. Ernst, *Org. Lett.*, 2000, **2**, 4111–4113.
83 M. Z. Chalaca, and J. D. Figueroa-Villar, *J. Mol. Struct.*, 2000, **554**, 225–231.
84 A. Foris, *Magn. Reson. Chem.*, 2000, **38**, 813–819.
85 B. Andresen, F. Duus, S. Bolvig, P. E. Hansen, *J. Mol. Struct.*, 2000, **552**, 45–62.
86 S. Bolvig, P. E. Poul, H. Morimoto, D. Wemmer, and P. Williams, *Magn. Reson. Chem.*, 2000, **38**, 525–535.
87 B. Wrackmeyer, G. Seidel, and R. Koster, *Magn. Reson. Chem.*, 2000, **38**, 520–524.
88 R. E. Hoffman, N. Treitel, E. Shabtai, R. Benshafrut, and M. Rabinovitz, *J. Chem. Soc., Perkin 2*, 2000, 1007–1011.
89 E. Wielogorska, and K. Jackowski, *Pol. J. Chem.*, 2000, **74**, 567–572.
90 S. Bolvig, and P. E. Hansen, *Curr. Org. Chem.*, 2000, **4**, 19–54.

91 B. Wrackmeyer, E. Garcia-Baez, F. J. Zuno-Cruz, G. Sanchez-Cabrera, and M. J. Rosales, *Z. Naturforsch., Chem. Sci.*, 2000, **55**, 185–188.
92 H. J. Reich, and J. L. Thompson, *Org. Lett.*, 2000, **2**, 783–786.
93 P. E. Hansen, *Magn. Reson. Chem.*, 2000, **38**, 1–10.
94 M. Michalik, M. Hein, and M. Frank, *Carbohydr. Res.*, 2000, **237**, 185–218.
95 M. Nath, S. Pokharia, and R. Yadav, *Coord. Chem. Rev.*, 2001, **215**, 99–149.
96 J. Gorte and D. White, *Micropor. Mesopor. Mater.*, 2000, **35–36**, 447–455.
97 G. E. Martin and C. E. Hadden, *J. Nat. Prod.*, 2000, **63**, 543–585.
98 L. M. Dickinson, R. K. Harris, J. A. Shaw, M. Chinn, and P. R. Norman, *Magn. Reson. Chem.*, 2000, **38**, 918–924.
99 R. A. Komoroski, *Magn. Reson. Imaging*, 2000, **18**, 103–116.
100 A. Johansson, A. Pettersson, and Ö. Davidsson, *J. Organomet. Chem.*, 2000, **608**, 153–163.
101 R. Nagel, Ch. Wickel, J. Senker, and H. D. Lutz, *Solid State Ionics*, 2000, **130**, 169–173.
102 R. Stoyanova, E. Zhecheva, E. Kuzmanova, R. Alcantara, P. Lavela and J. L. Tirado, *Solid State Ionics*, 2000, **128**, 1–10.
103 R. J. Accardi and R. F. Lobo, *Micropor. Mesopor. Mater.*, 2000, **40**, 25–34.
104 K. Nakamura, H. Ohno, K. Okamura, Y. Michihiro, I. Nakabayashi, and T. Kanashiro, *Solid State Ionics*, 2000, **135**, 143–147.
105 M. C. Wintersgill, J. J. Fontanella, P. E. Stallworth, S. A. Newman, S. H. Chung, and S. G. Greenbaum, *Solid State Ionics*, 2000, **135**, 155–161.
106 D. Golodnitsky, E. Livshits, Yu. Rosenberg, E. Peled, S. H. Chung, Y. Wang, S. Bajue, and S. G. Greenbaum, *J. Electroanal. Chem.*, 2000, **491**, 203–210.
107 P. P. Chu, D. L. Huang, and G. T. K. Fey *J. Power Sources*, 2000, **90**, 95–102.
108 H-L. Wang, H-M. Kao, and T-C. Wen, *Macromolecules*, 2000, **33**, 6910 6912.
109 M. Shamsipur and T. Madrakian, *Polyhedron*, 2000, **19**, 1681–1685.
110 S. Levasseur, M. Menetrier, E. Suard, and C. Delmas, *Solid State Ionics*, 2000, **128**, 11–24.
111 T. Akai, *J. Non-Crystalline Solids*, 2000, **262**, 271–275.
112 K. Guerin, M. Menetrier, A. Fevrier-Bouvier, S. Flandrois, B. Simon, and P. Biensan, *Solid State Ionics*, 2000, **127**, 187–198.
113 N. C. Mello, T. J. Bonagamba, H. Panepucci, K. Dahmouche, P. Judeinstein, and M. A. Aegerter, *Macromolecules*, 2000, **33**, 1280–1288.
114 A. Goto, R. Miyabe, T. Shimizu, H. Kitazawa, K. Hashi, H. Abe, G. Kido, K. Shimamura, and T. Fukuda, *Physica B: Condensed Matt.*, 2001, **298**, 585–589.
115 A. R. Lim and S. Y. Jeong, *J. Phys. Chem. Solids*, 2001, **62**, 881–885.
116 K. Hayamizu, Y. Aihara, and W. S. Price, *Electrochim. Acta*, 2001, **46**, 1475–1485.
117 A. C. Bloise, C. C. Tambelli, R. W. A. Franco, J. P. Donoso, C. J. Magon, M. F. Souza, A. V. Rosario, and E. C. Pereira, *Electrochim. Acta*, 2001, **46**, 1571–1579.
118 E. Tambelli, J. P. Donoso, A. M. Regiani, A. Pawlicka, A. Gandini, and J. -F. LeNest, *Electrochim. Acta*, 2001, **46**, 1665–1672.
119 Y. Wang, V. Yufit, X. Guo, E. Peled and S. Greenbaum, *J. Power Sources*, 2001, **94**, 230–237.
120 R. Pankiewicz, G. Schroeder, B. Gierczyk, G. Wojciechowski, B. Brzezinski, F. Bartl, G. Zundel, *Biopolym. -Biospectr. Sect.*, 2001, **62**, 173–182.
121 O. H. Han, J. K. Jung, M-Y. Yi, J. H. Kwak, and Y. J. Shin, *Solid State Commun.*, 2000, **117**, 65–68.

122 Y. Onoda, S. H. Chung, A. Watanabe, and T. Mitsuhashi, *Solid State Ionics,* 2000, **136-137**, 365–370.
123 M. Janssen and H. Eckert, *Solid State Ionics,* 2000, **136-137**, 1007–1014.
124 F. Angeli, J-M. Delaye, T. Charpentier, J-C. Petit, D. Ghaleb, and P. Faucon, *J. Non-Cryst. Solids,* 2000, **276**, 132–144.
125 J-C. Buhl, F. Stief, M. Fechtelkord, T. M. Gesing, U. Taphorn and C. Taake, *J. Alloys Compd.,* 2000, **305**, 93–102.
126 S. Ding and C. A. McDowell, *Chem. Phys. Lett.,* 2000, **320**, 316–322.
127 R. Martens and W. M. Warmuth, *J. Non-Cryst. Solids,* 2000, **265**, 167–175.
128 S. Prabakar, R. M. Wenslow, and K. T. Mueller, *J. Non-Cryst. Solids,* 2000, **263-264**, 82–93.
129 Q. Zengl, H. Nekvasil, and C. P. Grey, *Geochim. Cosmochim. Acta,* 2000, **64**, 883–896.
130 A. Belkebir, J. Rocha, A. P. Esculcas, P. Berthet, S. Poisson, B. Gilbert, Z. Gabelica, G. Llabres, F. Wijzen, and A. Rulmont, *Spectrochim. Acta Part A: Mol. Biomol. Spectr.,* 2000, **56**, 423–434.
131 G. Schroeder, B. Gierczyk, B. Brzezinski, B. Rozalski, F. Bartl, G. Zundel, J. Sonicki, and E. Grech, *J. Mol. Struct.,* 2000, **516**, 91–98.
132 P. Cahen, M. Luhmer, C. Fontaine, C. Morat, J. Reisse, and K. Bartik, *Biophys. J.,* 2000, **78**, 1059–1069.
133 S. Ding and C. A. McDowell, *Chem. Phys. Lett.,* 2001, **333**, 413–418.
134 M. Fechtelkord, S. Stief, J.-C. Buhl, *Am. Mineral.,* 2001, **86**, 165–175.
135 M. Nyman, B. X. Gu, L. M. Wang, R. C. Ewing, and T. M. Nenoff, *Micropor. Mesopor. Mater.,* 2000, **40**, 115–125.
136 M. Chiba, S. Ueda, T. Yanagimoto, M. Toda, and T. Goto, *Physica B: Conden. Matt.,* 2000, **284-288**, 1529–1530.
137 S. H. Park, P. Daniels, and H. Gies, *Micropor. Mesopor. Mater.,* 2000, **37**, 129–143.
138 H. Iijima, T. Kato, and O. Soderman, *Langmuir,* 2000, **16**, 318–323.
139 F. Cecconi, C. A. Ghilardi, S. Midollini, and A. Orlandini, *Inorg. Chem. Commun.,* 2000, **3**, 350–353.
140 L. Ciavatta, M. Iuliano, R. Porto, P. Innocenti, and A. Vacca, *Polyhedron,* 2000, **19**, 1043 -1048.
141 K. J. D. MacKenzie, C. M. Sheppard, and C. McCammon, *J. Eur. Ceram. Soc.,* 2000, **20**, 1975–1985.
142 S. Kroeker and J. F. Stebbins, *Am. Mineral.,* 2000, **85**, 1459–1464.
143 H. Sakamoto, H. Tou, H. Ishii, Y. Maniwa, E. A. Reny, and S. Yamanaka, *Physica C: Supercond.,* 2000, **341–348**, 2135–2136.
144 K. J. D. MacKenzie, T. Kemmitt, R. H. Meinhold, M. Schmücker, and L. Mayer, *J. Eur. Ceram. Soc.,* 2000, **20**, 645–650.
145 K. J. D. MacKenzie and R. H. Meinhold, *Ceram. Int.,* 2000, **26**, 87–92.
146 K. Ueda, T. Kohara, D. A. Gajewski, and M. B. Maple, *Physica B: Condensed Matt.,* 2000, **281–282**, 400–401.
147 A. L. Hector, W. Levason, and M. Webster, *Inorg. Chim. Acta,* 2000, **298**, 43–49.
148 T. Fukamachi, Y. Kobayashi, T. Miyashita, and M. Sato, *J. Phys. Chem. Solids,* 2001, **62**, 195–198.
149 D. Padro, A. P. Howes, M. E. Smith, and R. Dupree, *Solid State Nucl. Magn. Reson.,* 2000, **15**, 231–236.
150 L. L. G. Justino, M. L. Ramos, M. M. Caldeira, and V. M. S. Gil, *Inorg. Chim. Acta,* 2000, **311**, 119–125.

151 Q. Wu and G. Meng, *Solid State Ionics*, 2000, **136–137**, 273–277.
152 B. Alonso, J. Maquet, and C. Sanchez, *J. Non-Cryst. Solids*, 2000, **277**, 58–62.
153 M. Itoh, N. Akimoto, H. Yamada, M. Isobe, and Y. Ueda, *Physica C:*, 2000, **341–348**, 2133–2134.
154 L. I. Kuznetsova, N. I. Kuznetsova, L. G. Detusheva, M. A. Fedotov, and V. A. Likholobov, *J. Mol. Catal. A*, 2000, **158**, 429–433.
155 T. Blasco, L. Fernandez, A. M. Arias, M. S. Sanchez, P. Conception, and J. M. L. Nieto, *Micropor. Mesopor. Mater.*, 2000, **39**, 219–228.
156 L. A. Boyarsky, S. P. Gabuda, and S. G. Kozlova, *Physica. B: Condensed Matt.*, 2000, **284–288**, 1454–1455.
157 M. Itoh, N. Akimoto, M. Tsuchiya, H. Yamada, M. Isobe, and Y. Ueda, *Physica. B: Condensed Matt.*, 2000, **281–282**, 606–607.
158 T. Ohama, M. Isobe and Y. Ueda, *Physica. B: Condensed Matt.*, 2000, **281–282**, 650–651.
159 I. Andersson, S. Angus-Dunne, O. Howarth, and L. Pettersson, *J. Inorg. Biochem.*, 2000, **80**, 51–58.
160 H. Schmidt, I. Andersson, D. Rehder, and L. Pettersson, *J. Inorg. Biochem.*, 2000, **80**, 149–151.
161 K. Nomiya, S. Matsuoka, T. Hasegawa, and Y. Nemoto, *J. Mol. Catal. A*, 2000, **156**, 143–152.
162 M. Hassan Zahedi-Niaki, S. M. Javaid Zaidi, and S. Kaliaguine, *Appl. Catal. A*, 2000, **196**, 9–24.
163 A. A. Shubin, O. B. Lapina, and D. Courcot, *Catal. Today*, 2000, **56**, 379–387.
164 J. L. Lakshmi, T. R. B. Jones, M. Gurgi, and J. M. Miller, *J. Mol. Catal. A*, 2000, **152**, 99–110.
165 J. M. Miller and L. J. Lakshmi, *Appl. Catal. A*, 2000, **190**, 197–206.
166 Q. Wu and G. Meng, *Mater. Res. Bull.*, 2000, **35**, 85–91.
167 S. I. Wolke, R. Buffon, and U. P. R. Filho, *J. Organomet. Chem.*, 2001, **625**, 101–107.
168 K. Oyaizu, E. L. Dewi, and E. Tsuchida, *J. Electroanal. Chem.*, 2001, **498**, 136–141.
169 R. S. G. Ferreira, P. G. P. de Oliveira, and F. B. Noronha, *Appl. Catal. B: Environ.*, 2001, **29**, 275–283.
170 H. Kim, S. I. Woo, J. Noh and O-B. Yang, *Appl. Catal. A: General*, 2001, **207**, 69–77.
171 J. L. Lakshmi, N. J. Ihasz, and J. M. Miller, *J. Mol. Catal., A: Chem.*, 2001, **165**, 199–209.
172 J. J. Fitzgerald, S. Prasad, J. Huang, and J. S. Shore, *J. Am. Chem. Soc.*, 2000, **122**, 2556–2566.
173 F. E. Kuhn, A. M. Santos, A. D. Lopez, I. S. Gonsalvez, E. Herdtweck, and C. C. Romao, *Mol. Catal. A*, 2000, **164**, 25–38.
174 M. Luisa Ramos, M. Madalena Caldeira, and V. M. S. Gil, *Carbohydr. Res.*, 2000, **329**, 387–397.
175 A. J. Barton, J. Connolly, W. Levason, A. M. Jalon, S. D. Orchard, and G. Reid, *Polyhedron*, 2000, **19**, 1373–1379.
176 F. E. Kuhn, A. D. Lopez, A. M. Santos, E. Herdtweck J. J. Haider C. C. Romao, and A. G. Santos, *J. Mol. Catal. A*, 2000, **151**, 147–160.
177 C. Hamard, O. Pena, and M. Le Floch, *Solid State Commun.*, 2000, **113**, 489–494.
178 I. S. Gonsalves, A. M. Santos, C. C. Romao, A. D. Lopes, J. E. Rodriguez-

Borges, M. Pillinger, P. Ferreira, J. Rocha, and F. E. Kuhn, *J. Organomet. Chem.*, 2001, **626**, 1–10.
179 F. E. Kuhn, A. M. Santos, A. D. Lopes, I. S. Gonsalves, J. E. Rodriguez-Borges, M. Pillinger, and C. C. Romao, *J. Organomet. Chem.*, 2001, **621**, 207–217.
180 A. Ostuni and M. T. Pope, *Comp. Rend. Ser.* IIC, 2000, **3**, 199–204.
181 Z. G. Sun, Q. Liu, and J. F. Liu, *Inorg. Chem. Commun.*, 2000, **3**, 328–330.
182 K. Nomiya, Y. Arai, Y. Shimizu, M. Takahashi, T. Takayama, H. Weiner, T. Nagata, J. A. Widegren, and R. G. Finke, *Inorg. Chim. Acta*, 2000, **300–302**, 285–304.
183 R. Contant, S. Piro-Sellem, J. Canny, and R. Thouvenot, *Comp. Rend. Acad. Sci., Ser. IIC, Chem.*, 2000, **3**, 157–161.
184 Z-G. Sun, Q. Liu and J-F. Liu, *Polyhedron*, 2000, **19**, 125–128.
185 X. Wang, J. Liu, J. Li, and J. Liu, *Inorg. Chem. Commun.*, 2001, **4**, 372–374.
186 L. Meng, X. P. Zhan, M. Wang, and J-F. Liu, *Polyhedron*, 2001, **20**, 881–885.
187 S. Himeno, M. Yoshihara, and M. Maekawa, *Inorg. Chem. Commun.*, 2001, **4**, 5–8.
188 V. P. Pashchenko, A. A. Shemyakov, V. K. Prokopenko, V. N. Derkachenko, O. P. Cherenkov, V. I. Mihajlov, V. N. Varyukhin, V. P. Dyakonov, and H. Szymczak, *J. Magn. Magn. Mater.*, 2000, **220**, 52–58.
189 B. S. Dumesh, V. A. Panfilov, A. M. Tikhonov and D. N. Fourzikov, *Phys. B, Condensed Matt.*, 2000, **284–288**, 1623–1624.
190 P. DeShong, E. D. Soli, G. A. Slough, D. R. Sidler, V. Elango, P. J. Rybczynski, L. J. S. Vosejpka, T. A. Lessen, T. X. Le, G. B. Anderson, W. Philipsborn, M. Völher, D. Rentsch, and O. Zerbe, *J. Organomet. Chem.*, 2000, **593–594**, 49–62.
191 C. G. Kalodimos, I. P. Gerothanassis, R. Pierattelli, and A. Troganis, *J. Inorg. Biochem.*, 2000, **79**, 371–380.
192 B. Wrackmeyer, A. Ayazi, H. E. Maisel, and M. Herberhold, *J. Organomet. Chem.*, 2001, **630**, 263–265.
193 M. Buhl, S. Gaemers, and C. J. Elsevier, *Eur. J. Chem.*, 2000, **6**, 3272–3280.
194 E. H. C. P. Sinnecker, I. S. Oliveira, P. Tiberto, and A. P. Guimaraes, *J. Magn. Magn. Mater.*, 2000, **218**, 132–136.
195 M. S. Reis, I. S. Oliveira, F. Garcia, A. Y. Takeuchi, and A. P. Guimaraes, *J. Magn. Magn. Mater.*, 2000, **217**, 49–54.
196 H. Sugita, S. Wada, K. Miyatani, T. Tanaka and M. Ishikawa, *Physica B: Condensed Matt.*, 2000, **284–288**, 473–474.
197 C. Sizun, P. Kempgens, J. Raya, K. Elbayed, P. Granger, and J. Rose, *J. Organomet. Chem.*, 2000, **604**, 27–33.
198 M. Itoh and M. Nagawatari, *Physica B: Condensed Matt.*, 2000, **281–282**, 516–517.
199 T. Suzuki, S. Kaizaki, and K. Kashiwabara, *Inorg. Chim. Acta*, 2000, **298**, 131–140.
200 M. Buehl, M. Hkansson, A. H. Mahmoudkhani, and L. Oehrstroem, *Organometallics*, 2000, **19**, 5589–5596.
201 F. Asaro, M. Lenarda, G. Pellizer, and L. Storaro, *Spectrochim. Acta Part A: Mol. Biomol. Spectr.*, 2000, **56**, 2167–2175.
202 D. Horton and O. Varela, *Carbohydr. Res.*, 2000, **328**, 425–429.
203 F. D. Rochon and L. M. Gruia, *Inorg. Chim. Acta*, 2000, **306**, 193–204.
204 Y. Kohori and T. Kohara, *Physica B: Condensed Matt.*, 2000, **284–288**, 1283–1284.
205 H. Junicke, Y. Arendt, and D. Steinborn, *Inorg. Chim. Acta*, 2000, **304**, 224–229.

206 C. Sacht and M. S. Datt, *Polyhedron*, 2000, **19**, 1347–1354.
207 R. Ros, A. Tassan, G. Laurenczy, and R. Roulet, *Inorg. Chim. Acta*, 2000, **303**, 94–99.
208 W. Oberhauser, T. Stampfl, C. Bachmann, R. Haid, C. Langes, H. Kopacka, K. H. Ongania, and P. Bruggeller, *Polyhedron*, 2000, **19**, 913–923.
209 G. Uccello-Barretta, R. Bernardini, R. Lazzaroni, and P. Salvadori, *J. Organomet. Chem.*, 2000, **598**, 174–178.
210 T. Oswald, M. Keller, C. Janiak, M. Kolm, and H. Prinzbach, *Tetrahedron Lett.*, 2000, **41**, 1631–1635.
211 S. R. Ali Khan, S. Huang, S. Shamsuddin, S. Inutsuka, K. H. Whitmire, Z. H. Siddik, and A. R. Khokhar, *Bioorg. Med. Chem.*, 2000, **8**, 515–521.
212 S. U. Dunham and E. H. Abbott, *Inorg. Chim. Acta*, 2000, **297**, 72–78.
213 H. Baek, Y. Cho, O. K. Chong, Y. S. Sohn, *Anti-Cancer Drugs*, 2000, **11**, 715–725.
214 N. Nedelec and F. D. Rochon, *Inorg. Chim. Acta*, 2001, **319**, 95–108.
215 V. F. Plyusnin, E. M. Glebov, V. P. Grivin, Y. V. Ivanov, A. B. Venediktov and H. Lemmetyinen, *J. Photochem. Photobiol. A: Chem.*, 2001, **141**, 159–167.
216 H.-J. Drexler, I. Starke, M. Grotjahn, E. Kleinpeter, and H. -J. Holdt, *Inorg. Chim. Acta*, 2001, **317**, 133–142.
217 M. I. Garcia-Seijo, A. Castineiras, B. Mahieu, L. Janosi, Z. Berente, L. Kollar, and M. E. Garcia-Fernandez, *Polyhedron*, 2001, **20**, 855–868
218 S. Dey, V. K. Jain, and B. Varghese, *J. Organomet. Chem.*, 2001, **623**, 48–55.
219 C. Audo, J. F. Lambert, M. Che, and B. Didillon, *Catal. Today*, 2001, **65**, 157–162.
220 B. B. Eran, D. Singer, J. Pickardt, and K. Praefcke, *J. Organomet. Chem.*, 2001, **620**, 249–255.
221 A. A. Gippius, E. V. Antipov, O. Klein, and K. Lüders, *Physica B: Condensed Matt.*, 2000, **284–288**, 935–936.
222 J. Kimura, T. Ida, M. Mizuno, K. Endo, M. Suhara, and K. Kihara, *J. Mol. Struct.*, 2000, **522**, 61–69.
223 P. E. Stallworth, J-F. Guillemoles, J. Flowers, J. Vedel, and S. G. Greenbaum, *Solid State Commun.*, 2000, **113**, 527–532.
224 P. E. Stallworth, J-B. d'Espinose de la Caillerie, J. Maquet, F. Babonneau, J-F. Guillemoles, M. Powalla, V. Lyakovitskaya, M. Yakushev and B. Tomlinson, *Thin Solid Films*, 2001, **387**, 235–238.
225 M. Tansho, C. A. Fyfe, H. Grondey, T. Markus, and H. Wada, *Solid State Ionics*, 2000, **132**, 87–92.
226 K. Nomiya, R. Noguchi, and M. Oda, *Inorg. Chim. Acta*, 2000, **298**, 24–32.
227 F. H. Larsen, J. Skibsted, H. J. Jakobsen, and N. C. Nielsen, *J. Am. Chem. Soc.*, 2000, **122**, 7080–7086.
228 S. Sakida, M. Shojiya, and Y. Kawamoto, *Solid State Commun.*, 2000, **115**, 553–558.
229 A. J. Matysik, G. Nachtegaal, H. J. Van Gorkom, A. J. Hoff, and H. J. M. De Groot, *Biochemistry*, 2000, **39**, 6751–6755.
230 H. Xia and G. D. Rayson *Adv. Environ. Res.*, 2000, **4**, 67–74.
231 K. Hiraoka, K. Murakami, S. Tomiyoshi, T. Hihara, T. Shinohara, and K. Kojima, *Physica B: Condensed Matt.*, 2000, **281–282**, 173–174.
232 D. J. Sullivan, J. S. Shore, and J. A. Rice, *Am. Mineral.*, 2000, **85**, 1022–1029.
233 S. Sakida, M. Shojiya, and Y. Kawamoto, *J. Non-Crystal. Solids*, 2001, **284**, 22–26.

234 J. S. Casas, E. E. Castellano, A. Macias, N. Playa, A. Sanchez, J. Sordo, J. M. Verela, and E. M. Vezquez-Lopez, *Polyhedron,* 2001, **20**, 1845–1850.
235 W. Oberhauser, T. Stampfl, R. Haid, C. Langes, C. Bachmann, H. Kopacka, K-H. Ongania, and P. Brrugeller, *Polyhedron,* 2001, **20**, 727–740.
236 X. Almagro, W. Clegg, L. Cucurull-Sanchez, P. Gonzalez-Duarte, and M. Traveria, *J. Organomet. Chem.*, 2001, **623**, 137–148.
237 J. M. Oliva and C. Vinas, *J. Mol. Struct.*, 2000, **556**, 33–42.
238 A. N. Gashti, J. C. Huffman, A. Edwards, G. Szekeley, A. R. Siedle, J. A. Karty, J. P. Reilly, and L. J. Todd, *J. Organomet. Chem.*, 2000, **614–615**, 120–124.
239 R. M. Garrioch, G. M. Rosair, and A. J. Welch, *J. Organomet. Chem.*, 2000, **614–615**, 153–157.
240 J. Knizek and H. Nösh, *J. Organomet. Chem.*, 2000, **614–615**, 168–187.
241 H. Fang, J. Bould, J. Braddock-Wilking, and L. Barton, *J. Organomet. Chem.*, 2000, **614–615**, 223–230.
242 T. Takaishi, J. Jin, T. Uchino, T. Yoko, *J. Am. Ceram. Soc.*, 2000, **83**, 2543–2548.
243 W-F. Du, K. Kuraoka, T. Akai, and T. Yazawa, *J. Mater. Sci.*, 2000, **35**, 4865–4871.
244 K. Naka, T. Umeyama, and Y. Chujo, *Macromolecules,* 2000, **33**, 7467–7470.
245 W-F. Du, K. Kuraoka, T. Akai, and T. Yazawa, *J. Mater. Sci.*, 2000, **35**, 3913–3921.
246 H. Yamashita, H. Yoshino, K. Nagata, H. Inoue, T. Nakajin, and T. Maekawa, *J. Non-Cryst. Solids,* 2000, **270**, 48–59.
247 J. K. Jung, S. K. Song, T. H. Noh, and O. H. Han, *J. Non-Cryst. Solids,* 2000, **270**, 97–102.
248 J. Cho, S. W. Martin, B. Meyer, K. H. Kim, and D. R. Torgeson, *J. Non-Cryst. Solids,* 2000, **270**, 205–214.
249 B. Boizot, G. Petite, D. Ghaleb, N. Pellerin, F. Fayon, B. Reynard, and G. Calas, *Nucl. Instrum. Methods Phys. Res. Sect. B,* 2000, **166–167**, 500–504.
250 R. Martens and W. Müller-Warmuth, *J. Non-Cryst. Solids,* 2000, **265**, 167–175.
251 F. Zhang, X. Guo, X. Wang, G. Li, Q. Zhao, X. Bao, X. Han, and L. Lin, *Appl. Catal. A,* 2000, **192**, 157–163.
252 J. S. Hartman and J. A. W. Shoemaker, *Polyhedron,* 2000, **19**, 165–176.
253 B. Gierczyk, G. Schroeder, G. Wojciechowski, B. Leska, V. I. Rybachenko, and B. Brzezinski, *J. Mol. Struct.*, 2000, **516**, 153–156.
254 T. Shirasaki, A. Derre, M. Menetrier, A. Tressaud, and S. Flandrois, *Carbon,* 2000, **38**, 1461–1467.
255 C. Shao, Y. Miyazaki, S. Matsuoka, K. Yoshimura, and H. Sakashita, *Macromolecules,* 2000, **33**, 19–25.
256 R. Millini, L. C. Carluccio, A. Carati, and W. O. Parker, Jr., *Micropor. Mesopor. Mater.*, 2001, **46**, 191–201.
257 S. Kiyooka, R. Fujiyama, T. Kawai, H. Fujimoto, and K. Goh, *Tetrahedron Lett.*, 2001, **42**, 4151–4153.
258 R. Frankel, U. Kernbach, M. Bakola-Christianopoulou, U. Plaia, M. Suter, W. Ponikwar, H. Nöth, C. Moinet, and W. P. Fehlhammer, *J. Organomet. Chem.*, 2001, **617–618**, 530–545.
259 H. Mori, H. Kono, M. Terano, A. Nosov, and V. A. Zakharov, *J. Mol. Catal. A: Chem.*, 2000, **164**, 235–243.
260 S. Sakida, M. Shojiya, and Y. Kawamoto, *J. Fluor. Chem.*, 2000, **106**, 127–131.
261 A. S. Best, M. Forsyth, and D. R. MacFarlane, *Solid State Ionics,* 2000, **136–137**, 339–344.

262 A. Gola, B. Rebours, E. Milazzo, J. Lynch, E. Benazzi, S. Lacombe, L. Delevoye, and C. Fernandez, *Micropor. Mesopor. Mater.*, 2000, **40**, 73–83.
263 I. Heinmaa, S. Vija, and E. Lippmaa, *Chem. Phys. Lett.*, 2000, **327**, 131–136.
264 A. G. Potapov, V. V. Terskikh, G. D. Bukatov, and V. A. Zakharov, *J. Mol. Catal. A: Chem.*, 2000, **158**, 457–460.
265 M. L. Occelli, A. Auroux, and G. J. Ray, *Micropor. Mesopor. Mater.*, 2000, **39**, 43–56.
266 C. J. H. Jacobsen, C. Madsen, T. V. W. Janssens, H. J. Jakobsen, and J. Skibsted, *Micropor. Mesopor. Mater.*, 2000, **39**, 393–401.
267 J. A. Chudek, G. Hunter, M. R. Jones, S. N. Scrimgeour, P. C. Hewlett, and A. B. Kudryavtsev, *J. Mater. Sci.*, 2000, **35**, 4275–4288.
268 M. A. Aramendia, V. Borau, C. Jimenez, J. M. Marinas, J. R. Ruiz, and F. J. Urbano, *Solid State Nucl. Magn. Reson.*, 2000, **16**, 217–224.
269 D. H. Kim, S. I. Woo, and O. B. Yang, *Appl. Catal. B: Environ.*, 2000, **26**, 285–289.
270 T. Yano, T. Nagano, J. Lee, S. Shibata, and M. Yamane, *J. Non-Cryst. Solids*, 2000, **270**, 163–171.
271 L. Fischer, V. Harie, S. Kasztelan, and J. B. d'Espinose de la Caillerie, *Solid State Nucl. Magn. Reson.*, 2000, **16**, 85–91.
272 W. P. Gates, P. Komadel, J. Madejova, J. Bujdak, J. W. Stucki, and R. J. Kirkpatrick, *Appl. Clay Sci.*, 2000, **16**, 257–271.
273 F. Angeli, J-M. Delaye, T. Charpentier, J-C. Petit, D. Ghaleb, and P. Faucon, *Chem. Phys. Lett.*, 2000, **320**, 681–687.
274 I. G. Kim, T. H. Yeom, S. H. Choh, K. S. Hong, Y. M. Yu, and E. S. Choi, *Solid State Commun.*, 2000, **114**, 311–314.
275 G. H. Kuehl, and H. K. C. Timken, *Micropor. Mesopor. Mater.*, 2000, **35–36**, 521–532.
276 M. H. Zahedi-Niaki, S. M. J. Zaidi, and S. Kaliaguine, *Appl. Catal. A: General*, 2000, **196**, 9–24.
277 W-S. Jung and S-K. Ahn, *Mater. Lett.*, 2000, **43**, 53–56.
278 J. Jin, S. Sakida, T. Yoko and M. Nogami, *J. Non-Cryst. Solids*, 2000, **262**, 183–190.
279 B. C. Schmidt, T. Riemer, S. C. Kohn, H. Behrens, and R. Dupree, *Geochim. Cosmochim. Acta*, 2000, **64**, 513–526.
280 J. Aguado, D. P. Serrano and J. M. Escola, *Micropor. Mesopor. Mater.*, 2000, **34**, 43–54.
281 J. M. Egan, R. M. Wenslow, and K. T. Mueller, *J. Non-Cryst. Solids*, 2000, **261**, 115–126.
282 F. C. Hawthorne, M. D. Welch, G. Della Ventura, S. Liu, J-L. Robert, and D. M. Jenkins, *Am. Mineral.*, 2000, **85**, 1716–1724.
283 J. Klein, M. Ushio, L. S. Burrell, B. Wenslow, and S. L. Hem, *J. Pharmac. Sci.*, 2000, **89**, 311–321.
284 C. Magnenet, D. Massiot, I. Klur, and J. P. Coutures, *J. Mater. Sci.*, 2000, **35**, 115–121.
285 Y. Ba, C. I. Ratcliffe, and J. A. Ripmeester, *Adv. Mater.*, 2000, **12**, 603–606.
286 J. C. C. Chan and H. Eckert, *J. Non-Cryst. Solids*, 2001, **284**, 16–21.
287 M. Karabulut, E. Metwalli, and R. K. Brow, *J. Non-Cryst. Solids*, 2001, **283**, 211–219.
288 J. McManus, S. E. Ashbrook, K. J. D. MacKenzie, and S. Wimperis, *J. Non-Cryst. Solids*, 2001, **282**, 278–290.

289 E. Robert, A. Whittington, F. Fayon, M. Pichavant, and D. Massiot, *Chem. Geol.*, 2001, **174**, 291–305.
290 D. Champmartin, P. Rubini, A. Lakatos and T. Kiss, *J. Inorg. Biochem.*, 2001, **84**, 13–21.
291 D. Ma, F. Deng, R. Fu, X. Han, and X. Bao, *J. Phys. Chem. B*, 2001, **105**, 1770–1779.
292 A. Vazquez, T. Lopez, R. Gomez and X. Bokhimi, *J. Mol. Catal. A: Chem.*, 2001, **167**, 91–99.
293 J-A. Ke and I. Wang, *Mater. Chem. Phys.*, 2001, **68**, 157–165.
294 C-L. Tsai, B. Chou, S. Cheng, and J-F. Lee, *Appl. Catal. A: General*, 2001, **208**, 279–289.
295 T. Mimani, *J. Alloys Comp.*, 2001, **315**, 123–128.
296 D. H. Kim, S. I. Woo, J. Noh, and O-B. Yang, *Appl. Catal. A: General*, 2001, **207**, 69–77.
297 B. H. Wouters, T. Chen, and P. J. Grobet, *J. Phys. Chem. B*, 2001, **105**, 1135–1139.
298 Z. Y. Yuan, T. H. Chen, J. Z. Wang, and H. X. Li, *Colloids Surf. A*, 2001, **179**, 253–259.
299 M. Sychev, R. Prihod'ko, K. Erdmann, A. Mangel, and R. A. van Santen, *Appl. Clay Sci.*, 2001, **18**, 103–110.
300 A. R. Thompson and R. E. Botto, *Energy Fuels*, 2001, **15**, 176–181.
301 D. Massiot, R. Revel, C. Magnenet, and D. Bazin, *Solid State Nucl. Magn. Reson.*, 2000, **16**, 103–108.
302 M. I. M. Prata, A. C. Santos, C. F. G. C. Geraldes, and J. J. P. de Lima, *J. Inorg. Biochem.*, 2000, **79**, 359–363.
303 A. Belkebir, J. Rocha, A. P. Esculcas, P. Berthet, S. Poisson, B. Gilbert, Z. Gabelica, G. Llabres, F. Wijzen and A. Rulmont, *Spectrochim. Acta A*, 2000, **56**, 423–434.
304 K. Okumura, K. Nishigaki, and M. Niwa, *Micropor. Mesopor. Mater.*, 2001, **44–45**, 509–516.
305 D. Ma, Y. Shu, C. Zhang, W. Zhang, X. Han, Y. Xu, and X. Bao, *J. Mol. Catal. A: Chem.*, 2001, **168**, 139–146.
306 S. H. Kim, S. D. Kim, Y. C. Kim, C.-S. Kim, and S. B. Hong, *Micropor Mesopor. Mater.*, 2001, **42**, 121–129.
307 A. M. Panich and Th. Doert, *Solid State Commun.*, 2000, **114**, 371–375.
308 M. Michalik, M. Hein, and M. Frank, *Carbohydr. Res.*, 2000, **327**, 185–218.
309 S. Failla, P. Finocchiaro, and G. A. Consiglio, *Heteroatom Chem.*, 2000, **11**, 493–504.
310 V. Busico and R. Cipullo, *Prog. Polym. Sci.*, 2001, **26**, 443–533.
311 Y. Pang, and E. R. P. Zuiderweg, *J. Am. Chem. Soc.*, 2000, **122**, 4841–4842.
312 M. Hong, *J. Am. Chem. Soc.*, 2000, **122**, 3762–3770.
313 J. Schraml, *Appl. Organomet. Chem.*, 2000, **14**, 604–610.
314 J. Casanovas, F. Illas, and G. Pacchioni, *Chem. Phys. Lett.*, 2000, **326**, 523–529.
315 M. G. Mortuza, R. Dupree, and D. Holland, *J. Mater. Sci.*, 2000, **35**, 2829–2832.
316 W. P. Gates, P. Komadel, J. Madejova, J. Bujdak, J. W. Stucki, and R. J. Kirkpatrick, *Appl. Clay Sci.*, 2000, **16**, 257–271.
317 J. Brus, and J. Dybal, *Polymer*, 2000, **41**, 5269–5282.
318 J. Parmentier, P. R. Bodart, L. Audoin, G. Massouras, D. P. Thompson, R. K. Harris, P. Goursat, J-L. Besson, *J. Solid State Chem.*, 2000, **149**, 16–20.
319 T. M. Alam and M. Henry, *Phys. Chem. Chem. Phys.*, 2000, **2**, 23–28.

320 Y. Takeuchi, M. Nishikawa, K. Tanaka, T. Takayama, M. Imanari, K. D. Eguchi, T. Fujito, and Y. Sugisaka, *Chem. Commun.*, 2000, 687–688.
321 M. Nath, S. Pokharia, and R. Yadav, *Coord. Chem. Rev.*, 2001, **215**, 99–149.
322 G. M. Maksimov, M. A. Fedotov, S. V. Bogdanov, G. S. Litvak, A. V. Golovin, and V. A. Likholobov, *J. Mol. Catal. A: Chem.*, 2000, **158**, 435–438.
323 M. Kemmer, H. Dalil, M. Biesemans, J. C. Martins, B. Mahieu, E. Horn, D. de Vos, Edward, R. T. Tiekink, R. Willem, and M. Gielen, *J. Organomet. Chem.*, 2000, **608**, 63–70.
324 P. A. Robles-Dutenhefner, E. M. Moura, G. J. Gama, H. G. L. Siebald, and E. V. Gusevskaya, *J. Mol. Catal. A: Chemical*, 2000, **164**, 39–47.
325 U. Englich, K. Ruhlandt-Senge, and F. Uhlig, *J. Organomet. Chem.*, 2000, **613**, 139–147.
326 N. Lenze, B. Neumann, H-G. Stammler, and P. Jutzi, *J. Organomet. Chem.*, 2000, **608**, 86–88.
327 M. Lopez-Cardoso, P. Garcia, A. Rogers-Sakuma, and R. Cea-Olivares, *Polyhedron*, 2000, **19**, 1539–1543.
328 E. Siebel, R. Dieter Fischer, N. A. Davies, D. C. Apperley, and R. K. Harris, *J. Organomet. Chem.*, 2000, **604**, 34–42.
329 B. Wrackmeyer and S. V. Ponomarev, *J. Organomet. Chem.*, 2000, **598**, 211–214.
330 H. Yano, Y. Furukawa, Y. Kuranaga, K. Yamada, and T. Okuda, *J. Mol. Struct.*, 2000, **520**, 173–178.
331 U. Herzog and G. Rheinwald, *J. Organomet. Chem.*, 2001, **627**, 23–36.
332 M. I. Garcia-Seijo, A. Casteneiras, B. Mahieu, Z. Berente, L. Kollar, and M. E. Garcia-Fernandez, *Polyhedron*, 2001, **20**, 855–868.
333 T. Lebl, J. Holecek, M. Dymak, and D. Steinborn, *J. Organomet. Chem.*, 2001, **625**, 86–94.
334 J. A. Marshall and K. Gill, *J. Organomet. Chem.*, 2001, **624**, 294–299.
335 C. Audo, J. F. Lambert, M. Che, and B. Didillon *Catal. Today*, 2001, **65**, 157–162.
336 (a) D. L. Tierney, P. J. Moehs, and D. L. Hasha, *J. Organomet. Chem.*, 2001, **620**, 211–226, (b) D. L. Hasha, *J. Organomet. Chem.*, 2001, **620**, 296–302.
337 T. Lee, S. W. Lee, H. G. Jang, S. O. Kang, and J. Ko, *Organometallics*, 2001, **20**, 741–748.
338 X. Fang, X. Song, and Q. Xie, *J. Organomet. Chem.*, 2001, **619**, 43–48.
339 N. Lenze, B. Neumann, A. Salmon, A. Stammler, H-G. Stammler, and P. Jutzi, *J. Organomet. Chem.*, 2001, **619**, 74–87.
340 S. Garden, W. T. A. Harrison, R. A. Howie, H. Rufino, and J. L. Wardell, *J. Organomet. Chem.*, 2001, **619**, 226–234.
341 A. Jansco, T. Gajda, A. Szorcik, T. Kiss, B. Henry, G. Vanko, and P. Rubini, *J. Inorg. Biochem.*, 2001, **83**, 187–192.
342 T. M. Klapötke, B. Krumm, M. Niemitz, K. Polborn, and C. M. Rienäcker, *J. Fluor. Chem.*, 2000, **104**, 129–133.
343 D. A. Bussian and G. S. Harbison, *Solid State Commun.*, 2000, **115**, 95–98.
344 D. Christendat, J. H. Wosnick, I. S. Butler, D. F. R. Gilson, A-M. Lebuis, and F. G. Morin, *J. Mol. Struct.*, 2001, **559**, 235–243
345 G. E. Martin, C. E. Hadden, *J. Nat. Prod.*, 2000, **63**, 543–585.
346 C. M. Rienstra, M. Hohwy, M. Hong, R. G. Griffin, *J. Am. Chem. Soc.*, 2000, **122**, 10979–10990.
347 A. Medek, P. J. Hajduk, J. Mack, and S. W. Fesik, *J. Am. Chem. Soc.*, 2000, **122**, 1241–1242.

348 A. Bagno, *J. Phys. Org. Chem.*, 2000, **13**, 574–578.
349 T. Kuivalainen, J. El-Bahraoui, R. Uggla, R. Kostiainen, and M. R. Sundberg, *J. Am. Chem. Soc.*, 2000, **122**, 8073–8074.
350 U. Brenn, H. Ernst, D. Freude, R. Herrmann, R. Jähnig, H. G. Karge, J. Kärger, T. König, B. Mädler, U-T. Pingel, D. Prochnow, and W. Schwieger, *Micropor. Mesopor. Mater.*, 2000, **40**, 43–52.
351 V. Tsikaris, V. Moussis, M. Sakarellos-Daitsiotis, and C. Sakarellos, *Tetrahedron Lett.*, 2000, **41**, 8651 8654.
352 Y. Machida, S. Kuroki, M. Kanekiyo, M. Kobayashi, I. Ando, and S. Amiya, *J. Mol. Struct.*, 2000, **554**, 81–90.
353 W. H. Casey, B. L. Phillips, M. Karlsson, S. Nordin, J. P. Nordin, D. J. Sullivan, and S. Neugebauer-Crawford, *Geochim. Cosmochim. Acta*, 2000, **64**, 2951–2964.
354 W. H. Casey and B. L. Phillips, *Geochim. Cosmochim. Acta*, 2001, **65**, 705–714.
355 S. K. Lee and J. F. Stebbins, *J. Non-Cryst. Solids*, 2000, **270**, 260–264.
356 J. F. Stebbins, J. V. Oglesby, and S. K. Lee, *Chem. Geol.*, 2001, **174**, 63–75.
357 G. Wu and S. Dong, *Chem. Phys. Lett.*, 2001, **334**, 265–270.
358 T. M. Alam, M. Celina, R. A. Assink, R. L. Clough, and K. T. Gillen, *Radiat. Phys. Chem.*, 2001, **60**, 121 127.
359 J. V. Oglesby, S. Kroeber, and J. F. Stebbins, *Am. Mineral.*, 2001, **86**, 341–347.
360 B. G. Pfrommer, F. Mauri, and S. G. Louie, *J. Am. Chem. Soc.*, 2000, **122**, 123–129.
361 S. Dong, R. Ida, and G. Wu, *J. Phys. Chem. A*, 2000, **104**, 11194–11202.
362 K. Jackowski, *J. Mol. Struct.*, 2001, **563–564**, 159–162.
363 C. Hamard, V. Auffret, O. Pena, M. Le Floch, B. Nowak and A. Wojakowski, *Phys. B: Condensed Matt.*, 2000, **291**, 339–349.
364 P. Mathur, P. Payra, S. Ghose, M. M. Hossain, C. V. V. Satyanarayana, F. O. Chicote, and R. K. Chadha, *J. Organomet. Chem.*, 2000, **606**, 176–182.
365 P. Mathur, S. Ghosh, A. Sarkar, A. L. Rheingold, and I. A. Guzei, *Tetrahedron*, 2000, **56**, 4995–5000.
366 A. J. Barton, J. Connolly, W. Levason, A. Mendia-Jalon, S. D. Orchard, and G. Reid, *Polyhedron*, 2000, **19**, 1373–1379.
367 V. Bereau and J. A. Ibers, *Comp. Rend. Acad. Sci., Ser. II; Chem.*, 2000, **3**, 123–129.
368 G. Pilloni, B. Longato, and G. Bandoli, *Inorg. Chim. Acta*, 2000, **298**, 251–255.
369 C. Rosenhahn, S. E. Hayes, B. Rosenhahn, and H. Eckert, *J. Non-Cryst. Solids*, 2001, **284**, 1–8.
370 M. R. Burgess and C. P. Morley, *J. Organomet. Chem.*, 2001, **623**, 101–108.
371 (a) K. Hiraki, T. Takahashi, R. Kondo, S. Kagoshima, T. Hasegawa, T. Mochida, and Y. Iwasa, *Synth. Metals*, 2001, **120**, 917–918; (b) K. Hiraki, T. Takahashi, R. Kondo, S. Kagoshima, T. Hasegawa, T. Mochida, and Y. Iwasa, *J. Phys. Chem. Solids*, 2001, **62**, 401–403.
372 A. K. Singh and S. Sharma, *Coord. Chem. Rev.*, 2000, **209**, 49–98.
373 H. A. S. Citeau and D. M. Giolando, *J. Organomet. Chem.*, 2001, **625**, 23–31.
374 V. Garcia-Montalvo, A. Marcelo-Polo, R. Montoya, R. A. Toscano, S. Hernandez-Ortega, and R. Cea-Olivares, *J. Organomet. Chem.*, 2001, **623**, 74–80.
375 M. Michalik, M. Hein, and M. Frank, *Carbohydr. Res.*, 2000, **327**, 185–218.
376 S. Y. Troitski, M. A. Serebriakova, M. A. Fedotov, S. V. Ignashin, A. L. Chuvilin, E. M. Moroz, B. N. Novgorodov, D. I. Kochubey, V. A. Likholobov, B. Blanc, and P. Gallezot, *J. Mol. Catal. A: Chem.*, 2000, **158**, 461–465.
377 C. Parks, P. Stachowiak, and N. Sullivan, *J. Low Temp. Phys.*, 2000, **121**, 489–494.

378 B. Nagasaka, T. Eguchi, H. Nakayama, N. Nakamura, and Y. Ito, *Radiat. Phys. Chem.*, 2000, **58**, 581–585.
379 J. Wolber, A. Cherubini A. M. O. Leach, and A. Bifone, *Magn. Reson. Medicine*, 2000, **43**, 491–496.
380 M-A. Springuel-Huet, J-L. Bonardet, A. Gedeon, Y. Yue, V. N. Romannikov, and J. Fraissard, *Micropor. Mesopor. Mater.*, 2001, **44–45**, 775–784.
381 R. W. Mair, M. D. Hurlimann, P. N. Sen, L. M. Schwartz, S. Patz, and R. L. Walsworth, *Magn. Reson. Imaging*, 2001, **19**, 345–351.

4
Theoretical Aspects of Spin–Spin Couplings

BY H. FUKUI AND T. BABA

1 Introduction

Nuclear magnetic resonance (NMR) spectroscopy is one of the most applied experimental techniques since it is able to provide useful information about a wide variety of systems investigated in organic and inorganic chemistry. Many theoretical investigations have been devoted to compute and predict NMR spectroscopic observables, *i.e.*, chemical shielding and indirect nuclear spin–spin coupling tensors, from the first principles of quantum theory. In particular, the calculation of nuclear spin–spin coupling tensors has been one of the most challenging tasks because of the poor evaluation at the Hartree–Fock level. The aim of this review is to provide readers with information about important developments in theoretical aspects of spin–spin couplings in the last year.

2 Relativistic Calculation of Spin–Spin Couplings

Since the presentation of theory of indirect nuclear spin–spin couplings by Ramsey[1] in 1953, there has been a great effort to make theoretical predictions agree with observed couplings. However, Ramsey's theory is based on the nonrelativistic quantum theory and the relativistic effects are not taken into account.[2] It has long been known that a relativistic treatment of systems containing heavy elements is necessary even for a qualitatively correct description of bonding.[3–6] Since NMR spin–spin couplings are determined by features of the wave function at or very close to the nuclei, one may expect enormously large relativistic effects on spin–spin couplings. A relativistic analogue of Ramsey's nuclear spin–spin coupling theory was presented by Pyykkö[7] in 1977. After that a more sophisticated theory of relativistic effects on spin–spin couplings appeared (about ten years ago).[8]

Autschbach and Ziegler[9–12] performed the relativistic calculations of spin–spin coupling constants (isotropic part) and anisotropies in heavy atom compounds with the two-component zeroth-order regular approximation (ZORA) method.[13–15] The experimentally determined reduced spin–spin coupling tensor elements $K_{jk}(A,B)$ between two magnetically active nuclei, A and

Nuclear Magnetic Resonance, Volume 31
© The Royal Society of Chemistry, 2002

B, with nuclear magnetic moments, $\vec{\mu}_A = \gamma_A \hbar \vec{I}_A$ and $\vec{\mu}_B = \gamma_A \hbar \vec{I}_B$, respectively, are connected with the total electronic energy E of the system by

$$K_{jk}(A,B) = (\partial^2 E/\partial \mu_{Bk})_{\vec{\mu}_A=0,\vec{\mu}_B=0} \tag{4.1}$$

The reduced coupling constant K is the isotropic part of the tensor, *i.e.*, $K = (1/3)(K_{xx}+K_{yy}+K_{zz})$. Experimentally it is obtained from the observed coupling constants $J(A,B)$ as

$$J(A,B) = (h/4\pi^2)\gamma_A\gamma_B K(A,B), \tag{4.2}$$

where the γ's are the nuclear gyro-magnetic ratios. If we apply a double perturbation theory[16] and the Hellmann-Feynman theorem[17,18] to calculate the second-order derivative of the electronic energy with respect to the nuclear magnetic moments, we will have

$$K_{jk}(A,B) = \langle \Psi^{(0,0)}|\hat{H}^{(1,1)}|\Psi^{(0,0)}\rangle + 2\mathrm{Re}\langle \Psi^{(0,0)}|\hat{H}^{(1,0)}|\Psi^{(0,1)}\rangle \tag{4.3}$$

The superscripts (1,0) *etc*, denote the order of perturbation with respect to the perturbation parameters μ_{Aj} and μ_{Bk}, *i.e.*,

$$\Psi^{(0,1)} = (\partial\Psi/\partial\mu_{Bj})_{\vec{\mu}_B=0,\vec{\mu}_A=0} \tag{4.4}$$

$$\hat{H}^{(1,1)} = (\partial^2\hat{H}/\partial\mu_{Aj}\partial\mu_{Bk})_{\vec{\mu}_A=0,\vec{\mu}_B=0}. \tag{4.5}$$

etc. The perturbation Hamiltonians, $\hat{H}^{(1,1)}$ and $\hat{H}^{(1,0)}$, are derived from the ZORA Hamiltonian.

The standard representation of the four-component relativistic Dirac equation[19] for a single particle in an electrostatic potential $V(\vec{r})$ and a vector potential $\vec{A}(\vec{r})$ reads

$$(\hat{H}^D - E)\Psi^D = [c\vec{\alpha}\cdot\vec{\pi} + (\beta-1)c^2 + V - E]\Psi^D = 0. \tag{4.6}$$

Here, atomic units ($\hbar = 1$, $e = 1$, $m_e = 1$, $4\pi\varepsilon_0 = 1$, $c \cong 137.036$) are used. $\vec{\alpha}$ and β are the 4×4 Dirac matrices, which are written as

$$\vec{\alpha} = \begin{bmatrix} 0 & \vec{\sigma} \\ \vec{\sigma} & 0 \end{bmatrix} \text{and } \beta = \begin{bmatrix} I & 0 \\ 0 & -I \end{bmatrix} \tag{4.7}$$

where $\vec{\sigma}$ is the 2×2 Pauli spin matrix vector and I is the 2×2 unit matrix. The wave function Ψ^D is the 4×1 column vector function and called a four-component spinor. Usually, the upper two components of Ψ^D are called large components and the lower two components called small components. In order to account for the presence of electromagnetic fields, which are represented by the vector potential $\vec{A}$, we have to use the kinematic momentum $\vec{\pi} = \vec{p} + \vec{A}$ in $\hat{H}^D$ for an electron of charge e. In a two-component relativistic formulation, the coupling between the large and small components has to be eliminated. In the absence of the electrostatic potential $V(\vec{r})$, the Dirac Hamiltonian is exactly decoupled to the two component Hamiltonian[20] by a kind of unitary transformation, called the Foldy–Wouthuysen (FW) transformation.[21]

Unfortunately, in the presence of $V(\vec{r})$, the unitary matrix giving the exact decoupling is not found in a closed form. A number of different approximations to the exact FW transformation have been suggested and analyzed in the literature.[20,22–24] With the special choice of approximations to the exact decoupling, the effective two-component ZORA Hamiltonian in the presence of electromagnetic fields is

$$\hat{H}^Z = V + \frac{1}{2}\vec{\sigma}\cdot\vec{\pi}\mathcal{K}\vec{\sigma}\cdot\vec{\pi} \tag{4.8}$$

where

$$\mathcal{K} = [1 - V/2c^2]^{-1} \tag{4.9}$$

The factor $\mathcal{K}$ (not to be confused with the reduced coupling constant K) yields the relativistic effect. The nonrelativistic limit, which is given by taking $c \to \infty$, yields $\mathcal{K} = 1$ and eq. (4.8) leads to the nonrelativistic Hamiltonian in the electromagnetic fields.[25] We may insert $\vec{\pi} = \vec{p} + \vec{A}$ into the right-hand side of eq. (4.8) to obtain

$$\hat{H}^Z = V + \frac{1}{2}(\vec{p}\mathcal{K}\cdot\vec{p} + i\vec{\sigma}\cdot\vec{p}\mathcal{K}\times\vec{p} \tag{4.10a}$$

$$+ \vec{p}\mathcal{K}\cdot\vec{A} + \mathcal{K}\vec{A}\cdot\vec{p} + i\vec{\sigma}\cdot[\vec{p}\mathcal{K}\times\vec{A} + \mathcal{K}\vec{A}\times\vec{p})] \tag{4.10b}$$

$$+ \mathcal{K}\vec{A}^2) \tag{4.10c}$$

Equation (4.10a) is the electrostatic potential, scalar relativistic (SR), and spin–orbit (SO) terms of the ZORA Hamiltonian in the absence of electromagnetic fields. The remaining part, (4.10b) and (4.10c), represents the hyperfine terms due to the presence of the nuclear magnetic moments, $\vec{\mu}_A$ and $\vec{\mu}_B$.

If we insert

$$\vec{A} = \vec{A}_A + \vec{A}_B = \frac{1}{c^2}(r_A^{-3}\vec{\mu}_A\times\vec{r}_A + r_B^{-3}\vec{\mu}_B\times\vec{r}_B) \tag{4.11}$$

into eq. (4.10c) $\mathcal{K}\vec{A}_A\cdot\vec{A}_B$ yields the ZORA relativistic analogue of the diamagnetic spin–orbit (DSO) term,

$$\begin{aligned}\hat{H}_{ZDSO} &= \mathcal{K}\vec{A}_A\cdot\vec{A}_B \\ &= (\mathcal{K}/c^4)r_A^{-3}r_B^{-3}[(\vec{\mu}_A\cdot\vec{\mu}_B)(\vec{r}_A\cdot\vec{r}_B) - (\vec{\mu}_A\cdot\vec{r}_B)(\vec{\mu}_B\cdot\vec{r}_A)]\end{aligned} \tag{4.12}$$

The first two terms of eq. (4.10b) may be rewritten as

$$\hat{H}_{ZPSO} = \hat{H}^A_{ZPSO} + \hat{H}^B_{ZPSO} \tag{4.13a}$$

$$\hat{H}^N_{ZPSO} = \frac{1}{2c^2 i}\vec{\mu}_N\cdot\left(\frac{\mathcal{K}}{r_N^3}\vec{r}_N\times\vec{\nabla} + \vec{r}_N\times\vec{\nabla}\frac{\mathcal{K}}{r_A^3}\right), \quad N = A \text{ or } B \tag{4.13b}$$

The nonrelativistic limit of this operator yields the paramagnetic spin–orbit (PSO) contribution of Ramsey's theory. The remaining terms in eq. (4.10b) result in the ZORA relativistic spin–orbit Hamiltonian,

$$\hat{H}_{ZSO} = \hat{H}^{A}_{ZSO} + \hat{H}^{B}_{ZSO}, \tag{4.14a}$$

$$\hat{H}^{N}_{ZSO} = \frac{1}{2c^2}\vec{\sigma}\cdot\left[\vec{\mu}_N\left(\vec{\nabla}\mathcal{K}\cdot\frac{\vec{r}_N}{r_N^3}\right) - \left(\vec{\mu}_N\cdot\vec{\nabla}\mathcal{K}\frac{\vec{r}_N}{r_N^3}\right)\right], \quad N = A \text{ or } B \tag{4.14b}$$

The parentheses in $\left(\vec{\nabla}K\cdot\frac{\vec{r}_N}{r_N^3}\right)$ and $\left(\vec{\mu}_N\cdot\vec{\nabla}K\frac{\vec{r}}{r_N^3}\right)$ in eq. (4.14b) indicate that $\vec{\nabla}$ operates solely on the inside of the parentheses. The nonrelativistic limit of this operator corresponds to the sum of the Fermi-contact (FC) and spin–dipolar (SD) terms of Ramsey's theory. Second-order differentiation of eq. (4.12) with respect to μ_{Aj} and μ_{Bk} gives

$$\hat{H}^{(1,1)} = (\mathcal{K}/c^4)r_A^{-3}r_B^{-3}\left[\delta_{jk}(\vec{r}_A\cdot\vec{r}_B) - r_{Ak}r_{Bj}\right] \tag{4.15}$$

Differentiating eqs. (4.13) and (4.14) with respect to μ_{Aj} yeilds

$$\hat{H}^{(1,0)} = \hat{H}^{(1,0)}_{ZPSO} + \hat{H}^{(0,1)}_{ZSO} \tag{4.16a}$$

with

$$2c^2 i\hat{H}^{(1,0)}_{ZPSO} = \frac{\mathcal{K}}{r_A^3}\left(\vec{r}_A\times\vec{\nabla}\right)_j + (\vec{r}_A\times\vec{\nabla})_j\frac{\mathcal{K}}{r_A^3} \tag{4.16b}$$

$$2c^2\hat{H}^{(1,0)}_{ZSO} = \sigma_j\left(\vec{\nabla}\mathcal{K}\cdot\frac{\vec{r}_A}{r_A^3}\right) - \vec{\sigma}\cdot\left(\nabla_j\mathcal{K}\frac{\vec{r}_A}{r_A^3}\right) \tag{4.16c}$$

Similar expressions with A and j replaced by B and k, respectively, arise for the $\hat{H}^{(0,1)}$ operator.

We make use of partial integration to avoid derivatives of $\mathcal{K}$ in the matrix elements of eqs. (4.16b) and (4.16c). That is,

$$2c^2 i\langle\mathcal{X}_r|\hat{H}^{(1,0)}_{ZPSO}|\mathcal{X}_s\rangle = \int \mathrm{d}\tau\frac{\mathcal{K}}{r_A^3}\left[\vec{r}_A\times\left(\mathcal{X}_r\vec{\nabla}\mathcal{X}_s - \mathcal{X}_s\vec{\nabla}\mathcal{X}_r\right)\right]_j \tag{4.17a}$$

$$\begin{aligned}2c^2\langle\mathcal{X}_r|\hat{H}^{(1,0)}_{ZSO}|\mathcal{X}_s\rangle = &-\sigma_j\int \mathrm{d}\tau\mathcal{K}\frac{\vec{r}_A}{r_A^3}\cdot\left(\mathcal{X}_r\vec{\nabla}\mathcal{X}_s + \mathcal{X}_s\vec{\nabla}\mathcal{X}_r\right)\\ &+\vec{\sigma}\cdot\int \mathrm{d}\tau\mathcal{K}\frac{\vec{r}_A}{r_A^3}\left(\mathcal{X}_r\nabla_j\mathcal{X}_s + \mathcal{X}_s\nabla_j\mathcal{X}_r\right)\end{aligned} \tag{4.17b}$$

In the nonrelativistic limit, $c\to\infty$, eq. (4.16c) yields the well-known Fermi-contact operator and the spin–dipolar interaction operator because

$$\nabla\frac{r_j}{r^3} = \frac{4\pi}{3}\delta_{ij}\delta(\vec{r}) + \frac{\delta_{ij}}{r^3} - \frac{3r_ir_j}{r^5} \tag{4.18}$$

In the relativistic treatment, however, the situation is much different. A relativistic four-component Dirac wave function in a point-nucleus approximation diverges at the nuclei.[26] We should recall that the two-component ZORA wave function is proportional to the large components of the respective four-component wave function,[27] therefore showing similar divergences for s-type orbitals in a point-nucleus approximation. However, the factor $\mathcal{K}$ becomes

zero more rapidly than the divergency of the wave function at the nuclei, so that all integrals of $\mathcal{K}\delta(\vec{r}_N)$ vanish at the nucleus N. In this case, nonzero contributions come from derivatives of $\mathcal{K}$.

Autschbach and Ziegler presented relativistic spin–spin coupling constants based on the two-component ZORA formulation. They published four papers.[9–12] In the first paper[9] of their series, only the scalar relativistic part was included, and a full inclusion of the ZORA effects was implemented in the second paper.[10] They used the density functional theory (DFT) approach. The first paper showed that scalar relativistic calculations are able to reproduce major parts of the relativistic effects on the one-bond metal–ligand couplings of systems containing ^{183}W, ^{195}Pt, ^{199}Hg and ^{207}Pb. It was found that the relativistic effects on the coupling constants can be even larger in magnitude than the respective total nonrelativistic values. The relativistic effects were attributed to the relativistic increase of valence orbital density in the very vicinity of the heavy nucleus. The second paper of Autschbach and Ziegler[10] presented the spin–spin coupling constants and anisotropies for the XF (X = Cl, Br, I) and TlX (X = F, CL, Br, I) series, for which experimental and/or computational data[28] are available. In the second paper, the spin–orbit term was included. Especially in the TlX systems, spin–orbit effects were very important and necessary to obtain even qualitatively correct coupling tensors. Only with the inclusion of spin–orbit coupling, in particular the large negative ZSO-ZPSO cross term, brought the couplings in good agreement with the experimental results.

In the third paper[11] of their series, they calculated coordination effects of solvent molecules on one-bond metal–ligand spin–spin coupling constants of coordinatively unsaturated compounds containing ^{195}Pt and ^{199}Hg. It was shown earlier[9] that too small coupling constants, in comparison with the experimental values, are systematically obtained for the linear $Hg(CN)_2$ and H_3C–Hg–X (X = CH_3, Cl, Br, I) and the square planar $PtX_2(P(CH_3)_3)_2$ (X = H, Cl) complexes. Since these Hg and Pt systems mentioned above are not coordinatively saturated, solvent molecules may coordinate the heavy atom. This will not be the case for tetrahedral or octahedral systems such as the W and Pb compounds which were investigated in ref. 9. The poor results for the coordinatively unsaturated compounds may be attributed to the influence of solvent molecules since the experimental data were obtained in solution. Astschbach and Ziegler[11] obtained a good agreement with experimental data for the one-bond metal–ligand spin–spin coupling constants for $Hg(CN)_2$, H_3C–Hg–X, and $PtX_2(P(CH_3)_3)_2$ by ZORA relativistic DFT computations with explicit accounting for coordination of the heavy atom by solvent molecules. Fully optimized geometries for the solvated molecules were obtained from the quasi-relativistic DFT method developed by Ziegler *et al.*[29,30] Up to four solvent molecules were considered for the Hg complexes. The computed ^1J(Hg,C) spin–spin coupling constants are shown in Table 4.1. Table 4.1 shows that the calculated spin–spin coupling constants increase substantially with increasing number of solvent molecules coordinating the heavy atom, Hg, thereby approaching the experimental values. A similar result was obtained for

Table 4.1 *Computed one-bond spin–spin couplings* ^1K(Hg,C) *for the solvated compounds HgMeX (Me = CH_3, X = Me, Cl, Br, I) and $Hg(CN)_2$, in 10^{20} kg m^{-2} S^{-2} A^{-2} (taken from ref. 11)*

Cmpd	*Solvent*	*No solv.*[a,b]	*+2 solv.*[a,c]	*+3 solv.*[a,c]	*+4 solv.*[a,c]	*Exptl.*	$\bar{R}$[d]
HgMeCl	$CHCl_3$	195.5	223.5	233.5	277.1 261.5[f]	263.1[i]	3.25
	DMSO		260.3	295.2		307.8[i]	2.65[g]
HgMeBr	$CHCl_3$	197.8	218.9	227.2		256.3[i]	3.28
	DMSO		253.8	293.6		299.9[i]	2.69[g]
HgMeI	$CHCl_3$	182.7	192.9	241.2		239.2[i]	3.28
	DMSO		251.0	295.4		283.1[i]	2.66[g]
$HgMe_2$[e]	$CHCl_3$	82.7	108.0	121.8		126.6[i]	3.28
	DMSO		118.5	130.7		133.4[i]	2.89
$Hg(CN)_2$[e]	MeOH	440.8	513.1		576.2 560.7[f]	577.8[j]	2.59[h]
	THF		511.5		581.8	558.5[k]	2.58[h]

[a] Scalar ZORA: FC + PSO + DSO coupling. [b] Ref. 9. [c] Coupling constant including the number of specified solvent molecules. [d] Mean distance between the heavy metal and the closest O or Cl solvent atoms in Å. [e] Mean value of both Hg–C coupling constants. [f] ZORA spin–orbit computation including the SD term. [g] For three DMSO. One DMSO is at a distance of ~ 3.5 Å. [h] For two solvents. With four solvent molecules whose distances are 2.67 Å for MeOH and 2.68 Å for THF, respectively. [i] Ref. 31. [j] Ref. 32. [k] Ref. 33.

the Pt complexes where up to two solvent molecules were considered. The strong increase of the spin–spin coupling at the presence of solvent molecules can be explained by the coordination of the heavy atom by solvent atoms with lone pairs. The solvent will donate electrons into the metal–ligand bonds, which in turn leads to an increase of the metal–ligand spin–spin coupling constants.

In their fourth paper, Autschbach and Ziegler[12] presented a theoretical interpretation of the remarkable nuclear spin–spin coupling pattern in $[(NC)_5Pt–Tl(CN)]^-$ (**1**). Compounds which have a direct bond between two different heavy nuclei and which are stable in solution are rare. A class of such compounds, $[(NC)_5Pt–Tl(CN)_n]^{n-}$, $n = 0–3$, with unbridged Pt–Tl bonds has been described by Glaser and co-workers.[34,35] In particular, the complex $[(NC)_5Pt–Tl(CN)]^-$ has been experimentally extensively investigated by multinuclear NMR and Raman spectroscopy. The NMR spectra show three magnetically nonequivalent carbons, which we label with A, B and C.[34–36] Apart from the very large Pt–Tl spin–spin coupling of ~ 57 kHz, one of the most remarkable features of the NMR spectrum of **1** is the fact that the two-bond coupling $^2J(Tl,C^A)$ is much larger than the one-bond coupling $^1J(Tl,C^B)$, provided that the structure shown in **1**,[35] which is based on the NMR and Raman spectra, is correct. Autschbach and Ziegler[12] performed ZORA relativistic DFT calculations with explicit consideration of solvent molecules. Table 4.2 lists the experimentally observed and theoretically computed spin–spin couplings for the complex, **1**.

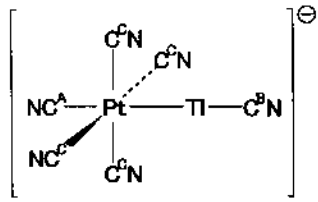

1

Table 4.2 *Spin–spin coupling constants in complex 1, in Hz (taken from ref. 12)*

Coupling[a]	*nrel*[b]	*rel*[c]	*rel, 4aq*[d]	*so, 4aq*[e]	*Exptl*[f]
^1J(Pt,Tl)	5410	18976	43102	40292	57020
^1J(Tl,C^B)	−1222	−5692	3081	3001	2446
^2J(Tl,C^A)	3428	5670	7983	7537	9743
^2J(Tl,C^C)[g]	−249	−484	−381	−392	452
^1J(Pt,C^A)	682	1382	1037	1007	843
^1J(Pt,C^C)[g]	444	890	954	920	821
^2J(Pt,C^B)	62	151	158	141	200
^3J(C^A,C^B)	36	39	20	24	30

[a] Couplings refer to ^{205}Tl, ^{195}Pt, and ^{13}C. FC + PSO + DSO contribution included in the scalar relativistic computations, SD contribution additionally present in spin–orbit computations. [b] Nonrelativistic couplings from scalar relativistically optimized geometry, no solvent. [c] Scalar relativistic couplings from scalar relativistically optimized geometry, no solvent. [d] Scalar relativistically optimized geometry including four water molecules. [e] Relativistic spin–orbit computation based on scalar relativistic geometry. [f] Ref. 35, sign not determined. [g] Mean value of the four coupling constants.

The computational results shown in Table 4.2 lead to the conclusion that the experimentally proposed structure involving a nonbridged Pt–Tl bond is most likely correct. The calculations reproduce the experimental fact that ^2J(Tl,C^A) is much larger than ^1J(Tl,C^B), provided that both relativity and water solvent effects are taken into account. A second conclusion can be drawn from the data obtained for the free complex in comparison with the solvated one. In the free complex, both ^1J(Tl,C^B) and ^2J(Tl,C^A) are of the same magnitude, but different in sign. Charge donation from the solvent to the heavy atom shifts both values positively, with the one-bond coupling being much more strongly affected than the two-bond coupling. Finally both coupling constants are positive, with ^2J(Tl,C^A) >> ^1J(Tl,C^B). Nevertheless, the question arises why ^2J(Tl,C^A) is already so large in comparison with the magnitude of ^1J(Tl,C^B) in the unsolvated complex. The complex **1** has been described[35] as being composed of a $[Pt^{II}(CN)_5]^{3-}$ fragment forming a dative bond to $Tl^{III}(CN)^{2+}$, thereby donating electrons into the Tl 6*s* orbital and reducing Tl to a formal oxidation state of <III. Obviously, upon formation of the complex, ^1J(Tl,C^B) undergoes a large negative shift and the resultant magnitude of ^1J(Tl,C^B) in the free complex is smaller than that of ^2J(Tl,C^A).

The accurate computation of heavy atom spin–spin coupling constants is a challenging task. Although a four-component *ab initio* calculation for nuclear spin–spin couplings at the Hartree–Fock level has been reported only recently,[37,38] the results are rather poor due to the missing treatment of electron correlation. Autschbach and Ziegler[9–12] showed that substantially improved accuracy for heavy atom spin–spin couplings can be achieved by employing a two-component ZORA relativistic DFT method.

Khandogin and Ziegler[39] calculated one-bond metal–ligand nuclear spin–spin coupling constants using two approximate frozen-core scalar relativistic (SR) schemes. In the first scheme, SRI, the quasirelativistic approach was incorporated into the nonrelativistic coupling calculation. In the second scheme, SRII, the scaling factor for the *s*-type orbitals at the heavy nucleus as introduced in the evaluation of the FC contribution without changing the nonrelativistic orbital expansion coefficients. The SRII method was able to reproduce the experimental trends in different ligand environments, whereas the SRI scheme failed almost completely. Furthermore, they showed that the difference between *cis* and *trans* configurations arises mainly from the difference in the electronic nature.

3 Density Functional Theory

In practice, the accurate calculation of spin–spin coupling constants has proved to be considerably more difficult than the calculation of other second-order properties such as quadratic force constants, polarizabilities, magnetizabilities, and nuclear shielding constants.[40] The reasons for these difficulties are the following. First, at the nonrelativistic level, several distinct mechanisms contribute to the spin–spin couplings:[1] the diamagnetic spin–orbit (DSO) mechanism, the paramagnetic spin–orbit (PSO) mechanism, the Fermi-contact (FC) mechanism, and the spin–dipole (SD) mechanism. All mechanisms may be important and none can be *a priori* neglected. Second, the indirect spin–spin coupling constants involve triplet perturbations, whose accurate calculation requires a highly flexible description of the electronic system. The Hartree–Fock model, the basic model of *ab initio* theory, gives notoriously poor results. As a result, there are currently no levels of *ab initio* theory available for the calculation of spin–spin coupling constants of large systems. Third, the often dominant FC contribution to the spin–spin couplings depends critically on the electron density at the nuclei; the basis set convergence is consequently slow and large basis sets must be employed for the results to be useful.

Recently, there have been several successful attempts at the calculation of spin–spin coupling constants at the density functional theory (DFT) level.[41–44] In view of the success of the DFT methodology, it would in particular be interesting to see how well DFT performs with respect to the calculation of spin–spin coupling constants. In particular, recent results demonstrated that DFT does not suffer from the triplet-instability problems that have plagued the application of Hartree–Fock theory to the calculation of spin–spin

coupling constants. Malkin *at al.* [41] and Dickson and Ziegler[43] demonstrated that the accuracy achieved by DFT with respect to calculation of spin–spin coupling constants is sufficiently high to be useful in the application of DFT to the solution of chemical problems in NMR.

Sychrovský *et al.*[45] performed, for the first time, a complete implementation of coupled perturbed density functional theory (CPDFT) for the calculation of spin–spin coupling constants with pure and hybrid DFT. They analyzed the dependence of DFT with respect to the calculation of coupling constants on the exchange-correlation (XC) functionals used. They demonstrated the importance of electron correlation effects and showed that the hybrid functional B3LYP[46,47] leads to the best accuracy of calculated spin–spin coupling constants. The CPDFT results were compared with sum-over-states density functional perturbation theory (SOS-DFPT)[48] results and it was shown that the former method is superior to the latter because it explicitly considers the dependence of the Kohn–Sham (KS) operator on the perturbed orbitals in DFT. The occupied first order spin orbitals $\psi_{k\sigma,t}^{(B),X}$ ($t \in x, y, z$; $X \in \mathrm{PSO, FC, SD}$; B is the perturbed nucleus), which are the response to the introduction of the t component of the magnetic moment of nucleus B, is given by

$$|\psi_{k\sigma,t}^{(B),X}\rangle = \sum_{a}^{vir}\sum_{\sigma'}(\varepsilon_k - \varepsilon_a)^{-1}\langle\psi_{a\sigma'}^{(0)}|F_{B,t}^{X}|\psi_{k\sigma}^{(0)}\rangle|\psi_{a\sigma'}^{(0)}\rangle \tag{4.19}$$

where $F_{B,t}^{X}$ is the first-order term of the perturbed KS operator. As the KS operator F depends on the KS orbitals through the electron density, $F_{B,t}^{X}$ depends on $|\psi_{k\sigma,t}^{(B),X}\rangle$. We can write $F_{B,t}^{X}$ as

$$F_{B,t}^{X} = H_{B,t}^{X} + \tilde{F}_{B,t}^{X} \tag{4.20a}$$

$$\tilde{F}_{B,t}^{X} = \sum_{k}^{occ}\sum_{\sigma}\int \mathrm{d}^3r(\delta F/\delta\psi_{k\sigma})\psi_{k\sigma,t}^{(B),X} \tag{4.20b}$$

Here, $H_{B,t}^{X}$ is the one-electron perturbation Hamiltonian operator. Equation (4.19) has to be solved simultaneously with eqs. (4.20) in a self-consistent fashion by CPDFT. This self-consistent procedure is avoided in SOS-DFPT, where the approximation $F_{B,t}^{X} \approx H_{B,t}^{X}$ is invoked. The spin–spin coupling constants for benzene calculated by Sychrovský *et al.*[45] with the B3LYP functional are shown in Table 4.3. A good agreement between the calculated and measured spin–spin coupling constants is obtained for J(C,C), J(C,H), and J(H,H).

Helgaker *et al.*[52] presented a fully analytical implementation of spin–spin coupling constants at the DFT level. They used the standard procedure for linear response theory to evaluate second-order properties of PSO, FC and SD mechanisms. Their calculation involves all four contributions of the nonrelativistic Ramsey theory. They tested three different XC functionals – LDA (local density approximation),[53] BLYP (Becke–Lee–Yang–Parr),[54,55] and B3LYP (hybrid BLYP).[46,47] All three levels of theory represent a

Table 4.3 *NMR spin–spin coupling constants for benzene calculated with the B3LYP functional*[a] *(taken from ref. 45)*

Coupling	K^{DSO}	K^{PSO}	K^{FC}	K^{SD}	K^{total}	J^{total}	J^{expt}
^1J(C,C)	0.30	−9.49	84.58	1.78	77.17	58.6	56.0
^2J(C,C)	−0.03	0.09	−1.47	−1.17	−2.58	−2.0	2.5[b]
^3J(C,C)	−0.01	0.69	11.09	2.52	14.29	10.9	10.0
^1J(C,H)	0.25	0.09	52.09	0.04	52.47	158.5	158.4
^2J(C,H)	−0.12	−0.28	1.02	0.01	0.63	1.9	1.1
^3J(C,H)	−0.16	0.13	2.58	−0.02	2.53	7.6	7.6
^4J(C,H)	−0.15	0.14	−0.41	0.01	−0.41	−1.2	−1.3
^3J(H,H)	−0.03	0.02	0.62	0.00	0.61	7.3	7.7[c]
^4J(H,H)	−0.15	0.15	0.11	0.00	0.11	1.3	1.4[c]
^5J(H,H)	−0.15	0.15	0.05	0.01	0.06	0.7	0.6[c]

[a] K values in SI units (10^{19} kg m^{-2} s^{-2} A^{-2}), J values in Hz. Experimental spin–spin coupling constant values are taken if not otherwise noted from ref. 49. Calculations with the basis (11*s*7*p*2*d*/6*s*2*p*) [7*s*6*p*2*d*/4*s*2*p*] (basis III in ref. 50) at the experimental geometry: r(C–C) = 1.399 Å, r(C–H) = 1.101 Å. [b] Sign unknown. [c] Ref. 51.

significant improvement on restricted Hartree–Fock (RFH) theory in the sense that the RHF instability problems are absent in DFT. It was shown that there is a steady improvement in the quality of the calculated spin–spin couplings in the sequence LDA, BLYP, and B3LYP. The results obtained by Helgaker *et al.*[52] are shown in Table 4.4. From the results in Table 4.4, it is clear that the calculated DFT spin–spin coupling constants represent a significant improvement on the Hartree–Fock constants. For example, the CC couplingsof C_2H_4 is reduced from 1236 Hz at the Hartree–Fock level to 50 Hz at the LDA level, in fair agreement with the experimental value of 68 Hz. Similar improvements are observed for the CN coupling in HCN and for the couplings in N_2 and CO, all of which are poorly described at the Hartree–Fock level. The poor description of the triplet perturbations at the Hartree–Fock level are solved at the LDA level.

Kamieńska-Trela *et al.*[73] performed DFT calculations of ^1J(C,C) coupling constants for variously mono- and disubstituted pyridine N-oxides and monosubstituted pyridines. The DFT data reproduced very well the experimental coupling values and revealed that the FC contribution is the dominating factor which governs the magnitude of the CC coupling across one bond.

Galasso and Carmichael[74] calculated ^1J(C,C) and ^2J(C,C) coupling constants for selected organic compounds containing the ultrashort (bent and unbent) or overlong CC single bond or the shortest C···C nonbonding distance between saturated carbon atoms, reported in the literature so far, by means of the DFT/B3LYP/6-31G(*d*,*p*). They showed that the nature of these extraordinary bonds is rationalized with the *s* and *p* orbital compositions of the atomic hybrid orbitals of the involved carbon atoms. The theoretical values of the ^1J(C,C) and ^2J(C,C) coupling constants, calculated by DFT methodologies, are fully consistent with available experimental evidence and

Table 4.4 *Indirect nuclear spin–spin coupling constants (Hz); all calculations have been carried out at the equilibrium geometry in the HIII basis,[a] except as noted for some MCSCF calculations; in the MCSCF calculations, a 6331 CAS was used except that RAS was used for HCN and full-valence CAS for H_2 and C_2H_4; all experimental results are vibrationally averaged except for H_2, HF and CH_4 for which R_e values are used (taken from ref. 52)*

		RHF	*LDA*	*BLYP*	*B3LYP*	*CAS*	*Exptl.*
H_2	^1J(H,D)	47.3	29.5	44.6	42.6	36.9	41.1[b]
HF	$^1J(^{19}F,H)$	632.7	385.5	373.3	419.5	517.7[c]	500 ± 20[d]
H_2O	$^1J(^{17}O,H)$	−97.1	−6.23	−67.8	−71.8	−74.5[c]	−80.6[e]
NH_3	$^1J(^{14}N,H)$	51.9	34.9	41.8	42.4	42.3[d]	43.6[g]
CH_4	$^1J(^{13}C,H)$	146.1	94.0	123.1	122.4	116.7[d]	120.9[h]
HCN	$^1J(^{15}N,^{13}C)$	−119.7	−7.9	−11.7	−17.2	−19.8[c]	18.5[i]
N_2	$^1J(^{14}N,^{15}N)$	−15.0	3.9	2.9	1.6	0.8[j]	1.8[k]
CO	$^1J(^{13}C,^{17}O)$	−5.0	26.1	22.8	19.5	16.1[j]	16.4[l]
C_2H_4	$^1J(^{13}C,^{13}C)$	1235.9	49.9	66.1	70.1	75.7[m]	67.5[n]
mean err	Hz	127.2	−15.4	−4.5	−7.0	2.2	
mean abs. err.	Hz	170.7	24.4	24.1	11.2	4.9	
stand. dev.	Hz	395.7	39.9	49.0	27.7	7.2	
mean err.	%	119.1	−2.6	12.3	−2.3	−6.5	
mean abs. err.	%	409.7	41.7	30.5	8.4	11.6	
stand. dev.	%	722.9	54.5	40.3	10.6	19.7	

[a] Refs. 56 and 57. [b] Refs. 58 and 59. [c] Ref. 60. [d] Refs. 61, 62 and 63. [e] Ref. 64. [f] HIV basis, ref. 40. [g] Ref. 65. [h] Refs. 66 and 67. [i] Ref. 68. [j] (12*s*7*p*3*d*/8*s*4*p*3*d*) basis, ref. 69. [k] Ref. 70. [l] Ref. 71. [m] *qz* + 2*d*1*f* basis, ref. 40. [n] Ref. 72.

expectation. In particular, the theory predicted an unusually large value of ^1J(C,C) for the ultrashort unbent bond in the bipolyhedron systems, a normal cyclopropanic positive value of ^1J(C,C) for the ultrashort bent bond in the tricyclo[2.1.0.0^{2,5}]pentane derivative, a reduced alkanic value of ^1J(C,C) for the overlong bond in the cyclobutaarene derivatives, and a large negative value of ^2J(C,C) for the shortest nonbonding C···C interaction in the quaternary 1-bicyclo [1.1.1]pentane salt.

Bagno[75] performed the DFT calculations of ^{1}H nuclear shieldings and ^{1}H–^{1}H spin–spin coupling constants in several aromatic and aliphatic organic molecules. Their results showed that the calculation of the FC term is generally sufficient for an estimation of ^{1}H couplings, although this is due to a cancellation of the other two major terms, PSO and DSO. They have also found that, among the various combinations of XC functionals and basis sets, NMR calculations (shieldings and couplings) run at the B3LYP/cc-pVTZ level with B3LYP/6-31G(*d*,*p*) geometry optimizations yield a good compromise between accuracy and cost. The data calculated in this way were directly employed to simulate the observed ^{1}H NMR spectrum at a given frequency.

Berger *et al.*[76] investigated experimentally and theoretically the stereochemical influence on the olefinic ^1J(C,C) coupling constants. The theoretical

values for ^1J(C,C) couplings were evaluated using *ab initio* (MP2/6-31G(*d*)) and DFT(B3LYP/6-31G(*d*)) calculations for model compounds. The calculated and experimental data were in good agreement. The olefinic ^1J(C,C) coupling constants did not show a distinct stereochemical dependence on the distortion of the double bonds. This result was attributed to the fact that the FC contribution to the coupling constants is transmitted *via* the sp^2-type σ-orbitals, whereas the π-type orbitals with a nodal plane at the position of the nuclei do not contribute to the ^{13}C–^{13}C couplings.

Peralta *et al.*[77] implemented calculations of the SD contribution to spin–spin coupling constants within a DFT scheme using the finite perturbation theory (FPT) approach. They tested their FPT-DFT method for calculating the SD term on a set of small molecules, *i.e.*, FH, CO and N_2, and obtained results in excellent agreement with values taken from the literature,[78] which were obtained with the inclusion of electron correlation. They also calculated the SD contribution to J(^{19}F,^{13}C), J(^{19}F, ^{19}F), and J(^{19}F, ^{1}H) couplings in 1,2-, 1,3-, and 1,4-difluorobenzenes. They found an important SD contribution to ^3J(^{19}F, ^{19}F)(*ortho*) and ^5J(^{19}F, ^{19}F)(*para*) couplings, which suggests that the conjugation between the π-type F lone pair orbital and the π-bonding orbital is the main transmission mechanism of the SD interaction.

Case *et al.*[79] analyzed vicinal spin–spin coupling constants, ^3J, in polypeptides using DFT in combination with molecular dynamics (MD) computer simulations. The potential of coupling constants for conformational analysis using NMR data has been recognized in the early days of liquid-state NMR. The establishment of a formal relationship by Karplus[80,81] between a vicinal coupling constant of two spins and their intervening torsion angle has produced a great deal of works and it continues today. Case *et al.* calculated eight ^3J coupling constants of proteins involving the φ and ψ backbone torsion angles. They found that static Karplus curves, which are fitted to the computed couplings as a function of the φ-torsion angle, are generally in good agreement with empirical Karplus curves[82] reported for several proteins if substantial motional averaging effects are taken into account. It was shown that the DFT calculation enhances the power of J-coupling analysis as a unique probe of structural dynamics of biomolecules.

Cloran *et al.*[83] performed DFT calculations of spin–spin coupling constants involving ^{13}C (*i.e.*, J(C,H) and J(C,C) over one, two, and three bonds) in 2-deoxy-D-ribofuranose. The computed J-couplngs were compared to those reported previously to assess the effect of bond rotation on coupling constants within the furanose ring and hydroxymethyl side chain. The results confirmed prevous predictions of correlations between ^2J(C,H), ^3J(C,H), ^2J(C,C), and ^3J(C,C), and ring conformation. Cloran *et al.*[84] also computed ^2J(C-O-C) spin–spin coupling constants across glycosidic linkages as a function of bond angle by the FPT-DFT method at the B3LYP level. The computed coupling data were used to determine torsion angles.

Czernek *et al.*[85] determined the ^3J(H,H), ^2J(H,H) and ^1J(C,H) spin–spin coupling constants for relatively large organic molecules, anhydrodeoxythymidines, both experimentally and theoretically using NMR spectroscopy

and DFT calculations. They obtained a very good agreement between DFT predicted and NMR measured values.

4 *Ab Initio* Calculations

4.1 Correlation Effects. – Core valence correlation (CVC) is known to significantly affect many molecular properties such as bond lengths, harmonic frequencies, dissociation energies, and weak interactions in transition metal complexes.[86–88] However, less is known about the influence of CVC on hyperfine properties, *i.e.*, the nuclear shielding, nuclear spin–spin coupling and nuclear quadrupole coupling tensors. Lantto and Vaara[89] investigated the CVC effect on nuclear spin–spin coupling constants with *ab initio* calculations based on multiconfigurational self-consistent field (MCSCF) reference states. They calculated the ^1J(X,H) and ^2J(H,H) coupling constants in first- and second-row hydrides to examine the effect of including the core and semicore orbitals in the active molecular orbital space. They considered the effects of using a multireference wave function instead of a single-reference one, as well as different numbers of electrons in the virtual orbitals. In second-row hydrides, the inclusion of semicore orbitals in the active space was found to be necessary for accurate calculation of ^1J(X,H) couplings involving the heavy nuclei. A smaller but nonnegligible semicore effect was observed for the ^2J(H,H) couplings.

Jaszuński and Ruud[90] presented accurate *ab initio* calculations of the indirect spin–spin coupling constants of acetylene. They used very large basis sets (the largest basis was an uncontracted (20*s*9*p*5*d*3*f*1*g*/11*s*4*p*2*d*1*f*)) and large MCSCF expansions. The best values calculated by them are ^1J(C,C) = 184.68 Hz, ^1J(C,H) = 244.27 Hz, ^2J(C,H) = 53.08 Hz, and ^3J(H,H) = 10.80 Hz. The experimental values recently obtained (by adding the nuclear motion corrections to the equilibrium geometry values)[91,92] are ^1J(C,C) = 185.04 Hz, ^1J(C,H) = 242.70 Hz, ^2J(C,H) = 53.82 Hz and ^3J(H,H) = 10.89 Hz. The calculated coupling constants are in good agreement with the experimental estimates. In percentage terms, the difference between the computed and experimental values is 1.4% for ^2J(C,H) and below 1% for the other constants.

4.2 Scalar Couplings as a Function of Interatomic Distance. – In previous work, Bacskay[93] presented a theoretical analysis of the effect of bond stretching on the ^1J(H,D) coupling of HD for a large range of interatomic H–D distances, R. A dramatic increase of about seven orders of magnitude was found for the FC contribution to the ^1J(H,D) coupling in the range between the equilibrium distance ($\sim$ 1.4 a.u.) and a distance of $\sim$ 11 a.u. This enormously large increase of ^1J(H,D) was ascribed to the near degeneracy of the ground $^1\Sigma_g^+$ and first excited $^3\Sigma_u^+$ states of the system for large interatomic distances. Vizioli and Ruiz de Azúa[94] made a theoretical study of the dependence of the ^1J(H,D) coupling in HD on the interatomic distance R in the presence of a static uniform magnetic field $\vec{B}_0$. They performed full

configuration interaction (FCI) calculations for the effect of a uniform static magnetic field $\vec{B}_0$ (which could be thought of as the spectrometer field in an NMR measurement) on the ^1J(H,D) *vs.* R curve. They found that the interaction of electrons with the field $\vec{B}_0$ produces a splitting of the $^3\sum_u^+$ level and an energy degeneracy with the $^1\sum_g^+$ level occurs at a shorter interatomic distance than that obtained when the magnetic field is absent. Thus, the ^1J(H,D) coupling constant is affected strongly by the presence of the magnetic field $\vec{B}_0$. They found that the FC term of ^1J(H,D) is initially independent of B_0 and increases by several orders of magnitude, in agreement with the previous results by Bacskay,[93] until a critical distance $R(B_0)$ is reached, but beyond which it suddenly vanishes. The quenching of ^1J(H,D) at $R(B_0)$ is due to the splitting of the $^3\sum_u^+$ state in the presence of the field $\vec{B}_0$.

Pecul[95] calculated the dependence of the He–He nuclear spin–spin coupling constant $^1J(^3\text{He},^3\text{He})$ for the helium dimer on the interatomic distance R using FCI and equation-of-motion coupled cluster singles and doubles (EOM-CCSD) methods. They found that the FC contribution to the $^1J(^3\text{He},^3\text{He})$ coupling has a nonnegligible value of 1.3 Hz at $R = 5.6$ a.u., while the other noncontact contributions are zero there. This suggests that nuclear spin–spin coupling constants transmitted through van der Waals interactions are a much more common phenomenon than previously thought. It was concluded that the scalar nuclear spin–spin coupling can be transmitted through van der Waals interactions (which are much weaker than the hydrogen-bonding interactions). All contributions to the $^1J(^3\text{He},^3\text{He})$ coupling constant exhibited sharp exponential decays with the internuclear distance R.

4.3 Anisotropy of the Spin–Spin Coupling Tensor. – In NMR experiments performed in anisotropic liquid crystal (LC) phases or in the solid state, the anisotric part of an indirect nuclear spin–spin coupling tensor $\hat{J}$ appears combined with the direct dipolar coupling D. The NMR spin Hamiltonian appropriate for spin 1/2 nuclei in molecules partially oriented in uniaxial LC solvents can be written in the high field approximation as

$$\mathcal{H} = -(B_0/2\pi)\sum_i \gamma_i(1-\sigma_i)I_{iz} + \sum_{i<j} J_{ij}^{iso}\vec{I}_i\cdot\vec{I}_j + \sum_{i<j}(D_{ij} + 1/2J_{ij}^{aniso})(3I_{iz}I_{jz} - \vec{I}_i\cdot\vec{I}_j) \tag{4.21}$$

where B_0 is the strength of the static magnetic field of the spectrometer $\vec{B}_0$ (in the z direction of the laboratory-fixed frame), γ_i, $\vec{I}_i$, and σ_i are the gyromagnetic ratio, dimensionless nuclear spin operator, and nuclear shielding (sum of the isotropic and anisotropic contributions) of nucleus i, respectively. The direct dipolar coupling D_{ij} is defined as

$$D_{ij} = -(\mu_o\hbar\gamma_i\gamma_j/8\pi^2)\langle S_{ij}/r_{ij}^3\rangle \tag{4.22}$$

where μ_0 is the permeability of a vacuum, r_{ij} is the length of the internuclear

vector $\vec{r}_{ij}$, and S_{ij} is called the order parameter of $\vec{r}_{ij}$ with respect to the magnetic field $\vec{B}_0$. S_{ij} is defined as[96]

$$S_{ij} = (3\cos^2\theta - 1)/2, \tag{4.23}$$

where θ is the angle between $\vec{r}_{ij}$ and $\vec{B}_0$. The experimental $1/2J_{ij}^{aniso}$ is given by the difference between the experimentally determined $(D_{ij} + 1/2H_{ij}^{aniso})$ and the calculated D_{ij} couplings. Lantto *et al.*[97] obtained all spin–spin coupling tensors $\hat{J}$ of the fluoromethanes, *i.e.*, CH_3F, CH_2F_2 and CHF_3, theoretically by multiconfiguration self-consistent field linear response (MCLR)[98,99] *ab initio* calculations. Furthermore, they determined the principal values and the orientations of the principal axes of each theoretical $\hat{J}$ tensor. The computed theoretical values for $J^{iso} = (J_{x'x'} + J_{y'y'} + J_{z'z'})/3$, $\Delta J = J_{z'z'} - 1/2(J_{x'x'} + J_{y'y'})$, and $J_{x'x'} - J_{y'y'}$ were compared with the experimentally determined values. Here, the z' axis is parallel with the molecular symmetry axis. A very good agreement was obtained between the calculated and experimental isotropic couplings, and a reasonable agreement was found for the anisotropic values. For example, in the case of CHF_3, the calculated and experimental values for $\Delta^2 J(\mathrm{F,F})$ are -232 Hz and -200 Hz, respectively.

Bryce and Wasylishen[100] investigated symmetry properties of indirect nuclear spin–spin coupling tensors of ClF_3 and OF_2. The full coupling tensor $\hat{J}$ may be decoupled into three parts: isotropic (J^{iso}), symmetric ($\hat{J}^{sym}$), and antisymmetric ($\hat{J}^{antisym}$) parts.[101–104] The isotropic portion is defined as one-third the trace of the tensor. The symmetric portion of the tensor, which is constructed from $\hat{J}$ and its transpose $\hat{J}^T$, is defined as

$$\hat{J}^{sym} = (\hat{J} + \hat{J}^T)/2 - J^{iso}1 \tag{4.24}$$

$\hat{J}^{sym}$ may posses up to five independent elements. The antisymmetric portion of $\hat{J}$ may have up to three independent elements and is defined as

$$\hat{J}^{antisym} = (\hat{J} - \hat{J}^T)/2 \tag{4.25}$$

It has long been known that, for powdered samples containing tightly coupled spin systems observed under the condition of magic-angle spinning, $\hat{J}^{antisym}$ should affect the observed spectrum.[105] Nevertheless, no experimental determinations of $\hat{J}^{antisym}$ exist. The MCSCF calculation by Bryce and Wasylishen showed that not only $\hat{J}^{antisym}$ exists, but also there is no reason to presume that these components will be small compared to their symmetric counterparts.

4.4 Effects of Internal Rotation and Bond Stretching. – Pecul and Sadlej[106] calculated the effects of internal rotation and bond stretching on the spin–spin coupling constants in CH_3OH and CH_3NH_2 molecules at the MCSCF level. Furthermore, they estimated the effects of water solvent (whose dielectric constant is 78.54) using the reaction field theory.[107] They optimized the molecular geometry (bond distances and bond angles) for each value of the internal rotation angle (dihedral angle). The internal rotation caused consider-

able changes not only in ^3J(H,H) but in ^1J(C,H), ^2J(O,H), and ^2J(N,H) as well. The coupling constants in the methyl group and some of the geminal couplings in polar moieties, ^2J(O,H), ^2J(N,H), and ^2J(H–N–H), exhibited a differential sensitivity to bond length variations. This phenomenon did not emerge for the ^1J couplings involving nuclei with lone pairs. The solvent effects were substantial for the ^1J coupling constants and for some of the ^2J coupling constants but negligible for ^3J(H,H). It was found that the solvent effects in ^1J(C,H) and ^2J(H–C–H) couplings depend considerably on the molecular conformation. All effects were dominated by the changes in the FC contribution.

Sauer and Raynes[108] investigated differential sensitivities of nuclear spin–spin coupling constants to bond stretching in BH_4^-, NH_4^-, and SiH_4 using correlated *ab initio* calculations of the second-order polarization propagator approximation (SOPPA)[109–111] and SOPPA-CCSD.[112] They found that stretching one of the Si–H bonds in silane from its equilibrium value increases the ^1J(Si,H) coupling of the other three bonds by more than the increase of ^1J(Si,H) of the stretched bond. This "unexpected differential sensitivity", or UDS for short,[113] in silane was considerably greater in terms of reduced coupling constants K than the same effect discovered previously in methane.[114,115] Similar UDS effects in ^1J(X,H) couplings were also found to occur in the BH_4^- and NH_4^+ ions. It was shown that these UDS effects come overwhelmingly from the FC term. For the ^2J(H,H) coupling, the UDS due to the stretch of a single bond was found earlier in methane. The UDS in the ^2J(H,H) coupling occurred also in NH_4^+, but did not appear in BH_4^- and SiH_4. They discussed the origins of UDS and the sign of the derivatives of the coupling constants. It is evident from earlier studies that the presence of UDS occurs only in the absence of lone pairs on each of the nuclei involved and that it is usually a correlation effect.

Grayson and Sauer[116] computed the coefficients in a Karplus-type equation[80,81] of the spin–spin coupling constants for a series of rotated ethane geometries. The coupling constants were calculated at the SCF, SOPPA, and SOPPA-CCSD levels and compared with results of previous calculations and experimental data. It was found that the coefficients in the Karplus equation calculated at the SOPPA-CCSD level are in good agreement with coefficients derived from experimental coupling constant data or results of MCSCF calculations.

5 Through-space and Hydrogen Bond Scalar Couplings

5.1 Through-space Scalar Coupling. – Arnold *et al.*[117] calculated the long-range $^nJ(^{19}F,^{19}F)$ ($n > 3$) couplings in small organic molecules by using the DFT method. The calculated results reproduced the exponential distance dependence of J seen experimentally, demonstrated the dominance of the FC contribution, and ruled out any significant covalent or through-bond contributions to J in the investigated systems. The calculation was also able to clearly elucidate the abnormally small J-coupling seen previously in phenanthrenes

and cyclohexenes by more distorted but less sterically hindered structures in these molecules where the F–F distances are increased and the $J(^{19}F,^{19}F)$ couplings are thereby reduced. All that is required for through-space scalar couplings is Fermi contact and the close spatial proximity of atoms. This result is of considerable current interest in the context of hydrogen bond *J*-couplings in macromolecules.

5.2 Hydrogen Bond Scalar Couplings. – Del Bene and Jordan[118] calculated the $^{2h}J(^{35}Cl,^{15}N)$ coupling constant of the hydrogen-bonded complex $ClH{:}NH_3$ at the EOM-CCSD level. They previously investigated the equilibrium Cl–N distances and proton-stretching frequencies as a function of the strength of external electric fields applied along the hydrogen-bonding Cl–H–N direction.[119] They found in ref. 119 that the Cl–N distances and anharmonic proton-stretching frequencies change as a function of field strength. In the present paper, they showed that relationships exist among the Cl–N distance, the anhormonic proton-stretching frequency, the ^1H NMR chemical shift, and the $^{2h}J(^{35}Cl,^{15}N)$ spin–spin coupling constant in the $ClH:NH_3$ complex. Since both ^{35}Cl (I = 3/2) and ^{37}Cl (I = 3/2) have nonzero quadrupole moments, Cl–N coupling constants have not been experimentally observed.

Del Bene and Bartlett[120] performed EOM-CCSD calculations of $^{2h}J(^{15}N,^{15}N)$ coupling constants in complexes with N–H···N hydrogen bonds. They found that the relationship between the $^{2h}J(^{15}N,^{15}N)$ spin–spin coupling constant across the hydrogen bond and the equilibrium intermolecular N–N distance R_e holds for all complexes, irrespective of the hybridization of the nitrogen in the proton-donor and proton-acceptor molecules. All the computed points were therefore fitted by the same $^{2h}J(^{15}N,^{15}N)$ *vs.* R_e curve. The $^{2h}J(^{15}N,^{15}N)$ coupling constant obtained from the curve at an equilibrium distance of 2.90 Å is 7.4 Hz, which is in good agreement with the experimental value of 7 Hz observed for the $^{2h}J(^{15}N,^{15}N)$ coupling constants across N–H···N hydrogen bonds in the adenine–uracil (A-U) and guanine–cytosine (G–C) base pairs.[121] Del Bene *et al.*[122] performed EOM-CCSD calculations to evaluate the $^{4h}J(^{31}P,\ ^{31}P)$ coupling constants across an $N–H^+–N$ hydrogen bond in a model system. They computed $^{4h}J(^{31}P,\ ^{31}P)$ coupling constants as a function of N–N distance *R*. The calculated $^{4h}J(^{31}P,\ ^{31}P)$ values were in good agreement with an experimentally measured value of the $^{4h}J(^{31}P,\ ^{31}P)$ coupling constant.

Chapman *et al.*[123] calculated the $^{2h}J(^{35}Cl,^{15}N)$ spin–spin coupling constant in the hydrogen-bonded complex ClH:pyridine at the EOM-CCSD level without and with external electric fields. The equilibrium structure at each field strength was calculated using the second-order Møller–Plesset perturbation theory (MP2) method. They showed that the magnitude of the $^{2h}J(^{35}Cl,^{15}N)$ coupling constant across the hydrogen bond initially increases as the field strength increases, exhibits a maximum at the field of 0.0040 a.u., and then decreases with increasing field strength. The equilibrium Cl–N distance and the proton-stretching frequency showed the same trend as the coupling constant.

However, the chemical shift of the hydrogen-bonded proton had a maximum at a field of 0.0040 a.u., but it did not decrease dramatically at higher fields. It was shown that the IR frequency and NMR coupling constant are fingerprints of hydrogen bond type from which the intermolecular distance in a complex, *R*, may be determined. An external field preferentially stabilizes more polar structures, so the hydrogen bond type changes from traditional, to proton-shared, and finally to ion-pair as the field strength increases.

Pecul *et al.*[124] evaluated both intra- and intermolecular spin–spin coupling constants for the models of biological systems: formamide–formamide (Fa–Fa) and formamide-formamidine (Fa–Fi) dimers using the MCSCF method. The Fa–Fa complex was chosen as a model of hydrogen bonding in peptides while the Fa–Fi complex serves as a model of interaction between complementary pairs of nucleic bases (adenine–thymine (A–T) in DNA or adenine–uracil (A–U) in RNA).[125–127] The geometries of the Fa–Fa and Fa–Fi complexes were optimized using the MP2 (frozen core)/aug-cc-pVDZ calculations. It is indicated that the performance of DFT rapidly deteriorates with the number of lone pairs borne by the coupled nuclei.[42] Therefore, they calculated the scalar spin–spin coupling constants by using the linear response MCSCF method[40,58] with the inclusion of all four terms contributing to the isotropic couplings. They showed that the intramolecular coupling constants of ^{1}J(N,H) and ^{2}J(N,H) are significantly changed by the hydrogen bond formation. The hydrogen-bond transmitted coupling constants, ^{1h}J(N,H) and ^{2h}J(N,H), calculated for the Fa–Fi dimer were in agreement with recent experimental results for nucleic acids. The ^{1h}J(N,H) and ^{2h}J(N,H) couplings were dominated by the FC term and decreased rapidly with increase in the distance between the coupled nuclei, *R*. On the other hand, the proton–proton intermolecular coupling constants were dominated by the DSO and PSO terms and were less distance dependent.

Barfield *et al.*[128] calculated the FC contributions to scalar coupling constants in the imino hydrogen-bonding region of Hoogsteen–Watson–Crick T·A–T and C^{+}·G–C triplets as a function of the distance between proton donor and acceptor nitrogen atoms, *R*, using the FPT-DFT method at the unrestricted B3PW91/6-311G** level.[46,129,130] All three scalar couplings and all three chemical shifts were strongly interrelated and exhibited monotonic changes with *R*. These correlations were in conformity with experimental data for the 32-nucleotide DNA triplex. In addition to the FPT-DFT calculation, they presented a simple three-orbital model of the N–H···N bond and an SOS analysis. This model reproduced the basic features of the H-bond coupling effect.

Bango[131] presented the FC contribution calculation of through-hydrogen bond spin–spin coupling constants in the formamide dimer and ubiquitin with the use of the FPT-DFT/B3LYP method. They showed that the magnitude of ^{3h}J(N,C) coupling constant in the hydrogen-bonded foramide dimer is relatively insensitive to the dihedral angle between the two amide planes. They also calculated scalar coupling constants in fragments of the ubiquitin protein in which all amino acids except those involved in hydrogen bonding were

removed. Although calculated ^{3h}J(N,C) values were sometimes overestimated, they generally correlated with the corresponding experimental values.[132] The hydrogen bond plays an essential role in maintaining the three-dimensional structure of proteins, nucleic acids, and carbohydrates.[133] Fiernan *et al.*[134] calculated the FC contribution to ^{2h}J(H,H) scalar coupling constants between hydrogen-bonded hydroxyl groups (O–H···O–H) at the FPT-DFT level with an MP2/6-31G* geometry optimization and found the calculated results to be in general agreement with experimental data.

6 References

1 N. F. Ramsey, *Phys. Rev.*, 1953, **91**, 303.
2 P. Pyykkö, *Theor. Chem. Acc.*, 2000, **103**, 214.
3 P. Pyykkö, *Chem. Rev.*, 1988, **88**, 563.
4 T. Zieglar, J. G. Snijders, and E. J. Baerends, *J. Chem. Phys.*, 1981, **74**, 1271.
5 J. G. Snijders and P. Pyykkö, *Chem. Phys. Lett.*, 1980, **75**, 5.
6 T. Ziegler, J. G. Snijders, and E. J. Baerends, *Chem. Phys. Lett.*, 1980, **75**, 1.
7 P. Pyykkö, *Chem. Phys.*, 1977, **22**, 289.
8 G. A. Aucar and J. Oddershede, *Int. J. Quantum Chem.*, 1993, **47**, 425.
9 J. Autschbach and T. Ziegler, *J. Chem. Phys.*, 2000, **113**, 936.
10 J. Autschbach and T. Ziegler, *J. Chem. Phys.*, 2000, **113**, 9410.
11 J. Autschbach and T. Ziegler, *J. Am. Chem. Soc.*, 2001, **123**, 3341.
12 J. Autschbach and T. Ziegler, *J. Am. Chem. Soc.*, 2001, **123**, 5320.
13 E. van Lenthe, E. J. Baerends, and J. G. Snijders, *J. Chem. Phys.*, 1993, **99**, 4597.
14 E. van Lenthe, E. J. Baerends, and J. G. Snijders, *J. Chem. Phys.*, 1994, **101**, 9783.
15 E. van Lenthe, R. van Leeuwen, E. J. Baerends, and J. G. Snijders, *Int. J. Quantum Chem.*, 1996, **57**, 281.
16 S. T. Epstein, in *The Variation Method in Quantum Chemistry*, Academic, New York, 1974.
17 H. Hellmann, *Z. Phys.*, 1933, **85**, 180.
18 R. P. Feynman, *Phys. Rev.*, 1939, **56**, 340.
19 P. A. M. Dirac, in *The Principles of Quatum Mechanics*, Clarendon, London, 4th Edn., 1983.
20 W. Kutzelnigg, *Chem. Phys.*, 1997, **225**, 203.
21 L. L. Foldy and S. A. Wouthuysen, *Phys. Rev.*, 1950, **78**, 29.
22 A. J. Sadlej, J. G. Snijders, E. van Lenthe, and E. J. Baerends, *J. Chem. Phys.*, 1995, **102**, 1758.
23 W. Kutzelnigg, *J. Chem. Phys.*, 1999, **110**, 8283.
24 J. Autschbach and W. H. E. Schwarz, *Theor. Chem. Acc.*, 2000, **104**, 82.
25 H. Fukui, *Prog. Nucl. Mang. Reson. Spectrosc.*, 1999, **35**, 267.
26 A. Messiah, in *Quantum Mechanics*, North-Holland, Amsterdam, 1961.
27 R. van Leeuwen, E. van Lenthe, E. J. Baerends, and J. G. Snijders, *J. Chem. Phys.*, 1994, **101**, 1272.
28 D. L. Bryce and R. Wasylishen, *J. Am. Chem. Soc.*, 2000, **122**, 3197.
29 T. Ziegler, V. Tschinke, E. J. Baerends, J. G. Snijders, and W. Ravenek, *J. Phys. Chem.*, 1989, **93**, 3050.
30 G. Schreckenbach, T. Ziegler, and J. Li, *Int. J. Quantum Chem.*, 1995, **56**, 477.

31 A. J. Brown, O. W. Howarth, and P. Moore, *J. Chem. Soc., Dalton Trans.*, 1976, 1589.
32 A. Sebald and B. Wrackmeyer, *J. Magn. Reson.*, 1985, **63**, 397.
33 P. L. Goggin, R. J. Goodfellow, D. M. McEwan, A. J. Griffiths, and K. Kessler, *J. Chem. Res.*, 1979, (*M*), 2315.
34 K. E. Berg, J. Glaser, M. C. Read, and I. Tóth, *J. Am. Chem. Soc.*, 1995, **117**, 7550.
35 M. Maliarik, K. E. Berg, J. Glaser, M. Sandström, and I. Tóth, *Inorg. Chem.*, 1998, **37**, 2910.
36 M. R. Russo and N. Kaltsoyannis, *Inorg. Chim. Acta*, 2001, **312**, 221.
37 L. Visscher, T. Enevoldsen, T. Saue, H. J. Aa. Tensen, and J. Oddershede, *J. Comput. Chem.*, 1999, **20**, 1262.
38 T. Enevoldsen, L. Visscher, T. Saue, H. J. Aa. Jensen, and J. Oddershede, *J. Chem. Phys.*, 2000, **112**, 3493.
39 J. Khandogin and T. Ziegler, *J. Phys. Chem. A*, 2000, **104**, 113.
40 T. Helgaker, M. Jaszuński, and K. Ruud, *Chem. Rev.*, 1999, **99**, 293.
41 V. G. Malkin, O. L Malkina, and D. R. Salahub, *Chem. Phys. Lett.*, 1994, **221**, 91.
42 O. L Malkina, D. R. Salahub, and V. G. Malkin, *J. Chem. Phys.*, 1996, **105**, 8793.
43 R. M. Dickson and T. Ziegler, *J. Phys. Chem.*, 1996, **100**, 5286.
44 V. G. Malkin, O. L Malkina, M. E. Casida, and D. R. Salahub, *J. Am. Chem. Soc.*, 1994, **116**, 5898.
45 V. Sychrovský, J. Gräfenstein, and D. Cremer, *J. Chem. Phys.*, 2000, **113**, 3530.
46 A. D. Becke, *J. Chem. Phys.*, 1993, **98**, 5648.
47 P. J. Stephens, F. J. Devlin, C. F. Chabalowski, and M. J. Frisch, *J. Chem. Phys.*, 1994, **98**, 11623.
48 V. G. Malkin, O. L. Malkina, L. A. Eriksson, and D. R. Salahub, in *Modern Density Functional Theory*, ed. J. M. Seminario and P. Politzer, Elsevier, Amsterdam, 1995.
49 H. O. Kalinowski, S. Berger, and S. Braun, in *^{13}C-NMR-Spektroskopie*, Georg Thieme Verlag, Stuttgart, 1984.
50 W. Kutzelnigg, U. Fleischer, and M. Schindler, in *NMR – Basic Principles and Progress*, Springer, Heidelberg, 1990, Vol. 23, p. 165.
51 S. Castellano and C. Sun, *J. Am. Chem. Soc.*, 1966, **88**, 4741.
52 T. Helgaker, M. Watson, and N. C. Handy, *J. Chem. Phys.*, 2000, **113**, 9402.
53 S. J. Vosko, L. Wilk, and M. Nusair, *Can. J. Phys.*, 1980, **58**, 1200.
54 A. D. Becke, *Phys. Rev. A*, 1988, **38**, 3098.
55 C. Lee, W. Yang, and R. G. Parr, *Phys. Rev. B*, 1988, **37**, 785.
56 S. Huzinaga, in *Approximate Atomic Functions*, University of Alberta, Edmonton, 1971.
57 S. Huzinaga, *J. Chem. Phys.*, 1965, **42**, 1293.
58 O. Vahtras, H. Ågren, P. Jørgensen, H. J. Aa. Jensen. S. B. Padkjaer, and T. Helgaker, *J. Chem. Phys.*, 1992, **96**, 6120.
59 Y. I. Neronov and A. E. Barsach, *Zh. Eksp. Teor. Fiz.*, 1975, **69**, 1872.
60 T. Helgaker, M. Jaszuński, K. Ruud, and A. Gorska, *Theor. Chem. Acc.*, 1998, **99**, 175.
61 S. M. Bass, R. L. DeLeon, and J. S. Muenter, *J. Chem. Phys.*, 1987, **86**, 4305.
62 J. S. Muenter and W. Klemperer, *J. Chem. Phys.*, 1970, **52**, 6033.
63 P.-O. Åstrand, K. Ruud, K. V. Mikkelsen, and T. Helgaker, *J. Chem. Phys.*, 1999, **110**, 9463.

64 N. M. Sergeyev, N. D. Sergeyeva, Y. A. Strelenko, and W. T. Raynes, *Chem. Phys. Lett.*, 1997, **277**, 142.
65 R. A. Bernheim and H. Batis-Hernandez, *J. Chem. Phys.*, 1964, **40**, 3446.
66 B. Bennett, W. T. Raynes, and C. W. Anderson, *Spectrochim. Acta, Part A*, 1989, **45**, 821.
67 F. A. L. Anet and D. J. O'Leary, *Tetrahedron Lett.*, 1989, **30**, 2755.
68 G. Dombi, P. Diehl, J. Lounila, and R. Wasser, *Org. Magn. Reson.*, 1984, **22**, 573.
69 O. Vahtras, H. Ågren, P. Jørgensen, T. Helgaker, and H. J. Aa. Jensen, *Chem. Phys. Lett.*, 1993, **209**, 201.
70 J. O. Friedrich and R. E. Wasylishen, *J. Chem. Phys.*, 1985, **83**, 3707.
71 R. E. Wasylishen, J. O. Friedrich, S. Mooibroek, and J. B. Macdonald, *J. Chem. Phys.*, 1985, **83**, 548.
72 J. Kaski, P. Lantto, J. Vaara, and J. Jokisaari, *J. Am. Chem. Soc.*, 1998, **120**, 3993.
73 K. Kamieńska-Trela, L. Kania, P. Bernatowicz, M. Bechcicka, L. Kaczmarek, and J. Wójcik, *Spectrochim. Acta, Part A*, 2000, **56**, 2079.
74 V. Galasso and I. Carmichael, *J. Phys. Chem. A*, 2000, **104**, 6271.
75 A. Bagno, *Chem. Eur. J.*, 2001, **7**, 1652.
76 S. Berger, A. Krebs, B. Thölke, and H-U. Siehl, *Magn. Reson. Chem.*, 2000, **38**, 566.
77 J. E. Peralta, V. Barone, M. C. Ruiz de Azúa, and R. H. Contreras, *Mol. Phys.*, 2001, **99**, 655.
78 J. Geertsen, J. Oddershede, W. T. Raynes, and G. E. Scuseria, *J. Magn. Reson.*, 1991, **93**, 458.
79 D. A. Case, C. Scheurer and R. Brüschweiler, *J. Am. Chem. Soc.*, 2000, **122**, 10390.
80 M. Karplus, *J. Chem. Phys.*, 1959, **30**, 11.
81 M. Karplus, *J. Am. Chem. Soc.*, 1963, **85**, 2870.
82 A. C. Wang and A. Bax, *J. Am. Chem. Soc.*, 1995, **117**, 1810.
83 F. Cloran, I. Carmichael, and A. S. Serianni, *J. Am. Chem. Soc.*, 2001, **123**, 4781.
84 F. Cloran, I. Carmichael, and A. S. Serianni, *J. Am. Chem. Soc.*, 2000, **122**, 396.
85 J. Czernek, J. Lang, and V. Sklenár, *J. Phys. Chem. A*, 2000, **104**, 2788.
86 J. Styszynski, *Chem. Phys. Lett.*, 2000, **317**, 351.
87 M. Urban and A. J. Sadlej, *J. Chem. Phys.*, 2000, **112**, 5.
88 C. W. Bauschlicher, Jr., S. R. Langhoff, and P. R. Taylor, *J. Chem. Phys.*, 1988, **88**, 2540.
89 P. Lantto and J. Vaara, *J. Chem. Phys.*, 2001, **114**, 5482.
90 M. Jaszuński and K. Ruud, *Chem. Phys. Lett.*, 2001, **336**, 473.
91 K. Jackowski, M. Wilczek, M. Pecul, and J. Sadlej, *J. Phys. Chem. A*, 2000, **104**, 5955.
92 R. D. Wigglesworth, W. T. Raynes, S. Kirpekar, J. Oddershede, and S. P. A. Sauer, *J. Chem. Phys.*, 2000, **112**, 3735.
93 G. B. Bacskay, *Chem. Phys. Lett.*, 1995, **242**, 507.
94 C. V. Vizioli and M. C. Ruiz de Azúa, *Mol. Phys.*, 2000, **98**, 891.
95 M. Pecul, *J. Chem. Phys.*, 2000, **113**, 10835.
96 J. Lounila and J. Jokisaari, *Prog. Nucl. Magn. Reson. Spectrosc.*, 1982, **15**, 249.
97 P. Lantto, J. Kaski, J. Vaara, and J. Jokisaari, *Chem. Eur. J.*, 2000, **6**, 1395.
98 P. Jørgensen, H. J. Aa. Jensen, and J. Olsen, *J. Chem. Phys.*, 1988, **89**, 3654.
99 J. Olsen, D. L. Yeager, and P. Jørgensen, *Chem. Phys.*, 1989, **91**, 381.

100 D. L. Bryce and R. E. Wasylishen, *J. Am. Chem. Soc.*, 2000, **122**, 11236.
101 A. D. Buckingham and J. A. Pople, *Trans. Faraday Soc.*, 1963, **59**, 2421.
102 A. D. Buckingham and I. Love, *J. Magn. Reson.*, 1970, **2**, 338.
103 J. B. Robert and L. Wiesenfeld, *Phys. Rep.*, 1982, **86**, 363.
104 R. E. Wasylishen, in *Encyclopedia of Nuclear Magnetic Resonance*, ed. D. M. Grant and R. K. Harris, Wiley Inc., Chichester, 1996, p. 1685.
105 E. R. Andew and L. F. Farnell, *Mol. Phys.*, 1968, **15**, 157.
106 M. Pecul and J. Sadlej, *Chem. Phys.*, 2000, **255**, 137.
107 P.-O. Åstrand, K. V. Mikkelsen, P. Jørgensen, K. Ruud, and J. Helgaker, *J. Chem. Phys.*, 1998, **108**, 2528.
108 S. P. A. Sauer and W. T. Raynes, *J. Chem. Phys.*, 2000, **113**, 3121.
109 E. S. Nielsen, P. Jørgensen, and J. Oddershede, *J. Chem. Phys.*, 1980, **73**, 6238.
110 M. J. Packer, E. K. Dalskov, T. Enevoldsen, H. J. Aa. Jensen, and J. Oddershede, *J. Chem. Phys.*, 1996, **105**, 5886.
111 K. L. Bak, H. Koch, J. Oddershede, O. Christiansen, and S. P. A. Sauer, *J. Chem. Phys.*, 2000, **112**, 4173.
112 S. P. A. Sauer, *J. Phys. B*, 1997, **30**, 3773.
113 W. T. Raynes, J. Geertsen, and J. Oddershede, *Chem. Phys. Lett.*, 1992, **197**, 516.
114 J. Geertsen, J. Oddershede, W. T. Raynes, and T. L. Marvin, *Mol. Phys.*, 1994, **82**, 29.
115 R. D. Wigglesworth, W. T. Raynes, S. P. A. Sauer, and J. Oddershede, *Mol. Phys.*, 1997, **92**, 77.
116 M. Grayson and S. P. A. Sauer, *Mol. Phys.*, 2000, **98**, 1981.
117 W. D. Arnold, I. Mao, H. Sun, and E. Oldfield, *J. Am. Chem. Soc.*, 2000, **122**, 12164.
118 J. E. Del Bene and M. J. T. Jordan, *J. Am. Chem. Soc.*, 2000, **122**, 4794.
119 M. J. T. Jordan and J. E. Del Bene, *J. Am. Chem. Soc.*, 2000, **122**, 2101.
120 J. E. Del Bene and R. J. Bartlett, *J. Am. Chem. Soc.*, 2000, **122**, 10480.
121 A. J. Dingley and S. Grzesiek, *J. Am. Chem. Soc.*, 1998, **120**, 8293.
122 J. E. Del Bene, S. A. Perera, R. J. Bartlett, I. Alkorta, and J. Elguero, *J. Phys. Chem. A*, 2000, **104**, 7165.
123 K. Chapman, D. Crittenden, J. Bevitt, and M. J. T. Jordan, *J. Phys. Chem. A*, 2001, **105**, 5442.
124 M. Pecul, J. Leszczynski, and J. Sadlej, *J. Phys. Chem. A*, 2000, **104**, 8105.
125 N. Zhanpeisov and J. Leszczynski, *J. Phys. Chem. A*, 1999, **103**, 8317.
126 J. Sponer and P. Hobza, *Chem. Phys. Lett.*, 1997, **267**, 263.
127 J. Sponer and P. Hobza, *J. Phys. Chem. A*, 2000, **104**, 4592.
128 M. Barfield, A. J. Dingley, J. Feigon, and S. Grzesiek, *J. Am. Chem. Soc.*, 2001, **123**, 4014.
129 Y. Wang and J. P. Perdew, *Phys. Rev. B*, 1991, **44**, 13298.
130 J. P. Perdew and Y. Wang, *Phys. Rev. B*, 1992, **45**, 13244.
131 A. Bagno, *Chem. Eur. J.*, 2000, **6**, 2925.
132 F. Cordier and S. Grzesiek, *J. Am. Chem. Soc.*, 1999, **121**, 1601.
133 G. A. Jeffrey and W. Saenger, in *Hydrogen Bonding in Biological Structures*, Springer, New York, 1991.
134 M. Fierman, A. Nelson, S. I. Khan, M. Barfield, and D. J. O'Leary, *Org. Lett.*, 2000, **2**, 2077.

5
Applications of Spin–Spin Couplings

BY KRYSTYNA KAMIEŃSKA-TRELA AND JACEK WÓJCIK

1 Introduction

The material in this chapter covers the period from 1 June 2000 to 31 May 2001. It has been arranged as was done previously,[1] *i.e.* according to (i) the increasing atomic number of the nuclei involved, and (ii) the number of the bonds separating them. We follow the IUPAC[2] recommendations with one notable exception, namely, the nucleus with the smaller mass is given first. For the sake of simplicity the following symbols were used throughout the paper: H for ^{1}H, D – ^{2}H, T – ^{3}H, Li – ^{6}Li, Be ^{9}Be, B – ^{11}B, C – ^{13}C, N – ^{15}N, O – ^{17}O, F – ^{19}F, Al – ^{27}Al, Si – ^{29}Si, P – ^{31}P, Mn – ^{35}Mn, Fe – ^{57}Fe, Co – ^{59}Co, Cu – ^{65}Cu, Se – ^{77}Se, Y – ^{89}Y, Nb – ^{93}Nb, Ru – ^{99}Ru, Tc – ^{99}Tc, Rh – ^{103}Rh, Ag – ^{109}Ag, Cd – ^{113}Cd, Sn – ^{119}Sn, Te – ^{125}Te, I – ^{127}I, Cs – ^{133}Cs, W – ^{183}W, Os – ^{187}Os, Pt – ^{195}Pt, Hg – ^{199}Hg, Tl – ^{205}Tl, Pb – ^{207}Pb. All the other isotopes are described explicitly.

An extensive review on the angular dependence of spin–spin couplings has been written by Contreras and Peralta.[3]

An interesting introductory review on recently discovered hydrogen bond scalar couplings has been written by Dingley *et al.*[4] Riek *et al.*[5] have briefly reviewed the use of the TROSY concept in measurements of $^{h}J_{NN}$ couplings across hydrogen bonds in very large molecules in solution, and in a comprehensive review Mollova and Pardi[6] have collected new methods for determination of couplings across hydrogen bonds in nucleic acids.

Multinuclear chemical shift and coupling NMR data of azo dyes and their metal complexes have been collected and discussed by Lyčka.[7] Recent studies on tautomerism in solution and in the solid state, which also included some *J* coupling results, have been reviewed by Kleinpeter.[8] A review of studies on the *ortho* Mannich bases containing various substituents in the phenyl ring on the basis of ^{1}H, ^{13}C and ^{15}N NMR spectra in various solvents and at various temperatures has been presented by Sobczyk.[9]

An elegant review on long-range ^{1}H–^{15}N heteronuclear shift correlation at natural abundance, which also contains a wealth of ^{1}H–^{15}N couplings for a variety of compounds of different size, has been written by Martin and Hadden.[10]

A review on fluorinated 1,3-diketones, 2-trifluoroacetyl phenols and their

Nuclear Magnetic Resonance, Volume 31
© The Royal Society of Chemistry, 2002

derivatives, in which also through-space F-F couplings are discussed, has been written by Schoth *et al.*[11]

Several interesting papers have been devoted to determination of the structure of carbohydrates. This includes a review by Duus *et al.*[12] devoted to modern NMR methods and their limitations and a short review written by Ferrier[13] on the use of $^{n}J_{HC}$ and $^{n}J_{CC}$ couplings and other NMR parameters in conformational analysis of saccharides.

The use of heteronuclear $^{1}J_{HC}$ and homonuclear $^{3}J_{HH}$ couplings, including $^{3}J_{HC,OH}$, for structure elucidation of gangliosides has been reviewed by Acquotti and Sonnino.[14] The couplings have been used to obtain information on the types of monosaccharides, their conformation, anomeric configuration and hydrogen bonding network.

A very large set of couplings of fluorinated carbohydrates has been collected by Michalik and co-workers.[15] This includes $^{n}J_{HF}$, $^{n}J_{CF}$ and $^{n}J_{FF}$ (where $n = 1$ up to 7) couplings for 130 compounds. The dependence of the coupling on the relative substituent orientation is also pointed out by the authors.

A review on carbohydrate complexes of platinum-group metals containing some coupling data has been written by Steinborn and Junicke.[16]

A comprehensive review on measurement of proton–proton couplings in the sugar part of a DNA molecule has been given by Kennedy and co-workers.[17] The authors explored the influence of stereo-selective deuteration, selective excitation, decoupling and *J*-doubling on the accuracy of the measured couplings.

Structure determination of membrane-associated proteins by the use of NMR data including proton–proton vicinal couplings has been discussed in a short review by Baleja.[18]

The papers in which the DFT method has been applied to calculate structural properties of molecules such as vibrations, relative energies, NMR chemical shifts and spin–spin couplings have been reviewed by Springborg.[19]

2 New Methods

Recent progress in editing and selective detection methods for ^{1}H NMR spectroscopy has been presented by Liu and Lindon.[20] Among other topics, they discuss MAXY-based NMR experiments and their application to the measurements of spin–spin couplings of neurotensin. It is a short peptide but the signals in its spectrum overlap strongly and cannot be separated by other standard methods.

Gerwick and co-workers[21] have applied the BIRD sandwich sequence for a rapid and accurate determination of $^{3}J_{HH}$ couplings in higher order spin systems present in the spectra of unsaturated fatty acids. Furihata and Seto[22] have proposed new pulse sequences, J_{HH}- and J_{CH}-resolved-HMQC for determination of the $^{3}J_{HH}$ coupling in strongly coupled spin systems. The authors have increased the accuracy of information on H–H *J*-splittings

observed with HMQC cross peaks by incorporating the *J*-scaling method in the HMQC pulse sequence.

Zhu and co-workers[23] have presented a 2D sensitivity-enhanced MJ-HMQC experiment which can amplify $^3J_{HNH\alpha}$ couplings and is more sensitive than experiments of that type reported earlier. Bazzo and co-workers[24] have designed an N,C-filtered HNHA experiment to measure homonuclear $^3J_{HNH\alpha}$ couplings of unlabelled peptides complexed with labelled proteins. Delaglio *et al.*[25] have described an amplitude-constrained multiplet evaluation method (ACME), an interactive computer procedure which determines homonuclear couplings from fitting the cross-peak multiplets in regular phase-sensitive COSY spectra. The authors have shown that, on average, *J* values derived from the widely used HA(CA)HB spectrum underestimate the true couplings. The ACME fit yields correct coupling values in proteins.

Garza-García *et al.*[26] have proposed a modified *J*-doubling method which makes it possible to analyse 2D multiplets and measure couplings as small as 0.11 Hz with the accuracy of ± 0.03 Hz.

Several new pulse sequences have been designed for the detection of heteronuclear long-range couplings. This includes a new 2D pulse sequence (BIRD-HMBC) proposed by Burger *et al.*[27] and new broadband XLOC and *J*-HMBC experiments suitable for the measurement of J_{HH} and J_{HX} couplings in small molecules, designed by Meissner and Sørensen.[28]

Liu and Zhang[29] have introduced multiple-quantum *J*-resolved spectroscopy (MQ-JRES) and applied this technique for the measurement of relative signs of couplings in the SI_3–M spin system. They found $^3J_{HH} = 7.25$ Hz and $^2J_{HC} = -4.57$ Hz in the $^{13}CH_3$–^{12}CH group in alanine.

Bazzo and co-workers[30] have proposed an optimised 2D HMBC method of higher sensitivity for the measurement of the $^3J_{HC}$ couplings. Parella and Belloc[31] have presented simple 1D HMQC and HSQC pulse schemes which allow the $^3J_{HC}$ sign and magnitude measurement for samples at natural carbon abundance.

A new pulse sequence which detects a wide range of one-bond proton–carbon couplings using accordion optimisation (accordion-optimised direct correlation single quantum coherence, ADSQC) has been published by Hadden and Angwin.[32] The antibiotic ceftiofur has been employed as a model molecule since in this compound the $^1J_{HC}$ couplings range from 130 Hz (the aliphatic fragment) up to 210 Hz (the furan moiety). Schmidt and co-workers[33] have modified HMQC-ECOSY to allow quantitative determination of heteronuclear $^3J_{H\alpha C\gamma}$ couplings in ^{13}C-enriched proteins. The method is applicable to amino acid residues lacking protons in the position γ. Pelupessy and Chiarparin[34] have discussed the usefulness of the 2D TOCSY experiment with selective excitation of I spins for evaluation of the accurate value and sign of long-range heteronuclear $^nJ_{IS}$ couplings. The method may be applied to peptides with natural abundance of S spins. A new, HMQC and HSQC based, pulse sequence for measuring ^1H–^{13}C couplings has been designed by Ding.[35]

Permi and co-workers[36] has described a TROESY-based α/β-HN(CO)CA-*J*

experiment designed for accurate measurement of the $^3J_{H\alpha(i-1)Ni}$ couplings in doubly labelled proteins.

Sørensen and co-workers[37] have developed new sequences for the measurement of the $^3J_{HP}$ couplings in the backbone of DNA duplexes. The $^3J_{HP}$ and $^3J_{CP}$ couplings have been measured in ^{13}C-labelled oligonucleotides by Schwalbe and co-workers[38] using a new method, 2D *constant time* Γ-DQ/ZQ-HCP.

A new accordion approach for measurement of J_{CC} couplings without a priori estimation of their magnitudes has been proposed by Koźmiński.[39]

Löhr and Rüterjans[40] have proposed a HN(CO)CG-[^{1}H–^{15}N]-TROSY sequence for the simultaneous determination of the $^3J_{C\gamma N}$ and $^3J_{C'C\gamma}$ couplings related to the side chain χ_1 angle of aromatic residues in ^{13}C,^{15}N -enriched proteins. Two methods which are based on simplified 2D ^{13}C$_\alpha$-coupled ^{15}N SE-HSQC spectra for thee measurement of $^1J_{C\alpha N}$ and $^2J_{C\alpha N}$ couplings in doubly labelled proteins have been described by Heikkinen *et al.*[41] The method has been tested by measuring a spectrum of uniformly ^{15}N/^{13}C labelled human ubiquitin.

The modified 2D J_{NN}-correlated [^{15}N,^{1}H] TROESY sequence has been proposed by Zhu and co-workers[42] for direct measurement of $^hJ_{HN}$ couplings in large nucleic acids.

Two sequences, the 'straight-through' (H6)N6N3H2 and 'out-and-back' H2N6N3 experiments have been presented by Majumdar and co-workers[43] for observing internucleotide $^{2h}J_{NN}$ couplings. These experiments are designed for measurement of scalar $^{2h}J_{N6N3}$ couplings across the (A)N6H$_2$···N3(G) hydrogen bond under exchange-broadening conditions.

The first pulsed field gradient experiment based on the PFG esHSQC sequence for the detection of natural abundance ^{15}N NMR parameters, including J_{NP} couplings, through ^{31}P has been described by Carbajo and López-Ortiz.[44] High quality spectra of *P*-(diphenyl)methyl(*N*-methoxycarbonyl)phosphazene and α-azidophosphazene have been recorded to demonstrate the usefulness of the method proposed. In particular the latter compound which contains four nitrogen atoms presented a challenging example.

The sensitivity of the measured values of couplings on conformational averaging has been studied by van Gunsteren and co-workers.[45] The authors showed that the same average value of J may correspond to the diversity of conformation distribution.

3 One-bond Couplings to Hydrogen

The dependence of the $^1J_{HD}$ coupling in HD on the interatomic distance R in the presence of an external magnetic field has been studied by Vizioli *et al.*[46] A disappearance of the PSO, DSO and SD terms with the increasing distance has been observed.

Effects of temperature and isotopic substitution on a $^1J_{HH}$ coupling in the cationic ruthenium complex [Cp*Ru(dppm)(H$_2$)]$^+$ have been studied by Law

et al.[47] in order to verify the theoretical DFT predictions made by Gelabert *et al.*[48] that the H–H bond distance in this molecule would be sensitive to isotopic substitution. The results obtained by Law *et al.*[47] provided experimental proof of the theoretical studies and were attributed to the extremely flat and highly anharmonic potential energy surface that defines the H–H and M–H interactions in the complex studied.

An analysis of the solvent dependence of the $^1J_{HC}$, $^1J_{DC}$ and $^3J_{HH}$ couplings combined with an analysis of the changes in the IR first overtone carbonyl bond intensities and theoretical calculations allowed Abraham and co-workers[49] to determine directly the conformational equilibria in 2-bromocyclohexanone, a model compound, by the use of which the authors illustrated an improved method of conformational analysis of substituted cyclohexanones.

The effect of the substitution on $\delta(^1H)$, $\delta(^{13}C)$ NMR chemical shifts and $^1J_{HC}$ couplings in heparin derivatives containing various sulfation patterns has been studied by Yates *et al.*[50] They have observed that the $^1J_{HC}$ couplings at the glycosidic linkage positions varied between free-amino and *N*-sulfated compounds, by up to 9 Hz, indicating that an overall conformational change takes place upon sulfonation of the compounds.

Afonin and co-workers[51] have continued their interesting studies on the application of $^1J_{HC}$ couplings on the steric and electronic properties of heteroaromatic compounds. Recently, they have published the ^1H and ^{13}C NMR data obtained for a series of 2-(pyridyl)pyrroles which have been shown to exist as two conformers with *syn* and *anti* arrangement of the heterorings.

$^1J_{HC}$ couplings have been measured at low and high temperatures for the conjugate carbanion of *p*-trifluoromethanesulfonylbenzyltriflone by Gromova *et al.*,[52] who studied the rotational isomerism in this compound by the use of the dynamic NMR.

A set of $^1J_{HC}$ and J_{HH} couplings has been reported by Sélambarom *et al.*[53] for a novel compound, [1*S*,2*S*,6*S*,7*S*]-1,6-diaza-4,9-dioxa-2,7-dimethoxycarbonylbicyclo[4.4.1]undecane obtained as an adduct of L-serine methyl ester hydrochloride with paraformaldehyde. The $^1J_{HC}$ and $^3J_{HH}$ couplings have been measured by Wałejko *et al.*[54] for a series of glycosides of vitamin E.

A somewhat confusing interpretation of the obtained results has been offered by Hon and Lee,[55] who measured the ^{13}C proton-coupled spectra of triphenylphosphonium and triphenylarsonium salts of acetic, benzoic and formic acids under fast intermolecular exchange conditions. This did not allow them to observe the one-bond C–H coupling in the methylenic group of these compounds. The authors assumed that the coupling value drops to zero, $^1J_{HC} = 0$ Hz, which is an obvious mistake since the magnitude of the couplings under consideration is most probably quite typical, of *ca.* 135 Hz (though not observed!), as was found in the same work for the corresponding bromides and *p*-toluenosulfates where the proton–proton exchange process is for the obvious reason much slower.

An agostic $^1J_{HC}$ coupling of 112 Hz has been observed by Dani *et al.*[56] in the spectrum of the $[Ru(C_6H_3\{CH_2PPh_2\}_2\text{-}2,6)(C_6H_4\{CH_2PPh\}\text{-}1,3]^+[CF_3SO_3]^-$

complex measured at $-70\,^{\circ}C$. A $^1J_{HC}$ coupling of 156 Hz has been observed in the spectrum of the free ligand.

$^1J_{HC}$ and $^1J_{HN}$ couplings have been applied by Grothjahn *et al.*[57] in order to obtain structural information on the bis(benzo crown ether)s and their complexes with alkali metal cations.

Proton transfer equilibrium in a large series of *N*-(R-salicylidene)-alkylamines has been elucidated by Schilf *et al.*[58] on the basis of the temperature dependence of the $\delta(^{15}N)$ chemical shifts and $^1J_{HN}$ couplings.

$^1J_{HN}$ couplings of *ca.* 102 Hz have been observed by Schraml *et al.*[59] for parts *Z* of several dihydroxamic acids $HONHCO(CH_2)_nCONHOH$, $n = 0, 1, 6$.

$^1J_{HN}$ couplings have been measured by Weisz and co-workers[60] and used as a measure of strength of hydrogen bonds in complexes of 2′-deoxyadenosine with 2′-deoxyuridine.

The values of the $^1J_{HSi}$ and $^1J_{CSi}$ couplings have been measured by Troitski *et al.*[61] for a series of siloles of the general formula C_4Ph_4SiRH (R = Cl, Ph, H, Me, *t*-Bu). A linear dependence of $^1J_{HSi}$ on Taft's substituent constant has been observed.

$^1J_{H117/119Sn}$ couplings of 1695.6/1774.5 Hz have been reported by Schumann *et al.*[62] for the first generation metallodendrimer $Si(CH_2CH_2SnH_3)_4$.

$^1J_{DC}$ couplings measured for 4′-cyanobiphenyl 2-deutero- and 6-deuterohexanoate in the isotropic phase have been applied by Canlet and Fung[63] in their studies on the determination of dipolar couplings in these compounds by the use of mono-deuterated liquid crystals.

$^1J_{DPt}$ couplings have been determined by Sabounchei[64] for several *trans* $[PtDX(PEt_3)_2]$ complexes where X denotes CN, Cl, SCN/NCS ligands, which provides the first examples of this type of couplings.

4 One-bond Couplings not Involving Hydrogen

Several important papers have been recently published on the theoretical aspects of spin–spin coupling. A fully analytical implementation of the NMR spin–spin couplings at the DFT level has been presented by Helgaker *et al.*[65] The implementation involves all four contributions of the non-relativistic Ramsey theory. The convergence of FPT-DFT calculations of the Fermi contact contribution to NMR couplings has been highlighted by Peralta *et al.*[66] They have also published a paper on an implementation of the FPT-DFT approach for calculation of the spin–dipolar contribution to the NMR spin–spin coupling.[67] A complete implementation of coupled perturbed DTF (CPDFT) for the calculation of NMR spin–spin couplings with pure and hybrid DFT has been presented by Sychrovský *et al.*,[68] and the Perdew-Zunger self-interaction correction (SIC) has been implemented self-consistently within a molecular density functional theory program by Patchkovskii *et al.*[69]

The scalar spin–spin coupling has been calculated by Pecul[70] for the helium dimer using full configuration interaction and EOM-CCSD methods. The

Fermi contact has been found to have the nonnegligible value of 1.3 Hz, whereas the remaining contributions are zero.

Li–C couplings have been collected for a series of lithium reagents by Reich and co-workers,[71] who studied their chelation and aggregation with potential 5-, 6-, and 7-ring chelating ether and amine *ortho* substituents. The couplings have been also applied by Hilmersson and Malmros[72] in their studies on mixed dimer and mixed trimer complexes of *n*-BuLi and a chiral lithium amide.

Dynamic NMR studies performed on cyclopropyldifluoroborane, vinyldifluoroborane and phenyldifluoroborane by Pawar *et al.*[73] also included measurement and analysis of $^1J_{BF}$ and $^2J_{FF}$ couplings.

$^1J_{BP}$ couplings of *ca.* 95 Hz have been measured for 1,3-(dioxa, oxaza or diaza)-2-phospholanes and their borane adducts by Peralta-Cruz *et al.*;[74] $^1J_{PSe}$ couplings of *ca.* 950 Hz have been found for the corresponding selenium adducts.

Accurate *ab initio* calculations of the NMR indirect spin–spin couplings in acetylene have been performed by Jaszuński and Ruud.[75] In order to achieve better agreement between the theoretical and experimental values the nuclear motion corrections (Wigglesworth *et al.*[76,77]) have been taken into account by the authors.

All NMR parameters including the $^1J_{CC}$ coupling have been measured by Jackowski *et al.*[78] for 1,2-^{13}C-enriched acetylene in various solvents. They have found that the $^1J_{CC}$ coupling is the most sensitive to intermolecular interactions; it varies from 174.78 Hz for an isolated molecule to 165.8 Hz for the molecule dissolved in acetone.

The DFT calculations which very well reproduced the experimental data obtained earlier have been performed by Biedrzycka and Kamieńska-Trela[79] for a series of variously substituted silylacetylenes.

Ab initio MO and DFT calculations have been performed by Cloran *et al.*[80] for 2-deoxy-β-D-ribofuranosylamine in its unprotonated and protonated forms. An analysis of the *J* data obtained led them to the conclusion that one- and two-bond J_{HC} and J_{CC} values appear more influenced by O→N substitution and by N-protonation than vicinal $^3J_{HC}$ and $^3J_{CC}$ values.

Extensive experimental and DFT studies on the influence of substituents on $^1J_{CC}$ couplings in heteroaromatic compounds have been performed by Kamieńska-Trela and co-workers; this included data for variously 2- and 3-substituted thiophenes[81–83] and for a large set of variously substituted pyridines and their *N*-oxides.[84–86] Particularly interesting results have been obtained for 2-lithiothiophenes where very small $^1J_{CC}$ coupling values of *ca.* 30 Hz only have been measured.[82,83] The experimental values have been very well reproduced by the DFT calculations. Similarly low coupling values are predicted for 2-lithiopryridines and their *N*-oxides.[84]

Configurational and conformational analysis of *O*-vinylketoximes by the use of ^{1}H and ^{13}C NMR parameters among which $^1J_{CC}$ couplings played an important role has been performed by Afonin *et al.*[87] $^1J_{CC}$ couplings measured by Schraml[88] allowed the author to discriminate between *E*- and *Z*-isomers of derivatives of hydroxamic acids.

$^1J_{CC}$, $^1J_{CN}$ and $^2J_{CN}$ couplings for some mesoionic oxadiazoles and thiadiazoles have been determined by Jaźwiński *et al.*[89] All $^1J_{CH}$ and $^1J_{CC}$ couplings have been determined by Bednarek *et al.*[90] for 5-halogenouracils and used for assigning the carbon signals. $^1J_{CC}$ couplings have been measured by Sommer *et al.*[91] for some di- and trisubstituted pyrazines and by Cmoch *et al.*[92] for *N*(1)-oxide and *N*(3)-oxide forms of pyridofuroxan[1,2,5]oxodiazolo[3,4-*b*]pyridine oxide.

Ab initio calculations of the NMR spectra including a set of couplings ($^1J_{CC}$, $^2J_{CC}$ etc.) have been performed by Pecul *et al.*[93] for [1.1.1]propellane and bicyclo[1.1.1]pentane.

Homans and co-workers[94] described an approach for the measurement of the $^1J_{C\alpha C'}$ and $^1J_{H\alpha C\alpha}$ couplings in a protein that is isotopically enriched exclusively in backbone nuclei.

$^1J_{CC}$ coupling values measured by Canisius *et al.*[95] for several multiply ^{13}C-labelled cuprate π-complexes have been interpreted by the authors in terms of a deformation of the cuprate alkene complex from the expected idealised square plane.

One-bond CC couplings across a double bond have been determined by Wrackmeyer *et al.*[96] for (*Z*)-1-chloro(dimethyl)silyl-1-(9-bora-bicylo[3.3.1]-non-9-yl)-3,3-dimethyl-but-1-ene and 2-[(*Z*)-1-(3,3-dimethyl)butenylidene]-1,3-dihydro-1,1,4-trimethyl-1-sila-3-(9-bora-bicylo[3.3.1]non-9-yl)-4-aza-6a-aza-pentalene.

$^1J_{CC}$ couplings have been measured by Norrild[97] for D-sorbitol before and after complexation with (*S,S*)-2-(*N,N*-dimethyl-1-aminoethyl)ferroceneboronic acid. The results obtained provided strong evidence that a 2,3,5-bound sorbitol complex is formed.

2D INADEQUATE spectra have been used to establish the structure of a series of β-propiothiolactones,[98] of a series of precursor polymers towards poly(*p*-phenylene vinylene),[99] of 1,16-di(2-carbomethoxy-2-propyl)-1,16-dihydro[60]fullerene[100] and of the C_{70}^{6-} fullerene anion.[101] One-bond carbon–carbon couplings have been determined for the latter compound and compared with those published for the neutral molecule.

A $^1J_{CF}$ coupling has been found by Abraham and co-workers[102] to be a valuable tool in their studies on the rotational isomerism in methyl fluoroacetate and methyl difluoroacetate.

$^1J_{CF}$ and $^2J_{CF}$ couplings have been applied by Bouillon *et al.*[103] in order to establish the regiochemistry of newly synthesised 4-fluoro-5-(perfluoroalkyl)-pyrazoles and reported by Charris *et al.*[104] for some fluoro derivatives of 3-amino-9-methyl-1*H*-pyrazolo[3,4-*b*]-4-quinolones.

The relationship between $^1J_{CF}$ couplings and the isotope effect on the chemical shift of ^{19}F bonded through one or two bonds to the isotopes ^{35}Cl and ^{37}Cl has been studied by Tordeux *et al.*[105]

$^1J_{CSi}$ and $^1J_{CSn}$ couplings have been used by Wrackmeyer *et al.*[106] in order to follow the reaction between 1-boraadamantane and di(1-alkynyl)silicon and -tin compounds of the type $(Me_2M(C{\equiv}C)R)_2$, M = Si or Sn, and to characterise some novel 7-metalla-2,5-diboranorbornane derivatives obtained as products.

$^1J_{CP}$ couplings of 18.2, 45.7 and 57.2 Hz have been measured by Heckmann *et al.*[107] in the heteroatom-substituted γ^3-phosphaalkynes (Me_3Si)-*i*-PrNCP, K^+[*i*-PrNCP]$^-$ and KOCP·2DME, respectively (DME = 1,2-dimethoxyethane). The following mesomerism has been suggested for the anion studied:

$$[i-\mathrm{Pr}\underline{\overline{\mathrm{N}}}\mathrm{C}\equiv\mathrm{P}]^- \leftrightarrow [i-\mathrm{Pr}\overline{\mathrm{N}}=\mathrm{C}=\underline{\overline{\mathrm{P}}}]^-$$

$^1J_{CP}$ couplings have been found by Nazarski *et al.*[108] to be very useful for elucidation of the configuration of *O,O*-dialkyl 1-oxoalkanephosphonate hydrazones (see Figure 1).

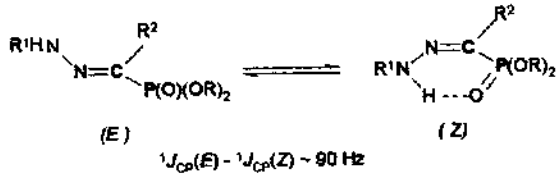

Figure 1

The conformational preferences and rotational dynamics of tetramesityldiphosphane have been studied by McFarlane[109] and co-workers by the use of NMR spectroscopy including analysis of $^1J_{CP}$ and $^2J_{CP}$ couplings.

A full spectral characteristics including $^1J_{CP}$ couplings has been reported by Schmutzler and co-workers[110] for (±)-2,2-diethyl-3,4-dihydro-2*H*-1,4-benzothiazin-3-yl dimethylphosphine oxide and (±)-2,2-diethyl-3,4-dihydro-2*H*-1,4-benzothiazin-3-yl dimethylphosphine sulfide.

An interesting study on glycosylmanganese pentacarbonyl complexes, (glycosyl)$Mn(CO)_5$, has been performed by DeShong *et al.*[111] The complexes have been characterised, among others, by $^1J_{CMn}$ couplings and ^{55}Mn NMR chemical shifts; $^1J_{C(1)Mn}$ of 45–48 Hz have been reported for these compounds.

$^1J_{CSn}$ coupling values and the relationships of Lockhart and Manders[112] and Holecek and Lyčka[113] have been applied by Girasolo *et al.*[114] in their studies on the structure elucidation of L-methionyl-L-histidine complexes with $R_2Sn(IV)$ ions (R = Me, *n*-Bu, Ph), and by Papadaki *et al.*,[115] who studied 1:2 adducts of dimethyltin(IV)dichloride with aromatic *N*-oxides such as isoqinoline-*N*-oxide, 6-methoxyquinoline-*N*-oxide and 4-phenylpyridine-*N*-oxide, and also by Nádvorník and Pejchal,[116] who analysed the structure of substituted tributyltin(IV) phenolates. The same relationship has been used by Tudela *et al.*[117] in their theoretical and experimental study on tri- and tetrahalodiorganostannate(IV) salts.

It has been shown by Sutton *et al.*[118] that $^nJ_{CSn}$ couplings (n = 1–4) measured in isotopically enriched dibutyltin dichloride, dibutyltin di-iodide, tributyltin chloride, tributyltin iodide, diphenyltin dichloride, triphenyltin chloride and triphenyltin iodide are solvent dependent.

Rather small $^1J_{CH3Sn}$ couplings of *ca.* 35–50 Hz only have been reported by

Fraenkel and Qiu[119] for two allylic stannanes. Typical couplings of this type are about ten times larger.

$^1J_{C(1)Pt}$ and $^1J_{C(2)Pt}$ coupling values measured by Asaro *et al.*[120] for $Pt^0(PPh_3)_2$(alkene) compounds containing asymmetric olefins (shown in Figure 2) are in agreement with a stronger interaction of Pt with carbon C(1) than with C(2), the consistently larger coupling values being observed for C(1).

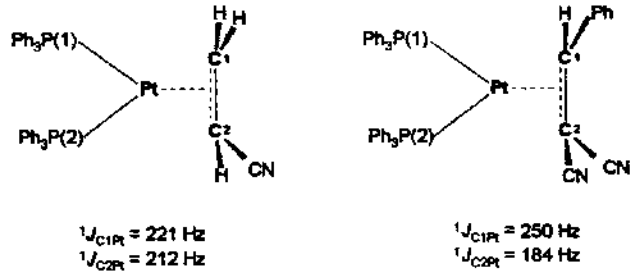

Figure 2

A theoretical DFT study of $^1J_{CHg}$ and $^1J_{PPt}$ couplings which also included solvent effects on these parameters has been carried out by Autschbach and Ziegler.[121]

The accurate measurement of $^1J_{14NPt}$ in $K[Pt(NH_3)Cl_3]$ performed by Gore[122] by complete line analysis yielded the value of 235.3 ± 0.2 Hz. This is in agreement with the value of 234 Hz calculated from the published value of $^1J_{NPt}$, whereas ^1J of 230.4 Hz was determined from the peak separation.

$^1J_{NP}$ couplings have been reported by Peralta-Cruz[74] for a series of 1,3-(dioxa, oxaza or diaza)-2-phospholanes and their sulfur, selenium and borane adducts. Considerably smaller $^1J_{NP}$ values have been observed for the endocyclic than exocyclic N–P bonds, *ca.* 50 and 70–90 Hz, respectively.

A $^1J_{NPt}$ coupling of 250 Hz has been observed by Schröder and Preetz[123] in the ^{15}N NMR spectrum of the mixture of isotopomers of $(n\text{-}Bu_4N)_2[Pt(^{15}NN_2)_n(N_2{}^{15}N)_{6n}]$, $n = 0 - 6$.

The small tip angle NMR techniques recently developed by Pennington *et al.*[124–126] allowed them to measure nuclear spin–spin couplings between neighbouring ^{17}O and $^{63/65}Cu$ nuclear spins in the high-temperature superconductor $YBa_2Cu_3O_7$.[127] The measurements have been performed on the ^{17}O enriched sample at T = 4.2 K in the superconducting state of the sample. Nevertheless, the authors hoped that the results obtained would be valid also for the normal state.

Chemical shifts and $^1J_{FAl}$ coupling have been determined by Petrosyants *et al.*[128] for the AlF_4^- anion in donor solvents.

Simulations of the ^{19}F MAS NMR spectra performed by Du *et al.*[129] for potassium heptafluoroniobate, K_2NbF_7, yielded $^1J_{FNb}$ of 204 Hz and $\delta_{iso}(^{19}F)$ of 76.28 ppm.

Alkali metal complexes of hexafluoro[130] and tetrafluoro[131] cage compounds have been studied by Takemura and co-workers. A F–Cs coupling of 35 Hz

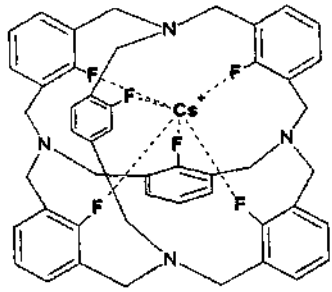

$^1J_{FCs}$ = 35.1 Hz

Figure 3

has been observed in the ^{19}F NMR spectrum of the Cs^+ complex of the hexafluoro compound and of 54.9 Hz in the spectrum of the tetrafluoro cage compound. This observation provided unambiguous and very rare evidence of the C–F···Cs^+ interaction. The structure of the hexafluoro compound is shown in Figure 3.

A $^1J_{FW}$ coupling of 69 Hz has been found by Weinert *et al.*[132] in the spectrum of the $[Bu_4N]_2[W_6Cl_8F_6]$ cluster.

$^1J_{SiSi}$, $^1J_{SiSe}$ and $^1J_{SiTe}$ couplings have been applied by Herzog *et al.* in order to characterise 2,5,7-trichalcogena-1,3,4,6-tetrasilanorbornanes,[133] a series of tellurobutyl-substituted silanes[134] and a large number of five- and six-membered ring group 14 chalcogenides of the types $(Me_2ME)_3$ (M = Si, Ge, Sn), $E(Si_2Me_4)_2E$, $Me_4Si_2(E)_2MRx$ (MRx = $C(CH_2)_5$, $SiMe_2$, $GeMe_2$, $SnMe_2$, $SnMe_2$, $SnPh_2$, BPh) and $[Me_4Si_2(E)_2SiMe\text{-}]_2$ (E = S, Se, Te).[135] A good linear $^1J_{SiTe}$ *vs* $^1J_{SiSe}$ relationship has been observed for the compounds studied.

A $^1J_{SiY}$ coupling of 59 Hz has been observed by Cai *et al.*[136] in the low temperature spectrum of $[Y(\eta^5\text{-}C_5H_5)_3Si\{[N(CH_2\text{-}t\text{-}Bu)]_2C_6H_4\text{-}1,2\}]\cdot C_7H_8$ complex.

$^1J_{PP}$ couplings and δ(P) NMR chemical shifts have been measured and assigned for all twelve possible molecules $P_5S_nSe_{2-n}X$ (n = 0–2; E = S, Se, X = Cl, Br or I) by Tattershall *et al.*[137] Additionally, approximate calculations of differences in J couplings using Natural Bond Orbital analysis and McConnell's equation have been performed by the authors.

Phosphorus chemical shift and spin–spin coupling P–P tensors have been determined by Gee *et al.*[138] for tetramethyldiphosphine disulfide.

$^1J_{PCu}$ couplings ranging from 1.23 to 1.46 kHz have been observed by Ainscough *et al.*[139] in the ^{31}PCPMAS NMR spectra of three-coordinate, monomeric 1:2 complexes of tribenzylphosphine with copper halides, $[Cu(PBz_3)_2X]$ (X = Cl, Br or I); significantly larger couplings of *ca.* 1.54 kHz have been measured for two-coordinated $[Cu(PBz_3)_2][CuX_2]$ compounds reflecting a transfer of electron density away from the Cu–P bonds with coordination of the halide.

$^1J_{PSe}$ couplings have been applied by Grossmann *et al.*[140] to confirm the structure of a series of variously substituted 1,3-diselena-2,4-diphosphetane-2,4-diselenides.

Interdependence of phosphorus–selenium couplings in bicyclic phosphorus selenide compounds has been studied by Tattershall and Sandham.[141] The knowledge of the rules which govern this parameter facilitates considerably an analysis of the spectra of new compounds, in particular symmetrical ones.

$^1J_{PAg}$ couplings have been measured by Bowmaker *et al.*[142] for bis(triphenylphosphine)silver(I) sulfate, selenate and phosphate compounds, $[Ag_2(PPh_3)_4(EO_4)]\cdot 2H_2O$ (E = S or Se), $[Ag_2(PPh_3)_4(HEO_4)]\cdot H_2O$ (E = S or Se) and $[Ag_2(PPh_3)_4(H_2EO_4)]\cdot 2EtOH$ (E = S or Se). An inverse correlation has been found between these couplings and the Ag–P bond length.

A linear correlation between $\delta(^{183}W)$ and $^1J_{PW}$ has been observed by Gudat *et al.*[143] in $[W(OTf)(bipy)(CO)_2(L)]$ complexes, where OTf denotes 1,3-dimesityl-4-chloro-1,3,2-diazaphospholenium triflate and L are CO, PPh_3, MeCN or OTf: $^1J_{PW} = 0.426 \times \delta(^{183}W) + 1393$ (r = 0.987)

A new series of metallocryptates that bind Tl(I) ion in the absence of attractive ligand interactions through metallophilic connections has been synthesised by Catalano *et al.*[144] $^1J_{PPt}$ of 4436 Hz and $^1J_{PtTe}$ of 5560 Hz have been measured for $[Pt_2Tl(2,9\text{-bis(diphenylphosphino)-1,10-phenathroline})_3](NO_3)$ compound; the corresponding *J* values found for $[Pt_2Tl(6,6'\text{-bis(diphenylphosphino)-2,2'-bipyridine})_3](NO_3)$ were 4436 and 6100 Hz, respectively.

The trends in chemical shifts $\delta(^{31}P)$ NMR and $^1J_{PPt}$ couplings have been applied by Fernández *et al.*[145] in their studies on the X ligand exchange substitution reactions in [Pt(triphos)X]Cl and [Pt(triphos)X]Br complexes, where triphos denotes $Ph_2PC_2H_4P(Ph)C_2H_4PPh_2$. $^1J_{PPt}$ couplings of typical of *trans* compounds values have been observed in the spectrum of the *trans*-$[PtCl_2(PPh_3)_2]$ complex.[146]

$^1J_{MnSn}$ of 139 Hz and $^1J_{MnPb}$ of 228 Hz have been measured by Christendat *et al.*[147] in the CP MASI spectra of bis(pentacarbonylmanganese)diphenyltin and bis(pentacarbonylmanganese)diphenyllead complexes, respectively.

An analysis of the $^1J_{Se^{203/205}Tl}$ and $^2J_{^{203/205}Tl^{203/205}Tl}$ couplings observed for $Tl_4Se_5^{4-}$ and $Tl_4Se_6^{4-}$ anions allowed Campbell *et al.*[148] to establish the solution structures of these novel cubanoid anions.

$^1J_{^{119/117}Sn^{119/117}Sn}$ of 8332 Hz has been observed by Eichler and Power[149] in the spectrum of 2,6-$Trip_2H_3C_6Sn(II)$-$Sn(IV)(Me)_2C_6H_3$-2,6-$Trip_2$ (Trip denotes C_6H_2-2,4,6-*i*-Pr_3), which represents the first example of a stable molecule with bonding between two-coordinate, bivalent tin and four-coordinate tetravalent tin. A considerably smaller $^1J_{SnSn}$ coupling of *ca.* 4050 Hz only has been found in its related lithium derivative, 2,6-$Trip_2H_3C_6Sn(IV)(Li)(Me)$-$Sn(IV)(Me)C_6H_3$-2,6-$Trip_2$.

The full spectral characteristics which included $^1J_{PtPt'}$ of 550.9 Hz, $^1J_{C(A)Pt}$ of 1281.5 Hz and $^1J_{C(B)Pt}$ of 1595.7 Hz have been reported by Xu *et al.*[150] for hexacarbonyldiplatinum, $[\{Pt(CO)_3\}_2]^{2+}$, the first homoleptic, dinuclear, cationic platinum carbonyl complex.

Studies have been continued by Glaser and his co-workers[151] on platinum–thallium clusters. Very large $^1J_{PtTl}$ couplings ranging from 48 to 66 kHz have been observed by them for $[(NC)_5PtTl(en)_{n-1}]$ (n = 1–3) complexes where *en* denotes ethylenediamine.

The values of the $^1J_{HgHg}$ coupling found by Malleier *et al.*[152] in solution of the asymmetric dimercury (2+) complexes with the stoichiometric Hg^{2+}/18-crown-6 and Hg^{2+}/18-crown-6/15-crown-5 are equal to 220.3 and 284.1 kHz, respectively. These are the largest scalar couplings measured so far. However, it should be noted that the authors did not observe the outer lines of the corresponding AB systems; the coupling values have been estimated from the positions of the inner lines of the systems and the shifts ν_A and ν_B measured for isotopomers containing one ^{199}Hg nucleus.

5 Two-bond Couplings to Hydrogen

$^2J_{HH}$ couplings have been applied in numerous cases as a useful parameter, which helped to establish the structure of the compounds studied or to assign their spectra. Thus, $^2J_{HH}$ couplings have been used by Ribeiro *et al.*,[153] who studied axial/equatorial populations in α-hetero-substituted cyclohexanone oximes and *O*-methyl oximes, by Shaikhutdinov *et al.*,[154] who performed a conformational study of four *cis*-fused *N*-substituted hexahydrocyclopent[*e*][1,3]oxazin-4-ones and by Balázs *et al.*,[155] who investigated tautomerism and *Z*/*E* isomerisation of a series of chromogenic calix[4]arene indophenols. $^2J_{HH}$ and $^3J_{HH}$ couplings have been applied by Costa *et al.*[156] for complete ^{1}H and ^{13}C NMR signal assignments in the spectra of glaucolide B. A set of $^nJ_{HH}$ (n = 2–4) couplings has been reported by Vialemaringe *et al.*[157] for isofenchylic alcohol derived from a functionalised pinene oxide and measured for four hispanane diterpenoids isolated from *Ballota hispanica* by Rodríguez and Savona.[158]

Geminal and vicinal proton–proton couplings have been collected and applied by Hughes *et al.*[159] in their studies on the structure of six alkaloids of the Lythraceae group, *i.e.* decinine, decodine, decamine, verticillatine, decaline and vertaline, and by Krajewski *et al.*,[160] who studied solution conformation of the alkaloid chelidonine and its protonated form.

Differences in the proton–proton couplings of the N^+–CH_2–CH_2 protons of some betaines, N^+–$(CH_2)_n$–COO^- (n = 2, 3), and their complexes in solutions have been analysed by Szafran *et al.*[161] in order to get insight into the conformations of the compounds studied.

Two-bond proton–proton couplings of *ca.* 16 Hz have been reported by Suárez *et al.*[162] for a series of 1,4,5,6,7,8-hexahydroquinolines and their oxa-analogues 5,6,7,8-tetrahydro-4*H*-chromenes.

Structural and conformational investigation of two series of 2,4,6-tris(amino)-s-triazines by the use of ^{1}H and ^{13}C NMR including $^2J_{HH}$ and $^3J_{HH}$ couplings has been made by Amm *et al.*[163]

A complete analysis of the higher-order ^{1}H NMR spectra of dimethylpropylsilane, its alkyl analogue, 2-methylpentane, and dimethylethylsilane has been performed by Bain *et al.*[164] yielding two- and three-bond proton–proton couplings for these compounds.

$^2J_{HH}$ and $^2J_{HN}$ couplings have been found by Duckett *et al.*[165] to be very

useful in monitoring the reaction between dihydrogen and the cationic iridium(I) complex $[Ir(BPM)(CO)_2][BPH_4]$ (BPM = bis(pirazol-1-yl)methane), and in the elucidation of the structure of the four major products obtained.

It has been recently suggested by Murata and co-workers[166] that a reliable conformational–configurational analysis of flexible organic molecules can be performed by the use of two- and three-bond H–C couplings. A similar approach has been applied by Ciminiello *et al.*,[167] who studied a new cytotoxin isolated from mussels from the northern Adriatic sea, and by Bassarello *et al.*,[168] who studied the structure of sphinxolide, a potent anti-tumour marine macrolide.

Novel platinum(VI) complexes with acetylated carbohydrates have been characterised by Steinborn and co-workers[169] by the use of NMR. $^2J_{HPt}$ couplings of *ca.* 80 Hz have been measured in these compounds.

A $^2J_{HPt\,trans}$ coupling of 50 Hz has been found by Mathew and Jagirdar[170] in the spectrum of the *trans*-$[(Ph_2CH_2CH_2PPh_2)_2Ru(\eta^2\text{-}H_2)(PF(OMe)_2)][BF_4]_2$ complex. This is the first observation of such a large coupling between a bound dihydrogen and a *trans*-phosphorus ligand.

Two papers have been devoted by Carlton[171,172] to the complexes of the type $[Rh(X)(H)(SnPh_3)(PPh_3)(L)]$ and $[Rh(X)(H)(SnPh_3)(PPh_3)_2(L)]$ which contain the three-centre Rh–H–Sn bonds; L = 1-methylimidazole, pyridine or substituted pyridines; X = $NCBPh_3$, $N(CN)_2$, NCS, NCO *etc.* An analysis of the NMR data obtained for these and some related compounds and in particular an inspection of $^2J_{HSn}$ couplings and their relationship to $\delta(^{103}Rh)$ and $^2J_{RhSn}$ (approximately linear) allowed the author to conclude that the value of $^1J_{HSn}$ correlates with the electron density on rhodium and that the structure of the compounds studied is reflected by the structures shown in Figure 4.

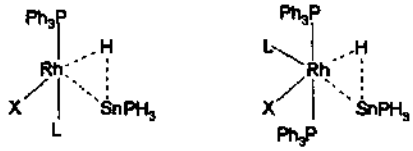

Figure 4

Very large H–Sn couplings have been observed by Schneider *et al.*[173] in the spectra of $[(\eta^6\text{-}C_7H_8)(\mu\text{-}OH)(H)Fe\{Sn[CH(SiMe_3)_2]_2\}_2]$ and $[(\eta^6\text{-}Cp)(\mu\text{-}OH)(H)Mo\{Sn[CH(SiMe_3)_2]_2\}_2]$, 630 and 593 Hz, respectively. These large coupling values combined with a very large Sn–Sn coupling of 4370 ± 100 Hz found for the $[(\eta^6\text{-}C_7H_8)(\mu\text{-}OH)(H)Fe\{Sn[CH(SiMe_3)_2]_2\}_2]$ complex have been invoked by the authors as strong evidence of the existence of three-centre Fe (or Mo), H, Sn interactions in the compounds studied (see Figure 5).

The correlation between the literature $^2J_{H(methyl)Pt}$ data and $d_{C\text{-}Pt}$ for some D_3PtMe_3 complexes, where D_3 denotes the same donor atoms but not ligands, has been analysed by Fekl *et al.*[174] In this analysis also the data obtained by

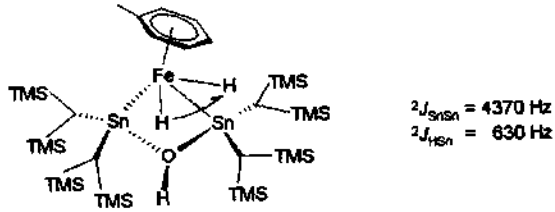

Figure 5

the authors for $Tp(CF_3)_2PtMe_3$ and $TpMe_2PtMe_3$, where $Tp(CF_3)_2$ = hydridotris(3,5-bis(trifluoromethyl)pyrazolyl)borate, have been included.

6 Two-bond Couplings not Involving Hydrogen

The $^2J_{C\text{-}(N)\text{-}P}$ couplings measured by Herberhold *et al.*[175] for a series of tri(tert-butyl)plumbyl-phosphanes allowed the authors a unequivocal elucidation of the preferred conformation of the amino group with respect to an axis representing the assumed orientation of the lone pair of electrons at the phosphorus atom. A large and positive coupling corresponds to the *syn*-orientation of the N-C bond with respect to the lone pair of electrons, and a small and of either sign $^2J_{C\text{-}N\text{-}P}$ coupling reflects the *anti* orientation.

A two-bond C–P coupling of 10.8 Hz observed by Szafert *et al.*[176] in the spectrum of $[(\eta^5\text{-}C_5Me_5)Re(NO)(PPh_3)(=C=C=C=C=CAr_2)]^+BF_4^-$ provided unequivocal proof of the presence of the P–Re=C fragment.

Typical trends have been observed in two-bond C–P couplings measured by Sánchez *et al.*[177] for two series of the new molybdenum and tungsten carbonyl complexes $[M(CO)_4(o\text{-}Ph_2PC_6H_4\text{–}CH{=}NR)]$ (M = Mo, W; R = Alk), the *trans* couplings (*ca.* 35 Hz) being significantly larger than the *cis* ones (3–9 Hz).

$^2J_{CP}$ couplings have been used by Keglevich *et al.*[178] to establish the structure of the oxidised products of the Diels–Alder addition of *N*-phenylmaleimide to 2,4,6-trialkylphenylphospholes.

A series of very interesting papers on the determination of two-bond couplings between two magnetically equivalent quadrupolar nuclei has been published recently by Bernatowicz and Szymański.[179–181] It has been shown by one of the authors[182] that the spectrum of a spin 1/2 nucleus coupled to a group of magnetically equivalent nuclei of spin >1/2 can be dependent on the magnitude of the scalar coupling between such nuclei. This phenomenon occurs when the spin relaxation of the equivalent nuclei is nonnegligible. The iterative lineshape analysis has been carried out by the authors for the ^{14}N NMR spectra of the $N{=}N{=}N^+$ ion in solution[180] and 2,1,3-benzoselenadiazole[179] as model compounds.

$^2J_{FF}$ and $^3J_{FF}$ couplings have been determined by Przyborowski *et al.*[183] from an analysis of the low-temperature spectrum of 1′-isopropyloamino-1′-phenyl-1-methylene-3,3,4,4-tetrafluorocyclopentan-2,5-dione, a member of a newly synthesised series of fluorinated β-enaminoketones. Two-bond F–F

couplings of *ca.* 55 Hz have been observed in the spectra of two pnictogen pentafluorides, 1,3-dimesitylimidazolium-2- and 1,3-dimesityl-4,5-dichloroimidazolium pentafluorophosphates.[184]

A large number of the two-bond Si–Se, Si–Te, Sn–Se and Sn–Te couplings has been collected by Herzog and Rheinwald[135] for a large number of five- and six-membered ring Group 14 chalcogenides of the types $(Me_2ME)_3$ (M = Si, Ge, Sn), $E(Si_2Me_4)_2E$, $Me_4Si_2(E)_2MRx$ (MRx = $C(CH_2)_5$, $SiMe_2$, $GeMe_2$, $SnMe_2$, $SnMe_2$, $SnPh_2$, BPh) and $[Me_4Si_2(E)_2SiMe]_2$, (E = S, Se, Te).

A reaction of triphenylmethylphosphine with norbornadiene tetracarbonyl molybdenum yielded the *cis*-$[(Ph_3CPH_2)_2Mo(CO)_4]$ complex.[185] The analysis of its spectrum has been performed under the assumption that the $(PH_2)_2$ fragment represents an AA′BB′MM′ system. Its solution yielded $^2J_{PP}$ = 14.7 Hz. Generally, a steady increase in the magnitude of $|^2J_{PMoP}|$ coupling in the $(RPXY)_2Mo(CO)_4$ series of complexes has been observed in order: (R = trityl) X,Y = F,F > H,F > H,Cl > H,H. This result has been attributed by the authors to the increasing electron-withdrawing power of the substituents attached to the phosphorus atom.

It has been shown by Edwards *et al.*[186] that a linear correlation exists between the $\delta(^{13}C)$ NMR chemical shift of C_α and the corresponding $^2J_{PP}$ coupling in the seven-membered nickelacycles $[NiBr\{o\text{-}C_\alpha(R^1)=C(R^2)C_6H_4\text{-}CH_2PPh_2\}L$ complexes. Two separate equations have been obtained for L = PEt_3 and PBz_2Ph. The more electron-deficient was the α-carbon, the smaller was the observed coupling.

An analysis of the ^{31}P NMR spectrum of the $[Ru(C_6H_3\{CH_2PPh_2\}_2\text{-}2,6)(C_6H_4\{CH_2PPh\}\text{-}1,3)]^+[CF_3SO_3]^-$ complex (an ABMN system) performed by Dani *et al.*[56] yielded a full set of $^2J_{PP}$ couplings which varied from 26.7 Hz up to 245.7 Hz.

A $^2J_{^{117}Sn^{119}Sn}$ coupling of 790 Hz has been reported by Wrackmeyer *et al.*[187] for 1,1′-di(trimethylstannyl)-2-allylboryl-pentadiene-1,4 obtained in the reaction of the corresponding mono-1-alkynyltin with triallylborane, and of 348.0 Hz for 1,1-bis(methoxy-ethynyl)(dimethylstannyl)ethene.[188]

Two-bond ^{183}W–^{183}W couplings in the range of 20–27 Hz observed by Contant *et al.*[189] in the spectrum of a novel Dawson-type tungstophosphate, $[H_4PW_{18}O_{62}]^{7-}$ have been used to confirm the structure of this compound.

7 Three-bond Hydrogen–Hydrogen Couplings

An analysis of $^3J_{HNH\alpha}$ couplings measured for unfolded lasozym, lactoalbumin and ubiquitin performed in dipeptide pairs by Schwalbe and co-workers[190] has revealed the influence of the (i-1) residue type on the value of the coupling. Bai *et al.*[191] used $^3J_{HNH\alpha}$ couplings in search of the potential folding sites in the unfolded doubly labelled *apo* plastocyanin. Madalengoitia and co-workers[192] have used $^3J_{HH}$ couplings to study conformation of 3-azabicyclo[3.1.0]hexane system which was composed to mimic a poly-L-proline type II peptide. Vicinal

Table 5.1 *Peptides and proteins for which the solution structure has been calculated with $^3J_{HH}$*

Name	*a*	*b*	*Ref.*
KL III and KL VI, pseudokonins from the fungus *Trichoderma pseudokoningii*	10	5	193
Scylichornin I, two analogues of	10	8	194
P775 peptide, an inhibitor bound to the [C/N] NS3 protein of human hepatitis C virus	10+180	8	24
Kassinin, the tachykinin nuropeptide	12	8	195
α-Conotoxin SI	13	9	196
Two synthetic α-helix – β-hairpin peptides, designed using 'Lego approach'	17	12	197
RTD-1, a cyclic antimicrobial defensin from rhesus macaque leukocytes	18	7	198
E6ap, papillomavius E6 interacting peptide of E6AP residues 391–408	18	17	199
PNNP, SM50 intracrystalline biomineralization protein, residues 411–430	20	12	200
Beta-4, a synthetic four stranded β-sheet peptide	26	11	201
ω-conotixon TxVII from the venom of *Conus textile*	26	20	202
BmPO2, from the venom of the Chinese scorpion *Buthus martensi* Karsch	28	13	203
Conotoxin TVIIA from the venom of the piscivorous cone snail *Conus tulipa*	30	27	204
HpTX2, a toxin from *Heteropoda ventoria* spider	30	19	205
hPTH, the osteogenic fragment of the human parathyroid hormone, residues 1–31	31	5	206
Maurocalcine, a toxin from the venom of *Scorpio maurus*	33	29	207
[N] NPY, neuropeptide Y	36	12	208
LB_6, the sixth ligand-binding module of the human low-density lipoprotein receptor, Ca^{2+}	39	32	209
BuTX, butantoxin from the venoms of Brazilian scorpions	40	47	210
DLP-2, defensin-like peptide-2 from platypus venom	42	24	211
[C/N] Nedd4 WWII, domain of rat ubiquitin ligase complexed with EnaC P2 peptide	48+15	22	212
PLN [F41C], phospholamban	52	5	213
[N] TyrR residues 258–318, C-terminal DNA-bindin domain of the TyrR from *Haemophilus influenzae*	61	34	214
[N] Ccc2A apo, yeast copper transporter domain	72	35	215
[N] Atx1 Cu^{1+}, yeast metallochaperone	73	42	216
[C/N] RPB5, RNA polymerase subunit from *Methanobacterium thermoautotrophicum*	77	41	217
[C/N] PyJ, the N-terminal, DnaJ-like domain of murine polyomavirus tumor antigens	79	44	218

Cont'd

Table 5.1 *Cont'd*

Name	*a*	*b*	*Ref.*
LB_{1-2}, the first and second ligand-bindin modules of the human low-density lipoprotein receptor, Ca^{2+}	93	32	219
[N] oxidized plastocyanin Cu^{2+}, from the cyanobacterium *Synechocrystis* PCC6803	98	28	220
[N] $p13^{MTCP1}$, the human oncogenic protein	105	80	221
[C/N] C1-T1, NaProPI residues 25–135, derived from a circular precursor protein from *Nicotiana alata*	111	32	222
[C/N] TNFR-DD, the death domain of the tumor necrosis factor receptor-1, residues 315–426	112	55	223
[C/N] PH domain from the *C. elegans* muscle protein UNC-89, residues 341–458	118	44	224
[N] α-sarcin, the cytotoxic ribonuclease	150	119	225
[N] $^{6}F1\ ^{1}F2\ ^{2}F2$, fragment from human fibronectin residues 274–433	160	69	226
[C/N] Ap_4A hydrolaze from *Lupinus angustifolius* L.	160	94	227

[a] The number of amino acid residues.
[b] The total number of vicinal backbone and side chain proton–proton couplings measured.
[c] Number not reported.

Table 5.2 *Nucleosides, nucleotides and oligonucleotides for which $^3J_{HH}$ has been used as a structural parameter*

Name	*Ref.*
A series of seco type *C*-nucleosides	232
A series of bicyclic nucleosides	233
Tricyclic nucleosides derived from D-glucose	234
Deoxyxylothymidyl-3′-*O*-acethylthymidyl (3′,5′)-*O*-(2-cyanoethyl)-phosphorothioate	235
d(GCATTAATGC)$_2$, 2′-S or 2′-R deuterium labelled	230
d(CGCGAATTCGCG)$_2$ and d(CGCG^{d}A^{d}ATTCGCG)$_2$ ^{d} = H2″ deuterated	17
d(GGCAAAAAACGG)/d(CCGTTTTTTGCC) containing an A-tract	236
r(cucuccuucucuu)(GAGAGGAAGAGAA)	237

proton–proton couplings have been utilised in 3D structure calculations of numerous peptides and proteins listed in Table 5.1.

The products of degradation of ethenoadenosine have been studied by Speina *et al.*[228] using $^3J_{HH}$ couplings and simultaneously, the structures of bi-imidazole nucleosides obtained by ring opening of etheno derivatives of adenosine have been established by Kronberg and co-workers.[229] The conformation of the sugar ring in 2′-*R* and 2′-*S* deuterium-labelled DNA decamer has been studied by Kyogoku and co-workers[230] using proton–proton couplings. The conformational dynamics of two α-containing duplexes, d(GCGAAT-3′-3′- αT-5′-5′-CGC)$_2$ and d(ATTG-3′-3′- αT-5′-5′-GCTC)·r(gagcaccau), has been studied by Germann and co-workers[231] using molecular dynamics and time-averaged NMR restraints; the *J*-data served as an independent experimental parameter for evaluation of the calculated structure ensembles. Further examples of nucleotide structures evaluated by the use of $^3J_{HH}$ couplings are given in Table 5.2.

The structure of the apigeninidin and luteolinidin-5-glucoside from the Gesneriad *Sinningia cardinalis* has been solved with the help of $^3J_{HH}$ couplings by Swinny and co-workers.[238] The conformational behaviour of fucosyl- and carbafucosyl mimetics has been studied by Jiménez-Barbero and co-workers.[239] The validity of the predictions obtained by the molecular mechanics calculations was tested using *J* values. The flexibility of the aldopyranosyl ring of α- and β-D-idopyranose has been described by Tobiason *et al.*[240] using computed Altona–Hasnoot-modified Boltzmann-averaged vicinal proton–proton couplings. MM3 modelling of ribose and 2-deoxyribose ring puckering by the use of $^3J_{HH}$ couplings has been performed by Dowd and co-workers.[241] Their results indicate that the investigated compounds exist in several tautomeric forms and in multiple conformations in solution. The $^3J_{HH}$ coupling value of 9 Hz has been observed by Lewis *et al.*[242] for the signal of the anomeric proton of a *C*-glycoside fragment of spinosin, a *C*-glycoside flavonoid isolated from the plant *Desmodium tortuosum*.

Solvent-dependent conformational changes in a mono-functionalized β-cyclodextrine, mono-(3-Tyr-3-deoxy-*altro*)- β-CD, have been followed by

Table 5.3 *Carbohydrates for which $^3J_{HH}$ couplings have been used as a structural parameter*

Name	*Ref.*
α- and β-D-idopyranose	240
2,6:3,4-dianhydro-α-D-altropyranoside	244
N-functionalized D-*arabino*-hex-2-ulosonic acid	245
Methyl 4,6-*O*-benzylidene-3-deoxy-3-phthalimido-α-D-altropyranoside derivatives	246
A series of flavone glycosides from *Sideritis hyssopifolio*	247
A series of five tri- and tetrasaccharides from *Asparagus ocinalis* L.	248
A new phenylpropanoid glycoside from *Scrophularia scorodonia* L.	249
β-D-(1→3,1→6)-linked glucans	250
SanOrg34006, the antithrombotic synthetic pentasaccharide	251
Templated cellodextrins T-*x* and T-*x*-*x* (where *x* = 1–4, 8), a mimic for cellulose I	252
Carbohydrates for which $^3J_{HC,OH}$ couplings have been also used	
A series of sixteen disaccharides with 1,3-, 1,4- and 1,6-linkages	253
Lactose, cellobiose, maltose, sucrose, agarose, *N*,*N*-diacetylchitobiose and hyaluronates	254
β-D-Glc*p*NAc-(1→4)-β-D-Glc*p*NAc-*N*-Asn; β-D-Gal*p*-(1→3)-α-D-Gal*p*NAc-*O*-Ser	255
α-L-Fuc*p*-(1→2)-β-D-(Gal*p*-(1→3)[α-L-Fuc*p*-(1→4)]-β-D-Glc*p*NAc-1-O$(CH_2)_2$NHCOCHCH_2	256

Berthault and Birlirakis[243] by the use of vicinal proton–proton couplings. In particular, a formation of a stable self-inclusion complex accompanied by a local structural modification of the substituted altrose ring has been observed by the authors.

Several examples of carbohydrates whose structure and/or conformation have been found using proton–proton vicinal couplings are listed in Table 5.3.

A full set of proton–proton couplings, mainly vicinal $^3J_{HH}$ couplings, has been measured for 35 mammalian brain metabolites by Maudsley and co-workers.[257]

$^3J_{HH}$ couplings have been extensively used by Arnó *et al.*[258] in order to determine the ratio of the different conformers in the six-membered C-ring of the podocarpene derivatives, by Chang *et al.*,[259] who elucidated the structure of a series of five new carbolactone-containing bishomoscalarane sesterterpenes isolated from the marine sponge *Phyllospongia lamellosa* and by Cerda-Garcia-Rojas *et al.*,[260] who performed detailed NMR studies of two acetyl derivatives of copteroside E, a triterpenoid saponin, isolated from the flowers and leaves of *Verbesina suncho* Blake, a shrub which grows in northern Argentina. A conformational analysis by the use of vicinal proton–proton couplings has been performed by Perry *et al.*[261] for the sesquiterpene lactone goyazensolide isolated from the Brazilian species *Lychnophora passerina*, by Flores-Sandoval *et al.*[262] for the tricyclic sesquiterpene β-panasinsene, the essential oil of the commercially widespread roots of *Panax ginseng* and its two

derivatives, and by Oberlies *et al.*[263] for two novel clerodane diterpenoids, intrapetacins A and B isolated from *Likania intrapetiolaris*. The stereochemistry of a sesquiterpene alcohol ledol isolated from the leaves of *Renealmia chrysotrycha* has been established by Kaplan *et al.*[264] mainly by the use of vicinal proton–proton couplings and NOE interactions. The chamigrenes johnstonol, pacifenediol, pacifidiene and pacifenol have been isolated from the Brazilian mollusc *Aplysia dactilomela*; a complete analysis of the ^{1}H and ^{13}C NMR spectra of these highly substituted sesquiterpenes has been performed by Kaiser *et al.*[265] yielding also a set of proton–proton couplings. The structural study of the various sulfite derivatives of a 6 α-sesquiterpene lactone vulgarin isolated from *Artemisia canariensis* has been performed by Garcia-Granados *et al.*;[266] for a series of these compounds $^{3}J_{HH}$ couplings have been calculated by the use of the Haasnoot–Leeuw–Altona[267] equation and compared with the experimental data when available.

Mori and co-workers[268] have solved the structure of the synthetic triterpene with the help of vicinal proton couplings and have disproved in this way the structure of naurol A, a cytotoxic metabolite of a Pacific sponge, proposed earlier. Garson and co-workers[269] reported vicinal proton couplings for three new sesquiterpenes from a tropical marine sponge *Dysidea* sp., namely 6-hydroxyfurodysinin-*O*-methyllactone, 2-(2′,4′-dibromophenoxy)-4,6-dibromoanisole and dehydroherbadysidolide. Podányi and co-workers[270] have used $^{3}J_{HH}$ couplings for structure elucidation of fumagillin-related natural products.

The total stereochemical elucidation of the structure of a cytotoxic 6-tetraacetyl-oxyheptenyl-5,6-dihydro-α-pyrone from *Hyptis spicigera* has been carried out by Pereda-Miranda and co-workers[271] with the use of molecular mechanics and $^{3}J_{HH}$ couplings analysis.

The pattern of vicinal proton–proton couplings measured for six unnaturally configured 13-*epi* steroids has been analysed by Fielding *et al.*[272] in order to get insight into the conformation of the C-D rings of these compounds.

$^{3}J_{HH}$ couplings have been of some help in the elucidation of the structure of a new C_{22}-quassinoid isolated from *Picrolemma sprucei* Hook by Vieira *et al.*[273]

Determination of the dihedral angles using extended Karplus equations has been performed for new analogous progesterone haptens by Korde *et al.*[274]

Three- and four-bond proton–proton couplings have been measured by Siergiejczyk *et al.*[275] for (*E*)-asarone, ([(*E*)-1-propenyl]trimethoxybenzene) and its five isomers, the compounds which exhibit significant hypolipidemic activity.

Configurational assignments of four diastereomers of the γ-lactone 2-ethyl-4-methyl-5-oxotetrahydrofuran-3-carboxylic acid by the use of $^{3}J_{HH}$ couplings and molecular modelling have been made by Stortz and Maier.[276]

The full spectral characteristics including $\delta(^{1}H)$ and $\delta(^{13}C)$ chemical shifts and proton–proton couplings have been reported by Molero *et al.*[277] for a series of derivatives of 3,5-disubstituted tetrahydro-2*H*-1,3,5-thiadiazine-2-thione, by Sonnenburg *et al.*[278] for a series of bis-(2-chloroethyl)amino-substituted diazaphosphorinones and by Georgescu *et al.*[279] for 3-substituted

quinazolin-4(3*H*)-ones. Furthermore, $^3J_{HH}$ have been reported for a series of unsaturated hexenones and heptenones,[280] for *cis*- and *trans*-3-hexenoic acids,[281] for several hydroxycyclopentylpropenone derivatives,[282] and for four 2,4,6,8-tetraaryl-3,7-diazabicyclo[3.3.1]nonan-9-ones[283] whose skeleton is present in the lupin alkaloids. $^3J_{HH}$ couplings have been employed by Nazarski and Leśniak[284] in their studies on the configuration and conformation of some bicyclic lactams. The vicinal proton–proton couplings played an important role in the conformational analysis performed by Kurteva and Lyapova[285] on 4,5,6-triphenyltetrahydro-1,3-thiazine-2-thiones, their *N*-alkyl derivatives and some 1-methyl-2,3,4-triphenylazetidines, and by Dvořáková *et al.*[286] on some tetrahydropyran derivatives prepared by hetero-Diels–Alder reaction between ethyl vinyl ether and 1-oxa-1,3-butadienes bearing a chiral substituent in position 4. The stereochemistry of 1,3-oxazino[3,2-*d*][1,5]benzodiazepine-1-ones has been studied by Xu *et al.*[287] by the use of vicinal couplings; the same parameter has been applied by Pandiarajan[288] and Ivanov[289] to establish the conformational preferences in some derivatives of piperidines,[288] methyl esters and dimethylamides of diastereomeric 4-cyano-3,4-diphenylbutanoic acids.[289]

$^3J_{H2'H3'}$ couplings of 2.9–4.4 Hz have been measured for a series of *N*-(3-hydroxy-2-methyl-3-phenylpropionyl)- and *N*-(3-hydroxy-2-methylbutanoyl)-hexahydrobenzoxazolidin-2-ones,[290] which are the products of the aldol condensation between *cis*- and *trans*-oxazolidin-2-ones and the corresponding aldehydes. These coupling values allowed the authors to assign the *syn* relative configuration at the newly created centres. $^3J_{H2'H3'}$ of 7–9 Hz is expected for the *anti* diastereoisomers. $^3J_{HH}$ couplings of rather typical values have been measured by Karpyak *et al.*[291] for a series of (*E*)-1-aryl-3-(4-nitrofenoksy)propenes.

A series of optically active *cis*-3 bis-adducts of C_{60} has been synthesised by Kessinger *et al.*[292] *via* regio- and stereoselective Bingel macrocyclization of C_{60} with bismalonates, which contain optically active tethers derived from 1,2-diols; for one of these compounds shown in Figure 6, a coupling of 7.9 Hz between the vicinal glycolic H-atoms has been found, which is in agreement with the *ap* conformation. This result in combination with the theoretical data allowed the authors to assign the ^{f}C-configuration to the inherently chiral addition pattern.

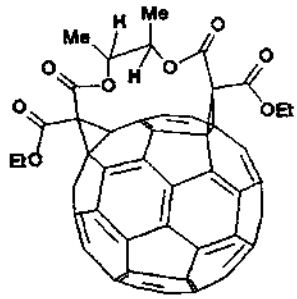

$^3J_{HH}$ = 7.9 Hz

Figure 6

Extensive use of vicinal proton–proton couplings has been made by Fraenkel and Qiu[119] in their studies on the structure and dynamic behaviour of several methyl substituted allylic lithium compounds, by Shestakova *et al.*,[293] who studied the structure of the complex between lanthanum(III) nitrate and 1,9 diaza-18-crown-6, and by Goto *et al.*[294] whose subjects of interest have been square-planar ternary platinum(II) complexes with *N*-ethyl- or *N*-benzyl-1,2-ethanediamine and 2,2′-bipyridine or 1,10-phenanthroline.

The full spectral characteristics which also included vicinal proton–proton couplings have been reported by Maeyama *et al.*[295] for the adduct of acetylene at sulfur in an oxygen- and sulfur-bridged open cubane cluster complex of tungsten isolated as $K_{0.5}(Hpy)_{3.5}[W_3(\mu^3\text{-}S)(\mu\text{-}O)(\mu\text{-}S)(\mu\text{-}SCH{=}CH_2)(NCS)_9]$.

An analysis of the mechanism governing the coupling between the vicinal protons in ethane and fluoroethane has been studied by Contreras and co-workers[296] by the developed by them method of natural bond orbital interactions between bonds and antibonds, $\sigma_m \rightarrow \sigma^*_n$. The authors have concluded that the main contribution to $^3J_{HH}$ comes from the through space term while the introduction of a fluorine changes this term and yields a direct contribution to the coupling.

$\delta(^1H)$ chemical shifts and proton–proton couplings of several simple aromatic and aliphatic organic molecules have been calculated by Bagno[297] by the use of the DFT method. The calculated parameters have been furthermore used for a simulation of the ^1H NMR spectra of the molecules with more complex spin systems. Very good agreement with the experimental spectra with no prior knowledge of the involved parameters has been observed by the author.

8 Three-bond Couplings Between Hydrogen and Heteronuclei

Hennig *et al.*[298] have measured a full set of heteronuclear $^3J_{C\alpha HN}$ and $^3J_{C\alpha C\alpha}$ couplings in the protein ubiquitin. The authors suggested a non-Karplus-type dependence of these couplings on the torsional angle of the proceeding residue. Several examples of proteins whose solution structure has been elucidated with the help of heteronuclear couplings are listed in Table 5.4.

Bundle and co-workers[306] experimentally re-calibrated the Karplus relationship of $^3J_{HC}$ couplings in carbohydrates. They found that the numerical values for the coupling across the oligosaccharide glycosidic bond for torsional angle close to 180° were underestimated by 10–20%. The values of experimentally measured $^3J_{HC}$ and $^3J_{HH}$ couplings have been used by Momany and Willett[307] to test computed conformations in DFT studies on maltose and cyclodextrins. Serianni and co-workers have continued their interesting theoretical and experimental studies on J_{HC} and J_{CC} couplings in saccharides.[308,309] Recently they have published the results concerning the effect of C4–C5 bond rotation on structural parameters of 2-deoxy-β-D-*erythro*-pentafuranose.[308] The structures of this compound have been optimised with the DFT and the corresponding $^nJ_{HC}$ and $^nJ_{CC}$ (where n = 1, 2, 3) couplings have been calculated with the same method. Predicted averaged $^1J_{HC}$ and $^3J_{CC}$ couplings have been

Table 5.4 *Peptides and proteins for which heteronuclear couplings have been used as a structural parameter in 3D structure calculations*

Name	*a*	*b*	*c*	*Ref.*
[β-iPrPhe[3]]deltorphin I	7	19	$^3J_{HC}$	299
[N] USH-F1, a zinc finger from the FOG family protein, residues 202–235	36	32	$^3J_{HN}$	300
[N] USH-F6, a zinc finger from the FOG family protein, residues 1113–1146	36	29	$^3J_{HN}$	300
[C/N] DinI, from *E. coli*	81	63	$^3J_{CC}$, $^3J_{CN}$	301
[C/N] AFX-DBD residues 92–181, complexed with DNA 16-mer	90+	[d]	$^3J_{HN}$	302
[N] MNEL, a single chain monellin	96	184	$^3J_{hn}$	303
[C/N] MotNF, the transcriptional activation domain of the bacteriophage T4 protein	96	[d]	$^3J_{CC}$, $^3J_{CN}$	304
]C/N] PAH2-SID complex, PAH2 = mSin3A (295–383), SID = Mad 1 (6–21)	109+16	124	$^3J_{HN}$, $^3J_{CC}$, $^3J_{CN}$	305

[a] Number of residues.
[b] Total number of vicinal couplings measured (homonuclear $^3J_{HH}$ couplings are also included if measured).
[c] Types of heteronuclear couplings measured.
[d] Number not reported.

calculated by Mazeau *et al.*[310] using MM3(92) force field for four combinations of β(1→4) linked glucosamine and *N*-acetylglucosamine.

The structures of two new pyrrolidine alkaloids, pandamarilactonine-A and -B isolated from *Pandanus amaryllifolius* Roxb, have been deduced by Takayama and co-workers[311] with the help of vicinal J_{HC} and J_{HH} couplings. Girault and co-workers[312,313] have determined conformations of free and ribosome-bound macrolide antibiotics using NMR and molecular modelling. The authors analysed $^3J_{HC}$ and $^3J_{HH}$ couplings of the proline and sugar part of lincomycin and clindamycin[312] and of the macrocycle as well as desosamine part of HMR 3647 (telithromycin).[313]

The three-dimensional structure of the antibiotic 6-*O*-methylerythromycin in water has been determined by Steinmetz *et al.*[314] by the use of torsional constraints obtained from proton–proton and proton–carbon vicinal couplings and distance constraints obtained from NOESY, ROESY and GOESY spectra.

A conformational analysis of naproxen anion[315] and monensin sodium[316] has been performed by the use of the $^3J_{HC}$ couplings. Especially extensive use of these couplings has been made by the authors in the case of the latter compound. They concluded that the conformation of monoensin in solution is very close to that in crystals. Further examples of the application of vicinal proton–carbon couplings in the conformational analysis of compounds include the NMR and quantum-chemical study of the stereochemistry of spiroepoxides obtained by oxidation of (*Z*)-3-arylidene-1-thioflavan-4-ones performed by Tóth *et al.*,[317] and the elucidation of the structure of isomalyngamides A and B isolated from a collection of the cyanobacterium *Lyngbya majuscula* from Hawaiian waters by Kan *et al.*[318]

The recently designed HECADE method has been applied by Koźmiński *et al.*[319] to the measurement of long-range ^1H–^{13}C couplings in tautomeric β-sulfonylenamines. The results obtained allowed the authors the qualitative characterisation of rotational degrees of freedom in all the isomers of the compounds studied.

The reaction between disubstituted 1,3-diynes such as 5,5-dimethyl-1-trimethylsilyl-1,3-hexadiyne with metallocenes $M(\eta^5\text{-}C_5H_5)_2$ studied by Baumann *et al.*[320] yielded a complex with the intact diyne when M = Ti and a σ,π-alkynyl-bridged dinuclear complex when M = Zr. These two types of compounds could be easily discriminated by the use of $^3J_{HC}$ couplings observed between the terminal carbon atoms of the 1,3-diyne moiety and the protons either of the t-Bu or the $SiMe_3$ group.

$^3J_{HH}$ and $^3J_{HF}$ couplings have been measured by Grée *et al.*[321] for a series of allylic fluorides and for the products of the Diels–Alder addition of these compounds to butadienes. The experimental coupling values have been subsequently compared with the couplings calculated for the predicted conformers of the compounds under study. This procedure allowed the authors to establish the conformational preferences in both groups of compounds.

The $^3J_{HP}$ and $^{2,3}J_{CP}$ couplings of uridine diphosphoglucose have been measured under a variety of conditions by du Penhoat and co-workers.[322]

They have found that magnesium ions lead to a significant increase in the average length of the molecule studied. Other examples of structural and conformational analysis of nucleotides by means of heteronuclear couplings are listed in Table 5.5.

The full NMR characteristics of a series of new class of bisphosphorus ligands, alkyl-tethered bisphosphoryl compounds with two 1,3,2-benzodiazaphosphorinone units and products of their oxidation have been reported by Fei *et al.*[333] $^3J_{HP}$ of 12–16 Hz have been observed for the MeNP fragments of the starting compounds and $^3J_{HP}$ of 8 Hz for the corresponding phosphoryl compounds. $^3J_{HP}$ and $^3J_{HH}$ couplings have been reported by Doherty *et al.*[334] for the $[Fe_4(CO)_{11}(\mu\text{-}PPh_2)_2\{\mu\text{-}\eta^1{:}\eta^2{:}\eta^1{:}\eta^2\text{-}(H)C{=}CHCHCHC{=}CH_2\}]$ complex and by Siedentop *et al.*[335] for spacer modified phosphorylated glucose derivatives (other examples are given in Table 5.6).

It has been found by Peralta-Cruz *et al.*[74] that the relative sign of the $^3J_{HP}/^2J_{CP}$ couplings is positive for the methylene and methyl groups of the sulfur and selenium adducts of 1,3-(dioxa, oxaza or diaza)-2-phospholanes; the sign changes for the corresponding borane adducts and for the compound with a phosphorus lone pair.

$^3J_{HSn}$ couplings provide useful information on the arrangment of the substituents around the double carbon–carbon bond, the *trans* couplings being significantly larger than the *cis* ones. Using this relationship Senda *et al.*[347] have assigned *Z* configuration to a series of 1-aryl-2-germyl-1-(stannyl)ethenes synthesised by them by the catalytic addition of tributyl(triethylgermyl)stannane to arylacetylenes.

J_{HTe} couplings across two and three bonds have been observed by Citeau and Giolando[348] in the ^{125}Te NMR spectra of a series of alkyl hex-1-ynyl tellurides recently synthesised by them.

$^3J_{HPt}$ couplings of *ca.* 35 Hz have been determined for some *cis*-Pt(II) complexes with amine and carboxylate ligands.[349]

Very large $^3J_{HTl}$ and $^4J_{HTl}$ coupling values combined with a large $^1J_{NTl}$ coupling observed in the spectra of a thallium(III) iminophenolate cryptate have been invoked by Drew *et al.*[350] as evidence of covalency in the Tl–N bond in this compound (see Figure 7).

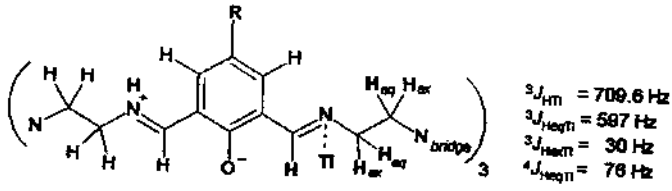

Figure 7

Table 5.5 *Nucleosides, nucleotides and oligonucleotides for which heteronuclear vicinal couplings have been used as a structural parameter*

Name	*a*	Ref.
UDP-Glc, uridine diphosphoglucose in presence of Mg^{2+}	$^{3}J_{HP}$, $^{2,3}J_{CP}$	322
5′-O-DMT-2′deoxythymidine 3′-*O*-(*S*-methyl-methanephosphonoselenolate)s	$^{3}J_{HP}$, $^{2,3}J_{CP}$	323
5′-O-DMT-2′deoxythymidine 3′-*O*-(*Se*-methyl-methanephosphonoselenolate)s	$^{3}J_{HP}$, $^{2,3}J_{CP}$	323
r[GCAm^{1}G-p-O(CH_2CH_2O)$_6$-p-UGCC]	$^{3,4}J_{HP}$	324
5′-CGCTAGCG-3′, a self-complementary octamer	$^{3}J_{HP}$	37
5′-CGCUUUUGCG-3′ hairpin, U = ^{13}C labelled uridine	$^{3}J_{HP}$, $^{3}J_{CP}$	38
r(GGAC)d(TTCG)2′F-a(GTCC), a hybrid hairpin, 2′F-ANA/RNA	$^{2,3,5}J_{HF}$, $^{3,5}J_{HP}$	325
5′-d(GAAGC-TTT-GCTTC)-3′, T_3 loop of the Adenoassociated Virus 2	$^{3,4}J_{HP}$, $^{2,3}J_{CP}$	326
d(GGGGCCCC)	$^{3}J_{HP}$	327
5′-d(AGGCG*CCT)$_2$, G* – guanines linked *via* a trimethylene interstrand cross-link	$^{3}J_{HP}$	328
[C/N] the conserved 690 hairpin from *E. coli* 16S rTNA, 687–700	$^{3}J_{HP}$	329
SL1 VBS RNA, 5′GGAG<u>A</u>CGC[GAUUC]GCGCUCC-3′, <u>A</u> – bulged	$^{3}J_{HP}$	330
Chimeric DNA, d(^{m}CG^{m}CGC$_L$G$_L$^{m}CG^{m}CG)·d(^{m}CG^{m}CGC$_L$G$_L$^{m}CG^{m}CG)	$^{n}J_{HP}$, $^{n}J_{CP}$	332

[a] Type of vicinal heteronuclear couplings measured; $^{3}J_{HH}$ homonuclear couplings have been also measured in most cases.

Table 5.6 *Carbohydrates for which heteronuclear couplings have been used as a structural parameter in conformational analysis*

Name	*a*	Ref.
2-Deoxy-β-D-ribofurosylamine	$^{1\text{-}4}J_{HC}$, $^{1\text{-}4}J_{CC}$	80
A series of phosphitylated monosaccharides	$^{3,4,6}J_{PP}$	336
α-D-Man*p*-(1→3)-β-D-Glc*p*-OMe	$^{3}J_{HC}$	337
N-Acetylneuraminosyl-(2→3)-lactose	$^{2,3}J_{HC}$	338
$[PtMe_3L]BF_4$, a series of four trimethyl-(carbohydrateplatinum tetrafluoroborate complexes	$^{2}J_{HPt}$	169
3,6-di-O-(α-D-mannopyranosyl)-α-D-mannopyranoside	$^{3}J_{HC}$	339
$(HSO_3)_2$-2,6Manα-2Glcα-1-*sn*-2,3-*O*-alkylglycerol	$^{3}J_{HC}$, $^{3}J_{HC,OH}$	340
[C-specific] $[PtMe_3L]BF_4$, L = α-D-mannofuranose or β-D-allofuranose	$^{3}J_{HC}$, $^{3}J_{CC}$	341
bis- and trissaccharidoguanidines	$^{1}J_{HC}$	342
2′-Fucosyllactose	$^{3}J_{HC}$	343
Sulfated derivatives of heparin	$^{1}J_{HC}$,	50
[C] hepta- and polysaccharide of the cell wall of *S. mitis J22*	$^{3}J_{HC}$, $^{3}J_{CC}$	344,345
ECA, a cyclic enterobacterial common antigen	$^{3}J_{HC}$	346

[a] Type of couplings measured.

9 Three-bond Couplings not Involving Hydrogen

Schwalbe and co-workers[351] have measured $^{3}J_{C\alpha C\alpha}$ and $^{3}J_{HNH\alpha}$ couplings in unfolded ubiquitin. The authors have found that the measured carbon–carbon couplings which are related to the ψ torsion angles are small with a mean value of 0.85 ± 0.2 Hz. This means that individual amino acids of the unfolded ubiquitin sample have both positive and negative torsion angles. The authors also observed that the measured proton–proton couplings fit in well with the predicted values, which supports the model of local conformational preferences in the denatured polypeptide chain.

The $^{3}J_{CC}$ couplings of several bis-^{13}C-labelled derivatives of farnesyl and geranylgeranyl have been measured in a variety of solvents by Zahn *et al.*[352] Since the measured coupling value does not depend on the solvent type it proves that the prenyl chain exists in all the solvents in an extended conformation.

The carbon–carbon one- and three-bond couplings have been determined for *cis* and *trans* cinnamic acids by Hanai *et al.*[353]

Long-range C–N couplings have been reported by Lyčka *et al.*[354] for the product of the coupling of benzenediazonium chloride with 1,3-dihydroxynaphthalene and benzenediazonium chloride with 1,5-dihydroxynaphthalene.

A set of $^{n}J_{CF}$ (n = 1–4), $^{n}J_{HF}$ (n = 3–5) and $^{n}J_{HH}$ (n = 3–5) has been published by Hametner *et al.*[355] for a series of nitrogen-containing bi- and trihetaryl compounds.

Ding[356] has measured $^{2,3}J_{CP}$ and $^{3,4}J_{HP}$ couplings in the fructose-1,6-diphosphate anion.

The *E* configuration has been assigned to (*E*)-2-(dialkylamino)alkenyl phosphonates by the use of vicinal C–P couplings. The compounds have been obtained *via* the regio- and stereospecifically proceeding addition of secondary amines to alkynylphosphonates.[357] Long-range C–P couplings have been determined by Reddy *et al.*[358] for 2-aryloxy/alkyl/phenyl-6-methyl-4*H*-1,3,2-dioxaphosphorino[5,4-*b*]pyridine-2-oxides and applied by Karataeva *et al.*[359] to establish the geometry of *N*-(thiophosphoryl)-*S*-organylbenzimidothioates.

The relationship $|^3J_{CSn}(trans)| > |^3J_{CSn}(cis)|$ has been applied by Wrackmeyer *et al.*[360] to establish the configuration of 4-(1-trimethylstannyl)butylideno- and 4-(2,2′-dimethyl-1-trimethylstannyl)propylideno-3-borahomoadamantanes.

Two- and three-bond C–Hg couplings of 140.4 Hz and 233.1 Hz, respectively, have been reported for 5-chloromercurio-2-thienylethanoic acid by Popović *et al.*[361]

Six homo- and heteronuclear Karplus relationships of vicinal couplings related to the φ torsional angle have been analysed with MD/DFT calculations and model peptides by Case *et al.*[362] It appeared that the average φ-torsion angle fluctuation amplitudes of ±24° had to be taken into account for ubiquitin in order to fit the calculated coupling values to the experimental ones. In addition, the authors have suggested that the ψ related $^3J_{NN}$ coupling does not obey the usual Karplus type relationship.

$^3J_{FF}$ and $^4J_{FF}$ couplings have been reported by Foris[363] for a large series of chlorofluorocarbons and hydrochlorofluorocarbons. A set of J_{CF} and J_{FF} couplings, which included those across three and more bonds, has been measured by Arfaoui and Haloui[364] for *p*-tetrafluorobenzoquinone. These data (also the signs of the couplings studied have been determined unambiguously) have been applied to study the orientation of the compound in four nematic liquid crystals.

It has been shown by Peralta *et al.*[67] that a spin-dipolar term might play an important role in the spin–spin F–F coupling across three and five bonds.

10 Couplings over More than Three Bonds and Through Space

The vicinal and allylic four-bond proton–proton couplings for ribafutinol, a reduced form of a naphthalenic ansamycin (ribafutin) have been applied by Santos *et al.*[365] in the elucidation of the three-dimensional structure of this compound. Full sets of the J_{HH} couplings have been reported for both ribafutin and ribafutinol.

The effect of stereoelectronic interactions on three- and four-bond proton–proton couplings in hydrocarbons has been studied by Sproviero and Burton.[366]

The substituted triazine, a dye, shown in Figure 8, undergoes internal rotation of the substituents about the triazine ring. This is reflected in the ^{1}H NMR variable-temperature spectra of the H(3′)H(5′)H(6′) system, an analysis of which has been performed by Birkett *et al.*[367] for the H3′ proton only yielding the relevant four- and five-bond proton–proton couplings. The

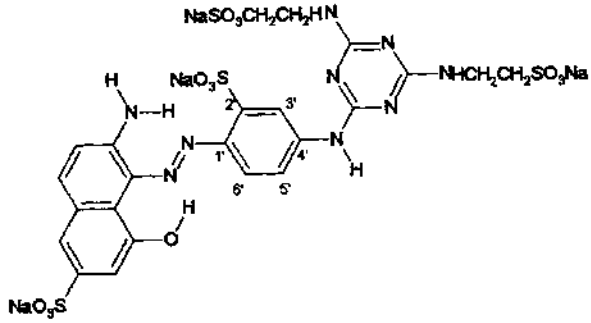

Figure 8

obtained results have been analysed in order to get insight into the exchange processes occurring in this molecule.

The proton–proton couplings across three, four and five bonds have been determined and analysed by Kania *et al.*[368] in their studies on the structure of a series of derivatives of 5,6,11-trimethyl-6*H*-indolo[2,3-*b*]quinolinium methylsulfate.

The stereospecifity of the proton–proton couplings across five bonds has been applied by Garrigues[369] in elucidation of the conformation of derivatives of thiophene in solution.

Long-range $^4J_{HH}$, $^5J_{HH}$ and $^3J_{HH}$ couplings have been extensively used by Therien and co-workers[370] in the structure determination of the unusually rigid π-stacked porphyrin-bridge-quinone system.

The presence of a through-space, formally across seven bonds, proton–proton coupling of 0.4 Hz has been observed by Bhacca *et al.*[371] in the spectrum of alkaloid tiliacorine extracted from the plant *Tiliacora racemosa*. It has been shown by the authors that the two protons which are located in different benzene rings are unusually close to one another in space (see Figure 9).

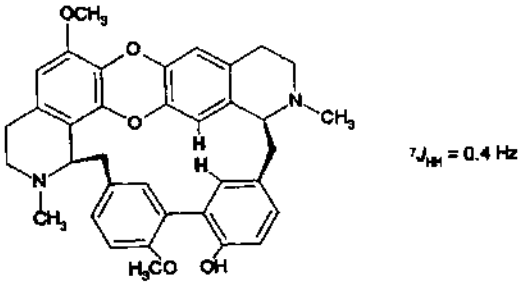

Figure 9

Small $^4J_{HC}$ couplings (less than 2.3 Hz) between the *N*-methyl protons and the quaternary carbons of the tolyl group have been reported by Tokunaga *et al.*[372] for several triarylstibanes bearing an amino side chain. No clear relationship between these couplings and the steric parameters has been observed.

$^6J_{HF}$ of 1.8 Hz between the 3-CF_3 fluorines and the hydrogens of the platinum-bound methyl groups has been observed by Fekl *et al.*[174] in the spectrum of the novel platinum(IV) complex, $Tp(CF_3)_2PtMe_3$, where $Tp(CF_3)_2$ denotes hydridotris(3,5-bis(trifluoromethyl)pyrazolyl)borate. This is the first example of a formal $^6J_{F\text{-}H(\text{-}C)}$ coupling in complexes involving hydridotris(pyrazolyl)borate ligands

The ^{1}H NMR spectra of *N,N*-dibenzyl- and *N*-methyl,*N*-benzylphosphoramidochloridic acid 4-methylphenyl esters revealed a splitting of the signal of the Me group of *p*-cresol caused by a seven-bond H–P coupling, $^7J_{HP}$ of 1.2–1.5 Hz.[373] No such splitting has been observed in their fluoridic analogues.

Abraham and his co-workers[374] have continued their studies on conformational analysis of small aliphatic molecules. Recently, they have published a paper devoted to NMR, solvation and theoretical investigation of conformational isomerism in *N,N*-dimethylfluoroacetamide and *N,N*-dimethyl-α-fluoropropionamide, where $^5J_{CF}$, $^1J_{CF}$ and $^4J_{CF}$ analysed by solvation theory played an important role. It has been shown by the authors that all these couplings measured in different solvents are sensitive to the F–C–C=O orientation.

The presence of the through-space C–P coupling of 2.3 Hz, analogous to that observed in $W(CO)_5(\eta^1\text{-}PPh_2CH_2PPh_2)$,[375] has been suggested by Jiang *et al.*[376] for the $(OC)_3(Me_3P)_2OsW(CO)_5$ complex.

A $^4J_{FF}$ coupling is the largest coupling occurring in the ^{19}F NMR spectra of perfluoroalkyl groups ($^4J_{FF} > {}^3J_{FF} \approx {}^5J_{FF}$). This observation facilitated considerably the assignment of the signals in the spectra of a series of bis(*n*-perfluoroalkyl)zinc compounds, $Zn(n\text{-}C_mF_{2m+1})_2{\cdot}2THF$ (m = 4, 6, 7, 8) and $Zn(n\text{-}C_6F_{13})_2{\cdot}2CH_3CN$, synthesised and studied by Schorn *et al.*[377]

Almost all possible fluoro derivatives of dimethyl bicyclo[1.1.1]pentane-1,3-dicarboxylate have been synthesised and their spectra measured by Michl and his co-workers.[378] The couplings across four bonds have been found to be particularly large (50–100 Hz), showing an inverse linear dependence on the calculated F–F distance in the range of 2.43–2.58 Å.

Recently Mallory and his group[379] have measured J_{FF} couplings for a set of eighteen compounds structurally related to 1,8-difluoronaphthalene for which an exponential relationship has been found with d_{FF}. (These results have been interpreted in terms of pσ interactions of the in-plane p_F lone pairs on the coupled fluorines. This conclusion has been corroborated by theoretical calculations performed by Peralta *et al.*,[380] who deconvoluted DFT and *ab initio* Fermi contact-derived couplings into conceptually familiar localised orbital contributions. They, however, have also drawn attention to the previously unrecognised importance of angular effects and X–F bond–bond coupling contributions. The DFT calculations of through-space F–F couplings for a number of model compounds have been also performed by Arnold *et al.*[381]

The small P–P coupling of 0.4 Hz across formally up to eight bonds has been observed by Pouysègu *et al.*[336] in the spectrum of methyl 2,3,4,6-tetrakis-*O*-(4,4,5,5-tetramethyl-1,3-dioxa-2-phospholanyl)-α-D-mannopyranoside. The

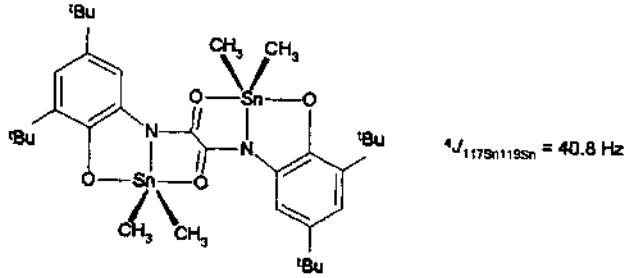

Figure 10

authors suggest that the dominant interaction in these couplings is *via* O→P coordination between neighbouring phosphite groups.

The P(III)–Se coupling across formally five bonds, $^5J_{PSe}$ of 54 Hz, and $^4J_{PP}$ of 53 Hz have been observed by Karaçar *et al.*[382] in the spectrum of a selenium derivative of 1,8-bis(diphenylphosphino)naphthalene and interpreted in terms of the through-space interaction due to the close proximity of the λ^3 and λ^5 phosphorus substituents at the peri-positions of the naphthalene backbone.

The presence of the four-bond ^{119}Sn–^{117}Sn coupling of 40.8 Hz observed by Contreras *et al.*[383] in the spectrum of the reaction product of bis(2-hydroxy-3,5-di-*tert*-butylphenylanilido)oxalic acid with dimethyltin dichloride shown in Figure 10 provided unambiguous evidence that the molecule contains two equivalent tin atoms.

11 Couplings Through Hydrogen Bonds

Recently detected couplings across hydrogen bonds have become an object of great interest. Theoretical studies on this topic have been performed by Del Bene *et al.*, who analysed the parameters which determine N–N and O–O couplings, $^{2h}J_{XX}$ across X–H···X hydrogen bonds,[384] and considered to what extent the bonding at the nitrogens influences $^{2h}J_{NN}$.[385] Comprehensive *ab initio* studies of the nuclear magnetic resonance shielding and couplings in XH–O hydrogen-bonded complexes of simple organic molecules have been performed by Pecul *et al.*[386] It has been concluded by the authors that the $^{1h}J_{HY}$ and $^{2h}J_{XY}$ couplings are substantial and dominated by the Fermi contact term. Quantum chemical modelling of the through-hydrogen bond spin–spin coupling in amides and ubiquitin has been performed by Bagno.[387]

A large $^{2h}J_{NN}$ coupling of 8.7 Hz across the hydrogen bond mediated by the proton has been reported by Pietrzak *et al.*[388] for the well-known proton sponge 1,8-bis(dimethylamino)naphthalene, DMANH$^+$. It was a rather difficult spectroscopic problem to solve since the ^{15}N atoms involved are magnetically equivalent. It was overcome by a synthesis of the ^{15}N doubly labelled compound and an analysis of the corresponding higher-order spectra measured at different magnetic fields.

A $^{2h}J_{NN}$ coupling of 8.5 Hz has been measured by Claramunt *et al.*[389] in 6-aminofulvene-1-aldimine, which represents an example of a new class of compounds exhibiting couplings across the hydrogen bond. No significant effect was observed when protium was replaced by deuterium.

Several very interesting papers were published last year on couplings across the hydrogen bond in molecules of biological importance. They include studies of the nature of this coupling and its dependence on the pressure and temperature. The most spectacular achievements include a detailed analysis of α-helix formation in a peptide and structural changes of the protein imposed by ligand binding.

The chemical nature of hydrogen bonding in proteins has been studied by Arnold and Oldfield.[390] The authors have drawn the conclusion that the $^{3h}J_{NC'}$ coupling is mediated by a closed shell non-covalent interaction between the donor hydrogen atom and the acceptor oxygen atom. Using the DFT method, Barfield *et al.*[391] have studied the dependence of $^{1h}J_{HN}$ and $^{2h}J_{NN}$ couplings on the distance between the donor and acceptor atoms in a DNA triplex. They have also determined a positive sign for the $^{2h}J_{NN}$ couplings from an E.COSY experiment.

Both increased and decreased $^{3h}J_{C'N}$ couplings have been observed by Li *et al.*[392] in the uniformly $^{13}C/^{15}N$-labelled immunoglobulin binding domain of streptococcal protein G measured under 30 and 2000 bar. Jaravine *et al.*[393] in a very elegant paper have traced TFE induced helix formation in the S-peptide of Ribonuclease A. Populations of H-bond estimated from the measured $^{3h}J_{C'N}$ couplings for each residue of the S-peptide fit in well with the populations predicted by the use of the Lifson-Roig model. Cordier *et al.*[394] have measured forty $^{3h}J_{C'N}$ couplings in free and ligand-bounded form of the chicken c-Src SH_3 domain. This is the first application of scalar couplings to examine ligand-induced structural changes at picometer resolution. Correlations between $^{1}J_{C'N}$ and $^{3h}J_{C'N}$ couplings in the hydrogen-bonding network of human ubiquitin have been studied by Juranić and Macura.[395]

Kainosho and co-workers[396] have studied temperature dependence of $^{2h}J_{NN}$ couplings in ^{15}N-selectively enriched DNA oligomers. The authors observed a significant decrease of the coupling value with the rise of the temperature.

Several other interesting couplings measured in protein and nucleic acids are listed in Table 7.

EOM-CCSD and MP2 calculations have been performed by Chapman *et al.*[403] on the equilibrium structure of the hydrogen-bonded complex, ClH : pyridine, at different field strengths in order to calculate the ^{15}N–^{35}Cl spin–spin coupling across the hydrogen bond. The authors found that this coupling has a distinct maximum at a field of 0.0040 a.u. and therefore, by analogy to proton-stretching frequency, can be a useful indicator of the hydrogen-bond type and intermolecular distance.

The NMR and IR spectra measured by Jasim and Perutz[404] for two platinum bifluoride complexes, *trans*-$[Pt(PCy_3)_2H(FHF)]$ and *trans*-$[Pt(PPr_3)_2H(FHF)]$ have shown that the bifluoride ligand in these compounds

Table 5.7 *Compounds for which scalar couplings were measured through the hydrogen bond*

Name	*a*	*b*	*c*	*Ref.*
[N] $tRNA^{Trp}$ A73 mutant from *B. subtilis*, 25 kDa	N–**H**···N	$^{1h}J_{HN}$	13	42
$d(CGCGAATTCGCG)_2$ with C-G and A-T ^{15}N enriched	N–**H**···N	$^{1h}J_{HN}$	2	397
CopA29, the RNA hairpin	N–H···N	$^{2h}J_{NN}$	9	398
[C/N] $d(GGGTTCAGG)_2$, a G3-A7 mismatch	N–H···N	$^{2h}J_{N6N3}$	1	43
[C/N] $d(GGGCAGGT)_4$, a G3-A7 mismatch	N–H···N	$^{2h}J_{N6N3}$	1	43
DNA triplex		$^{1h}J_{HN}$, $^{2h}J_{NN}$	51	391
[C/N] human FKBP12, side chain–side chain, Arg71-Asp100	N_ε–H···O=C_γ	$^{3h}J_{C\gamma N\varepsilon}$	1	399
[C/N] human FKBP12, backbone–side chain, Met49-Glu54	N–H···O=C_δ	$^{3h}J_{\delta N}$	1	400
FMN–[N] flavodoxin complex	N–H···O–**P**	$^{3h}J_{NP}$	1	401
FMN–flavodoxin complex	N(or O)–**H**···O–**P**	$^{2h}J_{HP}$	8	401
[C/N]HTLV-1 Rex peptide – [C/N] RNA aptamer complex	N–H···N	$^{2h}J_{NN}$	3	402
[C/N] S-peptide	N–H···O=C	$^{3h}J_{NC'}$	11	393
[N/C] chicken c-Src SH_3 domain, free nad ligand-bound	N–H···O=C	$^{3h}J_{NC'}$	40	394
[N/C] chicken c-Src SH_3 domain, backbone–side chain	N–H···O=C	$^{3h}J_{NC}$	2	394

[a] Hydrogen bond type, symbols of nuclei involved are given in bold.
[b] Type of couplings measured.
[c] Number of couplings measured.

involves a hydrogen bond Pt–F···H–F. A $^{2h}J_{FF}$ coupling of 103 Hz has been found for both compounds in their low temperature NMR spectra.

EOM-CCSD calculations have been performed by Del Bene *et al.*[405] to evaluate theoretically the $^{4h}J_{PP}$ coupling through N–H^+–N hydrogen bond in a model system; the theoretical values calculated *versus* the P–P distance have been compared with the experimental value, $^{4h}J_{PP}$ of 3 Hz, determined earlier (in 1993) by Laynez and co-workers[406] for 1,8-bis(dimethylamino)naphthalene in which both dimethylamino groups were replaced by iminophosphorano groups. Reasonably good agreement has been found between the J value calculated for $d = 5.79$ Å and the experimental one.

12 References

1 K. Kamieńska-Trela and J. Wójcik, *Specialist Periodical Report: Nuclear Magnetic Resonance*, 2001, **30**, 132.
2 R.K. Harris, J. Kowalewski, S. Cabral de Menezes, *Pure Appl. Chem.*, 1997, **69**, 2489.
3 R.H. Contreras, J.E. Peralta, *Prog. NMR Spectrosc.*, 2000, **37**, 321.
4 A.J. Dingley, F. Cordier, S. Grzesiek, *Concepts Magn. Reson.*, 2001, **13**, 103.
5 R. Riek, K. Pervushin, K. Wüthrich, *Trends Biochem. Sci.*, 2000, **25**, 462.
6 E.T. Mollova, A. Pardi, *Curr. Opin. Struct. Biol.*, 2000, **10**, 298.
7 A. Lyčka, *Annu. Rep. NMR Spetrosc.*, 2000, **42**, 1.
8 E. Kleinpeter, *Adv. Mol. Struct. Res.*, 2000, **6**, 97.
9 L. Sobczyk, *Appl. Magn. Reson.*, 2000, **18**, 47.
10 G.E. Martin, C.E. Hadden, *J. Nat. Prod.*, 2000, **63**, 543.
11 R.M. Schoth, D. Sevenard, K. Pashkevich, G.V. Roschenthaler, *Coord. Chem. Rev.*, 2000, **210**, 101.
12 J.O. Duus, C.H. Gotfredsen, K. Bock, *Chem. Rev.*, 2000, **100**, 4589.
13 R.J. Ferrier, *Carbohydr. Chem.*, 2000, **31**, 312.
14 D. Acquotti, S. Sonnino, *Methods Enzymol.*, 2000, **312**, 247.
15 M. Michalik, M. Hein, M. Frank, *Carbohydr. Res.*, 2000, **327**, 185.
16 D. Steinborn, H. Junicke, *Chem. Rev.*, 2000, **100**, 4283.
17 J.P. Yang, K. McAteer, L.A.P. Silks, R.L. Wu, N.G. Isern, C.J. Unkefer, M.A. Kennedy, *J. Magn. Reson.*, 2000, **146**, 260.
18 J.D. Baleja, *Anal. Biochem.*, 2001, **288**, 1.
19 M. Springborg, *Chem. Modell.*, 2000, **1**, 306.
20 M. Liu, J.C. Lindon, *Curr. Org. Chem.*, 2001, **5**, 351.
21 R.T. Williamson, J.R. Carney, W.H. Gerwick, *J. Nat. Prod.*, 2000, **63**, 876.
22 K. Furihata, H. Seto, *Tetrahedron Lett.*, 2001, **42**, 899.
23 Y.L. Xia, X.M. Kong, N. Ip, G. Zhu, *J. Magn. Reson.*, 2000, **146**, 228.
24 D.O. Cicero, G. Barbato, U. Koch, P. Ingallinella, E. Bianchi, S. Sambucini, P. Neddermann, R. De Francesco, A. Pessi, R. Bazzo, *J. Biomol. NMR*, 2001, **20**, 23.
25 F. Delaglio, Z.R.Wu, A. Bax, *J. Magn. Reson.*, 2001, **149**, 276.
26 A. Garza-García, G. Ponzanelli-Velázquez, F. del Río-Portilla, *J. Magn. Reson.*, 2001, **148**, 214.
27 R. Burger, C. Schorn, P. Bigler *Magn. Reson. Chem.*, 2000, **38**, 963.

28 A. Meissner, O.W. Sørensen, *Magn. Reson. Chem.*, 2001, **39**, 49.
29 M.L. Liu, X. Zhang, *J. Magn. Reson.*, 2000, **146**, 277.
30 D.O. Cicero, G. Barbato, R. Bazzo, *J. Magn. Reson.*, 2001, **148**, 209.
31 T. Parella, J. Belloc, *J. Magn. Reson.*, 2001, **148**, 78.
32 C.E. Hadden, D.T. Angwin, *Magn. Reson. Chem.*, 2001, **39**, 1.
33 F. Löhr, C. Pérez, R. Köhler, H. Rüterjans, J.M. Schmidt, *J. Biomol. NMR*, 2000, **18**, 13.
34 P. Pelupessy, E. Chiarparin, *Conc. Magn. Reson.*, 2000, **12**, 103.
35 K.Y. Ding, *Chem. J. Chin. Univ.*, 2001, **22**, 863.
36 P. Permi, I. Kilpeläinen, A. Annila, *J. Magn. Reson.*, 2000, **146**, 255.
37 C.H. Gotfredsen, A. Meissner, J.Ø. Duus, O.W. Sørensen, *Magn. Reson. Chem.*, 2000, **38**, 692.
38 C. Richter, B. Reif, C. Griesinger, H. Schwalbe, *J. Am. Chem. Soc.*, 2000, **122**, 12728.
39 W. Koźmiński, *Mol. Phys. Rep.*, 2000, **29**, 183.
40 F. Löhr, H. Rüterjans, *J. Magn. Reson.*, 2000, **146**, 126.
41 S. Heikkinen, P. Permi, I. Kilpeläinen, *J. Magn. Reson.*, 2001, **148**, 53.
42 X.Z. Yan, X.M. Kong, Y.L. Xia, K.H. Sze, G. Zhu, *J. Magn. Reson.*, 2000, **147**, 357.
43 A. Majumdar, A. Kettani, E. Skripkin, D.J. Patel, *J. Biomol. NMR*, 2001, **19**, 103.
44 R.J. Carbajo, F. López-Ortiz, *J. Magn. Reson.*, 2001, **148**, 165.
45 R. Bürgi, J. Pitera, W.F. van Gunsteren, *J. Biomol. NMR*, 2001, **19**, 305.
46 C.V. Vizioli, M.C. R. de Azua, *Mol. Phys.*, 2000, **98**, 891.
47 J.K. Law, H. Mellows, D.M. Heinekey, *J. Am. Chem. Soc.*, 2001, **123**, 2085.
48 R. Gelabert, M. Moreno, J.M. Lluch, A. Lledós, *J. Am. Chem. Soc.*, 1997, **119**, 9840.
49 M.P. Freitas, R. Rittner, C.F. Tormena, R.J. Abraham, *J. Phys. Org. Chem.*, 2001, **14**, 317.
50 E.A. Yates, F. Santini, B. De Cristofano, N. Payre, C. Cosentino, M. Guerrini, A. Naggi, G. Torri, M. Hricovini, *Carbohydr. Res.*, 2000, **329**, 239.
51 A.V. Afonin, I.A. Ushakov, O.V. Petrova, L.N. Sobenina, A.I. Mikhaleva, V.K. Voronov, B.A. Trofimov, *Russ. J. Org. Chem.*, 2000, **36**, 1043.
52 M. Gromova, C.G. Béguin, R. Goumont, N. Faucher, M. Tordeux, F. Terrier, *Magn. Reson. Chem.*, 2000, **38**, 655.
53 J. Sélambarom, S. Monge, F. Carré, A. Fruchier, J.P. Rogue, A.A. Pavia, *Carbohyd. Res.*, 2001, **330**, 43.
54 P. Wałejko, S. Witkowski, I. Wawer, T. Szczepanik, *Mol. Phys. Rep.*, 2000, **29**, 192.
55 Y.-S. Hon, C.-F. Lee, *Tetrahedron*, 2000, **56**, 7893.
56 P. Dani, A.M. Toorneman, G.P.M. van Klink, G. van Koten, *Organometallics*, 2000, **19**, 5287.
57 M. Grotjahn, S. Lehmann, J. Aurich, H.-J. Holdt, E. Kleinpeter, *J. Phys. Org. Chem.*, 2001, **14**, 43.
58 W. Schilf, B. Kamieński, T. Dziembowska, Z. Rozwadowski, A. Szady-Chełmieniecka, *J. Mol. Struct.*, 2000, **552**, 33.
59 J. Schraml, M. Kvičalová , V. Blechta, L. Soukupová , O. Exner, H.-M. Boldhaus, F. Erdt, C. Bliefert, *Magn. Reson. Chem.*, 2000, **38**, 795.
60 A. Dunger, H.-H. Limbach, K. Weisz, *J. Am. Chem. Soc.*, 2000, **122**, 10109.
61 N.A. Troitski, S.N. Tandura, S.P. Kolesnikov, S.B. Choi, P. Boudjouk, *Main Group Met. Chem.*, 2001, **24**, 1.

62 H. Schumann, B.C. Wassermann, M. Frackowiak, B. Omotowa, S. Schutte, J. Velder, S.H. Mühle, W. Krause, *J. Organomet. Chem.*, 2000, **609**, 189.
63 C. Canlet, B.M. Fung, *J. Phys. Chem. B*, 2000, **104**, 6181.
64 S.J. Sabounchei, *Ultra Sci. Phys. Sci.*, 2000, **12**, 34.
65 T. Helgaker, M. Watson, N.C. Handy, *J. Chem. Phys.*, 2000, **113**, 9402.
66 J.E. Peralta, M.C. de Azua, R.H. Contreras, *Theor. Chem. Acc.*, 2000, **105**, 165.
67 J.E. Peralta, V. Barone, M.C.R. de Azúa, R.H. Contreras, *Mol. Phys.*, 2001, **99**, 655.
68 V. Sychrovský, J. Gräfenstein, D. Cremer, *J. Chem. Phys.*, 2000, **113**, 3530.
69 S. Patchovskii, J. Autschbach, T. Ziegler, *J. Chem. Phys.*, 2001, **115**, 26.
70 M. Pecul, *J. Chem. Phys.*, 2000, **113**, 10835.
71 H.J. Reich, W.S. Goldenberg, A.W. Sanders, C.C. Tzschucke, *Org. Lett.*, 2001, **3**, 33.
72 G. Hilmersson B. Malmros, *Chem. Eur. J.*, 2001, **7**, 337.
73 D.M. Pawar, R. Parks, M. Price, D. Reese, E.A. Noe, *J. Mol. Struct.*, 2000, **525**, 209.
74 J. Peralta-Cruz, V.I. Bakhmutov, A. Ariza-Castolo, *Magn. Reson. Chem.*, 2001, **39**, 187.
75 M. Jaszuński, K. Ruud, *Chem. Phys. Lett.*, 2001, **336**, 473.
76 R.D. Wigglesworth, W.T. Raynes, S. Kirpekar, J. Oddershede, S.P.A. Sauer, *J. Chem. Phys.*, 2000, **112**, 736.
77 R.D. Wigglesworth, W.T. Raynes, S. Kirpekar, J. Oddershede, S.P.A. Sauer, *J. Chem. Phys.*, 2000, **112**, 3735.
78 K. Jackowski, M. Wilczek, M. Pecul, J. Sadlej, *J. Phys. Chem. A*, 2000, **104**, 5955.
79 Z. Biedrzycka, K. Kamieńska-Trela, *Mol. Phys. Rep.*, 2001, **33**, 50.
80 F. Cloran, Y. Zhu, J. Osborn, I. Carmichael, A.S. Serianni, *J. Am. Chem. Soc.*, 2000, **122**, 6435.
81 K. Kamieńska-Trela, A. Dąbrowski, E. Nieczyporuk, J. Wójcik, *Mol. Phys. Rep.*, 2000, **29**, 161.
82 A. Dąbrowski, K. Kamieńska-Trela, J. Wójcik, *Spectrochim. Acta A*, 2000, **56**, 91.
83 A. Dąbrowski, K. Kamieńska-Trela, *Mol. Phys. Rep.*, 2001, **33**, 47.
84 K. Kamieńska-Trela, L. Kania, P. Bernatowicz, M. Bechcicka, Ł. Kaczmarek, J. Wójcik, *Spectrochim. Acta*, 2000, **56**, 2079.
85 K. Kamieńska-Trela, A. Dąbrowski, E. Nieczyporuk, P. Bernatowicz, J. Wójcik, *Mol. Phys. Rep.*, 2000, **29**, 164.
86 K. Kamieńska-Trela, E. Dvornikova, M. Bechcicka, J. Wójcik, *Mol. Phys. Rep.*, 2001, **33**, 54.
87 A.V. Afonin, I.A. Ushakov, S.V. Zinchenko, O.A. Tarasova, B.A. Trofimov, *Magn. Reson. Chem.*, 2000, **38**, 994.
88 J. Schraml, *Appl. Organometal. Chem.*, 2000, **14**, 604.
89 J. Jaźwiński, O. Staszewska, J.W. Wiench, L. Stefaniak, S. Araki, G.A. Webb, *Magn. Reson. Chem.*, 2000, **38**, 617.
90 E. Bednarek, J.C. Dobrowolski, K. Dobrosz-Teperek, L. Kozerski, W. Lewandowski, A.P. Mazurek, *J. Mol. Struct.*, 2000, **554**, 233.
91 H. Sommer, H.-J. Bertram, G.E. Krammer, C.O. Schmidt, W. Stumpe, P. Werkhoff, M. Zviely, *Magn. Reson. Chem.*, 2000, **38**, 907.
92 P. Cmoch, B. Kamieński, K. Kamieńska-Trela, L. Stefaniak, G.A. Webb, *J. Phys. Org. Chem.*, 2000, **13**, 480.

93 M. Pecul, H. Dodziuk, M. Jaszuński, O. Lukin, J. Leszczyński, *Phys. Chem. Chem. Phys.*, 2001, **3**, 1986.
94 A.W. Giesen, L.C. Bae, C.L. Barrett, J.A. Chyba, M.M. Chaykovsky, M.-C. Cheng, J.H. Murray, E.J. Oliver, S.M. Sullivan, J.M. Brown, F.W. Dahlquist, S.W. Homans, *J. Biomol. NMR*, 2001, **19**, 255.
95 J. Canisius, T.A. Mobley, S. Berger, N. Krause, *Chem. Eur. J.*, 2001, **7**, 2671.
96 B. Wrackmeyer, H. Maisel, W. Milius, A. Badshah, E. Molla, A. Mottalib, *J. Organomet. Chem.*, 2000, **602**, 45.
97 J.C. Norrild, *J. Chem. Soc., Perkin Trans. 2*, 2001, 719.
98 H.B. Lee, H.-Y. Park, B.-S. Lee, Y.G. Kim, *Magn. Reson. Chem.*, 2000, **38**, 468.
99 A.J.J.M. van Breemen, M.M. de Kok, P.J. Adriaensens, D.J.M. Vanderzande, J.M.J.V. Gelan, *Macromol. Chem. Phys.*, 2001, **202**, 343.
100 W.T. Ford, T. Nishioka, F. Qiu, F. D'Souza, J.-P. Choi, *J. Org. Chem.*, 2000, **65**, 5780.
101 T. Sternfeld, R.E. Hoffman, I. Aprahamian, M. Rabinovitz, *Angew. Chem. Int. Ed.*, 2001, **40**, 455.
102 R.J. Abraham, C.F. Tormena, R. Rittner, *J. Chem. Soc., Perkin Trans. 2*, 2001, 815.
103 J.P. Bouillon, B. Didier, B. Dondy, P. Doussot, R. Plantier-Royon, C. Portella, *Eur. J. Org. Chem.*, 2001, 187.
104 J.E. Charris, J.N. Dominguez, G. Lobo, M.I. Cordero, S.E. López, B. Méndez, S. Pekerar, F. Riggione, *Magn. Reson. Chem.*, 2000, **38**, 1039.
105 M. Tordeux, C. Wakselman, O. Jarjayes, C.G. Béguin, *Magn. Reson. Chem.*, 2001, **39**, 301.
106 B. Wrackmeyer, W. Milius, E.V. Klimkina, Y.N. Bubnov, *Chem. Eur. J.*, 2001, **7**, 775.
107 G. Heckmann, G. Becker, S. Horner, H. Richard, H. Kraft, P. Dvortsak, *Z. Naturforsch., Teil B*, 2001, **56**, 146.
108 R. Nazarski, D.K. Gralak, Z.H. Kudzin, *Bull. Pol. Acad. Sci. Chem.*, 2000, **48**, 27.
109 W. McFarlane, N.H. Rees, L. Constanza, M. Patel, I.J. Colquhoun, *J. Chem. Soc., Dalton Trans.*, 2000, 4453.
110 H. Gröger, J.R. Goerlich, R. Schmutzler, J. Martens, *Phosphorus, Sulfur and Silicon*, 2000, **166**, 253.
111 P. DeShong, E.D. Soli, G.A. Slough, D.R. Sidler, V. Elango, P.J. Rybczynski, L.J.S. Vosejpka, T.A. Lessen, T.X. Le, G.B. Anderson, W. von Philipsborn, M. Vöhler, D. Rentsch, O. Zerbe, *J. Organomet. Chem.*, 2000, **593–594**, 49.
112 T.P. Lockhart, W.F. Manders, *J. Am. Chem. Soc.*, 1987, **109**, 7015.
113 J. Holecek, A. Lyčka, *Inorg. Chim. Acta*, 1986, **118**, L15.
114 M.A. Girasolo, T. Pizzino, C. Mansueto, G. Valle, G.C. Stocco, *Appl. Organometal. Chem.*, 2000, **14**, 197.
115 H. Papadaki, A. Christofides, J.C. Jeffery, T. Bakas, *J. Coord. Chem.*, 1999, **47**, 559.
116 M. Nádvorník, V. Pejchal, *Sci. Pap. Univ. Pardubice, Ser. A*, 1999, **5**, 165.
117 D. Tudela, M. Diaz, D.A. Alvaro, J. Ignacio, L. Seijo, V.K. Belsky, *Organometallics*, 2001, **20**, 654.
118 P.G. Sutton, C.F. Harrington, B. Fairman, E.H. Evans, L. Ebdon, T. Catterick, *Appl. Organometal. Chem.*, 2000, **14**, 691.
119 G. Fraenkel, F. Qiu, *J. Am. Chem. Soc.*, 2000, **122**, 12806.
120 F. Asaro, M. Lenarda, G. Pellizer, L. Storaro, *Spectrochim. Acta, A*, 2000, **56**, 2167.

121 J. Autschbach, T. Ziegler, *J. Am. Chem. Soc.*, 2001, **123**, 3341.
122 E.S. Gore, *Magn. Reson. Chem.*, 2001, **39**, 203.
123 S. Schröder, W. Preetz, *Anorg. Allgm. Chem.*, 2001, **627**, 390.
124 K.R. Gorny, O.M. Vyaselev, S. Yu, C.H. Pennington, W.L. Hults, J.L. Smith, *Phys. Rev. Lett.*, 1998, **81**, 2340.
125 T. Goullion, C.H. Pennington, *Chem. Phys. Lett.*, 1998, **290**, 88.
126 S. Yu, R.K. Gorny, J.A. Martindale, C.H. Pennington, W.L. Hults, J.L. Smith, *Phys. Rev. Lett.*, 1999, **83**, 3924.
127 C.H. Pennington, S. Yu, K.R. Gorny, M.J. Buoni, W.L. Hults, J.L. Smith, *Phys. Rev. B*, 2001, **63**, 63054513.
128 S.P. Petrosyants, A.M. Shpirt, Y.A. Buslaev, *Russ. J. Inorg. Chem.*, 2001, **46**, 880.
129 L.-S. Du, R.W. Schurko, K.H. Lim, C.P. Grey, *J. Phys. Chem. A*, 2001, **105**, 760.
130 H. Takemura, S. Nakashima, N. Kon, T. Inazu, *Tetrahedron Lett.*, 2000, **41**, 6105.
131 H. Takemura, N. Kon, M. Kotoku, S. Nakashima, K. Otsuka, M. Yasutake, T. Shinmyozu, T. Inazu, *J. Org. Chem.*, 2001, **66**, 2778.
132 C.S. Weinert, C.L. Stern, D.F. Shriver, *Inorg. Chim. Acta*, 2000, **307**, 139.
133 U. Herzog, U. Böhme, G. Rheinwald, *J. Organomet. Chem.*, 2001, **627**, 144.
134 U. Herzog, *Main Group Met. Chem.*, 2001, **24**, 31.
135 U. Herzog, G. Rheinwald, *J. Organomet. Chem.*, 2001, **627**, 23.
136 X. Cai, B. Gehrhus, P.B. Hitchcock, M.F. Lappert, *Can. J. Chem.*, 2000, **78**, 1484.
137 B.W. Tattershall, R. Blachnik, A. Hepp, *J. Chem. Soc., Dalton Trans.*, 2000, 2551.
138 M. Gee, R.E. Wasylishen, K. Eichele, J.F. Britten, *J. Phys. Chem. A*, 2000, **104**, 4598.
139 E.W. Ainscough, A.M. Brodie, A.K. Burrell, G.H. Freeman, G.B. Jameson, G.A. Bowmaker, J.V. Hanna, P.C. Healy, *J. Chem. Soc., Dalton Trans.*, 2001, 144.
140 G. Grossmann, G. Ohms, K. Krüger, K. Karaghiosoff, K. Eckstein, J. Hahn, A. Hopp, O.L. Malkina, P. Hrobařik, *Anorg. Allgm. Chem.*, 2001, **627**, 1269.
141 B.W. Tattershall, E.L. Sandham, *J. Chem. Soc., Dalton Trans.*, 2001, 1834.
142 G.A. Bowmaker, J.V. Hanna, C.E.F. Rickard, A.S. Lipton, *J. Chem. Soc., Dalton Trans.*, 2001, 20.
143 D. Gudat, A. Haghverdi, M. Nieger, *J. Organomet. Chem.*, 2001, **617-618**, 383.
144 V.J. Catalano, B.L. Bennett, R.L. Yson, B.C. Noll, *J. Am. Chem. Soc.*, 2000, **122**, 10056.
145 D. Fernández, P. Sevillano, M.I. García-Seijo, A. Castiñeiras, L. Jánosi, Z. Berente, L. Kollár, M.E. Garcia-Fernández, *Inorg. Chim. Acta*, 2001, **312**, 40.
146 M.H. Johansson, S. Otto, *Acta Crystallogr., Sect. C, Cryst. Struct. Commun.*, 2000, **56**, e12.
147 D. Christendat, J.H. Wosnick, I.S. Butler, D.F.R. Gilson, A.-M. Lebuis, F.G. Morin, *J. Mol. Struct.*, 2001, **559**, 235.
148 J. Campbell, H.P.A. Mercier, D.P. Santry, R.J. Suontamo, H. Borrmann, G.J. Schrobilgen, *Inorg. Chem.*, 2001, **40**, 233.
149 B.E. Eichler, P.P. Power, *Inorg. Chem.*, 2000, **39**, 5444.
150 O. Xu, B.T. Heaton, C. Jacob, K. Mogi, Y. Ichihashi, Y. Souma, K. Kanamori, T. Eguchi, *J. Am. Chem. Soc.*, 2000, **122**, 6862.
151 G.B. Ma, M. Kritikos, J. Glaser, *Eur. J. Inorg. Chem.*, 2001, 1311.

152 R. Malleier, H. Kopacka, W. Schuh, K. Wurst, P. Peringer, *Chem. Commun.*, 2001, 51.
153 D.S. Ribeiro, P.R. Olivato, R. Rittner, *Magn. Reson. Chem.*, 2000, **38**, 627.
154 R.A. Shaikhutdinov, K.D. Klika, F. Fülöp, K. Pihlaja, *Magn. Reson. Chem.*, 2001, **39**, 141.
155 B. Balázs, G. Tóth, G. Horváth, A. Grün, V. Csokai, L. Töke, I. Bitter, *Eur. J. Org. Chem.*, 2001, 61.
156 A. Vidal Costa, L.C. de Almeida Barbosa, J.L. Callegari Lopes, D. Piló-Veloso, *Magn. Reson. Chem.*, 2000, **38**, 675.
157 M. Vialemaringe, M.J. Bourgeois, E. Montaudon, C. Courseille, B. Barbe, I. Pianet, *Magn. Reson. Chem.*, 2000, **38**, 785.
158 B. Rodríguez, G. Savona, *Magn. Reson. Chem.*, 2000, **38**, 802.
159 D.W. Hughes, I.D. Spenser, J.T. Wróbel, *Magn. Reson. Chem.*, 2000, **38**, 707.
160 P. Krajewski, L. Kozerski, G. Grynkiewicz, E. Bednarek, J. Sitkowski, *Magn. Reson. Chem.*, 2000, **38**, 757.
161 M. Szafran, Z. Dega-Szafran, B. Nowak-Wydra, M. Pietrzak, *J. Mol. Struct.*, 2001, **563–564**, 555.
162 M. Suárez, D. Molero, E. Salfran, N. Martín, Y. Verdecia, R. Martinez, E. Ochoa, L. Alba, M. Quinteiro, C. Seoane, *Magn. Reson. Chem.*, 2001, **39**, 105.
163 M. Amm, N. Platzer, J.P. Bouchet, J.P. Volland, *Magn. Reson. Chem.*, 2001, **39**, 77.
164 A.D. Bain, M.A. Brook, P. Hazendonk, D. Reid, R.S. Stan, *Magn. Reson. Chem.*, 2000, **38**, 894.
165 S.B. Duckett, L.D. Field, B.A. Messerle, W.J. Shaw, L.P. Soler, *J. Chem. Soc., Dalton Trans.*, 2000, 2251.
166 N. Matsumori, D. Kaneno, M. Murata, H. Nakamura, K. Tachibana, *J. Org. Chem.*, 1999, **64**, 866.
167 P. Ciminiello, E. Fattorusso, M. Forino, M. Di Rosa, A. Ianaro, R. Poletti, *J. Org. Chem.*, 2001, **66**, 578.
168 C. Bassarello, G. Bifulco, A. Zampella, M.V. D'Auria, R. Riccio, L. Gomez-Paloma, *Eur. J. Org. Chem.*, 2001, 39.
169 H. Junicke, R. Kluge, D. Steinborn, *J. Inorg. Biochem.*, 2000, **81**, 43.
170 N. Mathew, B.R. Jagirdar, *Inorg. Chem.*, 2000, **39**, 5404.
171 L. Carlton, *Appl. Organometal. Chem.*, 2001, **15**, 157.
172 L. Carlton, *Inorg. Chem.*, 2000, **39**, 4510.
173 J.J. Schneider, J. Hagen, N. Czap, C. Krüger, S.A. Mason, R. Bau, J. Ensling, P. Gütlich, B. Wrackmeyer, *Chem. Eur. J.*, 2000, **6**, 625.
174 U. Fekl, R. van Eldik, S. Lovell, K.I. Goldberg, *Organometallics*, 2000, **19**, 3535.
175 M. Herberhold, C. Köhler, V. Tröbs, B. Wrackmeyer, *Z. Naturforsch., Teil B*, 2000, **55**, 939.
176 S. Szafert, P. Haquette, S.B. Falloon, J.A. Gladysz, *J. Organomet. Chem.*, 2000, **604**, 52.
177 G. Sánchez, J.L. Serrano, C.M. Lopez, J. Garcia, J. Pérez, G. López, *Inorg. Chim. Acta*, 2000, **306**, 168.
178 G. Keglevich, M. Trecska, B. Dajka, P. Bele, A. Dobo, I. Toko, *Heteroatom Chem.*, 2000, **11**, 271.
179 P. Bernatowicz, O. Bjørlo, E.H. Mørkved, S. Szymański, *J. Magn. Reson.*, 2000, **145**, 152.
180 P. Bernatowicz, S. Szymański, *Mol. Phys. Rep.*, 2000, **29**, 98.
181 P. Bernatowicz, S. Szymański, *J. Magn. Reson.*, 2001, **148**, 455.

182 S. Szymański, *J. Magn. Reson.*, 1997, **127**, 199.
183 J. Przyborowski, E. Lork, G.-Y. Röschenthaler, *J. Fluor. Chem.*, 2000, **104**, 207.
184 A.J. Arduengo III, F. Davidson, R. Krafczyk, W.J. Marshall, R. Schmutzler, *Monatsch. Chem.*, 2000, **131**, 251.
185 V. Plack, P. Sakhaii, M. Freytag, P.G. Jones, R. Schmutzler, *J. Fluorine. Chem.*, 2000, **101**, 125.
186 A.J. Edwards, S.A. Macgregor, A.D. Rae, E. Wenger, A.C. Willis, *Organometallics*, 2001, **20**, 2864.
187 B. Wrackmeyer, O.L. Tok, E. Klimkina, Y.N. Bubnov, *Inorg. Chim. Acta*, 2000, **300-302**, 169.
188 B. Wrackmeyer, S.V. Ponomarev, *J. Organomet. Chem.*, 2000, **598**, 211.
189 R. Contant, S. Piro-Sellem, J. Canny, R. Thouvenot, *C. R. Acad. Sci. Paris IIc, Chim.*, 2000, **3**, 157.
190 W. Peti, L.J. Smith, C. Redfield, H. Schwalbe, *J. Biomol. NMR*, 2001, **19**, 153.
191 Y.W. Bai, J. Chung, H.J. Dyson, P.E. Wright, *Protein Sci.*, 2001, **10**, 1056.
192 A. Mamai, R. Zhang, A. Natarajan, J.S. Madalengoitia, *J. Org. Chem.*, 2001, **66**, 455.
193 S. Rebuffat, C. Goulard, S. Hlimi, B. Bodo, *J. Pept. Sci.*, 2000, **6**, 519.
194 S. Rodziewicz-Motowidło, A. Łęgowska, X.-F. Qi, C. Czaplewski, A. Liwo, P. Sowiński, W. Mozga, J. Ołczak, J. Zabrocki, K. Rolka, *J. Pept. Res.*, 2000, **56**, 132.
195 R.C.R. Grace, A.M. Lynn, S.M. Cowsik, *J. Biomol. Struct. Dyn.*, 2001, **18**, 611.
196 A.J. Benie, D. Whitford, B. Hargittai, G. Barany, R.W. Janes, *FEBS Lett.*, 200, **476**, 287.
197 C. Das, C. Shankaramma, P. Balarm, *Chem. Eur. J.*, 2001, **7**, 840.
198 M. Trabi, H.J. Schirra, D.J. Craik, *Biochemistry*, 2001, **40**, 4211.
199 X.B. Be, Y.H. Hong, J. Wei, E.J. Androphy, J.J. Chen, J.D. Baleja, *Biochemistry*, 2001, **40**, 1293.
200 B. Zhang, G.Z. Xu, J.S. Evans, *Biopolymers*, 2000, **54**, 464.
201 C. Das, V. Nayak, S. Raghothama, P. Balaram, *J. Pept. Res.*, 2000, **56**, 307.
202 K. Kobayashi, T. Sasaki, K. Sato, T. Kohno, *Biochemistry*, 2000, **39**, 14761.
203 Y.Q. Xu, J.H. Wu, J.M. Pei, Y.Y. Shi, Y.H. Ji, Q.C. Tong, *Biochemistry*, 2000, **39**, 13669.
204 J.M. Hill, P.F. Alewood, D.J. Craik, *Eur. J. Biochem.*, 2000, **267**, 4649.
205 C. Bernard, C. Legros, G. Ferrat, U. Bischoff, A. Marquardt, O. Pongs, H. Darbon, *Protein Sci.*, 2000, **9**, 2059.
206 Z.G. Chen, P. Xu, J.-R. Barbier, G. Willick, F. Ni, *Biochemistry*, 2000, **39**, 12766.
207 A. Mosbah, R. Kharrat, Z. Fajloun, J.-G. Renisio, E. Blanc, J.-M. Sabatier, M. El Ayeb, H. Darbon, *Prot. Struct. Funct. Genet.*, 2000, **40**, 436.
208 R. Bader, A. Bettio, A.G. Beck-Sickinger, O. Zerbe, *J. Mol. Biol.*, 2001, **305**, 307.
209 D. Clayton, I.M. Brereton, P.A. Kroon, R. Smith, *FEBS Lett.*, 2000, **479**, 118.
210 S.K. Holaday, Jr., B.M. Martin, P.L. Fletcher, Jr., N.R. Krishna, *Arch. Biochem. Biophys.*, 2000, **379**, 18.
211 A.M. Torres, G.M. de Plater, M. Doverskog, L.C. Birinyi-Strachan, G.M. Nicholson, C.H. Gallagher, P.W. Kuchel, *Biochem. J.*, 2000, **348**, 649.
212 V. Kanelis, D. Rotin, J.D. Forman-Kay, *Nat. Struct. Biol.*, 2001, **8**, 407.
213 S. Lamberth, H. Schmid, M. Muenchbach, T. Vorherr, J. Krebs, E. Carafoli, C. Griesinger, *Helv. Chim. Acta*, 2000, **83**, 2141.
214 Y.J. Wang, S. Zhao, R.L. Somerville, O. Jardetzky, *Protein Sci.*, 2001, **10**, 592.

215 L. Banci, I. Bertini, S. Ciofi-Baffoni, D.L. Huffman, T.V. O'Halloran, *J. Biol. Chem.*, 2001, **276**, 8415.
216 F. Arnesano, L. Banci, I. Bertini, D.L. Huffman, T.V. O'Halloran, *Biochemistry*, 2001, **40**, 1528.
217 A. Yee, V. Booth, A. Dharamsi, A. Engel, A.M. Edwards, C.H. Arrowsmith, *Proc. Natl. Acad. Sci. USA*, 2000, **97**, 6311.
218 M.V. Berjanskii, M.I. Riley, A.Y. Xie, V. Semenchenko, W.R. Folk, S.R. Van Doren, *J. Biol. Chem.*, 2000, **275**, 36094.
219 N.D. Kurniawan, A.R. Atkins, S. Bieri, C.J. Brown, I.M. Brereton, P.A. Kroon, R. Smith, *Protein Sci.*, 2000, **9**, 1282.
220 I. Bertini, S. Ciurli, A. Dikiy, C.O. Fernàndez, C. Luchinat, N. Safarov, S. Shumilin, A.J. Vila, *J. Am. Chem. Soc.*, 2001, **123**, 2405.
221 L. Guignard, A. Padilla, J. Mispelter, Y.S. Yang, M.H. Stern, J.M. Lhoste, C. Roumestand, *J. Biomol. NMR*, 2000, **17**, 215.
222 H.J. Schirra, M.J. Scanlon, M.C.S. Lee, M.A. Anderson, D.J. Craik, *J. Mol. Biol.*, 2001, **306**, 69.
223 J.-B.Telliez, G.-Y. Xu, J.D. Woronicz, S. Hsu, J.-L. Wu, L. Lin, S.F. Sukits, R. Powers, L.-L. Lin, *J. Mol. Biol.*, 2000, **300**, 1323.
224 N. Blomberg, E. Baraldi, M. Sattler, M. Saraste, M. Nilges, *Structure*, 2000, **8**, 1079.
225 J.M. Pérez-Cañadillas, J. Santoro, R. Campos-Olivas, J. Lacadena, A.M. del Pozo, J.G. Gavilanes, M. Rico, M. Bruix, *J. Mol. Biol.*, 2000, **299**, 1061.
226 A.R. Pickford, S.P. Smith, D. Staunton, J. Boyd, I.D. Campbell, *EMBO J.*, 2001, **20**, 1519.
227 J.D. Swarbrick, T. Bashtannyk, D. Maksel, X.-R. Zhang, G.M. Blackburn, K.R. Gayler, P.R. Gooley, *J. Mol. Biol.*, 2000, **302**, 1165.
228 E. Speina, J.M. Cieśla, J. Wójcik, M. Bajek, J.T. Kuśmierek, B. Tudek, *J. Biol. Chem.*, 2001, **276**, 21821.
229 J. Mäki, R. Sjöholm, L. Kronberg, *J. Chem. Soc. Perkin Trans. 1*, 2000, 4445.
230 C. Kojima, E. Kawashima, T. Sekine Y. Ishido, A. Ono, M. Kainosho, Y. Kyogoku, *J. Biomol. NMR*, 2001, **19**, 19.
231 J.M. Aramini, A. Mujeeb, N.B. Ulyanov, M.W. Germann, *J. Biomol. NMR*, 2000, **18**, 287.
232 E.S.H. El Ashry, L.F. Awad, *Nucleosides, Nucleotides & Nucleic Acids*, 2001, **20**, 103.
233 J. Ravn, P. Nielsen, *J. Chem. Soc., Perkin Trans. 1*, 2001, 985.
234 P. Nielsen, M. Petersen, J.P. Jacobsen, *J. Chem. Soc., Perkin Trans. 1*, 2000, 3706.
235 M.J. Potrzebowski, X.-B. Yang, K. Misiura, W.R. Majzner, M.W. Wieczorek, S. Kanźmierski, S. Olejniczak, W.J. Stec, *Eur. J. Org. Chem.*, 2001, 1491.
236 D. MacDonald, K. Herbert, X.L. Zhang, T. Polgruto, P. Lu, *J. Mol. Biol.*, 2001, **306**, 1081.
237 E. Hantz, V. Larue, P. Ladam, L. Le Moyec, C. Gouyette, T.H. Dinh, *Int. J. Biol. Macromol.*, 2001, **28**, 273.
238 E.E. Swinny, S.J. Bloor, H. Wong, *Magn. Reson. Chem.*, 2000, **38**, 1031.
239 M. Carpintero, A. Fernández-Mayoralas, J. Jiménez-Barbero, *Eur. J. Org. Chem.*, 2001, 681.
240 F.L. Tobiason, D.D. Swank, G. Vergoten, P. Legrand, *J. Carbohydr. Chem.*, 2000, **19**, 959.
241 M.K. Dowd, A.D. French, P.J. Reilly, *J. Carbohydr. Chem.*, 2000, **19**, 1091.

242 K.C. Lewis, A.R. Maxwell, S. McLean, W.F. Reynolds, R.G. Enriquez, *Magn. Reson. Chem.*, 2000, **38**, 771.
243 P. Berthault, N. Birlirakis, *Tetrahedron Asymmetry*, 2000, **11**, 2463.
244 B. Coxon, *Carbohydr. Res.*, 2000, **329**, 131.
245 J. Andersch, L. Hennig, H. Wilde,*Carbohydr. Res.*, 2000, **329**, 693.
246 B. Coxon, R.C. Reynolds, *Carbohydr. Res.*, 2001, **331**, 461.
247 M.L. Rodriguez-Lyon, A.M. Díaz-Lanza, M. Bernabé, L. Villaescusa-Castillo, *Magn. Reson. Chem.*, 2000, **38**, 684.
248 E. Fukushi, S. Onodera, A. Yamamori, N. Shiomi, J. Kawabata, *Magn. Reson. Chem.*, 2000, **38**, 1005.
249 J. de Santos Galíndez, A.M. Diaz-Lanza, L.F. Matellano, A.R. Sánchez, *Magn. Reson. Chem.*, 2000, **38**, 688.
250 Y.-T. Kim, E.-H. Kim, C. Cheong, D.L. Williams, C.-W. Kim, S.-T. Lim, *Carbohydr. Res.*, 2000, **328**, 331.
251 J. Bootsma, G. Wagenaars, E. Dreef, F. Hout, E. Kellenbach, *Magn. Reson. Chem.*, 2001, **39**, 288.
252 B. Bernet, J.-W. Xu, A. Vasella, *Helv. Chim. Acta*, 2000, **83**, 2072.
253 I. Ivarsson, C. Sandström, A. Sandström, L. Kenne, *J. Chem. Soc., Perkin Trans. 2*, 2000, 2147.
254 B. Bernet, A. Vasella, *Helv. Chim. Acta*, 2000, **83**, 2055.
255 L. Kindahl, C. Sandström, T. Norberg, L. Kenne, *J. Carbohydr. Chem.*, 2000, **19**, 1291.
256 S. Bekiroglu, C. Sandström, T. Norberg, L. Kenne, *Carbohyd. Res.*, 2000, **328**, 409.
257 V. Govindaraju, K. Young, A.A. Maudsley, *NMR Biomed.*, 2000, **13**, 129.
258 M. Arnó, M.A. González, M.L. Marín, R.J. Zaragozá, *Magn. Reson. Chem.*, 2000, **38**, 1019.
259 L.C. Chang, S. Otero-Quintero, G.M. Nicholas, C.A. Bewley, *Tetrahedron*, 2001, **57**, 5731.
260 C.M. Cerda-Garcia-Rojas, G. Zamorano, M.I. Chávez, C.A.N. Cataláan, P. Joseph-Nathan, *Magn. Reson. Chem.*, 2000, **38**, 494.
261 K.S.P. Perry, E. Miguez, M.B. de Amorim, M.A.D. Boaventura, A.J.R. da Silva, *Magn. Reson. Chem.*, 2001, **39**, 219.
262 C.A. Flores-Sandoval, C.M. Cerda-García-Rojas, P. Joseph-Nathan, *Magn. Reson. Chem.*, 2001, **39**, 173.
263 N.H. Oberlies, J.P. Burgess, H.A. Navarro, R.E. Pinos, D.D. Soejarto, N.R. Farnsworth, A.D. Kinghorn, M.C. Wani, M.E. Wall, *J. Nat. Prod.*, 2001, **64**, 497.
264 M.A.C. Kaplan, H.R.L. Pugialli, D. Lopes, H.E. Gottlieb, *Phytochemistry*, 2000, **55**, 749.
265 C.R. Kaiser, L.F. Pitombo, A.C. Pinto, *Magn. Reson. Chem.*, 2001, **39**, 147.
266 A. García-Granados, E. Melguizo, A. Parra, Y. Simeó, B. Viseras, J.A. Dobado, J. Molina, J.M. Arias, *J. Org. Chem.*, 2000, **65**, 8214.
267 C.A.G. Haasnoot, F.A.A.M. Leeuw, C. Altona, *Tetrahedron*, 1980, **36**, 2783.
268 D. Nozawa, H. Takikawa, K. Mori, *J. Chem. Soc., Perkin Trans. 1*, 2000, 2043.
269 G.M. Cameron, B.L. Stapleton, S.M. Simonsen, D.J. Brecknell, M.J. Garson, *Tetrahedron*, 2000, **56**, 5247.
270 J. Halász, B. Podányi, L. Vasvári-Debreczy, A. Szabó, F. Hajdú, Z. Böcskei, J. Hegednús-Vajda, A. Győrbíró, I. Hermecz, *Tetrahedron*, 2000, **56**, 10081.
271 R. Pereda-Miranda, M. Fragoso-Serrano, C.M. Cerda-García-Rojas, *Tetrahedron*, 2001, **57**, 47.

272 L. Fielding, Y. Diepeveen, D. Fletcher, N. Hamilton, *Magn. Reson. Chem.*, 2001, **39**, 323.
273 I.J.C. Vieira, E. Rodrigues-Filho, J.B. Fernandes, M.F.G.F. da Silva, P.C. Vieira, *Magn. Reson. Chem.*, 2000, **38**, 805.
274 S.S. Korde, R.A. Udasi, G.K. Trivedi, *J. Ind. Chem. Soc.*, 1999, **76**, 557.
275 L. Siergiejczyk, J. Popławski, B. Łozowicka, A. Dubis, B. Lachowska, *Magn. Reson. Chem.*, 2000, **38**, 1037.
276 C.A. Stortz, M.S. Maier, *J. Chem. Soc., Perkin Trans. 2*, 2000, 1832.
277 D. Molero, R. Pérez, R. Martinez, M. Suárez, H. Rodriguez, N. Martín, C. Seoane, *Magn. Reson. Chem.*, 2001, **39**, 222.
278 R. Sonnenburg, I. Neda, H. Thönnessen, P.G. Jones, R. Schmutzler, *Anorg. Allgm. Chem.*, 2000, **626**, 412.
279 F. Georgescu, E.I. Georgescu, M.T. Caproiu, C. Draghici, *Rev. Roum. Chim.*, 1999, **44**, 341.
280 D.C. Byrd, K.W. Stewart, J.B. Grutzner, *Magn. Reson. Chem.*, 2000, **38**, 479.
281 H.G. Niessen, D. Schleyer, S. Wiemann, J. Bargon, S. Steines, B. Diessen-Hoelscher, *Magn. Reson. Chem.*, 2000, **38**, 747.
282 R. Le Lagadec, M.I. Chávez, L. Rubio, A. Cabrera, *Magn. Reson. Chem.*, 2001, **39**, 215.
283 V. Vijayakumar, M. Sundaravadivelu, S. Perumal, M.J.E. Hewlins, *Magn. Reson. Chem.*, 2000, **38**, 883.
284 R.B. Nazarski, S. Leśniak, *Bull. Pol. Acad. Sci. Chem.*, 2000, **48**, 19.
285 V.B. Kurteva, M.J. Lyapova, *Phosphorus, Sulfur Silicon*, 2000, **161**, 239.
286 H. Dvořáková, R. Hrabal, L. Kniežo, *Magn. Reson. Chem.*, 2000, **38**, 738.
287 H. Xu, J. Xu, X. Liu, S. Jin, Y. Cui, *Bopuxue Zazhi*, 2000, **17**, 363.
288 K. Pandiarajan, A. Manimekalai, G. Rajarajan, *Indian J. Chem., Sect. B: Org. Chem. Incl. Med. Chem.*, 2000, **39**, 517.
289 P.M. Ivanov, *J. Mol. Struct.*, 2000, **553**, 141.
290 C.A. de Parrodi, A. Clara-Sosa, L. Pérez, L. Quintero, V. Marañón, R.A. Toscano, J.A. Aviña, S. Rojas-Lima, E. Juaristi, *Tetrahedron Asymmetry*, 2001, **12**, 69.
291 V.V. Karpyak, N.D. Obushak, V.L. Mizyuk, N.I. Ganushchak, *Russ. J. Org. Chem.*, 2000, **36**, 83.
292 R. Kessinger, C. Thilgen, T. Mordasini, F. Diderich, *Helv. Chim. Acta*, 2000, **83**, 3069.
293 A.K. Shestakova, V.A. Chertkov, H.-J. Schneider, K.A. Lysenko, *Org. Lett.*, 2001, **3**, 325.
294 M. Goto, M. Sumimoto, T. Matsumoto, M. Iwasaki, Y. Tanaka, H. Kurosaki, K. Yuto, Y. Yoshikawa, *Bull. Chem. Soc. Jpn.*, 2000, **73**, 1589.
295 M. Maeyama, G. Sakane, R. Pierattelli, I. Bertini, T. Shibahara, *Inorg. Chem.*, 2001, **40**, 2111.
296 A.L. Esteban, M.P. Galache, F. Mora, E. Diéz, J. Casanueva, J.S. Fabián, V. Barone, J.E. Peralta, R.H. Contreras, *J. Phys. Chem. A*, 2001, **105**, 5298.
297 A. Bagno, *Chem. Eur. J.*, 2001, **7**, 1652.
298 M. Hennig, W. Bermel, H. Schwalbe, C. Griesinger, *J. Am. Chem. Soc.*, 2000, **122**, 6268.
299 S. Liao, M. Shenderovich, K.E. Kövér, Z. Zhang, K. Hosohata, P. Davis, F. Porreca, H.I. Yamamura, V.J. Hruby, *J. Pept. Res.*, 2001, **57**, 257.
300 C.K. Liew, K. Kowalski, A.H. Fox, A. Newton, B.K. Sharpe, M. Crossley, J.P. Mackay, *Structure*, 2000, **8**, 1157.

301 B.E. Ramirez, O.N. Voloshin, R.D. Camerini-Otero, A. Bax, *Protein Sci.*, 2000, **9**, 2161.
302 J. Weigelt, I. Climent, K. Dahlman-Wright, M. Wikström, *Biochemistry*, 2001, **40**, 5861.
303 R. Spadaccini, O. Crescenzi, T. Tancredi, N. De Casamassimi, G. Saviano, R. Scognamiglio, A. Di Donato, P.A. Temussi, *J. Mol. Biol.*, 2001, **305**, 505.
304 N. Li, W.X. Zhang, S.W. White, R.W. Kriwacki, *Biochemistry*, 2001, **40**, 4293.
305 K. Brubaker, S.M. Cowley, K. Huang, L. Loo, G.S. Yochum, D.E. Ayer, R.N. Eisenman, I. Radhakrishnan, *Cell*, 2000, **103**, 655.
306 S.A. Wacowich-Sgarbi, C.C. Ling, A. Otter, D.R. Bundle, *J. Am. Chem. Soc.*, 2001, **123**, 4362.
307 F.A. Momany, J.L. Willett, *Carbohydr. Res.*, 2000, **326**, 210.
308 F. Cloran, I. Carmichael, A.S. Serianni, *J. Am. Chem. Soc.*, 2001, **123**, 4781.
309 A.S. Serianni, I. Carmichael, *Polym. Prep.*, 2001, **42**, 80.
310 K. Mazeau, S. Peréz, M. Rinaudo, *J. Carbohyd. Chem.*, 2000, **19**, 1269.
311 H. Takayama, T. Ichikawa, T. Kuwajima, M. Kitajima, H. Seki, N. Aimi, M.G. Nonato, *J. Am. Chem. Soc.*, 2000, **122**, 8635.
312 L. Verdier, G. Bertho, J. Gharbi-Benarous, J.-P. Girault, *Bioorg. Med. Chem.*, 2000, **8**, 1225.
313 N. Evrard-Todeschi, J. Gharbi-Benarous, C. Gaillet, L. Verdier, G. Bertho, C. Lang, A. Parent, J.-P. Girault, *Bioorg. Med. Chem.*, 2000, **8**, 1579.
314 W.E. Steinmetz, J.D. Sadowsky, J.S. Rice, J.J. Roberts, Y.K. Bui, *Magn. Reson. Chem.*, 2001, **39**, 163.
315 E. Bednarek, W. Bocian, J.C. Dobrowolski, L. Kozerski, N. Sadlej-Sosnowska, J. Sitkowski, *J. Mol. Struct.*, 2001, **559**, 369.
316 A. Nagatsu, R. Tanaka, H. Mizukami, Y. Ogihara, J. Sakakibara, *Tetrahedron*, 2001, **57**, 3369.
317 G. Tóth, J. Kovács, A. Lévai, E. Kleinpeter, A. Koch, *Magn. Reson. Chem.*, 2001, **39**, 251.
318 Y. Kan, B. Sakamoto, T. Fujita, H. Nagai, *J. Nat. Prod.*, 2000, **63**, 1599.
319 W. Koźmiński, E. Bednarek, W. Bocian, J. Sitkowski, P.E. Hansen, B. Kwiecień, L. Kozerski, *Magn. Reson. Chem.*, 2000, **38**, 839.
320 W. Baumann, P.-M. Pellny, U. Rosenthal, *Magn. Reson. Chem.*, 2000, **38**, 515.
321 D. Grée, L. Vallerie, R. Grée, *J. Org. Chem.*, 2001, **66**, 2374.
322 C. Monteiro, S. Neyret, J. Leforestier, C.H. du Penhoat, *Carbohyd. Res.*, 2000, **329**, 141.
323 E. Gács-Baitz, L.A. Wozniak, M. Kajtár-Peredy, *Chirality*, 2000, **12**, 675.
324 M.-O. Ebert, B. Jaun, W. Pils, R. Micura, *Helv. Chim. Acta*, 2000, **83**, 2336.
325 J.-F. Trempe, C.J. Wilds, A.Y. Denisov, R.T. Pon, M.J. Damha, K. Gehring, *J. Am. Chem. Soc.*, 2001, **123**, 4896.
326 S.-H. Chou, Y.-Y. Tseng, B.-Y. Chu, *J. Biomol. NMR*, 2000, **17**, 1.
327 R. Štefl, L. Trantírek, M. Vorlíčková , J. Koča, V. Sklenář, J. Kypr, *J. Mol. Biol.*, 2001, **307**, 513.
328 P.A. Dooley, D. Tsarouhtsis, G.A. Korbel, L.V. Nechev, J. Shearer, I.S. Zegar, C.M. Harris, M.P. Stone, T.M. Harris, *J. Am. Chem. Soc.*, 2001, **123**, 1730.
329 S.V. Morosyuk, P.R. Cunningham, J. SantaLucia, Jr., *J. Mol. Biol.*, 2001, **307**, 197.
330 J.-S. Yoo, H.-K. Cheong, B.J. Lee, Y.-B. Kim, C. Cheong, *Biophys. J.*, 2001, **80**, 1957.
331 O. Mauffret, C. El Amri, F. Santamaria, G. Tevanian, B. Rayner, S. Fermandjian, *Nucl. Acids Res.*, 2000, **28**, 4403.

332 N. Tjandra, S.-i. Tate, A. Ono, M. Kainosho, A. Bax, *J. Am. Chem. Soc.*, 2000, **122**, 6190.
333 Z. Fei, H. Thönnessen, P.G. Jones, L. Crowe, R.K. Harris, R. Schmutzler, *Anorg. Allgm. Chem.*, 2000, **626**, 1763.
334 S. Doherty, G. Hogarth, M. Waugh, W. Clegg, M.R.J. Elsegood, *Organometallics*, 2000, **19**, 5696.
335 T. Siedentop, I. Neda, R. Schmutzler, *Z. Naturforsch., Teil B*, 2000, **55**, 956.
336 L. Pouységu, B. De Jéso, J.C. Lartigue, M. Pétraud, M. Ratier, *Magn. Reson. Chem.*, 2000, **38**, 668.
337 C. Höög, G. Widmalm, *J. Phys. Chem. A*, 2000, **104**, 9443.
338 J. Schulte, J. Lauterwein, U. Höweler, *Magn. Reson. Chem.*, 2000, **38**, 751.
339 E.W. Sayers, J.H. Prestegard, *Biophys. J.*, 2000, **79**, 3313.
340 N. Iida-Tanaka, K. Fukase, H. Utsumi, I. Ishizuka, *Eur. J. Biochem.*, 2000, **267**, 6790.
341 H. Junicke, A.S. Serianni, D. Steinborn, *J. Org. Chem.*, 2000, **65**, 4153.
342 G. Tóth, T. Gáti, I. Pintér, J. Kovács, R. Haessner, *Magn. Reson. Chem.*, 2001, **39**, 283.
343 T. Rundlöf, G. Widmalm, *Magn. Reson. Chem.*, 2001, **39**, 381.
344 M. Martin-Pastor, C.A. Bush, *Biopolymers*, 2000, **54**, 235.
345 M. Martin-Pastor, C.A. Bush, *J. Biomol. NMR*, 2001, **19**, 125.
346 M. Staaf, C. Höög, B. Stevensson, A. Maliniak, G. Widmalm, *Biochemistry*, 2001, **40**, 3623.
347 Y. Senda, Y-i. Oguchi, M. Terayama, T. Asai, T. Nakanao, T. Migita, *J. Organomet. Chem.*, 2001, **622**, 302.
348 H.A.S. Citeau, D.M. Giolando, *J. Organomet. Chem.*, 2001, **625**, 23.
349 F.D. Rochon, L.M. Gruia, *Inorg. Chim. Acta*, 2000, **306**, 193.
350 M.G.B. Drew, O.W. Howarth, N. Martin, G.G. Morgan, J. Nelson, *J. Chem. Soc., Dalton Trans.*, 2000, 1275.
351 W. Peti, M. Hennig, L.J. Smith, H. Schwalbe, *J. Am. Chem. Soc.*, 2000, **122**, 12017.
352 T.J. Zahn, M. Eilers, Z.M. Guo, M.B. Ksebati, M. Simon, J.D. Scholten, S.O. Smith, R.A. Gibbs, *J. Am. Chem. Soc.*, 2000, **122**, 7153.
353 K. Hanai, A. Kuwae, T. Takai, H. Senda, K.K. Kunimoto, *Spectrochim. Acta A*, 2001, **57**, 513.
354 A. Lyčka, Z. Vrba, M. Vrba, *Dyes Pigments*, 2000, **47**, 45.
355 C. Hametner, G. Hattinger, J. Röhrling, J. Fröhlich, P. Stanetty, M.D. Mihovilovic, *Magn. Reson. Chem.*, 2001, **39**, 417.
356 K. Ding, *Chin. J. Magn. Reson.*, 2000, **17**, 271.
357 A.E. Panarina, A.V. Dogadina, V.I. Zakharov, B.I. Ionin, *Tetrahedron Lett.*, 2001, **42**, 4365.
358 C.D. Reddy, M.S. Reddy, C.N. Raju, *Indian J. Chem., Sect. B: Org. Chem. Incl. Med. Chem.*, 2000, **39**, 426.
359 F. Karataeva, F.D. Kh. Sokolov, N.G. Zabirov, *Russ. J. Gen. Chem.*, 2000, **70**, 529.
360 B. Wrackmeyer, E.V. Klimkina, Y.N. Bubnov, *J. Organomet. Chem.*, 2001, **620**, 51.
361 Z. Popović, Ž. Soldin, J. Plavec, D. Vikić-Topinć, *Appl. Organomet. Chem.*, 2000, **14**, 598.
362 D.A. Case, C. Scheurer, R. Brüschweiler, *J. Am. Chem. Soc.*, 2000, **122**, 10390.
363 A. Foris, *Magn. Reson. Chem.*, 2000, **38**, 813.

364 Y. Arfaoui, E. Haloui, *Magn. Reson. Chem.*, 2000, **38**, 639.
365 L. Santos, F. Fant, M.A. Medeiros, F.A.M. Borremans, M.C. Costa, M.J.M. Curto, *Magn. Reson. Chem.*, 2000, **38**, 937.
366 E.M. Sproviero, G. Burton, *Molecules*, 2000, **5**, 539.
367 H.E. Birkett, R.K. Harris, P. Hodgkinson, K. Carr, M.H. Charlton, J.C. Cherryman, A.M. Chippendale, R.P. Glover, *Magn. Reson. Chem.*, 2000, **38**, 504.
368 L. Kania, K. Kamieńska-Trela, Ł. Kaczmarek, *Pol. J. Chem.*, 2000, **74**, 1599.
369 B. Garrigues, *Roum. Chem. Q. Rev.*, 2000, **8**, 55.
370 P.M. Iovine, M.A. Kellett, N.P. Redmore, M.J. Therien, *J. Am. Chem. Soc.*, 2000, **122**, 8717.
371 N.S. Bhacca, G.P. Juneau, D.C. Lankin, B. Mukherjee, T. Seal, J.O. Escobedo, R.M. Strongin, *Org. Lett.*, 2000, **2**, 3813.
372 T. Tokunaga, H. Seki, S. Yasuike,M. Ikoma, J. Kurita, K. Yamaguchi, *Tetrahedron*, 2000, **56**, 8833.
373 K. Gholivand, S. Dehghanpour, G. Gerivani, H.R. Bijanzadeh, *Phosphorus, Sulfur and Silicon*, 2000, **157**, 11.
374 C.F. Tormena, R. Rittner, R.J. Abraham, E.A. Basso, R.M. Pontes, *J. Chem. Soc., Perkin Trans. 2*, 2000, 2054.
375 J.W. Benson, R.L. Keiter, E.A. Keiter, A.L. Rheingold, G.P.A. Yap, V.V. Main, *Organometallics*, 1998, **17**, 4275.
376 F. Jiang, H.A. Jenkins, K. Biradha, H.B. Davis, R.K. Pomeroy, M.J. Zaworotko, *Organometallics*, 2000, **19**, 5049.
377 C. Schorn, D. Naumann, H. Scherer, J. Hahn, *J. Fluorine. Chem.*, 2001, **107**, 159.
378 A.B. Shtarev, E. Pinkhassik, M.D. Levin, I. Stibor, J. Michl, *J. Am. Chem. Soc.*, 2001, **123**, 3484.
379 F.B. Mallory, C.W. Mallory, K.E. Butler, M.B. Lewis, A.Q. Xia, E.D. Luzik, Jr., L.E. Fredenburgh, M.M. Ramanjulu, O.N. Van, M.M. Francl, D.A. Freed, C.C. Wray, C. Hann, M. Nerz-Stormes, P.J. Carroll, L.E. Chirlian, *J. Am. Chem. Soc.*, 2000, **122**, 4108.
380 J.E. Peralta, J.P. Snyder, R.H. Contreras, *Chem. Commun.*, 2000, 2025.
381 W.D. Arnold, J. Mao, H. Sun, E. Oldfield, *J. Am. Chem. Soc.*, 2000, **122**, 12164.
382 A. Karaçar, M. Freytag, H. Thönnessen, J. Omelanczuk, P.G. Jones, R. Bartsch, R. Schmutzler, *Zeit. Anorg. Allg. Chem.*, 2000, **626**, 2361.
383 R. Contreras, V.M. Jimenez-Perez, C. Camacho-Camacho, M. Gûizado-Rodriguez, B. Wrackmeyer, *J. Organomet. Chem.*, 2000, **604**, 229.
384 J.E. Del Bene, S.A. Perera, R.J. Bartlett, *J. Phys. Chem. A*, 2001, **105**, 930.
385 J.E. Del Bene, R.J. Bartlett, *J. Am. Chem. Soc.*, 2000, **122**, 10480.
386 M. Pecul, J. Leszczyński, J. Sadlej, *J. Chem. Phys.*, 2000, **112**, 7930.
387 A. Bagno, *Chem. Eur. J.*, 2000, **6**, 2925.
388 M. Pietrzak, J. Wehling, H.-H. Limbach, N.S. Golubev, C. López, R.M. Claramunt, J. Elguero, *J. Am. Chem. Soc.*, 2001, **123**, 4338.
389 R.M. Claramunt, D. Sanz, S.H. Alarcón, M.P. Torralba, J. Elguero, C. Foces-Foces, M. Pietrzak, U. Langer, H.-H. Limbach, *Angew. Chem., Int. Ed.*, 2001, **40**, 420.
390 W.D. Arnold, E. Oldfield, *J. Am. Chem. Soc.*, 2000, **122**, 12835.
391 M. Barfield, A.J. Dingley, J. Feigon, S. Grzesiek, *J. Am. Chem. Soc.*, 2001, **123**, 4014.
392 H. Li, H. Yamada, K. Akasaka, A.M. Gronenborn, *J. Biomol. NMR*, 2000, **18**, 207.
393 V.A. Jaravine, A.T. Alexandrescu, S. Grzesiek, *Protein Sci.*, 2001, **10**, 943.

394 F. Cordier, C.Y. Wang, S. Grzesiek, L.K. Nicholson, *J. Mol. Biol.*, 2000, **304**, 497.
395 N. Juranine, S. Macura, *J. Am. Chem. Soc.*, 2001, **123**, 4099.
396 C. Kojima, A. Ono, M. Kainosho, *J. Biomol. NMR*, 2000, **18**, 269.
397 Z.R. Wu, A. Ono, M. Kainosho, A. Bax, *J. Biomol. NMR*, 2001, **19**, 361.
398 B. Luy, J.P. Marino, *J. Am. Chem. Soc.*, 2000, **122**, 8095.
399 A.Z. Liu, W.D. Hu, A. Majumdar, M.K. Rosen, D.J. Patel, *J. Biomol. NMR*, 2000, **17**, 305.
400 A.Z. Liu, W.D. Hu, A. Majumdar, M.K. Rosen, D.J. Patel, *J. Biomol. NMR*, 2000, **17**, 79.
401 F. Löhr, S.G. Mayhew, H. Rüterjans, *J. Am. Chem. Soc.*, 2000, **122**, 9289.
402 A.Z. Liu, A. Majumdar, F. Jiang, N. Chernichenko, E. Skripkin, D.J. Patel, *J. Am. Chem. Soc.*, 2000, **122**, 11226.
403 K. Chapman, D. Crittenden, J. Bevitt, M.J.T. Jordan, J.E. Del Bene, *J. Phys. Chem. A*, 2001, **105**, 5442.
404 N.A. Jasim, R.N. Perutz, *J. Am. Chem. Soc.*, 2000, **122**, 8685.
405 J.E. Del Bene, S.A. Perera, R.J. Bartlett, I. Alkorta, J. Elguero, *J. Phys. Chem. A*, 2000, **104**, 7165.
406 J. Laynez, M. Menéndez, J.L.S. Velasco, A.L. Llamaz-Saiz, C. Foces-Foces, J. Elguero, P. Molina, M. Alajarin, A. Vidal, *J. Chem. Soc., Perkin Trans. 2*, 1993, 709.

6
Nuclear Spin Relaxation in Liquids and Gases

BY R. LUDWIG

1 Introduction

The aim of this report is to cover the progress of work in the field of magnetic relaxation and self-diffusion in liquids and gases over a period of twelve months from June 2000 to May 2001, and is a continuation of the report given last year.[1]

As in previous periods, this review is limited to work on comparatively simple liquids and solutions of physico-chemical and chemical interest, as publications in the field of macromolecules and biological chemistry are covered elsewhere in this volume. Of course, such a distinction is sometimes problematic, as innovative work dealing with solutions of complex molecules may be of interest for research in the field covered here. Thus, at the risk of duplication, some interesting studies dealing with more complex systems are mentioned briefly.

At the beginning of this chapter it is convenient to quote some authoritative reviews in the subject area. More specialized reviews will be discussed in the corresponding subsections. Also, some important general trends are briefly highlighted here. Details will be discussed later in this chapter.

Lippens and Jeener[2] reviewed the dipolar interaction under all angles. They considered both static and dynamics aspects of the dipolar interaction between two magnetic moments. The static distribution describes the situation of a powder sample, where different spin pairs corresponding to atom pairs on the individual molecules can have all possible orientations in space. The dynamics of the trajectory relates to the situation in a liquid, where every individual spin pair will adopt all orientations over time. Burnell *et al.*[3] presented a review of relaxation theory with special attention to molecular exchange between sites that are associated with different relaxation rates. They studied aqueous solution of nonionic surfactants as a function of composition, spectral frequency and temperature. Monasterio[4] determined rate constants by NMR for reactions controlled by diffusion. A review of Nicolay *et al.*[5] focuses on molecular diffusion in NMR spectroscopy. They used diffusion-weighted magnetic resonance spectroscopy to non-invasively quantify the translational displacement of metabolites in tissues. Luypaert *et al.*[6] reviewed the basic physics principles underlying diffusion and perfusion in magnetic resonance energy. A review of Leibfritz and Dreher[7] deals with magnetization transfer

Nuclear Magnetic Resonance, Volume 31
© The Royal Society of Chemistry, 2002

effects observed *in vivo* NMR spectroscopy. The basic experimental methods, the underlying kinetic mechanism as well as the evaluation of measured data to particular models are described. Ohno *et al.*[8] reviewed the new technique of oxygen-enhanced magnetic resonance ventilation imaging. Its usefulness for diagnostic radiology is discussed. De Graaf and Rothman[9] summarized the *in vivo* detection and quantification of scalar coupled ^{1}H NMR resonance. Proton transfer processes were studied by the deuterium isotope effect. Dziembowska and Rozwadowski[10] focus on the specific application of this method.

A couple of years ago, the traditional framework of NMR spectroscopy was challenged through a series of simple experiments performed by Warren and co-workers.[11–13] The pulse sequences used consisted of a few gradient pulses, and the samples were mixtures of simple molecules. The spectra showed unexpected crosspeaks between spins in different molecules. In order to explain these results, two basic assumptions had to be revisited: the high-temperature approximation of the Boltzmann distribution at equilibrium and the cancellation of dipolar couplings in solution. By taking a close look at the physics the authors showed that correlations between spins in separate molecules exist even after a single pulse, and that dipolar couplings can make these correlations visible in the presence of gradient pulses. Richter and Warren[14] gave a comprehensive description of the effect and presented some future applications. Chen and Zhong[15] found unconventional diffusion behavior of intermolecular multiple-quantum coherences (MQC) in NMR. They analyzed a number of physical effects such as molecular diffusion, variation in dipolar correlation distance, radiation damping, inhomogeneous broadening, spin relaxation, all of which may alter the NMR signal. Their results provide independent evidence to support the intermolecular MQC theory proposed by Warren and co-workers.

In further studies Zhang *et al.*[16] investigated the behavior of intermolecular multiple-quantum coherences in a variety of simple liquids with different chemical and magnetic properties experimentally and modeled it by numerical simulations based on modified Bloch equations. Hereby the authors examined the effects of spin concentration, temperature, intramolecular conformational flexibility, chemical exchange, and spin–spin coupling on the formation of high order coherences. Lin *et al.*[17] could show experimentally and theoretically that two readily observed effects in solution NMR, namely radiation damping and the dipolar field, combine to generate bizarre spin dynamics even with extraordinarily simple sequences. Details about these experiments based on simple pulse sequences and simple liquids are discussed later in the next chapter.

The research activity in the field of supercritical fluids is increasing steadily since the end of the 1980s.[18] There are several reasons for the increasing interest in supercritical fluids. First, new technical processes were developed. Reaction kinetics can be strongly effected in the supercritical region by varying temperature and pressure. Second, the supercritical state presents the intermediate state between the liquid and the gas phase. Physicochemical properties

can be changed continuously from high liquid like to low gas like values without phase transition by varying pressure and temperature. Nakahara *et al.*[19] elucidated the hydrogen bonding state of supercritical water by measuring spin–lattice relaxation times. Structural data obtained by NMR confirmed that hydrogen bonding is still present in supercritical water.[20] Yamaguchi *et al.*[21] used the gas phase approximation to determine NMR properties in supercritical water. In further spin-relaxation measurements a number of alcohols were studied under sub- and supercritical conditions.[22,23] Gaemers and Elsevier[24] gave an outline of the use of supercritical solvents in NMR spectroscopy with emphasis on instrumentation and applications. Especially discussed are the advantages of the low viscosity of supercritical solvents, resulting in appreciable reductions of the line width of NMR resonance of quadrupolar nuclei. They also studied numerous amines and nitrogen-containing heterocycles in liquefied gases and supercritical fluids.[25] Supercritical xenon is used to solve organic liquids and to transfer polarization to ^{1}H and ^{13}C simultaneously.

The techniques of optical pumping and spin exchange, together with the availability of intense lasers at the relevant wavelengths, yield remarkably large nuclear spin polarizations in ^{3}He and ^{129}Xe gases.[26,27] These large nuclear spin polarizations are useful for a variety of applications in NMR[28] and MRI. Hyperpolarized gases are ideal for lung-space MRI, as they are chemically inert and can provide the large signals needed for high special[29] and temporal[30] resolution, despite the low spin density of gases. Hyperpolarized gases have also been proposed of materials for pores and cracks.[31] NMR of hyperpolarized xenon has been used both to study adsorbed layers on low surface spins.[32–34] Direct chemical interest in hyperpolarized gases is limited because the technique is restricted to the inert gas. The largest application of NMR, however, is in the solution state, both on small organic molecules and biological molecules. If the ^{129}Xe polarization of 20% that has been achieved could be transferred to ^{1}H, sensitivity enhancement of solution-state NMR by a factor of about 4000 would be effected. Large enhancement would occur for lower frequency nuclei such as ^{13}C and ^{15}N. The wide applicability of sensitivity enhancement depends critically on an efficient method of transfer of hyperpolarization to a variety of organic or biological molecules.[35] Leawoods *et al.*[36] reported the progress towards the goal of efficient polarization transfer through the use of supercritical solutions of organic solutes in hyperpolarized xenon. Further progress in the field of using polarized noble gases is described in detail in Chapter 4.

Relaxation and self-diffusion techniques in solution are widely used to study hydrogen-bonded systems. The nuclear quadrupole coupling constant (NQCC) presents a sensitive probe for the strength of hydrogen bonding. Unfortunately in the liquid phase this property cannot be measured in a direct way. Two new indirect methods are now presented for determining NQCC in H-bonded liquids. Ferris and Farrar[37,38] showed that for the OD deuteron of ethanol the DQCC is related to the chemical shift of the hydroxy proton by a linear equation. Thus the straightforward measurement of the chemical shift

provides an accurate value for the DQCC. Along with measured deuteron relaxation times, those DQCC allow the determination of molecular correlation times. In the past, an expensive and time consuming combination of dipolar- and quadrupolar-relaxation time experiments was required to provide ^{2}H, ^{14}N and ^{17}O nuclear quadrupole coupling constants in H-bonded liquids. Hardy *et al.*[39] presented a self-consistent method, which allows the determination of both the NQCC as well as the rotational dynamic isotope effect in liquids. The authors successfully tested the method on deuterated benzene[40] and now present data for liquid acetonitrile and acetonitrile water mixtures.[41] The method is also appropriate to study the isotope effect on the translational and rotational motion in liquid water and ammonia.[42] These measured data are of importance for the correct interpretation of all kinds of experiments on both liquids, where isotopic substitutions are involved. The anisotropies of the reorientational motion of benzene is studied for the neat liquid as well as for solutions containing polystyrene.[43]

2 General, Physical and Experimental Aspects of Nuclear Spin Relaxation

2.1 General Aspects. – Underlying physical phenomena of NMR are extremely well understood. This is certainly the case for liquid-state high-resolution NMR spectroscopy. Thus it was surprising when Warren and co-workers[11–13] performed a series of experiments whose results seemed to contradict conventional NMR theory. In these experiments, extremely short pulse sequences were applied to sometimes extremely simple spin systems. Applying their CRAZED or HOMOGENIZED sequences resulted in spectra showing large peaks at positions where there was no peak expected. The peaks were found at positions that would be produced by intermolecular multiple-quantum transitions, which had not been observed before in liquids. Some classical explanations were given, but they lack the predictive and intuitive power of the quantum mechanical picture. Warren and co-workers state that two assumptions made in all textbooks have to be discarded. The two assumptions concerning the equilibrium density operator for the spin systems and the dipolar interactions between spins predict experimental results correctly, as long as there are no gradient pulses in the pulse sequence. In their review the authors gave a comprehensive description of the effect and presented some potential applications. In principle, any order of intermolecular multiple-quantum coherences may be achieved through the proper pulse sequence. Hence they called the general method the 'intermolecular multiple-quantum coherence' (iMQC) method. The strength of this method is that interactions and relationships between spins can be measured on a mesoscopic distance scale. Further improvements are also expected for functional magnetic resonance imaging (fMRI). Chen and Zhong[15] designed two variations of a two-pulse CRAZED sequence to accurately measure and characterize MQC diffusion rates during the evolution period. They were used to investigate the equivalence between intermolecular MQC[11,12,14,17] and demagnetization treat-

ments.[44–48] Physical effects such as molecular diffusion, variation in dipolar correlation distance, radiation damping, inhomogeneous broadening and spin relaxation were analyzed both theoretically and experimentally. The general results derived from both intermolecular MQC and demagnetization field treatments could reasonably explain new observations of diffusion phenomena in nonlinear spin echoes by Kimmich and co-workers.[49,50] The authors could demonstrate that the function dependence of the diffusion rate on coherence order is general. Thus this results provide independent evidence to support the iMQC theory proposed by Warren and co-workers. Zhang *et al.*[16] investigated the behavior of iMQC in a variety of simple liquids with different chemical and magnetic properties experimentally as well as theoretically. They examined the effects of spin concentration, temperature, intramolecular conformational flexibility, chemical exchange, and spin–spin-coupling on the formation of high-order coherences. It could be shown that any process that makes the Larmor frequency time-dependent may interfere with the formation of these coherences. As shown above, recent work on dipolar field effects in simple liquids has explained previously unexpected spectral features such as iMQC and has predicted some new applications but has not challenged the essentially predictable and reproducible nature of this approach. In contrast, Lin *et al.*[17] present experimental and numerical evidence that two readily observed effects in concentrated solutions – radiation damping and the dipolar field – combine to generate chaotic dynamics even with extraordinary simple sequences.

2.2 Experimental Aspects. – Luchinat *et al.*[51] developed NMR instrumentation to achieve excitation of large bandwiths in high-resolution spectra at high field. A prototype 2.5 mm ^{1}H high-resolution probe for an 18.8 T NMR spectrometer has been designed, together with a dedicated amplifier capable of delivering up to 1 kW of power. This probe permits a 90 degree pulse length of 2 μs to be achieved at 300 W, corresponding to an excitation band with of ±125 Hz. The authors could show that this probe is useful for a wide range of applications at high magnetic field, especially in the study of systems characterized by very broad and far-shifted resonance and in experiments that require high-power radiofrequency irradiation.

A low-temperature, high-power probe head has been designed by Damayanovich, Peternelj and Pintar.[52] This probe eliminates the problem of electric discharge commonly experienced during radiofrequency pulse cycling in a helium environment. This design was used in the 4.6 K to 77 K temperature range for RF pulse durations less than or equal to 50 ms and longer for low RF amplitudes. A pressure-resisting cell system for high-pressure high-resolution NMR measurements up to a maximum pressure of 600 MPa has been built by Yamada *et al.*.[53] This cell system is capable of performing high-pressure experiments with any standard spectrometer, including modern high-field NMR machines. A full description of the high-pressure NMR assembly mounted on a 750 MHz spectrometer is presented along with a detailed explanation of the procedure for preparing the pressure-resisting quartz and glass cells.

The quality factor, Q, of the magnetic resonance probe and the manner in which the probe is coupled to the spectrometer play important roles in the quality of the obtained experimental data, affecting the signal-to-noise (SNR), the probe recovery time, radiation damping, and the coupling between multiple coils. For example, high SNR often requires a high-Q probe, while a short recovery time to observe of broad signals generally requires low Q. Miller *et al.*[54] discuss effecting a compromise between SNR and recovery time by adjusting the coupling of the probe and preamplifier by mismatching their impedances. Lips *et al.*[55] presented the design, construction, and performance of a low-inductance solenoidal coil with high B_0 homogeneity for fast-field-cycling NMR. It consists of six concentric layers. The coil is liquid cooled and produces a B_0 field of 0.95 T at 800 A.

Luong *et al.*[56] developed an optimal control technique for magnet design in inside-out nuclear magnetic resonance. A magnet built from this design showed excellent agreement between the measured and computed data and validated the numerical method. Jeglic *et al.*[57] modeled the static fringe field of superconducting magnets. The model takes into account the actual design of the high-homogeneity magnet coil system that consists of the main coil and the cryoshim coils and enables a precise calibration of the on-axis magnetic field gradient and the resonance frequency inside and outside of the super conducting coil. Sigmund *et al.*[58] have studied the temporal instability of a high field resistive Bitter magnet through NMR. This instability leads to transverse spin decoherences in repeated and accumulated NMR experiments as is normally performed during signal averaging. The authors could show that the CPMG sequence with short pulse delays is successful in recovering the intrinsic spin–spin relaxation even in the presence of magnetic field temporal instability.

Olt *et al.*[59] introduced ^{23}Na NMR micro imaging to map the sodium distribution in living plants. The experiments were performed at 11.71 T with a double resonant ^{23}Na–^{1}H probe-head. The ^{23}Na micro imaging promises great potential for physiological studies of the consequences of salt stress on the macroscopic level and thus may become a unique tool for characterizing plants with respect to salt tolerance and salt sensitivity.

2.3 Relaxation in Coupled Spin Systems. – The phenomenon of NMR involves placing magnetically active nuclear spins embedded in a gas, liquid or solid phase in a constant, large and uniform magnetic field, causing a splitting of magnetic energy levels. Energy can be absorbed by these spins from a resonant radiofrequenc field causing transitions between these levels. Immediately following this absorption, the spins start to exchange this energy among themselves and also pass it on to other degrees of freedom, that is, the spins start to relax. Relaxation is central to the NMR phenomenon as a necessary prerequisite for its detection. It is also a probe for obtaining information on the local environment of the spins and about the dynamics of the molecules in which the spins are embedded. One of the most important interactions that couples nuclear spins to each other and to the environment is the dipole–dipole interaction between spins. In liquids, the intramolecular dipolar interaction,

between the spins of the same rigid molecule, becomes time dependent due to rapid molecular reorientations. Intermolecular interactions (between spins of two different molecules) become time dependent additionally due to translational motion. There are dipolar interactions between several spins at the same time, many of which have identical time dependences arising from the same reorientational or translational motion. Additionally, there are other sources of relaxation for the nuclear spins. The simultaneous presence of various mechanisms gives rise to cross terms between these mechanisms. These cross terms are known as cross-correlations. In high-resolution liquid state NMR, the effects of cross-correlations were observed in double resonance experiments used for studying the relaxation of coupled spins.[60–64] Kumar, Grace and Madhu[65] reviewed the recent progress in the field of cross relaxation phenomena in equivalent and strongly coupled spins and their influence on line broadening of resolved multiplets and relaxation.

In liquid-state NMR, spin relaxation due to cross-correlation of two anisotropic spin interactions can provide useful information about molecular structure and dynamics. These effects are manifest as differential line widths or line intensities in the NMR spectra. Recently, new experiments were developed for the accurate measurement of numerous cross-correlated relaxation rates in scalar coupled multi-spin systems. The recently introduced concept of transverse relaxation optimized spectroscopy (TROSY) is also based on cross-correlated relaxation. Brutscher[66] outlined the basic concepts and experimental techniques necessary for understanding and exploiting cross-correlated relaxation effects in macromolecules. In addition, he presented some examples showing the potential of cross-correlated relaxation for high-resolution NMR studies of proteins and nucleic acids.

Kover and Batta[67] presented two new sensitivity enhanced gradient NMR experiments for measuring interferences effects between CSA and dipolar coupling interactions in a scalar coupled two-spin system both in the laboratory and rotating frame. The authors could demonstrate that the standard heteronuclear T_1, T_2 and steady-state NOE autocorrelations experiments augmented by cross-correlation measurements provide sufficient experimental data to quantitatively separate the structural and dynamic contribution to these relaxation rates when the simplifying assumptions of isotropic overall tumbling and an axially symmetric chemical shift tensor are valid. Ferrage *et al.*[68] could show that selective single-transition cross-polarization (ST-CP) may be achieved in four-level systems such as encountered in NMR of scalar-coupled two-spin system (for example, ^{15}N–^{1}H groups in peptides), by employing two selective resonant fields applied to a pair of connected transitions with RF amplitudes much weaker than the separation of parallel transition (*e.g.* the scalar coupling constant $J(^{15}N, ^{1}H)$). The method proposed is quite general provided the selectivity is sufficient to confine the evolution of the single-transition coherences within two mutually exclusive subspaces of the Liouville space. As the authors pointed out this method should be useful to study differential relaxation of multiplet components.

Lambert *et al.*[69] proposed a new two-dimensional pulse sequence for T_2

measurements of protons directly coupled to ^{13}C-spins. The sequence measures the transverse relaxation time of heteronuclear proton single-quantum coherence under conditions of free precession and is therefore well suited to evaluate relaxation losses of proton magnetization during preparation delays of heteronuclear pulse experiments in analytical NMR. The relevant part of the pulse sequence can be inserted as a 'building block' into any direct or inverse detecting H,C correlation pulse sequence if proton spin–spin relaxation is to be investigated. The authors inserted the 'building block' into a HECTOR as well as into a HMQC pulse sequence. Fedin *et al.*[70] studied the anisotropic hyperfine interaction-induced (HFI) spin relaxation in a low magnetic field. It has been correctly considered for a radical with one magnetic nucleus in a framework of Redfield relaxation theory. The authors pointed out that the HFI-induced relaxation is very different in a low magnetic field from that in a high magnetic field. The traditional high-field expressions for calculating T_1 and T_2 are no longer valid.

Prompers and Brüschweiler[71] showed by quasiharmonic analysis that the conformational partition function of a globular protein sampled on the ns time scale can be factorized in good approximation into purely reorientational part, which determines heteronuclear NMR spin relaxation, and a remaining part that includes other types of intramolecular motions. Thus a thermodynamic interpretation of NMR relaxation parameters in proteins in the presence of motional correlations can be given.

Assuming that an original distribution is a probabilistic measure and the Laplace transforms are known only for a finite number of points that are affected by errors, Steinbrecher *et al.*[72] developed a method for reconstructing weak-sense mean values obtained by integrating smooth functions with the measure. Their method is useful if the NMR signal can be represented as a superposition of exponential terms. It was tested for an accurate reconstruction of spin–spin relaxation data. Skrynnikov *et al.*[73] could show that the relative orientation of peptide planes in proteins is reflected in carbonyl–carbonyl chemical shift anisotropy cross-correlated spin relaxation. NMR spin relaxation methods for characterization of disorder and folding in proteins were presented by Bracken.[74] Apel and Bychkov[75] studied the relaxation that is weakly coupled to a quantum mechanical environment. Starting from the microscopic description, the authors derived a system of coupled relaxation equations within the adiabatic approximation. These are valid for arbitrary I and also for a general stationary nonequilibrium state of the environment. In the case of equilibrium, the stationary solution of the equations becomes the correct Boltzmann equilibrium distribution for a given spin I. The relaxation towards the stationary solution is characterized by a set of relaxation times, the longest of which can be shorter, by a factor of up to $2I$, than the relaxation time in the corresponding Bloch equations calculated in the standard perturbative way. Kaikkonen and Kowalewski[76] calculated a relaxation network for multipolar AMX systems under application of a spin-locking RF field. All possible auto- and cross-correlation terms involving dipolar, quadrupolar and CSA interactions have been taken into account. The results show the presence

of spectral densities at zero frequency for interactions associated with the locked nuclei, which are nonvanishing in the absence of fast motion.

2.4 Dipolar Couplings and Distance Information. – In general, molecular geometries can be derived by cross-relaxation rates that depend on the internuclear distance. Usually, two routine types of experiments are used to determine macromolecular structures: NOESY[77] investigates the longitudinal cross correlation, while ROESY[78] makes use of the cross-relaxation of transverse magnetization spin-locked to a strong r.f. field close to resonance. An important aspect of ROESY is that crosspeak intensity increases monotonically with correlation time. The weak r.f. field guarantees the extreme narrowing limit $\omega\tau_c << 1$) for all values of τ_c and ω of practical interest. Unlike NOESY, therefore, ROESY crosspeak intensities will not tend to zero when $\omega\tau_c \approx 1$, which often appears to be the case at high fields for small molecules. A second advantage of ROESY is that NOE's generated in a linear chain of spins alternate in sign which makes it possible to distinguish whether a weak ROE crosspeak derives from transfer *via* an intermediate spin, chemical exchange or is an authentic long-range ROE. In conventional NOESY spectra of larger molecules, all crosspeaks are of the same sign regardless of the presence of 'spin-diffusion' or chemical exchange.

Almond *et al.*[79] investigated how aqueous dynamical simulations of flexible molecules can be compared against NMR data. The methodology compares state-of-the-art NMR residual dipolar coupling, NOESY and ^{13}C relaxation, to molecular dynamics simulations in water over several nanoseconds. In contrast to many previous applications of residual dipolar couplings in structure investigation of biomolecules, the approach described here uses MD simulations to provide a dynamic representation of the molecules.

The algorithms available today that use dipolar coupling data for macromolecular structures determination require the independent determination of two parameters, D-a(PQ) and R. Methods exist for obtaining these parameters when the set of dipolar couplings available is large and the orientations of the interatomic vectors on which they report is isotropically distributed. These methods are less satisfactory when the set is small and anisotropic. Thus Warren and Moore[80] described a maximum likelihood method for determining accurate values for D-a(PQ) and R from small sets of dipolar coupling data. Kramer *et al.*[81] optimized phase-cycle Carr–Purcell-type multiple-pulse sequences for coherence and polarization transfer in homonuclear Hartmann–Hahn experiments applied to partially oriented samples. Compared to previously suggested experiments, the sequences yield considerable improved scaling factors for residual dipolar coupling constants, resulting in improved transfer efficiency.

The measurement of residual dipolar couplings in weakly aligned proteins can potentially provide unique information on their structure and dynamics in the solution state. The challenge is to extract the information of interest from the measurements, which normally reflect a convolution of the structural and dynamic properties. Tolman *et al.*[82] discussed a formalism which allows a first

order separation of their effect, and thus, a simultaneous extraction of structural and motional parameters from residual dipolar coupling data. Mueller *et al.*[83] described a method for incorporating dipolar coupling restraints into calculations. Heteronuclear dipolar couplings were used by Chou *et al.*[84] to study conformational rearrangement and refinement of structural homology models.

Neubauer *et al.*[85] also demonstrated for carbohydrates that residual dipolar couplings have dramatically improved the accuracy and precision of high-resolution NMR structures in recent years. Significant differences between the solution and X-ray crystal structure exist. These results indicate that residual dipolar coupling data may provide a more complete and dynamic model of carbohydrates in particular, and small molecules in general. The superposition of scalar and residual dipolar couplings give rise to so-called cylindrical mixing Hamiltonians in dipolar coupling spectroscopy. Luy and Glaser[86] presented general analytical polarization and coherence transfer functions for three cylindrically coupled spin $\frac{1}{2}$ under energy-matched conditions. Hennig *et al.*[87] presented a residual dipolar coupling TOSCY for direct through space correlations of base protons and phosphorous nuclei in biomolecules. Meiler *et al.*[88] presented a model-free approach to the dynamic interpretation of residual dipolar couplings in globular proteins.

2.5 Exchange Spectroscopy. – Two-dimensional (2D) exchange spectroscopy and its numerous derivatives play a crucial role in the NMR study of small molecules and macromolecules in solution. Exchange spectroscopy is designed to monitor incoherent magnetization transfer, which in solution encompasses chemical exchange and cross relaxation. The beauty of the method is that it studies the dynamics in the equilibrium systems and spans a range of a few orders of magnitude of the exchange rate constant. The lower bound for the exchange rate constant is determined by the relaxation times of the spins involved. A principle disadvantage is that in complex systems cross-relaxation is indistinguishable from chemical exchange. Furthermore, when two processes occur in the same two spins in 'unfavorable' conditions they can cancel each other. Various modifications of the basic experiment have been proposed to differentiate chemical exchange from cross-relaxation. But none of the methods applies to cross-relaxation and chemical exchange among uncoupled spins when the system is in the extreme narrowing motional regime. Zhang and Mao[89] applied NMR two-dimensional exchange spectroscopy to measure the chemical exchange rate constant between water and hydroxyl protons in three natural organic compounds which contain four to eight hydroxyl groups. In data treatment, the simple geometric average method has been used.

It has recently become more widely appreciated that the presence of rotational diffusional anisotropy in proteins and other macromolecules can have a significant affect on the interpretation of NMR relaxation data in terms of molecular motion. Andrec *et al.*[90] showed how commonly used NMR relaxation data (T_1, T_2 and NOE) obtained at two spectrometer frequencies can be analyzed using a Bayesian statistical approach to reliably detect and

quantify the degree of rotational diffusion anisotropy. The Bayesian statistics also readily separate the effects of chemical exchange from rotational anisotropy. Based on the measurement of cross-correlation rates between ^{15}N CSA and ^{15}N–^{1}H dipole–dipole relaxation Renner and Holak[91] proposed a procedure for separating exchange contributions to transverse relaxation rates T_2 from effects caused by anisotropic rotational diffusion in a protein molecule. This approach determines the influence of anisotropy and chemical exchange processes independently and therefore circumvents difficulties associated with the currently standard use of T_1/T_2 ratios to determine the rotational diffusion tensor.

The McConnell equations combine the differential equations for a simple two-state chemical exchange process with the Bloch differential equations for a classical description of the behavior of nuclear spins in a magnetic field. This equation system provides a useful starting point for the analysis of slow, intermediate and fast chemical exchange studied using a variety of NMR experiments. The McConnell equations are in the mathematical form of an homogeneous system of first-order differential equations. Helgstrand *et al.*[92] rewrote the McConnell equations in a homogeneous form in order to facilitate fast and simple numerical calculation of the solution to the equation system. As the authors pointed out the McConnell equations can only treat equilibrium chemical exchange. They now present a homogeneous equation system that can handle both equilibrium and non-equilibrium chemical processes correctly, as long as the kinetics is of first-order. The same method of rewriting the inhomogeneous form of the McConnell equations into a homogeneous form is applied to a quantum mechanical treatment of a spin system in chemical exchange. Both treatments were tested experimentally.

An efficient sparse-matrix-based numerical method is constructed by Dumont and Assalone[93] to simulate two-dimensional NMR spectra of many-spin systems including the effects of chemical exchange and/or relaxation. The authors tested their method in simulations of double-quantum-filter correlation spectroscopy and exchange spectroscopy experiments on five- and seven-spin systems with two sites. Chernysh *et al.*[94] reported a technique to suppress a magnetic polarization of coherent transfer that makes it possible to use 2D exchange spectroscopy to study exchange processes. Only one nucleus from the couple's spin system undergoing the spin exchange is excited, which is referred to as multiplet selective excitation (MUSEX). In general, at excitation of this type the spin system behaves as an uncoupled system with multisite exchange. Juranic *et al.*[95] revisited two-dimensional exchange spectroscopy accounting for the number of participating spins. Although an accurate description of global tumbling of a protein is essential for correct analysis of internal motion, proper distinction between the effects of anisotropic rotational diffusion and conformational exchange has remained a challenge. Pawly *et al.*[96] presented a novel method for distinguishing between anisotropic tumbling and chemical exchange in analysis of ^{15}N relaxation parameters.

Monlien *et al.*[97] studied the cyanide exchange on a square planar tetracyanoplatinate complex under high pressure and over a large pH range.

Schneppensieper *et al.*[98] studied water exchange in water-soluble iron(III) porphyrins with high pressure ^{17}O NMR. Corsi *et al.*[99] investigated the same effects of a cationic macrocyclic gadolinium(III) complex. The sites of hydroxyl radical reaction with amino acids were identified by Nukuna *et al.*[100] by ^{2}H NMR detection of induced $^{1}H/^{2}H$ exchange. Aime *et al.*[101] used the same method to study the molecular pathways of hydrogen in organometallics. Traore *et al.*[102] studied the dynamics of water in gelatin by T_2 measurements using the Carr–Purcell–Meiboom–Gill pulse sequence. The authors interpreted their observations in terms of chemical exchanges between water protons and those of the macromolecules in the sol state.

2.6 Radiation Damping. – As NMR spectroscopy continues to move towards higher magnetic fields, accompanying advances must be made in the design of probes and pulse sequences capable of dealing with the effects of the enormous fields on NMR spectra. One such effect that routinely plagues the liquids NMR spectroscopist is radiation damping.[103] Radiation damping is the presence of a reaction field induced by coupling of precessing magnetization to tuned resonant circuits. Evidence for this effect was observed first in transient free precession experiments where the decay rate of the free induction signal could be controlled by varying the quality factor of an r.f. tank circuit.[104] More recently it has been shown that radiation damping effects can complicate the measurement of spin–lattice and spin–spin reaction times, as well as alter the appearance of multidimensional spectra.[105] There have been several methods developed to attenuate radiation damping effects. One approach essentially involves a feedback scheme that maintains zero voltage in the r.f. sample coil.[106] By canceling out the current induced by the precessing magnetization in the coil, the reaction field and radiation damping effects can be reduced substantially. Other strategies focus on the major magnetization component in the sample, primarily solvent. A combination of perdeuterated solvents with solvent suppression techniques that interleave pulsed field gradients with r.f. pulses can truncate radiation damping. It has been more practical to eliminate the nuisance of radiation damping rather than bother with the great difficulty of understanding its nonlinear effects,[107] because they do not lend themselves to standard techniques of analysis as applied to pulsed signal spectroscopy. Rourke and Augustine[108] showed that nonlinear evolution of the Landau–Lifshitz type can be exactly linearized. Special cases include the radiation-damped spin system and the superradiant system in the semiclassical regime, in the presence of time-varying driving fields. For these, the resultant linear system is simply that of a spin $\frac{1}{2}$ particle, with the radiation damping rate, or superradiant characteristic time, manifested as an imaginary addition to the spin's resonance frequency. Consequently, methods from inverse scattering theory can be used to design driving fields. Price *et al.*[109] examined the effects of macroscopic background gradients due to susceptibility differences at the sample interfaces and of radiation damping on pulsed-gradient spin-echo (PGSE) experiments. Both phenomena can lead to the seemingly strange effect of the echo signal growing as the gradient strength increases at

low applied gradient strength. The effects of radiation damping can also result in the attenuation curve being nonlinear but, different from the effect of background gradients, the nonlinearity does not change with the polarity of the applied gradient.

There are several examples in the literature where effects of inhomogeneous broadening on radiation damping of free precession signals have been described using a phenomenological 1/T2* term in the Bloch equations. Augustine and Hahn[110] demonstrated the inappropriate use of this model for specific cases. The authors could showed that correct signal shapes are predicted only when isochromat solutions of Bloch's equations are integrated over the spectrum of the inhomogeneous field. The observation of NOEs between bound water and biological macromolecules such as proteins and nucleic acids can be improved by inverting the water resonance selectivity while compensating for radiation damping effects.[111] Ramanthan and Bowtell[112] applied the COSY-revamped by asymmetric *z*-gradients experiment to a wide range of problems from functional magnetic resonance imaging to structure determination in porous media. The authors investigated the temporal dynamics of the experiment in the regime where the linear approximation for the signal evolution is no longer valid. Numerical solutions of the nonlinear evolution equations were obtained with and without radiation damping.

So far radiation damping has been mainly regarded as an annoyance in NMR experiments and techniques for eliminating or reducing radiation damping were discussed widely. However, radiation damping may have benefits. Louis-Joseph *et al.*[113] have shown that by amplification of radiation damping obtained by electronic feedback between consecutive transients of a Jump-Return (JR) experiment, residual in-plan water magnetization is suppressed, leading to substantial enhancement of water suppression.

2.7 Quadrupolar Interactions. – Quadrupolar coupling constants are sensitive probes of hydrogen bonding. Their accurate knowledge is a major prerequisite when trying to extract dynamical information from relaxation data of quadrupolar nuclei. If the relaxing nucleus is covalently bound, the NQCC is determined by the electric field gradient (efg) arising from the intramolecular charge distribution at the nuclear site. Liquid phase values for NQCC can be obtained only in an indirect way. The standard procedure is to first determine correlation times for molecular reorientation from dipole–dipole relaxation rates. For example, the molecular reorientation time obtained from dipolar ^{13}C–^{1}H relaxation data is used to determine the deuteron NQCC in ^{13}C–^{2}H from quadrupolar relaxation. In this particular case the procedure is correct, because the principle axis of the efg tensor coincides with the direction of the dipole–dipole interaction. The method also works for ^{1}H–^{17}O and ^{2}H quadrupolar interaction in the OH group of water[114,115] and alcohols.[116] In pure liquids and in various binary mixtures it could be shown that the obtained ^{2}H NQCC show large medium and temperature effects. Details are very difficult to interpret without the help of theoretical calculations. As noted in previous reports,[1] there are now theoretical methods to predict the efg in the liquid

state. The first method is based on Molecular Dynamics Simulations (MD). From the bulk configurations, molecular clusters are chosen and used in supra molecular *ab initio* calculations. This technique has been successfully applied by Huber *et al.*[117,118] to determine ^{2}H and ^{17}O NQCC in liquid water. In a second method, molecular clusters were calculated by pure *ab initio* methods. A Quantum Cluster Equilibrium (QCE) Model,[119,120] which is fully based on quantum thermodynamics treatment, generates temperature- and pressure-dependent molecular cluster populations. Changing cluster distributions leads to temperature-dependent H-bond-sensitive properties such as NQCC, chemical shifts and vibrational frequencies, which are calculated for each of the clusters. With this procedure the temperature dependence of ^{2}H NQCC for liquid alcohols[121] as calculated by pure theoretical methods. In a third method, Wendt and Farrar[122] presented an indirect method for the measurement of deuterium quadrupole coupling constants in liquids. They could demonstrate that in methanol the deuterium quadrupole coupling parameter is related to the deuterium chemical shift by a linear equation. The straightforward measurement of the chemical shift thus provides an accurate value for the NQCC which in turn provides along with measured deuteron relaxation times a value for the molecular correlation time. This method was applied to ethanol as a function of composition with CCl_4[38] and temperature.[37] In a fourth method Hardy *et al.*[39] presented a self-consistent method, which allows the determination of both the NQCC as well as the rotational dynamic isotope effect in liquids. By this new method NQCC and the isotopic effect were studied for acetonitrile and acetonitrile–water mixtures[41] as well as for neat water, ammonia[42] and benzene.[40]

Magnetic multipoles of rank higher than one become active in spin systems with $I > \frac{1}{2}$ and their contribution to relaxation depends on dynamics. The appearance of multipole terms complicates the relaxation description and supports the multiexponential behavior of relaxation. Nosel *et al.*[123] presented the effects of high rank multipoles on lineshape and longitudinal relaxation of $I=3$ systems. Results obtained from both numerical simulation and experimental data show that longitudinal and transverse relaxation are strongly influenced by these multipole terms, especially at lower temperatures where, due to molecular mobility, the extreme narrowing condition is not fulfilled.

Vaara and Pyykkö[124] presented a theory for the magnetic-field-dependent quadrupole splitting in the ^{131}Xe NMR spectra in isotropic media and tested it by *ab initio* electronic structure calculations. Evidence exists only for even-power magnetic field dependence. The dominant mechanism is verified to be the electric field gradient caused by the diamagnetic distortion of the atomic electron cloud, quadratic in the magnetic field. NQCC for diatomic molecules were calculated by Bryce and Wasylishen.[125] Turner *et al.*[126] performed a systematic computational study of the geometrical dependence of the deuteron quadrupole interaction parameters (DQCC and asymmetry parameter) for the water–formaldehyde model system. Bernatowicz and Szymanski[127] studied NMR spectra of a spin $\frac{1}{2}$ nucleus scalar coupled to two equivalent spin-1 nuclei

in the limit of slow quadrupolar relaxation. Lehoux *et al.*[128] developed a faster way to characterize water molecules strongly bound to macromolecules in solution by triple-quantum filtered ^{17}O NMR. Bagno *et al.*[129] detected hydrogen bonding by NMR quadrupolar relaxation of the acceptor nuclei. Quadrupole coupling constants of aluminium chlorides were studied by Mains *et al.*.[130]

2.8 Intermolecular Dipolar Interaction in Diamagnetic and Paramagnetic Solution. – The T_1 and T_2 relaxation rate enhancements produced by dissolved paramagnetic solutes is called the NMR paramagnetic relaxation enhancement or NMR-PRE. Because the unpaired electron spin has a magnetic moment which is about 10^3 times larger than the nuclear magnetic moments, and because the NMR-PRE depends on the square of the electron and the nuclear magnetic moment, the relaxation pathway provided by unpaired electron spins is very potent. It is frequently the case that micro- or millimolar concentrations of paramagnetic solutes provide the predominant relaxation pathway for nuclear spins on the solvent and ligand species. The physical mechanisms of the NMR-PRE was first analyzed by Solomon,[131] and independently by Bloembergen[132] and Bloembergen and Morgan.[133] The early physical picture is generally applicable to organic radicals and to spin-1/2 paramagnetic metal ions such as Cu(II). However, the large majority of paramagnetic transition metal ions in their common oxidation state have spin $S \geq 1$, and, for these ions, the theory of Solomon, Bloembergen and Morgan (SBM) is often physically inappropriate. SBM theory assumes a Zeeman quantization of both the nuclear and electron spin motion. While this is certainly valid approximately for nuclear spins in liquids, it is often not valid for electron spins $S \geq 1$, which are subject to the zero field splitting (zfs) interaction. The zfs is comparable in order of magnitude to the Zeeman interaction in many NMR experiments. When the zfs energy is greater than the Zeemann energy, the electron spin motion, which is determined by the driving Hamiltonian, is the primary determinant of the properties of the NMR-PRE. In a nice progress report, Sharp, Lohr and Miller[134] gave a formal theoretical description of these phenomena. The discussion focuses on the relationship of the NMR-PRE to the electron spin motion, which is driven by a spin Hamiltonian that consists of Zeeman and zfs contributions. The authors could show that the electron spin motion is the determining factor of the properties of the NMR-PRE. Their approach has been recently developed.[135–137] Related work is reported by a group in Florence,[138–140] mainly focusing to provide computational methods useful for analyzing NMR relaxometry data in systems of chemical and biochemical interest. A different approach, based on the Stochastic Liouville Equation of the motion of the coupled electron and nuclear spin systems was developed some time ago by Swedish workers[141–147] and has been discussed in earlier issues of this report. Miller *et al.*[136] tested one of the central predictions of the theory of paramagnetic enhancement of NMR relaxation rates in solution for spins $S \geq 1/2$ by measuring the axial/equatorial T_1 ratio for $S = 1$ in the zero-field splitting limit. In another article the same

authors[137] reported the NMR-PRE in the zfs-limit for a S = 3/2 complex. The NMR-PRE behavior was found to be different from that of the analogues S = 1 complex as well as from other previously studied S = 1 model compounds.

Rast *et al.*[148] studied the mechanisms of the intermolecular NMR relaxation dispersion of the tetramethylammonium protons in Gd^{3+} heavy-water solutions. The standard dipolar nuclear relaxation formalism of Solomon–Bloembergen, valid for the used frequency range between 10 and 800 MHz, leads to overall good agreement with the measured data without any adjustable parameters. Madhu *et al.*[149] reported experimental observation and numerical simulation of a two-dimensional multiplet effect in the heteronuclear correlation spectrum of a paramagnetic protein that depends on molecular geometry. Bertini *et al.*[150] performed solution structure calculations through self-orientation in a magnetic field of a cerium(III) substituted calcium-binding protein. This work showed that Ce(III), like low-spin Fe(III) in hemoproteins, is sufficiently magnetically anisotropic to induce self-orientation to an extent which can be exploited for solution structure determination. Ma *et al.*[151] measured longitudinal paramagnetic dipolar relaxation rates in plastocyanin from *Anabaena variabilis*. Hus *et al.*[152] used orientational and novel long-range order restraints available from paramagnetic systems to determine the backbone solution structure of the cytochrome c′ protein to atomic resolution in the complete absence of restraints derived from the nuclear Overhauser effect. Aroulmoji and Rao[153] measured T_1 and T_2 proton relaxation times in highly viscous glycerine–water and less viscous dioxan–water systems, both containing paramagnetic ions. Khomeriki[154] investigated the nonequilibrium behavior of nuclear spin systems with dipolar interaction in parallel pumping magnetic field. The highly polarized paramagnetic phase of nuclear spins is examined.

2.9 Slow Motions in Glasses. – Studies of slow molecular motions in supercooled and glassy systems using NMR techniques have become more popular and the number of papers increased steadily during the past few years. In particular the homogeneous *versus* heterogeneous scenario for the dynamics of glass-forming polymers was discussed intensively.[155–158] In the heterogeneous scenario the nonexponentiality of the α relaxation is attributed to a superposition of relaxation rates, whereas in the homogeneous scenario the nonexponentiality is intrinsic in nature. Although it has been long recognized that dynamics in supercooled liquids might be spatially heterogeneous, only in the past few years has clear evidence emerged to support this view. In his review article Ediger[159] addressed the recent progress in the field of glass-forming materials including important multidimensional NMR work. Richert[160] derived the time resolved inhomogeneous broadening line shape from analytical theory for a liquid which exhibits spatial heterogeneity regarding the solvent response time. The results demonstrate that it is the heterogeneous nature of supercooled liquids which gives rise to asymmetric lines and to a maximum in the linewidth as a function of time while average emission energy

experiences a redshift. Qian and Heuer[161] studied the exchange rates of dynamic heterogeneities in a glass-forming liquid by multidimensional NMR. Viot *et al.*[162] examined some of the consequences, and their connection to experiments on supercooled liquids, of a scaling model of heterogeneous relaxation that is based on the theory of frustration-limited domains. Their model is in agreement with a heterogeneous picture of the alpha relaxation for fragile supercooled liquids. Temperature and composition effects of spatially heterogeneous dynamics in thermoset resins below the glass-transition temperature were investigated by Wang and Ediger.[163] In contrast to homopolymer systems, a bimodal distribution of local relaxation times developed with the addition of the second component. Diezemann[164] presented a method that can be used for a clearcut distinction of homogeneously and heterogeneously broadened susceptibilities as they occur in the slow primary relaxation of supercooled liquids and other disordered materials.

Reinsberg *et al.*[165] presented the first direct measurement of the length scale of dynamic heterogeneity in a low molecular weight glass former without the perturbing effect of probe molecules or confinement. Using a multidimensional ^{13}C solid-sate exchange NMR experiment, 1 nm heterogeneities were found in glycerol for temperatures ranging from 199 K to 207 K. This small size and weak temperature dependence allows some distinctions to be made among different models of the glass transition. Long and Lequeux[166] studied the heterogeneous dynamics at the glass transition in van der Waals liquids, in the bulk and in thin films. The authors proposed first a thermodynamical model for van der Waals liquids, which accounts for experimental results regarding the bulk modulus of polymer melts and the evolution of the density with temperature.

Vogel *et al.*[167] investigated benzene in polystyrene systems as models for binary glass formers by applying multidimensional ^{2}H NMR experiments. It is demonstrated that the large molecular component of these systems essentially behaves as a neat glass former, whereas the small benzene molecules show a completely different scenario. Vogel and Rössler[168] studied the Johari-Goldstein beta process of organic glass formers by one- and two-dimensional ^{2}H NMR. The authors concluded that reorientations with an amplitude $\chi > 1$ degrees do not occur on a time scale of μs to ms for the majority of the molecules in glassy glycerol and polystyrene. Intramolecular motions in simple liquids at the glass transition were investigated by Sillescu *et al.*[169] The spin–lattice relaxation times of the selected ring deuterated, fragile glass formers propylene carbonate and toluene were compared with those measured for species which were specifically labeled at the methyl groups. Qiu *et al.*[170] measured ^{13}C NMR T_1, NOE and $T_{1\rho}$ for an atactic polypropylene melt as a function of Larmor frequency and temperature. The data fit very well with a model for C–H vector orientation composed of very fast librational relaxation, intermediate segmental relaxation, and a normal mode contribution described by Rouse dynamics modified for entanglement effects. Mortuza *et al.*[171] performed high-resolution NMR to measure relaxation times T_1 in alkali silicate glasses. The results for all systems were explained in terms of phase

separation. Senker and Rössler[172] discussed the liquid polyamorphisms of triphenyl phosphite. In particular, the problems of experimentally identifying amorphous–amorphous or liquid–liquid transitions were considered. McLaughlin *et al.*[173] studied the structure of alkali tellurite glasses. The molecular mobility in two similar organic glass formers, namely sorbitol and maltitol, were studied by Margulies *et al.*[174] in order to understand their differences in the cross-over between alpha and beta relaxation, far above their respective glass transition temperatures.

Hollander and Prins[175] investigated the effect of pressure on the glass-transition temperature T_g in atactic polypropylene in the pressure range up to 5000 bar. The decay rate of the deuteron-NMR quadrupole echo was used to monitor the glass transition. In further papers the same authors also studied the methyl group, segmental and chain motions of this molecular system.[176,177]

Kumar *et al.*[178] used spectroscopic techniques such as NMR to study the properties and structures of mixed glass systems. Rosenhahn *et al.*[179] obtained insight into the structure and dynamics of the binary As–Se glass system from high temperature ^{77}Se NMR studies of molten salts. *Ab initio* molecular orbital calculations have been carried out for silicate, aluminosilicate and aluminate clusters to study the NMR characteristics of various types of hydroxyl that are possibly present in hydrous silicate glasses and melts. Xue and Kanzaki[180] in particular studied the specification and dynamics of dissolved water in the silicate glasses.

2.10 Models for Molecular Dynamics. – Some years ago, a model-free approach to the interpretation of NMR relaxation in macromolecules was suggested by Lipari and Szabo.[181,182] For both isotropic and anisotropic overall motion, it was shown that the unique information about fast internal motions contained in relaxation experiments can be completely specified by two model-independent quantities: a generalized order parameter, S, which is a measure of the spatial restriction of the motion, and an effective correlation time, τ_e, which is a measure of the rates of motion. Palmer[183] reviewed the application of the model-free approach for characterizing intramolecular and overall rotational motions in proteins. Andrec *et al.*[184] explored connections between the Lipari–Szabo formalism and reduced spectral density mapping, and showed how spectral density estimates can be associated with Lipari–Szabo parameters *via* a simple geometric construction which they called Lipari–Szabo mapping. Practical applications of Lipari–Szabo mapping in conjunction with more traditional analysis methods were discussed.

Meiler *et al.*[88] applied the model-free approach to the dynamic interpretation of residual dipolar couplings in globular proteins. Ishima *et al.*[185] compared the methyl rotation axis order parameters derived from the model-free analyses of the ^{2}H and ^{13}C longitudinal and transverse relaxation rates measured in the same protein sample. Best *et al.*[186] reported the results of molecular dynamics simulations compared with NMR relaxation experiments for maltose and isomaltose. Using the model-free formalism they could estimate reliable order parameters. Baber *et al.*[187] used an 'extended model-

free approach' to analyze the slow interdomain motion of macromolecules. It was possible to uniquely determine all model-free parameters without any *a priori* assumptions regarding their magnitude by simultaneously least-square fitting the relaxation data measured at two different magnetic fields.

An automated model-based approach for NOE assignment was described by Duggan *et al.*[188] The use of the semi-automated iterative approach assists in the identification of errors in the NOE assignments to short-cut the path to an NMR solution structure. Kannan *et al.*[189] reported ^{1}H NMR spin–lattice relaxation times T_1 in glycine phosphite which is ferroelectric below 244 K. To describe the Larmor frequency dependence a model was proposed based on the Bloembergen–Purcell–Pound (BPP) theory. Masuda[190] studied the solvent effect on rotational relaxation time of ammonium ion. The observed solvent dependence of the rotational relaxation times showed a poor correlation with those for predicted from a hydrodynamic (Stokes–Einstein–Debye) model or an electro hydrodynamic (Hubbard–Onsager–Felderhof) model, where as a much better linear relation was found for the plot of the logarithms of the observed rotational relaxation times *versus* Gutmann's solvent donor numbers. A numeric algorithm which is suitable for calculating lineshape of cross-polarization spectra influenced by isotropic and anisotropic tumbling is proposed by Mayer.[191] It is based on a description of the cross-polarization process using single-transition operators combined with rotational diffusion represented by a stationary Markov operator. The applicability of the algorithm is demonstrated on supercooled glycerol as a model system.

It has recently become more widely appreciated that the presence of rotational diffusional anisotropy in proteins and other macromolecules can have a significant affect on the interpretation of NMR relaxation data in terms of molecular motion. Andrec *et al.*[90] used a Bayesian statistical method for the detection and quantification of rotational diffusion anisotropy from NMR relaxation data. Sturz and Dölle[192] examined the reorientational motion of toluene in neat liquid by using ^{13}C relaxation measurements. The relaxation rates were analyzed by rotational diffusion models. Chen *et al.*[193] measured self-diffusion coefficients for fluid hydrogen and fluid deuterium at pressures up to 200 MPa and in the temperature range 171–372 K by the spin echo method. The diffusion coefficients D were described by the rough sphere (RHS) model invoking the rotation translational coupling parameter A = 1.

3 Selected Applications of Nuclear Spin Relaxation

3.1 Pure Liquids. – Precise temperature dependent ^{1}H, ^{2}H, ^{13}C and ^{14}N relaxation measurements on liquid acetonitrile were presented by Hardy *et al.*[41] For the first time ^{2}H induced nuclear Overhauser enhancements on ^{13}C were reported. The new method allowed the determination of the acetonitrile quadrupole coupling constant. Lewandowska and Lewa[194] performed ^{1}H relaxation time measurements of liquid derivates of benzene and pyridine with regard to the effect of dipole interactions on the structure of close packing.

Sturz and Dölle[192] measured the temperature dependent dipolar spin–lattice relaxation rates and cross-correlation rates between the dipolar and the chemical-shift anisotropy relaxation mechanisms for different ^{13}C nuclei in toluene. They found that the reorientation about the axis in the molecular plane is approximately 2 to 3 times slower than the one perpendicular to the C-2 axis. Suchanski *et al.*[195] measured spin–lattice relaxation times T_1 and NOE factors of chemically non-equivalent carbons in *meta*-fluoroaniline. The analysis showed that the correlation function describing molecular dynamics could be well described in terms of an asymmetric distribution of correlation times predicted by the Cole–Davidson model. In a comprehensive simulation study of neat formic acid Minary *et al.*[196] found good agreement with NMR relaxation time experiments in the liquid phase. Iwahashi *et al.*[197] measured self-diffusion coefficients and ^{13}C spin–lattice relaxation times to study the dynamical conformation of n-saturated and unsaturated fatty acids.

3.2 Non-electrolyte Solutions. – Effemey *et al.*[198] measured ^{13}C spin–lattice and spin–spin relaxation rates as well as NOE for sucrose in a viscous cryosolvent, D_2O/DMSO, at several magnetic fields and two temperatures. The results, which were outside the extreme narrowing regime, were interpreted using the Lipari–Szabo formalism. NMR relaxation data were compared with molecular dynamics simulations of dimethyl sulfoxide (DMSO) and DMSO/water mixtures by Vishnyakov *et al.*[199] Banas *et al.*[200] proposed a simple two-motion model of molecular dynamics for cellulose/water systems on the basis of proton NMR relaxation time dependencies on temperature and frequency. The parameters, activation energies and correlation times, describing the model may be correlated with structure features such as level of crystallinity of cellulose with different origin. Rampp *et al.*[201] studied the density and temperature dependence of the viscosity and the self-diffusion coefficients in some aqueous carbohydrate solutions. Water diffusion showed no differences in all systems. Analysis of the data by the Vogel–Fulcher–Tammann equation yields the result that at a given concentration the self-diffusion coefficients of the sugar and the viscosity are described by identical ideal glass transition temperatures, while the diffusion of the water molecule decouples from these properties.

3.3 Electrolyte Solutions. – The self-association of relatively small hydrophobic organic components in aqueous mixtures has been investigated by Sacco.[202] He determined the association aparameter A(22), which is essentially obtained from experimental intermolecular dipole–dipole relaxation data of ^1H nuclei and from NMR measurements of the self-diffusion coefficients of the organic solvents. The effect of electrolytes and non-electrolytes has been studied. The chemical shifts and relaxation times T_1 and T_2 of ^3He and ^{129}Xe nuclei of noble gas atoms as well as those of ^7Li and ^{133}Cs nuclei of isoelectronic Li^+ and Cs^+ ions have been measured in aqueous solutions by Mazitov *et al.*[203] Ruso *et al.*[204] studied the self-association of weakly self-associating propranolol hydrochloride in aqueous electrolyte solutions by

NMR techniques. The same measurements were performed to study the self-aggregation of sodium n-hexyl sulfate in aqueous solution.[205]

Hallwass *et al.*[206] measured the sodium self-diffusion coefficients in aqueous solutions containing various amounts of crown ether using pulsed field gradients NMR techniques. The addition of very small amounts of crown ether can cause an anion-sensitive suppression of sodium diffusion which, for some electrolytes, was found to be quite significant. Wintersgill *et al.*[207] measured ^{7}Li relaxation times of polypropylene glycol and polyethylene glycol containing lithium salts. The results provided further evidence that ionic conductivity is controlled by large-scale segmental motions of the polymer chain. Saito *et al.*[208] investigated conduction properties of lithium gel electrolytes by impedance spectroscopy and pulsed-field gradient NMR with electric field. The reaction of lithium-manganese oxide for the cathode materials of rechargeable lithium batteries with nonaqueous electrolyte was studied by Nagayama *et al.*.[209] Hayamizu *et al.*[210,211] correlated the NMR self-diffusion and relaxation measurements with ionic conductivity in polymer electrolytes.

3.4 Transition Metal Complexes. – Self-diffusion coefficients of transition-metal complex ions, ion pairs and higher aggregates have been measured by Zuccaccia *et al.*[212] using pulsed field gradient spin-echo NMR measurements. Jasim and Perutz[213] studied hydrogen bonding in transition metal complexes. Orrell[214] performed dynamic NMR spectroscopy in inorganic and organometallic chemistry. Luukkanen *et al.*[215] investigated the photochemical reactivity of halogen-containing transition-metal complexes. Changes in the NMR proton spectra suggested that the release of the CO ligand is followed by reorganization of the halogen ligands and attachment of the one solvent molecule. Spin–lattice relaxation times of ^{59}Co and ^{31}P in CoRhP were measured by Nishihara *et al.*[216] The relaxation rates obey Korringa relations at high temperatures. NMR relaxation studies in oxovanadium(IV) complexes of *N*-D-gluconylamino acids were performed by Gyurcsik *et al.*[217] Buglyo *et al.*[218] measured ^{1}H relaxation times of VO(IV) complexes with several *O*-donor containing ligands. The data strongly suggest an equilibrium between the two isomers of the bis complexes. A series of new heterotrinuclear transition-metal complexes were synthesized and characterized by Chen *et al.*[219] The structures and dynamics in different solutions and temperatures were investigates by NMR spectra and relaxation times. The ^{2}H T_1 relaxation and deuterium quadrupole coupling constants in transition metal complexes were measured by Bakhmutov *et al.*[220] Castellanos *et al.*[221] reported fast ^{1}H NMR relaxation in some ruthenium hydrides. The relaxation is much faster than expected for a dipole–dipole process involving the two dihydrogen-bonded protons, but no origin for the effect could be suggested. Chaudhuri *et al.*[222] studied the electronic structure of transition-metal complexes containing radical ligands. Deblon *et al.*[223] synthesized and measured highly distorted rhodium complexes in solution by NMR techniques. Frohnapfel and Templeton[224] reported the bonding and structure of transition-metal vinyl complexes.

3.5 Molten Salts. – The solubility and the polymerization of polyacrylonitrile in low temperature molten salts was investigated by Hettrich *et al.*[225] The chemical interaction between the molten salt and the polymer was studied by ^{13}C NMR spectroscopy. Noda *et al.*[226] measured pulsed-gradient spin-echo ^{1}H and ^{19}F ionic diffusion coefficients of molten salts. The NMR properties of ^{133}Cs in binary melts of caesium trifluoroacetate with lithium, sodium and potassium were determined by Mirny *et al.*[227] The nature of the intra- and intermolecular paramagnetic contribution is discussed. Dupont *et al.*[228] studied CH-π interactions in the solid and the solution structure of molten salts by ^{1}H NOESY NMR. Forsyth *et al.*[229] reported conductivities at T_g in polymer electrolytes. ^{1}H NMR T_2 relaxation measurements suggest that T_g decreases with increasing salt content and confirms that the material is glassy at room temperature and hence that the conductivity is significantly decoupled from the structural relaxation.

4 Nuclear Spin Relaxation in Gases

In the past, nuclear magnetic relaxation in monoatomic noble gases has provided a good test of our understanding of nuclear relaxation mechanisms. Today, there again is significant interest in this problem in relation to the rapidly growing area of NMR and MRI with optically polarized noble gases.[26,28,230] The optimization of the production and storage[231] of hyperpolarized gases is a very important problem in extending and exploring novel applications to medical[232–234] and material sciences.[235–238] This requires a detailed understanding of the relaxation processes that eventually destroy the hard-won polarization and ultimately set the limits to the utilization of hyperpolarized nobel gases. Theoretical findings agree very well, and these were used quite successfully in the optimization of the production and storage of hyperpolarized ^{3}He. The relaxation in ^{3}He is a well-understood phenomenon. The situation is different for ^{129}Xe in the gas phase. Only a limited set of experimental data, dating back to the early 1960s[239–241] is available, and this restricted to the high-density region between 100 and 250 amagat. ^{129}Xe T_1 data have not been reported. A theoretical description of ^{129}Xe gas-phase relaxation has been given several times,[242,243] but because of the problem only semiquantitative treatments have been reported. Thus Moudrakovski *et al.*[244] revisited the gas-phase nuclear magnetic relaxation in ^{129}Xe. They combined experimental measurements with theory and numerical calculations to study the mechanism and rate of ^{129}Xe relaxation in the gas phase in a previously unstudied range of densities. A significant new discovery from field-dependent studies is that, in addition to the previously identified field-independent spin–rotation relaxation operative in the bulk gas, there is a contribution from the modulation of the chemical shift that depends on the square of the applied magnetic-field strength.

Polarization transfer from hyperpolarized gas to ^{1}H, ^{13}C *etc.* holds great promise for sensitivity enhancement of solution-state NMR. Leawoods *et al.*[36]

explored a route that uses hyperpolarized, supercritical xenon as solvent for the organic solute. A method is described for preparation of supercritical xenon solutions with little polarization loss. High-pressure ^{129}Xe NMR experiments have been performed by Nagasaka *et al.*[245] Using a newly designed probe the authors studied supercritical xenon interacting with polymers. Dimitrov *et al.*[246] used intermolecular ^{129}Xe–^{1}H nuclear Overhauser effects and ^{129}Xe longitudinal relaxation time measurements to demonstrate that the dipole–dipole coupling is the dominant relaxation mechanism for ^{129}Xe in water at room temperature. Desvaux *et al.*[247] found direct evidence of a magnetization transfer between laser-polarized xenon and protons of a cage-molecule in water. Mazitov *et al.*[203] measured relaxation times of ^{3}He and ^{129}Xe in aqueous solutions.

The large diffusion coefficient of gases result in significant spin motion during the application of gradient pulses that typically last a few milliseconds in most NMR experiments. In restricted environments, such as the lung, this rapid gas diffusion can lead to violation of the narrow pulse approximation, a basic assumption of the standard Stejskal–Tanner method of diffusion measurements. Mair *et al.*[248] therefore investigated the effect of a common, biologically inert buffer gas, sulfur hexafluoride, on ^{129}Xe NMR and diffusion. They concluded that SF_6 will not sufficiently reduce ^{129}Xe diffusion to allow accurate surface-area/volume ratio measurements in human alveoli using time-dependent gas diffusion NMR. To study how highly magnetized liquids behave in NMR experiments, Sauer *et al.*[249] have preformed low-field NMR on laser-polarized liquid ^{129}Xe, with nuclear polarization of up to 6%. The authors discussed the key role of long-range dipolar coupling in such spin systems. Wong *et al.*[250] used a novel NMR scheme to observe persistence in 1D gas diffusion. Medical imaging with laser-polarized noble gas was reviewed by Chupp and Swanson.[251] Piegay and Tastevin[252] have studied bulk longitudinal spin relaxation time T_1 in hyperpolarized liquid $^{3}He/^{4}He$ mixtures at saturated vapor pressure and at low magnetic field. Kopu and Thuneberg[253] calculated the NMR line shape in rotating ^{3}He–B taking into account the broadening effects of magnetic field inhomogeneity and Leggett-Takagi spin relaxtion. Thuneberg[254] also gave a hydrostatic theory of superfluid ^{3}He–B. Johnson *et al.*[255] performed ^{1}H and ^{3}He magnetic resonance microscopy of the lung.

Taha and True[256] measured pressure-dependent NMR properties of gas-phase formamide. The results indicate that internal rotation of this molecule follows statistical kinetics. Jackowski[257] performed ^{17}O and ^{33}S NMR spectroscopy on gaseous compounds. Kaiser *et al.*[258] used dynamic NMR microscopy to study xenon gas undergoing Poiseulle flow in the regime where deterministic and stochastic motions are the same order of magnitude. Jackowski *et al.*[259] determined NMR properties of acetylene in gaseous mixtures with xenon and carbon dioxide. Kuethe *et al.*[260] imaged an inert insoluble gas, SF_6, in rat lungs using a technique that clearly differentiates obstructed and normal ventilation. Ahlberg *et al.*[261] studied solvated CH_5^+ in liquid superacid. Arroyo *et al.*[262] compared the proton transfer reaction in N–H···O=C molecular association in solution and the gas phase.

5 Self-diffusion in Liquids

5.1 Experimental and Theoretical Aspects. – When NMR diffusion experiments are performed at temperatures different from ambient temperature, temperature gradients due to probe design can cause thermal convection and therefore significantly affect the signal amplitude. Fourier transformation of the signal amplitude give rise to a diffusion-broadened velocity spectrum, which contains information about the convection velocity. Mao and Kohlmann[263] showed that when the diffusion broadening factor is smaller than the maximum velocity, the broadening has little effect on the determination of the maximum velocity. Thus, convection velocity can be determined in the presence of diffusion. Damberg *et al.*[264] proposed a practical method for an accurate measurement of translational diffusion coefficients. Usually for NMR probes equipped with pulsed field gradients coils, which are not optimized for gradient linearity, the precision and accuracy of experimentally measured translational diffusion coefficients are limited by the linearity of the gradient pulses over the sample volume. The authors showed that the gradient experiment can be significantly improved by mapping the gradient z-profile and by using the mapped calibration parameters in the data analysis. Scharfenecker *et al.*[265] performed diffusion measurements with the aid of nutation spin echoes appearing after two inhomogeneous radiofrequency pulses in inhomogeneous magnetic fields. Applications to logging NMR, surface coil NMR, toroid cavity NMR *etc.* are suggested. Usmanov *et al.*[266] presented a numerical solution of an inverse task of a self-diffusion. Jeglic *et al.*[267] evaluated analytically the resonance frequency-space and the frequency gradient-space relations for the static fringe magnetic field of superconducting magnets used in the NMR diffusion measurement. Price *et al.*[109] studied the macroscopic background gradient and radiation damping effects on high-field PGSE NMR diffusion measurements. Both effects have serious implications for accurate diffusion measurements determination. Preston *et al.*[268] calibrated the stray field gradient by a heteronuclear method and by field profiling. Both methods compare very favorably with the conventional method of calibration which uses a standard with a known self-diffusion constant. Balibanu *et al.*[269] investigated the response of the spin system by numerical simulations in the case of a NMR experiment performed in inhomogeneous static and radiofrequency fields.

5.2 Selected Examples. – Pulsed magnetic field gradient (PFG) NMR is today a routine method for the determination of self-diffusion coefficients. However, a remaining goal is the improvement of the precision of the method. The best procedure for the determination of accurate diffusion coefficients by PFG NMR is a calibration with a sample of precisely known D value. Thus Holz *et al.*[270] presented temperature-dependent self-diffusion coefficients of water and six selected molecular liquids. The gained accurate self-diffusion data are suited for an elaborate check of theoretical approaches in the physics of molecular liquids. Price *et al.*[271] examined the translational diffusion

coefficients of supercooled heavy water at atmospheric pressure using pulsed-gradient spin-echo NMR diffusion measurements down to 244 K. Price *et al.*[272] also studied the translational and rotational motion of isolated water molecules in nitromethane using ^{17}O NMR.

Gross *et al.*[273] studied the influence of hydrogen bonds upon diffusion of simple and binary mixtures of ammonia. Hardy *et al.*[42] measured the isotope effect on the translational and rotational motion in liquid water and ammonia. Hallwass *et al.*[206] determined the sodium self-diffusion coefficients in aqueous solutions containing various amounts of crown ether using PFG NMR techniques. Self-diffusion dynamics of quercetin in solutions were measured by Zhang and Mao.[274] Gong *et al.*[275] measured self-diffusion of water, ethanol and decafluoropentane in perfluorosulfonate ionomer. The same property was studied by Chen *et al.* for fluid hydrogen and deuterium. The self-diffusion of n-saturated and unsaturated fatty acids were measured by Iwahashi *et al.*[197] Engelsen and Perez[276] measured self-diffusion coefficients of trehalose in aqueous solutions. Rampp *et al.*[201] reported self-diffusion coefficients for some aqueous carbohydrates solutions. Self-diffusion coefficients of water molecules and lithium and sodium counter-ions in gel-type resin were measured by Ohuchi *et al.*[277]

6 References

1 R. Ludwig, in *Nuclear Magnetic Resonance*, ed. G. A. Webb, Specialist Periodical Reports, The Royal Society of Chemistry, Cambridge, 2000, **30**, p.181–213.
2 G. Lippens and J. Jeener, *Concepts Magn. Res.*, 2001, **13**, 8.
3 E. E. Burnell, D. Capitani, C. Casieri and A. L. Segre, *J. Phys. Chem. B*, 2000, **104**, 8782.
4 O. Monasterio, *Methods*, 2001, **24**, 97.
5 K. Nicolay, K. P. J. Braun, R. A. de Graaf, R. M. Dijkhuizen and M. J. Kruiskamp, *NMR in Biomed.*, 2001, **14**, 94.
6 R. Luypaert, S. Boujraf, S. Sourbron and M. Osteaux, *Eur. J. Radiol.*, 2001, **38**, 19.
7 D. Leibfritz and W. Dreher, *NMR in Biomed.*, 2001, **14**, 65.
8 Y. Ohno, Q. Chen and H. Hatabu, *Eur. J. Radiol.*, 2001, **37**, 164.
9 R. de Graaf and D. L. Rothman, *Concepts Magn. Res.*, 2001, **13**, 32.
10 T. Dziembowska and Z. Rozwadowski, *Curr. Org. Chem.*, 2001, **5**, 289.
11 Q. He, W. Richter, S. Vathyam and W. S. Warren, *J. Chem. Phys.*, 1993, **98**, 6779.
12 W. S. Warren, W. Richter, A. H. Andreotti and B. T. Farmer III, *Science*, 1993, **262**, 2005.
13 W. Richter, S. Lee, W. S. Warren, Q. He, *Science*, 1995, **267**, 654.
14 W. Richter and W. S. Warren, *Concepts Magn. Res.*, 2001, **12**, 396.
15 Z. Chen and J. H. Zhong, *J. Chem. Phys.*, 2001, **114**, 5642.
16 H. M. Zhang, N. Lisitsa, R. G. Bryant and W. S. Warren, *J. Magn. Reson.*, 2001, **148**, 200.
17 Y. Y. Lin, N. Lisitza, S. D. Ahn and W. S. Warren, *Science*, 2000, **290**, 118.
18 D. Broll, C. Kaul, A. Krämer, P. Krammer, T. Richter, M. Jung, H. Vogel and P. Zehner, *Angew. Chem. Int. Ed.*, 1999, **38**, 2998.

19 M. Nakahara, N. Matubayasi, C. Wakai and Y. Tsujino, *J. Mol. Liq.*, 2001, **90**, 75.
20 M. C. Bellissent-Funel, *J. Mol. Liq.*, 2001, **90**, 313.
21 Y. Yamaguchi, N. Yasutake and N. Nagaoka, *Chem. Phys. Lett.*, 2001, **340**, 129.
22 T. Tsukahara, M. Harada, Y. Ikeda and H. Tomiyasu, *Chem. Lett.*, 2001, 420.
23 S. Mussig, E. U. Franck and M. Holz, *Z. Phys. Chem.*, 2000, **214**, 957.
24 S. Gaemers and C. J. Elsevier, *Chem. Soc. Rev.*, 1999, **28**, 135.
25 S. Gaemers and C. J. Elsevier, *Magn. Reson. Chem.*, 2000, **38**, 650.
26 T. G. Walker and W. Happer, *Rev. Mod. Phys.*, 1997, **69**, 629.
27 R. Tycko and J. A. Reimer, *J. Phys. Chem.*, 1996, **100**, 13240.
28 G. Navon, Y.-Q. Song, T. Room, S. Appelt, R. E. Taylor and A. Pines, *Science*, 1996, **271**, 1848.
29 M. Viallon, G. P. Cofer, S. A. Suddarth, H. E. Möller, X. J. Chen, M. S. Chawla, L. W. Hedlund, G. A. Cremillieux and G. A. Johnson, *Magn. Reson. Med.*, 1999, **41**, 787.
30 B. Saam, D. A. Yablonskiy, D. S. Gierada and M. S. Conradi, *Magn. Reson. Med.*, 1999, **42**, 507.
31 C. H. Tseng, R. Mair, G. Wong, D. Williamson, D. Cory and R. Walsworth, *Phys. Rev. E*, 1999, **59**, 1785.
32 H. J. Jänsch, T. Hof, U. Ruth, J. Schmidt, D. Stahl and D. Fick, *Chem. Phys. Lett.*, 1998, **296**, 146.
33 D. Raftery, E. Macnamara, G. Fisher, C. V. Rice and J. Smith, *J. Am. Chem. Soc.*, 1997, **119**, 8746.
34 D. Raftery, H. Long, T. Meersmann, P. J. Grandinetti and L. Reven, *Phys. Rev. Lett.*, 1991, **66**, 584.
35 K. L. Sauer, R. J. Fitzgerald and W. Happer, *Chem. Phys. Lett.*, 1997, **277**, 153.
36 J. C. Leawoods, B. T. Saam and M. S. Conradi, *Chem. Phys. Lett.*, 2000, **327**, 359.
37 T. D. Ferris and T. C. Farrar, *Z. Phys. Chem.*, 2000, **214**, 1659.
38 T. D. Ferris, M. D. Zeidler and T. C. Farrar, *Mol. Phys.*, 2000, **98**, 737.
39 E. H. Hardy, R. Witt, A. Dölle and M. D. Zeidler, *J. Magn. Reson.*, 1998, **134**, 300.
40 E. H. Hardy, P. J. Merkling. R. Witt and A. Dölle, *Z. Phys. Chem.*, 2000, **214**, 1687.
41 E. H. Hardy, A. Zygar and M. D. Zeidler, *Z. Phys. Chem.*, 2000, **214**, 1633.
42 E. H. Hardy, A. Zygar, M. D. Zeidler, M. Holz and F. D. Sacher, *J. Chem. Phys.*, 2001, **114**, 3174.
43 R. Witt, L. Sturz, A. Dölle and F. Müller-Plathe, *J. Chem. Phys. A*, 2000, **104**, 5716.
44 J. Jeener, A. Vassenbroek and P. Broekaert, *J. Chem. Phys.*, 1995, **103**, 1309.
45 M. H. Levitt, *Concepts Magn. Reson.*, 1996, **8**, 77.
46 I. Ardelean and R. Kimmich, *J. Chem. Phys.*, 1999, **110**, 3708.
47 I. Ardelean, R. Kimmich, S. Stapf and D. E. Demco, *J. Magn. Reson.*, 2000, **132**, 138.
48 J. Jeener, *Phys. Rev. Lett.*, 1999, **82**, 1772.
49 I. Ardelean and R. Kimmich, *J. Magn. Reson.*, 2000, **143**, 101.
50 I. Ardelean and R. Kimmich, *J. Chem. Phys.*, 2000, **112**, 5275.
51 C. Luchinat, M. Piccioli, R. Pierattelli, F. Engelke, T. Marquardsen and R. Ruin, *J. Magn. Reson.*, 2001, **150**, 161.
52 A. Z. Damayanovich, J. Peternelj and M. M. Pintar, *J. Magn. Reson.*, 2000, **144**, 1.

53 H. Yamada, K. Nishikawa, M. Honda, T. Shimura, K. Akasaka and K. Tabayashi, *Rev. Sci. Instrum.*, 2001, **72**, 1463.
54 J. B. Miller, B. H. Suits, A. N. Garroway and M. A. Hepp, *Concepts Magn. Reson.*, 2000, **12**, 125.
55 O. Lips, A. E. Privalov, S. V. Dvinskikh and F. Fujara, *J. Magn. Reson.*, 2001, **149**, 22.
56 B. Luong, J. C. Goswami, A. Sezginer and D. Davies, *IEEE Trans. Magn.*, 2001, **37**, 1015.
57 P. Jeglic, A. Lebar, T. Apih and J. Dolinsek, *J. Magn. Reson.*, 2001, **150**, 39.
58 E. E. Sigmund, E. S. Calder, G. W. Thomas, V. F. Mitrovic, H. N. Bachman, W. P. Halperin, P. L. Kuhns and A. P. Reyes, *J. Magn. Reson.*, 2001, **148**, 309.
59 S. Olt, E. Krotz, E. Komor, M. Rokitta and A. Haase, *J. Magn. Reson.*, 2000, **144**, 297.
60 R. R. Ernst, *J. Chem. Phys.*, 1966, **45**, 3845.
61 A. Kumar and B. D. N. Rao, *Mol. Phys.*, 1968, **15**, 377.
62 A. Kumar, N. R. Krishna and B. D. N. Rao, *Mol. Phys.*, 1970, **18**, 11.
63 A. Kumar and S. L. Gordon, *J. Chem. Phys.*, 1971, **54**, 3207.
64 B. D. N. Rao, *Adv. Magn. Reson.*, 1970, **4**, 271.
65 A. Kumar, R. C. R. Grace and P. K. Madhu, *Prog. Nucl. Magn. Reson. Spectrosc.*, 2000, **37**, 191.
66 B. Brutscher, *Concepts Mag. Reson.*, 2000, **12**, 207.
67 K. E. Kover and G. Batta, *J. Magn. Reson.*, 2001, **150**, 137.
68 F. Ferrage, T. R. Eykyn and G. Bodenhausen, *J. Chem. Phys.*, 2000, **113**, 1081.
69 J. Lambert, S. Haiber and H. Herzog, *J. Magn. Reson.*, 2001, **150**, 175.
70 M. V. Fedin, P. A. Purtov, E. G. Bagryanskaya, *Chem. Phys. Lett.*, 2001, **339**, 395.
71 J. J. Prompers and R. Brüschweiler, *J. Phys. Chem. B*, 2000, **104**, 11416.
72 G. Steinbrecher, R. Scorei, V. M. Cimpoiasu and I. Petrisor, *J. Magn. Reson.*, 2000, **146**, 321.
73 N. R. Skrynnikov, R. Konrat, D. R. Muhandiram and L. E. Kay, *J. Am. Chem. Soc.*, 2000, **122**, 7059.
74 C. Bracken, *J. Mol. Graph. Model.*, 2001, **19**, 3.
75 W. Apel, Y. A. Bychkov, *Phys. Rev. B*, 2001, **6322**, 4405.
76 A. Kaikkonen and J. Kowalewski, *J. Magn. Reson.*, 2000, **146**, 297.
77 J. Jeener, B. H. Meier, P. Bachmann and R. R. Ernst, *J. Chem. Phys.*, 1979, **71**, 4546.
78 A. Bax and D. G. Davis, *J. Magn. Reson.*, 1985, **63**, 207.
79 A. Almond, J. Bunkenborg, T. Franch, C. H. Gotfredsen and J. O. Duus, *J. Am. Chem. Soc.*, 2001, **123**, 4792.
80 J. J. Warren and P. B. Moore, *J. Magn. Reson.*, 2001, **149**, 271.
81 F. Kramer, W. Peti, C. Griesinger and S. J. Glaser, *J. Magn. Reson.*, 2001, **149**, 58.
82 J. R. Tolman, H. M. Al. Hashami, L. E. Kay and J. H. Prestegard, *J. Am. Chem. Soc.*, 2001, **123**, 1416.
83 G. A. Mueller, W. Y. Choy, N. R. Skrynnikov and L. E. Kay, *J. Biomol. NMR*, 2000, **18**, 183.
84 J. J. Chou, S. P. Li and A. Bax, *J. Biomol. NMR*, 2000, **18**, 217.
85 H. Neubauer, J. Meiler, W. Peti and C. Griesinger, *Helv. Chim. Acta*, 2001, **84**, 243.
86 B. Luy and S. J. Glaser, *J. Magn. Reson.*, 2001, **148**, 169.

87 M. Hennig, T. Carlomagno and J. R. Williams, *J. Am. Chem. Soc.*, 2001, **123**, 3395.
88 J. Meiler, J. J. Prompers, W. Peti, C. Griesinger and R. Brüschweiler, *J. Am. Chem. Soc.*, 2001, **123**, 6098.
89 T. Zhang and X. A. Mao, *Appl. Magn. Reson.*, 2001, **20**, 189.
90 M. Andrec, K. G. Inman, D. J. Weber, R. M. Levy and G. T. Montelione, *J. Magn. Reson.*, 2000, **146**, 66.
91 C. Renner and T. A. Holak, *J. Magn. Reson.*, 2000, **145**, 192.
92 M. Helgstrand, T. Hard and P. Allard, *J. Biomol. NMR*, 2000, **18**, 49.
93 R. S. Dumont and R. Assalone, *J. Chem. Phys.*, 2000, **113**, 4505.
94 Y. E. Chernysh, B. S. Luk'yanov, G. S. Borodkin, V. Y. Vdovichenko, S. E. Krivonosov and N. V. Stankevich, *Russ. J. Phys. Chem.*, 2000, **74**, 1207.
95 N. Juranic, Z. Zolnai and S. Macura, *J. Serb. Chem. Soc.*, 2000, **65**, 285.
96 N. H. Pawly, C. Y. Wang, S. Koide and L. K. Nicholson, *J. Biomol. NMR*, 2001, **20**, 149.
97 F. J. Monlien, A. Abou-Hamdan, L. Helm and A. E. Merbach, *High Pressure Res.*, 2000, **18**, 319.
98 T. Schneppensieper, A. Zahl and R. van Eldik, *Angew. Chem. Int. Ed.*, 2001, **40**, 1678.
99 D. M. Corsi, L. Vander Elst, R. N. Mueller, H. van Bekkum and J. A. Peters, *Chem. Eur. J.*, 2001, **7**, 1383.
100 B. N. Nukuna, M. B. Goshe and V. E. Anderson, *J. Am. Chem. Soc.*, 2001, **123**, 1208.
101 S. Aime, W. Dastru, R. Gobetto, F. Reineri, A. Russo and A. Viale, *Organometallics*, 2001, **20**, 2924.
102 A. Traore, L. Foucat and J. P. Renou, *Eur. Biophys. J. Biophys. Lett.*, 2000, **29**, 159.
103 N. Bloembergen and R. V. Pound, *Phys. Rev.*, 1954, **95**, 8.
104 A. Szöke and S. Meiboom, *Phys. Rev.*, 1959, **93**, 99.
105 X. A. Mao and C. H. Ye, *J. Chem. Phys.*, 1993, **99**, 7455.
106 P. Broekaert and J. Jeener, *J. Magn. Reson. A*, 1995, **113**, 60.
107 S. Bloom, J. *Appl. Phys.*, 1957, **28**, 800.
108 D. E. Rourke and M. P. Augustine, *Phys. Rev. Lett.*, 2000, **84**, 1685.
109 W. S. Price, P. Stilbs, B. Jonsson and O. Soderman, *J. Magn. Reson.*, 2001, **150**, 49.
110 M. P. Augustine and E. L. Hahn, *Concepts Magn. Reson.*, 2001, **13**, 1.
111 B. Cutting, J. H. Chen, D. Moskau and G. Bodenhausen, *J. Biomol. NMR*, 2000, **17**, 323.
112 C. Ramanthan and R. Bowtell, *J. Chem. Phys.*, 2001, **114**, 10854.
113 A. Louis-Joseph, D. Abergel, I. Lebars and J. Y. Lallemand, *Chem. Phys. Lett.*, 2001, **337**, 92.
114 J. R. C. van der Maarel, D. Lankhorst, J. de Bleijser and J. C. Leyte, *Chem. Phys. Lett.*, 1985, **122**, 541.
115 R. Ludwig, F. Weinhold and T. C. Farrar, *J. Chem. Phys.*, 1996, **103**, 6941.
116 R. Ludwig, M. D. Zeidler and T. C. Farrar, *Z. Phys. Chem.*, 1995, **189**, 19.
117 R. Eggenberger, S. Gerber, H. Huber, D. Searles and M. Welker, *J. Chem. Phys.*, 1992, **97**, 5898.
118 R. Eggenberger, S. Gerber, H. Huber, D. Searles and M. Welker, *Mol. Phys.*, 1993, **80**, 1177.
119 F. Weinhold, *J. Chem. Phys.*, 1998, **109**, 367.

120 F. Weinhold, *J. Chem. Phys.*, 1998, **109**, 373.
121 M. Huelsekopf and R. Ludwig, *J. Mol. Liq.*, 2000, **85**, 105.
122 W. Wendt and T. C. Farrar, *Mol. Phys.*, 1998, **95**, 1077.
123 W. Nosel, S. Capuani, D. Capitani and F. de Luca, *J. Magn. Reson.*, 2001, **150**, 178.
124 J. Vaara and P. Pyykkō, *Phys. Rev. Lett.*, 2001, **86**, 3268.
125 D. L. Bryce and R. E. Wasylishen, *J. Chem. Educ.*, 2001, **78**, 124.
126 G. W. Turner, R. L. Johnston and K. D. M. Harris, *Chem. Phys.*, 2000, **256**, 159.
127 P. Bernatowiz and S. Szymanski, *J. Magn. Reson.*, 2001, **148**, 455.
128 A. Lehoux, M. Krystyniak and E. Baguet, *J. Magn. Reson.*, 2001, **148**, 11.
129 A. Bagno, S. Gerard J. Kevelam, E. Menna and G. Scorrano, *Chem. Eur. J.*, 2000, **6**, 2915.
131 I. Solomon, *Phys. Rev.*, 1955, **99**, 555.
132 N. Bloembergen, *J. Chem. Phys.*, 1957, **34**, 842.
133 N. Bloembergen and L. O. Morgan, *J. Chem. Phys.*, 1961, **34**, 842.
134 R. Sharp, L. Lohr and J. Miller, *Prog. Nucl. Mag. Res.*, 2001, **38**, 115.
135 J. C. Miller, S. M. Abernathy and R. R. Sharp, *J. Phys. Chem. A*, 2000, **104**, 4839.
136 J. C. Miller and R. R. Sharp, *J. Chem. Phys. A*, 2000, **104**, 4889.
137 J. C. Miller, S. Abernathy, L. L. Lohr and R. R. Sharp, *J. Chem. Phys. A*, 2000, **104**, 9481.
138 I. Bertini, C. Luchinat, M. Mancini and G. Spina, *J. Magn. Reson.*, 1984, **59**, 213.
139 L. Banci, I. Bertini and C. Luchinat, *Nuclear and Electron Relaxation*, VCH, New York, 1991, Chap. 5.
140 I. Bertini, O. Galas, C. Luchinat and G. Parigi, *J. Magn. Reson., Ser. A*, 1995, **113**, 151.
141 N. Benetis, J. Kowalewski, L. Nordenskiold, H. Wennerström and P.-O. Westlund, *Mol. Phys.*, 1983, **48**, 329.
142 N. Benetis, J. Kowalewski, L. Nordenskiold, H. Wennerström and P.-O. Westlund, *J. Magn. Reson.*, 1984, **58**, 282.
143 P.-O. Westlund, N. Benetis and H. Wennerström, *Mol. Phys.*, 1987, **61**, 177.
144 J. Kowalewski, T. Larsson and P.-O. Westlund, *J. Magn. Reson.*, 1987, **74**, 56.
145 P.-O. Westlund and P. T. Larsson, *Acta Chem. Scand.*, 1991, **45**, 11.
146 J. Svoboda, T. Nilsson, J. Kowalewski, P.-O. Westlund and P. T. Larsson, *J. Magn. Reson.*, 1996, **121**, 108.
147 T. Nilsson, J. Svoboda and P.-O. Westlund, *J. Chem. Phys.*, 1998, **109**, 6364.
148 S. Rast, E. Beloritzky, P. H. Fries and J. P. Travers, *J. Phys. Chem. B*, 2001, **105**, 1978.
149 P. K. Madhu, R. Grandori, K. Hohenthanner, P. K. Mandal and N. Müller, *J. Biomol. NMR*, 2001, **20**, 31.
150 I. Bertini, M. B. L. Janik, G. H. Liu, C. Luchinat and A. Rosato, *J. Magn. Reson.*, 2001, **148**, 23.
151 L. X. Ma, A. M.M. Jorgensen, G. O. Sorensen, J. Ulstrup and J. J. Led, *J. Am. Chem. Soc.*, 2000, **122**, 9473.
152 J. C. Hus, D. Marion and M. Blackledge, *J. Mol. Biol.*, 2000, **298**, 927.
153 V. Aroulmoji and A. S. Rao, *Phys. Chem. Liq.*, 2000, **38**, 723.
154 R. Khomeriki, *Physica A*, 2000, **284**, 1714.
155 A. Heuer and H. W. Spiess, *Phys. Rev. Lett.*, 1999, **82**, 1335.
156 A. Arbe, J. Colmenero, M. Monkenbusch and D. Richter, *Phys. Rev. Lett.*, 1998, **81**, 590.

157 R. Böhmer, G. Hinze, G. Diezemann, B. Geil and H. Sillescu, *Europhys. Lett.*, 1996, **36**, 55.
158 A. M. George, P. Richet and J. F. Stebbins, *Am. Mineral.*, 1998, **83**, 1277.
159 M. D. Ediger, *Ann. Rev. Phys. Chem.*, 2000, **51**, 99.
160 R. Richert, *J. Chem. Phys.*, 2001, **114**, 7471.
161 J. Qian and A. Heuer, *Eur. Phys. J. B*, 2000, **18**, 501.
162 P. Voit, G. Tarjus and D. Kivelson, *J. Chem. Phys.*, 2000, **112**, 10368.
163 C. Y. Wang and M. D. Ediger, *J. Polym. Sci., B: Polym. Phys.*, 2000, **38**, 2232.
164 G. Diezemann, *Europhys. Lett.*, 2001, **53**, 604.
165 S. A. Reinsberg, X. H. Qiu, M. Wilhelm, H. W. Spiess and M. D. Ediger, *J. Chem. Phys.*, 2001, **114**, 7299.
166 D. Long and F. Lequeux, *Eur. Phys. J. E*, 2001, **4**, 371.
167 T. Vogel, P. Medick and E. Rössler, *J. Mol. Liq.*, 2000, **86**, 103.
168 M. Vogel and E. Rössler, *J. Chem. Phys.*, 2001, **114**, 5802.
169 H. Sillescu, R. Böhmer, A. Doss, T. Jorg and F. Qi, *Abstr. Pap. Am. Chem. Soc.*, 2000, **220**, 114.
170 X. H. Qiu, N. E. Moe, M. D. Ediger and L. J. Fetters, *J. Chem. Phys.*, 2000, **113**, 2918.
171 M. G. Mortuza, R. Dupree and D. Holland, *J. Non-Cryst. Solids*, 2001, **281**, 108.
172 J. Senker and E. Rössler, *Chem. Geol.*, 2001, **174**, 143.
173 J. C. McLaughlin, S. L. Tagg and J. W. Zwanziger, *J. Phys. Chem. B*, 2001, **105**, 67.
174 M. M. Margulies, B. Sixou, L. David, G. Vigier, R. Dolmazon and M. Albrand, *Eur. Phys. J. E.*, 2000, **3**, 55.
175 A. G. S. Hollander and K. O. Prins, *J. Non-Cryst. Solids*, 2001, **286**, 1.
176 A. G. S. Hollander and K. O. Prins, *J. Non-Cryst. Solids*, 2001, **286**, 12.
177 A. G. S. Hollander and K. O. Prins, *J. Non-Cryst. Solids*, 2001, **286**, 25.
178 S. Kumar, S. Murugavel and K. J. Rao, *J. Phys. Chem. B*, 2001, **105**, 5862.
179 C. Rosenhahn, S. E. Hayes, B. Rosenhahn and H. Eckert, *J. Non-Cryst. Solids*, 2001, **284**, 1.
180 X. Y. Xue and M. Kanzaki, *J. Phys. Chem. B*, 2001, **105**, 3422.
181 G. Lipari and A. Szabo, *J. Am. Chem. Soc.*, 1982, **104**, 4546.
182 G. Lipari and A. Szabo, *J. Am. Chem. Soc.*, 1982, **104**, 4559.
183 A. G. Palmer, *Annu. Rev. Biop. Biom.*, 2001, **30**, 129.
184 M. Andrec, G. T. Montelione and R. M. Levy, *J. Biolmol. NMR*, 2000, **18**, 83.
185 R. Ishima, A. P. Petkova, J. M. Louis and D. A. Torchia, *J. Am. Chem. Soc.*, 2001, **123**, 6164.
186 R. B. Best, G. E. Jackson and K. J. Naidoo, *J. Phys. Chem. B*, 2001, **105**, 4742.
187 J. L. Baber, A. Szabo and N. Tjandra, *J. Am. Chem. Soc.*, 2001, **123**, 3953.
188 B. M. Duggan, G. B. Legge, H. J. Dyson and P. E. Wright, *J. Biomol. NMR*, 2001, **19**, 321.
189 R. Kannan, K. P. Ramesh and J. Ramakrishna, *Phys. Status Solidi B*, 2001, **225**, 157.
190 Y. Masuda, *J. Phys. Chem. A*, 2001, **105**, 2989.
191 C. Mayer, *J. Magn. Reson.*, 2000, **145**, 216.
192 L. Sturz and A. Dölle, *J. Phys. Chem. A*, 2001, **105**, 5055.
193 L. P. Chen, T. Gross, H. Krienke and H. D. Lüdemann, *Phys. Chem. Chem. Phys.*, 2001, **3**, 2025.
194 D. Lewandowska and C. J. Lewa, *Spectrosc. Lett.*, 2000, **33**, 917.
195 W. Suchanski, P. Minkin and S. Jurga, *J. Mol. Struct.*, 2001, **559**, 179.

196 P. Minary, P. Jedlovszky, M. Mezei and L. Turi, *J. Phys. Chem. B*, 2000, **104**, 8287.
197 M. Iwahashi, Y. Kasahara, H. Matsuzawa, K. Yagi, K. Nomura, H. Terauchi, Y. Ozaki and M. Suzuki, *J. Phys. Chem. B*, 2000, **104**, 6186.
198 M. Effemey, J. Lang and J. Kowalewski, *Magn. Reson. Chem.*, 2000, **38**, 1012.
199 A. Vishnyakov, A. P. Lyubartsev and A. Laaksonen, *J. Phys. Chem. A*, 2001, **105**, 1702.
200 K. Banas, B. Blicharska, W. Dietrich and M. Kluza, *Holzforschung*, 2000, **54**, 501.
201 M. Rampp, C. Buttersack and H. D. Lüdemann, *Carbohydr. Res.*, 2000, **328**, 561.
202 A. Sacco, *Z. Phys. Chem.*, 2000, **214**, 917.
203 R. Mazitov, R. Seydoux, P. Diehl, K. Enikeev, A. Il'yasov and R. Haselmeier, *Z. Phys. Chem.*, 2000, **214**, 1671.
204 J. M. Ruso, P. Taboada, D. Attwood, V. Mosquera and F. Sarmiento, *Phys. Chem. Chem. Phys.*, 2000, **2**, 1261.
205 J. M. Ruso, D. Attwood, P. Taboada, V. Mosquera and F. Sarmiento, *Langmuir*, 2000, **16**, 1620.
206 F. Hallwass, M. Engelsberg, A. Simas and W. Barros, *Chem. Phys. Lett.*, 2001, **335**, 43.
207 M. C. Wintersgill, J. J. Fontanella, P. E. Stallworth, S. A. Newman, S. H. Chung and S. G. Greenbaum, *Solid State Ionics*, 2000, **135**, 155.
208 Y. Saito, H. Kataoka, T. Sakai and S. Deki, *Electrochim. Acta*, 2001, **46**, 1747.
209 K. Nagayama, K. Kamioka, E. Iwata, H. Oka, Y. Tokunaga and T. Okada, *Electrochemistry*, 2001, **69**, 6.
210 K. Hayamizu, Y. Aihara and W. S. Price, *J. Chem. Phys.*, 2000, **113**, 4785.
211 K. Hayamizu, Y. Aihara and W. S. Price, *Electrochim. Acta*, 2001, **46**, 1475.
212 C. Zuccaccia, G. Bellachioma, G. Cardaci and A. Macchioni, *Organometallics*, 2000, **19**, 4663.
213 N. A. Jasim and R. N. Perutz, *J. Am. Chem. Soc.*, 2000, **122**, 8685.
214 K. G. Orrell, *Annu. Rep. NMR Spectrosc.*, 1999, **37**, 1.
215 S. Luukkanen, M. Haukka, E. Eskelinen, T. A. Pakkanen, V. Lehtovuori, J. Kallionen, P. Myllyperkio and J. Korppi-Tommola, *Phys. Chem. Chem. Phys.*, 2001, **3**, 1992.
216 H. Nishihara, T. Yoshida, T. Matsukawa, T. Kanomata, G. Strijkers, W. J. M. de Jonge, F. Wagatsuma and T. Shinohara, *J. Alloy Compd.*, 2001, **317**, 258.
217 B. Gyurcsik, T. Jakusch and T. Kiss, *J. Chem. Soc., Dalton Trans.*, 2001, 1053.
218 P. Buglyo, E. Kiss, I. Fabian, T. Kiss, D. Sanna, E. Garribba and G. Micera, *Inorg. Chim. Acta*, 2000, **306**, 174.
219 Z. Chen, S. H. Cai, J. L. Ye, Q. S. Xie, G. T. Lu and L. N. Zhang, *Chin. J. Struct. Chem.*, 2000, **19**, 199.
220 V. I. Bakhmutov, C. Biachini, F. Maseras, A. Lledos, M. Peruzzini and E. V. Vorontsov, *Chem. Eur. J.*, 1999, **5**, 3318.
221 A. Castellanos, J. A. Ayllon, S. Sabo-Etienne, B. Donnadieu, B. Chaudret, W. B. Yao, K. Kavallieratos and R. H. Crabtree, *C. R. Acad. Sci. II*, 1999, **2**, 359.
222 P. Chaudhuri, C. N. Verani, E. Bill, E. Bothe, T. Weyhermüller and K. Wieghardt, *J. Am. Chem. Soc.*, 2001, **123**, 2213.
223 S. Deblon, H. Ruegger, H. Schonberg, S. Loss, V. Gramlich and H. Grutzmacher, *New J. Chem.*, 2001, **25**, 83.
224 D. S. Frohnapfel and J. L. Templeton, *Coord. Chem. Rev.*, 2000, **206**, 199.
225 K. Hettrich, S. Fischer, E. Brendler and W. Voigt, *J. Appl. Polym. Sci.*, 2000, **77**, 2113.

226 A. Noda, K. Hayamizu and M. Watanabe, *J. Phys. Chem. B*, 2001, **105**, 4603.
227 V. N. Mirny, V. V. Trachnevski and T. A. Mirnaya, *Z. Naturforsch. A*, 2001, **56**, 288.
228 J. Dupont, P. A. Z. Suarez, R. F. De Souza, R. A. Burrow and J. P. Kintzinger, *Chem. Eur. J.*, 2000, **6**, 2377.
229 M. Forsyth, J. Z. Sun and D. R. MacFarlane, *Electrochim. Acta*, 2000, **45**, 1249.
230 T. Pietrass and H. C. Gaede, *Adv. Mater.*, 1995, **7**, 826.
231 S. Breeze, S. Lang, I. Moudrakovski, C. I. Ratcliffe, J. A. Ripmeester, G. Santyr, B. Simard and I. Zuger, *J. Appl. Phys.*, 2000, **87**, 8013; S. Breeze, S. Lang, I. Moudrakovski, C. I. Ratcliffe, J. A. Ripmeester, B. Simarda and G. Santyr, *ibid.*, 1999, **86**, 4040.
232 H. Middleton, R. D. Black, B. Saam, G. D. Cates, G. P. Cofer, R. Guenther, W. Happer, L. W. Hedlund, G. A. Johnson, K. Juvan and J. Swartz, *Magn. Reson. Med.*, 1995, **33**, 271.
233 M. S. Albert, G. D. Cates, B. Driehuys, W. Happer, B. Saam, C. S. Springer, Jr. and A. Wishnia, *Nature*, 1994, **370**, 199.
234 J. P. Mugler III, B. Driehuys, J. R. Brookeman, G. D. Cates, S. S. Berr, R. G. Bryant, T. M. Daniel, E. E. deLange, J. H. Downs, C. J. Erickson, W. Happer, D. P. Hinton, N. F. Kassel, T. Maier, C. D. Phillips, B. T. Saam, K. L. Sauer and M. E. Wagshul, *Magn. Reson. Med.*, 1997, **37**, 809.
235 T. Pietrass, R. Seydoux and A. Pines, *J. Magn. Reson.*, 1998, **133**, 299; T. Room, S. Appelt, R. Seydoux, A. Pines and E. L. Hahn, *Phys. Rev. B*, 1997, **55**, 11604; T. Pietrass, A. Bifone and A. Pines, *Surf. Sci.*, 1995, **334**, L730.
236 Y.-Q. Song, H. C. Gaede, T. Pietrass, G. A. Barrall, G. C. Chingas, M. R. Ayers and A. Pines, *J. Magn. Reson., Ser. A*, 1995, **115**, 127.
237 R. Mair, G. Wong, D. Hoffmann, M. Hurlimann, S. Patz, L. Schwartz and R. Walsworth, *Phys. Rev. Lett.*, 1999, **83**, 3324.
238 Y.-Q. Song, B. M. Goodson, B. Sheridan, T. M. Swiet and A. Pines, *J. Chem. Phys.*, 1998, **108**, 6223.
239 R. L. Streever and H. Y. Carr, *Phys. Rev.*, 1961, **121**, 20.
240 E. R. Hunt and H. Y. Carr, *Phys. Rev.*, 1963, **130**, 2302.
241 D. Brinkmann, E. Brun and H. H. Staub, *Helv. Phys. Acta*, 1962, **35**, 431.
242 H. C. Torrey, *Phys. Rev.*, 1963, **130**, 2306.
243 B. Shizgal, *Chem. Phys.*, 1974, **5**, 464.
244 I. L. Moudrakovski, S. R. Breeze, B. Simard, C. I. Ratcliffe, J. A. Ripmeester, T. Seideman, J. S. Tse and G. Santyr, *J. Chem. Phys.*, 2001, **114**, 2173.
245 B. Nagasaka, H. Omi, T. Eguchi, H. Nakayama and N. Nakamura, *Chem. Phys. Lett.*, 2001, **340**, 473.
246 I. E. Dimitrov, R. Reddy and J. S. Leigh, *J. Magn. Reson.*, 2000, **145**, 302.
247 H. Desvaux, T. Gautier, G. Le Goff, M. Petro and P. Berthault, *Eur. Phys. J. D*, 2000, **12**, 289.
248 R. W. Mair, D. Hoffmann, S. A. Sheth, G. P. Wong, J. P. Butler, S. Patz, G. P. Topulos and R. L. Walsworth, *NMR Biomed.*, 2000, **13**, 229.
249 K. L. Sauer, F. Marion, P. J. Nacher and G. Tastevin, *Phys. Rev. B*, 2001, **6318**, 4427.
250 G. P. Wong, R. W. Mair, R. L. Walsworth and D. G. Cory, *Phys. Rev. Lett.*, 2001, **86**, 4156.
251 T. Chupp and S. Swanson, *Adv. Atom. Mol. Opt. Phys.*, 2001, **45**, 41.
252 N. Piegay and G. Tastevin, *Physica A*, 2000, **284**, 315.
253 J. Kopu and E. V. Thuneberg, *Physica B*, 2000, **284**, 256.

254 E. V. Thuneberg, *J. Low Temp. Phys.*, 2001, **122**, 657.
255 G. A. Johnson, G. P. Cofer, L. W. Hedlund, R. R. Maronpot and S. A. Suddarth, *Magn. Reson. Med.*, 2001, **45**, 365.
256 A. N. Taha and N. S. True, *J. Phys. Chem. A*, 2000, **104**, 8609.
257 K. Jackowski, *J. Mol. Struct.*, 2001, **563**, 159.
258 L. G. Kaiser, J. W. Logan, T. Meersmann and A. Pines, *J. Magn. Reson.*, 2001, **149**, 144.
259 K. Jackowski, M. Wilczek, M. Recul and J. Sadlej, *J. Phys. Chem. A*, 2000, **104**, 5955.
260 D. O. Kuethe, A. Caprihan, H. M. Gach, I. J. Lowe and E. Fukushima, *J. Appl. Physiol.*, 2000, **88**, 2279.
261 P. Ahlberg, A. Karlsson, A. Goeppert, S. O. N. Lill, P. Diner and J. Sommer, *Chem. Eur. J.*, 2001, **7**, 1936.
262 S. T. Arroyo, J. A. S. Martin and A. H. Garcia, *Chem. Phys.*, 2001, **265**, 207.
263 X. A. Mao and O. Kohlmann, *J. Magn. Reson.*, 2001, **150**, 35.
264 P. Damberg, J. Jarvet and A. Graslund, *J. Magn. Reson.*, 2001, **148**, 343.
265 A. Scharfenecker, I. Ardelean and R. Kimmich, *J. Magn. Reson.*, 2001, **148**, 363.
266 S. M. Usmanov, E. D. Shakir'yanov and G. E. Zaikov, *Oxid. Commun.*, 2001, **24**, 52.
267 P. Jeglic, A. Lebar, T. Apih, J. Dolinsek, *J. Magn. Reson.*, 2001, **150**, 39.
268 A. R. Preston, P. Kinchesh and E. W. Randall, *J. Magn. Reson.*, 2000, **146**, 359.
269 F. Balibanu, K. Hailu, R. Eymael, D. E. Demco and B. Blümich, *J. Magn. Reson.*, 2000, **145**, 246.
270 M. Holz, S. R. Heil and A. Sacco, *Phys. Chem. Chem. Phys.*, 2000, **2**, 4740.
271 W. S. Price, H. Ide, Y. Arata and O. Soderman, *J. Phys. Chem. B*, 2000, **104**, 5874.
272 W. S. Price, H. Ide and Y. Arata, *J. Chem. Phys.*, 2000, **113**, 3686.
273 T. Gross, L. Chen and H. D. Lüdemann, *High Pressure Res.*, 2000, **18**, 257.
274 Y. F. Zhang and X. A. Mao, *Acta Phys. Chim. Sin.*, 2001, **17**, 300.
275 X. Gong, A. Bandis, A. Tao, G. Meresi, Y. Wang, P. T. Inglefield, A. A. Jones and W. Y. Wen, *Polymer*, 2001, **42**, 6485.
276 S. B. Engelsen and S. Perez, *J. Phys. Chem. B*, 2000, **104**, 9301.
277 M. Ohuchi, P. Meadows, H. Horiuchi, Y. Sakai and K. Furihata, *Polym. J.*, 2000, **32**, 760.

7
Solid-state NMR Spectroscopy

BY A.E. ALIEV AND R.V. LAW

1 Introduction

Approximately 400 references published in July 2000 to June 2001 are included in the current report. The report covers mainly papers that include solid-state NMR and related terms in either the title or in the keywords section. The report is divided into two main parts. The first part is of general interest and includes reviews, theoretical and experimental aspects (Sections 2–4). The second part (Section 5) includes various applications of NMR for structural and dynamic studies of solid materials and is subdivided further by material type (Subsections 5.1–5.11). As this report is primarily intended for those specialising in the area of solid-state NMR we have organised references by nucleus type (from ^{1}H to ^{207}Pb) for easier browsing within each Subsection 5.1–5.11.

2 Reviews

The review by Frydman presents a perspective on the basic phenomena underlying solid-state NMR and their improved understanding that have made the recent progress in solid-state SNMR possible and describes the new opportunities and challenges that are being opened for spin-1/2 and quadrupole nuclei spectroscopies.[1]

Relevant reviews published in 'Annual Reports on NMR Spectroscopy' have encompassed recent developments in dipolar recoupling under MAS conditions,[2] characterization of porous media using NMR methods,[3] NMR studies of molecular motions in solids,[4] recent progress in solid-state NMR of low γ nuclei[5] and ^{59}Co NMR.[6]

Recent advances in high-resolution solid-state NMR spectroscopy have been briefly reviewed by Schwalbe and Bielecki.[7]

Reviews on subjects of biological interest have included structural characterizaton of peptides and protein fibrils and membrane-bound peptides and proteins using advanced solid-state NMR techniques,[8] single ^{15}N labelled polypeptides reconstructed into oriented membranes by static or ^{2}H, ^{15}N and ^{31}P MAS solid-state NMR techniques,[9] new physicochemical approaches based on recently developed DRAWS pulse sequence for examination of fibrils

Nuclear Magnetic Resonance, Volume 31
© The Royal Society of Chemistry, 2002

and the fibrillogenesis of peptide models of β-amyloid,[10] ways of customizing of model membranes and samples for both solution and solid-state NMR studies of complex membrane proteins[11] and elucidation of CO and O_2 binding geometries in respiratory proteins using ^{13}C and ^{17}O NMR.[12]

Hydrogen bonding studies, including both structural and dynamic aspects, using ^{1}H T_1 measurements have been reviewed.[13] Two classical examples are presented to illustrate recent developments: tautomerism in centrosymmetric dimers as a prototypical example for proton transfer and the strong symmetric hydrogen bond in the potassium hydrogen maleate as a model for the intermediate state in the proton transfer chemical reaction. Applications of ^{1}H NMR for studies of adsorbed molecules and free surface energy of carbon adsorbents have been reviewed by Turov.[14] MacKenzie[15] has reviewed applications of multinuclear solid-state NMR techniques for structural characterization of ceramic materials. Recent studies using solid-state ^{15}N NMR for the examination of the fate of biogenic nitrogen in soils have been summarized by Knicker.[16] Finally, recent applications of Monte Carlo methods for the study of cation ordering in minerals including computation of quantities measured in an NMR experiment have been reviewed by Warren.[17]

3 Theory

An introduction to Floquet theory has been presented.[18] The potential of this theoretical approach has been demonstrated using explicit calculations of the sideband patterns in MAS NMR. It has been shown that the Floquet theory works by expanding the periodic (due to sample spinning) Hamiltonian into a Fourier series, and that, regardless of the complexity of the time dependence of the Hamiltonian, the Floquet approach is the same.

The use of van Vleck's contact transformation method for the study of time-dependent interactions in solid-state NMR by Floquet theory has been proposed.[19] Floquet theory has been used for studying the spin dynamics of MAS NMR experiments. The contact transformation method is an operator method in time-independent perturbation theory and has been used to obtain effective Hamiltonians in molecular spectroscopy. This has been combined with Floquet theory to study the dynamics of a dipolar coupled spin ($I = 1/2$) system.

The existence of sidebands at $\pm \nu_r$ in MAS spectra due to the radial component of the RF field at the edges of the coil has been described theoretically and illustrated experimentally.[20] It has been shown that the height of the radial-field sidebands does not depend on the spinning speed and may contribute significantly to the intensity of spinning sidebands of MAS modulated internal interactions for a sample placed in a rotor of length exceeding the solenoid coil or a small volume sample placed at the edge of the coil.

The combination of MAS and multiple-pulse sequences for line-narrowing in solids with homogeneous spin interactions has been analyzed using Floquet

theory.[21] It has been shown that, for quasi-static conditions and for special synchronization conditions, line-narrowing is possible while for other conditions destructive interference of the two techniques takes place. For optimum line-narrowing conditions, fundamental limitations with respect to the achievable linewidth have been found. The implications of these results with respect to improving existing line-narrowing techniques or techniques for the design of specific Hamiltonians have been discussed.

It has been recently shown that utilizing double frequency sweeps (DFSs) instead of pulses can lead to increased efficiencies in population and coherence transfer in half-integer quadrupolar spin systems. A theoretical approach developed by Vega and co-workers has been extended to DFS induced adiabatic transfer phenomena in spin-3/2 and spin-5/2 systems.[22] A fully analytical description has been presented covering the whole adiabaticity range resulting in an accurate description of actual experiments. It has been shown that both population and coherence transfer are governed by the same principles. The ^{27}Al resonance in an α-Al_2O_3 single crystal has been inspected to demonstrate that the efficiency of DFS-induced population and coherence transfer in spin-5/2 systems depends on the direction of the DFS.

A theoretical treatment of the DREAM adiabatic homonuclear recoupling experiment has been given using Floquet theory.[23] An effective Hamiltonian has been derived analytically and the time evolution of the density operator in the adiabatic limit has been described. Shape cycles have been proposed and characterized experimentally. Application to spin-pair filtering as a mixing period in a 2D correlation experiment has been explored and the experimental results have been compared to theoretical predictions and exact numerical simulations.

An accurate and efficient formalism has been presented for simulating the effects of molecular motion on satellite and central transition NMR spectra of half-integer quadrupole nuclei.[24] The approach is based on the principles of the density operator and the stochastic Liouville–von Neumann equation and may be applied for both rotating and nonrotating samples. The symmetry properties of nuclear spin ensembles have been used to rewrite the stochastic Liouville–von Neumann equation in the form of a linear homogeneous system of coupled first-order differential equations among the alignments and coherences. The properties of Cartan–Weyl operators have been used to obtain the most efficient solution for secular interactions. The methodology has been incorporated into computer programs to simulate the effects of motion for any half-integer quadrupole nucleus. These programs include the first- and second-order quadrupole and first-order shielding interactions. The formalism has been used to calculate central transition ^{17}O NMR spectra of representative model systems. The calculations have revealed several interesting and important properties of central transition NMR spectra that have been discussed in terms of the functional form of the line shape. The validity of the methodology has been demonstrated experimentally by simulating VT central transition ^{17}O NMR spectra of the silicate (SiO_2) mineral cristobalite for both rotating and static samples. The simulations have allowed the structural and dynamical

details of the α–β phase transition in cristobalite to be separated. It has been shown that the line shapes can only be simulated if the effects of motion are included and are consistent with a model where the oxygen atoms reorient between six different orientations. The observed changes in the quadrupole and shielding parameters have been shown not to be the results of motional averaging but derive from an abrupt structural change associated with the first-order character of the α–β phase transition.

A density matrix description of the polarization inversion process has been presented enabling the visualization of the role of the process in the suppression of zero-frequency peaks in SLF-2D NMR experiments based on the dipolar oscillations during CP.[25] It has been shown that, during this process, a doubling of the amplitude of the oscillatory component occurs accompanied by a reduction of the initial intensity of the non-oscillatory component to zero.

The theory of satellite transition MAS NMR of half-integer quadrupolar spins has been presented and a 2D experiment that uses satellite transitions to obtain isotropic NMR spectra has been described.[26] Pulse sequences of the 2D satellite transition experiment have been described. Satellite transition excitation and coherence transfer have been studied using numerical simulations. Experimental results with model samples show high efficiencies of the experiment for acquisition of high-resolution isotropic NMR of half-integer quadrupolar nuclei.

The recoupling of homonuclear dipolar interactions between quadrupolar nuclei under MAS conditions caused by the first-order quadrupolar interaction has been discussed.[27] This recoupling leads to NMR linewidths displaying a nonmonotonic dependence on the spinning frequency and broader lines may result as the spinning rate is increased. It has been shown that the effect depends on geometrical parameters of the spin system, making it suitable for distance measurements and for obtaining the relative orientations of dipolar and quadrupolar tensors. A theoretical model of the dipolar recoupling based on average Hamiltonian theory has been proposed, and it has been shown to be in good agreement with numerically exact simulations and experiments on $I = 3/2$ systems.

General symmetry principles for rotor-synchronized pulse sequences in MAS solid-state NMR have been presented.[28] The symmetry theory has been extended to the case of generalized Hartmann–Hahn sequences, in which rotor-synchronized r.f. irradiation is applied simultaneously to two isotopic spin species. The symmetry theory has been used to design pulse sequences which implement heteronuclear dipolar recoupling at the same time as decoupling homonuclear spin–spin interactions, and which also suppress CSAs. Experimental demonstrations of heteronuclear 2D correlation spectroscopy, heteronuclear MQ spectroscopy, and the estimation of internuclear dipolar couplings have been given.

An exact solution to the problem of dynamic balancing in a NMR double rotor system enabling high speed spinning about two intersecting axes has been presented.[29] An exact expression for imbalance due to asymmetric distribution of weights about the rotation axes has been provided.

The generalization of the residual dipolar couplings for arbitrary quadrupolar/Zeeman ratios has been presented.[30] The predictions of the essentially numerical treatment compare well with previously derived high-field analytical models, as well as with experimental solid state NMR spectra observed in a borane compound possessing a ^{11}B–^{75}As spin pair. An alternative analytical variant that can account for these effects in the low-field limit has also been derived on the basis of average Hamiltonian theory; its results agree well with the predictions obtained from general numerical calculations of 1D spectra, but present peculiarities in the 2D NMR line shapes whose origins are briefly discussed.

Density functional gauge-including-atomic-orbitals (GIAO) calculations of the orientations of ^{15}N CSA tensors in peptides have been presented.[31] A comparison of the calculated ^{15}N CSA orientations with the available experimental values from single-crystal and powder studies shows excellent agreement after a partial, constrained optimization of some of the crystal structures used in the calculation. The results from this study suggest that the orientation as well as the magnitudes of ^{15}N CSA tensors may vary from molecule to molecule. Hydrogen bonding has been shown to have a negligible effect on the orientation of ^{15}N CSA tensor in accordance with recent theoretical predictions. Furthermore, it has been demonstrated that the orientation of the ^{15}N CSA can be calculated accurately with much smaller basis sets than is needed to calculate the chemical shift, suggesting that the routine application of *ab initio* calculations to the determination of ^{15}N CSA tensor orientations in large biomolecules might be possible.

The coordinates of crystallographically different atomic types of Si–O(H)–Al Brönsted centers within five H-form aluminosilicate frameworks have been optimized using a full periodic *ab initio* Hartree–Fock scheme at the STO-3G level.[32] Single-point calculations have been carried out to obtain the ^{2}H, ^{27}Al, and ^{17}O respective QCCs and e.f.g. anisotropies. The latter have been discussed and compared to the experimental values measured for different zeolites.

A computer program for fast and accurate numerical simulation of solid-state NMR experiments has been described.[33] The program is designed to emulate a NMR spectrometer by letting the user specify high-level NMR concepts such as spin systems, nuclear spin interactions, RF irradiation, free precession, phase cycling, coherence-order filtering, and implicit/explicit acquisition. These elements have been implemented using the Tcl scripting language to ensure a minimum of programming overhead and direct interpretation without the need for compilation, while maintaining the flexibility of a full-featured programming language. There are no intrinsic limitations to the number of spins, types of interactions, sample conditions (static or spinning, powders, uniaxially oriented molecules, single crystals, or solutions), and the complexity or number of spectral dimensions for the pulse sequence. The applicability ranges from simple 1D experiments to advanced multiple-pulse and multiple-dimensional experiments, series of simulations, parameter scans, complex data manipulation/visualization, and iterative fitting of simulated to

experimental spectra. A major effort has been devoted to optimizing the computation speed using state-of-the-art algorithms for the time-consuming parts of the calculations implemented in the core of the program using the C programming language. Modification and maintenance of the program are facilitated by releasing the program as open source software (General Public License) at http://nmr.imsb.au.dk. The general features of the program have been demonstrated by numerical simulations of various aspects for REDOR, rotational resonance, DRAMA, DRAWS, HORROR, C7, TEDOR, POST-C7, CW decoupling, TPPM, F-SLG, SLF, SEMA-CP, PISEMA, RFDR, QCPMG-MAS, and MQ MAS experiments.

The NMR WEBLAB program package has been described, providing an interactive tool for analyzing NMR spectra of solids and anisotropic liquids to elucidate their molecular dynamics.[34] It is a collection of programs freely available over the Internet at http://www.mpip-mainz.mpg.de/weblab40/ that permit the interpretation of 1D NMR spectra in the case of motions occurring on a cone and of 2D exchange NMR data for discrete jumps. The programs have been described in detail and analytical formulae for the averaged interaction tensor components that govern the spectra in the fast motional limit have been derived. To facilitate the validation of the results obtained from the WEBLAB, examples for two- and three-site jumps and complex motions around more than one axis have been presented.

4 Experiment

4.1 New Technique Developments. – *4.1.1 ^1H NMR.* A new solid-state NMR experiment that yields a significant reduction in proton linewidths for powdered organic solids under CRAMPS decoupling conditions has been reported.[35] This experiment, which relies on a constant-time acquisition of the proton transverse magnetization, removes the contribution of nonrefocusable broadening from the proton linewidths. Its feasibility on two model samples, L-alanine and the dipeptide Ala-Asp has been demonstrated. In both cases a significant linewidth reduction has been obtained for most of the proton resonances.

The possibility of exciting and detecting proton NMR DQ coherences in inhomogeneous static and r.f. magnetic fields has been investigated.[36] For this purpose specialized pulse sequences which partially refocus the strongly inhomogeneous evolution of the spin system and generate DQ buildup and decay curves have been implemented on the NMR MOUSE (mobile universal surface explorer). The theoretical justification of the method has been developed for the simple two spin-1/2 system. The performances of the same pulse sequences have also been tested on a solid-state high-field NMR spectrometer. It has been shown that DQ decay curves have a better signal-to-noise ratio in the initial time regime than DQ buildup curves. The DQ buildup and decay curves have been recorded for a series of cross-linked natural rubber samples. These curves give access to quantitative values of the ratio of proton total

residual dipolar couplings which are in good agreement with those measured in homogeneous fields.

A new 3D experiment that allows direct probing of proton spin-diffusion process between resolved proton spectra obtained under Lee–Goldburg homonuclear decoupling has been reported.[37] It is anticipated that this class of experiments will soon be used to study poorly crystalline hybrid materials as well as finely divided or porous inorganic materials.

4.1.2 Fast MAS. The inverse cubic dependency of the acceleration of a rotor on its diameter allows for mechanical dynamics comparable to spin dynamics in coupled spin systems. Rotor acceleration up to 300 kHz/s has been measured by Samoson and co-workers.[38] It has been shown that this feature can be used to simplify existing experiments and explore entirely new ones in the study of spin topologies and material properties.

Mixing sequences for total through-bond correlation spectroscopy in solids (TOBSY) have been developed for fast MAS experiments.[39] Possible sequences with the desired Hamiltonian (the homonuclear isotropic J interaction) have been identified using lowest order average Hamiltonian theory combined with numerical simulations as a function of the MAS frequency. An experimental TOBSY spectrum of a uniformly ^{13}C-labelled decapeptide at 20 kHz MAS has been obtained using one of the new sequences. The spectrum allows to assign the ^{13}C resonances to the respective spin systems.

Novel procedures for the spectral assignment of peaks in high-resolution solid-state ^{13}C NMR have been presented.[40] These methods are based on the observation that at moderate and already widely available MAS rates (10–14 kHz), CH and CH_2 moieties behave to a large extent as if they were effectively isolated from the surrounding proton reservoir. Dipolar-based analogs of editing techniques that are commonly used in liquid-state NMR such as APT and INEPT can then be derived, while avoiding the need for periods of homonuclear ^{1}H–^{1}H multipulse decoupling. The resulting experiments are essentially 'tuning-free', and capable of establishing unambiguous distinctions among CH/CH_2 and C/CH3 carbon sites. The principles underlying such sequences have been explored using both numerical calculations and experimental measurements, and once validated their editing applications have been illustrated on a number of compounds.

A new technique to recouple homonuclear dipolar couplings between dilute spin pairs such as ^{13}C- ^{13}C systems under very fast MAS has been presented.[41] The presented technique, finite pulse r.f. driven recoupling (fpRFDR), restores homonuclear dipolar interactions based on constructive usage of finite pulse-width effects in a phase- and symmetry-cycled π-pulse train in which a rotor-synchronous π pulse is applied every rotation period. The restored effective dipolar interaction has the form of a ZQ dipolar Hamiltonian for static solids, whose symmetry in spin space is different from that obtained by conventional r.f. driven recoupling (RFDR) techniques. It has been demonstrated that the efficiency of recoupling by fpRFDR is not strongly dependent on chemical shift differences or resonance offsets in contrast to previous recoupling

methods under very fast MAS. For distance measurements without effects of spin relaxation, a constant-time version of fpRFDR (CT-fpRFDR) has been introduced, in which the effective evolution period is varied by refocusing dipolar evolution with a rotor-synchronized solid echo while the total recoupling period is kept constant. From CT-fpRFDR experiments at a spinning speed of 30.3 kHz in a field of 17.6 T, the ^{13}C–^{13}C distance of [1-^{13}C]Ala-[1-^{13}C]Gly-Gly was determined to be 3.27 Å, which agrees well with the value of 3.20 Å obtained by X-ray diffraction. Possibility of high throughput determination of global main-chain structures based on ^{13}C shifts obtained from 2D $^{13}C/^{13}C$ chemical-shift correlation for uniformly/segmentally ^{13}C-labeled protein/peptide samples under very fast MAS has also been discussed.

A 2D solid-state NMR technique for measurements of dipole–dipole couplings in many-spin systems under high-speed MAS has been described.[42] By incorporating fpRFDR into a multiple-pulse cycle based on the Waugh–Huber–Haeberlen (WAHUHA) homonuclear decoupling cycle, a constant-time t_1 evolution period is created. The constant-time tl period minimizes distortions of the experimental data due to various pulse sequence imperfections. The CT-fpRFDR technique has been demonstrated experimentally using ^{13}C NMR of carboxylate-labeled, polycrystalline L-alanine. 2D fpRFDRCT spectra correlate the dipole-coupled lineshape of the ^{13}C carboxylate groups with their isotropic chemical shift. Good agreement has been obtained between the experimental second and fourth moments of the dipole-coupled line shapes and calculated moments based on the L-alanine crystal structure and an average Hamiltonian analysis of the fpRFDR sequence. Applications in structural investigations of biologically relevant systems are anticipated.

4.1.3 2D Correlation Spectroscopy. A simple, qualitative approach has been described for the determination of membrane protein secondary structure and topology in lipid bilayer membranes.[43] The new approach is based on the observation of wheel-like resonance patterns in the NMR ^{1}H–$^{15}N/^{15}N$ polarization inversion with spin exchange at the magic angle (PISEMA) and $^{1}H/^{15}N$ HETCOR spectra of membrane proteins in oriented lipid bilayers. These patterns, named Pisa wheels, have been previously shown to reflect helical wheel projections of residues that are characteristic of α-helices associated with membranes. This study extends the analysis of these patterns to β-strands associated with membranes and demonstrates that, as for the case of α-helices, Pisa wheels are extremely sensitive to the tilt, rotation, and twist of β-strands in the membrane and provide a sensitive, visually accessible, qualitative index of membrane protein secondary structure and topology.

New isotropic mixing sequences suitable for scalar correlation experiments in solids have been designed using symmetry principles similar to those employed in the construction of the C7 dipolar recoupling sequence.[44] Compared with existing methods, the new isotropic mixing sequences are

appropriate for use with faster MAS rates and show improved magnetization transfer efficiencies.

A simple method for obtaining ^{1}H–^{13}C HETCOR solid-state NMR spectra reflecting only medium- and long-range ^{1}H–^{13}C correlation peaks has been presented.[45] It has been shown that by dephasing the magnetisation of protons directly bonded to a ^{13}C nucleus, the short-range correlation peaks, which contain limited structural information, can be cleanly suppressed without reducing the long-range cross peaks significantly. The resulting reduction of resonance overlap simplifies spectral assignment. The dephasing of the intensity of a given peak in the HETCOR spectrum traces out a ^{1}H–^{13}C distance-dependent REDOR curve. This medium- and long-distance (MELODI) HETCOR experiment is demonstrated on a mixture of amino acids with ^{13}C in natural abundance. It is useful for resonance assignment of proteins and other organic solids with partial or no ^{13}C labeling.

Signal enhancement in HETCOR spectra as well as signal selection in ^{1}H experiments can be achieved through inverse, *i.e.*, ^{1}H-detection in the solid state under fast MAS conditions. Using recoupled polarization transfer (REPT), a heteronuclear ^{1}H–^{15}N single-quantum correlation (HSQC) experiment has been presented,[46] symmetrical design of which allows the frequency dimensions to be easily interchanged. By observing the ^{15}N dimension indirectly and detecting on ^{1}H, the sensitivity is found to be increased by factors between 5 and 10 relative to conventional ^{15}N detection. In addition, the inverse ^{1}H–^{15}N REPT-HSQC scheme can be readily used as a filter for the ^{1}H signal. As an example, the combination of such a heteronuclear filter with a subsequent ^{1}H–^{1}H DQ experiment, yielding 2D ^{15}N-edited ^{1}H–^{1}H DQ MAS spectra, has been presented. It has been shown that specific selection or suppression of ^{1}H resonances is possible in this way, by use of which the resolution can be improved and information can be unravelled in ^{1}H spectra.

A new through-bond ^{1}H–^{13}C correlation technique, the MAS-J-HSQC experiment, has been described for solid-state NMR.[47] The new pulse scheme has been compared experimentally with the previously proposed MAS-J-HMQC experiment in terms of proton resolution on a model sample of powdered L-alanine. It has been shown that for natural abundance compounds, the MAS-J-HMQC and MAS-J-HSQC experiments give about the same proton resolution, whereas, for ^{13}C-labeled materials, narrower proton linewidths are obtained with the MAS-J-HSQC experiment. In addition we show that in scalar as well as in dipolar heteronuclear shift correlation experiments, when the proton chemical shift is encoded by the evolution of a single-quantum coherence, the proton resolution can be enhanced by simply adding a ^{13}C π pulse in the middle of the t_1 evolution time.

An in-depth account of the effects of homonuclear couplings and multiple heteronuclear couplings has been given for a recently published technique for ^{1}H–^{13}C dipolar correlation in solids under very fast MAS, where the heteronuclear dipolar coupling is recoupled by means of REDOR π-pulse trains.[48] The method bears similarities to well-known solution NMR techniques, which form the framework of a heteronuclear MQ experiment. The so-called

recoupled polarization-transfer (REPT) technique is versatile in that rotor-synchronized ^{1}H–^{13}C shift correlation spectra can be recorded. In addition, weak heteronuclear dipolar coupling constants can be extracted by means of spinning sideband analysis in the indirect dimension of the experiment. These sidebands are generated by rotor encoding of the reconversion Hamiltonian. Generalized variants of the initially described heteronuclear multiple-quantum correlation (HMQC) experiment have been presented. Using these techniques, measurements on model compounds with ^{13}C in natural abundance confirm the very weak effect of ^{1}H–^{1}H homonuclear couplings on the spectra recorded with spinning frequencies of 25–30 kHz. The effect of remote heteronuclear couplings on the spinning-sideband patterns of CH groups has been discussed, and ^{13}C spectral editing of rigid organic solids has been shown to be practicable with these techniques.

Three resonances corresponding to the three crystallographically distinct fluorine sites have been resolved in the high-resolution ^{19}F MAS spectrum of chiolite ($Na_5Al_3F_{14}$) collected at a field strength of 19.6 T and at a spinning speed of 40 kHz.[49] In contrast, only one broad resonance is observed in the ^{19}F MAS NMR spectrum of the isostructural compound $Na_5W_3O_9F_5$. Thus, a combination of ^{19}F MAS, $^{19}F \rightarrow {}^{23}Na$ CP, and ^{23}Na–^{19}F HETCOR NMR experiments has been applied to resolve the resonances from the different local environments.

A 3QMAS/HETCOR experiment between spin-5/2 nuclei (^{27}Al) and spin-1/2 nuclei (^{31}P) has been applied to aluminophosphate molecular sieves.[50] It has been shown that a reasonable sensitivity of the experiment can be achieved even on a narrow-bore NMR spectrometer that allows only low r.f. fields, if the conversion from the aluminium triple quantum into single quantum level and CP from aluminium to phosphorus nuclei are carefully optimized. The application of ANAFOR processing to the 3QMAS/HETCOR data has also been demonstrated and it has been shown that in this way the required experimental time can be reduced, approximately, by a factor of ten.

4.1.4 2D MQ MAS. A new MQ MAS NMR experiment of quadrupolar nuclei has been demonstrated, which uses two different MQ coherences in t_1 to refocus the quadrupolar broadening.[51] It has been shown that this experiment has the potential of achieving improved resolution over current techniques.

A rigorous examination of the various MQ MAS sequences has been carried out with reference to sensitivity enhancement in the isotropic dimension and the lineshapes of the corresponding MAS peaks in the anisotropic dimension.[52] An echo efficiency parameter has been defined as an indicator of the performance aspects of the various sequences. A consequence of the systematic analysis has been the combination of a spin-lock pulse for excitation of MQ coherences and an amplitude-modulated pulse for their conversion into observable single-quantum coherences. This approach has resulted in an improved performance over other sequences with respect to both the anisotropic lineshapes and the isotropic intensities.

A systematic experimental and numerical evaluation of several basic

approaches to MQ MAS NMR is presented for spin-3/2 nuclei.[53] The approaches use identical MQ excitation, *via* a single r.f. pulse of high power, and three types of methods for conversion into observable coherence: (a) nutation by strong CW pulse; (b) rotation-induced adiabatic coherence transfer (RIACT), and (c) fast amplitude modulation (FAM-1). The optimization strategies and maximum achievable MQ MAS efficiencies of ^{87}Rb in $RbNO_3$ and $LiRbSO_4$ have been investigated using several coherence transfer schemes under a wide range of experimental parameters. These parameters include the strength of the r.f. magnetic field ν_{rf}, the sample rotation speed ν_r, the length of the conversion period, and the modulation frequency in FAM-1. The data provide new insights into the spin dynamics involved in these techniques and the experimental guidelines for achieving the best sensitivity. The r.f. requirements for maximum efficiency of conversion is shown to depend on the method to be used. In general, FAM-1 performs better than the nutation and RIACT methods in terms of efficiency and off-resonance behavior, especially when ν_r is small compared to the quadrupole frequency ν_Q. The experiments performed using nutation, RIACT, and FAM-1 methods yield similar resolution in the isotropic dimension, regardless of ν_{rf}.

The sensitivity of single- and MQ NMR experiments of half-integer quadrupolar nuclei can be increased significantly by introducing so-called double frequency sweeps (DFS) in various pulse schemes. These sweeps consist of two sidebands generated by an amplitude modulation of the RF carrier. Using a time-dependent amplitude modulation the sidebands can be swept through a certain frequency range. A detailed analysis has been carried out to show that the efficiency of this process is a function of the adiabaticity with which the various spin transitions are passed during the sweep.[54] The effects of sweep rate, sweep range, and RF field strength have been investigated both numerically and experimentally. Using a DFS as a preparation period has led to significantly enhanced central transition powder spectra under both static and MAS conditions, compared to single pulse excitation. DFSs have proved to be very efficient tools also for coherence transfer, which can be exploited for the multiple- to single-quantum transfer in MQ MAS experiments. It has been demonstrated that DFSs are capable of transferring both quintuple-quantum and triple-quantum coherence into single-quantum coherence in $I = 5/2$ spin systems. This leads to a significant enhancement in signal-to-noise ratio and strongly reduces the r.f. power requirement compared to pulsed MQ MAS experiments, thus extending their applicability. This has been demonstrated by ^{27}Al 3QMAS experiments on $9Al_2O_3{\cdot}2B2O_3$ and the mineral andalusite.

It has been shown that rotary resonances between r.f. field strength, ω_1, and MAS frequency, ω_R, dramatically enhance the sensitivity of triple quantum preparation and mixing in the MQ MAS experiment, particularly for quadrupolar nuclei having low gyromagnetic ratios or experiencing strong quadrupole couplings.[55] Triple quantum excitation efficiency minima occur when $2\omega_1 = n\omega_R$, where n is an integer, with significant maxima occurring between these minima. For triple quantum mixing, maxima have been observed when $\omega_1 = n\omega_R$. These rotary resonance conditions have been combined into a new

experiment called FASTER MQ MAS, which enables a factor of three enhancement in sensitivity in comparison to conventional MQ MAS.

The rotor assisted population transfer (RAPT) sequence has been used to enhance the sensitivity of the RIACT(II) experiment for spin-3/2 quadrupolar nuclei.[56] A detailed theoretical analysis of the polarizations that contribute to different types of MQ MAS experiments has been provided. In particular, two polarization pathways have been distinguished for the creation of triple-quantum coherence. The existence of these pathways has been experimentally demonstrated by comparing the sensitivities of different sequences with and without RAPT preparation.

Major advances in instrumentation have made it feasible to begin studying the spectroscopically challenging mineral zoisite, which has octahedral aluminium sites with QCCs of 8.0 and 18.5 MHz. Initial results have been presented from single-pulse excitation MAS, selective Hahn echo MAS, and two different types of 3QMAS studies.[57] The selective Hahn echo and the single-pulse excitation spectra have provided nearly identical values for the isotropic chemical shift, QCC, and asymmetry parameter for each AlO_6 site. In the 3QMAS work, using double frequency sweeps generated by amplitude-modulated pulses for more efficient conversion of triple-quantum coherence into single-quantum coherence have resulted in a higher signal-to-noise ratio compared to the frequently used z-filtered three-pulse 3QMAS experiment. Zoisite has been shown to be a particularly good sample for testing a variety of solid-state NMR techniques and advances in instrumentation.

A new approach to combining CP with MQ MAS in a 2D NMR experiment has been demonstrated, involving CP from ^1H to the single-quantum coherences of a quadrupolar nucleus.[58] In two separate methods, pure-absorption line shapes have been obtained using a z-filter and a 'reversed split-t_1' method.

CP from ^1H to the MQ coherences of a quadrupolar nucleus has been used in combination with the 2D MQ MAS NMR experiment in order to extract high-resolution CPMAS NMR spectra.[59] The technique has been demonstrated on ^{23}Na ($S = 3/2$), ^{17}O, ^{27}Al (both $S = 5/2$), and ^{45}Sc ($S = 7/2$) nuclei, showing the applicability of MQ CP to systems with differing spin quantum number, gyromagnetic ratio, and relative nuclide abundance. The utility of this 2D MAS NMR experiment for spectral editing and site-specific measurement of CP intensities has been demonstrated. The possibility of direct CP to higher order MQ coherences has also been considered and three-, five-, and seven-quantum cross-polarized ^{45}Sc MAS NMR spectra have been presented.

4.1.5 Other Experiments. A 2D DQ experiment under rotational resonance (R^2) conditions has been introduced for evaluating dipolar couplings in rotating solids.[60] It has been shown that the contributions from the R^2-recoupled dipolar interaction and the J coupling can be conveniently separated in the resulting 2D R^2-DQ spectrum, so that the unknown dipolar coupling can readily be extracted, provided that the values of the involved J coupling constants are known. The results of the theoretical models have been applied

to both ^{13}C and ^{1}H nuclei to extract dipolar couplings in uniformly ^{13}C labeled L-alanine and a cross-linked natural rubber.

As shown experimentally the combination of selective inversion and dipolar recoupling schemes, such as DANTE and C7, allows DQ coherences to be selectively generated between distinct types of spins.[61] In such selective inversion and MQ excitation experiments, the DQ coherences are excited between spins with identical polarization, but not between spins with opposite polarization. It has been shown that by investigating the decay of longitudinal magnetisation or the build-up of DQ coherences, the respective dipolar pair couplings can be individually measured in the presence of perturbing couplings, which may significantly exceed the coupling of interest.

By combining two dipolar DQ MAS experiments, a homonuclear DQ-DQ MAS exchange experiment has been designed, which probes the reorientation of dipolar tensors and allows the observation of slow molecular dynamics, in particular the determination of reorientation angles and rates.[62] The dipolar coupling between two distinct spins is used to generate a DQ coherence, and the orientation-dependent coupling is measured by means of the DQ MAS sideband pattern before and after a mixing time. In the course of a reduced 3D experiment, the two DQ sideband patterns are correlated, resulting in a DQ-DQ sideband pattern, which is sensitive to the reorientation angle. By referencing the DQ-DQ time signal, the information content of the pattern can be divided into the sidebands and the centerband, with the former reflecting only the moieties which have undergone a reorientation, and the latter predominantly containing contributions from moieties in their initial position. Hence, a single sideband pattern provides access to both the reorientation angle and the relative number of moieties subject to the motional process. As a first example, such DQ-DQ MAS experiments have been performed on the ^{13}C–^{13}C spin pairs of an enriched poly(ethylene) sample. In its crystallites, the dynamics of a known chain-flip motion have been investigated.

2D spin-echo MAS NMR experiments have been carried out on polycrystalline [2,3-$^{13}C_2$]-L-alanine, so that two unusual resonance lines emerged along the F_1 axis.[63] To examine the spectral structure observed in the F_1 direction more closely the 2D NMR experiment has been undertaken using a sufficiently small t_1 increment, yielding many more resonance lines on a spectrum sliced along the F_1 axis. In addition, it has been shown that the intensities of resonance lines are largely dependent on the dipolar interaction.

The use of ^{1}H–^{31}P CP-edited radio frequency dipolar recoupled (RFDR) 2D NMR exchange experiments for the study of surface dissolution species in solution-aged metaphosphate glass has been reported.[64] It has been demonstrated that use of CP allows the resonances of phosphate tetrahedral species within the hydrated dissolution surface to be selectively and cleanly edited from the bulk unaged phosphate species. Incorporating the CP-editing into a 2D RFDR exchange experiment also has allowed the local spatial connectivity between these surface dissolution phosphate species to be directly addressed.

It has been shown that appropriate modulation of the r.f. amplitude in the two-pulse phase-modulation (TPPM) ^{1}H decoupling sequence provides an

appreciable improvement in the decoupling efficiency.[65] The effect of the amplitude modulation on TPPM has been examined using the average Hamiltonian theory, and the improvement in the decoupling efficiency is ascribed to third averaging. Improved decoupling is demonstrated with ^{13}C MAS NMR in glycine and uniformly ^{13}C,^{15}N-labeled glycylisoleucine.

A simple and efficient method, based on finding the optimal spinning rate with a mathematical algorithm and subsequently treating the spectra with filtering functions, for filtering the SSBs in 1D MAS NMR spectra has been described.[66]

Solid-state NMR signal enhancements of about two orders of magnitude (100–400) have been observed in dynamic nuclear polarization (DNP) experiments performed at high magnetic field (5 T) and low temperature (10 K) using the nitroxide radical 4-amino TEMPO as the source of electron polarization.[67]

The cross-relaxation rate constants for a three spin system involving hyperpolarized ^{129}Xe, ^{13}C, and ^{1}H nuclei have been determined over a wide temperature range (136–216 K) through observation of the polarization enhancements from spin polarization induced nuclear Overhauser effect (SPINOE) experiments.[68] A model system of methoxy groups adsorbed on high surface area silica has been studied. A maximum polarization enhancement of 3.4 has been observed for the methoxy carbon. Possible improvements for the SPINOE experiment have been suggested including alternative substrates which would retard xenon diffusion across the surface and improve xenon–carbon cross-relaxation leading to significantly larger SPINOE enhancements.

An illumination set-up using solid-state NMR for studies of photosynthetic reaction centers has been described.[69]

A home-built solid-state NMR spectrometer with stochastic excitation has been described.[70] An overview of the instrument has been given and the control unit and the module for the pulse generation have been described. A static probe with crossed coils for the transmitter and receiver circuits and the data processing part of the spectrometer software have been presented. Several examples of NMR measurements have been shown, including selective excitation in solids and the acquisition of static ^{2}H solid-state NMR spectra with a spectral width of up to 185 kHz.

A 2D solid-state NMR technique has been presented that can be used to determine the ^{15}N chemical shift and ^{1}H–^{15}N dipolar coupling tensors in powder samples of polypeptides containing ^{15}N isotopes at multiple sites.[71] The magnitudes of the principal elements of the ^{15}N CSA tensors and their orientations in the molecular frame for *N*-acetyl-^{15}*N*-L-Val-^{15}*N*-L-Leu (NAVL) and *N*-acetyl-^{15}*N*-D,L-Val (NAV) powder samples have been determined using this method.

The utility of simple rotary resonance experiments for the determination of the magnitude and orientation of ^{13}C chemical shift tensors relative to one or more ^{13}C–^{14}N internuclear axes from ^{13}C MAS NMR experiments has been explored.[72] The method has been demonstrated by experiments and numerical simulations for the $^{13}C_{\alpha}$ spins in powder samples of L-alanine and glycine with

^{13}C in natural abundance. To investigate the potential of the experiment for determination of relative/absolute tensor orientations and backbone dihedral angles in peptides, the influence from long-range dipolar coupling to sequential ^{14}N spins in a peptide chain as well as residual quadrupolar dipolar coupling cross-terms have been analyzed numerically.

A general and optimized strategy for implementing the QUADRAMA technique for measurements of ^{2}H quadrupolar couplings under MAS conditions has been described.[73] The new technique does not require any knowledge of the size of the coupling. Experimental tests of the optimized protocol demonstrate that, by judicious choices of a combination of scaling factors and recoupling times, ^{2}H quadrupole couplings ranging over an order of magnitude from 3 to 42 kHz can be measured.

A composite-pulse sequence to cancel the spurious signals has been described.[74] The main advantage of this sequence over the Hahn echo sequence has been shown to be in the simplicity of optimizing the line intensity: the optimization of only one pulse duration for this sequence but of two pulse durations and the interpulse delay for the Hahn echo sequence. The effects of the first-order quadrupole interaction during the pulses have been considered (spin $I = 3/2$ nuclei). It has been shown that the size of the sample must be much smaller than that of the r.f. coil in order for the r.f. magnetic field to become homogeneous for the sample.

A novel way of extracting information from a series of severely overlapped ^{13}C CPMAS NMR spectra using multivariate data analysis techniques has been presented.[75]

4.2 Distance and Angle Measurements by REDOR and Other Solid-state NMR Techniques. – The possibility of performing ^{13}C-observed REDOR in ^{1}H–^{13}C systems has been presented, where very-fast MAS with spinning frequencies of up to 30 kHz is used to successfully suppress the perturbing homonuclear couplings among the protons, which would usually be expected to hamper a proper data analysis.[76] Simple modifications of the REDOR experiment have been presented which lead to a 2D experiment in which heteronuclear multi-spin MQ modes are excited, the evolution of which is monitored in the indirect frequency dimension. The existence of higher quantum orders in the proton subspace of these heteronuclear coherences has been proven by performing a phase-incremented spin-counting experiment, while a phase cycle can be implemented which allows the observation of specific selected coherence orders in the indirect dimension of 2D shift correlation experiments. The significance of the heteronuclear approach to spin counting has been discussed by comparison with well-known homonuclear spin-counting strategies. For the shift correlation, the high resolution of ^{1}H chemical shifts in the indirect dimension is achieved by the use of high B_0 fields (700.13 MHz) combined with very-fast MAS, and dipolar coupling information can be extracted by analyzing either peak intensities or spinning-sideband patterns in the indirect frequency dimension. The method is termed dipolar heteronuclear multiple-spin correlation (DIP-HMSC).

A new heteronuclear dipolar interaction recoupling scheme suitable for the characterization of heteronuclear dipolar couplings for multiple-spin systems under very fast MAS condition has been proposed.[77] The new technique has been shown to be superior to the rotational echo double resonance method and other recoupling schemes as far as the interference of homonuclear dipolar interaction is concerned. The potential of the technique is illustrated for fluorapatite sample at a spinning frequency of 25 kHz.

An experimental strategy has been developed for measuring multiple dipole–dipole interactions in inorganic compounds using REDOR NMR.[78] Numerical simulations have been carried out on a three-spin system of type SI_2 in order to assess the effect of the I–I homonuclear dipole–dipole coupling and the influence of experimental imperfections such as finite pulse length and misadjustments of the π pulses applied to the I-spin species. The simulations show that within the initial data range the effects of such misadjustments can be internally compensated by a modified sequence having an additional π pulse on the I channel in the middle of the dipolar evolution periods. Experimental $^{27}Al\{^{31}P\}$ REDOR results on the multispin systems $Al(PO_3)_3$, $AlPO_4$, $[AlPO_4]_{12}(C_3H_7)_4NF$ and Na_3PO_4 confirm the general utility of the new approach. Thus, for applications to unknown systems the compensation strategy obviates calibration procedures with model compounds

$^{11}B\{^{23}Na\}$ REDOR NMR has been used to probe the spatial relationship between the network former (boron) and the network modifier (sodium) species in sodium borate glasses.[79] Under conditions of fast MAS, site resolved REDOR data have been obtained, revealing that the trigonal and tetrahedral units interact more or less equally strongly with the sodium ions.

The complex hydrogen-bonding arrangement in the biologically important molecule bilirubin IX α has been probed by using ^1H DQ MAS NMR.[80] An analysis of ^1H DQ MAS spinning-sideband patterns has allowed the quantitative determination of proton–proton distances and the geometry. The validity of this procedure has been proven by simulated spectra for a model three-spin system, which show that the shortest distance can be determined to a very high degree of accuracy. The distance between the lactam and pyrrole NH protons in bilirubin has been determined to be 1.86 ± 0.02 Å (corresponding to a dominant dipolar coupling constant of 18.5 ± 0.5 kHz). The analysis also yields a distance between the lactam NH and carboxylic acid OH protons of 2.30 ± 0.08 Å (corresponding to a perturbing dipolar coupling constant of 9.9 ± 1.0 kHz).

Rotary resonance recoupling of heteronuclear ^{13}C–^1H dipolar interactions in ^{13}C NMR spectra (recorded under conditions of ^1H decoupling at frequency ν_1 and MAS at frequency ν_r) has been studied for three examples of molecular solids (adamantane, ferrocene and hexamethylbenzene) in which substantial molecular motion is known to occur.[81] It has been shown that when rotary resonance conditions are satisfied (*i.e.* $\nu_1/\nu_r = n$, for $n = 1$ or 2), the recoupling can lead to motionally averaged Pake-like powder patterns from which information on ^{13}C–^1H internuclear distances and/or molecular motion can be derived.

REDOR technique has been applied to natural abundance ^{13}C nuclei coupled to a singly labeled ^{15}N nucleus to determine the ^{13}C, ^{15}N interatomic distances simultaneously in crystalline ammonium [^{15}N] L-glutamate monohydrate with a precision of ± 0.15 Å.[82]

A new MAS NMR experiment has been described for selective ^{13}C–^{15}N distance measurements in uniformly ^{13}C,^{15}N-labeled solids, where multiple ^{13}C–^{15}N and ^{13}C–^{13}C interactions complicate the accurate measurement of structurally interesting, weak ^{13}C–^{15}N dipolar couplings.[83] The experiment, termed FSR (frequency selective REDOR), combines the REDOR pulse sequence with a frequency selective spin-echo to recouple a single ^{13}C-^{15}N dipolar interaction in a multiple spin system. The ^{13}C–^{15}N coupling of interest is extracted by a least-squares fit of the experimentally observed modulation of the ^{13}C spin-echo intensity to the analytical expression describing the dipolar dephasing in an isolated heteronuclear spin pair under conventional REDOR. The experiment is demonstrated in three uniformly ^{13}C,^{15}N-labeled model systems.

A novel site-directed solid-state NMR distance measurement approach, using ^{13}C–^{19}F REDOR, has been used to measure a ligand-induced change of 1.0 ± 0.3 Å in the distance between helices α_1 and α_4 of the ligand-binding domain in the intact, membrane-bound serine receptor.[84]

Carbon–caesium distances have been measured in the supramolecular inclusion guest–host system by ^{13}C–^{133}Cs REDOR NMR to illustrate the utility of solid-state NMR for the structural characterization of metal ions trapped by organic host compounds.[85] Caesium cation was chosen for study because of the importance of removing its radionucleotide from waste products. The results have shown that the ^{133}Cs nucleus has suitable properties for REDOR NMR.

Solid-state NMR has been used to study the new aluminophosphate material $AlPO_4$-ZON.[86] The location of fluorine in the $AlPO_4$-ZON framework has been verified by measuring the internuclear distances between ^{19}F and all ^{27}Al sites using the MQ-REDOR technique. MQ-REDOR has been also used to measure the distances between ^{1}H and ^{27}Al nuclei in this material.

A solid-state NMR technique for the determination of peptide backbone conformations at specific sites in unoriented samples under MAS has been described and demonstrated on labeled samples of tripeptide AlaClyGly and 17-residue peptide.[87] Experiments and simulations show that both ϕ and ψ backbone dihedral angles can be extracted from a single data set. This technique, called DQCSA spectroscopy, may be especially useful when analyzing the backbone conformation of a polypeptide at a particular doubly labeled site in the presence of additional labeled carbons along the sequence.

Reintroduction of dipolar coupling between spin-1/2, nuclei (*e.g.* ^{13}C, ^{15}N) and spin-1 ^{2}H, using phase-modulated deuterium dephasing pulses, has been shown to provide a simple and efficient basis for obtaining peptide backbone torsion angles (ϕ and ψ) in specific stable-isotope enriched samples.[88] The consequences of ^{13}C homonuclear interactions present during ^{13}C-observed,

^{2}H-dephased REDOR measurements have been explored and the theoretical basis of the experimentally observed effects has been investigated.

4.3 NMR Parameters: Experimental and Theoretical Studies. – *^{1}H* – A quantum chemical *ab initio* study of ^{1}H NMR chemical shifts has been undertaken to allow the elucidation of structural arrangements in solid-state molecular ensembles.[89] Using the hexabenzocoronene (HBC) molecule as an example, it has been shown that the new combined experimental and theoretical approach allows the observed ^{1}H chemical shifts to be related in a quantitative manner to the intermolecular structure. In the quantum chemical calculations, a series of model systems of stacked HBC oligomers have been used. On account of the marked dependence of the ^{1}H chemical shift to ring currents arising from nearby aromatic rings, the calculated ^{1}H chemical shifts have been found to be very sensitive to the stacking arrangement of the HBC molecules. Moreover, the ring current effect has been found to be particularly long range, with a considerable influence of the second neighbour, at a distance of 700 pm, being observed.

^{1}H and ^{13}C – The paramagnetic metallocenes and decamethylmetallocenes $(C_5H_5)_2M$ and $(C_5Me_5)_2M$ with M = V, Mn, Co and Ni have been studied by ^{1}H and ^{13}C solid-state MAS NMR.[90] Near room temperature spinning sideband manifolds cover ranges of up to 1100 and 3500 ppm, and isotropic signal shifts appear between −260 and 300 ppm and between −600 and 1640 ppm for ^{1}H and ^{13}C NMR spectra, respectively. The isotropic paramagnetic signal shifts, which are related to the spin densities in the s orbital of ligand atoms, have been discussed. A Herzfeld–Berger spinning sideband analysis of the ring carbon signals has yielded the principal values of the paramagnetic shift tensors, and for metallocenes with a small g-factor anisotropy the electron spin density in the ligand π system has been determined from the CSA. The unusual features of the ^{1}H and ^{13}C solid-state NMR spectra of manganocene have been related to its chain structure while temperature-dependent ^{1}H MAS NMR studies reflected antiferromagnetic interaction between the spin centers.

^{2}H and ^{13}C – The magnitudes and orientations of the principal elements of the ^{13}C CSA tensor in the molecular frame of the formate ion in β-calcium formate have been determined using 1D dipolar-shift spectroscopy: $\sigma_{11} = 104$ ppm, $\sigma_{22} = 179$ ppm, and $\sigma_{33} = 233$ ppm, with the least shielding element of the ^{13}C CSA tensor, σ_{33}, collinear with the C–H bond.[91] The temperature dependence of the ^{13}C CSA and the ^{2}H quadrupole coupling tensors in β-calcium formate have been analyzed for a wide range of temperature (173–373 K). It has been found that the span of the ^{13}C CSA and the magnitude of the H-2 quadrupole coupling interactions are averaged with the increasing temperature. The experimental results have also shown that the ^{2}H quadrupole coupling tensor becomes more asymmetric with increasing temperature. A librational motion about the σ_{22} axis of the ^{13}C CSA tensor has been used to model the temperature dependence of the ^{13}C CSA tensor and the ^{2}H quadrupole coupling tensor.

^{11}B – The application of solid-state NMR techniques at moderate (9.4 T)

and high (17.6 T) magnetic field strengths to characterize the boron CSA tensors in trimesitylborane ($BMes_3$) and triphenyl berate ($B(OPh)_3$) has been reported.[92] The boron CSA tensor of the former compound exhibits a remarkably large span (121 ppm), which encompasses the known range of isotropic chemical shifts for tricoordinate boron compounds. Conversely, the effect of the boron CSA tensor on the ^{11}B NMR spectra of $B(OPh)_3$ is difficult to observe and quantify even at field strengths as high as 17.6 T. The observed difference in the boron shielding tensors has been reproduced by a series of *ab initio* and DFT calculations with a range of basis sets. The difference has been rationalized in the context of Ramsey's theory of nuclear magnetic shielding by considering contributions to the paramagnetic shielding in the tricoordinate boron plane. Experimental and calculated boron nuclear quadrupolar coupling constants and asymmetry parameters have also been reported. A combination of experimental and theoretical results have provided the orientation of the CSA and e.f.g. tensors in the molecular framework.

^{13}C – ^{13}C CSA tensors for various carbon sites of polypeptides, and for carbon sites in α-helical and β-sheet conformations of poly-L-alanine, and polyglycine, have been presented.[93] The results suggest that the spans of carbonyl CSA tensors of alanine and glycine residues in various peptides are similar, even though the magnitude of individual components of the CSA tensor and the isotropic chemical shift are different. The δ_{22} element has been found to be the only component of the carbonyl CSA tensor that significantly depends on the CO···HN hydrogen-bond length.

An approach to the determination of the orientation of the carbonyl CSA tensor in a ^{13}C–^{15}N–^{1}H dipolar coupled spin network has been proposed.[94] The method involves the measurement of the Euler angles of the ^{13}C–^{15}N and ^{15}N–^{1}H dipolar vectors in the ^{13}C CSA tensor principal axes system, respectively, *via* a ^{13}C–^{15}N REDOR experiment and by a 2D relayed anisotropy correlation of the ^{13}C CSA (ω_2) and ^{15}N–^{1}H dipolar interaction (ω_1). *Via* numerical simulations the sensitivity of the ω_1 cross sections of the 2D spectrum to the Euler angles of the ^{15}N–^{1}H bond vector in the ^{13}C CSA frame has been shown. The orientation of the ^{13}C CSA tensor in the peptide plane of the dipeptide AibAib-NH_2 (Aib = α-aminoisobutyric acid) has been determined.

^{13}C and ^{15}N – In a dipolar-coupled spin-1/2 network of the type $^{15}N1$–^{13}C–$^{15}N2$, an assessment of the sensitivity of the N → C and C → N TEDOR sideband intensities to the Euler angles defining the orientation of the two heteronuclear dipolar vectors in the ^{13}C and ^{15}N CSA tensor principal axes system has been carried out *via* numerical calculations.[95] The results have clearly indicated the potential of TEDOR MAS NMR for the characterization of the CSA tensor orientation in the molecular frame. The efficiency of the method has been experimentally illustrated by TEDOR studies on a polycrystalline sample of [1,3-$^{15}N_2$, 2-^{13}C]uracil, which is one of the four bases in RNA.

^{17}O – The first experimental solid-state ^{17}O NMR and theoretical study of the ^{17}O e.f.g. and chemical shielding tensors in a free nucleic acid base, thymine, has been reported.[96]

A solid-state ^{17}O NMR study of [α-^{13}C,^{17}O]benzamide has been presented.[97] The orientations of the ^{17}O e.f.g. and chemical shift tensors have been determined from the analysis of MAS and static ^{17}O NMR spectra. It has been shown that the principal component of the ^{17}O chemical shift tensor with the least shielding is approximately 18° off the C=O bond and that the component with the most shielding is perpendicular to the amide plane.

High-resolution 'isotropic' ^{17}O (I = 5/2) NMR spectra of the powdered solids have been obtained using three- and five-quantum MAS NMR at magnetic field strengths of 9.4 and 16.4 T for two ^{17}O-enriched hydrous magnesium silicates, the minerals hydroxyl-chondrodite ($2Mg2SiO_4 \cdot Mg(OH)_2$) and hydroxyl-clinohumite ($4Mg2SiO_4 \cdot Mg(OH)_2$).[98] The MQ MAS spectra were analyzed to yield the ^{17}O isotropic chemical shifts and quadrupolar parameters of the distinct oxygen sites resolved in each sample. The values obtained were compared with those found previously for forsterite (Mg_2SiO_4). The ^{17}O resonances of the protonated (hydroxyl) sites were recorded and assigned with the aid of $^{17}O-\{^1H\}$ CP and comparison with the spectrum of ^{17}O-enriched brucite ($Mg(OH)_2$). Complete assignments of the five crystallographically inequivalent oxygen sites in hydroxylchondrodite and of the nine such sites in hydroxyl-clinohumite have been suggested. The validity of these assignments have been supported by the observation of a correlation between ^{17}O isotropic chemical shift and Si–O bond length.

^{17}O static and MAS NMR spectra have been reported from three crystalline cyclic titanodiphenylsiloxanes at magnetic fields of 5.6, 14.1 and 17.6 T.[99] These compounds allow the NMR parameters characteristic of Ti–O–Si environments to be determined. It has been shown that the quadrupole interaction of such environments is in the range of 3–3.5 MHz. The relatively large isotropic chemical range observed suggests that for structurally and atomically disordered titanosilicate-based materials the very highest applied magnetic field may not produce the best ^{17}O solid-state NMR spectra.

^{19}F and ^{93}Nb – A variety of NMR interactions have been characterized by solid-state NMR in potassium heptafluoroniobate, K_2NbF_7, with fluorine atoms arranged about a central niobium atom in a heptacoordinate, capped trigonal prism arrangement.[100] Simulations of ^{93}Nb MAS NMR spectra acquired at 11.7 T and at high spinning speeds (35 kHz) yielded the QCC, χ, the asymmetry parameter, η, and the isotropic chemical shift, δ_{iso}. From the analysis of ^{93}Nb NMR spectra of stationary samples of K_2NbF_7, the niobium chemical shielding anisotropy and the relative orientation of the e.f.g. and CSA tensors have been determined. The ^{93}Nb MAS NMR spectra acquired at lower spinning speeds, where the spinning sidebands are not separated from the centerband, have also been simulated by using an efficient time propagation algorithm based on Floquet theory. Slightly distorted ten-peak multiplets have been observed in the solid-state ^{19}F MAS NMR spectra, which arise from *J*-coupling and residual dipolar coupling between the ^{19}F and ^{93}Nb nuclei. Simulations of the ^{19}F MAS NMR spectra yield values of $^1J(^{93}Nb,^{19}F) = 204$ Hz and $\delta_{iso}(^{19}F) = 76$ ppm. An irreversible phase transition has been identified at *ca.* 160 °C by ^{19}F and ^{93}Nb NMR.

^{23}Na – High-temperature ^{23}Na MAS NMR experiments up to 873 K for a number of different sodalites have been reported.[101] The quadrupolar interaction for the thiocyanate sodalite, the nitrate aluminosilicate and germanate sodalite decreases strongly, passing a coalescence state on heating, while the quadrupolar interaction of the iodide and nitrite sample shows nearly no change. The temperature dependence of the quadrupolar interaction has been shown to be a function of the sodalite β-cage expansion. Two conceivable jump mechanisms have been proposed for a tetrahedral two-site jump between occupied and unoccupied tetrahedral sites.

The paramagnetic effects of oxygen molecules on the sodium cations in zeolite LiNaX (approximate to 70% Li; 30% Na) have been investigated using VT ^{23}Na MAS NMR and ^{23}Na MQ MAS NMR.[102] ^{23}Na MQ MAS NMR has been used to calculate the isotropic chemical shifts, quadrupolar shifts, and the quadrupolar coupling constants.

^{23}Na and ^{27}Al – The ^{23}Na and ^{27}Al satellite transition spectroscopy of NMR MAS spectra of polycrystalline of natural blue sodalite ($Na_8Cl_2(AlSiO_4)_6$) has been used to determine the electric field gradient and chemical shift tensors at both the ^{23}Na and ^{27}Al lattice sites.[103] The e.f.g. values are smaller than those of previously studied similar systems. The principal values of the e.f.g. and chemical shift tensors and the relative orientations of their principal axes have been obtained by computer simulating the spectra at two different applied magnetic fields.

^{29}Si – ^{29}Si solid-state NMR of the amino-functionalized silyllithium compounds tris(tetrahydrofuran)[bis(diethylamino)phenylsilyl]lithium (4.3THF) and tris(tetrahydrofuran)[(diethylamino)bisphenylsilyl]lithium (7.3THF) has been presented.[104] The apparently unusual experimental values of the ^{29}Si NMR resonance signals at $\delta = 20.3$ (for 7.3THF) and $\delta = 28.4$ ppm (for 4.3THF) have been explained by DFT-IGLO calculations and are a consequence of the combination of electronegative and electropositive substituents at the silicon center.

^{31}P and ^{77}Se – An intergrown crystal of two phases of bis(dineopentoxyphosphorothioyl) diselenide has been investigated by goniometer ^{31}P NMR.[105] From the angular dependence of the chemical shift, the tensors of a triclinic and a monoclinic phase have been determined. The principal values σ_{11}, σ_{22} and σ_{33} of the absolute nuclear magnetic shielding tensors for the triclinic phase are 134, 227 and 375 ppm and for the monoclinic phase are 132, 228. and 374 ppm, respectively. In both cases, the principal axis 3 of the ^{31}P tensor is directed nearly along the P=S bond and the principal axis 2 is nearly perpendicular to the S=P–Se plane. Calculations of the ^{31}P and ^{77}Se nuclear magnetic shielding tensors have been performed for molecules of both phases and for model compounds by the sum-over-states density functional perturbation theory IGLO method.

^{51}V – Magnitudes and relative orientations of ^{51}V quadrupole coupling and chemical shift tensors have been determined from ^{51}V MAS NMR spectra at 14.1 T for seven divalent metal pyrovanadates using least-squares fitting of the integrated spinning sideband intensities observed for the central and satellite

transitions.[106] A linear correlation has been observed between the principal elements for the ^{51}V quadrupole coupling tensors and calculated e.f.g. tensor elements, obtained from point-monopole calculations.

^{207}Pb – ^{207}Pb NMR has been used to investigate 20 lead(IV) tetracarboxylates both in solution and in the solid state.[107] From an analysis of the range of, and trends in, the NMR chemical shifts, circumstantial evidence has been presented for augmentary coordination by Lewis basic ortho-aromatic substituents of the carboxylate groups. The ^{207}Pb CSA parameters have been extracted from analysis of the spinning sideband manifolds of the CPMAS spectra. Thirteen of the 20 CSA analyses performed show effectively axial CSA tensors. A simple shielding model which rationalizes this typical CSA pattern has been presented

Correlation and relativistic effects on Pb–Pb and Pb–O interactions in β-PbO have been examined using *ab initio* calculations and ^{207}Pb NMR CSA tensor analysis.[108] It has been shown that a covalent-like Pb^{2+}–Pb^{2+} interaction accounts for many facets of the NMR and the X-ray absorption near-edge structure, as well as other spectroscopic properties.

4.4 Exotic and Troublesome Nuclei. – *^{14}N* MAS NMR of the nitrate ion[106] and *^{25}Mg* solid-state NMR of Mg(II) adenosine 5′-triphosphate complex have been reported.[109]

^{47}Ti, ^{49}Ti solid-state NMR spectra of TiO_2 nanoparticles have been reported.[110] The corresponding $^{47,49}Ti$ NMR spectra have been simulated by using the NMR interaction parameters determined from bulk polycrystalline TiO_2.

^{59}Co solid-state powder NMR spectra of ten simple inorganic cobalt(III) complexes at 11.75 and, in most cases, 4.7 T have been analyzed.[111] The relevant chemical shift components have been determined from the simulations of the powder line shapes. These simulations also provided the relative orientations of the CSA and e.f.g. tensors, as well as magnitude and asymmetry of the ^{59}Co quadrupolar coupling. Using symmetry arguments and *ab initio* calculations, as appropriate or necessary, the orientations of the e.f.g. tensors in the molecular frame have been deduced.

^{67}Zn solid-state NMR spectroscopic studies of the minimal DNA binding domain of human nucleotide excision repair protein XPA have been reported.[112]

^{89}Y MAS NMR and powder X-ray diffraction have been applied in order to elucidate the crystal growth process, Eu doping process, and Eu distribution in a red phosphor, Eu-doped Y_2O_2S (Eu-Y_2O_2S) fired at varying temperatures, as well as the correlation between such material properties and the phosphor quality.[113] The interrelation between the brightness, the linewidth and T_1 in ^{89}Y NMR, the amount of effective Eu, and the crystallinity of Eu-Y_2O_2S has been elucidated.

^{203}Tl and ^{205}Tl solid-state NMR have been applied to study crystallographically characterized thallium alkoxides $[Tl(OCH_2CMe_3)]_4$ and $[Tl(OAr)]_\infty$, where OAr = $OC_6H_3Me_2$-2,6 and $OC_6H_3(CHMe_2)_2$-2,6.[114]

5 Applications

5.1 Organic Solids. – *^2H* – ^{2}H NMR has been used to study the molecular behaviour of selectively deuterated *n*-alkanes of variable length that serve as guest molecules in channel-forming inclusion compounds, made from urea, cyclophosphazene or α-cyclodextrin.[115] ^{2}H NMR line shape and relaxation experiments have been performed which provide a deeper insight into the motional characteristics as well as the ordering behaviour of such spatially confined guest molecules. The analysis of these experiments has revealed the presence of chain motions that are found to depend strongly on the particular host matrix.

Clathrate hydrates formed by a water host structure and guest molecules of tetrahydrofuran have been studied using solid-state ^{2}H NMR.[116] ^{2}H NMR results for THF/D_2O suggest that there are at least two dynamically distinguishable types of water molecule, both undergoing four-site tetrahedral jump motions but with different rates. The population ratio can be assigned as 3:1, consistent with the known crystal structure. From analysis of the ^{2}H NMR line shapes, the jump rates have been determined as a function of temperature, and activation parameters have been estimated. The ^{2}H NMR spectra for THF-d_8/H_2O have been interpreted in terms of the THF-d_8 guest molecules undergoing an approximately isotropic motion in the rapid regime, but with a distribution of slightly anisotropic characteristics associated with the reorientational motions of different guest molecules. These conclusions have been complemented by information determined from ^{2}H NMR spin–lattice relaxation time measurements.

^2H, ^{13}C – Novel 1:1 complexes of acetone with *p-tert*-butylcalix[4]arene and *p-tert*-butylcalix[6]arene have been characterized by ^{13}C and ^{2}H solid-state NMR.[117] It has been shown that the behaviour of both molecules towards acetone is very similar, with the same orientation of the guest, and the same activation energy for the rotation of the C–D bond of acetone about its threefold axis.

^2H, ^{13}C, ^{15}N – Trinuclear MAS NMR, involving naturally abundant (^{13}C,^{15}N) and easily deuterated (^{2}H) nuclei, has been shown to offer newer opportunities to study molecular self-assembly in noncrystalline supramolecular systems.[118] This has been demonstrated using the cyanuric acid-melamine system.

^2H, ^{15}N – Dynamics of nano- to picosecond proton transfer processes in the ^{15}N labeled polycrystalline tetraaza[14]annulene have been studied by a combination of 9.1 MHz ^{15}N T_1 relaxation time measurements under CPMAS conditions and by 46 MHz ^{2}H T_1 relaxation time measurements of a static sample of a doubly deuterated sample.[119]

^{13}C – The dicyclohexylamine/thiourea inclusion compound has been studied by ^{13}C CPMAS NMR.[120] The results have shown that the guest (dicyclohexylamine) molecules are freely rotating and that the channels are perfect van der Waals cavities.

N-(ω-Carboxyalkyl)morpholine hydrochlorides, $OC_4H_8N(CH_2)_nCOOH{\cdot}HCl$,

n = 1–5, have been analyzed by ^{13}C CPMAS) NMR.[121] Contrary to the solution, non-equivalence of the ring carbon atoms has been found in the ^{13}C CPMAS NMR spectra. ^{13}C chemical shifts in solids have been linearly correlated with the shielding constants calculated from the PM3 geometry of ion pairs.

^{13}C solid-state NMR has been applied to study 4-acetyl-, formyl- and carboxy-benzo-9-crown-3 ether.[122] Chemical shift differences of *ca.* 8.5 ppm have been observed between the two aryl–O–C carbons and are explained using results of *ab initio* calculations previously performed on anisole. Chemical shift assignments have been verified by the use of selectively deuterated derivatives.

The stereolabile helical enantiomers of dimesityl sulfoxide and sulfone have been characterized by ^{13}C CPMAS NMR, which show that the helical enantiomers are stable in the crystalline state.[123]

A study of the tautomerism of dehydroacetic acid, using ^{13}C CPMAS and other techniques, has showed that this compound exists as the 3-acetyl-4-hydroxy-6-methyl-2*H*-pyran-2-one in the solid state.[124]

Two polymorphic forms of *cis*-cinnamic acid have been characterized using ^{13}C CPMAS NMR.[125]

The 3-alkyl, benzyl and phenyl derivatives of 1-(2-hydroxy-4-bromophenyl)-3-methyl-4-imidazolin-2-one have been studied by solid-state ^{13}C CPMAS NMR.[126] The differences in chemical shifts $\Delta = \delta(\text{liquid}) - \delta(\text{solid})$ are significant for aromatic carbons C_3 (−2.9 ppm), C_4 (3.6 ppm) and C_5 (−3.9 ppm) and C_7 (−1.5 ppm), which are adjacent to N_1–C_4, and are subject to the largest changes of the environment during reorientation of the imidazolin-2-one moiety.

The 5-carboxymethyl-1,2,4-triazole and 5-oxo-1,2,4-triazine derivatives have been examined by ^{13}C CPMAS NMR.[127]

Crystalline α-D-galacturonic acid monohydrate has been studied by ^{13}C CPMAS NMR and X-ray crystallography.[128] The molecular dynamics have been investigated by evaluating ^{13}C spin–lattice relaxation in the rotating frame ($T_{1\rho}$) and CSA properties of each carbon. It has been found that only limited molecular motions can be detected in the low frequency ($<10^4$ Hz) range by $T_{1\rho}(^{13}C)$ measurements and changes of CSA properties as a function of temperature.

The structure and conformational equilibrium of the monooximes of 1,2-naphthoquinone have been studied by ^{13}C solid and liquid state NMR and non-empirical quantum-chemical calculations.[129]

Solid-state NMR techniques have been applied to study two of the three conformational polymorphs of dimethyl-3,6-dichloro-2,5-dihydroxyterephthalate,[130] which have been previously characterized by X-ray. In these two polymorphs, named white and yellow due to their colour, the major structural difference is the torsional angle between the ester group and the aromatic ring. There are also differences in the hydrogen-bonding patterns, with the white form having intermolecular hydrogen bonds and the yellow form having intramolecular hydrogen bonds. The carbon isotropic chemical shift values

and the chlorine e.f.g. tensor information have been extracted from the ^{13}C MAS spectra, and the principal values of the chemical shift tensors of the carbons are obtained from 2D FIREMAT experiments. The differences between the spectral data on the two polymorphs are discussed in terms of the known electronic and structural differences.

Protonated cyclic GMP, which has an important biological role as a second messenger, has been studied by ^{13}C CPMAS NMR.[131]

^{13}C, ^{15}N – Two Schiff bases (*N,N'*-bis(5-bromosalicylidene)-1,2-diaminoethane and 7-[(1-(5-bromo-2-hydroxyphenyl)methylidene)amino]-4-methylcoumarin), and two appropriate Schiff–Mannich bases (*N,N'*-bis(5-bromo-3-[(diethylamino)methyl]salicylidene)-1,2-diaminoethane and 7-[(1-(5-bromo-3-[(diethylamino)methyl]-2-hydroxyphenyl)methylidene)amino]-4-methylcoumarin) capable of intramolecular hydrogen bonding have been investigated by multinuclear NMR methods in both solid and liquid phases.[132] In all of the compounds under investigation tautomeric equilibrium involving an intramolecular hydrogen bond has been found. In the solid state the tautomeric process is frozen and only one H-bonded form is present. On the basis of ^{13}C and ^{15}N CPMAS NMR spectra this is identified as the form with hydrogen bonds involving the imino groups.

The solid state ^{13}C and ^{15}N CPMAS NMR have been applied to study 3,5-di-*tert*-butyl-1,2,4-diazaphosphole and 3,5-diphenyl-1,2,4-diazaphosphole.[133] The X-ray structure of the first compound was already known (a cyclic dimer with localized N–H protons) while the structure of the second cannot be determined due to the difficulty of growing suitable single crystals. NMR results pointed out that 3,5-di-*tert*-butyl-1,2,4-diazaphosphole is a 'classical' compound while 3,5-diphenyl-1,2,4-diazaphosphole is probably a tetramer showing intermolecular solid-state proton transfer. GIAO/*lab initio* calculations have been carried out to estimate the absolute ^{1}H, ^{13}C and ^{15}N shieldings and to assign the signals of carbons C-3 and C-5.

^{13}C, ^{19}F – The supramolecular 1:1 host–guest inclusion compound *p-tert*-butylcalix[4]arene/α,α,α-trifluorotoluene has been characterized by ^{19}F and ^{13}C solid-state NMR.[134] The $^{19}F\{^{1}H\}$ NMR spectrum obtained under CPMAS conditions shows a single isotropic resonance with a significant spinning sideband manifold. The static $^{19}F\{^{1}H\}$ CP NMR spectrum consists of a powder pattern dominated by the contributions of the anisotropic chemical shift and the homonuclear dipolar interactions. The ^{19}F MREV-8 experiment, which minimizes the ^{19}F–^{19}F dipolar contribution, has been used to identify the chemical shift contribution. The full static $^{19}F\{^{1}H\}$ CP NMR spectrum has been analyzed using subspectral analysis and subsequently simulated as a function of the ^{19}F–^{19}F internuclear distance (2.25 ± 0.01 Å) of the rapidly rotating CF_3 group without including contributions from additional libration motions and the anisotropy in the scalar tensor. The shielding span is found to be 56 ppm. The width of the centerband in the $^{19}F\{^{1}H\}$ sample-spinning CP NMR spectrum is very sensitive to the angle between the rotor and the magnetic field, thus this sample is an attractive standard for setting the magic angle for NMR probes containing a fluorine channel with a proton-decoupling facility.

5.2 Organometallic and Coordination Compounds. – *^{11}B, ^{13}C* – The inclusion compounds formed between β-cyclodextrin (β-CD) and the tetrafluoroborate salts $[Cp'Mo(\eta^4\text{-}C_6H_8)(CO)_2]$ $[BF_4]$ and the neutral derivatives Cp′ $Mo(\eta^3\text{-}C_6H_7)(CO)_2$ [Cp′ = Cp ($\eta^5\text{-}C_5H_5$) have been studied by ^{13}C and ^{11}B MAS NMR.[135]

^{13}C – 1,11-bisbenzyl-5,7,7-trimethyl-1,4,8,11-tetraazaundeca-4-ene nickel(II) perchlorate has been studied using X-ray and ^{13}C CPMAS NMR.[136]

5′-GMP with Ca(II) and 5′-CMP with Cd(II) and Mg(II) complexes have been studied using ^{13}C CPMAS NMR.[137]

Four polymorphic forms of nickel(II) and two of zinc(II) dibenzoylmethanates have been characterized with solid-state ^{13}C CPMAS NMR and other techniques.[138]

A gallium citrate complex $(NH_4)_3[Ga(C_6H_5O_7)_2]\cdot 4H_2O$ has been studied by ^{13}C CPMAS NMR.[139] The number and intensities of the resolved resonances in the spectrum are found to be consistent with the X-ray structure.

^{13}C, ^{15}N – Crystal adducts of diethyldithiocarbamate complexes of zinc(II) and copper(II) with piperidine, and their solvated forms with the outer-sphere molecules of benzene, pyridine, and morpholine, have been characterized by EPR and high-resolution solid-state ^{13}C, ^{15}N NMR.[140]

^{13}C, ^{19}F – Copper(I) perfluorinated carboxylates complexes with 1,2-bis(diphenylphosphine)ethane have been characterized by ^{13}C, ^{19}F NMR in the solid state and by VT ^{31}P, ^{63}Cu NMR spectra in solution.[141]

^{13}C, ^{31}P – New copper(I) perfluorinated carboxylate complexes with bis(diphenylphosphine)methane have been characterized by ^{13}C and ^{31}P CPMAS NMR.[142]

^{13}C and ^{31}P CPMAS have also been employed to study a series of solid, peculiar ketenes, also known as η^1-ketenyl derivatives, bearing as substituents a PPh_3 moiety and a coordinatively unsaturated Pt(II) fragment.[143] The general utility of the CPMAS NMR technique in the study of unstable or insoluble complexes has been discussed.

^{15}N – Natural abundance ^{15}N CPMAS NMR has been shown to be a useful tool for investigating metal binding to nucleotides in the solid state.[144]

^{23}Na – A systematic solid-state ^{23}Na NMR study of sodium complexes with crown ethers, cryptands, and naturally occurring antibiotic ionophores has been reported.[145] Precise information about ^{23}Na QCCs and chemical shifts has been determined from analysis of ^{23}Na MAS NMR spectra. It has been shown that the experimental ^{23}Na chemical shifts can be related to an empirical parameter, *i.e.* a function of the atomic valence of the donor ligand, the Na^+-ligand distance, and the coordination number (CN) around the Na ion of interest. A reasonably good correlation has also been observed between the ^{23}Na quadrupole parameters measured in $CDCl_3$ solution and those measured in the solid state, indicating that the cation exchange is slow in $CDCl_3$.

^{31}P – The ^{31}P CPMAS technique has been used to establish the ratio between the amorphous and crystalline phases of deoxyxylo-thymidyl-3′-*O*-acetylthymidyl (3′,5′)-*O*-(2-cyanoethyl)phosphorothioate, and to test the progress of crystallization.[146] The differences in the ^{31}P δ_{33} principal elements of

the chemical shift tensor for crystalline and amorphous phases have been calculated.

Dithiophosphate zinc(II) complexes with eight different *O,O'*-dialkyldithiophosphate ligands have been studied by means of ^{31}P CPMAS NMR.[147] All ^{31}P resonances, corresponding to dithiophosphate ligands with different structural functions (*i.e.* terminal chelating or bridging between two metal atoms in bi- and tetranuclear complexes), have been assigned on the basis of comparative analyses of chemical shift data for solid complexes, their melts and chloroform solutions at various concentrations. In addition, novel molecular and crystal structures of the binuclear *O,O'*-dicyclohexyldithiophosphate zinc(II) complex have been resolved by single-crystal X-ray diffraction analysis, and useful correlations with ^{31}P NMR data for this complex have been obtained.

Dimeric phenoxide derivatives of zinc and cadmium have been characterized in the solid state using ^{31}P CPMAS NMR.[148]

Three-coordinate, monomeric 1:2 complexes of tribenzylphosphine (PBz_3) with copper(I) halides, $[Cu(PBz_3)_2X]$ (X = Cl, Br or I), have been synthesized and characterized by single crystal structure determinations and solid-state ^{31}P CPMAS NMR.[149] The two PBz_3 ligands show different conformational structures and this is reflected in a distorted 'P_2CuX' geometry for each complex. Solid-state ^{31}P CPMAS spectra show asymmetric quartets with $^1J(^{31}P–^{63}Cu)$ ranging from 1.23 to 1.46 kHz.

5.3 Natural Products. – *^1H, ^{13}C* – Solid-state NMR and FTIR have been used to study the degradation of cellulose in the form of transformer insulating paper and Whatman filter paper.[150] The NMR studies included ^1H wide line T_1 and $T_{1\rho}$ measurements and ^{13}C MAS experiments. The ^1H spectra and relaxation times have indicated the presence of absorbed water and oxygen in the papers. The ^{13}C-NMR spectra and FTIR spectra indicated the formation of aromatic structures on degradation above 250 °C, the conversion being essentially complete at 450 °C.

^2H – Mobility of water in cellulose has been studied by solid-state ^1H and high-resolution ^2H NMR as a function of moisture content within the unfreezable moisture range (0–19% dry basis).[151] Measurements of relative mobilities were based on relative intensities, transverse and longitudinal relaxation times and line shape analysis. At 2–16% moisture content (dry basis), water molecules reoriented anisotropically, suggesting an interaction with cellulose fibers. At moisture content below the monolayer value (2.8%, dry basis), 90% of the protons were immobile and no liquid deuterium signal was detected. A sharp increase in liquid or mobile ^1H intensity (accompanied by a decreased LW) and increases in ^2H NMR T_1 and T2 relaxation times were observed as moisture increased above 9% (dry basis).

^{13}C – Cellulose from flax, hemp, kenaf and sorghum has been investigated by solid-state NMR, vibrational spectroscopy and X-ray diffractometry. CPMAS ^{13}C NMR revealed the presence of I-α and I-β forms in all the samples.[152] The progressive loss in the crystalline phase is evidenced by ^{13}C

CPMAS T_1 measurements; ^{1}H CPMAS $T_{1\rho}$ measurement revealed an analogous loss in phase dimension for the ordered phase, but similar dimension values for the paracrystalline and amorphous phases.

Solid state ^{13}C NMR techniques have also been applied to study structures of (+)-catechin–formaldehyde reaction products (Stiasny precipitates) under strong acid conditions on the basis of the ^{13}C chemical shifts of (+)-catechin,[153] Eucalyptus tar pitches and their polymerization products characterized,[154] changes in cellulose fibril aggregation during kraft pulping and drying of kraft pulps,[155] and effects of dehydration on the crystalline structure and strength of developing cotton fibers.[156]

High-resolution solid-state ^{13}C NMR has been applied for the qualitative and quantitative analysis of the supramolecular structure and the quantitative phase analysis of Na-cellulose as an intermediate in cellulose ether manufacturing.[157]

Solid-state ^{13}C NMR has been used in the molecular characterization of the undegraded wheat straw and degraded samples.[158] The ^{13}C NMR spectra confirmed the increase in carboxyl content but indicated that the overall lignin and methoxyl contents remained relatively constant, although some nonsystematic variations were observed. The spectra also showed a decrease in amorphous noncellulosic polysaccharides in relation to the crystalline cellulose upon degradation.

Photoyellowing of lignocellulosic materials has been studied with a new technique based on solid-state ^{13}C NMR analysis of ^{13}C-enriched dehydrogenation polymer in cell wall tissue.[159] The ^{13}C NMR analysis of unirradiated and irradiated tissue revealed a decrease in the relative amount of coniferaldehyde and/or coniferyl alcohol end-groups during irradiation.

A detailed CPMAS ^{13}C NMR study of supermolecular changes in the cellulose and hemicellulose structure during kraft pulping has been described.[160] Two consecutive changes in the supermolecular structure have been observed in the CPMAS ^{13}C NMR spectra of the pulps as cooking proceeds: an increase in cellulose crystallinity and a change in order and/or structure of hemicellulose. A gradual change in the spectral behaviour of the hemicelluloses has been observed during the kraft pulping as a consequence of changes in intermolecular aggregation of the hemicelluloses.

The structure of a crystalline form of *Bombyx mori* silk fibroin (silk I) has been investigated using wide angle X-ray scattering and ^{13}C CPMAS NMR.[161] This study has been further extended using 2D spin-diffusion NMR under off MAS and REDOR.[162] A sequential peptide $(Ala\text{-}Gly)_{15}$ was used as a model. The torsional angles of $(Ala\text{-}Gly)_{15}$ with the structure similar to that of silk I were determined. The formation of the intra-molecular hydrogen bonding along the chain was confirmed from REDOR NMR by determination of the inter-atomic distance between the nitrogen and carbon atoms comprising the intra-molecular hydrogen bonding.

^{13}C, ^{15}N – The degree of acetylation of various samples has been evaluated by ^{1}H liquid-state NMR and ^{13}C and ^{15}N CPMAS solid-state NMR.[163] The ^{13}C and ^{15}N CPMAS experiments have allowed the evaluation of the chitin

degree of acetylation and content in the structural polysaccharides in a fungus named *Aspergillus niger*. The fungus structural carbohydrates mainly consist in pure chitin associated with glucans.

5.4 Biochemical, Medical and Pharmaceutical Applications. – *5.4.1 Proteins.* *^{2}H* – Proton magnetic spin–lattice relaxation in the effective field ^{2}H acting in the doubly rotating frame (DRF) was first applied to the study of slow internal protein dynamics in the submillisecond range of correlation times in the solid state.[164] In this method the local dipolar magnetic field is reduced by the magic-angle rotating-frame method so that the resonance frequency of the relaxation experiment may be set below the value of the local field. The measurements of the spin–lattice relaxation time in the DRF within a wide temperature range have been performed in dry and hydrated α-crystallin powders. This is the major protein in the eye lens. The results demonstrate that the protein hydration does not change the amplitude of slow side-chain motions but significantly shortens its correlation time: from about 50 to about 0.5 ms in dry and hydrated samples, respectively.

^{13}C – CPMAS solid-state NMR has been used to investigate the dependence of ^{13}C sugar chemical shifts on specific conformational parameters of a variety of ribonucleotides and ribonucleosides. The distinct effects of sugar puckering on the C_1', C_4', and C_5' resonances of C_2' endo (S type) and C_3' endo (N type) furanoid conformations allow us to separate them into two groups.[165]

Solid-state ^{13}C NMR spectroscopic methods were used to investigate changes in maize and sorghum proteins on wet cooking and popping.[166] Solid-state ^{13}C NMR, using the technique of CP/MAS, showed shifts of the protein carbonyl carbon and α-carbon resonances upfield on cooking in all samples, also indicating a change in protein secondary structure from α-helical to β-sheet conformation.

^{13}C, ^{15}N – 1D and 2D solid-state NMR experiments on a uniformly labeled intrinsic membrane–protein complex at ultra-high magnetic fields are presented.[167] 2D backbone and side-chain correlations for a [U-^{13}C,^{15}N] labeled version of the LH2 light-harvesting complex indicate significant resolution at low temperatures and under MAS. Tentative assignments were attributed to the α-helical segments of the protein.

The backbone and side-chain ^{13}C and ^{15}N signals of a solid 62-residue (U-^{13}C,^{15}N)-labelled protein containing the α-spectrin SH_3 domain were assigned by 2D MAS ^{15}N–^{13}C and ^{13}C–^{13}C dipolar correlation spectroscopy at 17.6 T.[168] The side-chain signal sets of the individual amino acids were identified by 2D ^{13}C–^{13}C proton-driven spin diffusion and dipolar recoupling experiments.

Low-temperature ^{15}N and ^{13}C CPMAS NMR has been used to analyze BChl–histidine interactions and the electronic structure of histidine residues in the light-harvesting complex II (LH2) of *Rhodopseudomonas acidophila*.[169] Comparison of the 2D MAS NMR homonuclear (^{13}C–^{13}C) dipolar correlation spectrum of [^{13}C(6),^{15}N(3)]-histidines in the LH2 complex with model systems in the solid state reveals two different classes of electronic structures from the

histidines in the LH2. ^{15}N–^{13}C double-CPMAS NMR data provide also evidence for the electronic structure of the histidines.

^{13}C, ^{31}P – A combination of solid-state ^{31}P and ^{13}C NMR, X-ray diffraction, and model building is used to show that the B and C forms of fibrous macromolecular DNA consist of two distinct nucleotide conformations, which correspond closely to the BI and BII nucleotide conformations known from oligonucleotide crystals.[170]

5.4.2 Peptides. ^{2}H – The correlation of deuterium quadrupolar tensors by spin diffusion under slow magic-angle-spinning conditions can provide accurate measurements of their relative orientation.[171] This work showed the technique applied to the cyclo-β-peptide cyclo[(*S*)-β-homoalanyl-(*R*)-β-homoalanyl-(*S*)-β-homoalanyl-(*R*)-β-homoalanyl] with its amide hydrogens labeled by deuterons. From the 2D spin-diffusion spectrum, the mutual orientation of the amide deuteron quadrupolar coupling tensors were found. Eight conformations that are all consistent with the NMR measurement were determined.

^{13}C, ^{15}N – ^{13}C–^{15}N interatomic distances of mono-dispersed sequential oligopeptides, [1-^{13}C]Leu(8 [^{15}N]Ala(12)-labeled (Phe-Leu-Ala)(6) were determined, and a variety of its derivatives in which Leu, at the residue 11, was replaced by Ala, Phe, Gly or D-Ala, by means of rotational echo double resonance (REDOR) experiments.[172]

Cells of the abscission zone of a monocotyledon fruit, the oil palm *Elaeis guineensis* have been studied by solid state ^{13}C CPMAS NMR.[173]

Solid-state ^{13}C CPMAS spectrum of the fibroin prepared from cocoons spun by larvae fed with [^{13}C]formate revealed that serine C_3 was labelled specifically with ^{13}C, suggesting that the reverse conversion from glycine into serine took place in the silkworm.[174]

Ternary phase diagrams have been constructed of systems with dioleoylphosphatidylcholine (DOPC) and water, and two α-helical membrane-spanning model peptides, KKLAKK16[KK(LA)(6)KK] and KKLAKK20[KK(LA)(8) KK].[175] When MAS ^{31}P NMR experiments were performed on samples four different isotropic chemical shifts were observed. The isotropic chemical shifts could be assigned to the phases, using spinning sidebands to calculate the CSA corresponding to each isotropic shift. MAS ^{13}C NMR also indicated a difference in the aggregational state of the peptides. ^{2}H solid-state NMR structural and dynamic studies of biotinylated gramicidins have been performed.[176]

5.4.3 Lipids and Membranes. Mastoparan X was studied by both high-resolution and solid-state ^{2}H NMR techniques to determine the structure and orientation of MPX when associated with bicelles.[177] Membrane elasticity in the presence of cholesterol and detergents.[178]

Solid-state NMR line shape, carbonyl chemical shifts and 2D exchange of protein backbone carbonyl nuclei were applied to structural studies of the membrane-bound HN-I fusion peptide.[179]

^{2}H – Location and dynamic reorientation of the fluorophore 7-nitrobenz-2-

oxa-1,3-diazol-4-yl (NBD) covalently attached to a short (C6) or a long (C12) sn2 acyl chain of a phosphatidylcholine molecule was investigated by fluorescence and solid-state NMR. ^{2}H NMR lipid chain order parameters indicate a perturbation of the phospholipid packing density in the presence of NBD.[180] Solid-state ^{2}H NMR was used to study and characterize the conformation and order of bolaform lipid membranes. A series of ^{2}H-labeled bolaform phosphatidylcholines has been synthesized and their properties compared to a [D-4] dimyristoylphosphatidylcholine (DMPC) and a [D-8]-32 macrocyclic phosphatidylcholine.[181] ^{31}P NMR measurements establish that the aqueous dispersions of these lipids adopt lamellar phases. Solid-state ^{2}H NMR was used to study the reorientation of magnetically ordered bicelles in the presence of the paramagnetic lanthanide Eu^{3+}.[182] Bicelles were composed of 1,2-dimyristoyl-sn-glycero-3-phosphocholine (DMPC) plus 1,2-dihexanoyl-sn-glycero-3-phosphocholine plus either the anionic lipid 1,2-dimyristoyl-sn-3-phosphoglycerol or the cationic lipid 1,2-dimyristoyl-3-trimethyl ammonium propane. Mastoparan X was studied by both high-resolution and solid-state ^{2}H NMR techniques to determine the structure and orientation of MPX when associated with bicelles.[177]

$^{2}H,^{13}C$ – Bicelle-forming mixtures of short-chain 1,2-dicaproyl-sn-glycero-3-phosphocholin (DHPC) and long-chain 1,2-dimyristoyl-sn-glycero-3-phosphocholine (DMPC) exhibit complicated phase behaviour.[183] The phase state of both lipids and the alignment of lipid monolayers in the magnetic field were determined by solid-state ^{2}H and ^{31}P NMR. MAS nuclear Overhauser effect ^{1}H NMR spectrometry revealed intensive intermolecular cross-relaxation among DMPC and among DHPC molecules but no detectable magnetization exchange between DMPC and DHPC.

Solid state NMR line shape, carbonyl chemical shifts and 2D exchange of protein backbone carbonyl nuclei were applied to structural studies of the membrane-bound HN-I fusion peptide.[179]

$^{2}H,^{13}C$ – This study reports the solid-state NMR spectroscopic characterization of a long chain phospholipid bilayer system which spontaneously aligns in a static magnetic field.[184] Magnetically aligned phospholipid bilayers or bicelles are model systems which mimic biological membranes for magnetic resonance studies with ^{2}H and ^{31}P NMR. Paramagnetic lanthanide ions (Yb^{3+}) were added to flip the bilayer discs such that the bilayer normal was parallel with the static magnetic field.

^{13}C – 11-*Z*-[8,9,10,11,12,13,14,15,19,20-^{13}C(10)]Retinal prepared by total synthesis was reconstituted with opsin to form rhodopsin in the natural lipid membrane environment.[185] The ^{13}C shifts are assigned with MAS NMR dipolar correlation spectroscopy in a single experiment and compared with data of singly labeled retinylidene ligands in detergent-solubilized rhodopsin. The use of multispin labeling in combination with 2D correlation spectroscopy improves the relative accuracy of the shift measurements. Accumulation of cholesteryl esters (CEs) is a key event in the formation of aeherosclerotic plaques.[186] Total CEs quantified by ^{13}C MAS (NIAS) NMR in excised plaques from human carotid arteries and rabbit aortic arteries were in good agreement

with the amounts determined by subsequent standard chemical assays. Combining MAS and off-MAS NMR isotropic (liquid), CEs from anisotropic (liquid-crystalline) CEs in plaque tissues were distinguished.

^{15}N – Solid-state NMR was employed to study the molecular dynamics of the colicin Ia channel domain in the soluble and membrane-bound states.[187] In the soluble state, the protein executes small-amplitude librations in the backbone and larger-amplitude motions in the side chains. Upon membrane binding, the motional amplitudes increase significantly for both the backbone and side chains as manifested by the reduction in the C–H and H–H dipolar couplings and ^{15}N CSA. These motions occur not only on the pico- to nanosecond time scales, but also on the microsecond time scale, as revealed by the ^{1}H rotating frame-spin–lattice relaxation times. It was proposed that the large mobility of the membrane-bound colicin Ia channel domain is a prerequisite for channel opening in the presence of a voltage gradient.

^{31}P – The composition of bovine casein micelles was analyzed by ^{31}P MAS solid-state NMR,[188] by looking at isotropic and anisotropic ^{31}P chemical shift parameters, resonance line shapes, the combination of single-pulse and ^{1}H to ^{31}P CP spectra.

The influence of melittin on two DMPA membrane systems at pH 4.2 and 8.2 has been investigated by solid-state ^{31}P and ^{2}H NMR, as a function of temperature and peptide concentration.[189] High-resolution ^{31}P MAS NMR is presented as a direct and non-perturbing method for measuring changes in surface charge density occurring in mixed phospholipid membranes upon binding of charged surface-active peptides.[190] ^{31}P MAS NMR was used to investigate mixed lipid membranes of neutral phosphatidylcholine and negatively charged phosphatidylglycerol.

5.4.4 Biomedical Applications. Spin–lattice relaxation times T_1 and T_{1d} as well as NMR second moment were employed to study the molecular dynamics of riboflavin (vitamin B-2) in the temperature range 55–350 K.[191] The broad and flat T_1 minimum observed at low temperatures is attributed to the motion of two non-equivalent methyl groups. The motion of the methyl groups is interpreted in terms of Haupt's theory, which takes into account the tunneling assisted relaxation.

^{1}H ^{31}P – High-resolution solid-state NMR was used for a better understanding of bone structure and bone implant.[192] In particular it is efficient to estimate osteoformation *via* bioceramics bone colonization using ^{1}H and ^{31}P NMR.

^{2}H ^{13}C ^{15}N – Several biologically active derivatives of the cardiotonic steroid ouabain have been made containing NMR isotopes (^{13}C, ^{2}H, and ^{19}F) in the rhamnose sugar and steroid moieties.[193] Deuterium NMR spectra of ^{2}H-labeled inhibitors revealed that the sugar group was only loosely associated with the binding site. CPMAS NMR showed that chemical shifts of inhibitors ^{13}C-labeled in the sugar group moved downfield by 0.5 ppm after binding to the digitalis site, suggesting that the sugar was close to aromatic side groups. A ^{19}F, ^{13}C-rotational-echo double-resonance NMR strategy was used to deter-

mine the structure of an inhibitor in the digitalis receptor site, and it showed that the ouabain derivatives adopt a conformation in which the sugar extends out of the plane of the steroid ring system.

^{13}C, ^{15}N – For powder diffraction data determination the key step is the generation of reliable trial structures for final refinement.[194] The subject of the study reported here is the pharmaceutical material anhydrous theophylline (3,7-dihydro-1,3-dimethyl-1*H*-purine-2,6-dione), which contains both oxygen and nitrogen as possible hydrogen bond acceptor atoms. Solid-state NMR spectra of a commercial sample not only confirmed immediately that there was only one molecule in the crystallographic asymmetric unit but also produced distinctive ^{13}C and ^{15}N chemical shifts.

5.5 Coal, Soil Organic Matter and Other Related Materials. – *5.5.1 Coals and Carbonaceous Materials. ^{13}C* – The extract from carbon disulfide/*N*-methyl-2-pyrrolidinone mixed solvent extraction of Upper Freeport coal at room temperature has been fractionated with acetone and pyridine into three fractions, and solid-state ^{13}C NMR measurements of these fractions have been measured.[195]

Carbonaceous compounds deposited on aluminosilicate mesoporous molecular sieves of the MCM-41 type during conversion of cyclohexene at various temperatures have been investigated using ^{13}C solid-state NMR and other techniques.[196]

It has been shown that detailed structural information on carbonaceous solids with complex molecular structures may be obtained using a combination of three advanced solid-state NMR techniques, *i.e.*, dipolar dephasing with variable dephasing times, ^{13}C CPMAS spectral editing, and an isotropic–anisotropic correlation experiment called PHORMAT.[197] The possibility of determining the ratio of protonated to non-protonated aromatic carbons with high accuracy has been demonstrated by the conventional dipolar dephasing experiment with variable dephasing times.

Carbon materials produced through the thermal decomposition of biomass (rice hulls) and a polymer (poly(vinyl chloride) have been investigated by ^{13}C high-resolution solid-state NMR using two different magnetic fields (2.0 and 9.4 T).[198]

5.5.2 Soils. ^{13}C – The structural composition of soil organic matter (SOM) has been determined in 27 soils with different vegetation from several ecological zones of Australia and Pakistan using solid-state ^{13}C CPMAS NMR.[199]

Binding of protons, Cu(II) and Pb(II) to a soil fulvic acid, humic acid, and two different size fractions of the humic acid has been investigated solid-state ^{13}C NMR combined with other techniques.[200]

The study of SOM, and dissolved organic carbon (DOC) in soil solutions and stream samples in clear-cut and uncut sites at the Hubbard Brook Experimental Forest in New Hampshire using DOC fractionation techniques and solid-state ^{13}C NMR has been presented.[201]

The molecular composition of fulvic acid and humic acid fractions from a German natural lake have been characterized by solid-state ^{13}C NMR.[202]

Solid state CPMAS ^{13}C NMR study of the insoluble organic fraction isolated by HF/HCl treatment under an inert atmosphere from the Orgueil and Murchison carbonaceous meteorites has been reported.[203]

A method has been developed to demineralize sediment trap material and marine sediments containing labile organic matter, in preparation for solid-state ^{13}C CPMAS NMR analysis.[204]

Using solid-state ^{13}C NMR the chemical structure of organic carbon in both surface plankton and sinking particulate matter from the Pacific Ocean and the Arabian Sea has been characterized.[205]

Humic acids extracted from olive mill pomace after a certain number of days of composting have been studied using ^{13}C CPMAS NMR.[206]

Dipolar dephasing has been investigated as a means for quantitatively differentiating protonated and non-protonated and molecularly mobile and rigid components in soil organic matter.[207] Cellulose, hemicelluloses, lignin, a protein, chitin, charcoal, palmitic acid and two waxes have been used as model systems for components of soil organic matter.

Black carbon (BC), occurring ubiquitously in soils and sediments, and produced by incomplete combustion of fossil fuels and vegetation, has been studied using ^{13}C MAS NMR and other techniques.[208]

Six soil organic matter fractions have been characterized using liquid- and solid-state ^{13}C NMR.[209]

New information on the chemical structure of a peat humic acid has been obtained using a series of 2D ^{1}H–^{13}C solid-state NMR HETCOR experiments with different contact times and with spectral editing by dipolar dephasing and ^{13}C transverse relaxation filtering.[210]

^{15}N – Soil contaminated with 2,4,6-trinitrotoluene (TNT) and spiked with [^{14}C]- and [$^{15}N_3$]-TNT has been subjected to an anaerobic–aerobic soil slurry treatment and subsequently analyzed by radiocounting and solid-state ^{15}N NMR.[211]

Humic isolates from different layers of an organic matter rich algal sapropel from Mangrove Lake, Bermuda, have been analyzed using solid-state ^{15}N NMR in order to reveal chemical structural interrelationships that allow delineation of diagenetic pathways.[212]

5.6 Polymers. – *^{1}H* – Blends of poly(vinylphenol-co-methyl methacrylate) (PVPh-co-PMMA) with poly(ethylene oxide) (PEO) were prepared by solution casting from tetrahydrofuran (THF) solution.[213] The miscibility behaviour and hydrogen bonding of blends were investigated by many techniques, including solid-state NMR. Experimental results indicate that PEO was miscible with PVPh-co-PMMA. Solid-state NMR reveals single-exponential decay of proton spin–lattice relaxation times in the rotating frame ($T_{1\rho}(H)$) in the amorphous PVPh-co-PMMA phase. Quantitative characterization of the inner structure of core-shell latex particles by ^{1}H solid-state NMR has been reported.[214]

High-resolution proton DQ MAS NMR is used as a new technique that is capable of revealing complex motional processes in entangled polymer melts.[215] Theoretical analysis shows the connection of quantities relating anisotropic polymer dynamics to data obtained from our DQ-MAS NMR experiment. With this technique, dynamic chain ordering as well as scaling laws consistent with the reptation model was previously observed for polybutadiene (PB).

This work investigates the behaviour of elastomeric chains (polybutadienes of identical molecular weight but different microstructures) in the close vicinity of carbon black surfaces in order to attain a better understanding of the structure and properties of interphases.[216] Elastomer–filler interactions are assessed through the study of the thermal properties and NMR relaxation characteristics of the corresponding materials. ^{1}H MAS solid-state NMR provides information on the effect exerted by polymer–filler interactions on the mobility of the various constitutive species of the macromolecular backbone.

The shape of the solid-state proton NMR free induction decay (FID) of a molten polyethylene (PE) sample has been examined as a function of time during isothermal crystallization *in situ*.[217] The crystallization rate as a function of crystallization temperature is derived and the results discussed within a thermodynamic framework.

Polyelectrolyte multilayers on silica colloids are investigated here using a combination of fast MAS and DQ solid-state ^{1}H NMR techniques.[218] 2D DQ ^{1}H NMR spectra of the bulk complex and the multilayer films are found to be similar, revealing complexation between the alternating layers of poly(sodium 4-styrenesulfonate) (PSS) and poly(diallyldimethylammonium chloride) (PDADMAC).

Curing and thermal ageing of EPDM synthetic elastomers has been studied using both ^{13}C high-resolution and ^{1}H wideline solid-state NMR experiments based on structural and dynamic parameter measurements.[219]

The miscibility of poly(4-vinylpyridine) (P4VP) with poly(4-vinylphenol) (PVPh) blends was investigated over a wide range of compositions by other techniques and high-resolution solid-state NMR.[220] Relaxation times were studied as a function of blend composition. T_1(H) and $T_{1\rho}$(H) results demonstrate that the spin diffusion can completely average out the entire relaxation process. It was also found that the intimate mixing of the polymer blends restricts the local chain mobility.

This article establishes the processing-microstructure-motion-property relationship of high-speed melt-spun nylon-6 fibers.[221] Solid-state ^{1}H NMR $T_{1\rho}$ relaxation studies were used to study the structure.

The network structure of W-cured acrylates was analyzed by dynamic mechanical experiments, ^{1}H T_2 NMR relaxation, and ^{13}C NMR.[222]

Solid-state ^{1}H – ^{19}F-CPMAS, ^{19}F – ^{1}H CPMAS, and ^{1}H fast MAS NMR spectra have been investigated for a semicrystalline polymer, namely poly(vinyl fluoride) (PVF), together with its solution-state ^{19}F spectrum and static solid-state ^{1}H pulsed and broad line NMR measurements.[223]

^{2}H – Deuterium solid-state NMR techniques at high pressure are used to

study the chain dynamics in the amorphous polymer atactic polypropylene.[224] The arrest of the structural relaxation above the glass-transition temperature T_g was investigated using 1D and 2D deuteron NMR spectra.

The interface in composite materials containing an ultrathin layer of poly(methyl acrylate)-d(3) (PMA-d(3)) on silica was studied using deuterium NMR.[225]

^{13}C – The phases of *n*-butylvinyl ether (C_4VE) and *n*-octadecylvinyl ether (C18VE) crosslinked with triethylene glycol divinyl ether or divinylbenzene were investigated by means of solid-state ^{13}C CPMAS NMR and ^{1}H HR MAS NMR in suspended-state.[226]

Different hydrogen-bonded states of OH groups in poly(vinyl alcohol) (PVA) films with different tacticities have been characterized by ^{1}H combined rotation and multiple pulse spectroscopy (CRAMPS),[227] solid-state ^{13}C NMR and 2D (2D) ^{1}H–^{13}C HETCOR analyses.

The hydration process and resulting hydrogen bonding for atactic poly(vinyl alcohol) (A-PVA) films have been investigated by high-resolution solid-state NMR.[228]

High-resolution solid-state ^{13}C CPMAS NMR was used to study the evolution of a polysaccharide (scleroglucan) conformation from the anhydrous to the hydrated form.[229]

A hydroxy-terminated polybutadiene (HTPB)/isophorone diisocyanate (IPDI) elastomer is commonly used as propellant binder material.[230] Solid-state NMR relaxation times have been used as a means to predict the mechanical properties of the binder as a function of ageing time.

The microstructure of segmented block copoly(ether esters) composed of poly(tetramethylene oxide) (PTMO) 'soft' blocks and poly(butylene terephthalate) (PBT) 'hard' blocks was investigated by a variety of analytical techniques, including ^{13}C solid-state NMR.[231]

The chemical structures of two poly(*p*-phenylene vinylene) (PPV) derivatives, one a copolymer formed by a random succession of phenylene vinylene and ether groups and the other characterized by a pendant side chain containing ether groups, were characterized by ^{13}C solid-state NMR and other techniques.[232]

Cyclic olefin copolymer (COC, poly(norbornene-co-ethylene)) catalyzed by ansa-ethylenebis-(indenyl)zirconium dichloride ($Et[Ind](2)ZrCl_2$)/methylaluminoxane (MAO) gives rise to phenomenal increase of T_g upon annealing. Unaveraged solid-state ^{13}C NMR resonance of the CH carbons in the norbornene (53 and 49 ppm) evidenced the different conformation conversions.[233]

Two resole-type phenol formaldehyde resins were synthesized and their structure on curing examined by ^{13}C CP-MAS solid-state NMR.[234]

The results of a study of the relation between the oriented structure and drawn poly(ε-caprolactone) specimens including $CaCO_3$ particles, their dynamic mechanical properties and line shape analyses of ^{13}C CP MAS NMR spectra are presented.[235] Solid state studies of ^{13}C NMR study of poly(methyl acrylate) ionomer have been reported.[236]

Novel model compounds based on 3,5-dimethylphenol were used to deter-

mine the structure of graphitisable 3,5-dimethylphenol resins which ^{13}C CP-MAS NMR showed to have a predominately linear structure, highly condensed but with few crosslinks.[237]

The rotating-frame spin–lattice relaxation time for protons, $T_{1\rho}$,(^{1}H), was measured indirectly from ^{13}C CPMAS/DD NMR to probe possible molecular scales of heterogeneity in the miscible poly(benzyl methacrylate)/poly(ethylene oxide) blend over the whole composition range.[238]

The light stability of wood panel treated with acetic anhydride, succinic anhydride, maleic anhydride, and phthalic anhydride was compared. Results from the solid state CPMAS ^{13}C NMR analyses revealed that the esterification of holocelluloses occurred mainly at the C-6 position in the amorphous cellulose component.[239]

Solid-state carbon NMR with MAS has been used to study the structure and dynamics of semicrystalline polycaprolactone (PCL) and its inclusion complexes formed with α- and γ-cyclodextrins (α- and γ-CDs), which are shown to have channel structures occupied by single and two parallel, side-by-side chains, respectively.[240]

Greatest drawability was studied for blend films with branched low molecular weight polyethylene (B-LMWPE) and ultra-high molecular weight polyethylene (UHMWPE) prepared by gelation/crystallization from solutions. The morphology of B-LMWPE–UHMWPE dry gel film was determined by solid-state ^{13}C NMR and other techniques.[241]

The relationship between the morphology and the mechanical properties of copolymer ethylene–methyl methacrylate (EMMA) was estimated as a function of temperature by using polarized light scattering, X-ray diffraction and ^{13}C solid-state NMR.[242]

Structural changes during the creep process of ultrahigh-strength polyethylene fiber (UHSPE) were investigated using X-ray and the solid-state NMR techniques. As the creep strain increases, the quantity of the amorphous phase area estimated by the ^{13}C NMR method increases until the final creep rupture.[243]

The conformation and molecular mobility of the noncrystalline chains for syndiotactic polypropylene (sPP) samples well crystallized have been characterized at different temperatures by high-resolution solid-state ^{13}C NMR.[244] The purposes are to investigate the cause inducing the high *trans* fraction of sPP chains in the noncrystalline state just after quenching at 0 °C from the melt and to know some correlation with the crystallization of form III with the planar zigzag conformation around 0 °C.

The morphology and mechanical properties of PVA were studied using atactic poly(vinyl alcohol) (at-PVA) dry gel films prepared by crystallization from solutions in dimethyl sulfoxide and water mixtures. The ^{13}C NMR measurements suggested changes in the hydrogen bonds.[245]

Synthesis of polydiacetylenes from novel monomers having two diacetylene units linked by an arylene group were characterized by solid-state ^{13}C NMR.[246]

Poly(ethylene-co-acrylic acid) copolymers (*i.e.*, $(-CH_2CH_2-)(x)[CH_2CH$

(CO^2H)](y)) with different levels of acrylic acid were synthesized and covalently bonded to silica *via* glycidoxypropyl or aminopropyl linkages. ^{13}C CPMAS NMR was used to characterize the new reversed-phase materials.[247]

The structure of laboratory-made polyhigh internal phase emulsion (poly-HIPE) was successfully characterized by CPMAS, solid-state ^{13}C NMR experiments.[248]

A copolymer based on α-methylstyrene was investigated by NMR. The styrene-co-α-methylstyrene was analyzed by solution and solid-state NMR techniques.[249]

A series of ethylene–vinyl alcohol copolymers (EVOH) with different comonomer contents were studied by both solution state and solid-state high-resolution ^{13}C-NMR.[250]

Three kinds of aromatic poly(amic acid)s that contain acetylene groups in the main chain were cured in air at temperatures up to 400 °C to give intermolecular crosslinked polyimides. The crosslink reactions occurred at the internal acetylene units and the chemical structures thus generated have been investigated by high resolution solid-state ^{13}C CPMAS NMR.[251]

A detailed analysis of the temperature dependent solid-state ^{13}C MAS NMR spectrum of a low molecular weight polyethylene fraction that was isothermally crystallized in extended chain forms is reported.[252]

The crystallization process of syndiotactic polypropylene (sPP) quenched from the melt or concentrated solutions has been investigated by high-resolution solid-state ^{13}C NMR in order to make clear the formation of the planar zigzag form at 0 °C.[253]

NMR spectroscopy in solution and solid state was applied to obtain the response of the chemical behavior of commercial poly(α-methylstyrene).[254]

The structure and thermal behavior of two organometallic polymers, poly (ferrocenyl dimethylsilane) (I) and poly(ferrocenyl di-*n*-butylsilane) (II), have been characterized by solid-state ^{13}C NMR spectra acquired for a wide range of ^{1}H–^{13}C contact times.[255]

^{13}C spin–lattice relaxtion times for polystyrene nanolatex particles were investigated. It was found that the dramatic increase at 80 degrees annealing temperature is well below the T_g temperature of bulk polystyrene, the increase of relaxation time of aromatic carbons is larger than that of for aliphatic carbons at transition annealing temperature.[256]

Blend films of poly(L-lactide) (PLLA) and poly(vinyl alcohol) (PVA) were synthesized. The component interaction, crystallization behavior, and miscibility of these blends were studied by solid-state NMR.[257]

The liquid study of propargylic monomers during heat treatment has shown the formation of secondary phenolic products in the reaction mixture and solid-state ^{13}C CPMAS NMR has confirmed the structure of the final polymer.[258]

The first direct evidence for second-order nonlinearity in partially cross-linked polyacrylonitrile is reported. The crosslinking in γ-ray-induced polymerized neat acrylonitrile is supported by ^{13}C CPMAS solid-state NMR.[259]

Poly(dimethylsiloxane) and polyacrylonitrile have been observed to form inclusion complexes (ICs) with γ-cyclodextrin. CP-MAS ^{13}C-NMR spectra of

the ICs show that γ-cyclodextrin, in the presence of a polymer guest, adopts a more symmetric conformation when compared to its pure state.[260]

The ceramization process of poly(Si-isocyanato-Si-methylpolysilazane) (MPZ-6) was investigated by means of the ceramic yield on pyrolysis, carbon content analysis, and solid-state CPMAS NMR spectra.[261]

Insoluble diorganotin functionalized polymers of the type (P–H)(1 – *t*)(P–(CH_2)(*n*)SnBuX_2)(*t*), with *n* = 4, 6, X = Ph, Cl, and *t* being the degree of functionalization, P = crosslinked polystyrene support. The tin-functionalized polystyrenes were characterized by elemental analysis, IR, and Raman as well as solid-state ^{117}Sn and ^{13}C NMR.[262]

Carbon-13 spin–lattice relaxation times are measured for poly(octadecyl acrylate) above and below the melting point of the crystalline side chains.[263]

The behaviours of lithium ions in a polyether poly(urethane urea) (PEUU) were investigated by ^{13}C MAS solid-state NMR.[264]

Wang resin has been transformed into an initiator for copper(I)-mediated living radical polymerization of methacrylates. The immobilized initiator was characterized by gel phase ^{13}C NMR, and solid-state CPMAS ^{13}C NMR using two different spinning frequencies as well as a TOSS pulse sequence.[265]

Carbon-13 dynamic MAS NMR is used to determine the π-flip rates of the phenyl rings in the low-molecular-weight members of the polyaryl ethers series (phenyl-O(-phenylene-O)(*n*)-phenyl).[266]

^{19}F – The radiation chemistry of poly(tetrafluoroethylene-co-perfluoropropylene) copolymers has been studied using Co-60 γ-radiation at temperatures of 300 and 363 K. New structure formation in the copolymers was analysed by solid-state ^{19}F NMR.[267,268]

At MAS speeds above 5 kHz, two major fluorine-19 resonances can be resolved in the acid form of the perfluorosulfonate ionomer Nafion (DuPont trademark). Xenon-129 NMR is used as an alternative probe of morphologically based sorption environments in Nafion. The xenon-129 spectrum of xenon sorbed into Nafion under a pressure of 12 atm shows two resonances corresponding to two sorption environments.[269]

^{13}C ^{19}F – Solid-state ^{19}F high-speed MAS, ^{19}F CRAMPS, and ^{19}F–^{13}C CPMAS NMR spectra have been investigated for an amorphous fluoropolymer (CYTOP) having a five-membered heteroring in the main chain. In the ^{19}F MAS spectra, spinning at 35 kHz is necessary to ensure no spectral overlap of spinning sidebands (SSB) with the isotropic signals.[270] Sensitivity enhancement was carred out using solid-state ^{13}C NMR in synthetic polymers and biopolymers by ^{1}H NMR detection with high-speed MAS.[271]

5.7 Glasses and Amorphous Solids. – *^{1}H* Powdered samples of glasses with the composition 16 R^2O.10 CaO.74 SiO_2 (= Na, K, Cs) and a concentration of water in glass were studied by solid state ^{1}H MAS NMR.[272]

^{1}H,^{13}C,^{15}N – Since the prediction of the potential extraordinary mechanical properties of crystalline β-C_3N_4, many authors have attempted its synthesis. To aid this ^{1}H, ^{13}C and ^{15}N solid-state NMR measurements for the determination of the bonding types in amorphous CN_x films are given.[273]

$^{1}H, ^{19}F, ^{27}Al, ^{31}P$ – The crystallization of needle-like apatite from a glass ceramic of composition (mol%) 61.5 SiO_2–9.4 Al_2O_3–9.2 Na_2O–7.7 K_2O–6.0 CaO–1.9 P_2O_5– 2.5 F with minor additional components of CeO_2, ZrO_2, TiO_2, Li_2O and B_2O_3, was monitored by high-resolution solid-state NMR utilizing the magnetic moments of ^{1}H, ^{19}F, ^{27}Al, and ^{31}P.[274]

$^{1}H, ^{13}C, ^{29}Si$ – The preparation of amorphous inorganic networks in the system Si/B/N/C, starting from molecular single source precursors results in high performance ceramics with outstanding and unprecedented high temperature and mechanical properties. These were studied using conventional multinuclear ^{11}B, ^{13}C and ^{29}Si MAS NMR and advanced double resonance techniques such as ^{29}Si–{^{11}B} rotational echo adiabatic passage double resonance (REAPDOR), ^{13}C–{^{11}B} REAPDOR or ^{11}B–{^{29}Si} rotational echo double resonance (REDOR) NMR.[275]

$^{11}B, ^{15}N$ – Polyborazilene, a precursor for hexagonal boron nitride (h-BN) ceramics, has been extensively characterized by ^{15}N and ^{11}B MAS NMR.[276]

^{17}O – ^{17}O MAS NMR, non-spinning, ^{1}H-decoupled, ^{1}H-^{17}O CP, and triple-quantum MAS NMR experiments were performed at two different magnetic fields on crystalline potassium hydrogen disilicate ($KHSi_2O_5$) and hydrous and anhydrous potassium tetrasilicate ($K_2Si_4O_9$), sanidine ($KAlSi_3O_8$), and haplogranite ($KAlSi_3O_8$-$NaAlSi_3O_8$–SiO_2) glasses.[277]

A quantitative approach was applied to the 3Q-MAS spectra of ^{17}O to characterize a four-oxide sodium aluminoborosilicate glass composition and the alteration film that formed on its surface during aqueous alteration.[278]

^{27}Al – The structural and textural properties of 'Two-Phase Porous Silica' consisting of a mesoporous pore system formed by finely dispersed silica-gel inside the original pores of a macroporous glass framework have been carefully investigated by ^{27}Al MAS NMR.[279] Modern high-resolution NMR spectroscopic techniques were applied to study the local environments of several aluminium fluoride-based glasses and the model crystalline compound AlF3. Through the combined application of MAS, ^{27}Al triple-quantum MAS, as well as CPMAS and rotational echo double resonance methods, a physical model concerning the short-range order has been developed for the glasses.[280]

2D ^{27}Al MQ MAS NMR is used to extract the isotropic chemical shifts and quadrupolar parameters of five amorphous aluminosilicates, all of approximately mullite composition (3Al(2)O(3).2SiO(2)) but of widely differing synthetic origin. Three principal types of Al site are apparent in each sample: two of these are conventionally assigned to 4- and 6-coordinate Al, while the nature of the third site, observed at a shift of delta approximate to 30 ppm, remains a subject of debate.[281]

Glass-forming characteristics, properties and structural features of glasses in the La_2O_3-Al_2O_3-P_2O_5 system-have been investigated by ^{27}Al MAS NMR.[282]

^{27}Al MAS NMR spectra of 12 fluoroaluminate crystals with known crystal structures and $40AlF_{(3)}.(20-x)BaF_2.xBaCl_{(2)}.20CaF_{(2)}.17YF_{(3)}.3EuF_{(3)}$. glasses ($x = 0$, 3, 6, 9 and 12) in mol% were measured to examine the anion coordination environments around Al^{3+} in the glasses. All the glasses gave

NMR spectra with very similar line profiles, indicating that the anion coordination environments around Al^{3+} are almost the same, and that only F^- bonds to Al^{3+} regardless of the substitution of Cl for F.[283]

Solid-state ^{27}Al NMR studies have been carried out of the aluminium coordination environments in TaAl tellurite glasses containing from 60 to 95 cation-% TeO_2. These data show the presence of 4-, 5- and 6-coordinate aluminium in all glasses.[284]

$^{27}Al, ^{29}Si$ – Changes in the structural properties of sodium alumine-silicate glasses of general formula $Na_2O.xAl(_2)O(_3).(3-x)SiO_2$ were investigated as a function of Al_2O_3 concentration. The experimental evidences provided by density, elastic modulus, glass chemical resistance measures, ^{29}Si and ^{27}Al MAS NMR investigations were complemented by molecular dynamics simulations.[285]

Samples of impactite glass, known as Libyan Desert Glass (LDG), were analyzed by NMR MAS in order to study the coordination of silicon and aluminium.[286]

Various 1D and 2D high-resolution solid-state NMR techniques have been applied to hydrous silicate and aluminosilicate glasses: simple acquisition, CPMAS, HETCOR, dipolar dephasing, spin counting, DQ correlation, and rotational echo double resonance (REDOR).[287]

$^{27}Al, ^{31}P$ – Solid-state ^{31}P /^{27}Al and ^{31}P /^{23}Na TRAPDOR NMR experiments have been used to investigate the spatial distribution of aluminium and sodium cations with respect to the phosphate backbone for a series of sodium aluminophosphate glasses, $xAl(_2)O(_4).50Na(_2)O.(50-x)P_2O_5$ $(0 \leq x \leq 17.5)$.[288]

$^{27}Al, ^{71}Ga, ^{125}Te$ – The structures of M_2O_3-TeO_2 (M = Al and Ga) glasses have been investigated by means of ^{125}Te, ^{27}Al, and ^{71}Ga NMR spectroscopies. The structural units of respective cations in M_2O_3-TeO_2 glasses were quantitatively analyzed.[289]

^{29}Si – Lead silicate glasses having different mole ratios of SiO_2 to PbO and containing different amounts of alkali/alkaline earth metal oxides were prepared by conventional melt-quench method. The different structural units of Si present in these glasses were identified by ^{29}Si MAS NMR.[290]

High-resolution NMR has been used to measure relaxation times, T_1, in alkali silicate glasses. Two-component relaxation was observed in lithium silicate glasses. In glasses close to the sodium disilicate composition, the relaxation was one component but, with decreasing sodium content, this becomes two component. In heat-treated sodium silicate glasses two components appear to grow from the single component and the extent of growth depends upon the heat-treatment temperature and time.[291]

$^{29}Si, ^{31}P$ – Solid state ^{29}Si and ^{31}P MAS NMR have been used to investigate the microstructural changes occurring in phosphosilicate gels during their conversion from a gel into the corresponding gel-derived glasses by heating. The studied gels have the molar compositions $10P(_2)O(_5).90SiO(_2)$ and $30P(_2)O(_5).70SiO(_2)$.[292]

In SiO_2–Al_2O_3–CaO–P_2O_5–K_2O–F-glasses, either spherical or needle-like fluorapatite crystals can be formed depending on the heat-treatment schedule.

On the basis of the combination of ^{31}P MAS NMR spectrometry a crystallization model capable of explaining the morphology change is derived.[293,294]

^{31}P – 1D MAS and 2D DQ solid-state ^{31}P NMR investigations have been carried out on $(MgO)(x)(P_2O_5)(1-x)$ glasses over the compositional range from $x = 0.44$ to 0.59.[295]

An X-ray diffraction and ^{31}P MAS NMR study of rare-earth phosphate glasses of composition $(R_2O_3)(x)P_2O_5)(1-x)$ where $x = 0.175$–0.263 and R = La–Er (except for Pm), is presented. The structures of these materials were investigated as a function of (a) rare-earth atomic number and (b) glass composition. The results show an increase in rare-earth coordination number from six to seven as the rare-earth ion increases in size.[296]

$PbO–P_2O_5$ glasses have been reported in which part of the PbO or P_2O_5 has been replaced by Sb_2O_3 and characterized ^{31}P MAS NMR.[297]

The short- and intermediate-range order of the polyphosphate glass network of the composition $xZnO + (1-x)P_2O_5$ is investigated, with $0.35 \leq x \leq 0.80$. The short-range order is probed using ^{31}P solid-state MAS NMR, liquid-state NMR and Raman spectroscopy.[298]

^{109}Ag – ^{109}Ag MAS-NMR spectra of AgI-based glasses containing frozen α-AgI nanocrystals were measured extensively for $AgI–Ag_2O–M_xO_y$ ($M_xO_y = B_2O_3$, GeO_2) systems.[299]

An ^{109}Ag solid-state NMR study on $(AgI)(x)(AgPO_3)(1-x)$ glasses is reported. We demonstrate that, all over the glass formation region ($0 < x < 0.6$), the number of Ag carriers is nearly equal to the fraction of silver ions introduced by AgI.[300]

^{109}Ag NMR in the highly conductive glass was investigated from 230 to 433 K. The ^{109}Ag NMR spectra reveal for the first time three well-resolved lines corresponding to three kinds of chemically speciated Ag ions in sites with different chemical shifts in a macroscopically homogeneous glass.[301]

^{113}Cd – ^{113}Cd MAS NMR spectra of crystalline CdF_2, $KCdF_3$ and $CdCl_2$ with known crystal structures and vitreous $50CdF_2 \cdot 30NaCl \cdot (20-x)BaF_2 \cdot xBaCl_2$ have been measured to reveal the anion-coordination environments around Cd^{2+} in the glasses.[302]

5.8 Cements. – *^{29}Si, ^{113}Cd* – Two kinds of Cd-containing calcium silicates, Cd/Ca silicate hydrates prepared by coprecipitation and Cd-exchanged C–S–H, have been characterized by ^{29}Si and ^{113}Cd MAS NMR X-ray diffraction, and EXAFS.[303]

^{29}Si – Hydraulic activity of municipal solid waste incinerator fly-ash-slag-blended eco-cement has been investigated using X-ray diffraction and ^{29}Si MAS NMR.[304]

Various techniques, including ^{29}Si MAS NMR, have been used to follow the reactive evolution of the alkaline activated slag cements.[305]

5.9 Micro- and Mesoporous Solids. – *^{1}H, ^{29}Si* – The distribution and strength of the Brönsted acid sites in three Mu-14 samples with different Si/Al ratios (17, 28 and 35) have been studied by ^{1}H MAS, $^{1}H–\{^{27}Al\}$ TRAPDOR

(transfer of population in double resonance), ^{1}H–^{29}Si CPMAS and HETCOR.[306] The ^{1}H MAS NMR spectra exhibit two different types of bridging OH groups associated with proton chemical shifts of *ca.* 4.2 and 5.3 ppm. From the ^{1}H–^{29}Si HETCOR experiments a single Brönsted Q^3 site Si–$(OSi)_3(OAl)$, resonating at $\delta(^{29}Si) = -108$ ppm, can be distinguished from two different Q^3 sites Si-$(OSi)_3(OH)$, at $\delta(^{29}Si) = -101$ and -104 ppm, and one of the Q^4 sites resonating at $\delta(^{29}Si) = -108.5$ ppm.

^{13}C, ^{29}Si – Mesoporous silica materials (MCM-41) have been characterized by ^{13}C and ^{29}Si MAS NMR.[307] ^{13}C chemical shifts reveal a high content of *gauche* conformations in the chain of cationic surfactant molecules within the nanopores. Measured $T_1(^{13}C)$ and T_{CH} values have demonstrated that the surfactant inside the pores exhibits anisotropic motions progressively reduced from the chain end toward the polar head. VT ^{13}C MAS NMR spectra show a strong thermal dependence of the motions and highlight a gel-like aggregation of the surfactant. The transfer of magnetization from the surfactant protons to the silicons on the pore surface has been found to be efficient as observed by CP dynamics following the nonprotonated silicon atoms. Silicons and carbons receive magnetization from the same proton system, because of the unique $T_{1\rho}(^{1}H)$ measured from the ^{13}C and ^{29}Si experiments.

Siliceous MEL-type (silicalite-2) zeolite nanocrystals with average particle size of less than 100 nm have been investigated by ^{13}C and ^{29}Si MAS NMR.[308]

^{23}Na – ^{23}Na DOR NMR studies for intrazeolite anchoring of rhodium carbonyl clusters have been reported.[309]

^{23}Na, ^{27}Al, ^{29}Si – Barrerite from Alaska has been investigated by ^{29}Si, ^{27}Al and ^{23}Na MAS NMR both in its untreated and heated forms.[310] The chemical shift of the ^{29}Si NMR lines of the natural phase revealed the presence of three different Si(*n*Al) configurations. The ^{27}Al NMR signal of the natural phase, positioned in the region of tetrahedrally coordinated Al, becomes more shielded with increasing temperature, in agreement with the changes of the Al–O–Si bond angles caused by the distortion of the framework. Changes in the ^{27}Al NMR linewidth have also been correlated with the degree of dehydration at high temperature. The shift of the ^{23}Na resonance line towards higher fields in the heated phase has been interpreted as a consequence of the increased coordination number.

^{23}Na, ^{113}Cs – Through the application of high-temperature ^{23}Na and ^{133}Cs MAS NMR, the mobility of sodium and caesium ions in dehydrated zeolites Y and X in the sodium form, after exchange with caesium cations and after impregnation with caesium hydroxide, has been investigated.[311]

^{27}Al – Copper and zinc containing mesoporous molecular sieves Al-MCM-41 have been studied by ^{27}Al MAS NMR and other techniques.[312]

The dealumination of zeolite MCM-22 by calcination or hydrothermal treatment has been investigated by conventional multinuclear solid-state NMR and checked by ultrahigh-field NMR experiments (19.6 T) with a fast spin rate (19.1 kHz).[313] The presence or variation of different species, such as silanol nest, 4-coordinated framework, 6-coordinated and 5-coordinated extraframework aluminium, during or after dealumination has been detected, and their

changes have been followed. Four tetrahedral framework aluminium sites have been identified from the ^{27}Al MAS NMR experiments at 61.5, 57.0, 53.5, and 50.0 ppm.

Using ^{27}Al MAS and ^{27}Al MQ MAS NMR, dealumination of zeolite H-β has been observed at specific T-positions in the framework.[314] ^{27}Al MQ MAS NMR was able to resolve aluminium in the T_1 and T_2 positions from the other (T_3–T_9) positions in the framework. A quantitative analysis of the ^{27}Al MQ MAS NMR spectra has shown that aluminium atoms in positions T_1 and T_3 resist dealumination and do not adopt an octahedral coordination. It has also been shown that a heat treatment of NH_4-β gives a single type of fairly symmetric framework octahedral aluminium, which can be reconverted into framework tetrahedral aluminium by ammonia treatment.

^{27}Al, ^{31}P – Novel alumina-pillared γ-zirconium phosphate materials have been characterized using solid-state NMR.[315] ^{31}P MAS NMR has been used to show the existence of P–O–Al groups, and ^{27}Al NMR analysis by means of the 2D five-quanta MQ MAS technique has revealed the coexistence of octahedral, tetrahedral, and pentacoordinated aluminium species.

^{27}Al, ^{29}Si – The dealumination of Nd-, Sm-, Gd-, and Dy-containing Y zeolites has been studied using ^{29}Si and ^{27}Al MAS NMR measurements.[316] Except for the Sm^{3+} treated sample, the Nd^{3+}, Gd^{3+}, Dy^{3+} samples could not have their tetrahedral and octahedral aluminium signal detected due to the high concentration of the paramagnetic ions with a large effective number of Bohr magnetons.

^{27}Al, ^{29}Si, ^{113}Cd – ^{113}Cd MAS NMR has been applied to study the structure of the guest clusters $Cd(OH)^+$, CdO and CdS located at the β cage of Y zeolite.[317] Resonance lines at 115, 114 and 100 ppm have been identified, corresponding to CdO–NaY, CdS_{10}–NaY and CdS_{20}–NaY, respectively. The results illustrate that the coordination environment of the Cd^{2+} ions located at the β cage of Y zeolite is similar to that of bulk CdO with the cubic halite structure. In addition, the ^{29}Si and ^{27}Al MAS NMR results have shown that several aluminium ions were removed from the framework of zeolite NaY in the period of preparation of guest cluster with ion exchange and sulfidation treatment.

^{29}Si – A silylated and calcined mesoporous Ti-MCM-48 has been characterized using ^{29}Si MAS NMR and other techniques.[318]

Highly crystalline microporous titano-alumino-silicate ETAS-10 materials with different framework aluminium contents (Al/Ti molar ratio 0.1–0.48) have been studied by ^{29}Si MAS NMR.[319]

Epitaxial FAU zeolite films have been prepared on micrometresized EMT support crystals and have been characterized using ^{29}Si MAS NMR.[320]

The characterization of polysiloxane-modified mesoporous silica gels derived from the acid catalyzed hydrolysis of tetraethoxysilane and oligomeric silanol terminated polydimethylsiloxane using ^{29}Si CPMAS NMR has been reported.[321]

^{31}P – ^{31}P MAS NMR has been applied to study novel open framework molecular sieves, titanium(IV) phosphates TCM-7 and -8 (Toyota Composite

Materials), with new mesoporous cationic framework topologies obtained by using both cationic and anionic surfactants.[322]

Mesostructured AlPOs with different structures have been characterized using ^{31}P CPMAS NMR.[323] It has been shown that hexagonal materials have much faster CP kinetics than lamellar materials, which is reflected in shorter CP times (T_{PH}) and $T_{1\rho}(^1H)$. T_{PH} increases with the increasing degree of condensation of the inorganic component, which is consistent with the increased ^{1}H–^{31}P distance. The CP dynamics of P sites connected to the surfactant head groups are affected by the fast motions of the protons in the -N(CH$_3$)$_3$ group.

^{51}V – A comparative study of calcined and rehydrated VSiB zeolite A by photoluminescence and ^{51}V NMR spectroscopies has led to the suggestion that there is a correlation between the vibrational energy of the V=O bond and the corresponding chemical shift of the ^{51}V NMR signal.[324]

^{207}Pb – ^{207}Pb and ^{27}Al – ^{207}Pb double resonance NMR data have been reported for a series of lead-containing zeolites.[325] It has been proposed that lead cations are strongly affected by the sorption of water, with the NMR spectra of the resulting material consistent with a chemical equilibrium between Pb^{2+} cations and $PbOH^+$ cations. Double resonance experiments on dehydrated samples have yielded Pb–Al distances consistent with reported X-ray structure.

5.10 Surface Science and Catalysis. – *^1H* – High-resolution ^{1}H MAS NMR has been employed to study water environments in a C-18 bonded silica phase,[326] the structure of hybrid siloxane-based networks and the interaction with quartz filler,[327] properties of chemisorbed hydrogen species on Ag-A zeolite partially reduced with hydrogen,[328] and properties of hydrogen over silica-supported rhodium catalyst.[329]

^2H – ^{2}H wideline NMR has been applied to investigate the time scale of the catalytic loop motion in triosephosphate isomerase using deuterated tryptophan.[330]

^{10}B, ^{11}B – 10B and ^{11}B MAS NMR has been conducted to characterize cubic boron nitride films prepared by plasma chemical vapor deposition.[331] Similarities and differences between cubic boron nitride films and polycrystals synthesized at high pressure and high temperature have been clarified by chemical shift and linewidth.

^{13}C – ^{13}C NMR data, obtained as a function of temperature with MAS and either CP or direct polarization, have been reported to study acetone adsorbed on dry silica gel.[332] It has been concluded that the main linewidth contributions, which increase at lower temperatures, are a dispersion of chemical shifts in the hydrogen-bonded state, associated with the inhomogeneous character of the silica surface, the interference between MAS and motional averaging of the CSA, and chemical exchange broadening.

Using ^{13}C CPMAS NMR, the first evidence has been obtained for *n*-pentane carbonylation with carbon monoxide into C-6 aldehydes, ketones and carboxylic acids on a sulfated zirconia catalyst.[333]

1D and 2D VT ^{13}C MAS NMR studies on the adsorption of methane on zeolite HY at temperatures ranging from 295 K to 135 K have been presented.[334]

Sonochemically prepared octadecyltrihydrosilane ($CH_3(CH_2)_{17}SiH_3$)-coated titania particles have been characterized using ^{13}C NMR.[335]

In situ ^{13}C NMR has been applied to understand the chemistry of acetone on the silico-aluminophosphate catalyst HSAPO-34.[336] The results of this investigation are interpreted in the context of methanol-to-olefin chemistry on HSAPO-34.

^{13}C, ^{27}Al – ^{13}C and ^{27}Al MAS NMR has been used to characterize a novel heterogeneous cocatalyst, partially hydrolyzed trimethylaluminium.[337]

^{13}C, ^{29}Si – Solid-state ^{29}Si and ^{13}C CPMAS NMR have been used to characterize three different reversed-phase materials for high-performance liquid chromatography, obtained by sorption of poly(methyloctylsiloxane) onto bare silica, titanized silica and zirconized silica pores[338] and to study the coupling of γ-methacryloxypropyltrimethoxysilane on experimental nano-porous silica fillers.[339]

^{13}C, ^{29}Si, ^{31}P – A multinuclear (^{13}C, ^{29}Si and ^{31}P) solid-state NMR characterization of the first phosphonate and phosphonic acid-modified porous silicas and polysilsesquioxanes has been presented.[340]

^{13}C, ^{31}P – The coking during propene oligomerization over silica-supported heteropoly acid $H_3PW_{12}O_{40}$ and its palladium-doped form and subsequent catalyst regeneration have been studied using ^{13}C and ^{31}P MAS NMR.[341]

^{19}F, ^{27}Al – *In situ* X-ray diffraction and ^{19}F, ^{27}Al and $^{19}F \rightarrow {}^{27}Al$ CP NMR methods have been used to follow the structural changes that occur during the dismutation reaction of $CHClF_2$ over γ-alumina.[342]

^{23}Na – $^{1}H/^{23}Na$ double resonance NMR techniques have been employed to study the modification of surface hydroxyls on γ-Al_2O_3 by sodium ions.[343] A $^{1}H \rightarrow {}^{23}Na$ CP experiment has been used resolve three kinds of sodium cations that are closely associated with surface hydroxyl groups. $^{1}H\{^{23}Na\}$ spin echo double resonance experiments reveal the surface modification in more detail.

^{27}Al – The detection of all of the aluminium present in steamed zeolite H-Y catalysts by ^{27}Al MAS NMR at 9.4 T, 14.4 T and 18.8 T has been reported.[344] It has been shown that ^{27}Al MAS and MQ MAS NMR measurements can be used to clearly identify four separate aluminium environments and to unambiguously assign their coordinations. Average chemical shift and quadrupolar coupling parameters have been used to accurately simulate the ^{27}Al MAS NMR spectra at 9.4 T, 14.4 T and 18.8 T in terms of these four aluminium environments. In addition, these average chemical shift and quadrupolar coupling parameters have been used to calculate peak positions in the ^{27}Al MQ MAS isotropic dimension that are in good agreement with the experimental data acquired at 9.4 and 18.8 T.

^{29}Si – Solid-state ^{29}Si NMR, including 2D heteronuclear and homonuclear NMR measurements, has been employed to study molecularly ordered inorganic frameworks in layered silicate surfactant mesophases.[345]

^{31}P – ^{31}P MAS NMR has been used to characterize $VOPO_4 \cdot {}^{2}H_2O$.[346]

^{51}V – ^{51}V NMR, applied to investigate the nature of the vanadium species present on V_2O_5/Al_2O_3 catalysts, has revealed the presence of V^{5+} in tetrahedral symmetry at low vanadium loading.[347]

^{71}Ga – ^{71}Ga MAS NMR, used to characterize MFI-type gallosilicalite and galloaluminosilicate, has confirmed that the Ga^{3+} cations are located in the zeolite framework.[348] Quantitative MAS NMR results have suggested that the incorporation of the Ga^{3+} cations is seriously inhibited by that of the Al^{3+} cations if they existed together, while the reverse process is not observed.

5.11 Inorganic and Other Related Materials. – *^{1}H* – Surface proton sites in mixed oxides MgO/Al_2O_3, MgO/Ga_2O_3 and $MgO/Al_2O_3/Ga_2O_3$ have been determined by ^{1}H MAS NMR and the results have been compared with those for the pure oxides.[349] Silver hydro sodalite $[Ag_3(H_2O)_4]_2[Al_3Si_3O_{12}]_2$ has been characterized using a combination of powder X-ray Rietveld refinement, ^{1}H MAS NMR and other techniques. ^{1}H MAS NMR spectra have revealed that the hydrogen atoms (which were not found in the Rietveld analysis) of the water molecules are involved in hydrogen bonding of different strengths and dynamics.[350]

^{1}H, ^{2}H – Silanol groups in protonated magadiite (H-magadiite) have been characterized by ^{1}H and ^{2}H solid-state NMR. In the ^{1}H NMR spectrum, silanol groups of H-magadiite showed two signals at 3.75 and 5.70 ppm, associated with weak and strong hydrogen bonding, respectively.[351] The ^{2}H NMR spectra of deuterated magadiite were measured in the temperature range from 150 to 440 K. Below 294 K, silanol groups showed Pake patterns composed of two components corresponding to the two types of silanol groups. Both silanol groups produced wobbling motions with increasing temperature. Above 294 K, the profile of the Pake pattern was transformed gradually into a near triangular pattern, indicating that the silanol groups underwent also other motions, such as a two-site jump.

^{1}H, ^{2}H, ^{31}P – The binding position and the electronic properties of acidic proton in anhydrous dodecatungstophosphoric acid, $H_3PW_{12}O_{40}$, have been studied by means of ^{1}H, ^{2}H NMR, and ^{1}H–^{31}P spin-echo double resonance (SEDOR) NMR techniques.[352] ^{1}H wide line NMR spectrum showed a bell-type resonance line shape with 4.7 kHz linewidth and the MAS NMR spectrum has a single resonance peak, suggesting that the hetero-polyanion $PW_{12}O_{40}^{3-}$ provides a single site to the acidic proton. The ^{2}H NMR spectrum leads to the QCC of 210 kHz and the asymmetry parameter of the e.f.g. tensor, η, of 0.15. The value of QCC suggests that the deuterons are static and bonded to oxygen atoms in the hetero-polyanion very rigidly. A remarkable decay of the ^{1}H–^{31}P SEDOR signal was observed, due to the dipolar interaction between the central ^{31}P and three protons strongly bonded to the hetero-polyanion. The P–H distance was evaluated by simulating the decay behavior of the echo to be 0.50 ± 0.02 nm.

^{1}H, ^{13}C, ^{17}O – A combination of X-ray techniques and multinuclear (^{1}H, ^{13}C, ^{17}O) solid-state NMR has been employed to follow the structural development of nanocrystalline zirconia.[353] ^{17}O MAS NMR of sol–gel-

produced undoped ZrO_2 shows unequivocally that oxygen sites in the initial gel are monoclinic-like. For sol–gel-produced ZrO_2, ^{13}C NMR shows that loss of all of the organic fragments occurs prior to crystallization. The ^{1}H NMR experiments determined that the proton content remains significant until well above the crystallization temperature.

^{1}H, ^{14}N – The improper ferroelastic phase letovicite $(NH_4)_3H(SO_4)_2$ has been studied by ^{1}H MAS NMR and static ^{14}N NMR experiments in the temperature range 296–425 K.[354] The ^{1}H MAS NMR resonance from ammonium protons can be well distinguished from that of acidic protons, and a third resonance appears just below the phase transition temperature due to the acidic protons in the paraelastic phase. 2D ^{1}H NOESY spectra indicate a chemical exchange between ammonium protons and the acidic protons of the paraphase. The static ^{14}N NMR spectra confirm the temperature of the motional changes of the ammonium tetrahedra.

^{1}H, ^{23}Na – Static and MAS ^{23}Na and MAS ^{1}H NMR experiments at temperatures down to 100 K as well as high temperature static and ^{23}Na MAS NMR experiments up to 873 K have been carried out to study the dynamics of the sodium cation in nitrate cancrinite.[355] Low temperature ^{23}Na NMR experiments show almost no change in signal, whereas the ^{1}H MAS NMR spectra show the freezing of cage water motion. Two ^{23}Na NMR signals exist at high temperatures above 673 K, a quadrupolar pattern and a Lorentzian signal. The strong quadrupolar coupling results from the loss of cage water and the near planar O atom coordination of Na in the epsilon-cage, while the interaction of Na^+ in the channel remains similar.

^{1}H, ^{29}Si – The use of 2D solid-state NMR correlation techniques to probe the chemical homogeneity of organically modified silicate networks has been presented.[356] Specifically, $^{29}Si\{^{1}H\}$ HETCOR NMR experiments have revealed the spatial proximity of the two types of Si units present in a gel obtained from co-hydrolysis of methyldiethoxysilane and triethoxysilane. Similar information has also been obtained by using 2D ^{1}H homonuclear correlation NMR spectroscopy. Such experiments were only possible by combining the use of high magnetic field (14.10 T) with fast MAS spinning rate (30 kHz).

^{6}Li – Three different lithium manganese(III) oxides (the orthorhombic $LiMnO_2$ phase, monoclinic layered $LiMnO_2$ and tetragonal $Li_2Mn_2O_4$) have been studied using ^{6}Li MAS NMR.[357] Much smaller shifts of 36–143 ppm have been reported for the Mn(III) phases, which has been explained by the Fermi-contact interaction. The ^{6}Li NMR shift of the resonances of the monoclinic and tetragonal phases show very little change with temperature in the range studied (−136 to 283 °C), implying that short-range antiferromagnetic interactions between Mn cations also exist for these phases.

^{6}Li MAS NMR has been used to study the local structure of the cathode material $LiNi_xMn_{2-x}O_4$ ($x = 0.05$, 0.1, 0.3, 0.5).[358] For $x = 0.05$ and 0.1, several resonances are observed, which are assigned to lithium local environments containing different numbers of Mn^{3+} and Mn^{4+} ions. By $x = 0.5$, only Mn^{4+} ions are present, and only one major resonance, due to the lithium local

environment $Li(ONi^{2+})_3(OMn^{4+})_9$, is observed; this is consistent with Mn/Ni ordering on the octahedral sites of the spinel structure. The VT NMR behavior is indicative of different magnetic behavior for the undoped and doped materials.

^7Li – $LiMn_2O_4$ has been studied using ^{7}Li MAS NMR.[359] 1D MAS NMR shows three Li resonances assigned to different crystallographic sites. At low temperatures an extra peak appears, indicating charge ordering of Mn^{3+} and Mn^{4+}. Rotor-synchronized 2D exchange NMR has been used to directly monitor the lithium dynamics. The activation energies and Li jump rates have been derived and are in agreement with those determined macroscopically.

Lithium insertion in pristine and partially oxidized graphite has been investigated by solid-state ^{7}Li NMR methods.[360] Both untreated and partially oxidized graphite exhibit three kinds of reversible Li sites, one at an average position of 43 ppm for both intercalation compounds LiC_6 and LiC_{12}, and at 3 ppm for LiC_{24}. Changes in the NMR spectra have been attributed to graphite structural changes.

^6Li, ^7Li, ^{59}Co – ^{6}Li, ^{7}Li and ^{59}Co MAS NMR has been applied to polytypes of $LiCoO_2$ at three different magnetic field strengths (4.7, 7.1, and 11.7 T).[361] The ^{59}Co and ^{6}Li, ^{7}Li quadrupole and anisotropic shift tensors have been determined by iterative fitting of the NMR line shapes at the three magnetic field strengths. Calculations of the shift and quadrupole coupling parameters have been performed by using a point dipole and point monopole model, respectively.

^{13}C – Solid-state ^{13}C NMR has been used to examine the crystalline quality of cubic diamond produced either *via* firing of explosive compositions, or through compression of mixtures containing carbonaceous precursors with metallic matrix.[362] In particular, the MAS technique has been used to estimate sp^3/sp^2 phase ratios for the obtained condensed carbon, whereas functionality of surface carbon atoms has been studied using the CPMAS method.

One out of four modifications of CaC_2, so-called metastable calcium carbide CaC_2-III, has been characterized using ^{13}C CPMAS.[363]

The superconducting fulleride $(NH_3)^xNaK_2C_{60}$ has been investigated using SQUID magnetometry and NMR in two differently doped samples.[364] ^{13}C NMR relaxation measurements validate the interpretation of the spin susceptibility in terms of density of states and rule out the presence of strong antiferromagnetic correlations in the Fermi liquid.

Dynamic and isothermal powder X-ray diffraction and solid-state ^{13}C NMR have been employed to provide an insight into the dehydration mechanism and the nature of solid-state phase transformation during the dehydration of nedocromil magnesium pentahydrate.[365]

^{17}O – Solid-state ^{17}O NMR of hybrid TiO_2–SiO_2 based materials has shown to be a useful tool for clearly distinguishing Si–O–Si, Si–O–Ti, and Ti–O–Ti linkages.[366] Spectra have been reported at applied magnetic fields from 5.6 to 14.1 T, allowing their NMR parameters to be deduced. The quantitative accuracy of these spectra has been investigated and the implications for detecting nanoscale phase separation have been discussed.

^{17}O, ^{27}Al, ^{89}Y – Phase diagrams of several compounds belonging to Y_2O_3–Al_2O_3 have been investigated by means of ^{27}Al, ^{17}O and ^{89}Y NMR.[367]

^{19}F – The study of the origin of paramagnetism in fluorinated graphite by means of EPR and ^{19}F NMR T_1 measurements has been presented. It has been shown that paramagnetism in fluorinated graphite is caused by local magnetic moments of dangling bonds. Localized spins in the high fluorine concentration region behave like isolated spins.[368]

^{23}Na, ^{27}Al – ^{23}Na and ^{27}Al MAS and DOR NMR spectra have been reported for the mullite-type crystalline compound $NaAl_9O_{14}$ and its amorphous precursor using a range of applied magnetic fields (8.45–16.9 T).[369] The crystalline compound has been shown by ^{27}Al NMR to contain aluminium in one octahedral and two tetrahedral sites. By contrast, two approximately equally populated non-identical Na sites have been distinguished by ^{23}Na NMR. Spectral simulation indicates these sites to be of slightly different distortion but of similar isotropic chemical shift. These measurements have illustrated the ability of NMR techniques to distinguish small variations in atomic environments, which are not resolved in the averaged X-ray structure.

^{27}Al – The microscopic properties of the hexagonal ZrNiAl, a model compound for a wide family of intermetallic compounds, have been studied using ^{27}Al NMR.[370] The line shape of static and MAS NMR spectra as a function of magnetic field strength (4.7–9.4 T) and temperature (5–300 K) has been investigated.

^{27}Al NMR spectra have been reported for the crystalline aluminates $CaAl_4O_7$ and $CaAl_{12}O_{19}$ at three different magnetic fields (8.45, 11.7, 14.1 T) using conventional and fast 3Q MAS NMR techniques.[371] For $CaAl_4O_7$ two distinct aluminate tetrahedra have been observed, both of which are in triclusters and can be assigned on the basis of the structural distortion index. The NMR interaction parameters deduced for these units have allowed useful comparison with other tetrahedra in triclusters. Comparison has been made with previous NMR studies of $CaAl_{12}O_{19}$ and with the structurally closely related phase $StAl_{12}O_{19}$.

^{29}Si – A ^{29}Si MAS-NMR study of a Cd-pyroxmangite of nominal composition $Cd_7[Ge_6Si]O_7$ has revealed considerable Si clustering, as GeSiSiSiGe triples corresponding to the wollastonite-like units of the siebener chain.[372] Ordering of Si-rich unit cells and of unit cells having no Si has been proposed as the reason for the occurrence of the superperiods in Cd-pyroxmangite.

The stability of yttrium silicate apatite has been investigated by studying the influence of iron as a 'stabilising cation' using X-ray diffraction and ^{29}Si MAS NMR.[373]

Carbon-silica hybrid precursors have been characterized using solid-state ^{29}Si MAS NMR.[374] In the case that the crystallites are held at small size during heat treatments, the powders show three signals, at −16, −20 and −25 ppm, in the NMR spectra. After coarsening of the crystallites and grains with heat treatment, the broad signal at −19 ppm and a small signal at −16 ppm are observed. The signal at −19 ppm has been assigned to the β-SiC structure disordered by α-SiC areas.

The crystal structure of α-eucryptite, $LiAlSiO_4$, has been reinvestigated by combining ^{29}Si NMR and single-crystal X-ray diffraction.[375] The silicon coordination in α-eucryptite of three different samples (two of natural, one of synthetic origin) has been shown to be identical on a local scale by means of ^{29}Si MAS NMR, suggesting a well-ordered arrangement of Si and Al within the crystal structure of α-eucryptite and the presence of two symmetrically non-equivalent sites for silicon.

^{31}P – A variety of solid complexes containing PBr_4^+ (*e.g.* $PBr_4^+AsF_6^-$, $PBr_4^+AlBr_4^-$, $PBr_4^+GaBr_4^-$, PI_4^+ (*e.g.* $PI_4^+AlCl_4^-$, $PI_4^+AlBr_4^-$, $PI_4^+GaBr_4^-$) or the mixed species $PBr_nI_4^{n+}$ has been studied by solid-state ^{31}P MAS NMR.[376] The influence of the counter-ion on the chemical shift has been discussed. Evidence for the existence of the hitherto unknown mixed bromoiodophosphonium cations PBr_3I^+, PBr_2I^{2+} and $PBrI_3^+$ has been confirmed by spin–orbit corrected density functional calculations of isotropic ^{31}P chemical shifts for $PBr_nI_4^{n+}$.

The crystal structures of lead hydroxyapatites at different degrees of cadmium substitution for lead (4.9, 10.0, 22.4 and 29.0% Cd atoms) have been investigated by X-ray powder pattern fitting and ^{31}P MAS NMR.[377] The different environments of the phosphate group demonstrated by ^{31}P NMR spectroscopic data have been discussed in relation to structural data.

A novel hydrated magnesium phosphate $Mg_3(PO_4)_2{\cdot}4H_2O$ has been characterized by ^{31}P MAS NMR.[378]

^{31}P, ^{77}Se – 1,3-Diselena-2,4-diphosphetane-2,4-diselenides $(RPSe_2)_2$ with R = Me, Et, *t*-Bu, Ph, 4-$Me_2NC_6H_4$, 4-$MeOC_6H_4$ have been investigated by ^{31}P and ^{77}Se solid-state NMR.[379] The structure of the investigated compounds has been confirmed by the isotropic and anisotropic values of the chemical shifts and the $^1J_{PSe}$ coupling constants. In addition, two new 1,2,4-triselena-3,5-diphospholane-3,5-diselenides, $(RPSe_2)_2Se$ (R = Me, Et), have been investigated. For $(t\text{-}BuPSe_2)_2$ the experimentally obtained principal values of ^{31}P and ^{77}Se shielding tensors are compared with values from IGLO calculations and the calculated orientations of the principal axes are discussed.

^{77}Se – Pure $Na_{12}(SeO_6)(SeO_4)_3$ has been characterized by ^{77}Se MAS NMR.[380]

^{87}Rb – ^{87}Rb NMR and ^{35}Cl NQR have been used to investigate phase transitions and modulation wave motions in Rb_2ZnCl_4.[381] ^{87}Rb 2D exchange-difference NMR has been used to study atomic motions in the incommensurate and paraelectric phases to elucidate the nature of the phase transition.

Solid-state NMR of the ^{87}Rb has been employed to investigate the phase transitions in polycrystalline $LiRbSO_4$.[382] The spin–lattice relaxation time T_1 and the NMR line shape have been measured using MAS and MQ MAS methods between 373 and 488 K. The QCC, χ, the asymmetry parameter, η, and the isotropic chemical shift, δ, have been determined from the analysis of MAS and MQ MAS spectra. The anomalies of χ near the phase transition were associated with the deformation of the local environment of the Rb ions in the crystal lattice.

Structural phase transition at 290 K and the implication on the intermediate

phase above 290 K in powdered $RbMnCl_3$ have been observed by using solid-state ^{87}Rb NMR.[383] Quadrupole parameters χ and η, and the relative peak intensities for two physically non-equivalent Rb sites, Rb(I) and Rb(II), have been determined from nonlinear least-squares fits to the ^{87}Rb NMR powder patterns in the temperature range 260 to 330 K.

^{93}Nb – ^{93}Nb (I = 9/2) MQ MAS NMR spectra of a series of inorganic niobates have been measured.[384] ^{93}Nb MQ MAS yields spectra with typically an order of magnitude higher resolution than that obtainable with ^{93}Nb MAS and ^{93}Nb dynamic-angle spinning (DAS) spectroscopy. For example, the full-width at half-maximums of the ^{93}Nb resonances of $LiNbO_3$ were 9 (MAS), 5.8 (DAS), and 0.7 kHz (MQ MAS). Broadening of the ^{93}Nb MAS and DAS spectra is due to the second-order quadrupolar and homonuclear dipolar interactions, respectively. The quadrupolar products and isotropic chemical shifts of the ^{93}Nb resonances of $LiNbO_3$, $NaNbO_3$, $PbNb_2O_6$, $Pb_2Nb_2O_7$, $Pb_3Nb_2O_8$, $Pb_5Nb_4O_{15}$, $Pb_3Nb_4O_{13}$, and $Pb_{1.83}Nb_{1.71}Mg_{0.29}O_{6.39}$ were determined from MQ MAS spectra. The applicability and limitations of MQ MAS spectroscopy in studying inorganic niobates containing multiple ^{93}Nb resonances have been addressed.

^{93}Nb, ^{119}Sn – Tin niobates ($Sn_{1+x}Nb_2O_{6+x}$, $x = 0.0$, 0.5, and 1.0) have been characterized by solid-state ^{119}Sn NMR.[385] ^{119}Sn MAS NMR supports the presence in synthetic foordite of Sn(II) in eight-fold coordination. ^{93}Nb NMR indicates a fairly distorted local environment for niobium in synthetic foordite, much more so than in the $Sn_2Nb_2O_7$ pyrochlore.

^{119}Sn – Mixed oxide samples of $Sn_{1-x}TixO_2$ ($0.0 \leq x \leq 1.0$), have been investigated by powder X-ray diffraction and ^{119}Sn MAS NMR.[386]

6 References

1 L. Frydman, *Annu. Rev. Phys. Chem.*, 2001, **52**, 463.
2 S. Dusold and A. Sebald, *Annu. Rep. NMR Spectrosc.*, 2000, **41**, 185.
3 P. J. Barrie, *Annu. Rep. NMR Spectrosc.*, 2000, **41**, 265.
4 M. J. Duer, *Annu. Rep. NMR Spectrosc.*, 2001, **43**, 1.
5 M. E. Smith, *Annu. Rep. NMR Spectrosc.*, 2001, **43**, 121.
6 J. C. C. Chan and S. C. F. Au-Yeung, *Annu. Rep. NMR Spectrosc.*, 2000, **41**, 1.
7 H. Schwalbe and A. Bielecki, *Angew. Chem. Int. Ed.*, 2001, **40**, 2045.
8 R. Tycko, *Annu. Rev. Phys. Chem.*, 2001, **52**, 575.
9 B. Bechinger, *Mol. Membr. Biol.*, 2000, **17**, 135.
10 D. G. Lynn and S. C. Meredith, *J. Struct. Biol.*, 2000, **130**, 153.
11 C. R. Sanders and K. Oxenoid, *Biochim. Biophys. Acta Biomembr.*, 2000, **1508**, 129.
12 L. K. Sanders, W. D. Arnold and E. Oldfield, *J. Porphyrins Phthalocyanines*, 2001, **5**, 323.
13 F. Fillaux, *Int. Rev. Phys. Chem.*, 2000, **19**, 553.
14 V. V. Turov and R. Leboda, 2001.
15 K. J. D. MacKenzie, *Br. Ceram. Trans.*, 2000, **99**, 231.
16 H. Knicker, *J. Environ. Quality*, 2000, **29**, 715.

17 M. C. Warren, M. T. Dove, E. R. Myers, A. Bosenick, E. J. Palin, C. I. Sainz-Diaz, B. S. Guiton, and S. A. T. Redfern, *Mineralog. Mag.*, 2001, **65**, 221.
18 A. D. Bain and R. S. Dumont, *Concepts Mag. Reson.*, 2001, **13**, 159.
19 R. Ramesh and M. S. Krishnan, *J. Chem. Phys.*, 2001, **114**, 5967.
20 P. Tekely and M. Goldman, *J. Magn. Reson.*, 2001, **148**, 135.
21 C. Filip and S. Hafner, *J. Magn. Reson.*, 2000, **147**, 250.
22 H. Schafer, D. Iuga, R. Verhagen, and A. P. M. Kentgens, *J. Chem. Phys.*, 2001, **114**, 3073.
23 R. Verel, M. Ernst, and B. H. Meier, *J. Magn. Reson.*, 2001, **150**, 81.
24 J. H. Kristensen and I. Farnan, *J. Chem. Phys.*, 2001, **114**, 9608.
25 N. Sinha and K. V. Ramanathan, *Chem. Phys. Lett.*, 2000, **332**, 125.
26 Z. H. Gan, *J. Chem. Phys.*, 2001, **114**, 10845.
27 M. Eden and L. Frydman, *J. Chem. Phys.*, 2001, **114**, 4116.
28 A. Brinkmann and M. H. Levitt, *J. Chem. Phys.*, 2001, **115**, 357.
29 A. Chakraborty, *Spectrochim. Acta Part A Mol. Biomol. Spectrosc.*, 2000, **56**, 2725.
30 S. Wi, V. Frydman, and L. Frydman, *J. Chem. Phys.*, 2001, **114**, 8511.
31 J. R. Brender, D. M. Taylor, and A. Ramamoorthy, *J. Am. Chem. Soc.*, 2001, **123**, 914.
32 A. V. Larin and D. P. Vercauteren, *Int. J. Quantum Chem.*, 2001, **82**, 182.
33 M. Bak, J. T. Rasmussen, and N. C. Nielsen, *J. Magn. Reson.*, 2000, **147**, 296.
34 V. Macho, L. Brombacher, and H. W. Spiess, *Appl. Magn. Reson.*, 2001, **20**, 405.
35 A. Lesage, L. Duma, D. Sakellariou, and L. Emsley, *J. Am. Chem. Soc.*, 2001, **123**, 5747.
36 A. Wiesmath, C. Filip, D. E. Demco, and B. Blumich, *J. Magn. Reson.*, 2001, **149**, 258.
37 D. Massiot, B. Alonso, F. Fayon, F. Fredoueil, and B. Bujoli, *Solid State Sci.*, 2001, **3**, 11.
38 A. Samoson, T. Tuherm, and J. Past, *J. Magn. Reson.*, 2001, **149**, 264.
39 E. H. Hardy, R. Verel, and B. H. Meier, *J. Magn. Reson.*, 2001, **148**, 459.
40 E. De Vita and L. Frydman, *J. Magn. Reson.*, 2001, **148**, 327.
41 Y. Ishii, *J. Chem. Phys.*, 2001, **114**, 8473.
42 Y. Ishii, J. J. Balbach, and R. Tycko, *Chem. Phys.*, 2001, **266**, 231.
43 F. M. Marassi, *Biophys. J.*, 2001, **80**, 994.
44 A. S. D. Heindrichs, H. Geen, C. Giordani, and J. J. Titman, *Chem. Phys. Lett.*, 2001, **335**, 89.
45 X. L. Yao, K. Schmidt-Rohr, and M. Hong, *J. Magn. Reson.*, 2001, **149**, 139.
46 I. Schnell, B. Langer, S. H. M. Sontjens, M. H. P. van Genderen, R. P. Sijbesma, and H. W. Spiess, *J. Magn. Reson.*, 2001, **150**, 57.
47 A. Lesage and L. Emsley, *J. Magn. Reson.*, 2001, **148**, 449.
48 K. Saalwachter, R. Graf, and H. W. Spiess, *J. Magn. Reson.*, 2001, **148**, 398.
49 L. S. Du, A. Samoson, T. Tuherm, and C. P. Grey, *Chem. Mater.*, 2000, **12**, 3611.
50 G. Mali, J. P. Amoureux, and E. Kaucic, *Phys. Chem. Chem. Phys.*, 2000, **2**, 5737.
51 A. Jerschow, J. W. Logan, and A. Pines, *J. Magn. Reson.*, 2001, **149**, 268.
52 A. Goldbourt, P. K. Madhu, S. Kababya, and S. Vega, *Solid State Nucl. Magn. Reson.*, 2000, **18**, 1.
53 M. Pruski, J. W. Wiench, and J. P. Amoureux, *J. Magn. Reson.*, 2000, **147**, 286.
54 D. Iuga, H. Schafer, R. Verhagen, and A. P. M. Kentgens, *J. Magn. Reson.*, 2000, **147**, 192.

55 T. Vosegaard, P. Florian, D. Massiot, and P. J. Grandinetti, *J. Chem. Phys.*, 2001, **114**, 4618.
56 H. T. Kwak, S. Prasad, Z. Yao, P. J. Grandinetti, J. R. Sachleben, and L. Emsley, *J. Magn. Reson.*, 2001, **150**, 71.
57 L. B. Alemany, R. L. Callender, A. R. Barron, S. Steuernagel, D. Iuga, and A. P. M. Kentgens, *J. Phys. Chem. B*, 2000, **104**, 11612.
58 S. E. Ashbrook and S. Wimperis, *Chem. Phys. Lett.*, 2001, **340**, 500.
59 S. E. Ashbrook and S. Wimperis, *J. Magn. Reson.*, 2000, **147**, 238.
60 C. Filip, X. Filip, M. Bertmer, D. E. Demco, and B. Blumich, *J. Magn. Reson.*, 2001, **150**, 184.
61 I. Schnell and A. Watts, *Chem. Phys. Lett.*, 2001, **335**, 111.
62 I. Schnell, A. Watts, and H. W. Spiess, *J. Magn. Reson.*, 2001, **149**, 90.
63 D. Kuwahara, T. Nakai, J. Ashida, and S. Miyajima, *Mol. Phys.*, 2001, **99**, 939.
64 T. M. Alam and D. P. Lang, *Chem. Phys. Lett.*, 2001, **336**, 385.
65 K. Takegoshi, J. Mizokami, and T. Terao, *Chem. Phys. Lett.*, 2001, **341**, 540.
66 A. K. Khitrin, C. Canlet, and B. M. Fung, *Solid State Nucl. Magn. Reson.*, 2001, **19**, 63.
67 C. T. Farrar, D. A. Hall, G. J. Gerfen, S. J. Inati, and R. G. Griffin, *J. Chem. Phys.*, 2001, **114**, 4922.
68 L. J. Smith, J. Smith, E. MacNamara, K. Knagge, and D. Raftery, *J. Phys. Chem. B*, 2001, **105**, 1412.
69 J. Matysik, Alia, J. G. Hollander, T. Egorova-Zachernyuk, P. Gast, and H. J. M. de Groot, *Indian J. Biochem. Biophys.*, 2000, **37**, 418.
70 O. Hirsch, G. Scheler, and C. Jager, *Rev. Sci. Instr.*, 2001, **72**, 1734.
71 D. K. Lee, Y. F. Wei, and A. Ramamoorthy, *J. Phys. Chem. B*, 2001, **105**, 4752.
72 L. Odgaard, M. Bak, H. J. Jakobsen, and N. C. Nielsen, *J. Magn. Reson.*, 2001, **148**, 298.
73 H. C. Jarrell and D. J. Siminovitch, *Solid State Nucl. Magn. Reson.*, 2001, **19**, 87.
74 Y. Millot and P. P. Man, *J. Magn. Reson.*, 2001, **150**, 10.
75 J. B. Hauksson, U. Edlund, and J. Trygg, *Magn. Reson. Chem.*, 2001, **39**, 267.
76 K. Saalwachter and H. W. Spiess, *J. Chem. Phys.*, 2001, **114**, 5707.
77 J. C. C. Chan, *Chem. Phys. Lett.*, 2001, **335**, 289.
78 J. C. C. Chan and H. Eckert, *J. Magn. Reson.*, 2000, **147**, 170.
79 M. Janssen and H. Eckert, *Solid State Ionics*, 2000, **136**, 1007.
80 S. P. Brown, X. X. Zhu, K. Saalwachter, and H. W. Spiess, *J. Am. Chem. Soc.*, 2001, **123**, 4275.
81 S. J. Kitchin, K. D. M. Harris, A. E. Aliev, and D. C. Apperley, *Chem. Phys. Lett.*, 2000, **323**, 490.
82 K. Nishimura, K. Ebisawa, E. Suzuki, H. Saito, and A. Naito, *J. Mol. Struct.*, 2001, **560**, 29.
83 C. P. Jaroniec, B. A. Tounge, J. Herzfeld, and R. G. Griffin, *J. Am. Chem. Soc.*, 2001, **123**, 3507.
84 O. J. Murphy, F. A. Kovacs, E. L. Sicard, and L. K. Thompson, *Biochemistry*, 2001, **40**, 1358.
85 E. Hughes, J. Jordan, and T. Gullion, *J. Phys. Chem. B*, 2001, **105**, 5887.
86 A. Bailly, J. P. Amoureux, J. W. Wiench, and M. Pruski, *J. Phys. Chem. B*, 2001, **105**, 773.
87 F. J. Blanco and R. Tycko, *J. Magn. Reson.*, 2001, **149**, 131.
88 I. Sack, Y. S. Balazs, S. Rahimipour, and S. Vega, *J. Magn. Reson.*, 2001, **148**, 104.

89 C. Ochsenfeld, S. P. Brown, I. Schnell, J. Gauss, and H. W. Spiess, *J. Am. Chem. Soc.*, 2001, **123**, 2597.
90 H. Heise, F. H. Kohler, and X. L. Xie, *J. Magn. Reson.*, 2001, **150**, 198.
91 K. J. Hallock, D. K. Lee, and A. Ramamoorthy, *J. Chem. Phys.*, 2000, **113**, 11187.
92 D. L. Bryce, R. E. Wasylishen, and M. Gee, *J. Phys. Chem. A*, 2001, **105**, 3633.
93 Y. F. Wei, D. K. Lee, and A. Ramamoorthy, *J. Am. Chem. Soc.*, 2001, **123**, 6118.
94 B. Heise, J. Leppert, H. Wenschuh, O. Ohlenschlager, M. Gorlach, and R. Ramachandran, *J. Biomol. NMR*, 2001, **19**, 167.
95 J. Leppert, B. Heise, and R. Ramachandran, *Solid State Nucl. Magn. Reson.*, 2001, **19**, 1.
96 G. Wu, S. Dong, and R. Ida, *Chem. Commun.*, 2001, 891.
97 G. Wu and S. Dong, *Chem. Phys. Lett.*, 2001, **334**, 265.
98 S. E. Ashbrook, A. J. Berry, and S. Wimperis, *J. Am. Chem. Soc.*, 2001, **123**, 6360.
99 C. Gervais, F. Babonneau, D. Hoebbel, and M. E. Smith, *Solid State Nucl. Magn. Reson.*, 2000, **17**, 2.
100 L. S. Du, R. W. Schurko, K. H. Lim, and C. P. Grey, *J. Phys. Chem. A*, 2001, **105**, 760.
101 M. Fechtelkord, *Solid State Nucl. Magn. Reson.*, 2000, **18**, 70.
102 R. J. Accardi, R. F. Lobo, and M. Kalwei, *J. Phys. Chem. B*, 2001, **105**, 5883.
103 S. W. Ding and C. A. McDowell, *Chem. Phys. Lett.*, 2001, **333**, 413.
104 C. Strohmann, O. Ulbrich, and D. Auer, *Eur. J. Inorg. Chem.*, 2001, 1013.
105 G. Grossmann, D. Scheller, O. L. Malkina, V. G. Malkin, G. Zahn, H. Schmitt, and U. Haeberlen, *Solid State Nucl. Magn. Reson.*, 2000, **17**, 22.
106 H. J. Jakobsen, H. Bildsoe, J. Skibsted, and T. Giavani, *J. Am. Chem. Soc.*, 2001, **123**, 5098.
107 J. E. H. Buston, T. D. W. Claridge, S. J. Heyes, J. L. Bretherton, M. G. Moloney, and M. Stevenson, *Magn. Reson. Chem.*, 2001, **39**, 68.
108 C. Dybowski, S. P. Gabuda, S. G. Kozlova, G. Neue, D. L. Perry, and V. V. Terskikh, *J. Solid State Chem.*, 2001, **157**, 220.
109 C. V. Grant, V. Frydman, and L. Frydman, *J. Am. Chem. Soc.*, 2000, **122**, 11743.
110 C. Gervais, M. E. Smith, A. Pottier, J. P. Jolivet, and F. Babonneau, *Chem. Mater.*, 2001, **13**, 462.
111 C. W. Kirby and W. P. Power, *Can. J. Chem.-Rev. Canad. Chim.*, 2001, **79**, 296.
112 A. S. Lipton, G. W. Buchko, J. A. Sears, M. A. Kennedy, and P. D. Ellis, *J. Am. Chem. Soc.*, 2001, **123**, 992.
113 T. Harazono, R. Adachi, Y. Shimomura, and T. Watanabe, *Phys. Chem. Chem. Phys.*, 2001, **3**, 2943.
114 C. A. Zehmann, T. J. Boyle, D. M. Pedrotty, T. M. Alam, D. P. Lang, and B. L. Scott, *Inorg. Chem.*, 2001, **40**, 2177.
115 J. Schmider, G. Fritsch, T. Haisch, and K. Muller, *Mol. Cryst. Liq. Cryst.*, 2001, **356**, 99.
116 M. Bach-Verges, S. J. Kitchin, K. D. M. Harris, M. Zugic, and C. A. Koh, *J. Phys. Chem. B*, 2001, **105**, 2699.
117 F. Benevelli, W. Kolodziejski, K. Wozniak, and J. Klinowski, *Phys. Chem. Chem. Phys.*, 2001, **3**, 1762.
118 K. Damodaran, G. J. Sanjayan, P. R. Rajamohanan, S. Ganapathy, and K. N. Ganesh, *Org. Lett.*, 2001, **3**, 1921.

119 U. Langer, L. Latanowicz, C. Hoelger, G. Buntkowsky, H. M. Vieth, and H. H. Limbach, *Phys. Chem. Chem. Phys.*, 2001, **3**, 1446.
120 N. Yutronic, V. Manriquez, P. Jara, O. Wittke, and G. Gonzalez, *Supramol. Chem.*, 2001, **12**, 397.
121 Z. Dega-Szafran, I. Gaszczyk, D. Maciejewska, M. Szafran, E. Tykarska, and I. Wawer, *J. Mol. Struct.*, 2001, **560**, 261.
122 G. W. Buchanan, M. F. Rastegar, and G. P. A. Yap, *J. Mol. Struct.*, 2001, **561**, 43.
123 D. Casarini, S. Grilli, L. Lunazzi, and A. Mazzanti, *J. Org. Chem.*, 2001, **66**, 2757.
124 M. Z. Chalaca and J. D. Figueroa-Villar, *J. Mol. Struct.*, 2000, **554**, 225.
125 K. Hanai, A. Kuwae, T. Takai, H. Senda, and K. K. Kunimoto, *Spectrochim. Acta Part A, Mol. Biomol. Spectrosc.*, 2001, **57**, 513.
126 M. K. Cyranski, I. Wawer, A. Zielinska, A. Mrozek, V. Koleva, and C. Lozanova, *J. Phys. Org. Chem.*, 2001, **14**, 323.
127 E. Bednarek, B. Modzelewska-Banachiewicz, M. K. Cyranski, J. Sitkowski, and I. Wawer, *J. Mol. Struct.*, 2001, **562**, 167.
128 H. R. Tang, P. S. Belton, S. C. Davies, and D. L. Hughes, *Carbohydr. Res.*, 2001, **330**, 391.
129 G. Ivanova and V. Enchev, *Chem. Phys.*, 2001, **264**, 235.
130 M. Strohmeier, A. M. Orendt, D. W. Alderman, and D. M. Grant, *J. Am. Chem. Soc.*, 2001, **123**, 1713.
131 A. Tinti, V. Tugnoli, M. R. Tosi, and D. Casarini, *J. Mol. Struct.*, 2001, **565**, 247.
132 W. Schilf, B. Kamienski, A. Szady-Chelmieniecka, and E. Grech, *Solid State Nucl. Magn. Reson.*, 2000, **18**, 97.
133 R. M. Claramunt, C. Lopez, A. Schmidpeter, A. Willhalm, J. Elguero, and I. Alkorta, *Spectrosc. Int. J.*, 2001, **15**, 27.
134 E. B. Brouwer, R. Challoner, and R. K. Harris, *Solid State Nucl. Magn. Reson.*, 2000, **18**, 37.
135 S. Lima, I. S. Goncalves, P. Ribeiro-Claro, M. Pillinger, A. D. Lopes, P. Ferreira, J. J. C. Teixeira-Dias, J. Rocha, and C. C. Romao, *Organometallics*, 2001, **20**, 2191.
136 G. Mendoza-Diaz, L. Ruiz-Ramirez, and R. Moreno-Esparza, *Polyhedron*, 2000, **19**, 2149.
137 M. de la Fuente, J. M. Gavira-Vallejo, A. Hernanz, and R. Navarro, *J. Mol. Struct.*, 2001, **565**, 265.
138 D. V. Soldatov, A. T. Henegouwen, G. D. Enright, C. I. Ratcliffe, and J. A. Ripmeester, *Inorg. Chem.*, 2001, **40**, 1626.
139 G. E. Hawkes, P. O'Brien, H. Salacinski, M. Motevalli, and I. Abrahams, *Eur. J. Inorg. Chem.*, 2001, 1005.
140 A. V. Ivanov, W. Forsling, O. N. Antzutkin, and E. V. Novikova, *Russ. J. Coord. Chem.*, 2001, **27**, 158.
141 E. Szlyk, R. Kucharek, and I. Szymanska, *J. Coord. Chem.*, 2001, **53**, 55.
142 R. Szlyk, R. Kucharek, and I. Szymanska, *Pol. J. Chem.*, 2001, **75**, 337.
143 L. Pandolfo, A. Sassi, and L. Zanotto, *Inorg. Chem. Commun.*, 2001, **4**, 145.
144 K. Barbarossou, A. E. Aliev, I. P. Gerothanassis, J. Anastassopoulou, and T. Theophanides, *Inorg. Chem.*, 2001, **40**, 3626.
145 A. Wong and G. Wu, *J. Phys. Chem. A*, 2000, **104**, 11844.
146 M. J. Potrzebowski, X. B. Yang, K. Misiura, W. R. Majzner, M. W. Wieczorek, S. Kazmierski, S. Olejniczak, and W. J. Stec, *Eur. J. Org. Chem.*, 2001, 1491.

147 A. V. Ivanov, O. N. Antzutkin, A. C. Larsson, M. Kritikos, and W. Forsling, *Inorg. Chim. Acta*, 2001, **315**, 26.
148 D. J. Darensbourg, J. R. Wildeson, J. C. Yarbrough, and J. H. Reibenspies, *J. Am. Chem. Soc.*, 2000, **122**, 12487.
149 E. W. Ainscough, A. M. Brodie, A. K. Burrell, G. H. Freeman, G. B. Jameson, G. A. Bowmaker, J. V. Hanna, and P. C. Healy, *J. Chem. Soc, Dalton Trans.*, 2001, 144.
150 S. Soares, N. Ricardo, S. Jones, and F. Heatley, *Eur. Polym. J.*, 2001, **37**, 737.
151 E. Vittadini, L. C. Dickinson, and P. Chinachoti, *Carbohydr. Polym.*, 2001, **46**, 49.
152 B. Focher, M. T. Palma, M. Canetti, G. Torri, C. Cosentino, and G. Gastaldi, *Ind. Crops Prods.*, 2001, **13**, 193.
153 N. Saito, M. Reilly, and Y. Yazaki, *Holzforschung*, 2001, **55**, 205.
154 M. J. Prauchner, V. M. D. Pasa, C. Otani, and S. Otani, *Energy Fuels*, 2001, **15**, 449.
155 E. L. Hult, P. T. Larsson, and T. Iversen, *Polymer*, 2001, **42**, 3309.
156 X. P. Hu and Y. L. Hsieh, *Textile Res. J.*, 2001, **71**, 231.
157 J. Kunze, A. Ebert, and H. P. Fink, *Cellulose Chem. Technol.*, 2000, **34**, 21.
158 C. H. Vane, S. C. Martin, C. E. Snape, and G. D. Abbott, *J. Agric. Food Chem.*, 2001, **49**, 2709.
159 J. Parkas, M. Paulsson, U. Westermark, and N. Terashima, *Holzforschung*, 2001, **55**, 276.
160 E. L. Hult, P. T. Larsson, and T. Iversen, *Nord. Pulp Paper Res. J.*, 2001, **16**, 33.
161 T. Asakura, T. Yamane, Y. Nakazawa, T. Kameda, and K. Ando, *Biopolymers*, 2001, **58**, 521.
162 T. Asakura, J. Ashida, T. Yamane, T. Kameda, Y. Nakazawa, K. Ohgo, and K. Komatsu, *J. Mol. Biol.*, 2001, **306**, 291.
163 L. Heux, J. Brugnerotto, J. Desbrieres, M. F. Versali, and M. Rinaudo, *Biomacromolecules*, 2000, **1**, 746.
164 A. G. Krushelnitsky, A. E. Mefed, A. A. Kharitonov, and V. D. Fedotov, *Appl. Magn. Reson.*, 2001, **20**, 207.
165 M. Ebrahimi, P. Rossi, C. Rogers, and G. S. Harbison, *J. Magn. Reson.*, 2001, **150**, 1.
166 K. G. Duodu, H. Tang, A. Grant, N. Wellner, P. S. Belton, and J. R. N. Taylor, *J. Cereal Sci.*, 2001, **33**, 261.
167 T. A. Egorova-Zachernyuk, J. Hollander, N. Fraser, P. Gast, A. J. Hoff, R. Cogdell, H. J. M. de Groot, and M. Baldus, *J. Biomol. NMR*, 2001, **19**, 243.
168 J. Pauli, M. Baldus, B. van Rossum, H. de Groot, and H. Oschkinat, *Chembiochem*, 2001, **2**, 272.
169 Alia, J. Matysik, C. Soede-Huijbregts, M. Baldus, J. Raap, J. Lugtenburg, P. Gast, H. J. van Gorkom, A. J. Hoff, and H. J. M. de Groot, *J. Am. Chem. Soc.*, 2001, **123**, 4803.
170 L. van Dam and M. H. Levitt, *J. Mol. Biol.*, 2000, **304**, 541.
171 H. C. Le, T. Hintermann, T. Wessels, Z. H. Gan, D. Seebach, and R. R. Ernst, *Helv. Chim. Acta*, 2001, **84**, 208.
172 S. Kimura, A. Naito, H. Saito, K. Ogawa, and A. Shoji, *J. Mol. Struct.*, 2001, **562**, 197.
173 J. Henderson, H. A. Davies, S. J. Heyes, and D. J. Osborne, *Phytochemistry*, 2001, **56**, 131.
174 M. Osanai and M. Okudaira, *Amino Acids*, 2001, **20**, 113.

175 E. Strandberg, T. Sparrman, and G. Lindblom, *Adv. Colloid Interface Sci.*, 2001, **89**, 239.
176 A. Anastasiadis, F. Separovic, P. C. A. van der Wel, and R. E. Koeppe, *Biophys. J.*, 2001, **80**, 610.
177 J. A. Whiles, R. Brasseur, K. J. Glover, G. Melacini, E. A. Komives, and R. R. Vold, *Biophys. J.*, 2001, **80**, 280.
178 G. V. Martinez, S. Lope-Piedrafita, E. M. Dykstra, and M. F. Brown, *Biophys. J.*, 2001, **80**, 2402.
179 J. Yang, P. D. Parkanzky, B. A. Khunte, C. G. Canlas, R. Yang, C. M. Gabrys, and D. P. Weliky, *J. Mol. Graphics Modelling*, 2001, **19**, 129.
180 D. Huster, P. Muller, K. Arnold, and A. Herrmann, *Biophys. J.*, 2001, **80**, 822.
181 L. A. Cuccia, F. Morin, A. Beck, N. Hebert, G. Just, and R. B. Lennox, *Chem. – Eur. J.*, 2000, **6**, 4379.
182 K. J. Crowell and P. M. Macdonald, *Biophys. J.*, 2001, **81**, 255.
183 E. Sternin, D. Nizza, and K. Gawrisch, *Langmuir*, 2001, **17**, 2610.
184 E. K. Tiburu, D. M. Moton, and G. A. Lorigan, *Biochim. Biophys. Acta Biomembr.*, 2001, **1512**, 206.
185 M. A. Verhoeven, A. F. L. Creemers, P. H. M. Bovee-Geurts, W. J. De Grip, J. Lugtenburg, and H. J. M. de Groot, *Biochemistry*, 2001, **40**, 3282.
186 S. Q. Peng, W. Guo, J. D. Morrisett, M. T. Johnstone, and J. A. Hamilton, *Arteriosclerosis Thromb. Vascul. Biol.*, 2000, **20**, 2682.
187 D. Huster, L. S. Xiao, and M. Hong, *Biochemistry*, 2001, **40**, 7662.
188 M. Bak, L. K. Rasmussen, T. E. Petersen, and N. C. Nielsen, *J. Dairy Sci.*, 2001, **84**, 1310.
189 T. Pott, J. C. Maillet, C. Abad, A. Campos, J. Dufourcq, and E. J. Dufourc, *Chem. Phys. Lipids*, 2001, **109**, 209.
190 B. Bonev, A. Watts, M. Bokvist, and G. Grobner, *Phys. Chem. Chem. Phys.*, 2001, **3**, 2904.
191 E. R. Andrew and S. Glowinkowski, *Solid State Nucl. Magn. Reson.*, 2000, **18**, 89.
192 A. P. Legrand, B. Bresson, and J. M. Bouler, 2000.
193 D. A. Middleton, S. Rankin, M. Esmann, and A. Watts, *Proc. Nat. Acad. of Sci. U.S.A.*, 2000, **97**, 13602.
194 E. D. L. Smith, R. B. Hammond, M. J. Jones, K. J. Roberts, J. B. O. Mitchell, S. L. Price, R. K. Harris, D. C. Apperley, J. C. Cherryman, and R. Docherty, *J. Phys. Chem. B*, 2001, **105**, 5818.
195 H. Kawashima and T. Takanohashi, *Energy Fuels*, 2001, **15**, 591.
196 M. Rozwadowski, M. Lezanska, J. Wloch, K. Erdmann, R. Golembiewski, and J. Kornatowski, *Chem. Mater.*, 2001, **13**, 1609.
197 J. Z. Hu, M. S. Solum, C. M. V. Taylor, R. J. Pugmire, and D. M. Grant, *Energy Fuels*, 2001, **15**, 14.
198 J. C. C. Freitas, T. J. Bonagamba, and F. G. Emmerich, *Carbon*, 2001, **39**, 535.
199 R. Ahmad, R. S. Kookana, A. M. Alston, and J. O. Skjemstad, *Environ. Sci. Technol.*, 2001, **35**, 878.
200 I. Christl, C. J. Milne, D. G. Kinniburgh, and R. Kretzschmar, *Environ. Sci. Technol.*, 2001, **35**, 2512.
201 K. H. Dai, C. E. Johnson, and C. T. Driscoll, *Biogeochemistry*, 2001, **54**, 51.
202 F. J. Gonzalez-Vila, U. Lankes, and H. D. Ludemann, *J. Anal. Appl. Pyrolysis*,

203 A. Gardinier, S. Derenne, F. Robert, F. Behar, C. Largeau, and J. Maquet, *Earth Planet. Sci. Lett.*, 2000, **184**, 9.
204 Y. Gelinas, J. A. Baldock, and J. I. Hedges, *Org. Geochem.*, 2001, **32**, 677.
205 J. I. Hedges, J. A. Baldock, Y. Gellnas, C. Lee, M. Peterson, and S. G. Wakeham, *Nature*, 2001, **409**, 801.
206 U. Tomati, E. Madejon, E. Galli, D. Capitani, and A. L. Segre, *Compost Sci. Utilization*, 2001, **9**, 134.
207 R. J. Smernik and J. M. Oades, *Eur. J. Soil Sci.*, 2001, **52**, 103.
208 M. W. I. Schmidt, J. O. Skjemstad, C. I. Czimczik, B. Glaser, K. M. Prentice, Y. Gelinas, and T. A. J. Kuhlbusch, *Global Biogeochem. Cycles*, 2001, **15**, 163.
209 X. Y. Dai, C. L. Ping, R. Candler, L. Haumaier, and W. Zech, *Soil Sci. Soc. Am. J.*, 2001, **65**, 87.
210 J. D. Mao, B. Xing, and K. Schmidt-Rohr, *Environ. Sci. Technol.*, 2001, **35**, 1928.
211 H. Knicker, C. Achtnich, and H. Lenke, *J. Environ. Qual.*, 2001, **30**, 403.
212 H. Knicker and P. G. Hatcher, *Org. Geochem.*, 2001, **32**, 733.
213 S. W. Kuo and F. C. Chang, *Macromolecules*, 2001, **34**, 4089.
214 M. Valtier, X. Drujon, M. Wilhelm, and H. W. Spiess, *Macromol. Chem. Phys.*, 2001, **202**, 1262.
215 T. Dollase, R. Graf, A. Heuer, and H. W. Spiess, *Macromolecules*, 2001, **34**, 298.
216 R. Mansencal, B. Haidar, A. Vidal, L. Delmotte, and J. M. Chezeau, *Polymer Int.*, 2001, **50**, 387.
217 P. E. Kristiansen, E. W. Hansen, and B. Pedersen, *Polymer*, 2001, **42**, 1969.
218 L. N. J. Rodriguez, S. M. De Paul, C. J. Barrett, L. Reven, and H. W. Spiess, *Adv. Mater.*, 2000, **12**, 1934.
219 P. Palmas, L. Le Campion, C. Bourgeoisat, and L. Martel, *Polymer*, 2001, **42**, 7675.
220 J. Wang, M. K. Cheung, and Y. L. Mi, *Polymer*, 2001, **42**, 3087.
221 S. Y. Kwak, J. H. Kim, and J. C. Lee, *J. Polym. Sci. Part B, Polym. Phys.*, 2001, **39**, 993.
222 V. M. Litvinov and A. A. Dias, *Macromolecules*, 2001, **34**, 4051.
223 S. Ando, R. K. Harris, P. Holstein, S. A. Reinsberg, and K. Yamauchi, *Polymer*, 2001, **42**, 8137.
224 A. G. S. Hollander and K. O. Prins, *Int. J. Thermophys.*, 2001, **22**, 357.
225 W. Y. Lin and F. D. Blum, *J. Am. Chem. Soc.*, 2001, **123**, 2032.
226 S. Bachmann, C. Hellriegel, J. Wegmann, H. Handel, and K. Albert, *Solid State Nucl. Magn. Reson.*, 2000, **17**, 39.
227 K. Masuda, H. Kaji, and F. Horii, *Polymer J.*, 2001, **33**, 190.
228 K. Masuda, H. Kaji, and F. Horii, *Polymer J.*, 2001, **33**, 356.
229 M. Jeannin, S. A. Rezzoug, Z. Maache-Rezzoug, S. Cohendoz, and K. Allaf, *Int. J. Polym. Anal. Characteriz.*, 2000, **6**, 177.
230 R. A. Assink, D. P. Lang, and M. Celina, *J. Appl. Polym. Sci.*, 2001, **81**, 453.
231 W. Gabrielse, M. Soliman, and K. Dijkstra, *Macromolecules*, 2001, **34**, 1685.
232 C. Dridi, N. Blel, A. Chaieb, M. Majdoub, M. S. Roudesli, J. Davenas, H. Ben Ouada, and H. Maaref, *Eur. Polym. J.*, 2001, **37**, 683.
233 P. P. J. Chu, M. H. Cheng, W. J. Huang, and F. C. Chang, *Macromolecules*, 2000, **33**, 9360.
234 K. Lenghaus, G. G. Qiao, and D. H. Solomon, *Polymer*, 2001, **42**, 3355.
235 T. Ito, Y. Yamaguchi, H. Watanabe, and T. Asakura, *J. Appl. Polym. Sci.*, 2001, **80**, 2376.
236 J. S. Kim and A. R. Lim, *Abstr. Papers Am. Chem. Soc.*, 2000, **220**, 87.

237 K. Lenghaus, G. G. H. Qiao, and D. H. Solomon, *Polymer*, 2001, **42**, 7523.
238 R. H. Lin, E. M. Woo, and J. C. Chiang, *Polymer*, 2001, **42**, 4289.
239 S. T. Chang and H. T. Chang, *Polym. Degrad. Stabil.*, 2001, **71**, 261.
240 J. Lu, P. A. Mirau, and A. E. Tonelli, *Macromolecules*, 2001, **34**, 3276.
241 Y. Z. Bin, L. Ma, R. Adachi, H. Kurosu, and M. Matsuo, *Polymer*, 2001, **42**, 8125.
242 L. Ma, Y. Bin, Y. Sakai, Q. Chen, H. Kurosu, and M. Matsuo, *Macromolecules*, 2001, **34**, 4802.
243 Y. Ohta, A. Kaji, H. Sugiyama, and H. Yasuda, *J. Appl. Polym. Sci.*, 2001, **81**, 312.
244 Y. Ohira, F. Horii, and T. Nakaoki, *Macromolecules*, 2001, **34**, 1655.
245 M. Matsuo, Y. Bin, and M. Nakano, *Polymer*, 2001, **42**, 4687.
246 H. Matsuzawa, S. Okada, A. Sarkar, H. Matsuda, and H. Nakanishi, *Polym. J.*, 2001, **33**, 182.
247 J. Wegmann, K. Albert, M. Pursch, and L. C. Sander, *Anal. Chem.*, 2001, **73**, 1814.
248 A. Mercier, S. Kuroki, I. Ando, H. Deleuze, and O. Mondain-Monval, *J. Polym. Sci. Part B, Polym. Phys.*, 2001, **39**, 956.
249 R. F. Nogueira and M. I. B. Tavares, *J. Appl. Polym. Sci.*, 2001, **81**, 261.
250 Q. J. Zhang, W. X. Lin, and Q. Chen, *Acta Polym. Sin.*, 2000, 800.
251 K. Nakamura, S. Ando, and T. Takeichi, *Polymer*, 2001, **42**, 4045.
252 T. Nakaoki, R. Kitamaru, R. G. Alamo, W. T. Huang, and L. Mandelkern, *Polym. J.*, 2000, **32**, 876.
253 T. Nakaoki, Y. Ohira, and F. Horii, *Polymer*, 2001, **42**, 4555.
254 R. F. Nogueira and M. I. B. Tavares, *Polym. Test.*, 2001, **20**, 379.
255 J. Rasburn, F. Seker, K. Kulbaba, P. G. Klein, I. Manners, G. J. Vancso, and P. M. Macdonald, *Macromolecules*, 2001, **34**, 2884.
256 Y. L. Tang, X. Z. Qu, L. S. Chen, and X. G. Jin, *Chin. Chem. Lett.*, 2001, **12**, 353.
257 X. Shuai, Y. He, N. Asakawa, and Y. Inoue, *J. Appl. Polym. Sci.*, 2001, **81**, 762.
258 S. Richer, S. Alamercery, O. Paisse, G. Raffin, C. Sanglar, H. Waton, and M. F. Grenier-Loustalot, *Polym. Polym. Composites*, 2001, **9**, 81.
259 S. Pethkar, J. A. Dharmadhikari, A. A. Athawale, R. C. Aiyer, and K. Vijayamohanan, *J. Phys. Chem. B*, 2001, **105**, 5110.
260 F. E. Porbeni, E. M. Edeki, I. D. Shin, and A. E. Tonelli, *Polymer*, 2001, **42**, 6907.
261 T. Gunji, Y. Suzuki, and Y. Abe, *Nippon Kagaku Kaishi*, 2000, 871.
262 F. A. G. Mercier, M. Biesemans, R. Altmann, R. Willem, R. Pintelon, J. Schoukens, B. Delmond, and G. Dumartin, *Organometallics*, 2001, **20**, 958.
263 M. Giotto, D. Azar, J. Gosselin, P. T. Inglefield, and A. A. Jones, *J. Polym. Sci. Part B, Polym. Phys.*, 2001, **39**, 1548.
264 H. L. Wang, H. M. Kao, M. Digar, and T. C. Wen, *Macromolecules*, 2001, **34**, 529.
265 S. Angot, N. Ayres, S. A. F. Bon, and D. M. Haddleton, *Macromolecules*, 2001, **34**, 768.
266 D. Reichert, G. Hempel, H. Zimmermann, H. Schneider, and Z. Luz, *Solid State Nucl. Magn. Reson.*, 2000, **18**, 17.
267 J. S. Forsythe, D. J. T. Hill, S. Mohajerani, and A. K. Whittaker, *Radiat. Phys. Chem.*, 2001, **60**, 439.
268 J. S. Forsythe, D. J. T. Hill, and A. K. Whittaker, *Radiat. Phys. Chem.*, 2001, **60**, 609.

269 G. Meresi, Y. Wang, A. Bandis, P. T. Inglefield, A. A. Jones, and W. Y. Wen, *Polymer*, 2001, **42**, 6153.

270 S. Ando, R. K. Harris, J. Hirschinger, S. A. Reinsberg, and U. Scheler, *Macromolecules*, 2001, **34**, 66.

271 Y. Ishii, J. P. Yesinowski, and R. Tycko, *J. Am. Chem. Soc.*, 2001, **123**, 2921.

272 W. Storek, C. Peuker, and H. Geissler, *Glass Sci. Technol., Glastech. Ber.*, 2000, **73**, 373.

273 J. C. Sanchez-Lopez, C. Donnet, F. Lefebvre, C. Fernandez-Ramos, and A. Fernandez, *J. Appl. Phys.*, 2001, **90**, 675.

274 A. J. Schmedt, K. Meise-Gresch, H. Eckert, W. Holand, and V. Rheinberger, *Glass Sci. Technol., Glastech. Ber.*, 2000, **73**, 90.

275 L. van Wullen and M. Jansen, *J. Mater. Chem.*, 2001, **11**, 223.

276 C. Gervais, J. Maquet, F. Babonneau, C. Duriez, E. Framery, M. Vaultier, P. Florian, and D. Massiot, *Chem. Mater.*, 2001, **13**, 1700.

277 J. V. Oglesby, S. Kroeker, and J. F. Stebbins, *Am. Mineral.*, 2001, **86**, 341.

278 F. Angeli, T. Charpentier, S. Gin, and J. C. Petit, *Chem. Phys. Lett.*, 2001, **341**, 23.

279 D. Enke, K. Otto, F. Janowski, W. Heyer, W. Schwieger, and W. Gille, *J. Mater. Sci.*, 2001, **36**, 2349.

280 J. C. C. Chan and H. Eckert, *J. Non-Cryst. Solids*, 2001, **284**, 16.

281 J. McManus, S. E. Ashbrook, K. J. D. MacKenzie, and S. Wimperis, *J. Non-Cryst. Solids*, 2001, **282**, 278.

282 M. Karabulut, E. Metwalli, and R. K. Brow, *J. Non-Cryst. Solids*, 2001, **283**, 211.

283 S. Sakida, M. Shojiya, and Y. Kawamoto, *J. Fluorine Chem.*, 2000, **106**, 127.

284 R. E. Youngman and B. G. Aitken, *J. Non-Cryst. Solids*, 2001, **284**, 9.

285 C. Leonelli, G. Lusvardi, M. Montorsi, M. C. Menziani, L. Menabue, P. Mustarelli, and L. Linati, *J. Phys. Chem. B*, 2001, **105**, 919.

286 G. Pratesi, D. Capitani, C. Cipriani, G. Giuli, and F. Ziarelli, *J. Non-Cryst. Solids*, 2001, **279**, 88.

287 E. Robert, A. Whittington, F. Fayon, M. Pichavant, and D. Massiot, *Chem. Geol.*, 2001, **174**, 291.

288 D. P. Lang, T. M. Alam, and D. N. Bencoe, *Chem. Mater.*, 2001, **13**, 420.

289 S. Sakida, S. Hayakawa, and T. Yoko, *J. Am. Ceram. Soc.*, 2001, **84**, 836.

290 J. Djordjevic, V. Dondur, R. Dimitrijevic, and A. Kremenovic, *Phys. Chem. Chem. Phys.*, 2001, **3**, 1560.

291 M. G. Mortuza, R. Dupree, and D. Holland, *J. Non-Cryst. Solids*, 2001, **281**, 108.

292 N. J. Clayden, S. Esposito, P. Pernice, and A. Aronne, *J. Mater. Chem.*, 2001, **11**, 936.

293 T. Hoche, C. Moisescu, C. Russel, and W. D. Heerdegen, *Glass Sci. Technol., Glastech. Ber.*, 2000, **73**, 119.

294 T. Hoche, C. Moisescu, I. Avramov, C. Russel, and W. D. Heerdegen, *Chem. Mater.*, 2001, **13**, 1312.

295 F. Fayon, D. Massiot, K. Suzuya, and D. L. Price, *J. Non-Cryst. Solids*, 2001, **283**, 88.

296 J. M. Cole, E. R. H. van Eck, G. Mountjoy, R. Anderson, T. Brennan, G. Bushnell-Wye, R. J. Newport, and G. A. Saunders, *J. Phys.-Condensed Matter*, 2001, **13**, 4105.

297 V. Sudarsan and S. K. Kulshreshtha, *J. Non-Cryst. Solids*, 2001, **286**, 99.

298 B. Tischendorf, J. U. Otaigbe, J. W. Wiench, M. Pruski, and B. C. Sales, *J. Non-Cryst. Solids*, 2001, **282**, 147.

299 N. Kuwata, J. Kawamura, Y. Nakamura, K. Okuda, M. Tatsumisago, and T. Minami, *Solid State Ionics*, 2000, **136**, 1061.
300 P. Mustarelli, C. Tomasi, A. Magistris, and L. Linati, *Phys. Rev. B*, 2001, **6314**, 4203.
301 T. Akai, S. W. Martin, and F. Borsa, *Phys. Rev. B*, 2001, **6302**, 4303.
302 S. Sakida, M. Shojiya, and Y. Kawamoto, *J. Non-Cryst. Solids*, 2001, **284**, 22.
303 M. P. Pomies, N. Lequeux, and P. Boch, *Cement Concrete Res.*, 2001, **31**, 563.
304 K. S. Wang, K. L. Lin, and Z. Q. Huang, *Cement Concrete Res.*, 2001, **31**, 97.
305 A. Fernandez-Jimenez and F. Puertas, *Mater. Construccion*, 2001, **51**, 53.
306 A. Simon, R. D. Gougeon, J. L. Paillaud, V. Valtchev, and H. Kessler, *Phys. Chem. Chem. Phys.*, 2001, **3**, 867.
307 R. Simonutti, A. Comotti, S. Bracco, and P. Sozzani, *Chem. Mater.*, 2001, **13**, 771.
308 J. P. Dong, Y. J. Sun, and Y. C. Long, *Chem. Lett.*, 2001, 516.
309 J. G. C. Shen, *J. Phys. Chem. B*, 2001, **105**, 2336.
310 A. Sani, L. Delmotte, C. Marichal, Z. Gabelica, and C. Forte, *Eur. J. Mineral.*, 2001, **13**, 101.
311 M. Hunger, U. Schenk, and A. Buchholz, *J. Phys. Chem. B*, 2000, **104**, 12230.
312 M. Hartmann, 2000.
313 D. Ma, F. Deng, R. Q. Fu, X. W. Dan, and X. H. Bao, *J. Phys. Chem. B*, 2001, **105**, 1770.
314 J. A. van Bokhoven, D. C. Koningsberger, P. Kunkeler, H. van Bekkum, and A. P. M. Kentgens, *J. Am. Chem. Soc.*, 2000, **122**, 12842.
315 E. Rodriguez-Castellon, A. Jimenez-Lopez, P. Maireles-Torres, J. Merida-Robles, P. Braos-Garcia, G. Aguilar-Armenta, E. Flores-Loyola, F. Marmottini, and E. Felici, *Langmuir*, 2001, **17**, 3769.
316 J. G. Nery, M. V. Giotto, Y. P. Mascarenhas, D. Cardoso, F. M. Z. Zotin, and E. F. Sousa-Aguiar, *Microporous Mesoporous Mater.*, 2000, **41**, 281.
317 Y. S. Zhang, M. Qi, Z. Y. Xue, and Q. Z. Li, *Acta Chim. Sin.*, 2001, **59**, 253.
318 M. L. Pena, V. Dellarocca, F. Rey, A. Corma, S. Coluccia, and L. Marchese, *Microporous Mesoporous Mater.*, 2001, **44**, 345.
319 Z. Lin, J. Rocha, A. Ferreira, and M. W. Anderson, *Colloids Surf. A Physicochem. Eng. Aspects*, 2001, **179**, 133.
320 A. M. Goossens, B. H. Wouters, P. J. Grobet, V. Buschmann, L. Fiermans, and J. A. Martens, *Eur. J. Inorg. Chem.*, 2001, 1167.
321 K. Noble, A. B. Seddon, M. L. Turner, P. Chevalier, and I. A. Mackinnon, *J. Sol–Gel Sci. Technol.*, 2000, **19**, 807.
322 A. Bhaumik and S. Inagaki, *J. Am. Chem. Soc.*, 2001, **123**, 691.
323 Y. Z. Khimyak and J. Klinowski, *Phys. Chem. Chem. Phys.*, 2001, **3**, 2544.
324 S. Dzwigaj, M. Matsuoka, M. Anpo, and M. Che, *Catal. Lett.*, 2001, **72**, 211.
325 H. G. Niessen, M. Van Buskirk, C. Dybowski, D. R. Corbin, J. A. Reimer, and A. T. Bell, *J. Phys. Chem. B*, 2001, **105**, 2945.
326 M. Coen, J. C. Lindon, C. Gavaghan, E. Holmes, E. Humpfer, I. D. Wilson, P. D. Stanley, and J. K. Nicholson, *Analyst*, 2001, **126**, 548.
327 J. Brus and M. Skrdlantova, *J. Non-Cryst. Solids*, 2001, **281**, 61.
328 T. Baba, Y. Tohjo, T. Takahashi, H. Sawada, and Y. Ono, *Catal. Today*, 2001, **66**, 81.
329 Z. S. Chao, T. H. Wu, J. L. Ye, G. Z. Chen, and H. L. Wan, *Sci. China Ser. B, Chem.*, 2001, **44**, 103.
330 S. Rozovsky and A. E. McDermott, *J. Mol. Biol.*, 2001, **310**, 259.

331 W. J. Zhang, M. Tansho, S. Matsumoto, and T. Mori, *J. Appl. Phys.*, 2001, **89**, 1734.
332 T. Tao, V. H. Pan, J. W. Zhou, and G. E. Maciel, *Solid State Nucl. Magn. Reson.*, 2000, **17**, 52.
333 M. V. Luzgin, A. G. Stepanov, V. P. Shmachkova, and N. S. Kotsarenko, *Mendeleev Commun.*, 2001, 23.
334 U. Seidel, E. Brunner, J. Karger, and H. Pfeifer, *Z. Phys. Chem . – Int. J. Res. Phys. Chem. Chem. Phys.*, 2001, **215**, 63.
335 K. Shafi, A. Ulman, X. Z. Yan, N. L. Yang, M. Himmelhaus, and M. Grunze, *Langmuir*, 2001, **17**, 1726.
336 W. G. Song, J. B. Nicholas, and J. F. Haw, *J. Phys. Chem. B*, 2001, **105**, 4317.
337 A. Koppl, H. G. Alt, and M. D. Phillips, *J. Appl. Polym. Sci.*, 2001, **80**, 454.
338 S. Bachmann, L. F. C. Melo, R. B. Silva, T. A. Anazawa, I. Jardim, K. E. Collins, C. H. Collins, and K. Albert, *Chem. Mater.*, 2001, **13**, 1874.
339 J. Z. Luo, J. Lannutti, and R. Seghi, *J. Adhesion Sci. Technol.*, 2001, **15**, 267.
340 A. Aliev, D. L. Ou, B. Ormsby, and A. C. Sullivan, *J. Mater. Chem.*, 2000, **10**, 2758.
341 I. V. Kozhevnikov, S. Holmes, and M. R. H. Siddiqui, *Appl. Catal. A, Gen.*, 2001, **214**, 47.
342 P. J. Chupas, M. F. Ciraolo, J. C. Hanson, and C. P. Grey, *J. Am. Chem. Soc.*, 2001, **123**, 1694.
343 F. Deng, Y. Yue, Y. R. Du, C. H. Ye, Y. H. Kong, G. X. Wang, and X. D. Li, *Chin. Sci. Bull.*, 2001, **46**, 188.
344 C. A. Fyfe, J. L. Bretherton, and L. Y. Lam, *J. Am. Chem. Soc.*, 2001, **123**, 5285.
345 S. C. Christiansen, D. Y. Zhao, M. T. Janicke, C. C. Landry, G. D. Stucky, and B. F. Chmelka, *J. Am. Chem. Soc.*, 2001, **123**, 4519.
346 J. K. Bartley, C. J. Kiely, R. P. K. Wells, and G. J. Hutchings, *Catal. Lett.*, 2001, **72**, 99.
347 R. S. G. Ferreira, P. G. P. de Oliveira, and F. B. Noronha, *Appl. Catal. B, Environ.*, 2001, **29**, 275.
348 D. Ma, Y. Y. Shu, C. L. Zhang, W. P. Zhang, X. W. Han, Y. D. Xu, and X. H. Bao, *J. Mol. Catal. A, Chem.*, 2001, **168**, 139.
349 M. A. Aramendia, V. Borau, C. Jimenez, J. M. Marinas, J. R. Ruiz, and F. J. Urbano, *Mater. Lett.*, 2000, **46**, 309.
350 S. Eiden-Assmann, A. M. Schneider, P. Behrens, G. Engelhardt, H. Mandar, and J. Felsche, *Eur. J. Inorg. Chem.*, 2001, 1527.
351 Y. Komori, M. Miyoshi, S. Hayashi, Y. Sugahara, and K. Kuroda, *Clays Clay Miner.*, 2000, **48**, 632.
352 T. Ueda, T. Tatsumi, T. Eguchi, and N. Nakamura, *J. Phys. Chem. B*, 2001, **105**, 5391.
353 A. V. Chadwick, G. Mountjoy, V. M. Nield, I. J. F. Poplett, M. E. Smith, J. H. Strange, and M. G. Tucker, *Chem. Mater.*, 2001, **13**, 1219.
354 M. Fechtelkord, A. Engelhardt, J. C. Buhl, L. Schwalowsky, and U. Bismayer, *Solid State Nucl. Magn. Reson.*, 2000, **17**, 76.
355 M. Fechtelkord, F. Stief, and J. C. Buhl, *Am. Mineral.*, 2001, **86**, 165.
356 F. Babonneau, V. Gualandris, J. Maquet, D. Massiot, M. T. Janicke, and B. F. Chmelka, *J. Sol–Gel Sci. Technol.*, 2000, **19**, 113.
357 Y. J. Lee and C. P. Grey, *Chem. Mater.*, 2000, **12**, 3871.
358 Y. J. Lee, C. Eng, and G. P. Grey, *J. Electrochem. Soc.*, 2001, **148**, A249.
359 V. W. J. Verhoeven, I. M. de Schepper, G. Nachtegaal, A. P. M. Kentgens, E. M. Kelder, J. Schoonman, and F. M. Mulder, *Phys. Rev. Lett.*, 2001, **86**, 4314.

360 Y. Wang, V. Yufit, X. Guo, E. Peled, and S. Greenbaum, *J. Power Sources*, 2001, **94**, 230.
361 R. Siegel, J. Hirschinger, D. Carlier, S. Matar, M. Menetrier, and C. Delmas, *J. Phys. Chem. B*, 2001, **105**, 4166.
362 J. B. Donnet, E. Fousson, L. Delmotte, M. Samirant, C. Baras, T. K. Wang, and A. Eckhardt, *C. R. Acad. Sci. Ser. C, Chim.*, 2000, **3**, 831.
363 J. Glaser, S. Dill, M. Marzini, H. A. Mayer, and H. J. Meyer, *Z. Anorg. Allg. Chem.*, 2001, **627**, 1090.
364 M. Ricco, T. Shiroka, A. Sartori, F. Bolzoni, and M. Tomaselli, *Europhys. Lett.*, 2001, **53**, 762.
365 H. J. Zhu and D. J. W. Grant, *Int. J. Pharm.*, 2001, **215**, 251.
366 C. Gervais, F. Babonneau, and M. E. Smith, *J. Phys. Chem. B*, 2001, **105**, 1971.
367 P. Florian, M. Gervais, A. Douy, D. Massiot, and J. P. Coutures, *J. Phys. Chem. B*, 2001, **105**, 379.
368 A. M. Panich, A. I. Shames, and T. Nakajima, *J. Phys. Chem. Solids*, 2001, **62**, 959.
369 K. J. D. MacKenzie, M. E. Smith, M. Schmucker, H. Schneider, P. Angerer, Z. Gan, T. Anupold, A. Reinhold, and A. Samoson, *Phys. Chem. Chem. Phys.*, 2001, **3**, 2137.
370 B. Nowak and S. Hayashi, *Solid State Nucl. Magn. Reson.*, 2000, **18**, 59.
371 C. Gervais, K. J. D. MacKenzie, and M. E. Smith, *Magn. Reson. Chem.*, 2001, **39**, 23.
372 M. Czank, M. D. Welch, and S. Liu, *Phys. Chem. Miner.*, 2000, **27**, 713.
373 J. Parmentier, K. Liddell, D. P. Thompson, H. Lemercier, N. Schneider, S. Hampshire, P. R. Bodart, and R. K. Harris, *Solid State Sci.*, 2001, **3**, 495.
374 M. Narisawa, Y. Okabe, K. Okamura, T. Taki, and T. Kamiyama, *J. Ceram. Soc. Jpn.*, 2000, **108**, 1110.
375 P. Daniels and C. A. Fyfe, *Am. Mineral.*, 2001, **86**, 279.
376 C. Aubauer, M. Kaupp, T. M. Klapotke, H. Noth, H. Piotrowski, W. Schnick, J. Senker, and M. Suter, *J. Chem. Soc., Dalton Trans.*, 2001, 1880.
377 B. Badraoui, A. Bigi, M. Debbabi, M. Gazzano, N. Roveri, and R. Thouvenot, *Eur. J. Inorg. Chem.*, 2001, 1261.
378 K. O. Kongshaug, H. Fjellvag, and K. P. Lillerud, *Solid State Sci.*, 2001, **3**, 353.
379 G. Grossmann, G. Ohms, K. Kruger, K. Karaghiosoff, K. Eckstein, J. Hahn, A. Hopp, O. L. Malkina, and P. Hrobarik, *Z. Anorg. Allg. Chem.*, 2001, **627**, 1269.
380 H. Haas and M. Jansen, *Z. Anorg. Allgem. Chem.*, 2001, **627**, 1313.
381 L. Muntean, R. K. Subramanian, and D. C. Ailion, *Appl. Magn. Reson.*, 2000, **19**, 403.
382 H. J. Kim, M. Pruski, J. W. Wiench, D. Y. Jeong, and S. H. Choh, *Phys. Rev. B*, 2001, **6305**, 4107.
383 A. J. Woo, Y. S. Park, and S. Y. Jeong, *Solid State Nucl. Magn. Reson.*, 2000, **17**, 15.
384 S. Prasad, P. Zhao, J. Huang, J. J. Fitzgerald, and J. S. Shore, *Solid State Nucl. Magn. Reson.*, 2001, **19**, 45.
385 L. P. Cruz, J. M. Savariault, J. Rocha, J. C. Jumas, and J. D. P. de Jesus, *J. Solid State Chem.*, 2001, **156**, 349.
386 S. K. Kulshreshtha, R. Sasikala, and V. Sudarsan, *J. Mater. Chem.*, 2001, **11**, 930.

8
Multiple Pulse NMR

BY I. BARSUKOV

1 Introduction

The majority of publications in the reported year can be characterised as optimisation of the existing experiments or extension of the existing methods for measurements of new parameters. Very often the improvements can only be achieved in special cases and the new parameters that can be measured are of a limited interest. So no major update to the existing pulse sequence library is required. Still there are some exceptions that are worth implementing. Adiabatic pulses were successfully used for homonuclear H,H and C,C isotropic mixing transfer. This offers an improvement in HCCH and TOCSY experiments at very high fields. Additional experiments were suggested for monitoring slow processes in macromolecules. The use of cross-correlated relaxation to estimate hydrogen bond length was demonstrated. Residual dipolar couplings in protein side chains were utilised to derive structural information. As before the new and improved experiments are summarised in Table 8.1 at the end of the chapter.

2 Shaped Radiofrequency Pulses and Solvent Suppression

2.1 Adiabatic Pulses and Isotropic Mixing. – Wide excitation range of adiabatic pulses stimulated development of their use for isotropic mixing transfer at high magnetic fields. Peti *et al.*[1] demonstrated strong dependence of the transfer efficiency in H,H and C,C TOCSY sequences on the shape of adiabatic pulse and supercycle used. Theoretical simulations and experimental data were presented. The popular WURST pulse has bandwidth transfer efficiency that is inferior to non-adiabatic DIPSI sequences and thus unsuitable for the applications. At the same time tanh/tan and BIR-4 pulses have wider bandwidth than DIPSI sequences when expanded in proposed P9M16 supercycle for C,C transfer and P5P9M16 supercycle for H,H transfer. Additionally the sequences tolerate significant pulse miscalibration and B_1 inhomogeneity. The authors present a modified HCCH-TOCSY sequence with z-magnetisation transfer and a z-filter which offers performance improvement. Kupce *et al.*[2] demonstrated good performance of adiabatic pulses for isotropic mixing transfer under conditions of low magnetic field homogeneity of nanoprobes

Nuclear Magnetic Resonance, Volume 31
© The Royal Society of Chemistry, 2002

when MAS in liquids is used. The analysis of the effect of fast sample spinning on the efficiency of the transfer lead to conclusion that the best performance is achieved under the rotational resonance conditions when the sample appears static in the nutation reference frame.

A combination of isotropic mixing and selective spin inversion with soft pulses in COIN TACSY experiment[3] was used to reduce the effective size of the spin system during isotropic mixing transfer. The new mixing sequence consists of a set of isotropic mixing DIPSI periods separated by selective inversion periods. The overall effect of the sequence is averaging on two different time–scales: fast broadband isotropic mixing and slow averaging of selected couplings. The removal of additional couplings increases the transfer efficiency between non-affected spins.

Decoupling sidebands are the main drawback of heteronuclear adiabatic decoupling. No ideal solution has been found yet so publications addressing this problem continue to appear. An analytical equations for amplitudes and phases of the sidebands were presented by Zhang and Gorenstein.[4] The analysis of the equations shows that the sidebands can be reduced by addition of spectra with different initial decoupling period. Sidebands in the indirect dimension are removed with the proposed synchronised adiabatic decoupling scheme.[5] The decoupling period or the initial decoupling time is adjusted for each value of increment so that the sampling always occurs at the end of complete decoupling period. As a result the effects of J couplings completely average out for all data points leading to the disappearance of the sidebands and corresponding intensity increase for the centre band.

2.2 Shaped Pulses and Other Homonuclear Experiments. – The interference of two soft pulses applied simultaneously at nearby frequencies was analysed by Steffen *et al.*[6] For the on-resonance pulse the frequency shift caused by the second soft pulse affects the resulting flip-angle of the on–resonance pulse. Adjustment of the carrier frequency to follow the induced on-resonance frequency shift restores the performance of the on-resonance pulse. An unexpected effect of a soft pulse presaturation was reported by Kupce and Freeman.[7] When a rectangular presaturation envelope was replaced by a shaped one the authors observed inversion of some signals flanking water resonance. It was concluded that the leading and trailing edges of the shaped pulse act as adiabatic sweeps causing the coupling magnetisations of spins close to on-resonance to be spin-locked. This leads to Hartmann–Hahn coherence transfer and, for the spin lock duration of $1/2J$, to the inversion of the signals.

The excitation sculpting method was expended to the selective inversion of z-magnetisation.[8] The method utilises DANTE train of hard pulses combined with gradient suppression of transverse magnetisation. Application of the selective inversion to z-magnetisation reduces relaxation loses and extends selective methods to larger molecule. Use of shaped pulses in DANTE train produces band-selective inversion. The proposed inversion method can be

combined with selective gradient echo to achieve water suppression in addition to selective inversion.

Signal separation in NMR spectra is not restricted to NMR parameters. Other physical properties can be used to create indirect spectral dimensions. He *et al.*[9] reported 3D EP COSY experiment which utilises electrophoretic migration rates to separate resonances from individual components in mixed solutions. Additional modulation of COSY resonances is introduced in the experiment by a stepwise increase of the electric field. Due to the presence of gradient pulses in the sequence the amplitude of the resonances has a cosine dependence on the field strength with the period depending on the electrophoretic mobility. In the processed spectra, COSY spectra of individual components are observed in separate planes.

Translational diffusion coefficients are commonly measured with gradient-based experiments. The accuracy of the results depends on the gradient linearity. Several methods to minimise this effect were proposed before. Damberg *et al.*[10] suggested a different approach to improve the accuracy of the measurements in non-linear gradient fields. In the proposed method the experimental gradient profile is used for correction at the data analysis stage. This allowed authors to derive accurate diffusion coefficients using full sample volume.

3 NOE, Chemical Exchange and Relaxation

3.1 NOE and Chemical Exchange. – Compared to the previous year hardly any developments have been reported in this area. Cutting *et al.*[11] suggested a sensitivity improvement for the 2D NOE-NOESY experiment detecting water–solute NOEs. The experiment requires highly selective inversion of water magnetisation achieved with long shaped pulses. The performance of the pulses is affected by radiation dumping. As a remedy a hardware feedback circuit was proposed previously to generate a radiation damping compensation field. Cutting *et al.*[11] demonstrated that a compensation field can be successfully generated if the secondary compensation RF field is superimposed directly on the waveform of the excitation pulse. The required compensation field is calculated from the ideal trajectory of the magnetisation during the selective pulse. No hardware modification is required in the new method.

Dalvit *et al.*[12] demonstrated a use of magnetisation transfer from the bulk water to small molecules for detection of weak protein–ligand interactions. The water signal is either saturated or selectively inverted and magnetisation transfer is detected in 1D or 2D mode with the proposed waterLOGSY experiment. The interacting ligands are identified by negative water–ligand NOEs transferred from the bound to the free state of the ligand. Use of the bulk water results in high sensitivity of the experiment.

A modification of GOESY experiment was proposed by Dixon *et al.*[13] In the new version of the experiment called M-GOESY the target proton is selectively excited using 'excitation sculpting' method but not decoded before NOE

transfer as in DPFGSE sequence. The decoding is performed after the NOE transfer, which reduces spectral artefacts. No subtraction of a reference spectrum is required to detect NOEs.

3.2 Relaxation Rate Measurements. – Measurement and analysis of traditional laboratory frame heteronuclear relaxation parameters R_1, R_2 and NOE were summarised by Palmer[14] in a review. The publication concentrates on the dynamic processes on ps–ns time scale in proteins. The theoretical part has a general character, while the experimental section and examples deal mainly with ^{15}N relaxation. A source of systematic error in the commonly used T_2 CPMG measurements was highlighted by Korzhnev *et al.*[15] The authors observed offset-dependent difference between T_2 and $T_{1\rho}$ values. This difference was attributed to the off-resonance effects of ^{15}N 180° pulses. When uncorrected, the error can be misinterpreted as a contribution from a slow conformational exchange. The authors suggested a numerical correction procedure.

The interpretation of relaxation data is most often performed either with 'reduced spectral density' or the Lipari–Szabo approach. The first is easy to implement as the values of spectral density at discrete frequencies are derived from a linear combinations of relaxation rates, but it does not provide any insight into a physical model of the motion. The second approach provides parameters that are related to the model of the internal motion, but the data analysis requires non-linear optimisation and a selection of a suitable model. A graphical way to relate the two approaches is described by Andrec *et al.*[16] Comparison of calculated parametric curves correlating J_H and J_N values for different Lipari–Szabo models of the internal motion with the experimental values provides a range of parameter values compatible with the data and allows to select a suitable model. The method is particularly useful at the initial stage of the data analysis.

A graphical approach was also used by Millet and Pons[17] to analyse anisotropy of rotational diffusion in proteins. The values of $D_\perp$ and $D_\perp/D_\parallel$ compatible with R_1/R_2 ratios are presented as a contour plot. The intersection of the contour plots for different residues provides the values of anisotropy parameters compatible with experimental data. The obtained parameters can be used as starting values for further optimisation. The method is applicable to axially symmetric rotation. A combination of approximate and exact methods was used by Ghose *et al.*[18] to reduce the computational time of the determination of rotational diffusion tensor from NMR relaxation data. The initial values of the tensor components and its orientation are evaluated from the approximate solution, which substantially reduces the search space during the exact calculations. The method was applied for the estimation of relative domain orientation of a dual domain protein.

Canet *et al.*[19] found that the standard Lipari–Szabo approach was inadequate for the analysis of multifield ^{15}N relaxation parameters of a 86 residue protein even when the extended model or anisotropy of the overall motion were introduced. To remedy the situation they used the correlation function in

the form $A + B/(1 + \omega^2\tau^2_s)$ with τ_s representing residue-specific effective correlation time. Variation of τ_s on the residue basis resulted in the successful fit of all relaxation data. The CSA values evaluated from the relaxation data during the suggested analysis showed no significant variation with the position of the residue in the structure. In contrast to this Barber *et al.*[20] successfully applied 'extended model-free approach' to analyse multifield relaxation data of calmodulin. The authors found evidence of a slow interdomain motion in the protein.

Direct experimental measurement of side chain dynamics on μs–ms time scale have been demonstrated for $NH_2$21 and Me-groups.[22] Exchange contribution into T_2 relaxation was evaluated using relaxation dispersion experiment monitoring the cross-peak intensity dependence on the spacing between 180° pulses of the constant-time CPMG element. A similar method was used previously for backbone ^{15}N exchange contribution measurement. Relaxation processes with the rates between 350 and 850 s^{-1} were detected for NH_2 groups and of the order of 1200 s^{-1} for Met Me-groups in T4 lysozyme.

Successful use of the 1D super-WEFT method for the determination of paramagnetic broadening was reported by Ma *et al.*[23] The method allows selective observation of broad resonances in the spectra that can be subsequently curve fitted to deduce paramagnetic broadening.

3.3 Cross-correlated Relaxation Experiments. – The measurements of cross-correlated relaxation rates in constant-time experiments are affected by systematic errors from undesired relaxation effects before and after constant time period. Such errors were analysed for two HNCO-based *J*-resolved Γ experiments[24] proposed earlier for measurement of backbone CSA/DD cross-correlated relaxation rates in proteins. The analytical equations derived for statistical errors were used to optimise the duration of constant time period to minimise the error. It was demonstrated that the systematic error could be removed by recording several experiments at different values of constant time. The equations derived are also applicab-spin coupling on cross-correlated relaxation rates was analysed by Dorai and Kumar.[25] A method based on a set of longitudinal multiple-quantum modes was suggested to derive cross-correlation information in case of strong coupling. The applicability of the method was demonstrated for a small molecule but the approach is also valid in case of macromolecules.

The usefulness of cross-correlated relaxation measurements for deriving structural information was described previously in several publications. More examples of that appeared in the reviewed year. Kloiber and Konrat[26] presented a method for measurement of $^{13}C^{\alpha}_{i}$–$^{1}H^{\alpha}_{i}$ (DD) / $^{13}C'_{i-1}$ (CSA) cross-correlated relaxation. The *J*-resolved experiment is based on HNCO/HNCA sequences creating two-spin coherences between C^{α} and $^{13}C'$ spins which evolve during a constant-time delay. The cross-correlated relaxation rate is evaluated from the intensities of the multiplet components centred at the carbonyl chemical shift and separated by $^{1}J(C^{\alpha},H^{\alpha})$. The relaxation rate correlates with the dihedral angle φ and can be used for its evaluation. It was

also suggested that the experiment could be used to monitor anisotropic backbone dynamics. Vincent and Zwahlen[27] demonstrated efficient magnetisation transfer across glycosidic bond in polysaccharides through ^{1}H–^{13}C DD/^{1}H–^{13}C DD cross-correlated relaxation between dipole pairs centred on the same carbon atom, $C^{1}H^{1}/C^{1}H^{n}$ and $C^{n}H^{n}/C^{n}H^{1}$. The experiment is performed at natural abundance. At the initial state antiphase ^{13}C coherence is created followed by constant-time chemical shift evolution. During the evolution the coherence is transferred into antiphase coherence involving the proton across the glycosidic bond from carbon. The latter is converted into antiphase proton coherence refocused during acquisition. The period for the efficient cross-correlation transfer is substantially smaller than thar required for the HMBC experiment which can make the experiment more sensitive than HMBC for large systems to achieve sequential correlation in polysaccharides.

Riek[28] demonstrated the correlation between hydrogen bond length in Watson–Crick base pairs with ^{1}H (CSA)/$^{15}N\cdots{}^{1}H^{N}$ (DD with proton acceptor) cross-correlated relaxation rates. The measurements are performed with modified 2D ^{15}N–^{1}H–ZQ TROSY experiment. The cross-correlated relaxation rates are evaluated from the cross-peaks ratio in the spectra where the relaxation is either active or deactivated with a selective pulse. The hydrogen bond length is estimated from the ratio of cross-correlated relaxation rate involving DD interaction with the acceptor to the rate of the relaxation in the reference experiment involving DD interaction with the donor.

Backbone torsion angles α and ζ in oligonucleotides can be estimated from the ^{1}H–^{13}C DD/ ^{31}P CSA cross-correlated relaxation. A modified *J*-resolved 2D CT Γ-DQ/ZQ-HCP experiment was proposed by Richter *et al.*[29] for the relaxation rate measurement. The rate is evaluated from the intensities of the multiplet component of DQC and ZQC cross-peaks observed in a single spectrum. The cross-correlated relaxation has a complex dependence on several torsion angles some of which can be determined from the values of $^{3}J(H,P)$ and $^{3}J(C,P)$.

In addition to structural information cross-correlated relaxation is used to monitor local dynamics on different time-scales. Combinations of cross-correlated relaxation rates involving backbone atoms can be used to analyse fast backbone motions.[30] The authors suggested an experiment based on the HNCO sequence that allows one to measure $\Gamma^{DD/DD}(C'C^{\alpha},NH^{N}) + \Gamma^{DD/DD}(C'H^{N},NC^{\alpha})$, $\Gamma^{CSA/DD}(N,NC^{\alpha}) + \Gamma^{CSA/DD}(N,C'C^{\alpha})$ and $\Gamma^{CSA/DD}(C',NH^{N}) + \Gamma^{CSA/DD}(N,NH^{N})$ combinations of cross-relaxation rates. All the rates are obtained using a single experiment from the time dependence of DQ/ZQ multiplet components. Two versions of the experiment were proposed, a 3D and a 2D with the separation of multiplet components corresponding to α and β states of H^{N} into different sub-spectra. The latter reduces spectral overlap. The analysis of the measured rates suggested a concerted motion of the α helix in ubiquitin. Cross-correlated ^{13}C–^{1}H DD/^{13}C–^{1}H DD relaxation within a CH_2 group was used to examine side chain dynamics in proteins.[31] The rates were measured in a modified 2D HCCH experiment from the differential intensities of cross-peak multiplet components. A significant difference in the

mobility of the residues in the active site and the structural part of the protein was found.

A new method to monitor slow dynamics on μs–ms time-scale was proposed in two publications.[32,33] The method is based on the observation that cross-correlated chemical shift modulation has different effects on the relaxation of ZQ and DQ coherences. The most efficient source of the cross-correlation is conformational exchange, which leads to significant changes in chemical shifts. The rates of cross-correlated relaxation for C^{α}–C^{β} group in protein side chains can be evaluated from the difference between DQ and ZQ C–C relaxation directly measured with a modified HNCOCA experiment as suggested by Fruh *et al.*[33] The evidence for the slow motions affecting side chains was found in the loop regions. A different method was used by Kloiber *et al.*[32] to measure relaxation induced by cross-correlated chemical shift modulation in the backbone NH groups of protein. They based the experiment on the observation that differential ZQ and DQ relaxation leads to the exchange of the two-spin coherence terms $2I_xS_x$ and $2\ I_yS_y$. Thus the relaxation difference can be measured in a modified 2D HSQC experiment by comparing the cross-peak intensities originated from each term. In the case of NH groups in proteins the main source of cross-correlated chemical shift modulation is associated with the formation and breaking of hydrogen bonds.

4 Coupling Constants Measurements

4.1 Scalar Couplings. – Several modifications of the existing methods were proposed for measurement of coupling constants in proteins. A sensitivity improvement of the *J*-multiplication HSQC method was proposed by Xia *et al.*[34] The method combines the ^{15}N chemical shift evolution and the evolution with $^{3}J(H^{N},H^{\alpha})$ coupling resulting in HSQC cross-peaks exhibiting the proton homonuclear spin–spin coupling splitting in ^{15}N dimension. By substituting HSQC with HMQC sequence in the new MJ-HMQC experiments the authors achieved ~34% sensitivity enhancement for a ~100 residue protein, as well as some line-width reduction. Lohr *et al.*[35] suggested a modification of constant-time 3D heteronuclear relayed E.COSY experiment to measure $^{3}J(H^{\alpha},C^{\gamma})$ couplings. The sequence utilises triple-quantum coherence within a $C^{\beta}H_2$ group that has favourable relaxation properties and avoids scalar coupling evolution between the spins involved in the coherence. The coherence is excited in the initial stage of the pulse-sequence and then transferred to the H^{α} for observation. The resulting cross-peaks have E.COSY multiplet structure. The method is applicable to the side chains with unprotonated C^{γ} groups. The coupling constant is extracted by numerical line-shape simulation and used for the estimation of the torsion angle $\chi 1$.

Sensitivity and resolution improvements offered by the TROSY method have been utilised in two modified sequences for measuring coupling constants in proteins. Permi *et al.*[36] proposed a 3D α/β-HN(CO)CA-J TROSY sequence for evaluation of $^{3}J(N,H^{\alpha})$ couplings related to the torsion angle ψ. The $^{1}H^{\alpha}$

acts as a passive spin during the ^{15}N and $^{13}C^{\alpha}$ coherences. The desired E.COSY cross-peak pattern is generated from a combination of two spectra in which the $^{13}C^{\alpha}$ magnetisation is edited with respect to the spin state of directly bound proton using a spin-state selective filter element. As a result the multiplet components are separated by the coupling constant of interest, $^{3}J(N,H^{\alpha})$ in one dimension and by a scaled coupling, $^{1}J(C^{\alpha},H^{\alpha})$ in another. The resolution in the ^{15}N dimension is enhanced with semi-constant-time TROSY evolution. The signal separation in the spectrum is better then in the HCACO{N} experiment suggested earlier for measurement of the same couplings due to the high dispersion of the HN-resonances. Lohr and Ruterjans[37] proposed a sequence for measurement of $^{3}J(N,C^{\gamma})$ and $^{3}J(C',C^{\gamma})$ in aromatic residues using quantitative *J*-correlation method. The sequence is based on a 3D HN(CO)CG-TROSY experiment with HMQC-type ^{15}N–$^{13}C'$ transfer that allows longer dephasing period with $^{3}J(N,C^{\gamma})$ coupling than the HSQC version. The reference peaks are present in the in the same spectrum as the *J*-transferred peaks which makes it possible to extract all the coupling from a single spectrum.

4.2 Couplings across Hydrogen Bonds. – Two publications suggested improvements in the methods of detection and measurement of couplings across hydrogen bonds in nucleotides. Yan *et al.*[38] addressed the problem of broadening of fast relaxing component of ^{15}N doublet with the increase of nucleotide molecular weight. This can lead to the decrease in the intensity and inability to deduce $^{h}J(N,N)$ couplings from J_{NN}-TROSY experiment. In the modified experiment two separate spectra are recorded corresponding to individual multiplet components. For the spectrum registering the fast relaxing component the corresponding coherence is active only during evolution time t_1, while the coherence transfer across the hydrogen bond is achieved through slow relaxing component. The positions of the cross-peaks in the two spectra differ only by the value of the coupling constant. The intensities of the peaks corresponding to the multiplet components are close. Majumdar *et al.*[39] suggested a modification of the method of detection of hydrogen bonds in nucleotides through non-exchangeable protons in the case of exchange broadening of imino/amino proton resonances. The experiment extends the range of magnetisation transfer by involving protons separated by four bonds from NH···N moiety. This is crucial for detection of $N6H_2$···N3 hydrogen bond in AG pairs where the nearest non-exchangeable proton H2 is separated by four bonds from donor N6. Two sequences were described: 'straight-through' (H6)N6N3H2 and 'out-and-back' H2N6N3. Both experiments detect $^{2h}J(N6,N3)$ coupling and utilise coherence transfer through $^{3}J(H2,C6)$ interaction.

Detection of very small coupling $^{3h}J(N^{\varepsilon},C'^{\gamma})$ between Arg and Asp side chains was demonstrated by Liu *et al.*[40] To improve sensitivity a modified 2D soft CPD-H(N)CO experiment was used. The main sensitivity enhancement is produced by the use of band-selective CPD decoupling of $^{13}C^{\delta}$ of Arg during the entire N–C′ transfer periods. This decoupling removed DD relaxation contribution from $^{13}C^{\delta}$. Additionally, $^{15}N^{\varepsilon/\eta}$ pulses were used to reduce signal

from backbone NH groups. The value of the coupling constant was estimated to be smaller than the analogous constant $^{3b}J(N,C')$ through backbone hydrogen bonds.

4.3 Residual Dipolar Couplings. – The high informational content of residual dipolar couplings and a large number of possible combinations of couplings in different systems stimulated a substantial number of publications. The couplings involving backbone nuclei are usually measured with modified triple-resonance experiments. The residual dipolar couplings obtained for different nuclei can be used to derive the orientation of the alignment tensor. As pointed out in ref. 41 the instability of the alignment system can lead to systematic deviations if the couplings are measured in separate experiments. To improve the situation the authors proposed to obtain two or more different couplings from a single experiment by introducing the evolution with the couplings of interest in two indirect dimensions. The resonance overlap due to the increased number of multiplet components is alleviated with IPAP method of individual multiplet component selection. The main drawback of the method is reduced sensitivity due to the additional multiplet splitting which is partly compensated for by obtaining two values for each coupling from the same spectrum. The method is illustrated on 3D HNCO-based 3D (HA)CA(CO)NH-based experiments that combine the measurement of $^1D(H,N)$ with $^1D(C^\alpha,C')$ or $^1D(C^\alpha,H^\alpha)$.

TROSY variants of the experiments were used to improve the sensitivity. Chou *et al.*[42] suggested an improved method of measuring of $^1D(N,C')$ coupling. The main difficulty in obtaining accurate results for this coupling is the small value of residual dipolar splitting due to low magnetogyric ratio of both nuclei involved. The proposed experiment is based on TROSY-HNCO sequence and uses a quantitative J correlation method to derive the coupling. The value of the coupling is calculated from the relative cross-peak intensities in two spectra obtained with $^1J(N,C')$ dephasing interval set to $\sim 1/(2^1J(N,C'))$ (reference) and $\sim 1/^1J(N,C')$. It was shown that the error in the measured coupling is inversely related to the signal-to-noise ratio in the spectra and can be less then 0.3 Hz for a medium size protein. An extension of the measurement of $^1D(C^\alpha,C^\beta)$ to large proteins was proposed by Evenas *et al.*[43] The method is based upon HN(CO)CA TROSY and requires deuteration of the protein. Coupling constants are evaluated either in 2D mode from the modulation of ^1H–^{15}N HSQC-type cross-peaks with the evolution due to $^1J(C^\alpha,C^\beta)$ or in a 3D mode where this evolution is present in $^{13}C^\alpha$ dimension. Both approaches produce comparable results.

An experiment for a simultaneous measurement of $^1D(H^\beta,C^\beta)$ and $^1D(H^\alpha,C^\alpha)$ was proposed by Chow and Bax.[44] The sequence is based on a 3D CB(CA)CONH experiment with the use of a quantitative approach to evaluate the coupling. Three spectra with different positions of ^1H 180° pulse in the constant-time period are recorded in an interleaved fashion and the couplings are derived with a least-square minimisation routine. For methylene groups only the sum of $^1J(C,H)$ couplings is available from the experiment. The

comparison of $^1D(H^\beta,C^\beta)$ with the residual dipolar couplings involving C^α can be used to deduce the value of dihedral angle $\chi 1$.

The evolution in the indirect dimension of a ^{15}N–^1H HSQC spectrum is affected by $^1J(N,C^\alpha)$ and $^2J(N,C^\alpha)$ couplings, creating the possibility for extraction of the coupling from the spectrum. The main difficulty in the measurement is imposed by small values of the couplings and overlap of the multiplet components. A solution suitable for small proteins was presented by Heikkinen *et al.*[45] The method is based on the ^{13}C-HSQC-TOCSY-^{15}N-HSQC sequence combined with an IPAP spin-state selection. The spin-state selective filter for $^{13}C^\alpha$ is introduced prior the H^α to H^N coherence transfer by isotropic TOCSY mixing. As the result two HSQC spectra are produced in which corresponding cross-peaks are displaced with the larger $^1J(N,C^\alpha)$ coupling. Cross-peaks in each of the spectra have in-phase doublet structure with respect to $^2J(N,C^\alpha)$ coupling. The small linewidth in the ^{15}N dimension for small proteins allows one to resolve and measure this coupling while the $^1J(N,C^\alpha)$ coupling is obtained from the spectra corresponding to different spin-states.

Experiments for measurement of residual carbon–proton and proton–proton couplings in protein side chains were proposed in several publications. Two methods are based on modified HSQC sequences. Carlomagno *et al.*[46] proposed a SPITZE-HSQC sequence that allows simultaneous measurement of one-bond homonuclear and heteronuclear couplings in CH_2 groups. The experiment utilises spin-state selective S^3E transfer to generate spectra containing only one of the multiplet components of $^{13}C/^1H$ cross-peak thus reducing cross-peak overlap. The couplings are derived from the comparison of four spectra containing different multiplet components. The method was demonstrated for Gly residues. A sequence for selection of individual outside multiplet components of ^{13}C quartet in the ^1H-^{13}C CT-HSQC spectrum was proposed by Kontaxis and Bax.[47] An additional dephasing delay followed by a z-filter is introduced prior to the CT evolution time of the HSQC spectrum. The variation of this delay has different effect on the multiplet components. The individual components can be generated from a linear combination of four spectra acquired at different dephasing delays. The value of $^1D(C,H)$ is extracted from the cross-peak displacements between the two IPAP sub-spectra.

The $^1D(H,H)$ can be measurement in the 2D DiM experiment.[48] The method is based on the observation that residual dipolar coupling leads to line splitting even in the isolated Me-group producing a triplet with relative intensities 1:2:1. The central component can be suppressed in the proposed modified HSQC experiment resulting in antiphase multiplet structure. The coupling is evaluated from the distance between the multiplet components. The accuracy of the method is reduced for the small values of the splitting due to the partial overlap of the multiplet components. In the first approximation $^1D(H,H) \approx 2.3\ ^1D(C,H)$ in Me-groups, making the information from both couplings redundant.

Residual dipolar couplings can be used for coherence transfer in the same manner as the scalar ones. This feature was utilised in the proposed CT-COSY

based method for measurement of residual homonuclear D(H,H) couplings.[49] The couplings are evaluated from the ratio of cross-peak to auto-peak amplitudes. The method produces reasonably accurate results only in the case of small number of coupled spins as the evolution with passive couplings affects cross-peak intensity. The accuracy can be somewhat improved by recording several spectra at different values of the constant time. The sensitivity of the experiment is comparable to the sensitivity of NOESY experiment. As additional advantages no indirect coherence transfer occurs when residual dipolar coupling are used and the cross-peak intensities are inversely proportional to the third rather than the sixth power of the interproton distance. Their properties make the experiment a valid supplement to NOESY distance estimates. A 3D ^{15}N-resolved version of the experiment was also presented. An analogous method was used by Hennig *et al.*[50] to detect correlation between base protons and phosphorous nuclei in nucleotides. The proposed experiment, 2D RADAR TOCSY, provides a direct link between phosphate backbone and nucleotide bases. The sequence is a straightforward extension of hetero-TOCSY experiment. A substantial sensitivity improvement of the method was achieved by applying band-selective homonuclear decoupling in the acquisition period. This decoupling removes residual homonuclear proton coupling which otherwise broadens the signals. The Hartmann–Hahn transfer in the presence of scalar and residual dipolar couplings was analysed by Luy and Glaser.[51] The analytical functions were derived for polarisation and coherence transfer in a coupled three-spin system. The efficiency of the transfer is analysed as a function of the relative coupling constants.

Two methods were proposed for deriving structural information from heteronuclear couplings in nucleotides. In one of them the residual dipolar coupling D(H3′,P) in nucleotides was measured by the traditional difference method with a 2D CT-NOESY sequence.[52] The coupling is evaluated from the relative cross-peak intensity in two experiments where the evolution with ^{31}P–^{1}H coupling is either present or refocused during the constant-time evolution. The evolution with the residual homonuclear proton coupling was removed by selective refocusing of H3′ resonances in the constant-time evolution period leading to line-width reduction. The use of NOESY experiment provided good signal separation in the method and a possibility of the coupling from several different cross-peaks. Due to the relatively uniform H3′–P distance in B-DNA the coupling constant value can be used to determine the vector orientation.

The ratio between one-bond and internucleotide ^{15}N–^{1}H dipolar couplings in nucleotides was used to derive the length of the hydrogen bond.[53] The coupling was measured with a modified 2D HNN sequence. The ST2P-TROSY element was used for the selection of slow-relaxing ^{15}N doublet component during ^{15}N–^{15}N transfer. Two spectra were recorded with ^{1}H spin-state flipped or remaining the same before ^{15}N evolution resulting in the relative cross-peak displacement with the corresponding ^{15}N–^{1}H coupling between them. Assuming the perfect linear geometry of H-bonds a significant difference between the hydrogen bond length was observed between C–G and

A–T basepairs. The method has high precision although the absolute value of the distance depends on the quality of the nucleotide structure used for data interpretation.

5 Inverse Proton Detected Correlation Spectroscopy

5.1 Isotope Filtered Experiments. – High-quality suppression of ^{13}C-labelled protein resonances using the WURST-based filter scheme was demonstrated for a protein–DNA complex by Iwahara *et al.*[54] The method was applied either as [F1,F2] single-stage filters or [F2] double-stage filter in a 2D NOESY experiment, similar to the original scheme. The intensities obtained from both described experiments are directly comparable, as proton magnetisation is transverse for the same duration in each experiment. The sensitivity of the WURST-based double experiment is higher than that of the corresponding experiment based on hard pulses as the filter duration is shorter. Melacini[55] proposed to separate resonances of protons attached to ^{13}C and ^{12}C using *J*-resolved method, thus combining isotope filtering and editing in a single experiment. The method is implemented with 4D quadrature-free constant-time NOESY-HSQC experiment. The constant-time *J*-resolved evolution is combined with semi-constant-time chemical-shift evolution prior NOE transfer. A standard HSQC sequence follows NOE mixing period. The resulting spectrum has an additional *J*-resolved dimension as compared to a 3D NOESY-HSQC spectrum. In the *J*-resolved dimension cross-peaks of ^{12}C-bound protons are observed in the plane $J = 0$ Hz and the ^{13}C-bound ones in the plane $J = {}^{1}J(\mathrm{H,C})/2$. The variation in $^{1}J(\mathrm{H,C})$ does not affect the separation of cross-peaks from labelled and unlabelled molecules. Adiabatic ^{13}C pulses were applied for uniform inversion over the whole range of ^{13}C chemical shifts.

Two publications described the use of filtered experiments to facilitate coupling constants measurement. The $^{1}J(\mathrm{H^N,H^\alpha})$ couplings of unlabelled peptide in complex with ^{13}C,^{15}N-protein can be measured with 2D C,N-filtered HNHA experiment.[56] In the proposed sequence the $\mathrm{H^N}$ to $\mathrm{H^\alpha}$ transfer period is combined with ^{13}C,^{15}N-filter eliminating signals of ^{13}C and ^{15}N-bound protons. Resulting 2D homonuclear spectrum contains only cross-peaks of unlabelled peptide. The coupling constants are evaluated in a 'quantitative' manner from the ratio of diagonal- and cross-peak intensities. The sign and magnitude of long-range ^{1}H–^{19}F couplings in F-labelled sugar bases containing CHF groups can be obtained from X-filtered E.COSY experiment.[57] The filter is tuned for $^{2}J(\mathrm{H2',F2'})$ coupling and selects fluorine-coupled proton resonances. Following the selection the magnetisation is transferred to nearby protons using NOESY or TOCSY mixing. The resulting spectrum contains cross-peaks of E.COSY multiplet patterns with respect to ^{1}H–^{19}F couplings. The large $^{2}J(\mathrm{H2',F2'})$ coupling provides effective multiplet component separation and allows measurement of small long-range ^{1}H–^{19}F couplings.

5.2 Isotope Edited Experiments. – Methods of selection according to the number of protons attached to individual carbons were developed further. The MUSIC scheme was incorporated into more experiments. The method uses spin-topology selection with double and triple-quantum filters and has been implemented in various triple-resonance experiments previously. Sequences for two more experiments were presented: 3D MUSIC CBCANH and 3D MUSIC CBCA(CO)NH[58] allowing selection of resonances of side chains containing CH_2 or CH_3 groups. Meissner and Sorensen[59] introduced DEPT-based multiplicity editing into 3D HCCH-COSY and HCCH-TOCSY experiments. The editing is combined with polarisation transfer which reduces intensity loses due to transverse relaxation. The selection of the resonances corresponding to the required multiplicity is achieved by a linear combination of spectra recorded with different flip angles of proton editing pulses. In the double-filter scheme nine spectra are measured in total and all possible transfer combinations CH_n–CH_m with n,m = 1, 2, 3 are extracted at the processing stage. In addition to simplification of the spectra the intensities of the diagonal peaks are reduced.

Schubert *et al.*[60] proposed two triple-resonance experiments for selection of amide resonances of residues sequential to proline in ^1H–^{15}N HSQC spectra. The selection is based upon the absence of amino proton in proline residues. For the selection of resonances from the residues preceding proline the coherence transfer starts from $^1H^\alpha$ of the preceding residue, is transferred to the ^{15}N of proline for the selection and then to the $^1H^N$ of the preceding residue for detection. In the experiment selecting resonances from residues following proline the transfer starts on $^1H^\alpha$ of proline, is transferred to intraresidue ^{15}N for selection and then to $^1H^N$ of the following residue for detection. In both experiments when coherence is on ^{15}N of proline the evolution with $^1J(H,N)$ couplings is induced for non-proline residues and when the coherence is antiphase it is removed by ^1H decoupling. The experiments are executed in 2D mode with indirect ^{15}N dimension corresponding to the chemical shift of either proline or sequential residue depending on the choice of the chemical shift evolution time in the sequence. Thus the experiments can be additionally used to establish sequential connectivity for the residues neighbouring proline. The sensitivity of the experiment is low due to long coherence transfer delays.

A 1D filtering scheme based upon carbon spin-state selection was described by Parella and Belloc.[61] The authors demonstrated that incorporation of an additional 90° ^{13}C pulse prior to the acquisition into HMQC or HSQC sequence allows the selection of the proton multiplet component corresponding to the α or β state of carbon depending on the phase of the pulse. The selected spin state can be propagated to other protons with appropriate mixing schemes in order to measure long-range proton–carbon coupling constants. When carbon-selective INEPT transfer is applied the method can be used for 1D ^{13}C spectrum editing, allowing coupling constant measurement in 1D mode in crowded spectra.

5.3 Heteronuclear Double Resonance Experiments. – *5.3.1 HSQC/HMQC.* A number of modifications were proposed for detection of long-range ^1H–^{13}C

correlations in small molecules. A 2D HMSC experiment was designed by Burger *et al.*[62] for simultaneous detection of single-bond and long-range correlations. The sequence has an additional BIRD element incorporated into long-range transfer period of HMBC experiment. This element is tuned for ^1J(H,C) coupling and provides the labelling of single-bond coherences. The single-bond or long-range cross-peaks are separated into different subspectra by adding or subtracting two spectra recorded in the interleaved fashion with different phases of ^{13}C pulses. The main advantage of the method is the reduction in number of required experiments for resonance assignments in small molecules. Differentiation between two-bond and three-bond long-range carbon–proton correlation can be achieved in 2D ^2J,^3J-HMBC experiments.[63] The method is based on combining the long-range transfer with the coherence evolution due to homonuclear couplings using the ACCORDION method. This results in the E.COSY-type multiplet structure of cross-peaks. The presence of non-zero ^3J(H,H) in case of ^2J(C,H) transfer leads to the skewed appearance on the C/H cross-peak in the spectrum. In case of ^3J(C,H) transfer the coupling constant ^4J(H,H) is negligibly small and there is no skewness in the multiplet structure. The reliance on the homonuclear coupling does not allow the transfer range differentiation for quaternary carbons. An echo-antiecho type sensitivity enhancement was introduced into a gradient-selection HMBC experiment.[64] The proposed sequence is a straightforward implementation of the method and offers the usual $\sqrt{2}$ enhancement.

A new element for simultaneous indirect detection of ^{13}C and ^{15}N signals in labelled proteins was proposed by Uhrin *et al.*[65] The CT-^{13}CH$_3$, VT-^{15}N-HSQC sequence combines constant-time carbon evolution with variable delay nitrogen evolution. This is achieved by the variation of the position of a 90° ^{15}N pulse creating transverse coherence within the ^{13}C constant-time period. The maximum indirect acquisition time for both nuclei is determined by constant-time period set to $1/^1J$(C,C) = 28.6 ms. The method is best suited for detection of CH$_3$ signals due to their slower relaxation. The proposed element was incorporated into NOESY-based experiments resulting in 3D NOESY-CH$_3$NH and 3D ^{13}C,^{15}N HSQC-NOESY-CH$_3$NH sequences. The experiments have high resolution in the ^{13}C dimension but suffer from relaxation intensity losses, thus being applicable mainly to small proteins. A similar method of simultaneous indirect detection of ^{13}C and ^{15}N signals was also implemented into the experiments for detection of NOE involving aromatic protons 3D H$_{aro}$-NOESY-CH$_3$NH and 3D C$_{aro}$-NOESY-CH$_3$NH.[66] The selection of aromatic ^{13}C-signals was achieved with shaped pulses.

Heteronuclear coherence transfer periods of HSQC or HMQC experiments are often incorporated into semi-constant-time proton chemical shift evolution to reduce the effective relaxation and thus improve sensitivity. This method was further extended by Bazzo *et al.*[67] to utilise ^{15}N chemical shift evolution period of HMQC-NOESY experiment for further reduction of the proton effective relaxation rate. This is achieved by changing the position of refocusing ^{1}H pulse in the middle of the heteronuclear MQ evolution period when ^{1}H evolution is encoded. As the result the MQ evolution period that is

normally used only to monitor heteronuclear evolution is fully incorporated into the ^{1}H chemical shift evolution period. As the MQ evolution period increases the effective proton relaxation decreases. The resulting cross-peak is narrower in the indirect proton dimension while the integral intensity remains unchanged. The expected sensitivity increase is 55–5% for proton relaxation times 5–20 ms. The method is applicable to XH groups such as backbone NH or aromatic CH. Sequences for 3D ^{1}H-^{13}C HMQC-NOESY and 3D ^{1}H-^{15}N HMQC-NOESY experiments were described and tested.

Two heteronuclear correlation experiments involving ^{31}P were described. Kaikkonen and Otting[68] proposed to use a DQ-^{31}P experiment to detect $^{1}H5'/^{31}P$ and $^{1}H5'/^{31}P$ correlations in nucleotides. In the method the homonuclear $^{1}H5'/^{1}H5'$coherence is exited, transferred to ^{31}P for chemical shift mapping and returned back to the protons for monitoring. As the proton antiphase coherence is not refocused prior acquisition cross-peaks have doubly antiphase multiplet structure in the acquisition dimension. This multiplet structure is advantageous in case of large line-width. The use of DQ coherence allows the suppression of $^{1}H4'/^{31}P$ cross-peaks, thus improving resolution in the spectra. The extension of the experiment into 3D was described. The high sensitivity of ^{31}P nuclei and 100% natural abundance can be utilised for detection of ^{15}N–^{31}P correlations in phosphorus–nitrogen compounds.[69] The suggested 2D 31P, 15N{1H} HSQC experiment is a straightforward adaptation of proton-based HSQC to the direct detection of ^{31}P nuclei. The resonances from ^{14}N–^{31}P groups are suppressed with gradient coherence selection. Echo–antiecho gradient scheme was used for sensitivity enhancement.

5.3.2 TROSY. The number of publications in this area was substantially reduced relative to the previous year. A new TROSY element was proposed by Riek *et al.*[70] The method utilises ^{13}C–^{13}C DD/^{13}C CSA cross-correlation in addition to previously used ^{13}C–^{13}C DD/^{13}C CSA cross-correlation to reduce ^{13}C relaxation in nucleotides. Both TROSY enhancements were introduced into a HCN experiment in a concatenated fashion, resulting in a simple and robust sequence TROSY-HCN. The sequence achieves ^{1}H–^{13}C–^{15}N coherence transfer with both mechanisms of relaxation compensation active when ^{13}C coherence is transverse. Two variants of the experiment were proposed, with and without suppression of the anti-TROSY component. The first version is used for small molecules, while the second is applicable to the large molecules where the intensity of anti-TROSY component is negligible. The additional ^{13}C–^{13}C DD/^{13}C CSA relaxation compensation mechanism of the new experiment provided 15% sensitivity enhancement in a 17 kDa protein–DNA complex relative to the experiment that utilises only ^{13}C–^{13}C DD/^{13}C CSA compensation. Quantitative comparison of different relaxation compensation schemes including the use of multiple-quantum coherence was presented.

Other publications dealt with optimisations of the previously proposed sequences. Pervushin *et al.*[71] proposed a new element ^{15}N,^{1}H/^{13}C,^{1}H-TROSY

for simultaneous detection of ^{15}N–^{1}H and ^{13}C–$^{1}H_{aro}$ in aromatic rings. The element is a direct combination of the individual TROSY elements. To improve cross-peak separation the ^{15}N–^{1}H and ^{13}C–$^{1}H_{aro}$ correlations are extracted by addition or subtraction of two interleaved sub-spectra with the opposite phase of ^{13}C excitation pulse. The delays of the back-transfer INEPT part of the sequence was adjusted for optimum intensity of ^{15}N–^{1}H and ^{13}C–$^{1}H_{aro}$ signals. In addition, the signals of the NH_2 groups, which are suppressed in a conventional TROSY spectra, are observed with high sensitivity. The new element was incorporated into 3D [^{1}H,^{1}H]-NOESY-^{15}N,^{1}H/^{13}C,^{1}H-TROSY experiment and used to detect NOEs in a perdeuterated 80 kDa protein in detergent micelles.

Pellecchia *et al.*[72] described a modification of TROSY for selective observation of solvent-exposed amide protons. The selection is based on magnetisation transfer from water. The proposed SEA-TROSY experiment starts with a ^{15}N double filter that eliminates all amide proton magnetisation with minimum affect on equilibrium water magnetisation. The filter is followed by magnetisation transfer delay during which solvent accessible amide proton acquire magnetisation from the solvent. Finally a water flip-back version of TROSY is used to acquires the spectrum. As the result the spectrum contains only cross-peaks from amide groups in fast exchange with solvent. The filter element can be easily added to other experiments. A version of the 3D SEA-HNCA experiment was described. It was suggested that the filtering method is particularly useful in binding studies for large proteins. The experimental data were presented for a 70 kDa protein. A straightforward addition of the standard TROSY element to produce 3D and 4D ^{15}N/^{15}N HSQC-NOESY-TROSY experiments was reported elsewhere.[73]

5.4 Heteronuclear Triple Resonance Experiments. – A very small number of new triple-resonance experiments was reported. A version of the 3D HNCA experiment was presented[74] that suppresses coherence transfer through $^{1}J(N,C^{\alpha})$. The method is based on the scalar couplings of sequential ^{15}N and $^{13}C^{\alpha}$ to the same $^{13}C'$ which is not the case for the intraresidue ^{15}N and $^{13}C^{\alpha}$. During ^{15}N to $^{13}C^{\alpha}$ transfer the antiphase coherence relative to $^{13}C'$ is created and then refocused when the $^{13}C^{\alpha}$ coherence is transverse, which is only possible for the sequential transfer. The presented TROSY version of the experiment reduces signal losses due to relaxation. The experiment was suggested as a replacement of the HN(CO)CA experiment for sequential assignment when using very high magnetic field, as the large value of $^{13}C'$ CSA under those conditions increases $^{13}C'$ relaxation and makes the later experiment less sensitive.

A TROSY version of the 3D HNCAN experiment was described by Lohr *et al.*[75] The experiment correlates chemical shifts of backbone NH group with ^{15}N resonances of preceding and following residues. The out-and-back coherence transfers through $^{1}J(N,C^{\alpha})$ and $^{2}J(N,C^{\alpha})$ couplings in sequential manner. During indirect detection of the sequential ^{15}N resonances the $^{1}J(N,H)$ decoupling is achieved with a pair of 180° pulses to preserve the TROSY

component. Two variants of the experiment were proposed that differ in the final step of $^{13}C^{\alpha}$–$^{15}N_{Pro}$ transfer. In one variant HSQC sequence was used. It has a shorter time of transverse $^{13}C^{\alpha}$ coherence evolution, but the efficiency of the transfer is reduced. In the other variant a HMQC sequence was used with better transfer efficiency, higher resolution, but larger relaxation losses. The choice of method mainly depends on the relaxation rate of $^{13}C^{\alpha}$. The main suggested use of the experiment is to establish sequential links across proline residues for resonance assignment. Additionally the experiment can be used to supply extra sequential information for other residues.

To overcome the problem of low dispersion of sugar resonances in nucleotides Hu *et al.*[76] proposed to incorporate HCN transfer into HCCH-type sequences resulting in 3D MQ-HCN-CCH-TOCSY and 3D MQ-HCN-CCH-COSY experiments. The coherence transfer pathway starts with H1′-C1′ transfer followed by an out-and-back transfer to N1/N9 for indirect detection and subsequent transfer through ^{13}C network. As a result the CCH spectra are additionally resolved with ^{15}N chemical shift. During the C′–N1/N9 transfer MQ H1′/C1′ coherence is active to reduce the relaxation losses due to ^{13}C relaxation. The experiments were successfully applied to a 23-mer RNA aptamer.

Table 8.1 *Summary of new or improved experiments and methods*

Experiment/method	*Aims*	*Ref.*
Adiabatic pulses and isotropic mixing		
Use of adiabatic pulses for C,C and H,H TOCSY transfer, HCCH-TOCSY	Efficient broad-band transfer. Low sensitivity to misadjustments. High fields.	1
2D adiabatic TOCSY MAS	Efficient TOCSY transfer in MAS liquid samples at low homogeneity of magnetic filed. Applicable to nanoprobes	2
Analytical expression for amplitudes and phases of adiabatic decoupling sidebands	Minimisation off adiabatic decoupling artefacts	4
Synchronised adiabatic decoupling	Removal of sidebands from the adiabatic decoupling in the indirect dimension	5
COIN TACSY	Selective isotropic mixing transfer. Simplification of spin coupled network	3
Shaped pulses and homonuclear experiments		
Theoretical analysis of simultaneous application of two soft pulses	Optimisation of shaped-pulse inversion	6
Adiabatic effect of the shaped pulse presaturation	Inversion of water-flanking signals during shaped pulse presaturation	7
Excitation sculpting for longitudinal magnetisation	Multiplet-selective excitation, band-selective excitation, water suppression	8
3D EP-COSY	Separation of resonances on the basis of electrophoretic migration rates.	9

Diffusion coefficient measurement in non-linear field gradients	Improve accuracy and make use of the full sample volume	10
NOE and chemical exchange		
Selective water inversion in 2D NOE-NOESY	Improve observation of NOEs between bound water and protein	11
WaterLOGSY	Detection of NOEs between protein bound water and a small ligand. Evidence of ligand–protein interaction	12
1D M-GOESY	Modified GOESY experiment for 1D NOE measurements in small molecules	13
Relaxation rate measurement		
Review on relaxation rate measurements	Experimental methods, theory, analysis, protein applications	14
Off-resonance effects of ^{15}N T_2 CPMG	Systematic up to 10% ^{15}N T_2 overestimation in 180° CPMG train	15
Graphical approach to Lipari–Szabo mapping	Evaluation of Lipari–Szabo parameters without non-linear fit	16
Graphical analysis of anisotropic relaxation data	Estimation of components of axially symmetrical rotational diffusion tensor	17
Multi-field analysis of ^{15}N relaxation data	Use of residue-specific effective correlation time to analyse relaxation data	19
Rotational diffusion tensor from a combination of exact and approximate methods	Reduction of computation time	18
Analysis of slow interdomain motions	Use of relaxation data at two magnetic fields to derive 'extended model-free' parameters	20
^{15}N Relaxation dispersion experiment	μs–ms dynamics of Asn and Gln side chains	21
^{13}C Relaxation dispersion experiment	μs–ms dynamics of side chain Me groups in proteins	22
Super-WEFT application	Determination of paramagnetic line-broadening in metalloproteins	23
Cross-correlated relaxation experiments		
Analysis of errors in the measurement of cross-correlated relaxation rates	Optimisation of CT cross-relaxation rate measurement experiments to reduce systematic errors	24
3D HNCO/HNCA-based *J*-resolved experiment	Measurement of $^{13}C^{\alpha}_{i}$-$^{1}H^{\alpha}_{i}$ (dipole) / $^{13}C'_{i-1}$ (CSA) cross-correlated relaxation	26
2D HSQC-based	Measurement of differential DQ-ZQ relaxation in HN groups. Characterisation of slow dynamics	32
2D HMBC-based	Use of ^{1}H–^{13}C DD/^{1}H–^{13}C DD cross-correlated relaxation for transfer across glycosidic bond in polysaccharides	27

3D, 2D HNCO-based	Measurement of $\Gamma^{DD/DD}(C'C^{\alpha},NH^{N}) + \Gamma^{DD/DD}(C'H^{N},NC^{\alpha})$, $\Gamma^{CSA/DD}(N,NC^{\alpha}) + \Gamma^{CSA/DD}(N,C'C^{\alpha})$, $\Gamma^{CSA/DD}(C',NH^{N}) + \Gamma^{CSA/DD}(N,NH^{N})$	30
2D HCCH-based	Measurement of C-H DD/C-H DD cross-correlated relaxation in protein side chains CH_2 groups	31
Theoretical analysis of cross-correlated relaxation in strongly coupled systems	Evaluation of cross-correlated relaxation rates in strongly coupled systems. Small molecules.	25
2D ^{15}N–^{1}H-ZQ TROSY	Measurement of ^{1}H CSA/^{1}H–^{15}N DD cross-correlated relaxation in Watson–Crick H-bonds	28
2D CT Γ-DQ/ZQ-HCP	Measurement of ^{1}H–^{13}C DD/ ^{31}P CSA cross-correlated relaxation. α and ζ torsional angles in nucleotides	29
2D HNCOCA-based	Measurement of differential DQ–ZQ relaxation in C^{α}–C^{β} groups of proteins. Characterisation of slow dynamics	33
Scalar couplings		
2D and 3D HTQC-COSY	E.COSY determination of $3J(H^{\alpha},C^{\gamma})$	35
2D MJ-HSQC	Measurement of $^{3}J(H^{N},H^{\alpha})$	34
3D α/β-HN(CO)CA-J TROSY	Measurement of $^{3}J(H^{\alpha},N)$ coupling	36
3D HN(CO)CG-TROSY	Measurement of $^{3}J(N,C^{\gamma})$ and $^{3}J(C',C^{\gamma})$ in aromatic residues	37
Measurement of homonuclear couplings from 2D COSY	Non-linear cross-peak fitting procedure to derive coupling constants	77
Couplings across hydrogen bonds		
2D soft CPD-H(N)CO	H-bonds for Arg side-chains	40
2D H2N6N3 2D (H6)N6N3H2	H-bond detection in nucleotides *via* remote non-exchangeable protons	39
J_{NN}-TROSY	Measurement of $^{h}J(N,N)$ in nucleotides. E.COSY-type	38
Residual dipolar couplings		
3D TROSY-HNCO-based	Quantitative measurement of $^{1}D(N,C')$	42
3D HNCO-based 3D (HA)CA(CO)NH-based	Simultaneous measurement of several one-bond couplings when protein is unstable. IPAP strategy.	41
2D ^{13}C IPAP-TOCSY- ^{15}N HSQC	Measurement of $^{1}J(N,C^{\alpha})$ and $^{2}J(N,C^{\alpha})$	45
2D and 3D HN(CO)CA TROSY based	Measurement of $^{1}D(C^{\alpha},C^{\beta})$	43
3D CB(CA)CONH-based	Quantitative measurement of $^{1}D(C^{\alpha},C^{\beta})$	44
SPITZE-HSQC	$^{1}D(C,H)$ and $^{1}D(H,H)$ simultaneously in CH_2 groups. Spin state selective transfer	46

2D IPAP ^{13}C–$^{1}H_3$ CT-HSQC	Measurement of ^{1}D(H,C) in Me-groups	47
2D CT-COSY	Measurement of ^{1}H–^{1}H residual dipolar couplings	49
2D DiM	Measurement of ^{1}D(H,C) in Me-groups	48
2D RADAR TOCSY	Correlation of base proton and phosphorous resonances through residual dipolar couplings	50
Theoretical analysis of Hartmann–Hahn transfer in the presence of scalar and residual dipolar couplings		51
2D CT-NOESY 31P difference	D(H3′,P) in nucleotides	52
2D HNN	Measurement of $^{1}H^{N}\cdots^{15}N$ residual dipolar coupling across H-bond	53
Isotope filtered experiments		
2D WURST-based ^{13}C-filtered NOESY	Demonstration of adiabatic filtering application in 2D NOESY experiments on a protein–DNA complex	54
4D *J*-resolved NOESY-HSQC	Separation of proton signals from labelled and non-labelled molecules	55
2D C,N-filtered HNHA	Measurement of $^{3}J(HN,H^{\alpha})$ of unlabelled peptide in protein/peptide complexes	56
2D X-filtered E.COSY-type	Measurement of *J*(H,F) in fluorolabelled RNA	57
Isotope edited experiments		
3D HCCH-COSY 3D HCCH-TOCSY	Editing on the basis of the number of carbon-bound protons.	59
1D ^{13}C spin-state selective HMQC and HSQC-based	1D ^{13}C editing for resonance assignments in small molecules	61
3D MUSIC CBCANH 3D MUSIC CBCA(CO)NH	CH_2 and CH_3 spin-system based selection of residue type resonances	58
2D Pro-HSQC	Selective observation of resonances of pro-connected residues	60
Heteronuclear double resonance		
2D HMSC	Simultaneous detection of single-bond and long-range ^{1}H–^{13}C correlations	62
2D ^{2}J,^{3}J-HMBC	Long-range heteronuclear correlation differentiating between ^{2}J and ^{3}J couplings for protonated carbons	63
2D GE-HMBC	Long-range heteronuclear coupling in small molecules at natural abundance	64
2D CT-$^{13}CH_3$, VT-^{15}N-HSQC 3D NOESY-CH_3NH 3D ^{13}C,^{15}N HSQC-NOESY-CH_3NH	Simultaneous use of CT ^{13}C and VT ^{15}N evolutions to acquire high-resolution combined ^{13}C, ^{15}N HSQC spectrum. Detection of NOEs involving Mc and HN groups	65
3D Haro-NOESY-CH_3NH 3D Caro-NOESY-CH_3NH	Detection of NOEs between aromatic protons and Me and HN groups	66

3D ^{1}H–^{13}C HMQC-NOESY 3D ^{1}H–^{15}N HMQC-NOESY	Use of INEPT delays to reduce apparent 1H relaxation. Applicable to NH and CH groups	67
2D and 3D DQ-^{31}P	$^{1}H5'/^{31}P$ and $^{1}H5'/^{31}P$ correlation in nucleotides with improved sensitivity	68
2D 31P, 15N{1H} HSQC	Indirect detection of natural abundance ^{15}N through ^{31}P in phosphorous–nitrogen compounds	69
TROSY		
[C-13,C-13] -TROSY	TROSY element based on ^{13}C–^{13}C DD/^{13}C CSA compensation. Sensitivity improvement of triple resonance experiments for nucleotide bases	70
SEA-TROSY	Detection of solvent-exposed amides	72
2D $^{15}N,^{1}H/^{13}C,^{1}H$-TROSY 3D [$^{1}H,^{1}H$]-NOESY-$^{15}N,^{1}H/^{13}C,^{1}H$-TROSY	Simultaneous detection of ^{15}N–^{1}H, ^{13}C–$^{1}H_{aro}$ and N–H_2 groups in large proteins	71
3D and 4D $^{15}N/^{15}N$ HSQC-NOESY-TROSY	Sensitivity enhancement and line-width reduction	73
Heteronuclear triple resonance		
3D sequential HNCA-TROSY	Modification of HNCA to suppress correlation through $^{1}J(N,C^{\alpha})$. Only intraresidue cross-peaks are observed	74
3D TROSY-HNCAN	Backbone resonance correlation for sequential assignments across Pro residues	75
3D MQ-HCN-CCH-TOCSY 3D MQ-HCN-CCH-COSY	Resonance assignments of ribose spin systems	76

6 References

1 W. Peti, C. Griesinger and W. Bermel, *J. Biomol. NMR*, 2000, **18**, 199.
2 E. Kupce, P. A. Keifer and M. Delepierre, *J. Magn. Reson.*, 2001, **148**, 115.
3 T. Carlomagno, T. Prasch and S. N. J. Glaser, *J. Magn. Reson.*, 2001, **149**, 52.
4 S. M. Zhang and D. G. Gorenstein, *J. Magn. Reson.*, 2000, **144**, 316.
5 S. M. Zhang and D. G. Gorenstein, *J. Magn. Reson.*, 2000, **147**, 110.
6 M. Steffen, L. M. K. Vandersypen and I. L. Chuang, *J. Magn. Reson.*, 2000, **146**, 369.
7 E. Kupce and R. Freeman, *J. Magn. Reson.*, 2000, **146**, 240.
8 C. Roumestand and D. Canet, *J. Magn. Reson.*, 2000, **147**, 331.
9 Q. H. He, W. Lin, Y. M. Liu and E. C. Li, *J. Magn. Reson.*, 2000, **147**, 361.
10 P. Damberg, J. Jarvet and A. Graslund, *J. Magn. Reson.*, 2001, **148**, 343.
11 B. Cutting, J. H. Chen, D. Moskau and G. Bodenhausen, *J. Biomol. NMR*, 2000, **17**, 323.
12 C. Dalvit, P. Pevarello, M. Tato, M. Veronesi, A. Vulpetti and M. Sundstrom, *J. Biomol. NMR*, 2000, **18**, 65.
13 A. M. Dixon, G. Widmalm and T. E. Bull, *J. Magn. Reson.*, 2000, **147**, 266.

14 A. G. Palmer, *Annu. Rev. Biophys. Biomol. Struct.*, 2001, **30**, 129.
15 D. M. Korzhnev, E. V. Tischenko and A. S. Arseniev, *J. Biomol. NMR*, 2000, **17**, 231.
16 M. Andrec, G. T. Montelione and R. M. Levy, *J. Biomol. NMR*, 2000, **18**, 83.
17 O. Millet and M. Pons, *J. Biomol. NMR*, 2001, **19**, 181.
18 R. Ghose, D. Fushman and D. Cowburn, *J. Magn. Reson.*, 2001, **149**, 204.
19 D. Canet, P. Barthe, P. Mutzenhardt and C. Roumestand, *J. Am. Chem. Soc.*, 2001, **123**, 4567.
20 J. L. Baber, A. Szabo and N. Tjandra, *J. Am. Chem. Soc.*, 2001, **123**, 3953.
21 F. A. A. Mulder, N. R. Skrynnikov, B. Hon, F. W. Dahlquist and L. E. Kay, *J. Am. Chem. Soc.*, 2001, **123**, 967.
22 N. R. Skrynnikov, F. A. A. Mulder, B. Hon, F. W. Dahlquist and L. E. Kay, *J. Am. Chem. Soc.*, 2001, **123**, 4556.
23 L. X. Ma, E. Philipp and J. J. Led, *J. Biomol. NMR*, 2001, **19**, 199.
24 T. Carlomagno and C. Griesinger, *J. Magn. Reson.*, 2000, **144**, 280.
25 K. Dorai and A. Kumar, *J. Magn. Reson.*, 2000, **145**, 8.
26 K. Kloiber and R. Konrat, *J. Biomol. NMR*, 2000, **17**, 265.
27 S. J. F. Vincent and C. Zwahlen, *J. Am. Chem. Soc.*, 2000, **122**, 8307.
28 R. Riek, *J. Magn. Reson.*, 2001, **149**, 149.
29 C. Richter, B. Reif, C. Griesinger and H. Schwalbe, *J. Am. Chem. Soc.*, 2000, **122**, 12728.
30 T. Carlomagno, M. Maurer, M. Hennig and C. Griesinger, *J. Am. Chem. Soc.*, 2000, **122**, 5105.
31 L. Banci, I. Bertini, I. C. Felli, P. Hajieva and M. S. Viezzoli, *J. Biomol. NMR*, 2001, **20**, 1.
32 K. Kloiber and R. Konrat, *J. Biomol. NMR*, 2000, **18**, 33.
33 D. Fruh, J. R. Tolman, G. Bodenhausen and C. Zwahlen, *J. Am. Chem. Soc.*, 2001, **123**, 4810.
34 Y. L. Xia, X. M. Kong, N. Ip and G. Zhu, *J. Magn. Reson.*, 2000, **146**, 228.
35 F. Lohr, C. Perez, R. Kohler, H. Ruterjans and J. M. Schmidt, *J. Biomol. NMR*, 2000, **18**, 13.
36 P. Permi, I. Kilpelainen and A. Annila, *J. Magn. Reson.*, 2000, **146**, 255.
37 F. Lohr and H. Ruterjans, *J. Magn. Reson.*, 2000, **146**, 126.
38 X. Z. Yan, X. M. Kong, Y. L. Xia, K. H. Sze and G. Zhu, *J. Magn. Reson.*, 2000, **147**, 357.
39 A. Majumdar, A. Kettani, E. Skripkin and D. J. Patel, *J. Biomol. NMR*, 2001, **19**, 103.
40 A. Z. Liu, W. D. Hu, A. Majumdar, M. K. Rosen and D. J. Patel, *J. Biomol. NMR*, 2000, **17**, 305.
41 E. de Alba, M. Suzuki and N. Tjandra, *J. Biomol. NMR*, 2001, **19**, 63.
42 J. J. Chou, F. Delaglio and A. Bax, *J. Biomol. NMR*, 2000, **18**, 101.
43 J. Evenas, A. Mittermaier, D. W. Yang and L. E. Kay, *J. Am. Chem. Soc.*, 2001, **123**, 2858.
44 J. J. Chou and A. Bax, *J. Am. Chem. Soc.*, 2001, **123**, 3844.
45 S. Heikkinen, P. Permi and I. Kilpelainen, *J. Magn. Reson.*, 2001, **148**, 53.
46 T. Carlomagno, W. Peti and C. Griesinger, *J. Biomol. NMR*, 2000, **17**, 99.
47 G. Kontaxis and A. Bax, *J. Biomol. NMR*, 2001, **20**, 77.
48 A. Kaikkonen and G. Otting, *J. Am. Chem. Soc.*, 2001, **123**, 1770.
49 F. Tian, C. A. Fowler, E. R. Zartler, F. A. Jenney, M. W. Adams and J. H. Prestegard, *J. Biomol. NMR*, 2000, **18**, 23.

50 M. Hennig, T. Carlomagno and J. R. Williamson, *J. Am. Chem. Soc.*, 2001, **123**, 3395.
51 B. Luy and S. J. Glaser, *J. Magn. Reson.*, 2001, **148**, 169.
52 Z. R. Wu, N. Tjandra and A. Bax, *J. Biomol. NMR*, 2001, **19**, 367.
53 Z. R. Wu, A. Ono, M. Kainosho and A. Bax, *J. Biomol. NMR*, 2001, **19**, 361.
54 J. Iwahara, J. M. Wojciak and R. T. Clubb, *J. Biomol. NMR*, 2001, **19**, 231.
55 G. Melacini, *J. Am. Chem. Soc.*, 2000, **122**, 9735.
56 D. O. Cicero, G. Barbato, U. Koch, P. Ingallinella, E. Bianchi, S. Sambucini, P. Neddermann, R. De Francesco, A. Pessi and R. Bazzo, *J. Biomol. NMR*, 2001, **20**, 23.
57 B. Luy and J. P. Marino, *J. Biomol. NMR*, 2001, **20**, 39.
58 M. Schubert, H. Oschkinat and P. Schmieder, *J. Magn. Reson.*, 2001, **148**, 61.
59 A. Meissner and O. W. Sorensen, *J. Biomol. NMR*, 2001, **19**, 69.
60 M. Schubert, L. J. Ball, H. Oschkinat and P. Schmieder, *J. Biomol. NMR*, 2000, **17**, 331.
61 T. Parella and J. Belloc, *J. Magn. Reson.*, 2001, **148**, 78.
62 R. Burger, C. Schorn and P. Bigler, *J. Magn. Reson.*, 2001, **148**, 88.
63 V. V. Krishnamurthy, D. J. Russell, C. E. Hadden and G. E. Martin, *J. Magn. Reson.*, 2000, **146**, 232.
64 D. O. Cicero, G. Barbato and R. Bazzo, *J. Magn. Reson.*, 2001, **148**, 209.
65 D. Uhrin, J. Bramham, S. J. Winder and P. N. Barlow, *J. Biomol. NMR*, 2000, **18**, 253.
66 Y. L. Xia, D. Man and G. Zhu, *J. Biomol. NMR*, 2001, **19**, 355.
67 R. Bazzo, G. Barbato and D. O. Cicero, *J. Biomol. NMR*, 2001, **19**, 261.
68 A. Kaikkonen and G. Otting, *J. Biomol. NMR*, 2001, **19**, 273.
69 R. J. Carbajo and F. Lopez-Ortiz, *J. Magn. Reson.*, 2001, **148**, 165.
70 R. Riek, K. Pervushin, C. Fernandez, M. Kainosho and K. Wuthrich, *J. Am. Chem. Soc.*, 2001, **123**, 658.
71 K. Pervushin, D. Braun, C. Fernandez and K. Wuthrich, *J. Biomol. NMR*, 2000, **17**, 195.
72 M. Pellecchia, D. Meininger, A. L. Shen, R. Jack, C. B. Kasper and D. S. Sem, *J. Am. Chem. Soc.*, 2001, **123**, 4633.
73 Y. L. Xia, K. H. Sze and G. Zhu, *J. Biomol. NMR*, 2000, **18**, 261.
74 A. Meissner and O. W. Sorensen, *J. Magn. Reson.*, 2001, **150**, 100.
75 F. Lohr, S. Pfeiffer, Y. J. Lin, J. Hartleib, O. Klimmek and H. Ruterjans, *J. Biomol. NMR*, 2000, **18**, 337.
76 W. D. Hu, L. C. Jiang and Y. Q. Gosser, *J. Magn. Reson.*, 2000, **145**, 147.
77 F. Delaglio, Z. R. Wu and A. Bax, *J. Magn. Reson.*, 2001, **149**, 276.

9
NMR of Proteins and Nucleic Acids

BY S.J. MATTHEWS

1 Introduction

The application of NMR to proteins and nucleic acids has continued to grow throughout this year. Increased usage of deuteration, applications of transverse relaxation optimised spectroscopy (TROSY) and liquid crystal NMR have seen the most development. Furthermore, the NMR application to structure elucidation of membrane bound systems is rapidly emerging.[1] On the technical side highly sensitive cryo-probes are almost essential additions for serious protein NMR protagonists as will be access to magnetic fields in excess of 800 MHz. Structural genomic studies (the high-throughput structure determination of proteins) are now well established and are beginning to produce tangible results. NMR, as expected, has had a significant role in such developments; for example in the rapid screening of folded material, structure determination of 'difficult to crystallise' targets and the ratification of homology models (leading web sites include http://www.jcsg.org/, http://www.mcsg.anl.gov/, http://www.nysgrc.org/, http://www.nysgrc.org/, http://www.secsg.org/ and http://www.doe-mbi.ucla.edu/TB/).

2 Emerging NMR methodology

In the last year TROSY techniques and liquid crystal NMR have dominated new NMR methodological developments. The contents of this section reflect this.

2.1 Dipolar Couplings. – The use of residual dipolar couplings has revolutionized the refinement of NMR-derived solution structures of biological macromolecules, particularly in circumstances where distance information, obtainable from nuclear Overhauser effect (NOE) data, is sparse; for example, in structural studies of multi-domain proteins, macromolecular complexes and deuterated molecules. An excellent array of alignment media are available and this year further additions to this list have been made. The behaviour of biomacromolecules within the aqueous phase of polyacrylamide gels has been described.[2] Weak alignment of the solute macromolecules is achieved within such gels by vertical or radial compression or by the embedding of magneti-

Nuclear Magnetic Resonance, Volume 31
© The Royal Society of Chemistry, 2002

cally oriented purple membrane fragments. The methods were successfully applied to derive residual dipolar couplings for human HIV-1 Nef and ubiquitin. Ruckert and Otting showed that n-alkyl-poly(ethylene glycol)/n-alkyl alcohol and glucopone/n-hexanol mixtures formed dilute liquid crystalline phases, which are suitable for partial alignment of biological macromolecules in a magnetic field.[3] Advantages include commercial availability and cost. They are also uncharged, insensitive to pH and salt, and tolerant against high protein concentrations. Hansen *et al.* demonstrated that Pf1 filamentous phage represents a simple and versatile method for generating partially ordered nucleic acids in solution.[4] These dipolar couplings improve the local structure of nucleic acids and importantly they contain information on the global structure, such as DNA bending, which cannot be obtained by standard NMR methods.

Ma and Opella showed that twelve amino acid residues corresponding to an 'EF-hand' calcium-binding site could be added to the N-terminus of a protein and magnetically aligned by specific binding of a lanthanide ion.[5] Also, the same laboratory showed that lanthanide ion binding to adventitious sites would align membrane proteins in micelles.[6] The weak orientation induced by the magnetic field facilitated the measurement of residual dipolar couplings that are suitable for the structural analysis. A similar method utilizes a zinc finger tag fused at either the N- or the C-terminus of a protein and substituting zinc with cobalt or manganese.[7] This was demonstrated with retroviral gag protein onto the C-terminus of barnase, a ribonuclease produced by *Bacillus amiloliquifaciance*. The observed paramagnetic anisotropy induced by cobalt binding to the metal binding tag also permitted measurement of dipolar shifts. Substitution of manganese into the metal binding tag permitted the measurement of unpaired electron–amide proton distances using paramagnetic relaxation enhancement methodology. The availability of both amide proton dipolar shifts and unpaired electron to amide proton distances permitted the direct calculation of z-coordinates for individual amide protons. This approach is robust and will prove powerful for global fold determination of proteins identified in genome initiatives. Also Bertini *et al.* substituted calcium with Ce(III), Yb(III) and Dy(III) within the Ca-2 calbindin protein and demonstrated substantial alignment in high magnetic fields due to the high anisotropy of the metal magnetic susceptibility. This property has allowed the measurement of residual dipolar couplings of asparagine and glutamine NH_2 moieties and therefore aids the structural characterization of these groups.[8]

The experimental strategies for measuring dipolar coupling are becoming increasingly efficient, enabling different couplings to be measured and better defined structures. Heteronuclear dipolar couplings of the protein backbone have proven to have a big impact on the accuracy of protein NMR structures. Recent efforts have been directed at the measurement of multiple bond homonuclear proton dipolar couplings which contain useful distance information as well as angular. An intensity-based constant-time COSY (CT-COSY) method has also been described for measuring ^1H–^1H residual dipolar couplings of proteins in weakly aligned media.[9] For small proteins, the overall sensitivity of

this experiment is comparable to the NOESY experiment. These measurements provide useful orientational constraints for protein structure determination. The $1/r^3$ distance dependence of directly observed dipolar couplings can provide longer range distance information at favorable angles. An interactive computer procedure has also been described which determines ^{1}H–^{1}H couplings from fitting the cross-peak multiplets in regular phase-sensitive COSY spectra.[10] A method has been presented that combines both heteronuclear and homonuclear dipolar couplings to investigate the local conformation of methylene groups. Carlomagno and co-workers have developed a new pulse sequence (SPITZE-HSQC) that allows the two C,H and H,H dipolar couplings to be measured at the same time.[11] The new method has been applied to the methylene groups of glycines in the protein ubiquitin. The C,H and the H,H dipolar couplings might have a key role in fast stereospecific assignment of protons in CH_2 groups.

Luy *et al.* have described a sensitive X-filtered-E.COSY-type method that measures both the sign and magnitude of long-range ^{1}H–^{19}F dipolar couplings in selectively fluorine labeled RNA oligonucleotides oriented in solution by a liquid crystalline medium. Experimentally measured ^{1}H–^{19}F dipolar couplings for the 2′-deoxy-2′-fluoro-sugars located in the helical region of an RNA hairpin were found to be in excellent agreement with values predicted using canonical A-form helical geometry.[12] The ratios of cross-peak intensities in a selective constant-time NOESY experiment, recorded with and without 31P decoupling, yield values for the sum of the H3′–P scalar and dipolar couplings. The vicinal H3′–P scalar and dipolar couplings in the DNA oligomer d(CGCGAATTCGCG)(2) were measured in both isotropic solution, and in a liquid crystalline phase. Dipolar couplings are in excellent agreement with the NMR structure for this dodecamer, and to a somewhat lesser extent with the X-ray structures.[13] Kontaxis and Bax have described a simple spectral editing procedure for generating separate subspectra of methyl multiplet components of ^{1}H–^{13}C HSQC spectra.[14] The resulting spectra permit rapid and reliable measurement of ^{1}H–^{13}C J and dipolar couplings. The editing procedure is illustrated for a Ca^{2+}-calmodulin sample in isotropic and liquid crystalline phases. Giesen *et al.* proposed the use of protein samples that are selectively isotopically enriched only in the backbone atoms and conventional heteronuclear single quantum correlation (HSQC) techniques to obtain accurate dipole–dipole couplings between protein backbone nuclei.[15] Evenas *et al.* have presented TROSY-based HN(CO)CA 2D and 3D pulse schemes for the measurement of ^{13}C (alpha)–^{13}C (beta) dipolar couplings in high molecular weight proteins.[16] Chou *et al.* proposed a quantitative J type method for measuring the $^1J_{C'N}$ splitting from the relative intensity in two 3D TROSY-HNCO spectra with selected $^1J_{C'N}$ dephasing intervals.[17]

NMR residual dipolar couplings have great potential to provide rapid structural information for proteins in the solution state. This information even at low resolution may be used to advantage in proteomics projects that seek to annotate large numbers of gene products for entire genomes. Numerous groups have made several contributions to towards this goal. Meiler *et al.* have

written a useful computer program, DipoCoup, which allows one to search the protein data bank for proteins that have a homologous three-dimensional fold.[18] The search uses secondary structure alignment based on chemical shifts and dipolar couplings or pseudocontact shifts for the three-dimensional orientation of secondary structure elements. Furthermore, the program offers additional tools for handling and analyzing dipolar couplings. Fowler *et al.* have devised a strategy based on residual dipolar couplings that provides a route to the rapid determination of protein folds.[19] Allowing the alignment of previously identified secondary structural elements with respect to each other enables this. The authors illustrated this with the *Escherichia coli* acyl carrier protein and the NodF protein from *Rhizobium leguminosarum*. Andrec and co-workers have described a novel approach to the structural interpretation of dipolar couplings, which is based on structural motif pattern recognition, where a predefined gapless structural template for a motif is used to search a set of residual dipolar couplings for good matches.[20] Mueller *et al.* have published two papers describing the use of dipolar coupling in the determination of the global folds. As an alternative to direct refinement against measured dipolar couplings, an approach where discrete orientations are calculated for each peptide plane on the basis of the dipolar couplings is described. The techniques were applied the large maltose-binding protein in complex with the substrate beta-cyclodextrin.[21,22] Another approach has been described for rapidly determining protein structures using dipolar couplings. It utilizes proteins containing ^{13}C-methyl labeled Val, Leu, and Ile (delta1) and protonated Phe and Tyr in a deuterated background. Using this strategy, the key NOEs together with comprehesive list of dipolar couplings can be obtained.[23] Also, Chou *et al.* showed that dipolar couplings decrease the backbone root-mean-square-deviation between various homology models of calmodulin (CaM) and its crystal structure.[24]

The use of residual dipolar couplings has become increasingly important in the refinement NMR-derived solution structures of biological macromolecules to high resolution. Particularly when long-range order constraints are needed, for example in macromolecular complexes, multidomains protein and nucleic acids. Clore has developed a simple and rapid method for solving the three-dimensional structures of protein–protein complexes in solution using intermolecular NOE data and dipolar couplings.[25] The method is demonstrated for the 40 kDa complex of enzyme I and the histidine phosphocarrier protein. It involves the application of rigid body minimization using a target function composed of only three terms, namely experimental NOE-derived intermolecular interproton distance and dipolar coupling restraints, and a simple intermolecular van der Waals repulsion potential. The same group used similar approach to orient the two halves of the domain-swapped HIV-inactivating protein cyanovirin-N dimmer.[26] The local structure of nucleic acids can be determined from traditional solution NMR techniques, but it is usually not possible to uniquely define the global conformation of DNA or RNA double helices. Vermeulen *et al.* have presented results that show the inclusion of dipolar coupling constraints makes it possible to accurately and precisely

reproduce the overall helical bend in a DNA duplex.[27] Wu *et al.* showed that the ratio of the internucleotide dipolar coupling and the corresponding one-bond imino ^{15}N–^{1}H dipolar coupling provides a measure for the NH/H-N distance ratio.[28] These measurements were carried out on the labeled dodecamer d(CGCGAATTCGCG)(2) and, assuming H-bonds to be perfectly linear, dipolar data indicate time-averaged hydrogen bond lengths of 1.80 ± 0.03 Å for A-T and 1.86 ± 0.02 Å for C-G. Furthermore, Al-Hashimi *et al.* have described a new NMR procedure for determining the three-dimensional fold of C2-symmetric nucleic acid homodimers that relies on long-range orientational constraints derived from the measurement of two independent sets of residual dipolar couplings under two alignment conditions.[29]

2.2 Transverse Relaxation Optimized Spectroscopy (TROSY). – TROSY and CRINEPT are new techniques for solution NMR studies of molecular and supramolecular structures. They allow the collection of high-resolution spectra of structures with molecular weights >100 kDa, significantly extending the range of macromolecular systems that can be studied by NMR in solution. TROSY has already been used to map protein–protein interfaces, to conduct structural studies on membrane proteins and to study nucleic acid conformations in multimolecular assemblies. A number of reviews have been published this year that cover the TROSY technique since its inception.[30–32]

The number of pulse sequences incorporating TROSY type magnetization transfer has steadily grown over the last year. The discovers of TROSY describe a ^{15}N–^{1}H/ ^{13}C–^{1}H-TROSY experiment for the simultaneous acquisition of the heteronuclear chemical shift correlations of backbone amide ^{15}N–^{1}H groups, side-chain ^{15}N–$^{1}H_2$ groups and aromatic ^{13}C–^{1}H groups.[33] The correlations are extracted from two subspectra of the same data set, thus preventing possible spectral overlap of aromatic and amide protons in the proton dimension. The side-chain ^{15}N–$^{1}H_2$ groups, which are suppressed in conventional TROSY, are observed with high sensitivity. The experiment was demonstrated on the membrane protein OmpA reconstituted in detergent micelles of molecular weight 80 000 Da, which enabled the detection of numerous NOEs between backbone amide protons and both aromatic protons and side-chain ^{15}N–$^{1}H_2$ groups. The same group also showed that TROSY-type triple resonance experiments on the uniformly ^{2}H, ^{13}C, ^{15}N-labeled 7,8-dihydroneopterin aldolase (DHNA) from *Staphylococcus aureus*, which is a symmetric homooctamer protein of molecular mass 110 kDa, provide at least a 20-fold sensitivity gain when compared to conventional triple resonance NMR experiments.[34] Also, Reik *et al.* introduced a novel TROSY element that exploits cross-correlation effects between ^{13}C–^{13}C dipole–dipole coupling and chemical shift anisotropy of aromatic carbons.[35] Although these ^{13}C–^{13}C effects are smaller than the previously described ^{13}C–^{1}H-TROSY effects for aromatic ^{13}C,^{1}H moieties, their constructive use resulted in further transverse relaxation-optimization by up to 15% for the resonances in a 17 kDa protein–DNA complex. Two- and three-dimensional versions of the HCN experiment for obtaining ribose-base and intrabase correlations in the nucleotides of DNA

and RNA were designed. Lohr and coworkers have described a TROSY-based triple-resonance pulse scheme, which correlates backbone amide chemical shifts of an amino acid residue with the ^{15}N chemical shifts of both the sequentially preceding and following residues.[36] One benefit is that N–N connectivities are obtained irrespective of whether the neighbouring amide nitrogens are protonated or not, which makes the experiment suitable for the assignment of proline resonances. Meissner and Sorensen presented a further experiment for improving the sequential assignment of large proteins. The sequential HNCA experiment is described and leads to a spectrum exhibiting exclusively interresidue correlations as in the conventional HN(CO)CA.[37] This removes the problem associated with increasing static magnetic fields where the chemical shift anisotropy relaxation mechanism of carbonyl carbons becomes more efficient, leading to a degradation of the HN(CO)CA sensitivity. Pellecchia *et al.* have developed a method, called SEA-TROSY, for resolving the of spectral overlap problems associated with very large proteins by selecting solvent exposed amides with TROSY.[38]

Precision in the determination of the 3D structures of proteins by NMR depends on obtaining an adequate number of NOE restraints. Ambiguity in the assignment of NOE cross-peaks is an impediment to high quality structure determination. Xia *et al.* have described a number of new NOESY experiments benefiting from the introduction of TROSY elements[39,40] In order to obtain NOEs for protons in large proteins with degenerate chemical shifts 3D and 4D ^{15}N–^{15}N separated NOESY experiments are essential. TROSY sections replacing the latter or both HSQC parts of the 3D and 4D ^{15}N–^{15}N separated HSQC-NOESY-HSQC pulse sequences enhance signal sensitivity and improve resolution. The sensitivities are enhanced by up to 62% for a 27 kDa protein at 5 °C.[40] Two pulse sequences, 3D H-aro-NOESY-CH3NH and 3D C-aro-NOESY-CH3NH, have also been proposed. These 3D experiments provide NOE information between aromatic protons and methyl or amide protons and provide important restraints for protein structure calculations.[39]

Recent developments in the direct observation of J couplings across hydrogen bonds in proteins and nucleic acids provide additional information for structure and function studies of these molecules by NMR spectroscopy. Yan *et al.* proposed a modified J(N,N)-correlated ^{15}N–^{1}H TROSY experiment which enables direct measurement of $^{h}J_{HN}$ in large nucleic acids.[41] Also, Lohr *et al.* use TROSY techniques to present direct experimental evidence for hydrogen bonds involving the phosphate moiety of FMN in *Desulfovibrio vulgaris* flavodoxin.[42] Riek *et al.* have shown that accurate hydrogen bond lengths in Watson–Crick base pairs can be characterized by cross-correlated relaxation between ^{1}H chemical shift anisotropy and dipole–dipole coupling of ^{1}H and its hydrogen bond acceptor ^{15}N.[43] Permi *et al.* have described a TROSY experiment for the measurement of three-bond scalar coupling constant between 1H(i-1alpha) and 15N(i), which defines the dihedral angle.[44]

There are still relatively few examples of real applications where TROSY techniques have been essential to derive meaningful information. This is just a matter of time and this year has seen a few landmark illustrations. In a first

step towards detailed structural studies Mulder *et al.* have used 4D-TROSY triple resonance NMR spectroscopy to obtain complete ^{1}H(N), ^{15}N, ^{13}C(alpha), ^{13}(CO) and ^{13}C(beta) resonance assignments of the 67 kDa dimeric form p53 tumor suppressor protein.[45] Fernandez and co-workers have assigned, identified secondary structure and computed a fold for the 148-residue integral membrane protein OmpX from *Escherichia coli* reconstituted with dihexanoyl phosphatidylcholine (DHPC) of molecular mass of about 60 kDa.[46] Using TROSY triple resonance and NOE spectra complete sequence-specific NMR assignments for the polypeptide backbone were obtained. Furthermore ^{13}C chemical shifts and the nuclear Overhauser effect data resulted in the identification of the regular secondary structure elements and conformational constraints for the computation of the global fold of the protein. This data is some of the first to demonstrate that relaxation-optimized NMR techniques open novel avenues for the study of integral membrane protein structure and function. Oxenoid *et al.* used TROSY NMR to study the misfolding of a mutant form of diacylglycerol kinase (s-DAGK), a 40 kDa homotrimeric protein having nine transmembrane segments. A 100 kDa complex of s-DAGK with detergent micelles exhibits a single additional set of resonances from the misfolded form. Differences in NMR chemical shift dispersion and temperature-dependent line widths exhibited by folded and misfolded s-DAGK support the notion that they represent very different structural states. This work appears to represent the first documentation of conformationally specific misfolding of an integral membrane protein.[47]

2.3 General Methodology. – A few improvements to the conventional triple-resonance strategy for assigning protein spectra have also been published this year. Conventional assignment strategies use ^{1}H–^{15}N-correlations as a starting point and therefore have problems when proline appears in the amino acid sequence, which lacks a signal in these correlations. Schubert *et al.* have detailed a set of amino acid selective pulse sequences, which provide the information to link the amino acid on either side of proline residues and thus complete the sequential assignment.[48] The amide protons are correlated with their own nitrogen or with that of the proline. Meissner *et al.* introduced a novel three-dimensional HCCH NMR experiment, which involves COSY or TOCSY coherence transfer plus two independent editing steps according to the number of protons attached to the individual carbons. This double editing leads to simplification of HCCH protein side-chain spectra that otherwise are prone to spectral overlap.[49] Iwahara *et al.* demonstrated the utility of a modified 2D F1,F2 ^{13}C-filtered NOESY experiment that employs a $^{1}J_{HC}$ *versus* chemical shift optimized adiabatic C-13 inversion pulse. They also showed that the targeted replacement of an interfacial aromatic residue in the DRI-DBD:DNA complex substantially reduces line broadening within its NMR spectra. The spectral changes are dramatic, salvaging a protein–DNA complex that was originally ill-suited for structural analysis by NMR.[50]

Two methods for the measurement of $^{2}J_{NCalpha}$ and $^{1}J_{NCalpha}$ in ^{15}N ^{13}C-labeled small and medium-size proteins are described by Heikkinen and co-

workers.[51] The current approach is based on simplified ^{13}C (alpha)-coupled ^{15}N HSQC spectra, where the two $^{2}J_{NCalpha}$ doublets are separated into two subspectra corresponding to the alpha and beta spin states of the residue's own alpha carbon. In one method *J*-multiplication is utilized by introducing an additional coupling evolution period making it possible to scale the peak-to-peak separation. Xia proposed an improvement to *J*-multiplied HSQC experiment, which amplifies *J* coupling constants and allows direct observation of coupling constants in peptides and proteins. They replaced the PEP-HSQC pulse sequence by a sensitivity-enhanced HMQC section, which shortens the total decay time for the *J*-coupling and the chemical shift evolution by a period of t1. This experiment affords narrower line-width and enhances the sensitivity by 34%.[52]

3 Solution Structures

Structure elucidation of small macromolecules by NMR is largely routine, which has lead to rapid rise solution structures being deposited in the protein databank (http://www.rcsb.org/pdb/holdings.html). In order to avoid a monotonous section describing hundreds of structures, I present only papers that have had a major impact.

3.1 Free Proteins. – As the size limit has increased, NMR now has the ability to tackle more interesting systems. In early years NMR was limited to single domains whereas larger fragments of modular proteins can now be studied. Pickford *et al.* presented elegant work describing the solution structure of the (6)F1(1)F2(2)F2 fragment from the gelatin-binding region of fibronectin.[53] Interestingly, the structure reveals an extensive hydrophobic interface between the non-contiguous (6)F1 and (2)F2 modules. The hairpin topology may facilitate intramolecular contact between matrix assembly regions, which flank the gelatin-binding domain, but is not consistent with the view that fibronectin is simply a linear string of beads. The same group revealed the structure of the first two EGF domains from the LDL receptor, using residual dipolar couplings in the refinement.[54] Their results facilitated a detailed assessment of the consequences of mutations associated with familial hypercholesterolaemia. Yuzawa and co-workers have described the structure of Grb2, which is an adaptor protein composed of a single SH2 domain flanked by two SH3 domains.[55] Grb2 is a flexible protein in which the C-terminal SH3 domain is connected to the SH2 domain *via* a flexible linker, which is in contrast to the previously described compact crystal structure.

Other notable free protein structures include the following. Uniquely, Hung and co-workers have determined the high-resolution structure of Mu B, a protein required for the strand transfer step of bacteriophage Mu DNA transposition, at extreme salt concentrations *i.e.* 1.5 M NaCl. Their approach for structural determination in high salt may be generally applicable for proteins that do not crystallize or those that are plagued by solubility problems

at low ionic strength.[56] Also from a bacteriophage, Maxwell *et al.* determined the solution structure of protein W (gpW) that is required for the stabilization of DNA in lambda.[57] It possesses a novel fold consisting of two alpha helices and a single two-stranded beta sheet arranged around a well-packed hydrophobic core with a flexible C-terminus, which is essential for function. Wang *et al.* revealed that ThiS, a sulfur carrier protein that plays a central role in thiamin biosynthesis in *Escherichia coli*, is a ubiquitin fold but only shares 14% homology with ubiquitin.[58] Their work establishes the importance of structure determination in establishing evolutionary links between proteins in which structure and function have been conserved through eons of evolution despite loss of sequence identity. Spadaccini *et al.* have described the solution structure of an engineered sweet protein, MNEI, composed of linked chains from dimeric monellin. MNEI shows close similarity to the crystal structures of wild-type monellins.[59] Berglund *et al.* reported structural studies of FADD (also known as MORT-1), an essential adapter protein of transmembrane receptors Fas (CD95) and tumor necrosis factor receptor-1 (TNF-R1).[60] The structure is composed of six alpha helices joined by short loops and displays overall similarity to the death domain of the Fas receptor. An emerging model for FasL-induced FADD recruitment to Fas and caspase-8 activation is proposed. Horita have presented the solution structure of the chromo domain from the cryptic loci regulator protein Clr4, which is known to regulate silencing and switching at the mating-type loci and to affect chromatin structure at centromeres. Their structure highlights a conserved surface that may be involved in chrome domain–ligand interactions.[61]

Three papers have reported structures of novel antimicrobial peptides. Gonzalez *et al.* described the solution structure of bacteriocin AS-48, a 70-residue cyclic polypeptide from *Enterococcus faecalis*, which consists of five alpha-helices enclosing a compact hydrophobic core.[62] A similar five-helix structural motif has been found in the antimicrobial NK-lysin, an effector of T and natural killer (NK) cells, which may suggest a common mechanism of antibacterial action. Campos-Olivas and co-workers revealed the three-dimensional solution structure of AFP1, which is a recently discovered anti-fungal, chitin-binding protein from *Streptomyces tendae* Tu901.[63] The protein contains two antiparallel P-sheets that pack against each other in a parallel P-sandwich. The authors classify AFP1 as a new member of the py-crystallin superfamily and based on sequence comparisons with cellulose and chitin-binding proteins, they postulate a putative sugar-binding site for AFP1. Ohki *et al.* also described the identical structure for SKLP, the first killer toxin-like protein for yeasts identified in *Streptomyces*.[64] SKLP has a unique electrostatic surface potential distribution; one surface of the beta-barrel fold has a large negatively charged region, with an isolated positive charge in the center and positively charged residues surround edge of this surface. They hypothesise that this unusual surface charge distribution might be related to the target binding of SKLP.

3.2 Protein–Small Molecule Complexes. – In this section, we address the recognition of small organic molecules or short peptides. Binding constants

can be weak and labeling strategies difficult, so varied NMR techniques are required to study such complexes. Chemical shift mapping of protein–peptide interaction provides a fast and efficient means for identifying binding sites.

The Ena-VASP family of proteins act as molecular adaptors linking the cytoskeletal system to signal transduction pathways. Their N-terminal EVH1 domains use groups of exposed aromatic residues to specifically recognize 'FPPPP' motifs found in the mammalian zyxin and vinculin proteins, and the ActA protein of *Listeria monocytogenes*. Ball *et al.* used a combination of peptide library screening, fluorescence titration and NMR chemical shift mapping after the determination of solution structure of the VASP EVH1 domain to reveal a second affinity-determining epitope.[65] They propose that this epitope, which is absent in the sequences of the native EVH1-interaction partners zyxin and vinculin, may provide the pathogen with an advantage when competing for the recruitment of host VASP and Mena proteins. Also involved in host cell cytoskeletal rearrangement is intimin which is primarily responsible for intimate attachment of enteropathogenic and enterohaemorrhagic *Escherichia coli*. Intimin targets the translocated intimin receptor (Tir), which is exported by the bacteria and integrated into the host cell plasma membrane. Batchelor *et al.* localized the Tir-binding region of intimin to the C-terminal 190 amino acids and determined the high-resolution solution structure, which is composed of an immunoglobulin domain that is intimately coupled to a novel C-type lectin domain.[66] The interpretation of NMR-titration and mutagenesis data enabled the authors to identify, for the first time, the binding site for Tir, which is located at the extremity of the molecule. Kozlov *et al.* have determined the solution structure of the C-terminal quarter of human poly(A)-binding protein (hPABP).[67] The protein fragment contains a protein domain, PABC (for poly(A)-binding protein C-terminal domain), which is also found associated with the HECT family of ubiquitin ligases. Also, by using chemical shift perturbation analysis they identify the peptide binding site in PABC and the major elements involved in peptide recognition.

Zhang *et al.* have reported the full three-dimensional structure of the catalytic domain of human collagenase-3 (MMP-13) complexed to a potent sulfonamide hydroxamic acid inhibitor.[68] Inhibitor binding placed the methoxy phenyl ring in the S1′ pocket with the remainder of the molecule primarily solvent exposed. The binding mode for this inhibitor was found to be similar with respect to stromelysin-1 and collagenase-1; however, subtle comparative differences in the interactions between inhibitor and enzyme were consistent with their respective binding potencies. Xu *et al.* completed a similarly comprehensive study on the Acyl carrier protein (ACP) in apo and hole forms.[69] Comparison of the structure of free ACP with the bound form of ACP in the ACP–ACPS complex reveals a displacement of helix II. The same group elucidated the solution structure of the 144-residue C-terminal domain of *E. coli* ZipA, which is an essential component of cell division and interacts with the FtsZ protein.[70] ZipA is composed of three alpha helices and a beta sheet where the alpha helices and the beta sheet form surfaces directly opposite

each other. A C-terminal peptide from FtsZ binds in a hydrophobic channel formed by the beta-sheet.

3.3 Protein–Metal Complexes. – The Bertini group produced a breakthrough in metalloproteins structure determination, in that they elucidated the structure of oxidized plastocyanin from the cyanobacterium *Synechocystis* that includes paramagnetic copper. The detection of broad hyperfine-shifted signals and their full assignment allowed the identification of the copper(II) ligands and the determination of the Cu–S–C–H dihedral angle for the coordinated cysteine.[71] The same group is involved in the NMR solution structure determination of the Cu(I)-bound form of Atx1, a 73-amino acid metallochaperone protein from the yeast *Saccharomyces cerevisiae*.[72] The structure is composed of four antiparallel beta strands, two alpha helices and a copper ion placed between the sulfur atoms of Cys15 and Cys18. Comparison of the Cu(I) and apo conformations of the protein reveals that the Cu(I) binding cysteines move from a buried site in the bound metal form to a solvent-exposed conformation on the surface of the protein after copper release.

Plant homeodomain (PHD) domains are found in >400 eukaryotic proteins, many of which are transcriptional regulators. Naturally occurring point mutations or deletions of this domain contribute to a variety of human diseases, including ATRX syndrome, myeloid leukemias and autoimmune dysfunction. The first structural characterization of a PHD domain has been reported; Capili *et al.* reveal that the PHD domain from KAP-1 corepressor binds zinc in a cross-brace topology between anti-parallel beta-strands reminiscent of RING (really interesting new gene) domains.[73] They also defined the structural features required for transcriptional repression by KAP-1 and explain naturally occurring, disease-causing mutations in PHD domains of other proteins. The TAZ2 (CH3) domain of the transcriptional adapter protein CBP has been implicated in direct functional interactions with numerous cellular transcription factors and viral oncoproteins. De Guzman *et al.* identified that the novel helical fold adopted by TAZ2 (CH3) domain is stabilised by three zinc ions, each of which is bound to one histidine and three cysteine ligands in HCCC-type motifs.[74] Each zinc-binding site is formed from the carboxy terminus of an alpha helix, a short loop, and the amino terminus of the next alpha helix. A peptide derived from the N-terminal transactivation domain of p53 binds specifically to one face of the TAZ2 domain.

3.4 Protein–Protein Complexes. – On of the most significant reports of a protein complex structure this year is Wang *et al.*'s description of the solution structure of the second protein–protein complex of the phosphoenolpyruvate–sugar phosphotransferase system. The complex between histidine-containing phosphocarrier protein (HPr) and glucose-specific enzyme IIA(Glucose) (IIA(Glc)) was determined using dipolar couplings to provide long-range orientational information and the newly developed rigid body minimization and restrained simulated annealing method.[75] Comparisons with the structures of the enzyme I-HPr and IIA(Glc)-glycerol kinase complexes reveal how

similar binding surfaces can be formed with underlying backbone scaffolds that are structurally dissimilar and highlights the role of redundancy and side-chain conformational plasticity.

Sin3A or Sin3B are components of a corepressor complex that mediates repression by transcription factors such as the helix-loop-helix proteins Mad and Mxi. Members of the Mad/Mxi family of repressors play important roles in the transition between proliferation and differentiation by down-regulating the expression of genes that are activated by the proto-oncogene product Myc. Spronk *et al.* have determined the solution structure of the second paired amphipathic helix (PAH) domain (PAH2) of Sin3B in complex with a peptide comprising the N-terminal region of Mad1. This complex exhibits a novel interaction fold; four alpha helices of PAH2 form a hydrophobic cleft that accommodates an amphipathic Mad1 alpha helix.[76]

Liu *et al.* have described the solution structure of a mutant of the homodimer protein transcription factor 1, TF1. The dimeric core, consisting of the N-terminal helices and beta sheets, is more tightly packed than wire type, and this might be responsible for its increased thermal stability.[77] Also, Gordon-Smith *et al.* reported the dimeric structure of a C-terminal fragment of Bovine IF1, which inhibits the hydrolytic action of the F1F0 ATP synthase in mitochondria under anaerobic conditions. Most unusually, the molecule forms an anti-parallel coiled-coil in which three histidine residues occupy key positions at the dimer interface.[78]

MAP kinases (MAPKs) control mitogenic signal transduction in all eukaryotic organisms and are inactivated by dual specificity MAPK phosphatases (MKPs). MKP-3, a prototypical MKP, achieves substrate specificity through its N-terminal domain binding to the MAPK ERK2, resulting in the activation of its C-terminal phosphatase domain. Farooq *et al.* have elucidated the solution structure and biochemical analysis of the ERK2 binding (EB) domain of MKP-3 and shown that regions that are essential for ERK2 binding partly overlap with sites that interact with the C-terminal catalytic domain.[79] They suggested a novel mechanism by which the EB domain binding to ERK2 is transduced to cause a conformational change of the C-terminal catalytic domain, resulting in the enzymatic activation of MKP-3. TRADD is a multifunctional signaling adaptor protein that is recruited to TNFR1 upon ligand binding. The C-terminal of TRADD comprises the 'death domain' that is responsible for association of TNFR1 and other death domain-containing proteins such as FADD and RIP. The solution structure of N-TRADD revealed a novel protein fold. A combination of NMR, BIAcore, and mutagenesis experiments was used to identify the site of interaction of N-TRADD with C-TRAF2.[80] The inhibitor-of-apoptosis proteins (IAPs) regulate programmed cell death by inhibiting members of the caspase family of enzymes. Liu *et al.* described the structure of the BIR3 domain of X-linked IAP (XIAP) complexed with a functionally active nine-residue peptide derived from the N terminus of Smac.[81] The peptide binds across the third beta strand of the BIR3 domain in an extended conformation with only the first four residues contacting the protein. Petros *et al.* reveal that the structures of the

two isoforms of Bcl-2 are virtually identical and that differences are observed in the ability of the proteins to bind to a 25-residue peptide from the proapoptotic Bad protein and a 16-residue peptide from the proapoptotic Bak protein.[82] The results suggest that there are subtle differences in the hydrophobic binding groove in Bcl-2 that may translate into differences in anti-apoptotic activity for the two isoforms.

3.5 Protein–Nucleic Acid Complexes. – Some of the most impressive NMR structures have been protein–nucleic complexes. The RNA genome of the human immunodeficiency virus type-1 (HIV- 1) contains a 120 nucleotide Psi-packaging signal that is recognized by the nucleocapsid (NC) domain of the Gag polyprotein during virus assembly. The Psi-site contains four stem-loops (SL1-SL4) that possess overlapping and possibly redundant functions. Amarasinghe and co-workers determined the structure of the NC-SL2 complex. The structural features are similar to those observed previously in the NMR structure of NC bound to SL3 but other features of the complex are substantially different. Most notably, the N-terminal zinc knuckle interacts with an A-U-A base triple platform in the minor groove of the SL2 RNA stem, but binds to the major groove of SL3. These findings demonstrate that NC binds in an adaptive manner to SL2 and SL3 *via* different subsets of inter- and intra-molecular interactions, and support a genome recognition/packaging mechanism that involves interactions of two or more NC domains of assembling HIV-1 Gag molecules with multiple Psi-site stem-loop packaging elements.[83,84]

Nucleolin is an abundant 70 kDa nucleolar protein involved in many aspects of ribosomal RNA biogenesis. The central region of nucleolin contains four tandem consensus RNA-binding domains (RBD). The two most N-terminal domains (RBD12) bind with nanomolar affinity to an RNA stem-loop containing the consensus sequence UCCCGA in the loop. Allain *et al.* determined the solution structure of nucleolin RBD12 in its free form and have studied its interaction with a 22 nt RNA stem-loop.[85] The two RBDs are separated by a 12 amino acid flexible linker and do not interact with one another in the free protein. This linker becomes ordered when RBD12 binds to the RNA. Analysis of the observed NOEs between the protein and the RNA indicates that both RBDs interact with the RNA loop *via* their beta sheet. The polypyrimidine tract binding protein (PTB), also known as hnRNP-I, was originally identified as a nuclear factor, which binds specifically to the polypyrimidine tract of pre-mRNA introns. PTB is a homodimer, which functions mainly as a negative regulator of pre-mRNA splicing by binding to high affinity sequence motifs in the introns downstream and upstream of regulated exons and repressing their incorporation in mature RNA. In the present study the solution structure of PTB-C198 has been investigated, showing a novel fold for one of the two RBD domains.[86] The two linked RBD domains also appear to tumble independently in solution, showing no fixed relative orientation with each other.

A number of studies report novel DNA binding interfaces. Wojciak *et al.*

have determined the solution structure of the complex between the 'winged-helix' enhancer-binding domain of the Mu repressor protein and its cognate DNA site. The structure reveals an unusual use for the 'wing', which becomes immobilized upon DNA binding where it makes intermolecular hydrogen bond contacts deep within the minor groove. Although the wing is mobile in the absence of DNA, it partially negates the large entropic penalty associated with its burial by maintaining a small degree of structural order in the DNA-free state. Extensive contacts are also formed between the recognition helix and the DNA, which reads the major groove of a highly conserved region of the binding site through a single base-specific hydrogen bond and van der Waals contacts.[87] Vaughn *et al.* have determined the high-resolution NMR solution structure of the novel DNA binding domain of the *Bacillus subtilis* transition state regulator AbrB.[88] Comparisons of the AbrB DNA binding domain with DNA binding proteins of known structure show that it is a member of a completely novel class of DNA recognition folds that employs a dimeric topology for cellular function. This new DNA binding conformation is referred to as the looped-hinge helix fold.

In vertebrates, the biological consequences of DNA methylation are often mediated by protein factors containing conserved methyl-CpG binding domains (MBDs). Mutations in the MBD protein MeCP2 cause the neuro-developmental disease Rett syndrome. Ohki *et al.* reported the solution structure of the MBD of the human methylation-dependent transcriptional regulator MBD1 bound to methylated BRA.[89] DNA binding causes a loop in MBD1 to fold into a major and novel DNA binding interface. The *E. coli* protein Ada specifically repairs the S-p diastereomer of DNA methyl phosphotriesters in DNA by direct and irreversible transfer of the methyl group to its own Cys 69, which is part of a zinc-thiolate center. Lin *et al.* have presented a highly refined solution structure of the 10 kDa N-terminal domain, N-Ada10, which reveals structural details of the nonspecific DNA interaction of N-Ada10 during the repair process and provides a basis for understanding the mechanism of the conformational switch triggered by methyl transfer.[90] Methylation of N-Ada induces a structural change, which enhances the promoter affinity of a remodeled surface region that does not include the transferred methyl group.

4 Protein Relaxation and Dynamics

As a result of the recent improvements in measurement methods and data interpretation, multinuclear relaxation in large biological molecules is fast becoming a mature subject. Information obtained from NMR dynamics experiments provides insights into specific structural changes or configurational energetics associated with function. A variety of applications, in which studies of protein dynamics provide insights into protein–protein interactions, target recognition, ligand binding, and enzyme function, have been reviewed by Ishima and Torchia.[91] A number of reports have described improved

strategies or experiments for the measurement and interpretation of relaxation data in biological macromolecules. Tolman and co-workers addressed the challenge of extracting structural and dynamic properties from residual dipolar couplings measured in weakly aligned proteins. They discussed a formalism that allows a first order separation of their effects and a simultaneous extraction of structural and motional parameters.[92] De la Torre *et al.* have written a computer program using bead models, HYDRONMR, which calculates the rotational diffusion tensor and other properties of proteins from their detailed, atomic-level structure. The orientation of dipoles can be extracted and combined with the hydrodynamic information to predict relaxation times.[93] Andrec and colleagues explored simple connections between the Lipari–Szabo formalism and reduced spectral density mapping. They showed how spectral density estimates can be associated with Lipari–Szabo parameters *via* a geometric construction.[94] Baber *et al.* demonstrated how the extended MF can be used to analyze multifield 15N backbone relaxation data acquired at three different field strengths for *Xenopus* Ca^{2+}-ligated calmodulin and derive parameters by simultaneous least-squares fitting without any prior assumptions regarding their magnitudes.[95] This procedure provides a useful first-order description of complex internal motions in macromolecules despite neglecting the coupling of overall and interdomain motions. Also, Canet *et al.* showed that all data obtained at five magnetic field strengths are consistently fitted to a simple MF approach in which a specific effective correlation time associated with slow motions is defined for each residue. The strategy makes needless elaborate approaches that are based on the combination of several slow motions or possible anisotropy.[96] Osborne and Wright have described a detailed analysis of the effects of rotational anisotropy on the m.[97] Their findings show that the small degree of anisotropy exhibited by DHFR introduces erroneous motional parameters to over 50% of the NH spins analyzed when isotropic tumbling is assumed. Tugarinov *et al.* proposed an alternative to the extended model-free (IMF) approach, which is the two-body Slowly Relaxing Local Structure (SRLS) model.[98] SRLS accounts for dynamical coupling between the global diffusion of the protein and the internal motion of the N–H bond vector. They showed that experimental NMR data are sensitive to the presence of mixed modes and MF can significantly overestimate order parameters and underestimate local motion correlation times in proteins.

Although not directly relevant to relaxation analysis but nevertheless an important development is the ingenious method devised by Skalicky *et al.* for characterizing the flipping kinetics of phenylalanine and tyrosine rings within proteins.[99] NMR spectroscopy of BPTI is performed with supercooled water for the first time at temperatures between -3 and $-16.5\,°C$. At the lower temperature flip broadening of aromatic NMR lines is reduced beyond detection and averaging of NOEs through ring-flipping is abolished. They demonstrated that supercooling is an effective means to harvest potential benefits of stalled ring-flipping for refining NMR solution structures, recruit additional aromatic rings for investigating protein dynamics, and use multiple

slowly flipping rings to probe cold denaturation. Orekhov *et al.* have described the dynamics and structure of (1-36)bacteriorhodopsin solubilized in chloroform/methanol mixture under a hydrostatic pressure of 2000 bar.[100] It was shown that the peptide retains its spatial structure at high pressure. The model free analysis of the relaxation data for the helical 9–31 fragment revealed that the high pressure decreases the overall rotation and translation diffusion, as well as apparent order parameters of fast picosecond internal motions but has no effect on internal nanosecond motions. Kitahara *et al.* also demostrated high-pressure 15N/1H two-dimensional NMR on folate-bound dihydrofolate reductase (DHFR) up to 2000 bar.

The number of publications quoting relaxation measurements for biological macromolecules is vast, therefore a selection of key results is presented. Several of these reports have measured relaxation measurements in monomeric proteins and identified significant correlations with macromolecular recognition and structure. Uhrinova and co-workers have reported the structure and backbone dynamics of monomeric phosphoglycerate mutase (PGAM) from *Schizosaccharomyces pombe*.[101] Interestingly, ^{15}N relaxation indicates that PGAM tumbles isotropically with a rotational correlation time of 8.7 ns and displays a range of dynamic features, which includes 77 amides requiring a chemical exchange term in the MF analysis. In contrast to most analyses, slow exchange residues appeared to correlate with architectural features (*i.e.* helices) in the enzyme rather than ligand binding sites. The same group described the anisotropy of rotational diffusion from ^{15}N relaxation data for two modules from the *Vaccinia* virus complement control protein (VCP).[102] They conclude that the time-averaged structure is more compact than suggested by proton NOEs, which is consistent with the presence of many intermodular orientations, some of which are kinked, undergoing interconversion on a 10^{-8}–10^{-6} timescale. In contrast, Gao *et al.* observed conformational exchange fluctuations in the matrix metalloproteinase (MMP)-inhibitory domain, which map to the sites of MMP-induced fit at the AB and CD loops.[103] Analysis of 15N backbone relaxation parameters shows that dynamic motion of regions directly linked to DNA binding exhibit motion on the microsecond–millisecond timescale. Similarly, Vaughn *et al.* showed that dynamic motion of regions of AbrB involved in DNA binding, a *Bacillus subtilis* protein responsible for gene regulation, show concerted motion on the microsecond–millisecond timescale.[104] Also using the MF formalism, Huang and colleagues extracted the backbone dynamics of TEP-I, a member of a novel subclass of the lipolytic enzymes with a distinctive GDSLS motif. The results reveal that the core structure of the central beta sheet and the long alpha helices is rigid, while the binding pocket appears to be rather flexible.[105] The presence of a flexible substrate-binding pocket may also facilitate binding to a wide range of substrates and confer the versatile functional property of this protein. Suh *et al.* used ^{15}N relaxation measurements to probe the backbone dynamics of an N-terminally truncated monomeric pilin from *P. aeruginosa*.[106] Analysis using MF approach revealed that regions of well-defined secondary structure exhibited consistently low-amplitude spatial fluctuations, while the terminal

and loop regions showed larger amplitude motions in the subnano- to picosecond range. Interestingly, the C-terminal disulfide loop region that contains the receptor binding domain was found to be relatively rigid on the pico- to nanosecond timescale but exhibited motion in the micro- to millisecond timescale. This slower millisecond timescale motion is likely to be crucial for conferring a range of specificity of interactions.

Changes in dynamics observed in complex formation provide insights into the interactions responsible for protein–ligand recognition. A number of papers describe the rigidifying of backbone and side-chain mobility upon binding. Kristensen and co-workers analyzed the backbone dynamics of the C-terminal SH2 domain from the regulatory subunit F85 of phosphoinositide 3-kinase in complex with a phosphotyrosine-containing peptide.[107] Upon binding of the phosphotyrosine peptide, NOE values increase to values observed for regular secondary structure and the exchange contributions vanish. This indicates loss of backbone flexibility upon ligand binding. The results suggest that ligand binding is accompanied by a loss of conformational flexibility on the ligand binding face of the protein. Lu *et al.* showed that the backbone dynamics of holo-cellular retinol-binding protein II are restricted throughout the polypeptide.[108] Also, T2 derived backbone exchange rates indicate that the microsecond to second timescale conformational exchange has been suppressed in the hole form when compared to the the apo form. Huntley *et al.* examined the backbone and tryptophan side-chain dynamics of the metallo-beta-lactamase from *B. fragilis* in the presence and absence of a tight-binding inhibitor.[109] Overall they reveal that the metallo-beta-lactamase molecule is rigid and shows little flexibility except in loops. Furthermore, the large-amplitude motions that were observed for the flexible flap region (residues 45–55) in the absence of the inhibitor were completely damped out in the presence of the inhibitor. Similarly, Zajicek *et al.* concluded that complexation of human plasminogen (K1(Pg)) with ligand reduced fast internal motions and magnitudes of the chemical exchange.[110] Also using relaxation measurements, McCallum and colleagues disclosed that GSH binding to glutathione transferases reduces the exchange rate of residues in proximity to its binding site.[111]

Yun *et al.* have controversially described the backbone dynamics of Delta (5)-3-ketosteroid isomerase (KSI) from *Pseudomonas testosteroni* in complex with its steroid ligand.[112] The majority of the residues exhibit reduced order parameters upon ligand binding, in particular regions involved in the dimer interaction. These results differ from those of previous studies on the backbone dynamics of monomeric proteins, in which high-frequency internal motions are typically restricted upon ligand binding. However, similar observations have been revealed in other systems. Chi *et al.* have characterised the backbone dynamics of the human acidic fibroblast growth factor (hFGF-1) in its free and sucrose octasulfate (SOS)-bound states.[113] They reveal that upon binding to SOS there is a marked decrease in the overall flexibility of the hFGF-1 molecule. However, the segment consisting of residues 103–111 shows increased flexibility in the presence of SOS. Significant correlation is found

between residues that show high flexibility and the putative receptor binding sites on the protein. Sahu *et al.* studied the backbone dynamics of free barnase and its complex with unlabelled barstar.[114] An overall increase in the order parameter is observed upon complex formation by the changes are not uniform along the backbone. For about five residues near the binding interface there is actually a significant decrease in the order parameters on complex formation. Furthermore, Mine *et al.* found that the number of residues in (NAG)(3)-bound human and hen lysozymes showed an increase or decrease in the order parameters at or near active sites on the binding of (NAG)(3), indicating the increase in picosecond to nanosecond.[115] These results suggested that the immobilization of residues upon binding (NAG)(3) resulted in an entropy penalty and that mobilizing other residues compensated this penalty. Also, differences in the internal motions between both ligand-bound human and hen lysozymes reflected a subtle difference in the substrate-binding mode or efficiency of activity between them.

Most NMR relaxation studies on protein concentrate on backbone motions, largely because of the ease with which measurements can be made and interpreted. A few studies report side-chain measurements. Mulder *et al.* have presented a new NMR experiment for the measurement of μs–μs dynamics of Asn and Gin side-chains in proteins. Exchange contributions to the ^{15}N line widths of side-chain residues are determined *via* a relaxation dispersion experiment in which the effective nitrogen transverse relaxation rate is measured as a function of the number of refocusing pulses in constant-time, variable spacing CPMG intervals. They showed that many of the side-chain amide groups of Asn and Gin residues in the C-terminal domain of the protein are affected by a chemical exchange process which may be important in facilitating the rapid binding of hydrophobic ligands to the cavity.[116] Wilkinson *et al.* used the MF formalism to interpret the dynamics of the corresponding N-epsilon-H-epsilon bond vectors of human immunodeficiency virus type 1 (HIV-1) Rev protein.[117] Results indicate that a number of arginine side-chains display a surprising degree of conformational freedom when bound to RNA, and that arginine residues having known importance for specific Rev Response element (RRE) recognition show striking differences in side-chain mobility. The observed dynamical behavior of the arginine side-chains at the protein–RNA interface is likely to play an important role in the specificity and affinity of complex formation. Lou and co-workers have described the methyl side-chain dynamics of three forms of Cdc42Hs, a signal transduction protein that is involved in cytoskeletal growth, from measurements of deuterium T^1 and $T_{1\rho}$ relaxation times. A wide variation in flexibility was observed throughout the protein, with methyl axis order parameters ranging from 0.2 to 0.4 in regions near the binding site to 0.8–1.0 in some helices.[118] Banci *et al.* have monitored the mobility of beta CH2 moieties in oxidized and reduced cytochrome b(5) by analysis if the ^{13}C relaxation of *J*-split components. It is found that higher mobility is present in the alpha helices forming the heme pocket, whereas the beta strands, which form the hydrophobic core of the molecule, have the lowest mobility.[119]

5 Protein Folding

NMR has continued to play a central role in the study of protein folding. Structural and kinetic information can be revealed under denatured and partially denatured conditions providing insight into the structure of folding intermediates and transition states. Equilibrium and quenched-flow hydrogen exchange labeling in combination stopped-flow fluorescence, stopped-flow circular dichroism experiments dominate the experimental protein-folding scene.[120] Although protein-folding intermediates are not accessible to the usual structural studies, hydrogen exchange methods have been able to detect and characterize intermediates in both kinetic and equilibrium modes. A burst phase in the early folding of the four-helix two-state folder protein acyl-coenzyme A binding protein (ACBP) was detected using quenched-flow hydrogen exchange by Teilum *et al.*[121] Several of the burst phase structures coincide with a structure consisting of eight conserved hydrophobic residues at the interface between the two N and C-terminal helices. Samuel *et al.* measured the unfolding and refolding rates of human fibroblast growth factor (hFGF-1) in urea and found that it proceeds through an accumulation of kinetic intermediates.[122] The results of the quenched-flow hydrogen exchange experiments revealed that the hydrogen bonds linking the N- and C-terminal ends are the first to form rather than a hydrophobic interface. Kuwata *et al.* used ultrarapid mixing techniques in conjunction with fluorescence and hydrogen exchange labeling to define the structural and dynamic properties of an early folding intermediate of beta-lactoglobulin.[123] Well-protected amide protons indicative of the stable hydrogen bonded folding core of beta-lactoglobulin were found within the 2 ms of refolding. Nishimura *et al.* characterized the folding pathway of apoleghemoglobin using stopped-flow circular dichroism, heteronuclear NMR pulse labeling techniques and mass spectrometry. The A and B helices are not stabilized until later stages of the folding process. It was found that the pathway of folding differed significantly from that of a protein of the same family, apomyoglobin,[124] although both proteins appear to fold through helical burst phase intermediates.[125] Also, equilibrium NMR measurements for the unfolded state of apomyoglobin formed at pH 2.3 provided insights into the regions of the polypeptide that spontaneously undergo local hydrophobic collapse and sample native-like secondary structure.[126]

Equilibrium amide exchange in destabilized states is useful in the characterization of molten globule and proposed intermediates. The acid-induced collapse of Sac7d, from pH 2 to pH 0, does not lead to a molten globule but proceeds directly to the native state. These results demonstrate that formation of a molten globule is not a general property of proteins that are refolded by acid.[127] However, molten globules are commonly present at acid pH. Kobayashi *et al.* characterized the molten globule structure of equine beta-lactoglobulin at acidic pH using hydrogen exchange protection of the backbone amide protons.[128] The pattern of protection is consistent with a native-like beta-sheet formation by principal strands and formation of the major helix, which is packed against the sheet as in the native structure. However, the

alpha helices in molten globule of canine milk lysozyme are more stabilized than in the homologous alpha-lactalbumin and equine milk lysozyme. These results emphasise the importance of the cooperative interaction in the stability of the molten globule state.[129] Hodsdon and Frieden also showed, using equilibrium amide exchanges at various concentrations of urea, that there are regions in the all beta sheet intestinal fatty acid binding protein which appear to act in a concerted manner at intermediate steps in refolding.[130]

Previous experimental and theoretical studies have produced high-resolution descriptions of the native and folding transition states of chymotrypsin inhibitor 2 (C12), In similar fashion, a combination of NMR experiments and molecular dynamics simulations have been used to examine the conformations populated by C12 in the denatured state.[131] The denatured state is highly unfolded, but there is some residual native helical structure along with hydrophobic clustering in the center of the chain. The lack of persistent nonnative structure in the denatured state reduces barriers that must be overcome, leading to fast folding through a nucleation-condensation mechanism. Yi *et al.* used chemical shifts and paramagnetic relaxation enhancement to characterize structure within the denatured state of a destabilized protein L variant in 2 M guanidine[132] While Bai *et al.* used coupling constants, NOEs, and 15N relaxation parameters to conclude that the an unfolded state of apo-plastocyanin is also noncompact, but with some evidence of native and nonnative local structuring.[133]

This year has seen a continued refinement of real-time NMR studies. Several groups report real-time 1D and 2D NMR experiments for monitoring the kinetics of protein folding. Wirmer and co-workers have explored the kinetics of ion dependent protein folding by time-resolved NMR. Kunn and Schwalbe showed that the refolding of metal binding proteins can be induced by photolysis of photolabile ion chelators, the subsequent release of Ca^{2+} ions can induce protein folding, and the changes in resonance positions can be monitored by time-resolved NMR spectroscopy. The precedure was demonstrated on the refolding of alpha-lactalbumin, or protein containing a Ca^{2+} binding site.[134,135] Balbach used real-time NMR diffusion experiments to monitor compaction during protein folding.[136] The same group measured a series of 128 very fast 2D N-15-HMQC spectra, to observe the kinetics of individual backbone amides within S54G/P55N ribonuclease T1. They found that the intermediate is as compact as the native protein with many native chemical shifts and the intermediate has already gained 40% of the Gibbs free energy of refolding with many protected amides in not-yet-native regions.[137]

Other strategies for investigating protein folding have also emerged. Vugmeyster *et al.* interpret ^{15}N R_1 rho relaxation measurements and show that they facilitate the determination of ultrafast protein folding rates.[138] Myers and Oas fitted the lineshape of a single histidine resonance as a function of denaturant in order to give folding and unfolding rate constants. They report that fast-folding proteins utilize a diffusion–collision mechanism, with the preorganization of one or more elements of secondary structure in the unfolded state.[139] Hill *et al.* examined the roles of intramolecular conforma-

tional dynamics and folding kinetics using novel NMR spin relaxation methods.[140] Chemical exchange line-broadening resulting from the folding equilibrium of alpha D-2 was investigated for four leucine ^{13}C-alpha spins. Folding and unfolding rate constants were measured. The ^{13}C-alpha chemical shifts for unfolded and folded forms of alpha D-2 indicate that the ensemble of unfolded states includes transiently structured helical conformations. Results suggest avenues for improvement of the native-like properties of alpha D-2. Inoue *et al.* have identified a unique equilibrium unfolding intermediate I in the Ras binding domain of the Ral guanine nucleotide dissociation stimulator using 2D NMR spectroscopy at pressures from 30 to 2000 bar. It is characterized by a local melting of specific structural elements near hydrophobic cavities while the overall folded structure is maintained[141] Results from NMR studies of independently interacting protein fragments have implications for protein folding. Jourdan and Searle used NMR to show that peptide fragments corresponding to the N- and C-terminal portions of bovine ubiquitin associate in solution and form a complex of modest stability, which has features characteristic of a native-like structure.[142]

6 References

1 H. J. M. de Groot, *Curr. Opin. Struct. Biol.*, 2000, **10**, 593–600.
2 H. J. Sass, G. Musco, S. J. Stahl, P. T. Wingfield, and S. Grzesiek, *J. Biomol. NMR*, 2000, **18**, 303–309.
3 M. Ruckert and G. Otting, *J. Am. Chem. Soc.*, 2000, **122**, 7793–7797.
4 M. R. Hansen, P. Hanson, and A. Pardi, *J. Biomol. Struct. Dyn.*, 2000, 365–369.
5 C. Ma and S. J. Opella, *J. Magn. Reson.*, 2000, **146**, 381–384.
6 G. Veglia and S. J. Opella, *J. Am. Chem. Soc.*, 2000, **122**, 11733–11734.
7 V. Gaponenko, A. Dvoretsky, C. Walsby, B. M. Hoffman, and P. R. Rosevear, *Biochemistry*, 2000, **39**, 15217–15224.
8 I. Bertini, I. C. Felli, and C. Luchinat, *J. Biomol. NMR*, 2000, **18**, 347–355.
9 F. Tian, C. A. Fowler, E. R. Zartler, F. A. Jenney, M. W. Adams, and J. H. Prestegard, *J. Biomol. NMR*, 2000, **18**, 23–31.
10 F. Delaglio, Z. R. Wu, and A. Bax, *J. Magn. Reson.*, 2001, **149**, 276–281.
11 T. Carlomagno, W. Peti, and C. Griesinger, *J. Biomol. NMR*, 2000, **17**, 99–109.
12 B. Luy and J. P. Marino, *J. Biomol. NMR*, 2001, **20**, 39–47.
13 Z. R. Wu, N. Tjandra, and A. Bax, *J. Biomol. NMR*, 2001, **19**, 367–370.
14 G. Kontaxis and A. Bax, *J. Biomol. NMR*, 2001, **20**, 77–82.
15 A. W. Giesen, L. C. Bae, C. L. Barrett, J. A. Chyba, M. M. Chaykovsky, M. C. Cheng, J. H. Murray, E. J. Oliver, S. M. Sullivan, J. M. Brown, F. W. Dahlquist, and S. W. Homans, *J. Biomol. NMR*, 2001, **19**, 255–260.
16 J. Evenas, A. Mittermaier, D. W. Yang, and L. E. Kay, *J. Am. Chem. Soc.*, 2001, **123**, 2858–2864.
17 J. J. Chou, F. Delaglio, and A. Bax, *J. Biomol. NMR*, 2000, **18**, 101–105.
18 J. Meiler, W. Peti, and C. Griesinger, *J. Biomol. NMR*, 2000, **17**, 283–294.
19 C. A. Fowler, F. Tian, H. M. Al-Hashimi, and J. H. Prestegard, *J. Mol. Biol.*, 2000, **304**, 447–460.
20 M. Andrec, P. C. Du, and R. M. Levy, *J. Am. Chem. Soc.*, 2001, **123**, 1222–1229.

21 G. A. Mueller, W. Y. Choy, N. R. Skrynnikov, and L. E. Kay, *J. Biomol. NMR*, 2000, **18**, 183–188.
22 G. A. Mueller, W. Y. Choy, D. W. Yang, J. D. Forman-Kay, R. A. Venters, and L. E. Kay, *J. Mol. Biol.*, 2000, **300**, 197–212.
23 A. Medek, E. T. Olejniczak, R. P. Meadows, and S. W. Fesik, *J. Biomol. NMR*, 2000, **18**, 229–238.
24 J. J. Chou, S. P. Li, and A. Bax, *J. Biomol. NMR*, 2000, **18**, 217–227.
25 G. M. Clore, *Proc. Natl. Acad. Sci. USA*, 2000, **97**, 9021–9025.
26 C. A. Bewley and G. M. Clore, *J. Am. Chem. Soc.*, 2000, **122**, 6009–6016.
27 A. Vermeulen, H. J. Zhou, and A. Pardi, *J. Am. Chem. Soc.*, 2000, **122**, 9638–9647.
28 Z. R. Wu, A. Ono, M. Kainosho, and A. Bax, *J. Biomol. NMR*, 2001, **19**, 361–365.
29 H. M. Al-Hashimi, A. Majumdar, A. Gorin, A. Kettani, E. Skripkin, and D. J. Patel, *J. Am. Chem. Soc.*, 2001, **123**, 633–640.
30 K. Pervushin, *Q. Rev. Biophys.*, 2000, **33**, 161–197.
31 K. Wuthrich, K. Pervushin, R. Riek, M. Salzmann, and G. Wider, *Abstr. Pap. Am. Chem. Soc.*, 2000, **219**, 11–PHYS.
32 R. Riek, K. Pervushin, and K. Wuthrich, *Trends Biochem. Sci.*, 2000, **25**, 462–468.
33 K. Pervushin, D. Braun, C. Fernandez, and K. Wuthrich, *J. Biomol. NMR*, 2000, **17**, 195–202.
34 M. Salzmann, K. Pervushin, G. Wider, H. Senn, and K. Wuthrich, *J. Am. Chem. Soc.*, 2000, **122**, 7543–7548.
35 R. Riek, K. Pervushin, C. Fernandez, M. Kainosho, and K. Wuthrich, *J. Am. Chem. Soc.*, 2001, **123**, 658–664.
36 F. Lohr, S. Pfeiffer, Y. J. Lin, J. Hartleib, O. Klimmek, and H. Ruterjans, *J. Biomol. NMR*, 2000, **18**, 337–346.
37 A. Meissner and O. W. Sorensen, *J. Magn. Reson.*, 2001, **150**, 100–104.
38 M. Pellecchia, D. Meininger, A. L. Shen, R. Jack, C. B. Kasper, and D. S. Sem, *J. Am. Chem. Soc.*, 2001, **123**, 4633–4634.
39 Y. L. Xia, D. Man, and G. Zhu, *J. Biomol. NMR*, 2001, **19**, 355–360.
40 Y. L. Xia, K. H. Sze, and G. Zhu, *J. Biomol. NMR*, 2000, **18**, 261–268.
41 X. Z. Yan, X. M. Kong, Y. L. Xia, K. H. Sze, and G. Zhu, *J. Magn. Reson.*, 2000, **147**, 357–360.
42 F. Lohr, S. G. Mayhew, and H. Ruterjans, *J. Am. Chem. Soc.*, 2000, **122**, 9289–9295.
43 R. Riek, *J. Magn. Reson.*, 2001, **149**, 149–153.
44 P. Permi, I. Kilpelainen, and A. Annila, *J. Magn. Reson.*, 2000, **146**, 255–259.
45 F. A. A. Mulder, A. Ayed, D. W. Yang, C. H. Arrowsmith, and L. E. Kay, *J. Biomol. NMR*, 2000, **18**, 173–176.
46 C. Fernandez, K. Adeishvili, and K. Wuthrich, *Proc. Natl. Acad. Sci. USA*, 2001, **98**, 2358–2363.
47 K. Oxenoid, F. D. Sonnichsen, and C. R. Sanders, *Biochemistry*, 2001, **40**, 5111–5118.
48 M. Schubert, L. J. Ball, H. Oschkinat, and P. Schmieder, *J. Biomol. NMR*, 2000, **17**, 331–335.
49 A. Meissner and O. W. Sorensen, *J. Biomol. NMR*, 2001, **19**, 69–73.
50 J. Iwahara, J. M. Wojciak, and R. T. Clubb, *J. Biomol. NMR*, 2001, **19**, 231–241.
51 S. Heikkinen, P. Permi, and I. Kilpelainen, *J. Magn. Reson.*, 2001, **148**, 53–60.

52 Y. L. Xia, X. M. Kong, N. Ip, and G. Zhu, *J. Magn. Reson.*, 2000, **146**, 228–231.
53 A. R. Pickford, S. P. Smith, D. Staunton, J. Boyd, and I. D. Campbell, *Embo J.*, 2001, **20**, 1519–1529.
54 S. Saha, J. Boyd, J. M. Werner, V. Knott, P. A. Handford, I. D. Campbell, and A. K. Downing, *Structure*, 2001, **9**, 451–456.
55 S. Yuzawa, M. Yokochi, H. Hatanaka, K. Ogura, M. Kataoka, K. Miura, V. Mandiyan, J. Schlessinger, and F. Inagaki, *J. Mol. Biol.*, 2001, **306**, 527–537.
56 L. H. Hung, G. Chaconas, and G. S. Shaw, *Embo J.*, 2000, **19**, 5625–5634.
57 K. L. Maxwell, A. A. Yee, V. Booth, C. H. Arrowsmith, M. Gold, and A. R. Davidson, *J. Mol. Biol.*, 2001, **308**, 9–14.
58 C. Y. Wang, J. Xi, T. P. Begley, and L. K. Nicholson, *Nat. Struct. Biol.*, 2001, **8**, 47–51.
59 R. Spadaccini, O. Crescenzi, T. Tancredi, N. De Casamassimi, G. Saviano, R. Scognamiglio, A. Di Donato, and P. A. Temussi, *J. Mol. Biol.*, 2001, **305**, 505–514.
60 H. Berglund, D. Olerenshaw, A. Sankar, M. Federwisch, N. Q. McDonald, and P. C. Driscoll, *J. Mol. Biol.*, 2000, **302**, 171–188.
61 D. A. Horita, A. V. Ivanova, A. S. Altieri, A. J. S. Klar, and R. A. Byrd, *J. Mol. Biol.*, 2001, **307**, 861–870.
62 C. Gonzalez, G. M. Langdon, M. Bruix, A. Galvez, E. Valdivia, M. Maqueda, and M. Rico, *Proc. Natl. Acad. Sci. USA*, 2000, **97**, 11221–11226.
63 R. Campos-Olivas, I. Horr, C. Bormann, G. Jung, and A. M. Gronenborn, *J. Mol. Biol.*, 2001, **308**, 765–782.
64 S. Ohki, E. Kariya, K. Hiraga, A. Wakamiya, T. Isobe, K. Oda, and M. Kainosho, *J. Mol. Biol.*, 2001, **305**, 109–120.
65 L. J. Ball, R. Kuhne, B. Hoffmann, A. Hafner, P. Schmieder, R. Volkmer-Engert, M. Hof, M. Wahl, J. Schneider-Mergener, U. Walter, H. Oschkinat, and T. Jarchau, *Embo J.*, 2000, **19**, 4903–4914.
66 M. Batchelor, S. Prasannan, S. Daniell, S. Reece, I. Connerton, G. Bloomberg, G. Dougan, G. Frankel, and S. Matthews, *Embo J.*, 2000, **19**, 2452–2464.
67 G. Kozlov, J. F. Trempe, K. Khaleghpour, A. Kahvejian, I. Ekiel, and K. Gehring, *Proc. Natl. Acad. Sci. USA*, 2001, **98**, 4409–4413.
68 X. L. Zhang, N. C. Gonnella, J. Koehn, N. Pathak, V. Ganu, R. Melton, D. Parker, S. I. Hu, and K. Y. Nam, *J. Mol. Biol.*, 2000, **301**, 513–524.
69 G. Y. Xu, A. Tam, L. Lin, J. Hixon, C. C. Fritz, and R. Powers, *Structure*, 2001, **9**, 277–287.
70 F. J. Moy, E. Glasfeld, L. Mosyak, and R. Powers, *Biochemistry*, 2000, **39**, 9146–9156.
71 I. Bertini, S. Ciurli, A. Dikiy, C. O. Fernandez, C. Luchinat, N. Safarov, S. Shumilin, and A. J. Vila, *J. Am. Chem. Soc.*, 2001, **123**, 2405–2413.
72 F. Arnesano, L. Banci, I. Bertini, D. L. Huffman, and T. V. O'Halloran, *Biochemistry*, 2001, **40**, 1528–1539.
73 A. D. Capili, D. C. Schultz, F. J. Rauscher, and K. L. B. Borden, *Embo J.*, 2001, **20**, 165–177.
74 R. N. De Guzman, H. Y. Liu, M. Martinez-Yamout, H. J. Dyson, and P. E. Wright, *J. Mol. Biol.*, 2000, **303**, 243–253.
75 G. S. Wang, J. M. Louis, M. Sondej, Y. J. Seok, A. Peterkofsky, and G. M. Clore, *Embo J.*, 2000, **19**, 5635–5649.
76 C. Spronk, M. Tessari, A. M. Kaan, J. F. A. Jansen, M. Vermeulen, H. G. Stunnenberg, and G. W. Vuister, *Nat. Struct. Biol.*, 2000, **7**, 1100–1104.

77 W. D. Liu, H. M. Vu, E. P. Geiduschek, and D. R. Kearns, *J. Mol. Biol.*, 2000, **302**, 821–830.
78 D. J. Gordon-Smith, R. J. Carbajo, J. C. Yang, H. Videler, M. J. Runswick, J. E. Walker, and D. Neuhaus, *J. Mol. Biol.*, 2001, **308**, 325–339.
79 A. Farooq, G. Chaturvedi, S. Mujtaba, O. Plotnikova, L. Zeng, C. Dhalluin, R. Ashton, and M. M. Zhou, *Mol. Cell*, 2001, **7**, 387–399.
80 D. H. H. Tsao, T. McDonagh, J. B. Telliez, S. Hsu, K. Malakian, G. Y. Xu, and L. L. Lin, *Mol. Cell*, 2000, **5**, 1051–1057.
81 Z. H. Liu, C. H. Sun, E. T. Olejniczak, R. P. Meadows, S. F. Betz, T. Oost, J. Herrmann, J. C. Wu, and S. W. Fesik, *Nature*, 2000, **408**, 1004–1008.
82 A. M. Petros, A. Medek, D. G. Nettesheim, D. H. Kim, H. S. Yoon, K. Swift, E. D. Matayoshi, T. Oltersdorf, and S. W. Fesik, *Proc. Natl. Acad. Sci. USA*, 2001, **98**, 3012–3017.
83 G. K. Amarasinghe, R. N. De Guzman, R. B. Turner, and M. F. Summers, *J. Mol. Biol.*, 2000, **299**, 145–156.
84 G. K. Amarasinghe, R. N. De Guzman, R. B. Turner, K. J. Chancellor, Z. R. Wu, and M. F. Summers, *J. Mol. Biol.*, 2000, **301**, 491–511.
85 F. H. T. Allain, D. E. Gilbert, P. Bouvet, and J. Feigon, *J. Mol. Biol.*, 2000, **303**, 227–241.
86 M. R. Conte, T. Grune, J. Ghuman, G. Kelly, A. Ladas, S. Matthews, and S. Curry, *Embo J.*, 2000, **19**, 3132–3141.
87 J. M. Wojciak, J. Iwahara, and R. T. Clubb, *Nat. Struct. Biol.*, 2001, **8**, 84–90.
88 J. L. Vaughn, V. Feher, S. Naylor, M. A. Strauch, and J. Cavanagh, *Nat. Struct. Biol.*, 2000, **7**, 1139–1146.
89 I. Ohki, N. Shimotake, N. Fujita, J. G. Jee, T. Ikegami, M. Nakao, and M. Shirakawa, *Cell*, 2001, **105**, 487–497.
90 Y. X. Lin, V. Dotsch, T. Wintner, K. Peariso, L. C. Myers, J. E. Penner-Hahn, G. L. Verdine, and G. Wagner, *Biochemistry*, 2001, **40**, 4261–4271.
91 R. Ishima and D. A. Torchia, *Nat. Struct. Biol.*, 2000, **7**, 740–743.
92 J. R. Tolman, H. M. Al-Hashimi, L. E. Kay, and J. H. Prestegard, *J. Am. Chem. Soc.*, 2001, **123**, 1416–1424.
93 J. G. de la Torre, M. L. Huertas, and B. Carrasco, *J. Magn. Reson.*, 2000, **147**, 138–146.
94 M. Andrec, G. T. Montelione, and R. M. Levy, *J. Biomol. NMR*, 2000, **18**, 83–100.
95 J. L. Baber, A. Szabo, and N. Tjandra, *J. Am. Chem. Soc.*, 2001, **123**, 3953–3959.
96 D. Canet, P. Barthe, P. Mutzenhardt, and C. Roumestand, *J. Am. Chem. Soc.*, 2001, **123**, 4567–4576.
97 M. J. Osborne and P. E. Wright, *J. Biomol. NMR*, 2001, **19**, 209–230.
98 V. Tugarinov, Z. C. Liang, Y. E. Shapiro, J. H. Freed, and E. Meirovitch, *J. Am. Chem. Soc.*, 2001, **123**, 3055–3063.
99 J. J. Skalicky, J. L. Mills, S. Sharma, and T. Szyperski, *J. Am. Chem. Soc.*, 2001, **123**, 388–397.
100 V. Y. Orekhov, P. V. Dubovskii, H. Yamada, K. Akasaka, and A. S. Arseniev, *J. Biomol. NMR*, 2000, **17**, 257–263.
101 S. Uhrinova, D. Uhrin, J. Nairn, N. C. Price, L. A. Fothergill-Gilmore, and P. N. Barlow, *J. Mol. Biol.*, 2001, **306**, 275–290.
102 C. E. Henderson, K. Bromek, N. P. Mullin, B. O. Smith, D. Uhrin, and P. N. Barlow, *J. Mol. Biol.*, 2001, **307**, 323–339.

103 G. Gao, V. Semenchenko, S. Arumugam, and S. R. Van Doren, *J. Mol. Biol.*, 2000, **301**, 537–552.

104 J. L. Vaughn, V. A. Feher, C. Bracken, and J. Cavanagh, *J. Mol. Biol.*, 2001, **305**, 429–439.

105 Y. T. Huang, Y. C. Liaw, V. Y. Gorbatyuk, and T. H. Huang, *J. Mol. Biol.*, 2001, **307**, 1075–1090.

106 J. Y. Suh, L. Spyracopoulos, D. W. Keizer, R. T. Irvin, and B. D. Sykes, *Biochemistry*, 2001, **40**, 3985–3995.

107 S. M. Kristensen, G. Siegal, A. Sankar, and P. C. Driscoll, *J. Mol. Biol.*, 2000, **299**, 771–788.

108 J. Y. Lu, C. L. Lin, C. G. Tang, J. W. Ponder, J. L. F. Kao, D. P. Cistola, and E. Li, *J. Mol. Biol.*, 2000, **300**, 619–632.

109 J. J. A. Huntley, S. D. B. Scrofani, M. J. Osborne, P. E. Wright, and H. J. Dyson, *Biochemistry*, 2000, **39**, 13356–13364.

110 J. Zajicek, Y. Chang, and F. J. Castellino, *J. Mol. Biol.*, 2000, **301**, 333–347.

111 S. A. McCallum, T. K. Hitchens, C. Torborg, and G. S. Rule, *Biochemistry*, 2000, **39**, 7343–7356.

112 S. G. Yun, D. S. Jang, D. H. Kim, K. Y. Choi, and H. C. Lee, *Biochemistry*, 2001, **40**, 3967–3973.

113 Y. H. Chi, T. K. S. Kumar, I. M. Chiu, and C. Yu, *J. Biol. Chem.*, 2000, **275**, 39444–39450.

114 S. C. Sahu, A. K. Bhuyan, J. B. Udgaonkar, and R. V. Hosur, *J. Biomol. NMR*, 2000, **18**, 107–118.

115 S. Mine, T. Ueda, Y. Hashimoto, and T. Imoto, *Protein Sci.*, 2000, **9**, 1669–1684.

116 F. A. A. Mulder, N. R. Skrynnikov, B. Hon, F. W. Dahlquist, and L. E. Kay, *J. Am. Chem. Soc.*, 2001, **123**, 967–975.

117 T. A. Wilkinson, M. V. Botuyan, B. E. Kaplan, J. J. Rossi, and Y. Chen, *J. Mol. Biol.*, 2000, **303**, 515–529.

118 A. P. Lou, N. Pawley, L. K. Nicholson, and R. E. Oswald, *Biochemistry*, 2001, **40**, 4590–4600.

119 L. Banci, I. Bertini, I. C. Felli, P. Hajieva, and M. S. Viezzoli, *J. Biomol. NMR*, 2001, **20**, 1–10.

120 S. W. Englander, *Annu. Rev. Biophys. Biomol. Struct.*, 2000, **29**, 213–238.

121 K. Teilum, B. B. Kragelund, J. Knudsen, and F. M. Poulsen, *J. Mol. Biol.*, 2000, **301**, 1307–1314.

122 D. Samuel, T. K. S. Kumar, K. Balamurugan, W. Y. Lin, D. H. Chin, and C. Yu, *J. Biol. Chem.*, 2001, **276**, 4134—4141.

123 K. Kuwata, R. Shastry, H. Cheng, M. Hoshino, C. A. Batt, Y. Goto, and H. Roder, *Nat. Struct. Biol.*, 2001, **8**, 151–155.

124 C. Garcia, C. Nishimura, S. Cavagnero, H. J. Dyson, and P. E. Wright, *Biochemistry*, 2000, **39**, 11227–11237.

125 C. Nishimura, S. Prytulla, H. J. Dyson, and P. E. Wright, *Nat. Struct. Biol.*, 2000, **7**, 679–686.

126 J. Yao, J. Chung, D. Eliezer, P. E. Wright, and H. J. Dyson, *Biochemistry*, 2001, **40**, 3561–3571.

127 J. L. Bedell, B. S. McCrary, S. P. Edmondson, and J. W. Shriver, *Protein Sci.*, 2000, **9**, 1878–1888.

128 T. Kobayashi, M. Ikeguchi, and S. Sugai, *J. Mol. Biol.*, 2000, **299**, 757–770.

129 Y. Kobashigawa, M. Demura, T. Koshiba, Y. Kumaki, K. Kuwajima, and K. Nitta, *Proteins*, 2000, **40**, 579–589.

130 M. E. Hodsdon and C. Frieden, *Biochemistry*, 2001, **40**, 732–742.
131 S. L. Kazmirski, K. B. Wong, S. M. V. Freund, Y. J. Tan, A. R. Fersht, and V. Daggett, *Proc. Natl. Acad. Sci. USA*, 2001, **98**, 4349–4354.
132 Q. Yi, M. L. Scalley-Kim, E. J. Alm, and D. Baker, *J. Mol. Biol.*, 2000, **299**, 1341–1351.
133 Y. W. Bai, J. Chung, H. J. Dyson, and P. E. Wright, *Protein Sci.*, 2001, **10**, 1056–1066.
134 J. Wirmer, T. Kuehn, and H. Schwalbe, *Faseb J.*, 2000, **14**, 428.
135 T. Kuhn and H. Schwalbe, *J. Am. Chem. Soc.*, 2000, **122**, 6169–6174.
136 J. Balbach, *J. Am. Chem. Soc.*, 2000, **122**, 5887–5888.
137 C. Steegborn, H. Schneider-Hassloff, M. Zeeb, and J. Balbach, *Biochemistry*, 2000, **39**, 7910–7919.
138 L. Vugmeyster, C. D. Kroenke, F. Picart, A. G. Palmer, and D. P. Raleigh, *J. Am. Chem. Soc.*, 2000, **122**, 5387–5388.
139 J. K. Myers and T. G. Oas, *Nat. Struct. Biol.*, 2001, **8**, 552–558.
140 R. B. Hill, C. Bracken, W. F. DeGrado, and A. G. Palmer, *J. Am. Chem. Soc.*, 2000, **122**, 11610–11619.
141 K. Inoue, H. Yamada, K. Akasaka, C. Hermann, W. Kremer, T. Maurer, R. Doker, and H. R. Kalbitzer, *Nat. Struct. Biol.*, 2000, **7**, 547–550.
142 M. Jourdan and M. S. Searle, *Biochemistry*, 2000, **39**, 12355–12364.

10
NMR of Carbohydrates, Lipids and Membranes

BY E.F. HOUNSELL

1 Introduction

With the rapid rise in available gene sequences of various species, the post-genomic age is fast approaching. In the context of the subject under review herein, we are going beyond proteomic approaches, which follow the expressed genes as far as protein products, to the characterisation of the further products of protein enzymes, *i.e.* the secondary metabolites and natural products. Previous reviews in this series[1,2] have concentrated on other areas of NMR analysis, largely in the mammalian structure/function field and I have directed the readership to the journals of extensive body of data on natural products. The unprecedented rise in such data has prompted me to present an overview this time of the structure of natural products. In addition, a recent review by Duus *et al.*[3] covers the former area well *via* a survey of structural assignment by NMR; NMR methods and limitations; coupling constant data; analysis of linkage and sequence; long range ^{13}C–^{1}H coupling constants; isotopic labelling strategies; and gradient enhanced versions of COSY (gCOSY) which have shown superior sensitivity for observing cross peaks between proton pairs with small coupling constants *e.g.* $^{3}J_{H\text{-}1,H\text{-}2}$ in β-D-Man.

New approaches from the body of data on natural products include toxicogenetic approaches where characterised natural products, as toxins, cytokines or cell stimulants, can be studied by their effects in cell culture assayed by changing DNA/RNA expression characterised by gene micro-array techniques. Relational data bases can be used to correlate gene sequences with micro-array analysis results and structural data of the natural products produced from NMR characterisation followed by mass spectrometric profiling. In addition, in genomics, annotation of the genome requires that we unravel the parts which both code for structural protein (proteomics) and for the large amount of the genome that is given over to the enzymes which synthesise natural products and natural products (metabolomics) and catalyse the post-translational modifications of proteins (glycoproteomics?). New understanding of the glycosylation of bacterial proteins and the genes that encode the glycosyltransferases responsible for this and other glycoconjugates such as lipopolysaccharide (LPS) is exemplified by our study of *Porphyromonas gingivalis*.[4] Knowledge of the structures leads to the genes encoding the glycosyl transferases. This is important not only in bacteria, but also plants

Nuclear Magnetic Resonance, Volume 31
© The Royal Society of Chemistry, 2002

and fungus which have an equal diversity in natural product structure and functions and for which genomic data are being rapidly produced.

No-one has yet expressed the need to define 'lipomics' as a separate field, but it is obvious to many that the ubiquity of the lipids and their conjugates, together with studies on membranes and molecular interactions in membranes, is an essential aspect of our post-genomic understanding. NMR is an essential tool in the characterisation of their structure and dynamics. Aspects of this are covered in the review along with NMR studies of the ubiquity of lipids and proteins that are glycosylated and of glycoproteins anchored into the membrane by glycosylphosphatidylinositol (GPI).

2 Bacterial Natural Products

2.1 Bacteria Causing Mammalian Pathogenesis. – In addition to glycosylated proteins mentioned above, bacteria have classically been characterised by their conjugates and polysaccharides (PS): the LPS, which consists of the lipid A component and the *O*-polysaccharide (OPS); secreted exopolysaccharides (EPS); and the capsular PS (CPS). The diversity of the polysaccharide structures of bacteria knows no bounds. Only detailed NMR studies are capable of distinguishing the species and strain differences. The following are some recent examples of their novelty: Bergstrom *et al.*[5] have characterised a unique teichoic acid-like polysaccharide of *Streptococcus mitis* which has a heptasaccharide phosphate repeating unit which contains neither ribitol nor glycerol phosphate as classical teichoic acids do. The group O antigen of this organism has a *C*-polysaccharide similar to that of *S. pneumoniae* having phosphocholine and galactosamine residues (the latter mostly *N*-acetylated in *S. mitis*). Strains of *Bordetella bronchiseptica* have LPS polysaccharide structures consisting of (α1-4)-linked 2,3-diacetamido-2,3-dideoxy-L-galacturonic acid repeating units with 2,3,4-trideoxy-α-galacturonamide derivatives at their non-reducing ends, a monosaccharide first defined in nature in this paper.[6] The derivative was found to be further complicated by having a strain specific pattern of acylation with variations of *N*-formyl-L-alanyl, *N*-alanyl, *N*-2-methoxypropionyl, *N*-acetyl and *O*-formyl. The distributions of the acyl groups were determined by NMR using long range ^{1}H–^{13}C correlation (HMBC).

The structure of the core oligosaccharides of *Campylobacter jejuni* O2 LPS was found to contain 3-deoxy-D-*manno*-octulosonic acid (Kdo), L-glycero-D-manno-heptose (LD-Hep), D-Gal, D-Glc and phosphoethanolamine based on ^{1}H, ^{13}C and ^{31}P NMR.[7] Molecular mimicry in *C. jejuni* LPS has been implicated in the pathogenesis of Guillain-Barre syndrome by inducing antibodies to human gangliosides.

Other examples include: a branched trisaccharide of the type 1A group B *Streptococcus* capsular polysaccharide,[8] GlcNAc(β1-3)[Glc(β1-6)]Glc, was synthesised and characterised using HSQC and ^{31}P NMR; Schaffer *et al.*[9] characterised a pyrophosphate bridge which links the pyruvate-containing

secondary cell wall polymer of *Paenibacillus alvei* CCM 2051 to muramic acid, the secondary cell wall polymer of the peptidoglycan which, in addition to the surface layer (S-layer) glycoproteins are the major cell wall components; the structure of an *O*-acetylated acidic polysaccharide of *Proteus vulgaris* O46 was elucidated[10] following solvolysis of the *O*-deacetylated polysaccharide with trifluoromethansulfonic acid, demonstrating the tetrasaccharide building block-4)Glc*p*6Ac(α1-3)Glc*p*A4Ac(β1-3)Glc*p*NAc(a1-3)Glc*p*A4Ac(β1-, *i.e.* glucuronic acid, acetylated at C-4, alternating with glucose, acetylated at C-6, or GlcNAc.

Yildirim *et al.*[11] reported the NMR characterisation of the OPS of *Escherichia coli* O77LPS and reviewed the OPS structure and antigenicty of *E. coli*. *E. coli*, a facultative anaerobic Gram negative rod, is the predominant species in the colonic flora of animals and man. There are three general clinical syndromes that result from infections with pathogenic *E. coli* enteric/diarrhoeal, urinary tract and septicaemia/meningitis. The species is subdivided into serotypes O, K and H based on their immunogenicity where O is the polysaccharide portion of the LPS, K is the capsular polysaccharide and H is the flagella antigen. More than 170 different O antigens and over 100 capsular polysaccharides have been identified in the species.

Marshall *et al.*[12] reported on the diverse structures of the EPS from streptococci, lactobacilli and lactococci. Whilst the main constituent sugars are frequently Gal, Glc and Rha there is no obvious pattern in the frequency at which they occur. The complexity of the structures is further compounded by the variety of linkages that exist between the monosaccharides. For example these authors report a heptasaccharide repeating unit of the EPS of *Streptococcus thermophilus* containing β-D-Gal*p*, α-D-Gal*p*, β-L-Rha*p*, α-L-Rha*p*, β-D-Glc*p* and α-D-Gal*f*. Obviously this type of complexity and mixture of D/L and *p*/*f* can only be deconvoluted by detailed NMR studies using the gamut of available pulse sequences.

It is also obvious that we have a long way to go to unravel the complexity of such organisms. A recent review[13] on current methods in the structural elucidation of polysaccharides, including recently developed methodologies (in particular pulse field gradients), has concentrated on bacterial polysaccharides with most of the techniques being illustrated using O-polysaccharides from *Proteus mirabilis* (which as previous studies have shown has a large strain specific variety in its LPS structure). Although the review set out to discuss the significance of polysaccharides, in general, in (a) biological functions, (b) the growing range of polysaccharide-based drugs and (c) their multiple industrial applications polysaccharides, it is no surprise that the bacterial polysaccharides were chosen as examples. These are also ideal for conformational studies as they are easily isotopically labelled. Martin-Pastor and Bush have continued studies from this group on bacterially derived, labelled oligosaccharides (also see the literature of the group of Homans and this review last year). In the latest 2001 study[14] the refined structure of a flexible heptasaccharide is reported using ^{1}H–^{13}C and ^{1}H–^{1}H NMR and characterisation of residual dipolar coulpings in concert with NOE and long range scalar coupling

constants of the cell wall *S. mitis* J22, (*NB*, a different strain to that reported at the beginning of this section).

2.2 Bacteria Causing Disease in Plants. – The last section concentrated on the lipid-linked PS of bacteria, ignoring the secreted polysaccharides which normally are seen as contaminants in the PS preparation from the LPS. These can be readily identified by NMR spectroscopy.[4] Such mannans and glucans so far characterised have homologues in fungal excreted PS fractions. Several of these have now been characterised from bacteria causing disease in plants. The first reported mannan EPS from a phytopathogenic bacterium was reported from the Gram negative bacterium *Pseudomonas syringae* pv. *ciccaronei* which is the pathogenic agent responsible for the leaf spots of carob plants.[15] Full ^{1}H NMR data were reported for an oligosaccharide having a (1-6)-linked backbone with (1-2)-linked side chains and an occasional (1-3)-linkage. This shows a similar population composition as yeast *Saccharomyces cerevisiae* mannan which has been shown to be recognised by human antibodies and has been implicated in brewers and bakers allergy to occupationally exposed yeast.[16,17]

Xanthomonas campestris pv. *Vitians* (proposed new names: *X. hortorum* pv. *Vitians*/*X. axonopodis* pv. *Vitians*) is the causal agent of leaf spot and head rot of lettuce studied by Molinaro *et al.*[18] The LPS constitutive components implicated in the events of pathogenicity were characterised. From the aqueous phase of the phenol/water treatment of the dried bacterium cells a glucan rich LPS was extracted. As usual, mild acid hydrolysis gave the *O*-specific polysaccharide. This consisted of only 3-linked L-Rha residues which by ^{1}H and ^{13}C NMR were also shown to be present in the phenol phase after Smith degradation (*i.e.* complexed with other PS). The full structure was shown to be -(α-L-Rha*p*)$_2$-(β-L-Rha*p*)$_1$-. A similar LPS structure was reported[19] in the genus *Stenotrophomona*, a genus which was created to accommodate the organism originally known as *Pseudomonas maltolhila* and subsequently as *Xanthomonas maltophilia*. The species has potential for bioremediation and the biological control of plant pathogens and has emerged as a multi-drug resistant opportunistic pathogen responsible for nosocomial infections (hospital inpatients) and a particular threat to the cystic fibrosis population. The lipid A of *S. maltophilia* contains a distinctive set of branched-chain fatty acids, GalA is released during mild acid hydrolysis of the LPS and the core lacks heptose, but includes D-Man. The authors compared the OPS structure of the O14 antigen obtained by 1D and 2D NMR to that of *X. campestris* discussed above, but here the OPS contains a backbone of all α-Rha, all D rather than L and one in three linked (1-2) rather than (1-3). The O16 antigen of *S. maltophilia* on the other hand also characterised by 1D and 2D NMR[20] is very different having the repeating structure-4)Glc*p*NAc (β1-3)[Rib*f*(α1-4)]Man*p*NAc(β1-.

2.3 Marine Bacteria. – Faulkner[21] has reviewed marine natural products putting into context those containing glycosides with others and with the natural products of marine microorganisms (fungi and bacteria). As further

examples of their diversity: an acidic polysaccharide from a marine bacterium *Pseudoalteromonas distincta* was shown[22] to contain 5-acetamido-3,5,7,9-tetra-deoxy-7-formamido-L-glycero-L-manno-nonulosonic acid (Pse5Ac7Fo), a derivative of pseudaminic acid (this was linked with QuipNAc in a repeating backbone unit with less unusual sugars forming the side chain); the OPS from the LPS of the marine gram negative bacterium *Pseudoalteromonas tetrodonis* IAM 14160 has been characterised[23] to contain 3,6-dideoxy-L-*xylo*-hexose (D-colitose) as part of a hexasaccharide repeat both in the backbone and also as a non-reducing terminus of the side chain. As well as one of the most potent nerve toxins known, tetrodotoxin, a range of biologically active compounds such as antibiotics, enzymes, anti-toxins, anti-tumour and anti-viral agents were isolated from this species.

3 Fungal Natural Products

Series of bacterial, fungal and plant PS are being explored for their potential in the food, agriculture and neutriceutical industries. Structural analysis of a series of β-D-(1-3, 1-6)-linked glucans (laminaran, curdlan, yeast glucan, pachyman, pustulan, sclerglucan *etc.* was performed using two-dimensional NMR spectroscopy.[24] These have the ability of enhancing and stimulating the immune system. Sources included *Laminaria digita*, *Umbiliaria papullosa*, *saccharomyces cerevisiae*, *Alcaligenes faecalis*, *Poria cocos* and *Sclerotium glucanicum*. Carboxymethyl pullulans (maltotriose repeats containing two (α1-4) linkages and one (α1-6) linkage) were also characterised further by NMR.[25] Other natural products of fungi having biomedical properties include: two novel lactones isolated from *Aspergillus versicolor* fermentation broth which exhibited insecticidal activity against *Staphylinidae*;[26] novel fungal metabolites as cell wall active anti-fungals (against *Candida* and *Aspergillus*) were isolated from the fermentation broth of another fungus and identified as peptides containing amino acids such as alanine, aminoisobutyric acid, proline, leucine, valine, glycine and a previously identified β-ketoacid, 2-methyl-3-oxotetradecanoic acid.[27] Roselipins from the marine fungus *Gliocladium roseum* KF-1040 are highly methylated glycolipids, possibly propionates, that inhibit the enzyme diacylglycerol acyl transferase.[28–30]

4 Plant Natural Products Characterised by ^{1}H and ^{13}C NMR

A high molecular weight fructan was isolated from garlic (*Allium sativum* L) and the structure determined by enzymatic, chemical and NMR (COSY and HSQC) methods.[31] It was found that the garlic fructan belongs to the neoketose family. It has a (2-1)-linked β-D-Fru*f* backbone with (2-6) β-D-Fru*f* side chains. A structural model was postulated for a degree of polymerisation of about 58. This model was substantiated using an endo-inulinase purified from *Aspergillus ficuum* and by ^{1}H and ^{13}C NMR spectroscopy. Arabinoxylan

polysaccharides are found in the cell walls of a number of different plants and have been studied extensively by NMR over the past 10 years resulting in the elucidation of a number of plant oligosaccharide structures with varied distribution in specifc plants. These are reviewed in ref. 32 which also describes the application of nano-probe NMR for structure determination of low amounts of oligosaccharides fractionated by analytical HPAEC-PAD. Stable aqueous suspensions of purified and homogenised sugar beet pulp cellulose, subjected to various TFA treatments, induced flocculation of the suspension and the release of a number of polysaccharides.[33] Among these a 4-*O*-methyl glucuronoxylan, with an α-D-GlcA linked to 1/7 of (1-4)-linked β-D-Xyl, was characterised from 1D ^{1}H and ^{13}C NMR data.

The following are some recent examples of the low molecular weight natural products of plants characterised by ^{1}H and ^{13}C NMR: new ellagitannins from *Pelargonium reniforme*[34] having a fully aromatic ester substituted rhamnose galloyl glycoside; the first total synthesis of a dimeric ellagitannin, coriariin A;[35] a new flavone diglycoside from *Carthanus tinctorius* seeds;[36] sulfonated triterpenoid saponins from *Fagona indica* characterised by a combination of homonuclear and heteronuclear 1D and 2D NMR experiments which defined the structure and conformation of three glycoside rings and one sterol structure;[37] a novel oligosaccharide antibiotic from *Micromonospora carbonaceae* active against multi-drug resistant bacteria having eight partially methylated glycoside rings flanked by two mono-chlorinated aromatic rings;[38] room temperature (^{1}H and ^{13}C) and variable temperature (^{1}H)NMR studies on spinosin from the plant *Desmodium tortuosum*[39] including 2D homo- and hetero-nuclear 2D experiments gave an aromatic glycoside of Glc(β1-2) Glc(β1-; cytotoxic norbisabolane glycosides from *Phyllanthus acidus*;[40] two new acylated flavanoid glycosides from *Vicia ameurensis* were characterised from FABMS and HMBC correlations showing a glycoside of ferulyl-L-6dGul(β1-6)[L-6dGul(β1-2)]Gal;[41] tetrasacchairde multi-esters and xanthone glycosides from the roots of *Polygala arillata* and *P. watteraii*;[42] four new phenyl propanoid esters from *Polygonum perfoliatum*;[43] three new simple glycosides from the fruits of *Morinda citrifolia*;[44] four new bisanthraquinone glycosides of *Hypericum perforatum*,[45] chromones and anthrones from *Aloe marlothi* and *A. rupestris* leaf exudates,[46] triterpene glycosides of *Schefflerpsis angkae* characterised as glycosides of oleanic and ursolic acids;[47] new triterpine saponinins from *Chenopodium quinoa* seeds, *e.g.* those containing phytolaccagenic acid;[48] steroidal saponins from the leaves of *Cestrum sendtenerianum*,[49] where one of the compounds, a spirostanol triglycoside, showed weak cytotoxic activity on HL-60 human promyelocytic leukemia cells; saponin and flavanoid glycosides from *Nigella sativa L*;[50] bioactive oleanolic acid saponins from the roots of *Viguiera decurrens* which showed insecticidal activity;[51] the flavanoids apigenin and luteolin glycosides from the aerial parts of alfalfa;[52] novel acylated nonlinear tetrasaccharide resin glycoside, soldanelline B, a macrolactone and its fatty acid derivative soldanellic acid B from *Calystegia soldanella*;[53] triterpene glycosides from cultures of *Phytolacca americana*;[54] and a new nortriterpenoid glycoside from *Sinofranchetia chinensis*, named sinofoside A.[55]

5 Other Organisms

Aurantosides with anti-fungal activity were isolated from the Japanese lithistid *Siliquariaspngia japonica*[56] which also contained a related series of tetramic acid glycosides, called rubrosides, that induced large intracellular vacuoles in rat fibroblasts.[57] An additional aurnatoside was isolated from the lithistid sponge *Homophymia conferta* from the Philippines.[58] Triterpene glycosides which defend the Caribbean reef sponge *Erylus formosus* from predatory fish-antifeedant metabolites were isolated by bio-assay guided fractionation of extracts and identifed by NMR spectroscopy[59] to have a penasterol triterpene core and an *N*-acetylgalactosamine formaside.

Sulfated polysaccharides are widely distributed among marine invertebrates which are reveiwed in ref. 60. Several of these animals possess polysaccharides with unique structures such as sulfated L-galactans, sulfated L-fucans or glycosaminoglycan polymers, but they differ from mammalian compounds due to additional sugar branches or to distinguishing sulfation patterns. In the case of marine sponges, the sulfated polysaccharides have been associated with cell interaction processes between sponge cells. Sulfated PS of algae have been reviewed previously[1,2] as anti-complement factors, *i.e.* of use in dampening down the immune response. Other sulfate esters include the starfish aphelasteroside C and aphelaketotriol, two new haemolytic polar steroids from a starfish *Aphelasterias japonica*[61] sulfated at C-4 of 6dGlc and on the steroid aglycon.

6 Lipid Conjugates

α-Galactosyl cerebrosides have been synthesised and characterised by NMR in $CDCl_3$ and had been shown previously to have immunostimulating properties.[62] Some α-galactosyl ceramides with phytosphingosine structures isolated from the marine sponge *Agela mauritianus* were shown to have strong *in vivo* anti-tumour activities against several murine tumour cells.[63] Monoglycosylated ceramides (cerebrosides) are the simplest class of glycosphingolipids. Galactosyl cerebrosides have been shown to possess important functions in promoting the regulation of nerve cells, regulating protein kinasae C activities and modulating the function of hormone receptors. This is one of a very large number of possible structures of glycolipids and gangliosides (those having sialic acid residues). A very useful review with 57 references has been published[64] on the use of NMR in the evaluation of ganglioside structure, conformation and dynamics giving the choice of solvent and temperature in the NMR experiments of gangliosides and their primary and secondary structure. A particular subset of blood group ABO(H) active gangliosides have been characterised in type AB erythrocytes and structural analysis described of type A-active ganglioside variants in type A human erythrocytes.[65]

In lower organisms: the structural analysis was reported[66] of a new glycosphingolipid (GSL) from the LPS-lacking *Sphingomonas adhaesiva* (whilst in

most Gram negative bacteria the major glycolipid in the outer membrane is the LPS, in bacteria belonging to the family *Sphingomonadaceae* this is replaced by GSLs); new lipopeptides were isolated from a marine red cyanobacterium, *Lyngbya majuscula*, which exhibited cytoxicity against mammalian tumour cells;[67] the a-factor lipopeptide (farnesylated) pheromone of *Saccharomyces cerevisiae* was characterised by NMR spectroscopy[68] and the bioactivity measured by fluorescent analysis of the binding to vesicles (isoprenylation is now recognised as a common post-translational modification of proteins in this yeast as well as mammals); eight compounds isolated from an extract of central Asian lichens comprised new glucosides having murolic, protoconstipatic and allo-murolic acids as the aglycons and a sacchararide moiety linked at C-18 made up of four glucoses;[69] novel triphonooctaosyl ceramides from the eggs of the sea hare, *Aplysia kurodai*.[70]

7 Glycosylphosphatidylinositol Anchors

The glycan units of GPI membrane anchors are interesting targets for drug design. For example the GPI anchor of *Trypanosoma brucei* contains the α-galactosylated sequence Gal(α1-2)Gal(α1-6)[Gal(α1-2)]Gal(α1-3)[Protein-6) Man(α1-2)Man(α1-6)]Man(α1-4)GlcN(α1-6)InsP. Up to a tetrasaccharide sequence having the Galα- linked to Man which is also substituted by the other two Man residues has been synthesised as the allyl glycoside[71] and characterised by NMR in D_2O. *Trypanosoma cruzi* NMR assignments for glucosylated and galactosylated *N*-acetylhexosaminitols from *O*-linked mucins of the trypanosome GPI anchored surface mucins[72] and the structure of *O*-glycosidically linked oligosacchrides of their glycoproteins – evidence for *O*-linked sialyl oligosaccharidedes – was presented.[73] Although *Trypanasoma brucei* and *Trypanasoma cruzi* cause millions of deaths and morbidity in humans, the most famous GPI anchored protein of the moment is the prion. In the absence of X-ray crystallographic data, NMR remains the only experimental source of conformational data which has helped elucidate some of the details of the structure/function of these molecules.[74–86]

NMR analysis of molecules containing phosphate has been aided considerably by studies on model compounds, for example to study the mechanism of action of cleavage enzymes. Venugopal *et al.*[87] have made a valuable contribution by their synthesis and IR, ^{1}H, ^{31}P and mass spectral data on cyclic phosphoramidate/phosphate/phosphorothioates of gluco- and xylofuranoses. The regulation of protein degradation and protease expression by mannose in maize root tips has been studied using *in vivo* and *in vitro* ^{13}C and ^{31}P NMR to follow the effects of mannose on Pi sequestration.[88] Occurrance of an unusual phosphorylated *N*-acetyllactosamine in hose colostrum,[89] another in a series of milk oligosaccharides having phosphate as the aglycon, has been reported.

8 Membranes Studies

Ternary phase diagrams have been constructed[90] from experiments including NMR data of systems with dioleoylphosphatidylcholine (DOPC) and water and two α-helical membrane spanning model peptides of the known lysine containing type, KKLAKK[KK(LA)$_n$KK]. Several complementary NMR approaches have been used[91] to study the interactions of a 14-residue peptide toxin (mastoparan) from wasp venom with lipid membranes – the 3D structure of mastoparan was determined using ^{1}H-NMR NOESY experiments in perdeuterated (SDS-d$_{25}$) micelles, solid state ^{2}H-NMR binding of mastoparan to lipid layers composed of headgroup-deuterated dimyristoylglycerophosphocholine (DMPC-d$_4$) and dimyristoylphosphatidylglycerol (DMPG) with correlation of the deuterium quadrupole splittings and the insertion and orientation of a specifically ^{15}N-labelled mastoparan in the bilayer environment investigated by solid-state ^{15}N NMR using macroscopically-orientated samples. The solution structure of human immunodeficiency virus type 1 peptide residues 13–33 in micelles was studied by NMR and CD spectroscopy and it was found[92] that this forms an amphipathic leucine-zipper-like 1-helix that serves as a basis for interactions with a variey of viral and cellular factors. Lipid organisation and dynamics were studied in the liquid phase of the monostearyolglycerol(MSG)–water system with fully labelled [^{2}H$_{35}$]-MSG and selectively labelled [11-^{2}H$_2$]-MSG.[93] The lipid charge density at the bilayer surface modulating the effects of melittin on membranes was investigated by solid state ^{31}P and ^{2}H as a function of temperature and peptide concentration.[94] For the system at pH 4.2 and at a high temperature, a lipid-to-peptide molar ratio of 30 was sufficient to transform the whole system (with DMPA) into an isotropic phase, proposed to be an inverted micelle. When the system was cooled down towards the gel phase, an intermediate hexagonal phase was observed in a narrow range of temperature. Similar results[95] regarding structural phases at specific temperatures and concentrations of magnetically alignable lipid mixtures were found using small-angle neutron scattering (SANS). The results were compared to NMR results using variously DMPC, DHPC (dihexanoylphosphatidylcholine) and DMPG. ^{1}H NMR was used to quantify dolichols cholesterols, choline-containing phospholipids and double bonds in unsaturated acyl chains in lipid extracts of four types of thyroid tissue and changes in cancer shown.[96] Characterisation of sterically stabilised cisplatin liposomes was carried out by NMR in studies of improving drug delivery of potent platinum anti-cancer drugs.[97]

9 Mammalian Glycoproteins and Carbohydrate–Protein Recognition Studies

9.1 Structural Studies. – O-linked oligosaccharides of rabbit brain glycoproteins having mannose as the linkage sugar were proposed based on detailed 1D and 2D ^{1}H and ^{13}C NMR of alditols released by alkaline borohydride degradation from non-dialysable brain glycopeptides.[98] GlcNAc(β1-2)Man

core with and without Gal(β1-4), Neu5Ac(α2-3)Gal(β1-4) and Le^x substitutions. Krishna *et al.*[99] have contributed to the *Advances in Carbohydrate Chem. Biochem.* series of excellent reviews in NMR characterisation over the years with an overview concerning the ubiquity and structural variability of carbohydrate–protein linkage regions for various kinds of proteoglycans. This is the latest in a series of papers on the characterisation of oligosacchride structure and function from the chondroitin sulfates.[100–109] A brief survey of NMR spectroscopic and molecular modelling approaches applicable to structural analysis of these complex carbohydrates is provided along with a compilation of ^{1}H NMR chemical shifts for comparative structural studies.

9.2 Conformational Studies. – The recent appreciation of the enormous coding capacity of oligosaccharide chains of natural glycoconjugates *via* the glycosyltransferases as direct gene products and their specific recognition as information molecules has been explored *via* NMR data, together with X-ray crystallography, molecular modeling and thermodynamic analysis of engineered ligands and receptors.[110] Meanwhile the data from conformational studies of the Le related antigens and their interactions with carbohydrate binding protein continues. Bekiroglu *et al.*[111] have looked at the hydroxy protons in a Le^b tetrasaccharide derivative in aqueous solution by NMR spectroscopy. Having taken the precaution to remove all traces of ionic impurities that can catalyse the exchange of the hydroxy protons with water and adjusted the pH to around neutral values (in order to keep the exchange rate low), nine cross peaks of the hydroxy protons could be observed in the DQF-COSY spectra. Additional data were found from the NOESY spectra. The data did not show any evidence for persistent hydrogen bonds participating in the structure. On the other hand for glycopeptides more extensive conformational data were obtained. A series of NMR experiments have been carried out on representative glycopeptides of the membrane-bound mucin leukosialin or CD43, a glycoprotein involved in cell adhesion and associated with acute myelogenous leukemia.[112] The experiments provided a large number of NOE interaction and coupling restraints which when used in molecular dynamics revealed a well defined conformation with extended conformation as found previously by others in mucin type glycopeptides (reviewed[1,2]). NMR solution studies[113] of hamster galectin-3 and EM visualisation of surface absorbed complexes showed oligomerisation of substratum absorbed galectin through N- and C-terminal domain interactions which could be relevent to the positive cooperativity observed in binding of lectin to immobilised multi-glycosylated proteins.

Other information on oligosaccharide–protein interaction is being obtained from non-mammalian systems. Large amounts of data have now accumulated on the carbohydrate binding modules of fungal and bacterial cellulases. The structural basis for the ligand specificty of family 2 CBMs has been explored recently using comprehensive NMR studies of the CBM–ligand interactions.[114] Analysis of oligosaccharide conformation by NMR spectroscopy utilising ^{1}H,^{1}H and ^{1}H, ^{13}C residual dipolar couplings in a dilute liquid crystalline

phase based on ^{1}H, ^{1}H COSY and a *J*-coupling procedure confirms that dipolar coupling data are essential for conformational inferences to be drawn from oligosaccharides. Understanding of the detailed mechanisms of gelling of glucomannan polysaccharides and their interactions with proteins was obtained by combining ^{1}H and ^{13}C NMR spectra of glucomannan gels in water.[115] NMR has been used to characterise three isomeric mono-2-, 3-, or 6-permethylated cyclodextrins[116] and the complexation of peptides by amino-cyclo dextrins.[117]

9.3 ***In vivo* studies.** – Many natural compounds and therapeutic drugs form glycosides during transport through the gastrointestinal tract. Mortenson *et al.*[118] have used directly coupled LC-^{1}H NMR to various acylated isomers of the glucuronide of S-naproxen in human urine samples. This technique has also been used to study the metabolic variation in rats to identify metabolic populations in urine.[119]

References

1 E. F. Hounsell, *RSC Specialist Periodical Reports in NMR*, 2000, **29**, 406–418.
2 E. F. Hounsell, *RSC Specialist Periodical Reports in NMR*, 2001, **30**, 360–376.
3 J. O. Duus, C. H. Gotfredson and K. Bock, *Chem. Rev.*, 2000, **100**, 4589–4614.
4 N. Paramonov, D. Bailey, M. Rangarajan, A. Hashim, G. Kelly, M. Curtis and E. F. Hounsell, *Eur. J. Biochem.*, 2001, **268**, 4698–4707.
5 N. Bergstrom, P.-E. Jansson, M. Kilian and U. B. S. Sorensen, *Eur. J. Biochem.*, 2000, **267**, 7147–7157.
6 E. Vinogradov, M. S. Pepplera and M. B. Perry, *Eur. J. Biochem.*, 2000, **267**, 7230–7236.
7 O. M. Hanniffy, A. S. Shashkov, A. P. Moran, S. N. Senchenkova and A. V. Savage, *Carbohydr. Res.*, 2000, **330**, 223–229.
8 S. Mehta and D. M. Whitfield, *Tetrahedron*, 2000, **56**, 6415–6425.
9 C. Schaffer, N. Muller, P. K. Mandel, R. Christian, S. Zayni and P. Messner, *Glycocon. J.*, 2000, **17**, 681–690.
10 A. V. Perepelov, S. N. Senchenkova, A. Torzewska, B. Bartodziejska, A. S. Shashkov, A. Rozalski and Y. A. Knirel, *Carbohydr. Res.*, 2000, **328**, 229–234.
11 H. Yildirim, A. Weintraub and G. Widmalm, *Carbohydr. Res.*, 2000, **333**, 179–183.
12 V. M. Marshall, H. Dunn, M. Elvin, N. McLay, Y. Gu and A. P. Laws, *Carbohydr. Res.*, 2000, **331**, 413–422.
13 G. Kogan and D. Uhrin, *New Adv. Anal. Chem.*, 2000, P1/73-P1/134.
14 M. Martin-Pastor and C. A. Bush, *J. Biomol. NMR*, 2001, **19**, 125–139.
15 M. M. Corsaro, A. Evidente, R. Lanzetta, P. Lavermicocca and A. Molinaro, *Carbohydr. Res.*, 2000, **330**, 271–277.
16 M. Young, M. J. Davies, D. Bailey, M. J. Gradwell, B. Smestad-Paulsen, J. K. Wold, R. M. R. Barnes and E. F. Hounsell, *Glycoconjug. J.*, 1998, **15**, 815–822.
17 P. R. Ashton, E. F. Hounsell, N. Jayaraman, T. M. Nilsen, N. Spencer, J. F. Stoddart and M. Young, *J. Org. Chem.*, 1998, **63**, 3429–3437.
18 A. Molinaro, A. Evidente, R. Lanzetta, M. Parrilli and A. Zoina, *Carbohydr. Res.*, 2000, **328**, 435–439.

19 A. M. Winn and S. G. Wilkinson, *Carbohydr. Res.*, 2000, **330**, 215–221.
20 A. M. Winn and S. G. Wilkinson, *Carbohydr. Res.*, 2000, **330**, 279–283.
21 D. J. Faulkner, *Nat. Prod. Rep.*, 2001, **18**, 1–49.
22 J. Muldoon, A. S. Shashkov, S. N. Senchenkova, S. V. Tomshich, N. A. Komandrova, L. A. Romanenko, Y. A. Knirel and A. V. Savage, *Carbohydr. Res.*, 2000, **330**, 231–239.
23 J. Muldoon, A. V. Perepelov, A. S. Shashkov, R. P. Gorshkova, E. L. Nazarenko, V. A. Zubkov, E. P. Ivanova, Y. A. Knirel and A. V. Savage, *Carbohydr. Res.*, 2000, **331**, 41–46.
24 Y.-T. Kim, E.-H. Kim, C. Cheong, D. L. Williams, C.-W. Kim and S.-T. Lim, *Carbohydr. Res.*, 2000, **328**, 331–341.
25 K. Glinel, J. Paul Sauvage, H. Oulyadi and J. Huguet, *Carbohydr. Res.*, 2000, **328**, 343–354.
26 M. R. Carvalho, L. C. d. A. Barbosa, J. H. de Queiroz and O. W. Howarth, *Tetrahedron Lett.*, 2001, **42(5)**, 809–811.
27 V. R. Hegde, J. Silver, M. Patel, V. P. Gullo, R. Yarborough, E. Huang, P. R. Das, M. S. Puar, B. J. Di Domenico, D. Loebenberg, *J. Antibiot.*, 2001, **54 (1)**, 74–83.
28 S. Omura, H. Tomada, N. Tobata, Y. Ohyama, T. Abe and M. Namikoshi, *J. Antibiot.*, 1999, **52**, 586.
29 H. Tomada, Y. Ohyama, T. Abe, N. Tobata, M. Namikoshi, Y. Yamaguchi, R. Masuma and S. Omura, *J. Antibiot.*, 1999, **52**, 689.
30 N. Tabata, Y. Ohyama, H. Tomoda, T. Abe, M. Namikoshi and S. Omura, *J. Antibiot.*, 1999, **52**, 815.
31 S. Baumgartner, T. G. Dax, W. Praznik and H. Falk, *Carbohydr. Res.*, 2000, **328**, 177–183.
32 A. Broberg, K. K. Thomsen and J. O. Duus, *Carbohydr. Res.*, 2000, **328**, 375–382.
33 E. Dinand and M. R. Vignon, *Carbohydr. Res.*, 2000, **330**, 285–288.
34 K. P. Latte and H. Kolodziej, *Phytochemistry*, 2000, **54**, 701–708.
35 K. S. Feldman and M. D. Lawlor, *J. Am. Chem. Soc.*, 2000, **122**, 7396–7397.
36 Kh. M. Ahmed, M. S. Marzouk, E. A. M. El-Khrisy, A. Abdel Wabab and S. S. El-Din, *Pharmazie*, 2000, **55**, 621–622.
37 K. H. Shaker, M. Bernhardt, M. H. A. Elgamal and K. Seifert, *Z. Naturforsch., Sect. C*, 2000, **55**, 520–523.
38 M. Chu, R. Mierzwa, Patel, J. Jenkins, P. Das, B. Pramanik and T.-M. Chan, *Tetrahedron Lett.*, 2000, **41**, 6689–6693.
39 K. C. Lewis, A. R. Maxwell, S. McLean, W. F. Renolds and R. G. Enriquez, *Magn. Reson. Chem.*, 2000, **38**, 771–774.
40 N. Vongvanich, P. Kittakoop, J. Kramyu, M. Tanticharoen and Y. Thebtaranonth, *J. Org. Chem.*, 2000, **65**, 5420–5423.
41 S. S. Kang, Y. S. Chang and J. S. Kim, *Chem. Pharm. Bull.*, 2000, **48**, 1242–1245.
42 W. Kobayashi, T. Miyase, S. Suzuki, H. Noguchi and X.-M. Chen, *J. Nat. Prod.*, 2000, **63**, 1066–1069, 1121–1126.
43 X. Sun, M. L. Zimmermann, J.-M. Campagne and A. T. Sneden, *J. Nat. Prod.*, 2000, **63**, 1094–1097.
44 M. Wang, H. Kikuzaki, Y. Jin, N. Nakatani, N. Zhu, K. Csiszar, C. Boyd, R. T. Rosen, G. Ghai and C.-T. Ho, *J. Nat. Prod.* 2000, **63**, 1182–1183.
45 A. Wirz, U. Simmen, J. Heilmann, I. Calis, B. Meier and O. Stitcher, *Phytochemistry*, 2000, **55**, 941–947.

46 D. Bisrat, E. Dagne, B.-E. van Wyk and A. Viljoen, *Phytochemistry*, 2000, **55**, 949–952.
47 A. S. Stolyarenko, V. I. Grishkovets, A. S. Shashkov and V. Y. Chirva, *Chem. Nat. Compd.*, 2000, **36**, 295–298.
48 I. Dini, O. Schettino, T. Simioli and A. Dini, *J. Agric. Food Chem.*, 2001, **49**, 741–746.
49 M. Haraguchi, Y. Mimaki, M. Motidome, H. Morita, K. Takeya, H. Itokawa, A. Yokosuka and Y. Sashida, *Phytochemistry*, 2000, **55**, 715–720.
50 A. B. Singab, T. I. Khalifa, T. Okuyama and S. Fushiya, *Al-Azhar J. Pharm. Sci.*, 1999, **24**, 1–9.
51 S. Marquina, N. Maldonado, M. Luisa Garduno-Ramirez, E. Aranda, M. Luisa Villarreal, V. Navarro, R. Bye, G. Delgado and L. Alvarez, *Phytochemistry*, 2001, **56**, 93–97.
52 A. Stochmal, S. Piacente, C. Pizza, F. De Riccardis, R. Leitz and W. Oleszek, *J. Agric. Food Chem.*, 2001, **49**, 753–758.
53 E. M. M. Gaspar, *Eur. J. Org. Chem.*, 2001, 369–373.
54 H. Takahashi, Y. Namikawa, M. Tanaka and Y. Fukuyama, *Chem. Pharm. Bull.*, 2001, **49**, 246–248.
55 J. Xiong, Q. D. Jin and Y. L. Xu, *Chin. Chem. Lett.*, 2001, **12**, 51–54 (Eng).
56 N. U. Sata, S. Matsunaga, N. Fusetani and R. W. M. van Soest, *J. Nat. Prod.*, 1999, **62**, 969.
57 N. U. Sata, S. Wada, S. Matsunaga, S. Watabe, R. W. M. van Soest and N. Fusetani, *J. Org. Chem.*, 1999, **64**, 2331.
58 D. Wolf, F. J. Schmitz, F. Qui and M. Kelly-Borge, *J. Nat. Prod.*, 1999, **62**, 170.
59 J. Kubanek, J. R. Pawlik, T. M. Eve and W. Fenical, *Mar. Ecol.: Prog. Ser.*, 2000, **207**, 69–77.
60 M. S. Zierer and P. A. S. Mourao, *Carbohydr. Res.*, 2000, **328**, 209–216.
61 N. V. Ivanchina, A. A. Kicha, A. I. Kalinovsky, P. S. Dmitrenok, V. A. Stonik, R. Riguera and C. Jimenez, *J. Nat. Prod.* 2000, **63**, 1178–1181.
62 S. Figueroa-Perez and R. R. Schmidt, *Carbohydr. Res.*, 2000, **328**, 95–102.
63 K. Lycknert, A. Maliniak and G. Widmalm, *J. Phys. Chem.*, 2001, **105**, 5119–5122
64 D. Acquotti and S. Sonnino, *Methods Enzymol.*, 2000, **312**, 247–272.
65 Y. Kushi, M. Shimizu, K. Watanabe, T. Kasama, S. Watarai, T. Ariga and S. Handa, *Biochim. Biophys. Acta*, 2001, **1525 (1–2)**, 58–69.
66 K. Kawahara, B. Lindner, Y. Isshiki, K. Jakob, Y. A. Knirel and U. Zahringer, *Carbohydr. Res.*, 2000, **331**, 87–93.
67 J. I. Jimenez and P. J. Scheuer, *J. Nat. Prod.*, 2001, **64**, 200–203.
68 H. Xie, J. M. Becker and F. Naider, *Pept, New Millenium, Proc. Am. Pept. Symp., 16th*, 1999 (pub. 2000), 330–331.
69 T. Rezanka and I. A. Guschina, *Phytochemistry*, 2001, **56**, 181–188.
70 S. Araki, S. Yamada, S. Abe, H. Waki, K. Kon, S. Itonori, M. Sugita and S. Ando, *J. Biochem.*, 2001, **129**, 93–100.
71 T. Ziegler, R. Dettmann and M. Duszenko, *Carbohydr. Res.*, 2000, **327**.
72 A. R. Todeschini, R. Adriane, E. X. Da Silveira, C. Jones, R. Wait, J. O. Previato and L. Mendoca-Previato, *Glycobiology*, 2001, **11**, 47–55.
73 C. Jones, J. O. Previato and L. Mendonca-Previato, *Carbohydr. Res.*, 2000, **328**, 321–330.
74 D. R. Brown, *Biochem. J.*, 2000, **352**, 511–518.
75 C. Guilbert *et al.*, *Biopolymers*, 2000, **54**, 406–415.

76 M. Horiuchi *et al.*, *Proc. Natl. Acad. Sci. USA*, 2000, **97**, 5836–5841.
77 M. Horiuchi *et al.*, *J. Biol. Chem.*, 2001, **276**, 15489–15497.
78 F. Lopez-Garcia *et al.*, *Proc. Natl. Acad. Sci. USA*, 2000, **97**, 8334–8339.
79 R. K. Meyer *et al.*, *J. Biol. Chem.*, 2000, **48**, 38081–38087.
80 O. G. Parchment and J. W. Essex, *Proteins: Struct., Function, Gen.*, 2000, **38**, 327–340.
81 S. A. Priola *et al.*, *J. Virol.*, 2001, **75**, 4673–4680.
82 W. Swietnicki *et al.*, *Biochemistry*, 2000, **39**, 424–431.
83 B. Vincent *et al.*, *J. Biol. Chem.*, 2000, **275**, 35612–35616.
84 J. Warwicker, *Biochem, Biophys. Res. Commun.*, 2000, **278**, 646–652.
85 R. Zahn *et al.*, *Proc. Natl. Acad. Sci. USA.*, 2000, **97**, 145–150.
86 N. K. C. Wong, D. V. Renouf, S. Lehmann and E. F. Hounsell, *J. Mol. Model. Graph.*, 2000, **18**, 126–134.
87 M. Venugopal, C. D. Reddy, M. F. S. Babu and C. S. Reddy, *Heterocycl. Commun.*, 2000, **6**, 533–538.
88 R. Brouquisse, A. Evrard, D. Rolin, P. Raymond and C. Roby, *Plant Physiol.*, 2001, **125**, 1485–1498.
89 T. Nakamura, S. Amikawa, T. Harada, T. Saito, I. Arai and T. Urashima, *Biochim. Biophys. Acta*, 2001, **1525**, 13–18.
90 E. Strandberg, T. Sparrman and C. Lindblom, *Adv. Colloid Interface Sci.*, 2001, **89–90**, 239–261.
91 Y. Hori, M. Demura, M. Iwadate, A. S. Ulrich, T. Niidome, H. Aoyagi and T. Asakura, *Eur. J. Biochem.*, 2001, **268(2)**, 302–309.
92 A. Engler, T. Stangler and D. Willbold, *Eur. J. Biochem.*, 2001, **268**, 389–395.
93 V. Chupin, J.-W. Boots, J. A. Killian, R. A. Demel and B. de Kruijff, *Chem. Phys. Lipids*, 2001, **109**, 15–28.
94 T. Pott, J.-C. Maillet, C. Abad, A. Campos, J. Dufourcq and E. J. Dufourcq, *Chem. Phys. Lipids*, 2001, **109(2)**, 209–223.
95 M.-P. Nieh, C. J. Glinka, S. Krueger, R. S. Prosser and J. Katsaras, *Langmuir*, 2001, **17(9)**, 2629–2638.
96 Y. Yoshioka, J. Sasaki, M. Yamamoto, K. Saitoh, S. Nakaya and M. Kubokawa, *NMR Biomed.*, 2000, **13**, 377–383.
97 T. Peleg-Shulman, D. Gibson, R. Cohen, R. Abra and Y. Barenholz, *Biochim. Biophys. Acta*, 2001, **1510**, 278–291.
98 H. Kogelberg, W. Chai, T. Feizi and A. M. Lawson, *Carbohydr. Res.*, 2000, **331**, 393–401.
99 N. R. Krishna and P. K. Agrawal, *Adv. Carbohydr. Chem. Biochem.*, 2001, **56**, 201–234.
100 T. N. Huckerby, R. M. Lauder, G. M. Brown, M. Gavin, I. A. Nieduszynski, K. Anderson, J. Boocock, P. L. Sandall and S. D. Weeks, *Eur. J. Biochem.*, 2001, **268**, 1181–1189.
101 A. Oohira, F. Matsui, Y. Tokita, S. Yamanuchi and S. Aono, *Arch. Biochem. Biophys.*, 2000, **374**, 24–34.
102 K. Sugahara and S. Yamada, *Trends Glycosci. Glycotechnol.*, 2000, **12**, 321–349.
103 C. Ucoka, N. Kaneda, I. Okazaki, S. Nadanaka, T. Muramatsu and K. Sugahara, *J. Biol. Chem.*, 2000, **275**, 37407–37413.
104 N. Maeda, K. Ichihara-Tanaka, T. Kimura, K. Kadomatsu, T. Muramatsu and M. Noda, *J. Biol. Chem.*, 1999, **274**, 12474–12479.
105 H. Kawashima, M. Hirose, J. Hirose, D. Nagakuba, A. H. Plaas and M. Miyasaka, *J. Biol. Chem.*, 2000, **275**, 35448–35456.

106 J. Hirose, H. Kawashima, O. Yoshie, K. Tashiro and M. Miyasaka, *J. Biol. Chem.*, 2001, **275**, 5228–5234.
107 K. Zou, H. Muramatsu, S. Ikematsu, S. Sakuma, R. H. Salama, T. Shinomura, K. Kimata and T. Muramatsu, *Eur. J. Biochem.*, 2000, **267**, 4046–4053.
108 K. Sugahara and H. Kitagawa, *Curr. Opin. Struct. Biol.*, 2000, **10**, 518–527.
109 O. Habuchi, *Biochim. Biophys. Acta*, 2000, **1474**, 115–127.
110 T. Kondo, D. Yamamoto, A. Yokota, A. Suzuki, H. Nagasawa and S. Sakuda, *Biosci. Biotechnol. Biochem.*, 2000, **64**, 2388–2394.
111 S. Bekiroglu, C. Sandstrom, T. Norberg and L. Kenne, *Carbohydr. Res.*, 2000, **328**, 409–418.
112 D. H. Live, R. A. Kumar, L. Williams and D. Sames, *Pept. New Millenium, Proc. Am. Pept. Symp., 16th*, 1999 (pub. 2000), 525–527.
113 B. Birdsall, J. Feeney, I. J. D. Burdett, S. Bawumia, E. A. M. Barboni and C. R. Hughes, *Biochemistry*, 2001, **40**, 4859–4866.
114 P. J. Simpson, H. Xie, D. N. Bolam, H. J. Gilbert and M. P. Williamson, *J. Biol. Chem.*, 2000, **275**, 41137–41142.
115 I. C. Baianu and E. Ozu, *Polym. Prepr. (Am. Chem. Soc. Div. Polym. Chem.)*, 2001, **42**, 65–66.
116 H. Cousin, P. Cardinael, H. Oulyadi, X. Pannecoucke and J. C. Combret, *Tetrahedron: Asymmetry*, 2001, **12 (1)**, 81–88.
117 F. Hacket, S. Simova and H.-J. Schneider, *J. Phys. Org. Chem.*, 2001, **14**, 159–170.
118 R. W. Mortensen, O. Corcoran, C. Cornett, U. G. Sidelmann, J. Troke, J. C. Lindon, J. K. Nicolson and S. H. Hansen, *J. Pharm. Biomed. Anal.*, 2001, **24**, 477–485.
119 C. L. Gavaghan, J. K. Nicholson, S. C. Connor, I. D. Wilson, B. Wright and E. Holmes, *Anal. Biochem.*, 2001, **291**, 245–252.

11
Synthetic Macromolecules

BY HIROMICHI KUROSU AND TAKESHI YAMANOBE

1 Introduction

For synthetic macromolecules, NMR has been the most powerful method to characterize and to investigate the relationship between the structure and the physical properties at the atomic level. In the field of synthetic macromolecules, NMR is used not only as the routine analytical method but also as the method that has infinite possibility. In this chapter, NMR applications are reviewed by categorizing primary structure, liquid crystal, characterization of the synthetic macromolecules, dynamics of the synthetic macromolecules, gels and crosslinking macromolecules and polymer blends and diffusion of the synthetic macromolecules.

Ando *et al.* have described the principles and applications of NMR to polymers.[1] They covered the wide range of NMR applications to polymers. They started from the basis of NMR including NMR parameters (chemical shift, spin–spin coupling and relaxation times) and structure relationship and basic NMR techniques (solution, solid state and imaging), followed by the application of NMR to polymers in solution (determination of tacticity, sequence distribution, end group, branch and so on), solid polymers (conformation, crystal structure), the dynamics of polymers, polymer gels and imaging methods. Other reviews have been published about NMR imaging,[2] stretching of polymers[3] and crystalline and liquid crystalline polymers.[4]

2 Primary Structure

The primary structure of polymers is the most basic information for estimating physical properties. Table 11.1 summarizes the lists of papers in which NMR is used to characterize the tacticity, regioregularity, end group, branch, degradation and so on.

3 Liquid Crystalline Polymers

A variable-director ^{13}C NMR method was used to investigate the order and dynamics of aromatic polyamides in lyotropic liquid crystalline phases.[311] In

Nuclear Magnetic Resonance, Volume 31
© The Royal Society of Chemistry, 2002

Table 11.1

Polymer	*Nucleus*	*Contents*	*Ref.*
poly(*N*-acylethyleneimine)	H	end group, molecular weight	5
(2-hydroxypropyl)cellulose	H	substitution	6
aliphatic polyacetylene		configuration	7
aliphatic polyether epoxy		branch	8
allylcellulose, crotylcellulose	H,C	branch, conformation	9
cellulose,ester,2,2-difluoroethoxy, 2,2,3,3,4,4,5,5-octafluoropentoxy substituents	H,F	substitution	10
cellulose-*graft*-poly(*N*-acetylethylenimine)	C	graft	11
copolyamide,4I-PIP(20), isophthaloyl chloride,4,4'-diaminodiphenyl sulfone, piperazine	H	sequence distribution	12
copolycarbonate,2,2-dibutyl-2-stanna-1,3-dioxepane,bisphenol-A bischloroformate	C	sequence distribution	13
copolyester, 1,1′-binaphthalene-2,2′-diyl	C	composition, sequence distribution	14
copolymethyl-epoxysilsesquioxane	H,Si	graft	15
cyano-substituted polycarbosilane	H,C,Si	substitution	16
cycloolefin copolymer, norbornene	C	conformation	17
dendrimer, polyamide,5-[3-(4-aminophenyl)propionylamino]isophthalic acid		end group, branch	18
ethylene-propylene-diene rubber, EPDM, polypropylene		crosslink	19
fluorinated terpolymer, XC2000S, vinylidene fluoride, tetrafluoroethylene, allyloxypropandiol	H,F	assignment	20
modified poly(hydroxy ether of bisphenol-A)	H,C	composition, sequence distribution	20
natural rubber	C	configuration	22
natural rubber	H,C	degradation	23
natural rubber, synthetic rubber	H,C	degradation	24
nitrile rubber	H	composition,graft	25
nylon6, nylon11, nylon12, nylon66, nylon69, nylon610, nylon612	C	end group, conformation	26
nylon6/12 copolyamide	C	sequence distribution	27
oligo(allyl methacrylate)	C	end group, tacticity	28
perfluorinated polyimide	H,N,F	end group	29
phenol–formaldehyde resin	C	cure mechanism	30
phenol–formaldehyde resin	C	cure mechanism	31
phenol–resorcinal–formaldehyde resin	H	composition,molecular weight	32
poly(1,1-dimethyl-2-phenylsilacyclobutane)	C,Si	regioregularity	33
poly(1,2-*O*-isopropylidene-D-xylofuranose-3, 5-cyclic carbonate-co-w-pentadecalactone)	H,C	sequence distribution	34
poly(1,3-butylene adipate)	H,C	end group, molecular weight	35
poly(1,4-benzophenone)	C	regioselectivity	36

poly(1-dimethylsiloxypentamethyltrisiloxane), poly(1-diphenylmethoxy dimethylsiloxy-pentamethyltrisiloxane),poly(1′-phenylethyl dimethylsiloxypentamethyltrisiloxane-*co*-2′-phenylethyldimethylsiloxypentamethyl trisiloxane)	H,C,Si	end group, molecular weight	38
poly(1-hexene)	H,C	tacticity	38
poly(1-octadecene), poly(ethylene-co-1-octadecene)	C	composition	39
poly(1-octadecene), poly(ethylene-co-1-octadecene)	C	composition	40
poly(1-pentene),poly(1-hexene),poly(1-octene), poly(1-decene)	H	tacticity	41
poly(2,3-bis(4-ethoxy-4-oxobutyl)-1,3-butadiene), poly(2,3-bis(4-ethoxy-4-oxobutyl)-1,3-butadiene-*co*-styrene)	H	configuration	42
poly(2-(1-naphthyl)-2-phenyl-5,5-dimethyl-1-oxa-2,5-disilacyclopentane)	C	stereoselectivity	43
poly(2-(2-methoxyethoxy)ethanol-*co*-diacetone D-glucofuranose)	H	composition	44
poly(2-(dimethylamino)ethyl methacrylate),	H	end group	45
poly(2-(dimethylamino)ethylmethacrylate), poly(2-(dimethylamino)-ethylmethacrylate-block-tert-butylaminoethyl methacrylate)	H	block, end group	46
poly(2-(*N*-phthalimido)-2-methylpropylacrylate*co*-acrylonitrile)	H	composition	47
poly(2-(trimethylsiloxy)ethyl methacrylate), poly[2-(hydroxyethyl) methacrylate], poly[2-[(3,5-dinitrobenzoyl)oxy]ethyl methacrylate]	H	composition	48
poly(2-butene-*co*-ethylene)	C	composition	49
poly(2-butyl malic acid ester), poly(3,3-dimethyl-2-butyl malic acid ester)	C	configuration	50
poly(2-cyanomethyl-1,3-butadiene-*co*-styrene), poly(2-cyanomethyl-1,3-butadiene-*co*-acrylonitrile)		sequence distribution	51
poly(2-hydroxyethyl methacrylate-*co*-t-butyl acrylate)	H	sequence distribution, stereoregularity	52
poly(2-isopropenyl-3-phenyloxirane-*co*-styrene)	H	composition	53
poly(2-N-phthalimido-ethyl methacrylate-*co*-methyl methacrylate)	H	composition	54
poly(3,5-diaminobenzoic acid)	H	branch	55
poly(3-(4-aminophenoxy)benzoic acid), poly(3,5-bis(4-aminophenoxy)benzoic acid)	H,C	branch,composition	56
Poly(3-alkylthienylenevinylenes)		regioregularity	57
poly(3-aminobenzenesulfonic acid-*co*-2-methoxyaniline)	H,C	block, sequence distribution	58
poly(3-hydroxyalkanoates), copolyester,3-hydroxy-7-oxooctanoate, 3-hydroxy-5-oxohexanoate, 8-acetoxy-3-hydroxyoctanoate, 6-acetoxy-3-hydroxyhexanoate, 4-acetoxy-3-hydroxybutyrate	H,C	composition	59
poly(4-(4′-chlorocinnamoyl)phenyl methacrylate-*co*-methyl methacrylate)	H,C	composition	60

Table 11.1 *contd.*

poly(4-(tert-butyldimethylsilyl)oxystyrene), poly(3-(tert-butyldimethylsilyl)oxystyrene), poly(4-(tert-butyldiphenylsilyl)oxystyrene)	C	tacitcity	61
poly(4-vinylphenylamine), poly(*N*-isopropyl-4-vinylbenzylamine)	H	graft	62
poly(5-(Me methacryloyl isocyanate) bicyclo[2.2.1]hept-2-ene), poly(methyl methacrylate)	H,C	configuration	63
poly(5-(*N*-carbazolyl methylene)-2-norbornene)		block	64
poly(5-benzoxymethyl-1,3-oxathiolane-2-thione)	H	molecular weight	65
poly(5-methyl-5-benzyloxycarbonyl-1,3-dioxan-2-one-*co*-trimethylene carbonate)	H,C	sequence distribution	66
poly(7-methylbicyclo[2.2.1]hepta-2,5-diene)	C	configuration	67
poly(acrylamide-*co*-acrylic acid-*co*-acrylonitrile)	C	branch	68
poly(alkyl acetylene)	H	stereoregularity	69
poly(alkyl α-chloroacetoxymethacrylate)	H	degree quaternization	70
poly(alkyl sorbate-*co*-oxygen)		sequence distribution	71
poly(alkylacrylamide-*co*-arylalkylacrylamide)		composition	72
poly(alkylated thiophene-*co*-2,2′-bipyridine)	H	sequence distribution, regioregularity	73
poly(α-alkyl-β,L-aspartate), poly(alpha-n-octadecyl-β,L-aspartate), poly(α-n-octadecyl-β,L-aspartate-*co*-α-n-benzyl β,L-aspartate)		composition, sequence distribution	74
poly(α-methylstyrene)	H,C	tacticity	75
poly(amic acid methyl ester), fluoro-containing copolymer	H	sequence distribution	76
poly(amide-enaminonitrile)	H	regioregularity	77
poly(amidoamine-organosilicon)		composition, end group, branch	78
poly(amine methacrylate), 2-(dimethylamino)ethyl methacrylate, 2-(diethylamino)ethyl methacrylate, 2-(*N*-morpholino)ethyl methacrylate, (tert-butylamino)ethyl methacrylate	H	end group,block	79
poly(amine thioether), 4-aminobenznethiol, 1,4-phenylene diacrylate	H,C	regioselectivity	80
poly(aniline-*co*-xylidine)	H	composition	81
poly(aryl ether oxazole)	H	branch	82
poly(benzaldehyde formaldehyde azine), poly(1-phenyl-2,3-diaza-1,3-butadiene)	H	configuration	83
poly(β-butyrolactone-*co*-ε-caprolactone), poly(β-butyrolactone-*co*-δ-valerolactone)	H,C	sequence distribution	84
poly(β-hydroxybutyrate)	C	stereosequence, tacticity	85
poly(β-malic acid)-*block*-poly(β-malic acid alkyl ester)	H	block	86
poly(bicyclic bis-γ-lactone-*co*-spiro orthocarbonate)	H	sequence distribution	87

poly(bisphenol-A carbonate), poly(ε-caprolactone)	H,C	transesterification	88
poly(butadiene-*co*-styrene)	H	configuration	89
poly(butylene terephthalate-*co*-*p*-oxybenzoate)	H	sequence distribution	90
poly(carbon monooxide-*co*-ethylene)	H,P	sequence distribution	91
poly(carbosilane),poly(carbosiloxane)	H,C,Si	end group, stereoregularity	92
poly(CO-*co*-styrene), poly(CO-*co*-dicyclopentadiene), poly(CO-*co*-methylcyclopentadiene), poly(1,4-ketone)	H,C	tacticity, sequence distribution	93
poly(cyanoquinodimethane), poly(cyanobenzocyclobutene-*block*-styrene)	H,C	block end group	94
poly(cycloalkene oxide-*co*-CO_2)	C	tacticity	95
poly(cyclohexadiene)		tacticity, configuration	96
poly(cyclohexyl acrylate)	C	branch	97
poly(cyclopentene-*co*-norbornene)	C	sequence distribution, tacticity	98
poly(D,L-3-methylglycolide-*co*-glycolide)	H	composition	99
poly(dimethyl siloxane)	Si	chain scission	100
poly(dimethyl siloxane)	Si	composition	101
poly(ε-caprolactone)	H,C	end group	102
poly(ε-caprolactone), poly(ε-caprolactone-*block*-isobutylene-*block*-ε-caprolactone)	C	end group	103
poly(ε-caprolactone), poly(ω-pentadecalactone), poly(ε-caprolactone-*co*-ω-pentadecalactone)	C	tacticity, sequence distribution	104
poly(ε-caprolactone)-*block*-poly(tert-butyl acrylate), poly(ε-caprolactone)-*block*-poly(acrylic acid)	H	degradation	105
poly(ε-caprolactone-*co*-maleic acid)		composition	106
poly(ε-caprolactone-*co*-w-pentadecalactone)	C	sequence distribution	107
poly(εster-amide), dimethyladipate, 1,4-butanediol,dimethyl-7, 12-diaza-6, 13-dioxo-1, 18-octadecanedioate	H	block, sequence distribution	108
poly(ether ketone)	H,F	branch, end group	109
poly(ethyl 1-cyanocyclopropanecarboxylate)	H	tacticity	110
poly(ethyl methacrylate)	H	tacticity	111
poly(ethylene carbonate-*co*-ε-caprolactone), poly(ethylene-*co*-δ-valerolactone)	H	sequence distribution	112
poly(ethylene glycol), polyisobutylene, poly(ehtylene glycol-*co*-isobutylene)	H,C	block	113
poly(ethylene oxide)	C	conformation	114
poly(ethylene terephthalate), copolyester	H	end group, composition	115
poly(ethylene terephthalate), poly(ε-caprolactone)	H	transesterification	116
poly(ethylene terephthalate), poly(ethylene naphthalene-2,6-dicarboxylate)	H	end group, transesterification	117
poly(ethylene terephthalate), poly(succinic anhydride-*co*-ethylene oxide)	H	sequence distribution	118
poly(ethylene terephthalate-*co*-isophthalate)	H	sequence distribution	119
poly(ethylene terephthalate-*co*-isophthalate)	C	sequence distribution	120
poly(ethylene terephthalate-*co*-nitroisophthalate)		sequence distribution	121

Table 11.1 *contd.*

poly(ethylene-*alt*-1,9-decadiene)	C	sequence distribution	122
poly(ethylene-*alt*-chlorotrifluoroethylene)	C	dehydrohalogenation	123
poly(ethylene-*co*-1-hexene)	C	sequence distribution	124
poly(ethylene-*co*-1-hexene)	C	composition, branch	125
poly(ethylene-*co*-1-hexene)	C	sequence distribution	126
poly(ethylene-*co*-10-undecen-1-ol), poly(ethylene-*co*-10-undecenyl Me ether), poly(ethylene-*co*-10-undecenyl trimethylsilyl ether), poly(ethylene-*co*-1-undecene)		composition	127
poly(ethylene-*co*-4-methyl-1-pentene), poly(ethylene-*co*-1-hexene), poly(ethylene-*co*-1-decene), poly(ethylene-*co*-1-hexadecene)	C	sequence distribution	128
poly(ethylene-*co*-5-norbornene-2-methanol-*co*-5-norbornene-2-carboxlic acid)	C	composition	129
poly(ethylene-*co*-HALS), poly(propylene-*co*-HALS); *HALS(Hindered amine light stabilizer)	C	branch, stereoregularity, sequence distribution	130
poly(ethylene-*co*-norbornene)	C	composition, sequence distribution	131
poly(ethylene-*co*-propylene)	C	sequence distribution	132
poly(ethylene-*co*-propylene), poly(ethylene-*co*-octene-1), poly(ethylene-*co*-propylene-*co*-octnene-1)	C	composition, sequence distribution	133
poly(ethylene-*co*-styrene)	C	sequence distribution	134
poly(ethylene-*co*-vinyl acetate)	H	graft	135
poly(ethylene-*co*-vinyl acetate-*co*-vinyl alcohol)	H	conposition	136
poly(ethylene-norbornene)	C	sdequence distribution	137
poly(glycidyl methacrylate)	H,C	tacticity	138
poly(hydrogenmethylsiloxane-*co*-dimethylsiloxane)	H,Si	stereosequence, sequence, distribution	139
poly(hydrogenmethylsiloxane-*co*-dimethylsiloxane)	Si	sequence distribution, block	140
poly(hydroxy ether of bisphenol-A)	H,C	sequence distribution	141
poly(hydroxyacetic acid), polyglycolide	C,Na	polymerization mechanism	142
poly(vinyl acetate-*co*-ethylene)	H	composition	143
poly(iso-butyl vinyl ether-*co*-maleic anhydride)	C	sequence distribution, composition	144
poly(isobutylene), polystyrene	H	end group	145
poly(isobutylene-*co*-*p*-methylstyrene)	H	sequence distribution	146
poly(L-lactide)	H,C	polymerization mechanism	147
poly(L-lactide)-*block*-poly(ε-caprolactone)	H,C	degradation	148
poly(lactic acid)	H	tacticity, block, stereoblock	149
poly(lactic acid)	H	end group	150
poly(*m*-phenylenevinylene-*co*-*p*-henylenevinylene)	H	composition	151
poly(maleic anhydride)-*block*-polystyrene		sequence distribution, block	152

poly(Me methacrylate)	H	end group	153
poly(Me methacrylate-*co*-*N*-phenylmaleimide), poly(styrene-*co*-*N*-phenylmaleimide)	H,C	stereoregularity, sequence distribution	154
poly(methyl acrylate), poly(butyl acrylate)	H	end group	155
poly(methyl methacrylate)	H,C	tacticity	156
poly(methyl methacrylate)	H	end group	157
poly(methyl methacrylate)	C	end group	158
poly(methyl methacrylate)	H	tacticity	159
poly(methyl methacrylate)	H	end group	160
poly(methyl methacrylate), poly(*N*-(*p*-carboxy phenyl) methacrylamide-*co*-acrylamide)	H	composition	161
poly(methyl methacrylate), poly(methyl methacrylate-*co*-styrene)	H	end group	162
poly(methyl methacrylate), polystyrene, poly(dimethylaminoethyl methacrylate), poly(γ-butyrolactone)	H	end group	163
poly(methyl methacrylate), poly(methyl methacrylate) derivatives	H,C	composition	164
poly(methyl methacrylate)-*graft*-polystyrene	H	end group branch	165
poly(methyl methacrylate-*co*-butyl methacrylate)	C	sequence distribution, configurational sequence	166
poly(methyl methacrylate-*co*-dimethyl acrylamide)		composition	167
poly(methyl methacrylate-*co*-ethyl acrylate)	C	tacticity, composition, sequence distribution	168
poly(methyl methacrylate-*co*-ethyl acrylate)	C	composition, sequence distribution	169
poly(methyl methacrylate-*co*-ethyl methacrylate)	H	sequence distribution	170
poly(methyl methacrylate-*co*-n-hexyl methacrylate)	H	composition	171
poly(methyl methacrylate-*co*-styrene)		end group	172
poly(methylene terephthalate), poly(methylene terephthalate-*co*-ethylene terephthalate)	H	composition	173
poly(*N*,*N*-diallyl-*N*-methylamine-*co*-3-(*N*,*N*-diallyl-*N*-methylammonia)propanesulfonate)	C	conformation, sequence distribution	174
poly(*N*,*N*-dimethylacrylamide), poly(ethylene oxide)	F	end group	175
poly(*N*-[3,5-di(tert-butyldimethylsilyloxy) phenyl]-4-fluorophthalimide), poly(ether imide)		branch	176
poly(*N*-vinylcarbazole)	H,C	assignment	177
poly(norbornene-2-carboxylic acid)	C	regioregularity	178
poly(oxy(1,3-diphenyl-1,3,5,5-tetramethyl-1,3,5-trisiloxane-1,5-diyl)), poly(oxy(1,3-dimethyl-1,3,5,5-tetraphenyl-1,3,5-trisiloxane-1,5-diyl))	H,C,Si	stereoregularity	179
poly(oxy-1-chloromethylethylene), poly(oxy-1-chloromethyl-ethylene-*co*-oxyethylene)	C	end group	180
poly(*p*-chloro-α-methylstyrene), poly(*p*-chloro-α-methylstyrene-co-isobutylene)	H	tacticity, sequence distribution	181
poly*p*-methylstyrene-*co*-styrene)-*block*-poly(ethylene-*co*-butene)-*block*-poly(*p*-methylstyrene-*co*-styrene)	H,C	halogenation, bromination	182

Table 11.1 *contd.*

poly(*p*-phenylene vinylene), poly(*p*-phenylene(1-butylsulfinyl)ethylene), poly(*p*-phenylene(1-butylsulfanyl)ethylene)	C	assignment	183
poly(*p*-phenylenebenzimidazole)	H	composition, end group	184
poly(*p*-toylsilane)	H,C,Si	tacticity	185
poly(*p*-phenylene vinylene), poly(*p*-xylylene α-tetrahydrothiophenium bromide)	C	sequence distribution	186
poly(phenacyl methacrylate-*co*-glycidyl methacrylate)	H,C	composition	187
poly(phenacyl methacrylate-*co*-*N*-vinyl-2-pyrrolidone)	H,C	composition, sequence distribution	188
poly(phenylenevinylene)	H	configuration	189
poly(phosphinoborane), poly(isobutylphosphinoborane)	H,B,C,P	branch, crosslink	190
poly(propylene *co*-1-octene)	C	sequence distribution	191
poly(propylene)	C	tacticity, end group	192
poly(propylene-*co*-styrene-ethylene)	C	configuration	193
poly(silyl ether), (1,2-bis(phenyldihydridosilyl)ethane, 1,4-bis(phenyldihydridosilyl)benzene, 1,4-bis(phenyldihydridosilyl)naphthalene)	H,C	stereoregularity	194
poly(silylenevinylene)		branch	195
poly(sodium styrenesulfonate-*block*-vinylnaphthalene)	H	composition	196
poly(styrene-*block*-butadiene)	C	block	197
poly(styrene-*co*-acrylonitrile)	C	sequence distribution	198
poly(styrene-*co*-acrylonitrile)	H	composition	199
poly(styrene-*co*-Bu methacrylate), poly(styrene-*co*-Et methacrylate), poly(styrene-*co*-Me methacrylate), poly(styrene-*co*-octyl methacrylate), poly(styrene-*co*-vinyl acetate), poly(styrene-*co*-*N*,*N*-dimethylacrylamide), poly(styrene-*co*-2-(dimethylamino)ethyl acrylate)	H	block	200
poly(styrene-*co*-C_{60}), poly(methyl methacrylate-*co*-C_{60})	C	composition, branch	201
poly(styrene-*co*-ethyl acrylate)	C	sequence distribution, composition	202
poly(styrene-*co*-ethylene glycol dimethacrylate)	H,C	composition	203
poly(styrene-*co*-ethylene)	H,C	sequence distribution, block, composition, tacticity	204
poly(styrene-*co*-methacrylate)	F	end group	205
poly(styrene-*co*-methacrylonitrile)	H	end group, composition	206
poly(styrene-*co*-methyl methacrylate), poly(tetrafluoroethylene-*co*-hexafluoropropylene)		end group	207
poly(styrene-*co*-n-butyl methacrylate)	H	composition	208
poly(styrene-*co*-vinylidene chloride)	H,C	tacticity	209
poly(styrene-co-vinylidene chloride)	H,C	tacticity	210
poly(succinic anhydride-*co*-ethylene oxide)-*block*-poly(L-lactide)	H,C	block	211

poly(sulfone-*co*-amine)	H	branch	212
poly(t-butyl acrylate), poly(t-butyl acrylate-*co*-ethyl methacrylate)	C	block	213
poly(tert-butyl acrylate), poly(tert-butyl acrylate)-*block*-polystyrene-*block*-poly(methyl acrylate)	H	block	214
poly(tert-butylacetylene)	H,C	polymerization mechanism	215
poly(tert-butylacrylate)	H	tacticity	216
poly(thiophene dimethyldihydropyrene)	H	configuration	217
poly(*trans*-4-acryloyloxyazobenzene-co-methyl methacrylate)		composition, assignment	218
poly(trifluoroethylene)	F	tacticity	219
poly(trifluoroethylene-*co*-vinylidene fluoride)		dehalogenation	220
poly(trimethylene carbonate)	H	end group	221
poly(trioxane-*co*-dioxolane)	H	sequence distribution	222
poly(trisubstituted ehtylene-*co*-styrene), Me 2-cyano-3-phenyl-2-propenoate	H,C	composition	223
poly(vinyl acetate)	C	tacticity	224
poly(vinyl acetate)-*block*-polystyrene	H	block	225
poly(vinyl acetate-*co*-n-butyl acrylate)	C	branch, sequence distribution	226
poly(vinyl alcohol)	H,C	tacticity	227
poly(vinyl alcohol), partially hydrolyzed PVA	H,C	sequence distribution	228
poly(vinyl chloride)	C	substitution, tacticity	229
poly(vinyl chloride)	H,C	degradation	230
poly(vinyl chloride)-*blend*-natural rubber, poly(vinyl chloride)-*blend*-Epoxyprene 50, poly(vinyl chloride)-*blend*-natural rubber-*blend*-Epoxyprene 50	C	degradation	231
poly(vinyl chloride)-*blend*-nitrile rubber, poly(vinyl chloride)-*blend*-Epoxyprene 50	C	degradation	232
poly(vinyl ether)	H,C	end group	233
poly(vinylacetate)	C	branch	234
poly[1,4-bis(4-alkyl-2-thienyl)-2,5-disubstituted phenylene]	H,C	regioregularity	235
poly[1-(trimethylgermyl)-1-propyne]	C	configuration	236
poly[6,8-dioxabicyclo[3.2.1]octane-*block*-(ethylene glycol)-*b*-6,8-dioxa bicyclo[3.2.1] octane]	H,C	block	237
poly[*N*-(2-hydroxyethyl)-ethyleneimine-*co*-3,4,5,6-tetrahydrophthalic anhydride]	H	composition	238
poly{1,4-bis[3-(4′-butylphenyl)thienyl]-2,5-di(2′-ethylhexyloxy)phenylene}	H,C	regioregularity	239
polyacrylamide, manganese peroxidase, basidiomycete *Bjerkandera adusta*	C	tacticity	240
polyacrylonitrile, poly[(acrylamide)-*co*-(sodium acrylate)]	C	composition	241
polyaniline	H,C	regioselectivity	242
polybutadiene	H,C,Sn	end group	243
polybutadiene	H,C,Sn	end group	244
polycaprolactone-*block*-poly(ethylene glycol)-*block*-polylactide	H	composition, block	245
polycarbonate, 5-methyl-5-benzyloxycarbonyl-1,3-dioxane-2-one, trimethylene carbonate	C	sequence distribution	246

Table 11.1 *contd.*

polycarbonate, bisphenol A, 2,2′-bis[(4-chloroformyl)oxyphenyl]propane	H,C	regioselectively	247
polydicyclopentadiene	C	configuration	248
polydimethylsiloxane-*block*-polystyrene-*block*-polydimethylsiloxane		end group, molecular weight	249
polyester urethane	H,C	end group	250
polyester, 2,2-dibutyl-2-stanna-1,3-dioxepane, bis(4-chlorothiophenyl)suberate	H	end group	251
polyethylene	C	branch	252
polyethylene	H,D,C	branch	253
polyethylene	C	branch	254
polyethylene	C	branch	255
polyethylene	C	branch	256
polyethylene	H,C	crosslink mechanism	257
polyethylene	C	branch	258
polyethylene	C	branch	259
polyethylene	C	branch	260
polyethylene	C	branch	261
polyethylene, poly(ethylene-*co*-1-hexene)	C	composition	262
polyethyloxazoline		end group	263
polyglycerol	C	branch	264
polyimide, 2,2-bis(3,4-dicarboxyphenyl) hexafluoropropane dianhydride), 3,3′,4,4′-diphenyl sulfonetetracarboxylic dianhydride	H	branch	265
polyimide, copolyimide, n-alkyl norbornene dicarboxyimide	H,C	composition, tacticity	266
polyimide,4,4′-(hexafluoro-isopropylindene) diphthalic anhydride and 3,3′-dihydroxy-4,4′-diaminobiphenyl	H	crosslink	267
polyisocyanate		conformation	268
polyisocyanurate,poly(propylene glycol), 4,4′-diisocyanatodiphenylenemethane	H,C	degradation	269
polyisoprene	C	crosslink	270
polyisoprene	H,C	configuration, regioregularity	271
polylactide	H,C	stereosequence	272
polymethacrylate, poly(imidazoylethyl methacrylate)	H	sequence distribution, block, composition	273
polymethacrylic acid-*graft*-ethylene glycol)	H	composition	274
polymethylsiloxane	H,C,Si	ladderlike polymer	275
polynorbornene	C	stereoregularity	276
polyphenylazomethine		conformation	277
polyphenylene		configuration, branch	278
polypropylene	C	tacticity	279
polypropylene	H	regioselectivity, end group	280
polypropylene	C	tacticity	281
polypropylene	C	graft	282
polypropylene	C	tacticity, end group	283
polypropylene, poly(ethylene-*co*-propylene)	C	tacticity, sequence distribution	284
polysiloxane, (*S*,*S*)-1,3-dimethyl-1,3-diphenyldisiloxanediol,	H,C	stereoregularity	285

bis(dimethylamino)dimethylsilane, bis(dimethylamino)diphenylsilane			
polysiloxane, polysiloxane-acrylic emulsion	H,C,Si	composition	286
polystyrene	H	end group	287
polystyrene	C	tacticity	288
polystyrene	C	tacticity, end group	289
polystyrene	H	end group	290
polystyrene	H	end group	291
polystyrene, monosaccharide	H,C	end group	292
polystyrene, poly(vinyl chloride), polyethylene		end group	293
polystyrene-*block*-poly(4-hydroxystyrene)-*block*-poly(methyl methacrylate), polystyrene-*block*-poly(4-urethano propyl triethoxysilylstyrene)-*block*-poly(methyl methacrylate)		block	294
polystyrene-*block*-poly(butyl acrylate), polystyrene-*block*-poly((butyl acrylate)-*co*-styrene))		block	295
polystyrene-*block*-poly(ethylene-*co*-1-butene)-*block*-polystyrene		block	296
polystyrene-*block*-poly(methyl methacrylate)	H	block	297
polystyrene-*block*-poly(styrene-*co*-acrylonitrile)	H	block	298
polystyrene-*graft*-poly(ethylene glycol)	H	graft	299
polystyrene-*graft*-poly(methyl methacrylate), polystyrene-*graft*-poly(methylacrylate)		end group, graft	300
polyurethane	H,C,P	degradation	301
polyurethane	H,C,P	degradation	302
polyurethane	H,C,P	degradation	303
polyurethane, [n]-polyurethane	H,C	composition	304
polyurethane, poly(tetramethylene oxide), 4,4-methylene diphenyl diisocyanate, 1,4-butanediol, polydimethylsiloxane		composition	305
polyurethane, *p*-isocyanatobenzyl isocyanate, ethylene glycol	C	regioregularity	306
polyurethane,poly(tetramethylene adipate), 4,4′-diphenylmethane diisocyanate, butanediol, poly(oxytetramethylene)	H,C	composition	307
saccharide polymer, poly(2,6-anhydro-3,4,5-tri-O-benzoyl-1-desoxy-β-*D*-arabino-hex-1-enopyranose), poly(2,6-anhydro-3,4,5-tri-*O*-acetyl-1-desoxy-β-D-arabino-hex-1-enopyranose)	H,C	composition	308
sexi(3-n-octylthiophene), star polymer	H,C	regioregularity	309
sodium polysialate	Si	composition	310

the magnetic field, polyamides in liquid crystalline phase align to the magnetic field macroscopically. Peak position of ^{13}C spectrum shift if the ordered fluid is rotated away from equilibrium. Based on an exchange model involving molecular reorientation of the polymer chains, the macromolecular order and dynamics of the liquid crystal were discussed.

The conformation of a spacer group in the liquid crystalline state of poly(ester imide)s was discussed.[312] In the liquid crystalline state of poly(ester

conformations in the smectic crystalline phase contain ordered *trans-trans*-conformations.

The interaction between polysaccharides and water was discussed.[313] From NMR results, it was shown that water in the liquid crystalline phase is in a state ranging from a non-rigid solid to viscous liquid and that the motion of counter-ions is profoundly influenced by the molecular motion of water.

The dynamic behavior of AB block copolymers in nematic solvents was investigated by ^{2}H NMR.[314] NMR studies were also carried out for poly(aroylbis(oxyarylates))[315] and starch[316] in the liquid crystalline phase.

4 Characterization of the Synthetic Macromolecules

The conformation of poly(ethylene oxide), PEO, in molecular complexes with resorcinol (RES) and *p*-nitrophenol (PNP) was investigated by solid-state NMR. The two-dimensional double-quantum NMR spectrum shows that all OC–CO bonds in the PEO/RES molecular complex are *gauche* with $\psi = 74 \pm 9°$ and a torsion angle distribution with a width $\sigma < 10°$. The spectra of the PEO/PNP complex, however, show that $33 \pm 8\%$ of the OC–CO bonds are *trans* with $\sigma < 7°$.[317] The solid-state ^{1}H MAS, ^{2}H static, ^{15}N CP/MAS and ^{15}N–H dipolar CSA NMR spectra of two different modifications of Cα-deuterated ^{15}N-polyglycine, namely PG I and PG II (-CO-CD$_2$-^{15}NH-)*n* have been measured. From these measurements, while in the PG II system the ^{15}N CSA tensor is collinear with the amide plane, in the PG I system the CSA tensor is tilted *ca.* 16° with respect to the (δ_{11} δ_{22}) CSA plane.[318] FT-IR, CD, DSC, 2D-NOESY, ^{1}H NMR and ^{23}Na NMR measurements were carried out on complexes of 80:20 ethylene oxide (EO)-propylene oxide (PO) block copolymers, 75:25 EO-PO random copolymers and helical sodium poly(α,L-glutamate).[319] The microstructure of the poly(vinylimidazole)-silica hybrids (PVI-SiO$_2$) containing various proportions of silica was examined by high-resolution solid-state ^{29}Si and ^{13}C NMR spectroscopy. The ^{29}Si–^{1}H CP process revealed that the Q3 and Q4 species had different CP efficiency. The spin–lattice relaxation time in rotating frame ($T_{1\rho}^{H}$) of hybrids suggested that the ^{1}H spin-diffusion between imidazole and siloxane units were on a nanometre scale estimated by spin-diffusion path length.[320] Samples of poly(Me acrylate) (PMA) and of poly(Me acrylate-*co*-sodium methacrylate) (PMA-Na) containing 6.9 mol% of ionic groups were prepared and studied by ^{13}C CP/MAS NMR as well as measurement of the ^{13}C spin-lattice relaxation time in a rotating frame as a function of temperature. The 1-Me carbon atoms of PMA-Na showed significantly slower motion than those in PMA.[321] Two poly(ethylene-*co*-1-octene) samples (4 and 40 mol% 1-octene content) were prepared and the acquisition of the 1D ^{13}C NMR, 2D HMQC and 2D HMBC NMR spectra was performed. Effects of variation of polymer concentration and temperature on spectrum properties were studied.[322] The structure of poly(dimethylsiloxane)-vanadate hybrid materials was fully investigated. In particular, the use and interpretation of thermogravimetric analysis, IR, Raman and multi-

nuclear NMR (^{1}H, ^{13}C, ^{17}O, ^{29}Si, ^{51}V) spectroscopies allowed an accurate description of their structure on the nanometric scale.[323] The structure of poly(chloromethyldisilane-*co*-styrene) obtained from polymerization of styrene and chloromethyldisilanes has been investigated by HR liquid and solid-state NMR techniques. ^{1}H–^{13}C DEPT and ^{1}H–^{29}Si HMBC investigations indicate that the system has to be considered as a polymer blend consisting of poly(chloromethylsilane) and polystyrene.[324] The existence and the average size of free volume in bisphenol-A polycarbonate (PC), low-density polyethylene (LDPE), poly(2,6-dimethyl-phenyleneoxide) (PPO) and polytetrafluoroethylene (PTFE) were studied by positron annihilation and ^{129}Xe NMR measurements. The ^{129}Xe NMR chemical shifts for xenon adsorbed in the polymers indicated that the average pore size of the free volume increased in the following order: PC, LDPE, PPO, and PTFE.[325] Both liquid- and solid-state ^{13}C-NMR spectroscopies were employed to investigate the cure-acceleration effects of three carbonates [polyene carbonate (PC), sodium carbonate (NC), and potassium carbonate (KC)] on liquid and cured phenol–formaldehyde (PF) resins. The liquid-phase ^{13}C NMR spectra showed that the cure-acceleration mechanism in the PC-added PF resin seemed to be involved in increasing reactivity of the phenol rings, while the addition of both NC and KC into PF resin apparently resulted in the presence of *ortho–ortho* methylene linkages.[326] ^{13}C CP/MAS NMR and ^{1}H $T_{1\rho}$ experiments of polyglycine (PG), poly(L-alanine) (PLA), and PG/PLA blends prepared from dichloroacetic acid solution have been carried out, in order to elucidate the confomational stability of these polypeptides in the solid state. From these experimental results, it was clarified that the conformations of PG and PLA in their blends are strongly influenced by intermolecular hydrogen-bonding interactions that cause their miscibility at the molecular level.[327] The changes in phase structure under uniaxial deformation of block copolymers of poly(butylenes terephthalate)(PBT) and poly(tetramethylene oxide) (PTMO) were investigated using ^{13}C solid state NMR spectroscopy and IR spectroscopy on *in situ* stretched samples. It became obvious that a minimum stress level in the material is necessary for the strain-induces PTMO crystals to form and to be stable at room temperature.[328] Analysis of β-CH_2 signals in the ^{13}C NMR spectra of the methyl methacrylate-ethyl acrylate copolymers has been performed. A simulation of the DEPT sub-spectrum shows that it is possible to determine the distribution of configurational-compositional tetrads providing a tool for microstructure analysis of acrylic copolymers.[329] Permeability and morphology of Nafion ionomers were studied by ^{19}F and ^{129}Xe NMR spectroscopy. Diffusion of ethanol in Nafion and the morphology of Nafion in the presence of ethanol were determined.[330] Solid-state NMR techniques were used to evaluate the size of the dispersed domains and the interface between the minor and the major phase in hetero-ordering for styrene-isobutylene block copolymer.[331] $^{13}C(^{19}F)$ rotational-echo double-resonance (REDOR) NMR experiments were performed on fifth-generation poly(benzyl ether) dendrimers synthesized by convergent methods. The ^{19}F label was incorporated in the first generation by coupling of two dendritic benzyl ethers containing a benzylic

bromide focal-point functionality to the two phenolic sites of 1-fluoro-3,5-dihydroxybenzene. These experiments show that a first-generation ^{19}F label of one dendrimer molecule is about equally distant to either the third- or fifth-generation ^{13}C labels of its neighbors.[332] ^{13}C CP/MAS and PST/MAS spectra of 10% ^{13}C-labeled n-tetracosane adsorbed on the surface of silica gel were measured by means of high resolution solid-state ^{13}C NMR. From these experimental results, it is found that adsorbed n-tetracosane is in three regions with different molecular motion. In the immobile region, n-tetracosane takes a layer structure with triclinic-like form. In the mobile region, n-tetracosane is undergoing a fast transition between *trans* and *gauche* conformations and fast rotation along the chain axis.[333] The utility of ^{1}H–^{19}F chemical shift correlation 2D NMR experiments for the characterization of fluorinated compounds was demonstrated.[334] The structure of ultrahigh molecular weight polyethylene fibers has been investigated by solid-state NMR. A structural model for ultradrawn PE fibers is proposed.[335] A detailed analysis of the temperature-dependent solid state ^{13}C spectrum of a low molecular weight polyethylene fraction, that was isothermally crystallized in extended chain forms is reported. It was concluded that conformational disordering of the chain-end sequence takes place at temperatures well below the fusion range.[336] The microstructure of a series of copolymers obtained from the chemical modification of poly(-hydroxy ether of bisphenol-A) with different degrees of modification has been investigated by ^{1}H and ^{13}C NMR spectroscopy.[337] The principal values of the ^{13}C chemical shift tensors and the ^{1}H–^{13}C separated-local-field patterns are reported for the all-*trans* structures with long and short T_1 as well as the more and less mobile amorphous segments in polyethylene.[338] Four propylene/ethylene, methallocene-catalyzed random copolymers, with ethylene mole fractions of 0.8% to 7.5% and melt crystallization histories of cooling at 1 °C/min, were studied by ^{13}C solid-state NMR techniques to determine the partitioning of ethylene defect residues within the semicrystalline morphology of isotactic poly(propylene/ethylene) copolymers.[339] ^{1}H, ^{13}C and ^{27}Si NMR spectroscopy was used to study the terminal structures, stereoregularity and optical activity of silicon-containing polymers.[340] Poly(ethylene oxide) (PEO) included in tris(*o*-phenylenedioxy)cyclotriphosphazine (TPP) and polyethylene included in the same matrix have been characterized by ^{13}C MAS NMR. TPP molecules provide a unique environment where the aromatic rings face the included polymer chains.[341] A method of incremental calculation of chemical shifts in the ^{13}C NMR spectra for different configurational compositional sequences, developed for copolymer of ethylene methacrylate and ethylene acrylate, PMMA/EA, has been applied to poly(Me methacrylate) samples of different tacticity.[342] NMR analysis of quadrupolar nuclei is shown to be a robust and powerful tool for studying glass transition of elastomeric nano-composites. In the case of polydimethylsiloxane-vanadate (PDMSV) materials, single pulses on ^{17}O and ^{61}V nuclei allow an observation of the effect on the quadrupolar splitting of motional changes above the calometric glass transition (177 ± 1 K).[343] Morphology effects on molecular mobility have been studied for solid state ultrahigh molecular weight polyethylenes crystallized

from the melt and from solution or during polymerization.[344] Solid-state proton NMR with fast MAS has been used to study the structure and dynamics of polymers and the water interface in porous glass composites. The composites were prepared by photopolymerizstion of poly(Et acrylate) and other acrylate formulations in a high surface area rigid glass matrix with 40 Å interconnected pores.[345] The complete ^{1}H, ^{13}C and ^{15}N NMR assignments of two closely related quinoacridinium salts, 8,13-diethyl-6-methyl-8*H*-quino[4,3,2-kl]acridinium iodide and 8,13-diethyl-3,6,11-trimethyl-8*H*-quino[4,3,2-kl]acridinium iodide, are described. The multinuclear NMR and 2D shift correlated NMR were applied, accompanied by *ab initio* GIAO CPHF calculations of shielding constants.[346] Solid-state ^{13}C and ^{1}H NMR were used to study the effects of melamine and fire retardant on the thermal degradation of a flexible polyether-polyurethane foam.[347] The structure of networks obtained by UV curing of triethylene-glycol divinyl ether (DVE3) and its mixtures with diethylene-glycol monovinyl ether (HDVE2) were investigated by high resolution ^{1}H and ^{13}C NMR spectroscopy. By working in swelled systems, signals with good resolution were obtained and were assigned to the different structures.[348] The γ-irradiated oxidation of pentacontane ($C_{50}H_{102}$) and the polymer polyisoprene was investigated as a function of oxidation level using ^{17}O NMR spectroscopy. It is demonstrated that by using ^{17}O labeled O_2 gas during the γ-irradiation process, details about the oxidative degradation mechanisms can be directly obtained from the analysis of the ^{17}O NMR spectra.[349] The crystallization process of syndiotactic polypropylene quenched from the melt or solutions has been investigated by high-resolution solid-state ^{13}C NMR spectroscopy in order to make clear the formation of the planar zigzag form at 0 °C.[350] ^{13}C NMR spectra of two poly(vinyl acetate)s with different tacticities (r-diad, 0.54 and 0.57) were measured, and their peak intensities were compared with the calculated ones. The methane carbon signals were assigned with pentads in the order of mmmm, mmmr+rmmr, rmrr+mmrr, rrrr, mmrm, rmrm, mrrr, mrrm from low field.[351] Solid-state ^{19}F NMR in combination with fast MAS at a speed of 35 kHz has been applied to examine the morphology of poly(vinylindene fluoride) samples by effectively suppressing dipolar interactions of the same order. A Lorentzian lineshape fitting analysis applied to the fast MAS was able to determine accurately the relative contents for the various domains: crystalline phase, 41%; amorphous regions, 54%; defect segments, 5%; with ± 3% error limits.[352] ^{27}Al MAS NMR spectroscopy has been used to study the surface aluminium compounds formed upon interaction of the supported $TiCl_4$/donor/$MgCl_2$ catalyst with $AlEt_3$ in the presence or absence of the external donor. It was found that there is no influence of internal and/or external donors on the state of aluminium in adsorbed $AlEt_2Cl$ in spite of a decrease of the aluminium content in the presence of external donor.[353] Solid state NMR results showed that nylon 6 in the presence of clay particles adopted both α and γ crystal phases in about equal amounts. Since only the α phase was observed in the nylon 6, the presence of the γ phase in the nanocomposite must result from interaction with clay.[354] The ^{13}C NMR spectra of model mono- to tetra-amides containing CO,

$(CH_2)_5$ and $(CH_2)_{11}$ groups in varied sequential arrangements have been used to reinterpret assignments previously proposed for signals in the spectra of nylon 6/12 random copolyamides.[355] The peak splitting effect due to different phase structures of some methane and methylene carbon peaks is observed in ^{13}C CP/MAS spectra of ethylene-vinyl alcohol copolymers at 353 K, which is 20–30 K higher than T_g of the samples.[356] ^{19}F NMR spectroscopy has been used to study imide materials in solution.[357] The stereochemical configuration of poly(glycidyl methacrylate) has been analyzed by ^1H and ^{13}C NMR spectroscopy.[358] Variable temperature solid-state ^{13}C CP/MAS NMR of poly(bis-n-propylurethane of 5,7-dodecadin-1,12-diol) was studied to probe the structure changes that are responsible for a thermochromic transition. The changes in the side chain conformation showed a significant influence on the backbone conformation of the conjugated unit.[359] The effect of weather and aging on the properties of polymer coatings was studied using solid state NMR spectroscopy.[360] The examination of an H_2O_2-initiated hydroxytelechelic polyisoprene by ^1H and ^{13}C NMR allowed the characterization of the microstructure.[361] Polyaniline doped with a single enantiomer of camphorsulfonic acid exhibits optical activity. NMR spectroscopy is used to determined the main-chain structure of these doped polymers in the solid state.[362] The poly(methyl acrylate) (PMA) and poly(methyl acrylate-*co*-sodium methacrylate) containing 6.9 mol% of ionic groups (PMANa-6.9) were studied by ^{13}C CP/MAS NMR. The ^{13}C spin–lattice relaxation times in a rotating frame, $T_{1\rho}$, have been measured as a function of temperature. The mobility, the correlation time for the PMA and activation energy for the PMANa-6.9 were discussed by using T_{1r} spin–lattice relaxation times.[363] A combination of solid state ^{13}C NMR and *in situ* ^1H NMR measurements have been used to elucidate the evolution of the condensed phase structure as PVC dehydrochlorination proceeds at 300 °C.[364] High-resolution solid-state ^{13}C NMR spectra were obtained for four polyethylene samples, at temperatures from 20 to 100 °C. The samples varied in crystallinity, lamellar thickness, and molecular weight. From the chemical shift of the peak corresponding to the amorphous phase, the fraction of *gauche* conformers was determined. By assuming a Boltzmann distribution of *trans* and gauche conformations, the energy difference between the *trans* and *gauche* states was 6.4 ± 0.5 kJ mol^{-1}. This is higher than values found previously for polyethylene and alkane chains in melt and solution states, and can be attributed to effects of the semi-crystalline morphology.[365] Both liquid- and solid-state ^{13}C NMR spectroscopies were used to investigate the cure acceleration effects of three carbonates (propylene carbonate, sodium carbonate, and potassium carbonate) on liquid and cured phenol–formaldehyde (PF) resins.[366] Solid state NMR was used to probe the inorganic phase structure and the effects of the temperature and composition on the dynamic behavior of the ionic species and the polymer chains of hybrid organic–inorganic conductors which were obtained by dissolution of $LiClO_4$ into silica/poly(-ethylene glycol) matrix.[367] A series of precursor polymers towards poly(*p*-phenylene vinylene) has been analyzed by different complementary NMR techniques. Resonance assignments were achieved by the use of one- and two-

dimensional NMR techniques, such as ^{1}H, ^{13}C, APT, 2D-HETCOR, FLOCK, COSY and INADEQUATE.[368] ^{13}C enriched polyethylene was subjected to γ-irradiation in the presence of air at 25 and 80 °C for total doses ranging from 71 to 355 kGy. Significant quantities of hydroperoxides were detected in the 25 °C irradiated sample by ^{13}C MAS NMR spectroscopy.[369] ^{1}H and ^{2}H NMR measurements of partially deuterated polybutadiene elastomers with systematically varied elastic properties are reported. A combined study of proton and deuteron NMR relaxation and the behavior under mechanical deformation was performed.[370] ^{2}H NMR measurements of partially deuterated polybutadiene elastomers with systematically varied elastic properties were performed. ^{2}H NMR spectroscopy has been applied to investigate the behavior under uniaxially mechanical deformation.[371] A study of drawn fibers prepared from an isotactic polypropylene modified by an ethylene-aminoalkyl acrylate copolymer has been done using the broad line of ^{1}H NMR. NMR spectra were measured on the set of fibers prepared with a draw ratio λ from *q* to 5.5 at two temperatures, one of them corresponding to the onset of segmental motion and the other one is the middle of the temperature interval as determined by decrease of the second moment M_2.[372] 2D time-domain ^{1}H NMR was used to investigate annealed isotactic polypropylene in the solid phase. The T_1 and $T_{1\rho}$ were correlated with the shape of the FID to identify and characterize relaxation components over the temperature range from −120 to 120 °C. Several phase transitions were observed, and three distinct solid phases, with identified as regions with different chain mobilities, were detected.[373] The cure reactions of phenylethylene end-capped polyimides were investigated using solid-state ^{13}C MAS NMR. A ^{13}C-labeled model compound, 13C-PEPA-3,4′-ODA, was studied.[374] The methyl-d_3 dynamics of two relatively similar polymers, poly(α-methylstyrene) and polymethylphenylsilane, were investigated *via* deuterium (^{2}H) NMR relaxation experiments.[375] The large strain uniaxial tensile deformation behaviour of nylon 6 plasticized by deuterium oxide is investigated by an *in situ* stretching device built in a ^{2}H NMR probe.[376] Structure, size and dynamics of domains of hybrid siloxane networks were studied by several techniques of solid-state ^{1}H and ^{29}Si NMR spectroscopy as well as by *ab initio* quantum chemical calculations.[377] High resolution solid-state ^{13}C NMR experiments were performed on the two series of aryl-aliphatic copolyamides. The local motions were studied by following the temperature dependence of ^{13}C chemical shift anisotropies and ^{13}C–^{1}H dipolar couplings.[378] The cohesive interaction among polymer chains in a polyacrylamide (PAAm)–D_2O solution has been studied by NMR relaxation. The NMR relaxation times of PAAm in the good solvent D_2O were measured at local viscosity an it was found that its relaxation characteristic is soft-solid-like.[379] Pulsed-gradient spin-echo NMR spectroscopy was use to study the molecular interaction between poly(vinyl alcohol) and the small diffusant ethylene glycol.[380] Structure of degraded microporous polyurethane elastomer was investigated by means of ^{1}H-, ^{13}C- and ^{31}P-NMR spectroscopy.[381] $^{1}H/^{13}C/^{119}Sn$ triple resonance 3D-NMR was used to obtain information about the tin-containing polybutadiene chain end structure. By combining data from

1D, 2D and 3D experiments, all ^{1}H, ^{13}C and ^{119}Sn chemical shifts for four postulated Sn species could be resolved unambiguously.[382,383] Variable temperature and variable stress NMR spectroscopic and imaging studies are reported for a sample of high impact polystyrene. NMR microscopy and solid state stray field imaging studies indicated that imposed stress affects the molecular chain dynamics only of the polybutadiene region and not of the polystyrene(PS) matrix.[384] The principal values of the ^{13}C chemical shift tensors and the ^{1}H–^{13}C separated-local field pattern are reported for the all-*trans* structures with long and short T_1 as well as the more and less mobile amorphous segments in polyethylene.[385] NMR and wide-angle X-ray scattering reveal the influence of residual groups of vinyl alcohol–ethylene copolymers on the structure of the polymer.[386] ^{2}H NMR lineshapes of carbon black (N 220) filled *cis*-1,4-polybutadiene networks have been examined. The effect of the susceptibility of the filler on the NMR lineshape has been considered.[387] Liquid chromatography at the critical adsorption point with online NMR detection (online LC CAP NMR) was utilized for analysis of tacticity distribution of stereoregular poly(ethylene methacrylate)s (PEMAs). The tacticity distribution in a particular PEMA sample with mm/mr/rr = 2/45/53 and narrow molar mass distribution of Mw/Mn = 1.05 has been revealed by the LC CAP NMR technique.[388]

5 Dynamics of the Synthetic Macromolecules

A specially designed solid-state ^{2}H NMR probe was used to examine the effect of uniaxial elongation on the chain mobility in the amorphous region of semicrystalline nylon 6. In measurements conducted near the glass transition temperature, there was measurable deformation-induced enhancement of the mobility of the amorphous chains up to the yield point.[389] High-resolution solid-state ^{13}C NMR spectra of (ethylene–vinyl alcohol)copolymers (EVOH) with various ethylene contents in the solid state and their ^{13}C T_1 were measured, in order to elucidate the structure and dynamics of the copolymers. From these experimental results, the structural change of thee EVOHs with changes of the ethylene content was successfully elucidated. Further, it is found that the ^{13}C T_1 for the CH carbon of the vinyl alcohol unit is mainly composed of two components. The fractions of short and long T_1 components increase and decrease with an increase in the ethylene fraction, respectively. From these experimental results, it can be said that changes of the ethylene content in the copolymers lead to large changes in their structure and dynamics.[390] The structure of silk fibroin fibers was determined by solid-state NMR spectroscopy. The dynamics of the fibroin samples were also determined by ^{2}H NMR spectroscopy.[391] The dynamics of water molecules and cations (lithium and sodium counter-ions) in cation-exchange resins were investigated by measuring relaxation time and self-diffusion coefficients of ^{1}H, ^{7}Li, and ^{23}Na NMR.[392] ^{2}H NMR spectroscopy was applied to a study of conformational dynamics of alkyl chains in the lamellar phase of a $C_{12}E_3$ (nonionic

surfactant)–water system.[393] ^{2}H NMR experiments were performed on a selectively deuterated aryl-aliphatic copolyamide in order to investigate the local dynamics of the phenyl rings as a function of temperature. The activation energy of the phenyl ring flip motion was determined by dielectronic relaxation for the β transition.[394] NMR lineshapes and ^{1}H T_1 and ^{2}H nuclei of poly[(*R*)-3-hydroxy-butyric acid] have been measured in the temperature range 100–413 K. The results provide information on the local dynamics of the polymer.[395] The use of NMR measurements for a series of nearly monodisperse polybutadiene and polyisoprene polymers covering a range of molecular weights and encompassing the dilute, semidilute and entangled regimes is described. Assuming chain dynamics are isotropic, the relaxation time associated with the transition from liquid-like to pesudo-solid-like behavior is linearly dependent on the polymer molecular weight.[396] NMR relaxation time measurements and molecular dynamics simulations were done for polyethylene and atactic polypropylene. The ability to accurately describe the segmental relaxation time distribution in homopolymers opens up many possibilities to characterize polymers.[397] The *trans/gauche* ratio of backbone bonds in atactic polyacrylonitrile (aPAN) was characterized by several 2D solid-state NMR experiments using 15% $^{13}CH_2$-carbon labeled aPAN. An estimation of the conformational ratio was obtained from double-quantum filtered NMR experiments. The orientation of the chemical shift tensor was determined in auxiliary experiments. The backbone conformation of two successive bonds was characterized by double-quantum NMR spectroscopy, which correlates the orientation-dependent ^{13}C chemical shifts of two adjacent $^{13}CH_2$ segments.[398] Selective 1D and 2D ^{13}C solid state NMR studies have been carried out to obtain detailed interpretation of the dynamics in form I, II, and II polymorphs of isotactic poly-1-butene.[399] Solid state ^{13}C NMR was used to measure the structure and dynamics of the polycaprolactone in the inclusion complex with α-cyclodextrin. The magnetization exchange did not occur. The inclusion complex showed incomplete spin diffusion between the polymer and the host matrix.[400] MAS $^{13}C\{^{1}H\}$- and $^{13}C\{^{19}F\}$-recoupling NMR experiments were performed on two polycarbonates with F substituents on every fourth ring in the main chain.[401] ^{13}C NMR T_1, NOE and $T_{1\rho}$ were measured for an atactic polypropylene (aPP) melt at 4, 25, 75 and 125 MHz ^{13}C Larmor frequencies from 43 °C to 260 °C. The data fit very well with a model for C–H vector reorientation composed of very fast librational relaxation, intermediate segmental relaxation, and a normal mode contribution described by Rouse dynamics modified for entanglement effects.[402] ^{13}C NMR T_1 and NOE measurements are reported for linear polyethylene, polyethylene with long branches and linear polyethylene with infrequent short branches at 75 MHz over the temperature range 400–535 K. A quantitative description of the segmental dynamics of the main chain methylene units and the branch points is obtained for linear polyethylene with ethylene branches.[403] MAS ^{13}C-$\{^{1}H\}$ recoupling NMR experiments have been performed on two series of poly(ester carbonate) block copolymers. These experiments show that all the bisphenol A blocks ring flip faster than 10 kHz at 300 K in the poly(ester carbonate)s, just as they do in PC itself, and

none of the tetramethylbisphenol A blocks (T) rings flip, either in tetramethyl PC homopolymer or in the T-based poly(ester carbonate)s.[404] Temperature dependent data of ^{13}C T_1 and NOE factors for methylene carbons at 50.3 MHz and 125.5 MHz have been used to probe the local chain dynamics of poly(butylenes terephthalate) (PBT) in solution phase.[405] High-resolution ^{1}H double quantum MAS NMR is used as a new technique that is capable of revealing complex motional processes in entangled polymer melts. The influence of rigid confinements represented by immobile moieties attached to one or both chain ends of the polybutadiene block on chain dynamics and ordering have been investigated.[406] The local dynamics of polypropylene in solution was studied by ^{13}C NMR relaxation and by molecular dynamics simulation *via* the orientational autocorrelation function of C–H bonds.[407] The ^{1}H NMR technique is used to study the motion of monomer units on the interface PEO chains grafted on silica.[408]

6 Gels and Crosslinking Macromolecules

^{1}H pulse NMR and solid-state ^{13}C NMR spectra of ethylene–vinyl alcohol copolymer (EVOH) gels were measured as a function of ethylene content, and furthermore, the ^{13}C T_1 and the ^{1}H T_2 have been measured, to elucidate the structure and dynamics of the mobile and immobile regions in the gels. From the ^{1}H pulse NMR experimental results, it is found that the ^{1}H T_2 signal is mainly composed of two or three kinds of components with different molecular motions. The long T_2 component is assigned to correspond to the mobile region, which comes from an un-crosslinked region, the short T_2 component corresponds to the immobile region, which comes from the crosslinked region, and the intermediate T_2 component corresponds to the intermediate region, which comes from the vicinity of the crosslinked region in the EVOH gel. From solid-state ^{13}C NMR results, it is found that the formation of hydrogen bonds between the hydroxyl groups in vinyl alcohol parts of EVOH copolymers with high vinyl alcohol fraction and the formation of hydrophobic interactions between the methylene groups in the ethylene parts of EVOH copolymers with high ethylene fraction contributes to its gel formation.[409] ^{17}O NMR spectra of PVA gel as prepared by repeating the freezing/thawing cycle were measured, in order to elucidate the structure and dynamics of water in PVA gel.[410] The network of dicumyl peroxide(DCP)/triallyl cyanurate (TAC) crosslinked *cis*-1,4-polyisoprene was studied by solid-state NMR techniques such as direct polarization (DP), CP and ^{1}H T_2 experiments. Line broadening and *cis/trans* isomerization of mobile carbons were observed in the DP experiments. Information on rigid carbons of network structures was observed with the CP technique. Motional heterogeneity was examined by ^{1}H T_2 relaxation experiments.[411] The crosslinking of PVA with glutaraldehyde at 80 °C was characterized by viscosity and pulse field gradient NMR techniques. NMR signified an initial dormant period of ~6 h, in which the self-diffusion coefficient of PVA was constant and independent of time. During the next 7 h,

this induction period was succeeded by a fast decay of the self-diffusion coefficient of rate $9.13 \pm 0.45 \times 10^{-5}$ sec^{-1} followed by a slower decay rate of $3.22 \pm 0.30 \times 10^{-5}$ sec.$^{-1}$ [412]

7 Polymer Blend and Diffusion of the Synthetic Macromolecules

The morphology of blends of PS microgels with linear PS were studied using NMR spectroscopy. Three techniques were employed to assess the intimacy of mixing: isothermal CP/MAS dipolar dephasing ^{13}C NMR, temperature-dependent ^{13}C CP/MAS NMR and one-pulse ^{1}H MAS NMR. The experimental data show that linear PS can penetrate the core of soft microgels, whose network strands are substantially larger than the linear chains. When the microgels highly crosslinked, however, such penetration is prevented.[413] The effect of addition of poly(propylene oxide) (PPO) and PS with low molecular weight (LPS) to PS was investigated by blending these polymers in a Haake internal mixer. The blends were analyzed by DSC and ^{13}C NMR in the solid state, using CP/MAS and ^{1}H $T_{1\rho}$.[414] Solid state 1D and 2D ^{13}C CP/MAS NMR and ^{1}H-CRAMPS and Raman spectroscopy, X-ray scattering and DSC were used to investigate the structure, morphology and dynamics behavior of blends of two semicrystalline polymers, PC and PEO.[415] The kinetics of the ester-amide exchange in solution blends of the random liquid-crystal polyester copoly(oxybenzonate- terephthalate) and polyamide 6 were studied with ^{13}C NMR spectroscopy.[416] ^{1}H $T_{1\rho}$ was measured to probe possible molecular scales of heterogeneity in the miscible poly(benzyl methacrylate) (PBzMA)/PEO blend over the whole composition range. According to the NMR results, only one phase was observed for the blends in which the PEO component is less than 16%. This miscible amorphous phase with PBzMA and PEO chains was mixed at the molecular level.[417] Various blends of atactic, low-MW (~4000), metal-sulfonated PS (MSOS) and a higher-MW (~25 000) poly(amide) were studied by a solid-state ^{13}C and ^{1}H NMR technique which includes multi-pulse irradiation, CP and MAS. This study is an investigation of the morphology of these MSPS(n)/PA blends (n = 100x mole fraction sulfonate = 2.3, 7.0 or 11.9) as functions of blend composition and sufonation level.[418] The miscibility and transesterification of poly(butylenes naphthalate) and novel P-containing copolyester blends were studied by ^{31}P and ^{1}H NMR, X-ray diffraction and DSC.[419] The formation of intermolecular hydrogen bonds in blends of novolac type phenolic and poly(hydroxyl ether) of bisphenol A was investigated by studying its T_g behaviour, excess volume and solid state ^{13}C NMR spectra. The T_g and parameters of solid state ^{13}C NMR, such as the T_{CH} and ^{1}H $T_{1\rho}$, indicate that London dispersion forces significantly affect the intermolecular hydrogen bonding of the blend.[420]

8 References

1 I. Ando, M. Kobayashi, M. Kanekiyo, S. Kuroki, S. Ando, S. Matsukawa, H. Kurosu, H. Yasunaga, S. Amiya, *Exp. Methods Polym. Sci.*, 2000, 261–493.
2 B. Blumich, D.E. Demco, S. Stapf, U. Goerke, C. Chwatinski, L. Gasper, R. Giesen, R. Haken, S. Han, *Polym. Mater. Sci. Eng.*, 2000, **82**, 148.
3 C. O'Driscoll, *Chem. Br.*, 2000, **36**, 20.
4 F. Horii, *Polym. Mater. Sci. Eng.*, 2000, **82**, 139.
5 R. Weberskirch, J. Preuschen, H.W. Spiess, O. Nuyken, *Macromol. Chem. Phys.*, 2000, **201**, 995–1007.
6 Y. Xiao, A.M. Ritcey, *Langmuir*, 2000, **16**, 4252–4258.
7 M. Mitsuyama, K. Kondo, *Macromol. Chem. Phys.*, 2000, **201**, 1613–1618.
8 T. Emrick, H.-T. Chang, J.M.J. Frechet, *J. Polym. Sci., Part A: Polym. Chem.*, 2000, **38**, 4850–4869.
9 N.D. Sachinvala, D.L. Winsor, O.A. Hamed, K. Maskos, P. Walter, G.J. Tregre, W. Glasser, N.R. Bertoniere, *J. Polym. Sci., Part A: Polym. Chem.*, 2000, **38**, 1889–1902.
10 W.G. Glasser, J.G. Todd, *Carbohydr. Polym.* , 2000, **42**, 393–400.
11 U. Mais, W.H. Binder, S. Knaus, H. Gruber, *Macromol. Chem. Phys.*, 2000, **201**, 2115–2122.
12 S. Konagaya, O. Watanabe, A. Kaji, *J. Appl. Polym. Sci.*, 2000, **76**, 921–928.
13 H.R. Kricheldorf, Z. Gomourashvili, D. Langanke, *J. Macromol. Sci., Pure Appl. Chem.*, 2000, **37**, 1531–1545.
14 C.-F. Chen, M. Ai, Z. Li, H.-W. Liu, A.-J. Gong, F. Xi, *Chin. J. Polym. Sci.*, 2000, **18**, 443–447.
15 M. Cao, Z. Li, Y. Zhang, P. Xie, D. Dai, R. Zhang, Y. Lin, N.T. Chung, *React. Funct. Polym.*, 2000, **45**, 119–130.
16 M. Lienhard, C. Wiegand, T. Apple, L.V. Interrante, *Polym. Prepr.*, 2000, **41**, 570–571.
17 W.-J. Huang, F.-C. Chang, P.P.-J. Chu, *J. Polym. Sci., Part B: Polym. Phys.*, 2000, **38**, 2554–2563.
18 T. Hayakawa, Y. Yamakawa, M. Nomura, M. Okazaki, K. Takeuchi, M. Asai, M. Ueda, *Polym. J.*, 2000, **32**, 784–788.
19 M. Van Duin, *Rubber Chem. Technol.*, 2000, **73**, 706–719.
20 J.-P. Macheteau, H. Oulyadi, B. van Hemelryck, M. Bourdonneau, D. Davoust, *J. Fluorine Chem.*, 2000, **104**, 149–154.
21 A.M. De Ilarduya, J.J. Iruin, M.J. Fernandez-Berridi, *Polym. Int.*, 2000, **49**, 801–805.
22 J.Y. Buzare, G. Silly, J. Emery, G. Boccaccio, E. Rouault, *Eur. Polym. J.*, 2000, **37**, 85–91.
23 A.E. Somers, T.J. Bastow, M.I. Burgar, M. Forsyth, A.J. Hill, *Polym. Degrad. Stab.*, 2000, **70**, 31–37.
24 A.E. Somers, T.J. Bastow, M. Forsyth, A.J. Hill, *AIP Conf. Proc.*, 1999, **497**, 235–241.
25 N. Papke, J. Karger-Kocsis, *Eur. Polym. J.*, 2001, **37**, 547–557.
26 R.D. Davis, W.L. Jarrett, L.J. Mathias, *Polymer*, 2000, **42**, 2621–2626.
27 I. Goodman, D.J. Maitland, A.H. Kehayoglou, *Eur. Polym. J.*, 2000, **36**, 1301–1311.
28 T. Hirano, T. Kitayama, J. Cao, K. Hatada, *Polym. J.*, 2000, **32**, 961–969.

29 S. Ando, T. Matsuura, S. Sasaki, *Fluoropolymers*, ed. G. Hougham, Kluwer Academic/Plenum Publishers, New York, 1999, **2**, 277–303.
30 B.-D. Park, B. Riedl, *J. Appl. Polym. Sci.*, 2000, **77**, 841–851.
31 B.-D. Park, B. Riedl, *J. Appl. Polym. Sci.*, 2000, **77**, 1284–1293.
32 S.K. Datta, M. Higuchi, M. Morita, *J. Wood Sci.*, 1999, **45**, 411–416.
33 K. Matsumoto, M. Shinohata, H. Yamaoka, *Polym. J.*, 2000, **32**, 354–360.
34 A. Mahapatro, A. Kumar, R.R. Gross, *Polym. Prepr.*, 2000, **41**, 1826–1827.
35 C. Oriol-Hemmerlin, Q.T. Pham, *Polymer*, 2000, **41**, 4401–4407.
36 R.P. Quirk, W. Yu, *Polym. Prep.*, 2000, **41**, 95–96.
37 G. P. Cai, W.P. Weber, *Macromolecules*, 2000, **33**, 8976–8982.
38 E.Y. Tshuva, I. Goldberg, M. Kol, *J. Am. Chem. Soc.*, 2000, **122**, 10706–10707.
39 Quijada, R. Rojas, J. Guevara, A. Narvez, D. Delfin, G.B. De Galand, *Polimery*, 2000, **45**, 339–343.
40 Quijada, J.L. Guevara, R. Rojas, F.M. Rabagliati, *Chin. J. Polym. Sci.*, 2000, **18**, 249–254.
41 I. Kim, J.-M. Zhou, H. Chung, *J. Polym. Sci., Part A:Polym. Chem.*, 2000, **38**, 1687–1697.
42 D. Beery, M.K. Rath, V.V. Sheares, *Macromolecules*, 2001, **34**, 2469–2475.
43 Li, Y. Kawakami, *Macromolecules*, 2000, **33**, 1560–1564.
44 F.F. Stewart, M.K. Harrup, R.P. Lash, M.N. Tsang, *Polym. Int.*, 2000, **49**, 57–62.
45 F. Zeng, Y. Shen, S. Zhu, R. Pelton, *Macromolecules*, 2000, **33**, 1628–1635.
46 M.V.P. Baoez, K.L. Robinson, S.P. Armes, *Polym. Prepr.*, 2000, **41**, 206–207.
47 R. Balaji, N. Sivakumar, S. Nanjundan, *J. Polym. Mater.*, 2000, **17**, 207–213.
48 M. Orphanou, M.R. Simmons, C.S. Patrickios, *J. Polym. Sci., Part A: Polym. Chem.*, 2000, **38**, 1457–1465.
49 C.-H. Ahn, M. Tahara, T. Uozumi, J. Jin, S. Tsubaki, T. Sano, K. Soga, *Macromol. Rapid Commun.*, 2000, **21**, 385–389.
50 M.-M. Bear, S. Randriamahefa, V. Langlois, Ph. Guerin, *Polymer*, 2000, **41**, 3705–3712.
51 Y. Jing, V.V. Sheares, *Polym. Prepr.*, 2000, **41**, 44–45.
52 G. Martinez, M. Sanchez-Chaves, E.L. Madruga, C. Fernandez-Monreal, *Polymer*, 2000, **41**, 6021–6026.
53 O. Moriya, T. Koizumi, T. Kodama, Y. Matsubara, S. Tsubaki, T. Endo, *J. Polym. Sci., Part A: Polym. Chem.*, 2000, **38**, 3729–3735.
54 R. Jayakumar, R. Balaji, S. Nanjundan, *Eur. Polym. J*, 2000, **36**, 1659–1655.
55 Y. Ishida, A.C.F. Sun, M. Jikei, M. Kakimoto, *Macromolecules*, 2000, **33**, 2832–2838.
56 M. Jikei, K. Fujii, G. Yang, M. Kakimoto, *Macromolecules*, 2000, **33**, 6228–6234.
57 R.S. Loewe, R.D. McCullough, *Chem. Mater.*, 2000, **12**, 3214–3221.
58 I. Mav, M. Zigon, *Polym. Bull. (Berlin)*, 2000, **45**, 61–68.
59 K. Jung, R. Hany, D. Rentsch, T. Storni, T. Egli, B. Witholt, *Macromolecules*, 2000, **33**, 8571–8575.
60 R. Balaji, K. Subramanian, S. Nanjundan, A.V.R. Reddy, *J. Appl. Polym. Sci.*, 2000, **78**, 1412–1418.
61 H. Ito, A. Knebelkamp, S.B. Lundmark, C.V. Nguyen, V. Cattien, W.D. Hinsberg, *J. Polym. Sci., Part A: Polym. Chem.*, 2000, **38**, 2415–2427.
62 K. Se, R. Ohtomo, *J. Appl. Polym. Sci.*, 2000, 77(7), 1558–1567.
63 D.-J. Liaw, J.-S. Tsai, P. Wu, *Macromolecules*, 2000, **33**, 6925–6929.

64 D.-J. Liaw, C.-H. Tsai, *Polymer*, 2000, **41**, 2773–2780.
65 T. Endo, F. Sanda, W. Choi, *Macromol. Symp.*, 2000, **157**, 21–28.
66 T.F. Al-Azemi, J.P. Harmon, K.S. Bisht, *Biomacromolecules*, 2000, **1**, 493–500.
67 K.J. Ivin, A.M. Kenwright, E. Khosravi, J.G. Hamilton, *J. Organomet. Chem.*, 2000, **606**, 37–48.
68 B.D. Iyer, I.A. Mathakiya, A.K. Shah, A.K. Rakshit, *Polym. Int.*, 2000, **49**, 685–690.
69 M. Mitsuyama, R. Ishii, K. Kondo, *J. Polym. Sci., Part A: Polym. Chem.*, 2000, **38**, 3419–3427.
70 D. Avci, *Polym. Bull. (Berlin)*, 2000, **44**, 469–475.
71 A. Matsumoto, H. Higashi, *Macromolecules*, 2000, **33**, 1651–1655.
72 M. Camail, A. Margaillan, I. Martin, A.L. Papailhou, J.L. Vernet, *Eur. Polym. J.*, 2000, **36**, 1853–1863.
73 L. Trouillet, A. De Nicola, S. Guillerez, *Chem. Mater.*, 2000, **12**, 1611–1621.
74 R. Ramirez, M. Morillo, M.L. Arnal, F. Lopez-Carrasquero, A. Martinez de Ilarduya, S. Munoz-Guerra, *Polymer*, 2000, **41**, 8475–8486, 2000.
75 M. Osa, M. Sumida, T. Yoshizaki, H. Yamakawa, K. Ute, T. Kitayama, K. Hatada, *Polym. J.* , 2000, **32**, 361–369.
76 S. K. Park, S. Y. Park, C. J. Lee, *Eur. Polym. J.*, 2000, **36**, 2621–2628.
77 J.A. Moore, S. Kaur, *Macromolecules*, 2000, **33**, 3585–3589.
78 P.R. Dvornic, A.M. De Leuze-Jallouli, M.J. Owen, S.V. Perz, *Macromolecules*, 2000, **33**, 5366–5378.
79 M.V. de Paz Banez, K.L. Robinson, V. Butun, S.P. Armes, *Polymer*, 2000, **42**, 29–37.
80 L. Li, T. Hayakawa, K. Yonetake, M. Ueda, *Macromol. Chem. Phys.*, 2000, **201**, 1667–1672.
81 X.-G. Li, M.-R. Huang, Y. Yang, *Polym. J.*, 2000, **32**, 348–353.
82 Z.-H. Gong, C.-M. Leu, F.-I. Wu, C.-F. Shu, *Macromolecules*, 2000, **33**, 8527–8533.
83 A. Hashidzume, A. Tsuchiya, Y. Morishima, M. Kamachi, *Macromolecules*, 2000, **33**, 2397–2402.
84 F. Schue, C. Jaimes, R. Dobreva-Schue, O. Giani-Beaune, W. Amass, A. Amass, *Polym. Int.*, 2000, **49**, 965–974.
85 M. Arcana, O. Giani-Beaune, F. Schue, W. Amass, A. Amass, *Polym. Int.*, 2000, **49**, 1348–1355.
86 S. Cammas-Marion, M.-M. Bear, A. Harada, P. Guerin, K. Kataoka, *Macromol. Chem. Phys.*, 2000, **201**, 355–364.
87 F. Sanda, K. Chung, T. Takata, T. Endo, *Nettowaku Porima*, 2000, **21**, 1–8.
88 Z. Zhang, X. Luo, X. Lu, D. Ma, *Eur. Polym. J.*, 2000, **37**, 99–104.
89 V.A.E. Barrios, R.H. Najera, A. Petit, F. Pla, *Eur. Polym. J.*, 2000, **36**, 1817–1834.
90 C.-F. Ou, *J. Appl. Polym. Sci.*, 2000, **77**, 949–954.
91 H.-K. Luo, Y. Kou, X.-W. Wang, D.-G. Li, *J. Mol. Catal. A: Chem.*, 2000, **151**, 91–113.
92 Y. Kawakami, I. Imae, *Int. J. Polym. Anal. Charact.*, 2000, **5**, 437–455.
93 J.C. Yuan, S.-J. Lu, *J. Polym. Sci., Part A: Polym. Chem.* 2000, **38**, 2919–2924.
94 K. Chino, T. Endo, *J. Polym. Sci., Part A: Polym. Chem.*, 2000, **38**, 3434–3439.
95 M. Cheng, N.A. Darling, *Chem. Commun. (Cambridge)*, 2000, 2007–2008.
96 M. Nakano, Q. Yao, A. Usuki, S. Tanimura, T. Matsuoka, *Chem. Commun. (Cambridge)*, 2000, 2207–2208.

97 B. Yamada, M. Azukizawa, H. Yamazoe, D.J.T. Hill, P.J. Pomery, *Polymer*, 2000, **41**, 5611–5618.
98 B. Al Samak, V. Amir-Ebrahimi, D. G. Corry, J. G. Hamilton, S. Rigby, J. Rooney, J. M. Thompson, *J. Mol. Catal. A: Chem.*, 2000, **160**, 13–21.
99 C.M. Dong, K.Y. Qiu, Z.W. Gu, X.D. Feng, *Chin. Chem. Lett.*, 2000, **11**, 815–818.
100 D.J.T. Hill, C.M.L. Preston, A.K. Whittaker, S.M. Hunt, *Macromol. Symp.*, 2000, **156** (IUPAC 8th International Symposium on Macromolecule-Metal Complexes (MMC-8 Tokyo), 1999), 95–102.
101 J. Uilk, S. Bullock, E. Johnston, S.A. Myers, L. Merwin, K.J. Wynne, *Macromolecules*, 2000, **33**, 8791–8801.
102 G.A. Abraham, A. Gallardo, A.E. Lonzano, J.S. Roman, *J. Polym. Sci., Part A: Polym. Chem.*, 2000, **38**, 1355–1365.
103 R.F. Storey, J.W. Sherman, L.B. Brister, *Polym. Prepr.*, 2000, **41**, 690–691.
104 A. Kumar, R.A. Gross, *J. Am. Chem. Soc.*, 2000, **122**, 11767–11770.
105. Q. Zhang, E.E. Remsen, K.L. Wooley, *J. Am. Chem. Soc.*, 2000, **122**, 3642–3651.
106 R. Mani, J. Currier, M. Bhattacharya, *J. Appl. Polym. Sci.*, 2000, **77**, 3189–3194.
107 A. Kumar, B. Kalra, A. Dekhterman, R.A. Gross, *Macromolecules*, 2000, **33**, 6303–6309.
108 P.J. Dijkstra, H.R. Stapert, J. Feijen, *Macromol. Symp.*, 2000, **152**, 127–137.
109 H.Y. Lee, S.-Y. Kwak, *Polymer*, 2000, **42**, 1375–1382.
110 L. Kagumba, J. Penelle, *Polym. Prepr.*, 2000, **41**, 1313–1314.
111 T. Kitayama, M. Janco, K. Ute, R. Niimi, K. Hatada, D. Berek, *Anal. Chem.*, 2000, **72**, 1518–1522.
112 H. Shirahama, A. Kanetani, H. Yasuda, *Polym. J. (Tokyo)*, 2000, **32**, 280–286.
113 P. Kurian, S. Zschoche, J.P. Kennedy, *J. Polym. Sci., Part A: Polym. Chem.*, 2000, **38**, 3200–3209.
114 D.J. Harris, T.J. Bonagamba, M. Hong, K. Schmidt-Rohr, *Macromolecules*, 2000, **33**, 3375–3381.
115 X.-G. Li, M.-R. Huang, *Polym. Test*, 2000, **19**, 373–383.
116 Z.-P. Zhang, X.-L. Luo, Y.-C. Lu, D.-Z. Ma, *Chin. J. Polym. Sci.*, 2000, **18**, 405–412.
117 S. Collins, A.M. Kenwright, C. Pawson, S.K. Peace, R.W. Richards, W.A. MacDonald, P. Mills, *Macromolecules*, 2000, **33**, 2974–2980.
118 Y. Maeda, T. Maeda, K. Yamaguchi, S. Kubota, A. Nakayama, N. Kawasaki, N. Yamamoto, S. Aiba, *J. Polym. Sci., Part A: Polym. Chem.*, 2000, **38**, 4478–4489.
119 Y. Zhang, L. Gu, *Eur. Polym. J.*, 2000, **36**, 759–765.
120 A. Martinez de Ilarduya,D.P.R. Kint, S. Munoz-Guerra, *Macromolecules*, 2000, **33**, 4596–4598.
121 D.P.R. Kint, M. De Ilarduya, S. Munoz-Guerra, *J. Polym. Sci., Part A:Polym. Chem.*, 2000, **38**, 1934–1942.
122 T. Uozumi, G. Tian, C.-H. Ahn, J. Jin, S. Tsubaki, T. Sano, K. Soga, *J. Polym. Sci., Part A: Polym. Chem.*, 2000, **38**, 1844–1847.
123 S.E. Evsyukov, B. Thomas, R.B. Heimann, *Mater. Chem. Phys.*, 2000, **66**, 34–40.
124 K. Czaja, M. Bialek, *Polimery*, 2000, **45**, 353–357.
125 K.-J. Chu, J.B.P. Soares, A. Penlidis, *Macromol. Chem. Phys.*, 2000, **201**, 340–348.
126 K. Nomura, K. Oya, T. Komatsu, Y. Imanishi, *Macromolecules*, 2000, **33**, 3187–3189.

127 K. Hakala, T. Helaja, B. Lofgren, *J. Polym. Sci., Part A: Polym. Chem.*, 2000, 38(11), 1966–1971.
128 T. Uozumi, G.-H. Ahn, M. Tomisaka, G. Tian, T. Sano, K. Soga, *Macromol. Chem. Phys.*, 2000, **201**, 1748–1752.
129 R.A. Wendt, G. Fink, *Macromol. Chem. Phys.*, 2000, **201**, 1365–1373.
130 C.-E. Wilen, M. Auer, J. Stranden, J.H. Naesman, B. Rotzinger, A. Steinmann, R.E. King III, H. Zweifel, R. Drewes, *Macromolecules*, 2000, **33**, 5011–5026.
131 I. Tritto, C. Marestin, L. Boggioni, L. Zetta, A. Provasoli, *Macromolecules*, 2000, **33**, 8931–8944.
132 K. Takawaki, T. Uozumi, C.-H. Ahn, T. Sano, K. Soga, *Macromol. Chem. Phys.*, 2000, **201**, 1279–1282.
133 S. Li, Z. Zhou, Y. Xiao, F. Jing, D. Pang, B. Huang, *Chem. Res. Chin. Univ.*, 2000, **16**, 236–245.
134 Y. Fang, F. Zhu, S. Lin, *Gaofenzi Xuebao*, 2000, (1), 74–78.
135 J.S. Parent, K. Geramita, S. Ranganathan, R.A. Whitney, *J. Appl. Polym. Sci.*, 2000, **76**, 1308–1314.
136 E. Perez, M. Lujan, J.M. De Salazar, *Macromol. Chem. Phys.*, 2000, **201**, 1323–1328.
137 W.-J. Huang, F.-C. Chang, P.P.-J. Chu, *J. Polym. Res.*, 2000, **7**, 51–56.
138 M.H. Espinosa, P.J.O. delToro, D.Z. Silva, *Polymer*, 2001, **42**, 3393–3397.
139 P. Cancouet, E. Daudet, G. Helary, M. Moreau, G. Saubet, *J. Polym. Sci., Part A: Polym. Chem.*, 2000, **38**, 826–836.
140 P. Cancouet, S. Pernin, G. Helary, M. Moreau, G. Saubet, *J. Polym. Sci., Part A: Polym. Chem.*, 2000, **38**, 837–845.
141 A.M. Dellarduya, J.J. Iruin, M.J. Fernandez-Berridi, *Polym. Int.*, 2000, **49**, 801–805.
142 A.E. Aliev, L. Elizabe, B.M. Kariuki, H. Kirschnick, J.M. Thomas, M. Epple, K.D.M. Kenneth, *Chem. -Eur. J.* 2000, **6**, 1120–1126.
143 N. Gupta, R.K. Srivastava, V. Choudhary, I.K. Varma, S. Patnaik, *J. Therm. Anal. Calorim.*,1999, **58**(3), 509–515.
144 X. Hao, K. Fujimori, D.J. Tucker, P.C. Henry, *Eur. Polym. J.*, 2000, **36**, 1145–1150.
145 R.F. Storey, C.L. Curry, T.L. Maggio, *NATO Sci. Ser., Ser. E*, 1999, **359**(Ionic Polymerizations and Related Processes), 161–175.
146 J.R. Ashbaugh, C.R. Ruff, T.D. Shaffer, *J. Polym. Sci., Part A: Polym. Chem.*, 2000, **38**(9), 1680–1686.
147 K. Stridsberg, M. Ryner, A.-C. Albertsson, *Macromolecules*, 2000, **33**, 2862–2869.
148 H. Quian, J. Bei, S. Wang, *Polym. Degrad. Stab.*, 2000, **68**, 423–429.
149 T.M. Ovitt, G.W. Coates, *J. Polym. Sci., Part A: Polym. Chem.*,2000, **38**(Suppl.), 4686–4692.
150 G. Coullerez, C. Lowe, P. Pechy, H.H. Kausch, J. Hilborn, *J. Mater. Sci.*, 2000, **11**, 505–510.
151 H. Schlick, F. Stelzer, S. Tasch, G. Leising, *J. Mol. Catal. A: Chem.*, 2000, **160**, 71–84.
152 D. Benoit, C.J. Hawker, E.E. Huang, Z. Lin, T.P. Russell, *Macromolecules*, 2000, **33**(5), 1505–1507.
153 X.-P. Chen, K.-Y. Qiu, *New J. Chem.*, 2000, **24**, 865–869.
154 G.-R. Shan, Z.-X. Weng, Z.-M. Huang, Z.-R. Pan, *J. Appl. Polym. Sci.*, 2000, **77**, 2581–2587.

155 H. Uegaki, Y. Kotani, M. Kamigaito, M. Sawamoto, *ACS Symp. Ser.*, 2000, **760**, 196–206.
156 T. Stuhldreier, H. Keul, H. Hocker, *Macromol. Rapid Commun.*, 2000, **21**, 1093–1098.
157 D.-Q. Qin, S.-H. Qin, X.P. Chen, K.-Y. Qiu, *Polymer*, 2000, **41**, 7347–7353.
158 D. Baskaran, A.H.E. Muller, *Macromol. Rapid Commun.*, 2000, **21**, 390–395.
159 P. Carriere, Y. Grohens, J. Spevacek, J. Schultz, *Langmuir*, 2000, **16**, 5051–5053.
160 J.E. Lockey, J.R. Ebdon, S. Rimmer, B.J. Tabner, *Macromol. Rapid Commun.*, 2000, **21**, 841–845.
161 A. Mishra, V. Choudhary, *J. Appl. Polym. Sci.*, 2000, **78**, 259–267.
162 D.-Q. Qin, S.-H. Qin, K.-Y. Qiu, *Macromolecules*, 2000, **33**, 6987–6992.
163 Y. Shen, S. Zhu, F. Zeng, R. Pelton, *Macromolecules*, 2000, **33**, 5399–5404.
164 M. Sivakumar, K.P. Rao, *React. Funct. Polym.*, 2000, **46**, 29–37.
165 S.-H. Qin, K.-Y. Qiu, *Chin. J. Polym. Sci.*, 2000, **18**, 515–520.
166 T. Nishiura, T. Kitayama, K. Hatada, *Int. J. Polym. Anal. Charact.*, 2000, **5**, 401–413.
167 L.M. Muratore, T.P. Davis, *J. Polym. Sci., Part A: Polym. Chem.*, 2000, **38**, 810–817.
168 G. Nguye, M. Matlengiewicz, D. Nicole, *Analusis*, 1999, **27**, 847–853.
169 M. Matlengiewicz, G. Nguyen, D. Nicole, N. Henzel, *J. Polym. Sci., Part A: Polym. Chem.*, 2000, **38**, 2147–2155.
170 M.R. Giles, J.N. Hay, S.M. Howdle, *Macromol. Rapid Commun.*, 2000, **21**, 1019–1023.
171 M. Patnaik, V. Choudhary, I.K. Varma, *Indian J. Chem. Technol.*, 2000, **7**, 254–258.
172 K. Tanaka, B. Yamada, *Macromol. Chem. Phys.*, 2000, **201**, 1565–1573.
173 A.G. Pinkus, R. Hariharan, L.P. Thrasher, A.P. Kesse, *J. Macromol. Sci., Pure Appl. Chem.*, 2000, **37**, 1037–1051.
174 R.S. Armentrout, C.L. McCormick, *Macromolecules*, 2000, **33**, 2944–2951.
175 T.E. Hogen-Esch, H. Zhang, D. Xie, *ACS Symp. Ser.*, 2000, **765**, 179–203.
176 D.S. Thompson, L.J. Markoski, J.S. Moore, I. Sendijarevic, A. Lee, A.J. McHugh, *Macromolecules*, 2000, **33**, 6412–6415.
177 A. Karali, G.E. Froudakis, P. Dais, F. Heatley, *Macromolecules*, 2000, **33**, 3180–3183.
178 V. Montembault, J. Desbrosses, I. Campistron, D. Reyx, *Macromol. Chem. Phys.*, 2000, **201**, 973–979.
179 M. Oishi, I. Imae, Y. Kawakami, *Polym. Prep.*, 2000, **41**, 606–607.
180 M. Perez, J.A. Reina, A. Serra, J.C. Ronda, *Polymer*, 2000, **41**, 7331–7337.
181 L. Sipos, X. Cao, R. Faust, *Macromolecules*, 2001, **34**, 456–459.
182 R.C.-C. Tsiang, C.-Y. Tsai, *Polym. Prepr.*, 2000, **41**, 1407–1408.
183 A.J.J.M. Van Breemen, M.M. DeKok, P.J. Adriaensens, D.J.M. Vanderzande, J.M.J.V. Gelan, *Macromol. Chem. Phys.*, 2001, **202**, 343–353.
184 I. Yamaguchi, K. Osakada, T. Yamamoto, *Macromolecules*, 2000, **33**, 2315–2319.
185 B.J. Grimmond, J.Y. Corey, *Organometallics*, 2000, **19**, 3776–3783.
186 J.A. Sanborn, P.M. Lahti, *Des. Monomer Polym.*, 2000, **3**, 351–361.
187 C. Soykan, M. Ahmedzade, M. Coskun, *Eur. Polym. J.*, 2000, **36**, 1667–1675.
188 C. Soykan, M. Coskun, M. Ahmedzade, E. Ozdemir, *J. Macromol. Sci., Pure Appl. Chem.*, 2000, **37**, 1089–1101.
189 A. Izumi, M. Teraguchi, R. Nomura, T. Masuda, *J. Polym. Sci., Part A: Polym. Chem.*, 2000, **38**, 1057–1063.

190 H. Dorn, R.A. Singh, J.A. Massey, J. M. Nelson, C.A. Jaska, A.J. Lough, I. Manners, *J. Am. Chem. Soc.*, 2000, **122**, 6669–6678.
191 Z.-Q. Fan, T. Yasin, L.-X. Feng, *J. Polym. Sci., Part A: Polym. Chem.*, 2000, **38**, 4299–4307.
192 W. Weng, E.J. Markel, A.H. Dekmezian, *Macromol. Rapid Commun.*, 2000, **21**, 1103–1107.
193 L. Caporaso, L. Izzo, S. Zappile, L. Oliva, *Macromolecules*, 2000, **33**, 7275–7282.
194 Y. Li, M. Seino, Y. Kawakami, *Macromolecules*, 2000, **33**, 5311–5314.
195 Y. Xiao, R.A. Wong, D.Y. Son, *Macromolecules*, 2000, **33**, 7232–7234.
196 M. Nowakowska, S. Zapotoczny, A. Karewicz, *Macromolecules*, 2000, **33**, 7345–7348.
197 M. Caprio, A. Grassi, A. Zambelli, *Polym. Prepr.* 2000, **41**, 1899–1900.
198 P.G. Sanghvi, A.C. Patel, K.S. Gopalkrishnan, S. Devi, *Eur. Polym. J.*, 2000, **36**, 2275–2283.
199 A. Kavousian, F. Ziaee, S.M.S. Mohaghegh, M.H. Nekoomanesh, K. Zare, *Iran. J. Polym. Sci. Technol. (Persian Ed.)*, 1999, **12**, 23–28.
200 Y. Zou, L. Jian, R. Zhuang, J. Ye, L. Dai, L. Zheng, *Macromolecules*, 2000, **33**, 4745–4749.
201 W.T. Ford, T. Nishioka, S.C. McCleskey, T.H. Mourey, P. Kahol, *Macromolecules*, 2000, **33**, 2413–2423.
202 C. Vu, *Macromol. Symp.*, 2000, **151**, 535–541.
203 E. Szuromi, M. Berka, J. Borbely, *Macromolecules*, 2000, **33**, 3993–3998.
204 A. Grassi, M. Caprio, A. Zambelli, D.E. Bowen, *Macromolecules*, 2000, **33**, 8130–8135.
205 J.C. Bevington, B. Guyot, T.N. Huckerby, B.J. Hunt, R. Jones, *Eur. Polym. J.*, 2000, **36**, 657–661.
206 W.K. Busfield, C.I. Zayas-Holdsworth, S.H. Thang, *Polymer*, 2000, **41**, 4409–4414.
207 A.E. Feiring, E.R. Wonchoba, F. Davidson, V. Percec, B. Barboiu, *J. Polym. Sci., Part A: Polym. Chem.*, 2000, **38**, 3313–3335.
208 G.V.R. Reddy, V.S. Joseph, K.C. Mani, *J. Appl. Polym. Sci.* , 2000, **77**, 398–408.
209 A.S. Brar, S.K. Hekmatyar, *J. Appl. Polym. Sci.*, 2000, **79**, 544–554.
210 A.S. Brar, S.K. Hekmatyar, *J. Appl. Polym. Sci.*, 2000, **79**, 544–554.
211 Y. Maeda, A. Nakayama, I. Arvanitoyannis, K. Hayashi, N. Yamamoto, S. Aiba, *Polym. J.*, 2000, **32**, 307–315.
212 C. Gao, D. Yan, *Macromolecules*, 2001, **34**, 156–161.
213 T. Kitayama, M. Tabuchi, K. Hatada, *Polym. J. (Tokyo)*, 2000, **32**, 796–802.
214 K.A. Davis, K. Matyjaszewski, *Macromolecules*, 2000, **33**, 4039–4047.
215 T. Szymanska-Buzar, I. Czelusniak, *J. Mol. Catal. A: Chem.*, 2000, **160**, 133–144.
216 W. Liu, T. Nakano, Y. Okamoto, *Polymer*, 2000, **41**, 4467–4472.
217 M.J. Marsella, Z.-Q. Wang, R.H. Mitchell, *Org. Lett.*, 2000, **2**, 2979–2982.
218 A.S. Brar, M. Thiyagarajan, *Indian J. Chem., Sect. A: Inorg., Bio-inorg., Phys., Theor. Anal. Chem.*, 2000, **39**, 625–630.
219 S.A. Reinsberg, S. Ando, R.K. Harris, *Polymer*, 2000, **41**, 3729–3736.
220 T. Ramotowski, K. Hamilton, G. Kavarnos, Q. Zhang, V. Bharti, *Mater. R. Soc. Symp. Proc.*, 2000, **600**, 77–82.
221 H.R. Kricheldorf, A. Stricker, *Macromol. Chem. Phys.*, 2000, **201**, 2557–2565.
222 P. Dunn, N.-L. Yang, J.A. Grates, *Polym. Prepr.*, 2000, **41**, 381–382.
223 K. Kim, D.A. Blaine, L.M. Brtek, R.M. Flood, C.G. Krubert, A.M.T. Rizzo,

E.A. Sterner, S. De Armas, G.B. Kharas, K. Watson, *J. Macromol. Sci., Pure Appl. Chem.*, 2000, **37**, 841–851.
224 K. Katsuraya, K. Hatanaka, K. Matsuzaki, K. Yamaura, *Macromol. Rapid Commun.* , 2000, **21**, 697–700.
225 M. Destarac, B. Pees, B. Boutevin, *Macromol. Chem. Phys.*, 2000, **201**, 1189–1199.
226 D. Britton, F. Heatley, P.A. Lovell, *Macromolecules*, 2001, **34**, 817–829.
227 R. Fukae, K. Nakata, M. Takeo, T. Yamamoto, O. Sangen, *Sen'i Gakkaishi*, 2000, **56**, 254–258.
228 B.M. Budhlall, K. Landfester, D. Nagy, E.D. Sudol, V.L. Dimonie, D. Sagl, A. Klein, M.S. El-Aasser, *Macromol. Symp.* 2000, **155**, 63–84.
229 G. Martinez, J. Millan, *Macromol. Chem. Phys.*, 2000, **201**, 1709–1717.
230 C.M. Dick, C.E. Snape, J.J. Liggat, *Polym. Mater. Sci. Eng.*, 2000, **82**, 185.
231 M.C.S. Perera, U.S. Ishiaku, Z.A.M. Ishak, *Polym. Degrad. Stab.*, 2000, **68**, 393–402.
232 M.C.S. Perera, U.S. Ishiaku, Z.A.M. Ishak, *Polym. Degrad. Stab.*, 2000, **68**, 393–402.
233 M. Sangermano, S. Spera, R. Bongiovanni, A. Priola, C. Busetto, *Macromol. Chem. Phys.*, 2000, **201**, 2441–2446.
234 D. Britton, F. Heatley, P.A. Lovell, *Macromolecules*, 2000, **33**, 5048–5052.
235 J. Pei, W.-L. Yu, W. Huang, A.J. Heeger, *Macromolecules*, 2000, **33**, 2462–2471.
236 G. Kwak, T. Masuda, *J. Polym. Sci., Part A: Polym. Chem.*, 2000, **38**, 2964–2969.
237 C. Troeltzsch, T.E. Patten, *J. Polym. Sci., Part A: Polym. Chem.*, 2000, **38**, 4081–4087.
238 S.A. Pooley, G.S. Canessa, B.L. Rivas, *Bol. Soc. Chil. Quim.*, 2000, **45**, 251–258.
239 A.-L. Ding, J. Pei, Z.-K. Chen, Y.-H. Lai, W. Huang, *Thin Solid Films*, 2000, **363**, 114–117.
240 K. Iwahara, M. Hirata, Y. Honda, T. Watanabe, M. Kuwahara, *Biotechnol. Lett.*, 2000, **22**, 1355–1361.
241 I.V. Ermakov, A.I. Rebrov, A.D. Litmanovich, N.A. Plate, *Macromol. Chem. Phys.*, 2000, **201**, 1415–1418.
242 A.L. Cholli, J. Kumar, S. Tripathy, L. Samuelson, *Polym. Mater. Sci. Eng.*, 2000, **82**, 189–190.
243 W. Liu, A. Halasa, J. Visintainer, R. Hirst, P.L. Rinaldi, *Polym. Prepr.*, 2000, **41**, 26–27.
244 W. Liu, T. Saito, L. Li, P.L. Rinaldi, R. Hirst, A.F. Halasa, J. Visintainer, *Macromolecules*, 2000, **33**, 2364–2369.
245 H. Chen, J. Bei, S. Wang, *Polym. Adv. Technol.* , 2000, **11**, 180–184.
246 K.S. Bisht, T.F. Al-Azemi, *Polym. Prepr.*, 2000, **41**, 1865–1866.
247 T. Yashiro, K. Matsushima, A. Kameyama, T. Nishikubo, *Macromolecules*, 2000, **33**, 7737–7742.
248 M.J. Abadie, M. Dimonie, C. Couve, V. Dragutan, *Eur. Polym. J.*, 2000, **36**, 1213–1219.
249 J.R. Sargent, W.P. Weber, *Polym. Prepr.*, 2000, **41**, 476–477.
250 D.M. Lemaster, G. Hernadez, *Macromolecules*, 2000, **33**, 3569–3576.
251 H.R. Kricheldorf, K. Hauser, R.-P. Kruger, G. Schultz, *J. Macromol. Sci., Pure Appl. Chem.*, 2000, **37**, 379–394.
252 Y. Yuan, L. Wang, L. Feng, *Polym. Int.*, 2000, **49**, 1289–1292.
253 R. Blom, I.M. Dahl, O. Swang, *J. Catal.*, 2000, **194**(2), 352–363.

254 P.M. Wood-Adams, J.M. Dealy, A.W. deGroot, O.D. Redwine, *Macromolecules*, 2000, **33**, 7489–7499.
255 A.M. Striegel, M.R. Krejsa, *J. Polym. Sci., Part B: Polym. Phys.*, 2000, **38**, 3120–3135.
256 W. Li, Y. Yuan, L. Feng, Y. Wang, J. Pan, C. Ge, B. Ji, *Eur. Polym. J.*, 2000, **36**, 851–855.
257 B. Qu, Y. Xu, L. Ding, B. Ranby, *J. Polym. Sci., Part A: Polym. Chem.*, 2000, **38**, 999–1005.
258 Y. Ma, M. Xu, *Chin. J. Polym. Sci.*, 2000, **18**, 557–564.
259 F. Zhu, Y. Fang, H. Chem, S. Lin, *Macromolecules*, 2000, **33**, 5006–5010.
260 T. Dodge, M.A. Curtis, J.M. Russell, M. Sabat, M.G. Finn, R.N. Grimes, *J. Am. Chem. Soc.*, 2000, **122**, 10573–10580.
261 F. Zhu, Y. Huang, Y. Yang, S. Lin, *J. Polym. Sci., Part A: Polym. Chem.*, 2000, **38**, 4258–4263.
262 K. Nomura, W. Sidokmai, Y. Imanishi, *Bull. Chem. Soc. Jpn.*, 2000, **73**, 599–605.
263 U.S. Schubert, O. Nuyken, G. Hochwimmer, *J. Macromol. Sci., Pure Appl. Chem.*, 2000, A37(6), 645–658.
264 A. Sunder, H. Frey, R. Mulhaupt, *Macromol. Symp.*, 2000, **153**, 187–196.
265 J. Fang, H. Kita, K. Okamoto, *Macromolecules*, 2000, **33**, 4639–4646.
266 E. Khosravi, W.J. Feast, A.A. Al-Hajaji, T. Leejarkpai, *J. Mol. Catl. A: Chem.*, 2000, **160**, 1–11.
267 J. He, K. Horie, R. Yokota, *Polymer*, 2000, **41**, 4793–4802.
268 C.G. Wada, D.J. O'Leary, J. Roth, K.B. Armstrong, J.D. Thoburn, D.C. Miller, A. Pomerantz, *Polym. Prepr.*, 2000, **41**, 892.
269 C. Dick, E. Dominguez-Rosado, B. Eling, J.J. Liggat, C.I. Lindsay, S.C. Martin, M.H. Mohammed, G. Seeley, C.E. Snape, *Polymer*, 2000, **42**, 913–923.
270 D.D. Parker, J.L. Koenig, *J. Adhes.*, 2000, **73**, 299–311.
271 F. Burel, H. Oulyadi, C. Bunel, *Int. J. Polym. Anal. Charact.*, 2000, **6**, 193–212.
272 E.E. Paske, G.L. Baker, *Polym. Prepr.*, 2000, **41**, 1378.
273 C.S. Patrickios, M.R. Simmons, *Colloids Surf., A*, 2000, **167**, 61–72.
274 B. Drescher, A.B. Scranton, J. Klier, *Polymer*, 2001, **42**, 49–58.
275 C. Liu, Z. Liu, Y. Liu, P. Xie, R. Zhang, *Polym. Int.*, 2000, **49**, 1658–1664.
276 Q. Wu, Y. Lu, Z. Lu, *ACS Symp. Ser.*, 2000, **760** (Transition Metal Catalysis in Macromolecular Design), 165–173.
277 M. Higuchi, S. Shiki, K. Yamamoto, *Org. Lett.*, 2000, **2**, 3079–3082.
278 Z.B. Shifrina, M.S. Averina, A.L. Rusanov, M. Wagner, K. Muellen, *Macromolecules*, 2000, **33**, 3525–3529.
279 P. Viville, D. Daoust, A.M. Jonas, B. Nysten, R. Legras, M. Dupire, J. Michel, G. Debras, *Polymer*, 2000, **42**, 1953–1967.
280 I. Camurati, A. Fait, F. Piemontesi, L. Resconi, S. Tartarini, *ACS Symp. Ser.* 2000, **760**, 174–193.
281 K. Takawaki, T. Uozumi, C.-H. Ahn, G. Tian, T. Sano, K. Soga, *Macromol. Chem. Phys.*, 2000, **201**, 1605–1609.
282 A.C. Patel, R.B. Brahmbhatt, P.V. C. Rao, K.V. Rao, S. Devi, *Eur. Polym. J.*, 2000, **36**, 2477–2484.
283 W. Weng, E.J. Markel, A.H. Dekmezian, *Polym. Prep.*, 2000, **41**, 498–499.
284 J.C. Randall, C.J. Ruff, M. Ohkura, *ACS Symp. Ser.*, 2000, **749** (Olefin Polymerization), 130–150.
285 M. Oishi, Y. Kawakami, *Macromolecules*, 2000, **33**, 1960–1963.

286 Y. Yang, D. Chen, J. Wang, J. Wang, C. Wang, *Bopuxue Zazhi*, 2000, **17**, 329–334.
287 B. Ivan, T. Fonagy, *ACS Symp. Ser.*, 2000, **768**, 372–383.
288 P. Ravi, K. Udayasankar, S. Divakar, *J. Inclusion Phenom., Macrocycl. Chem.* 2000, **38**, 99–112.
289 J. Xu, J. Ouyang, Z. Fan, D. Chen, L. Feng, *J. Polym. Sci., Part A: Polym. Chem.*, 2000, **38**, 127–135.
290 Y. Kotani, M. Kamigaito, M. Sawamoto, *ACS Symp. Ser.* 2000, **768**, 168–181.
291 X.-P. Chen, K.-Y. Qiu, *J. Appl. Polym. Sci.*, 2000, **77**, 1607–1613.
292 S. Loykulnant, M. Hayashi, A. Hirao, *Polym. Prepr.*, 2000, **41**, 239–240.
293 D. Price, J.V. Dawkins, *Int. J. Polym. Anal. Charact.*, 2000, **5**, 313–329.
294 J. Wang, S. Kara, T.E. Long, T.C. Ward, *J. Polym. Sci., Part A: Polym. Chem.*, 2000, **38**, 3742–3750.
295 C. Farcet, M. Lansalot, R. Pirri, J.P. Vairon, B. Charleux, *Macromol. Rapid Commun.*, 2000, **21**, 921–926.
296 E. Passaglia, S. Ghetti, F. Picchioni, G. Ruggeri, *Polymer*, 2000, **41**, 4389–4400.
297 F. Liu, B. Liu, N. Luo, S. Ying, Q. Liu, *Chem. Res. Chin. Univ.*, 2000, **16**, 72–77.
298 M. Baumann, A.-I. Roland, G. Schmidt-Naake, H. Fischer, *Macromol. Mater. Eng.*, 2000, **280/281**, 1–6.
299 J.S. Shay, R.J. English, R.J. Spontak, C.M. Balik, S.A. Khan, *Macromolecules*, 2000, **33**, 6664–6671.
300 S. Liu, A. Sen, *Macromolecules*, 2000, **33**, 5106–5110.
301 K. Troev, Vl. Atanassov, R. Tzevi, *J. Appl. Polym. Sci.*, 2000, **76**, 886–893.
302 K. Troev, G. Grancharov, R. Tsevi, A. Tsekova, *Polymer*, 2000, **41**, 7017–7022.
303 K. Troev, G. Grancharov, R. Tsevi, *Polym. Degrad. Stab.*, 2000, **70**, 43–48.
304 S. Neffgen, J. Kusan, T. Fey, H. Keul, H. Hocker, *Macromol. Chem. Phys.*, 2000, **201**, 2108–2114.
305 L.F. Wang, Q. Ji, T.E. Glass, T.C. Ward, J.E. McGrath, M. Muggli, G. Burns, U. Sorathia, *Polymer*, 2000, **41**, 5083–5093.
306 A. Nishio, A. Mochizuki, J. Sugiyama, K. Takeuchi, M. Asai, K. Yonetake, M. Ueda, *J. Polym. Sci., Part A: Polym. Chem.*, 2000, **38**, 2106–2114.
307 P.J. Yoon, C.D. Han, *Macromolecules*, 2000, **33**, 2171–2183.
308 A. Glumer, E.-J. Yaacoub, *Macromol. Chem. Phys.*, 2000, **201**, 1521–1531.
309 J. Bras, S. Guillerez, B. Pepin-Donat, *Chem. Mater.*, 2000, **12**, 2372–2384.
310 V.F.F. Barbosa, K.J.D. MacKenzie, C. Thaumaturgo, *Int. J. Inorg. Mater.*, 2000, **2**, 309–317.
311 J. Grinshtein, D. McElheny, V. Frydman, L. Frydman, *J. Chem. Phys.*, 2001, **114**, 5415–5424.
312 C. Wutz, *Polymer*, 2000, **41**, 4957–4964.
313 H. Hatakeyama, T. Hatakeyama, *Hydrocolloids*, 1998, **1**, 261–270.
314 A. Schneider, S. Muller, H. Finkelmann, *Macromol. Chem. Phys.*, 2000, **20**, 184–191.
315 A.Y. Billibin, J.V. Solovjeva, N.V. Girbasova, G. Schwartz, *Macromol. Chem. Phys.*, 2000, **201**, 1088–1100.
316 T.A. Waigh, M.J. Gidley, B.U. Komanshek, A.M. Donald, *Carbonydr. Res.*, 2000, **328**, 165–176.
317 D.J. Harris, T.J. Bonagamba, M. Hong, K. Schmidt-Rohr, *Macromolecules*, 2000, **33**, 3375–3381.
318 I. Sack, S. Macholl, F. Wehrmann, J. Albrecht, H.H. Limbach, F. Fillaux, M.H. Baron, G. Buntkowsky, *Appl. Magn. Reson.*, 1999, **17**, 413–431.

319 K.P. Pemawansa, I.M. Khan, *Polym. Prepr. (Am. Chem. Soc., Div. Polym. Chem.)*, 2000, **41**, 965–966.

320 T.C. Chang, Y.T. Wang, Y.S. Hong, H.B. Chen, J.C. Yang, *Phosphorus, Sulfur Silicon Relat. Elem.*, 2000, **160**, 29–41.

321 J-S. Kim, A.R. Lim, *Polym. Prepr. (Am. Chem. Soc., Div. Polym. Chem.)*, 2000, **41**, 1165–1166.

322 W. Liu, P.L. Rinaldi, L.H. McIntosh, R.P. Quirk, *Polym. Prepr. (Am. Chem. Soc., Div. Polym. Chem.)*, 2000, **41**, 30–31.

323 B. Alonso, C. Sanchez, *J. Mater. Chem.*, 2000, **10**, 377–386.

324 E. Brendler, C. Jaeger, D. Dcheller, G. Roewer, *Macromolecules*, 2000, **33**, 8371–8374.

325 B. Nagasaka, T. Eguchi, H. Nakayama, N. Nakamura, Y. Ito, *Radiat. Phys. Chem.*, 2000, **58**, 581–585.

326 B.-D. Park, B. Ruedl, *J. Appl. Polym. Sci.*, 2000, **77**, 841–851.

327 J. Nakano, S. Kuroki, I. Ando, T. Kameda, H. Kurosu, T. Ozaki, A. Shoji, *Biopolymers*, 2000, **54**, 81–88.

328 A. Schmidt, C. Alves, M. Soliman, W.S. Veeman, *Annu. Tech. Conf. -Soc. Plast. Eng.*, 2000, **58th** (Vol. 3), 3288–3291.

329 M. Matlengiewicz, G. Nguyen, D. Nicole, N. Henzel, *J. Polym. Sci., Part A: Polym. Chem.*, 2000, **38**, 2147–2155.

330 P.T. Inglefield, G. Meredsi, Y. Wang, A.A. Jones, W.-Y. Wen, *Polym. Mater. Sci. Eng.*, 2000, **82**, 172–172.

331 C. Neagu, J.E. Puskas, M.A. Singh, A. Natansohn, *Macromolecules*, 2000, **33**, 5976–5981.

332 H.-M. Kao, A.D. Stefanescu, K.L. Wooley, J. Schaefer, *Macromolecules*, 2000, **33**, 6214–6216.

333 H. Kurosu, K. Takahashi, D. Inoue, I. Ando, *J. Mol. Struct.*, 2000, **516**, 177–184.

334 J.-P. Macheteau, H. Oulyadi, B. van Hemelryck, M. Bourdonneau, D. Davoust, *J. Fluorine Chem.*, 2000, **104**, 149–154.

335 W.-G. Hu, K. Schmidt-Rohr, *Polymer*, 2000, **41**, 2979–2987.

336 T. Nakaoki, R. Kitamaru, R.G. Alamo, W.T. Huang, L. Mandelkern, *Polym. J. (Tokyo)*, 2000, **32**, 876–882.

337 A.M. De Ilarduya, M. Antxon, J.J. Iruin, M.J. Fernadez-Berridi, *Polym. Int.*, 2000, **49**, 801–805.

338 J.Z. Hu, W. Wang, S. Bai, R.J. Pugmire, C.M. Taylor, D.M. Grant, *Macromolecules*, 2000, **33**, 3359–3367.

339 R.G. Alamo, D.L. VanderHart, M.R. Nyden, K. Mandelkern, *Macromolecules*, 2000, **33**, 6094–6105.

340 Y. Kawakami, I. Imae, *Int. J. Polym. Anal. Charact.*, 2000, **5**, 437–455.

341 R. Simonutti, P. Sozzani, S. Bracco, A. Comotti, *Polym. Mater. Sci. Eng.*, 2000, **82**, 161–162.

342 G. Nguyen, M. Matlengiewicz, D. Nicolo, *Analusis*, 1999, **27**, 847–853.

343 B. Alonso, J. Maquet, C. Sanchez, *J. Non-Cryst. Solids*, 2000, **277**, 58–62.

344 H. Uehara, T. Yamanobe, T. Komoto, *Macromolecules*, 2000, **33**, 4861–4870.

345 P.A. Mirau, S.A. Heffner, M. Schilling, *Solid State Nucl. Magn. Reson.*, 2000, **16**, 47–53.

346 J. Jaroszewska-Manaj, D. Maciejewska, I. Wawer, *Magn. Reson. Chem.*, 2000, **38**, 482–485.

347 C.M. Dick, J.J. Liggat, C.E. Snape, S.C. Martin, C. Denecker, G. Seeley, B. Eling, C. Lindsay, P. Chaffanjon, *Polym. Mater. Sci. Eng.*, 2000, **83**, 44.

348 M. Sangermano, S. Spera, R. Bongiovanni, A. Priola, C. Busetto, *Macromol. Chem. Phys.*, 2000, **201**, 2441–2446.
349 T.M. Alam, M. Celina, R.A. Assink, R.L. Clough, K.T. Gillen, *Radiat. Phys. Chem.*, 2001, **60**, 121–127.
350 T. Nakaoki, Y. Ohira, F. Horii, *Polymer*, 2001, **42**, 4555–4561.
351 K. Katsuraya, K. Hatanaka, K. Matsuzaki, K. Yamaura, *Macromol. Rapid Commun.*, 2000, **21**, 698–700.
352 T.W. Su, D.L. Tzou, *Polymer*, 2000, **41**, 7289–7293.
353 A.G. Potapov, V.V. Terskikh, G.D. Bukatov, V.A. Zakharov, *J. Mol. Catal. A:Chem.*, 2000, **158**, 457–460.
354 R.D. Davis, W.L. Jarrett, L.J. Mathias, *Polym. Mater. Sci. Eng.*, 2000, **82**, 272–273.
355 Goodman, D.J. Maitland, A.H. Kehayoglou, *Eur. Polym. J.*, 2000, **36**, 1301–1311.
356 Q. Zhang, W. Lin, Q. Chen, G. Yang, *Macromolecules*, 2000, **33**, 8904–8906.
357 C.D. Smith, R. Mercier, H. Waton, B. Sillion, *Fluoropolymers*, 1999, **2**, 371–399.
358 M.H. Espinosa, P.J.O. del Toro, D.Z. Silva, *Polymer*, 2001, **42**, 3393–3397.
359 A.L. Cholli, D.J. Sandman, *Polym. Mater. Sci. Eng.*, 2000, **82**, 146–147.
360 F. Separovic, H.D. Chau, M.I. Burgar, *Polymer*, 2001, **42**, 925–930.
361 F.O. Burel, C. Bunel, *Int. J. Polym. Anal. Charact.*, 2000, **6**, 193–212.
362 M.P. Espe, B.M. Gates, P.M. Schmeida, *Polym. Mater. Sci. Eng.*, 2000, **82**, 138.
363 A.R. Lim, J.-S. Kim, *Solid State Commun.*, 2000, **115**, 179–183.
364 C.M. Dick, C.E. Snape, J.J. Liggat, *Polym. Mater. Sci. Eng.*, 2000, **82**, 185.
365 M.B. Robertson, P.G. Klein, I.M. Ward, K.J. Oacker, *Polymer*, 2001, **42**, 1261–264.
366 B.-D. Park, B. Riedl, *J. Appl. Polym. Sci.*, 2000, **77**, 1284–1293.
367 N.C. Mello, T.J. Bonagamba, H. Panepucci, K. Dahmouche, P. Judeinstein, M.A. Aegerter, *Macromolecules*, 2000, **33**, 1280–1288.
368 A.J.J.M. Van Breemen, M.M. DeKok, P.J. Adriaensens, D.J.M. Vanderzande, J.M.J.V. Gelan, *Macromol. Chem. Phys.*, 2001, **202**, 343–353.
369 R.A. Assink, M. Celina, T.D. Dunbar, T.M. Alam, R.L. Clough, K.T. Gillen, *Macromolecules*, 2000, **33**, 4023–4029.
370 H. Menge, S. Hotopf, H. Schneider, *Polymer*, 2000, **41**, 3019–3027.
371 H. Menge, S. Hotopf, H. Schneider, *Polymer*, 2000, **41**, 4189–4201.
372 D. Olcak, L. Sevcovic, L. Mucha, *Acta Phys. Slovaca*, 2000, **50**, 259–266.
373 W.P. Weglarz, H. Peemoeller, A. Rudin, *J. Polym. Sci., Part B: Polym. Phys.*, 2000, **38**, 2487–2506.
374 X. Fang, X.-Q. Xie, C.D. Simone, M.P. Stevens, D.A. Scola, *Macromolecules*, 2000, **33**, 1671–1681.
375 R.D. O'Connor, E.J. Ginsburg, F.D. Blum, *J. Chem. Phys.*, 2000, **112**, 7247–7259.
376 L.S. Loo, R.E. Cohen, K.K. Gleason, *Polymer*, 2000, **41**, 7699–7704.
377 J. Brus, J. Dybal, *Polymer*, 2000, **41**, 5269–5282.
378 F. Beaume, F. Laupretre, L. Monnerie, *Polymer*, 2000, **41**, 2989–2998.
379 S.-Z. Mao, X.-D. Zhang, J.-M. Dereppe, Y.-R. Du, *Colloid Polym. Sci.*, 2000, **278**, 264–269.
380 L. Masaro, W.E. Baille, X.X. Zhu, *Polym. Prepr. (Am. Chem. Soc., Div. Polym. Chem.)*, 2000, **41**, 62–63.
381 K. Troev, Vl. Atanassov, R. Tzevi, *J. Appl. Polym. Sci.*, 2000, **76**, 886–893.

382 W. Liu, A. Halasa, J. Visintainer, R. Hirst, P.L. Rinaldi, *Polym. Prepr. (Am. Chem. Soc., Div. Polym. Chem.)*, 2000, **41**, 26–27.
383 L. Weixia, T. Saito, L. Li, P.L. Rinaldi, R. Hirst, A.F. Halasa, J. Visintainer, *Macromolecules*, 2000, **33**, 2364–2369.
384 F.M. Som, J.A. Chudek, G. Hunter, *J. Rubber Res. (Kuala Limpur)*, 1999, **2**, 169–182.
385 J.Z. Hu, W. Wang, S. Bai, R.J. Pugmire, C.M.V. Taylor, D.M. Grant, *Macromolecules*, 2000, **33**, 3359–3367.
386 M.L. Cerrada, R. Benavente, E. Perez, J.M. Perena, *J. Polym. Sci., Part B: Polym. Phys.*, 2000, **38**, 573–583.
387 P. Ekanayake, H. Menge, H. Schneider, M.E. Ries, M.G. Brereton, P.G. Klein, *Macromolecules*, 2000, **33**, 1907–1812.
388 T. Kitayama, M. Janco, K. Ute, R. Niimi, K. Hatada, D. Berek, *Anal. Chem.* 2000, **72**, 1518–1522.
389 L.S. Loo, R.E. Cohen, K.K. Gleason, *Science (Washington, DC)*, 2000, **288**, 116–119.
390 M. Kanekiyo, M. Kobayashi, I. Ando, H. Kurosu, S. Amiya, *Polymer*, 2000, **41**, 2391–2404.
391 T. Asakura, Y. Nakazawa, P.Y. Ghi, J. Ashida, T. Kameda, *Polym. Mater. Sci. Eng.*, 2000, **82**, 145.
392 M. Ohuchi, P. Meadows, H. Horiuchi, Y. Sakai, K. Furihata, *Polym. J. (Tokyo)*, 2000, **32**, 760–770.
393 A. Tonegawa, K. Ohno, H. Matsuura, K. Yamada, T. Okuda, *Chem. Lett.*, 2000, 324–325.
394 N. Garin, J. Hirschinger, F. Beaume, F. Laupretre, *Polymer*, 2000, **41**, 4281–4384.
395 F. Nozirov, Z. Fojud, E. Szczensiak, S. Jurga, *Appl. Magn. Reson.*, 2000, **18**, 37–45.
396 A.D. English, *Polym. Mater. Sci. Eng.*, 2000, **82**, 152.
397 M.D. Ediger, X. Qiu, *Polym. Mater. Sci. Eng.*, 2000, **82**, 153.
398 H. Kaji, K. Schmidt-Rohr, *Macromolecules*, 2000, **33**, 5169–5180.
399 D. Maring, M. Wilhelm, H. W. Spiess, B. Meurer, G. Weill, *J. Polym. Sci., Part B: Polym. Phys.*, 2000, **38**, 2611–2624.
400 A.E. Tonelli, J. Lu, D. Shin. P.A. Mirau, *Polym. Mater. Sci. Eng.*, 2000, **82**, 163–164.
401 J. Wu, C. Xiso, S.F. Yee, J.M. Goetz, *Macromolecules*, 2000, **33**, 6849–6852.
402 X. Qiu, N.E. Moe, M.D. Ediger, L.J. Fetters, *J. Chem. Phys.*, 2000, **113**, 2918–2926.
403 X. Qiu, M.D. Ediger, *J. Polym. Sci., Part B: Polym. Phys.*, 2000, **38**, 2634–2543.
404 J. Liu, A.F. Yee, J.M. Goetz, J. Schaefer, *Macromolecules*, 2000, **33**, 6853–6855.
405 H. Namgoong, J.-R. Rho, J.W. Lee, *Bull. Korean Chem. Soc.*, 2000, **21**, 1071–1076.
406 T. Dollase, R. Graf, A. Hruer, H.W. Spiess, *Macromolecules*, 2001, **34**, 298–309.
407 M. Destree, F. Laupretre, A. Lyulin, J.-P. Ryckaert, *J. Chem. Phys.*, 2000, **112**, 632–9644.
408 S. Azizi, T. Tajouri, H. Bouchriha, *Polymer*, 2000, **41**, 5921–5928.
409 M. Kanekiyo, M. Kobayashi, I. Ando, H. Kurosu and S. Amiya, *Macromolecules*, 2000, **33**, 7971–7976.
410 Y. Machida, S. Kuroki, M. Kanekiyo, M. Kobayashi, I. Ando, S. Amiya, *J. Mol. Struct.*, 2000, **554**, 81–90.

11 S.J. Oh, J.L. Koenig, *J. Polym. Sci., Part B: Polym. Phys.*, 2000, **38**, 1417–1423.
12 E.W. Hansen, A.M. Bouzga, B. Sommer, P.O. Kvernberg, *Polym. Adv. Technol.*, 2000, **11**, 185–191.
13 K.J. McGrath, C.M. Roland, M. Antonietti, *Macromolecules*, 2000, **33**, 8354–8360.
14 M.A.P.R. Torres, C.M.F. Oliveira, M.I.B. Tavares, *Int. J. Polym. Mater.*, 2000, **46**, 695–700.
15 J. Brus, J. Dybal, P. Schmidt, J. Kratochvil, J. Baldrian, *Macromolecules*, 2000, **33**, 6448–6459.
16 J.-C. Ho, K.-H. Wei, *J. Polym. Sci., Part B: Polym. Phys.*, 2000, **38**, 2124–2135.
17 R.-H. Lin, E.M. Woo, J.C. Chiang, *Polymer*, 2001, **42**, 4289–4297.
18 D.L. VanderHart, Y. Feng, C.C. Han, R.A. Weiss, *Macromolecules*, 2000, **33**, 2206–2227.
19 C.S. Wang, C.H. Lin, *Polymer*, 2000, **41**, 4029–4037.
20 H.-D. Wu, C.-C.M. Ma, F.-C. Chang, *Macronol. Chem. Phys.*, 2000, **201**, 1121–1127.

12
NMR in Living Systems

BY M.J.W. PRIOR

1 General Applications and New Methodologies

1.1 Applications, Methodologies and Instrumentation. – A review of NMR probeheads for *in vivo* applications has been produced with 86 references.[1]

The feasibility of using the praseodymium complex 10-(2-methoxyethyl)-1,4,7,10-tetraazacyclododecane-1,4,7-triacetate (Pr[MOE-DO3A]) for non-invasive measurement of temperature *in vivo* has been assessed. Calibration curves for the temperature dependent chemical shift of Pr[MOE-DO3A] in water and plasma were obtained which indicated that the maximum accuracy of the method would be $\pm 0.2^{\circ}$ *in vivo*.[2] In an investigation of the influence of subcutaneous fat on the measurement of oxygen consumption by near-infra red spectroscopy (NIRS), ^{31}P NMR was used to confirm the rate of oxygen consumption from changes in the level of phosphocreatine (PCr).[3] A method for the determination of body composition from ^{1}H NMR spectra has been proposed. ^{1}H NMR spectra of the chest to abdomen, abdomen to pelvis and pelvis to thigh regions were obtained from 16 healthy volunteers using single free induction decay measurements. The NMR-derived metabolite ratio was calculated as the ratio of fat methyl and methylene ^{1}H resonances to the water ^{1}H resonance. The peak areas for the chest to abdomen and pelvis to thigh regions were normalised to an external reference of 2200 g of benzene and the NMR-derived metabolite ratio for the two regions was calculated. Total body water was calculated for each subject by the $^{2}H_2O$ dilution method. The NMR-derived metabolite ratio for the abdomen to pelvis region correlated best with the ratio of body fat to lean body mass.[4]

1.2 Spectral Editing. – The use of ^{13}C NMR and inverse ^{1}H NMR in metabolic flux analysis has been reviewed.[5]

The method of time-share modulation for ^{19}F[-^{1}H] decoupling has been implemented on a 1.5 T clinical scanner. The method can give a threefold increase in signal-to-noise compared to a WALTZ-4 decoupling scheme when there is significant interaction between the decoupler and receiver. Data was collected from patients receiving 5FU chemotherapy.[6] Double-resonance J-edited ^{1}H NMR has been used to monitor the uptake of [6-^{13}C]-D-2-deoxyglucose into glioma cells, *via* the detection of the C6 methylene protons.[7]

The simultaneous detection of water (as an internal standard) and brain

Nuclear Magnetic Resonance, Volume 31
© The Royal Society of Chemistry, 2002

metabolites in NMR spectra of healthy volunteers has been demonstrated using oversampling to avoid digitisation errors.[8] A new scheme has been proposed for the separation of signals from ^{1}H attached to glutamate C3 and C4 which overlap at magnetic fields of up to 3 Tesla. The scheme involves the two steps of the POCE method combined with two steps where the relative phases of the C3 and C4 ^{1}H resonances are manipulated using zero and double quantum coherence pathways; spectra have the same sensitivity as spectra obtained by the POCE method.[9] A fast variant of ^{1}H spectroscopic U-FLARE imaging has been developed which incorporates an adjusted phase encoding scheme using prior knowledge of the peaks in the spectra. The number of phase encoding steps can be reduced by a factor of four in 1H spectroscopic imaging. Measurements were made in phantoms and rat brain.[10]

A method for obtaining ^{17}O-decoupled ^{1}H spin echo images and spectra has been developed which utilises a stimulated echo method, allowing detection using a surface coil. The method may have applications for the indirect detection of ^{17}O in measurements of blood flow and metabolism.[11] An implementation of the polarisation transfer technique INEPT using segmented adiabatic BIR4 RF pulses has been carried out using a surface coil. Localisation was also achieved by the use of ISIS applied to the coupled spins. The transfer and localisation capabilities were demonstrated in phantoms and data was also collected from the liver of a normal volunteer that showed enhanced signals from the phosphodiesters (PDE) peaks.[12]

1.3 Localisation. – A single-shot, three-dimensional 'non-echo' localisation method has been developed which has reduced sensitivity to B_1 variation and is suitable for the detection of signals with short T1 and T2 values. A T1-optimised outer volume suppression scheme using hyperbolic secant pulses allowed the suppression of strong lipid, muscle and glucose signals from outside of the rat brain whilst signals were detected from glycogen, aspartate, glutathione, γ-aminobutyric acid (GABA) C4, *N*-acetyl-containing moiety (NAc) and, C3 and C4 of glutamate (Glu) and glutamine (Gln).[13] A method for three-dimensional localisation of a two-dimensional ^{1}H–^{13}C correlation spectroscopy experiment has been developed. The experiment has the 180°(^{13}C) and 180°(^{1}H) pulses separated in time with the 180°(^{13}C) pulse applied at $1/(4J_{CH})$ before the 90°(^{1}H) polarisation transfer pulse. This means that slice-selective 90°(1H) RF pulses with gradients could be applied during the preparation period. The localisation capabilities were confirmed in a phantom before a 3D localised ^{1}H–^{13}C correlation experiment was performed in monkey brain following the injection of [1-^{13}C]glucose.[14]

1.4 Spectral Analysis. – A new method of analysis of ATP utilisation and resynthesis has been developed which simulates cellular ATP flux, mitochondrial oxidative phosphorylation and creatine kinase kinetics. The model was used to examine previously published ^{31}P NMR data of changes in PCr and Pi in resting muscle, muscle exercising during ischaemia and muscle in aerobic recovery. The model allowed estimation of the maximal velocity of oxidative

phosphorylation and of the net ATP flux in individuals at rest and during stimulation.[15] A method for the study of oxidation in the TCA cycle, by the analysis of ^{13}C isotopomers of Glu, has been presented.[16] A procedure for modelling intermediary metabolism and the analysis of labelling kinetics from ^{13}C NMR data has been proposed. The approach, which includes metabolite compartmentation and exchange, may be useful for the analysis other metabolic processes in intact biological systems.[17]

The application of LCModel to quality control and quantitative *in vivo* ^{1}H NMR has been assessed. Tests *in vivo* were performed on 13 metabolites, NAc, *N*-acetylaspartylglutamate, total creatine (tCr), choline-containing compounds (Cho), *myo*-inositol (mI), *scyllo*-inositol, GABA, Glu, Gln, glucose (Glc), lactate, alanine and taurine, in ^{1}H NMR spectra of the white matter and hippocampus of volunteers.[18] An analysis of the errors resulting from the use of Lorentzian lineshapes in the fitting of *in vivo* data has been produced. The use of mixed Lorentzian–Gaussian functions are demonstrated in the analysis of data from human brain.[19] The reliability of quantitative clinical data from single voxel PRESS spectra has been assessed in 84 *in vitro* and 30 *in vivo* measurements. The coefficients of variations for Cho, Cr and NAc ranged from 3.3% to 4.0% and from 3.8% to 6.4% for *in vitro* and *in vivo* measurements, respectively.[20] ^{1}H NMR spectra of earthworms (*Eisenia veneta*) exposed for 72 h to 3-trifluoromethyl-aniline have been analysed using pattern recognition techniques. The use of mean principal components plots in simplifying group data representation and highlighting the dose–response function was demonstrated. Identification and assignment of metabolite responses to toxicity were found *via* correlation coefficient shift plots. Alanine and other amino acids were the most significant metabolites measured by correlation coefficients, although elevated levels of glucose, citrate and succinate were noted as potential markers of toxicity.[21] The use of the continuous wavelet transform approach combined with the data shift accumulation technique (WT-DSA) has been assessed as a post-acquisition water suppression technique. Data were collected from two test solutions and the method was compared to that obtained using presaturation and WATERGATE water suppression techniques. The WT-DSA method showed promise as a method to remove the water component without affecting peaks near the water resonance.[22] Continuous wavelet transform analysis has been applied to the detection of lactate in human blood plasma and brain tumours.[23]

1.5 Data Analysis. – The vocabulary and principles used in stable isotope tracer studies have been reviewed.[24]

A network model of ATP free energy metabolism in muscle consisting of actomyosin ATPase, sarcoplasmic reticulum Ca^{2+}-ATPase and mitochondria has been developed. The model was used to analyse ATP metabolic flux and cytosolic ATP/ADP steady state at six contraction frequencies between 0 and 2 Hz measured in the forearm flexor muscle using ^{31}P NMR.[25]

1.6 Intracellular Ions. – A review of ^{23}Na NMR and its application in biomedicine has been produced.[26]

A pitfall in the determination of the concentration of free intracellular magnesium ($[Mg^{2+}]_i$) based on the measurement of hβ/α of the β- and α-ATP signals in ^{31}P NMR spectra has been highlighted. It was shown in studies with phantoms that although hβ/α varies with $[Mg^{2+}]_i$ the ratio was also affected by magnetic field inhomogeneity leading to possible problems in the assessment of $[Mg^{2+}]_i$.[27] A new equation for the correlation of the chemical shift of β-ATP to the $[Mg^{2+}]_i$ in human tissue has been produced.[28] The effects of oral magnesium supplement (12 mmol Mg Lactate daily for one month) on the biodistribution of Mg^{2+} in the body has been investigated in 30 young, healthy men. Plasma Mg^{2+} levels were determined by ion selective electrode and ^{31}P NMR was used to measure levels in the brain and skeletal muscle. The level of Mg^{2+} in the urine was found to increase following administration of the supplement, though, there was no other effect detected.[29]

1.7 Cellular Metabolites. – A review of methods for the measurement of mI has been produced with 95 references. It examines the quantitative measurement of mI by mass spectrometry and *in vivo* ^1H NMR.[30] The ^1H NMR chemical shifts and *J*-coupling values of 35 metabolites which can be detected by *in vivo* or *in vitro* investigations of the mammalian brain have been published.[31] The principles and recent applications of dynamic nuclear polarisation, which combines the sensitivity to oxygen of EPR and the tractability of NMR imaging, have been reviewed with 244 references.[32] A review of studies of intermediary metabolism, including the use of NMR in the analysis of substrate selection under *in vivo* conditions, has been produced.[33] A review has been produced, with 74 references, on the study of metabolic flux and subcellular transport of metabolites using ^{13}C NMR.[34]

The effects of gadolinium diethylenetriaminepentaacetic acid on the ^1H NMR relaxation properties of Cho, tCr and NAc have been investigated at 1.5 T. The modulation of peak intensities by T1- and T2-weighted sequences was assessed.[35] Diffusion weighted ^1H NMR has been used to measure the distribution of Glc and lactate between the intracellular and extracellular space of the rat brain. At large diffusion values the apparent diffusion coefficient (ADC) of Glc and lactate was similar to that for intracellular metabolites such as *N*-acetyl-containing compounds (NAc), Cr and Glu. At small diffusion weighting, the ADC of Glc and lactate was increased, indicating a decrease in the contribution of intracellular Glc and lactate to their total signals.[36]

The signal losses, due to magnetic field inhomogeneity, in non-localised whole brain measurements of NAc have been investigated. The whole-head ^1H NMR spectrum of the water signal from the head was integrated over the same frequency width as that used in the analysis of NAc. The ratio of this area/total-water-line was $75 \pm 5\%$ in five volunteers. The procedure was repeated with brain-only water signal obtained by summation of signals from brain in a 3D CSI data set. This method estimated that 10% of the signal

from the brain was lost.[37] A method for the accurate determination of lactate concentration in isolated exercising muscle has been presented and the possible sources of errors in the determination of lactate from ^{31}P and ^{1}H NMR spectra have been discussed.[38] The concentration of creatine in the myocardium has been measured by ^{1}H NMR in the Langendorff-perfused rat heart. The relaxation times for myocardial creatine were determined (1.1 ± 0.29 s and 56.4 ± 6.2 ms for T1 and T2, respectively, at 11.75 T) prior to the implementation of a quantitative ^{1}H NMR method. The concentration of creatine measured in extracts was 14.2 ± 1.9 mmol kg^{-1} wet weight, but ^{1}H NMR *in vivo* detected only 60% of this. Furthermore, the addition of the CHESS sequence for water suppression led to a further 30% decrease in the detection of the metabolite.[39]

1.8 pH. – Aminomethylphosphonate (NMePo) and 2-aminoethylphosphonate (NEthPo) have been evaluated with ^{31}P NMR for use as pH indicators in the isolated perfused rat liver. NMePo was found to remain in the extracellular space and NEthPo accumulated within cells but, without affecting the energetic status of the liver. The intracellular fraction of NEthPo was found to be stable enough to allow the determination of its T1 in the tissue. A comparison of the titration curves of Pi and NEthPo revealed that NEthPo was as accurate as Pi for the determination of cellular pH.[40]

2 Cells

The use of NMR for the measurement of biotransformations in the online assessment of industrial fermentation process has been reviewed with 34 references.[41]

2.1 Microorganisms. – A review of the metabolic behaviour of lactic and propionic acid bacteria, studied by NMR, has been produced with 43 references.[42] The use of NMR in the study of bacterial sugar transport has been reviewed with 46 references[43] and sugar transport and metabolism in fermentative bacteria has been reviewed with 19 references.[44] A review of a new method for the determination of metabolic activity in microorganisms using ^{31}P, ^{15}N and ^{13}C NMR has produced with 13 references[45] and the methods for analysis of metabolism from ^{13}C NMR data has been reviewed with 18 references.[46] The use of NMR in the study of microorganisms has been reviewed with 53 references[47] and the use of *in situ* NMR systems has been reviewed with 57 references.[48] A review of NMR investigations into polymer biosynthesis has been produced with 41 references[49] and the use of NMR in studies of yeast metabolism has been reviewed with 72 references.[50]

The influence of sudden oxygen depletion on *Saccharomyces cerevisiae*, grown in glucose limited chemostat culture, has been investigated with ^{31}P NMR. During the switch from aerobic to anaerobic conditions there was a rapid, significant decrease in ATP, phosphoenolpyruvate (PEP) and intracel-

lular pH (pH_i). These changes were accompanied by a transient increase of Pi which was shown not to be from polyphosphate.[51] The fermentation characteristics of recombinant *Zymomonas mobilis ZM4(pZB5)* and its parental strain, *ZM4*, have been investigated with ^{13}C and ^{31}P NMR. The levels of nucleoside triphosphates (NTP) in *ZM4(pZB5)* were lower when cells were grown on xylose compared to cells grown on Glc. When *ZM4(pZB5)* was grown on xylose, the lignocellulosic toxic compound HOAc was strongly inhibitory with xylose utilisation being completely inhibited at pH ≤ 5.0 in the presence of 10.9 g dm^{-3} HOAc. ^{31}P NMR demonstrated that treatment with HOAc caused a decrease in pH_i, NTP and sugar phosphates.[52] The metabolism of glucose by non-growing cells of *Lactococcus lactis* strain *FI7851*, constructed from the wild-type *L. lactis* strain *MG1363* by disruption of the lactate dehydrogenase gene, has been studied with ^{31}P and ^{13}C NMR. The kinetics of the build up and consumption of pools of mannitol-1-phosphate, fructose 1,6-bisphosphate, 3-phosphoglycerate and PEP as well as the utilisation of [1-^{13}C]glucose and the formation of lactate, acetate, mannitol, ethanol, acetoin and 2,3-butanediol were monitored with a time resolution of thirty seconds. A clear shift from the homolactic acid fermentation of the wild-type organism to a mixed acid fermentation was observed in strain *FI7851*. Furthermore, high levels of mannitol were produced and consumed once glucose was depleted; up 76 mM mannitol phosphate was accumulated by *Lactococcus lactis* strain *FI7851*.[53] The interactions between pyruvate and lactate metabolism have been investigated with ^{13}C NMR in cell suspensions of *Propionobacterium freudenreichii* subspecies *shermanii*. Pyruvate was consumed at apparent initial rates of 148 and 90 μmol min^{-1} g^{-1} (dry cell weight) when it was the sole substrate or co-metabolised with lactate, respectively. Lactate was consumed at an apparent initial rate of 157 μmol min^{-1} g^{-1} when it was co-metabolised with pyruvate.[54] The effects of mannose on the growth of *Plesiomonas shigelloides* has been investigated with ^{13}C and ^{31}P NMR *in vivo* and with ^{31}P NMR in cell extracts. *P. shigelloides* was shown to transport mannose by a phosphoenol pyruvate-dependent phosphorotransport system producing mannose-6-phosphate, though a toxic effect was observed when cells were grown in the presence of mannose. ^{13}C NMR *in vivo* showed that mannose-6-phosphate underwent no further metabolism and no mannose-6-phosphate isomerase activity was found in extracts. The level of PEP and Pi were measured by ^{31}P NMR *in vivo* to be relatively constant in starved cells and mannose-metabolising cells. However, in glucose-metabolising cells the level of PEP was lower and 80% of Pi was used during the first 10 min of metabolism.[55]

^{31}P NMR has been used to investigate the effects of three anti-microbial peptides isolated from Australian tree frogs *Litoria caerulea* and *L. genimaculata* on the cell membranes of *Bacillus cereus* and *Staphylococcus epidermidis*. The wide-spectrum antibiotic peptides caerin 1.1 and maculatin 1.1 disrupted cell membranes causing an increase in the isotropic ^{31}P NMR signal. However, caerin 4.1, a narrow-spectrum antibiotic, did not affect the ^{31}P spectra of these bacteria.[56]

2.2 Blood. – The study of the metabolism of 2,3-bisphosphoglycerate in human erythrocytes using NMR and computer simulation has been reviewed with 19 references.[57]

The effects of temperature on the distribution of non-electrolytes between erythrocytes and the surrounding medium *in vitro* has been investigated with ^{1}H NMR. The results indicated that between 4° and 37° the rate of uptake by erythrocytes was a function of temperature.[58] The inhibition of water-permeability by diffusion (P_d) through the erythrocyte membrane has been investigated using ^{1}H NMR. Maximal inhibition of 50% of P_d was achieved by 2 mM *p*-chloromercuri benzoate in 20 min. The maximal effect of *p*-chloromercuri benzoate was reduced by the presence of lipophilic solutes. However, lipophilic solutes alone caused a faster inhibition of P_d, though this was less efficient than that from *p*-chloromercuri benzoate.[59] A method has been developed to observe early phosphate penetration into erythrocytes. When the main extracellular cation was Na^+, 100 mM extracellular Pi penetrated the cells within one hour. When the main extracellular cation was K^+ the apparent penetration rate of Pi was reduced by 25%. The influx of Pi into erythrocytes was not accompanied by a change in pH_i.[60]

^{31}P NMR has been used to measure a decrease in 2,3-diphosphoglucose, an allosteric regulator of oxygen release from haemoglobin (Hb), in erythrocytes from $CeCl_3$-fed rats. Measurements of oxygen saturation curves for Hb demonstrated a change in the curve in response to dosing with $CeCl_3$. Furthermore, there was an increase in the Hb content of the erythrocytes following treatment.[61] The metabolism of [1-^{13}C]-L-ascorbic acid, [2-^{13}C]-L-ascorbic acid and their dehyro counter-parts has been monitored with ^{13}C NMR in human erythrocytes. Resonances were assigned to the metabolites diketogulonic acid and CO_2 when cells were incubated with or without Glc. No signals for lactate were observed, counter to a recent finding.[62] The accumulation of Na^+ in human erythrocytes following cryopreservation has been investigated with ^{23}Na NMR. When membrane permeability was modulated by the addition of nystatin (50 μg cm^{-3}) there was a rapid ninefold increase of intracellular Na^+ (Na^+_i) within 50 min. However, after cryopreservation saturation with Na^+ was achieved in only 18 min.[63] ^{19}F and ^{31}P NMR have been used to measure intracellular Ca^{2+} (Ca^{2+}_i) and intracellular Mg^{2+} (Mg^{2+}_i) in erythrocytes from subjects in two age groups. Following fasting, Mg^{2+}_i levels were lower and Ca^{2+}_i levels were higher in older (average age 71.1 years) compared to younger (average age 51.1 years) subjects; a correlation was seen between age and ion content. However, no differences were observed in ion content of erythrocytes from older compared to younger subjects with essential hypertension or type 2 diabetes.[64]

2.3 Cultured and Tumour Cells. – A review of ^{1}H NMR visible lipid signals from cells during life and death has been produced with 55 references.[65] The investigation of cell biochemistry using NMR has been reviewed with 20 references.[66] A review of NMR methods for the real-time observation of metabolites in living cells has been produced with 22 references.[67]

Diabetic and control cardiomycetes, encapsulated in agarose beads and perfused with modified medium 199, have been studied with ^{23}Na and ^{31}P NMR. Baseline Na^+ levels were higher and baseline βATP and PCr levels were lower in diabetic *vs.* control cells. When cells were perfused with 2-deoxyglucose (2DG) or ouabain there was a minimal effect on diabetic cardiomycetes whereas in control cells both agents caused significant increases in Na^+_i after 63 min exposure. Treatment with dinitrophenol, though, was associated with a large increase in Na^+_i and a decrease in PCr and βATP to below the level of detection in both cell types. However, neither 2DG nor ouabain caused a decrease in PCr or βATP that would have compromised sarcolemmal function in either cell type.[68] ^{31}P NMR has been used to monitor energy status in a study of the effect of continuous medium flow on the viability and structural organisation of hepatocytes entrapped at high density in alginate beads. Energetic status was stable during the experimental time and a physiological redox ratio was achieved after the first three hours of culture.[69] Diffusion-weighted ^1H NMR has been used to measure changes in cell volume of immobilised perfused F98 glioma cells exposed to NH_4Cl. Cellular swelling to 125% of control volumes was accompanied by a 130% increase in Gln and a decrease in cellular osmolytes (mI and taurine) measured by ^1H NMR in extracts. Inhibition of glutamate synthetase partially prevented the increase in water content.[70] ^{31}P and ^{13}C NMR have been used to investigate the metabolism of EMT6/Ro multicellular spheroids in the presence of glucose, glutamine, acetate and propionate. Stable NTP and PCr levels for up to 48 h were observed in the presence of glucose. The metabolism of [1-^{13}C]glucose was almost entirely to [3-^{13}C]lactate (88%) even though the perfusate was equilibrated with 95% O_2. Labelling was also observed primarily in alanine and α-glycerophosphate, though a low level was observed in C4 of glutamate; labelling of glutamate C2 and C2 was less than 20% of that in C4 and there was no evidence, even in extracts, of adjacent labelling in glutamate that would indicate multiple rounds of glutamate in the TCA cycle. Stable NTP and PCr levels, for up to 12 h, were seen in the presence of 2 mM glutamine and ≤ 0.5 mM glucose. In the presence of 2.5 mM acetate the bioenergetic status declined slowly and no label incorporation was observed even in extracts. However, in the presence of [3-^{13}C]propionate (with glucose and glutamine) the high energy phosphate levels declined and stabilised; label was incorporated into methylmalonate and C2 and C3 of glutamate. The addition of vitamin B_{12} resulted in the elimination of the methylmalonate signal and a variety of 2- and 3-labelled metabolites was observed.[71] The intracellular biochemical profiles of six cell lines, perfused in alginate beads, have been obtained with diffusion-weighted ^1H NMR. Spectral differences between groups of cell lines, including Cho, lactate and threonine were observed and the response of the cell lines to lonidamine, an antineoplastic agent, was investigated. A two- to ninefold increase in the lactate signal was observed in several cancer lines in response to treatment with lonidamine. Furthermore, there was a two- to threefold difference between the accumulation of lactate in melanoma cells and compared to that in some breast cell lines.[72]

^{31}P NMR has been used in an investigation of the effects of ammonia and lactate on the growth, metabolism and productivity of a BHK21 cell line expressing an IgG–IL2 fusion protein. Experiments showed that ammonia and lactate affected the cells leading to a decrease in pH_i and phosphomonoesters (PME) whilst the cellular energy status was maintained.[73] The effects of photodynamic therapy with Victoria Blue BO on TF-1 leukaemic cells has been investigated with ^{31}P NMR. In the absence of light, significant differences were observed between cells treated with Victoria Blue BO and untreated controls, including a reduction in PCr, UDP-hexose and PDE and a slightly reduced pH. Following exposure of treated cells to light, PCr became undetectable, Pi increased and there was a significant cellular acidification. Furthermore, there was an accumulation of CDP choline and a decrease in PDE in these cells.[74] The uptake and washout of two boron-containing neutron capture therapy agents have been investigated in M2R mouse melanoma cells grown on microspheres. The presence of inorganic boronate, borocaptate sodium and borono-phenylalanine was detected by ^{11}B NMR and, fluorinated borono-phenylalanine was detected with ^{19}F NMR. In the medium, borocaptate sodium formed a dimer and borono-phenylalanine readily reacted with glucose, though, borono-phenylalanine was converted within the cells into an unknown compound. The cellular accumulation of borono-phenylalanine was greater than borocaptate sodium, although the retention of borocaptate sodium was longer.[75] The effects of hepatocyte growth factor/scatter factor (HGF/SF) on perfused DA3 murine mammary cancer cells has been investigated with ^{31}P and ^{13}C NMR. Treatment with HGF/SF induced alterations in phospholipid metabolites and enhanced the rate of glucose phosphorylation. Measurements with ^{13}C NMR demonstrated that HGF/SF reduced the steady state levels of glucose and elevated those of lactate. Furthermore, HGF/SF increased oxygen consumption, decreased CO_2 levels and attenuated pH decrease.[76]

2.4 Reproductive. – ^{31}P and ^{1}H NMR have been used to monitor metabolites in turbot *(Psetta maxima)* spermatozoa prior to, and following, the initiation of motility. Compounds from seminal fluid and urine were detected by ^{1}H NMR. The analysis of urine revealed the presence of dimethylamine, trimethylamine and trimethylamine oxide whilst seminal fluid was shown to contain lipoproteins, formic acid and citric acid. ^{31}P NMR revealed the presence of PME, PDE, Pi, PCr and NTP. Following the activation of motility, there was a fall in nucleoside diphosphates, NTP, PCr and PME whilst Pi increased; ^{1}H NMR detected an increase in lactate at this time.[77] The metabolism of mature boar spermatozoa have been investigated using NMR and metabolic studies. Washed spermatozoa incubated with exogenous substrates maintained a high energy charge potential for at least 10 h, though the addition of bromopyruvate caused an immediate decrease in this potential. Some of the sources of metabolic substrates were identified: acetylcarnitine contributed acetyl groups early in the incubation, glycerophosphocholine was degraded to glycerol 3-phosphate and choline after about 5 h; acetate also accumulated after about

5 h. The presence of phosphorylcholine and phosphorylethanolamine later in the incubation indicated the degradation of phospholipids to glycerol.[78]

3 Plants and Algae

3.1 Cells. – ^{15}N NMR has been used to monitor nitrogen metabolism in transformed *Nicotiana tabacum L.* root cultures. The incorporation of ^{15}N-label from [^{15}N]ammonium and/or [^{15}N]nitrate into agropine, conjugated polyamines, GABA, Glu, Gln and nicotine was observed. The largest ^{15}N-labelled pool was agropine and it synthesis was maintained, to the detriment of the Gln pool, under conditions of nitrogen starvation. The addition of α-naphthaleneacetic acid and kinetin to the growth medium caused de-differentiation of the root culture and perturbed secondary nitrogen metabolism; the ratio of agropine to glutamine increased, but the total amount of agropine decreased.[79] The incorporation of label from $(^{15}NH_4)_2SO_4$ and $K^{15}NO_3$ in cultured cell suspensions of *Nicotiana plumbaginifolia* has been investigated using two-dimensional ^{15}N–^{1}H NMR with heteronuclear single-quantum-coherence spectroscopy and heteronuclear multiple-bond-coherence spectroscopy sequences. This enabled the observation of glutamine, aspartate and alanine, normally detected by one-dimensional spectroscopy, and several other amino acids such as serine, glycine and proline. Furthermore, the peak assigned as GABA in one-dimensional spectra was found to contain several components as did the peak for *N*-acetylated compounds. Label was also observed in the intermediates agmatine and putrescine.[80] The uptake of [^{13}C]methanol into sycamore (*Acer pseudoplantanus L.*) cells has been monitored *in vivo* and its subsequent metabolism to [3-^{13}C]serine, [$^{13}CH_3$]methionine and [$^{13}CH_3$]phosphatidylcholine was measured in extracts.[81]

The effects of salt stress have been investigated in perfused maize cells with ^{31}P and ^{23}Na NMR. In cells exposed to salt stress there was a significant increase in vacuolar pH whilst the cytoplasmic pH remained constant. In concentrations of up to approximately 300 mM Na^+, vacuolar pH and the rate of Na^+ uptake were dependent on the extracellular concentration; above 300 mM, vacuolar pH and Na^+ uptake were independent of the extracellular concentration. Na^+ uptake into the cell was accompanied by a rapid increase in vacuolar Pi, broadening of the ^{31}P resonances and a reduction in glucose monophosphate and UDPG.[82]

3.2 Seeds and Fruits. – Changes in metabolites and subcellular pH during development have been studied in the cherry tomato (*Lycopersicon esculentum Mill.* var. *cerasiformae*) with ^{31}P and ^{13}C NMR. Fruit compartments had a cytoplasmic pH around 7.1 from the cell division and expansion stages. The vacuolar pH, measured by ^{13}C NMR, decreased from 4.5 to 3.6 units. An accumulation of GABA was observed during the first 15 days after anthesis and glutamate decarboxylase activity increased tenfold during the first 8 days of development.[83]

3.3 Tissues. – A review of methods for the quantification of metabolic fluxes in metabolic engineering of secondary metabolism in plants has been produced with 42 references. It includes the use of *in situ* ^{31}P and ^{13}C NMR for the measurement primary metabolism and physiology.[84] The interaction of sucrose metabolism, starch storage and phloem export in source leaves, and the effects on sugar status in phloem, has been reviewed with 22 references.[85]

Metabolic modelling has been used in conjunction with [^{14}C]choline labelling experiments and ^{31}P NMR to define the constraints on glycine betaine synthesis in tobacco (*Nicotiana tabacum*) plants engineered to express spinach choline monooxygenase in the chloroplast.[86]

The metabolic response of cucumber (*Cucumis sativus L.*) roots grown under iron-deficiency conditions has been investigated with ^{31}P NMR. Iron starvation induced activation of metabolism, leading to consumption of stored carbohydrates, and an increase in ATP, NAD(P)H, PEP, glucose-6-phosphate (G6P) and fructose-6-phosphate (F6P). Furthermore, there was an slight increase in the vacuolar pH and cytosolic pH along with a dramatic fall in the vacuolar Pi concentration.[87] The intracellular phosphorous metabolites of mycorrhizal and nonmycorrhizal roots of cucumber, and those in the external mycelium of the arbuscular mycorrhizal fungus *Glomus intraradices Schenck & Smith*, have been studied with ^{31}P NMR.[88]

Ammonium-induced changes in the cytoplasmic and vacuolar pH values of excised maize (*Zea mays L.*) root tips, measured by ^{31}P NMR, have been correlated with the ammonium content of the tissue, determined by ^{14}N NMR. Calculations from these measurements showed that pH changes during exposure to 10 mM ammonium for 1 h at pH 9.0, and during recovery, were largely determined by the influx and efflux of NH_3. Carboxylate synthesis, determined by ^{13}C NMR, was stimulated, but the contribution of this process to pH regulation was insignificant. Similarly, ammonium assimilation did not significantly contribute to pH regulation.[89] ^{31}P NMR has been used to investigate the changes in phosphate metabolism and pH_i in intact maize (*Z. mays L.*) root segments under hyperosmotic shock. A large vacuolar alkalinization and a decrease in pH across the tonoplast membrane was observed under hyperosmotic shock along with a gradual build up of phosphocholine and a decrease of G6P and uridine diphosphoglucose. In gradual stress the root segments were able to adapt and maintain a pH gradient across the tonoplast with only marginal alkalinization of the vacuole.[90] ^{31}P NMR was used to measure pH in an investigation of the mechanism by which the elongation of stems of over-wintered tubers of *Potamogeton pectinatus (L.)* is strongly promoted by several days of oxygen free conditions.[91]

4 Animal Tissues

4.1 Brain. – The impact of exercise and fasting with subsequent glucose supplementation on glucose metabolism in rats has been studied with ^{1}H NMR to measure intracellular plus extracellular glucose and with microdia-

lysis to measure extracellular glucose. Exercise increased extracellular glucose whereas fasting caused a decrease, and infusion of glucose after fasting or exercise increased the level of extracellular glucose and the level of glucose detected by NMR.[92] ^{13}C NMR has been used to measure the rates of glutamate/glutamine cycling, *de novo* glutamine synthesis *via* anaplerosis and the TCA cycle rates in the rat cerebral cortex from the metabolism of infusions of [2-^{13}C]glucose and [5-^{13}C]glucose. Under normoammonaemic conditions anaplerosis was found to make up 19–26% of the total glutamine synthesis, while this fraction increased significantly to 32% during hyperammonaemia.[93]

The effects of creatine supplements on a transgenic mouse (R6/2) model of Huntington's disease has been investigated with ^{1}H NMR. Dietary creatine supplement significantly improved survival and slowed the development of brain atrophy. Furthermore, body weight and motor performance were significantly improved and the onset of diabetes was markedly delayed. ^{1}H NMR showed that brain tCr was increased and the decrease in NAc was delayed.[94] A large decrease in NAc has been detected in the brains of transgenic Huntington's disease mice. The 53% fall began at 6 weeks of age with the onset of symptoms. Nissl staining was used to demonstrate the absence of neuronal death in these mice, but the presence of nuclear inclusion bodies was detected.[95]

^{31}P NMR has been used to assess $[Mg^{2+}]_i$ in the rat brain following severe, diffuse traumatic brain injury and the results were compared to performance in a rotarod test of neurological function. It was found that an i.v. bolus of $MgSO_4$ or $MgCl_2$ at 30 min following brain injury significantly attenuated the decline in $[Mg^{2+}]_i$ and this was sustained for the entire week of the post injury monitoring period. The was a significant improvement in the neurological motor function in the magnesium treated rats and $[Mg^{2+}]_i$ was linearly correlated with the neurological motor function.[96] The effects of thrombolytic therapy on metabolic changes has been studied with 2D spectroscopic imaging and perfusion-weighted MRI in rats submitted to thromboembolic stroke. Reperfusion therapy was initiated at 1.5, 3.0 and 4.5 h after embolism by injection of recombinant tissue-type plasminogen activator (rt-PA). In untreated animals, there was a fall in perfusion signal intensity in the occluded hemisphere followed by an increase in lactate and a fall in NAc. Although thrombolysis partially restored blood flow, there was no recovery in the level of NAc. Five hours after the initiation of thrombolysis the average tissue lactate was 95, 111 and 139% of the early ischaemic value when treatment was initiated 1.5, 3.0 and 4.5 h after embolism.[97] The effects of vasospasm induced by the application of endothelin-1 (10^{-4} or 10^{-6} M) to the middle cerebral artery has been investigated in the rat brain. Treatment with endothelin-1 caused an immediate drop in pH_i, an increase in Pi and an increase in lactate. There was a gradual recovery to control values in the group treated with 10^{-6} M endothelin-1, but there was a loss of 10% of signal intensities of PCr and ATP in those treated with 10^{-4} M endothelin-1.[98]

The relationship between cerebral interstitial oxygen tension (Pt_{O2}) and cellular energetics has been investigated in mechanically ventilated anaesthetised rats during progressive acute hypoxia. Cerebral Pt_{O2}, measured by ESR

oximetry, decreased proportionally to the inspired oxygen fraction. There were no changes in Pi, PCr/Pi or pH when arterial blood oxygen tension (Pa_{O2}) was reduced from 145.1 ± 11.7 to 56.5 ± 4.4 mmHg (Pt_{O2} reduced to 15.1 ± 1.8 mmHg). There was an intracellular acidosis, a sharp rise in Pi and a decline in PCr/Pi when Pa_{O2} was decreased to 40.7 ± 2.3 mmHg (Pt_{O2} reduced to 15.1 ± 1.8 mmHg).[99] In a study of the effects of anoxia on oxidative phosphorylation in the new-born piglet brain ^{31}P NMR has been used to measure high energy phosphates whilst full spectral NIRS was used to determine changes in Hb oxidation and the oxidation state of cytochrome oxidase. ^{31}P spectra were obtained with a resolution of 10 s during transient (105 s) anoxia. There was no change in PCr or the oxidation state of cytochrome oxidase until there was a substantial decrease in the cerebral Hb oxygenation at which point cytochrome oxidase reduced simultaneously with the decline of PCr. After this decline there was a fall in the pH_i.[100]

The effects of hypoxia on foetal lamb brain metabolism has been studied with ^{1}H NMR. Hypoxia, induced by decreasing the oxygen supply to the pregnant ewe, caused a decrease in NAc whilst tCr, Cho and mI remained constant; lactate was detected only under hypoxia.[101] ^{31}P NMR has been used to monitor the energy metabolism in the brain of 7-day-old rat pups exposed to a 3 h period of hypoxic ischaemia. In rats pretreated with 0.1 mg kg^{-1} dexamethazone, the levels of NTP and PCr were elevated during exposure to hypoxic ischaemia compared to controls. Furthermore the treated group had little or no brain damage compared to the control group which had severe neuronal loss and cortical infarction.[102] In a study of the viability of tissue in and around focal ischaemia, a rat model has been studied with lactate-edited magnetic resonance spectroscopic imaging following the infusion of [1-^{13}C]glucose. There was no detected enrichment of lactate in the central core of the ischaemic region, but ^{13}C was incorporated in the boarder zone areas.[103] In an investigation of the mechanism by which systemic creatine supplementation prevents hypoxic seizures in 15-day-old rabbit pups ^{31}P NMR has been used to measure the rate of creatine kinase flux in rabbit brain slices from predominantly grey matter or predominantly white matter.[104] Cerebral metabolite changes in the rat brain 8 days after ligation of the middle cerebral artery have been investigated with NMR. Each rat exhibited accumulation of lactate and individual changes in PCr, Pi and PME whilst ATP ADP and pH were constant. Correlation analysis of these parameters were used to characterise regulatory changes in the system of cerebral metabolism.[105]

^{1}H NMR has been used to measure changes in NAc in the rat brain caused by exotoxic lesions of the medial prefrontal cortex (mPFC) which is connected to the striatum and ventral tegmental areas. Lesioned rats exhibited reductions in NAc and other brain metabolites in the prefrontal cortex, and reductions in NAc in the striatum. No changes were observed in the parietal cortex. The reduction in prefrontal NAc correlated with lesion extent.[106] The effects of alcohol treatment (4.5 g kg^{-1} ethanol in 2 of 12 daily feeding sessions) on the response of the neonatal rat brain to hypoxia has been investigated with ^{31}P NMR. Spectra were acquired in an atmosphere of 5% or 0% oxygen before

and after the second alcohol feedings on days four and nine. A decrease in PCr, ATP and pH, with an increase in Pi was observed in day four animals exposed to 0% oxygen; day nine animals did not tolerate this regime. There were no differences between groups exposed to 5% O_2 on day four, but a decrease in ATP and Pi was observed on day nine compared to pretreatment and control groups.[107] The effects of treatment with 3-nitropropionic acid have been investigated with ^{1}H NMR and diffusion-weighted MRI in the striatum of the rat brain. A significant decrease in NAc was detected nearly simultaneously with the appearance of lesions in the MR images and was preceded by an increase in the level of acetate. Shortly before NAc was at its lowest level the acetate peak reached its highest level and gradually declined.[108] The brain energy metabolism of rats affected by chronic hepatic encephalopathy due to portacaval shunting has been investigated with ^{31}P NMR. Portacaval shunting decreased the levels of PCr, NTP and $[Mg^{2+}]_i$ compared to controls. The levels of PCr, NTP and $[Mg^{2+}]_i$ were further reduced in shunted animals when they were exposed to ammonium acetate; the spectra from control animals were unaffected by exposure to ammonium acetate.[109]

The effects of substrate types on high energy phosphate (HEP) levels have been assessed in rat brain slices at 25° with a time resolution of 4 min. Measurements were made of the population excitatory post-synaptic potentials (EPSP) from granule cells in rat brain hippocampal slices in parallel experiments. During K^+-stimulation PCr decreased to a low level and recovered to control levels in artificial cerebrospinal fluid (ACSF) in about 10 min; population EPSP disappeared during stimulation and recovered in standard ACSF. Glucose was unable to support metabolism in iodoacetate-treated cells, but ACSF containing lactate or pyruvate allowed the recovery of PCr following K^+-stimulation. The half-time of recovery of PCr was longer when lactate replaced glucose in ACSF. When iodoacetate-treated slices were further subjected to fluorocitrate the recovery of PCr following K^+-stimulation was supported by pyruvate but not lactate.[110] ^{1}H NMR diffusion weighted spectroscopy has been used to assess the ADC of water and metabolites in rats brain slices. Aglycaemic hypoxia caused a reduction in the ADC of NAc from 0.15×10^{-3} mm^2 s^{-1} to 0.09×10^{-3} mm^2 s^{-1}, a reduction in the 'slow' diffusion coefficient of water from 0.51×10^{-3} mm^2 s^{-1} to 0.37×10^{-3} mm^2 s^{-1} and a 32 ± 11 % increase in the tissue water volume. Changes in the ADC of NAc and the 'slow' diffusion coefficient of water were abolished by the removal of external Ca^{2+}. Furthermore, in 10 mM Mg^{2+} these changes were delayed until after 40 min of hypoxia.[111]

Hyperpolarized ^{129}Xe has been detected in the rat brain following the injection of the gas, dissolved in a lipid emulsion, into the carotid artery. Spectra were recorded at 2.35 T over 51 s with a repetition time of 253 ms. Two peaks were detected and were assigned to intravascular xenon (194 ± 1 ppm) and xenon dissolved in brain tissue (199 ± 1 ppm).[112]

4.2 Eye. – ^{31}P NMR has been used to monitor changes in the rat eye during development of cataracts induced by 5, 15, 25 and 40% dietary galactose.

There was a significant rise in α-glycerophosphate in response to galactose followed by a decline to a steady value of 120% for all doses except the 40% galactose group which had a fall to 65% of baseline values. Choline phosphate decreased rapidly during all dose regimes, except in the 5% group, and remained constant after 2 weeks dosing. There was a significant decrease in ATP when the histological damage had progressed to the entire lens.[113]

4.3 Heart. – The applications of specific dynamic ^{13}C NMR methods to studies of myocardial pathophysiology have been reviewed.[114] A review has been produced with 36 references on the alterations in myocardial energetics observed in failing hearts of small animal models using ^{31}P NMR in combination with chemical assays.[115]

A new system for the metabolic investigation of the isolated perfused rat heart has been developed. The novel two surface-coil probe was combined with a dual perfusion system which allows spectra to be collected independently from the two coronary beds of the heart. The technique has been demonstrated in an experiment where ^{31}P NMR spectra were collected from a perfused rat heart in which the septum and right ventricle were made ischaemic whilst the left ventricle wall was fully perfused.[116] Spatially localised *in vivo* ^{31}P NMR and ^{1}H MRI have been used to measure mean murine myocardial PCr/ATP ratios of 2.0 ± 0.2 and left ventricular ejection fractions of $65 \pm 7\%$ at a physiological heart rate of approximately 600 beats min^{-1}.[117]

The systolic and diastolic concentration of intracellular Ca^{2+} ($[Ca^{2+}]_i$) in the Langendorff-perfused ferret heart has been estimated using ^{19}F NMR and five fluorinated Ca-indicators. A newly synthesised indicator, 1,2-bis-[2-bis-(carboxymethyl)-amino-4,5-difluorophenoxy]ethane (4,5FBAPTA), with a low affinity (K_d 2950 nM) was used to estimate $[Ca^{2+}]_i$ and the measurements were compared to those obtained using the following indicators which cover a range of affinities: 1,2-bis-[2-(1-carboxyethyl)(carboxymethyl)amino-5-fluorophenoxy]ethane (DiMe-5FBAPTA), 1,2-bis-[2-(1-carboxyethyl)(carboxymethyl)amino-4-fluorophenoxy]ethane (DiMe-4FBAPTA), 1,2-bis-[2-bis(carboxymethyl)amino-5-fluorophenoxy]ethane (5FBAPTA) 1,2-bis-[2-bis(carboxymethyl)amino-5-fluoro-4-methylphenoxy]ethane (MFBAPTA). The positive correlation observed between the indicator K_d and the end-diastolic and peak systolic $[Ca^{2+}]_i$ was used to estimate the unperturbed end-diastolic and peak-systolic $[Ca^{2+}]_i$ by extrapolation. The results agreed well with values measured in single cells and muscle strips.[118] ^{31}P NMR has been used to measure the level of ATP in the perfused rat heart in a study of the relationship between total and free intracellular Mg^{2+}.[119]

The effects of hypertonic perfusion during hypoxia has been investigated in the Langendorff-perfused rabbit heart. During 60 min of control hypoxia (295 mosM), Na^+_i rose from 22 to 100 meq kg dry $weight^{-1}$ whilst $[Ca^{2+}]_i$ rose from 347 to 1306 nM. In hearts perfused with 325 mosM buffer the increases in Na^+_i and Ca^{2+}_i were reduced by 65 and 60%, respectively. Hypertonic perfusion also diminished Na^+ uptake after normoxic acidification by 87%.[120] The role of creatine kinase (CK), high energy phosphates and Ca^{2+}-influx in

the genesis of myocardial injury in the rat heart compared to that in the hamster heart. Isolated hearts were perfused in the Langendorff mode at 37 °C for 30 min with normal Tyrode, for 15 min with Ca^{2+}-free Tyrode and then reperfused for 30 min with normal Tyrode. In the rat heart, ^{31}P NMR measured a decrease in HEP with 1 min of Ca^{2+}-reperfusion, a massive release of CK and a significant rise in Ca^{2+}-influx. However, in the hamster heart there was a preservation of HEP, no CK release and no rise in ^{45}Ca-influx upon reperfusion.[121]

The effects of regional ischaemia in the Langendorff-perfused pig heart on the uptake of K^+ has been investigated using Rb^+ as a K^+ congener; hearts were loaded with Rb^+ either prior to, or after, ischaemia. The uptake of Rb^+ was monitored by ^{87}Rb NMR and MRI and ^{31}P NMR was used to measure changes in high energy phosphates. Ischaemia resulted in infarction in the anterior wall and, at the end of reperfusion, the rate-pressure product and oxygen consumption rate decreased by 58 ± 10 and $74 \pm 4\%$ of there pre-ischaemic values, respectively. The levels of PCr and ATP and, pH_i decreased to 59 ± 17, $32 \pm 6\%$ and 6.7 ± 0.36 pH units, respectively. Ischaemia and reperfusion decreased the relative flux of Rb^+ in the anterior wall and increased the relative flux of Rb^+ in the posterior wall.[122] The methods of Rb^+-loading, in conjunction with ^{87}Rb NMR, have been used to investigate the response of the pig heart to 120 min of ischaemia and 60 min of reperfusion in a second study which also examined the Langendorff-perfused rat heart.[123] ^{23}Na and ^{31}P NMR have been used to assess the effects of trimetazidine on isovolumetric rat hearts following no-flow or low-flow ischaemia. During low-flow ischaemia trimetazidine caused a significant reduction in intracellular acidosis whereas in no-flow trimetazidine reduced the increase in Na^+_i. Furthermore, trimetazidine caused an attenuation of the accumulation of Na^+_i during early reperfusion, though this attenuation also occurred when hearts were perfused with glucose but not with palmitate.[124]

The mechanism by which the inhibition of Na^+/H^+ exchange by HOE642 (cariporide) improves post-ischaemic recovery of cardiac function has been investigated using ^{31}P NMR. Left ventricular developed pressure (LVDP) and end diastolic pressure were measured in isolated perfused rat hearts subjected to 30 min of non-flow ischaemia and 30 min of reperfusion with or without HOE642 15 min prior to ischaemia. Pre-ischaemic mechanical function, $[Ca^{2+}]$ and pH were unaffected by HOE642, though mechanical function after 30 min of reperfusion was improved. End-ischaemic $[Ca^{2+}]$ was lower in HOE642-treated hearts and the maximal Ca^{2+}-overload during the first 60 s of reperfusion was attenuated. The pH at the end of ischaemia was unaltered by the presence of HOE642 although re-alkalinization was delayed in the next three minutes.[125] The effects of 1-*cis*-diltiazem, diltiazem or niphedipine on the energy metabolism of the isolated guinea pig heart during 30 min ischaemia and 30 min reperfusion has been investigated with ^{31}P NMR. LVDP was decreased less by exposure to 10 mM 1-*cis*-diltiazem than exposure to 3 mM diltiazem or 500 nM niphedipine before ischaemia. Furthermore, 1-*cis*-diltiazem preserved ATP and attenuated the increase in end-diastolic pressure

during ischaemia and reperfusion and restored LVDP after reperfusion. Hearts treated with 1-*cis*-diltiazem or diltiazem had a higher pH_i at the end of ischaemia compared to niphedipine-treated or control hearts.[126] The interaction of β-adrenergic and insulin receptors in the regulation of $[Mg^{2+}]_i$ has been investigated with ^{31}P NMR in the rat heart. The separation of the α-ATP and β-ATP peaks was used to calculate the $[Mg^{2+}]_i$ using the dissociation constant of MgATP of 87 μM. In hearts perfused with phosphate-free Krebs–Henseleit buffer the $[Mg^{2+}]_i$ was approximately 0.2 mM. Insulin at physiological and pathological concentrations increase $[Mg^{2+}]_i$ and contractility in a dose dependent manner. When insulin was administered at >100 μM cm^{-3} it blocked the decrease in $[Mg^{2+}]_i$ caused by the administration isoprenaline and this effect of insulin was blocked by a protein kinase C inhibitor. Furthermore, isoprenaline caused a decrease in ATP in the heart and this effect was reduced by the administration of insulin.[127]

The effects of hydrogen peroxide on cardiac function and metabolism have been investigated in the Langendorff-perfused heart with ^{31}P and ^{19}F NMR. Exposure to 200–400 μmol dm^{-3} for 8 min resulted in a transient depression of LVDP and a delayed elevation of left ventricular end-diastolic pressure after the washout of hydrogen peroxide. The initial phase of dysfunction correlated with the accumulation of sugar phosphates and treatment with glibenclamide attenuated the initial depression of LVDP. The delayed elevation of end-diastolic pressure correlated with the total ATP depletion which was paralleled by the increase in $Ca^{2+}{}_i$ detected *via* a ^{19}F-labelled indicator.[128] ^{13}C NMR has been used to measure isotope kinetics in the neonate and adult rabbit heart. Hearts, oxidising 2.5 mM [2,4-^{13}C]butyrate, were subjected to either normal or high cytosolic redox state (2.5 mM lactate) to evaluate the recruitment of malate–aspartate activity and the resulting 2-oxyglutarate-malate carrier (OMC) flux. During development from neonate to adult, mitochondrial protein density in the heart increased from 19 ± 3 to 31 ± 2% whereas OMC expression decreased by 65% per mitochondrial protein content; the OMC flux was lower in adults by 76%. However, the responsiveness of the malate–aspartate shuttle to increase cytosolic NADH was similar in adults and neonates with an approximate increase in OMC flux of threefold.[129] Isolated perfused hearts from mice lacking the genes for the main muscle isoform of creatine kinase (M-CK) or lacking the genes for M-CK and the main mitochondrial isoform (Mt-CK) have been investigated with ^{31}P NMR. Developmental changes in the foetal isoform of creatine kinase (BB-CK) were unaffected by loses in the other isoenzymes. In hearts lacking M-CK and Mt-CK, the rate of synthesis of ATP from PCr was only 9% of that from oxidative phosphorylation; the intrinsic activities of the BB-CK and the M-CK isoforms were found to be equivalent. Furthermore, the combined loss of M-CK and Mt-CK prevented an increase in the amount of free energy released from ATP hydrolysis when pyruvate was provided as a substrate.[130] The influence of ATP compartmentation and ATP-Pi exchange on the forward CK-flux (F_f) and reverse CK flux (F_r) has been investigated in the isovolumetric perfused rat heart. The F_f should equal the F_r under steady state conditions, however,

when the effects of ATP-Pi exchange were masked by saturation of Pi, the ratio F_f/F_r was 0.80 ± 0.06 and 1.32 ± 0.06 when PCr or ATP was inverted, respectively. This discrepancy could be explained by a compartment of ATP not accessible to CK; under medium work loads this represents 20–33% of cellular ATP.[131]

The workload dependencies of the rate of oxygen consumption and changes in metabolic parameters in the Langendorff-perfused rat heart have been investigated with ^{31}P NMR. Measurement of metabolic changes during the transition from perfusion with glucose to perfusion with pyruvate showed an increase in PCr and its stability at increased work loads. In hearts without an active creatine kinase system there was a twofold decrease in the maximal developed tension and respiration rates. Data were analysed by a mathematical model of compartmentalised energy transfer which is independent of the classical concept of creatine kinase equilibrium.[132] The potential for a mechanism, mediated by substrate dependent proton production and pH_i, for the improved recovery of post-ischaemic hearts following stimulation of pyruvate dehydrogenase (PDH) has been investigated in the isolated rabbit heart. Stimulation of PDH was achieved by exposure to dichloroacetate (DCA) and pH_i was measured by ^{31}P NMR. When lactate was present during reperfusion, the effects of DCA on the recovery of the rate-pressure product were not supported nor was the effects of DCA on the recovery of pH_i to normal values.[133]

The effects of resveratol on the phosphate metabolism and contractility of the isolated Langendorff-perfused rat heart exposed to 20 min of no-flow ischaemia followed by 30 min of reperfusion have been investigated with ^{31}P NMR. During resveratol pretreatment basal phosphorylation potential dropped by 40% without affecting contractility; the level of effluent adenosine was increased by 65% in conjunction with a 50% increase in coronary flow. Furthermore, resveratol significantly improved post-ischaemic recovery of rate-pressure product.[134] The effects of angiotensing converting enzyme inhibitor temocaprilat and angiotensin II type 1 receptor antagonist CV-11974 on myocardial metabolism and contraction during ischaemia and reperfusion has been investigated with ^{31}P NMR in the Langendorff-perfused rabbit heart. Temocaprilat and/or CV-11974 were administered 40 min prior to 15 min of global ischaemia followed by 60 min of reperfusion. The presence of either or both drugs resulted in a significant inhibition of the overshoot of PCr during reperfusion compared to controls and a significant inhibition of decrease in ATP during ischaemia. Furthermore, the presence of CV-11974 with or without temocaprilat caused an early recovery of ATP during reperfusion compared to the other groups.[135]

The effects of ischaemic preconditioning on hexose transport has been investigated in the Langendorff-perfused heart. Four cycles of 5 min of ischaemia followed by 5 min of reperfusion was used to precondition the hearts prior to measurement of 2DG uptake detected by ^{31}P NMR measurements of the accumulation of 2-deoxy-glucose-6-phosphate (2DG6P). In preconditioned hearts, the accumulation of 2DG6P was greater than that in

control perfused heart. Wortmannin, an inhibitor of phosphatidylinositol 3-kinase, did not affect 2DG6P accumulation in preconditioned hearts; however, treatment with SB202190, an inhibitor of p38 MAP kinase, did. Furthermore, SB202190 did not affect 2DG6P accumulation in control hearts.[136] The role of the sarcoplasmic reticulum in ischaemic preconditioning has been investigated in the isolated rat heart. Treatment with 0.1 μM ryanodine or 50 μM cyclopiazonic acid was shown to eliminate the ability of the sarcoplasmic reticulum to accumulate calcium and caused a reduction of developed pressure by 75% and 59%, respectively. Following ischaemia the recovery of LVDP was greater in all hearts subjected to ischaemic preconditioning compared to their controls. However, exposure to ryanodine or cyclopiazonic acid did not cause any significant changes in the ATP and PCr content of the heart or the recovery of ATP and PCr following ischaemia.[137]

The contrast agent manganese dipyridoxyl diphosphate, normally used for obtaining contrast in MRI of the liver has been assessed for a possible role in investigation of coronary disease. The contrast agent normally releases Mn^{2+} when it is metabolised in the liver but was found to release Mn^{2+} in the isolated guinea pig heart perfused at a normal flow rate. Tissue manganese levels rose from 4.1 to 70.4 μmol 100 g^{-1} dry weight under normal conditions but, only rose to 16.6 μmol 100 g^{-1} dry weight in low flow ischaemia; T1 shortening closely paralleled myocardial Mn^{2+} elevations.[138] The effects of 30 min of graded low flow ischaemia and reperfusion have been investigated in the rat heart. At 69, 38 and 10% of coronary flow rate LVDP dropped to 71, 43 and 25% of pre-ischaemic values, respectively, without an increase in diastolic tone; LVDP returned to $92 \pm 3\%$ after 30 min of reperfusion. At 69, 38 and 10% coronary flow rate cytosolic phosphorylation potentials decreased from 74 ± 10 mM^{-1} to 40 ± 6, 25 ± 4 and 14 ± 4, respectively. Furthermore, lactate efflux increased and glycogen content decreased during under-perfusion.[139] The ADC of water, taurine and creatine have been measured during perfusion, ischaemia and reperfusion in the isolated rat heart. The values obtained were 1.06×10^{-3} mm^2 s^{-1}, 0.29×10^{-3} mm^2 s^{-1} and 0.26×10^{-3} mm^2 s^{-1} for water, taurine and creatine, respectively. Although the ADC for water and taurine remained constant during ischaemia, the ADC for creatine increased by 35% due to the hydrolysis of PCr to creatine. The average cardiomycete diameter was 40 μm in the perfused heart and 27 μm at the end of ischaemia.[140]

The effects of L-arginine on energy metabolism and coronary vessel function of ischaemic and reperfused rabbit myocardium have been investigated with ^{31}P NMR. Langendorff-perfused rabbit hearts were subjected to 180 min of ischaemia at 15° and then reperfused for 60 min at 37°. When L-arginine was added to the cardioplegia solution, coronary flow rate during reperfusion, ATP and PCr were improved.[141]

4.4 Liver. – The detailed mapping of glucose and lactate metabolism along the radius of the hepatic lobule has been investigated *in situ* in rat livers perfused with 1.5 mM lactate before and during perfusion with 5 mM fructose.

The majority of fructose was taken in the periportal region and 45% of this was converted into glucose. Periportal lactate uptake was markedly decreased by the addition of glucose. Basal perivenous lactate output, derived from glucose synthesised periportally, was increased in the presence of fructose. During fructose infusion there was a small decrease in cell pH periportally, but there was an acidification of up to 0.5 pH units perivenously. ^{31}P NMR showed that the concentration of PME changed very little periportally during fructose infusion, but there was an approximate twofold increase perivenously.[142] The presence of glucose and glucose-6-phosphate has been detected in the liver using ^{13}C NMR at 7 T following an infusion of [1-^{13}C]glucose. Partially resolved low-field shoulders of the glucose C1 resonances at 96.86 ppm (C1β) and 93.02 ppm (C1α) were detected.[143] The metabolism of [1-^{13}C] and [3-^{13}C]alanine has been followed with ^{13}C NMR *in vivo* and *in vitro* in the fasted and normal rat liver. The enrichment of the alanine pool was estimated to be 11% from L-alanine and 70% from D-alanine. Labelled alanine entered the TCA cycle mainly *via* pyruvate carboxylase. The ratio of flux from PEP through PEP kinase compared to the flux from PEP to Glc was approximately 42%.[144] The effects of 1,4-dideoxy-1,4-imino-D-arabinitol have been investigated on preparations of glycogen phosphorylase and in the liver of C57BL6J (ob/ob) mice using ^{13}C NMR.[145]

The effects of fatty acids (FA) on the liver carried by egg-lecithin liposomes (LIPO) compared to fatty acids carried by bovine serum albumin (BSA) has been investigated by ^{31}P and ^{13}C NMR. The ATP content decreased slowly, and the ATP turnover was similar, in livers perfused with saline or LIPO. However, LIPO induced an enhancement of the respiratory control ratio in isolated mitochondria. Tissue glycogen and glucose content decreased when FA (linoleate or linolenate) was perfused with BSA or LIPO, though glucose excretion was unchanged and lactate excretion tended to increase. Furthermore, FA carried by LIPO caused a dramatic fall in ATP, mitochondrial uncoupling and impairment of the phosphorylation activity, whereas perfusion with FA carried by BSA increased ATP degradation without affecting mitochondrial function.[146] ^{31}P NMR three-dimensional chemical shift imaging has been used to investigate metabolic changes in the rat liver at 1, 2 and 3 weeks post-ligation of the common bile duct. Quantification of metabolites was performed using an external standard. There were no significant changes in NTP levels relative to controls though, pH was significantly elevated at 2 and 3 weeks post-ligation.[147] The use of ^{31}P NMR as a tool for determining the safest period for chemotherapy after 70% hepatectomy has been investigated in adult male Fischer rats. In rats subjected to resection the ATP content of the liver fell 37% whereas in animals treated with 2′-deoxy-5-fluorouridine (100 mg kg^{-1} i.p. four times per day for 5 days) the fall in nucleotide levels was only 17%.[148] Cyclosporine, a specific inhibitor of mitochondrial permeability transition pore opening, has been used on a model of perfused rat liver to investigate whether mitochondrial dysfunction is linked to organ dysfunction. Liver energetics were monitored using ^{31}P NMR and mitochondrial functions were studied using top down control analysis. Ischaemia was not responsible for mitochon-

drial damage whereas reperfusion caused organ dysfunction and mitochondrial dysfunction which were prevented by cyclosporine.[149]

4.5 Muscle. – The diffusion of ATP and PCr in rat skeletal muscle has been measured using ^{31}P NMR. The spectra were optimised for the highest signal-to-noise of ATP by using a frequency selective stimulated echo sequence in combination with adiabatic RF pulses and surface coil acquisition. The variation of the ADC with time was used to assess the diffusion restriction with orientation effects eliminated by determining the trace of the diffusion tensor. When data were fitted to a cylindrical restriction model the unbounded diffusion coefficients were around 90% of their values *in vitro* and the diameters of the cylindrical restriction compartments were 16 and 22 μm for ATP and PCr, respectively; the diameters of rat skeletal muscle fibres are known to range from 60 to 80 μm.[150] The relationship between free cytosolic [ADP] and [Pi], and steady-state aerobic muscle work has been investigated in the rat gastrocnemius muscle stimulated at 0.1, 0.2, 0.3, 0.4, 0.5, 0.8. 1.0 and 2.0 Hz. In parallel experiments glycogen, lactate, pyruvate and total creatine were measured in freeze clamped muscles stimulated for 10 min. When muscle were stimulated by up to 0.5 Hz there was no significant change glycogen, lactate or the pyruvate/lactate ratio but at 0.8 Hz there was a 17% fall in glycogen, a 65% rise in lactate and a concomitant fall in pH. Above this frequency of stimulation glycogen fell rapidly, lactate continued to rise and ATP and pH declined. The results showed that calculated free ADP, Pi and tension time followed a Hill relationship with at least a second order function.[151] ^{1}H magnetisation transfer studies have been carried out on the hindleg muscle of wild type and transgenic mice, lacking cytoplasmic CK and/or mitochondrial CK. The magnetisation transfer effect was similar in wild type and the two single knock-out muscle types and slightly reduced in the tissue lacking both isoforms; ^{31}P NMR showed no off-resonance magnetisation transfer effects. The CK reaction flux was 0.2–0.3 s^{-1} in wild-type muscle and muscle deficient in the mitochondrial isoform whilst CK flux was negligible in the other two groups.[152]

A combination of ^{31}P and ^{13}C NMR has been used to assess mitochondrial energy coupling in skeletal muscle of awake rats to investigate the effects of increased levels of UCP13, a recently cloned uncoupling protein. ^{13}C NMR was used to determine rates of mitochondrial substrate oxidation and ^{31}P NMR was used to measure the unidirectional rate of ATP synthesis in control, 10-day triiodo-L-thyronine treated and 2,4-dinitrophenol treated rats. Following treatment with triiodo-L-thyronine, UCP13 mRNA and protein levels increased by 8.1-fold and 2.8-fold, respectively. The rates of TCA cycle flux were measured to be 61 ± 21, 148 ± 25 and 310 ± 48 nmol g^{-1} min^{-1} in control, triiodo-L-thyronine-treated and DNP-treated groups, respectively. The unidirectional rates of ATP synthesis flux were 83 ± 14, 84 ± 14 and 73 ± 7 nmol g^{-1} s^{-1} in control, triiodo-L-thyronine-treated and DNP-treated groups, respectively.[153] The effects of 48 h fasting on the energy coupling in the skeletal muscle of the rat has also been investigated using measurements of

TCA cycle flux and the unidirectional rate of ATP synthesis made by ^{13}C and ^{31}P NMR, respectively. However, there were no differences observed between fasted and fed rats despite a two- to threefold increase in UCP13 mRNA.[154]

The effects of different ion-transport inhibitors on the rate of pH recovery during hypercapnia, on energy turnover and on steady-state acid-base variables have been investigated in the body wall musculature of the marine worm *Sipunculus nudus* using ^{31}P NMR and oxygen consumption analysis. During acute hypercapnia recovery of pH_i was delayed at extracellular pH (pH_e) 7.5 compared with that at pH_e 7.9. Inhibition of Na^+/H^+ exchange with 5-(*N*,*N*-dimethyl)amiloride at pH_e 7.5 delayed recovery even further though this effect was much smaller at pH_e 7.9. However, inhibition of anion exchange by 4,4′-diisothiocyanatostilbene-2,2′-disulfonic acid prevented pH recovery at pH_e 7.5 and delayed recovery at pH_e 7.9.[155]

4.6 Smooth Muscle. – ^{31}P NMR has been used to assess the effects of smooth muscle energy state and pH_i on pulmonary arterial tone during hypoxia. Hypoxia caused early transient contraction followed by relaxation and late sustained contraction; there was a decrease in the energy state and pH_i during relaxation which recovered towards control values during late contraction. In femoral arterial rings, however, there was a higher energy state and lower pH_i in baseline conditions and no late contraction nor recovery of the energy state and pH_i during hypoxia. In glucose-free conditions, late contraction and the recovery of energy state and pH_i was abolished in pulmonary artery rings, though endothelial denudation abolished only late hypoxic contraction.[156] The influence of energy metabolism on contraction of porcine carotid artery smooth muscle has been investigated with ^{31}P NMR and, in parallel experiments, with tissue mechanics. During long-term contractions, linear and logarithmic regression analysis found the order of correlation with force to be highest for Pi, followed by pH, free energy, PCr, ATP, ADP and free Mg^{2+}.[157]

4.7 Tumour. – A review on the use of ^{19}F NMR for the study of fluoropyrimidine metabolism has been produced with 131 references.[158]

The effects of methotrexate and trimetrexate on the uptake and anabolism of 5FU has been assessed with ^{19}F NMR. In the Novikoff hepatoma both modulators increased the production of cytotoxic anabolites from 5FU. However, higher amounts of anabolites were produced and the peak level of anabolites was earlier following methotrexate pretreatment compared to trimetrexate pretreatment. The effects of the modulators on the metabolism of 5FU were also studied in excised samples of the Walker Carcinoma.[159] ^{19}F NMR has been used to assess the effects of carbogen (95% O_2–5% CO_2) breathing of the uptake and metabolism of 5-fluorouracil (5FU) in C38 murine colon tumours grown in C57B1/6 mice. Carbogen breathing started 1 min prior to the administration of 5FU and increased the level of the drug, its catabolites and its anabolites in the tumour; the maximum value being twofold higher compared to controls. However, no effect of carbogen breathing on the inhibition of tumour growth was observed.[160] The release of 5FU from a

glucuronic acid-conjugated carbamate derivative has been detected in two human colon tumour transplanted into nude mice.[161]

The metabolism and biochemical changes of C6 glioma spheroids in the right caudate nucleus of 15 rats has been investigated with PRESS ^{1}H NMR. Peaks for NAc, Cho, tCr, Glu/Gln, lipid and lactate were observed in control rats. The presence of C6 glioma caused a decrease in NAc reflected in a decrease of NAc/Cho and NAc/tCr. Furthermore, there was an increase in Cho/tCr and lactate.[162] In a study of the effects of bryostatin-1 on paclitaxel-induced tumour growth, mitotic entry and blood flow, ^{31}P NMR has been used to asses the impact of the drug on tumour energetics. It was found a dose of 80 μg kg^{-1} bryostatin-1 caused a decrease in pH_i and HEP.[163] ^{31}P NMR has been used to measure changes in the phosphorous metabolites of xenografted human hypopharynx carcinoma in an investigation of the predictability of response of the tumour to radiotherapy. Tumours were treated with 15 or 30 Gy and ^{31}P spectra were collected before treatment and 24, 48, 72 and 120 h after. Although treatment with 30 Gy induced increases in the PDE peak and decreases in the PME peak, no correlation was found between any change in the spectra and growth delay resulting from therapy.[164] The effects of chemotherapy with 1,3-bis(2-chloroethyl)-1-nitrosourea on subcutaneously implanted 9L gliomas have been investigated with ^{31}P NMR, single quantum (SQ) ^{23}Na NMR to measure total tissue sodium and triple-quantum-filtered (TQF) ^{23}Na NMR to measure Na^{+}_{i}. There were no differences observed in tumour size or spectral data from treated and untreated tumours one day after chemotherapy. Five days after therapy, treated tumours had 28 ± 16% lower SQ ^{23}Na signal intensity, 46 ± 20% lower TQF ^{23}Na intensity, a higher ATP/Pi ratio, a higher PCr/Pi ratio and a higher pH_i of 0.17 units.[165]

4.8 Whole Animal. – A review has been produced on metabolic and hormonal changes caused by irradiation. The article, which has 48 references, assesses the role of NMR in animal studies.[166]

Parameters of pH regulation and energy metabolism have been studied with ^{31}P NMR in three White Sea *Littorina* species (*L. littorea, L. saxatilis* and *L. obtusata*) during prolonged anaerobiosis in fresh water. Intracellular pH decreased significantly, especially during the early period of anaerobiosis, with the most rapid decrease in the least freshwater resistant species. The buffering capacities of the organisms were measured from tissue homogenates to further examine the mechanism of pH regulation.[167] The biosynthesis of alanine, and its incorporation into fibroin, has been investigated in the larvae of *Samia cynthia ricini* using multinuclear NMR. The incorporation of ^{13}C from [2-^{13}C]acetate into alanine C2 and C3, and glycine C2 of fibroin, along with the incorporation of the label into glutamate and glutamine, was observed *in vivo*.[168] The uptake and metabolism of 2DG in the filarial parasite *Acanthocheilonema viteae* using ^{31}P NMR. An unusually long retention time of 2DG6P was observed along with decreased ATP levels. When the therapeutic value of 2DG-treatment was investigated in infected *Mastomys coucha* there was an 73.6% activity against adult worms with 50% of surviving female worms being sterile.[169]

5 Clinical Studies

A review of cellular mechanisms of insulin resistance has been produced with 46 references.[170] The use of NMR to study glycogen in exercise has been reviewed with many references.[171] The quantification of the contribution of gluconeogenesis to glucose production in fasted human subjects, using stable isotopes and NMR, has been reviewed with 72 references.[172] A review of the use of magnetic resonance imaging and spectroscopy in biomedicine has been produced with 180 references.[173] The beginnings and later applications of NMR for clinical studies has been reviewed with 18 references.[174]

5.1 Brain. – An historical review of developments in the field of cerebral blood flow and metabolism has been produced with 34 references.[175] The use of NMR and magnetic resonance imaging in the study of function and dysfunction in the neonatal brain has been reviewed with 40 references.[176] The potential of ^{1}H and ^{31}P NMR in the assessment of cerebral metabolism in experimental models and human hydrocephalus has been reviewed with 110 references.[177] A review of the applications of ^{13}C-labelling to studies of the human brain has been produced with 90 references.[178] The detection of choline-containing phospholipids in acute and chronic neurodegeneration has been reviewed with 231 references.[179] The role of ^{1}H and ^{31}P NMR in the study of schizophrenia has been reviewed in two parts.[180,181] A review of the use of NMR in the study of phenylketonuria has been produced with 26 references[182] and comments on the text have also been published.[183]

In a study of the availability of central benzodiazepine receptors ^{1}H NMR has been used to measure changes in the brains of chronic alcoholics compared to age-matched controls. The mean (combined glutamine–glutamate peak)/tCr (Glx/tCr) ratio was significantly increased and the mean Cho/tCr ratio was significantly decreased in all areas of the brains of alcoholics, though the NAc/tCr ratio was unaffected. The spectroscopy results reflected the cerebral derangement associated with hepatic encephalopathy. Measurements, using positron emission tomography and ^{11}C-flumazenil, indicated an increase in the benzodiazepine receptor availability in the cortex, cerebellum and basal ganglia in patients compared to controls.[184] ^{1}H NMR has been used to investigate the neurobiological basis for alcohol-associated brain abnormalities in short-term and long-term abstinent alcoholics. Absolute concentrations of NAc, Cho, mI and tCr were determined in the anterior centrum semiovale, anterior cingulate gyrus and right thalamus of the two groups. Recently detoxified alcoholics had significantly higher mI in the thalamus compared with controls and long-term abstinent alcoholics and had significantly higher mI in the anterior cingulate gyrus compared with controls.[185]

Regional glucose metabolism, measured using 2-deoxy-2-[^{18}F]fluoro-glucose PET, and the concentration represented by the Glx peak, measured by ^{1}H NMR, have been investigated in multiple brain regions of 11 patients with medically intractable partial epilepsy. Studies were performed in the interictal state in seven patients and in the ictal/periictal state in four patients. Lower

glucose metabolism and lower Glx concentrations were found in the epileptic focus than in the contralateral normal cortex in patients in the interictal state, whereas higher glucose metabolism and higher Glx concentrations were found in the epileptic focus of the four patients studied in the ictal/periictal state. A significant correlation was found between Glx concentration and glucose utilisation in all brain regions.[186] ^{1}H spectroscopic imaging has been used to determine the distribution of metabolites along the long axis of the hippocampus in 14 control subjects and 9 patients with unilateral mesial temporal lobe epilepsy. There was a significantly lower ratio of NAc/(tCr+Cho) in the anterior compared to the posterior part of the hippocampus in control subjects. A similar change in the NAc/(tCr+Cho) ratio was seen over the ipsilateral and contralateral hippocampus in patients. However, the NAc/(tCr+Cho) ratio in the hippocampus of patients was reduced by 17% ipsilateral and 10% contralateral.[187] The levels of phenylalanine (Phe) in the brains of patients with phenylketonuria have been assessed with ^{1}H NMR. An abnormal concentration of Phe (determined from the ratio of Phe/tCr) was detected in all ten subjects investigated. However, there was a wide range of Phe detected in the plasma. In late detected subjects brain Phe concentration correlated better with clinical phenotype than did plasma Phe concentrations.[188]

^{1}H NMR has been used to compared the spectra from a voxel containing lesions, compared to normal-appearing white matter (NAWM), in primary-progressive (PP) and secondary-progressive (SP) multiple sclerosis patients. Resonances for NAc, tCr and Cho were detected in an 8 cm^3 voxel in the parieto-occipital region of 17 PP, 18 SP and 17 control subjects. There were significant reductions in NAc and the ratio of NAc/Cho in the PP-lesion, SP-lesion, PP-NAWM and SP-NAWM groups compared to controls.[189] The ratio of Cho/tCr has been shown to recover (increase) in the frontal and thalamic areas in Cushing's syndrome patients following correction for hypercotisolism. No change was observed in the ratio of NAc/tCr and no variation in the NAc, tCr and mI ratios relative to water was detected.[190] ^{1}H NMR spectroscopic imaging has been used to characterise unidentified T2 hyperintense lesions observed by magnetic resonance imaging in nine male patients with neurofibromatosis type 1. The distributions of Cho, NAc, and tCr were calculated in four axial 15 mm slices. Absolute metabolite concentrations within the hyperintense regions, the unaffected globus pallidus and thalami showed elevated Cho and preserved NAc in younger subjects and normal Cho and reduced NAc in older subjects. Significant decreases in NAc were only found in the thalami of patients with hyperintense regions in the globus pallidus.[191] The absolute concentrations of NAc, tCr and Cho in the subcortical white matter of the motor region in 16 patients with motor neuron disease (8 with bulbar onset and 8 with limb onset) have been measured with ^{1}H NMR. No differences were detected in metabolite concentrations of the patients compared to those detected in controls, however, there was significantly higher tCr in the bulbar-onset group compared to the limb-onset group.[192]

^{1}H NMR has been used to measure the metabolite levels in the centrum semiovale of patients with unilateral steno-occlusive carotid artery disease with

no cortical infarction. Regional blood flow, regional metabolic rate of oxygen ($rCMRO_2$) and regional oxygen extraction fraction (rOEF) of the cerebral cortex were measured by the steady-state method with ^{15}O gas and PET. The asymmetry index (ipsilateral compared to contralateral results) of the ratio of NAc/tCr correlated positively with the asymmetry index of $rCMRO_2$. The asymmetry index of Cho/tCr showed a significant positive correlation with the asymmetry index of rOEF; all but one patient showed an increase in rOEF of the ipsilateral cortex.[193] ^1H NMR has been used to examine the parietal grey and white matter of 30 patients with Alzheimer disease. There were no differences observed in the concentrations of NAc, tCr, Cho, mI, Glu, Gln or lactate found in the brains of patients compared to control subjects. Furthermore, the were no differences found between patients with early onset of the disease compared to those with late onset.[194] A two-dimensional chemical shift imaging technique has been used to characterise changes in brain metabolites during therapy for disseminated nocardiosis in an AIDS patient. Prior to treatment, a rise in the Cho/tCr ratio and a decrease in the NAc/tCr ratio were observed in the left anteromedial centrum semiovale. After 16 weeks of treatment the patient had recovered, showing no cerebral abscesses with MRI, and the spectra had returned to normal.[195]

^1H NMR has been used to measure NAc, Cho, tCr, mI and Glx in the frontal lobe and basal ganglia of subjects with familial schizophrenia, family members with mixed psychiatric diagnoses, unaffected family members and community controls. A negative correlation with age was observed for NAc, Cho, NAc, tCr and Glx in the frontal lobe. A subject with schizophrenia had a significant reduction in the ratio of NAc/Cho in the left frontal lobe compared with unaffected family members and community controls.[196] Measurements of the metabolite levels in the lenticular nuclei of 10 patients with simple schizophrenia have been made with ^1H NMR. Compared to 10 age-matched controls there were no differences in the ratios of Cho/tCr, NAc/tCr and NAc/Cho. Quantification of signals demonstrated a normal variation in the level of Cho, tCr and NAc in all patients.[197]

^1H NMR has been used to measure metabolite levels in the dorsolateral prefrontal area of the brain in patients with bipolar disorder. The ratios of NAc, Cho and mI to tCr were measured in bilateral 8 cm^3 voxels in 20 bipolar patients and 20 age- and gender-matched controls. The ratio of NAc/tCr was found to be lower in both hemispheres of patients compared to control subjects.[198] The levels of NAc in the brains of 21 adult subjects (12 medication-free bipolar affective disorder patients and 9 controls) have been measured with ^1H NMR. An increase in NAc content was observed following 4 weeks of Li^+ treatment. This increase was observed in all regions studied, including the frontal, temporal, parietal and occipital lobes.[199]

The ratios of NAc/tCr and NAc/(tCr+Cho) in the right and left thalami have been measured in 11 treatment-naive, non-depressed obsessive-compulsive disorder outpatients (8 to 15 year old) and 11 control subjects. A significant reduction in the ratios of NAc/tCr and NAc/(tCr+Cho) were observed in the right and left medial thalami in patients compared to control.

Furthermore, there was no difference in the ratios of NAc/tCr and NAc/(tCr+Cho) between the right and left medial thalami of control subjects, but reductions in the NAc level in the left thalamus in patients was inversely correlated with increase obsessive-compulsive disorder symptom severity.[200] The levels of NAc, aspartate, Cho, Glu, Gln, GABA, mI, glucose and lactate have been measured in 8 cm^3 voxels in the thalamus, cingulate, insula, sensorimotor, dorsolateral prefrontal and orbital frontal cortices in the left hemisphere of 16 healthy volunteers. Measurements were analysed in relation to anxiety, measured by the State-Trait Anxiety Inventory, and showed a relationship between anxiety and chemical composition of the orbital frontal cortices; high anxiety subjects showed a 32% increase in overall chemical concentrations within the orbital frontal cortices. Other brain regions showed no detectable anxiety dependence and the level of NAc in the orbital frontal cortices was identified as the strongest marker for anxiety.[201] ^{1}H NMR has been used to examine the hippocampus of seventeen patients receiving electroconvulsive therapy. No changes in the level of NAc were observed after electroconvulsive therapy, though a significant increase of 16% of the signal from Cho was observed after five or more treatments.[202] ^{1}H NMR has been used to examine the anterior cingulate cortex and the parietal white matter in 19 patients with major depressive episodes and 18 age-matched controls. Absolute concentrations for NAc, Cho, tCr, mI, Glx and Glu were estimated but a significant result was only found for a decrease in Glx in the anterior cingulate for depressed patients. If only severely depressed patients were considered then Glx and Glu showed a significant decrease.[203]

Changes in the metabolites of the hippocampus with age have been studied in 24 healthy adults from 36 to 85 years of age. Consistent with previous studies, MRI detected a 20% decrease in the size of the hippocampus with age. The ratio of NAc/Cho decreased by 24%, NAc/tCr decreased by 26%, whereas Cho/tCr remained constant.[204] The multi-chemical profile of the brain has been compared between 19 young adults and 16 middle-aged normal subjects across multiple brain regions for all metabolites of the ^{1}H NMR spectra relative to the level of tCr. For all subjects the concentration of metabolites was greatest in the prefrontal cortex. Middle-aged subjects were found to have significantly reduced total metabolite levels in the dorsolateral prefrontal, orbital frontal and sensorimotor cortices compared with younger subjects. Other brain regions showed no age-dependent differences.[205] The effects of fast repetitive off-resonance irradiation on the ^{1}H NMR resonances of the metabolites in the white matter has been investigated in 10 healthy young volunteers. A magnetisation transfer attenuation factor of 0.87 ± 0.05 was observed for the methyl resonances of tCr. However, the resonances of NAc, Cho, mI or Glx showed no attenuation.[206] The levels of GABA in the brains of 36 healthy volunteers have been detected using a J-resolved, two-dimensional ^{1}H NMR method. The concentrations of GABA in a 12 cm^3 voxel in the occipital lobe were measured to be 1.01 ± 0.36 μmol cm^{-3} for males and 1.1 ± 0.63 μmol cm^{-3} for females, respectively, without corrections for T1 and T2 effects.[207]

A mathematical model has been used to determine the metabolic rates in human grey and white matter from ^{13}C isotopic labelling data from ^{1}H-observed/^{13}C-edited NMR. Spectra were obtained from 22.5 cm^3 and 56 cm^3 voxels located in the grey and white matter, respectively. When partial volume affects were ignored the measured rate of the TCA cycle was 0.72 ± 0.22 and 0.29 ± 0.09 μmol min^{-1} g^{-1} in voxels of 70% grey and 70% white matter, respectively. After correction for partial volume effects the rate of the TCA cycle was 0.80 ± 0.10 μmol min^{-1} g^{-1} in grey matter and 0.17 ± 0.01 in white matter.[208] In a separate study the mean values of the TCA cycle rate were 0.88 ± 0.12 μmol min^{-1} g^{-1} in the occipital grey matter and 0.28 ± 0.13 μmol min^{-1} g^{-1} in the occipital white matter.[209]

^{1}H NMR has been used to measure brain alcohol levels and relaxation parameters in 20 light-drinking subjects administered 0.85 g k^{-1} ethanol; blood and breath alcohol concentrations were also obtained. The measured ^{1}H NMR relaxation times were shorter than given in previous reports and the brain alcohol signal decreased by 30% on application of on- or off-resonance saturation pulses. ^{1}H NMR measurements of brain alcohol concentration correlated highly with blood and breath concentrations after equilibration of alcohol in the brain.[210] Spectroscopic imaging has been used to determine the value of T2 of ethanol in the human brain. A frequency-selective refocusing pulse was used to suppress J-modulation of the ethanol triplet so that non-integral values of 1/J could be used for TE. The measured T2 values for the methyl resonances of ethanol, creatine and NAc in a mixture of grey and white matter were 82 ± 12, 148 ± 20 and 227 ± 25 ms, respectively.[211] The presence of methyldisulfonylmethane has been detected in the human brain following ingestion of the compound in a dietary supplement. The concentration of the compound was found to be 2.4 mM and the concentration of major metabolites of the brain (NAc, tCr Cho and mI) were found to be within normal limits.[212] ^{1}H NMR has been used to measure pH_i from the chemical shift of histidine following oral loading of 400 mg kg^{-1} 4–7 h prior to measurements.[213] ^{19}F NMR has been used to measure the pharmacokinetics of fluvoxamine and fluoxetine-norfluoxetine in the brains of patients treated for depression. The steady-state concentration of fluvoxamine in the brain was 12 μM and the brain-to-plasma concentration ratio was ten; similar results were seen for fluoxetine-norfluoxetine. The elimination half-life of fluvoxamine from the brain was 79 h whereas that for fluoxetine-norfluoxetine was 382 h.[214]

5.2 Heart. – The measurement of ATP, creatine and phosphocreatine by NMR in relation to energy metabolism of the heart in patients with cardiovascular diseases has been reviewed with 20 references.[215]

5.3 Liver. – ^{13}C NMR has been used to measure hepatic glycogen concentrations of young, lean type 1 diabetic and matched non-diabetic subjects in a study of the effects of acute improvement of metabolic control. Rates of net glycogen synthesis and breakdown were calculated from linear regression of the glycogen concentration time curves from 7:30 to 10:30 pm and from 10:30

pm to 8:30 am, respectively. In diabetic subjects the mean plasma glucose concentration was 2.4-fold higher and the rates of net glycogen synthesis and net glycogen breakdown were reduced by 74% and by 47%, respectively. During short-term intensified insulin treatment, the mean plasma glucose concentration in diabetic subjects was not different to that in controls, and net glycogen synthesis and breakdown was increased by 92% and 40%, respectively.[216] The mechanism by which metformin reduces endogenous glucose production in type 2 diabetes has been investigated inpatients before and after three months of metformin treatment. Rates of net hepatic glycogenolysis were estimated using ^{13}C NMR spectroscopy and the combined contribution of glycogenolysis and gluconeogenesis to glucose production was estimated from labelling of blood glucose from ingested $^{2}H_2O$. The rate of glucose production in diabetes was twice that found in controls but was reduced by 24% following treatment with metformin. The rate of gluconeogenesis was threefold higher in the diabetic subjects and metformin treatment reduced that by 36%. However, when the $^{2}H_2O$ method was used to estimate gluconeogenesis there was a twofold increase in the rate which was decreased by 33% following metformin treatment.[217]

5.4 Muscle. – The use of ^{31}P NMR in the study of human skeletal muscle has been reviewed with 68 references.[218] A review of the insights into muscle diseases gained from ^{31}P NMR has been reviewed with 166 references.[219]

The proximal histidyl $N_{\sigma}H$ signal from myoglobin (Mb) has been monitored during dynamic exercise whilst data was collected from NIRS. As the level of work increased an increase in Mb was observed and there was a linear relationship between Mb and oxygen consumption; a decrease in PCr and an increase in Pi was also observed. The results showed that NIRS reflected the oxygenation status of Mb not Hb.[220] A previously unassigned peak in the ^{1}H NMR spectra of human muscle has been assigned to the acetyl group of acetylcarnitine. Results of the application of ^{1}H NMR to several muscles under different exercise regimes were found to be in agreement with previous invasive measurements of acetylcarnitine.[221]

^{31}P NMR has been used to investigate the effects of two weeks of 21 g day^{-1} creatine supplementation on the kinetics of PCr metabolism during 50 plantar flexion extensions against weights. A surface coil placed under the calf muscle was used to record spectra at rest and during 1 min of either 40 or 70% maximal voluntary contractions (MVC) separated by 10 min rest in fourteen healthy male subjects. Creatine supplementation increased resting muscle PCr by 20% and increased PCr depletion by 15 and 10% during 40 and 70% MVC exercises, respectively. No change was observed in PCr repletion or the half-life of PCr repletion.[222] ^{31}P NMR has been used to measure the effect of creatine supplementation on energy metabolism during repeated plantar flexion isometric exercise at 32 ± 1 and 79 ± 4% of MVC. Resting muscle PCr increased from 18.3 ± 0.9 to 19.6 ± 1.0 mmol kg^{-1} wet weight after 9 days of 5 g day^{-1} creatine supplementation. At 79% of MVC, the changes in PCr, Pi and pH were similar after 4 days and 11 days of creatine supplementation.

However, PCr utilisation, Pi accumulation and pH acidification were lower after 9 days compared to 4 days supplementation during 32% of MVC.[223]

The effects of caffeine (6 mg kg^{-1}) on muscle glycogen consumption has been investigated with ^{13}C NMR in 20 muscle glycogen-loaded subjects exercising for 2 h at 65% of their maximal oxygen consumption; muscle glycogen content was increased to 140% above normal values on the trial day. After cycling for 2 h caffeine was associated with a greater plasma lactate, adrenaline and cortisol though, plasma free fatty acids increased and muscle glycogen decreased to the same extent in the caffeine-treated and control groups. Plasma β-endorphin levels were, however, almost doubled in the caffeine-treated group.[224] The effects of glycogen loading on the post-exercise recovery of muscle glycogen has been investigated with natural abundance ^{13}C and ^{31}P NMR. A seven day carbohydrate loading program was used to increase muscle glycogen from 63.2 ± 2.8 to 99.3 ± 4.0 mmol dm^{-3}. Subjects performed plantar flexion exercise at 50% of maximum voluntary contraction, before and after the glycogen loading protocol, until muscle glycogen concentrations decreased by 50 mmol dm^{-3}. The rate of glycogen re-synthesis was more rapid in glycogen loaded muscle during the first 15 min post-exercise. However, during the following 45 min glycogen re-synthesis was highest in the non-glycogen-loaded muscle and this trend continued for the next four hours.[225] ^{1}H and ^{13}C NMR have been used to determine the intramyocellular glycogen and lipid utilisation during prolonged exercise and resynthesis during recovery. Subjects ran on a treadmill at sub-maximal intensity until exhaustion. At the time of exhaustion, glycogen depletion was twofold greater in calf than in thigh muscle, though a significant amount of glycogen was left in both muscle groups. The glycogen content of forearm muscle decreased to 73% during the initial 5 hours of recovery. During exercise, the intramyocellular lipid content of the soleus muscle decreased to 67%, but recovered to 83% during rest.[226] The mechanism by which muscle glycogen limits its own synthesis has been investigated with ^{31}P NMR to measure G6P accumulation and ^{13}C NMR to measure muscle glycogen levels. Seven healthy volunteers were subjected to a euglycaemic-hyperinsulinaemic clamp which resulted in a 65% increase in muscle glycogen, a twofold increase in fasting plasma lactate concentrations and an ~30% decrease in plasma free fatty acids concentrations. Furthermore, there was an approximate 30% decrease in the insulin stimulated rate of muscle glycogen synthesis which was associated with a twofold increase in the i.m. G6P concentration. Glycogen loading also resulted in an approximate 30% increase in whole body glucose oxidation though there was no effect on insulin stimulated rates of whole body glucose uptake or glycogen turnover.[227]

^{13}C and ^{31}P NMR have been used to assess the effects of troglitazone on glucose uptake and metabolism in type 2 diabetes. Seven subjects were examined under hyperglycaemic-hyperinsulinaemic clamp before and after 3 months treatment with troglitazone. The rate of insulin-stimulated whole body glucose uptake increased by $58 \pm 11\%$ after treatment and this increase was associated with a threefold increase in glucose oxidation and muscle glycogen synthesis. After treatment, muscle G6P concentrations increased during hyper-

glycaemic-hyperinsulinaemic clamp whereas there was no detected rise in the concentration of G6P before treatment.[228] The levels of $[Mg^{2+}]_i$ in the calf muscle in patients with kidney disease have been investigated with ^{31}P NMR. Although no differences were observed in the level of $[Mg^{2+}]_i$ in patients compared to controls, patients did have a slightly more acidic pH_i which was more pronounced in those patients with insulin resistance. Furthermore, patients had a lower ratio of ATP/Pi and a higher ratio of PCr/ ATP.[229] ^{31}P NMR has been used to examine the muscle of 15 patients with fibromyalgia and 17 healthy control subjects. Increases in PDE and Pi were observed with no difference in pH_i.[230]

5.5 Tumour. – The use of ^{19}F NMR in the measurement of the pharmacokinetics of fluorinated antimetabolites has been reviewed with 136 references.[231]

^{1}H NMR has been used to assess 27 patients with recurrent primary brain tumour. The maximum Cho/NAc ratio was determined for high grade glioma ($n = 10$), brainstem glioma ($n = 7$), medulloblastoma/peripheral neuroectodermal tumour ($n = 6$), ependymoma ($n = 3$) and pineal germinoma ($n = 1$). The maximum Cho/NAc ratio ranged from 1.1 to 13.2 in tumours and the ratio for each histological subtype varied considerably; however, the max Cho/NAc ratio was less than 1.0 in normal appearing brain. Patients with a maximum Cho/NAc ratio greater than 4.5 had a median survival of 22 weeks; those with a ratio of less than 4.5 had a projected survival of more than 50% at 63 weeks.[232]

6 References

1 Haase, A., Odoj, F., Von Kieln, M., Warnking, J., Fidler, F., Weisser, A., Nittka, M., Rommel, E., Lanz, T., Kalusche, B. and Griswold, M. *Concepts Magn. Reson.*, 2000, **12(6)**, 361–388.

2 Hentschel, M., Findeisen, M., Schmidt, W., Frenzel, T., Wlodarczyk, W., Wust, P. and Felix, R. *Magn. Reson. Mater. Phys., Biol. Med.*, 2000, **10(1)**, 52–59.

3 Niwayama, M., Hamaoka, T., Kime, R., Lin, L., Shao, J., Kudo, N., Katoh, C., Katsumura, T. and Yamamoto, K. *Ther. Res.*, 2000, **21(6)**, 1520–1523.

4 Kamba, M., Kimura, K., Koda, M. and Ogawa, T. *Am. J. Clin. Nutr.*, 2001, **73(2)**, 172–176.

5 de Graaf, A. A. *NMR Microbiol.*, 2000, 73–103. Eds. Barbotin, J.-N. and Portais, J-C., Horizon Scientific Press, Wymondham, UK.

6 Li, B. S. Y., Payne, G. S., Collins, D. J. and Leach, M. O. *Magn. Reson. Med.*, 2000, **44(1)**, 5–9.

7 Knijn, A., Casieri, C., Carpinelli, G., Testa, C., Podo, F. and De Luca, F. *NMR Biomed.*, 2000, **13(3)**, 124–128.

8 van der Veen, J. W. C., Weinberg, D. R., Tedeschi, G., Frank, J. A. and Duyn, J. H. *Radiology (Oak Brrok, Ill.)* 2000, **217(1)**, 296–300.

9 Henry, P.-G., Roussel, R., Vaufrey, F., Dautry, C. and Bloch, G. *Magn. Reson. Med.*, 2000, **44(3)**, 387–394.

10 Ebel, A., Dreher, W. and Leibfritz, D. *J. Magn. Reson.*, 1999, **142(2)**, 241–253.

11 Charagundla, S. R., Duvvuri, U., Noyszewski, E. A., Dandora, R., Stolpen, A. H., Leigh, J. S. and Reddy, R. *J. Magn. Reson.*, 2000, **143(1)**, 39–44.
12 Payne, G. S. and Leach, M. O. *Magn. Reson. Med.*, 2000, **43(4)**, 510–516.
13 Choi, I.-Y., Tkac, I. and Gruetter, R. *Magn. Reson. Med.*, 2000, **44(3)**, 387–394.
14 Watanabe, H., Ishihara, Y., Okamoto, K., Oshio, K., Kanamatsu, T. and Tsukada, Y. *Magn. Reson. Med.*, 2000, **43(2)**, 200–210.
15 Vicni, P. and Kushmerick, M. J. *Am. J. Physiol.*, 200, **79(1, Pt. 1)**, C213–C224.
16 Sherry, D. A. and Malloy, C. R. *Biol. Magn. Reson.*, 1998, **15**(In vivo Carbon-13 NMR), 59–97.
17 Chatham, J. C. and Chance, E. M. *Biol. Magn. Reson.*, 1998, **15**(In vivo Carbon-13 NMR), 99–116.
18 Hajek, M., Burian, M. and Dezortova, M. *Magn. Reson. Mater. Phys., Biol. Med.*, 2000, **10(1)**, 6–17.
19 Marshall, I., Bruce, S. D., Higinbotham, J., MacLullich, A., Wardlaw, J. M., Ferguson, K. J. and Seckl, J. *Magn. Reson. Med.*, 2000, **44(4)**, 646–649.
20 Schirmer, T. and Auer, D. P. *NMR Biomed.*, 2000, **13(1)**, 28–36.
21 Warne, M. A., Lenz, E. M., Osborn, D., Weeks, J. M. and Nicholson, J. K. *Biomarkers* 2000, **5(1)**, 56–72.
22 Serrai, H., Senhadji, L., Clayton, D. and De Certaines, J. D. *Spectrosc. Lett.*, 2000, **33(1)**, 47–67.
23 Serrai, H., Nadal-Desbarats, L., Poptani, H., Glickson, J. D. and Senhadji, L. *Magn. Reson. Med.*, 200, **43(5)**, 649–656.
24 Laughlin, M. R., Kelleher, J. K. *Biol. Magn. Reson.*, 1998, **15**(In vivo Carbon-13 NMR), 1–57.
25 Jeneson, J. A. L., Westerhoff, H. V. and Kuhmerick, M. J. *Am. J. Physiol.*, 2000, **79(3, Pt. 1)**, C813–C832.
26 Tian, J.-G., Xia, Z.-F. and Ye, C.-H. *Bopuxue Zazhi* 2000, **17(5)**, 419–425.
27 Widmaier, S., Jung, W.-I. Dietze, G. J. and Lutz, O. *Magn. Reson. Mater. Phys., Biol. Med.*, 1999, **9(1–2)**, 1–4.
28 Constanczak, P., Schafer, A., Sperner, J. and Gunther, T. *Magnesium-Bull.*, 2000, **22(1)**, 20–25.
29 Wary, C., Brillault-Salvat, C., Bloch, G., Leroy-Willig, A., Roumenov, D., Grognet, J.-M., Leclerc, J. H. and Carlier, P. G. *Br. J. Clin. Pharmacol.*, 1999, **48(5)**, 655–662.
30 Shetty, H. U. and Huang, W. *Curr. Org. Chem.*, 2000, **4(1)**, 1–17.
31 Govindaraju, V., Young, K. and Maudsley, A. A. *NMR Biomed.*, 2000, **13(3)**, 129–153.
32 Grucker, D. *Prog. Nucl. Magn. Reson. Spectrosc.*, 2000, **36(3)**, 241–270.
33 Robitaille, P.-M. L. *Biol. Magn. Reson.*, 1998, **15**(In vivo Carbon-13 NMR), 215–238.
34 Lewandowski, E. D. *Biol. Magn. Reson.*, 1998, **15**(In vivo Carbon-13 NMR), 117–159.
35 Murphy, P. S., Leach, M. O. and Rowland, I. J. *Magn. Reson. Med.*, 1999, **42(6)**, 1155–1158.
36 Pfeuffer, J., Tkac, I. and Gruetter, R. *J. Cereb. Blood Flow Metab.* 2000, **20(4)**, 736–746.
37 Gonen, O. and Grossman, R. I. *Magn. Reson. Imaging*, 2000, **18(10)**, 1255–1258.
38 Hsu, A. C. and Dawson, M. J. *Magn. Reson. Med.*, 2000, **44(3)**, 418–426.
39 Schneider, J., Fekete, E., Weisser, A., Neubauer, S. and Von Kienlin, M. *Magn. Reson. Med.*, 2000, **43(4)**, 497–502.

40 Vidal, G., Thiaudiere, E., Canioni, P. and Gallis, J.-L. *NMR Biomed.*, 2000, **13(5)**, 289–296.
41 Brecker, L. and Ribbons, D. W. *Trends Biotechnol.*, 2000, **18(5)**, 197–202.
42 Boyaval, P. and Deborde, C. *NMR Microbiol.*, 2000, 283–307.
43 Gemmecker, G. and Erni, B. *NMR Microbiol.*, 2000, 191–210.
44 Bouvet, O. M. M. and Rager, M.-N. *NMR Microbiol.*, 2000, 349–361.
45 De Graaf, A. *BIOspektrum*, 2000, **6(5)**, 370–373.
46 Son, T.-D. *NMR Microbiol.*, 2000, 105–153.
47 Grivet, J.-P. *NMR Microbiol.*, 2000, 27–46.
48 Shanks, J. V. *NMR Microbiol.*, 2000, 47–72.
49 Gosselin, I., Barbotin, J.-N. and Portais, J.-C. *NMR Microbiol.*, 2000, 331–348.
50 Vogel, H. J. and Lohmeier-Vogel, E. M. *NMR Microbiol.*, 2000, 309–330.
51 Gonzalez, B., De Graaf, A., Renaud, M. and Sahm, H. *Yeast*, 2000, **16(6)**, 483–497.
52 Kim, I. S., Barrow, K. D. and Rogers, P. L. *Appl. Biochem. Biotechnol.*, 2000, **84–86**, 357–370.
53 Neves, A. R., Ramos, A., Shearman, C., Gasson, M. J., Almeida, J. S. and Santos, H. *Eur. J. Biochem.*, 2000, **267(12)**, 3859–3868.
54 Deborde, C. and Boyaval, P. *Appl. Environ. Microbiol.*, 2000, **66(5)**, 2012–2020.
55 Rager, M. N., Binet, M. R. B., Lonescu, GH. and Bouvet, O. M. M. *Eur. J. Biochem.*, 2000, **267(16)**, 5136–5141.
56 Chia, B. C. S., Lam, Y.-H., Dyall-Smith, M., Separovic, F. and Bowie, J. H. *Lett. Pept. Sci.*, 2000, **7(3)**, 151–156.
57 Kuchel, P. W. and Mulquiney, P. J. *NATO Sci. Ser.*, 3 2000, **74**(Technological and Medical Implications of Metabolic Control Analysis), 139–145.
58 Kucherenko, Y. V. and Zinchenko, V. D. *Spectrosc. Biol. Mol.: New Dir., Eur. Conf., 8th*, 1999, Eds. Greeve, J., Puppels, G. J. and Otto, C. 457–458.
59 Lahajnar, G., Macek, P. and Zupancic, I. *Bioelectrochemistry*, 2000, **52(2)**, 179–185.
60 Murayama, A., Takemori, S. and Yamaguchi, M. *Jikeikai Med. J.*, 1999, **46(4)**, 199–207.
61 Cheng, Y., Li, Y., Li, R., Lu, J. and Wang, K. *Chem.-Biol. Interact.*, 2000, **125(3)**, 191–208.
62 Himmelreich, U., Emling, M., Drew, K. N., Seranni, A. S. and Kuchel, P. W. *Free Radical Biol. Med.*, 2000, **28(11)**, 1607–1610.
63 Zinchenko, V. D. *Probl. Kriobiol.*, 2000, **(1)**, 95–96.
64 Barbagallo, M., Gupta, R. K., Dominguez, L. J. Resnick, L. M. *J. Am. Geriatr. Soc.*, 2000, **48(9)**, 1111–1116.
65 Haumki, J. M. and Kauppinen, R. A. *Trends Biochem. Sci.*, 2000, **25(8)**, 357–362.
66 Brindle, K. M. and Haggie, P. M. *NATO Sci. Ser., 3*, 2000, **74**(Technological and Medical Implications of Metabolic Control Analysis), 191–198.
67 Ramos, A., Neves, A. R., Almeida, J. and Santos, H. *Quimica (Lisboa)*, 2000, **77**, 6–16.
68 Doliba, Nat. M., Babsky, A. M., Werhli, S. L., Doliba, Nic. M., Friedman, M. F. and Osbakken, M. D. *Biochemistry (Moscow)*, 2000, **65(4)**, 502–508.
69 Miccheli, A., Tomassini, A., Capuani, G., Di Cocco, M. E., Sartori, E., Falasca, L., Devirgiliis, L. C., Manetti, C. and Conti, F. *Cytotechnology*, 2000, **32(3)**, 219–228.

70 Zwingmann, C., Flogel, U., Pfeuffer, J. and Leibfritz, D. *Dev. Neurosci. (Basal)*, 2000, **22(5–6)**, 463–471.

71 Wehrle, J. P., Ng, C. E., McGovern, K. A., Aiken, N. R., Shungu, D. C., Chance, E. M. and Glickson, J. D. *NMR Biomed.*, 2000, **13(6)**, 349–360.

72 Mardor, Y., Kaplan, O., Sterin, M., Ruiz-Cabello, J., Ash, E., Roth, Y., Ringel, I. and Cohen, J. S. *Cancer Res.*, 2000, **60(18)**, 5179–5186.

73 Cruz, H. J., Freitas, C. M., Alves, P. M., Moreira, J. L. and Carrondo, M. J. T. *Enzyme Micro. Technol.*, 2000, **27(1–2)**, 43–52.

74 Viola, A., Lutz, N. W., Maroc, C., Chabannon, C., Julliard, M. and Cozzone, P. J. *Int. J. Cancer*, 2000, **85(5)**, 733–739.

75 Panov, V., Salomon, Y., Kabalka, G. W., Bendel, P. *Radiat. Res.*, 2000, **154(1)**, 104–112.

76 Kaplan, O., Firon, M., Vivi, A. Navon, G. and Tsarfaty, I. *Neoplasia 2000*, **2(4)**, 365–377.

77 Dreanno, C., Seguin, F., Cosson, J., Suquet, M. and Billard, R. *J. Exp. Zool.*, 2000, **286(5)**, 513–522.

78 Jones, A. R. and Bubb, W. A. *J. Reprod. Fertil.*, 2000, **119(1)**, 129–135.

79 Ford, Y., Ratcliffe, R. G. and Robins, R. J. *Physiol. Plant.*, 2000, **109(2)**, 123–128.

80 Mesnard, F., Azaroual, N., Marty, D., Fliniaux, M.-A., Robins, R. J., Vermeersch, G. and Monti, J.-P. *Planta*, 2000, **210(3)**, 446–453.

81 Gout, E., Aubert, S., Bligny, R., Rebeille, F., Nonomura, A. R., Benson, A. A. and Douce, R. *Plant Physiol.*, 2000, **123(1)**, 287–296.

82 Gruwel, M. L. H., Rauw, V. W., Loewen, M. and Abrams, S. R. *Plant Sci. (Shannon, Irel.)*, 2001, **160(5)**, 785–794.

83 Rolin, D., Baldet, P., Just, D., Chevalier, C., Biran, M. and Raymond, P. *Aust. J. Plant Physiol.*, 2000, **27(1)**, 61–69.

84 Shanks, J. V., Rijhwani, S. K., Morgan, J., Vani, S., Bhadra, R. and Ho, C-H. *Plant Cell Tissue Cult. Prod. Food Ingredients, [Proc. Symp.]*, 1997 (Pub. 1999), Eds. Fu, T.-J., Singh, G. and Curtis, W. R. 45–60.

85 Komor, E. Aust. J. *Plant Physiol.*, 2000, **27(6)**, 497–505.

86 McNeil, S. D., Rhodes, D., Russell, B. L., Nuccio, M. L., Shachar-Hill, Y. and Hanson, A. D. *Plant Physiol.*, 2000, **124(1)**, 153–162.

87 Espen, L., DerliOrto, M., De Nisi, P. and Zocchi, G. *Planta*, 2000, **210(6)**, 985–992.

88 Rasmussen, N., Lloyd, D. C. and Ratcliffe, R. G. *Plant Soil*, 2000, **226(2)**, 245–253.

89 Gerendas, J. and Ratcliffe, R. G. *J. Exp. Bot.*, 2000, **51(343)**, 207–219.

90 Nagarajan, S., Dijkema, C. and Van As, H. *Indian J. Exp. Biol.*, 2000, **38(5)**, 477–482.

91 Summers, J. E., Racliffe, R. G. and Jackson, M. B. *J. Exp. Bot.*, 2000, **51(349)**, 1413–1422.

92 Bequet, F., Peres, M., Gomez-Merino, D., Berthelot, M., Satabin, P. Pierard, C. and Guezennec, C. Y. *J. Appl. Physiol.*, 2000, **88(6)**, 1949–1954.

93 Sibson, N. R., Mason, G. F., Shen, J., Cline, G. W., Herskovits, A. Z., Wall, J. E. M., Behar, K. L., Rothman, D. L. and Shulman, R. G. *J. Neurochem.*, 2001, **76(4)**, 975–989.

94 Ferrante, R. J., Andreassen, O. A., Jenkins, B. G., Dedeoglu, A., Kuemmerle, S., Kubilus, J. K., Kaddurah-Daouk, R., Hersch, S. M. and Beal, M. F. *J. Neurosci.*, 2000, **20(12)**, 4389–4397.

95 Jenkins, B. G., Klivenyi, P., Kustermann, E., Andreassen, O. A., Ferrante, R. J., Rosen, B. R. and Beal, M. F. *J. Neurochem.*, 2000, **74(5)**, 2108–2119.

96 Heath, D. L. and Vink, R. *J. Clin. Neurosci.*, 1999, **6(6)**, 505–509.

97 Franke, C., Brinker, G., Pillekamp, F. and Hoehn, M. *J. Cereb. Blood Flow Metab.*, 2000, **20(3)**, 583–591.

98 Domingo, Z., Bradley, J. K., Blamire, A. M., Brindle, K., Styles, P. and Rajagopalan, B. *NMR Biomed.*, 2000, **13(3)**, 154–162.

99 Rolett, E. L., Azzawi, A., Liu, K. J., Yongbi, M. N., Swartz, H. M. and Dunn, J. F. *Am. J. Physiol.*, 2000, **279(1 Pt. 2)**, R9–R16.

100 Springett, R., Wylezinska, M., Cady, E. B., Cope, M. and Delpy, D. T. *J. Cereb. Blood Flow Metab.*, 2000, **20(2)**, 280–289.

101 Van Walsum, A.-M. van C., Heerschap, A., Nijhuis, J. G., Oeseburg, B. and Jongsma, H. W. *Am. J. Obstet. Gynecol.*, 1999, **181(6)**, 1537–1545.

102 Dardzinski, B. J., Smith, S. L., Towfighi, J., Williams, G. D., Vanucci, R. C. and Smith M. B. *Pediatr. Res.*, 2000, **48(2)**, 248–255.

103 Dijkhuizen, R. M., De Graaf, R. A., Garwood, M., Tulleken, K. A. F. and Nicolay, K. *J. Cereb. Blod Flow Metab.*, 1999, **19(4)**, 376–379.

104 Kekelidze, T., Khait, I., Togliatti, A. and Holtzman, D. *Dev. Neurosci. (Basal)*, 2000, **22(5–6)**, 437–443.

105 Semenova, N. A., Topchyan, A. V., Mirzoya, R. S., Konraov, A. A. and Balasanyan, M. G. *Bul. Exp. Biol. Med.*, 2000, **128(10)**, 987–990.

106 Roffman, J. I., Lipska, B. K., Bertolino, A., Van Gelderen, P., Olson, A. W., Khaing, Z. Z. and Weinberger, D. R. *Neuropsychopharmacology*, 2000, **22(4)**, 430–439.

107 Cudd, T. A., Wasser, J. S., Chen, W.-J. A. and West, J. R. *Alcohol.: Clin. Exp. Res.*, 2000, **24(6)**, 865–872.

108 Lee, W.-T., Lee, C.-S., Pan, Y.-L. and Chang, C. *Magn. Reson. Med.*, 2000, **44(1)**, 29–34.

109 Astore, A. and Boicelli, C. A. *Magn. Reson. Mater. Phys., Biol. Med.*, 2000, **10(3)**, 160–166.

110 Yoshioka, K., Nisimaru, N., Yanai, S., Shimoda, H. and Yamada, K. *Neurosci. Res. (Shannon, Irel.)*, 2000, **36(3)**, 215–226.

111 Hakumaki, J. M., Pirttila, T. R. M. and Kauppinen, R. A. *J. Cereb. Blood Flow Metab.*, 2000, **20(2)**, 405–411.

112 Duhamel, G., Choquet, P., Leviel, J.-L., Steibel, J., Lamalle, L., Julien, C., Kober, F., Grillon, E., Derouard, J., Decorps, M., Ziegler, A. and Constantinesco, A. *C. R. Acad. Sci., Ser. III*, 2000, **323(6)**, 529–536.

113 Sakagami, K., Igarashi, H., Tanaka, K., Yoshida, A. *Hokkaido Igaku Zasshi*, 1999, **74(6)**, 457–466.

114 Weiss, R. G. and Gerstenblith, G. *Biol. Magn. Reson.*, 1998, **15**(In vivo Carbon-13 NMR), 161–180.

115 Tian, R. and Ingwall, J. S. *Heart Failure Rev.*, 1999, **4(3)**, 245–253.

116 Garlick, P. B., Parkes, H. G. and Cave, A. C. *J. Mol. Cell. Cardiol.*, 2000, **32(5)**, 853–858.

117 Chacko, V. P., Aresta, F., Chacko, S. M. and Weiss, R. G. *Am. J. Physiol.*, 2000, **279(5, Pt. 2)**, H2218–H2224.

118 Kirschenlohr, H. L., Grace, A. A., Vandenberg, J. I., Metcalfe, J. C. Smith, G. A. *Biochem. J.*, 2000, **346(2)**, 385–391.

119 Fatholahi, M., LaNoue, K., Romani, A. and Scarpa, A. *Arch. Biochem. Biophys.*, 2000, **374(2)**, 395–401.

120 Ho, H. S., Liu, H., Cala, P. M. and Anderson, S. E. *Am. J. Physiol.*, 2000, **278(5, Pt. 1)**, C953–C964.
121 Ray, M., Roy, R., Chowdhury, P. D., Srivastava, S., Dubey, M. P. *Pharmacol. Res.*, 2000, **41(3)**, 361–367.
122 Kupriyanov, V. V., Xiang, B., Sun, J., Dai, G., Jilkina, O., Dao, V. and Deslauriers, R. *Magn. Reson. Med.*, 2000, **44(1)**, 83–91.
123 Kupriyanov, V. V., Xiang, B., Sun, J., Jilkina, O., Dai, G. and Deslauriers, R. *Magn. Reson. Med.*, 2000, **44(2)**, 193–200.
124 El Banni, H., Bernard, M., Baetz, D., Cabanes, E., Cozzone, P., Lucin, A. and Feuvray, D. *Cardiovasc. Res.*, 2000, **47(4)**, 688–696.
125 Stromer, H., De Groot, M. C. H., Horn, M., Faul, C., Leupold, A., Morgan, J. P., Scholz, W. and Neubauer, S. *Circulation*, 2000, **101(23)**, 2749–2755.
126 Sakamoto, K., Ishikawa, M., Koga, K., Urushidani, T. and Nagao, T. *Jpn. J. Pharmacol.*, 2000, **83(3)**, 225–232.
127 Amano, T., Matsubara, T., Watanabe, J., Nakayama, S. and Hotta, N. *Br. J. Pharmacol.*, 2000, **130(4)**, 731–738.
128 Masumoto, Y., Kaneko, M., Iimuro, M., Fujise, Y. and Hayashi, H. *Mol. Cell. Biochem.*, 2000, **204(1&2)**, 97–106.
129 Griffin, J. L., O'Donnell, J. M., White, L. T., Hajjar, R. J. and Lewandowski, E. D. *Am. J. Physiol.*, 2000, **79(6, Pt. 1)**, C1704–C1709.
130 Saupe, K. W., Spindeler, M., Hopkins, J. C. A., Shen, W. and Ingwall, J. S. *J. Biol. Chem.*, 2000, **275(26)**, 19742–19746.
131 Joubert, F., Gillet, B., Mazet, J. L., Mateo, P., Beloeil, J.-C. and Hoerter, J. A. *Biophys. J.*, 2000, **79(1)**, 1–13.
132 Dos Santos, P., Aliev, M. K., Diolez, P., Duclos, F., Besse, P., Bonoron-Adele, S. Sikk, P., Canioni, P. and Saks, V. *J. Mol. Cell. Cardiol.*, 2000, **32(9)**, 1702–1734.
133 Griffin, J. L., White, L. T. and Lewandowski, E. D. *Am. J. Physiol.*, 2000, **279(1, Pt. 2)**, H361–H367.
134 Bradamante, S., Piccinini, F., Barenghi, L., Bertelli, A. A. E., De Jonge, R., Beemster, P. and De Jong, J. W. *Int. J. Tissue React.*, 2000, **22(1)**, 1–4.
135 Kawabata, H., Rymoto, T. and Ishikawa, K. *Jpn. Circ. J.*, 2000, **64(4)**, 276–282.
136 Tong, H., Chen, W., London, R. E., Murphy, E. and Steenbergen, C. *J. Biol. Chem.*, 2000, **275(16)**, 11981–11986.
137 Cave A. C. and Garlic P. B. *J. Ml. Cell. Cardiol.*, 2000, **32(3)**, 415–417.
138 Brurok, H., Skogland, T., Berg, K., Skarra, S., Karlsson, J. O. G. and Jynge, P. *NMR Biomed.*, 1999, **12(6)**, 364–372.
139 Askenasy, N. J. *Mol. Cell. Cardiol.*, 2000, **32(5)**, 791–803.
140 Liess, C., Radda, G. K. and Clarke, K. *Magn. Reson. Med.*, 200, **44(2)**, 208–214.
141 Zhang, Z., Gu, C., Zhang, X., Yan, D. and Gu, T. *Zhongguo Yike Daxue Xuebao*, 2000, **29(1)**, 60–61.
142 Burns, S. P., Murphy, H. C., Iles, R. A., Bailey, R. A. and Cohen, R. D. *Biochem. J.*, 2000, **349(2)**, 539–545.
143 Kunnecke, B., Kustermann, E. and Seelig, J. *Magn. Reson. Med.*, 2000, **44(4)**, 556–562.
144 Dolle, A. *NMR Biomed.*, 2000, **13(2)**, 72–81.
145 Fosgerau, K., Westergaard, N., Quistorff, B., Grunnet, N., Kristiansen, M. and Lungren, K. *Arch. Biochem. Biophys.*, 2000, **380(2)**, 274–284.
146 Delmas-Beauvieux, M. C., Leducq, N., Thiaudiere, E., Diolez, P., Gin. H., Canioni, P. and Gallis, J. L. *Magn. Reson. Mater. Phys., Biol. Med.*, 2000, **10(1)**, 43–51.

147 Zakian, K. L., DAngelica, M., Matei, C., Yoo, H.-H., Ercolani, M., Delman, K., Fong, Y. and Koutcher, J. A. *Magn. Reson. Imaging*, 2000, **18(2)**, 181–187.

148 Koby, D. A., Zakian, K. L., Challa, S. N., Matei, C., Petrowsky, H., Yoo, H.-H., Koutcher, J. A. and Fong, Y. *Cancer Res.*, 2000, **60(14)**, 3800–3806.

149 Leducq, N., Delmas-Beauvieux, M.-C., Bourdel-Marchasson, I., Duour, S., Gallis, J.-L., Canioni, P. and Diolez, P. *Transplant Proc.*, 2000, **32(2)**, 479–480.

150 De Graaf, R.A; Van Kranenburg, A. and Nicolay, K. *Biophys. J.*, 2000, **78(4)**, 1657–1664.

151 Cieslar, J. H. and Dobson, G. P. *J. Biol Chem.*, 2000, **275(9)**, 6129–6134.

152 Kruiskamp, M. J., Van Vliet, G. and Niolay, K. *Magn. Reson. Med.*, 2000, **43(5)**, 657–664.

153 Jucker, B. M., Dufour, S., Ren, J., Cao, X., Previs, S. F., Underhill, B., Cadman, K. S. and Shulman, G. I. *Proc. Natl. Acad. Sci. USA*, 2000, **97(12)**, 6880–6884.

154 Jucker, B., Ren, J., Dufour, S., Cao, X., Previs, S. F., Cadman, K. S. and Shulman, G. I. *J. Biol. Chem.*, 2000, **275(50)**, 39279–39286.

155 Portner, H. O., Bock, C. and Reipschlager, A. *J. Exp. Biol.*, 2000, **203(16)**, 2417–2428.

156 Leach, R. M., Sheehan, D. W., Chacko, V. P. and Sylvester, J. T. *Am. J. Physiol.*, 2000, **278(2, Pt. 1)**, L294–L304.

157 Dillon, P. F. *J. Vasc. Res.*, 2000, **37(6)**, 532 539.

158 Martino, R., Malet-Martino, M. and Gilard, V. *Curr. Drug Metab.*, 2000, **1(3)**, 271–303.

159 Katzir, I., Shani, J., Wolf, W., Chatterjee-Parti, S. and Berman, E. *Cancer Invest.*, 2000, **18(1)**, 20–27.

160 Kamm, Y. J. L., Heerschap, A. and Wagener, D. J. T. *Eur. J. Cancer*, 200, **36(9)**, 1180–1186.

161 Guerquin-Kern, J.-L., Volk, A., Chenu, E., Lougerstay-Madec, R., Monneret, C., Florent, J.-C., Carrez, D. and Croisy, A. *NMR Biomed.*, 2000, **13(5)**, 306–310.

162 Yin, H., Huang, Z., Li, L., Liu, M. and Zhao, H. *Disi Junyi Daxue Xuebao*, 2000, **21(4)**, 433–436.

163 Koutcher, J. A., Motwani, M., Zakian, K. L., Li, X.-K., Matei, C., Dyke, J. P., Ballon, D., Yoo, H. H. and Schwartz, G. K. *Clin. Cancer Res.*, 2000, **6(4)**, 1498–1507.

164 Jackel, M. C., Kopf-Maier, P., Baumgart, F., Ziessow, D. and Tausch-Treml, R. *J. Cancer Res. Clin. Oncol.*, 2000, **126(6)**, 325–331.

165 Winter, P. M., Poptani, H. and Bansal, N. *Cancer Res.*, 2001, **61(5)**, 2002–2007.

166 Ahlers, I. *NATO Sci. Ser., 2*, 1999, **55**(Fundamentals for the Assessment of Risks from Environmental Radiation), 389–394.

167 Sokolova, I. M., Bock, C. and Portner, H.-O. *J. Comp. Physiol., B*, 2000, **170(2)**, 105–115.

168 Osanai, M., Okudaira, M., Naito, J., Demura, M. and Asakura, T. *Insect Biochem. Mol. Biol.*, 2000, **30(3)**, 225–232.

169 Shukla-Dave, A., Roy, R., Bhaduri, A. P. and Chatterjee, R. K. *Physiol. Chem. Phys. Med. NMR*, 2000, **32(1)**, 1–12.

170 Shulman, G. I. *J. Clin. Invest.*, 2000, **106(2)**, 171–176.

171 Price, T. B., Rothman, D. L. and Shulman, R. G. *Proc. Nutr. Soc.*, 1999, **58(4)**, 851–859.

172 Landau, R. *Proc. Nutr. Soc.*, 1999, **58(4)**, 963–972.

173 Raghunathan, P. *PINSA – A: Proc. Indian Natl. Sci. Acad., Part A*, 1999, **65(6)**, 699–729.
174 Ross, B. D. *IUBMB Life*, 2000, **50(3)**, 177–187.
175 Sokoloff. L. *Keio Univ. Symp. Life Sci. Med.*, 2000, **6**(Ischemic Blood Flow in the Brain), 3–10.
176 Cooper, C. E. and Wyatt, J. S. *Biochem. Soc. Trans.*, 2000, **28(2)**, 121–126.
177 Braun, K. P. J., Vandertop, W. P., Gooskens, R. H. J. M., Tulleken, K. A. F. and Nicolay, K. *Neurol. Res.*, 2000, **22(1)**, 51–64.
178 Mason, G. F. *Biol. Magn. Reson.*, 1998, **15**(In vivo Carbon-13 NMR), 181–214.
179 Klein, J. *J. Neural Transm.*, 2000, **107(8–9)**, 1027–1063.
180 Stanley, J. A., Pettegrew, J. W. and Keshavan, M. S. *Biol. Psychiatry*, 2000, **48(5)**, 357–368.
181 Keshavan, M. S., Stanley, J. A. and Pettegrew, J. W. *Biol. Psychiatry*, 2000, **48(5)**, 369–380.
182 Moller, H. E., Ullrich, K. and Weglage, J. *Eur. J. Pediatr.*, 2000, **159(Suppl. 2)**, S121–S125.
183 Kreis, R. *Eur. J. Pediatr.*, 2000, **159(Suppl. 2)**, S126–S128.
184 Jalan, R., Turjanski, N., Taylor-Robinson, S. D., Koepp, M. J., Richardson, M. P., Wilson, J. A., Bell, J. D. and Brooks, D. J. *Gut*, 2000, **46(4)**, 546–552.
185 Schweinsburg, B. C., Taylor, M. J., Videen, J. S., Alhassoon, O. M., Patterson, T. L. and Grant, I. *Alcohol.: Clin. Exp. Res.*, 2000, **24(5)**
186 Pfund, Z., Chugani, D. C., Juhasz, C., Muzik, O., Chugani, H. T., Wilds, I. B., Seraji-Bozorgzad, N. and Moore, G. J. *J. Cereb. Blood Flow Metab.*, 2000, **20(5)**, 871–878.
187 Vermathen, P., Laxer, K. D., Matson, G. B., Weiner, M. W. *Radiology (Oak Brook, Ill.)*, 2000, **214(2)**, 403–410.
188 Leuzzi, V., Bianchi, M. C., Tosetti, M., Carducci, C. L., Carducci, C. A. and Antonozzi, I. *J. Inherited Metab. Dis.*, 2000, **23(6)**, 563–570.
189 Cucurella, M. G., Rovira, A., Rio, J., Pedraza, S., Tintore, M.-M., Montalban, X. and Alonso, J. *NMR Biomed.*, 2000, **13(2)**, 57–63.
190 Khiat, A., Bard, C., Lacroix, A. and Boulanger, Y. *Brain Res.*, 2000, **862(1, 2)**, 301–307.
191 Wang, P. Y., Kaufmann, W. E., Koth, C. W., Denckla, M. B. and Barker, P. B. *Ann. Neurol.*, 2000, **47(4)**, 477–484.
192 Ellis, C. M., Simmons, A., Glover, A., Dawson, J. M., Williams, S. C. R. and Leigh, P. N. *Amylotrophic Lateral Scler. Other Mot. Neuron Disord.*, 2000, **1(2)**, 123–129.
193 Tsuchida, C., Kimura, H., Sadato, N., Tsuchida, T., Tokuriki, Y. and Yonekura, Y. *J. Nucl. Med.*, 2000, **41(8)**, 1357–1362.
194 Stoppe, G., Bruhn, H., Pouwels, P. J. W., Hanicke, W. and Frahm, J. *Alzheimer Dis. Assoc. Disord.*, 2000, **14(2)**, 112–119.
195 Marcus, C. D., Taylor-Robinson, S. D., Cox, I. J., Sargentoni, J. and Shaunak, S. *Metab. Brain Dis.*, 1999, **14(4)**, 231–237.
196 Block, W., Bayer, T. A., Tepest, R., Traber, T. F., Rietschel, M., Muller, D. J., Schulze, T. G., Honer, W. G., Maier, W., Schild, H. H. and Falkai, P. *Neurosci. Lett.*, 2000, **289(2)**, 147–151.
197 Ohara, K., Isoda, H., Suzuki, Y., Takehara, Y., Ochiai, M., Takeda, H., Hattori, K., Igarashi, Y. and Ohara, K. *Prog. Neuro-Psychopharmacol. Biol. Psychiatry*, 2000, **24(4)**, 507–519.

198 Winsberg, M. E., Sachs, N., Tate, D. L., Adalsteinsson, E., Spielman, D. and Ketter, T. A. *Biol. Psychiatry*, 2000, **47(6)**, 475–481.
199 Moore, G. J., Bebchuk, J. M., Hasanat, K., Chen, G., Seraji-Bozorgzad, N., Wilds, I. B., Faulk, M. W., Koch, S., Glitz, D. A., Jolkovsky, L. and Manji, H. J. *Biol. Psychiatry*, 2000, **48(1)**, 1–8.
200 Fitzgerald, K. D., Moore, G. J., Paulson, L. A., Stewart, C. M. and Rosenberg, D. R. *Biol. Psychiatry*, 2000, **47(3)**, 174–182.
201 Grachev, I. D. and Apkarian, A. V. *Mol. Psychiatry*, 2000, **5(5)**, 482–488.
202 Ende, G., Braus, D. F., Walter, S., Weber-Fahr, W. and Henn, F. A. *Arch. Gen. Psychiatry*, 2000, **57(10)**, 937–943.
203 Auer, D. P., Putz, B., Kraft, E., Lipinski, B., Schill, J. and Holsboer, F. *Biol. Psychiatry*, 2000, **47(4)**, 305–313.
204 Schuff, N., Amend, D. L., Knowlton, R., Norman, D., Fein, G. and Weiner, M. W. *Neurobiol. Aging*, 1999, **20(3)**, 279–285.
205 Grachev, I. D. and Apkarian, A. V. *J. Neurochem.*, 2001, **76(2)**, 582–593.
206 Helms, G. and Frahm, J. *NMR Biomed.*, 1999, **12(8)**, 490–494.
207 Ke, Y., Cohen, B. M., Bang, J. Y., Yang, M. and Renshaw, P. F. *Psychiatry Res.*, 2000, **100(3)**, 169–178.
208 Mason, G. F., Pan, J. W., Chu, W.-J., Newcomer, B. R., Zhang, Y., Orr, Rt. and Hetherington, H. P. *J. Cereb. Blood Flow Metab.*, 1999, **19(11)**, 179–1188.
209 Pan, J. W., Stein, D. T., Telang, F., Lee, J. H., Shen, J., Brown, P., Cline, G., Mason, G. F., Shulman, G. I., Rothman, D. L. and Hetherington, H. P. *Magn. Reson. Med.*, 2000, **44(5)**, 673–679.
210 Fein, G., Meyerhoff, D. J. *Alcohol.: Clin. Exp. Res.*, 2000, **24(8)**, 1227–1235.
211 Sammi, M. K., Pan, J. W., Telang, F. W., Schuhlein, D., Molina, P. E., Volkow, N. D., Springer, C. S. and Hetherington, H. P. *Magn. Reson. Med.*, 2000, **44(1)**, 35–40.
212 Rose, S. E., Chalk, J. B., Galloway, G. J. and Doddrell, D. M. *Magn. Reson. Imaging*, 2000, **18(1)**, 95–98.
213 Vermathen, P., Capizzano, A. A. and Maudsley, A. A. *Magn. Reson. Med.*, 2000, **43(5)**, 665 -675.
214 Bolo, N. R., Hode, Y., Nedelec, J.-F., Laine, E., Wagner, G. and Macher, J.-P. *Neuropsychopharmacology*, 2000, **23(4)**, 428–438.
215 Clark, J. F. *Med. Sci. Symp. Ser.*, 2000, **4**(Creatine), 25–32.
216 Bischof, M. G., Krssak, M., Krebs, M., Bernroider, E., Stingl, H., Waldhausl, W. and Roden, M. *Diabetes*, 2001, **50(2)**, 392–398.
217 Hundal, R. S., Krssak, M., Dufour, S., Laurent, D., Lebon, V., Chandramouli, V., Inzucchi, S. E., Schumann,W. C., Petersen, K. F., Landau, B. R. and Shulman, G. I. *Diabetes*, 2000, **49(12)**, 2063–2069.
218 Heerschap, A., Houtman, C., In't Zandt, H. J. A., Van den Bergh, A. J. and Wieringa, B. *Proc. Nutr. Soc.*, 1999, **58(4)**, 861–870.
219 Agrov, Z., Lofberg, M. and Arnold, D. L. *Muscle Nerve*, 2000, **23(9)**, 1316–1334.
220 Jue, T., Tran, T. K., Mole, P., Chung, Y., Sailasuta, N., Hurd, R., Kreutzer, U. and Kuno, S. *Adv. Exp. Med. Biol.*, 1999, **471**(Oxygen Transport to Tissue XXI), 289–294.
221 Kreis, R., Jung, B., Rotman, S., Slotboom, J. and Boesch, C. *NMR Biomed.*, 1999, **12(7)**, 471–476.
222 Francaux, M., Demeure, R., Goudemant, J-F. and Poortmans, J. R. *Int. J. Sports Med.*, 2000, **21(2)**, 139–145.
223 Rico-Sans, J. *J. Appl. Physiol.*, 2000, **88(4)**, 1181–1191.

224 Laurent, D., Schneider, K. E., Prusaczyk, W. K., Franklin, C., Vogel, S. M., Krssak, M., Petersen, K. F., Goforth, H. W. and Shulman, G. I. *J. Clin. Endocrinol. Metab.*, 2000, **85(6)**, 2170–2175.

225 Price, T. B., Laurent, D., Petersen, K. F., Rothman, D. L. and Shulman, G. I. *J. Appl. Physiol.*, 2000, **88(2)**, 698–704.

226 Krssak, M., Petersen, K. F., Bergeron, R., Price, T., Laurent, D., Rothman, D. L., Roden, M. and Shulman, G. I. *J. Clin. Endocrinol. Metab.*, 2000, **85(2)**, 748–754.

227 Laurent, D., Hundal, R. S., Dresner, A., Price, T. B., Vogel, S. M., Petersen, K. F. and Shulman, G. I. *Am. J. Physiol.*, 2000, **278(4, Pt. 1)**, E663–E668.

228 Petersen, K. F., Krssak, M., Inzucchi, S., Cline, G. W., Dufour, S. and Shulman, G. I. *Diabetes*, 2000, **49(5)**, 827–831.

229 Sebekova, K., Stefikova, K., Krivosikova, Z. and Spustova, V. *Bratisl. lek. Listy*, 1999, **100(8)**, 411–416.

230 Sprott, H., Rzanny, R., Reichenbach, J. R., Kaiser, W. A., Hein, G. and Stein, G. *Rheumatology (Oxford)*, 2000, **39(10)**, 1121- 1125.

231 Wolf, W., Presant, C. A. and Walunch, V. *Adv. Drug Delivery Rev.*, 2000, **41(1)**, 55–74.

232 Warren, K. E., Frank, J. A., Black, J. L., Hill, R. S., Duyn, J. H., Aikin, A. A., Lewis, B. K., Adamson, P. C. and Balis, F. M. *J. Clin. Oncol.*, 2000, **18(5)**, 1020–1026.

13
Nuclear Magnetic Resonance Imaging

BY TOKUKO WATANABE

1 Introduction

NMR is successfully used in physics, chemistry, and biology to explore and characterize chemical reactions, molecular conformations, biochemical pathways, solid state materials and many other applications that elucidate invisible characteristics of matter and tissue. Recently, however, magnetic resonance methods, including magnetic resonance imaging (MRI), magnetic resonance spectroscopy (MRS), magnetic resonance spectroscopic imaging (MRSI) and functional magnetic resonance imaging (fMRI), have been used for the assessment of materials and *in vivo* subjects mentioned above. The number of papers concerning NMR imaging is increasing more and more in a variety of fields. This review is a continuation of the last five years[1] and covers the progress in the field of NMR imaging (NMRI), NMR microimaging or microscopy over a period from June 2000 to May 2001, based on papers recorded in the CA Select Proton Magnetic Resonance and Carbon & Heteroatom NMR. The topics were limited to mainly basic and technical aspects and the non-clinical research field, such as physicochemical, biological, physiological, pharmaceutical, geological, environmental and industrial applications carried out by employing a high-resolution NMR machine or a horizontal MRI machine for animal use.

In this period, development of functional magnetic resonance imaging (fMRI) has made marked progress. Brain blood flow and metabolites have long been subjects of great interest. The MRI-based functional brain imaging has become the most popular, quantitative method applicable to unanesthetized animals and man. The number of papers is increasing. Investigations of functional activity associated with administration of CBS-active drug were recently developed as phamacological MRI or neurophamacological fMRI. Optically pumped ^{129}Xe has received a great deal of attention because of its increased sensitivity of xenon NMR in gas phase imaging and this trend was further accelerated in this period, especially *in vivo* application and in porous materials. High quality NMR imaging machines with a horizontal high field magnet for animal use has been wide spread, resulting in unique results especially in fMRI. Therefore, many more papers are reviewed in section 12 *in vivo* and *ex vivo* in this review compared to reviews in past.[1] Dynamic images such as diffusion-weighted magnetic resonance imaging and flow

Nuclear Magnetic Resonance, Volume 31
© The Royal Society of Chemistry, 2002

analysis are performed in various research fields. Educational and practical review articles, including NMR apparatus for education, basic principles and pulse sequences, have been published timely.

A lot of papers on a clinically oriented MRI by using a whole body MRI machine have been published in the period, but almost all of such papers have not been picked up because of their clinical or medical bias. A recent technical development of the whole body MRI machine, however, allows us to observe micro-imaging of a tiny part of a human body, which has been included in this review. In some cases the technical development for imaging methods or pulse sequences precede in the clinical MRI machine rather than in the high-resolution NMR machine or MRI machine for animal use because of the much more severe, specific demands for using with patients. Such technical developments can be available in the high-resolution NMR machine and they have been partly picked up. Journals that concentrate on the development and applications within the field include *Journal of Magnetic Resonance, Magnetic Resonance in Medicine, Journal of Magnetic Resonance Imaging, Magnetic Resonance Imaging, NMR in Biomedicine, Magnetic Resonance in Chemistry, Journal of Computer Assisted of Tomography*, as well as more clinical publications: *Radiology, American Journal of Roentgenology, American Journal of Neuroradiology, Neuroimage and Investive Radiology*. Theoretical aspects of the field are often documented in *Medical Physics* and hardware developments regularly appear in the *Review of Scientific Instruments. Concepts in Magnetic Resonance* which present fundamental aspects of the technique and *Magnetic Resonance Quarterly* which contains review articles of various topics of the field are recommended from the educational view point. *Abstracts from the Annual Meeting of International Society for Magnetic Resonance in Medicine* (ISMRM) are recommended as a means of deriving concise, up to data information on developments within the subjects.

2 General Aspects and Reviews

Reviews including MRI, MRSI, and fMRI were published in large numbers. Some of these reviews include the basic principles of NMR as well.[2–5] The necessary background to comprehend molecular aspects of magnetic resonance applications in medicine was reviewed.[2] An introduction into the physical basis aims at an understanding of some molecular mechanisms without an extended mathematical treatment. The MR typical terminology is explained such that reading of original MR publications could be facilitated for non-MR experiments. Applications in MRI and MRS are intended to illustrate the consequences of molecular effects on images and spectra. This review is useful not only for medical people, but also beginners of NMR and NMR imaging. A review with 124 references summarizes the ways in which magnetic resonance spectroscopy (^{31}P- and ^{13}C-MRS) and related methods (fMRI, positron emission tomography and so on) can be used as windows on brain energy metabolism *in vivo*.[3] These methods are powerful but demanding techniques,

valuable in understanding both normal physiology and pathophysiology. However, discrepancies remain to be reconciled, and this will require increasing sophistication of both techniques and analytical models. An introduction to the use of NMR for the investigation of microbial physiology and metabolites was reviewed with 53 references.[5] NMR parameters, which determine the sensitivity and the resolution, are reviewed. A broad survey of current applications follows. Qualitative uses are described first, which include compound identification and localization. Quantitative aspects, such as pH, concentration and flux measurements are then examined, as well as the corresponding experimental constraints. The review ends with suggestions of possible future developments in instrument capabilities aimed at improving sensitivity: higher fields, spectroscopic and imaging microprobes. An overview with 180 references was made of the cardinal aspects of the MR physics governing the various signal encoding methodologies and the signal intensity contrast mechanisms, including MR angiography of flowing spins, effects of diffusion and perfusion on MR images, and image contrast enhancement with exogenous paramagnetic agents.[6]

Materials, Solid. Functional NMR imaging is also a useful technique for material research. Functional NMR imaging of materials was reviewed.[7] Work on molecular structure of elastmeric networks was reviewed (67 references) by Koenig.[8] Solid state NMR and NMR imaging was effectively used to study many different aspects of vulcanization. Details are given in Section 9.1. NMR imaging is a viable and useful approach to exploring spatial chemical and motional dynamics of a wide range of materials. Of fundamental importance for spatial resolution in solid state NMR imaging is the relations between NMR linewidth, imaging resolution, signal-to-noise ratio and measuring times. The line-broadening effect characteristic for dipolar and quadrupolar interactions must be surpassed in order to obtain better spatial resolution and better image contrast. Demco and Blumich have reviewed the current development of imaging methods employing strong field gradients as Part I with 43 references[9] and line-narrowing methods as Part II with 31 references,[10] as well as the principles of NMR with spatial resolution. Details are given in Section 5.

Hyperpolarized Noble Gases. The uses of hyperpolarized noble gases range from the study of surfaces over solutes to materials and medical imaging. A review outlining the physics underlying theoretical pumping process, practical aspects, techniques and applications in NMR and MRI is presented with 170 references.[11] The current performance and possible improvements of optical pumping techniques for the production of polarized ^{3}He gas were reported as a review with 47 references.[12] The specific properties and dynamics of the polarization inside the lungs are also discussed. A number of recent developments in ^{129}Xe NMR spectoscopy were reviewed with direct applications to the study of mesopore space in solids (37 references).[13] This includes the establishment of a relationship between pore size and chemical shifts for many controlled pore glasses and the exploration of hyperpolarized (HP) xenon for a number of NMR and microimaging application to porous solids.

Other Nuclei. Techniques of ^{13}C-NMR imaging and its applications to

materials and biological systems have been reviewed with 16 references.[14] This paper reviews techniques and schemes developed to overcome some of limitations due to low concentration as well as the low magnetogyric ratio of ^{13}C nucleus, and some of the practical applications of the ^{13}C-NMR imaging to plants and to elastomer blend systems.

The therapeutic efficiency of lithium (Li) for the long-term management of bipolar disorder is well recognized, along with the risk of Li-induced toxicity. A review was described with 26 references, including current findings of *in vivo* functional neuroimaging techniques with respect to the pharmacokinetics and pharmacodynamics of Li and their future potential for elucidating the drug's distribution and the neural mechanisms that produce its therapeutic effects.[15] A review with 20 references is presented regarding the quantification and imaging of myocardial sodium and creatine kinase metabolites by combination of ^{31}P MRS, ^{1}H MRS and ^{23}Na MRI techniques.[16] Details are given in Section 6.2.2.

Phamacokinetics. Synthesizing large molecular weight contrast agents has been targeted in order to modify the pharmacokinetic behavior of presently available small-sized compounds from a broad extracellular to an intravascular distribution. Dendrimers are currently under investigation as potential polymeric carriers of contrast agents for MRI, scintigraphy and X-ray techniques, *i.e.*, computed tomographies (CT). Dendrimers in diagnostics were reviewed with 144 references.[17] Evolution from empirical dynamic contrast-enhanced magnetic resonance imaging to pharmacokinetic MRI was presented and reviewed for antitumor drug pharmacokinetics.[18]

Trees. The major hypotheses that have been proposed to explain the patterns of decay development and its restriction in the wood (xylem) of living trees are outlined briefly.[19] Furthermore, the current understanding of the biochemical and physiological events that contribute to the protection of pre-existing functional sapwood was reviewed with particular reference to the formation of reaction zones at the host–pathogen interface in *Acer* species, especially the European sycamore maple (*Acer pseudoplatanus*).

Cartilage. Cartilage degenerative disease affects millions of people. MRI techniques for the early stages of cartilage disease were reviewed with 141 references, to the assessment of the whole joint, of cartilage as a whole (as an organ), of cartilage tissue, and of cartilage molecular compound and structure.[20] Culture studies, tissue-engineering systems, animal models studies, and *in vivo* studies in humans are included. Each of these levels is amenable to assessment by MRI and offers different information that, in the long run, will serve as an important element of cartilage imaging.

In Vivo Application: Medical. Brain (cerebral) blood flow (CBF) and metabolism have long been subjects of great interest, but progress in their study awaited development of quantitative methods applicable to unanesthetized animals and man. An historical review of developments in this field has been published with 34 references.[21] A review with 191 references, discussing the published studies on neuroimaging methods used for investigations of the pathophysiology of mood disorders, with a particular focus on studies that included bipolar disorder patients, has appeared.[22] Emerging findings in this

area were also reviewed and future strategies for investigations in this field were suggested. A review of neuroimaging studies was described from the viewpoint of how the apolipoprotein E genotype modulates the brain in aging and in Alzheimer's disease.[23]

A review with 66 references has been published. Topics discussed include clinical patterns and classification, imaging in the evaluation of early synovitis, pathol. features, infectious agents, autoantibodies, genetic considerations, and the development of a mechanistically based prognostic model.[24] Cardiac overexpression of β adrenergic receptors was reviewed with 51 references.[25] And the usefulness of the β1-receptor overexpressing mice as a model for heart failure in human patients will have to be evaluated. Molecular mechanisms and therapeutic implications of central nervous system processing of somatic and visceral sensory signals, *i.e.*, pathobiology of visceral pain, were reviewed.[26]

3 Instruments

3.1 NMR Apparatus for Education. – Two types of simple and inexpensive NMR spectroscopy and imaging apparatus for education have been presented; one is for a classical demonstration of the behavior of magnetic dipoles mainly to beginners and the other is a pulsed NMR method for an advanced course.[27,28] A set of simple, classical demonstrations of NMR and NMR imaging principles that illustrate the resonance condition associated with magnetic dipoles and the dependence of the resonance frequency on the environment are presented.[27] The mechanical analogy underpinning the demonstrations is the use of common orienteering compasses to represent the dipoles of magnetic nuclei in a static magnetic field provided by three collinear, strong permanent magnets. This experiment is readily extended to show the effects of electronic shielding, spin–spin coupling, magnetogyric ratio, and free induction decay, topics that are routinely discussed in more advanced treatments of magnetic resonance phenomena.

A simple yet versatile pulsed proton NMR apparatus is described, together with experiments for students joining a NMR research group or students in an advanced laboratory course.[28] The centerpiece of the apparatus is a 1.4 or 2.1 T permanent magnet with high field stability and uniformity. The magnet is used together with the original NMR probe and some of the electronics, resulting in a decrease in both the cost and time to construct the apparatus. If a computer with a data acquisition card is already available, the cost of the apparatus is under $3000. Several experiments are described, illustrating the principles of nuclear magnetism. These include free induction decays, transverse and longitudinal relaxation, spin echoes, motional averaging, Fourier analysis, high resolutional observation of chemical shifts and spin–spin splittings, and one-dimensional imaging.

3.2 Receiver Coil and Flux Guide. – Superconducting conductors such as (Bi, Pb)$_2$Sr$_2$Ca$_2$Cu$_3$O$_{10}$[29] or YBCO (Y, Ba, Cu oxide)[30] for receiver coils and a new

microstructured magnetic material for Rf flux guides[31] were developed. The response of long superconducting $(Bi,Pb)_2Sr_2Ca_2Cu_3O_{10}$ (Bi(2223)) based conductors fabricated by the Oxide Powder In Tube method has been studied when they were exposed to radiofrequency magnetic field excitation.[29] In particular, the authors have characterized their properties as a part of L-C resonator typical of pick-up coil devices in NMR imaging. In these conditions, Bi(2223) conductors cooled down to 77 K showed superior properties compared to already optimized copper based devices: the quality factor Q increased by more than one order of magnitude for a resonance frequency between 6 and 9 MHz, and there was an increase of the signal-to-noise ratio by a factor larger than three. This promising result opens new perspectives for Bi-based conductors in the field of the detection of weak high frequency signals.

A new-material contains microstructure designed according to concepts taken from the field of photonic band gap materials.[31] In the RF range, it has a magnetic permeability that can be produced to specification while exhibiting negligible-direct-current magnetism. The latter property is vital to avoid perturbing the static and audio-frequency magnetic fields needed to obtain image and spectral data. The new magnetic material and the concept offers novel possibilities for guiding RF flux from regions of interest, often deep within the body to the receiver coil, permitting a clear image to be obtained where none might otherwise be detectable.

3.3 Probe. – A high power NMR probe for low temperature studies has been designed, which eliminates the problem of electric arc discharge commonly experienced during radiofrequency pulse cycling in a helium environment.[32] In this design, the sample coil and all high-voltage elements can effectively be isolated in a vacuum, while at the same time permitting good thermal contact between the sample and cryogenic gas. This design was used in NMR studies in the $4.6 < T < 77$ K temperature range for RF pulse duration < 50 ms (and longer for low RF amplitudes) and amplitudes up to *ca.* 60 G.

4 Pulse Sequences and Data Processing

New approachs have been developed for ^{17}O-decoupled ^{1}H imaging by a surface coil,[33] magnetization-grating rotating-frame imaging (MAGROFI),[34] ^{13}C chemical shift-resolved ^{1}H second moment imaging[35] and proton MR spectroscopic imaging without water suppression.[36]

^{17}O-decoupled ^{1}H spin echo imaging has been reported as a means of indirect ^{17}O detection, with potential application to measurement of blood flow and metabolites.[33] Charagundla *et al.* developed an ^{17}O-decoupled proton stimulated echo sequence ('STEAM decoupling') to allow ^{17}O detection with a surface coil, instead of ^{17}O-decoupled proton spin echo imaging. A high B_1 amplitude is easily generated, allowing complete decoupling of ^{17}O and ^{1}H. Slice-selective, ^{17}O-decoupled ^{1}H image is readily performed and the sequence is easily adapted for localized spectroscopy by the surface coil.

A finite-difference approach was developed for precisely determining the diffusion coefficient and T_1 relaxation time in fluid samples analyzed by magnetization-grating rotating-frame imaging (MAGROFI) with either a surface coil or a toroid cavity detector (TCD).[34] This approach avoids the shortcoming of phenomenology based approximations, such as neglect of sample geometries with singularities at the confines of the sample volume, and accounts for the diffusive edge enhancement observed in fluid imaging. The new method was applied to the determination of the self-diffusion coefficient for MAGROFI experiments using TCDs filled with acetone.

Imaging of the ^{1}H NMR second moment with ^{13}C chemical-shift resolution was proposed for molecular mobility imaging of heterogeneous materials.[35] For evaluating the ^{1}H NMR second moment, the method relies on the curve fitting procedure using spin-echo shapes indirectly. The information of ^{1}H echo shapes is transferred to the ^{13}C signal amplitude through ^{1}H–^{13}C cross polarization and then the curve fitting is made using the ^{13}C signal amplitude. The second moment images obtained can reflect the molecular mobility at every molecular site separated by ^{13}C chemical shifts, yielding detailed information on the molecular mobility.

To improve reproducibility in ^{1}H MRSI in human brain, simultaneous acquisition of the internal water reference and metabolite signals was evaluated.[36] Use of singular value decomposition techniques and finite impulse response filters proved effective in separating water and metabolite signals and providing estimations of the metabolite concentrations.

5 Solid State NMR Imaging

Two reviews regarding solid state NMR imaging are presented.[9,10,37] Demco and Blumich reviewed the principles of NMR imaging and spatial information applicable to solid materials and examples of current development are given.[9,10] The NMR line-broadening effect characteristic for dipolar and quadrupolar solids or quasi-solids can be surpassed by strong field gradients or line-narrowing methods. In part I,[9] the principles of NMR with spatial resolution by frequency and phase encoding are introduced and then one class of NMR imaging methods, which use stray fields, strong oscillatory gradients, or multi-quantum coherences evolution, is discussed with 43 references. In part II,[10] the basic principles of the second class using line-narrowing methods by magic-echoes, magic-angle sample spinning, multi-pulse excitation, and magic-angle rotating frame techniques are presented with 31 references.

A spatial solid state NMR imaging approach, which is able to give maps of the heteronuclear dipolar interaction (in this case ^{1}H–^{13}C) and, therefore, of the rare-nuclei distribution in solids, was presented.[37] This approach uses the cross-relaxation mechanism based on the Hartmann–Hahn matching condition. The cross-relaxation map is also able to provide a mobile–rigid structure distribution as well as the spatial-dependent degree of crosslinking in solid polymers and elastomers.

Applications of solid state NMR are included in other topical sections below, such as polymer and hyperpolarized xenon.

6 Other Nuclei

6.1 Hyperpolarized Noble Gases. – Widespread applications of laser-polarized noble gases such as ^{3}He or ^{129}Xe have been found in various fields, especially *in vivo* use. Tremendous potential lies in transferring its large polarization to other nuclei which opens the possibility of spectral editing and surface selective NMR. The physics underlying the theoretical pumping process, practical aspects in the generation of optically polarized xenon, special NMR techniques coping with the non-equilibrium polarization, polarization transfer techniques, and finally its applications in NMR and MRI were reviewed.[11] Recent investigations in magnetic resonance imaging in animals and human subjects have demonstrated that laser polarized ^{3}He can be used to visualize airways and air spaces. Recent investigations in MRI in animals and human subjects, including specific properties and dynamics of the polarization inside lungs, are reviewed.[12]

6.1.1 Application to Dynamics. The transport process in porous materials is a crucial component of many important processes in science and technology. It was demonstrated how magnetic resonance microscopy with continuous flow laser-polarized noble gases makes it possible to light-up and thereby visualize, with unprecedented sensitivity and resolution, the dynamics of gases in samples of silica aerogels and zeolite molecular sieve particles.[38] The 'polarization-weighted' images of gas transport in aerogel fragments are corrected to the diffusion coefficient of xenon obtained from NMR pulsed-field gradient experiments.

The large xenon NMR signal provided by the laser-polarization technique allows more rapid imaging than one can achieve with thermally polarized gas–liquid systems, permitting shorter time-scale events such as rapid gas flow[39] and gas–liquid dynamics[40] to be observed. Dynamic NMR microscopy was used to study xenon gas undergoing Poiseuille flow in the regime where deterministic and stochastic motions are the same order of magnitude.[39] A spin echo version of the dynamic NMR experiment yields images exhibiting strong distortions for longer observation time due to fast diffusion under the 'natural' gradient from magnetic field inhomogeneity (compared to results obtained with a stimulated echo version). This effect is used as a edge-enhancement filter by employing a longer time duration of the imaging gradient in a stimulated echo experiment. NMR imaging of the flow and diffusion of laser-polarized ^{129}Xe gas undergoing convection above evaporating laser-polarized liquid xenon was demonstrated.[40] Two-dimensional velocity-encoded imaging shows convective gas above the evaporating liquid xenon, and also permits the measurement of enhanced gas diffusion near regions of large velocity variation.

High equilibrium spin polarizations in solid ^{129}Xe due to optical pumping and their applications were discussed.[41]

6.1.2 Chemical Shift. The relationship between pore size and chemical shifts for many controlled pore glasses has been established by the exploration of hyperpolarized xenon gas in the porous solids. A number of recent developments in ^{129}Xe NMR spectroscopy and microimaging were reported with direct applications to the study of mesopore space in solids (37 references).[42] Experiments illustrated include the rapid characterization of the void space in porous solids, including the *in situ* processes such as diffusion and dehydration, and imaging with chemical shift resolution. Chemical shift imaging with continuously flowing hyper-polarized xenon was applied to the characterization of materials.[43]

6.1.3 Application to In Vivo Systems. The need for standardized noble gas inhalation procedures that have been carefully tested, and for continuous physiological monitoring to ensure the safety of the subject, is much talked about. The physiological effects of various hyperpolarized helium and xenon MRI-compatible breathing protocols were investigated in 17 Sprague–Dawley rats, by continuous monitoring of blood oxygen saturation, heart rate, ECG, temperature and endotracheal pressure.[44] Authors found short breath-hold and alternate-breath protocols to be safe procedures for use in hyperpolarized noble gas MRI experiments.

Hyperpolarized ^{129}Xe was dissolved in a lipid emulsion and administered to anesthetized rats by manual injections into the carotid (approx. 1–1.5 mL in a max. time of 30 s).[45] During injection, ^{129}Xe NMR brain spectra at 2.35 T were recorded over 51 s, with a repetition time of 253 ms. Two peaks assigned to dissolved ^{129}Xe were observed (intravascular xenon at 194 ppm and xenon dissolved in the brain tissue at 199 ppm). Their kinetics revealed a rapid intensity increase, followed by a plateau (approx. 15 s duration) and then a decrease over 5 s. An identical experimental set-up was used to acquire a series of 2D projection of ^{129}Xe images on the phantom and the rat brain. Hyperpolarized ^{129}Xe NMR has been examined as a probe for blood oxygenation, *i.e.* for oxy and deoxy hemoglobins.[46] Detection of emphysema in rat lungs by using magnetic resonance measurements of ^{3}He diffusion was carried out.[47]

6.2 Other Nuclei. – *6.2.1 Application to Materials and Plants.* Techniques of ^{13}C-NMR imaging and its applications to plants and elastomer blend systems were reviewed.[14] In this review, the authors focused on the imaging of ^{13}C nuclei as a means to deal with the spatial distribution of molecules of interest other than water.

6.2.2 Application to In Vivo Systems. Brain ^{7}Li NMR spectroscopy findings have disassociated brain and blood Li concentrations and suggest a phamocokinetic basis for Li response and nonresponse.[15] The use of *in vivo* synaptic

activity measurements and neurochemical imaging is providing new knowledge related to the local neural activity associated with Li response and is contributing to the critical human testing of neuroprotective and signal-transduction models of Li's therapeutic effects. *In vivo* imaging of the phamacodynamics and phamacokinetics of Li have been reviewed with 26 references.

In vivo carbon-edited detection has been developed to detect metabolites of lactate[48] and glutamate/glutamine[49] in brain. The ischemic penumbra was differentiated from the core on the basis of the dynamics of lactate formation. This was tested in a rat model of focal cerebral ischemia by infusion of [1-^{13}C]glucose, using lactate-edited MRSI techniques.[48] Early identification of the potentially salvageable penumbra is critical for the determination of therapeutic intervention strategies in acute focal cerebral ischemia. The authors' findings suggest that this combination of ^{13}C-glucose infusion with the proposed MR methods may aid in differentiating the penumbra from the core in cerebral ischemia. A method for *in vivo* carbon-edited detection with proton echo-planar spectroscopic imaging (ICED PEPSI) was described.[49] This method is composed of an EP based acquisition implemented with ^{13}C–^{1}H *J* editing spectroscopy and is intended for high temporal and spatial resolution *in vivo* spectroscopic imaging of ^{13}C turnover, from D-[1, 6-^{13}C]glucose to [3, 4-$^{13}CH_2$]-glutamate and -glutamine, in the brain.

Quantitative determination of pharmacokinetics of ^{19}F-labeled drugs in target organs by ^{19}F-MRS and MRSI *in vivo* is quite useful for understanding and investigating the outcome of treatment modifications and side effects. Release of 5-fluorouracil derivatives in colon tumors,[50] a macromolecular conjugated anticancer drug in tumors,[51] and brain pharmacokinetics and tissue distribution of fluvoxamine and fluoxetine[52] has been presented. A paper on the tablet swelling and release of the drug by ^{19}F-NMR imaging is picked up together with other papers in Section 7.3.2 Drug Delivery. A glucuronic acid-conjugated carbamate derivatives of 5-fluorouracil (5-FU), originally designed as a prodrug for antibody-directed enzyme prodrug therapy, was used for direct *in vivo* observation of *in situ* 5-FU generation in two human colon tumors heterotransplanted into nude mice.[50] These tumors, when becoming necrotic, are rich enough in β-glucuronidase to allow ^{19}F-NMR spectroscopic monitoring, at the tumor level, of both prodrug elimination and 5-FU release without preliminary treatment by a specifically targeted enzyme conjugate. This method, which should allow overall estimation of the β-glucuronidase content of tumors, might also be helpful for selecting tumors as specific targets for nontoxic glucuronic acid-conjugated prodrugs without prior treatment with a fusion protein. This work is the first report evidencing a direct intratumor conversion of a glucuronic acid-conjugated prodrug into the expected active drug by ^{19}F-NMR spectroscopic monitoring and ^{19}F-NMR imaging.

The effective clinical use of radiosensitizers requires the development of drug targeting systems and the investigation of imaging techniques to noninvasively monitor the biodistribution of the agent. A ^{19}F-labeling technique in combina-

tion with a chemical shift selective ^{19}F-NMR imaging sequence was applied to map the biodistribution and pharmacokinetics of 3-aminobenzamide (3-ABA) in tumor-bearing animals.[51] 3-ABA is a potent agent which inhibits the repair of radiation-induced DNA strand breaks, and thus enhances the antitumor activity of radiotherapy. Fluvoxamine and fluoxetine-norfluoxetine distributions *in vivo* at steady state and quantitative kinetics in brain and plasma after drug therapy interruption have been investigated by ^{19}F-NMR spectroscopy, MRSI, and HPLC in subjects treated for depression.[52]

An inert gas, SF_6, in the lung after the partial obstruction of the left bronchi of rats was imaged with NMR using a technique that clearly differentiates obstructed and normal ventilation.[53] When the inhaled fraction of O_2 is high, SF_6 concentrates dramatically in regions of the lung with low ventilation-to-perfusion ratios (Va/Q); therefore, these regions are brighter in an image than where VA/Q values are normal or high.

For rapid *in vivo* monitoring of the chemotherapeutic response of mouse xenograft tumors propagated from human prostate cancer cell lines, a novel pulse sequence strategy uses weighted ^{23}Na NMR imaging.[54] An investigated pulse suppresses Na with long T_1, weighting the image toward intracellular Na nuclei. Comparing these weighted Na images before and 24 h after administration of antineoplastisity, the authors measured a *ca.* 36% increase in signal intensity.

Loss of membrane permeability caused by ischemia leads to cellular sodium accumulation and myocardial edema.[55] After prolonged coronary occlusion and complete reflow, the rate of myocardial sodium accumulation may be governed by microvascular integrity. Three-dimensional ^{23}Na MRI was used to monitor myocardial sodium content changes over time in an *in vivo* closed-chest canine model of myocardial infarction and reperfusion.

A review (20 refs) is presented regarding the quantification and imaging of myocardial sodium and creatine kinase metabolites by combination of ^{31}P MRS, ^{1}H MRS and ^{23}Na MRI techniques.[16] In order to accomplish analoguous accuracy of a MRI or MRS test to the clinical thallium (^{207}Tl) radionuclide imaging stress test for demonstrating metabolic alterations associated with non-viable infarcted tissue and/or ischemia, the sensitivity would need to be sufficient to detect changes in the entire heart that is at least comparable or better than radionuclide imaging. For ^{31}P, this may be advanced through the combination of phased-array detection and Overhauser enhancement technologies.

Transgenic mice are increasingly used to probe genetic aspects of cardiovascular pathophysiology. However, the small size and rapid-rates of murine heart make noninvasve, physiological *in vivo* studies of cardiac bioenergetic and contractility difficult. Modification of noninvasive cardiac magnetic resonance imaging with image-guided ^{31}P MRS technique used in humans to mice have been developed.[56] Using spatially localized, noninvasive ^{31}P NMR spectroscopy and imaging at 4.7 T, authors observed mean murine *in vivo* myocardial phosphocreatine-to-ATP ratios. Now, it is possible to noninvasively study *in vivo* myocardial bioenergetic, morphology, and contractile function in mice under physiological conditions. Phosphorus metabolites in

the jaundiced rat liver were studied by three-dimensional phosphorus chemical shift imaging. Quantitation of metabolites was performed using an external standard. Metabolite T_1 values were assessed in CSI experiments on normal untreated animals.[57] ^{31}P NMR CSI may be used to assess liver metabolites under conditions of stress such as jaundice. However, absolute quantitation requires careful attention to many factors including point spread function, correct T_1 values, and adequate signal-to-noise ratio.

K^+ uptake rates were measured in the anterior (An) and posterior (Pos) LV walls of pig hearts before and after regional ischemia and reperfusion using Rb^+ as a K^+ congener and 3D ^{87}Rb NMR imaging and spectroscopy as detection methods.[58] The hearts were perfused by the Langendorff method with Krebs–Henseleit (KH) buffer and loaded with Rb^+ (4.7 mM, Rb-KH) after 120-min ischemia and 60-min reperfusion. The intensities of the Rb images correlated with the Rb^+ content measured in tissue samples. ^{87}Rb MR imaging and spectroscopy were used to study the effects of ischemia on the properties of K^+ in cardiac tissue.[59] Isolated pig and rat hearts perfused by the Langendorff method with Krebs–Henseleit buffer were preloaded with Rb^+. The decreases in apparent line-width and increases in Rb^+ visibility can be explained by an increase in Rb^+ mobility caused by displacement of Rb^+ from anionic binding sites by H^+ (ischemic acidosis) and changes in intracellular compartmentalization of Rb^+.

7 Diffusion, Flow and Velocity Imaging

NMR spectroscopy or NMR imaging allows nondestructive and noninvasive quantification and visualization of both static and dynamic liquid transport phenomena. Diffusion, flow, mass transfer and transport processes can be measured by mapping the (proton) displacement in a defined time interval directly in a so-called pulsed field gradient (PFG) experiment. Other methods follow the local intensity in time-controlled sequential images of water or labeled molecules, or map the effect of contrast agents. Combining transport measurements with relaxation time information allows the discrimination of transport processes in different environments or of different fluids, even within a single picture element in an image of the porous biosystem. By proper choice of the applied NMR method, a time window ranging from milliseconds to weeks (or longer) can be covered. A lot of papers concerning this topic have been published.[60–77]

7.1 Diffusion. – Distribution of the diffusivitity of fluid in a horizontally oriented cylinder was demonstrated by NMR imaging in two papers on a granular flow system[60] and in the earth's magnetic field.[61] Correlation time (τ_c) and diffusion coefficient ($D = \langle u^2 \rangle \tau_c$) imaging (CTDCI) was applied to a granular flow system of 2 mm oil-filled sphere rotated in a half-filled horizontal cylinder, *i.e.* to an Ornstein–Uhlenbeck process with a velocity autocorrelation function.[60] Time dependent apparent diffusion coefficients are measured, and τ_c

and D are then calculated from the apparent diffusion coefficients images. This method is also applicable to study transport in systems involving turbulence and porous media flows. The influence of natural convection on NMR measurement of a self-diffusion coefficient of fluid in the earth's magnetic field was described.[61] The authors pointed out that even a slight temperature gradient can cause significant misinterpretation of measurements. The chaotic nature of convection enhances the apparent self-diffusion constant of the liquid.

Molecular motion in the polar organic solvent nitrobenzene, induced by both continuous and pulsed electronic fields, was studied by magnetic resonance imaging.[62] The resultant image correlation spectra indicate that the time scale of motion in a 9.6 kV cm^{-1} electric field is tens of milliseconds. The data were analyzed by the Fokker–Planck probability function for one-dimensional bounded diffusion.

7.2 Flow: Velocity, Rheometry. – Papers relating to the flow of hyperpolarized ^{3}He or ^{129}Xe gas are picked up in Sections 2 and 6 as well. Poiseuille flow in ^{129}Xe gas phase was studied by dynamic NMR microscopy.[39] The flow profile images are different for a short observation time than for a longer observation time.

Visualization of gas transport in silica aerogels and zeolite molecular sieves was demonstrated by the polarization-weighted images.[38]

Instead of polarized noble gases, thermally polarized ^{1}H NMR microimaging was used to study of liquid and gas flow in monolithic catalysts.[63] Two-dimensional spatial maps of flow velocity distributions for acetylene, propane, and butane flowing along the transport channels of shaped monolithic alumina catalysts were obtained at 7 T by ^{1}H NMR, with true in-plane resolution of 400 μm and reasonable detection times. The flow maps reveal the highly nonuniform spatial distribution of shear rates within the monolith channels of square cross-section, the kind of information essential for evaluation and improvement of the efficiency of mass transfer in shaped catalysts. The water flow imaging, for comparison, demonstrates the transformation of a transient flow pattern observed closer to the inflow edge of a monolith into a fully developed one further downstream.

The flow through an abrupt contraction[64] or a step stenosis[65] was demonstrated. The flow of liquid crystalline hydroxypropyl cellulose aqueous solutions, where polymer was flowing through an abrupt contraction, was imaged by pulsed field gradient NMR techniques.[64] Flow velocity was determined in the case of the flow through step stenosis.[65]

There is a need for improving the understanding of complex fluid and suspension flow behavior in mixing equipment. The concentration profiles obtained by MR imaging were used to monitor mixing with respect to axial position in a Kenics mixer, to which the two viscosity-matched test fluids were delivered at approximately the same volumetric flow rate.[66]

A tubular rheometry that is based on obtaining velocity profiles by NMR imaging and measuring pressure drop of the flow is used for polymer melts.[67] This technique allows one to obtain viscosity data potentially over many

decades of shear rate region in a single measurement for low-density of polyethylene melt as the flow medium.

7.3 Mass Transport: Absorption, Dissolution, Swelling, Drying. – Mass transportation is one of the typical application fields for NMR imaging. The characteristic features of these processes, such as the main mechanisms and the limiting stages of mass transport, and some factors which can alter the efficacy of mass transport, have been investigated in porous materials and bioreactors. Water absorption in cork,[68] adsorption of nitrobenzene adsorbate to activated carbon,[69] hydrates in sediments,[70] mass transport process in drying and adsorption,[71] in porous biosystems[72] and in drug release processes[73–76] are picked up in this section. An overview[77] of the principles of NMR and NMR imaging techniques to visualize and unravel complex, heterogeneous transport processes in porous biological systems has been presented with applications and limitations of these methods, based on results obtained in (model) biofilms, bioreactors, microbial mats and sediments. The operation of bioreactors and the metabolites of microorganisms in biofilms or soil/sediment systems are strongly dictated by the transport processes therein.

7.3.1 Water Absorption, Transport Process of Water. An NMR microscopy study has been performed to measure the imbibition of water into natural cork, extractives-free cork and de-suberized cork.[68] It was clearly indicated that suberin is the key constituent which determines the ability of cork to resist water uptake. Hydrates were generated in synthetic sediments in a laboratory cell.[70] After hydrate formation took place and the sediments were solidified, the samples were investigated both visually and by use of ^{1}H NMR imaging.

Drying and adsorption were studied by detecting the temporal evolution of the 1-dimensional spatial profiles or 2-D maps of liquid content without interrupting the process under study.[71] From the ^{1}H NMR microscopic data mass transport processes in porous materials, including individual catalyst support pellets and beds composed of porous gains, were discussed. The problem associated with the relaxation weighting of the NMR signals (often unavoidable for liquids permeating mesoporous solids) and the possibilities to overcome these problems were discussed. The disappearance of water in the paint drying process was monitored by NMR imaging.[72]

7.3.2 Drug Delivery. NMR techniques have been usually used to monitor the drug release processes, the hydration process of controlled release drugs, the porosity, compaction of tablets and so on. The potential of NMR microscopy is now higher for understanding the drug release mechanisms. Four articles relating to such topics appeared.[73–76] NMR microscopy of the uptake, distribution and mobility of dissolution media in small (sub-millimeter) drug delivery systems is presented.[73] The drug release process from lipophilic matrix theophylline beads, the change of mobility and distribution of liquid within fully liquid penetrated beads were measured by pulsed gradient field spin echo (PGSE) NMR and 3D-NMR imaging. A multi-slice multi-echo (MSME)

method was used to monitor the development of the hydrated layer gel as a function of time and the measurements of the spatial distribution of the T_2 relaxation time in this layer.[74] The single point imaging (SPI) method provides useful information about the porosity and compaction density within tablets.

A system for performing NMR imaging experiments on drug delivery devices within a flow-through dissolution apparatus (USP App. 4) has been developed.[75] This system was used to image the physical changes that occur in solid dosage forms during dissolution in the flow-through apparatus. Simultaneous cumulative drug release measurements were also made. The NMR images obtained under these conditions and the drug release data provide a better understanding of the process involving in the release of drugs from drug delivery systems based on diffusion, dissolution, and osmosis mechanisms.

The release behavior of two model drugs, triflupromazine-HCl and 5-fluorouracil, from swelling hydroxypropyl methyl cellulose (HPMC) tablets has been investigated.[76] The tablet swelling was restricted to 1-dimension and distributions of the water and model drugs were obtained by ^{1}H and ^{19}F imaging, respectively. The difference in the self-diffusion of two model drugs may be useful in predicting the mechanism of drug release from swelling hydrophilic matrix systems.

8 Porosity, Fluid Assisted Imaging

8.1 Porosity, Porosimetry, Structure. – The increase in experimental sensitivity by hyperpolarized xenon, is remarkable. A number of recent developments in ^{129}Xe NMR spectroscopy were reviewed with direct applications to the study of mesopore space in solids (37 references).[13] Experiments illustrated include the rapid characterization of the void space in porous solids, including the *in situ* study of processes such as diffusion and hydration, and imaging with chemical shift resolution.

8.1.1 Porosimetry. Mercury porosimetry data on a pore size distribution in porous media are corrected and interpreted by using a new method of NMR imaging techniques.[78,79] A new method for removing the so-called 'shielding' effect inherent in a pore size distribution of a porous medium obtained from the mercury porosimetry intrusion curve was presented.[78] The characterization of the macropore network of an alumina tablet obtained using the new methodology was compared with the results of a study of a similar sample using microscopy carried out by earlier workers. In conjunction with NMR spin density and spin–lattice relaxation time images the proposed deshielding method may be used to provide a spatially resolved pore-size distribution not possible with conventional methods. A new model of interpretation for the mercury porosimetry experiment was presented which would enable both the morphology and spatial geometrical changes in pellet structure, over several lengthscale (*ca.* 1 nm–1 mm), to be monitored during the deactivation of catalysts by coking.[79]

8.1.2 Cork and Coal. Magnetic resonance microimaging studies of the microstructure of cracking porous petroleum coke (oil sand bitumen),[80] structure of coal and interactions with solvents,[81] and the modeling and measurement of coke profiles in deactivated catalyst pellets[82] were reported. It was found that the distribution of mobile components was very heterogeneous, like the distribution of macerals, from the single-point imagings of coal structure and coal solvent swelling.[81]

8.2 Migration of Liquids in Porous Media. – Information on migration of liquids into porous media and on mobility of the absorbed fluids is of great relevance for theory and for many branches of the material science.[83–86] Migrations of water and chloroform into porous poly(vinyl alcohol) (PVA)[83] and 4-n-pentyl-4′-cyanobiphenyl (5CB) into poly(Bu-methacrylate) (PBMA)[84] were demonstrated by NMR microimaging. The images taken using gradient echo fast imaging (GEFI) and constant time imaging (CTI) methods show differences, which are assumed to reflect the restriction of mobility of water molecules due to formation of hydrogen bonds with hydrophilic PVA.[83] To examine solvent diffusion into materials, NMR imaging and Fourier-transform IR imaging (FTIRI) have been applied.[84] FTIRI micro-spectroscopy (fast FTIRI) is a new microanalytical technique, with a spatial resolution of 7 μm. This paper outlines FTIRI of liquid crystal 4-n-pentyl-4′-cyanobiphenyl (5CB) into poly(Bu-methacrylate) (PBMA). Time-dependent concentration profiles were obtained above and below the nematic to isotropic transition temperature. A sharp 5CB front penetrating the PBMA matrix, along with near-square root of time front progression indicates anomalous diffusion. Fast FTIRI correctly identified the diffusion as anomalous, whereas mass uptake analysis would have concluded Fickian diffusion. These methods are advantageous for detailed analysis and interpretation of chemical agent diffusion, sorption and desorption in polymeric materials of varying geometry.

Fluid–fluid displacement was studied in porous media by means of NMR imaging.[85] The displacement front was imaged as one fluid displaced the fluid that initially saturated the porous media. How the fluid rheology at various driving pressure gradients and porous medium configurations affect the displacement was investigated.

The study of penetration by waterborne wood preservatives into wood was reported.[86] Samples of three wood species, *i.e.* red maple (*Acer rubrum L.*), ponderosa pine (*Pinus ponderosa Dougl. ex Laws.*) and aspen (*Populus tremuloides*), containing different anatomical features, *e.g.* sapwood, heartwood, early-wood, late-wood, and knots, were air-dried and pressure-treated with water. MRI provides a useful method for assessment of the penetrability of wood by water and consequently waterborne preservatives.

8.3 Packed Beds, Granual Media: Flow, Voidage. – *8.3.1 Velocity and Voidage.* Single- and two-phase flows in fixed-bed reactors were visualized by three-dimensional NMR imaging and MRI velocimetry.[87] The fluid velocity vector is determined at a pore-scale resolution of 156 μm. Characteristics of

the individual pores are combined with the MRI velocity data to determine quantitative statistical information concerning flow through these pores. The ability of the lattice-Boltzmann simulations, the structure of the interparticle pore space and the single-phase flow field in a packed bed of alumina catalyst particles was fully characterized. A direct comparison of the MRI and lattice-Boltzmann results shows there is good agreement between the two methods, except close to the wall. A case study of the visualization of the extent of wetting of the packing as a function of time following start-up is presented.

Using a water substitution method to determine bed voidage, an independent relationship between bed height and bed voidage was observed for the trilobe (virgin and crushed) and cylindrical alumina supports.[88] Bed voidage values were approximately 6% larger in the 0.05 m i.d. column and could be attributed to a greater extent of wall zone voidage. Three-dimensional NMR imaging data were also used in conjunction with digital image analysis techniques to obtain one-dimensional radial profiles of voidage from comparable alumina catalyst support material. In all cases, the NMR imaging data yield voidage values that are consistently higher than those obtained from water substitution measurements. Local transitions in flow phenomena of glucose through packed beds have been identified by NMR imaging.[89]

8.3.2 Resin Column. Chemical sorption in ion-specific resin columns[90] and solvent flow through chromatographic columns[91] was demonstrated by NMR imaging. Physical transport and chemical sorption properties of a Gd ion tracer were characterized and assessed through ion-specific resin columns.[90] Trivalent Gd ion was selected based on its chemical similarity to typical high-level waste components, ^{241}Am and ^{244}Cm, and for its paramagnetic contrasting abilities in NMR experiments. NMR imaging results of flow experiments are provided showing a characteristic flow phenomena and resin column loading profiles. This technique can be applied to other complex flow systems such as environmental transport in radioactive waste reprocessing operations. NMR techniques have been used to measure and characterize solvent flow through chromatographic columns.[91] An injection of D_2O was tracked by NMR imaging and the flow-rate dependence of axial and transverse apparent diffusion was measured by PGSE (pulsed gradient spin echo) NMR, leading the spatial distribution of the local velocity and apparent diffusion through a cross-section of the column. Significant column wall effects were observed and these effects were found to be highly dependent upon the column packing density. The column performance was assessed in terms of the HETP (height equivalent to a theoretical plate) determined by the NMR techniques employed.

9 Polymers

9.1 Crosslinked Structures. – In vulcanization, chemical crosslinks are formed across elastomeric polymer chains, improving both the strength and elastic properties of the rubber. Koenig and co-workers have presented a lot of

work for understanding the formation, structure and stability of vulcanizates by using solid state NMR and NMR imaging, which is reviewed by Koenig.[8] In solid state NMR, several peaks appear in the ^{13}C spectrum of vulcanized rubber and these peaks were assigned to their respective vulcanizates structure based on model studies. NMR imaging has been used in the detection of internal inhomogeneities arising from inadequate mixing, gradients in crosslinking chemicals, filler distribution, blends, and coagents.

Relationships between microvoid heterogeneity and physical properties in crosslinked elastomers, poly-(isobutylene-*p*-methylstyrene-*p*-bromomethylstyrene) (PIB-PMS/BrPMS) terpolymers, were identified by a 3D-NMR imaging study.[92] Three-dimensional reconstruction of the sample images reveals that the voids are spherically shaped. The experimental results indicate that high microvoid density in cured elastomers leads to crack initiation and accelerated crack growth, thereby resulting in premature mechanism failure of the materials.

Single-point NMR imaging-based method for broad-line analysis was presented.[93] The technique was applied to obtaining spectroscopic information of a two-component covulcanized rubber sample. Natural rubber and styrene–butadiene rubber compounds were discriminated, resulting in chemical and mechanical characterization of the sample interface. A sharp interface of thickness less than 200 μm was found by the space-resolved chemical shift weighted measurements, on the other hand a wider interface, with a gradual crosslinked change extended to about 500 μm over the natural rubber component, was shown by spin–spin relaxation weighted profiles.

The paramagnetic effect of ^{1}H T_2 was effectively used to observe the crosslinking structure of the interfacial region between the two parts of composite poly(methacrylic acid) (PMMA) hydrogels with a different degree of crosslinking.[94] By using the relationship between the Mn^{2+} ion concentration and the ^{1}H T_2 values at 270 MHz NMR, the ^{1}H T_2 NMR image was converted into the Mn^{2+} ion concentration image. The spatial distribution of Mn^{2+} ions in the gel under the application of a 3 V DC electric field was determined as a function of elapsed time.

It has been previously demonstrated that calcium alginate gels prepared by dialysis often exhibit a concentration inhomogeneity such that the polymer concentration is considerably lower in the center of the gel than at the edges. The concentration gradient of alginate has been analyzed by measuring both the spatial distribution of calcium ions in sections of alginate gel spheres, by means of X-ray fluorescence spectroscopy, and the T_2 relaxation behavior on intact gel beads using magnetic resonance microimaging.[95] The experimentally determined gradients from three-dimensional gels provide data to reevaluate the parameter estimates in the recently reported mathematical model for alginate gel formation (A. Mikkaelsen and A. Elgsaeter, Biopolymers, 1995, Vol. 36, pp. 17–41). The model may account for the gels being less inhomogeneous when nongelling sodium or magnesium ions are added during gelation.

The volume-phase-transition in a thermoreversible gel is conveniently monitored through one-dimentional 1H-NMR imaging and images derived

from relaxation and diffusion weighted planar spin echo experiments.[96] This is demonstrated in the LCST gel, *N*-isopropylacryl-amide-ethyleneglycol-dimethacrylate copolymer swollen in water. Insight into the hydration state of water and the motional state of polymer, in fully swollen and collapsed states of the gel, was provided.

The crack growth resistance of polymers, being an important toughness parameter, was visualized by NMR imaging.[97] For this purpose a dedicated stretching device was developed to keep notched materials under load during the NMR measurements. Two polymers, ABS, a blend copolymer poly (styrene-*co*-acrylonitrile) with 28 wt% polybutadiene, and a block copolymer poly(butylene terephthalate)/poly(tetramethylene oxide) (PBT/PTMO), were investigated, resulting in quite different behaviors.

9.2 Swelling, Diffusion, Hydrophilicity. – Superabsorbing polymers, *i.e.* polyacrylate-based superabsorbing particles, were characterized by NMR imaging techniques.[98] Spatial differences in the crosslinked density were investigated by parameter-selective ^{1}H-NMR imaging of samples swollen with water. The T_2 relaxation time, self-diffusion coefficient of the absorbed water, local water mobility, and the time evolution of the swelling process are discussed. Moreover, MAS (magic angle spinning) NMR imaging method was applied to investigate the influence of mechanical load on the swollen particle by taking advantage of the centrifugal forces on the spinning sample. These experiments indicate the presence of two water components, one strongly adsorbed, while the other is relatively mobile.

The conventional method for determining the characteristics of the diffusion of solvents into the polymer is by measuring the mass uptake of the polymer while the solvent penetrates the matrix. The measurements at a macroscopic level, however, give little information relating to the properties of the solvent inside the polymer matrix and the mechanisms of the processes that control the diffusion. NMR imaging is used to monitor the transport of solvent into solid systems, such as rubber and hydrogels.[99,100] The potential applicability of NMR imaging techniques to polymer gel systems has been demonstrated on the diffusion of organic solvents in polymeric materials like natural rubber, nematic-like networks and hydrogels.[99] The transport of solvent into solid systems was monitored in real-time. Information about a quantitative measurement of the diffusion coefficient was provided by the density and the mobility of the solvent in materials in NMR imaging of solvent. Information about the network properties (mobility of network chains itself due to the softening influence of the solvent, de-crystallization and so on) during the swelling process was also given by the observation of the networks. For any polymer gel, the amount of solvent uptake is dependent upon the chemical nature of the gel and the nature of its environment, such as solvent component, temperature, pH, and so on. The use of different hydrogels based on crosslinked poly(*N*-isopropylacrylamide) and copolymers with basic or acidic groups as materials for flow control was discussed and then the design of a chemo-mechanical valve is described.[100] By NMR imaging, it is possible to

follow the transport processes inside the gel in real-time. With the present experimental arrangement the authors could show that sensitive polymers can be used for controlling the flow in dependence on temperature, pH and content of organic solvents in H_2O.

A novel physical parameter, saturation transfer ratio (STR), was proposed for evaluation of the hydrophilicity of synthetic copolymer gels in magnetic resonance imaging.[101] Good correlation was found between STR and hydrophilicity of copolymer gels based on 2-hydroxyethyl methacrylate (HEMA), glycidyl methacryrate (GMA), *N*-vinyl-2-pyrrolidinone (N-VP), and/or methylmethacryrate.

9.3 Dosimetry. – Polyacrylamide gels are a powerful tool to measure radiation dose by quantifying the NMR T_2 relaxation times of the irradiated gel. The exploitation of these radiation sensitive gels in clinical radiotherapy requires accurate mapping of T_2 values. The optimization strategy used to identify accurate and practical methods of measuring a typical range of T_2 values (140–700 ms) in the gel dosimeters has been presented.[102,103] Four sequences for measuring T_2 values and the choice of image acquisition parameters are compared and the results are analyzed in terms of accuracy, signal-to-noise ratio and acquisition times.[102] This paper reports the importance of careful selection and optimization of the NMR imaging sequences for accurate and reliable polyacrylamide gel dosimetry. Radiation-induced modifications in radiation dosimetry polymer gels (PAGs), which are composed of acrylamide, N,N′-methylene-bisacrylamide, gelatin, and H_2O, were studied by ^1H- and ^{13}C-NMR spectroscopy and FT-Raman spectroscopy.[103] The formation of a polyacrylamide network within the gelatin matrix follows a dose dependence nonlinearly correlated to the disappearance of the double bonds from the dissolved monomers within the absorbed dose range of 0–50 Gy. The T_2 values of PAGs irradiated to up to 50 Gy measured in a NMR spectrometer and a clinical magnetic resonance imaging scanner can be modeled using the spectroscopic intensity of the growing polymer network.

10 Plants: *In Vivo*

Some applications of NMR microimaging and EPR spectroscopy to the study of disease and senescence processes in plant organs are presented, with emphasis on the non-invasive nature of the techniques.[104] A particular strength of the use of NMR microimaging in research on live specimens is its ability to perform repeated measurements on the same specimen. From EPR spectroscopy information specifically on free radicals and paramagnetic metal-containing species was produced. Techniques to avoid the production of artifacts from sample preparation was described in both methods.

The major hypotheses that have been proposed to explain the patterns of decay development and its restriction in the wood (xylem) of living trees and the current understanding of the biochemical and physiological events that

contribute to the protection of pre-existing functional sapwood was reviewed.[19] Studies using conventional anatomical and biochemical approaches have been integrated with the application of advanced physical techniques such as NMR imaging, proton induced X-ray emission (PIXE) microanalysis and mapping and electron paramagnetic resonance (EPR) spectroscopy. As result, a model describing the development and function of reaction zones was proposed. The implications of our developing understanding of antimicrobial defense in trees on the practice of arboriculture were discussed briefly.

^{23}Na NMR microimaging was described to map the Na distribution in living plants at 11.75 T machine with a homebuilt double resonant ^{23}Na–^{1}H probe head for the first time.[105] As an example, a response of 6-day-old seedlings of *Ricinus communis* to exposure to NaCl concentration from 5 to 300 mM was examined. The spatial resolution (in-plane 156×156 μm) is enough to discern the different types of tissue in the hypocotyl and the measurement time within 85 min is shorter compared to the time scale of Na uptake and accumulation in the plant. The ^{23}Na microimaging promises great potential for physiological studies of the consequences of salt stress on the microscopic level and thus may become a unique tool for characterizing plants with respect to salt tolerance and salt sensitivity.

A double-quantum selective chemical shift imaging sequence was developed and applied to monitor the sucrose distribution in the stem of sugar cane (*Saccharum officinarum L.*) with a resolution of $0.4 \times 0.4 \times 6$ mm^3 to $0.645 \times 0.645 \times 6$ mm^3.[106] This ^{1}H spectroscopic imaging in combination with double-quantum filtering with magnetic field gradients is expected to be a useful tool for monitoring of metabolites *in vivo* systems because of its high selectivity and strong reduction of water signal.

Phloem loading of sucrose is decisive for the speed of mass flow, because sucrose is the dominant solute in the sieve tube sap of nearly all plant species. The interaction of sucrose metabolism, starch storage and phloem export in source leaves and the effects on sugar status in phloem was presented.[107] The sucrose concentrations was revealed by a NMR imaging method.

Water transportation, water binding and water status in plants have been presented.[108–110] A dynamic NMR imaging method is described to calculate the characteristics of water transport in plant stems.[108] The amount of stationary water, the amount of flowing water, the cross-sectional area of flow, the average linear flow velocity of the flowing water and the volume of flow were calculated per pixel without advance knowledge of the flow-profile in that pixel. NMR imaging and light microscopy and SEM were used to follow time-dependent morphology changes and water status changes of tulip bulbs during bulb storage for 12 weeks at 20 °C (non-chilled) and 4 °C (chilled) and after planting.[109] Water content and T_1, T_2, and the apparent diffusion coefficient of water molecules were reflected in the NMR imagings, which demonstrated redistribution of water between different bulb organs, as well as significant differences in the pattern of this redistribution between the chilled and non-chilled bulbs. Tissue structure and developmental changes occurring during active growth in the root tuber of *Zantedeschia Spreng* cv. *Chianti*, a

commonly significant cut flower, was examined by using NMR imaging and complementary analytical techniques.[110] Plants were observed during the period of leaf senescence and tuberization at the end of the first growth cycle of micropropagated plantlets and, following cool storage to break endodormancy, during development occurring after the replanting of ecodormant tubers. NMR imaging distinguished two distinct regions within the tuber, and the differences in the binding state of water in the two regions was reflected in differences in tissue morphology and function.

NMR microimaging was applied for examining the efficiency of grafting coniferous plants.[111] Results indicate that the quality of union between stock and scion depends very much on the grafting method and NMR imaging gives more information about the graft than microscopic images.

11 Food

Prediction models for residue transfer into eggs are being developed. Recent results indicate that the developing egg yolk serves as an important storage depot for chemical residues. From the view point of human food safety, the current study was conducted to visualize incorporation and potential compartmentalization of drug residues in developing egg yolks.[112] For details see Section 12.3.

For better characterization and understanding of meat characteristics, the potential of NMR spectroscopy and imaging has been illustrated.[113] Authors demonstrate the energy metabolites in muscle, fatty acid components of animal fat, a quantitative measurement of parameters closely correlated with meat properties such as pH, cooking yield and water holding capacity at each point of an NMR imaging and so on. It is concluded that NMR is a powerful tool for meat research in comparison with other less expensive techniques.

The presence of hollows in cooked rice grains was additionally confirmed for four more cultivars Koshihikari with various amylose contents.[114] The size, shape and total volume of hollows differed between cultivars. The hypothetical model for the formation of hollows has not been proved experimentally. ^{1}H-NMR microimaging was used to determine moisture distribution in boiled Japanese noodles (udon) made from different varieties of wheat.[115] The T_2 profile of a piece of boiled udon was monitored in time course measurements during and after boiling. Water permeation from the surface to the core was evaluated by the T_2 profile. Effect of moisture distribution on texture of boiled Japanese noodles was discussed.

12 *In Vivo* and *Ex Vivo*

12.1 In Vivo Applications. – *12.1.1 Sponges and Insects.* Until now, direct, non-invasive *in vivo* studies on water and metabolite distribution in living sponges have not been possible. NMR imaging was applied for the first time to

determine the spatial distribution of water in the marine sponge *Suberites domuncula*.[116] After transfer of the sponge into deuterated water (D_2O) for a short incubation period of 18 min, no significant water exchange was observed, neither in *S. domuncula*, nor in the hermit crab living in symbiosis with it. This suggests D_2O to be an ideal contrast-enhancing agent for NMR imaging of sponges. Thus, NMR imaging provides a promising technique for the detection (and possibly quantification) of the distribution and transport of water both by diffusion and active transport in a living sponge.

A range of NMR techniques, ^1H liquid spectroscopy and T_1 and T_2 relaxation measurements, and microimaging, have been used to observe changes taking place within the bodies of live samples of *Coccinella septempunctata* (*Coleoptera*: *Coccinellidae*) under a variety of conditions.[117] Various organs could be seen and identified. By changing the diet of the ladybird from aphids to a standard artificial diet, major changes took place in the insect's tissues. By using a combination of all three techniques, NMR could become a major tool in the non-destructive study of insects not just as a means of studying anatomy but also to observe changes in the nature of body tissue.

12.1.2 Apparent Diffusion Coefficient (ADC), DWI. Diffusion-weighted magnetic resonance imaging (DWI) with calculation of the apparent diffusion coefficient (ADC) of water is a widely used noninvasive method to measure movement of water from the extracellular to the intracellular compartment during cerebral ischemia.

Lamotrigine, a neuronal Na^+ channel blocker, has been shown to attenuate the increase in extracellular concentrations of excitatory amino acids (EAA) during ischemia and to improve neurological and histological outcome. To determine the effect of lamotrigine on intra- and extracellular water shifts during transient global cerebral ischemia, ADC was measured during ischemia and early reperfusion for fifteen New Zealand white rabbits.[118] The results suggest that the ADC decline may not be mediated by voltage-gated sodium influx and glutamate release. To determine if vasospasm induced by application of endothelin-1 (ET-1) in the rat brain would model the abnormalities attributed to vasospasm described in patients with subarachnoid hemorrhage (SAH) with reversible neurological deficits, DWI and MRS were performed.[119] The data suggest that the regions with persistently low ADC were metabolically compromised, with incomplete recovery of PCr and ATP, and represent irreversibly damaged tissue. This model is a potentially useful model of low flow as seen in clinical vasospasm following SAH. The relationship between ADC measured by MRI, anoxic depolarization, and glutamate efflux during experimental cerebral ischemia were compared.[120]

A range of liquids suitable as quality control test objects for measuring the accuracy of clinical MRI diffusion sequences (both ADC and tensors) has been identified and characterized.[121] The self-diffusion coefficients for 15 liquids (values at 22 °C range from 0.36 to 2.2×10^{-9} m^2 s^{-1}) were measured at 15–30 °C using an NMR spectrometer.

12.1.3 Flow, CBV, Ischemic Tissue. An historical review of developments in the field of cerebral blood flow (CBF) and metabolism has been given.[21] The review includes the development of the nitrous oxide method by Kety and Schmidt (1948), the autoradiogram, *i.e.* [^{131}I]trifluoro-iodomethane ($CF_3{}^{131}I$) method and its modification for use with ^{14}C autoradiogram and a nonvolatile tracer, first [^{14}C]antipyrine, and then [^{14}C]iodoantipyrine, and furthermore, MRI techniques. MRI-based functional brain imaging has become the most popular CBF-related technique in use today because of its non-invasiveness, lack of ionizing radiation, excellent spatial and temporal resolution, and repeatability. Although it may correlate with changes in CBF, however, it does not measure it.

Cerebral blood flow (CBF) and blood volume (CBV) was measured by MRI bolus tracking after acute stroke in pigs and compared with [^{15}O]H_2O positron emission tomography.[122] Authors examined the feasibility of using a novel method for measuring CBF of ischemic tissue based on MRI after middle cerebral artery occlusion (MCAO) in 13 pigs. Moreover, the regional correlation between CBF and CBV was investigated in the regions with acute ischemic stroke.

12.1.4 Magnetic Resonance Spectroscopic Imaging (MRSI). Quantitative NMR spectroscopic imaging is applied to the brain to quantify the amount of *N*-acetylaspartate (NAA),[123,124] choline,[124] creatine[124] and other metabolites. A non-localizing pulse sequence to quantify the total amount of *N*-acetylaspartate (NAA) in the whole brain (WBNAA) was introduced recently.[123] However, it is known that regional magnetic field inhomogeneities, ΔB_0s, arising from susceptibility differences at tissue interfaces, shift and broaden local resonances to outside the integration window, leading to an underestimation of the true amount of NAA in the entire brain. By using the procedure of summing signals only from voxels within that organ from a three-dimensional chemical shift imaging (3D CSI) set, it was indicated that <10% of the water signal loss occurred in the brain and, therefore, by analogy, WBNAA accounts for >90% of that metabolite. Quantitative ^{1}H MR spectroscopic imaging was applied to monitor the change of distribution of NAA, choline and creatin in early Rett syndrome.[124]

12.1.5 Therapy Effect. The effect of thrombolytic therapy on metabolic changes was studied in rat brains submitted to thromboembolic stroke by a MRSI.[125] Temporal changes in the cerebral methabolites lactate and *N*-acetylaspartate (NAA) were determined. In individual pixels, the probability of metabolic tissue recovery clearly declined with increasing lactate concentration before thrombolysis.

Laser therapy by low light doses shows promising results in the modulation of some cell functions. However, the mechanism behind it is still not completely understood. To explore the effect of a low-power diode laser (= 780 nm) on normal skin tissue, time-dependent contrast enhancement has been determined by MRI.[126] It can be observed that, after biomodulation with light of low energy and low power, wound healing improves and pain is

reduced. This effect might be explained by an increased blood flow in this area. Therefore, the use of this kind of laser treatment might improve the outcome of other therapeutic modalities such as tumour ionizing radiation therapy and local chemotherapy.

Recent studies suggest that tranilast inhibits a variety of agents implicated in neointimal growth and restenosis in experimental animal models and humans. A study evaluating the efficacy of tranilast was reported in the rat carotid artery balloon angioplasty model, a model that mimics many aspects of the percutaneous transluminal angioplasty procedure in humans.[127] Efficacy was determined based on *in vivo* and *ex vivo* magnetic resonance imaging as well as by histomorphometry.

The changes of tumor size after gene therapy treatment and its relationship with the changes of vascular volume was investigated by dynamic contrast-enhanced MRI, to investigate whether the vascular changes is predictive of tumor regression.[128] The study was carried out using a spontaneously regressing rat tumor model (C6 Glioma grown subcutaneously in rats). Three rats were treated with recombinant adenoviruses expressing three genes, mouse interleukin 1- (IL1-), mouse interferon (IFN-), and human transforming growth factor (TGF-), respectively. Two rats were treated with saline as controls. The vascularity changes measured by dynamic MRI may provide a means to serve for this purpose.

12.1.6 Pharmacological MRI and Neuropharmacological MRI. Various methods, including fMRI, have recently been developed to allow investigators to study functional activity in the living brain. Such techniques are now being used to investigate regionally specific brain activity associated with the administration of CNS-active drugs. fMRI in particular is increasingly recognized as being a relatively non-invasive way to perform pharmacological investigations in experimental animals, healthy human volunteers, and individuals with CNS disease. This use of fMRI, dubbed 'pharmacological MRI' or 'phMRI', holds the promise of providing relatively straightforward pharmacodynamic assays and can be used to establish brain-penetrability parameters, or dose-ranging information for novel therapeutic compounds. Pharmacological MRI was reviewed as a new application for fMRI.[129]

Regional brain activation by the GABA antagonist bicuculline was visualized by MRI.[130] Time-resolved assessment of bicuculline-induced changes in local cerebral blood volume was performed by using an intravascular contrast agent. The effects of dopamine receptor supersensitivity were detected using pharmacological MRI and correlations with PET.[131] Hypothalamic function following intraperitoneal glucose administration in a rat model was demonstrated by *in vivo* fMRI[132] and the effect of ethanol on BOLD response to acoustic stimulation was presented for the implications of neuropharmacological fMRI.[133]

12.1.7 BOLD Effect, High Field. The close correspondence between neural activity in the brain and cerebral blood flow (CBF) forms the basis for

modern functional neuroimaging methods. However, the temporal characteristics of hemodynamic changes induced by neuronal activity are not well understood. DeoxyHb can be detected by blood oxygenation level-dependent (BOLD) fMRI.[134] The temporal characteristics of CBF and BOLD changes elicited by somatosensory stimulation in rat were investigated by high field (9.4 T) MRI. The findings argue against the occurrence of an early loss of Hb oxygenation that precedes the rise in CBF and suggest that CBF and oxygen consumption increases may be dynamically coupled in this animal model of neural activation.

12.1.8 Gene Expression. The ability to increase cardiac frequency and contractility is essentially dependent on the stimulation of cardiac β-adrenergic receptors. Two receptors, *i.e.*, the β1-subtype and the β2-subtype, are coupled to an increase in the production of cAMP and increased opening of calcium channels. Transgenic mouse models with heart-specific overexpression generated for both receptor subtypes have been characterized to evaluate the effects by overexpression of each β subtype. A review was presented with 51 references.[25] *In vivo* NMR imaging also indicated a massive reduction of the ejection fraction, which was only about 20% at nine months of age, compared to about 60% in wild-type control mice. Thus, the data available so far suggest strikingly dissimilar phenotypes resulting from the heart-specific overexpression of the two β-adrenergic receptors.

Assessing gene expression *in vivo* has been performed by magnetic resonance imaging and spectroscopy[135–137] and briefly reviewed.[135]

12.1.9 Paramagnetic Effects: Endogenous. Non-heme iron is abundantly present in the brain in three different forms: 'low molecular weight' complexes, iron bound to 'medium molecular weight complexes' metalloproteins such as transferrin, and 'high molecules weight' complexes as ferritin and hemosiderin. Total amount and forms of iron may differ in health and disease, and MRI can possibly quantify and monitor such changes.

Using both *in vitro* specimens and intact tissue *in vivo*, it was demonstrated that MRI may be able to distinguish between hemosiderin- and ferritin-bound brain iron.[138] Ferritin is water soluble, and shortens both T_1 and T_2 relaxation, with resultant signal changes on the MRI, on the other hand the large cluster size of hemosiderin (*i.e.* a degradation product of ferritin) and its water insolubility explain a lack of significant T_1-shortening effect on T_1-weighted images. In humans, ferritin is mainly located in the liver, spleen and brain, and is involved in many diseases, such as hemochromatosis and Parkinson disease. Ferritin in different organs causes a darkening of T_2-weighted images in MRI, resulting from a fast proton transverse relaxation.[139] This phenomenon can be used as a non-invasive tool for estimating the ferritin concentration *in vivo*. However, the relaxation mechanism of water in the presence of ferritin is not understood. It was shown that the relaxation may be due to a proton exchange between the ferrihydrite iron core of ferritin and bulk water. Dynamic relaxometry was applied to iron uptake by ferritin.[140]

Influence of several nitrosyl-iron complexes on ^1H relaxation rates was assessed to establish a MR imaging technique for nitric oxide (NO).[141] To induce formation of nitrosyl-ion complexes in a biological tissue, isolated rat liver was perfused with a saline solution of the NO donor sodium nitroprusside (SNP), and the MR signal intensity was examined thereafter. Nitrosyl-iron complexes exhibit a contrast effect at MR imaging that can be exploited for NO imaging in living animals and patients with conventional ^1H MR imaging.

Due to its paramagnetic properties, manganese (Mn) can be effectively visualized by MRI. Mn accumulates selectively in the globus pallidus of basal ganglia, where it can produce high signals at brain magnetic resonance. These hyperintensities are bilateral, symmetric and visible in T_1-weighted magnetic resonance imaging of different manganese overload conditions. A review of the literature with 36 references shows identical findings in Mn exposed workers, hepatopatic patients, and patients undergoing total parenteral nutrition with excessive amount of manganese.[142] Two indicators of exposure and hyperintensity were considered, represented respectively by the concentration of Mn in total blood (MnB) and the pallidal index (PI). These two indicators show a possitive association, which indicates a possible continuum from normality to clinical stages both in workers occupationally exposed to Mn and in patients suffering from chronic liver disease. Since both MnB and PI show a high degree of variability, further research should be focused on the identification of more accurate indicators.

The brain pallidal T_1-weighed MRI signal hyperintensity was recorded in 10 women and 11 men (33–69 yrs) with chronic liver disease and the data were correlated with self-reported clinical neurological symptoms and blood serum Fe, Mn, bilirubin, alk. phosphatase and aspartate transaminase, erythrocyte Mn, and blood Hb and hematocrit levels.[143]

12.1.10 Paramagnetic Effect and Pharmacokinetics: Exogeneous. The evaluation of a Gd-carborane complex as a MR imaging and boron carrier agent was carried out *in vivo* by using tumor-bearing Donryu rats, MRI, ICP-AES, and a-autoradiogram.[144]

Dendrimers in diagnostics were reviewed with 144 references.[17] Major target indications of dendrimeric contrast agents include angiography, tissue perfusion determination and tumor detection and differentiation. The structures and sizes of these carriers are presently optimized. So far, however, no compound has reached the status of clinical application. Possible hurdles to overcome are synthetic problems such as drug uniformity, reproducible production of pure compounds and analytical issues, *e.g.* demonstrating purity. In principle, proof of concept for dendrimeric contrast agents as intravascular and tumor-targeting substances seems to have been established. However, a lot of effort is still necessary before a dendrimeric contrast agent will finally be available for wide-spread use in patients.

The extravasation properties of two macromolar MR imaging contrast media (CM) in relation to structural differences of the terminal vascular bed

were investigated in the hamster skinfold chamber to determine whether differentiation between normal (physiol.) and tumor (pathol.) tissue can be achieved by means of extravasation characteristics.[145] The CM studied showed different microvascular permeation properties. Faster leakage of Gd-DOTA cascade polymer (20 kDa) was observed in areas with neoplastic tumor vessels, whereas extravasation in physiological tissue was detected after a period of 5 min. Gd-DTPA-polylysine (50 kDa) demonstrated nonspecific leakage at later time points.

Tat peptide-derivatized magnetic nanoparticles allow *in vivo* tracking and recovery of progenitor cells.[146]

12.1.11 Toxicity. Caenorhabditis elegans (*C. elegans*) has proven useful in toxicity testing of known toxicants, but its potential for assessing the toxicity of new pharmaceuticals is relatively unexplored. The procedures used in aquatic testing of toxicants were modified to permit testing of small amounts (<40 mg) of Gd-based MRI compounds and five blind compounds were tested.[147] The toxicity of these compounds determined using *C. elegans* was compared to existing mammalian test system data (min. LD [MLD] values for mice). Testing with *C. elegans* is efficient and could markedly reduce the cost of screening potentially useful compounds.

Acute aflatoxin B1 (AFB1)-induced hepatotoxicity was assessed *in vivo* in male Sprague–Dawley rats (150–300 g) using MRI.[148] MRI results were compared to serum enzyme levels, histology and electron microscopy.

12.2 *Ex Vivo* Experiments. – *12.2.1 Cartilage.* To test the hypothesis that MRI results correlate with the biochemical composition of cartilage matrix and can therefore be used to evaluate natural tissue development and the effects of biological interventions. Chondrocytes harvested from day-16 chick embryo sterna were inoculated into an MRI-compatible hollow-fiber bioreactor. The response of engineered tissue, that formed over a period of 2–4 weeks, to biochemical agents was studied biochemically, histologically and with magnetic resonance microscopy.[149] Parameters, *i.e.* water T_1 and T_2 relaxation times, magnetization transfer value and self-diffusion coefficient of water, derived from MRI obtained non-invasively can be used to quantitatively assess the composition of cartilage tissue generated in a bioreactor.

Quantifying the diffusive transport of large molecules in a vascular cartilage tissue is important both for planning potential pharamacological treatments and for gaining insight into the molecular scale structure of cartilage. The diffusion coefficients of Gd-DTPA and Gd-labeled versions of four proteins – lysozyme, trypsinogen, ovalbumin and bovine serum albumin – have been measured in healthy and degraded calf cartilage. The experimental technique relies on the effect of the paramagnetic on the relaxation properties of the surrounding water, combined with the time course of a 1-dimensional spatial profile of the water signal in the cartilage sample.[150] Degradation of the cartilage led to increases in the diffusion coefficient of up to fivefold for the Gd-labeled proteins. These basic transport parameters yield insights into the

nature of pore sizes and chemical matrix interactions in the cartilage tissue and may prove diagnostically useful for identifying the degree and nature of damage to cartilage.

Comparison of results of scanning electron microscopy and MRI was done before and after administration of a radiographic contrast agent in the tendon of the deep digital flexor muscle obtained from horse cadavers.[151]

In vivo and *ex vivo* applications of MRI techniques in early stage of cartilage disease were reviewed in reference 20.

12.3 Miscellaneous. – The expression of leukocyte adhesion molecules in the intact brains of mice with experimental autoimmune encephalitis (EAE) was visualized by MRI through the use of a new, target-specific MR contrast agent.[152] Antibody-conjugated paramagnetic liposomes (ACPLs) were designed to achieve *in vivo* targeting of molecules expressed on vascular endothelium, while providing sufficient signal enhancement at these sites for detection by MRI. ACPLs targeted to intercellular adhesion molecule-1 (ICAM-1), an endothelial leukocyte receptor upregulated on cerebral microvasculature during EAE, were administered to diseased mice. High resolution MRI of mouse brains *ex vivo* demonstrated that ACPL binding conferred significant enhancement of signal intensity SI as compared to control images. These results suggest that ACPLs can be used as MRI contrast agents to visualize specific molecules expressed on vascular endothelium during disease.

Double-resonance *J*-edited ^{1}H-NMR detection of [6-^{13}C]-D-2-deoxyglucose uptake in glioma cells has been developed.[153] The C_6 methylene protons were selectively detected in ^{1}H-NMR spectra of intact glioma cells incubated with [6-^{13}C]-D-2-deoxyglucose (I), a ^{13}C-enriched glucose analog that is suitable for monitoring glucose utilization in brain tumors. Spectral editing *via* ^{1}H–^{13}C scalar coupling was performed with twin spin-echo double resonance (T-SEDOR), a pulse sequence which combines chemical specificity and high sensitivity, requires no solvent pre-saturation, and can easily be adapted to imaging protocols. This work demonstrates the suitability of the pulse sequence for monitoring the uptake of (I) in living cells *in vitro*, in spite of line-broadening and the occurrence of other strong signals in the spectral region of interest (3.5–4.4 ppm).

In vivo magnetic resonance imaging and relaxometry of a porous hydrogel implanted in the trapezius muscle of rabbits was studied.[154]

The drug magnevist (Gd-DTPA) was injected into hens to evaluate drug transfer into either early- or late-developing yolks.[112] High resolution MRI of drug residues were acquired using a 1.5 T clinical scanner by using an inversion time (T_1) weighted magnetization-prepared, rapid acquisition, gradient-recalled-echo (MPRAGE) pulse sequence. Following dosing, images of drug residues in eggs indicate that drugs can be incorporated and compartmentalized into ring structures within individual developing egg yolk.

13 Miscellaneous

The structure of a CH_4 hydrate layer from ice was argued by Moudrakovski *et al.* and L. A. Stern *et al.* A polemic is given answering the publication by Moudrakovski (Letter, 'Hydrate layers on ice particles and superheated ice: A ^1H NMR microimaging study' in *J. Phys. Chem.* 1999, **103**, 4969) by L. A. Stern *et al.*[155] The experimental conditions in both groups are completely different for the formation of CH_4 hydrate from ice and CH_4 gas, *i.e.* under high pressure (27–33 MPa) by Stern *et al.* and at lower pressures (5.7–11.9 MPa) by Moudrakovski's ^1H NMR microimaging experiments.

NMR imaging was used to study the spatial distribution of molecules with chemically induced dynamic nuclear polarization.[156] It is shown that heating of a system during the photolysis can cause a highly nonuniform distribution of reaction products due to a convective effect.

Proton NMR imaging of tobacco blends in cigarette rods was investigated to assess the feasibility of various imaging protocols to characterize and quantify the structure and component of multiphase plant materials *in situ*.[157] Single-point imaging (SPI) and a single-point ramped imaging with T_1 enhancement (SPRITE) were employed. Both 1D and 2D maps of proton spin density and relaxation (T_2*) were acquired.

14 References

1 T. Watanabe, *Nuclear Magnetic Resonance*, 1997, **26**, 447; *ibid.*, 1998, **27**, 431; *ibid.*, 1999, **28**, 468–484; *ibid.*, 2000, **29**, 509–533; *ibid.*, **30**, 453–476.

2 C. Boesch, *Mol. Aspects Med.*, 1999, **20** (4/5), 185–318.

3 P. F. Renshow, B. deB. Frederick, and L. C. Maas, III, *Brain Imaging Subst. Abuse*, ed. by M. J. Kaufman, Human Press Inc., NJ, 2001, 47–76.

4 G. J. Kemp, *Dev. Neurosci. (Basel)*, 2000, **22**(5–6), 418–428.

5 J.-P. Grivet, *NMR Microbiol.*, 2000, 27–46, ed. by J.-N. Barbotin, and J.-C. Portais, Horizon Scientific Press, Wymondham, UK.

6 P. Raghunathan, *Proc. India Natl. Sci. Acad. Part A*, 1999, **65** (6), 699–729.

7 B. Blumich, D. E. Demco, S. Stapf, U. Goerke, C. Chwatinski, L. Gasper, R. Giesen, R. Haken, and S. Han, *Polym. Mater. Sci. Eng.*, 2000, **82**, 148.

8 J. L. Koenig, *Rubber Chem. Technol.*, 2000, **73** (3), 385–404.

9 D. E. Demco, and B. Blumich, *Concepts Magn. Reson.*, 2000, **12** (4), 188–206.

10 D. E. Demco, and B. Blumich, *Concepts Magn. Reson.*, 2000, **12** (5), 269–288.

11 T. Pietrass, *Magn. Reson. Rev.*, 2000, **17**(4), 263–337.

12 G. Tastevin, *Phys. Ser. T*, 2000, **T86**, 46–50.

13 S. R. Breeze, S. J. Lang, A. V. Nosov, A. Sanchez, I. L. Moudrakovski, C. I. Ratcliffe, and J. A. Ripmeester, *Stud. Surf. Sci. Catal.*, 2000, **129** (Nanoporous Materials II, Proceedings of the Conference on Access in Nanoporous Materials, 2000), 491–499.

14 N. Chandrakumar, *Supramol. Colloidal Struct. Biomater. Biosubstrates*, Proc. R. Soc.–Unilever Indo-UK Forum Mater. Sci. Eng., 5th, 2000, Meeting Date 1999, 33–51, ed. M. Lal, Imperial College Press, London, UK.

15 C. D. Kilts, *J. Clin. Psychiatry*, 2000, **61** (Suppl. 9), 41–46.

16 P. A. Bottomley, R. F. Lee, C. D. Constantinides, R. Ouwerkerk, and R. G. Weiss, *Magn. Reson. Mater. Phys., Biol. Med.*, 2000, **11** (1–2), 39–41.
17 W. Krause, N. Hackmann-Schlichter, F. K. Maier, and R. Muller, *Top. Curr. Chem.*, 2000, **210** (Dendrimers II), 261–308.
18 J. S. Taylor, and W. E. Reddick, *Adv. Drug Delivery Rev.*, 2000, **41** (1), 91–110.
19 R. B. Pearce, *J. Arboriculture*, 2000, **26** (1), 1 11.
20 D. Burstein, A. Bashir, and M. L. Gray, *Invest. Radiol.*, 2000, **35** (10), 622–638.
21 L. Sokoloff, *Keio Univ. Symp. Life Sci. Med.*, 2000, **6** (Ischemic Blood Flow in the Brain), 3- 10.
22 J. C. Soares, and R. B. Innis, *Med. Psychiatry*, 2000, **15**, 227–252.
23 M. Lehtovirta, M. P. Laakso, G. B. Frisoni, and H. Soininen, *Neurobiol. Aging*, 2000, **21** (2), 293–300.
24 H. El-Gabalawy, *Arthritis Res.*, 1999, **1** (1), 31–36.
25 M. J. Lohse and S. Engelhardt, *Mol. Approaches Heart Failure Ther.*, 2000, 26–38. ed. G. Hasenfuss, and E. Marban. Dr. Dietrich Steinkopff Verlag GmbH & Co. KG, Darmstadt, Germany.
26 U. Ladabaum, S. Minoshima, and C. Owyang, *Am. J. Physiol.*, 2000, **279** (1), Pt. 1, G1–G6.
27 J. A. Olson, K. J. Nordell, M. A. Chesnik, C. R. Clark, A. B. Ellis, M. S. Rzchowski, S. Michael Condren, G. C. Lisensky, and J. W. Long, *J. Chem. Educ.*, 2000, **77** (7), 882–889.
28 D. A. Cornell, C. F. M. Clewett, and M. S. Conradi, *Concepts Magn. Reson.*, 2000, **12** (5), 257–268.
29 G. Grasso, A. Malagoli, N. Scati, P. Guasconi, and A. S. Siri, *Int. J. Mod. Phys. B*, 2000, **14** (25–27), 2902–2907.
30 A. A. Esmail, D. Bracanovic, S. J. Penn, D. Hight, S. Keevil, T. W. Button, and N. McNalford, *Inst. Phys. Conf. Ser.*, 2000, **167** (Applied Superconductivity 1999, Vol. 2), 299–302.
31 M. C. K. Wiltshire, J. B. Pendry, I. R. Young, D. J. Larkman, D. J. Gilderdale, and J. V. Hajnal, *Science*, 2001, **291** (5505), 849–851.
32 A. Z. Damyanovich, J. Peternelj, and M. M. Pintar, *J. Magn. Reson.*, 2000, **144** (1), 1–5.
33 S. R. Charagundla, U. Duvvuri, E. A. Noyszewski, R. Dandora, A. H. Stolpen, J. S. Leigh, and R. Reddy, *J. Magn. Reson.*, 2000, **143** (1), 39–44.
34 K. Woelk, B. L. J. Zwank, P. Trautner, E. Lehnhof, J. Bargon, R. J. Klingler, R. E. Gerald, II, and J. W. Rathke, *J. Magn. Reson.*, 2000, **145** (2), 276–290.
35 M. Nonaka, S. Matsui, and T. Inouye, *J. Magn. Reson.*, 2000, **145** (2), 315–318.
36 J. W. C. van der Veen, D. R. Weinberger, G. Tedeschi, J. A. Frank, and J. H. Duyn, *Radiology* (Oak Brook, Ill.), 2000, **217** (1), 296- 300.
37 F. Santoro, C. Casieri, and F. De Luca, *Solid State Commun.*, 2000, **116** (5), 293–296.
38 L. G. Lana, T. Meersmann, J. W. Logan, and A. Pines, *Proc. Natl. Acad. Sci., U.S.A.* 2000, **97** (6), 2414–2418.
39 L. G. Kaiser, J. W. Logan, T. Meersmann, and A. Pines, *J. Magn. Reson.*, 2001, **149** (1), 144–148.
40 R. W. Mair, C.-H. Tseng, G. P. Wong, and D. G. Cory, *Phys. Rev. E: Stat. Phys., Plasmas, Fluids, Relat. Interdiscip. Top.*, 2000, **61**(3), 2741–2748.
41 A. Honig, X. Wei, A. Lewis, E. ter Haar, and K. Seraji-Bozorgzad, *Physica B (Amsterdam)*, 2000, **284–288**, 2049–2050.

42 S. R. Breeze, S. J. Lang, A. V. Nosov, A. Sanchard, G. Santyr, and J. A. Ripmeester, *J. Magn. Reson.*, 2000, **144** (2), 372–377.

43 I. L. Moudrakovski, S. Lang, C. I. Ratcliffe, B. Simard, G. Santyr, and J. A. Ripmeester, *J. Magn. Reson.*, 2000, **144** (2), 372–377.

44 M. P. Ramirez, K. C. E. Sigaloff, L. V. Kubatina, M. A. Donahue, A. K. Venkatesh, and M. S. Albert, *NMR Biomed.*, 2000, **13**(4), 253–264.

45 G. Duhamel, P. Choquet, J.-L. Leviel, J. Steibel, L. Lamalle, C. Julien, F. Kober, E. Grillon, J. Derouard, M. Decorps, A. Ziegler, and A. Constantinesco, C. R. *Acad. Sci., Ser. III*, 2000, **323** (6), 529–536.

46 J. Wolber, A. Cherubini, M. O. Leach and A. Bifone, *Magn. Reson. Med.*, 2000, **43** (4), 491–496.

47 X. J. Chen, L. W. Hedlund, H. E. Moller, M. S. Chawla, R. R. Maronpot, and G. A. Johnson, *Proc. Natl. Acad. Sci. USA*, 2000, **97** (21), 11478–11481.

48 R. M. Dijkhuizen, R. A. De Graaf, M. Garwood, K. A. F. Tulleken, and K. Nicolay, *J. Cereb. Blood Flow Metab.*, 1999, **19** (4), 376–379.

49 F. Hyder, R. Renken, and D. L. Rothman, *Magn. Reson. Med.*, 1999, **42** (6), 997–1003.

50 J.-L. Guerquin-Kern, A. Volk, E. Chenu, R. Lougerstay-Madec, C. Monneret, J.-C. Florent, D. Carrez, and A. Croisy, *NMR Biomed.*, 2000, **13** (5), 306–310.

51 A. Schlicker, W. Mier, M. E. Bellemann, G. Brix, and P. Peschke, *Proc. Int. Symp. Controlled Release Bioact. Mater.*, 2000, **27**th, 522–523.

52 N. R. Bolo, Y. Hode, J.-F. Nedelec, E. Laine, G. Wagner, and J.-P. Macher, *Neuropsychopharmacology*, 2000, **23** (4), 428–438.

53 D. O. Kuethe, A. Caprihan, H. M. Gach, I. J. Lowe, and E. Fukushima, *J. Appl. Physiol.*, 2000, **88** (6), 2279–2286.

54 R. P. Kline, E. X. Wu, D. P. Petrylak, M. Szabolcs, P. O. Alderson, M. L. Weisfeldt, P. Cannon, and J. Katz, *Clin. Cancer Res.*, 2000, **6** (6), 2146–2156.

55 C. E. Rochitte, R. J. Kim, H. B. Hillenbrand, E.-L. Chen, and J. A. C. Lima, *Circ. Res.*, 2000, **87** (8), 648–655.

56 V. P. Chacko, F. Aresta, S. M. Chacko, and R. G. Weiss, *Am. J. Physiol.*, 2000, **279** (5, Pt 2), H2218–H2224.

57 K. L. Zakian, M. D'Angelica, C. Matei, H.-H. Yoo, M. Ercolani, K. Delman, Y. Fong, and J. A. Koutcher, *Magn. Reson. Imaging*, 2000, **18** (2), 181–187.

58 V. V. Kupriyanov, B. Xiang, J. Sun, G. Dai, O. Jilkina, V. Dao, and R. Deslauriers, *Magn. Reson. Med.*, 2000, **44** (1), 83–91.

59 V. V. Kupriyanov, B. Xiang, J. Sun, O. Jilkina, G. Dai, and R. Deslauriers, *Magn. Reson. Med.*, 2000, **44** (2), 193–200.

60 A. Caprihan and J. D. Seymour, *J. Magn. Reson.*, 2000, **144** (1), 96–107.

61 A. Mohoric and J. Stepisnik, *Phys. Rev. E: Stat. Phys., Plasmas. Fluids, Relat. Interdiscip. Top.*, 2000, **62** (5–A), 6628–6635.

62 S. A. Riley, and M. P. Augustine, *J. Magn. Reson.*, 2000, **144** (2), 288–296.

63 I. G. Koptyug, S. T. Altobelli, E. Sukushima, A. V. Matveev, and R. Z. Sagdeev, *J. Magn. Reson.*, 2000, **147**, (1), 36–42.

64 M. Gentzler, Y. Q. Song, S. J. Muller, and J. A. Reimer, *Polym. Mater. Sci. Eng.*, 2000, **82**, 149.

65 K. W. Moser, E. C. Kutter, J. G. Georgiadis, R. O. Buckius, H. D. Morris, and J. R. Torczynski, *Exp. Fluids*, 2000, **29** (5), 438–447.

66 K. L. McCarthy and M. J. McCarthy, *AT-PROCESS*, 2000, **5** (3,4), 94–103.

67 Y. Uludag, M. J. McCarthy, R. L. Powell, and G. Barall, *Annu. Tech. Conf. – Soc. Plast. Eng. 58th*, 2000, **1**, 1061–1064.

68 A. M. Gil, M. H. Lopes, C. P. Neto, and P. T. Callaghan, *J. Mater. Sci.*, 2000, **35** (8), 1891–1900.

69 F. B. Aarden, R. M. E. Valckenborg, L. Pel, P. J. A. M. Kerkhof, and K. Kopinga, *Adsorpt. Sci. Technol., Proc. Pac. Basin Conf., 2nd*, 2000, 26–30.

70 M. Mork, G. Schei, and R. Larsen, *Ann. NY Acad. Sci.*, 2000, **912** (NR: Gas Hydrates), 897–905.

71 I. V. Koptyug, R. Z. Sagdeev, L. Yu. Khitrina, and V. N. Parmon, *Appl. Magn. Reson.*, 2000, **18** (1), 13–28.

72 J. Middleton, *Polym. Paint Colour J.*, 2000, **190** (4432), 25–26.

73 S. Harding, H. Baumann, T. Gren, and A. Seo, *J. Controlled Release*, 2000, **66** (1), 81–99.

74 J. Tritt-Goc and N. Pislewski, *Mol. Phys. Rep.*, 2000, **28**, 126–132.

75 C. A. Fyfe, H. Grondey, A. I. Blazek-Welsh, S. K. Chopra, and B. J. Fahie, *J. Controlled Release*, 2000, **68** (1), 73–83.

76 C. A. Fyfe and A. I. Blazek-Welsh, *J. Controlled Release*, 2000, **68** (3), 313–333.

77 H. V. As and P. Lens, *J. Ind. Microbiol. Biotechnol.*, 2001, **26** (1/2), 43–52.

78 S. P. Rigby and L. F. Gladden, *Chem. Eng. Sci.*, 2000, **55** (23), 5599–5612.

79 S. P. Rigby, *Stud. Surf. Sci. Catal.*, 2000, **130 D** (Int. Congr. On Catalysis, 2000, Part D), 3267–3272.

80 E. B. Brouwer, I. Moudrakovski, K. H. Chung, G. Pleizier, J. A. Ripmeester, and Y. Deslandes, *Stud. Surf. Sci. Catal.*, 2000, **129** (Nanoporous Materials II, Proceedings of the Conference on Access in Nanoporous Materials), 509–516.

81 K. Saito, Y. Fujioka, M. Hatakeyama, and K. Katoh, 1998, *Sekitan Kagaku Kaigi Happyo Ronbunshu*, **35**, 261–266.

82 S. P. Rigby, *Stud. Surf. Sci. Catal.*, 2000, **130D** (International Congress on Catalysis), 3267–3272.

83 S. Kusmia, E. Szczesniak, and S. Jurga, *Mol. Phys. Rep.*, 2000, **28**, 106–108.

84 D. D. Parker, C. M. Snively, J. L. Koenig, C. E. Rogers, *Proc. ERDEC Sci. Conf. Chem. Biol. Def. Res.*, 1999 (Meeting Date 1998), 795–799.

85 J. Zhou, G. Metcalfe, L. Graham, and R. Hamilton, *Proc. Int. Congr. Rheol. 13th*, 2000, **2**, 297–299, ed. D. M. Binding, British Society of Rheology, Glasgow, UK.

86 B. E. Dawson-Andoh, J. M. Halloin, T. G. Cooper, D. P. Kamdem, and E. J. Potchen, *Wood Fiber Sci.*, 2001, **33** (1), 84–89.

87 M. D. Mantle, A. J. Sederman, and L. F. Gladden, *Chem. Eng. Sci.*, 2001, **56**(2), 523–529.

88 S. Sharma, M. D. Mantle, L. F. Gladden and J. M. Winterbottom, *Chem. Eng. Sci.*, 2001, **56** (2), 587–595.

89 M. L. Johns, A. J. Sederman, A. S. Bramley, L. F. Gladden, and P. Alexander, *AIChE J.*, 2000, **46** (11), 2151–2161.

90 D. F. Caputo, D. G. Cory, M. Draye, and K. R. Czerwinski, *Mater. Res. Soc. Symp. Proc.*, 2000, **608** (Scientific Basis for Nuclear Waste Management XXIII), 643–648.

91 S. G. Harding and H. Baumann, *J. Chromatogr. A*, 2001, **905** (1–2), 19–34.

92 P. Adriaensens, A. Pollaris, D. Vanderzande, J. Gelan, J. L. White, and M. Kelchtermans, *Macromolecules*, 2000, **33** (19), 7116–7121.

93 P. J. Prado, L. Gasper, G. Fink, and B. Blumich, *Appl. Magn. Reson.*, 2000, **18** (1), 177–185.

94 A. Yamazaki, Y. Hotta, H. Kurosu, and I. Ando, *J. Mol. Struct.*, 2000, **554** (1), 47–53.

95 B. Thu, O. Gaserod, D. Paus, A. Mikkelsen, B. G. Skjak, R. Toffanin, F. Vittur, and R. Rizzo, *Biopolym. J.*, 2000, **53** (1), 60–71.
96 S. Ganapathy, P. R. Rajamohanan, M. V. Badiger, A. B. Mandhare, and R. A. Mashelkar, *Polymer*, 2000, **41** (12), 4543–4547.
97 P. Adriaensens, L. Storme, R. Carleer, D. Vanderzande, J. Gelan, V. M. Litvinov, and R. Marissen, *Macromolecules*,, 2000, **33** (13), 4836–4841.
98 B. Traub, T. Fritzhanns, S. Hafner, and H. W. Spiess, *Colloid Polym. Sci.*, 2000, **278** (6), 547–552.
99 M. Knorgen, K.-F. Arndt, S. Richter, D. Kuckling, and H. Schneider, *J. Mol. Struct.*, 2000, **554** (1), 69–79.
100 K. F. Arndt, D. Kuckling, and A. Richter, *Polym. Adv. Technol.*, 2000, **11** (8–12), 496–505.
101 S. Matsushima, A. Takasu, Y. Inai, T. Hirabayashi, S. Era, M. Sogami, and Y. Kinosada, *Polym. J. (Tokyo)*, 2000, **32** (10), 828–833.
102 I. C. Baustert, M. Oldham, T. A. D. Smith, C. Hayes, S. Webb, and M. O. Leach, *Phys. Med. Biol.*, 2000, **45** (4), 847–858.
103 M. Lepage, A. K. Whittaker, L. Rintoul, and C. Baldock, *J. Appl. Polym. Sci.*, 2000, Volume Date, 2001, **79** (9), 1572–1581.
104 B. A. Goodman and S. M. Glidewell, *Phyton-Horn.*, 1997, **37** (3 Special Edition), 81–94.
105 S. Olt, E. Krotz, E. Komor, M. Rokitta, and A. Haase, *J. Magn. Reson.*, 2000, **144** (2), 297–304.
106 K. Wolf, A, Van der Toorn, K. Hartmann, L. Schreiber, W. Schwab, A. Haase, and G. Bringmann, *J. Exp. Bot.*, 2000, **51** (353), 2109–2117.
107 E. Komor, *Australian J. Plant Physiol*,. 2000, **27** (6), 497–505.
108 T. W. Scheenen, D. van Dusschoten, P. A. De Jager, and H. Van As, *J. Exp. Bot.*, 2000, **51**(351), 1751–1759.
109 A. Van der Toorn, H. Zemah, H. Van As, P. Bendel, and R. Kanenetsky, *J. Exp. Bot.*, 2000, **51** (348), 1277–1287.
110 A. Robinson, C. J. Clark, and J. Clemens, *J. Exp. Bot.*, 2000, **51** (353), 2009–2020.
111 R. Leszczynski, B. Byczkowski, S. Jurga, and S. Korszun, *Appl. Magn. Reson.*, 2000, **18** (1), 147–153.
112 D. J. Donoghue, and K. Myers, *J. Agric. Food Chem.*, 2000, **48** (12), 6428–6430.
113 W. Laurent, J. M. Bonny, and J. P. Renou, *Food Chem.*, 2000, **69** (4), 419–426.
114 A. K. Horigane, W. M. H. G. Engelaar, H. Toyoshima, H. Ono, M. Sakai, A. Okubo and T. Nagata, *J. Food Sci.*, 2000, **65** (3), 408–412.
115 T. Kojima-okiko, M. Sekine, T. Suzuki, A. Horigane, T. Nagata, *Nippon Shokuhin Kagaku Kogaku-Kaishi*, 2000, **47** (2), 142–147.
116 G. Bringmann, K. Wolf, T. Lanz, A. Haase, J. Hiori, P. Proksch, and W. E. G. Mueller, *Mar. Ecol. Progr. Ser.*, 1999, **189**, 307–310.
117 I. E. Geoghegan, J. A. Chudek, R. L. Mackay, C. Lowe, S. Moritz, R. J. Mcnicol, A. N. E. Birch, G. Hunter, and M. E. N. Majerus, *Eur. J. Entomol.*, 2000, **97** (4), 457–461.
118 H. Koenig, J. P. Williams, M. J. Quast, and M. H. Zornow, *Brain Res.*, 2000, **887** (2), 301–308.
119 Z. Domingo, J. K. Bradley, A. M. Blamire, K. Brindle, P. Styles, and B. Rajagopalan, *NMR Biomed.*, 2000, **13** (3), 154–162.
120 N. G. Harris, E. Zilkha, J. Houseman, M. R. Symms, T. P. Obrenovitch, and S. R. Williams, *J. Cereb. Blood Flow Metab.*, 2000, **20** (1), 28–36.

121 P. S. Tofts, D. Lloyd, C. A. Clark, G. J. Barker, G. J. M. Parker, P. McConville, P. C. Baldock, and J. M. Pope, *Magn. Reson. Med.*, 2000, **43** (3), 368–374.
122 M. Sakoh, L. Rohl, C. Gyldensted, A. Gjedde, and L. Ostergaard, *Stroke*, 2000, **31** (8), 1958–1964.
123 O. Gonen and R. I. Grossman, *Magn. Reson. Imaging*, 2000, **18**(10), 1255–1258.
124 A. Horska, S. Naidu, E. H. Herskovits, P. Y. Wang, W. E. Kaufmann, and P. B. Barker, *Neurology*, 2000, **54** (3), 715–722.
125 C. Franke, G. Brinker, F. Pillekamp, and M. Hoehn, *J. Cereb. Blood Flow Metab.*, 2000, **20** (3), 583–591.
126 M. Schaffer, H. Bonel, R. Sroka, P. M. Schaffer, M. Busch, M. Reiser, E. Duhmke, *J. Photochem. Photobiol. B*, 2000, **54** (1), 55–60.
127 E. H. Ohlstein, A. M. Romanic, L. V. Clark, R. D. Kapadia, S. K. Sarkar, R. Gagnon, and S. Chandra, *Cardiovasc. Res.*, 2000, **47** (4), 759–768.
128 M.-Y. Sua, J. A. Taylor, L. P. Villarreal, and O. Nalcioglu, *Magn. Reson. Imaging*, 2000, **18** (3), 311–317.
129 R. A. Leslie and M. F. James, *Trends Pharmacol. Sci.*, 2000, **21** (8), 314–318.
130 T. Reese, B. Bjelke, R. Porszasz, D. Baumann, D. Bochelen, A. Sauter, and M. Rudin, *NMR Biomed.*, 2000, **13** (1), 43–49.
131 T. V. Nguyen, A.-L. Brownell, Y.-I. Chen, E. Livni, J. T. Coyle, B. R. Rosen, F. Cavagna, and B. G. Jenkins, *Synapse (NY)*, 2000, **36** (1), 57–65.
132 S. Mahankali, Y. Liu, Y. Pu, J. Wang, C.-W. Chen, P. T. Fox, and J.-H. Gao, *Magn. Reson. Med.*, 2000, **43** (1), 155–159.
133 E. Seifritz, D. Bilecen, D. Hanggi, R. Haselhorst, E. W. Radu, S. Wetzel, J. Seelig, and K. Scheffler, *Psychiatry Res.*, 2000, **99** (1), 1–13.
134 A. C. Silva, S.-P. Lee, C. Iadecola, and S.-G. Kim, *Cereb. Blood Flow Metab.*, 2000, **20** (1), 201–206.
135 J. D. Bell and S. D. Taylor-Robinson, *Gene Ther.*, 2000, **7** (15), 1259–1264.
136 A. Y. Louie, M. M. Huber, E. T. Ahrens, U. Rothbacher, R. Moats, R. E. Jacobs, S. E. Fraser, and T. J. Meade, *Nat. Biotechnol.*, 2000, **18** (3), 321–325.
137 R. Weissleder, A. Moore, U. Mahmood, R. Bhorade, H. Benveniste, E. A. Chiocca, and J. P. Basilion, *Nat. Med. (NY)*, 2000, **6** (3), 351–354.
138 J. Vymazal, D. Urgosik, and J. W. M. Bulte, *Cell. Mol. Biol. (Paris)*, 2000, **46** (4), 835–842.
139 Y. Gossuin, *Phys. Mag.*, 2000, **22** (2), 101–115.
140 V. Herynek, J. W. M. Bulte, T. Douglas, and R. A. Brooks, *J. Biol. Inorg. Chem.*, 2000, **5** (1), 51–56.
141 B. Fichtlscherer and A. Mulsch, *Radiology*, 2000, **216** (1), 225–231.
142 R. Lucchini, E. Albini, D. Placidi, R. Gasparotti, M. G. Pigozzi, G. Montani, and L. Alessio, *Neurotoxicology*, 2000, **21** (5), 769–775.
143 E. A. Malecki, A. G. Devenyi, T. F. Barron, T. J. Mosher, P. Eslinger, C. V. Flaherty-Craig, and L. Rossaro, *Trace Elem. Man Anim.*, 2000, **10**, [Proc. Int. Symp.], 10th, Meeting Date 1999, 601–605, ed. A.-M. Roussel, R. A. Anderson, and A. E. Favier, Kluwer Academic/Plenum Pub.
144 H. Nakamura, H. Fukuda, F. Girald, T. Kobayashi, J. Hiratsuka, T. Akaizawa, H. Nemoto, J. Cai, K. Yoshida, and Y. Yamamoto, *Chem. Pharm. Bull.*, 2000, **48** (7), 1034–1038.
145 G. Schneider, R. Seidel, M. Uder, D. Wagner, H. J. Weinmann, and B. Kramann, *Invest. Radiol.*, 2000, **35** (9), 564–570.
146 M. Lewin, N. Carlesso, C.-H. Tung, X.-W. Tang, D. Cory, D. T. Scadden, and R. Weissleder, *Nat. Biotechnol.*, 2000, **18** (4), 410–414.

147 P. L. Williams, G. L. Anderson, J. L. Johnstone, A. D. Nunn, M. F. Tweedle, and P. Wedeking, *J. Toxicol. Environ. Health, Part A*, 2000, **61** (8), 641–647.
148 R. A. Towner, H. Hashimoto, and P. M. Summers, *Biochim. Biophys. Acta*, 2000, **1475** (3), 314–320.
149 K. Potter, J. J. Butler, W. E. Horton, and G. S. Richard, *Arthritis Rheum.*, 2000, **43** (7), 1580–1590.
150 B. D. Foy, and J. Blake, *J. Magn. Reson.*, 2001, **148** (1), 126–134.
151 R. M. Asperio, P. Marzola, A. Sbarbati, F. Osculati, and F. Addis, *Am. J. Vet. Res.*, 2000, **61** (3), 321–325.
152 D. A. Sipkins, K. Gijbels, F. D. Tropper, M. Bednarski, K. C. P. Li, and L. Steinman, *J. Neuroimmunol.*, 2000, **104** (1), 1–9.
153 A. Knijn, C. Casieri, G. Carpinelli, C. Testa, F. Podo, and F. De Luca, *NMR Biomed.*, 2000, **13**(3), 124–128.
154 A. S. Traore, S. Woerly, V. D. Doan, Y. Marois, and R. Guidoin, *Tissue Eng.*, 2000, **6** (3), 265–278.
155 L. A. Stern, S. H. Kirby, and W. B. Durham, *J. Phys. Chem A*, 2001, **105** (7), 1223–1224.
156 A. A. Obynochny, A. G. Maryasov, K. A. Ilyasov, I. Gnezdilov, and K. M. Salikhov, *Appl. Magn. Reson.*, 1999, **17** (4), 609–614.
157 D. E. Axelson and J. B. Wooten, *J. Agric. Food Chem.*, 2000, **48**(6), 2199–2207.

14
Oriented Molecules

C.L. KHETRAPAL, G.A. NAGANA GOWDA AND K.V. RAMANATHAN

1 Introduction

The report on the oriented molecules is published in alternate volumes of this series and the present one covers the available literature during the biennial period ending May 2001. The complete literature on the subject can be traced back by referring to earlier volumes of this series. As pointed out in the previous report[1] there has been a rapid development in certain branches in the field, while in other areas progress has been moderate. More specifically, use of weakly ordered media for orienting biological macromolecules has seen an explosive growth in the last couple of years with the literature covering a gamut of topics, from developments of new techniques to sophisticated molecular modeling procedures using dipolar couplings and other anisotropic parameters. Consequently, a large section of this report is devoted to this 'hot' topic. Interestingly, some new areas have also emerged where NMR of oriented molecules is likely to have a significant impact. One such area is the field of quantum computing. This nascent field has already utilized several advantages inherent in the use of molecules oriented in liquid crystalline media with potential for novel applications. A sub-section to highlight these developments has also been included in this report. It may be mentioned that the technique of oriented molecules initially gained importance owing to its potential in the study of molecular structure. The early interest revolved around the study of structure of small molecules in order to assess the scope of the technique. Severe limitations for studies of structure of molecules larger than about eight interacting nuclei were soon realized. This was essentially due to 'strong couplings' arising from large degrees of order of the materials used as the orienting media. Efforts were then directed to develop new techniques and evolve procedures for the simplification of the spectra including attempts to discover new materials with appropriate solubility properties and low molecular order in order to extend the scope of the method to larger molecules. It is essentially only during the past few years that significant success in this direction has been achieved with the use of low ordering media such as the bicelles which are formed as liquid crystalline arrays in aqueous mixtures of long chain phospholipids like dimyristoylphosphatidylcholine (DMPC) and dihexanoylphosphatidylcholine (DHPC).[2] This has resulted in enormous interest in studies of large biomolecules. Side by side, there has been a decline

Nuclear Magnetic Resonance, Volume 31
© The Royal Society of Chemistry, 2002

in the interest in the study of the structure of small organic molecules, which are essentially oriented by liquid crystalline media having a larger ordering effect on the solute, thus giving rise to rich, but complicated, spectra. This has been happening gradually over the years as pointed out earlier.[1] During the period under report, the interest in the study of structure of small molecules has declined so much that, unlike in the earlier issues, it was not considered necessary to have a separate section devoted to it. This topic has therefore been combined with the section on conformation and molecular order.

The classification of the topics is essentially the same as that followed in earlier volumes, with more weightage given to emerging areas. The available literature is presented under the following headings: Reviews, Theory and General Studies; New Techniques and Emerging Areas; Dynamic NMR Studies; Smectic, Lyotropic, Polymeric and Chiral Systems; Weak Ordering and Biomolecular Structural Studies; Membranes and the Molecules Oriented Therein; Relaxation Studies; Structure and Conformation of Small Molecules and Orientational Order.

2 Reviews, Theory and General Studies

An overview of the application of NMR to the field of liquid crystals over the past 50 years has been presented and the important aspects of proton and deuterium NMR have been delineated.[3] The use of liquid crystals as solvents in NMR spectroscopy has been reviewed.[4] Reviews on NMR studies of orientational order with 20 references,[5] rotational diffusion of liquid crystals in the nematic phase[6] and ^{2}H- NMR spectroscopy in liquid crystals and membranes[7] are available. A review on the application of spectroscopic methods to liquid crystalline phases has appeared during the period under report and it includes a discussion of the NMR methods.[8] NMR and other methods used to determine the order parameters of nematics have been reviewed.[9]

A molecular dynamics simulation has been performed on 4-n-pentyl-4(-cyanobiphenyl (5CB) in the nematic phase. Order parameters and dipolar couplings have been calculated and used to test theoretical models.[10] Theoretical models have also been developed to explain the shielding of a noble-gas atom in an anisotropic environment and applied to explain the medium-induced shielding of the noble gases ^{129}Xe and ^{21}Ne in the nematic liquid crystal 4(-ethoxybenzylidene-4-n-butylaniline (EBBA).[11,12]

The indirect spin–spin coupling tensors J_{XF} (X = H, C, F) in *p*-difluoro benzene have been determined using *ab initio* calculations and from NMR experiments performed in a nematic liquid crystalline phase. It has been suggested that the anisotropic contributions to J_{XF} can become important for accurate determination of geometry or orientation in the case of NMR of oriented fluorine-substituted systems.[13] Rotational energetics of the formyl group including solvent effects on the energetics and the formyl proton spin–spin coupling behaviour of 2,6-dichloro- and 2,6-dinitrobenzaldehydes have

been studied from dipolar couplings and the temperature dependence of the J couplings, obtained from the ^{1}H- NMR spectra including the ^{13}C- satellites in a liquid crystalline solvent.[14]

Transverse nuclear relaxation due to director fluctuations in liquid crystals for the slow motion regime has been considered; this leads to an analysis in detail of the transverse magnetization decay in different kinds of experiments.[15]

3 New Techniques and Emerging Areas

This section covers new techniques as well as improvements made in the already existing methodologies. The use of oriented molecules in quantum computing – a potentially important area – has also been included.

3.1 General. – Several broadband decoupling sequences for protons are compared.[16,17] A new sequence with the acronym SPINAL-64 for small phase incremental alternation with 64 steps is found to offer better results and has been applied to the liquid crystal 5CB and the solid L-tyrosine hydrochloride.[16] ^{13}C-spectra of liquid crystal molecules having a fluorine atom have been considered. Different proton decoupling sequences and their effect on the line-splittings and broadenings have been studied.[17] A 2-dimensional (2D) method for improved resolution and assignment of the ^{13}C- spectra of liquid crystalline samples has been proposed.[18] The method involves evolution of the spins at two different director orientations with respect to the magnetic field achieved by mechanical rotation of the sample. The problem of strong axial peaks in ^{1}H–^{13}C 2D experiments involving dipolar oscillations[19,20] has been addressed. To overcome this problem so as to resolve small dipolar couplings, the use of polarization inversion, rather than the direct polarization transfer, has been proposed.[21] A density matrix description of the process has also been given and the experimental implementation on 4(-methoxybenzylidene-4-n-butylaniline (MBBA) demonstrated. A two-dimensional experiment for correlating deuterium quadrupolar splittings with the ^{13}C- chemical shifts of the attached carbons has been proposed.[22] The experiment has been employed to measure and assign all the quadrupolar couplings for the perdeuterated liquid crystal 4-n-pentyl-4′-cyanobiphenyl. The utility of standard 2D-NMR methods for oriented systems has been investigated.[23] From the HMQC experiment, the magnitude of proton–proton dipolar couplings for an AA′MM′X system has been obtained. The use of this experiment in combination with the HSQC experiment has been demonstrated for 1,1-difluoro- and 1,2-dibromoethane and *p*-dibromobenzene.[23] Use of the deuterium NMR spectrum of a deuterated solute dissolved in the nematic phase of a liquid crystal has been suggested for setting the 'Magic Angle' in solid state NMR.[24] The utility of the method as a convenient and accurate means of setting the angle has been pointed out. The application of an electric field to alter the orientation of the director suitably so as to reduce the line-widths arising from the dipolar interactions in

pulsed field gradient NMR methods has been demonstrated.[25] To test the applicability of the method self-diffusion coefficients of 5CB have been measured in the nematic and isotropic phases. Problems associated with employing homonuclear decoupling sequences to suppress dipolar dephasing during gradient pulses in experiments to measure molecular diffusion coefficients have been addressed. A slice selection scheme has been suggested and the method demonstrated by ^{13}C- and ^{19}F- NMR experiments on a sample of caesium perfluorooctanoate (CsPFO) in D_2O in its liquid crystalline phase.[26,27] Molecular alignment by an electric field has been used to reintroduce quadrupolar couplings into the ^{2}H- NMR spectrum of polar liquids. Pulsed electric fields together with suitable radiofrequency pulse sequences have been used to carry out 2D- experiments that correlate isotropic chemical shifts with residual anisotropic couplings.[28] Two-dimensional NMR experiments have been discussed where AC electric fields are used in the indirect dimension to align a sample of neat nitrobenzene. Pulse sequences providing either dipolar coupling information or correlation between the isotropic chemical shifts through dipolar coupling for pairs of nuclei have been presented.[29]

3.2 Quantum Computing. – The idea of quantum computing was first proposed by Feynman in 1982.[30] However, experimental attempts to implement quantum computation started much later. That NMR could be one of the techniques to make quantum computing realistically accessible was suggested independently by Gershenfeld and Chuang[31] and Cory *et al.*[32] Since then, a number of papers dealing with NMR quantum computing has been published. The basic aspects and recent progress in this area are available.[33] There are several challenges in the use of NMR for quantum computing and the solution to some of these problems is provided by the use of molecules oriented in liquid crystalline media. In NMR quantum computing each spin represents a single qubit and the logic operations require that the spectral lines due to chemical shifts and J couplings are well separated. In this context the advantage of using oriented molecules, which have well dispersed spectra due to relatively large dipolar couplings, has been pointed out.[34] The other advantage is the shorter T_1 relaxation time that enables the computation to be speeded up. These ideas have been demonstrated with the successful implementation of a two-qubit Grover search algorithm and a two-bit controlled-NOT gate using $^{13}CHCl_3$ oriented in a liquid crystal[34] and with the generation of the Einstein–Podolsky–Rosen states.[35] The use of quadrupolar split energy levels of nuclei with spin greater than half oriented in a liquid crystal has several advantages such as an increase in the number of qubits without actually increasing the number of spins and increase in the speed of computation. Such systems have been exploited for the creation of pseudo-pure states[36,37] where all energy levels except one have the same population and for the implementation of a complete set of two-qubit reversible logic gates.[37] A simple method for the creation of a pair of pseudo-pure states has been presented and its implementation using $^{13}CH_3CN$ dissolved in a liquid crystalline solvent achieved.[38] The results of applying a C^2-NOT quantum logic gate on the

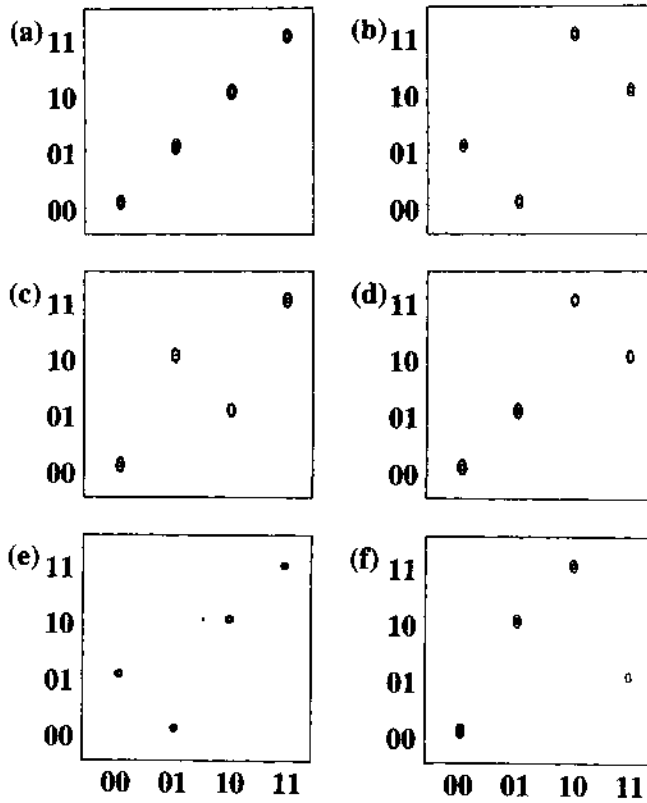

Figure 1 *^{13}C NMR spectra of oriented $^{13}CH_3CN$ corresponding to various 2-qubit gates implemented using transition selective pulses and two-dimensional NMR. They correspond to the following gates: (a) NOP (No Operation), (b) NOT2, (c) SWAP, (d) XOR2, (e) XNOR2, (f) SWAP + XOR2. The bits have been labeled 1 and 2 from left to right. (Ref. 42).*

pseudo states thus prepared are also presented. A method for preparing pseudo-pure states by transfer of population by the use of a multifrequency excitation pulse has been proposed and implemented for ^{133}Cs having eight energy levels (spin 7/2) in a liquid crystalline environment.[39] The method also provides improved sensitivity up to a factor of 4. Quantum simulation of the propagation of excitation along a one-dimensional chain of atoms has been illustrated with the use of the ^{133}Cs in a liquid-crystalline matrix.[40] Using a special seven-frequency pulse, the Hamiltonian corresponding to migration of excitation has been simulated and the propagation of population from a created pseudo-pure state monitored. Use of a spin 7/2 system as a three qubit system has been proposed and experimental implementation of a Half-Adder and Subtractor achieved using ^{133}Cs in a liquid crystalline medium.[41] It has been shown that the quantum states can be relabeled suitably so as to increase the efficiency of a computational task. Dipolar coupled methyl groups of

CH_3CN and $^{13}CH_3CN$ oriented in liquid crystalline matrices have been shown to provide 2 and 3 qubit systems corresponding to their symmetric A states (Figure 1).[42] By manipulation of the populations in these states with suitable transition selective and nonselective pulses and magnetic field gradients, pseudo-pure states have been created. Two and three bit gates have also been implemented using one- and two-dimensional NMR.

4 Dynamic NMR Studies

This section covers studies on molecular and director dynamics under applied electric and magnetic fields and sample spinning. ^{2}H-NMR spectroscopy has been used to study selectively- and per-deuterated samples of chloro- and iodo-cyclohexanes dissolved in a liquid crystalline medium.[43] Line shapes and 2D exchange spectra have been used to estimate the ratios of equatorial and axial conformers existing in dynamic equilibrium. From temperature variation studies the activation enthalpies for the internal processes have been estimated. The molecular order parameters and orientations of the main ordering axis for the two conformers at different temperatures have also been determined.[43] Electric field-induced director alignment of the smectic A phase of the liquid crystal 4-α, α-d_2-octyl-4′-cyanobiphenyl, with the electric field being orthogonal to the magnetic field has been investigated by deuterium NMR, as a function of time after the electric field was switched on.[44] At high electric fields, the director switches its orientation from one that is parallel to the magnetic field to the one that is parallel to the electric field. The time required for alignment along the electric field becomes larger as the electric field is lowered. During this induction period, the alignment behaviour of the director depends on the applied electric field and reveals a pattern in which the smectic layers breakdown into domains which are initially decoupled from each other, but eventually align with their directors more or less parallel to the electric field. Deuterium NMR spectroscopy has been employed to investigate electric field-induced director dynamics in 5CB deuterated in the α-position of the pentyl chain and confined between two glass plates.[45] From the spectra, obtained as a function of time after turning an electric field on and off, the rotational viscosity and the diamagnetic anisotropy have been determined Deuterium NMR has been employed to investigate the director distribution in a thin nematic cell confined between two glass plates, as a function of the electric field applied perpendicular to the magnetic field.[46] It is observed that the director orientation and distribution depend on the surface treatment of the glass plates and the anchoring conditions. A ^{2}H-NMR study of the alignment process of the directors in a smectic A phase by an external magnetic field has been reported.[47] This complex process is also influenced by the nature of the surface. Computer simulations of the process have also been carried out for understanding the process. ^{2}H-NMR has been used to study the alignment of the director in the smectic A phase of 4-octyl-4(-cyanobiphenyl (8CB) in a magnetic field.[48] The process of alignment of a droplet of this phase in glycerol

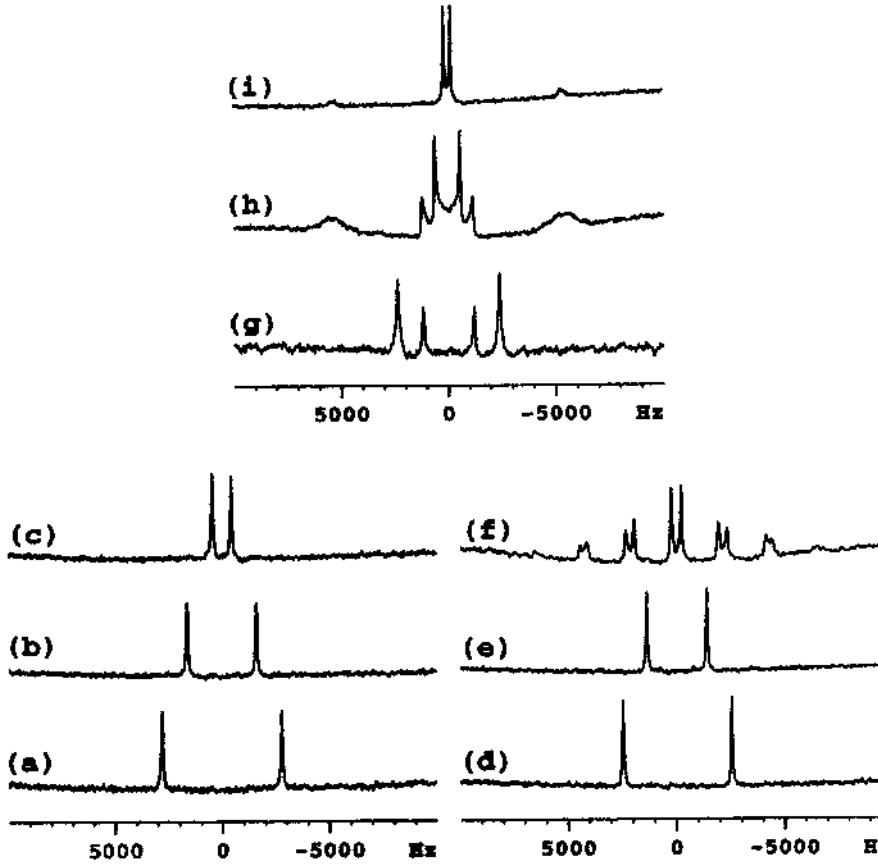

Figure 2 *^{2}H- NMR spectra of $CDCl_3$ dissolved in a mixture of liquid crystals with a slightly positive $\Delta\chi$ recorded at three nearly the same angles and three different spinning speeds. (a–c) spinning speed 1090 Hz and angles 42.9°, 47.8° and 52.8°, respectively; (d–f) spinning speed 2113 Hz and angles 44.1°, 48.8° and 53.7°, respectively; (g–i) spinning speed 5350 Hz and angles 44.5°, 49.6° and 54.0°, respectively. (Ref. 51).*

is found to be significantly different from that of the sample confined in a glass tube. The experiments have also been performed on a sample of 8CB deuterated at the α chains and a sample containing a small amount of *p*-xylene-d_{10} as a solute.[49] The director dynamics in nematic liquid crystals in the presence of both magnetic and electric fields has been studied by employing proton magnetic resonance experiments.[50] The experiments provide such parameters as the ratio of the diamagnetic anisotropy to the dielectric anisotropy and rotational viscosity. The dynamics of the director in mixtures of nematic liquid crystalline phases for which the macroscopic diamagnetic susceptibility anisotropy is nearly zero have been studied under variable angle spinning for different spinning speeds.[51] Deuterium NMR spectra of a deuterated probe molecule have been monitored. It is observed that a switch

over of the director orientation occurs as a function of the spinning speed and the angle the spinning axis makes with the magnetic field. The farther the angle between the spinning axis and the magnetic field from the magic angle, the higher the spinning speed required to effect such a switch-over. The switch-over takes place gradually accompanied by the appearance of a powder pattern (Figure 2).

5 Smectic, Lyotropic, Polymeric and Chiral Systems

Deuterium is the probe of choice for studying these phases while occasionally other nuclei have also been employed. The supramolecular structure of hydrogen bonded mesogens composed of dipyridyl and 4-(oligodimethylsiloxyl)alkoxybenzoic acids has been investigated.[52] The mesogens exhibit a cubic phase at a temperature below smectic A phase. While the X-ray studies suggest aggregation driven by nanophase separation, the ^{2}H-NMR measurements in the isotropic and smectic phases are indicative of aggregation and an oriented lamellar structure respectively. The collapse of the quadrupolar splittings at the lower temperatures is also consistent with the presence of a cubic phase. The solubility of two partially deuterated thio-indigo dopants in a smectic liquid crystal host has been evaluated by ^{2}H-NMR spectroscopy carried out at different temperatures and with different dopant concentrations. The study provides a means of determining the occurrence and the extent of microphase separation into smectic and isotropic phases; this has not been possible by polarized microscopy.[53] Inter-layer molecular exchange in the antiferroelectric smectic-C^*_A phase of deuterated 4-(1-methylheptyloxycarbonyl)phenyl 4'-octyloxybiphenyl-4-carboxylate (MHPOBC) has been studied by ^{2}H-NMR spectroscopy.[54] The varying field gradients produced by the anticlinic smectic layer structure of the system has been exploited for the purpose. ^{1}H-NMR studies of the molecular order in smectic C_2, smectic C* and the anticlinic smectic C phases of two liquid crystals have been carried out and the tilt angles obtained.[55] Deuterium NMR spectra of ferroelectric and antiferroelectric phases of liquid crystals have been studied and the interlayer exchange effects on the spectra used to confirm the alternating tilt structure of the smectic C_A* phase of the liquid crystals studied.[56] Deuterium NMR spectra of a deuterated sample of MHPOBC in its smectic C_A* phase obtained at different angles between the magnetic field direction and the normal to the smectic layers have been compared with calculated line shapes and the alternating tilt structure of the phase has been confirmed.[57] The polymorphism of the ternary system lecithin/alkanphosphondiethylesteric acid/water has been studied by means of phosphorous and deuterium NMR and a geometric model for the phase transition proposed.[58]

A ^{2}H-NMR study of the dynamics of the phenyl ring of a side-chain liquid crystal polymer has been carried out.[59] The rotation of the phenyl ring about its *para*-axis has been attributed to the relaxation process and a Gaussian distribution of the activation energy points to a dynamic heterogeneity of the

system. Computational methods have been employed to calculate director distribution in cylindrical samples of nematic liquid crystals.[60] These are used to interpret the process of reorientation of nematic monodomains in liquid crystal polymers in presence of a magnetic field. A procedure for ^{1}H-NMR imaging of residual dipolar couplings in cross-linked elastomers has been described.[61] Partially deuterated side-chain polymers with methoxybenzylbenzoate mesogenic groups have been studied by ^{1}H- and ^{2}H-NMR spectroscopies. The deuteration of the main chain provides separate access to the study of orientation effects of the side and the main chains.[62] Magnetisation exchange has been used to investigate proton residual dipolar couplings in crossed-linked elastomers. The study helps to test a filter that can be used to generate contrasts in NMR images of heterogeneous elastomers.[63]

^{2}H-NMR spectroscopy has been used to study a ring-deuterated chiral liquid crystal 4-(2-methylbutyl)oxycarbonylphenyl-4-(10-undecenyloxy)-benzoate.[64] Quadrapolar and Zeeman spin–lattice relaxation times have been measured as a function of temperature in the smectic A phase. The analysis of the data based on a rotational diffusional model seems to indicate that for this particular molecule the diffusion tensor is such that $D_\perp$ is greater than $D_\parallel$; this is different from non-chiral rod-like liquid crystals. Symmetry arguments have been used to show that the effective molecular point groups of solutes dissolved in any chiral liquid crystalline solvent are reduced from their normal molecular point groups.[65] When the molecules have a point group symmetry of either C_s, C_{2v}, S_4 or D_{2d}, this reduction in symmetry can be detected by NMR; this is illustrated by the example of acenaphthene-d_{10} dissolved in a chiral nematic solvent. A proton decoupled deuterium NMR study of labeled diastereomers with remote stereogenic carbons dissolved in various mixtures of poly-γ-benzyl-L-glutamate (PBLG) and poly-γ-benzyl-D-glutamate (PBDG) liquid crystalline solutions has been carried out.[66] The utility of the study for measuring diastereomeric as well as enantiomeric excesses of each diastereomer has been presented. A Cartesian spin operator formalism has been used for the description of natural abundance deuterium 2D-NMR spectra in weakly ordered liquid crystalline phases.[67] Several improvements of the basic sequences that make it possible to correlate the two components of the quadrupole doublets as well as assign each of them on the basis of chemical shifts have been proposed and discussed. Such experiments for the enantiomeric analysis through natural abundance deuterium NMR have also been described.[68] ^{2}H-NMR has been used to investigate diastereomeric shape recognition based on the difference in the induced orientation of the dissolved molecule in liquid crystals. It has been possible to observe spectroscopic discrimination of diastereomers with remote asymmetric centers up to nine bonds apart, using a chiral liquid crystalline solvent.[69] Use of organic solutions of poly-γ-benzyl-L-glutamate to generate a sufficient differential ordering effect to visualize enantiomers using multinuclear NMR methods at natural abundance has been presented.[70] Theoretical and experimental considerations involved in the use of NMR observables such as proton–proton, proton–carbon and carbon–carbon residual dipolar couplings, carbon chemical shift

anisotropies and deuterium quadrupolar splittings for the estimation of enantiomeric excess have been discussed.

6 Weak Ordering and Biomolecular Structural Studies

The progress in this area has been very rapid in the last two years. Several new techniques and methodologies have been developed and extensively employed in the studies of structure and interaction of proteins, nucleic acids and oligosaccharides. New orienting media that generate just the sufficient amount of weak ordering of the biomolecules have been experimented with and their utility reported. Considering the fact that till recently analyzing the spectrum and solving the structure of a molecule with as few as eight interacting nuclei was considered to be a difficult problem, it is amazing to see the rapid growth of the area and the application to such large macromolecules. The developments are in fact a 'dream' turned 'reality' and will guide future NMR studies of the structure of biomolecules. Though efforts in this direction were directed since the early days of the development of the technique of NMR of oriented systems, only limited success was achieved till recently in applying the technique to such large molecules due to complexities involved. The breakthrough was achieved only after the discovery of the novel liquid crystals with low order parameters and with appropriate solubility properties and the availability of high sensitivity and high-field instruments. The new liquid crystalline materials with low order parameters enable the observation of the anisotropic interactions only between the nearby nuclei resulting in the spectral simplicity; the high sensitivity enables one to get the spectra of dilute solutions of macromolecules and the high fields can induce small orientation effects in favourable cases and thus eliminate the use of external orienting media.

The field has aroused so much interest in the last few years that a review with 84 references presenting the elucidation of protein structure and dynamics through field-induced residual dipolar couplings, detailing all aspects from measurement of the couplings to structure determination protocols, has already been published.[71] A review of NMR of nucleic acids and proteins with 256 references has a substantial portion devoted to the description of the measurement of residual dipolar couplings in samples where the solute is partially oriented either by a magnetic field or due to alignment influence of the medium.[72] Recent advances in the use of various NMR methods including the use of residual dipolar couplings in biological systems have also been reviewed.[73] A review on the use of the bacteriophage Pf1 for macromolecular structure determination is also there.[74] Developments in the field of liquid crystals over the years with emphasis on their use for biomolecular structural studies have been reviewed.[75] Attention has also been drawn on the caution required while interpreting the NMR data in terms of molecular structure.

Study of proteins has generally attracted more attention and several methodologies have been applied to proteins to test their viability, though other macromolecular systems have also been occasionally used as a test case.

Therefore the rest of this section is presented under the following two subheadings: New Methodologies and Protein Studies; Nucleic Acids, Oligosaccharides and their Complexes.

6.1 New Methodologies and Protein Studies. – A three-dimensional experiment which allows quantitative measurement of the magnitude of the proton–proton dipolar couplings in partially oriented proteins has been reported.[76] The method enables resonance assignment, local structure refinement and study of protein folds. The changes in the chemical shifts of a solute between isotropic and liquid crystalline phases have been used to derive information on the magnitude and orientation of the chemical shielding tensors for the polypeptide backbone atoms such as the carbonyl carbon, nitrogen and the amide proton.[77] Perdeuterated ubiquitin dissolved in a medium containing a small volume fraction of phospholipid bicelles has been used for this purpose. The possibility of using residual dipolar couplings to provide rapid structural information for proteins in solution so as to apply the technique in proteomics projects that seek to annotate large number of gene products has been discussed.[78] The interpretation of dipolar couplings is based on pattern recognition where a predefined structural template for a motif is used to search a set of residual dipolar couplings for good matches. The method has been demonstrated for a helix-turn-helix motif and for a 20 residue template using experimental data available for the protein ubiquitin. The axial and rhombic components of the molecular alignment tensor of solute molecules aligned in liquid crystalline media constituted by colloidal suspensions of phage particles are shown to be modulated by the pH of the system.[79] It is also observed that a larger residual dipolar coupling is obtained for the longer phage particles. A method for measuring C^{β}–H^{β} dipolar couplings in proteins has been presented.[80] Utility of such a measurement for identifying the side-chain rotamer by comparison of the value obtained with selected backbone dipolar couplings is also discussed. The use of mineral liquid crystals such as an aqueous suspension of V_2O_5 for orienting biological molecules in a magnetic field so as to extract dipolar couplings that provide long range structural information has been proposed and the utility demonstrated for a pentasaccharide dissolved in the suspension.[81] Since the medium, prepared in D_2O, contains no protons or carbons it has the advantage that no isotope labeling of the studied molecule is necessary. A method to obtain the sign of the residual dipolar coupling in the case of methyl protons which is normally not possible otherwise, due to the absence of J couplings in the spectrum, has been proposed.[82] The pulse scheme proposed creates magnetization *via* one-bond ^{13}C–^{1}H coupling of the methyl group such that the sign of the cross-peak reflects the relative sign of D_{HH} and $^{1}J_{CH}$. A new type of bicelles which align with their major axes parallel to an external magnetic field constituted by 1-dodecanoyl-2-(biphenyl-4-acetyl)-*sn*-glycero-3-phosphocholine (DBPC) and 1,2-dihexanoyl-*sn*-glycero-3-phosphocholine (DHPC) have been employed.[83] The suitability of the system for NMR studies of biological molecules has been tested by recording a HMQC spectrum of a trisaccharide oriented in the bicelle. The effect of proton exchange on the

measurement of ^1H–^1H, ^1H–^2H and ^2H–^2H residual dipolar interactions in water molecules in bovine Achilles tendons has been investigated using Multiple Quantum filtered experiments. Using the theoretical expressions ^1H–^1H and ^1H–^2H residual dipolar couplings and the proton exchange rates have been obtained at temperatures where no dipolar splitting is evident in the spectrum.[84] An approach that significantly reduces the time required to solve structures of protein–protein complexes has been proposed. The method, involving the application of a minimization procedure using intermolecular interproton distances derived from NOE data, dipolar coupling restraints and a simple intermolecular van der Waals repulsion potential, has been demonstrated for the case of the complex of enzyme I and the histidine phosphocarrier protein.[85] The utility of the 2D-COSY experiments for the measurement of H^N–H^α residual dipolar couplings of positive sign in proteins has been presented.[86] These measurements, which obviate the need for isotopically enriched samples, has been demonstrated for the case of the basic pancreatic tripsin inhibitor oriented in bicelles. A new protocol for the inclusion of residual dipolar coupling restraints has been described.[87] It has better convergence properties than methods based on direct refinement strategies for large molecules with limited number of NOEs per residue. The method has been applied to the study of the global fold of maltose-binding protein in complex with the substrate β-cyclodextrin. The application of ^1H–^1H dipolar couplings for macromolecular structure refinement has been presented with the protein ubiquitin as an example.[88] The computational tools required for direct refinement of structure, including cases where the sign of the dipolar coupling is unknown and also where stereospecific assignments of the resonances have not been made have also been described. A method for measuring the sign and the magnitude of ^1H–^1H dipolar couplings based on the E-COSY technique has been presented and its advantages discussed.[89] The use of residual dipolar couplings in the determination of the structure of a small, unlabeled ligand complexed to an isotopically labeled protein has been reported.[90] This approach is observed to provide more precise and accurate structures of protein/ligand complexes, in comparison to only NOE based structures and promises an important step in structure-based ligand design. ^{15}N-chemical shifts, measured at 17.6 T, for hen lysozyme resulting from orientation of the protein in bicelles have been used to determine the orientation and magnitude of the ^{15}N- chemical shift tensor.[91] A new procedure for measuring homonuclear proton–proton couplings based on the analysis of a constant time COSY experiment has been proposed.[92] The method uses the fact that for a pair of spins having a scalar coupling J and dipolar coupling D, the cross-peak and auto-peak intensities are respectively proportional to $\sin\{\pi(J + D)\Delta\}$ and $\cos\{\pi(J + D)\Delta\}$, Δ being the constant time of evolution. The intensity measurements provide quantitative measure of the sum of the couplings and the method has been demonstrated for an oligosaccharide oriented in a bicelle medium. A method to predict both the magnitude and orientation of macromolecular alignment in dilute liquid crystalline phases due to steric interactions has been proposed.[93] Correlations between experimental dipolar couplings and

values calculated from shape-predicted alignment tensors for different protein–liquid crystal systems have been obtained. The method has the potential to distinguish degenerate solutions for the structure or to provide input on flexibility of multidomain proteins.

n-Alkyl-poly (ethylene glycol)/n-alkyl alcohol as well as glucopone (a technical product containing different n-alkylated carbohydrates)/n-hexanol mixtures have been reported to form dilute liquid-crystalline phases in aqueous solution; they are suitable for partial alignment of biological macromolecules in a magnetic field.[94] The suitability of these systems for measurement of residual dipolar couplings in proteins, DNA and a protein/DNA complexes has been demonstrated. An equimolar complex consisting of amphiphilic chelating agent, 1,11-bis[distearylamino]-diethylenetriamine pentaacetic acid and Tm^{3+} has been shown by ^{2}H-NMR to be useful in aligning model membranes consisting of DMPC and DHPC. The inherent paramagnetic shifts and line broadening effects have been studied by monitoring the ^{2}H-NMR spectra of the membrane binding peptide, Leu-enkephalin.[95] A new approach to produce weak alignment of biopolymers has been suggested; it requires that a protein be dissolved in an aqueous polymeric gel.[96] Anisotropy has been induced by straining the gel away from an initial isotropic state. Experimental results on a ^{15}N-labeled protein sample dissolved in cross-linked polyacrylamide gel have also been presented. Weak alignment of a membrane protein in lipid micelles in solution has been accomplished in a controlled way by adding a well-characterized calcium metal binding motif to the N-terminus of a protein.[97] This allows the measurement of residual dipolar couplings and other spectroscopic parameters resulting from the presence of a lanthanide ion in a unique, well-defined location. The use of more than one type of lanthanide ions enabled multiple orientations of the protein to be obtained in the magnetic field. The method is useful in eliminating ambiguities in orientational information. An approach to the determination of backbone protein structure using residual dipolar couplings alone has been presented and demonstrated for the case of the protein ubiquitin using experimental data.[98] The question of using a uniform value for the quadrupolar coupling constant for the analysis of ^{2}H-relaxation data measured at the methyl sites in proteins has been discussed.[99] By measuring and analyzing ^{2}H-quadrupolar and one-bond ^{13}C–^{13}C dipolar couplings at the methyl sites in a uniformly ^{13}C-labeled and fractionally ^{2}H-labeled protein weakly aligned in a dilute solution of the phage Pf1, it has been concluded that the use of uniform value for ^{2}H- quadrupolar coupling constant is indeed a good approximation. The use of oriented phospholipid bilayers which have been doped with a lipid derivatized with a polyethylene glycol polymer head group has been suggested for achieving magnetic orientation of NMR samples.[100] Factors like degree of orientation and sample stability have been discussed. An approach for determining protein backbone structure solely from dipolar couplings has been suggested.[101] The method, which uses a 'best-fit' of experimental dipolar couplings to data already available in Protein Data Bank for protein fragments, has been applied to the case of the protein ubiquitin and its utility demonstrated. An order matrix approach that enables

accurate structural parameters to be obtained even in the presence of significant internal motions has been proposed.[102] The method with the potential of providing a protein structure and simultaneously identifying dynamic regions of the protein, making exclusive use of dipolar coupling data, has been applied to the protein ubiquitin. The magnetic field-induced alignment of a polymer-grafted lipid-based complex fluid consisting of a quaternary mixture of water, a phospholipid, a lipopolymer and a zwitterionic surfactant has been reported and its potential as a medium for orienting biomolecules is discussed.[103] Band selective ^{1}H homonuclear decoupling during data acquisition has been suggested for suppressing residual proton–proton dipolar couplings which cause line broadening in partially oriented protein samples.[104] With the aim of establishing an acidic bicellar solution as a useful model membrane, ^{2}H-NMR spectroscopy has been used to investigate the DMPC/DHPC bicelles containing 25% w/w of either dimyristoylphosphatidylserine or dimyristoylphosphatidylglycerol. Study of the binding of a 14-residue peptide in both neutral and acidic bicelles shows the utility of these membrane mimetics.[105] The behaviour of the director of bicelles in variable angle spinning (VAS) experiments has been investigated by ^{31}P-NMR.[106] The utility of the VAS technique for determining the relative sign of the dipolar and scalar couplings has been presented. A method which obviates the use of the alignment tensor parameters in molecular structure calculations has been proposed and tested for the case of human ubiquitin.[107] Mixtures of ditetradecyl-phosphatidylcholine or didodecylphosphatidylcholine and dihexylphosphatidylcholine in water have been reported to form lyotropic liquid crystalline phases and have been used to measure ^{15}N–^{1}H dipolar couplings for ubiquitin over the pH range 2.3–10.4.[108] A procedure for obtaining molecular structure from molecular alignment data is available.[109] An experiment that allows determination of the sign of the residual dipolar ^{1}H–^{1}H coupling constants relative to the sign of one-bond ^{1}H–X coupling constants in linear three-spin systems has been reported.[110] The other features of the experiment are that it is sensitivity enhanced with diagonal peak suppression and with cross peaks being observed only between directly coupled protons. The possibility that nematic liquid crystalline phases can be oriented with the director at an arbitrary angle to the applied magnetic field by sample rotation has been extended to bicelles.[111] Switching the angle of spinning retains the monodomain character of the system for sufficiently long time, indicating the possibility of application to two-dimensional correlation experiments to proteins oriented in a bicellar solution. Dilute solution of cetylpyridinium bromide/hexanol/sodium bromide have been characterized and the liquid crystalline phases that orient in the magnetic field have been studied.[112] Three transverse relaxation optimized experiments (TROSY) for the measurement of scalar and dipolar couplings suitable for proteins dissolved in aqueous isotropic and anisotropic solutions have been presented.[113] A new pulse sequence that allows the measurement of ^{13}C–^{1}H and ^{1}H–^{1}H dipolar couplings at the same time using spin-state selective transfer has been reported.[114] The method has been applied to the methylene groups of glycines in the protein ubiquitin. A set of 3D experiments for measurement of residual

dipolar couplings in labeled proteins has been suggested and demonstrated on three proteins, viz., cardiac Troponin C, calerythrin and ubiquitin.[115] An approach that translates residual dipolar couplings into inter-vector projection angles which can then be used as restraints in the simulated annealing protocol has been proposed.[116] A suspension of cellulose crystallites has been suggested for orienting biological macromolecules in a magnetic field with a modest alignment necessary for the measurement of residual dipolar couplings.[117] 3D-pulse schemes for measuring ^{1}H–^{15}N, ^{15}N–^{13}C, ^{1}H–^{13}C, ^{13}C–^{13}C backbone dipolar couplings for a ^{15}N, ^{13}C, ^{2}H labeled protein based on the TROSY method have been presented.[118] Precise dipolar couplings have been obtained for a complex of β-cyclodextrin with maltose binding protein and human carbonic anhydrase II. Alignment of proteins within polyacrylamide gels due to mechanical stress or embedding of oriented purple membrane fragments has been studied and used to derive residual dipolar couplings for the proteins human HIV-1 Nef and ubiquitin.[119] A procedure to use dipolar coupling information for structure determination without reference to the orientation of the principal axes of the alignment tensor has been suggested and applied to the maltodextrin-binding protein.[120] The use of residual dipolar couplings not only for validation of structural models, but also for their refinement has been illustrated for calmodulin.[121] A method for incorporating dipolar coupling restraints into structure calculations in cases of axially symmetric alignment tensor has been proposed and applied to modeling studies on an α-helical protein.[122] The effect of incomplete sampling of the orientation space on the determination of orientational properties has been examined and the theoretical approach applied to the rotational diffusion and alignment tensors obtained from NMR data for several proteins to determine the accuracy of the estimation.[123] A constant-time COSY method is suggested for measuring ^{1}H–^{1}H residual dipolar couplings of proteins in weakly ordered media and the advantages of the technique discussed.[124] A method for the measurement of one bond $J_{C(N}$ coupling from the relative intensities of the cross peaks in two 3D-spectra has been proposed and the error in the measurement estimated.[125] A strategy designed to overcome the problem of the alignment tensor changing during the progress of the experiment has been suggested.[126] The method proposes the measurement of different types of one-bond dipolar couplings simultaneously. An expression for the dipolar coupling R-factor has been derived; it provides a quantitative and readily interpretable measure of the agreement between observed and calculated dipolar couplings.[127] The application has been demonstrated for the protein cyanovirin-N.

The problem of constraining relative orientations of protein-fragments based on a single set of residual dipolar couplings has been addressed. A procedure based on order tensor analysis in two alignment media has been suggested and demonstrated for ^{15}N–^{1}H residual dipolar coupling data acquired on the protein zinc rubredoxin from *Clostridium pasteurianum* dissolved in two different bicelle media.[128] ^{13}C and ^{15}N labeled peptides based on the N-terminal sequence of the protein adenosine diphosphate ribosylation factor 1 have been synthesized with and without an *N*-myristoyl anchor and

have been studied in micellar environment and in magnetically oriented bicelles.[129] It has been observed that *N*-myristoylation does not greatly influence the structure of the peptide which is α-helical in a lipid environment. The solution-state conformation of the maltodextrin-binding protein loaded with β-cyclodextrin has been determined on the basis of one-, two- and three-bond dipolar couplings involving the nuclei H^N, ^{15}N, $^{13}C_\alpha$ and $^{13}C'$.[130] Domain orientation studies of calcium-binding proteins in solution using partial replacement of Ca^{2+} by Tb^{3+} have been carried out.[131] The paramagnetic Tb^{3+} allows measurement of inter-domain pseudo-contact shifts as well as leading to partial alignment of the molecule such that residual dipolar couplings can be measured. The studies indicate the potential of the method for determining the relative orientations of domains in favorable cases. The utility of measuring anisotropic interactions such as residual dipolar couplings has been investigated for obtaining relative domain orientations in multi-domain proteins.[132] Such studies carried out on the protein barley lectin indicate that the two domains of the protein are not oriented as expected from the crystal structure of a homologous protein and that they experience different reorientational dynamics. Orientational and long-range order constraints available from paramagnetic systems such as paramagnetic pseudo-contact shifts, electron–nuclear dipolar cross-correlation effects and residual dipolar couplings have been used to determine the structure of cytochrome c′ protein to atomic resolution.[133] The use of residual dipolar couplings in combination with other constraints for identification of a protein fold has been described with application of the approach for the case of ^{15}N-labeled *Escherichia coli* acyl carrier protein and also for the case of another related protein from *Rhizobium leguminosarum*.[134] The lanthanide ions such as Yb^{3+} and Dy^{3+} have been shown to bind to three small membrane proteins, resulting in weak magnetic field alignment of these proteins in micelles; this enables the measurement of the residual dipolar couplings.[135] The use of residual dipolar couplings and deuterium labeling in combination with a minimal set of NOE-based constraints has been shown to be useful for structure-based drug design.[136] The method has been tested for the case of a fragment of the protein human fibroblast collagenase and its complex with an inhibitor. ^2H-NMR studies of gramicidin A in which the amino acid residues are shifted by one position towards the N-terminus have been carried out for oriented and non-oriented samples.[137] The orientations and dynamics of ^2H- labeled valine residues have been estimated and compared with the native molecule. The solution structure of the human protein GAIP (Gα interacting protein), a regulator of G- protein signaling, has been determined by utilizing dipolar couplings of the oriented protein in two different liquid crystalline media.[138] ^{15}N–^1H dipolar couplings measured in two different liquid crystalline media namely DMPC/DHPC bicelles and the filamentous bacteriophage Pf1 for residues 43–200 of the prokaryotic protein S4, augmenting NOE restraints, have been shown to help establish the relative orientation of the sub-domains of the protein in solution which is observed to be quite similar to that in the crystal structure.[139] The solution structure of the protein–protein complex of

the bacterial phosphoenolpyruvate/sugar phosphotransferase system between the N-terminal domain of enzyme I and the histidine-containing phosphocarrier protein HPr has been determined by NMR spectroscopy by including residual dipolar couplings that provide long-range structural information.[140] A method for measuring both the sign and magnitude of the H^N–H^α residual dipolar couplings has been suggested and applied to the FK506 binding protein complexed to FK506. Agreement between the experimental values and the values predicted from X-ray crystal structure indicate that these couplings provide accurate structural constraints.[141] The utility of a suspension of planar purple membrane fragments containing bacteriorhodopsin that provides a weak alignment of biological macromolecules in a strong magnetic field has been presented.[142] Measurement of one-bond dipolar couplings is demonstrated for two ^{15}N-labeled proteins, namely the V_α-domain of the human T-cell receptor and ubiquitin. The use of dipolar couplings has been shown to result in significant improvement in the accuracy of protein structure determination with only minimal NOE data sets employed. This is demonstrated for three systems for which experimental dipolar couplings have been measured, namely, B1 domain of streptococcal protein G, the monomer of the barrier-to-autointegration factor BAF and cyanovirin-N.[143] Residual dipolar couplings of neighbouring protons have been observed for a paramagnetic protein oriented in a lyotropic liquid crystal solvent with measurable splittings for several hyperfine-shifted proton lines, without excessive broadening.[144] The system studied is the protein cytochrome-c in the ternary system of cetyltrimethylammonium bromide/pentanol/water. Transient binding of the C-terminal transducin undecapeptide to rhodopsin after light-activation leads to weak ordering of the peptide. This has enabled residual ^{15}N–^{1}H dipolar couplings for the selectively ^{15}N labeled Leu5 and Gly9 residues to be determined, yielding the angles made by the corresponding N–H vectors with the normal to the rhodopsin containing disks.[145] Residual dipolar couplings have been measured and the restraints derived used in the refinement of the structure of the complex of DNA with three zinc fingers of transcription factor IIIA.[146] A sensitivity-enhanced HSQC experiment has been described and applied to measure one-bond scalar and dipolar couplings in ubiquitin and hepatitis C protease.[147] Large residual ^{15}N–^{1}H dipolar couplings have been measured for SH2 domain aligned in a medium containing Pf1 bacteriophage at a concentration an order of magnitude lower than that normally used for such alignment.[148] A good correlation has been observed between the measured dipolar couplings and values predicted from the solution structure. Magnetic field induced orientation of ^{15}N-enriched oxidized cytochrome-b562 has been used to obtain several one-bond residual dipolar couplings which have been used as constraints to improve the existing structure of the molecule.[149] The alignment of Ca_2 calbindin protein in which one calcium has been replaced by a lanthanide has been used to obtain residual dipolar coupling contributions to $^1J_{H\text{-}N}$ and $^2J_{H\text{-}H}$ couplings of asparagine and glutamine NH_2 moities, which in turn have been used to aid structural characterization of these groups.[150] The fragment spanning the last 85 C-terminal residues of the heterogeneous nuclear

ribonucleoprotein K has been studied and backbone residual dipolar couplings have been employed to improve structure quality.[151]

6.2 Nucleic Acids, Oligosaccharides and their Complexes. – The observation of weak dipolar couplings has also been exploited to study the structure and interactions of nucleic acids. A method for determining the global helical structure of RNA in solution has been reported.[152] A set of ^{1}H–^{15}N residual dipolar couplings have been measured in partially oriented samples of ^{15}N-labeled tRNA and used to determine the relative orientations of the helical arms in tRNA. A method for obtaining the relative orientations of the purine and pyrimidine bases in terms of the helical parameters by estimating the residual dipolar couplings has been proposed and demonstrated for the case of a DNA dodecamer.[153] The structure of a DNA dodecamer has been studied in an aqueous liquid crystalline medium made up of phospholipid bicelles.[154] Like in an earlier study[155] for a protein, in this case too a nearly complete set of one-bond ^{1}H–^{13}C dipolar couplings, supplemented by ^{1}H–^{15}N and ^{1}H–^{1}H dipolar couplings, has been obtained and used with torsion angles derived from *J* couplings and inter-proton distances obtained from NOEs to arrive at the structure. The precision of the determined structures has been discussed in terms of the uncertainty in the exact magnitude and rhombicity of the alignment tensor. From the ^{13}C–^{1}H, ^{15}N–^{1}H and ^{1}H–^{1}H dipolar couplings and NOE restraints several parameters such as sugar puckers, glycosyl torsion angles and other helical parameters have been determined. The use of ^{31}P-chemical shift anisotropy as an aid in determining nucleic acid structures in liquid crystalline media has been discussed.[156] The method is demonstrated for a sample of d(CGCGAATTCGCG)$_2$ in the presence and the absence of the phage particle Pf1 which is added to cause nematic liquid crystalline order. The HSQC spectrum in oriented phase shows substantial ^{31}P chemical shift changes in comparison to the spectrum in the isotropic phase and the results indicate the possibility of the use of such studies for oligonucleotide structure determination. Use of residual dipolar couplings has been suggested to test for specific conformational changes induced by drug binding to a target RNA and has been applied to the RNA oligonucleotide complexed to the antibiotics paromomycin and gentamicin, with and without partial alignment induced by the phage Pf1.[157] Molecular dynamics calculations performed with simulated constraints derived from two DNA duplex molecules show that dipolar couplings significantly improve the local as well as global structures.[158] The method enabled features such as the overall helical bend in a DNA duplex to be reproduced precisely. Advances in NMR solution structure determination of macromolecules utilizing residual dipolar couplings and the use of 2D- and 3D-NMR studies of isotopically labeled molecules are presented in the context of solution structure determination of nucleic acids.[159] The use of residual dipolar couplings in the refinement of the structure of a protein–RNA complex has been shown to improve the definition of the long-range properties of the RNA.[160] A procedure for determining the three-dimensional fold of C_2-symmetric nucleic acid homo-dimers that relies on long-range orientational

constraints derived from the measurement of two independent sets of residual dipolar couplings under two different alignment conditions has been proposed and demonstrated on a deoxyoligonucleotide sequence.[161] The use of filamentous bacteriophage Pf1 for producing weak alignment of macromolecules has been presented.[162] The procedure for obtaining dipolar couplings and their use for generating angular constraints for structure refinement of nucleic acids has been discussed. A method for obtaining direct through-space correlations of base protons and phosphorous nuclei in RNA has been proposed.[163]

Studies of the structure, conformation and dynamics in oligosaccharides have also attracted considerable attention during the period under report. ^{1}H and ^{13}C one-bond dipolar couplings in natural abundance have been measured for samples of the human milk oligosaccharides oriented in bicelles consisting of a mixture of DMPC/DHPC.[164] The dipolar coupling along with NOE data have been fitted to conformational models which confirm earlier models based on NOE and molecular dynamics simulations. A new approach for the determination of ligand geometry in protein binding sites that relies on orientational constraints derived from residual dipolar couplings of partially ordered macromolecular complexes has been proposed and demonstrated for the case of ^{13}C- labeled α-methyl mannoside bound to the 53 kDa mannose-binding protein.[165] The method has the advantage that relative orientations of the protein and the ligand at the binding site can also be determined which is not possible from other methods such as transfer NOE studies. The conformational and motional properties of an oligosaccharide, methyl 3,6-di-*O*-(α-D-mannopyranosyl)-α-D-mannopyranoside, have been studied.[166] By combining the residual dipolar couplings between protons and between protons and carbons, an order matrix is solved for each ring of the trimannoside and the relative amplitudes of the internal motion at the two linkages could be obtained. The results are further confirmed by measurements carried out in two different orienting media. The utility of dipolar couplings in determining the geometry of a ligand bound to a protein, having three symmetry related binding sites, has been illustrated for the case of interaction of a saccharide ligand, α-methyl-mannose, with a mannose binding protein.[167] The tetrasaccharide lacto-*N*-neotetraose has been investigated by measurements of residual dipolar couplings in two liquid crystalline media namely mixtures of DMPC and DHPC in water and the ternary system consisting of cetylpyridinium chloride/n-hexnanol/brine.[168] The molecular structures generated by computer simulation were used in the analysis of the experimental ^{13}C–^{1}H dipolar couplings. It indicated a small conformational difference for the oligosaccharide in the two media. Residual dipolar coupling measurement in a dilute liquid crystalline solvent has been used to determine the structure of the complex between the oligosaccharide moiety of globotriaosylceramide and the B-subunit homopentamer of verotoxin 1 and for identifying the binding site.[169] Residual ^{13}C–^{1}H dipolar coupling values have been measured for a pentasaccharide oriented in a mixture of DMPC and DHPC and the structural information has been derived.[170] ^{13}C–^{1}H and ^{1}H–^{1}H residual dipolar couplings have been obtained for raffinose and saccharose.[171] The relative orientation as

well as the dynamics of the monosaccharide moieties with respect to each other have been determined.

7 Membranes and Molecules Oriented Therein

The use of ^{2}H-NMR for structural and dynamical studies in oriented membranes and model systems has been employed for over three decades and has resulted in generating enormous information and literature on the subject. It is remarkable that the interest in this area still continues and hence the results are included in a separate section in this report. ^{2}H-NMR spectra of oriented samples of gramicidin A in dimyristoylphosphatidylcholine (DMPC) show large changes for the ^{2}H-resonances of tryptophan at position 9 when the leucine residue at position 10 is substituted by amino acids such as alanine, valine and phenylalanine. The results indicate that the leucine residue helps to stabilize an optimal orientation of tryptophan in gramicidin A channels in lipid bilayers.[172] A method for the determination of orientational and order parameter-distributions simultaneously from NMR spectra of partially oriented model membranes has been proposed.[173] Multiple Quantum experiments have been used to study rat and bovine skeletal muscles and the results presented to show that there is an orientation-dependent and magnetic field independent coupling in the lactate molecule; this has been attributed to the dipolar interaction.[174] Several polarization transfer methods for lipid membranes spinning at the 'Magic Angle' have been considered.[175] It is observed that refocused INEPT or NOE enhancement methods have advantages over normal cross polarization techniques. The polar interface of membranes containing phosphatidylglycerol or cholesterol has been studied by ^{2}H-NMR as a function of membrane hydration.[176] It has been observed that as spontaneous evaporation of inter-lamellar water occurs, there is a change of conformation and average orientation with respect to the membrane surface for the phosphatidylglycerol head group and for the cholesterol molecule the off-axis motion decreases. ^{15}N–^{2}H dipolar coupling measurements have been employed in hydrogen–deuterium exchange studies.[177] The structure of gramicidin M in a lipid bilayer and the mechanism of insertion of polypeptides in the bilayer have been investigated. Alignments of a voltage-sensing peptide in dodecylphosphocholine micelles and in oriented lipid bilayers have been investigated by multidimensional solution and solid state NMR methods, respectively.[178] 2D-NMR experiments that correlate ^{13}C-chemical shifts and ^{13}C–^{1}H dipolar couplings have been carried out on cholesterol oriented in lipid bilayers and order parameters of different C–H vectors obtained.[179]

^{2}H- and ^{31}P- NMR studies on the methyl-d_3 amide derivative of the antibiotic amphotericin B incorporated into mechanically aligned bilayers of DPPC have been reported.[180] Variations of the quadrupolar and dipolar splittings as a function of macroscopic sample orientation and temperature indicate that the amide derivative undergoes fast rotation about an axis parallel to the bilayer normal.

It has been shown that the secondary structure and topology of membrane proteins can be described by inspection of two-dimensional ^{1}H–^{15}N dipolar coupling / ^{15}N chemical shift polarization inversion spin exchange at the magic angle (PISEMA) spectra obtained from uniformly ^{15}N-labeled samples in oriented bilayers.[181,182] The characteristic wheel-like patterns of resonances observed in these spectra reflect the helical wheel projections of residues in both transmembrane and in-plane helices and hence provide direct indices of the secondary structure and topology of membrane proteins in phospholipid bilayers. The method has been illustrated for the transmembrane segment of the M2 peptide[181,182] and the antibiotic peptide magainin.[181]

The use of three-dimensional spectroscopy involving ^{1}H chemical shift/^{1}H-^{15}N dipolar coupling/^{15}N chemical shift correlation has been shown to improve spectral resolution in studies of membrane proteins with helices aligned parallel to the membrane surface.[183] Such a measurement on the antibiotic peptide magainin enabled the three-dimensional orientation of this helical peptide to be determined in the lipid bilayer. The orientation of the insect antiobiotic peptide cecropin A in the phospholipid bilayer membrane has been determined using ^{15}N solid-state NMR spectroscopy and the result discussed in relation to the mechanism of action of the peptide.[184]

8 Relaxation Studies

Relaxation rates of selectively deuterated dodecyltrimethylammonium chloride/water system in the micellar cubic phase have been studied by ^{2}H-NMR spectroscopy at several frequencies down to 0.5 MHz.[185] The results indicate that the residual order is small due to diffusion and aggregate rotation; these are also confirmed by the static quadrupole splittings in this phase. Proton spin–lattice relaxation has been studied over the frequency range 10^{3}Hz–10^{8} Hz for the liquid crystal propylcyanophenylcyclohexane in the nematic phase.[186] The anomalous behaviour of T_1-dependence on Larmor frequency over certain frequency range has been attributed to spin pair reorientational fluctuations. Molecular dynamics in the nematic and isotropic phases as well as in the polyphasic regions of the phase diagram of the ternary mixture of potassium laurate/1-decanol/water have been studied by proton spin–lattice relaxation dispersion measurements in a broad Larmor frequency range.[187] Evidence to show that director fluctuations are responsible for the spin–lattice relaxation dispersion behaviour at low Larmor frequencies in the nematic phase has been presented. The mechanisms responsible for the behaviour at higher frequencies and in other phases have also been dealt with. The ^{2}H-Zeeman and quadrupolar spin–lattice relaxation times of two deuterated isotopmers of 1-methylheptyl 4′-(4″-n-decyloxybenzoyloxy) biphenyl-4-carboxylate and [4-(2-methylbutyloxycarbonyl)phenyl] 4-n-heptyl-biphenyl carboxylate have been measured.[188] The variation of the spectral densities as a function of temperature has been discussed qualitatively in the phases in which the molecules do not align along the magnetic field direction. For the smectic

phase, a quantitative interpretation in terms of diffusion coefficients has been presented. ^{2}H-quadrupolar splittings and spin-lattice relaxation times have been measured for the ring-deuterated hexaoctyloxyrufigallol in the columnar phase and the diffusion constants for rotations of the molecule around and perpendicular to the columnar axis obtained.[189] Proton T_1-measurements have been reported for the aqueous solutions of n-dodecylhexaoxyethylene glycol as a function of composition, spectral frequency and temperature and the results interpreted in terms of the motion of the molecule in the different phases.[190] ^{2}H-NMR study of a chain-deuterated octyloxy benzoyloxy cynaobiphenyl (8OBCB) and deuterated 4-n-octyloxy-4(-cyanobiphenyl (8OCB) has been carried out at two different Larmor frequencies.[191,192] Deuterium spin–lattice relaxation times and quadrupolar splittings have been measured. The potential of the mean torque has been obtained from the quadrupolar splittings and the relaxation data have been used to obtain the motional parameters.[192] Similar studies have also been carried out in a mixture containing 72 wt% of 8OCB and 28 wt% of 6OCB exhibiting nematic and reentrant nematic phases.[193] Proton T_1-measurements have been made over the range 400 Hz to 80 MHz by field-cycling techniques in the nematic mesophase of butylcyano-phenylcyclohexane and the physical significance of the plateau in the relaxation profiles at low Larmor frequencies discussed.[194] Relaxation of proton dipolar order (T_{1D}) in the nematic phase of *para*-azoxyanisole having the methyl protons deuterated has been studied over a broad frequency range.[195] An isolated spin-pair model has been used to calculate the relaxation times. It predicts a lower rate of relaxation than experimentally observed. Possible reasons for the failure of the model have been discussed. Proton spin–lattice relaxation dispersion in the smectic phase of 4 cyano-4′-8-alkylbiphenyl and 4,4′-bis-heptyloxyazoxybenzene has been studied.[196] The T_1- dependence on Larmor frequency has been used to understand the molecular dynamics in the systems. ^{129}Xe- chemical shifts and relaxation times have been used to detect phase transitions and characterize the dynamics in binary and ternary reentrant nematic liquid crystal mixtures.[197] The results of the dynamics study have been compared in terms of the molecular packing and the dynamical modes responsible for nuclear spin relaxation.

9 Structure and Conformation of Small Molecules and Orientational Order

As mentioned earlier, the proton NMR spectra of small molecules oriented in nematic liquid crystals become rapidly complex with the increase of number of interacting nuclei. In order to obtain information on orientation and structure, it is therefore essential to develop strategies to interpret such spectra with the help of special techniques. Techniques such as 'Automatic Analysis' and the use of Multiple Quantum Spectroscopy have been employed for these purposes during the period under report. A method based on the Automatic Analysis of Multiple Quantum proton spectra of flexible molecules dissolved in liquid crystalline phases has been suggested for extracting starting parameters for the

analysis of the single quantum spectra and applied to molecules Ph-CH_2-X and 3-phenylprop-1-yne.[198] A strategy for analyzing complex NMR spectra of several solutes co-dissolved in liquid crystalline phases has been evolved.[199,200] Spectral parameters of solutes *m*- or *o*-xylene contained in a mixture were estimated by analyzing the 2D Multiple Quantum spectra. The calculated single quantum spectrum of one of the molecules was then subtracted from the composite spectrum, enabling spectral and structural parameters for the other solutes to be accurately estimated.[199] A similar strategy has also been exploited to simplify spectra of a mixture of three compounds which are co-solutes in a nematic phase.[200] Strategies based on the use of partially deuterated molecules, spin-echo and multiple quantum spectroscopy have been employed to analyze the proton spectra of the flexible molecule ethylbenzene oriented in four different liquid crystals.[201] Differences in the geometry of the molecule derived from the dipolar couplings to that obtained from molecular orbital calculations have been attributed to the latter being carried out for an isolated molecule. Conformational analysis of chain molecules in liquid crystalline phases by a rotational isomeric state scheme with maximum entropy method has been carried out.[202] Agreement with an analysis of experimental ^1H–^1H dipolar coupling data obtained for n-hexane, n-heptane, n-octane, n-nonane and n-decane dissolved in a nematic liquid crystal has also been obtained. Similarly ^2H-quadrupolar splittings observed for n-decane and 1,6-dimethoxy hexane dissolved in 4′-methoxybenzyline-4-n-butyl-aniline (MBBA) have been analyzed and the results reproduced by simulations.[203] A new approach based on integral curves and genetic algorithms has been proposed for the analysis of spectra of solutes oriented by liquid crystals.[204] The ^1H-NMR spectra of ethanol, *trans*-azobenzene and tolan in a nematic phase have been analyzed by this method. Experiments to selectively excite spin 3/2 nuclei exhibiting residual quadrupolar splittings have been used to acquire ^{23}Na-NMR spectra from samples containing sodium in ordered environments and approaches to the analyses of such spectra suggested.[205]

The orientation of *p*-tetrafluorobenzoquinone in four nematic liquid crystalline solvents with different aromaticities has been determined from the ^{19}F–^{19}F and the ^{19}F–^{13}C scalar and dipolar couplings.[206] Signs of $J_{F\text{-}F}$ and $J_{C\text{-}F}$ have also been determined. The geometry of the molecule has also been derived. The discrepancies between the experimentally derived geometry of the molecule and that obtained from other methods have been attributed to the formation of a charge-transfer molecular complex which was confirmed from UV spectrophotometric measurements though anisotropies of the ^{19}F–^{19}F indirect spin–spin couplings could also contribute significantly. The structures and conformations of methyl isonicotinate, methyl nicotinate and methyl picolinate have been investigated by the analysis of the proton spectra obtained at 296 K in the solvent ZLI-1167.[207] A conformer with a planar skeleton was detected for methyl isonicotinate. For the other two compounds *s-trans* and *s-cis* conformers were found and their relative abundance determined.

Several molecules having a bent structure with a 2-phenylindazole group in the core have been studied for their liquid crystalline properties.[208] From the

^{13}C- NMR studies it has been observed that the long molecular axis is nearly parallel to the *para*-axis of the phenyl moiety and hence the first few fragments of the chain attached to the indazole group are not along this axis. This requires that the alkoxy chain attached to the indazole group has at least six carbon atoms to promote liquid crystalline behaviour. The order parameters of 4′-cyanophenyl 4-heptylbenzoate have been obtained by using ^{13}C 2D-NMR spectroscopy.[209] Linear relationships between ^{13}C-chemical shifts and order parameters have been obtained. Phase behaviour of a mixture of this liquid crystal and its chain-perfluorinated analogue has also been studied.

Deuterium NMR has been employed to investigate the orientational order, molecular structure and phase transitions of the chiral smectic liquid crystal 1-methylheptyl 4′-(4-n-decyloxybenzoyloxy)biphenyl-4-carboxylate.[210] Orientational orders in the nematic and smectic phases formed by 4-(2-methylbutyl) phenyl-4′n-heptylbiphenyl-4-carboxylate have been investigated as also have the dynamics of the aromatic core by ^{2}H-relaxation time measurements.[211] Two partially deuterated liquid crystalline monomers and the corresponding polysiloxanes in which the aromatic mesogenic core is composed of a bis(oxybenzoate) unit and different chiral groups have been studied by ^{1}H and ^{2}H-NMR and the order parameters in all the cases and the biaxiality in the case of the monomers have been examined.[212] ^{2}H-quadrupolar splittings and spin–lattice relaxation times have been measured for the ring deuterated 1-fluoro-2,3,6,7,10,11-hexahexyloxytriphenylene as a function of temperature at two different Larmor frequencies and the dynamics and order in its columnar phase studied.[213] The microscopic origin of the photocontrol of smectic spacing has been investigated by a deuterium NMR study of the perturbation of the orientational order in the smectic A phase of the liquid crystal octylcyanobiphenyl caused by photo-induced *trans–cis* isomerization of a photo-sensitive dopant.[214] ^{2}H-NMR spectra of nitrobenzene-d_5 in the presence of strong electric fields revealed partial alignment of the molecule in the applied electric field.[215] A two-dimensional detection method has been used. Molecular order parameter and relative angle between the bond vectors have been obtained from the deuterium splittings. Dependence of the order parameter on the concentration of the molecule has also been studied. ^{2}H-NMR along with other techniques such as optical microscopy and X-ray diffraction have been used to map the phase diagram and to measure the nematic order parameter variation in the ternary mixture of ammonium pentadecafluorooctanoate/D_2O/NH_4Cl.[216] ^{2}H-NMR experiments on nematic single domains of vanadium pentoxide suspension in D_2O provide quadrupolar doublets characteristic of a uniaxial symmetry.[217] A simple model for the system could account for the value of the quadrupolar splittings and their concentration dependence. The reorientation of this nematic phase has also been investigated. Deuterium spectra and relaxation rates have been measured for 8CB confined in cylindrical cavities of Anopore membranes and 5CB in an embedded polymer network.[218,219] The data have been used to infer information on the effect of spatial constraints on molecular mobility and on the surface orientational order parameter. The method of selective deuterium labeling and

monitoring ^{13}C–^{2}H dipolar couplings in the ^{13}C- spectra proposed earlier[220] has been exploited for the case of 4′-cyanobiphenyl 2-deutero- and 6-deutero-hexanoate over the complete nematic range of the compounds.[221] The ^{2}H-NMR spectrum with homonuclear proton decoupling provides ^{2}H-quadrupolar and ^{1}H–^{2}H dipolar couplings. Two-dimensional spectroscopy has also been employed to provide ^{1}H–^{13}C dipolar couplings and the order parameters for the system studied. ^{2}H-NMR spectroscopy has been used to study the orientational order, tilt angle and layer organization of a chiral smectic liquid crystal.[222] Deuterium quadrupole splittings of benzyl alcohol-d_5 and a series of alkyl benzyl-d_5 ethers with linear aliphatic chains dissolved in anionic nematic lyotropic liquid crystals prepared with sodium decylsulfate and caesium decylsulfate have been measured and the two order parameters that describe the average orientation of the aromatic ring calculated.[223] The studies also provide information on the mechanism of incorporation of the solute molecules into the superstructure of the aggregate. ^{2}H-NMR spectra of deuterated molecules have been recorded in the chiral liquid crystal formed by PBLG and a co-solvent.[224] The deuterium quadrupolar couplings are found to provide large signal dispersion and also act as probes for obtaining local order. Banana shaped mesogens derived either from isophthalic acid or 4-bromoisophthalic acid have been synthesized and the mesophase identified as B_2 phase.[225]

Proton NMR study of molecular order has been reported for octylphenyl-2-chloro-4-(*p*-cyano-benzoyloxy) benzoate having three bilayer smectic phases.[226] Experimental dipolar couplings have been used to suggest models that provide the tilt angles associated with the phase. The dipolar oscillations observed during cross-polarization in liquid crystals[19] have been used to study the anti-ferroelectric chiral smectic liquid crystal MHPOBC.[227] Decay time for the oscillations has been used as a probe for monitoring intramolecular motions. Motion of the chiral chain in the anti-ferroelectric phase has been observed to be frozen, indicating the origin of the large transverse dipole moment observed.

Experimental orientational data have been obtained from proton NMR spectra of 1,4-difluorobenzene, 1,4-dichlorobenzene, 1,4-diboromobenzene and naphthalene dissolved in several nematic solvents at different temperatures.[228,229] The results indicate a relationship between the sign and magnitude of dielectric anisotropies of the nematic solvents and the temperature dependence of the orientational biaxiality ratio of the solutes dissolved in them.[228]

Temperature and concentration dependence of the degree of orientational order of acetonitrile in nematic esters 4-butyloxyphenyl 4-hexyloxybenzoate and 4-(4-ethoxyphenyloxycarbonyl)phenyl carbonate has been investigated.[230] Proton NMR studies of the nematic liquid crystal ZLI-1132 containing small amounts of the solutes 1,3,5-trichlorobenzene, *p*-dichlorobenzene and acetone have been carried out as a function of the pressure of a mixture of molecular hydrogen and deuterium gases.[231] The observed differences in the orientational behavior of the investigated molecules have been attributed to short range mechanisms and shape and size dependent hard body interactions. A general increase of solute orientational order with pressure has been observed.

10 References

1 C.L. Khetrapal, K.V. Ramanathan and G.A. Nagana Gowda, in *Nuclear Magnetic Resonance*, ed. G.A. Webb (Specialists Periodical Reports), The Royal Society of Chemistry, Cambridge, 2000, **29**, p. 534.
2 N. Tjandra and A. Bax, *Science*, 1997, **278**, 1111.
3 R. Blinc, *Liq. Cryst.*, 1999, **26**, 1295.
4 N. Suryaprakash, *Curr. Org. Chem.*, 2000, **4**, 85.
5 P. Ukleja and D. Finotello, in *Liquid Crystals*, ed. S. Kumar, Cambridge University Press, Cambridge, 2001, p. 155–196.
6 R. Righini, *EMIS Datarev. Ser.*, 2000, **25**, 464.
7 M.F. Brown and A.A. Nevzorov, *Colloids Surf. A.*, 1999, **158**, 281.
8 D. Bauman, *Proc. SPIE-Int. Soc. Opt. Eng.*, 2000, **4147**, 126.
9 S.J. Picken, *EMIS Datarev. Ser.*, 2000, **25**, 89.
10 B. Stevensson, A.V. Komolkin, D. Sandstrom and A. Maliniak, *J. Chem. Phys.*, 2001, **114**, 2332.
11 M. Ylihautala, J. Lounila and J. Jokisaari, *Chem. Phys. Lett.*, 1999, **301**, 153.
12 M. Ylihautala, J. Lounila and J. Jokisaari, *J. Chem. Phys.*, 1999, **110**, 6381.
13 J. Vaara, J. Kaski and J. Jokisaari, *J. Phys. Chem. A*, 1999, **103**, 5675.
14 J. Lounila, Y. Hiltunen, K. Tuppurainen, A. Pulkkinen and R. Laatikainen, *Can. J. Chem.*, 1999, **77**, 1788.
15 D. Frezzato, G. Kothe and G.J. Moro, *J. Phys. Chem. B*, 2001, **105**, 1281.
16 B.M. Fung, A.K. Khitrin and K. Ermolaev, *J. Magn. Reson.*, 2000, **142**, 97.
17 G. Antonioli, D.E. McMillan and P. Hodgkinson, *Chem. Phys. Lett.*, 2001, **344**, 68.
18 D. McElheny, M. Zhou and L. Frydman, *J. Magn. Reson.*, 2001, **148**, 436.
19 R. Pratima and K.V. Ramanathan, *J. Magn. Reson.* A, 1996, **118**, 7.
20 C.S. Nagaraja and K.V. Ramanathan, *Liq. Cryst.*, 1999, **26**, 17.
21 N. Sinha and K.V. Ramanathan, *Chem. Phys. Lett.*, 2000, **332**, 125.
22 D. Sandstrom and H. Zimmermann, *J. Phys. Chem. B*, 2000, **104**, 1490.
23 S. Vivekanandan and N. Suryaprakash, *Chem. Phys. Lett.*, 2001, **338**, 247.
24 C.S. Nagaraja and K.V. Ramanathan, *J. Magn. Reson.*, 2000, **146**, 165.
25 P. Holstein, M. Bender, P. Galvosas, D. Geschke and J. Karger, *J. Magn. Reson.*, 2000, **143**, 427.
26 S.V. Dvinskikh, R. Sitnikov and I. Furo, *J. Magn. Reson.*, 2000, **142**, 102.
27 S.V. Dvinskikh and I. Furo, *J. Magn. Reson.*, 2000, **144**, 142.
28 S.A. Riley and M.P. Augustine, *J. Phys. Chem. A*, 2000, **104**, 3326.
29 A. Peshkovsky and A.E. McDermott, *J. Magn. Reson.*, 2000, **147**, 104.
30 R.P. Feynman, *Int. J. Theor. Phys.*, 1982, **21**, 467.
31 N.A. Gershenfeld and I.L. Chuang, *Science*, 1997, **275**, 350.
32 D.G. Cory, A.F. Fahmy and T.F. Havel, *Proc. Natl. Acad. Sci. USA*, 1997, **94**, 1634.
33 J.A. Jones, *Prog. Nucl. Magn. Reson. Spectrosc.*, 2001 **38**, 325.
34 C.S. Yannoni, M.H. Sherwood, D.C. Miller, I.L. Chuang, L.M.K. Vandersypen and M.G. Kubinec, *Appl. Phys. Lett.*, 1999, **75**, 3563.
35 M. Marjanska, I.L. Chuang and M.G. Kubinec, *J. Chem. Phys.*, 2000, **112**, 5095.
36 A. Khitrin and B.M. Fung, *J. Chem. Phys.*, 2000, **112**, 6963.
37 N. Sinha, T.S. Mahesh, K.V. Ramanathan and A. Kumar, *J. Chem. Phys.*, 2001, **114**, 4415.
38 B.M. Fung, *Phys. Rev. A*, 2001, **63**, 022304.

39 A. Khitrin, H. Sun and B.M. Fung, *Phys. Rev. A*, 2001, **63**, 020301(R).
40 A. Khitrin and B.M. Fung, *Phys. Rev. A*, 2001, **64**, 032306.
41 K.V.R.M. Murali, N. Sinha, T.S. Mahesh, M.H. Levitt, K.V. Ramanathan and A. Kumar, *Phys. Rev. A*, (communicated).
42 T.S. Mahesh, N. Sinha, K.V. Ramanathan and A. Kumar, *Phys. Rev. A*, in press.
43 S. Ternieden, D. Zauser and K. Muller, *Liq. Cryst.*, 2000, **27**, 1171.
44 G.R. Luckhurst, T. Miyamoto, A. Sugimura and B.A. Timimi, *Mol. Cryst. Liq. Cryst.*, 2000, **347**, 147.
45 C.J. Dunn, G.R. Luckhurst, T. Miyamoto, H. Naito, A. Sugimura and B.A. Timmi, *Mol. Cryst. Liq. Cryst.*, 2000, **347**, 167.
46 G.R. Luckhurst, A. Sugimura and B.A. Timimi, *Mol. Cryst. Liq. Cryst.*, 2000, **347**, 53.
47 G.R. Luckhurst, *Mol. Cryst. Liq. Cryst.*, 2000, **347**, 121.
48 J.W. Emsley, G.R. Luckhurst and P. Pedrielli, *Chem. Phys. Lett.*, 2000, **320**, 255.
49 J.W. Emsley, J.E. Long, G.R. Luckhurst and P. Pedrielli, *Phys. Rev. E*, 1999, **60**, 1831.
50 M. Bender, P. Holstein and D. Geschke, *J. Chem. Phys.*, 2000, **113**, 2430.
51 S. Vivekanandan, H.S. Vinay Deepak, G.A. Nagana Gowda. K.V. Ramanathan and C.L. Khetrapal, *J. Mol. Struct.*, in press.
52 E. Nishikawa and E.T. Samulski, *Liq. Cryst.*, 2000, **27**, 1463.
53 K.E. Maly, G. Wu and R.P. Lemieux, *Liq. Cryst.*, 2001, **28**, 457.
54 B. Zalar, A. Gregorovic and R. Blinc, *Phys. Rev., E*, 2000, **62**, R37.
55 A. Carvalho, P.J. Sebastio, A. Ferraz, A.C. Ribeiro and H.T. Nguyen, *Eur. Phys. J. E*, 2000, **2**, 351.
56 R. Blinc, B. Zalar, A. Gregorovic, M. Simsic, A Zidansek and M. Neubert, *Ferroelectrics*, 2000, **245**, 1.
57 R. Blinc, A. Gregorovic and B. Zalar, *Z. Naturforsch. A*, 2000, **55**, 298.
58 A. Zheliaskova, R. Marinov and A. Derzhanski, *J. Mol. Struct.*, 1999, **513**, 9.
59 M. Geppi, S. Pizzanelli, C.A. Veracini, *Chem. Phys. Lett.*, 2001, **343**, 513.
60 A.F. Martins, A.E. Gomes, A. Polimeno and L. Orian, *Phys. Rev. E*, 2000, **62**, 2301.
61 M. Schneider, D.E. Demco and B. Blumich, *J. Magn. Reson.*, 1999, **140**, 432.
62 P. Holstein, E.B. Barmatov, D. Geschke, M. Bender and V.P. Shibaev, *Colloid Polym. Sci.*, 2000, **278**, 711.
63 L. Gasper, D.E. Demco and B. Blumich, *Solid State NMR*, 1999, **14**, 105.
64 R.Y. Dong, M. Cheng, K. Fodor-Csorba and C.A. Veracini, *Liq. Cryst.*, 2000, **27**, 1039.
65 D. Merlet, J.W. Emsley, P. Lesot and J. Courtieu, *J. Chem. Phys.*, 1999, **111**, 6890.
66 C. Canlet, D. Merlet, P. Lesot, A. Meddour, A. Loewenstein and J. Couriteu, *Tetrahedron: Asymmetry*, 2000, **11**, 1911.
67 D. Merlet, M. Sarfati, B. Ancian, J. Courtieu and P. Lesot, *Phys. Chem. Chem. Phys.*, 2000, **2**, 2283.
68 D. Merlet, B. Ancian, J. Courtieu and P. Lesot, *J. Am. Chem. Soc.*, 1999, **121**, 5249.
69 A. Meddour, C. Canlet, L. Blanco and J. Courtieu, *Angew. Chem. Int. Ed.*, 1999, **38**, 2391.
70 M. Sarfati, P. Lesot, D. Merlet and J. Courtieu, *Chem. Commun.*, 2000, 2069.
71 J.H. Prestegard, J.R. Tolman, H.M. Al-Hashimi and M. Andrec, *Biol. Magn. Reson.*, 1999, **17**, 311.

72 P.C. Driscoll, D. Esposito and M. Pfuhl, *Nucl. Magn. Reson.*, 2000, **29**, 340.
73 G. Siegal, J. van-Duynhoven and M. Baldus, *Curr. Opin. Chem. Biol.*, 1999, **3**, 530.
74 M.R. Hansen and P. Hanson and A. Pardi, *Methods Enzymol.*, 2000, **317**, 220.
75 C.L. Khetrapal, *J. Ind. Chem. Soc.*, 2001, **78**, 112.
76 M. Pellecchia, C.W. Vander Kooi, K. Keliikuli and E.R.P. Zuiderweg, *J. Magn. Reson.*, 2000, **143**, 435.
77 G. Cornilescu and A. Bax, *J. Am. Chem. Soc.*, 2000, **122**, 10143
78 M. Andrec, P. Du and R.M. Levy, *J. Am. Chem. Soc.*, 2001, **123**, 1222.
79 L.G. Barrientos, J.M. Louis and A.M. Gronenborn, *J. Magn. Reson.*, 2001, **149**, 154.
80 J.J. Chou and A. Bax, *J. Am. Chem. Soc.*, 2001, **123**, 3844.
81 H. Desvaux, J.-C.P. Gabriel, P. Berthault and F. Camerel, *Angew. Chem. Int. Ed*, 2001, **40**, 373.
82 A. Kaikkonen and G. Otting, *J. Am. Chem. Soc.*, 2001, **123**, 1770.
83 G. Cho, B.M. Fung and V.B. Reddy, *J. Am. Chem. Soc.*, 2001, **123**, 1537.
84 U. Eliav and G. Navon, *J. Magn. Reson.*, 1999, **137**, 295.
85 G. Marius Clore, *Proc. Natl. Acad. Sci. USA*, 2000, **97**, 9021.
86 E. Brunner, J. Ogle, M. Wenzler and H.R. Kalbitzer, *Biochem. Biophys. Res. Commun.*, 2000, **272**, 694.
87 G.A. Mueller, W.Y. Choy, D. Yang, J.D. Formankay, R.A. Venters and L.E. Kay, *J. Mol. Biol.*, 2000, **300**, 197.
88 N. Tjandra, J. Marquardt and G. Marius Clore, *J. Magn. Reson.*, 2000, **142**, 393.
89 W. Peti and C. Griesinger, *J. Am. Chem. Soc.*, 2000, **122**, 3975.
90 E.T. Olejniczak, R.P. Meadows, H. Wang, M. Cai, D.G. Nettesheim and S.W. Fesik, *J. Am. Chem. Soc.*, 1999, **121**, 9249.
91 J. Boyd and C. Redfield, *J. Am. Chem. Soc.*, 1999, **121**, 7441.
92 F. Tian, P.J. Bolon and J.H. Prestegard, *J. Am. Chem. Soc.*, 1999, **121**, 7712.
93 M. Zweckstetter and A. Bax, *J. Am. Chem. Soc.*, 2000, **122**, 3791.
94 M. Ruckert and G. Otting, *J. Am. Chem. Soc.*, 2000, **122**, 7793.
95 R.S. Prosser, H. Bryant, R.G. Bryant and R.R. Vold, *J. Magn. Reson.*, 1999, **141**, 256.
96 R. Tycko, F. J. Blanco and Y. Ishii, *J. Am. Chem. Soc.*, 2000, **122**, 9340.
97 C. Ma and S. J. Opella, *J. Magn. Reson.*, 2000, **146**, 381.
98 J.-C. Hus, D. Marion and M. Blackledge, *J. Am. Chem. Soc.*, 2001, **123**, 1541.
99 A. Mittermaier and L. E. Kay, *J. Am. Chem. Soc.*, 1999, **121**, 10608.
100 V. King, M. Parker and K.P. Howard, *J. Magn. Reson.*, 2000, **142**, 177.
101 F. Delaglio, G. Kontaxis and A. Bax, *J. Am. Chem. Soc.*, 2000, **122**, 2142.
102 J.R. Tolman, H.M. Al-Hashimi, L.E. Kay and J.H. Prestegard, *J. Am. Chem. Soc.*, 2001, **123**, 1416.
103 M.A. Firestone, D.M. Tiede and S. Seifert, *J. Phys. Chem. B*, 2000, **104**, 2433.
104 K.C.W. Vander, E. Kupce, E.P.R. Zuiderweg and M. Pellecchia, *J. Biomol. NMR*, 1999, **15**, 335.
105 J. Struppe, J.A. Whiles and R.R. Vold, *Biophys. J.*, 2000, **78**, 281.
106 F. Tian, J.A. Losonczi, M.W.F. Fischer and J.H. Prestegard, *J. Biomol. NMR*, 1999, **15**, 145.
107 S. Moltke and S. Grzesiek, *J. Biomol. NMR*, 1999, **15**, 77.
108 M. Ottiger and A. Bax, *J. Biomol. NMR*, 1999, **13**, 187.
109 N. Tjandra, *Structure*, 1999, **7**, R205.
110 G. Otting, M. Ruckert, M.H. Levitt and A. Moshref, *J. Biomol. NMR.*, 2000, **16**, 343.

111 G. Zandomeneghi, M. Tomaselli, J.D. van Beek and B.H. Meier, *J. Am. Chem. Soc.*, 2001, **123**, 910.
112 L.G. Barrientos, C. Dolan and A.M. Gronenborn, *J. Biomol. NMR*, 2000, **16**, 329.
113 P. Permi and A. Annila, *J. Biomol. NMR*, 2000, **16**, 221.
114 T. Carlomagno, W. Peti and C. Griesinger, *J. Biomol. NMR*, 2000, **17**, 99.
115 P. Permi, P.R. Rosevear and A. Annila, *J. Biomol. NMR*, 2000, **17**, 43.
116 J. Meiler, N. Blomberg, M. Nilges and C. Griesinger, *J. Biomol. NMR*, 2000, **16**, 245.
117 K. Fleming, D. Gray, S. Prasannan and S. Mathews, *J. Am. Chem. Soc.*, 2000, **122**, 5224.
118 D. Yang, R.A. Venters, G.A. Mueller, W.Y. Choy and L.E. Kay, *J. Biomol. NMR*, 1999, **14**, 333.
119 H.-J. Sass, G. Musco, S.J. Stahl, P.T. Wingfield and S. Grzesiek, *J. Biomol. NMR*, 2000, **18**, 303.
120 N.R. Skrynnikov and L.E. Kay, *J. Biomol. NMR*, 2000, **18**, 239.
121 J.L. Chou, S. Li and A. Bax, *J. Biomol. NMR*, 2000, **18**, 217.
122 G.A. Mueller, W.Y. Choy, N.R. Skrynnikov and L.E. Kay, *J. Biomol. NMR*, 2000, **18**, 183.
123 D. Fushman, R. Ghose and D. Cowburn, *J. Am. Chem. Soc.*, 2000, **122**, 10640.
124 F. Tian, C.A. Fowler, E.R. Zarter, F.A. Jenney, M.W. Adams and J.H. Prestegard, *J. Biomol. NMR*, 2000, **18**, 23.
125 J.J. Chou, F. Delaglio and A. Bax, *J. Biomol. NMR*, 2000, **18**, 101.
126 E. de Alba, M. Suzuki and N. Tjandra, *J. Biomol. NMR*, 2001, **19**, 63.
127 G. Marius Clore and D.S. Garrett, *J. Am. Chem. Soc.*, 1999, **121**, 9008.
128 H.M.Al-Hashimi, H. Valafar, M. Terrell, E.R. Zartler, M.K. Eidsness and J.H. Prestegard, *J. Magn. Reson.*, 2000, **143**, 402.
129 J.A. Losonczi, F. Tian and J.H. Prestegard, *Biochemistry*, 2000, **39**, 3804.
130 N.R. Skrynnikov, N.K. Goto, D. Yang, W.-Y. Choy, J.R. Tolman, G.A. Mueller and L.E. Kay, *J. Mol. Biol.*, 2000, **295**, 1265.
131 R.R. Biekofsky, F.W. Muskett, J.M. Schmidt, S.R. Martin, J.P. Browne, P.M. Bayley and J. Feeney, *FEBS Lett.*, 1999, **460**, 519.
132 M.W.F. Fischer, J.A. Losonczi, J.L. Weaver and J.H. Prestegard, *Biochemistry*, 1999, **38**, 9013.
133 J.-C. Hus, D. Marion and M. Blackledge, *J. Mol. Biol.*, 2000, **298**, 927.
134 C.A. Fowler, F. Tian, H.M. Al-Hashimi and J.H. Prestegard, *J. Mol. Biol.*, 2000, **304**, 447.
135 G. Veglia and S.J. Opella, *J. Am. Chem. Soc.*, 2000, **122**, 11733.
136 X. Huang, F. Moy and R. Powers, *Biochemistry*, 2000, **39**, 13365.
137 A.R. Jude, D.V. Greathouse, M.C. Leister and R.E. Koeppe II, *Biophys. J.*, 1999, **77**, 1927.
138 E. de Alba, L. De Vries, M.G. Farquhar and N. Tjandra, *J. Mol. Biol.*, 1999, **291**, 927.
139 M.A. Markus, R.B. Gerstner, D.E. Draper and D.A. Torchia, *J. Mol. Biol.*, 1999, **292**, 375.
140 D.S. Garrett, Y.-J. Seok, A. Peterkofsky, A.M. Gronenborn and G. Marius Clore, *Nat. Struct. Biol.*, 1999, **6**, 166.
141 M. Cai, H. Wang, E.T. Olejniczak, R.P. Meadows, A.H. Gunasekera, N. Xu and S.W. Fesik, *J. Magn. Reson.*, 1999, **139**, 451.
142 B.W. Koenig, J.-S. Hu, M. Ottiger, S. Bose, R.W. Hendler and A. Bax, *J. Am. Chem. Soc.*, 1999, **121**, 1385.

143 G. Marius Clore, M.R. Starich, C.A. Bewley, M. Cai and J. Kuszewski, *J. Am. Chem. Soc.*, 1999, **121**, 6513.
144 I. Bertini, F. Castellani, C. Luchinat, G. Martini, G. Parigi and S. Ristori, *J. Phys. Chem. B*, 2000, **104**, 10653.
145 B.W. Koenig, D.C. Mitchell, S. Konig, S. Grzesiek, B.J. Litman and A. Bax, *J. Biomol. NMR*, 2000, **16**, 121.
146 V. Tsui, L. Zhu, T.H. Huang, P.E. Wright and D.A. Case, *J. Biomol. NMR*, 2000, **16**, 9.
147 F. Cordier, A.J. Dingley and S. Grzesiek, *J. Biomol. NMR*, 1999, **13**, 175.
148 D.D. Ojennus, D. Deanna, F. Mitton, M. Rachel and D.S. Wuttke, *J. Biomol. NMR*, 1999, **14**, 175.
149 F. Arnesano, L. Banci. I. Bertini, K. Van der Watering, M. Czisch and R. Kaptein, *J. Biomol. NMR*, 2000, **17**, 295.
150 I. Bertini, I.C. Felli and C. Luchinat, *J. Biomol. NMR*, 2000, **18**, 347.
151 J.L. Baber, D. Libutti, D. Levens and N. Tjandra, *J. Mol. Biol.*, 1999, **289**, 949.
152 E.T. Mollova, M.R. Hansen and A. Pardi, *J. Am. Chem. Soc.*, 2000, **122**, 11561.
153 L. Trantirek, M. Urbasek, R. Stefl, J. Feigon and V. Sklenar, *J. Am. Chem. Soc.*, 2000, **122**, 10454.
154 N. Tjandra, S.-i. Tate, A. Ono, M. Kainosho and A. Bax, *J. Am. Chem. Soc.*, 2000, **122**, 6190.
155 M. Ottiger and A. Bax, *J. Am. Chem. Soc.*, 1998, **120**, 12334.
156 Z. Wu, N. Tjandra and A. Bax, *J. Am. Chem. Soc.*, 2001, **123**, 3617.
157 S.R. Lynch and J.D. Puglisi, *J. Am. Chem. Soc.*, 2000, **122**, 7853.
158 A. Vermeulen, H. Zhou and A. Pardi, *J. Am. Chem. Soc.*, 2000, **122**, 9638.
159 E.T. Mollova and A. Pardi, *Curr. Opin. Struct. Biol.*, 2000, **10**, 298.
160 P. Bayer, L. Varani and G. Varani, *J. Biomol. NMR*, 1999, **14**, 149.
161 H.M. Al-Hashimi, A. Majumdar, A. Gorin, A. Kettani, E. Skripkin and D.J. Patel, *J. Am. Chem. Soc.*, 2001, **123**, 633.
162 M.R. Hansen, P. Hanson and A. Pardi, *Proc. Conversation Biomol., Stereodyn.*, 2000, **11**, 365.
163 M. Hennig, T. Carlomagno and J.R. Williamson, *J. Am. Chem. Soc.*, 2001, **123**, 3395.
164 M. Martin-Pastor and C.A. Bush, *Biochemistry*, 2000, **39**, 4674.
165 P.J. Bolon, H.M. Al-Hashimi and J.H. Prestegard, *J. Mol. Biol.*, 1999, **293**, 107.
166 F. Tian, H.M. Al-Hashimi, J.L. Craighead and J.H. Prestegard, *J. Am. Chem. Soc.*, 2001, **123**, 485.
167 H.M. Al-Hashimi, P.J. Bolon and J.H. Prestegard, *J. Magn. Reson.*, 2000, **142**, 153.
168 C. Landersjo, C. Hoog, A. Maliniak, and G. Widmalm, *J. Phys. Chem. B*, 2000, **104**, 5618.
169 G.S. Thompson, H. Shimizu, S.W. Homans and A. Donohue-Rolfe, *Biochemistry*, 2000, **39**, 13153.
170 M. Martin-Pastor and C.A. Bush, *Carbohydr. Res.*, 2000, **323**, 147.
171 H. Neubauer, J. Meiler, W. Peti and C. Griesinger, *Helv. Chim. Acta*, 2001, **84**, 243.
172 R.E. Koeppe II, J. Hatchett, A.R. Jude, L.L. Providence, O.S. Andersen and D.V. Greathouse, *Biochemistry*, 2000, **39**, 2235.
173 E. Sternin, H. Schafer, I.V. Polozov and K. Gawrisch, *J. Magn. Reson.*, 2001, **149**, 110.

174 I. Asllani, E. Shankland, T. Pratum and M. Kushmerick, *J. Magn. Reson.*, 1999, **139**, 213.
175 D. E. Warschawski and P.F. Devaux, *J. Magn. Reson.*, 2000, **145**, 367.
176 V. Kurze, B. Steinbauer, T. Huber and K. Beyer, *Biophys. J.*, 2000, **78**, 2441.
177 M. Cotten, R. Fu and T.A. Cross, *Biophys. J.*, 1999, **76**, 1179.
178 K. Mattila, R. Kinder and B. Bechinger, *Biophys. J.*, 1999, **77**, 2102.
179 S. Massou, M. Tropis and A. Milon, *J. Chim. Phys. Phys.-Chim. Biol.*, 1999, **96**, 1595.
180 A.W. Hing, J. Schaefer and G.S. Kobayashi, *Biochem. Biophys. Acta*, 2000, **1463**, 323.
181 F.M. Marassi and S.J. Opella, *J. Magn. Reson.*, 2000, **144**, 150.
182 J. Wang, J. Denny, C. Tian, S. Kim, Y. Mo, F. Kovacs, Z. Song, K. Nishimura, Z. Gan, R. Fu, J.R. Quine and T.A. Cross, *J. Magn. Reson.*, 2000, **144**, 162.
183 F.M. Marassi, C. Ma, J.J. Gesell and S.J. Opella, *J. Magn. Reson.*, 2000, **144**, 156.
184 F.M. Marassi, S.J. Opella, P. Juvvadi and R.B. Merrifield, *Biophys. J.*, 1999, **77**, 3152.
185 M. Tornblom, R. Sitnikov and U. Henriksson, *Liq. Cryst.*, 2000, **27**, 943.
186 R.H. Acosta and D.J. Pusiol, *Phys. Rev. E*, 2000, **63**, 011707.
187 C.R. Rodriguez, F.V. Chavez, D.J. Pusiol, A.M.F. Neto and R.-O. Seitter, *J. Chem. Phys.*, 2000, **113**, 10809.
188 D. Catalano, M. Cifelli, M. Geppi and C.A. Veracini, *J. Phys. Chem. A*, 2001, **105**, 34.
189 R.Y. Dong and C.R. Morcombe, *Liq. Cryst.*, 2000, **27**, 897.
190 E.E. Burnell, D. Capitani, C. Casieri and A.L. Segre, *J. Phys. Chem. B*, 2000, **104**, 8782.
191 R.Y. Dong, A. Carvalho, P.J. Sebastiao and H.T. Nguyen, *Phys. Rev. E*, 2000, **62**, 3679.
192 R. Y. Dong, *Phys. Rev. E*, 1999, **60**, 5631.
193 R. Y. Dong and M. Cheng, *J. Chem. Phys.*, 2000, **113**, 3466.
194 D.J. Pusiol and F. Vaca Chavez, *Chem. Phys. Lett.*, 1999, **312**, 91.
195 O. Mensio, R.C. Zamar, D.J. Pusiol and S. Becker, *J. Chem. Phys.*, 1999, **110**, 8155.
196 R.H. Acosta and D.J. Pusiol, *Phys. Rev. E*, 1999, **60**, 1808.
197 J. Bharatam and C.R. Bowers, *J. Phys. Chem. B*, 1999, **103**, 2510.
198 F. Castiglione, G. Celebre, G. De Luca and M. Longeri, *J. Magn. Reson.*, 2000, **142**, 216.
199 R.T. Syvitski and E.E. Burnell, *J. Magn. Reson.*, 2000, **144**, 58.
200 R.T. Syvitski and E.E. Burnell, *Can. J. Chem.*, 1999, **77**, 1761.
201 C. Algieri, F. Castiglione, G. Celebre, G. De Luca, M. Longeri and J.W. Emsley, *Phys. Chem. Chem. Phys.*, 2000, **2**, 3405.
202 Y. Sasanuma, *Polym. J.*, 2000, **32**, 883.
203 Y. Sasanuma, *Polym. J.*, 2000, **32**, 890.
204 H. Takeuchi, K. Inoue, Y. Ando and S. Konaka, *Chem. Lett.*, 2000, 1300.
205 R. Kemp-Harper, B. Wickstead and S. Wimperis, *J. Magn. Reson.*, 1999, **140**, 351.
206 Y. Arfaoui and E. Haloui, *Mag. Reson. Chem.*, 2000, **38**, 639.
207 H. Kiyono, K. Inoue, H. Takeuchi and S. Konaka, *J. Mol. Struct.*, 1999, **476**, 73.
208 P. Berdague, P. Judeinstein, J.-P. Bayle, C.S. Nagaraja, N. Sinha and K.V. Ramanathan, *Liq. Cryst.*, 2001, **28**, 197.

209 H. Sun and B.M. Fung, *Liq. Cryst.*, 2000, **27**, 755.
210 D. Catalano, M. Cavazza, L. Chiezzi, M. Geppi and C.A. Veracini, *Liq. Cryst.*, 2000, **27**, 621.
211 L. Calucci, D. Catalano, K. Fodor-Csorba, C. Forte and C. A. Veracini, *Mol. Cryst. Liq. Cryst.*, 1999, **331**, 9.
212 D. Catalanoa, E. Chiellini, L. Chiezzi, K. Fodor-Csorba, G. Galli, E. Gacs-Baitz, S. Holly and C.A. Veracini, *Mol. Cryst. Liq. Cryst.*, 1999, **336**, 111.
213 R.Y. Dong, N. Boden, R.J. Bushby and P.S. Martin, *Mol. Phys.*, 1999, **97**, 1165.
214 B. Zalar, O.D. Lavrentovich, H. Zeng and D. Finotello, *Phys. Rev. E*, 2000, **62**, 2252.
215 A. Peshkovsky and A.E. McDermott, *J. Phys. Chem. A*, 1999, **103**, 8604.
216 V.P. Dmitriev and G.R. Ouriques, *Phys. Rev. E*, 1999, **60**, 1840.
217 O. Pelletier, P. Sotta and P. Davidson, *J. Phys. Chem. B*, 1999, **103**, 5427.
218 M. Vilfan, N. Vrbancic-Kopac, P. Ziherl and G.P. Crawford, *Appl. Magn. Reson.*, 1999, **17**, 329.
219 P. Ziherl, M. Vilfan, N. Vrbancic-Kopac, S. Zumer, R.J. Ondris-Crawford and G.P. Crawford, *Phys. Rev. E*, 2000, **61**, 2792.
220 A. Hohener, L. Muller and R.R. Ernst, *Mol. Phys.*, 1979, **38**, 909.
221 C. Canlet and B.M. Fung, *J. Phys. Chem. B*, 2000, **104**, 6181.
222 D. Catalano, M. Cifelli, K. Fodor-Csorba, E. Gacs-Baitz, M. Geppi, A. Jakli and C.A. Veracini, *Mol. Cryst. Liq. Cryst. A*, 2000, **351**, 245.
223 L. Weiss, E. Boris, G. Mino, R. Araya-Maturana and A.S. Tracey, *Langmuir*, 2000, **16**, 4040.
224 G. Szalontai, *Magn. Reson. Chem.*, 2000, **38**, 872.
225 H. Dehne, M. Potter, S. Sokolowski, W. Weissflog, S. Diele, G. Pelzl, I. Wirth, H. Kresse, H. Schmalfuss and S. Grande, *Liq. Cryst.*, 2001, **28**, 1269.
226 A. Carvalho, P.J. Sebastiao and H.T. Nguyen, *Mol. Cryst. Liq. Cryst.*, 1999, **331**, 89.
227 H. Fujimori, J.-P. Bayle and S. Miyajima, *J. Phys. Soc. Jpn.*, 2000, **69**, 3090.
228 G. Celebre, G. De Luca and M. Longeri, *Phys. Chem. Chem. Phys.*, 2000, **2**, 1883.
229 G. Celebre, G. de Luca and M. Longeri, *Mol. Phys.*, 2000, **98**, 559.
230 V.V. Aleksanndriiskii, I.V. Novikov, A.I. Pirogov and V.A. Burmistrov, *Izv. Vyssh. Uchebn. Zaved., Khim. Khim. Teknol.*, 1999, **42**, 39.
231 E.E. Burnell, C.A. deLange and S. Gaemers, *Chem. Phys. Lett.*, 2001, **337**, 248.

As a spectroscopic method, nuclear magnetic resonance (NMR) has seen spectacular growth over the past two decades, both as a technique and in its applications. Today the applications of NMR span a wide range of scientific disciplines, from physics to biology to medicine. Each volume of Nuclear Magnetic Resonance comprises a combination of annual and biennial reports which together provide comprehensive coverage of the literature on this topic. This Specialist Periodical Report reflects the growing volume of published work involving NMR techniques and applications, in particular NMR of natural macromolecules which is covered in two reports: "NMR of Proteins and Nucleic Acids" and "NMR of Carbohydrates, Lipids and Membranes".

For those wanting to become rapidly acquainted with specific areas of NMR, this title provides unrivalled scope of coverage. Seasoned practitioners of NMR will find this an invaluable source of current methods and applications.

ISBN 0-85404-337-3

9 780854 043378 >

SPECIALIST PERIODICAL REPORTS

Specialist Periodical Reports provide systematic and detailed review coverage in major areas of chemical research. Compiled by teams of leading authorities in the relevant subject areas, the series creates a unique service for the active research chemist, with regular, in-depth accounts of progress in particular fields of chemistry. Subject coverage within different volumes of a given title is similar and publication is on an annual or biennial basis.

Current subject areas covered are *Amino Acids, Peptides and Proteins, Carbohydrate Chemistry, Catalysis, Chemical Modelling: Applications and Theory, Electron Paramagnetic Resonance, Nuclear Magnetic Resonance, Organometallic Chemistry, Organophosphorus Chemistry, Photochemistry* and *Spectroscopic Properties of Inorganic and Organometallic Compounds*. From time to time, the series has altered according to the fluctuating degrees of activity in the various fields, but these volumes remain a superb reference point for researchers.